MEDICAL RADIOLOGY

Diagnostic Imaging

A. L. Baert
M. Knauth
K. Sartor

Spinal Imaging

Diagnostic Imaging of the Spine and Spinal Cord

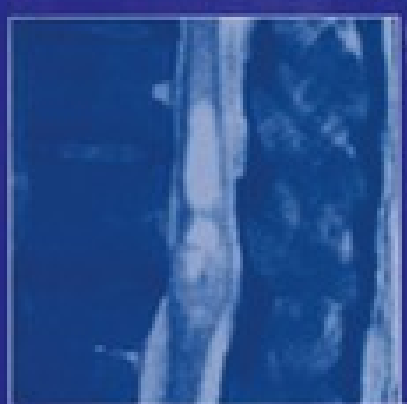

J. Van Goethem
L. van den Hauwe
P. M. Parizel
Editors

Springer

MEDICAL RADIOLOGY

Diagnostic Imaging

J. W. M. Van Goethem · L. van den Hauwe
P. M. Parizel (Eds.)

Spinal Imaging

Diagnostic Imaging of the Spine and Spinal Cord

With Contributions by

P. R. Algra · C. Andreula · D. Balériaux · S. M. Belkoff · R. G. Bhatia · B. C. Bowen
O. Boyunaga · A. Cama · S. Capoccia · R. Cartolari · A. Y. Choi · M. Colajacomo
C. Cristaudo · P. Demaerel · A. M. De Schepper · M. Gallucci · C. Gandolfo · N. Gültaşli
R. Gunzburg · S. H. M. Kahn · D. S. Katz · P. E. Kim · B. Koes · J. Kråkenes
S. J. Lypen · M. Maes · C. Manelfe · L. Manfré · M. Murrone · A. O. Ortiz · Ö. Özsarlak
P. M. Parizel · A. Rossi · R. Salgado · M. Szpalski · E. T. Tali · M. M. Thurnher
P. Tortori-Donati · G. Trasimeni · A. Van Campenhout · E. van de Kelft
L. van den Hauwe · J. W. M. Van Goethem · F. M. Vanhoenacker · M. van Tulder
M. Voormolen · C. S. Zee

Foreword by

A. L. Baert

With 477 Figures in 1218 Separate Illustrations, 36 in Color and 67 Tables

Springer

Johan W. M. Van Goethem, MD, PhD
Department of Radiology, University Hospital Antwerpen
Wilrijkstraat, 10
2650 Edegem, Belgium
and
Department of Radiology, Algemeen Ziekenhuis Nikolaas
Moerlandstraat 1
9100 Sint-Niklaas, Belgium

Luc van den Hauwe, MD
Department of Radiology, University Hospital Antwerpen
Wilrijkstraat 10
2650 Edegem, Belgium
and
Department of Radiology, AZ KLINA
Augustijnslei 100
2930 Brasschaat, Belgium

Paul M. Parizel, MD, PhD
Department of Radiology, University Hospital Antwerpen
Wilrijkstraat 10
2650 Edegem, Belgium

Medical Radiology · Diagnostic Imaging and Radiation Oncology
Series Editors:
A. L. Baert · L. W. Brady · H.-P. Heilmann · M. Knauth · M. Molls · C. Nieder · K. Sartor

Continuation of Handbuch der medizinischen Radiologie
Encyclopedia of Medical Radiology

Library of Congress Control Number: 2005929008

ISBN 978-3-540-21344-4 Springer Berlin Heidelberg New York

Springer is part of Springer Science+Business Media

http//www.springer.com

Printed in Germany

Medical Editor: Dr. Ute Heilmann, Heidelberg
Desk Editor: Ursula N. Davis, Heidelberg
Production Editor: Kurt Teichmann, Mauer
Cover-Design and Typesetting: Verlagsservice Teichmann, Mauer

Printed on acid-free paper – 21/3151xq – 5 4 3 2 1 0

Foreword

Medical imaging of the spine is among the most frequently performed diagnostic studies due to the high incidence of the very common clinical problem of acute or chronic back pain.

Radiologists have a whole range of diagnostic modalities at their disposal to study spine pathology. It is of the utmost importance that they be familiar with the advantages and disadvantages of these different diagnostic techniques and are able to apply, in each clinical situation, the method that is most likely to optimally solve the clinical problem and indicate its correct management.

Many authors, all well known specialists in their field, have contributed to this book which offers a very complete update of our current insights into and knowledge of common and less common disorders of the spine and the spinal cord.

The illustrations are numerous, highly informative and of impeccable technical quality.

I am very much indebted to the editors, J.W.M. Van Goethem, L. van den Hauwe and P.M. Parizel, for this superb volume which very much enriches the Medical Radiology series. It will be of great interest to radiologists in training, certified radiologists, as well as to neurosurgeons, neurologists and rheumatologists.

Leuven

Albert L. Baert

Preface

Diseases of the spine are very common. They affect up to 80% of the population worldwide and may cause pain, disability and economic loss. Pain or discomfort originating in the spine is usually a self-limiting condition. In more than 50% of patients, symptoms usually resolve spontaneously within 4–8 weeks, but there is a very high recurrence rate, estimated at about 85%. Back pain ranks seventh among the top costliest health conditions and is only preceded by heart disease, diabetes, hypertension, stroke-related conditions, osteoarthritis and pneumonia. Spinal imaging is one of the most common radiology procedures in general and is also the most performed MR imaging examination in many countries.

Although the indication for spinal imaging in specific spinal problems, such as trauma, is evident, the role of imaging in the diagnosis of neck and low back pain often remains controversial. Many so-called radiographic abnormalities seen on CT and MRI are commonly also encountered in asymptomatic individuals, a phenomenon carefully explained in this book.

This book aims to provide an overview of diagnostic spinal imaging. It is a comprehensive textbook with many illustrations and tables, yet easy to use with logical chapter-by-chapter coverage of different spinal pathologies. Extensive coverage of common spinal conditions, such as the degenerative diseases, spinal trauma, spinal surgery and imaging of the postoperative spine, spinal tumors, as well as spinal infection and inflammation, make this a very helpful book for everyday use in any practice involved with spinal imaging.

I would like to take the opportunity to thank everybody who made this project possible.

In the Name of Friendship

My thanks go first of all to my co-editors, Paul Parizel and Luc van den Hauwe, without whom this book would not have existed. Luc was the originator, pointing out the fact that a volume on spinal imaging was missing in the Diagnostic Imaging series. Additionally, I have to thank Prof. Albert Baert for believing in our ability and giving us the opportunity to write this book.

I also wish to thank the more than 40 contributors for their tremendous efforts in making this book possible; I know most of them personally and am very grateful to have been able to collaborate on this project with real friends. Finally, I have to thank Paul and Luc for their remarkable efforts in realizing this book together with me – it would not have been possible without them.

In the Name of Love and Family

This book could not have been completed without the continuing support of my wife, Isabelle, who, as a radiologist herself, not only understood my endeavours to complete this work, but who was also my most loyal supporter. As the mother of our three daughters, Alexia, Olivia and Félicia, she is also the cornerstone of our wonderful family and I wish to dedicate this book to these four women in my life.

Edegem — Johan W. M. Van Goethem

This book is dedicated first and foremost to the ones I love: Marleen, my wife, and our children Vincent, Isabel, Liesa and Marie. Our children, they are the future.

My thanks go to Paul and Johan, not only for teaching me neuroradiology, but primarily for their friendship. We have been working together for many years now in the spirit of the three musketeers (Les Trois Mousquetaires, a novel by Alexandre Dumas), inseparable men who chant the motto "One for all, and all for one".

Edegem — Luc van den Hauwe

I dedicate this book to:

- My wife, Vera, and to my son, Maxim, who mean everything to me
- My neuroradiology teachers in Antwerp, Boston, Brussels and Philadelphia, who programmed my brain with their wisdom and enthusiasm
- My friends and colleagues, Johan Van Goethem and Luc van den Hauwe, from whom I still learn everyday
- The happy coincidence which brought us all together: "in infinito vacuo, ex fortuita atomorum collisione"

Edegem — Paul M. Parizel

Contents

Congenital

Congenital Malformations of the Spine, Spinal Cord, and Cranio-Cervical Junction

1

Andrea Rossi, Carlo Gandolfo, Armando Cama, and Paolo Tortori-Donati

CONTENTS

1.1 Congenital Malformations of the Spine and Spinal Cord

1.1.1 Introduction

Congenital malformations of the spine and spinal cord are generally referred to as spinal dysraphisms. These conditions are usually diagnosed prenatally, at birth, or in early infancy; however, some may be discovered in older children or adults. Magnetic resonance imaging (MRI) has made the diagnosis of these disorders easier, faster, and more accurate, thereby enhancing the possibility of an early and case-tailored treatment, mainly thanks to its multiplanar imaging and tissue characterization capabilities. Classification of spinal dysraphisms requires a balanced correlation of clinical, neuroradiological, and embryological information. Use of classification schemes may prove helpful in making a diagnosis in everyday clinical practice (Tortori-Donati et al. 2000; Tortori-Donati et al. 2001; Rossi et al. 2004a,b; Tortori-Donati et al. 2005b). Although the MRI picture in patients with spinal cord malformations may appear complicated and puzzling even to the experienced observer, we believe that a rational approach focusing on a correlation among clinical, embryological, and neuroradiological data greatly facilitates the diagnosis. Neuroradiologists should pursue the maximum degree of collaboration with neurosurgeons and other specialists involved in the management of

A. Rossi, MD
Senior Staff Neuroradiologist, Department of Pediatric Neuroradiology, G. Gaslini Children's Research Hospital, Largo G. Gaslini 5, 16147 Genoa, Italy
C. Gandolfo, MD
Staff Neuroradiologist, Department of Pediatric Neuroradiology, G. Gaslini Children's Research Hospital, Largo G. Gaslini 5, 16147 Genoa, Italy
A. Cama, MD
Head, Department of Pediatric Neurosurgery, G. Gaslini Children's Research Hospital, Largo G. Gaslini 5, 16147 Genoa, Italy
P. Tortori-Donati, MD
Head, Department of Pediatric Neuroradiology, G. Gaslini Children's Research Hospital, Largo G. Gaslini 5, 16147 Genoa, Italy

KEY POINTS

Spinal Dysraphism

- General term used for congenital malformations of the spine and/or spinal cord. Spina bifida is widely used as a synonym but strictly speaking only indicates defective fusion
- Caused by embryological derangement between gestational weeks 2 and 6
- Open spinal dysraphism (OSD; characterized by exposure of nervous tissue through a congenital defect
  - Almost 99% are myelomeningoceles
  - Variable degree of sensorimotor deficits, bowel and bladder dysfunction
  - All patients with OSD have Chiari II
  - Role of MRI: anatomic characterization; presurgical evaluation; identification of cord splitting when present
- Closed spinal dysraphism (CSD) is covered by skin and has two main subtypes:
  - CSD with subcutaneous mass
    - In the vast majority this mass is a lipoma tethering the spinal cord: lipomyelo(meningo-)cele
  - CSD without subcutaneous mass are often clinically occult and several types are recognized among which:
    - Intradural lipoma
    - Filar lipoma
    - Tight filum terminale: conus inferior to L2
    - Dermal sinus: above the intergluteal cleft
    - Persistent terminal ventricle, usually asymptomatic except when very large
    - Diastematomyelia: split cord. Associated tight filum terminale, hydromyelia, vertebral anomalies, and/or scoliosis are common. Type I with osteocartilaginous spur, type II without spur
    - Caudal agenesis: total or partial agenesis of the caudal portion of the spine, anal imperforation, genital anomalies, renal dysplasia, pulmonary hypoplasia, and/or lower limb anomalies. Type I with high and abrupt-ending conus, type II with low and tethered conus.

Congenital malformations of the cranio-cervical junction

- Can be bony and/or nervous
- Measurements:
  - Chamberlain's line: hard palate – posterior margin foramen magnum
  - McGregor's line: hard palate – lowest point occipital bone
- Chiari-I malformation
  - Cerebellar tonsils >5 mm below basion-opisthion line or 3–5 mm and neurological signs or peg-like tonsils or syrinx
    - 14–56% neurologically normal
    - Significant incidence of hydrosyringomyelia and/or hydrocephalus
- Chiari-II malformation
  - Small posterior fossa
  - Downward displacement of vermis, brainstem and fourth ventricle
  - 90% has OSD
  - Associated brain malformations
- Chiari-III malformation
  - Chiari II + cephalocele
- Chiari-IV malformation
  - Severe cerebellar hypoplasia + myelomeningocele

these patients in order to improve their diagnostic capabilities and to provide more useful information for the management of these children.

In this chapter, the basic concepts about normal and deranged spinal cord embryogenesis are summarized, the principal malformations are described, and a practical approach to neuroradiological decision-making is offered. Additionally, because the Chiari-II malformation is part of the myelomeningocele malformative spectrum, the Chiari malformations are also discussed in this chapter.

1.1.2 Embryology

Spinal dysraphisms are caused by derangements that occur during a fairly limited period of time in the early embryological development, situated between gestational weeks 2 and 6. During this period, three consecutive stages occur, i.e., gastrulation (weeks 2–3), primary neurulation (weeks 3–4), and secondary neurulation (weeks 5–6) (Tortori-Donati et al. 2000; Tortori-Donati et al. 2001; Rossi et al. 2004a,b; Tortori-Donati et al. 2005b).

1.1.2.1 Gastrulation

During gastrulation, the bilaminar embryonic disk, formed by epiblast (future ectoderm) and primitive endoderm is converted into a trilaminar disk because of formation of an intervening third layer, the mesoderm (Fig. 1.1). This process begins by day 14 or 15 when the primitive streak, a stripe of thickened epiblast composed by totipotential cells, appears along the midline of the inferior portion of the dorsal surface of the embryo. The primitive streak has a knob-like cranial termination called Hensen's node. Epiblastic cells start migrating toward the primitive streak and pass inward at the primitive pit, a central depression of Hensen's node, to ingress the interface between the epiblast and the primitive endoderm. Subsequent waves of epiblastic cells migrating laterally along the interface form the interposed mesoderm, whereas cells migrating along the midline form the notochord. The notochord is the foundation of the axial skeleton and extends throughout the entire length of the future vertebral column. From the mesoderm surrounding the neural tube and notochord, the skull, vertebral column, and the membranes of the brain and spinal cord are developed. The notochord is traditionally believed to induce the overlying ectoderm that differentiates into neural ectoderm; however, it has been hypothesized that the default state of the ectoderm is neural ectoderm, and that the notochord is required to preserve such condition (Naidich et al. 2002).

1.1.2.2 Primary Neurulation

Establishment of the neural plate marks the onset of primary neurulation (Fig. 1.2). This occurs on about day 18, when the neural plate starts bending, forming paired neural folds. In the following days, these progressively increase in size and approach each other to eventually fuse in the midline to form the

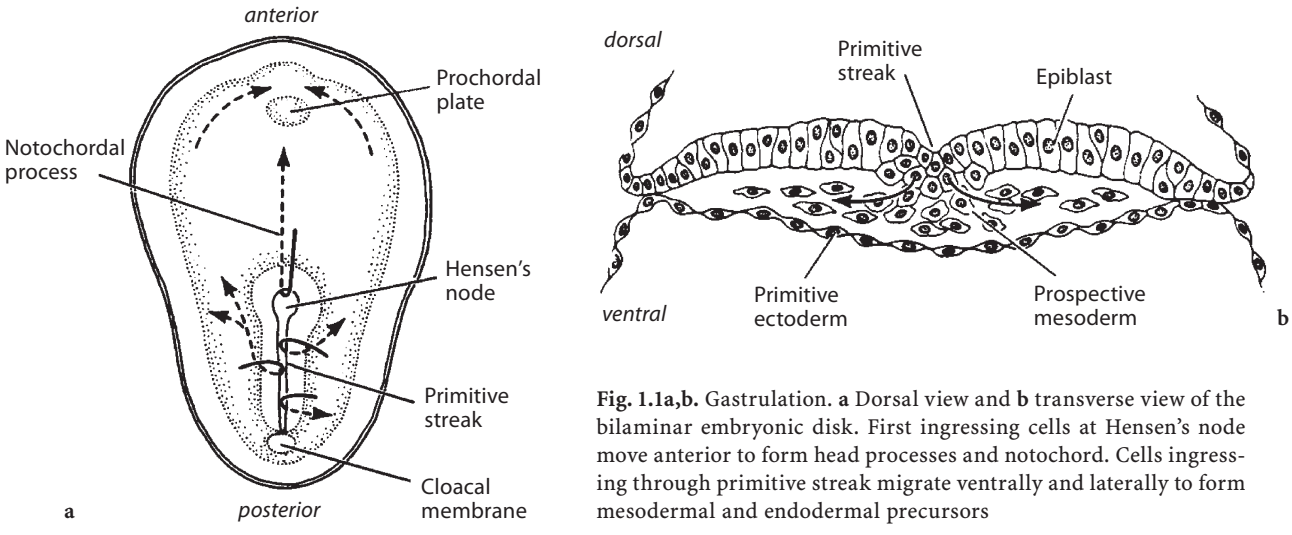

Fig. 1.1a,b. Gastrulation. **a** Dorsal view and **b** transverse view of the bilaminar embryonic disk. First ingressing cells at Hensen's node move anterior to form head processes and notochord. Cells ingressing through primitive streak migrate ventrally and laterally to form mesodermal and endodermal precursors

neural tube. According to the traditional "zipper" model, closure of the neural tube occurs first at level of the fourth somite (future craniocervical junction) and then proceeds both cephalad and caudad. The cranial extremity of the neural tube (rostral or anterior neuropore) closes at day 25, whereas the caudal extremity (caudal or posterior neuropore) closes at days 27 or 28. Closure of the posterior neuropore marks the termination of primary neurulation.

1.1.2.3 Secondary Neurulation

The posterior neuropore, corresponding to the caudal extremity of the primary neural tube, corresponds to the 32nd somite, i.e., the future third sacral metamere. The segment of the spine and spinal cord caudad to somite 32 is formed by secondary neurulation (Fig. 1.3). This embryological step begins immediately after completion of primary neurulation and proceeds until approximately gestational day 48. During secondary neurulation, the tail bud, a mass of cells deriving from the caudal portion of the primitive streak, lays down an additional part of the neural tube caudad to the posterior neuropore. This cord segment differs from the one formed by primary neurulation in several ways. While the primary neural tube results from an upfolding of the lateral borders of the neural plate which join at the midline, the secondary neural tube is formed by an infolding of the neural plate, creating an initially solid medullary cord that subsequently becomes cavitated (Catala 2002; Nievelstein et al. 1993). The fate of the secondary neural tube is to undergo an incompletely understood process of regression, degeneration, and further differentiation, called retrogressive differentiation. This process results in the formation of the tip of the conus medullaris, which contains the lower sacral and coccygeal cord metameres, and the filum terminale, a fibroconnectival structure practically devoid of neural elements. Notably, retrogressive differentiation has not been clearly demonstrated

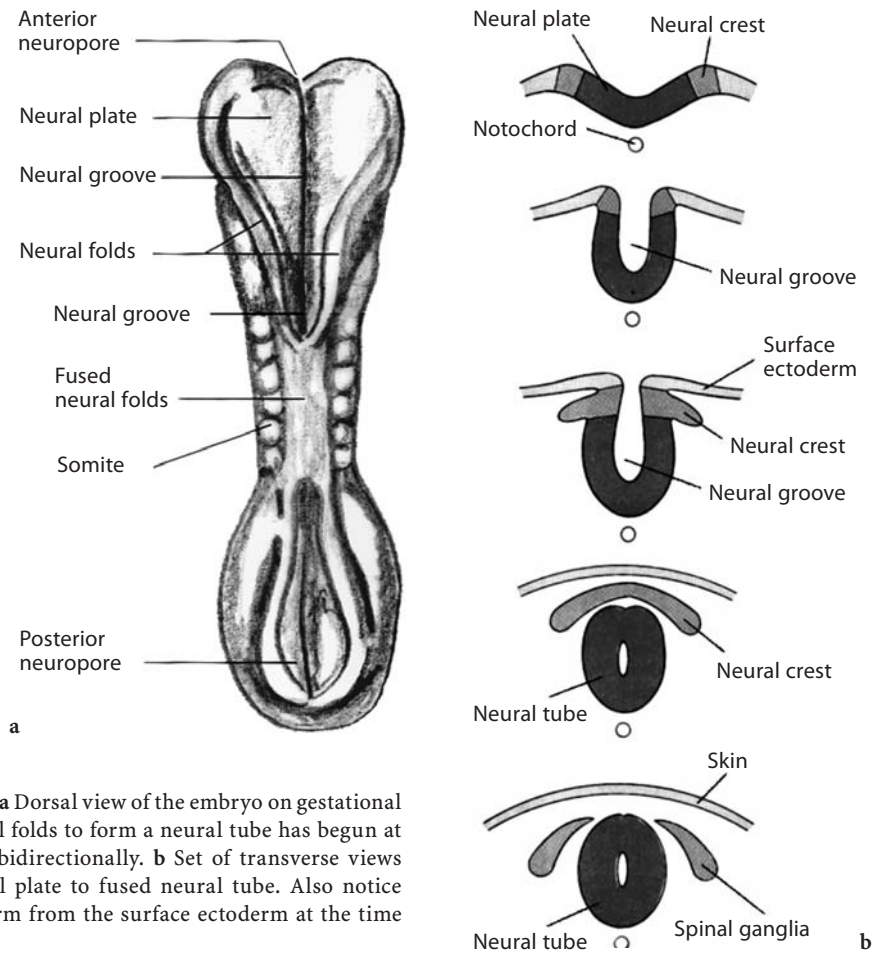

Fig. 1.2a,b. Primary neurulation. **a** Dorsal view of the embryo on gestational day 21 shows fusion of the neural folds to form a neural tube has begun at the cervical level and proceeds bidirectionally. **b** Set of transverse views shows evolution from flat neural plate to fused neural tube. Also notice disjunction of the neural ectoderm from the surface ectoderm at the time of neural tube fusion

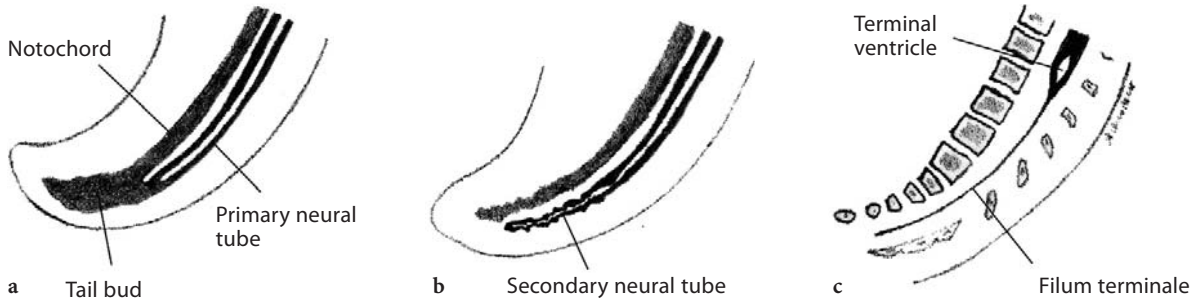

Fig. 1.3a-c. Secondary neurulation. **a** The tail bud forms as a result of coalescence of the neuroectoderm with the lower notochord. **b** A secondary neural tube connects cranially with the neural tube formed by primary neurulation. **c** Eventually, the tip of the conus medullaris and the filum terminale result from this process. The terminal ventricle is the sole remnant of the secondary neural canal (From Tortori-Donati et al. 2005a)

in humans, and a lack of proliferation, rather than regression or degeneration, could actually account for the rudimentary character of the filum terminale (M. Catala, pers. commun.). The conus medullaris contains a focal expansion of the ependymal canal called terminal ventricle, representing the remnant of the lumen of the secondary neural tube.

1.1.2.4 Development of the Vertebral Column

At first, the paraxial trunk mesoderm is unsegmented. As development proceeds, epithelial spheres, called somites, are formed in a cephalo-caudal gradient. These somites mature during development according to a cephalo-caudal gradient. This maturation leads to dissociation of the epithelial somite, forming the dermatome (dorsal), the myotome (intermediate), and the sclerotome (ventral). The dermatome is located underneath the surface ectoderm. It will give rise to dermal cells for the dorsal moiety of the body. The myotome gives rise to all striated muscle fibers of the body. The sclerotome differentiates into cartilaginous cells of the vertebrae, cells of the intervertebral discs and ligaments, and cells of the spinal meninges. Furthermore, the somite gives rise to endothelial cells. The sclerotome is first located ventrally, and then it spreads to enwrap the entire neural tube forming at its dorsal face, the so-called dorsal mesoderm that will insinuate itself between the neural tube and the surface ectoderm after disjunction. On a next step of differentiation, the sclerotomes divide in half horizontally; the bottom half of one fuses with the top half of another to form the vertebrae. Notochordal remnants between the vertebrae become the nucleus pulposus within the intervertebral disk.

1.1.3 Terminology

1.1.3.1 Open and Closed Spinal Dysraphisms

Etymologically "dysraphism" implies defective closure of the neural tube and should therefore be used to refer to abnormalities of primary neurulation only; however, the term has gained widespread use as a synonym to congenital spinal cord malformation.

Spinal dysraphisms are categorized into open spinal dysraphisms (OSD) and closed spinal dysraphisms (CSD) (Tortori-Donati et al. 2000; Tortori-Donati et al. 2001; Rossi et al. 2004a,b; Tortori-Donati et al. 2005b). The OSDs are characterized by exposure of nervous tissue to the environment through a congenital defect in the child's back. On the contrary, CSDs are covered by skin, although cutaneous birthmarks, such as angiomas, dimples, overgrowing hair, dyschromia, and dystrophy, are present in more than 50% of cases (Drolet 1998; Warder 2001). Use of the term "occult spinal dysraphisms" is discouraged as it suggests complete absence of external abnormalities, a condition that occurs only in a minority of CSDs (Tortori-Donati et al. 2000).

1.1.3.2 Spina Bifida

Strictly speaking, "spina bifida" indicates defective fusion of the vertebral neural arch (French 1983); however, it is widely used as a synonym of spinal dysraphism. The terminology "spina bifida aperta" (or "cystica") and "spina bifida occulta" refers to OSD and CSD, respectively (Sattar et al. 1996),

and is presently discouraged (Tortori-Donati et al. 2000; Tortori-Donati et al. 2001; Rossi et al. 2004a,b; Tortori-Donati et al. 2005b).

1.1.3.3 Placode

The placode is a segment of non-neurulated embryonic neural tissue, i.e., frozen at the neural plate stage (Tortori-Donati et al. 2000; Tortori-Donati et al. 2001; Rossi et al. 2004a,b; Tortori-Donati et al. 2005b). All OSDs are characterized by the presence of a placode that grossly corresponds to the segment of the spinal cord that is exposed externally. Several, but not all, forms of CSDs also have a placode, but in this case the integuments cover it. A placode may be categorized into terminal and segmental depending on location along the spinal cord. A terminal placode lies at the caudal end of the spinal cord and may in turn be either apical or parietal, depending on whether the defect involves the apex or a longer segment of the cord. Conversely, a segmental placode lies at an intermediate level along the spinal cord, which regains normal morphology and structure caudad to the abnormality (Tortori-Donati et al. 2000; Tortori-Donati et al. 2001; Rossi et al. 2004a,b; Tortori-Donati et al. 2005b).

1.1.3.4 Tethered Cord

Many researchers believe that the tethered cord is some sort of malformation, and especially confuse this term with the tight filum terminale, a CSD characterized by a short, rigid filum terminale. This common belief is entirely inappropriate, and the term should in fact be used to indicate a clinical condition, the tethered cord syndrome (TCS) (Tortori-Donati et al. 2000; Tortori-Donati et al. 2001; Rossi et al. 2004a,b; Tortori-Donati et al. 2005b). The TCS occurs as a consequence of traction on a low-lying conus medullaris with progressive neurological deterioration due to metabolic derangement (Warder and Oakes 1993, 1994) and may ensue as a complication of myelomeningocele repair or as the presentation of several forms of CSD, including spinal lipomas, the tight filum terminale, diastematomyelia, and caudal agenesis. The clinical picture of TCS includes sensorimotor dysfunction, muscle atrophy, decreased or hyperactive reflexes, urinary incontinence, spastic gait, and orthopedic deformities such as scoliosis or foot and hip deformity.

1.1.4 Building a Classification

Most authors have tried to classify spinal dysraphisms on the basis of a correlation of pathological–radiological features with specific developmental derangements that are believed to explain such features; however, traditional classification schemes are continuously challenged by new knowledge about both normal and deranged embryogenesis. Unfortunately, we are far from understanding the genetic factors that play a role in the normal and abnormal development of the spine and spinal cord. Until then, it will be unlikely that classifications will explain the full spectrum of abnormalities encountered, and individual cases will continue to escape rigid categorization. From a practical perspective, it is important to use a conceptual framework that relies on identifying those factors that critically restrict the scope of possible diagnoses (Table 1.1).

The initial step in this intellectual approach is clinical. Is the malformation exposed to air, or is there intact skin coverage? In other words, the most basic categorization is that between OSD and CSD (Fig. 1.4) (Tortori-Donati et al. 2000; Tortori-Donati et al. 2001; Rossi et al. 2004a,b; Tortori-Donati et al. 2005b).

1.1.4.1 Classifying Open Spinal Dysraphisms

Only four varieties of OSD exist, with myelomeningocele taking the lion's share (98.8% of cases) (Tortori-Donati et al. 2000). Clinically, myelomeningoceles are characterized by elevation of the neural placode by the underlying expanded subarachnoid space, whereas in myelocele the placode is flush with the surface of the back. Such differentiation is clinical and the neuroradiologist plays little part in it. Conversely, it is the neuroradiologist's role to identify the hemimyelocele and hemimyelomeningocele, very rare entities in which the closure defects affect one hemicord in patients with diastematomyelia. More importantly, the neuroradiologist plays a critical part in the assessment of the Chiari-II malformation, the associated hydrocephalus, and the complications of myelomeningocele repair (Herman et al. 1993; McLone and Dias 1992; Scott et al. 1986).

Table 1.1. Classification of spinal dysraphisms

Open spinal dysraphisms	Closed spinal dysraphisms	
	With subcutaneous mass	Without subcutaneous mass
Myelomeningocele Myelocele Hemimyelomeningocele Hemimyelocele	*Lumbosacral* • Lipomas with dural defect – Lipomyelomeningocele – Lipomyelocele • Terminal myelocystocele • Meningocele	*Simple dysraphic states* • Intradural lipoma • Filar lipoma • Tight filum terminale • Persistent terminal ventricle • Dermal sinus
	Cervico-thoracic • Nonterminal myelocystocele • Meningocele	*Complex dysraphic states* • Disorders of midline notochordal integration – Diastematomyelia – Neurenteric cysts – Dorsal enteric fistula • Disorders of segmental notochordal formation – Caudal agenesis – Segmental spinal dysgenesis

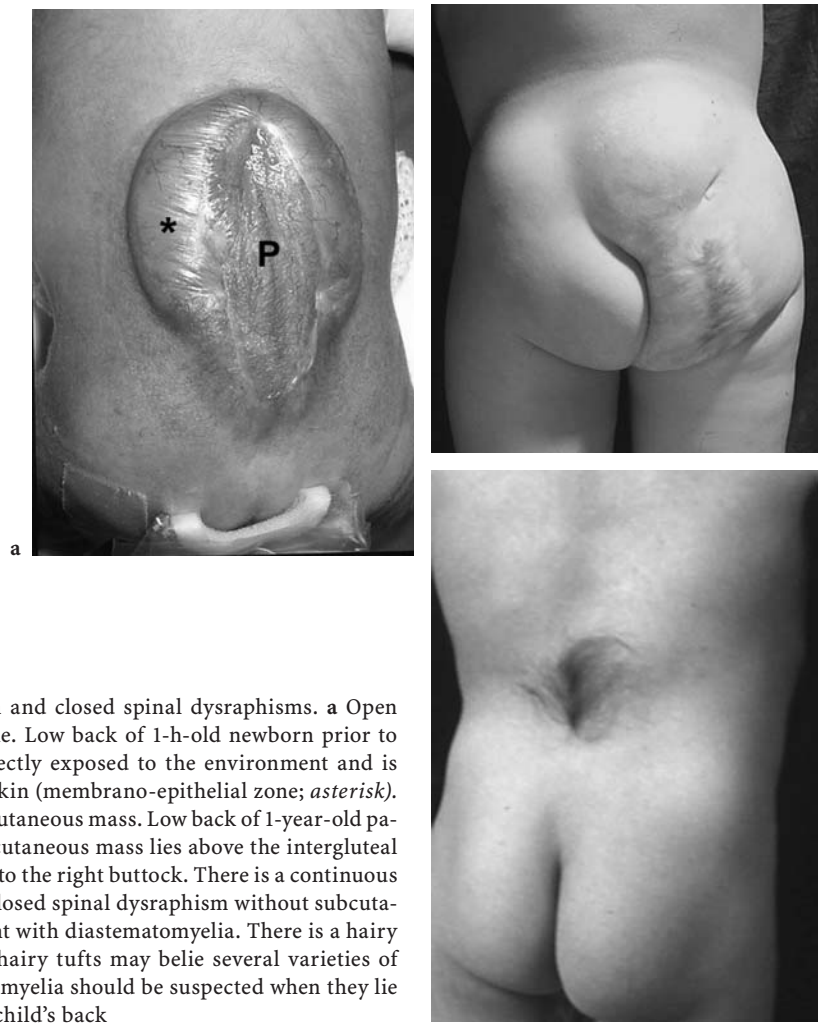

Fig. 1.4a-c. External features of open and closed spinal dysraphisms. **a** Open spinal dysraphism: myelomeningocele. Low back of 1-h-old newborn prior to surgery. The wide placode *(P)* is directly exposed to the environment and is surrounded by partially epithelized skin (membrano-epithelial zone; *asterisk).* **b** Closed spinal dysraphism with subcutaneous mass. Low back of 1-year-old patient with lipomyelocele. A large subcutaneous mass lies above the intergluteal crease and extends asymmetrically into the right buttock. There is a continuous skin coverage to the abnormality. **c** Closed spinal dysraphism without subcutaneous mass. Back of 2-year-old patient with diastematomyelia. There is a hairy tuft at high lumbar level. Although hairy tufts may belie several varieties of closed spinal dysraphism, diastematomyelia should be suspected when they lie at a relatively cranial level along the child's back

1.1.4.2 Classifying Closed Spinal Dysraphisms

The CSDs are much more heterogeneous than OSDs. Some are not clinically evident at birth, and patients are brought to medical attention later in infancy when complications, such as TCS, ensue. Clinical examination is significantly helpful to restrict the differential diagnosis. A critical factor in this evaluation is the presence of a subcutaneous mass on the patient's back.

1.1.4.2.1 CSDs with Subcutaneous Mass

In the vast majority of cases, such mass involves the lumbar or lumbosacral level. Only four malformations will present with a subcutaneous mass in this location, i.e., lipomyelocele, lipomyelomeningocele, meningocele, and terminal myelocystocele (Tortori-Donati et al. 2000; Tortori-Donati et al. 2001; Rossi et al. 2004a,b; Tortori-Donati et al. 2005b); among these, lipomyelocele and lipomyelomeningocele are much more common. In both these cases, the mass is represented by a lipoma, and the spinal cord is connected to the lipoma at the level of a placode. Differentiation between the two entities is based on the position of this attachment, the so-called placode–lipoma interface. In lipomyeloceles, the lipomatous tissue creeps into the spinal canal through a posterior bony spina bifida and attaches to the neural placode, i.e., the placode–lipoma interface lies within the spinal canal, whereas in lipomyelomeningoceles, expansion of the subarachnoid spaces pushes the neural placode out of the spinal canal, i.e., the placode–lipoma interface lies outside the spinal canal; therefore, the simple assessment of the location of the placode–lipoma interface with respect to the anatomical borders of the spinal canal will allow a confident diagnosis (Tortori-Donati et al. 2000; Tortori-Donati et al. 2001; Rossi et al. 2004a,b; Tortori-Donati et al. 2005b). The other two entities presenting with a subcutaneous mass in the lumbosacral region are meningoceles and terminal myelocystoceles. These entities are extremely rare, especially the latter. While meningoceles are herniations of a CSF-filled meningeal outpouching, terminal myelocystoceles are complex entities basically characterized by herniation of a hydromyelic cavity that involves the terminal portion of the cord into a meningocele.

The CSD with a tumefaction involving the cervical or thoracic spine are exceedingly rare and are basically represented by a spectrum of nonterminal myelocystoceles, either full-blown (i.e., containing a hydromyelic cavity) or abortive (i.e., composed of a fibroneural stalk that fans out from the posterior aspect of the spinal cord and crosses a skin-covered meningocele) (Rossi et al. 2004c), and by meningoceles

1.1.4.2.2 CSDs Without Subcutaneous Mass

The CSDs without a subcutaneous mass are very heterogeneous both from a clinical and a neuroradiological perspective. Often, they are clinically completely occult; however, thorough assessment of external features is very important to suspect their presence. Although this clinical information is critical in focusing one's attention to a specific subset of dysraphism, it is in the category of CSD without a subcutaneous mass that the neuroradiologist will be challenged most.

Several birthmarks are associated with underlying dysraphisms; among these, focal hirsutism is significantly associated with CSDs. When a hairy tuft lies relatively cephalad along the child's back, presence of diastematomyelia is likely (Tortori-Donati et al. 2000; Tortori-Donati et al. 2001; Rossi et al. 2004a,b; Tortori-Donati et al. 2005b).

Among cutaneous birthmarks, capillary hemangioma is the least sensitive in predicting underlying malformation, although capillary hemangiomas of the lumbar region are associated with spinal dysraphisms in greater than 10% of cases.

Dorsal dimples or ostia can indicate either a dermal sinus or a sacrococcygeal fistula. All fistula openings above the gluteal crease should be presumed to violate the subarachnoid space until proven otherwise. Conversely, skin pits located within the intergluteal cleft need no further investigation as they are related to simple sacrococcygeal cysts or fistulas.

Patients with caudal agenesis (also known as caudal regression syndrome) may have a rudimentary tail, lower limb abnormalities, or anorectal malformations. Imperforate anus is associated with surgically correctable intradural pathology in at least 10% of patients; therefore, all patients with imperforate anus should undergo MR imaging studies. Patients with segmental spinal dysgenesis, a rare entity embryologically related to caudal agenesis, typically

have a protuberance of bony consistence along their back, corresponding to the apex of a kyphotic gibbus at level of the focal bony aplasia, and are congenitally paraplegic or paraparetic.

1.1.5 Open Spinal Dysraphisms

1.1.5.1 Myelomeningocele and Myelocele

Myelomeningocele accounts for 98.8% of all OSDs (Tortori-Donati et al. 2000). In myelomeningocele (Fig. 1.5) the placode herniates, together with the meninges, through a more or less large defect in the midline of the back, typically at the lumbosacral level, and is therefore exposed to the environment. Expansion of the underlying subarachnoid space causes elevation of the surface of the placode above the skin surface. This feature distinguishes myelomeningoceles from the far less common myelocele (Fig. 1.6) or myeloschisis, in which the placode is flush with the cutaneous surface. The degree of motor deficit can be increased by direct injury to the exposed placode during vaginal delivery; therefore, cesarean section is indicated. Because placode ulceration and infection are leading causes of mortality in the untreated newborn, affected patients are operated on soon after birth. Unfortunately, surgery cannot restore complete functional recovery, and surgically treated patients usually exhibit a variable association of sensorimotor deficits of the lower extremities, bowel and bladder incontinence, hindbrain dysfunction, as well as intellectual and psychological disturbances. Intrauterine myelomeningocele repair has been shown to reduce the incidence of shunt-dependent hydrocephalus and the severity of the Chiari-II malformation that is typically associated with OSDs, and could become the standard treatment of myelomeningoceles in the future; however, conclusive evidence of the benefit of prenatal vs postnatal myelomeningocele repair has still to be presented (Walsh and Adzick 2003). It has been shown that leg movements, related to spinal segments caudal to the myelomeningocele, are typically present immediately after birth but are lost after the first postnatal week, indicating that progressive lower motor neuron dysfunction is not significantly affected by surgery, either postnatal or fetal (Sival et al. 2004). It is also estimated that a significant proportion (be-

Fig. 1.6 Myelocele, 12-h-old newborn. Sagittal T1-weighted images shows exposed, slightly funnel-shaped placode *(P)* lying flush with the skin surface. There is dehiscence of subcutaneous fat *(asterisks)*. The lack of expansion of subarachnoid spaces is the only difference from the much more common myelomeningocele (compare with Fig. 1.5)

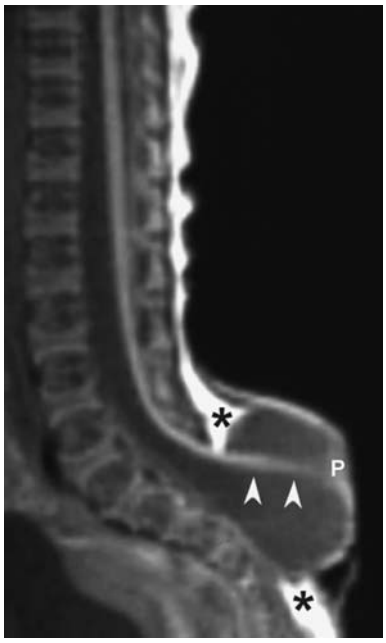

Fig. 1.5 Myelomeningocele, 8-h-old male newborn. Sagittal T1-weighted image of the lumbosacral spine shows the spinal cord *(arrowheads)* crosses the meningeal outpouching and ends with an exposed terminal apical placode *(P)*. Note dehiscent subcutaneous fat *(asterisks)*

tween 20 and 40%) of individuals with OSDs are allergic to latex. Allergic responses can vary from mild to anaphylaxis and occur when latex products touch the skin or mucous membranes. Latex-free devices must therefore be used in the MR environment when these patients are studied.

Embryologically, both myelomeningoceles and myeloceles result from a failure of primary neurulation with persistence of a portion of non-neurulated placode (Dias and Partington 2004). The vast majority involves the lumbosacral spine, and the placode is terminal; however, purely lumbar, thoracolumbar, and even thoracic myelomeningoceles have been described, in which the placode is segmental and the spinal cord caudad to the malformation is normal.

The exposed surface of the placode is what should have become the inner, ependymal surface of the spinal cord and is covered by a rich network of small and friable vessels. This area is called the medullovascular zone. The cutaneous ectoderm never detaches from the neural ectoderm and is forced to remain in a lateral position, resulting in a midline skin defect through which the placode becomes exposed to the environment. Because the mesenchyme cannot migrate behind the neural tube, bones, cartilage, muscles, and ligaments are forced to develop anterolaterally to the neural tissue, and therefore will appear everted. The ventral surface of the placode is what should have become the external surface of the spinal cord, from which the nerve roots originate, the anterior ones medially, and the posterior ones laterally. These nerve roots course obliquely through the subarachnoid space to reach their corresponding neural foramina.

Because these newborns are usually operated on soon after birth, only rarely are MRI studies performed prior to surgery; however, preoperative MRI investigation should be performed whenever possible to obtain: (a) anatomic characterization of the various components of the malformation, especially regarding the relationships between the placode and nerve roots; (b) presurgical evaluation of the entity and morphology of the malformation sequence (hydromyelia, Chiari-II malformation, and associated hydrocephalus); and (c) identification of rare cases with associated cord splitting (hemimyelomeningoceles and hemimyeloceles). MRI of untreated myelomeningoceles shows dehiscence of the subcutaneous fat, fascia, bone, and muscle at the level of the spina bifida, and a low position of the spinal cord that forms the dorsal wall of the defect. In myelomeningoceles, the placode is elevated above the cutaneous surface due to wide dilatation of the subarachnoid spaces, which are crossed by nerve roots that arise from the ventral surface of the placode. In myeloceles, the placode is flush with the skin.

Hydrocephalus usually appears within 48–72 h after surgical repair of the spinal malformation, and is preferentially treated by ventriculoperitoneal shunting. Evaluation of ventricular size is the major reason for referral to neuroradiological examinations during the subsequent clinical history. All patients with OSDs also harbor a Chiari-II malformation, which is an element, rather than an associated feature, of the disease commonly called "myelomeningocele," as well as of the other forms of OSDs and, very rarely, of some skin-covered myelocystoceles. The Chiari-II malformation is described in detail in a subsequent section of this chapter. Deterioration of a previously stable neurological function is another reason for neuroradiological evaluation of these children. This may be caused by retethering of the spinal cord at the surgical site, dysontogenetic masses, or hydromyelia. Retethering by scar is a difficult diagnosis on MRI. In fact, most postoperative MRI studies will show a close relationship between the dorsal surface of the placode and the surgical site also in patients without clinical signs of cord retethering; therefore, scar retethering is usually an exclusion diagnosis. Dysontogenetic masses, prevailingly dermoids, may result from inadvertent inclusion of epidermal cells during surgical repair of the spinal malformation. They are usually located in close vicinity to the surgical site and appear as masses that are usually slightly hyperintense to CSF both on T1- and T2-weighted images and that may enhance in cases of infection or abscessation. Hydromyelia may occur in as many as 80% of operated patients, and may predispose to scoliosis if untreated (Herman et al. 1993; McLone and Dias 1992; Scott et al. 1986).

1.1.5.2 Hemimyelomeningocele and Hemimyelocele

Myelomeningoceles and myeloceles are associated with diastematomyelia in 8–45% of cases (Breningstall et al. 1992; Pang et al. 1992); however, only when failure of neurulation involves one hemicord is the malformation called hemimyelocele (or hemimyelomeningocele when there is associated meningeal expansion). If the cord splitting lies at a different level than the placode, the resulting mal-

formation is merely an association between diastematomyelia and OSD. If such restrictive definition is adopted, then these anomalies become extremely rare (Tortori-Donati et al. 2000).

Affected patients show neurological impairment similarly to those with diastematomyelia, but with markedly asymmetric involvement of the lower limbs (Pang 1992). A hairy tuft bordering one side of an exposed placode is a strong indicator of an underlying cord splitting.

Embryologically, both hemimyeloceles and hemimyelomeningoceles are related to an abnormality of gastrulation with superimposed failure of primary neurulation of one hemicord.

1.1.6 Closed Spinal Dysraphisms

1.1.6.1 CSDs with Subcutaneous Mass

These abnormalities are characterized by a skin-covered mass that covers the underlying malformation. In most cases the mass lies at the lumbosacral level right above the intergluteal cleft. As previously stated, the corresponding anomalies in these cases are represented by the quite common lipomas with dural defect (lipomyelocele and lipomyelomeningocele) and the distinctly uncommon terminal myelocystocele and meningocele (Tortori-Donati et al. 2000; Tortori-Donati et al. 2001; Rossi et al. 2004a,b; Tortori-Donati et al. 2005b). Differential diagnosis basically includes sacrococcygeal teratomas, which are located more caudally, i.e., at or below the intergluteal cleft. The CSDs with associated subcutaneous masses involving the cervical and thoracic spine are exceptional and basically represented by the spectrum of nonterminal myelocystoceles as well as by meningoceles.

1.1.6.1.1 Lipomas with Dural Defect

Lipomyeloceles and lipomyelomeningoceles are characterized by a midline subcutaneous mass, corresponding to a lipoma, located at the lumbosacral level right above the intergluteal cleft and usually extending asymmetrically into one buttock (Naidich et al. 1983). Because the mass is clinically evident at birth, the diagnosis is usually made before significant neurological deterioration ensues; however, infants not treated before the age of 6 months develop hyposthenia and hypotrophy of the lower limb muscles, gait disturbances, urinary incontinence, and paresthesias. These clinical features progress over time if the child is left untreated.

Histologically, the mass is composed of clusters of mature adipocytes separated by collagenous bands, usually associated with other tissues such as striated muscle, cartilage, bone, nerve cells, ependyma, and aberrant neuroglial tissue. Sometimes, these aberrant tissues form hamartomatous masses, called dysraphic hamartomas, which may become macroscopically visible on imaging. Although congenital intraspinal lipomas are anatomically stable lesions (Pierre-Kahn et al. 1997), they may grow harmonically with the physiological increase of adipose tissue throughout childhood (Knittle et al. 1979), as well as in conditions such as pregnancy and obesity.

Embryologically, spinal lipomas are abnormalities of primary neurulation. According to traditional views, they originate from focal premature disjunction of the cutaneous ectoderm from the neuroectoderm, allowing the mesenchyme to penetrate into the neural tube and to contact the primitive ependyma, which induces it to differentiate into fatty tissue (Naidich et al. 1983). An alternative theory postulates an abnormality of the dorsal mesoderm that could either be primitive or secondary to defective induction from the neural tube (Catala (1997).

Lipomyelocele

In spinal lipomas with a dural defect, the anatomic position of the placode–lipoma interface varies depending on the size of the lipoma and the degree of expansion of the subarachnoid spaces. Lipomyeloceles (synonym: lipomyeloschisis) are characterized by a placode–lipoma interface located within the spinal canal. MRI is the imaging modality of choice to demonstrate both the bony defect and the subcutaneous fat extending into the spinal canal and attaching to the spinal cord (Fig. 1.7); the latter is typically low-lying, and the placode–lipoma interface may extend over several vertebral levels. It may be smooth and regular or large and irregular, with stripes of adipose tissue that permeate the spinal cord and penetrate into the ependymal canal. Hydromyelia is usually present in these cases. The size of the spinal canal may be increased in relation to the size of the lipoma, but the size of the subarachnoid space ventral to the cord is consistently normal, marking an important difference from lipomyelomeningoceles.

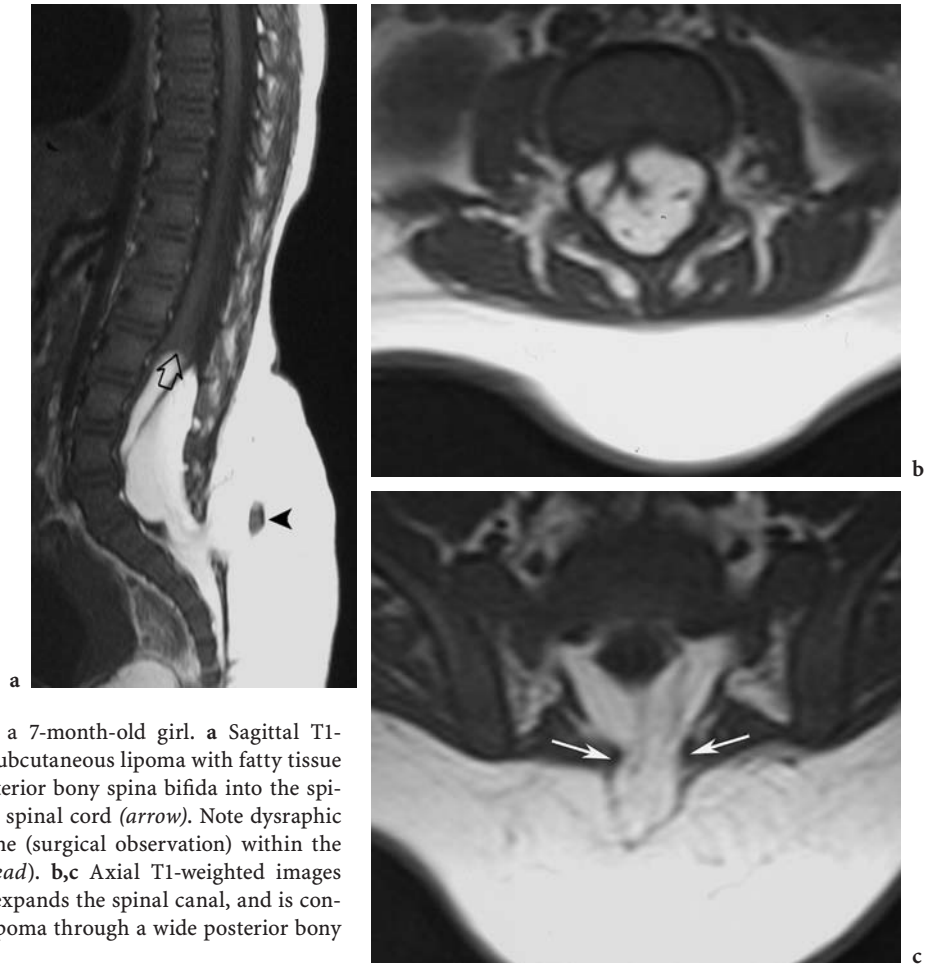

Fig. 1.7a-c. Lipomyelocele in a 7-month-old girl. **a** Sagittal T1-weighted image shows large subcutaneous lipoma with fatty tissue creeping through a wide posterior bony spina bifida into the spinal canal to connect with the spinal cord *(arrow)*. Note dysraphic hamartoma composed of bone (surgical observation) within the subcutaneous mass (*arrowhead*). **b,c** Axial T1-weighted images show lipoma obliterates and expands the spinal canal, and is continuous with subcutaneous lipoma through a wide posterior bony spina bifida (*arrows,* **c**)

Lipomyelomeningocele

In lipomyelomeningoceles, the placode–lipoma interface lies within a posterior meningocele, i.e., anatomically outside the anatomical borders of the spinal canal. Lipomyelomeningoceles may produce a constellation of MRI features and individual cases typically differ from one another because of the variable size of the meningocele and lipoma, as well as the variable orientation of the placode. An archetypal condition in which the placode–lipoma interface lies exactly along the midline is not the rule but rather an exception (Tortori-Donati et al. 2000; Tortori-Donati et al. 2001; Rossi et al. 2004a,b; Tortori-Donati et al. 2005b). In most cases, the placode is stretched and rotated eccentrically towards the lipoma on one side, whereas the meningocele develops on the other side (Fig. 1.8). In such an instance, the spinal roots that emerge from the side facing the meningocele have a redundant course and may be at greater risk for damage during surgery, whereas those lying on the side of the lipoma are shorter and cause cord tethering. Unlike with lipomyeloceles, the spinal canal is dilated because of expansion of the ventral subarachnoid spaces.

1.1.6.1.2 Meningocele

Posterior meningocele is composed of a CSF-filled sac, lined by dura and arachnoid, which herniates through a posterior bony spina bifida. Simple meningoceles are commonly lumbar or sacral in location, but thoracic and even cervical meningoceles are sporadically found. In general, spinal meningoceles are less common than is usually believed, accounting for only 2.4% of all CSDs (Tortori-Donati et al. 2000). Their embryological origin is unknown, although it has been speculated that they might result from ballooning of the meninges

a

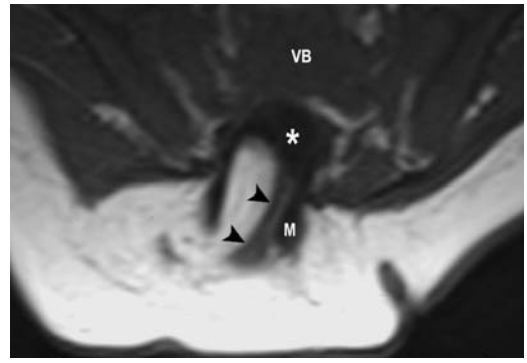

b

Fig. 1.8a,b. Lipomyelomeningocele in a 2-month-old girl. **a** Sagittal T1-weighted image shows large subcutaneous lipoma. The spinal cord, containing a slender dilatation of the ependymal canal (*arrow*) exits the spinal canal through a posterior sacral spina bifida to enter a small meningocele *(M)*. Note enlargement of the subarachnoid space ventral to the cord and concurrent sacral abnormality, which places this case within the setting of the caudal agenesis syndrome. **b** Axial T1-weighted image shows elongated, terminal parietal placode adjoining the lipoma to the right side (*arrowheads*) while a comparatively small meningocele (*M*) develops to the left. Note that, although fat is seen to extend into the spinal canal, the placode-lipoma interface is located outside the spinal canal. *Asterisk* spinal canal, *VB* vertebral body

through a posterior spina bifida due to the relentless pulsations of CSF (Tortori-Donati et al. 2000; Tortori-Donati et al. 2001; Rossi et al. 2004a,b; Tortori-Donati et al. 2005b). By definition, no part of the spinal cord enters the sac, although the nerve roots and, more rarely, a hypertrophied filum terminale may course within the meningocele. The spinal cord itself is completely normal structurally, although it usually is tethered to the neck of sacral meningoceles (Fig. 1.9). Associated anomalies, such as filar lipomas, diastematomyelia, and caudal agenesis, are not uncommon.

1.1.6.1.3 Myelocystocele

Myelocystoceles are rare malformations composed of a herniation of the spinal cord, containing a hydromyelic cavity, within a meningocele. In these skin-covered malformations, neurulation of the spinal cord is practically complete with the sole exception of a limited portion, corresponding to a small placode, that connects with the inner cutaneous surface (limited dorsal myeloschisis).

Myelocystoceles are classified into terminal and nonterminal, depending on whether the malformation involves the apex of the conus medullaris or an intermediate segment of the spinal cord.

Terminal Myelocystocele

Terminal myelocystoceles are located at the lumbosacral level and are composed of a cystic expansion of the central canal of the caudal spinal cord, produced by terminal hydromyelia ("syringocele") that herniates into an expanded dural sheath ("meningocele"). A subcutaneous lipoma is usually associated, so that the abnormality could perhaps be better defined as a "lipomyelocystocele" (Fig. 1.10) (Rossi et al. 2004a,b). The terminal spinal cord cyst communicates with the ependymal canal of the spinal cord and the outer dural sac communicates with the subarachnoid space, but the two cavities do not communicate with each other (Byrd et al. 1995; McLone and Naidich 1985; Peacock and Murovic 1989).

Patients with terminal myelocystoceles are markedly impaired neurologically, with no bowel or bladder control and poor lower-extremity function (Warder 2001). The prognosis is mainly related to the associated anomalies, usually belonging to the OEIS constellation (omphalocele, extrophy of the cloaca, imperforate anus, spinal anomalies) (Carey et al. 1978; Smith et al. 1992).

The embryological origin of terminal myelocystoceles has not yet been determined. Current theories postulate a perturbation of CSF dynamics (Byrd et al. 1995; McLone and Naidich 1985; Peacock and Murovic 1989). Inability of CSF to egress from the

a b

Fig. 1.9a,b. Posterior sacral meningocele in a 7-month-old girl with concurrent caudal agenesis and diastematomyelia. **a** Sagittal T1-weighted image show large sacral cerebrospinal fluid-filled mass *(M)*. The overlying skin is continuous, without dehiscence of the subcutaneous fat. The conus medullaris is low and tethered to the neck of the meningocele (*arrow*). Note concurrent sacrococcygeal agenesis. *Horizontal white line* shows scan plane level of image **b**. **b** Axial T1-weighted image shows associated diastematomyelia *(arrows)* with hydromyelia involving the right hemicord

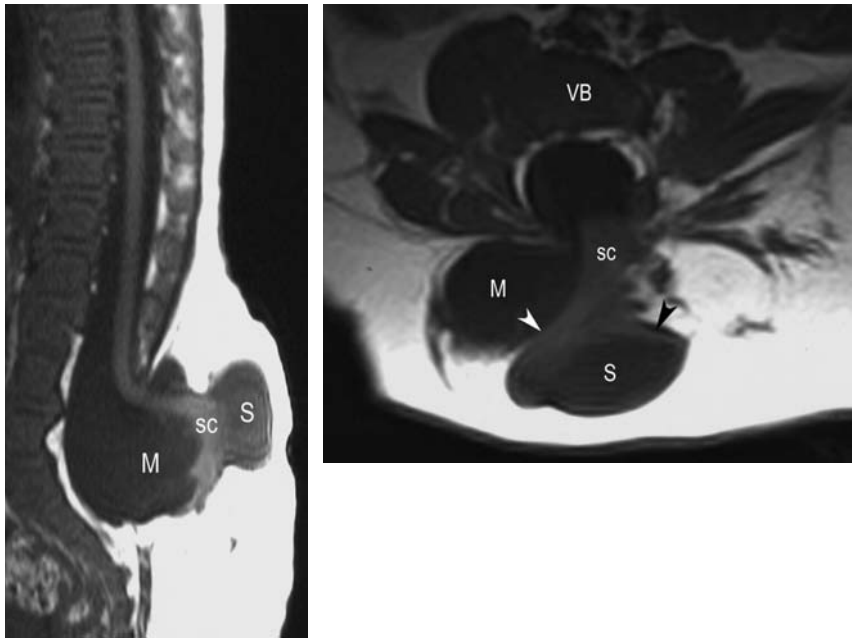

a b

Fig. 1.10a,b. Terminal myelocystocele in a 5-month-old girl. **a** Sagittal T1-weighted image shows complex mass comprised of a large subcutaneous lipoma containing a large meningocele (*M*) into which the spinal cord (*sc*) herniates. The fluid-filled cavity superficial to the cord corresponds to terminal hydromyelia, i.e., the syringocele (*S*). **b** Axial T1-weighted image shows the spinal cord (*sc*) exits the spinal canal and splays (*arrowheads*) to engulf a large terminal hydromyelic cavity, the syringocele (*S*). External to it, the meningocele (*M*) also is displayed. *VB* vertebral body. The overall picture is extremely complex, due to the markedly distorted anatomy. On initial imaging analysis, we were unable to recognize the real nature of the syringocele; therefore, our presumptive diagnosis was lipomyelomeningocele. Only on surgery, displaying continuity of the syringocele with the interior of the spinal cord, was the diagnosis of terminal myelocystocele eventually established. This case exemplifies why these lesions could perhaps be better defined as "lipomyelocystoceles."

neural tube could cause the terminal ventricle to balloon into a cyst that disrupts the overlying mesenchyme; therefore, the terminal myelocystocele could be viewed as a severe, disruptive variety of a persistent terminal ventricle (Tortori-Donati et al. 2000; Tortori-Donati et al. 2001; Rossi et al. 2004a,b; Tortori-Donati et al. 2005b).

Nonterminal Myelocystocele

The CSDs with a subcutaneous mass occurring at the cervical or thoracic level are exceedingly rare, and are significantly different from those occurring at the lumbosacral level. These lesions are characterized by a large skin-covered meningocele with a thin neck crossing a narrow posterior spina bifida. The contents of the sac may be represented by an expanded hydromyelic cavity lined by the posterior wall of the spinal cord (i.e., a nonterminal myelocystocele) or by a thin fibroneurovascular stalk that attaches to the dome of the meningocele, probably better defined as abortive forms of nonterminal myelocystocele (Rossi et al. 2006).

The embryogenesis of these rare malformations is believed to be a minimal abnormality of primary neurulation, represented by localized failure of the final fusion of the apposed neural folds after most of neurulation has been completed, a mechanism that was called limited dorsal myeloschisis (Pang and Dias 1993). This results in failure of the cutaneous ectoderm to separate from the neuroectoderm with a resulting fibroneurovascular stalk emanating from the dorsal aspect of the spinal cord and penetrating through a narrow dorsal dural opening to connect to the skin. The presence of a hydromyelic cavity that dissects the fibroneurovascular stalk results in the formation of a full-blown myelocystocele.

Clinically, patients with nonterminal myelocystoceles are significantly less impaired than those with terminal myelocystoceles, with most neonates having a normal neurological exam at birth. Neurological deterioration may ensue after surgical repair without release of the intraspinal tethering structures or due to associated diastematomyelia or hydrocephalus.

On MRI, full-blown nonterminal myelocystoceles show hydromyelia ballooning into a cyst that protrudes out of the spinal canal and into a meningocele (Fig. 1.11). In abortive myelocystoceles, a thin stalk emanating from the dorsal aspect of an otherwise normal spinal cord and fanning out into a posterior meningocele is detected. In both cases, the dome of the meningocele is covered by thick, squamous epithelium, and the spinal cord caudad to the abnormality is normal. A Chiari-II malformation may be associated in approximately 40% of cases (Pang and Dias 1993; Rossi et al. 2006).

1.1.6.2 CSDs without Subcutaneous Mass

1.1.6.2.1 Simple Dysraphic States

This category of abnormalities is embryologically heterogeneous, as it comprises defects related to both primary and secondary neurulation; however, they may be grouped from a clinical perspective, since they represent the most common abnormalities found in infants or children who complain with TCS but usually do not have significant low-back cutaneous stigmata (Raghavan et al. 1989; Tortori-Donati et al. 1990).

Intradural and Intramedullary Lipoma

Intradural and intramedullary lipomas differ from lipomas with dural defects in that they are contained within an intact dural sac but are otherwise similar to them both pathologically and embryologically. Intradural lipomas are located along the midline in the groove formed by the dorsal surface of the unapposed folds of the placode, and may bulge posteriorly in the subarachnoid spaces elevating the pia mater. Large lipomas may displace the cord laterally, resulting in an off-midline, flattened or bumped placode–lipoma interface (Fig. 1.12). In rare instances, lipomas are completely intramedullary. Intradural lipomas commonly involve the lumbosacral spine and usually present with TSC, whereas cervicothoracic lipomas generally produce insidious signs of spinal cord compression.

On MRI, lipomas are detected as masses that are isointense with subcutaneous fat on all sequences, including those acquired with fat suppression (Tortori-Donati et al. 2000; Tortori-Donati et al. 2001; Rossi et al. 2004a,b; Tortori-Donati et al. 2005b).

Filar Lipoma

Filar lipoma is an anomaly of secondary neurulation characterized by a fibrolipomatous thickening of the filum terminale. The incidental finding of fat within the filum terminale in the normal adult population, estimated from unselected MRI studies, is 1.5–5% (Brown et al. 1994; Uchino et al. 1991). In

a b

Fig. 1.11a,b. Thoracic nonterminal myelocystocele, 2-day-old male newborn. **a,b** Sagittal GRE T2*-weighted images show that the posterior aspect of the spinal cord is pinched posteriorly (*large arrowheads,* **b**) and stretched through a narrow posterior spina bifida, to then re-expand into a large, trapped hydromyelic cavity (*H*) contained within a large subcutaneous mass. The stretched walls of the spinal cord are visible (*arrowhead,* **a,b**) as they separate the hydromyelic cavity from external, slightly dilated subarachnoid spaces (*thick arrow,* **b**). Note localized hydromyelia just above the origin of the posterior stalk (*arrow,* **a**), a quite common occurrence with nonterminal myelocystoceles. (Case courtesy of J. Van Goethem)

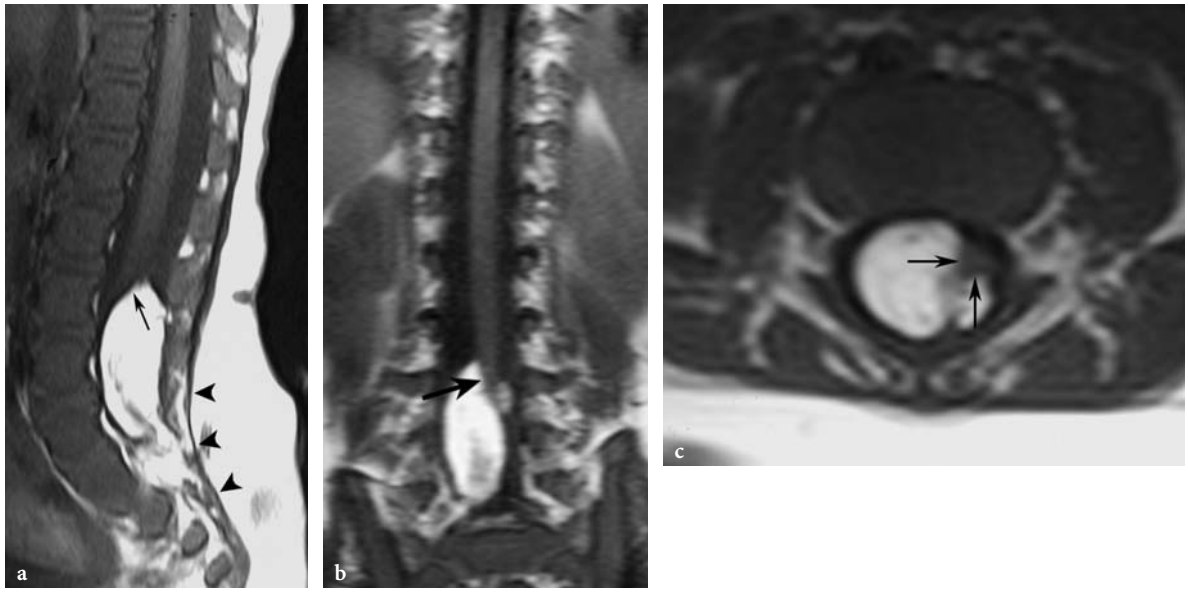

Fig. 1.12a-c. Intradural lipoma in a 4-month-old girl. **a** Sagittal T1-weighted image shows large lipoma filling the bottom of the thecal sac and connecting to a low-lying spinal cord (*arrow).* Note that there also is overgrowing subcutaneous tissue. This case could superficially resemble a lipomyelocele (compare with Fig. 1.7); however, note continuity of the superficial fascia (*arrowheads*) separating the subcutaneous from the intraspinal fat. **b** Coronal T1-weighted image shows the lipoma prevailingly develops to the right and connects to the right side of the conus tip (*arrow*). **c** Axial T1-weighted image shows the lipoma fills the thecal sac almost completely and engulfs the conus tip, which is displaced to the left (*arrows*)

the absence of TCS, a fatty filum is therefore considered an anatomic variant. The exact embryological mechanisms by which filar lipomas arise remains undetermined, although impaired canalization of the tail bud and persistence of cells capable of differentiating into adipocytes are suggested factors (Uchino et al. 1991).

On MRI (Fig. 1.13) adipose tissue with resultant thickening of the filum terminale is detected as a hyperintense stripe on sagittal T1-weighted images. Because the filum frequently lies slightly off the midline, axial and coronal T1-weighted images are also useful to identify this abnormality, especially when the lipoma itself is thin.

Tight Filum Terminale

The tight filum terminale is often misnamed as "tethered cord," a term that should only be used to describe the clinical syndrome (see section 1.1.3.4). A tight filum terminale is a short, hypertrophic filum that produces tethering and impaired ascent of the conus medullaris. Different from what is commonly believed, isolated cases are extremely uncommon, while the abnormality is more frequent in patients with diastematomyelia or dermal sinuses (Tortori-Donati et al. 2000; Tortori-Donati et al. 2001; Rossi et al. 2004a,b; Tortori-Donati et al. 2005b). A low-lying conus medullaris is frequently, albeit not necessarily, associated. The tip of the conus medullaris lies inferior to L2 in the vast majority of cases (Warder 2001).

Embryologically, the tight filum terminale has been related to abnormal retrogressive differentiation of the secondary neural tube (perhaps lack of apoptosis) producing a thicker-than-normal filum. Often, a subjective perception of an increased thickness of the filum on MRI (Fig. 1.14) remains unconfirmed, because an exact measurement cannot reliably be obtained; however, the filum terminale should not exceed 2 mm in diameter in normal individuals (Yundt et al. 1997).

Dermal Sinus

A dermal sinus is an epithelium-lined fistula that extends from the skin surface inward to a variable depth, and sometimes pierces the dura to reach the intradural compartment. The lumbosacral region is the most common location, although cervical, thoracic, and occipital locations are also described (Scotti and Harwood-Nash 1980; Barkovich et al. 1991). Clinical examination reveals a midline dimple or pinpoint ostium, often associated with a

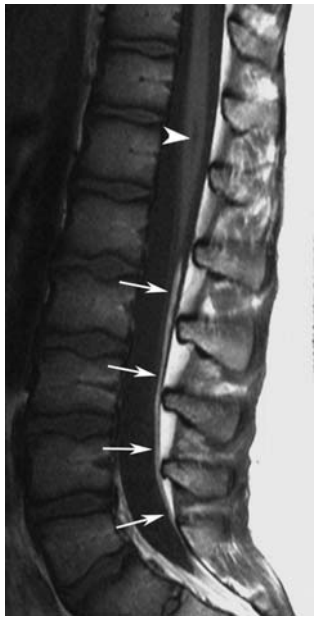

a

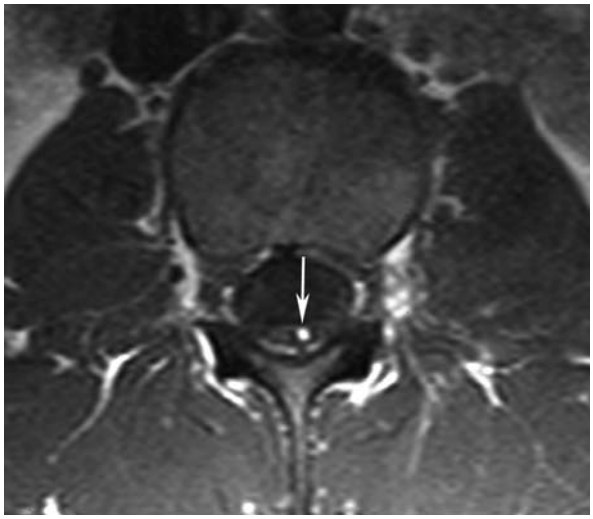

b

Fig. 1.13a,b. Filar lipoma in a 12-year-old girl with tethered cord syndrome. **a** Sagittal T1-weighted image shows that the filum terminale is largely replaced by fat *(arrows)*. The spinal cord is not low-lying (conus terminus at L1) but does show an excessive taper and contains slender hydromyelic cavity (*arrowhead*). **b** Axial T1-weighted image shows slightly off-midline filar lipoma (*arrow*). Note typical posterior position of the filar lipoma within the thecal sac, consistent with the normal anatomic location of the filum

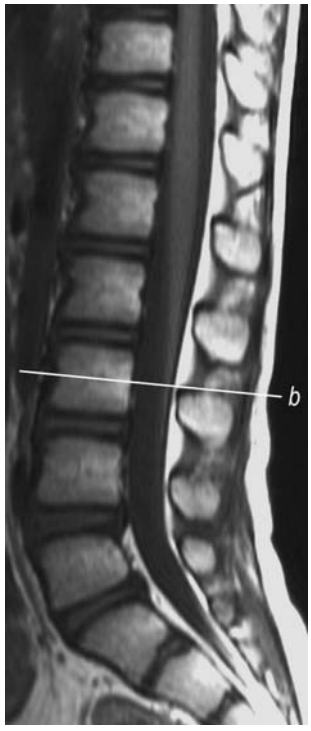

a

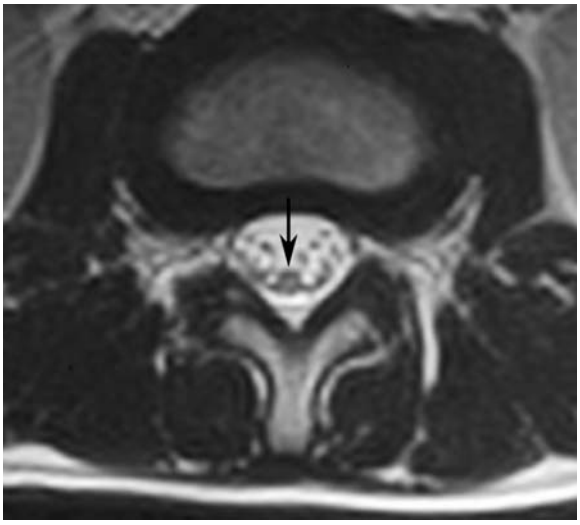

b

Fig. 1.14a,b. Tight filum terminale in a 9-year-old boy with tethered cord syndrome. **a** Sagittal T1-weighted image shows low-lying thickened filum terminale *(arrow)* with tethered, low conus medullaris. The spinal canal is abnormally large. *Horizontal white line* shows scan plane level of image *b*. **b** Axial T2-weighted image confirms thickening of the filum terminale *(arrow)* in its normal posterior position in the thecal sac

hairy nevus, capillary hemangioma, or dyschromic area. The location of the cutaneous opening of a dermal sinus tract differs from that of a sacrococcygeal fistula in that the dermal sinus tracts are found above the intergluteal cleft and usually are directed superiorly, whereas the sacrococcygeal pits are found within the natal cleft extending either straight down or inferiorly. Because the latter are anatomically located below the level of the bottom of the thecal sac, dysraphic abnormalities are typically not associated, and imaging studies are usually not required (Weprin and Oakes 2000). Although the ostium is usually evident at birth, some children are not brought to medical attention until complications such as local infection or meningitis ensue.

Embryologically, dermal sinus tracts are traditionally believed to result from focal incomplete disjunction of the neuroectoderm from the cutaneous ectoderm (Elton and Oakes 2001). They are easily recognized on sagittal MR images as thin hypointense stripes that course obliquely within the subcutaneous fat, more often in a caudally oblique direction (Fig. 1.15), whereas they are more difficult to detect on axial scans. While their course is quite easily recognized until the posterior elements of the spine are reached, the intraspinal portion of the tract is usually not detectable on MRI, which makes it difficult to assess the true extent of the tract itself and, particularly, whether it pierces the dura to involve the intradural compartment. In a considerable amount of cases, dermal sinuses are associated with dermoids, generally located at the level of the cauda equina or near the conus medullaris and probably resulting from an encasement of part of the dermal sinus tract (Fig. 1.15). Such an association was found in 11.3% of cases in our series (Tortori-Donati et al. 2000), but may be higher. Dermoids show variable MRI features depending on their content. Some portions may be hyperintense on T1-weighted images, but the mass may be isointense to CSF on both T1- and T2-weighted images and, therefore, may be difficult to discern. Infected dermoids display intense contrast enhancement that may become ring-like with abscessation.

Persistent Terminal Ventricle

The terminal ventricle, called "fifth ventricle" in the older scientific literature (Kernohan 1924), is a small cavity lined by ependyma within the conus medullaris, corresponding to the caudal end of the ependymal canal, that is always identifiable on postmortem examinations but must achieve a certain size to become visible on MRI (Coleman et al. 1995). It is embryologically related to preservation of the continuity of the terminal ventricle of secondary neurulation with the central canal of the spinal cord. The latter point is critical because fail-

ure of regression of the terminal ventricle associated with inefficient connection to the central canal may produce a terminal myelocystocele, which is a much more severe abnormality.

By itself, the persistent terminal ventricle is asymptomatic, but cases have been reported in which a huge cystic dilation was associated with low-back pain, sciatica, and bladder disorders (Sigal et al. 1991). It is unclear whether these "terminal ventricle cysts" are developmental variants or result from pathological changes eventually resulting into obstruction of the connection between the terminal ventricle and the central canal (Coleman et al. 1995). Differentiation of a persistent terminal ventricle from hydromyelia is based on the location within the conus medullaris immediately above the filum terminale; however, when continuity is detected with the central canal above, the distinction may become philosophical (Fig. 1.16). Intramedullary tumors are easily excluded by morphology, isointensity with CSF, and absence of gadolinium enhancement. The size of the cavity usually does not change on follow-up exams.

Fig. 1.15 Dermal sinus and dermoid in a 4-month-old girl. Sagittal T2-weighted image shows dermal sinus coursing obliquely through the subcutaneous fat *(arrows)*. Hyperintense dermoid (*D*) apparently originating from bottom of the dermal sinus (*open arrow*) connects with a low-lying conus medullaris. A fatty stripe along the posterior aspect of the cord generates chemical shift artifact (*arrowheads*)

1.1.6.2.2 Complex Dysraphic States

Gastrulation is characterized by the development of the notochord, a potent inductor that is involved in the formation of not only the spine and spinal cord, but also of several other organs and structures in the human body; therefore, spinal dysraphisms originating during this period will characteristically show a complex picture in which not only the spinal cord, but also other organs are impaired. Due to this complex picture, disorders of gastrulation are also called complex dysraphic states (Dias and Walker 1992). In the vast majority of cases, these abnormalities are covered by skin, and no telltale subcutaneous masses are present. The only exceptions are hemimyelocele and hemimyelomeningocele (see section 1.1.5.2).

Fig. 1.16 Persistent terminal ventricle in a 4-year-old boy. Sagittal T2-weighted image shows dilatation of the ependymal canal that slightly expands the conus medullaris

Embryologic Basis for Classification of Complex Dysraphic States

Failures of notochordal development have been categorized into two subsets: (a) disorders of midline notochordal integration; and (b) disorders of segmental notochordal formation (Tortori-Donati et al. 2000; Tortori-Donati et al. 2001; Rossi et al. 2004a,b; Tortori-Donati et al. 2005b). While the former results in longitudinal spinal cord splitting, the latter results in the absence of a notochordal

segment and, therefore, of the corresponding spine and spinal cord segment.

Disorders of Midline Notochordal Integration

Embryologically, prospective notochordal cells are derived from the Hensen's node, and stream in equal numbers from both sides of the node past the primitive pit to migrate between the hypoblast and the primitive endoderm in the midline. Midline integration is the process by which the two paired notochordal anlagen fuse in the midline to form a single notochordal process. The cause of failed midline notochordal integration has been the source of continuing debate among authors, and several possible explanations have been proposed (Faris and Crowe 1975; Pang et al. 1992; Prop and Fensdorf 1967). The eventual malformation depends on the severity of the abnormality and the outcome of the repair efforts of the embryo. Several malformations belong to this broad group. The full expression of the abnormality is the so-called dorsal enteric fistula, in which a connection between the skin surface and the bowel, crossing a complete duplication of the spine and spinal cord, is established due to persistence of the neurenteric canal, which connects the epiblast to the primitive endoderm during gastrulation. This condition is extremely rare and has only exceptionally been described (Hoffman et al. 1993). Malformations that may be embryologically related to the persistence and further differentiation of limited portions of the neurenteric canal are more frequent; these include bowel duplications, neurenteric cysts and fistulae, diastematomyelia, and according to some views, dermal sinuses.

Disorders of Segmental Notochordal Formation

Programmed cell death, or apoptosis, is a process of cell elimination that occurs during normal development and represents a crucial phenomenon in various steps of embryogenesis. According to one theory (Tortori-Donati et al. 2000; Tortori-Donati et al. 2001; Rossi et al. 2004a,b; Tortori-Donati et al. 2005b) prospective notochordal cells that are wrongly specified in terms of their rostrocaudal positional encoding could be eliminated so that, eventually, fewer cells or even no cells will form the notochord at a given abnormal segmental level. The consequences of such a segmental notochordal paucity are manifold and affect the development of the spinal column and spinal cord as well as of other notochord-induced organs. If the prospective notochord is depleted, a wide array of segmental vertebral malformations, including segmentation defects, indeterminate or block vertebrae, or absence of several vertebrae, will result. Moreover, lack of neural induction and absence of a floor plate will result in fewer prospective neuroectodermal cells, or even no cells at all, being induced to form the neural tube in the pathological segment. The resulting malformation will basically depend on the segmental level and the extent of the abnormality along the longitudinal embryonic axis, resulting in interference on the subsequent processes of primary and/or secondary neurulation. In the vast majority of cases, the abnormality involves the caudal extremity of the embryo, resulting in caudal agenesis. Much less frequently, the abnormality involves an intermediate notochordal segment, thereby resulting in segmental spinal dysgenesis (Tortori-Donati et al. 2000; Tortori-Donati et al. 2001; Rossi et al. 2004a,b; Tortori-Donati et al. 2005b).

Diastematomyelia

Diastematomyelia is the most frequent form of abnormal midline notochordal integration. Diastematomyelia (literally "split cord") refers to a variably elongated separation of the spinal cord in two, usually symmetric, halves. Whether this diastematomyelia represents true cord splitting or, rather, incomplete cord duplication has been the subject of enduring debate. Observations indicate that there is in fact a continuous spectrum of abnormality ranging all the way between a partially cleft cord contained in a single dural tube at one end, and a completely duplicated spinal cord contained within dual dural tubes with an intervening bony spur at the other end. The term "split cord malformations" (SCM) has been introduced to describe this malformative continuum (Pang 1992; Pang et al. 1992); however, we believe this is just an English translation of the originally from Greek derived term, diastematomyelia, which is deeply rooted into common use. We therefore encourage retaining the traditional denomination, which has the advantage of being widely recognized and accepted in the literature.

Embryologically, abnormal midline notochordal integration results into a variably elongated segment in which the midline notochord is replaced by two paired notochordal processes separated by intervening primitive streak cells. These "heminotochords" will join each other at either (i.e., cranial and caudal) end of the defect. Each "heminotochord" induces a separate "hemi"-neural plate, which will then neurulate independently to form a "hemi"-neural tube.

The resulting malformation essentially depends on the developmental fate of the intervening primitive streak tissue, which is a totipotential tissue capable of differentiating into ecto-, meso-, and endodermal lineages. If this intervening tissue differentiates into cartilage and bone, the two hemicords eventually will be contained into two individual dural sacs separated by an osteocartilaginous spur. Conversely, if the primitive streak tissue is reabsorbed or only results into a thin fibrous septum, the two hemicords eventually will lie within a single dural tube. This basic, albeit somewhat oversimplified, mechanism represents the foundation of the classification of diastematomyelia into two groups (Pang et al. 1992).

Diastematomyelia Type I

Diastematomyelia type I consists of two hemicords contained within individual dural tubes, separated by a bony or osteocartilaginous septum that extends from the vertebral body to the neural arches (Pang et al. 1992). This rigid septum is entirely extradural.

Clinically, patients often display a hairy tuft lying high relatively cephalad along the back, which is considered to be a very reliable clinical marker of diastematomyelia (Tortori-Donati et al. 2000; Tortori-Donati et al. 2001; Rossi et al. 2004a,b; Tortori-Donati et al. 2005b). Affected children usually present with scoliosis and a tethered cord syndrome (TCS).

Radiological abnormalities involve both the spine and spinal cord. Vertebral anomalies, including bifid lamina, widened interpediculate distance, hemivertebrae, bifid vertebrae, fused vertebrae, and narrowing of the intervertebral disk space, may already be apparent on conventional X-ray. Scoliosis is common and is seen in 30–60% of these individuals. The radiological hallmark (Naidich and Harwood-Nash 1983; Pang et al. 1992) is the osseous or osteocartilaginous septum (the "spur"), which divides the spinal canal into two separate halves, each containing an independent dural tube, in turn containing a hemicord. Although in the archetypal case the spur connects the vertebral body to the neural arch along a midsagittal plane, "atypical" spurs are common. The spur may course obliquely and may be incomplete, in which case it may originate either from the vertebral body or from the neural arch. In some cases, the spinal canal is divided unequally, resulting in two asymmetric hemicords. CT may be performed in order to obtain a three-plane evaluation of the spur for presurgical evaluation; however, especially in young children, the spur may be mostly cartilaginous and is therefore inadequately visualized on CT.

MRI is the imaging modality of choice for a thorough investigation of this abnormality (Fig. 1.17). In most cases, the spur is located at the thoracic or lumbar level and lies at the caudal end of the cord splitting. As a consequence, the two hemicords usually surround the spur tightly before fusing with each other to form a normal spinal cord below, whereas rostrally the splitting is much more elongated; therefore, there is a craniocaudal sequence of partial clefting, complete diastematomyelia within a single dural tube, diastematomyelia with dual dural tubes with intervening spur, and reunion of the two hemicords.

There may be a number of associated findings in this condition. Hydromyelia is very common and may involve the normal cord both above and below the splitting, as well as one or both hemicords (Schlesinger et al. 1986). A tight filum terminale is very commonly associated to diastematomyelia, in our experience more often than it exists as an isolated anomaly. Failure of neurulation of one hemicord produces a hemimyelocele or hemimyelomeningocele.

Diastematomyelia Type II

Diastematomyelia type II is embryologically a less severe form than type I. The basic difference is that there is not an osteocartilaginous spur to divide the spinal canal. As a consequence, there is a single dural tube housing both hemicords (Naidich and Harwood-Nash 1983; Pang et al. 1992). Patients may have a less severe neurological impairment than those with the type I, basically because TCS usually is not a factor (Pang 1992).

Three variants of diastematomyelia type II exist, i.e., absence of a septum, presence of an intervening fibrous septum, and partial cord splitting (Tortori-Donati et al. 2000; Tortori-Donati et al. 2001; Rossi et al. 2004a,b; Tortori-Donati et al. 2005b); of these, absence of whatever septum is, by far, the most common (Fig. 1.18). In such a case, the diagnosis is relatively straightforward both on correctly placed axial and coronal MRI sequences; however, it is commonplace that most radiologists basically rely on sagittal MR images for initial spinal assessment and further decision on if and how to proceed with additional sequencing. Unfortunately, diastematomyelia type II may be especially difficult to appreciate on sagittal MR images, where the only indicative sign is an apparent thinning of the spinal cord resulting from partial averaging with the intervening subarachnoid space between the two hemicords. A midline, nonrigid,

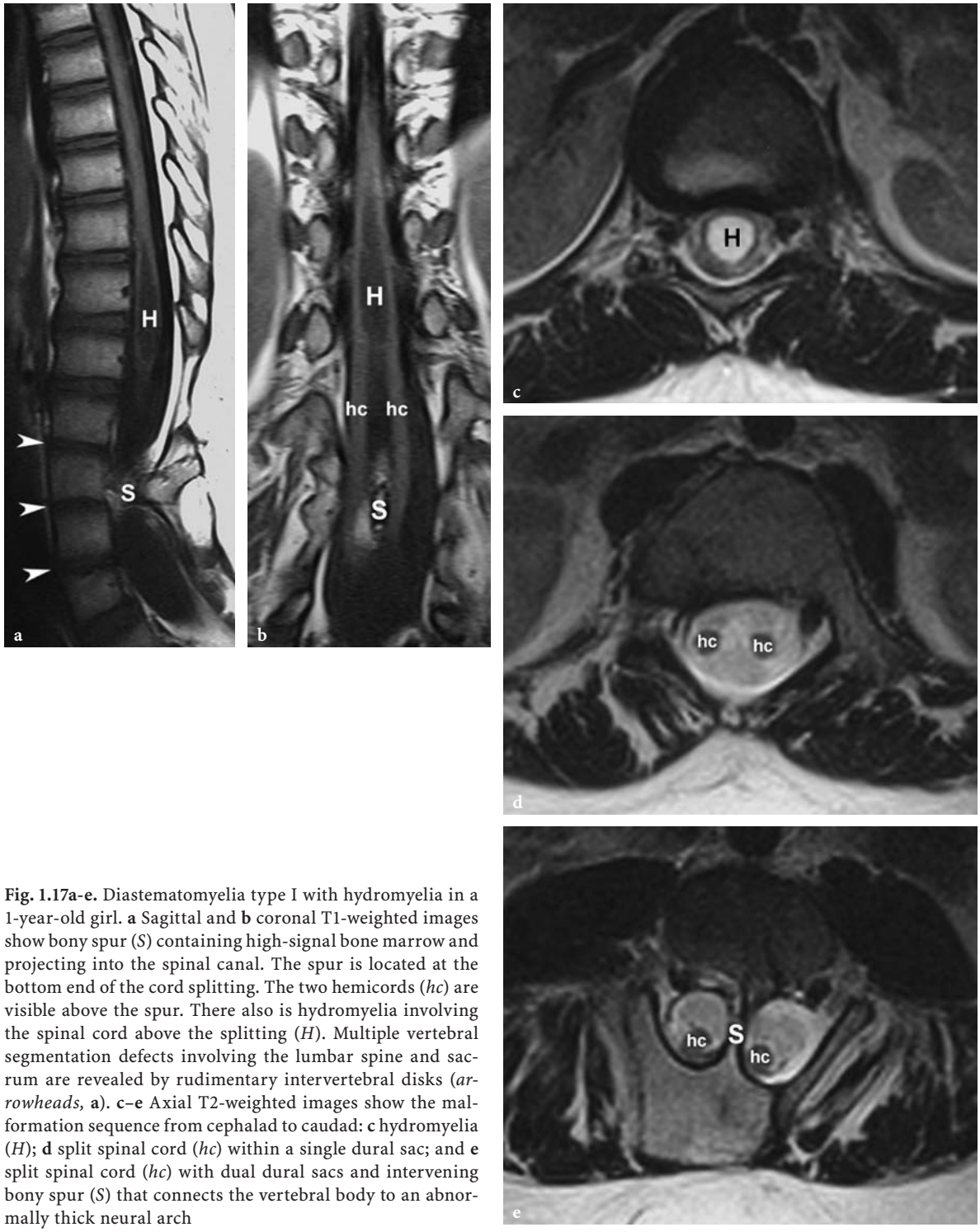

Fig. 1.17a-e. Diastematomyelia type I with hydromyelia in a 1-year-old girl. **a** Sagittal and **b** coronal T1-weighted images show bony spur (*S*) containing high-signal bone marrow and projecting into the spinal canal. The spur is located at the bottom end of the cord splitting. The two hemicords (*hc*) are visible above the spur. There also is hydromyelia involving the spinal cord above the splitting (*H*). Multiple vertebral segmentation defects involving the lumbar spine and sacrum are revealed by rudimentary intervertebral disks (*arrowheads*, **a**). **c–e** Axial T2-weighted images show the malformation sequence from cephalad to caudad: **c** hydromyelia (*H*); **d** split spinal cord (*hc*) within a single dural sac; and **e** split spinal cord (*hc*) with dual dural sacs and intervening bony spur (*S*) that connects the vertebral body to an abnormally thick neural arch

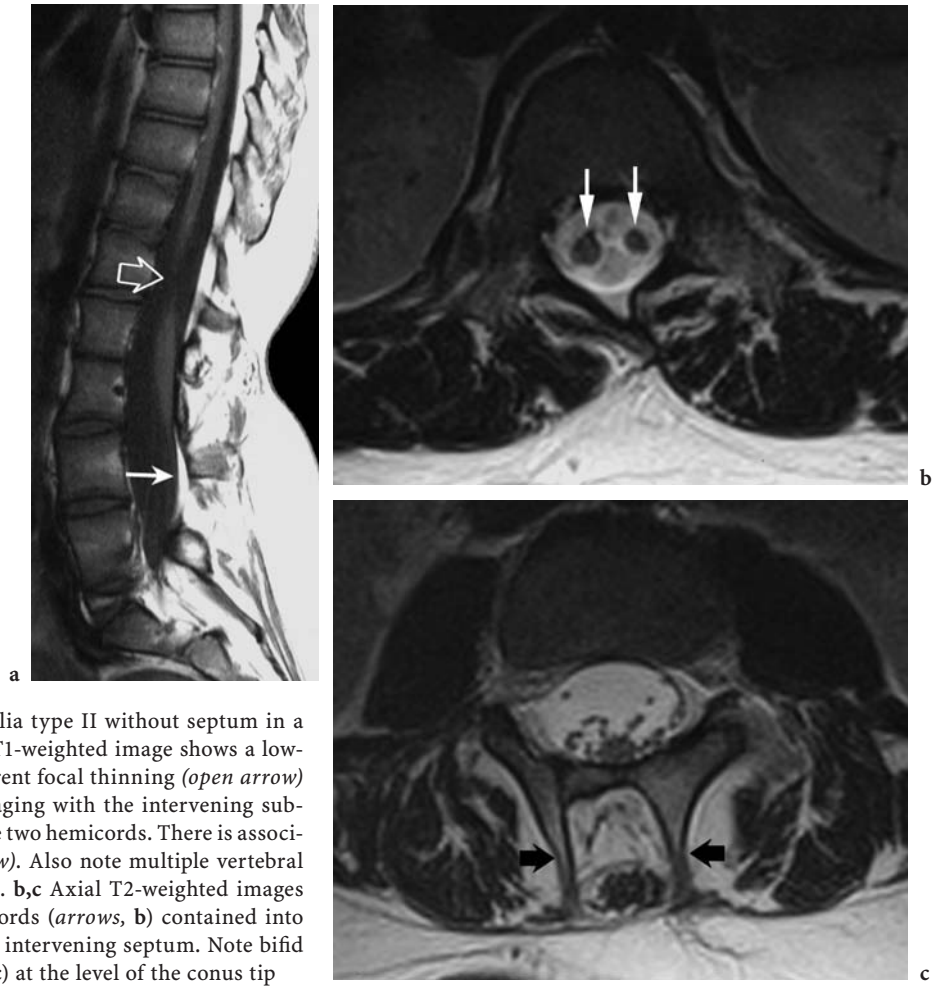

Fig. 1.18a-c. Diastematomyelia type II without septum in a 13-year-old girl. **a** Sagittal T1-weighted image shows a low-lying spinal cord with apparent focal thinning *(open arrow)* resulting from partial averaging with the intervening subarachnoid space between the two hemicords. There is associated filar lipoma *(thin arrow)*. Also note multiple vertebral segmentation abnormalities. **b,c** Axial T2-weighted images clearly show the two hemicords (*arrows,* **b**) contained into a single dural tube, with no intervening septum. Note bifid spinous processes (*arrows,* **c**) at the level of the conus tip

fibrous septum is sometimes detected at surgery, accounting for rare cases of TCS in the setting of diastematomyelia type II (Pang 1992). These septa may be identified on axial and coronal T2-weighted images as thin hypointense stripes interposed between the two hemicords. Rare cases of partial cord splitting are characterized by an incomplete separation of the two hemicords, which remain joined by a midline bridge; these are the mildest forms of diastematomyelia (Tortori-Donati et al. 2000; Tortori-Donati et al. 2001; Rossi et al. 2004a,b; Tortori-Donati et al. 2005b). Hydromyelia may be present with the same features as in diastematomyelia type I. The conus medullaris is typically low, and there is a strong association with a tight filum terminale. Associated vertebral anomalies are usually milder than in type I, and are represented by butterfly vertebrae in most cases. Posterior spina bifida is often present, whereas scoliosis is usually absent.

Caudal Agenesis (Caudal Regression Syndrome)

Caudal agenesis (CA), or caudal regression syndrome (Duhamel 1961), is a broad header grouping a heterogeneous constellation of anomalies that comprise total or partial agenesis of the caudal portion of the spinal column, anal imperforation, genital anomalies, bilateral renal dysplasia or aplasia, pulmonary hypoplasia, and lower limb abnormalities. The term caudal agenesis is preferred to caudal regression syndrome, as the latter implies a concept of excessive regression of the embryonic tail that cannot be adequately applied to tail-less animals, such as humans. Sacrococcygeal agenesis may be part of complex syndromes, such as OEIS (omphalocele, cloacal exstrophy, imperforate anus, and spinal deformities) (Carey et al. 1978), VACTERL (vertebral abnormality, anal imperforation, cardiac anomalies, tracheoesophageal fistula, renal abnormalities, limb deformities) (Smith et al. 1992), and

the Currarino triad (partial sacral agenesis, anorectal malformation, and presacral mass: teratoma and/or meningocele) (Currarino et al. 1981; Dias and Azizkhan 1998; Gudinchet et al. 1997). The association with maternal diabetes mellitus (1% of offspring of diabetic mothers) is well established. Also, in humans CA can be inherited as an autosomal-dominant condition (Catala 2002).

The degree of vertebral abnormality in CA may range extensively, from isolated agenesis of the coccyx to absence of the sacral, lumbar, and lower thoracic vertebrae; however, the vast majority of these anomalies involve absence of the coccyx and part of, or the whole, sacrum. The degree of sacral agenesis may vary, with S1 through S4 present in individual cases. Sacral aplasia may also be asymmetric, with resulting total or subtotal hemisacrum that may, in turn, be unilateral or bilateral (Pang 1993). Full appreciation of the heterogeneous spectrum of vertebral malformation requires anteroposterior and lateral X-ray films, which constitute an essential part of the neuroradiological work-up. Computed tomography may be necessary for clarification of particularly complex conditions.

Classically CA is categorized into two variants depending on the location and shape of the conus medullaris: either high and abrupt (type I) or low and tethered (type II). This categorization is very adequate in that it effectively groups patients into two quite homogeneous groups, characterized not only radiologically, but also by different embryology and clinical picture. Embryologically, CA is consistent with abnormal formation of a caudal segment of the notochord and corresponding paraxial mesoderm, resulting in a correspondingly segmental abnormality of neural induction. The cause of the original abnormality is unknown, but it may be related to abnormal genetics at the level of Hensen's node. Depending on the longitudinal extent of the defect, interference will be generated with either both primary and secondary neurulation (CA type I, more severe) or with secondary neurulation alone (CA type II, less severe); therefore, the crucial embryological watershed between the two varieties is the interface between primary and secondary neurulation (i.e., the junction between the true notochord and the tail bud) corresponding to the caudal end of the future neural plate (Tortori-Donati et al. 2000; Tortori-Donati et al. 2001; Rossi et al. 2004a,b; Tortori-Donati et al. 2005b). This site has been the source of continuing debate among authors: current evidence places it at S3 (Nievelstein et al. 1993). As a consequence, the degree of spinal cord aplasia correlates metamerically with the degree of the spinal malformation, with a greater elongation of vertebral aplasia in the type I than in the type II (Nievelstein et al. 1994).

Type-I CA

In type-I CA, not only the tail bud, but also part of the true notochord, fails to develop. As a consequence, there will be interference with both the processes of primary and secondary neurulation, and the final vertebra to form will be S3. In other words, depending on the severity of the original damage the eventual degree of vertebral aplasia may range from absence of the coccyx and lower midsacrum to aplasia of all coccygeal, sacral, lumbar, and lower thoracic vertebrae, although the last vertebra is L5 through S2 in the vast majority of patients.

Because absence of a notochord causes failed neural induction, there will be aplasia of the caudal metameres of the spinal cord, resulting in the typically abrupt (i.e., without normal taper) spinal cord terminus that nearly always is club or wedge shaped (Fig. 1.19) and high-lying (most often opposite T12, but sometimes opposite L1) (Barkovich et al. 1989; Pang 1993; Nievelstein et al. 1994). The cauda equina also has an abnormal course that has been termed the "double bundle shape" (Pang 1993). The thecal sac tapers below the cord terminus, and also ends at an unusually high level with a gross correspondence to the degree of cord aplasia, i.e., the higher the cord terminus, the higher the termination of the thecal cul-de-sac. Associated caudal anomalies, such as anterior meningoceles and teratomas, are sometimes found, although much less frequently than in type-II CA, and unlike in the latter, the cord is not tethered to these caudal anomalies. This accounts for the negligible incidence of the tethered cord syndrome and progressive neurological deterioration in these patients, contrary to those with type-II CA. In fact, children with type I typically have a stable neurological defect that is due to their "fixed" spinal cord dysplasia (Pang 1993). In particular, their motor deficit tends to parallel the extent of the bony abnormality, whereas sensory impairment is much less predictable from the radiographic appearance.

Type-II CA

In type-II CA, the whole or a part of the tail bud fails to develop, but the true notochord is unaffected; therefore, primary neurulation occurs normally, while there is interference only with the process of

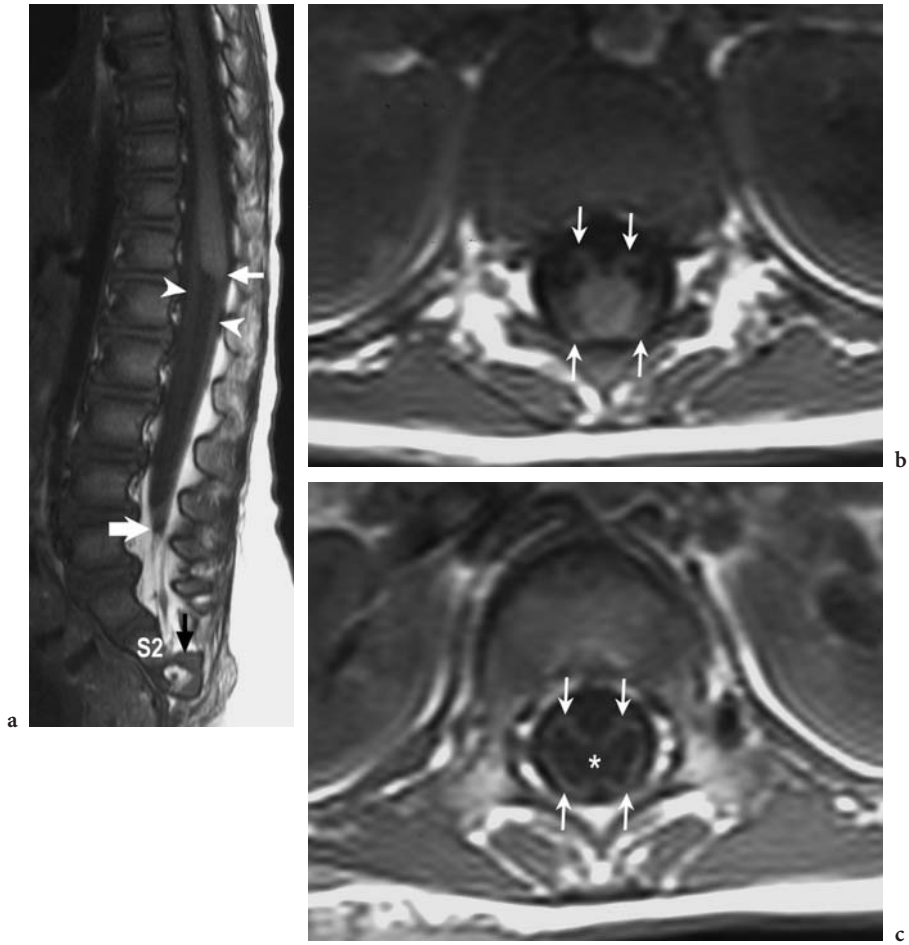

Fig. 1.19a-c. Type-I caudal agenesis in a 15-month-old girl. **a** Sagittal T1-weighted image shows subtotal sacrococcygeal agenesis, with S2 as the last visible vertebra, articulating with aberrant osteocartilaginous conglomerate (*black arrow*). The cord terminus is wedge-shaped and lies opposite T12 (*white arrow*). There is "double bundle" arrangement of the nerve roots of the cauda equina (*arrowheads*). The dural sac tapers abruptly and ends abnormally high (*thick arrow*). **b** Axial T1-weighted image at the level of T12 shows bulky cord terminus surrounded by anterior and posterior nerve roots (*arrows*). **c** Axial T1-weighted image at the level of L1 shows presence of the nerve roots (*arrows*) but absence of the conus tip (*asterisk*). This "ghost conus" appearance is a common and telltale occurrence with type-I caudal agenesis

secondary neurulation. As a consequence, the degree of vertebral dysgenesis is less severe than in type I, with at least S4 present as the last vertebra. Correspondingly, only the most caudal portion of the conus medullaris (corresponding to the metameres formed by secondary neurulation) is absent; however, the latter condition is difficult to recognize on imaging, because the conus itself is stretched caudally and tethered to a tight filum, lipoma (Fig. 1.20), terminal myelocystocele, lipomyelomeningocele, or the neck of an anterior sacral meningocele.

Because of this situation, children with type-II CA typically present with a tethered cord syndrome and are at risk for further neurological deterioration, which is why they often are referred for neurosurgical interventions. In a minority of cases, teratomas or other caudal tumors are found. On clinical examination, these low-back masses must be differentiated from overgrowing fatty tissue that is sometimes present in these patients at the level of the buttocks.

Imaging studies in the type-II CA may be difficult to interpret, especially when one is looking for small teratomatous masses along the walls of anterior meningoceles, in the presacral space, or deep within the pelvic cavity. In these cases, presaturation slabs must not be placed anterior to the spinal column in order not to miss possible presacral abnormalities.

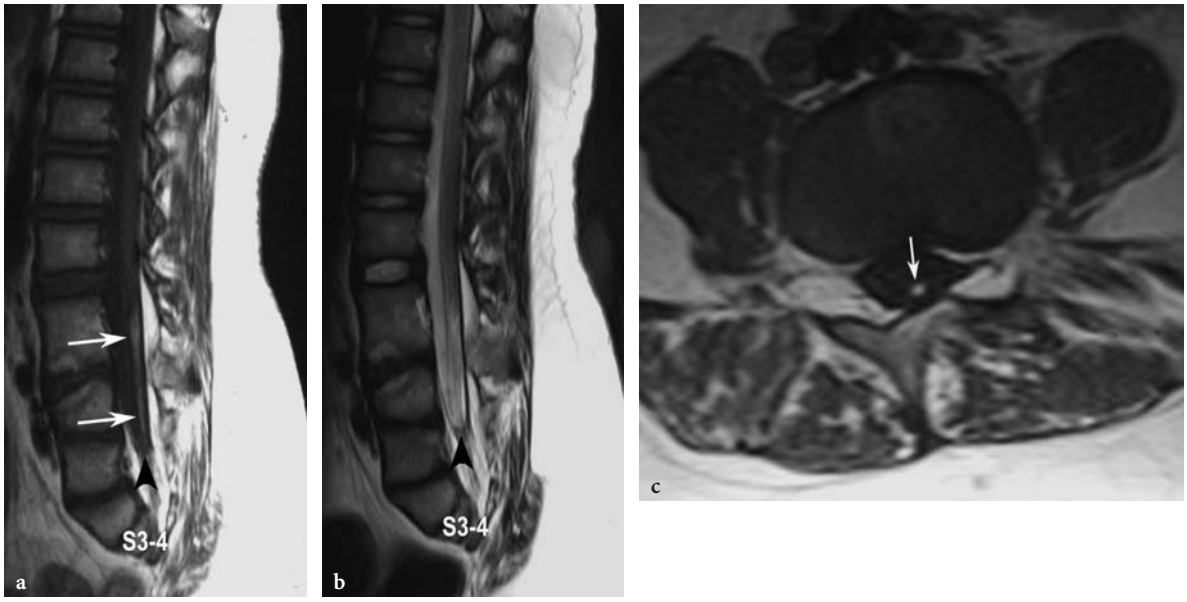

Fig. 1.20a-c. Type-II caudal agenesis in a 9-year-old boy with VACTERL association. **a** Sagittal T1-weighted and **b** sagittal T2-weighted images show the spinal cord is low and tethered to an intradural lipoma (*arrows,* **a**). The thecal sac terminates abnormally high (*arrowheads,* **a,b**). Notice extensive vertebral anomalies; however, the degree of sacrococcygeal abnormality is less severe than in the type I, with a nonsegmented S3-4 rudiment present in this case. **c** Axial T1-weighted images confirms filar lipoma (*arrow*) and shows abnormal vertebral neural arch

Segmental Spinal Dysgenesis

Segmental spinal dysgenesis (SSD) is defined as the association of: (a) segmental agenesis or dysgenesis of the lumbar or thoracolumbar spine; (b) segmental abnormality of the underlying spinal cord and nerve roots; (c) congenital paraplegia or paraparesis; and (d) congenital lower limb deformities (Tortori-Donati et al. 1999). Segmental vertebral anomalies may involve the thoracic, lumbar, or lumbosacral spine, but the thoracolumbar region is the most often involved. As with CA, the embryogenesis of SSD is believed to relate to a yet unknown genetic defect interfering with the normal function of Hensen's node and notochordal formation. Different from CA, however, an intermediate, rather than the most caudal, segment of the notochord is affected (Tortori-Donati et al. 1999). The consequences, however, are the same in that segmental notochordal abnormality causes segmental lack (or abnormality) of neural induction, resulting in a metameric correspondence between vertebral abnormality and spinal cord dysgenesis.

In the most severe cases, the spinal cord at the level of the abnormality is thoroughly absent, and the bony spine is focally aplastic. As a result, the spine and spinal cord are "cut in two," with resulting acute angle kyphosis (Fig. 1.21). Between the two spinal segments, the spinal canal is extremely narrowed or even totally interrupted. The lower spinal cord segment is invariably bulky and low-lying. A horseshoe kidney is typically lodged in the concavity of the kyphosis. Newborns with this severe form of SSD are paraplegic at birth and typically show hypotrophic and deformed lower limbs with equinocavovarus feet.

In less severe cases, the spinal cord is focally hypoplastic and will therefore appear narrower than normal on MRI studies, but is not interrupted. There is no disconnection of the bony spine either, although bony stenosis of the spinal canal and vertebral abnormalities typically involve the pathological segment (Tortori-Donati et al. 1999).

1.2 Congenital Abnormalities of the Cranio-Cervical Junction

Congenital or acquired abnormalities of the occipital bone, foramen magnum, or the first two cervical vertebrae may decrease the potential space for the lower brainstem and cervical cord and can therefore result in compression of the cerebellum,

Fig. 1.21a,b. Segmental spinal dysgenesis in 2-year-old girl. **a,b** Sagittal T2-weighted images show acute thoracolumbar kyphosis with complete interruption of the spinal column. There are two completely separated spinal cord segments (*sc*). The upper one ends several vertebral levels above the gibbus, whereas the lower one is bulky and low. Note horseshoe kidney (*K*) lodged into the kyphotic concavity, a typical arrangement in severe forms of segmental spinal dysgenesis

lower cranial nerves, cervical spinal cord, cervical nerve roots, or their vascular supply. Clinical findings may be variable. Often, patients present with a head tilt or torticollis. Pain may be present either due to compression of the C2 nerve root and greater occipital nerve or to local musculoskeletal dysfunction. Myelopathy may cause both motor and sensory disturbances; the former includes weakness, spasticity, hyperreflexia, and muscular atrophy; the latter includes paresthesia, loss of pain and temperature sensation, abnormal vibration sensation, and Lhermitte's sign. Brainstem and cranial nerve deficits include sleep apnea, internuclear ophthalmoplegia, nystagmus, hoarseness, dysarthria, and dysphagia.

1.2.1 Bony Abnormalities

1.2.1.1 Basilar Invagination

Basilar invagination indicates an occipitocervical dysplasia in which there is upward herniation of the margins of the foramen magnum into the posterior fossa, a process that may be accompanied by impingement of structures, such as the odontoid on the medulla oblongata with flexion of the head (Fig. 1.22). The term is not synonymous with basilar impression, which indicates a secondary form of invagination caused by bone softening (Castillo and Mukherji 1995) as in Paget's disease, rickets, or osteogenesis imperfecta, or by bone destruction related to tumor, infection, or trauma. Instead, the basilar invagination results from abnormal development of the endochondral bone at the skull base and/or abnormal development of the atlas and axis of the cervical spine (C1 and C2).

Measurements used to evaluate basilar invagination on skull radiographs and CT include (Zimmerman 2005):

Chamberlain's line, which joins the posterior margin of the foramen magnum to the posterior margin of the hard palate. In normal conditions, the tip of the odontoid should not be more than 5 mm above Chamberlain's line.

McGregor's line, which is from the lowermost point of the occipital squama through the posterior margin of the hard palate. The tip of the odontoid should not be more than 7 mm above McGregor's line.

Digastric line, which is drawn between the right and left digastric notches and can be visualized on an anteroposterior skull radiograph or on a coronally reconstructed CT. The digastric line is supposed to be 11 mm (±4 mm) above the middle of the atlanto-occipital joint. Basilar invagination is pres-

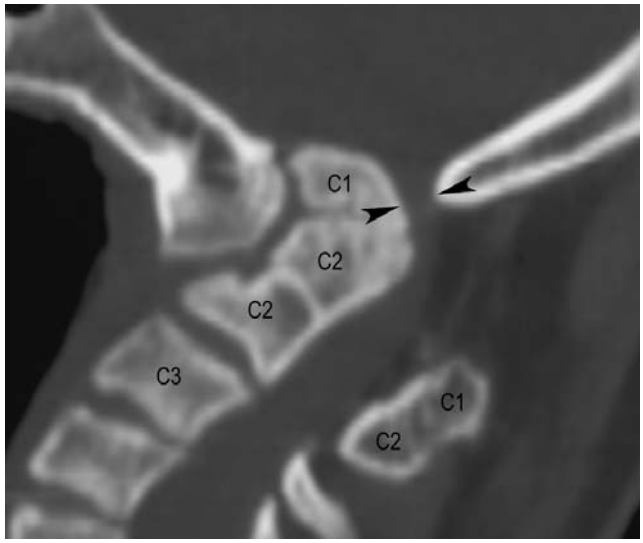

a

b

Fig. 1.22a,b. Complicated basilar invagination in an 18-year-old tetraplegic boy. **a** Sagittal reformatted CT scan shows assimilation of C1–C2, upward protrusion of the cervical spine with respect to the clivus, and marked stenosis of the foramen magnum (*arrowheads*). **b** Sagittal T2-weighted image shows hyperintensity of the bulbomedullary junction (*arrows*) related to edema due to mechanical compression

ent when the atlanto-occipital joint is at or above the digastric line.

The role of MRI is basically in the evaluation of the cervico-medullary junction for possible edema due to mechanic compression and the search of associated abnormalities, such as the Chiari-I malformation (Fig. 1.23).

1.2.1.2 Achondroplasia

Achondroplasia is autosomal dominant, with a frequency of 1 in 26,000 live births (Rousseau et al. 1994; Shiang et al. 1994) and as many as 80% spontaneous mutations. Clinical manifestations are characterized by short-limbed, short-trunked dwarfism with a large head (Hecht et al. 1985). Newborns with this condition may be hypotonic at birth, possibly as a result of brainstem compression, which may also cause sleep apnea and dysphagia. Most patients are intellectually normal.

On imaging, there is a small skull base involving the region of the sphenoid and a small posterior

Fig. 1.23 Basilar invagination associated with Chiari-I malformation (bulbar variant) in a 10-year-old boy. Sagittal T2-weighted image shows protrusion of the odontoid process above the Chamberlain line (*white line*). There is associated tonsillar descent (*thin arrow*). Also note cervicomedullary kink (*open arrow*) which, together with tonsillar ectopia and bulbar elongation, constitutes the so-called bulbar or myelencephalic variant of the Chiari-I malformation

fossa because of underdevelopment of portions of the sphenoid and occipital bones, which can produce compression of the cervicomedullary structures at the region of the foramen magnum (Fig. 1.24). The cross-sectional area of the foramen magnum is reduced in the vast majority of patients. Stenosis of the jugular foramina causes retrograde venous hypertension that hinders cerebrospinal resorption, frequently causing communicating hydrocephalus. Spinal canal stenosis is typical and especially involves the cervical and lumbar portions of the canal. The sacrum is horizontalized.

1.2.1.3 Down Syndrome

Anatomic abnormalities of the craniocervical juncture are common in patients with Down syndrome, and comprise C1 hypoplasia and assimilation, hypoplasia of the odontoid process of C2, and ligamentous laxity of the atlantooccipital and atlantoaxial joints (White et al. 1993). These conditions predispose to anterior or posterior subluxation with distortion of the subarachnoid spaces and compression of the medulla and/or spinal cord. Functional atlantoaxial instability may be demonstrated and measured dynamically both with conventional radiograms and CT as well as on MRI. It is crucial that trained personnel perform these potentially harmful maneuvers in order not to cause, or further aggravate, spinal cord compression.

1.2.1.4 Klippel-Feil Syndrome

The Klippel-Feil deformity is a complex of osseous and visceral anomalies that includes low hairline, platybasia, fused cervical vertebrae with short neck, and deafness (Fig. 1.25). The classical clinical triad consists of short neck, limitation of head and neck movements, and low-set posterior hairline. Bony malformations may entrap and damage the brain and spinal cord. The disorders of the lower vertebral region may become symptomatic in adolescence or adult life. The pathogenesis has been related to anomalous somitic segmentation between gestational weeks 4 and 8. Associated CNS abnormalities include occipital cephalocele, Chiari-I malformation, syringes, microcephaly, and hydrocephalus. Several associated abnormalities, such as scoliosis, posterior bony spina bifida, absence of ribs, conductive hearing loss, mirror movements, unilateral renal ectopia with dilated collecting system, microtia, and preaxial polydactyly, have also been reported. The pattern of bony fusion may involve more than one level, producing the "wasp waist sign" when two adjacent lev-

a

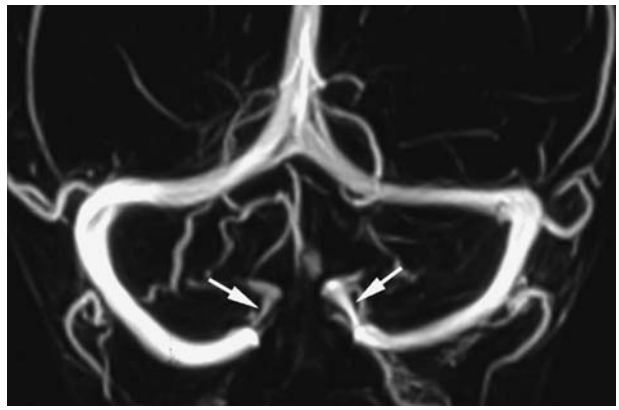

b

Fig. 1.24a,b. Achondroplasia in a 2-year-old boy. **a** Sagittal T2-weighted image shows stenosis of the foramen magnum caused by prominence of the posterior lip of the foramen magnum, indenting the posterior aspect of the bulbomedullary junction (*arrow*). Note stenosis of the spinal canal with the posterior margins of the intervertebral disks impinging on the ventral aspect of the thecal sac. **b** Coronal 2D time-of-flight MR angiogram shows the jugular foramen is also stenotic bilaterally (*arrows*), predisposing to venous hypertension and communicating hydrocephalus

Fig. 1.25 Klippel-Feil syndrome in an 8-year-old boy. Sagittal T1-weighted image shows fusion of most cervical and superior thoracic vertebral bodies, with only one individually recognizable normal intervertebral disk (*arrowhead*). Note also fusion of the posterior vertebral elements. The craniocervical junction and spinal canal are normal in this case

els are involved (Nguyen and Tyrrel 1993). Cervical spondylosis, disk herniation, and secondary degenerative changes are more common at levels adjacent to fused vertebrae (Ulmer et al. 1993). Spontaneous and progressive neurological sequelae and neurological injury may follow minor neck trauma.

1.2.2 Chiari Malformations

Chiari malformations are a heterogeneous group of abnormalities grouped under a common heading because they were initially described by the same Austrian pathologist H. Chiari, in two papers published at the end of the nineteenth century (Chiari 1891, 1896). The Chiari malformations comprise the common, widely known types I and II, the rare type III, and a fourth type whose definition and autonomous dignity is still debated among authors (Cama et al. 1995). Although all these entities share common features, such as a variable degree of reduction in size of the posterior fossa and (with the exception of the type IV) herniation of portions of the cerebellum into the foramen magnum, it is accepted that type I (resulting from a mesodermal hindbrain abnormality) should be separated from the other types that are related to neural tube closure defects (Tortori-Donati et al. 2005a).

1.2.2.1 Chiari-I Malformation

1.2.2.1.1 Background

The Chiari-I malformation is characterized by downward displacement of elongated, peg-like cerebellar tonsils through the foramen magnum into the upper cervical spinal canal, sometimes associated with descent and distortion of the bulbo-medullary junction and often complicated by hydrosyringomyelia and/or hydrocephalus. Although the extensive use of MRI has revealed that caudal tonsillar ectopia is much more common than was previously believed, understanding of the pathogenesis, clinical manifestations, and treatment of this abnormality is still controversial (Milhorat et al. 1999).

1.2.2.1.2 Pathogenesis

It is believed that the anomaly is primarily related to a disorder of the paraxial mesoderm and, particularly, to hypoplasia of the occipital bone due to underdevelopment of the occipital somites, with reduced volume and overcrowding of the posterior cranial fossa, which contains a normally developed hindbrain (Nishikawa et al. 1997). The possible association with other skeletal developmental abnormalities, such as basilar invagination, further reduces the size of the posterior fossa, thereby increasing overcrowding and downward herniation of nervous structures. The vast majority of cases occur sporadically.

The Chiari-I malformation is a primary malformative condition that should be differentiated from acquired forms of caudal herniation of the hindbrain that may occur secondary to CSF hypotension (either iatrogenic or spontaneous), raised intracranial pressure (i.e., in intracranial tumors), or venous hypertension (i.e., in arteriovenous malformations). While radiological findings may be at first glance indistinguishable from those of Chiari I, there is complete reversal of tonsillar descent after treatment of the predisposing condition, as is documented by follow-up MRIs. We believe that the term “acquired

Chiari-I malformation," sometimes used to describe this condition (Payner et al. 1994), is a misnomer that should be abandoned.

1.2.2.1.3 Clinical Findings

A significant proportion of patients (14–56% of cases; Elster and Chen 1992; Park et al. 1997; Meadows et al. 2000) are neurologically normal at presentation, and the diagnosis is made when an MRI is performed for another reason. The clinical significance and appropriate management of these patients often remains uncertain (Wu et al. 1999). When present, symptoms are often vague, ambiguous, and may last months to years prior to diagnosis. Initial symptomatology may include headache, head tilt, neck pain, dysphagia, numbness, weakness, incoordination, nystagmus, and ataxia, among other symptoms (Elster and Chen 1992; Park et al. 1997; Milhorat et al. 1999;Wu et al. 1999). Although the degree of tonsillar descent grossly correlates with the presence of signs and symptoms, cranial and brain measurements have not been found to correlate significantly with the prognosis and the incidence of complications (Christophe and Dan 1999). When present, hydrocephalus and hydrosyringomyelia generally overshadow other clinical manifestations. Scoliosis is found in 28% of cases (Milhorat et al. 1999).

1.2.2.1.4 Imaging Findings

Caudal ectopia of the cerebellar tonsils into the foramen magnum is the hallmark of the Chiari-I malformation (Fig. 1.26). Measurement of the degree of downward displacement is critical in order to make the diagnosis. The extent of this ectopia is measured on a midsagittal MR image from the tips of the cer-

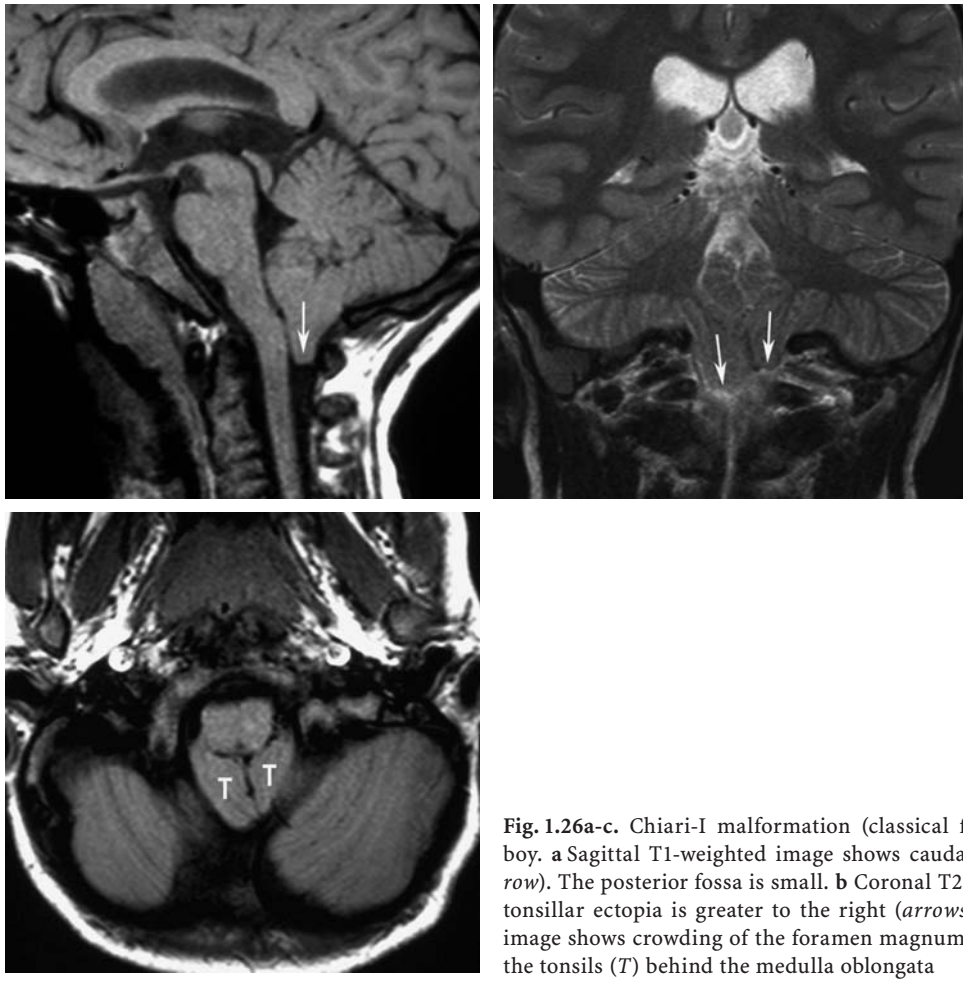

Fig. 1.26a-c. Chiari-I malformation (classical form) in a 12-year-old boy. **a** Sagittal T1-weighted image shows caudal tonsillar ectopia (*arrow*). The posterior fossa is small. **b** Coronal T2-weighted image shows tonsillar ectopia is greater to the right (*arrows*). **c** Axial T1-weighted image shows crowding of the foramen magnum due to the presence of the tonsils (*T*) behind the medulla oblongata

ebellar tonsils to a line drawn from the basion to the opisthion. There has been a significant amount of controversy concerning the exact degree of tonsillar ectopia that should be regarded as abnormal (Elster and Chen 1992; Milhorat et al. 1999). In our clinical experience we have used 3 mm as a cut-off for normal individuals in the pediatric age group, and considered ectopia greater than 5 mm to be definitely pathological. Mild (i.e., 3–5 mm) ectopia was considered significant in cases of: (a) neurological signs or symptoms that can be related to hindbrain compression; (b) peg-like deformation of the tonsils; or (c) a syrinx.

There is a significant incidence of hydrosyringomyelia and hydrocephalus in patients with Chiari-I malformations. The CSF cavities may extend over variable distances along the spinal cord (Fig. 1.27). They involve more often the cervical spinal cord, but may also be holocord. They involve the medulla (i.e., syringobulbia) in a minority of patients. Hydrocephalus is more common in patients who also have hydrosyringomyelia (Milhorat et al. 1999) due to the fact that both result from impaired CSF flow at the foramen magnum due to abnormal pulsatile motion of the cerebellar tonsils, producing a selective obstruction of CSF flow from the cranial cavity to the spine during systole. These phenomena may be dynamically observed on MRI using flow-sensitive techniques (Puyol et al. 1995). Because hydrosyringomyelia (HSM) is a significant contributor to the clinical picture and to the eventual outcome, it is critical that all patients with a diagnosis of Chiari-I malformation undergo MR imaging of the spinal cord. The reverse is also true, in that all patients with an apparently isolated HSM should be investigated for a possible Chiari-I malformation.

In a minority of cases, bulbar elongation with a prominent obex and, sometimes, a true posterior cervico-medullary kinking may be seen in association to the tonsillar descent. These cases have been referred to as the «bulbar» or «myelencephalic» variant of the Chiari-I malformation (Tortori-Donati et al. 2005a). This variant probably results from a smaller posterior fossa as compared with classical Chiari-I malformation, with an increased degree of neural overcrowding and downward displacement of the medulla. It is noteworthy that associated skeletal anomalies, such as platybasia and basilar invagination, are also relatively more common in patients with the bulbar variant (Fig. 1.23) than in classical Chiari-I malformation (Tortori-Donati et al. 2005a).

Fig. 1.27 Chiari-I malformation with hydromyelia in a 13-year-old girl. Sagittal T1-weighted image shows ectopic cerebellar tonsils in the foramen magnum (*arrow*). There is associated hydromyelia that involves the whole cord from C4 downwards to the conus medullaris (not shown). Multiple haustrations are a typical finding with Chiari-I-associated hydromyelia

1.2.2.2 Chiari-II Malformation

1.2.2.2.1 Background

The Chiari-II malformation is a congenital abnormality of the hindbrain characterized by a smaller than normal posterior cranial fossa with downward displacement of the vermis, brainstem, and fourth ventricle into the foramen magnum and cervical spinal canal. The Chiari-II malformation is found in all patients with open spinal dysraphisms (i.e., myelomeningoceles and myeloceles) (Cama et al. 1995; Tortori-Donati et al. 2000; Tortori-Donati et al. 2005a), although, because the severity of the hindbrain malformation may be extremely variable, a number of patients may have a nearly normal-sized posterior fossa with minimal, or even absent, caudal hindbrain displacement. Although greater than 90% of patients with Chiari-II malformation have open spinal dysraphisms, a minority of cases is dis-

covered in patients with closed spinal dysraphisms, especially myelocystoceles (Rossi et al. 2006).

1.2.2.2.2 Pathogenesis

According to the McLone and Knepper theory (McLone and Knepper 1989), the medial walls of the primitive central canal of the neural tube ("neurocele") normally appose and occlude the neurocele transiently during primary neurulation. Defective biosynthesis of cell surface glycoproteins causes the neurocele to remain patent, thereby allowing CSF to flow downwards and leak freely through the spinal defect into the amniotic cavity. This results in chronic CSF hypotension with collapse of the rhombencephalic vesicle (developing fourth ventricle) which in turn causes lack of induction of the perineural mesenchyme of the posterior cranial fossa. As a consequence, both the cerebellum and brainstem eventually are forced to develop within a smaller than normal posterior fossa to the extent that the vermis and cervicomedullary junction eventually herniate caudally through the foramen magnum.

1.2.2.2.3 Clinical Findings

The most common early symptom of this condition is respiratory stridor, often occurring within 1 or 2 weeks of birth and usually disappearing spontaneously within a few days, or at most 3 months. On occasion, it may be associated with signs of hindbrain dysfunction, such as difficult swallowing, intermittent apnea, aspiration, cessation of breathing, and arm weakness. Symptoms such as breathing and swallowing difficulties are probably related to the disorganization of brainstem nuclei rather than to mechanical distortion (Narayan et al. 2001). Hydrocephalus, usually appearing within 72 h of surgical correction of the spinal abnormality, presents with signs of raised intracranial pressure, that include bradycardia, opisthotonus, hypertonic upper limbs, hyperreflexia, headache, and seizures.

1.2.2.2.4 Imaging Findings

The Chiari-II malformation is characterized by a host of pathological features that generate a complex picture on neuroradiological investigations. Although caudal hindbrain displacement is the principal abnormality, there is a wide array of anomalies that involve the supratentorial compartment, the skull and meninges, and the spine and spinal cord; however, only the abnormalities pertaining the craniocervical junction are discussed here. As with other brain malformations, MRI is the single best neuroimaging modality; however, CT still plays a role in the depiction of bony abnormalities, other than in the follow-up of patients undergoing CSF shunting procedures. Shunt malfunctions, cord tethering, trapped fourth ventricle, and hydrosyringomyelia are frequent causes of relapsing ventricular dilatation. Because these children often undergo CT scanning for evaluating ventricular size, care should be employed to limit X-ray exposure.

As was previously detailed, the principal osseous abnormality is represented by a smaller than normal posterior cranial fossa, resulting from abnormal development of the occipital somites due to insufficient expansion of the rhombencephalic vesicle. The foramen magnum is enlarged in approximately three fourths of cases. The posterior margin of the odontoid process is frequently scalloped, and the upper portion of the cervical canal is widened. The posterior arch of the atlas is often incompletely developed; in such case, a thick fibroelastic band that constricts the underlying nervous structures bridges the intervening gap.

Because the posterior fossa is smaller than normal, there is a lack of vital space for the nervous structures of the hindbrain, which are squeezed out of the posterior fossa during their growth. This process results in the pathological hallmark of the Chiari-II malformation, i.e., a caudal displacement of the inferior vermis, medulla, cervicomedullary junction, and sometimes the fourth ventricle into the foramen magnum and upper cervical canal, forming a cascade of herniations that is particularly well depicted on sagittal MR images (Fig. 1.28). As a result, there is crowding of the foramen magnum with chronic constriction exerted by bony and fibrous structures on the herniating brain. This may result in mechanically induced ischemia of the inferior vermis and cervicomedullary junction, revealed by increased signal on T2-weighted MR images (Fig. 1.29). Notably, the cerebellar tonsils are not herniated even in severe cases, marking an important difference with the Chiari-I malformation.

The cervicomedullary deformities have been categorized into three types (Wolpert et al. 1988). In the type-1 deformity, the fourth ventricle and medulla do not descend through the foramen magnum,

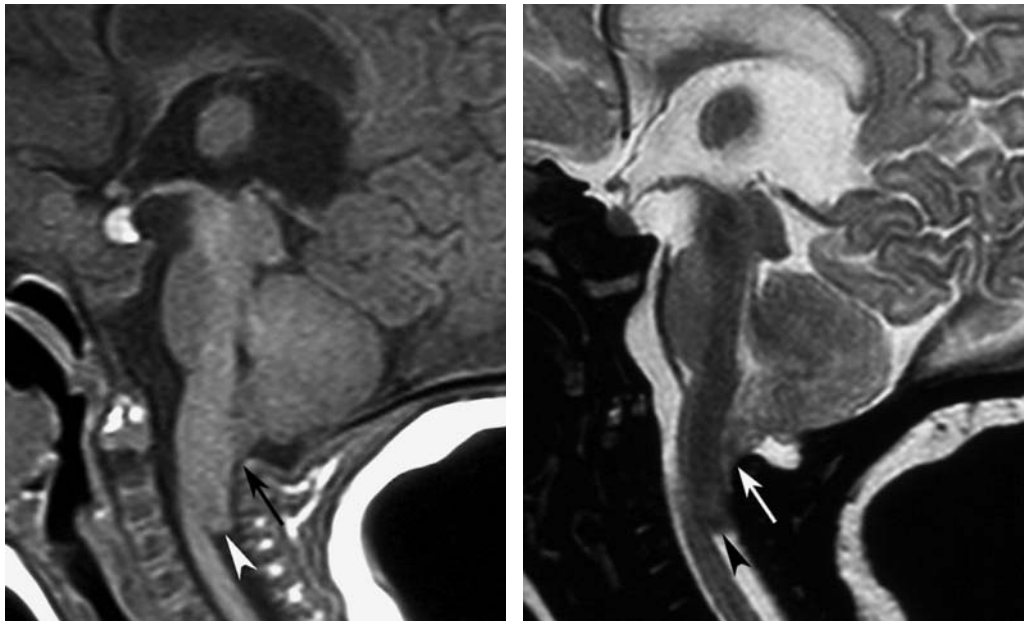

Fig. 1.28a,b. Chiari-II malformation in a 14-h-old male newborn with sacral myelomeningocele. **a** Sagittal T1-weighted image and **b** sagittal T2-weighted image show a very small posterior cranial fossa and the typical cascade of herniations constituting the hallmark of the Chiari-II malformation. Specifically, there is downward displacement of the vermis, forming the so-called cerebellar peg (*arrow*), while the medulla is also displaced caudally and buckles below the cervical spinal cord which is kept in place by the dentate ligaments, forming the cervicomedullary kink (*arrowhead*). In this case, the fourth ventricle is collapsed, making it a Wolpert's type-3a deformity (see text for discussion). Additional features include supratentorial hydrocephalus with a dilated suprapineal third-ventricular recess and a thickened quadrigeminal plate

Fig. 1.29 Chiari-II malformation with cerebellar peg edema in a 20-h-old female newborn with sacral myelomeningocele. Sagittal T2-weighted shows hyperintensity of the cerebellar peg extending upwards all the way to the nodulus (*arrows*) representing edema due to mechanical compression and vascular compromise. The posterior fossa is small and contains a correspondingly small fourth ventricle. Note that, unlike the previous case (see Fig. 1.28) there is no cervicomedullary kinking, making it a Wolpert's type-1 deformity (see text for discussion). Additional features include hypertrophic interthalamic mass and quadrigeminal plate. Note that hydrocephalus has not appeared yet

and the only deformity is a cerebellar peg through the foramen magnum. In type 2, the fourth ventricle descends vertically through the foramen magnum in front of the cerebellar peg. In type 3, the medulla is buckled below the spinal cord, forming the cervicomedullary kink behind the cord itself. This type is further categorized depending on whether the fourth ventricle is collapsed (type 3a) or dilated (type 3b).

1.2.2.3 Chiari-III Malformation

The original paper by Chiari (Chiari 1891) included the description of a case of cervical spina bifida combined with multiple hindbrain anomalies. Since then, the definition of the Chiari-III malformation has been expanded to include patients with herniation of the hindbrain in a low occipital and/or high cervical cephalocele in combination with pathological and imaging features of Chiari-II malformation, such as a small posterior fossa, tectal beaking, enlarged suprapineal third ventricular recess, and so forth (Castillo et al. 1992).

The cephalocele consistently involves the occipital bone below the inion, with possible extension into the high cervical (C1–C3) spine, and contains at least a part of the cerebellum, but may also contain the occipital lobe(s) (Fig. 1.30) and a severely distorted brainstem. Purely cervical cephaloceles must contain cerebellar tissue in order to match the Chiari-III definition.

1.2.2.4 Chiari-IV Malformation

In his 1896 paper, Chiari described a fourth type of hindbrain anomaly, corresponding to severe cerebellar hypoplasia (Chiari 1896); however, subsequent investigators discarded the term "Chiari-IV malformation." In 1996, Tortori-Donati reintroduced the term to designate the association of severe cerebellar hypoplasia in patients with myelomeningocele (Tortori-Donati et al. 1996). Such association appears to represent a well-defined, albeit rare, condition. Pathological and imaging findings of this condition (Fig. 1.31) include absent or severely hypoplastic cerebellum, small brainstem, and large posterior fossa CSF spaces, as opposed to caudal cerebellar displacement and collapsed posterior fossa CSF spaces seen in typical Chiari-II patients.

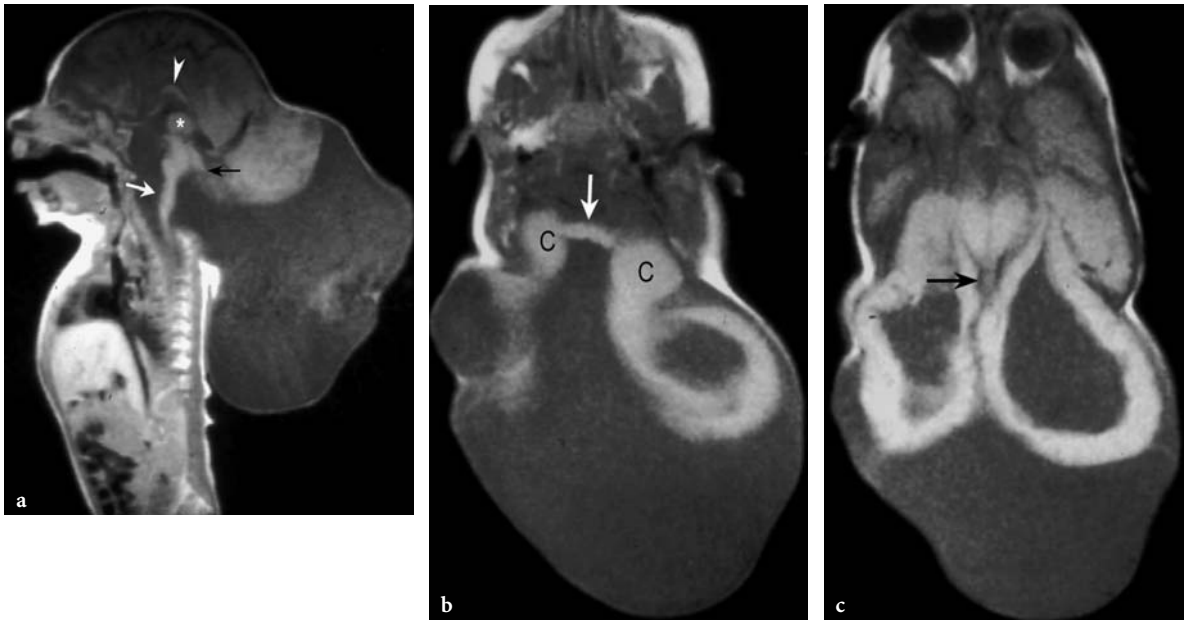

Fig. 1.30a-c. Chiari-III malformation in a 2-month-old girl. **a** Sagittal T1-weighted image shows enormous occipito-cervical cephalocele basically containing cerebrospinal fluid, but also brain. Additional findings include a hypoplastic brain stem (*white arrow*) tectal beak (*black arrow*) enlarged interthalamic mass (*asterisk*) and corpus callosum dysgenesis (*arrowhead*). **b,c** Axial T1-weighted images show both occipital lobes, containing markedly enlarged occipital horns, herniate into the cephalocele, while the cerebellar hemispheres (*C*) abridge the sessile base of the cephalocele. There is no vermis to be found. The pons is markedly hypoplastic (*white arrow,* **b**) and tectal beaking is confirmed (*black arrow,* **c**)

a b

Fig. 1.31a,b. Chiari-IV malformation in a 16-year-old boy operated for sacral myelomeningocele soon after birth. **a** Sagittal T1-weighted image shows a hypoplastic vermis with rudimentary foliation, a hypoplastic brain stem, and a very small fourth ventricle. Note that although the posterior fossa is smaller than normal, the subarachnoid spaces are wide and there is no hindbrain herniation. **b** Axial T1-weighted image shows hypoplastic cerebellar vermis (*V*) and hemispheres (*H*). The appearance of the cerebellum, with rudimentary foliation, and brain stem strongly favors the hypothesis of primitive hypoplasia, rather than secondary destruction, as the pathogenesis of this rare condition

References

Barkovich AJ, Raghavan N, Chuang SH (1989) MR of lumbosacral agenesis. Am J Neuroradiol 10:1223–1231

Barkovich AJ, Edwards MSB, Cogen PH (1991) MR evaluation of spinal dermal sinus tracts in children. Am J Neuroradiol 12:123–129

Breningstall GN, Marker SM, Tubman DE (1992) Hydrosyringomyelia and diastematomyelia detected by MRI in myelomeningocele. Pediatr Neurol 8:267–271

Brown E, Matthes JC, Bazan C III, Jinkins JR (1994) Prevalence of incidental intraspinal lipoma of the lumbosacral spine as determined by MRI. Spine 19:833–836

Byrd SE, Harvey C, Darling CF (1995) MR of terminal myelocystoceles. Eur J Radiol 20:215–220

Cama A, Tortori-Donati P, Piatelli GL, Fondelli MP, Andreussi L (1995) Chiari complex in children: neuroradiological diagnosis, neurosurgical treatment and proposal of a new classification (312 cases). Eur J Pediatr Surg 5:35–38

Carey JC, Greenbaum B, Hall BD (1978) The OEIS complex (omphalocele, exstrophy, imperforate anus, spinal defects). Birth Defects Orig Artic Ser 14:253–263

Castillo M, Mukherji SK (1995) Imaging of the pediatric head, neck, and spine. Lippincott-Raven, Philadelphia

Castillo M, Quencer RM, Dominguez R (1992) Chiari III malformation: imaging features. Am J Neuroradiol 13:107–113

Catala M (1997) Embryogenesis. Why do we need a new explanation for the emergence of spina bifida with lipoma? Childs Nerv Syst 13:336–340

Catala M (2002) Genetic control of caudal development. Clin Genet 61:89–96

Chiari H (1891) Über veränderungen des kleinhirns infolge von hydrocephalie des grosshirns. Dtsch Med Wochenschr 17:1172–1175

Chiari H (1896) Über veränderungen des kleinhirns, des pons und der medullaoblongata infolge von congenitales hydrocephalie des grosshirns. Dtsch Akad Wiss, Wien, pp 63–71

Christophe C, Dan B (1999) Magnetic resonance imaging cranial and cerebral dimensions: Is there a relationship with Chiari I malformation? A preliminary report in children. Eur J Paediatr Neurol 3:15–24

Coleman LT, Zimmerman RA, Rorke LB (1995) Ventriculus terminalis of the conus medullaris: MR findings in children. Am J Neuroradiol 16:1421–1426

Currarino G, Coln D, Votteler T (1981) Triad of anorectal, sacral, and presacral anomalies. Am J Roentgenol 137:395–398

Dias MS, Azizkhan RG (1998) A novel embryogenetic mechanism for Currarino's triad: inadequate dorsoventral separation of the caudal eminence from hindgut endoderm. Pediatr Neurosurg 28:223–229

Dias MS, Partington M (2004) Embryology of myelomeningocele and anencephaly. Neurosurg Focus 16:E1

Dias MS, Walker ML (1992) The embryogenesis of complex dysraphic malformations: a disorder of gastrulation? Pediatr Neurosurg 18:229–253

Drolet B (1998) Birthmarks to worry about. Cutaneous markers of dysraphism. Dermatol Clin 16:447–453

Duhamel B (1961) From the mermaid to anal imperforation: the syndrome of caudal regression. Arch Dis Child 36:152–155

Elster AD, Chen MYM (1992) Chiari I malformations: clinical and radiological reappraisal. Radiology 183:347–353

Elton S, Oakes WJ (2001). Dermal sinus tracts of the spine. Neurosurg Focus 10, Article 4. Available at: http://www.neurosurgery.org/focus/jan01/10-1-4.pdf. Accessed 26 July 2005

Faris JC, Crowe JE (1975) The split notochord syndrome. J Pediatr Surg 10:467–472

French BN (1983) The embryology of spinal dysraphism. Clin Neurosurg 30:295–340

Gudinchet F, Maeder P, Laurent T, Meyrat B, Schnyder P (1997) Magnetic resonance detection of myelodysplasia in children with Currarino triad. Pediatr Radiol 27:903–907

Hecht JT, Nelson FW, Butler IJ, Horton WA, Scott CI Jr, Wassman ER, Mehringer CM, Rimoin DL, Pauli RM (1985) Computed tomography of the foramen magnum: achondroplastic values compared to normal standards. Am J Med Genet 20:355–360

Herman JM, McLone DG, Storrs BB, Dauser RC (1993) Analysis of 153 patients with myelomeningocele or spinal lipoma reoperated upon for a tethered cord. Pediatr Neurosurg 19:243–249

Hoffman CH, Dietrich RB, Pais MJ, Demos DS, Pribram HF (1993) The split notochord syndrome with dorsal enteric fistula. Am J Neuroradiol 14:622–627

Kernohan JW (1924) The ventriculus terminalis: its growth and development. J Comp Neurol 38:10–125

Knittle JL, Timmers K, Ginsberg-Fellner F, Brown RE, Katz DP (1979) The growth of adipose tissue in children and adolescents. Cross-sectional and longitudinal studies of adipose cell number and size. J Clin Invest 63:239–246

McLone DG, Dias MS (1992) Complications of myelomeningocele closure. Pediatr Neurosurg 17:267–273

McLone DG, Knepper PA (1989) The cause of Chiari II malformation: a unified theory. Pediatr Neurosci 15:1–12

McLone DG, Naidich TP (1985) Terminal myelocystocele. Neurosurgery 16:36–43

Meadows J, Kraut M, Guarnieri M, Haroun RI, Carson BS (2000) Asymptomatic Chiari type I malformations identified on magnetic resonance imaging. J Neurosurg 92:920–926

Milhorat TH, Chou MW, Trinidad EM, Kula RW, Mandell M, Wolpert C, Speer MC (1999) Chiari I malformation redefined: clinical and radiological findings for 364 symptomatic patients. Neurosurgery 44:1005–1017

Naidich TP, Harwood-Nash DC (1983) Diastematomyelia. Part I. Hemicords and meningeal sheaths. Single and double arachnoid and dural tubes. Am J Neuroradiol 4:633–636

Naidich TP, McLone DG, Mutleur S (1983) A new understanding of dorsal dysraphism with lipoma (lipomyeloschisis): radiological evaluation and surgical correction. Am J Neuroradiol 4:103–116

Naidich TP, Blaser SI, Delman BN, McLone DG, Dias MS, Zimmerman RA, Raybaud CA, Birschansky SB, Altman NR, Braffman BH (2002) Embryology of the spine and spinal cord. Proc 40th Annual Meeting of the American Society of Neuroradiology, Vancouver, BC, Canada, pp 3–13

Narayan P, Mapstone TB, Tubbs RS, Grabb PA, Frye T (2001) Clinical significance of cervicomedullary deformity in Chiari II malformation. Pediatr Neurosurg 35:140–144

Nguyen VD, Tyrrel R (1993) Klippel-Feil syndrome: patterns of bony fusion and wasp-waist sign. Skeletal Radiol 22:519–523

Nievelstein RAJ, Hartwig NG, Vermeji-Keers C, Valk J (1993) Embryonic development of the mammalian caudal neural tube. Teratology 48:21–31

Nievelstein RAJ, Valk J, Smit LME, Vermeji-Keers C (1994) MR of the caudal regression syndrome: embryologic implications. Am J Neuroradiol 15:1021–1029

Nishikawa M, Sakamoto H, Hakuba A, Nakanishi N, Inoue Y (1997) Pathogenesis of Chiari malformation: a morphometric study of the posterior cranial fossa. J Neurosurg 86:40–47

Pang D (1992) Split cord malformation. Part II: clinical syndrome. Neurosurgery 31:481–500

Pang D (1993) Sacral agenesis and caudal spinal cord malformations. Neurosurgery 32:755–779

Pang D, Dias M (1993) Cervical myelomeningoceles. Neurosurgery 33:363–373

Pang D, Dias MS, Ahab-Barmada M (1992) Split cord malformation. Part I: A unified theory of embryogenesis for double spinal cord malformations. Neurosurgery 31:451–480

Park JK, Gleason PL, Madsen JR, Goumnerova LC, Scott RM (1997) Presentation and management of Chiari I malformation in children. Pediatr Neurosurg 26:190–196

Payner TD, Prenger E, Berger TS, Crone KR (1994) Acquired Chiari malformations: incidence, diagnosis, and management. Neurosurgery 34:429–434

Peacock WJ, Murovic JA (1989) Magnetic resonance imaging in myelocystoceles. Report of two cases. J Neurosurg 70:804–807

Pierre-Kahn A, Zerah M, Renier D, Cinalli G, Sainte-Rose C, Lellouch-Tubiana A, Brunelle F, Le Merrer M, Giudicelli Y, Pichon J, Kleinknecht B, Nataf F (1997) Congenital lumbosacral lipomas. Childs Nerv Syst 13:298–334

Prop N, Frensdorf EL (1967) A postvertebral endodermal cyst associated with axial deformities: a case showing the "endodermal–ectodermal adhesion syndrome". Pediatrics 39:555–562

Pujol J, Roig C, Capdevila A, Pou A, Marti-Vilalta JL, Kulisevsky J, Escartin A, Zannoli G (1995) Motion of the cerebellar tonsils in Chiari type I malformation studied by cine phase-contrast MRI. Neurology 45:1746–1753

Raghavan N, Barkovich AJ, Edwards M, Norman D (1989) MR imaging in the tethered spinal cord syndrome. Am J Neuroradiol 10:27–36

Rossi A, Biancheri R, Cama A, Piatelli G, Ravegnani M, Tortori-Donati P (2004a) Imaging in spine and spinal cord malformations. Eur J Radiol 50:177–200

Rossi A, Cama A, Piatelli G, Ravegnani M, Biancheri R, Tortori-Donati P (2004b) Spinal dysraphism: MR imaging rationale. J Neuroradiol 31:3–24

Rossi A, Piatelli G, Gandolfo C, Pavanello M, Hoffmann C, Van Goethem JW, Cama A, Tortori-Donati P (2006) Spectrum of nonterminal myelocystoceles. Neurosurgery 58:509–515

Rousseau F, Bonaventure J, Legeai-Mallet L, Pelet A, Rozet JM, Maroteaux P, Le Merrer M, Munnich A (1994) Mutations in the gene encoding fibroblast growth factor receptor-3 in achondroplasia. Nature 371:252–254

Sattar MT, Bannister CM, Turnbull IW (1996) Occult spinal dysraphism: the common combination of lesions and the clinical manifestations in 50 patients. Eur J Pediatr Surg 6 (Suppl I):10–14

Schlesinger AE, Naidich TP, Quencer RM (1986) Concurrent hydromyelia and diastematomyelia. Am J Neuroradiol 7:473–477

Scott RM, Wolpert SM, Bartoshesky LF, Zimbler S, Klauber GT (1986) Dermoid tumors occurring at the site of previous myelomeningocele repair. J Neurosurg 65:779–783

Scotti G, Harwood-Nash DC (1980) Congenital thoracic dermal sinus: diagnosis by computer assisted metrizamide myelography. J Comput Assist Tomogr 4:675–677

Shiang R, Thompson LM, Zhu YZ, Church DM, Fielder TJ, Bocian M, Winokur ST, Wasmuth JJ (1994) Mutations in the transmembrane domain of FGFR3 cause the most common genetic form of dwarfism, achondroplasia. Cell 78:335–342

Sigal R, Denys A, Halimi P, Shapeero L, Doyon D, Boudghène F (1991) Ventriculus terminalis of the conus medullaris: MR imaging in four patients with congenital dilatation. Am J Neuroradiol 12:733–737

Sival DA, van Weerden TW, Vles JS, Timmer A, den Dunnen WF, Staal-Schreinemachers AL, Hoving EW, Sollie KM, Kranen-Mastenbroek VJ, Sauer PJ, Brouwer OF (2004) Neonatal loss of function in human spina bifida aperta. Pediatrics 114:427–434

Smith NM, Chambers HM, Furness ME, Haan EA (1992) The OEIS complex omphalocele-exstrophy-imperforate anus-spinal defects: recurrence in sibs. J Med Genet 29:730–732

Tortori-Donati P, Cama A, Rosa ML, Andreussi L, Taccone A (1990) Occult spinal dysraphism: neuroradiological study. Neuroradiology 31:512–522

Tortori-Donati P, Fondelli MP, Rossı A, Raybaud CA, Cama A, Capra V (1999) Segmental spinal dysgenesis. Neuroradiologic findings with clinical and embryologic correlation. Am J Neuroradiol 20:445–456

Tortori-Donati P, Rossi A, Cama A (2000) Spinal dysraphism: a review of neuroradiological features with embryological correlations and proposal for a new classification. Neuroradiology 2000; 42:471–491

Tortori-Donati P, Rossı A, Biancheri R, Cama A (2001) Magnetic resonance imaging of spinal dysraphism. Top Magn Reson Imaging 12:375–409

Tortori-Donati P, Rossi A, Biancheri R (2005a) Brain malformations. In: Tortori-Donati P (ed) Pediatric neuroradiology. Springer, Berlin Heidelberg New York, pp 71–198

Tortori-Donati P, Rossi A, Biancheri A, Cama A (2005b) Congenital malformations of the spine and spinal cord. In: Tortori-Donati P (ed) Pediatric neuroradiology. Springer, Berlin Heidelberg New York, pp 1539–1596

Uchino A, Mori T, Ohno M (1991) Thickened fatty filum terminale: MR imaging. Neuroradiology 33:331–333

Ulmer JL, Elster AD, Ginsberg LE, Williams DW III (1993) Klippel-Feil syndrome: CT and MR of acquired and congenital abnormalities of cervical spine and cord. J Comput Assist Tomogr 17:215–224

Walsh DS, Adzick NS (2003) Foetal surgery for spina bifida. Semin Neonatol 8:197–205

Warder DE (2001) Tethered cord syndrome and occult spinal dysraphism. Neurosurg Focus (serial online] 10: Article 1. Available at http://www.neurosurgery.org/focus/jan01/10-1-1.pdf

Warder DE, Oakes WJ (1993) Tethered cord syndrome and the conus in a normal position. Neurosurgery 33:374–378

Warder DE, Oakes WJ (1994) Tethered cord syndrome: the low-lying and normally positioned conus. Neurosurgery 34:597–600

Weprin BE, Oakes WJ (2000) Coccygeal pits. Pediatrics 105: E69

White KS, Ball WS, Prenger EC, Patterson BJ, Kirks DR (1993) Evaluation of the craniocervical junction in Down syndrome: correlation of measurements obtained with radiography and MR imaging. Radiology 186:377–382

Wolpert SM, Scott RM, Platenberg C, Runge VM (1988) The clinical significance of hindbrain herniation and deformity as shown on MR images of patients with Chiari II malformation. Am J Neuroradiol 9:1075–1078

Wu YW, Chin CT, Chan KM, Barkovich AJ, Ferriero DM (1999) Pediatric Chiari I malformations. Do clinical and radiologic features correlate? Neurology 53:1271–1276

Yundt KD, Park TS, Kaufman BA (1997) Normal diameter of filum terminale in children: in vivo measurement. Pediatr Neurosurg 27:257–259

Zimmerman RA (2005) Skull development and abnormalities. In: Tortori-Donati P (ed) Pediatric neuroradiology. Springer, Berlin Heidelberg New York, pp 1271–1287

Pediatric Spine

The Spine and Spinal Cord in Children

2

Normal Radiologic Appearance, Variations, Infections and Tumors

E. Turgut Tali and Oznur Boyunaga

CONTENTS

E. T. Tali, Prof. Dr.; O. Boyunaga, Assoc. Prof.
Gazi University School of Medicine, Department of Radiology, Divisions of Neuroradiology and Pediatric Radiology, Besevler 06510 Ankara, Turkey

2.1 Introduction

Knowledge of the normal anatomy and development of vertebrae, as well as of the changes in the vertebral bone marrow and spinal cord according to age are mandatory to interpret radiological images of these regions accurately. Imaging of the spine can be performed by conventional radiography, ultrasonography (US), computerized tomography (CT), digital subtraction angiography (DSA) or magnetic resonance imaging (MRI). With conventional radiography, anteroposterior (AP), lateral, and oblique projections of the vertebral column, as well as specific structural imaging, should be obtained (e.g. AP open mouth for the odontoid process). Conventional radiographs provide valuable information regarding the bony structures of the spinal column, facet joints, disc spaces, and foramina, while only limited information regarding the paraspinal soft tissues can be obtained. The spinal cord is well seen with US in the first few months of life, but at a later age visualization of the cord is not satisfactory. US examination of the dural sac during spinal surgery is

KEY POINTS

- **Stages** of spinal development on MRI
  - **Stage I** (< 1 mo)
    - Ossified portion of the vertebral body is oval
    - Cartilaginous endplates are relatively large
    - T1-WI: bone marrow and nucleus pulposus are hypointense; cartilaginous endplates are hyperintense
  - **Stage II** (1–6 months)
    - Size and SI of ossified portion of vertebral body increases
    - T1-WI SI of cartilaginous structures decreases
    - Decrease of SI gradually in vertebral body by 2 years
    - Vertebral bodies have a horizontal band with high SI
  - **Stage III** (6 months–5 years)
    - Vertebral bodies become rectangular
    - T1-WI SI of the bodies exceeds that of discs
    - At 5 years the SI of vertebral bodies > discs on T1-WI
    - Vertebral body bone marrow has a relatively low SI, basivertebral plexus has high SI on T2-WI
    - Intervertebral discs are narrower compared to adults
    - Posterior elements are cartilaginous initially and have high SI on T2-WI compared to muscle; ossification begins by 1st year and become relatively hypointense on T2-WI
- **Atlantodental distance**
  - Neutral 2–3 mm
  - Increase ≥2 mm in flexion
- **Cervical interspinous distance**
  - Increases with flexion at C1–C2
  - Interspinous distance >1.5× compared to adjacent levels: ligamentous injury possible
- **Prevertebral soft tissue**
  - ≤ 6 mm at C3 in children
  - Widening in expiration
- **Normal variants** in the pediatric **cervical** spine:
  - Ossiculum terminale
  - Bifid odontoid
  - Cleft in posterior neural arches
  - Ponticulus posticus
  - Pseudosubluxation
  - Wedging of vertebral bodies
  - Pseudo widening of interpeduncular distance
  - Spina bifida occulta
- **Normal variants** in the pediatric **thoracic and lumbosacral** spine:
  - Neurocentral synchondroses
  - Cleft in posterior neural arches
  - Wedging of vertebral bodies
  - Spina bifida occulta
  - Vascular grooves
  - Ring apophyses
  - Pediculate thinning
  - "Bone-within-bone"
- Degenerative disc disease
  - More common than generally thought in children and adolescents
  - Scheuermann's disease, Schmorl's nodes and limbus vertebrae are different manifestations of degenerative disc disease
  - Not all degenerative discs are symptomatic
  - Why some children are affected is not known
    - Repeated, subclinical traumas
    - Individual susceptibility
- **Spondylodiscitis:** in children, persisting vascular channels may allow direct inoculation of the intervertebral disc. Following bacteremia, the infection begins within the disc and extends to the adjacent endplate
- **Spinal tumors:**
  - Intramedullary
    - Majority in children are astrocytoma followed by ependymoma
    - Hemangioblastoma, oligodendroglioma, and paraganglioma are rare in children
  - Intradural extramedullary
    - Less frequent in children: meningioma, nerve sheath tumors
    - More frequent in children: dermoids
  - Extradural
    - More frequent in children: osteosarcoma

helpful for imaging evaluation and surgical planning. Multislice CT demonstrates the vertebral column, vascular structures and discs very well together with better visualization of the spinal cord and paraspinal soft tissues, while conventional CT demonstrates the vertebral body and posterior elements very well with only limited visualization of the soft tissues and spinal cord. Color-3D images of the entire vertebral column, paraspinal soft tissues and vascular structures can be obtained with multislice CT. DSA is still the gold standard for imaging and interventional procedures of spinal vascular structures. However, DSA is a time consuming, invasive technique that has the disadvantage of high levels of radiation, the risk of nephrotoxicity due to the contrast agents, spinal cord ischemia, etc. In addition, spinal DSA also has limitations in patients with thoracoabdominal aortic aneurysm. MR imaging has become the modality of choice for imaging of the spinal cord, thecal sac, nerve roots, epidural space, vascular structures, neural foramina, vertebral body, intervertebral discs, facet joints, spinal ligaments and also paraspinal soft tissues. New MR imaging techniques such as diffusion (DWI), perfusion (PWI), functional imaging (fMRI) and magnetic resonance spectroscopy (MRS) provide more specific, detailed and physiological information about the spine and spinal cord and also enable quantitative evaluation. Contrast-enhanced (high dose) spinal MRA is a very promising technique, particularly for screening examinations of the spinal veins and arteries. Increased temporal and spatial resolution enable us to differentiate arteries and veins lying in close proximity. This differentiation may not be precise due to the bidirectional flow of the segmental arteries, course and/or anatomical similarities of the veins and arteries. However, spinal MRA can be used to demonstrate the anterior spinal artery and artery of Adamkiewicz and in screening for AVF and AVM (Backes et al 2004). Spinal CSF flow can also be demonstrated and measured reliably using MRI. The pulsatile motion of the cerebrospinal fluid (CSF) is characterized by a cranio-caudad flow during arterial systole, followed by a caudo-craniad flow during diastole and shows a biphasic pattern corresponding to the cardiac cycle. The CSF flow posterior to the spinal cord is slightly earlier than the flow anterior to the cord (Bhadelia et al. 1995, Henry-Feugeas et al 1993). Although CSF flow velocities are variable depending on the size of the dural sac and spinal canal, generally maximum systolic velocity is not more than 10 cm/s at the cervical level and even lower at the distal levels (Bhadelia et al. 1995, Henry-Feugeas et al 1993). It is also possible to differentiate syringomyelic circulating cysts from non-circulating cysts (Brugiéres et al 2004). Flow imaging is also helpful for the accurate diagnosis of transdural spinal cord herniation. Application of DWI in the spine and spinal cord has been limited and more research is required. The small size of the spinal cord, the surrounding CSF, their motions and also swallowing and breathing artifacts make spinal DWI difficult. Slight contamination due to partial volume effects of the surrounding CSF may confound quantitative measurements at the edge of the cord (Thurnher and Bammer 2004). Although there are several recently introduced DWI techniques for the spine and spinal cord, each with their advantages and disadvantages, there is still no consensus for the optimal diffusion weighted sequence. Animal studies have demonstrated that DWI is more sensitive for spinal cord injury, myelopathy and treatment monitoring. Although, it is not possible to distinguish between gray and white matter, diffusion maps showed lower diffusivity in the center of the cord while higher diffusivity was demonstrated in the lateral and posterior regions (Thurnher and Bammer 2004). Water diffusivity in the direction parallel to the fibers was found to be 2.5 times higher than the average diffusivity perpendicular to the fibers (Ries et al. 2000). Diffusion tensor imaging promises the characterization of the structural integrity of the spinal cord fibers (Ries et al. 2000). ADC values mainly depend on the size of the extracellular space, and correlate with quantitative measurements of axonal density. ADC values were found to be increased with the expansion of the extracellular space (Mottershed et al. 2003). Line-scan diffusion imaging was found to be a feasible technique for pediatric patients (Robertson et al. 2000). Spinal cord fMRI might have relevance for preoperative evaluation of tumors and to evaluate pain processing, although currently there are no clinical indications (Stracke et al. 2004). There are still major problems and limitations for spinal fMRI. The area of interest with expected neuronal activity is very small and very high spatial resolution and signal to noise ratio (SNR) are required. The imaging technique should be less susceptible for surrounding bony and ligamentous structures, and should include cardiac, respiratory and flow gating due to its motion of respiration, cardiac motion and surrounding CSF flow. The most important technique is echo planar imaging (EPI) gradient echo

imaging. Most of the research has been performed in the cervical and upper thoracic spine. The feasibility of fMRI of the spinal cord has been demonstrated, even though the time course of the hemodynamic response function is not yet known. fMRI of the spinal cord was performed initially with a motor task and also somatosensory stimulation (Stroman et al. 2002; Backes et al. 2001).

2.2 Development and Normal Radiological Appearance of the Pediatric Spine

The spinal column develops in three stages: membrane development, chondrification, and ossification (Kirks and Griscom 1998). The dorsal neural tube forms at the 25th gestational day. Lateral to the closing neural tube the mesenchyma forms somites which are precursors of the vertebrae. At 6–8 weeks of gestation, chondrification of vertebral bodies occurs, later at 9 weeks of gestation, ossification begins. The first ossification of the vertebral bodies occurs in the lower thoracic and upper lumbar spine and the first ossified neural arches occur in the cervical region. Between the vertebral bodies there are remnants of the notochord, which become part of the nucleus pulposus.

The cervical (C) and lumbar (L) lordosis and thoracic (T) kyphosis of the spinal column are less pronounced in neonates. As the child grows and after upright posture and walking are established, the normal curvatures of the spine becomes more prominent (Kirks and Griscom 1998; Swischuk 1997). When the neck is in neutral position, absence of lordosis can be seen in children up to 16 years of age (Lustrin et al. 2003).

2.2.1 Normal Radiological Appearances of the Cervical Vertebrae in Children

The atlas (C1) has three ossification centers: one anterior arch and two posterior neural arches. The anterior arch can be seen as an ossification center by the first year of life. It fuses with the neural arches by the seventh year of age. Fusion of the neural arches of C1 and C2 posteriorly occurs by the 3 years of age (Lustrin et al. 2003).

The axis (C2) has the most complex development of all vertebrae. It has four ossification centers at birth: two for the neural arches, one for the body, and one for the odontoid process. The os terminale, a secondary ossification center, appears at the tip of the odontoid process between 3–6 years of age and fuses by the age of 12 years. The body of C2 also fuses with the odontoid process by 3–6 years of age. This fusion line (the remnant of the cartilaginous synchondrosis) can be seen until the age of 11 (Lustrin et al. 2003).

C3 through C7 show a similar developmental pattern. Three ossification centers are present at each level: one for the vertebral body and two for the neural arches. The body fuses with the neural arches by age of 3–6 years and the neural arches fuse posteriorly by age of 2–3 years. Epiphyseal plates are seen as sclerotic lines at the superior and inferior aspects of the vertebral bodies, especially visible at the anterior corners on lateral plain film (Fig. 2.1a). They fuse with the vertebral bodies during early adulthood. Secondary ossification centers are also visible at the tips of the spinous and transverse processes and articulating facets just before puberty and may persist until the third decade (Lustrin et al. 2003). Uncinate processes, paired little projecting structures extending from superolateral aspect of the vertebral body, are present only in the cervical vertebrae. They articulate with the inferolateral aspect of the suprajacent cervical vertebra and form a joint that is often referred to as “uncovertebral joint” or “joint of Luschka” (Fig. 2.1b) (Jinkins 2000).

For a proper and correct evaluation of MRI of the pediatric spine, normal spinal development stages must also be known. The spinal development can be divided into three stages. Birth to 1 month is stage I, 1 month to 6 months is stage II, and 6 months to 5 years is stage III (Foster et al. 2004). At birth, the ossified portion of the vertebral body is oval and its cartilaginous endplates are relatively large. The vertebral bone marrow and nucleus pulposus are hypointense while the cartilaginous endplates are hyperintense on T1-WI (Fig. 2.2). In stage II, the size and signal intensity of the ossified portion of the vertebral body increases and the signal intensity of the cartilaginous structures decreases. This decrease in signal gradually spreads to the entire vertebral body by the second year of life (Fig. 2.3). Vertebral bodies have a high signal horizontal band that corresponds to the basivertebral plexus (Fig. 2.4). By stage III, the vertebral bodies have a rectangular shape and the signal intensity of the

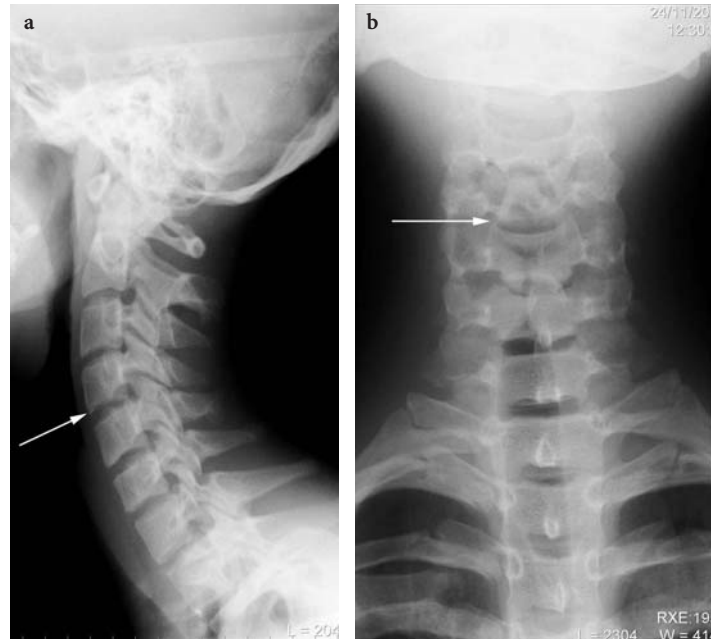

Fig. 2.1a,b. Lateral (**a**), and AP (**b**) radiographs demonstrate the epiphyseal plate as a sclerotic line at the inferior aspect of the C4 (*arrow*, **a**) in a 15-year-old boy. Note also the uncovertebral joints (joint of Luschka) (*arrow*, **b**)

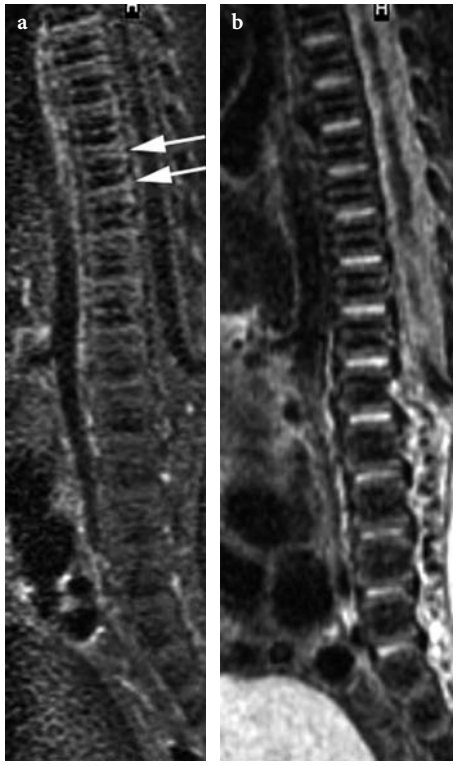

Fig. 2.2a,b. Sagittal T1-WI (**a**) shows large and hyperintense cartilaginous endplates (*arrows*) of the vertebral body while vertebral bone marrow and nucleus pulposus are hypointense in the newborn. Between the hyperintense cartilaginous endplates, hypointense vertebral body is also seen. T2-WI (**a**) demonstrates hyperintense intervertebral discs and hypointense cartilaginous endplates. Signals of vertebral bodies are more hypointense than endplates

Fig. 2.3a,b. Sagittal T1-WI (**a**) and T2-WI (**b**) of the lumbar spine show increased signal of the vertebral bodies in this 1-year-old infant. The cartilaginous structures show decreased signal when compared to images of the newborn baby

Fig. 2.4. Axial T2-WI demonstrates neural foramina with spinal nerves and basivertebral vein in a thoracic vertebral body

bodies exceeds that of the intervertebral discs. At 5 years of age, the signal intensity of the vertebral bodies is greater than that of the discs on T1-WI in more than 90% of the population (Figs. 2.5, 2.6) (Foster et al. 2004). Vertebral body bone marrow has a relatively low signal, while the basivertebral plexus has a high signal on T2-WI. The intervertebral discs are narrower when compared to the adults. The posterior elements are cartilaginous initially and have high signal on T2-WI compared to muscle. They begin to ossify by the first year of life and contain red marrow and become relatively hypointense on T2-WI (Foster et al. 2004).

Physiologic as well as pathologic marrow signal changes are readily detectable on MRI. Sagittal images are the most useful images for depicting bone marrow changes of the vertebral bodies. The signal of the marrow depends on the relative amounts of fat and water within the marrow and the selected sequence. T1-WI show anatomy and signal changes between fatty (yellow) and hematopoietic (red) marrow well. Children have more red marrow which has more cellular material, protein and water, and thus has longer T1 relaxation times than yellow marrow. On T1-WI, red marrow has similar or slightly higher signal intensity than muscle. Vertebral red marrow changes to yellow marrow when the child grows up (Lustrin et al. 2003). After the first decade, the signal intensity of the vertebral body marrow is higher on T1-WI than that of the intervertebral disc signal (Figs. 2.5, 2.6). Yellow marrow replaces the red marrow in a diffuse or focal spotted pattern over years (Foster et al. 2004).

2.2.1.1 Atlantodental Distance

The atlantodental distance is defined as the distance between the anterior aspect of the dens and the posterior aspect of the anterior arch of the atlas. In

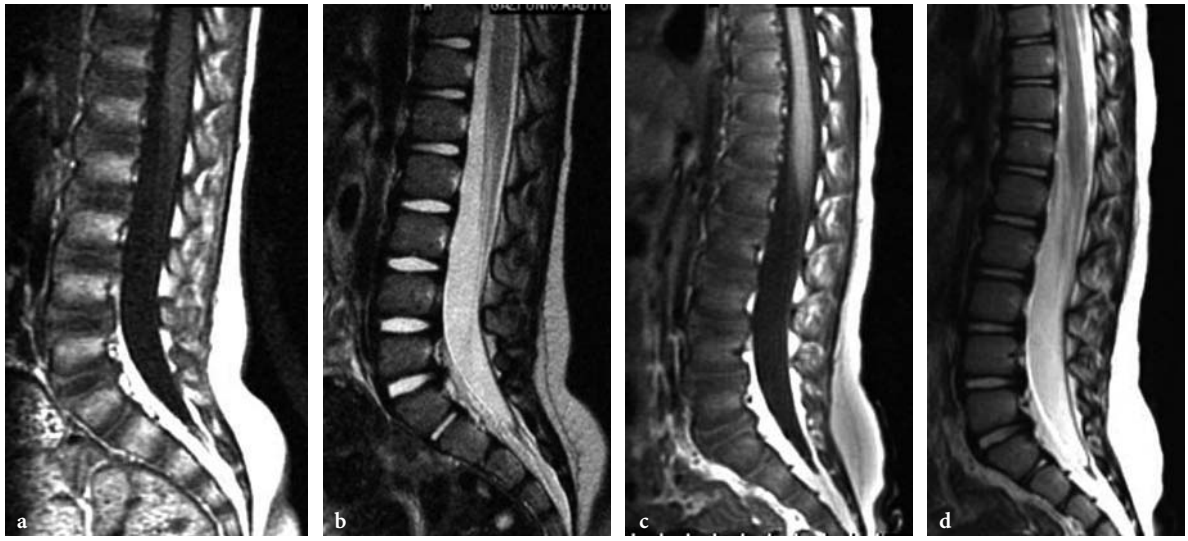

Fig. 2.5a–d. Sagittal T1-WI (**a**) and T2-WI (**b**) of a 2-year-old-boy, as well as T1-WI (**c**) and T2-WI (**d**) of 3-year-old boy demonstrate signal intensity changes of the vertebral bodies which exceed intervertebral disc signals during stage III (6 months–5 years old)

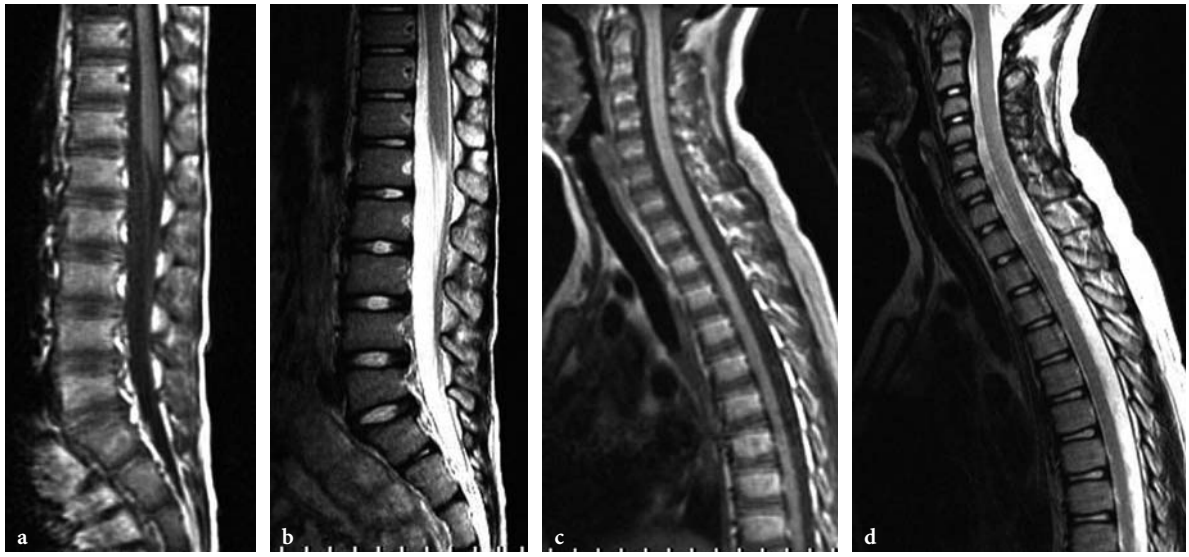

Fig. 2.6a-d. Sagittal T1-WI (**a**) and T2-WI (**b**) of 10-year-old girl and T1-WI (**c**) and T2-WI (**d**) of an 11-year-old boy illustrate that the signal intensity of vertebral body bone marrow is higher than the disc signal on T1-WI

neutral position, generally 2–3 mm distance is seen on lateral radiographs. A normal increase in the distance up to 2 mm (atlantodental distance should be less than 5 mm in total) is expected on flexion radiographs of the neck, but, if no increase is observed in the atlantodental distance, it is also considered normal (Swischuk 2002).

2.2.1.2 Interspinous Distance

Lack of lordosis in the neutral position of the neck may be a normal finding in children. Increase in distance between the tips of the spinous processes of C1 and C2 with flexion of the neck in children is a normal finding. If a ligamentous injury is present, the interspinous distance is more than 1.5 times greater than the upper and lower normal interspinous distances (Lustrin et al. 2003).

2.2.1.3 Prevertebral Soft Tissue Thickness

A prevertebral soft tissue thickness up to 6 mm at the level of C3 is normal in children. Widening of the prevertebral soft tissues can be a normal finding due to expiration. A lateral radiograph in inspiration and in mild extension should be obtained to evaluate the soft tissue thickness accurately (Lustrin et al. 2003).

2.2.2 Normal Variations of the Cervical Vertebrae in Children

Normal anatomic variations must also be known in order to prevent diagnostic pitfalls. Common normal findings of cervical vertebrae are given in Table 2.1.

2.2.2.1 Clefts of C1

Clefts in the anterior and posterior ring of C1 are normal findings and can be seen on CT (Fig. 2.7). They have smoothly corticated edges (Swischuk 1997, 2002).

2.2.2.2 Cervical Pseudosubluxation

A normal physiologic displacement can be seen between C2–3 and C3–4 on lateral radiographs of children. Pseudosubluxation of the cervical spine can also be seen at C4–5 (Swischuk 1997, 2002).

2.2.2.3 C3 and C4 Wedging

Anterior wedging of the vertebral bodies, especially at C3 and at times at C4, is also a normal find-

Table 2.1. Common normal findings of cervical vertebrae

• Ossiculum terminale
• Bifid odontoid
• Cleft in posterior neural arches
• Ponticulus posticus (a small bridge of bone resulting from complete ossification of the atlanto-occipital membrane reaching the posterior notch of C1)
• Pseudosubluxation
• Wedging of vertebral bodies
• Pseudo widening of interpeduncular distance
• Spina bifida occulta

Fig. 2.7. Axial CT image demonstrates clefts in the anterior and posterior arches of C1

ing, commonly seen in infants and young children. When the child grows up, this wedging resolves (Swischuk 1997).

2.2.3 Normal Radiological Appearances of the Thoracic and Lumbar Vertebrae in Children

In the thoracic and lumbar region, there are four chondrification centers, two for the vertebral body, and two for the posterior elements, separated by a dorsoventral sheath of notochord in the midline. The chondrification centers of the vertebral body and neural arches fuse in the midline anteriorly and posteriorly in that order. On lateral radiographs of neonates the vertebral bodies are rectangular in shape in the thoracic region and ovoid shape in the lumbar region. Synchondroses between the vertebral body and the posterior neural arches are easily seen in newborns (Fig. 2.8). Synchondroses between the vertebral bodies and the posterior arches begin to disappear first in the cervical region, reaching the lumbar region at 6 years of life. In contrast, the posterior arches of the lumbar vertebrae begin to fuse in the first year of life and this progresses cranially. The cervical laminae fuse lastly in the third year of life. Anterior and posterior vascular channels are also prominent in infants (Fig. 2.9). Lateral anterior vascular channels usually disappear. The

a

b

Fig. 2.8a,b. Conventional radiograph (**a**) and CT image (**b**) demonstrate synchondroses between the vertebral body and the posterior neural arches (*arrows*)

posterior vascular channels may still be visible in adulthood. Vertebral ring apophyses appear at approximately 6 years of age in the middle and lower thoracic and upper lumbar areas (Fig. 2.10). They fuse with vertebral bodies by the age of 18 (Kirks and Griscom 1998). The normal radiographic appearance of the vertebral column at different ages are shown in Figures 2.11 and 2.12.

There are three primary ossification centers of the sacrum: one for the body and two for the posterior neural arches. The sacrum is formed by five partially or completely fused segments. Fused transverse processes of the sacrum articulate laterally with the iliac bones and form the sacroiliac joints. There are four ventral and four dorsal sacral neural foramina. These foramina transmit the ventral and dorsal divisions of the upper sacral spinal nerves (S1–S4). The number of segments of the coccyx varies from three to five. These are fused or partially fused rudimentary vertebral segments (Jinkins 2000).

2.2.4 Normal Variations of the Thoracic and Lumbar Vertebrae in Children

Common normal variations of thoracic and lumbosacral vertebrae are given in Table 2.2.

Table 2.2. Common normal findings of thoracic and lumbosacral vertebrae

• Neurocentral synchondroses
• Cleft in posterior neural arches
• Wedging of vertebral bodies
• Spina bifida occulta
• Vascular grooves
• Ring apophyses
• Pediculate thinning
• "Bone-within-bone"

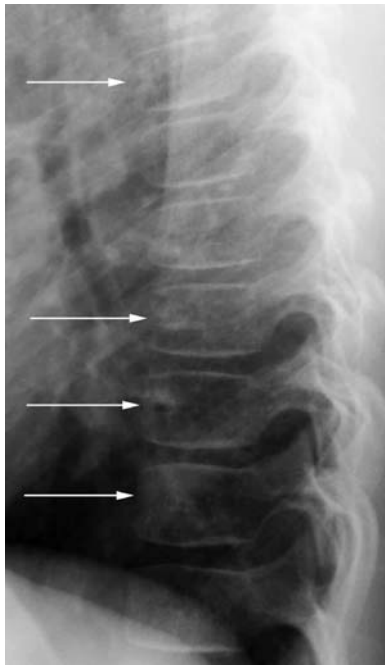

Fig. 2.9. Grooves of the anterior vascular canals of the vertebral bodies are seen (*arrows*)

Fig. 2.10. Lateral radiograph shows that the vertebral ring apophyses are visible in the anterior superior and anterior inferior corners of the vertebral bodies

Fig. 2.11. AP radiograph of a newborn demonstrates "bone-within-bone" appearance

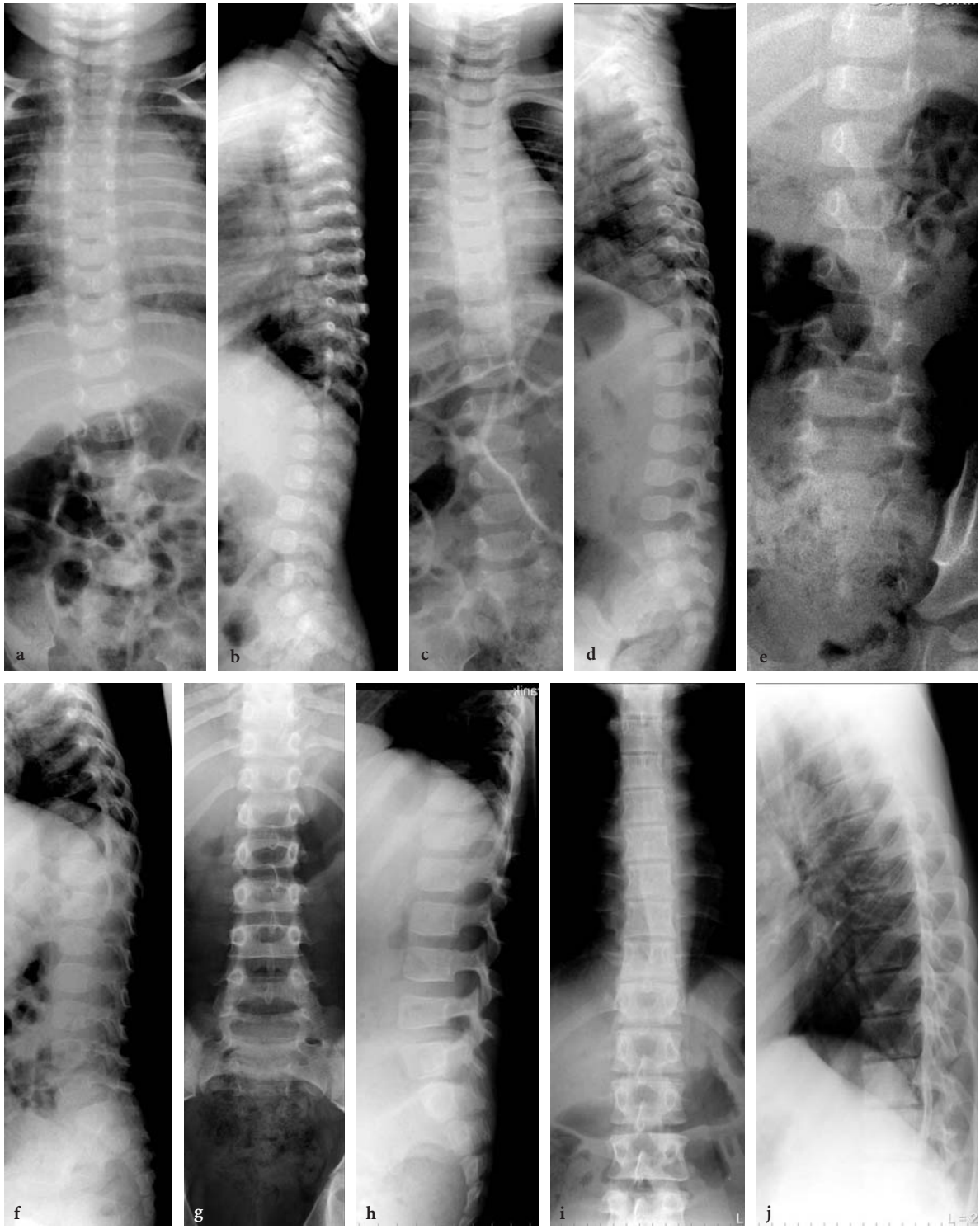

Fig. 2.12a–j. AP and lateral radiographs in children of different ages ranging between 8 months and 15 years [8 months (**a,b**), 1 year old (**c,d**), 2 years old (**e,f**), 6 years old (**g,h**), 15 years old (**i,j**)] demonstrate the changes in the shape of the vertebral bodies and posterior elements by age

2.2.4.1 Bone-Within-Bone

A "bone-within-bone" appearance of the thoracic and lumbar vertebral bodies is frequently seen on radiographs of normal neonates (Kirks and Griscom 1998) (Fig. 2.11).

2.2.4.2 Spina Bifida Occulta

The posterior neural arches are separated by a cartilaginous cleft and are seen as a narrow vertical lucent line on AP radiographs in infants. This cleft disappears through ossification by 3–5 years of age. A persisting cleft is most frequently seen at S1. Other persisting clefts may be present at L5, C1, C7 and T1 in decreasing order. When isolated, these clefts are benign conditions and called spina bifida occulta (Kirks and Griscom 1998).

At the cervicothoracic, thoracolumbar and lumbosacral levels some variations may be visible such as extra (cervical) ribs, hypoplastic or absent (12^{th}) ribs and lumbalization of the first sacral vertebra due to cranial shift of vertebral processes or as first lumbar ribs and sacralization of the fifth lumbar vertebra due to caudal shift of vertebral processes. These shifts occur in approximately 30% of people in different segments and different arrangements (Kuhn et al. 1993).

2.2.5 Other Structures of the Spine

2.2.5.1 Neural Foramina

The intervertebral neural foramina are the lateral pathways for the nerves. The boundaries of the neural foramina are: anteriorly, the posterior surface of the suprajacent and subjacent vertebrae and between them intervertebral disc, superiorly, the inferior aspect of the suprajacent vertebral pedicle, posteriorly, the anterior surface of the superior articular process, inferiorly, superior surface of the subjacent vertebral pedicle (Fig. 2.13a). The spinal neural foramina contain the spinal nerve/sheath complexes, meningeal nerves, blood vessels and fat (Figs. 2.4, 2.13).

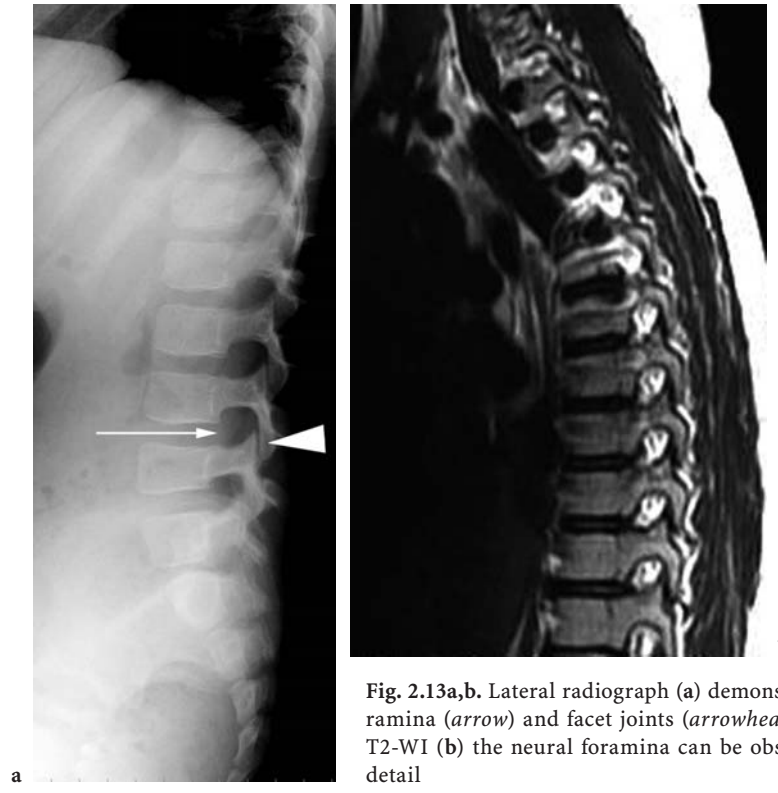

Fig. 2.13a,b. Lateral radiograph (**a**) demonstrates neural foramina (*arrow*) and facet joints (*arrowhead*). On a sagittal T2-WI (**b**) the neural foramina can be observed in greater detail

2.2.5.2 Facet Joints

The paired superior and inferior articular processes of the vertebrae form a pair of articulations between vertebral segments called facet (zygapophyseal) joints (Fig. 2.13). Facet joints vary in shape, size and spatial orientation according to the vertebral level.

2.2.5.3 Spinal Ligaments

The posterior longitudinal ligament (PLL) extends from the posterior surfaces of the bodies of C1–C2 to the posterior surface of the clivus and is called the tectorial membrane. The anterior longitudinal ligament (ALL) extends from the anterior surface of the body of C2 and anterior arch of C1 to the anterior surface of the clivus (Fig. 2.14). The anterior atlantooccipital membrane, the apical odontoid ligament, and the cruciate ligament can be found between the ALL and PLL (Jinkins 2000). The ALL and PLL cover the entire anterior and the posterior surfaces of the spinal column.

The alar ligaments are present between the odontoid tip and the occipital condyles bilaterally. The transverse atlantal ligament passes between the synovial joint (posterior to the odontoid process) and the tectorial membrane and extends horizontally between the lateral masses of C1 (Jinkins 2000). Ligamenta flava (yellow ligaments) are paired ligaments and originate and insert into the lamina of two adjacent vertebral bodies and are seen well on axial images of CT or MR. The interspinous ligaments connect the spinous processes. They are more prominent in the lumbar region and thinner in the thoracic region. The supraspinous ligament interconnects the tips of the spinous processes of C1–L5. It extends from C1 to the external protuberance of the occipital bone as the ligamentum nuchae.

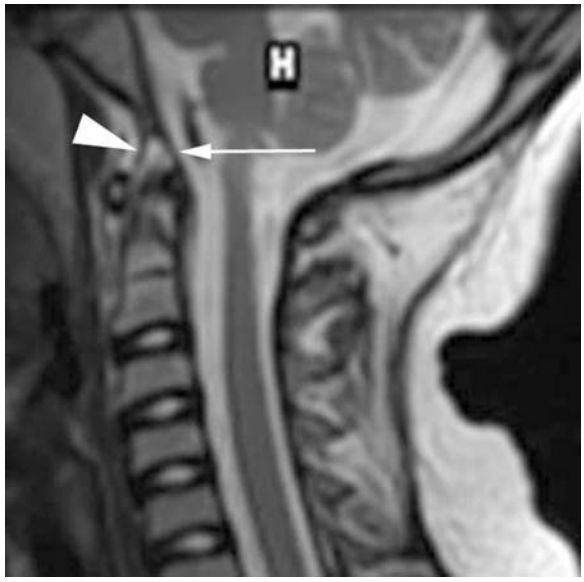

Fig. 2.14. Sagittal T2-WI demonstrates the tectorial membrane (extension of the posterior longitudinal ligament) (*arrow*) and anterior longitudinal ligament (*arrowhead*)

2.2.5.4 Discs

Intervertebral discs are present between C2–C3 up to the sacrum. Intervertebral discs have a central nucleus pulposus and an outer annulus fibrosus. The nucleus pulposus is large at birth and has mucoid material. Over time the mucoid material is replaced with fibrocartilage. The intervertebral discs are thickest in the lumbar spine and the thinnest in the upper thoracic spine (Jinkins 2000). The intervertebral disc spaces are seen on AP and lateral radiographs. Discs are demonstrated best on T2-WI, especially on sagittal images.

2.2.5.5 Arterial Supply and Venous Drainage of Spinal and Spinal Cord

Segmental spinal arteries supplying the vertebrae (e.g., intercostals, lumbar, sacral paraspinal arteries) originate from the aorta. A series of radiculomedullary arteries supply the spinal cord. Radiculomedullary arteries may originate from segmental spinal arteries, vertebral arteries, ascending cervical artery, deep cervical artery, intercostals arteries, lumbar and sacral paraspinal arteries, and iliac arteries. The anterior cervical and thoracic radiculomedullary arteries form the anterior spinal artery of the cord. The posterior cervical and thoracic radiculomedullary arteries form the posterior spinal artery of the cord.

The basivertebral vein drains the vertebral body and is located at its center (Fig. 2.4). There is a venous plexus around the vertebral body and posterior elements. Spinal segmental veins drain to the vena cava. An epidural venous plexus draining the spinal cord is located between the dura of the thecal sac and the periosteum of the vertebrae surrounding the spinal cord. Longitudinal anteromedian and posteromedian veins and a pair of anterior and

posterior radiculomedullary veins connects to the epidural venous plexus. Also, longitudinal anterolateral and posterolateral veins connect to the epidural venous plexus (Jinkins 2000).

2.2.5.6 Spinal Meninges

The meninges of the spine are continuous with cranial meninges and consist of pachymeninges (dura mater) and leptomeninges (arachnoid mater and pia mater). Vessels and nerves exiting and entering the thecal sac have a thin covering layer of leptomeningeal cells throughout their course in the subarachnoid space (Jinkins 2000).

2.2.5.7 Spinal Cord

The spinal cord ends at the level of L2 in newborns, and at the level of L1 in adults. The spinal cord is wider in the cervical region and gradually gets narrower through the thoracic region; later, a little widening is seen at the lumbar region. These changes in caliber of the cord are in harmony with the changes of the diameter of the spinal canal.

The spinal cord is clearly visualized with ultrasonography in neonates through the acoustic window of the incompletely ossified posterior spinal arches. The visibility of the cord decreases with age. The normal spinal cord is seen as a hypoechoic tubular structure that has hyperechoic outer contours that are formed by dura mater and a hyperechoic central part (central spinal canal or commissural tracts) on a longitudinal image on a sagittal view (Fig. 2.15). The anechoic space around the cord is the subarachnoid space. At its end the cord forms the conus medullaris that is continuous with the filum terminale which is seen as an echogenic linear structure surrounded by nerve roots. Vascular pulsations and movements of the cord by respiration and crying of the baby are seen in real time on US (Siegel 1996).

The brain stem–cervical spinal cord junction and cervical spinal cord are readily demonstrated on sagittal MRI. Sagittal MRI also shows the slightly bulbous but tapering conus medullaris at the L2 region and also distal to the cord the filum terminale and nerve roots called cauda equina. The thecal sac ends at S1 or S2, but sometimes lower down to S5. Sometimes the most distal portion of the central canal is dilated and oval shaped. This is called a "ventriculus terminalis" and is a normal variation (Swischuk 1997; Lustrin et al. 2003). The cervical spinal canal and cord is wider than the thoracic spinal canal and cord. Especially in the thoracic region, turbulent CSF flow dorsal to the cord forms heterogeneous signal areas, but laminar flow of the CSF ventral to the cord creates homogenous signal void areas in the subarachnoid space.

2.3 Degenerative Disc Disease in Childhood: Scheuermann's Disease, Schmorl's Nodes, and Limbus Vertebrae

Degenerative disc disease in older children and adolescents is more common than generally thought (Swischuk et al. 1998). There is a tendency to consider that Scheuermann's disease, Schmorl's nodes and limbus vertebrae are different manifestations of degenerative disc disease (Begg 1954; Heithoff et al. 1994). Disc degeneration is not completely understood and not all degenerative discs are symptomatic (Wood et al. 1995). Dehydration of discs occurs with increasing age so degenerative disc disease is a well known disease of adulthood, but why some children are affected is not known yet. It is probable that repeated, subclinical traumas and individual susceptibility play a role in the development of the disease process. With time, tears occur in the annulus fibrosus and fissures form in the vertebral

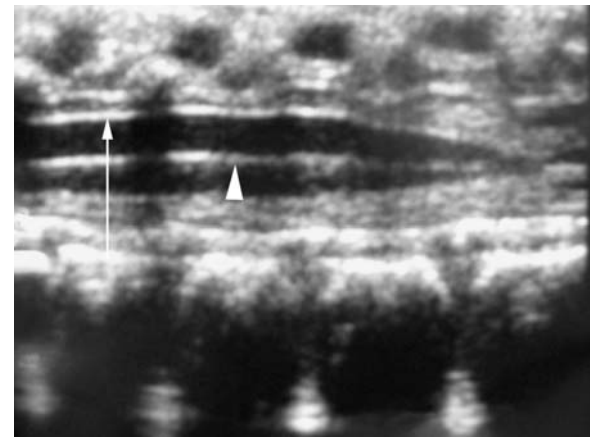

Fig. 2.15. Longitudinal sonographic image of the distal cord. The spinal cord is seen as a hypoechoic tubular structure. The dura forms the outer hyperechoic contours (*arrow*). Hyperechoic central line represents central spinal canal (*arrowhead*)

endplates. Under continuous high pressure, nuclear material can extrude through the vertebral endplates and later into the vertebral bodies, a process which results in the formation of Schmorl's nodes and limbus vertebrae. When small, numerous extrusions occur through the endplates Scheuermann's disease ensues (Begg 1954). These conditions can overlap and can be seen together in any patient. Schmorl's nodes can occur in different locations as central, anterior, posterior or lateral. On plain films, a notch at the vertebral endplate through the body is seen. The notch itself and high signal disc material within are visible on sagittal T2-WI (Fig. 2.16). Loss of disc space height, disc dehydration and herniation of disc material into the vertebral end plates are common findings in these disorders. So it seems reasonable to group these diseases together as degenerative disc disease (Swischuk et al. 1998).

The nuclear material can undermine the ring epiphysis anteriorly, posteriorly or laterally and separate it from the vertebral body so limbus vertebra occurs (Swischuk et al. 1998). On plain films, a triangular shaped bony fragment separated from the vertebral body is seen at the anterior or lateral corner of the body. High signal disc material separating the bony fragment from the body can be demonstrated easily with T2-WI.

Scheuermann's disease frequently occurs in the thoracic spine region but lumbar and even sacral regions can also be affected (Swischuk et al. 1998). Multiple disc spaces are narrowed and endplates have irregular shapes due to extrusions of the disc materials in Scheuermann's disease and these findings can be demonstrated with plain films and particularly on MRI clearly (Fig. 2.16). In most of the cases multiple levels are affected and the changes are extensive.

2.4 Spinal Infections

Spinal infection is a significant cause of morbidity and mortality. Inflammation of the spine can occur in pyogenic, granulomatous, autoimmune, idiopathic and iatrogenic conditions. Spinal infections can be thought of as a spectrum of diseases comprising spondylitis, discitis, spondylodiscitis, pyogenic facet arthropathy, epidural infection, meningitis, polyradiculopathy and myelitis. Despite the availability of advanced imaging techniques, the diagnosis of spinal infection remains challenging. The

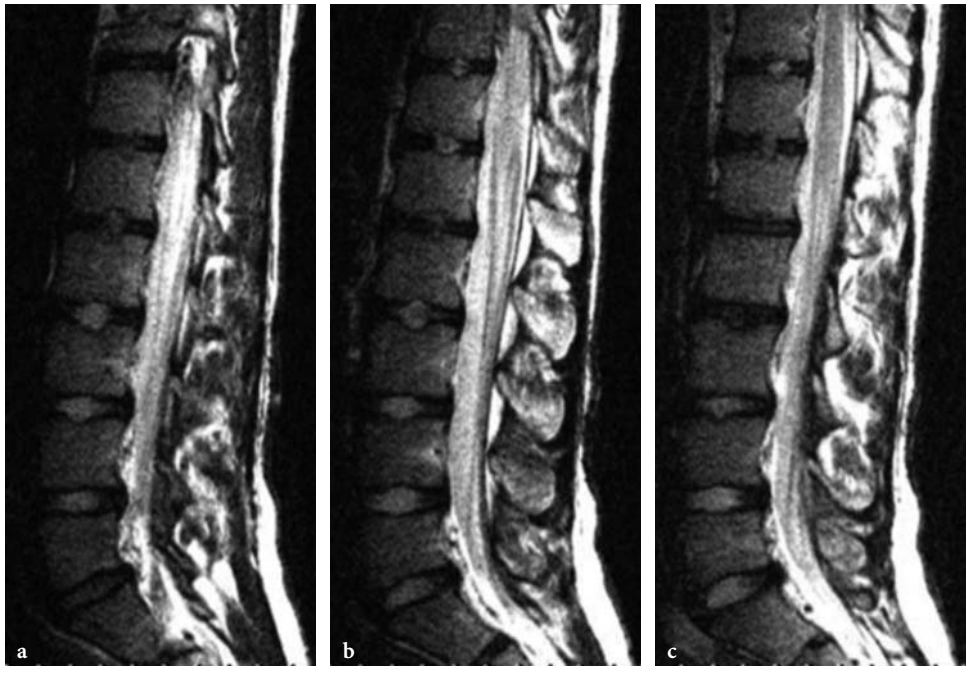

Fig. 2.16a–c. Sagittal T2-WI (**a–c**) demonstrate narrowed disc spaces and irregular endplates with Schmorl nodes in a 15-year-old girl with Scheuermann's disease. Decreased signal intensities of the discs are also evident

differential diagnosis with degenerative disease, non-infectious inflammatory lesions and spinal neoplasms is difficult, and the clinical features can be subtle and misleading. Delays in diagnosis can lead to increased morbidity and mortality (Bouchez et al. 1985; Danner and Hartmann 1987; Feldenzer et al. 1987). Appropriate and prompt diagnosis can be achieved through a combination of imaging and microbiological examination. Spinal infections can be categorized into three groups according to the involved compartment:

1. Extradural infections (osseous spine, epidural space, facet joints, and paraspinal soft tissues)
2. Intradural extramedullary infections
3. Intramedullary infections

The symptoms, radiological findings and treatment approaches may change depending on the involved compartment.

2.4.1 Extradural Infections

2.4.1.1 Osseous Spine (Spondylitis)

2.4.1.1.1 Pyogenic Spondylitis

The axial skeleton is a frequent site of infections and accounts for approximately 2%–7% of all cases of osteomyelitis (Tyrell et al. 1999; Dagirmanjian et al. 1999; Stabler and Reiser 2001). The lumbar spine is the most common site for pyogenic spondylitis, followed by the cervical spine. Involvement of pedicles, laminae and spinous process is much less common (3%–12%) and when it does occur, one should think of tuberculosis (TB) (Babinchak et al. 1997; Smith and Blaser 1991). Most cases of discitis and/or spondylitis are treated empirically according to the imaging findings. Therefore, it is difficult to compile correct statistical data regarding the etiologic microbial agents. However, *Staphylococcus aureus* accounts for approximately 60% of infections, followed by Diplococcus, Streptococcus and Enterobacter. The incidence of discitis and spondylitis caused by Salmonella is increased in patients with sickle cell disease.

In children, persisting vascular channels may allow direct inoculation of the intervertebral disc. Following bacteremia, the infection begins within the disc and extends to the adjacent endplate. In adults, micro-organisms arrive in the vertebrae via end-arteriolar arcades of metaphyseal equivalent areas which are subchondral plates adjacent to the disc, particularly in the anterior part of the vertebral body (Ross 1996). Through the disrupted cortical bone, the infection extends to subligamentous paravertebral, epidural spaces, to adjacent disc and to the contiguous vertebrae. An untreated infection may lead to significant deformity of the spine and to severe neurological deficits, particularly paraplegia and tetraplegia. Mortality ranges between 18%–31 % (Smith and Blaser 1991).

Plain radiographs are usually the initial imaging study, but their sensitivity and specificity is very low. Plain X-ray films usually fail to show early signs of infection and a negative result does not exclude the presence of the infection. The earliest radiographic signs depend on the initial location of the infection. Loss of definition and irregularity of the vertebral endplate, usually commencing anterosuperiorly, may be observed after 2–8 weeks if the infection is initially located in the vertebrae. An increase in disc space height may be demonstrated if the disc is the initial location. This is later followed by a decrease of disc height in both types of infection. Gradual development of osteolysis results in poorly defined endplates. Cortical erosions of the vertebral endplates on both sides of the narrowed disc and an associated paraspinal mass are the radiographic hallmarks of pyogenic infection. In a later stage, reactive changes with sclerosis, new bone formation with osteophytosis, kyphotic deformity and bony ankylosis may also be seen. Digital radiographs must be viewed with window settings for both bone and soft tissue for better evaluation.

The sensitivity of CT is higher, but it lacks specificity. Therefore, CT plays a minor role in the diagnosis of early spondylitis and disc space infection. CT provides fine bone detail, shows the amount of calcified bone tissue and also demonstrates the degree of spinal canal involvement in terms of lytic fragmentation and cortical erosion, disc hypodensity and gas within the disc, paraspinal soft tissue infiltration with obliteration of fat planes, and sclerosis. Epidural involvement may be missed due to beam hardening artifacts especially in the cervicothoracic region. Sagittal reformatted and 3D images demonstrate reduced disc height. Spiral CT with thin-slice collimation and multiplanar reconstructions is needed. New multi-detector row scanners provide a significant diagnostic advantage (Stabler and Reiser 2001). Percutaneous vertebral biopsy is usually performed under CT guidance.

MRI is the method of choice for diagnosing spondylitis. The increase in extracellular water content in the production of exudates containing WBC and fibrin within vertebral marrow (a manifestation of inflammatory reaction and associated ischemic changes) and reactive bone marrow stimulation are responsible for the abnormal signal which is a non-specific sign for the infection (Figs. 2.17–2.19). Decreased signal intensity on T1-WI probably results from a replacement of fat cells by non-neoplastic stimulated proliferating bone marrow cells producing WBC (Figs. 2.17–2.19) (Stabler and Reiser 2001). Spin echo sequences should be preferred over gradient echo sequences for T1-WI. In younger patients, on T1-WI, bone marrow edema may be masked by red marrow. High signal intensity of the affected areas of the vertebral body and disc is typically observed on T2-WI (Figs. 2.17–19). FSE images are not optimal for the evaluation of infectious diseases due to the bright signal of marrow and can mask the bone edema if fat saturation is not used. STIR technique has slightly higher sensitivity for detecting areas of involvement than T2-WI, but, STIR sequences do not depict fine anatomic detail. These sequences can help in showing vertebral and disc disease; epidural extension may not be adequately assessed, since the abnormal signal obtained may be isointense with the high signal of CSF. PDWI may be helpful, presumably because of the higher protein content of the inflammatory exudates. Bone marrow edema can also be evaluated by using opposed-phase gradient recall echo (Fig. 2.17). Normal marrow exhibits low signal intensity with signal subtraction of the water- and fat-bound proton components, whereas edema exhibits high signal intensity. Spinal diffusion weighted imaging has also been initiated and has proven to be helpful in the differentiation of long-standing infections (Fig. 2.17) (Calli et al. 2001).

The use of intravenously administered contrast material is mandatory. Enhancement is the earliest sign of infection; it is pathognomonic in the acute inflammatory episode and, even in subacute and chronic infection, contrast enhancement may persists to a varying degree for several weeks or months (Figs. 2.17–19). Contrast material also helps to differentiate the disc, the vertebral body and the phlegmon. It enhances inhomogeneously, and appears as a peripherally enhancing mass with a hypointense liquefactive center. This differentiation is important for treatment planning, surgery being indicated for an abscess, whereas there is a more conservative approach for phlegmon (Figs. 2.17, 2.18). When contrast enhancement no longer occurs, active inflammation can be excluded. Fat suppressed T1-WI can be helpful to improve contrast between tissues. Measuring the percentage of enhancement has been shown to be a reliable method to quantify diffuse bone marrow changes (Stabler and Reiser 2001).

MRI findings of spondylitis and discitis from acute to advanced stages include (Figs. 2.17–2.19):

1. The earliest sign of an infectious process is the altered signal intensity of the disc or bone marrow on both T1- and T2-WI. Typically, the disc shows a low signal intensity on T1-WI, and an increased signal on T2-WI. As the disease progresses, the intervertebral disc frequently cannot be distinguished from the infected vertebrae without contrast, and the disc height is invariably reduced.
2. Contrast enhancement of the infected area.
3. Blurring and loss of definition of the vertebral endplate(s).
4. Irregularity and destruction of the endplates with interruption of the normal signal void of cortical endplate.
5. Soft tissue involvement (epidural space and/or paraspinal soft tissues) with inhomogeneous signal change and inhomogeneous contrast enhancement.
6. Cervical instability may occur due to the lysis of transverse ligament during pyogenic osteomyelitis of C1–C2 vertebrae.
7. Cervical spondylitis can progress anteriorly and may cause the formation of an obstructing retropharyngeal abscess anteriorly and mediastinitis inferiorly.
8. Thoracic spondylitis can also cause mediastinitis, empyema and pericarditis, while lumbar spondylitis can cause peritonitis and subdiaphragmatic abscess.
9. Intravertebral vacuum clefts are pathognomonic; the signal in vertebral body is dramatically reduced on T1- and T2-WI because of the presence of gas within the dead bone (Rothman 1996).
10. Reactive bone changes, new bone formation, sclerosis, vertebral body height changes, kyphosis and ankylosis are also late stage changes of the spondylitis. Sclerosis is more common in pyogenic spondylitis than in TB (Rothman 1996).

The outcome of the treatment is influenced by the type of infection and by the degree of neurologic compromise before treatment. There is an increasing tendency towards conservative therapy, percutaneous drainage of abscess or a combina-

Fig. 2.17a–g. Sagittal T2-WI (**a**), precontrast T1-WI (**b**), postcontrast T1-WI (**c**), in-phase gradient echo (**d**), out-of-phase gradient echo (**e**), DWI (**f**) and ADC map (**g**) demonstrate L1–L2 aspergillus spondylodiscitis. There is signal intensity change of neighboring vertebrae with prominent destruction and loss of endplate cortical continuity at the caudal part of the L1 vertebral body. In- and out-of-phase images are helpful to demonstrate the infection. Discitis is also seen with signal change, contrast enhancement and disc space height decrease. DWI shows increased signals with increased ADC values corresponding to edema secondary to the inflammation

tion of both rather than surgical intervention. It is therefore critical to monitor treatment response, particularly in the immunodeficient population (Gillams et al. 1996).

MRI is also helpful in monitoring the treatment. Important milestones to remember are:

1. The earliest sign of improvement is reduction in paravertebral soft tissue swelling.
2. This is followed by he appearance of a high signal intensity rim at the edge of the lesion (mean 15 weeks).
3. Higher marrow signal on T1-WI and FSE-T2-WI than noninvolved marrow. (The reconstituted marrow is predominantly fatty and appears to be of higher signal intensity than normal marrow and degeneration of hematopoietic marrow is probably caused by obliteration of the intramedullary vessels, preventing repopulation with red marrow cells) (Stabler and Reiser 2001).
4. Low signal within the marrow on both T1- and T2-WI (may be a reflection of reactive sclerosis and fibrosis due to healing).

5. High marrow signal on STIR, PD- and T2-WI decreases.
6. The disc space remains narrowed, but high disc signal intensity decreases on STIR and T2-WI.
7. The new bone formation bridging the disc space can also be seen.
8. Resolution of canal compromise.
9. Progressive reduction in contrast enhancement. Increasing or persisting contrast enhancement with clinical improvement and increasing destruction does not necessarily indicate treatment failure (Stabler and Reiser 2001).

Several noninfectious conditions can mimic the appearance of pyogenic spondylitis. The differential diagnosis includes: degenerative endplate changes, dialysis arthropathy, Charcot joint, ankylosing spondylitis, rheumatoid arthritis, pseudoarthrosis, vertebral lymphoma, multiple myeloma, chordoma, metastases, avascular necrosis, hemophilia, chronic recurrent multifocal osteomyelitis and erosive intervertebral osteochondrosis.

2.4.1.1.2 Nonpyogenic Infections

A granulomatous reaction is a nonspecific response of tissues to an antigenic stimulus. Such a reaction has been identified in a wide range of diseases including bacterial, fungal or viral infections, neoplastic, autoimmune and idiopathic disorders. Bacterial granulomatous organisms that have been implicated in spinal infections including Mycobacterium and Brucella species.

2.4.1.1.3 Tuberculous Spondylitis

Tuberculosis of the spine accounts for 1% of all TB infections and 25%–60% of all bone and joint TB infections (Chotivichit et al. 1999; Sharif et al. 1995). Spinal involvement may be the initial manifestation in children. The incidence of TB has increased in recent years, not least due to the rise in AIDS cases. TB spondylitis may present with atypical findings that mimic metastatic disease (Villoria et al. 1995). The lower thoracic and lumbar vertebrae are the most commonly involved sites, whereas the sacrum and cervical region are less frequently implicated. Involvement of more than one vertebral segment is usual.

Neither the clinical examination nor the radiological findings may be reliable in differentiating atypical forms of spinal TB from other infections, or from neoplasm. The age of the lesion and its degree of caseation necrosis are possible explanations for the different appearances of TB. In many cases, the imaging findings are more suggestive of neoplasm than of the pyogenic spondylitis, since the disc spaces are spared (Fig. 2.18). Multiple vertebral body involvement is the rule and skip lesions occur in up to 4% of the cases; intervertebral joints are also common sites for TB (Fig. 2.18) (Gillams et al. 1996). The infection usually originates at the anterior subchondral bone, adjacent to the vertebral endplates (Fig. 2.18). The infection process spreads underneath the longitudinal ligaments, most frequently along the anterior longitudinal ligament (Fig. 2.18). Adjacent vertebrae and multiple vertebral bodies and discs may be involved and skip lesions can be encountered (Fig. 2.18). The intervertebral disc remains intact for a longer time and is destroyed more slowly in TB spondylitis than in pyogenic spondylitis; this may be due to the relative lack of proteolytic enzymes (Fig. 2.18) (Gillams et al. 1996). When both neighboring vertebral bodies are involved, the disc may lose its nutrition and be involved secondarily. During the destructive process, bony fragments may migrate into the surrounding structures, including spinal canal and perivertebral soft tissues (Fig. 2.18). Paraspinal involvement is frequent with formation of a large abscess that may extend to the hip, pelvis and into the lower limb. It may contain calcifications, and reaches a maximum size within 2 months with/without marked epidural extension, epidural abscess and even cutaneous fistula formation. Anterior vertebral osteolysis/wedging, compression fracture and gibbus deformity, as well as scoliosis are also common in untreated cases (Fig. 2.18). Generally, heterogeneous contrast enhancement is observed with a central non-enhancing portion and a peripheral enhancing rim. The involved ligaments, epidural mass and inflamed meninges may also enhance. Reactive new bone formation may simulate an ivory vertebra if it is abundant during the healing process. Ankylosis may also be seen. Odd locations and involvement of pedicles (very often affected), laminae and spinous processes with sparing of the vertebral body does occur (2%–10%) and all should raise suspicion of TB (Chotivichit et al. 1999; Sharif et al. 1995).

CT examinations show extensive destruction of the vertebral endplates with fragmentation, bone sequestration, large paravertebral abscess and frequently epidural infection. In contradistinction to pyogenic spondylitis, the cortical definition of the

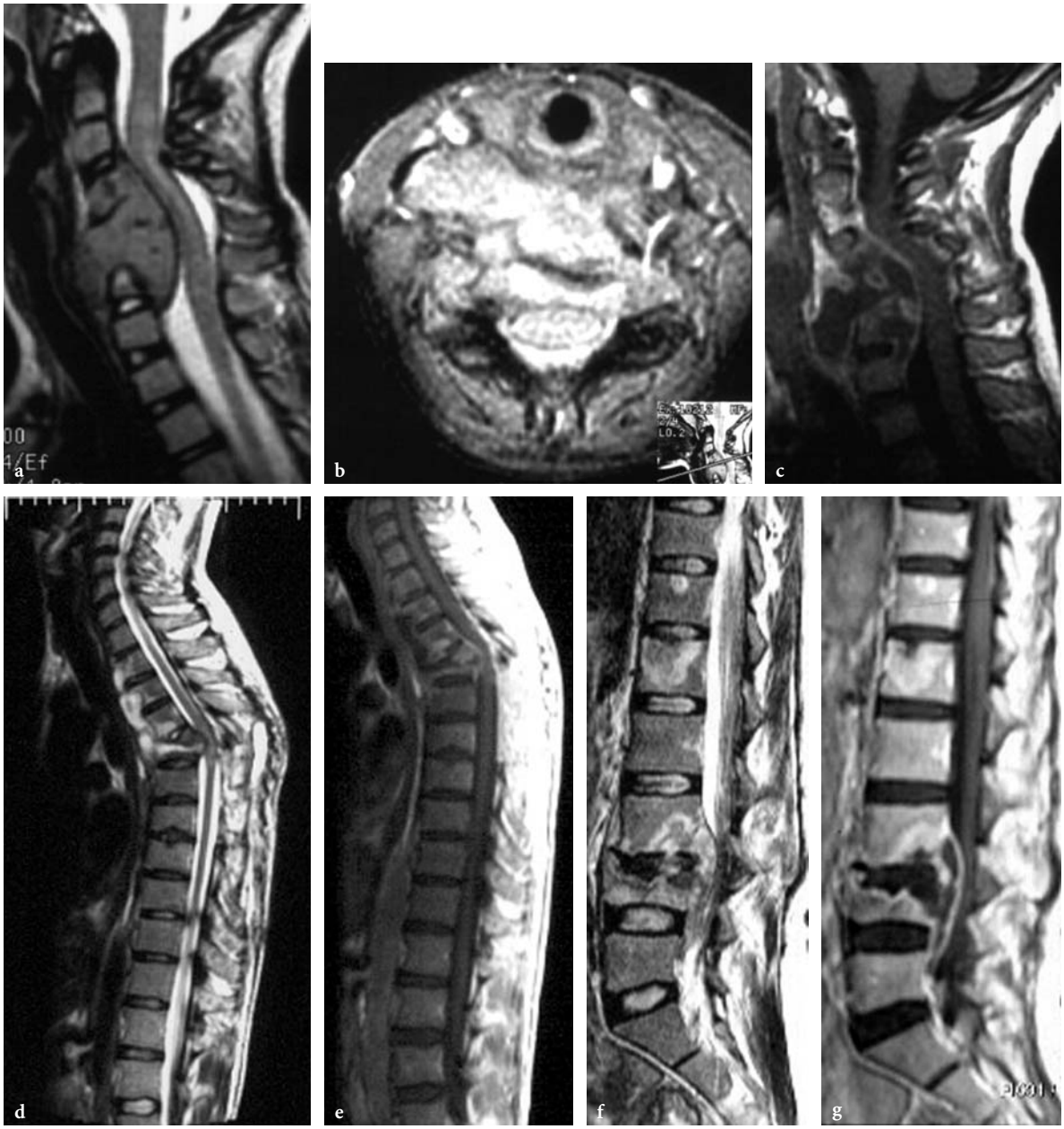

Fig. 2.18a–g. Sagittal (**a**), axial T2-WI (**b**), postcontrast sagittal T1-WI (**c**) demonstrate C4–C5 TB spondylitis mimicking a mass lesion. The C4 and C5 vertebral bodies and intervening discs were involved and destroyed while C3–4 and C5–6 discs are spared. Retropharyngeal and anterior epidural extension with marked impingement and posterior displacement of the spinal cord is seen. Also evident is a large paraspinal soft tissue abscess extending to the right and anteriorly. The postcontrast image shows peripheral contrast enhancement with central necrosis. Sagittal T2-WI (**d**) and postcontrast T1-WI (**e**) of another patient show TB involvement of multiple thoracic vertebrae with extension underneath the anterior longitudinal ligament, and sparing of the intervertebral discs. Due to the vertebral body collapse, a gibbus deformity is seen. Sagittal T2-WI (**f**) and postcontrast T1-WI (**g**) of a different case show involvement of multiple lumbar segments with skip lesions. There is marked destruction of the L4 vertebra. There is formation of an epidural abscess with peripheral contrast enhancement is also seen

affected vertebrae is invariably lost (Sharif et al. 1995). Migrating bony fragments into surrounding structures including the spinal canal can be demonstrated clearly with CT. Calcification of paraspinal mass with thick irregular rim contrast enhancement associated with vertebral osteomyelitis is pathognomonic for TB.

Differential diagnosis of TB spondylitis includes pyogenic spondylitis, metastasis, lymphoma, eosinophilic granuloma and fungal spondylitis. If there is sclerosis of a pedicle, one should also take into account osteoid osteoma, osteoblastoma and Brodie's abscess (Gillams et al. 1996).

2.4.1.1.4 Parasitic Infestations

Echinococcosis, onchocerciasis, toxoplasmosis and toxocariasis can also be seen in spine. Hydatid disease is found in bone in 0.5%–2% of all cases. Involvement of the vertebral column occurs in about one-half of the osseous cases (Akhan et al. 1991). Although all parts of a vertebra may be affected, there appears to be a predilection for the central part and pedicles of thoracic vertebrae as a result of portovertebral shunts (Iplikcioglu et al. 1991; Robinson 1959; Morhed 1977). Discs and disc space are usually not involved and the dura always remains intact (Sharif 1992). Vertebral lesions differ from cerebral lesions with their microvesicular configuration and invasiveness (Ozek 1994). Hydatid cysts involving the bone have thinner walls due to the reduced fibrotic and inflammatory response of the host. The hydatid cysts do not show their specific spherical shape but permeate and slowly destroy cancellous bone, where there is less resistance, until the cortex is reached and penetrated by the growing parasite (Fig. 2.18).

2.4.1.2 Facet Joint Infections

If there is no evidence of spondylitis, discitis or an epidural abscess, the facet joints should be evaluated carefully. CT abnormalities include loss of subchondral bone associated with the facet joint, loss of density of ligament flavum and obliteration of fat planes (Babinchak et al. 1997). MRI shows swelling of the capsule and periarticular soft tissue of the facet joint. Pus or joint effusion may be seen. Peripheral contrast enhancement is seen on postcontrast images. The differential diagnosis includes neoplastic diseases, erosive arthritis, histiocytosis and scleroderma.

2.4.1.3 Spinal Epidural Infections

Once thought to be a rare clinical entity, recent epidemiologic studies point to an increasing prevalence of spinal epidural infection (SEI) in which early diagnosis and appropriate treatment dramatically alters the clinical outcome (Smith and Blaser 1991; Van Tassel 1994). SEI may be classified as acute and chronic depending on the duration of the clinical symptoms.

SEI can be caused by many kinds of bacteria. *S. aureus* is the leading cause (62%–67%), followed by *M. tuberculosis* (Mendonca 2002). The most frequently involved sites are the lower thoracic and lumbar regions (Tang et al. 2002). Epidural abscesses are almost always located in the posterior portion of the spinal canal; there is a very low incidence of anterior location, unless there is an association with osteomyelitis. Epidural abscesses alone tend to be more extensive than those secondary to spondylitis (Post et al. 1988; Hitchon et al. 1992). Other pathologies such as meningitis, subdural abscesses, facet infection and retroperitoneal abscesses can be seen in association with SEI.

Plain radiographs are generally the initial modality used, but provide little information. CT is valuable to demonstrate paraspinal extension and associated bone destruction. Administration of an intrathecal contrast agent is useful to fully delineate the epidural collection and its relationship with spinal cord (Smith and Blaser 1991). However, MRI is the modality of choice with the highest sensitivity. MRI demonstrates a soft tissue mass within the epidural space encroaching upon the dural sac or spinal nerves (Fig. 2.18). Sagittal views are preferred for assessment of cranial or caudal extension. Axial views are useful to define the exact location of the epidural collection. The MRI signal depends on the contents of the lesion. Frequently, an elongated iso- or hyperintense epidural mass lesion is observed, with hypointense thickened, displaced dura on T1- and T2-WI. Cord compression is almost always the presenting clinical symptom of SEI and can be easily detected with MRI. Postcontrast images are helpful to differentiate the epidural phlegmon from abscess. Urgent surgical intervention is indicated for abscess while a more conservative approach is the favored treatment modality in the case of phlegmon. Without treatment, patients generally show a progressive downhill course (Van Tassel 1994; Tang et al. 2002). Epidural abscesses can occasionally be seen

as tiny loculations in the posterior epidural space which can be easily confused with CSF flow phenomenon particularly when located in the thoracic spine. The use of intravenous contrast medium or the application of gradient-echo sequences is relevant in such circumstances (Tyrrell et al. 1999). Associated spinal cord signal change presumed to represent edema may also be seen.

Spinal epidural TB infections are generally isointense when compared to the cord on T1-WI and show mixed signal intensity on T2-WI (Bernaerts et al. 2003). Uniform enhancement will be seen if the inflammatory process is phlegmonous and peripheral enhancement if abscess or caseation has occurred (Sharif et al. 1995). Hydatid disease of the epidural space is rare. The imaging appearance of a hydatid cyst usually comprises spherical lesion(s) with clearly defined borders containing fluid with intensity similar to that of CSF on both CT and MRI (Fig. 2.19) (Gupta and Chang 2001). Lack of periph-

Fig. 2.19a–f. Sagittal (**a**) and axial (**b**) T1-WI demonstrate extradural hydatid cysts located in the vertebral body, anterior epidural space and paravertebral soft tissues. The hydatid cyst with an ill-defined border is located at the left posterior part of the vertebrae. The spinal cord is displaced posteriorly by the epidural hydatid cyst. The sagittal images clearly show displacement of the dura by the hydatid cyst in the anterior epidural space. There is another hydatid cyst located on the left side in close proximity to the posterior wall of the aorta. Sagittal T2-WI (**c**) and postcontrast T1-WI (**d**) of another case demonstrate multiple intradural hydatid cysts in the lumbar region associated with vertebral body hydatid cyst. Axial T2-WI (**e**) and T1-WI (**f**) of a different patient demonstrate unique intramedullary hydatid cyst together with multiple intradural, extradural and paraspinal hydatid cysts located in the cervical region. (Images courtesy of Abdulhakim Coskun)

eral enhancement and mural components are the differentiating features from abscesses.

The differential diagnosis includes metastatic disease and epidural hematomas in different stages (Gupta and Chang 2001; Sharif 1992; Gero et al. 1991).

2.4.2 Intradural Extramedullary Infections

Spinal meningitis has a lower incidence when compared to its intracranial counterpart. The etiology varies with patient age, especially in pediatric cases. In neonates, Streptococci account for almost 50% of the infections followed by *E. coli* and Listeria, while in young infants *H. influenza* accounts for almost 60% of cases followed by Neisseria and Pneumococci. In older children Neisseria, Pneumococci and Staphylococci are the main causative agents (Van Tassel 1994). Subdural abscess is very rare compared to epidural abscess with less than 50 cases reported in the literature (Ozates et al. 2000).

Imaging studies are helpful for the precise diagnosis, identification of complications and treatment monitoring. Plain radiographs and CT have a limited role in the diagnosis. On MRI, precontrast T1-WI may be either normal or may reveal nonspecific abnormalities, unless there is an associated bone infection. T2-WI are of limited use since the bright signal intensity of the CSF obscures the meningeal structures. Postcontrast T1-WI may show inflamed dura or nerve sheath with possible involvement of the spinal cord. Three patterns of enhancement are defined: linear, nodular and diffuse. The linear enhancement is the most common pattern. However, no significant correlation has been found between the pattern of enhancement and the severity of symptoms or the causative agent of infection. In spinal meningitis, the severity of contrast enhancement does not correlate with the course of the disease in contrast to cranial meningitis (Rothman 1996). Unfortunately, MR imaging has a low specificity in differentiating infectious meningitis from a leptomeningeal neoplastic process.

As a granulomatous disease, TB leptomeningitis is unique among other types of meningitis because of its frequent association with the spinal cord and nerve roots. Intradural tuberculosis commonly presents itself simultaneously or shortly after an intracranial infection. Less often, it is associated with vertebral infection and rarely with a primary spinal meningitis (Chang et al. 1989). Tuberculoma formation may also occur in the inner aspect of the dura. The lesion tends to dig a crater into the cord so that it may be quite difficult to distinguish it from a dural disease or from an intramedullary tuberculoma (Fig. 2.21) (Sharif 1992).

Spinal TB leptomeningitis can occasionally cause subarachnoid block. MR imaging clearly outlines the extent of leptomeningeal involvement and also allows direct evaluation of intramedullary lesions and associated pathological processes of the spine (Figs. 2.20, 2.21) (Bernaerts et al. 2003). The imaging features of spinal TB leptomeningitis are diverse and include: cerebrospinal fluid loculations, obliteration of the spinal subarachnoid space with loss of outline of the spinal cord in the cervicothoracic spine and thickened, clumped nerve roots in the lumbar region (Figs 2.20, 2.21). Precontrast images are not valuable and cannot show the spinal cord and subarachnoid space as distinct entities. Postcontrast MRI is essential and very useful for the demonstration of meningeal involvement and associated cord disease (Figs. 2.20, 2.21) (Van Tassel 1994; Chang et al. 1989).

Fungal meningitis is extremely rare. Patients with AIDS living in endemic areas are particularly susceptible to coccidioidomycosis. Coccidioidal meningitis has recently been reported and is the most serious form of the disease. The basal cisterns and upper cervical subarachnoid space are prefer-

Fig. 2.20a–i. Axial precontrast (**a**), axial (**b**) and sagittal (**c**) postcontrast T1-WI demonstrate intradural extramedullary TB leptomeningitis which causes a subarachnoid block. Cerebrospinal fluid loculations and obliteration of the spinal subarachnoid space with loss of outline of the spinal cord at the thoracic spine are clearly seen. The infected areas show marked diffuse and linear enhancement. Sagittal pre- (**d**) and postcontrast (**e**) T1-WI demonstrate obliteration of the spinal subarachnoid space with loss of outline of the spinal cord in the cervical region due to Coccidioidal meningitis in another case. Linear meningeal enhancement is seen on postcontrast image starting from brain stem. (Images courtesy of Anton Hasso, USA). Sagittal (**f**), axial (**g**) T2-WI, sagittal (**h**), axial (**i**) postcontrast T1-WI demonstrate thickened and clumped roots in an arachnoiditis case. The exudative material around the nerve roots results in the obliteration of nerve root sheaths and subarachnoid space. Mild contrast enhancement is also evident

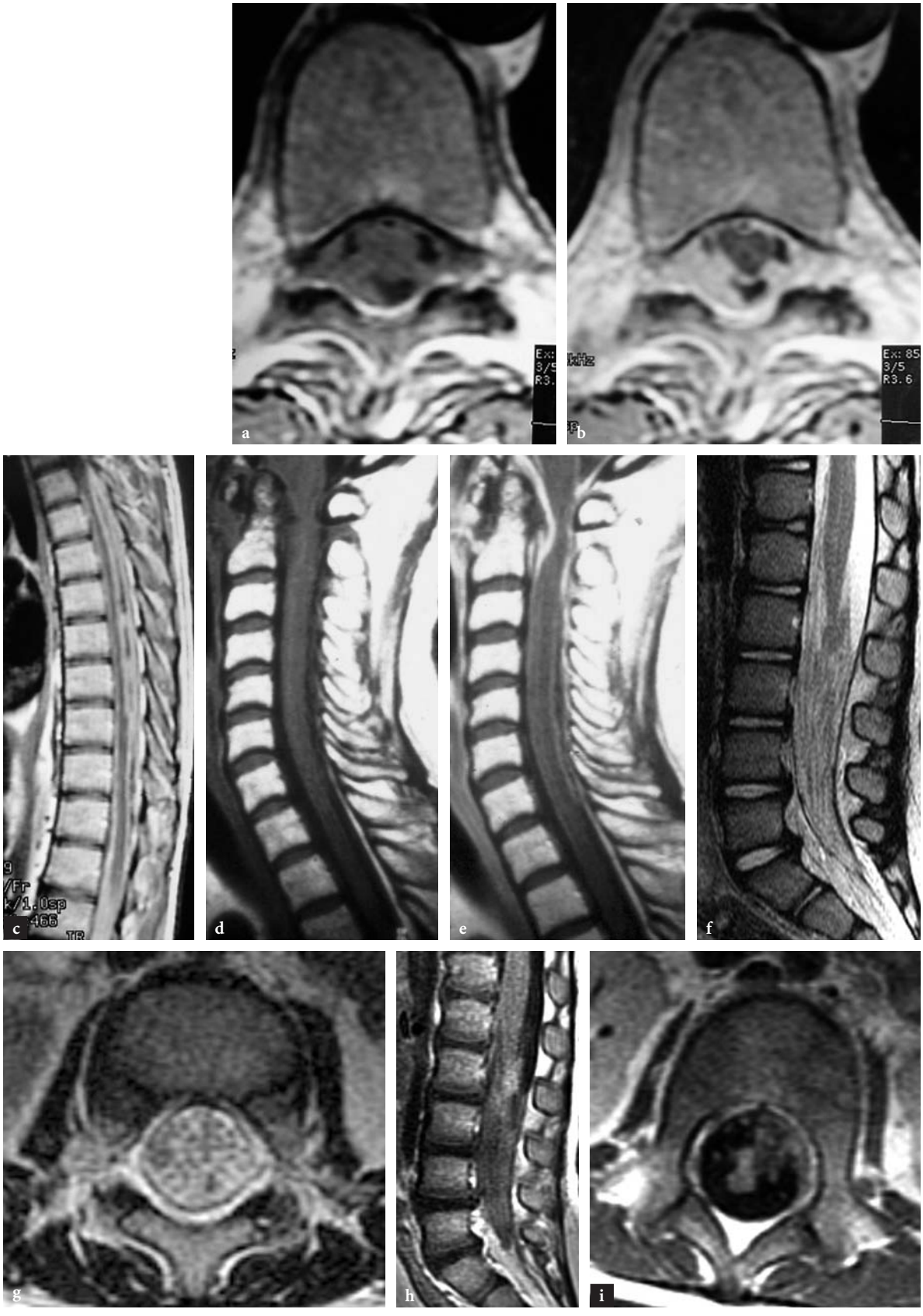
a
b
c
d
e
f
g
h
i

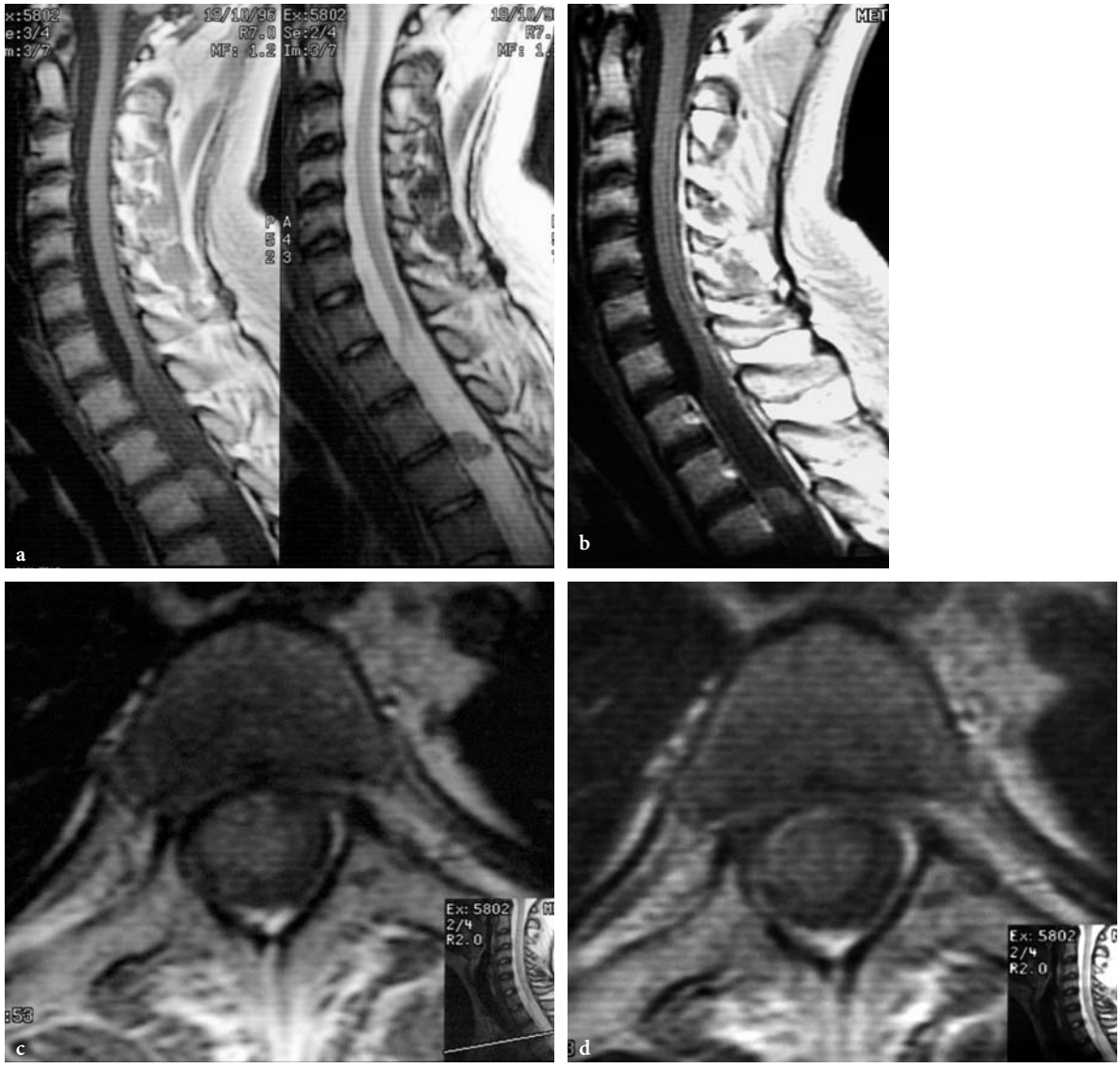

Fig. 2.21a–d. Sagittal precontrast T1- and T2-WI (**a**) and postcontrast T1-WI (**b**), axial pre- (**c**) and postcontrast (**d**) T1-WI demonstrate thickened leptomeninges and disappearance of anterior subarachnoid space with marked meningeal enhancement of TB meningitis and myelitis. Expansion of the cord is also evident. Tuberculoma is seen as a typically hypointense nodular lesion surrounded by high signal edema on T2-WI which enhances on the postcontrast image

entially involved (Fig. 2.20). Thickened, inflamed cervical meninges may cause spinal cord infarction and hydrocephalus (Van Tassel 1994). Candidiasis and histoplasmosis may also present as leptomeningitis.

Cysticercosis is the most common parasitic infection of the CNS. It is caused by systemic infestation of the larval form of Taenia solium. The occurrence of intradural-extramedullary cysticercosis is thought to be the result of direct CSF seeding of the larvae throughout the subarachnoid space from a source in the cerebrum. Spinal disease is rare. Leptomeningeal cysticercosis is more common than intramedullary disease. The rim enhancement of a discrete intradural-extramedullary cyst and homogeneously enhancing sheet-like arachnoiditis may be well demonstrated on contrast-enhanced MRI. Congenital lesions such as arachnoid and dermoid and hydatid cysts (Fig. 2.19) should be considered in the differential diagnosis of spinal cysticercosis (Mendonca 2002; Leite et al. 1997).

Arachnoiditis is an inflammatory process of the spinal leptomeninges, seen as intradural clumping of the spinal nerve roots (Fig. 2.20). The exudative material around the nerve roots eventually causes adhesions, finally resulting in the obliteration of nerve root sheaths and clumping of the roots. T2-WI in the axial plane can display centrally clumped or peripheral adherent roots (Fig. 2.20). Contrast enhancement of nerve roots is an infrequent finding that is often an uncertain and less helpful for the correct diagnosis (Smith and Blaser 1991; Van Tassel 1994; Mendonca 2002; Sharif 1992).

MRI findings in patients with intradural extramedullary infections are quite similar to those of leptomeningeal tumor spread. Fine linear enhancement of the cord surface may be also detected in sarcoidosis (Sharif 1992).

2.4.3 Intramedullary Infections

Infection of the spinal cord is relatively uncommon and may be caused by bacteria, viruses, fungi and parasites. Schistosomiasis is common in children (Rossi and Tortori-Donati 2004). The diagnosis of intramedullary infection in infants and children may be difficult and delayed due to the insidious course of the disease and late onset of clinical findings. Often the diagnosis is only made after irreversible neurologic impairment has already occurred (Simon et al. 2003). The clinical presentation can be acute or chronic. The process usually begins as myelitis and may progress to abscess. MRI may provide many valuable and useful clues leading to the correct diagnosis (Van Tassel 1994). MRI findings are variable and cover a wide spectrum from mild edema, swelling with mild or no contrast enhancement to prominent edema and abscess formation with diffuse, patchy or ring enhancement consistent with the stage of the infection. Intramedullary areas of high signal intensity, expansion of the cord and necrotic center are well seen on T2-WI (Figs. 2.21, 2.22). Without any known predisposing factors, the diagnosis can be exceedingly difficult. An infected syrinx may also simulate an intramedullary abscess particularly in the pediatric age group. Abnormal signal intensities on T2-WI and contrast enhancement diminish gradually during the treatment.

The incidence of intramedullary granulomatous infection is relatively low with TB as the most common cause. The MR findings are similar to intracranial tuberculomas. Focal spinal cord swelling, high signal edema, low signal nodular lesion (tuberculoma) on T2-WI (which is a differentiating feature from a pyogenic abscess) and nodular contrast enhancement on T1-WI are frequently detected findings (Fig. 2.21) (Bernaerts et al. 2003; Gero et al. 1991). Intramedullary high signal intensities, expansion of the cord and necrotic center are well seen on T2-WI. Diffuse, patchy or ring-shaped enhancement are consistent with the stages of the intramedullary abscess (Fig. 2.21). Syringohydromyelia, a well-known complication of tuberculous radiculomyelitis, generally results from inflammatory edema and ischemia in the early period of the disease, whereas chronic arachnoiditis is the hallmark of late-onset cases.

The imaging features of intramedullary tuberculosis are generally nonspecific. Therefore, the differential diagnosis is broad including neoplastic, inflammatory, demyelinating, vascular and other granulomatous disorders.

Viruses are the most common agents to infect the spinal cord; herpes virus, poliovirus, coxsackie genus and HIV are the most frequently encountered ones. Although encephalitis is the most common manifestation, some herpes viruses may also cause myelitis and polyradiculitis (Mendonca 2002). Herpes zoster infection may cause the subsequent onset of neurological symptoms after the appearance of a vesicular rash corresponding to dermatomal distribution. The etiology of the myelitis during herpes infection is still unclear and may be due to viral infection, allergic reaction, autoimmune vasculitis, etc. The virus is rarely isolated from the CSF, but antivirus antibody titers may be found to be elevated. MR features of herpes myelitis are nonspecific and indistinguishable from other forms of myelitis (Fig. 2.22). Intramedullary lesions usually tend to be located ipsilateral to the cutaneous rash. CMV is a common opportunistic virus that causes viral myelitis. Precontrast MR images demonstrate a thickened cauda equina with diffuse enhancement of the nerve roots, the surface of the conus and the meninges on postcontrast T1-WI. There are three kinds of polioviruses (types 1, 2 and 3) causing poliomyelitis by invading the motor neurons of the cord and brain stem causing flaccid asymmetric muscle weakness. On MRI, PD- and T2-WI reveal a hyperintense band along the entire ventral surface of the cord with no enhancement (Mendonca 2002). HIV-1 is the causative agent of AIDS and may itself alone cause spinal infection or the final immunologic deficit of AIDS also facilitates spinal infection. Viral

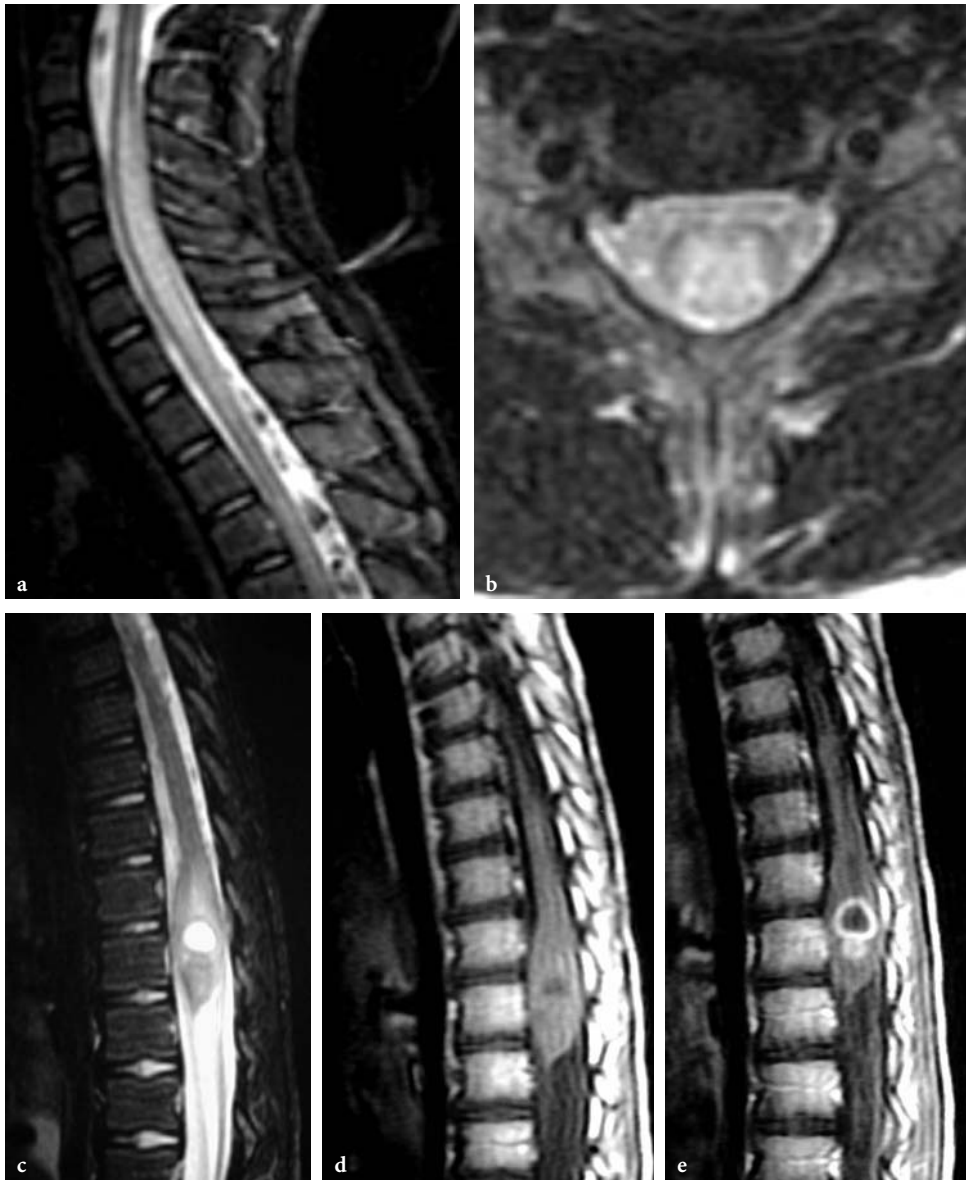

Fig. 2.22a–e. Intramedullary infection. Sagittal (**a**) and axial (**b**) T2-WI demonstrate fusiform enlargement of the cervical spinal cord due to viral myelitis. High signal is mostly seen in the posterior part of the cord, between the posterior roots. Sagittal T2-WI (**c**), pre- (**d**) and postcontrast (**e**) T1-WI of another patient demonstrate intramedullary cysticercosis. The cyst is located within the enlarged spinal cord with signal similar to CSF and shows peripheral enhancement. There is mild edema around the cyst

myelitis is among the many potential causes of acute transverse myelopathy. Vacuolar myelopathy and tract pallor are the other known causes of AIDS-related myelopathy. MRI plays an essential role in the evaluation of myelopathy in AIDS patients. MRI of vacuolar myelopathy is characterized by widespread signal abnormalities extending along the white matter tracts and symmetrically on multiple contiguous sections while tract pallor is characterized by gracile tract abnormality. Cord edema is not a prominent finding in HIV myelitis and vacuolar myelopathy, in contrast to toxoplasmosis and lymphoma (Mendonca 2002). The differential diagnosis of an enhancing lesion in the spinal cord in AIDS patients includes CMV, Herpes simplex virus type 2, fungal myelitis, lymphoma and other neoplasms. The presence of hemorrhage in the lesion may suggest Herpes simplex virus type 2. CMV and herpes infections, tuberculosis, nocardiosis, toxoplasmosis and lymphoma may all cause meningeal enhancement while this is not a usual imaging

feature in cryptococcal infection (Mendonca 2002). Toxoplasmic myelitis caused by T. gondii, which is an intracellular protozoan, should be suspected in immunocompromised patients with an intramedullary lesion. MR imaging shows diffuse hyperintensity on T2-WI with nodular enhancement. Differential diagnosis includes intramedullary tumors, inflammatory conditions such as multiple sclerosis, transverse myelitis, myelopathies and ADEM.

Fungal infections of the spinal cord can be caused by pathogenic and saprophytic fungi. A. fumigatus is the most common pathogen and invasive and life threatening forms are mostly seen in immunocompromised patients. Granuloma and abscess formation are also common. Fungal spinal cord abscesses have a nonspecific appearance of ring-enhancing medullary mass lesion. Candidiasis is generally an opportunistic disease. In the spine, the disease presents in different forms such as spondylodiscitis, intramedullary abscess and arachnoiditis. An intramedullary abscess cannot be differentiated by imaging alone but must be considered in the immunocompromised patient (Lindner et al. 1995).

In spinal cord involvement by cysticercosis, MRI typically shows cystic areas with similar signal intensity to that of CSF (Fig. 2.22). Occasionally, the scolex can be identified as an isointense mural nodule within the cyst cavity. With progressive degeneration, cysts may show irregular peripheral enhancement. Neoplasia (primary and secondary neoplastic cysts), hydatid cysts (Fig. 2.19) and posttraumatic changes (posttraumatic syrinx) should be considered in the differential diagnosis.

2.5 Spinal Tumors

Traditionally, spinal neoplasms are categorized by location as extradural, intradural extramedullary and intradural intramedullary, even though this classification sometimes represents an overgeneralization. Nevertheless, a topographic classification by compartment is useful because the symptoms, radiological findings, treatment planning and surgical approach all depend on the anatomic compartments in which the spinal tumors are localized rather than their histological characteristics.

The role of neuroradiology in spinal tumors consists of lesion detection, delineation, characterization, image-guided biopsies, treatment planning and treatment of patients with interventional procedures, such as vertebroplasty of the metastatic, painful compression fractures, and treatment monitoring. MRI is the imaging modality of choice for all spinal tumors. T1 acquisitions are very sensitive for the detection of these lesions and also demonstrate the morphology in detail. Vertebral body lesions usually are of low signal intensity surrounded by the higher signal of normal fat-containing marrow on T1-WI. However, the signal intensity of the vertebral body bone marrow is not very bright in young patients and in the patients with anemia or chronic diseases. Lesions can not be demonstrated well due to the low background signal. For this reason, SE or FSE with fat saturation, or STIR should be applied to improve the sensitivity. Vertebral lesions usually demonstrate high signal on T2-WI. FSE acquisitions must be used with caution because the persistent high marrow signal may obscure the pathology. In such conditions, fat saturated sequences may help. Contrast enhancement is helpful for differentiation of the tumor from normal marrow, delineation of the lesion, demonstration of epidural and soft tissue extension, demonstration of cord compression and also identification of more active tumor regions as targets for biopsy. Enhancing low signal lesions often become isointense with the surrounding high signal marrow-tissues and background and consequently become hardly detectable. For this reason, fat saturated postcontrast T1-WI are essential. Enhancement patterns are extremely variable. This variability of enhancement often occurs even in different metastatic lesions within the same patient. DWI sequences are helpful for differentiation of the osteoporotic fractures from either neoplastic or infectious causes of collapsed vertebrae. It was shown that all benign compression fractures were hypo-isointense to normal vertebrae while pathologic fractures were hyperintense and ADC values differs (Calli et al. 2001).

2.5.1 Extradural Tumors

Extradural tumors occur outside the dura and typically arise from the osseous spine and adjacent soft tissues. In the extradural space, nonneoplastic lesions are much more common than neoplasms. With the exception of vertebral hemangioma, benign tumors in the extradural space are infrequent compared to malignant lesions, especially to metastases.

2.5.1.1 Primary Extradural Tumors

2.5.1.1.1 Primary Benign Extradural tumors

Vertebral Hemangioma

Vertebral hemangiomas (VH) are slow-growing benign vascular tumors of the spinal column, present in approximately 11% of all patients (Schmorl and Junghans 1971). Approximately two thirds of the lesions are solitary and most of them are located in the vertebral body. A total of 60% occur in the thoracic region, while 29% are found in the lumbar region, 6% in the cervical region, and 5% in the sacrum (Schmorl and Junghans 1971). The majority of these lesions are asymptomatic and discovered incidentally. The thickened vertical trabeculae of hemangiomas cause parallel linear densities, which result in a striped "jail bar" or honey-combed appearance of the vertebral body on plain films. Extension into the posterior elements can occur. On axial CT and MR images, the thickened trabeculae seen in cross-section give a typical spotted appearance to the vertebral bodies (Fig. 2.23). Angiographic findings vary from normal to marked hypervascular strain. The sensitivity of the MRI is very high in the detection of hemangiomas and also demonstration of the paravertebral and epidural extension. VH are seen as round, relatively well-delineated lesions which tend to have increased signal intensity on both T1- and T2-WI (Fig. 2.23). This high signal reflects the adipose tissue (fat) in these lesions, rather than a hemorrhagic component. Hemangiomas can occasionally have a somewhat lower amount of fatty tissue and appear even diffusely hypointense. These lesions often enhance markedly with contrast material, and may be associated with an extradural soft tissue mass. Hemangiomas containing lower amounts of fatty tissue may be more aggressive (Tekkok et al. 1993). Extraosseous hemangioma may also be seen in association with or without VH and usually tends to lack fatty tissue and appears isointense on T1-WI with dural sac and spinal cord compression. Differential diagnosis consists of metastasis, and focal fat depositions (Masaryk 1991).

Osteoid Osteoma

Osteoid osteoma comprises 11%–12% of all benign bone tumors (Sze 2002). The most common locations in the spine are the lumbar region (59%), followed by the cervical (27%), thoracic (12%), and sacral (2%) regions (Gamba et al. 1984). Osteoid osteomas involve the posterior elements in 75% of cases while the vertebral body is affected in only 7% (Sze 2002).

Plain films and CT demonstrate the classic imaging findings of a lucent nidus surrounded by bony sclerosis (Swee et al. 1979). Some reports have stated that the lesion should be classified as osteoblastoma if the diameter is greater than 1.5 cm. However, this is not generally accepted and there are also reports stating that osteoblastoma is an entirely different histopathological entity (Orbay et al. 1999). A small amount of calcium can be present in the nidus. There may be extensive bony sclerosis which obscures the exact location of the nidus on plain films. If the initial plain films and CT are negative and clinical suspicion is still high for an osteoid osteoma, radionuclide bone scans, a highly sensitive method for detecting the nidus, are generally recommended. Osteoid osteomas are focally "hot" on bone scan. Osteoid osteomas demonstrate a heterogeneous appearance on MRI. Noncalcified portions of the nidus show increased signal intensity on the T2-WI while the calcified portion of the nidus and the surrounding bony sclerosis demonstrate low signal intensity on T1- and T2-WI. The nidus is frequently rich in vascularity and enhances markedly following contrast media administration. This enhancement may help not only to localize the nidus but also to differentiate it from nonenhancing lytic lesions, such as Brodie's abscess (Sze 2002). Associated reactive soft-tissue mass with inhomogeneous signal on T1-WI, and increased signal on T2-WI can also be demonstrated by MRI.

Osteoblastoma

Osteoblastomas are uncommon bone tumors. They account for 1% of all primary bone neoplasms and have a particular predilection for the spine, where 25%–50% of the cases are located (Sze 2002). Osteoblastomas occur most often in the posterior elements with a predilection for the lumbar spine, followed by the thoracic and cervical spine.

Plain films and CT typically show an expansile lytic lesion with a lucent or ossified center (Fig. 2.24). The margins are often, but not always, well defined. Although less pronounced than in osteoid osteoma, there may be a dense sclerotic reaction associated with osteoblastoma. CT also shows associated soft tissue masses and epidural extension (Fig. 2.24). Areas of hemorrhage or calcification show inhomogeneous signal on MRI. A thin rim of signal void as a result

Fig. 2.23a–d. Axial CT (**a**), axial (**b**) and sagittal (**c**) T2-WI and sagittal T1-WI (**d**) demonstrate thickened vertical trabeculae of L2 body with the typical spotted appearance on the right side. Vertebral hemangioma shows increased signal intensity on both T1- and T2-WI

of the bony shell may be visible (Fig. 2.24) (Nguyen and Hersh 1992). Irregular linear areas of signal void may be seen, corresponding to osseous trabeculae (Nguyen and Hersh 1992). Regions of vascularized stroma can be seen with high signal on T2-WI (Fig. 2.24). The lesion shows enhancement on post-contrast images. Associated reactive soft-tissue mass with inhomogeneous signal on T1-WI and increased signal on T2-WI can also be demonstrated by MRI.

Aneurysmal Bone Cyst

Aneurysmal bone cysts (ABC) are also encountered in the spine (12%–20%). They can be associated with other lesions such as giant cell tumor (GCT), chondroblastoma, chondromyxoid fibroma, fibrous dysplasia and nonossifying fibroma. Most of them occur in the lumbar spine and are located in the posterior elements. The pedicle and neural arch are the most frequently affected sites.

Plain films show a lytic, expansile lesion generally with intact cortex and honey-combed trabeculated appearance; the lesion may lead to vertebral collapse and vertebra plana. Extension into the spinal canal can also be seen. CT shows lucent and hyperdense areas, septations and lobulations in detail (Fig. 2.25). Following contrast media administration, particularly, septal enhancement show the lobulations in detail. MRI also demonstrates the lobulations and septations as a thin, well-defined low signal rim. The signal of the cystic sections of


a


b


c

Fig. 2.24a–c. Axial CT (**a**), T2-WI (**b**) and postcontrast T1-WI (**c**) demonstrate enlarged mass lesion of the left superior articular process of L2 of an osteoblastoma. Cortical breakthrough is seen at the posterolateral part of the tumor. Associated reactive soft-tissue changes with inhomogeneous signal on T1-WI and increased signal on T2-WI are also

the lesion depends on the contents of the cysts. They are usually hyperintense on T2-WI and iso-hypointense to cord on T1-WI. Fluid–fluid levels with various signal intensities representing hemorrhage of different age with various stages of evolution can also be observed (Fig. 2.25). The differential diagnosis includes osteoblastoma, GCT and telangiectatic osteosarcoma.

Sacrococcygeal Teratoma

Sacrococcygeal teratoma occurs rarely. It has malignant potential and is more frequent in girls. Plain film and CT show a pelvic mass with coccygeal erosion, calcifications and with bowel loops and bladder displacement. These lesions tend to be hypointense on T1-WI, hyperintense on T2-WI and the solid portion of the tumor enhances markedly.

2.5.1.1.2 Primary Malignant Extradural Tumors

Primary Lymphoma

Lymphoma can involve the spine as an isolated primary lesion or as part of a systemic disease. Over 85% of cases are non-Hodgkin's lymphoma (NHL). Plain X-ray films show a wide spectrum of radiographic manifestations, ranging from a permeative moth-eaten appearance to a more lytic geographic area of bony destruction and to rare osteosclerotic lesions. Infiltration of the vertebral bodies results in focal or diffuse areas of decreased signal on T1-WI

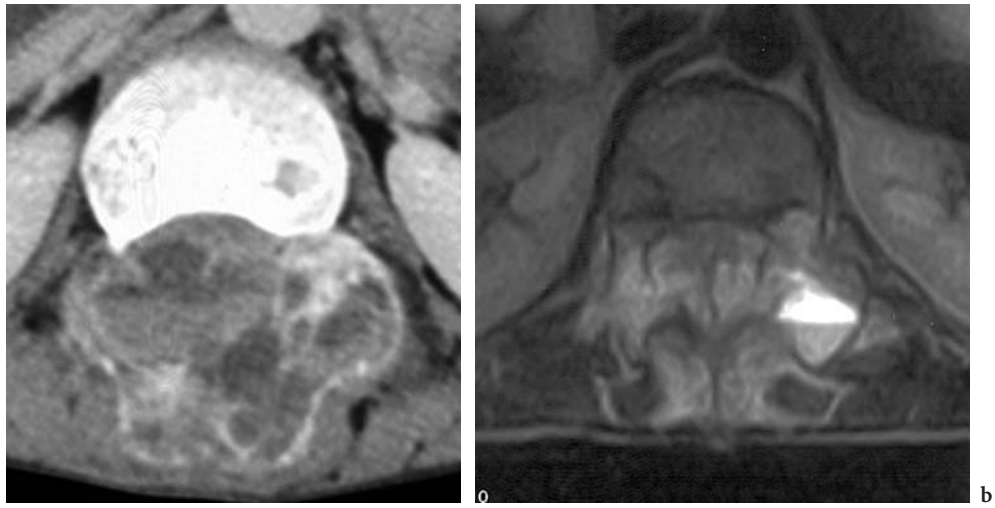

Fig. 2.25a,b. Axial CE-CT (**a**) shows lucent and hyperdense areas, lobulations and septations with septal enhancements in an aneurysmal bone cyst. Axial T2-WI (**a,b**) also demonstrate the thin, well-defined low signal rim of septations. Cysts are hyperintense on T2-WI with fluid–fluid levels. (Images courtesy of Alpay Alkan)

due to the replacement of fatty marrow by cellular elements. Focal areas of tumor infiltration typically show slightly increased signal intensity or even hypointensity on T2-WI. The appearance is suggestive but nonspecific and is identical to metastatic disease, particularly those of hypercellular primary tumors, as well as plasmacytoma or multiple myeloma.

Osteosarcoma

Osteosarcomas are malignant tumors of the pediatric age group. They are more frequent in boys. Primary spinal osteosarcomas are unusual. Secondary osteosarcomas are more common. Osteosarcomas are usually located centrally in the vertebral body. Osteoblastic and/or osteolytic lesions can be seen on plain X-ray films and CT with prominent destruction. MRI is superior to CT for detection and delineation. The content of the mass affects the signal intensity. Usually, areas of cortical thinning and loss of cortical continuity are seen. Osteosarcomas demonstrate heterogeneous signal on both T1- and T2-WI. Osteosarcoma enhances immediately; the enhancing areas should be chosen as targets for the biopsy.

Ewing Sarcoma

Primary spinal Ewing sarcoma of the spine is rare, while secondary tumors are relatively common. Ewing sarcoma is frequent before the second decade. Plain films and CT show lytic changes with lamellated periosteal reaction, bone spicules and a large soft tissue mass. They are hypointense on T1-WI and hyperintense on T2-WI with soft tissue involvement (Fig. 2.26). Ewing sarcoma enhances moderately (Fig. 2.26).

2.5.1.2 Secondary Extradural Tumors

2.5.1.2.1 Metastatic Disease to the Spine and Extradural Space

Metastasis is the most common extradural malignant spinal tumor. Almost every malignancy can involve the spine or the soft tissues in the epidural space, but Ewing sarcoma, neuroblastoma, osteogenic sarcoma, rhabdomyosarcoma, Hodgkin lymphoma and soft tissue sarcomas are the most common primary tumors that metastasize to the vertebrae (Figs. 2.26, 2.27) (Fornasier and Horne 1975).

Metastatic lesions may involve any portion of the vertebra and epidural space. The vertebral body is frequently the initial site followed by involvement of the epidural space and pedicles (Osborn 1994). Spinal metastatic lesions are most often destructive and lytic; less frequently, they can also be osteoblastic and sclerotic. Typically, 40%–50% bone destruction is required in order to detect the bone metastases on plain X-ray films (Parizel and Wilmink 1998). CT is well suited to demonstrate the destructive lesions with loss of cortical conti-

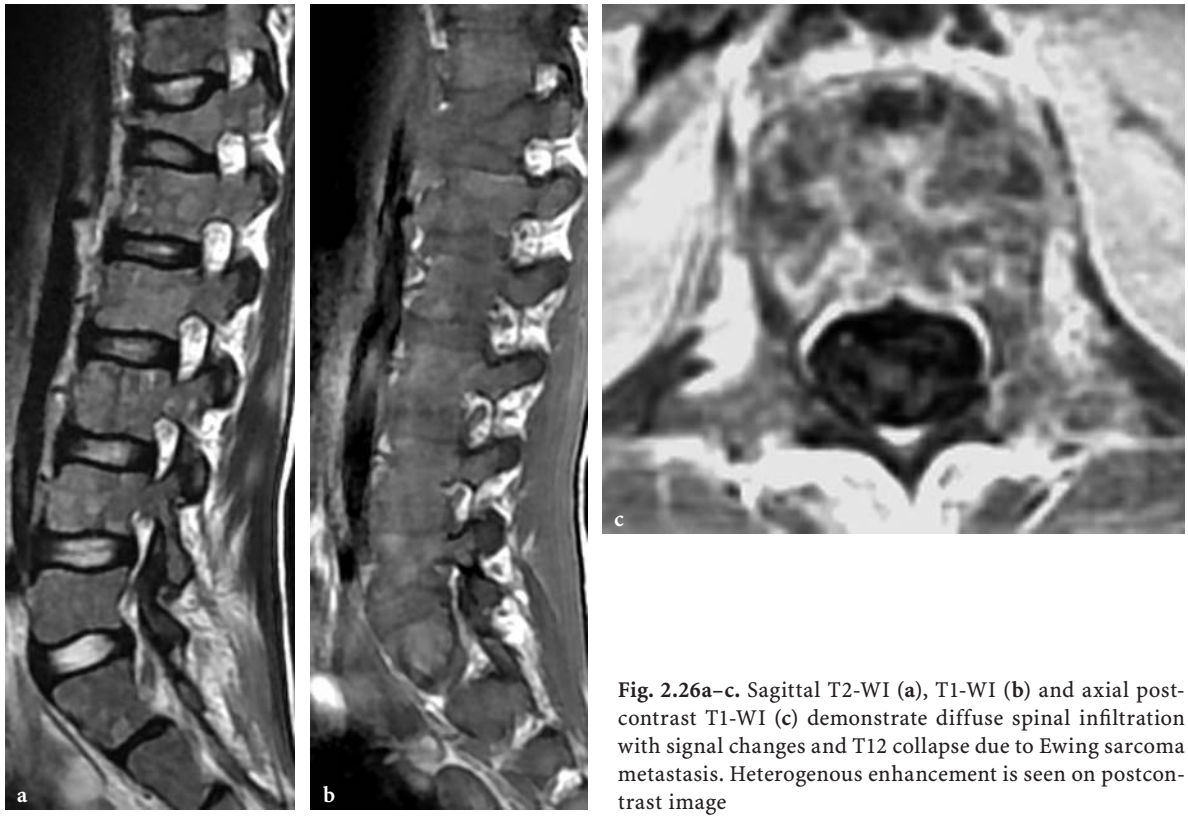

Fig. 2.26a–c. Sagittal T2-WI (**a**), T1-WI (**b**) and axial post-contrast T1-WI (**c**) demonstrate diffuse spinal infiltration with signal changes and T12 collapse due to Ewing sarcoma metastasis. Heterogenous enhancement is seen on postcontrast image

nuity and infiltrations. MRI is extremely sensitive and is certainly the modality of choice. The multiplicity of the lesions is strong evidence for a metastatic origin (Figs. 2.26, 2.27). In the case of single lesions, differentiation of a metastatic lesion from a primary tumor or from a lesion of another etiology is difficult. Biopsy is generally necessary in these cases. The signal intensity of spinal metastases varies according to the content of the lesions. Lesions are usually hypointense on T1-WI and heterogeneous on T2-WI, and most of them are hyperintense on STIR (Fig. 2.27). They enhance markedly. Post-contrast fat saturated T1-WI are very helpful to demonstrate extension in detail. DWI is helpful to differentiate pathologic fractures from osteopenic fractures. Epidural metastases tend to compress and encase the thecal sac. Displacement of the dura, extension through the foramina, and destruction of neighboring bony structures are the imaging findings of epidural metastasis (Fig. 2.28). They generally demonstrate heterogeneous enhancement, depending on the primary tumor (Fig. 2.28). Differential diagnosis consists of MM and multiple VH.

2.5.2 Intradural Extramedullary Tumors

Nerve sheath tumors and meningiomas account for 80%–90% of intradural-extramedullary tumors. Other benign tumors are uncommon.

2.5.2.1 Primary Intradural Extramedullary Tumors

2.5.2.1.1 Nerve-Sheath Tumors

In the general population, nerve-sheath tumors are the most common intraspinal lesions. The two main histologic types of nerve sheath tumors, i.e. schwannoma and neurofibroma, are frequent in the spine, while ganglioneuroma is relatively rare. Schwannomas are slightly more common than neurofibromas. In the pediatric population, nerve-sheath tumors probably constitute less than 10% of all intraspinal lesions. They are most commonly intradural extramedullary in location (58%) (Sze 2002). The remainder are purely extradural (27%), dumbbell-

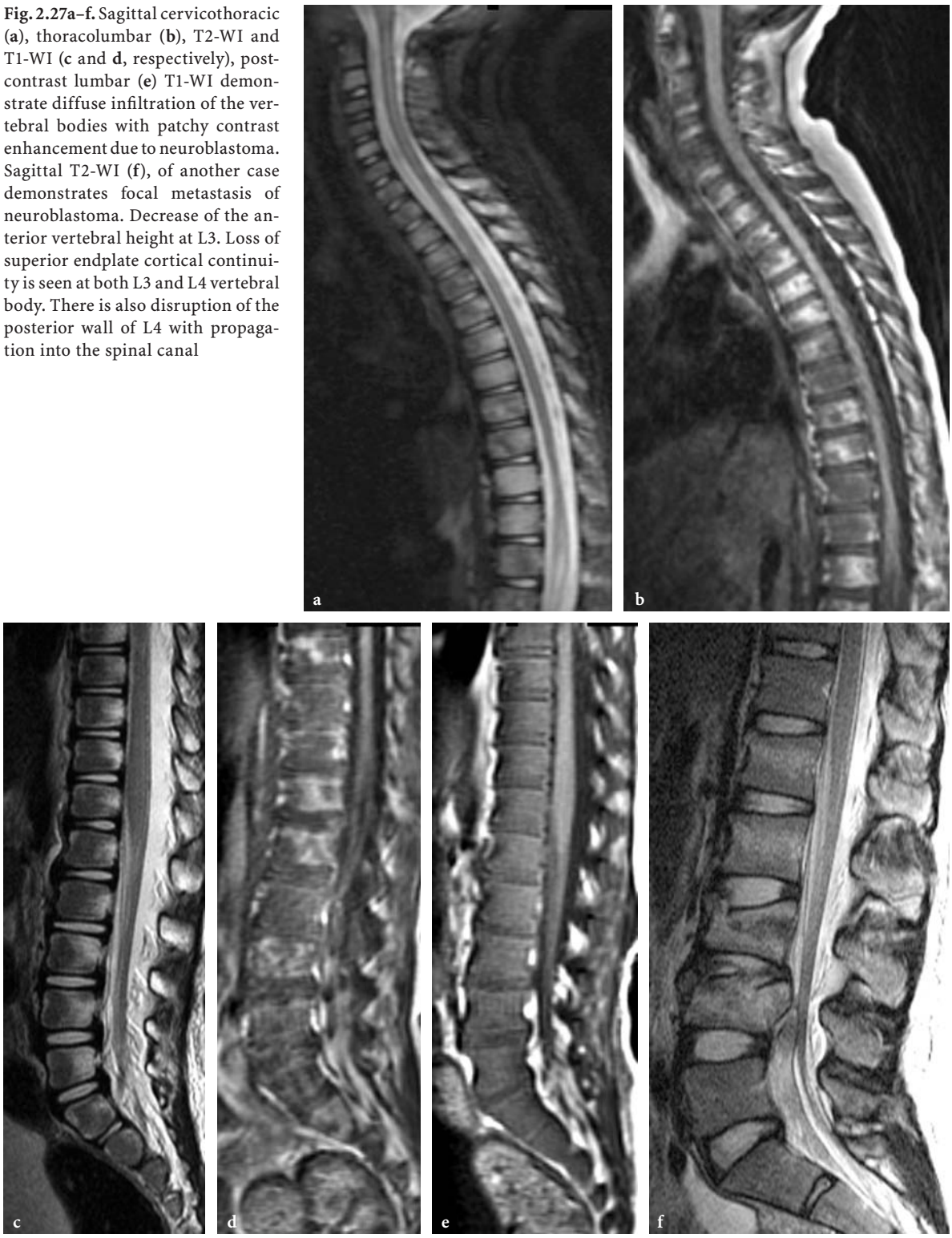

Fig. 2.27a–f. Sagittal cervicothoracic (**a**), thoracolumbar (**b**), T2-WI and T1-WI (**c** and **d**, respectively), post-contrast lumbar (**e**) T1-WI demonstrate diffuse infiltration of the vertebral bodies with patchy contrast enhancement due to neuroblastoma. Sagittal T2-WI (**f**), of another case demonstrates focal metastasis of neuroblastoma. Decrease of the anterior vertebral height at L3. Loss of superior endplate cortical continuity is seen at both L3 and L4 vertebral body. There is also disruption of the posterior wall of L4 with propagation into the spinal canal

Fig. 2.28a–f. Sagittal T2-WI (**a**), sagittal (**b**) and axial (**c**) postcontrast T1-WI demonstrate an epidural mass lesion of synovial sarcoma metastasis posterior to the L5 and S1 vertebral bodies, encasing the dural sac and enlarging the spinal canal. Dural elevation by the mass lesion is seen clearly on T2-WI. The mass lesion is extending laterally through the enlarged left neural foramen. The mass lesion enhances moderately and marked peripheral meningeal enhancement is seen. Almost all the vertebral bodies show heterogenous signal changes with heterogenous enhancement suggesting the metastatic infiltration. Sagittal T2-WI (**d**), postcontrast sagittal (**e**) and axial (**f**) postcontrast T1-WI (**g**) demonstrate thoracic epidural metastasis in a different patient compressing and shifting the dural sac and spinal cord to anterior. The mass lesion shows marked homogeneous enhancement

shaped with both an extradural and an intradural component (15%), and rarely, intramedullary (less than 1%) (Sze 2002). The most common location is the cervical region, followed by the lumbar and thoracic regions.

Schwannomas do not envelop the adjacent nerve root and are generally solitary. In contrast, neurofibromas envelop the dorsal sensory root, are frequently multiple, and usually are associated with neurofibromatosis, even when single (Sze 2002). Schwannomas are lobulated, encapsulated, well-circumscribed round or oval tumors that often show cystic degeneration, hemorrhage, and xanthomatous changes (Fig. 2.29). On the other hand, neurofibromas are unencapsulated, fusiform, less well-defined lesions (Osborn 1994). Necrosis and cystic degeneration are rare in neurofibromas (Fig. 2.29). In schwannomas, nerve fibers do not course through the tumor but are confined to the capsule. Neurofibromas usually can not be dissected from the parent nerve, because it typically runs through the lesion and nerve fibers are dispersed throughout the lesion (Osborn 1994).

Neurofibromatosis is a phacomatosis. The condition occurs spontaneously in 50% of cases and is an autosomal dominant in 50% of cases. Patients with neurofibromatosis have a predisposition to develop other neoplasms in addition to neurofibromas, including intramedullary lesions, such as astrocytomas, ependymomas and hamartomas. Malignant degeneration is uncommon in nerve-sheath tumors. Those cases associated with neurofibromatosis tend to occur at a young age and to have a worse prognosis.

Plain film findings of nerve-sheath tumors include posterior scalloping of the vertebral bodies, pedicle erosion and widening of the neural foramina. On CT, nerve sheath tumors show decreased attenuation values and present as paraspinal or intraspinal masses. Calcification and hemorrhage are rare. Nerve-sheath tumors on MRI tend to have increased signal intensity compared with muscle on T1-WI; it has been postulated that this may be secondary to shortening of the T1 relaxation time by mucopolysaccharide molecules interacting with high tissue water (Fig. 2.29). On T2-WI, these lesions show markedly increased signal intensity. The "target sign" is seen frequently with hyperintense rim and hypointense central area, which represents peripheral myxomatous and central fibrocollagenous tissue on T2-WI. These lesions usually enhance markedly and fairly homogeneously. Areas of cystic degeneration may cause heterogeneous contrast enhancement (Fig. 2.29).

2.5.2.1.2 Meningioma

Meningiomas of the spinal canal generally are found in the thoracic region (80%), followed by the cervical and lumbar regions; they are rare in children (Sze 2002). They tend to be encapsulated and are attached to the dura. When meningiomas are purely extradural, they tend to be malignant.

Meningiomas in the spine are typically well-circumscribed lesions, frequently located antero- or posterolateral to the spinal cord, and tend to displace the cord. The lesions are hypo- to iso-intense relative to the spinal cord on T1-WI while they are slightly hyperintense to the spinal cord on T2-WI (Fig. 2.29). Signal void areas represent calcifications. Meningiomas are hypervascular tumors which enhance immediately, intensely and homogeneously on postcontrast images (Fig. 2.29). Nerve-sheath tumors should be the first consideration in the differential diagnosis.

2.5.2.1.3 Dermoid and Epidermoid Tumors

Dermoid and epidermoid tumors are rare in the spinal canal. Histologically, dermoids are differentiated from epidermoids by their higher fat content. Dermoids appear slightly higher in signal intensity than CSF on T1-WI images and are hyperintense on T2-WI. Dermoids are found more commonly in the midline and most are diagnosed in children. MR distinguishes dermoid from lipoma by virtue of the nonfatty component of the lesion.

Epidermoids do not contain fat and show signal characteristics similar to CSF on T1- and T2-WI. Epidermoids are diagnosed on proton density-weighted, FLAIR or CISS images on the basis of their "cotton cheese" texture (Rubinstein 1972). Diffusion weighted scans are useful to show restricted diffusion, although in the spine this may be technically challenging. Both of these lesions can rupture and cause chemical meningitis.

2.5.2.2 Secondary Intradural Extramedullary Tumors

2.5.2.2.1 Spinal Leptomeningeal Tumors

Intracranial neoplasms as medulloblastoma, glioblastoma multiforme, anaplastic astrocytoma, and

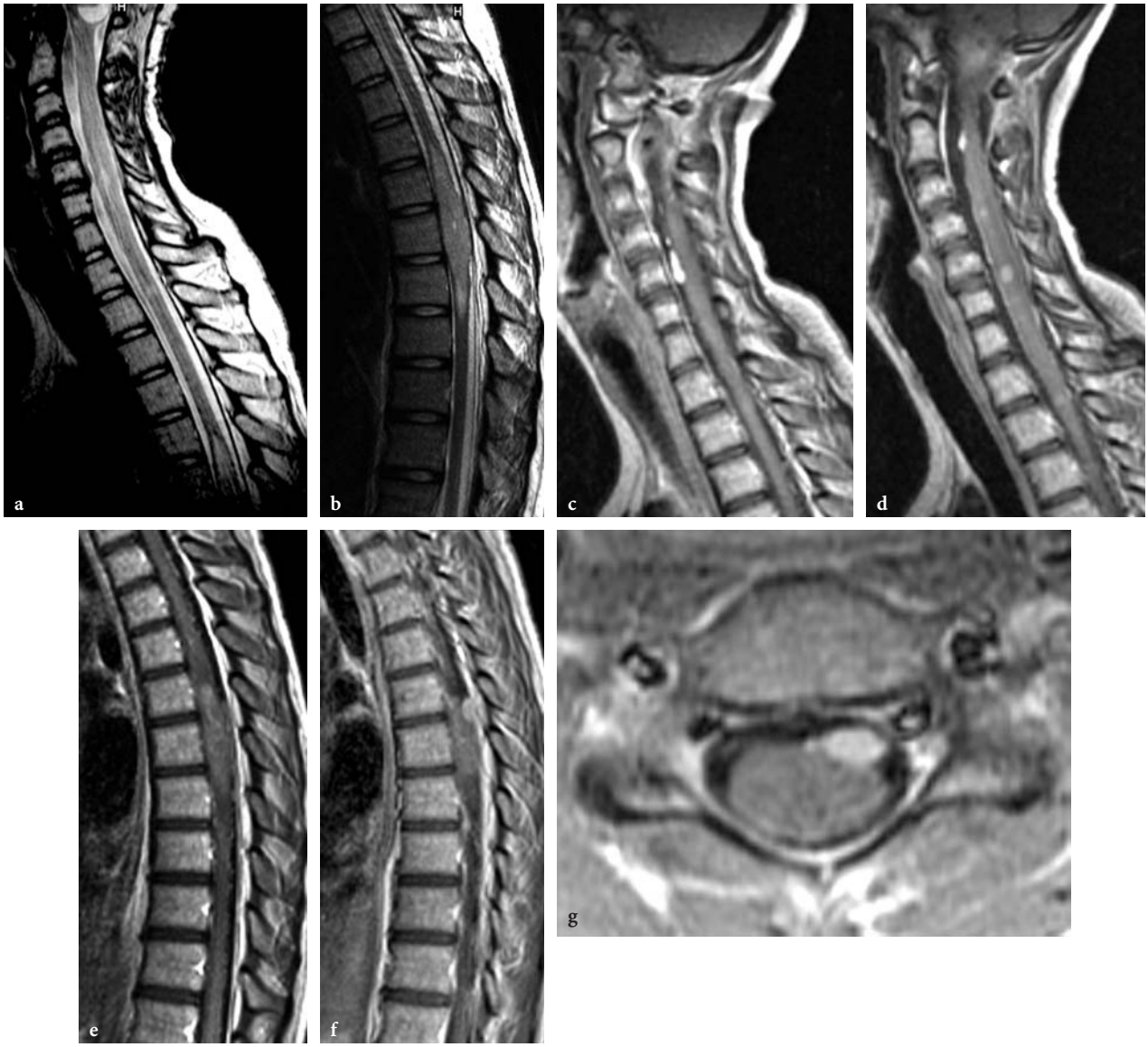

Fig. 2.29a–g. Sagittal cervical (**a**), thoracic (**b**) T2-WI, postcontrast cervical (**c,d**), thoracic (**e,f**) and axial (**g**) T1-WI demonstrate intramedullary tumors located both in cervical and thoracic levels with fusiform enlargements and heterogenous enhancements of neurofibromatosis. Markedly enhancing nodular lesions posterior to C2 and C5 are suggestive of nerve sheath tumors. Another markedly enhancing nodular lesion which has a broad-based dural location posterior to T7–T8 disc space is suggestive of meningioma

ependymoma, choroid plexus papilloma, choroid plexus carcinoma, pineal tumors and systemic tumors may spread via the CSF to the meninges. Establishing the presence of leptomeningeal metastasis with an intracranial tumor is very important and may significantly alter the treatment planning and spinal axis radiation should be employed. Systemic tumors may spread to the leptomeninges by many mechanisms, including direct extension into the subarachnoid space, peripheral lymphatic invasion, hematogenous dissemination or seeding via the choroid. Leptomeningeal tumors most often spread to the lumbosacral region (73%), probably because of the effects of gravity, with most of the tumor cells settling in this area (Dorwardt et al. 1981). These are the so-called drop metastases. However, leptomeningeal metastases can also be seen in the cervical and thoracic regions, where they are more commonly posteriorly located (Dorwardt et al. 1981). Contrast-enhanced MR

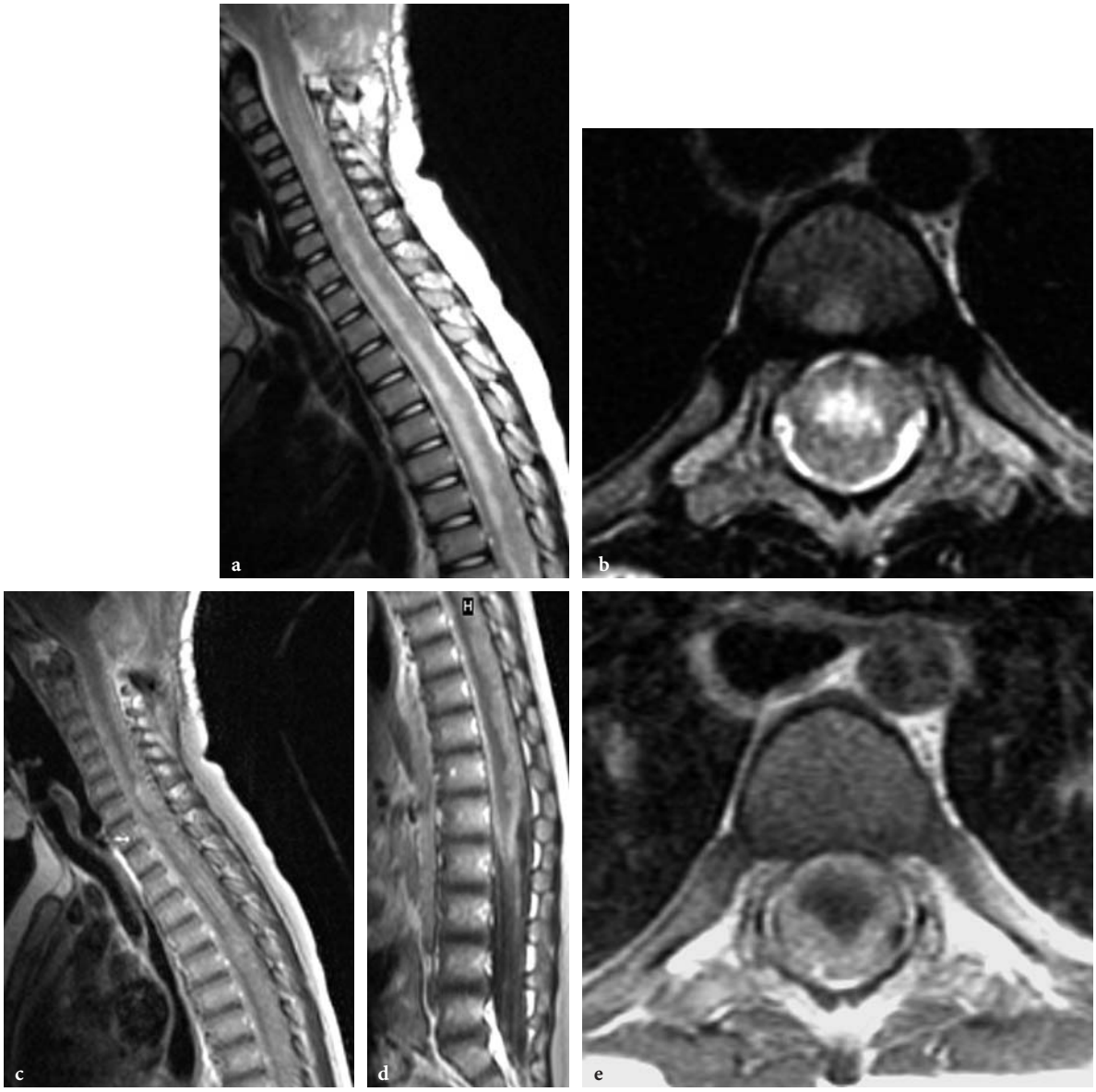

Fig. 2.30a–e. Cervicothoracic sagittal (**a**), axial (**b**) T2-WI, sagittal cervicothoracic (**c**), thoracolumbar (**d**) and axial (**e**) post-contrast T1-WI demonstrate a linear fine layer of enhancement of intradural leptomeningeal infiltration from brainstem to cauda caused by medulloblastoma. Cord is encased by the infiltration. There is also a long segment of centrally located intramedullary infiltration

examination is mandatory (Fig. 2.30). The higher sensitivity has made the MRI the modality of choice in the detection of metastatic tumors in the intradural extramedullary compartment of the spine. Tumor spread can have a variety of appearances. Tumor may coat the cord or the nerve roots as a fine layer of enhancement or may be very local as multiple nodules (Fig. 2.30). Enhancement of the entire thecal sac may also be seen due to tumoral infiltration in severe cases.

2.5.3 Intramedullary Tumors

2.5.3.1 Primary Intramedullary Tumors

Intramedullary spinal cord tumors represent 3% of all central nervous system tumors, and 25% of spinal tumors. Most spinal cord tumors are malignant. The majority of intramedullary tumors in children are

astrocytoma followed by ependymoma. Intramedullary hemangioblastoma, oligodendroglioma and paraganglioma are rare in children.

2.5.3.1.1 Astrocytoma

Astrocytomas most often are located in the cervical and thoracic regions. Multisegmental involvement is the rule, and many intramedullary astrocytomas involve both regions. The prevalence of astrocytomas decreases in the lower thoracic and lumbar regions, unlike the prevalence of ependymomas, which increases in the caudal spinal canal. It is rare for astrocytomas to be located in the filum terminale, which is a common site for ependymomas. Most astrocytomas are intramedullary, although rarely they can be exophytic and intradural extramedullary in location.

Cord enlargement with marked signal intensity changes such as hypointensity on T1- and hyperintensity on T2-WI are the imaging findings (Fig. 2.31). The infiltrative nature of the tumor often causes poorly defined and irregular margins. These lesions almost always enhance immediately (Fig. 2.31). Intratumoral and/or extratumoral cysts can also be seen. If there is no contrast uptake, extratumoral cysts tend to be benign. Signal intensity of both reactive and neoplastic cysts changes according to the content of the cyst. Complex benign syrinxes can resemble cystic astrocytomas with gliosis within their walls. This tissue can display increased signal intensity on T2-WI and can be indistinguishable from tumor. The use of a contrast agent is mandatory to evaluate the etiology of the syrinx.

2.5.3.1.2 Ependymoma

Ependymomas are the most common glial spinal cord tumors in adults; however, they may occur at any age, with male predominance (Sze 2002). The cervical cord is the most common site for the intramedullary ependymomas. Ependymoma is the most common primary cord tumor of the lower spinal cord, conus medullaris and filum terminale. The myxopapillary form is particularly common in the conus and the filum.

MRI demonstrates spinal cord enlargement or mass lesion, frequently near the conus but not uncommonly elsewhere in the spinal cord (Fig. 2.32). The lesions often have well-defined borders and are hypointense or isointense to the cord on T1-WI and are typically heterogeneous on T2-WI (Fig. 2.32). Areas of intratumoral hemorrhage cause a variable

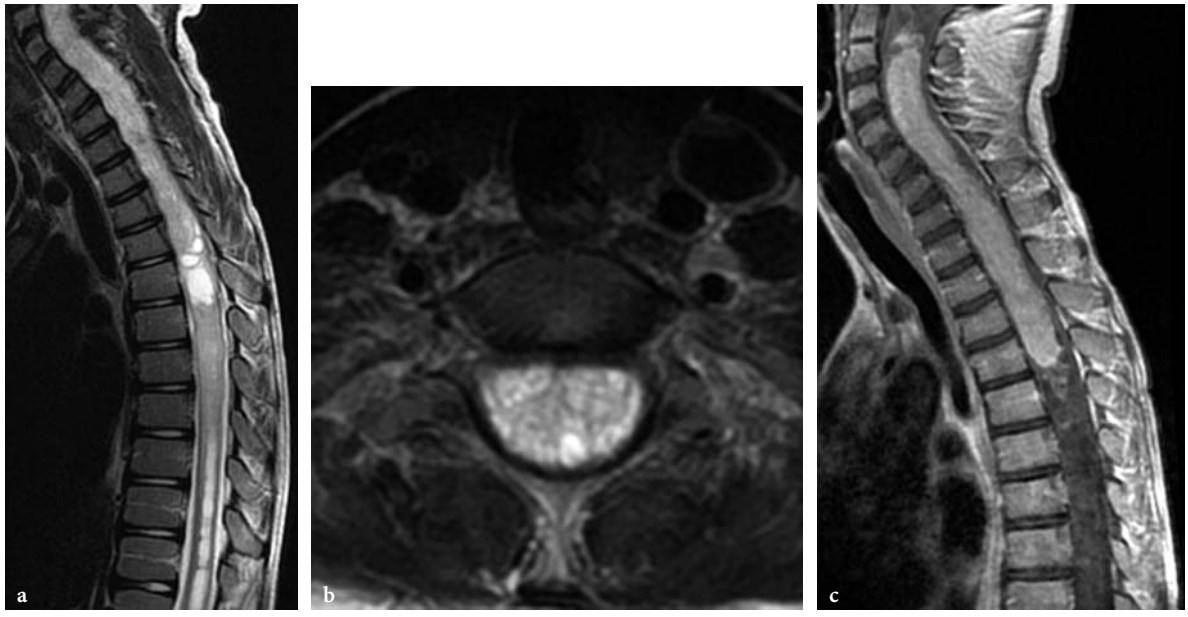

Fig. 2.31a–c. Sagittal (**a**), axial (**b**) T2-WI and sagittal postcontrast T1-WI (**c**) demonstrate cervicothoracic spinal cord enlargement with heterogeneous signal abnormalities of an intramedullary astrocytoma. There are multiple irregular cysts at the distal part of the tumor followed by syrinx. Subarachnoid space around the cord is obliterated. Marked homogenous contrast enhancement is evident on the postcontrast images

Fig. 2.32a–c. Sagittal T2-WI (**a**), sagittal (**b**) and axial (**c**) postcontrast T1-WI demonstrate an enlarged lumbar spinal cord and cauda with an associated mass lesion. Ependymoma fills the entire spinal canal and shows heterogeneous signal abnormalities with heterogeneous contrast enhancement

appearance with mixed signal intensities, due to the presence of different blood degradation products. Hemosiderin deposition is encountered frequently, particularly at the superior and inferior borders of the tumor, and appears as a "cap" with mildly hypointense signal on T1-WI and markedly hypointense signal on T2-WI. This finding is suggestive of, but not pathognomonic for, ependymoma. Ependymomas enhance markedly and heterogeneously following contrast media administration (Fig. 2.32). Astrocytoma should be the first consideration in the differential diagnosis.

MRI shows a widened cord, and associated edema, often extending for a considerable length with low signal intensity on T1-WI and high signal intensity on T2-WI than cord (Fig. 2.30). Metastatic lesions may be multiple and infiltrative with ill-defined borders. The nidus of the tumor can sometimes be visualized as a lower-intensity structure surrounded by the higher intensity edema on T2-WI. Use of an intravenously administered contrast agent is mandatory and metastases always enhance markedly (Fig. 2.30). Hemangioblastoma should be the first consideration in the differential diagnosis.

2.5.3.2 Secondary Intramedullary Tumors

2.5.3.2.1 Metastatic Disease of the Spinal Cord

Metastatic intramedullary tumors are rare, especially when compared with extradural metastases. The incidence of metastasis to the spinal cord in patients with systemic carcinomas has been estimated from 0.9% to 8.5% (Sze 2002). The thoracic cord is most often involved, followed by the cervical and the lumbar cord.

References

Akhan O, Dinçer A, Saatçi I et al. (1991) Spinal intradural hydatid cyst in a child. Br J Radiol 64:465–466

Babinchak TJ, Riley DK, Rotheram EB (1997) Pyogenic vertebral osteomyelitis of posterior elements. Clin Infect Dis 25:221–224

Backes WH, Mess WH, Wilmink JT (2001) Functional MR imaging of the cervical spinal cord by using median nerve stimulation and fist clenching. Am J Neuroradiol 22:1854–1859

Backes W, Nijenhuis RJ, Mull M et al. (2004) Contrast en-

hanced MRA of the spinal arteries: current possibilities and limitations. Rivista di neuroradiologia 17:282–291
Begg AC (1954) Nuclear herniations of the intervertebral disc: their radiological manifestations and significance. J Bone Joint Surg 36:180–193
Bernaerts A, Vanhoenacker FM, Parizel PM et al. (2003) Tuberculosis of the central nervous system: overview of the neuroradiological findings. Eur Radiol 13:1876–1890
Bhadelia RA, Bogdan AR, Wolpert SM (1995) Analysis of CSF flow waveforms with gated phasecontrast MR velocity measurements. Am J Neuroradiol 16:389–400
Bouchez B, Arnott G, Delfosse JM (1985) Acute spinal epidural abscess. J Neurol 231:343–344
Brugiéres P, Thomas P, Ruel L et al. (2004) CSF flow imaging of the spine. Rivista di neuroradiologia 17:300–308
Calli C, Yunten N, Kitis O et al. (2001) Diffusion weighted MRI in spondylodiscitis and vertebral malignancies. Neuroradiology 43:55
Chang KH, Han MH, Choi YW et al. (1989) Tuberculous arachnoiditis of the spine: findings of the myelography, CT and MR imaging. Am J Neuroradiol 10: 1255–1262
Chotivichit A, Buchowski JB, Lawson HC, Huckel CB (1999) Tuberculosis of spine. In: Osenbach RK, Zeidman SM (eds) Infections in neurological surgery. Diagnosis and management. Lippincott-Raven, Philadelphia, pp 281–297
Dagirmanjian A, Schils J, McHenry M (1999) MR imaging of spinal infections. Mag Reson Imaging Clin N Am 7:525–538
Danner RL, Hartmann BJ (1987) Update of spinal epidural abscess: 35 cases and review of the literature. Rev Infect Dis 9:265–274
Dorwart RH, Wara WM, Norman D et al. (1981) Complete myelographic evaluation of spinal metastases from medulloblastoma. Radiology 139:403–408
Feldenzer JA, McKeever PE, Schaberg DR et al. (1987) Experimental spinal epidural abscess: a pathophysiological model in rabbit. Neurosurgery 20:859–867
Fornasier VL, Horne JG (1975) Metastases to the vertebral column. Cancer 36:590–594
Foster K, Chapman S, Johnson K (2004) MRI of the marrow in the paediatric skeleton. Clin Radiol 58:651–673
Gamba JL, Martinez J, Apple J et al. (1984) CT of axial skeletal osteoid osteomas. AJR Am J Roentgenol 142:769–772
Gero B, Sze G, Sharif H (1991) MR imaging of intradural inflammatory diseases of the spine. Am J Neuroradiol 12:1009–1019
Gillams AR, Chaddha B, Carter AP (1996) MR appearances of the temporal evolution and resolution of infectious spondylitis. AJR Am J Roentgenol 166:903–907
Gupta RK, Chang KH (2001) Parasitic infections. In: Gupta RK, Lufkin RB (eds) MR imaging and spectroscopy of central nervous system infection. Kluwer Academic/Plenum Publishers, New York, Boston, Dordrecht, London, Moscow, pp 205–239
Heithoff KB, Gundry CR, Burton CV, Winter RB (1994) Juvenile discogenic disease. Spine 19:335–340
Henry-Feugeas MC, IdyPeretti I, Blanchet B (1993) Temporal and spatial assessment of normal CSF dynamics with MR imaging. Magn Reson Imag 11:1107–1118
Hitchon PW, Osenbach RK, Yuh WT et al. (1992) Spinal Infections. Clin Neurosurg 38:373–387
Iplikcioglu C, Kokes F, Bayar A (1991) Spinal invasion of pulmonary hydatidosis: computed tomographic demonstration. Neurosurgery 29:467–468
Jinkins JR (2000) Atlas of neuroradiologic embryology, anatomy, and variants. Lippincott Williams & Wilkins, Philadelphia
Kirks DR, Griscom NT (1998) Practical pediatric imaging. In: Young Poussaint T, Barnes PD, Ball WS (eds) Spine and spinal cord. Lippincott-Raven, Philadelphia, pp 269–272
Kuhn JP, Slovis TL, Haller JO (1993) Caffey's pediatric diagnostic imaging, 9th ed. In: The skull, spine and central nervous system, vol. I, section 1. Mosby, pp 116–125
Leite CC, Jinkins JR, Escobar BE et al. (1997) MR imaging of intramedullary and intradural-extramedullary spinal cysticercosis. AJR Am J Roentgenol 169:1713–1717
Lindner A, Becker G, Warmuth-Metz M et al. (1995) Magnetic resonance imaging findings of spinal intramedullary abscess caused by Candida albicans: case report. Neurosurgery 36:411–412
Lustrin ES, Karakas SP, Ortiz AO, Cinnamon J, Castillo M, Vaheesan K, Brown JH, Diamond AS, Black K, Singh S (2003) Pediatric cervical spine: normal anatomy, variants, and trauma. Radiographics 23:539–560
Mahboubi S, Morris MC (2001) Imaging of spinal infections in children. Radiol Clin North Am 39:215–222
Marani SAD, Canossi GC, Nicoli FA et al. (1990) Hydatid disease: MR imaging study. Radiol 175:701–706
Masaryk TJ (1991) Neoplastic disease of the spine. Radiol Clin North Am 29:829–845
Mendonca RA (2002) Spinal infection and inflammatory disorders. In: Atlas SW (ed) Magnetic resonance imaging of the brain and spine, 3rd ed. Lippincott-Raven, Philadelphia, pp 1854–1969
Morhed AA (1977) Hydatid disease of spine. Neurochirurgia 20:211–215
Mottershed JP, Scmierer K, Clemence M et al. (2003) High field MRI correlates of myelin content and axonal density in MS. J Neurol 250:1293–1301
Nguyen VD, Hersh M (1992) A rare bone tumor in an unusual location: osteoblastoma of the vertebral body. Comput Med Imag Graphics 16:11–16
Orbay T, Ataoglu O, Tali ET et al. (1999) Vertebral osteoblastoma: are radiological structural changes necessary for diagnosis? Surg Neurol 51:426–429
Osborn AG (1994) Tumors, cysts and tumorlike lesions of the spine and spinal cord. In: Osborn AG (ed) Diagnostic neuroradiology. Mosby Publishers, St. Louis, pp 876–918
Ozates M, Ozkan U, Kemaloglu S et al. (2000) Spinal subdural tuberculous abscess. Spinal Cord 38:56–58
Ozek MM (1994) Complications of central nervous system hydatid disease. Pediatr Neurosurg 20:84–91
Parizel PM, Wilmink JT (1998) Imaging of the spine: techniques and indications. In: Algra PR, Valk J, Heimans JJ (eds) Diagnosis and therapy of spinal tumors. Springer-Verlag, Berlin Heidelberg New York, pp 15–48
Post MJ, Quencer RM, Montalvo BM et al. (1988) Spinal infection: evaluation with MR imaging and intraoperative US. Radiology 169:765–771
Ries M, Jones RA, Dousset V et al. (2000) Diffusion tensor MRI of the spinal cord. Magn Reson Med 44:884–892
Robertson RL, Maier SE, Mulkern RV et al. (2000) MR Linescan diffusion imaging of the spinal cord in children. Am J Neuroradiol 21:1344–1348

Robinson RG (1959) Hydatid disease of spine and its neurologic complications. Br J Surg 47:301–306
Ross JS (1996) Discitis, osteomyelitis and epidural abscess. Core curriculum in neuroradiology, part II: neoplasms and infectious diseases, pp 201–206
Rossi A, Tortori-Donati P (2004) Pediatric spinal infections and inflammations Rivista di neuroradiologia 17:322–335
Rothman SL (1996) The diagnosis of infections of the spine by modern imaging techniques. Orthop Clin North Am 27:15–31
Rubinstein LJ (1972) Tumors of the central nervous system: atlas of tumor pathology, series 2, Armed Forces Institute of Pathology, Washington DC, Fascicle 6
Schmorl G, Junghanns H (1971) The human spine in health and disease, 2nd ed. Grune and Sratton, New York, p 325
Sharif HS (1992) Role of MR imaging in the management of spinal infections. Am J Roentgenol 158:1333–1345
Sharif HS, Morgan JL, al Shahed MS et al. (1995) Role of CT and MR imaging in the management of tuberculous spondylitis. Radiol Clin North Am 33:787–804
Siegel MJ (1996) Pediatric sonography. Lippincott-Raven Philadelphia New York
Simon JK, Lazareff JA, Diament MJ et al. (2003) Intramedullary abscess of the spinal cord in children: a case report and review of the literature. Pediatr Inf Dis J 22:186–192
Smith AS, Blaser SI (1991) Infectious and inflammatory processes of the spine. Radiol Clin North Am 29:809–827
Stabler A, Reiser MF (2001) Imaging of spinal infection. Radiol Clin N Am 39:115–135
Stracke P, Pettersson L, Möller-Hartman W et al. (2004) Functional MRI of the spinal cord. Rivista di neuroradiologia1 7:292–300
Stroman PW, Nance PW, Ryner LN (2002) BOLD fMRI of the human cervical spinal cord with stimulation of different sensory dermatomes. Magn Reson Imaging 20:1–6
Swee RG, McLeod RA, Beabout JW (1979) Osteoid osteoma. Radiology 130:117–123
Swischuck LE (1997) Imaging of the newborn, infant, and young child. Williams & Wilkins, Baltimore Philadelphia London
Swischuk LE, John SD, Allbery S (1998) Disk degenerative disease in childhood: Scheuermann's disease, Schmorl's nodes, and the limbus vertebra: MRI findings in 12 patients. Pediatr Radiol 28:334–338
Swischuk LE (2002) Imaging of the cervical spine in children. Springer-Verlag, Berlin Heidelberg New York
Sze G (2002) Neoplastic disease of the spine and spinal cord. In: Atlas SW (ed) Magnetic resonance imaging of the brain and spine, 3rd ed. Lippincott, Philedelphia, pp 1715–1767
Tang HJ, Lin HJ, Liu YC et al. (2002) Spinal epidural abscess experience with 46 patients and evaluation of prognostic factors. J Infect 45:76–81
Tekkok IH, Acikgoz B, Saglam S et al. (1993) Vertebral hemangioma symptomatic during pregnancy: report of a case and review of the literature. Neurosurg 32:302–306
Thurnher M, Bammer R (2004) Diffusion-weighted MRI of the spinal cord in spinal stroke. Rivista di neuroradiologia 17:314–321
Tyrrell PN, Cassar-Pullicino VN, McCall IW (1999) Spinal infection. Eur Radiol 9:1066–1077
Van Tassel P (1994) Magnetic resonance imaging of spinal infections. Top Magn Reson Imaging 6:69–81
Villoria MF, Fortea F, Moreno S et al. (1995) MRI and CT of CNS tuberculosis in the patients with AIDS. Radiol Clin North Am 33:805–819
Wood KB, Garvey TA, Gundry C, Heithoff KB (1995) Magnetic resonance imaging of the thoracic spine. Evaluation of asymptomatic individuals. J Bone Joint Surg 77:1631–1638

Biomechanics

Biomechanics of the Spine

3

Stephen M. Belkoff

CONTENTS

S. M. Belkoff, PhD
Associate Professor and Director, International Center for Orthopedic Advancement, Department of Orthopedic Surgery, Johns Hopkins University / Johns Hopkins Bayview Medical Center, 4940 Eastern Avenue, A674, Baltimore, MD 21224-2780, USA

3.1 Introduction

The purpose of the current chapter is to review the normal mechanics of the spine, i.e., the structure and function of the various components such as discs, vertebral bodies, and spinous ligaments, and to delineate how the normal behavior of these structures is altered by age and various clinical interventions. A growing segment of spine radiology involves not just imaging but musculoskeletal intervention as well. Radiologists now are performing tasks that previously were in the realm of neurosurgery and orthopaedics. Because procedures such as thermal ablation of the disc, vertebroplasty, and kyphoplasty not only address pain relief but also may alter the mechanical behavior of the disc and/or vertebral body, it is important to have a fundamental understanding of the biomechanics of the spine. Knowledge of the normal biomechanics can help the clinician understand the effect a given intervention may have.

3.2 Spine

3.2.1 Structure

The spine is a complex structure that can be divided into five regions: the cervical, thoracic, lumbar, and sacral spines; and the coccyx. Of primary interest are the unfused vertebrae of the cervical through the lumbar regions, although recently the fused vertebrae of the sacrum, especially with regard to insufficiency fractures, have been the subject of increasing clinical interest.

The cervical region has seven vertebrae (C1–C7), which form a lordotic curve. The upper two vertebra are different in design compared with the other un-

KEY POINTS

- Main spinal motions, minor spinal motions:
  - C0–C1: flexion/extension
  - C1–C2: rotation
  - C2–C7: flexion/extension rotation lateral bending
  - T1–T12: flexion/extension rotation lateral bending
  - L1–L5: flexion/extension lateral bending
- Cervical and lumbar lordosis and thoracic kyphosis make the spine function as a spring reducing impact forces
- The spine transmits loads from the upper body through the pelvis into the lower extremities. The anterior center of gravity creates anterior bending and axial compression
- Bone mineral density (BMD) determines compressive strength:
  - Compressive strength ≈ BMD^2
  - BMD < average - 1 SD = osteopenic
  - BMD < average - 2.5 SD = osteoporotic
- Vertebrae:
  - Bear the compressive load
  - Facet joints limit axial rotation
- Disc:
  - Nucleus: hydrophilic mucopolysaccharides – 70 to 90% water
  - Annulus fibrosus: multiple-angled collagen layers
  - Bears the same compressive load as the vertebrae
  - Shock absorber, resists torsion, tensile and shear loads
  - Traumatic disc herniations require not only compressive force but also flexion and lateral bending, and typically occur in the lower lumbar region
- Spinal ligaments:
  - Guide motion and restrict excessive motion
  - Mix of collagen and elastin fibers
  - Ligamentum flavum more elastin = more stretch (up to 100% strain before failure compared with 10 to 15% for most other ligaments)

fused vertebra of the spine. The specialized design permits the unique function of these levels. The atlas (C1) mates with the occiput of the skull, and the space between them allows for flexion and extension but almost no rotation (White and Panjabi 1990). The axis (C2) is below the atlas and, as its name implies, most of the rotation that occurs in the spine occurs through the C1–C2 junction. There is essentially no lateral bending, but some flexion and extension. The remainder of the cervical spine (C3–C7), is fairly flexible, allowing motion in flexion/extension, lateral bending, and rotation (White and Panjabi 1990).

In contrast, the thoracic spine has 12 vertebrae (T1–T12). By virtue of its interaction with the rib cage, the thoracic spine does not allow much flexion/extension or lateral bending, but it does allow for some axial rotation. The curvature of the thoracic spine is naturally kyphotic.

In the lumbar spine, which consists of five vertebrae (L1–L5), the dominant motion is flexion. There is some extension and lateral bending, but almost no rotation. The curvature of the lumbar spine is normally lordotic.

Regardless of the level and type of motion, motion of the spine occurs in the spaces between the vertebrae, i.e., in the disc and at the facet joints.

3.2.2 Function

The spine, which transmits loads from the upper body through the pelvis into the lower extremities, is conceptually divided into three columns: anterior, medial, and posterior columns (Denis 1983). Because the center of gravity of the human body is located anterior to the spinal column, the center of gravity creates a combined load resulting in axial compression and an anterior bending moment (Fig. 3.1). When the spine is in flexion, the instantaneous axis of rotation is generally in the vertebral bodies near the superior endplate (Panjabi et al. 1984). The instantaneous axis of rotation may be considered a fulcrum and, as such, tensile forces must be active posterior to the fulcrum to balance the anterior bending moment caused by the body's center of gravity. The balancing forces are provided

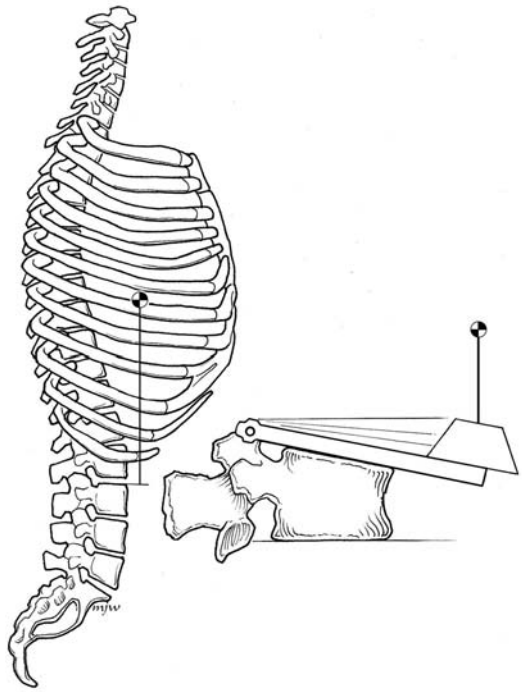

Fig. 3.1. The body's center of mass is located anterior to the spinal column and causes an anterior bending moment on the vertebral bodies. The anterior bending moment creates stresses on the anterior cortex of the vertebral body greater than would be expected from body weight alone

by the paraspinous muscles, posterior ligaments, and the posterior portion of the annulus fibrosis. During anterior flexion (e.g., bending over to tie a pair of shoes), the body's center of gravity moves anteriorly, increasing the bending moment on the spine and the compressive stresses on the anterior column. Bending over to pick up a load not only moves the center of gravity anteriorly, but it also increases the magnitude of the anteriorly located load, which, when combined with the increased moment arm, dramatically increases the compressive stresses on the anterior column. It is this excessive compressive stress that often results in vertebral compression fractures in osteoporotic patients. By definition, vertebral compression fractures exhibit disruption of the anterior column (Denis 1983).

3.2.3 Mechanical Behavior

Compressive vertebral strength is related roughly to the square of the vertebral bone mineral density (BMD) (Lang et al. 1988). When a patient's BMD is 1 standard deviation below the average for the sex-, height-, weight-, and race-matched young (20–30 years old) population, the patient is considered to be osteopenic. A patient with a BMD more than 2.5 standard deviations below that standard is considered osteoporotic (WHO Study Group 1994). In patients with osteoporosis, vertebral BMD might be half of what it was in their youth, which means their vertebral compressive strength may be as low as a one fourth of what it was when they were young. It is not surprising, then, that each year in the United States, more than 700,000 vertebral compression fractures are reported (Riggs and Melton 1995), 300,000–400,000 of which result in hospital admissions.

The lordotic and kyphotic curves of the spine function as a spring, allowing the spine to flex and thereby reduce impact magnitude and increase impulse time compared with what would be the case if the spine were a perfectly straight post. The viscoelastic nature of the spinous ligaments and intervertebral discs increases the impulse time even more, thereby reducing axial impacts.

3.3 Vertebrae

3.3.1 Structure

Except for the first and second cervical vertebrae, all vertebrae share the same basic structure. The roughly cylindrical anterior portion has a thin, hard, cortical shell filled with cancellous bone. The posterior portion, or neural arch, is composed of the pedicles and lamina. This bony ring protects the spinal canal and serves as the foundation for the articular, transverse, and spinous processes. The latter two processes serve as attachment sites of the muscles of the spine. The former process serves as the support for the inferior and superior facet joints.

3.3.2 Function

The primary mechanical function of the vertebrae is to support the axial compression of the body weight. The vertebral body bears most of the compressive

load, but the facets also are involved in resisting axial load. Some researchers report that the facet bears between 3 and 25% of the load (Lorenz et al. 1983; Yang and King 1984), and that if the facet joint is arthritic, it may bear 47% or more (Yang and King 1984). Although the facet joints bear some axial load, they serve to limit relative axial rotation between vertebrae. In fact, intervertebral discs can withstand 22° or more of axial rotation before they fail (Farfan et al. 1970), but the facets limit axial rotation to about 5° to prevent such disc injury (Gregersen and Lucas 1967). The neural arch also protects the spinal cord from injury. The interior of the vertebral body serves to support the endplates by means of the cancellous framework, but it also functions as a vascular space filled with marrow, fat, and blood. Part of the nutrition of the disc is supplied through the endplates.

3.3.3 Mechanical Behavior

Vertebral bodies increase in compressive strength (and size) from C1 to L5 (Brinckmann et al. 1989; Burklein et al. 2001; Moro et al. 1995), probably in response to the higher mechanical demands on the vertebral bodies secondary to the increasing body weight they bear from the superior to the inferior spine. The strength of a given vertebral level is a function primarily of its bone density. In theory, bone strength is a function of the square of the density, but studies have found a wide range of powers (1.2–27; Lotz et al. 1990). Vertebral bodies are strongest along the axis of the spine. In normal vertebral bodies, most of the compressive strength comes from the trabecular bone beneath the endplates. The trabeculae are arranged predominantly in a vertical fashion (as support columns) with some horizontal cross-bracing (Fig. 3.2). The compressive strength of the trabecular structure in the medial–lateral and anterior–posterior directions is approximately half that in the axial direction (Galante et al. 1970). Trabecular compressive strength is greatest in the center of the vertebral body, where it is most needed to resist endplate bending (Keller et al. 1989). The remaining compressive strength of the vertebral body comes from the cortical shell (Rockoff et al. 1969).

3.3.4 Effect of Aging

As the vertebral bodies age, the cortical shell bears a greater share of the load (Rockoff et al. 1969), perhaps as a consequence of the general decrease of cancellous bone associated with osteoporosis, i.e., the cortical shell may bear a greater percentage of the load because there is simply less cancellous bone with which to share the load. Cancellous bone density may also be off-loaded as the disc dehydrates and its health degenerates. Axial load tends to be transmitted through the nucleus pulposus in healthy discs, causing the endplates to deflect. In vertebral bodies with healthy discs that develop compression fractures, the predominant mode is endplate fracture (Rolander and Blair 1975) When the disc degenerates, the load is transmitted through the annulus into the cortical shell, bypassing the cancellous bone. In this instance, the fracture mode is predominantly that of cortical shell

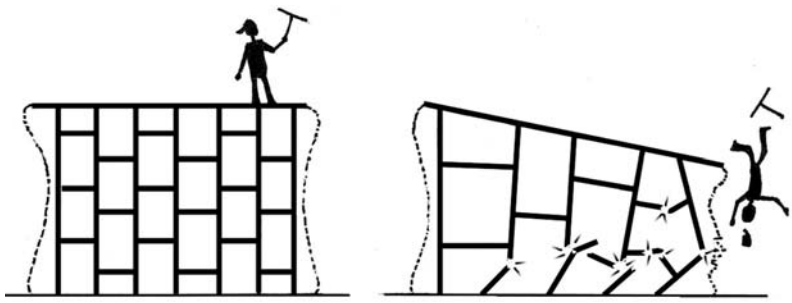

Fig. 3.2. The cancellous interior of each vertebral body functions as a scaffold supporting the endplates (*left*). As the spine becomes osteoporotic, the support columns become fewer and thinner, and there are fewer cross-braces. These changes conspire to weaken the scaffold, placing it at risk for collapse (*right*)

fractures. Because the load apparently is shunted toward the cortex, the lack of mechanical stimulation may encourage the cancellous bone underneath the endplate to resorb.

Bone density generally decreases as a function of aging. Because of the power-law relationship between bone density and strength, if bone density of a vertebral body decreases to half of its young healthy norm, then strength might be a quarter of what it once was in youth.

The bone density of osteoporotic vertebral bodies is at least 2.5 standard deviations below that of their young, sex-, race-, and weight-matched counterparts, as defined by the World Health Organization (Kanis and WHO Study Group 1994; WHO Study Group 1994). In addition to this diminished bone density, the organization of the remaining cancellous bone is altered as the horizontal crossbraces are resorbed (Bell et al. 1967), resulting in long rather than short columns. The load needed to cause a column to buckle is an inverse function of the square of the column length (Fig. 3.2); therefore, if the column's effective length doubles, the load needed to buckle it decreases by a factor of 4.

3.4 Disc

3.4.1 Structure

The disc comprises two major parts: the hydrated gel center (or nucleus pulposus) and the surrounding collagen-rich annulus fibrosus. The nucleus is composed of hydrophilic mucopolysaccharides. Approximately 70–90% of the nucleus is water (Panagiotacopulos et al. 1987). The annulus fibrosus, which wraps around the nucleus, is composed of several layers of fibrous tissue. The orientation of the collagen fibers in each layer (or lamina) is approximately 30° relative to the endplate (Fig. 3.3) (Inoue 1981).

3.4.2 Function

The disc serves many functions. It bears the compressive load of the body's weight above it as well as the resultant compressive load of active muscle contraction during activities of daily living. The disc is a hydrated viscoelastic structure and, as such, dampens the axial loads transmitted through the spine. It serves as a shock absorber between vertebral levels and resists tensile and shear loads that result from spine flexion/extension, lateral bending, and twisting.

3.4.3 Mechanical Behavior

The orientation of the fibers alternates from 30 to –30° with each subsequent layer (Inoue 1981). Presumably, the fiber orientation is an evolutionary optimization that allows the disc to resist torsion, shear, and tension. When the spine is subjected to a compressive load, the nucleus pulposus, which is essentially incompressible because of its high water content, forces the annulus fibrosus laterally. This lateral expansion places the collagen fibers of the annulus in tension to resist the compressive loading to which the composite structure of the disc is subjected. One might expect that severe compression would cause the collagen fibers to rupture and allow the nucleus to prolapse; however, herniation of the nucleus pulposus reportedly does not occur even under high compressive loads alone (Markolf and Morris 1974; Virgin 1951). Traumatic disc herniation requires a combined compressive load with flexion and lateral bending (Adams and Hutton 1982). In that study, discs prone to such injury typically were in the lower lumbar region, from the 40- to 49-year-old subgroup of donors, and had some apparent disc degeneration.

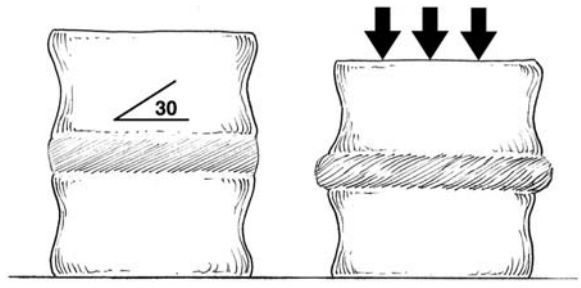

Fig. 3.3. The annulus fibrosis is composed of layers of collagen fibers. The collagen fibers are oriented at either 30 or –30° relative to the endplate. The orientation alternates with each successive layer (*left*). When a load is placed on the vertebral body, the hydrated nucleus pulposus becomes pressurized and pushes laterally against the annulus (*right*)

Discs, like other collagenous soft tissue structures of the body, are viscoelastic, i.e., the material behavior of the structure depends not only on the stress or strain that is applied, but also on the time period over which it is applied. When a disc is subjected to a compressive load, the disc will compress instantly, but it also will continue to compress until it reaches some equilibrium level. This compressive deformation as a function of time is called creep. The amount of creep deformation is a function of the load magnitude, the time period over which the load is applied, and the degree of degeneration of the disc. Degenerated discs creep more and creep more quickly than do healthy hydrated discs (Kazarian 1975), suggesting that degenerated discs lose some of their viscoelasticity and, therefore, some of their shock absorption characteristics. Viscoelasticity imparts a damage tolerance to tissues. If tissues are stressed or strained at high rates, their apparent modulus and failure strength increase and their ability to absorb energy increases.

3.5 Spinal Ligaments

3.5.1 Structure

The ligaments of the spine are composed of collagen and elastin fibers enmeshed in a hydrated gel. The relative amounts of collagen to elastin fibers dictates the mechanical response of a given ligament. For example, the ligamentum flavum, which runs from the lamina of one vertebral body to the lamina of the adjacent vertebral body, has the highest elastin content of all spinal ligaments. The high elastin-to-collagen content allows the ligament to stretch when the spine is in full flexion. Most ligaments fail at approximately 10–15% strain, but some, such as the ligamentum flavum and supraspinous ligament in the lumbar spine, reportedly withstand strains as high as 100% until failure (Fig. 3.4) (Pintar et al. 1992).

3.5.2 Function

Spinal ligaments, like other ligaments of the body, are tasked with connecting one bone to another – in this case, one vertebral body to another. They guide joint motion and permit flexibility of the spine without allowing excessive motion that would place the spinal cord at risk for injury. By tethering the vertebral bodies together, the spinal ligaments relieve the muscles about the spine of some of the burden of maintaining stability.

3.5.3 Mechanical Behavior

The ligaments exhibit nonlinear viscoelastic behavior. Because the dry weight of ligaments primarily is composed of collagen fibers, ligaments are designed to resist tension. They have no inherent resistance to compression, and they buckle easily. The low modulus response of ligaments in the "toe" region, the initial part of the stress-strain curve, allows the spine to be flexible without the need for spinous muscle to expend much energy overcoming ligament resistance. As the spine is placed in more extreme positions, the ligaments are stretched. As the ligament as a whole is stretched, the collagen fibers, which are generally wavy in the relaxed state, become straightened. Sequential straightening of the fibers increases the apparent modulus of the ligament. In this manner, the ligaments' resistance to stretching dramatically increases. If spinal motion continues, the ligaments are stretched further into the linear region of the stress-vs-strain curve. In this region, practically all of the collagen fibers have been straightened in an

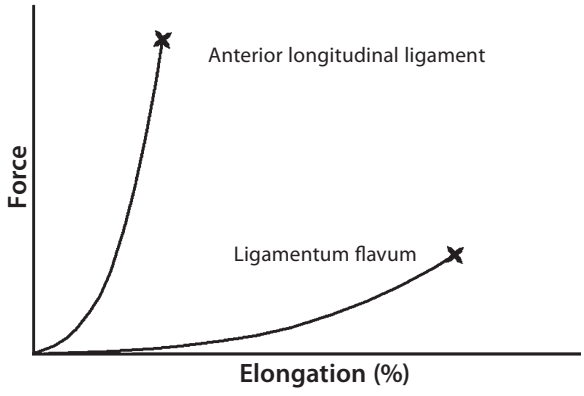

Fig. 3.4. The structure and function of ligaments are determined by the job each ligament needs to perform. Ligaments that need to be relatively strong and stiff, such as the anterior longitudinal ligament, have a high collagen to elastin ratio, whereas ligaments that need to be flexible, such as the ligamentum flavum, contain large percentages of elastin

attempt to prevent any further motion. If additional motion occurs, collagen fiber will rupture, resulting in a loss of stiffness, damage to the ligament, and eventual failure. Because ligaments are viscoelastic, the apparent strength and stiffness of a ligament is increased dramatically if the stretching rate is rapid (Fig. 3.5).

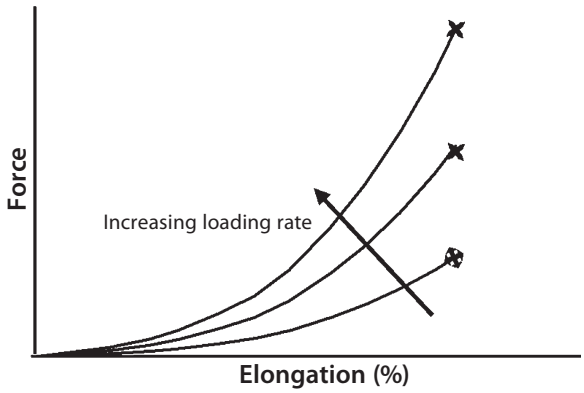

Fig. 3.5. Ligaments are viscoelastic and, as such, increase their apparent stiffness and strength when the rate at which they are loaded increases. They also are able to absorb more energy. These characteristics prevent damage during impact loading, such as typically happens with traumatic events

References

Adams MA, Hutton WC (1982) Prolapsed intervertebral disc. A hyperflexion injury. 1981 Volvo Award in Basic Science. Spine 7:184–191

Bell GH, Dunbar O, Beck JS et al. (1967) Variations in strength of vertebrae with age and their relation to osteoporosis. Calcif Tissue Res 1:75–86

Brinckmann P, Biggemann M, Hilweg D (1989) Prediction of the compressive strength of human lumbar vertebrae. Spine 14:606–610

Burklein D, Lochmuller EM, Kuhn V et al. (2001) Correlation of thoracic and lumbar vertebral failure loads with in situ vs ex situ dual energy X-ray absorptiometry. J Biomech 35:579–587

Denis F (1983) The three column spine and its significance in the classification of acute thoracolumbar spinal injuries. Spine 8:817–831

Farfan HF, Cossette JW, Robertson GH et al. (1970) The effects of torsion on the lumbar intervertebral joints: the role of torsion in the production of disc degeneration. J Bone Joint Surg 52A:468–497

Galante J, Rostoker W, Ray RD (1970) Physical properties of trabecular bone. Calcif Tissue Res 5:236–246

Gregersen GG, Lucas DB (1967) An in vivo study of the axial rotation of the human thoracolumbar spine. J Bone Joint Surg 49A:247–262

Inoue H (1981) Three-dimensional architecture of lumbar intervertebral discs. Spine 6:139–146

Kanis JA, WHO Study Group (1994) Assessment of fracture risk and its application to screening for postmenopausal osteoporosis: synopsis of a WHO report. Osteoporos Int 4:368–381

Kazarian LE (1975) Creep characteristics of the human spinal column. Orthop Clin North Am 6:3–18

Keller TS, Hansson TH, Abram AC et al. (1989) Regional variations in the compressive properties of lumbar vertebral trabeculae. Effects of disc degeneration. Spine 14:1012–1019

Lang SM, Moyle DD, Berg EW et al. (1988) Correlation of mechanical properties of vertebral trabecular bone with equivalent mineral density as measured by computed tomography. J Bone Joint Surg 70A:1531–1538

Lorenz M, Patwardhan A, Vanderby R Jr (1983) Load-bearing characteristics of lumbar facets in normal and surgically altered spinal segments. Spine 8:122–130

Lotz JC, Gerhart TN, Hayes WC (1990) Mechanical properties of trabecular bone from the proximal femur: a quantitative CT study. J Comput Assist Tomogr 14:107–114

Markolf KL, Morris JM (1974) The structural components of the intervertebral disc. A study of their contributions to the ability of the disc to withstand compressive forces. J Bone Joint Surg 56A:675–687

Moro M, Hecker AT, Bouxsein ML et al. (1995) Failure load of thoracic vertebrae correlates with lumbar bone mineral density measured by DXA. Calcif Tissue Int 56:206–209

Panagiotacopulos ND, Pope MH, Bloch R et al. (1987) Water content in human intervertebral discs. Part II. Viscoelastic behavior. Spine 12:918–924

Panjabi MM, Krag MH, Dimnet JC et al. (1984) Thoracic spine centers of rotation in the sagittal plane. J Orthop Res 1:387–394

Pintar FA, Yoganandan N, Myers T et al. (1992) Biomechanical properties of human lumbar spine ligaments. J Biomech 25:1351–1356

Riggs BL, Melton LJ III (1995) The worldwide problem of osteoporosis: insights afforded by epidemiology. Bone 17:505S–511S

Rockoff SD, Sweet E, Bleustein J (1969) The relative contribution of trabecular and cortical bone to the strength of human lumbar vertebrae. Calcif Tissue Res 3:163–175

Rolander SD, Blair WE (1975) Deformation and fracture of the lumbar vertebral end plate. Orthop Clin North Am 6:75–81

Virgin WJ (1951) Experimental investigations into the physical properties of the intervertebral disc. J Bone Joint Surg 33B:607–611

White AA III, Panjabi MM (1990) Kinematics of the spine. In: Clinical biomechanics of the spine, 2nd edn. Lippincott, Philadelphia, pp 85–125

WHO Study Group (1994) Assessment of fracture risk and its application to screening for postmenopausal osteoporosis. Report of a WHO Study Group. World Health Organ Tech Rep Ser 843:1–129

Yang KH, King AI (1984) Mechanism of facet load transmission as a hypothesis for low-back pain. Spine 9:557–565

Scoliosis

4

Johan W. M. Van Goethem and Anja Van Campenhout

CONTENTS

4.1 Introduction

The normal human spine has a series of curves in the sagittal plane, including a cervical lordosis that averages, depending on the end points, 20–50° (C2–C7) or 30–70° (C1–T1), a thoracic kyphosis averaging 30–35° (T5–T12), and a lumbar lordosis averaging 50–60° (T12–S1). The normal cervical lordosis is a circular arc.

In the frontal plane the normal load-bearing spine is straight. Scoliosis is defined as a deviation from the midline in a frontal plane. A small deviation (< 10°) is sometimes called spinal asymmetry, whereas "true" scoliosis has a deviation of ≥10°. This deviation is accompanied by a rotation that is maximally at the apex of the curve. In the thoracic region this rotation creates an asymmetry of the thoracic cage that produces the typical chest wall prominence known as the Adams sign.

Imaging in scoliosis is very important. Most cases of scoliosis are idiopathic and imaging is used routinely in monitoring the changes of the deformity that take place during growth. Imaging is also crucial in determining the underlying etiology in non-idiopathic cases of scoliosis. Finally, imaging is used in pre- and postoperative monitoring (Table 4.1).

Generally, scoliosis is treated by orthopedic surgeons with special training in spinal and pe-

J. W. M. Van Goethem, MD, PhD
Department of Radiology, University Hospital Antwerp, Wilrijkstraat 10, 2650 Edegem, Belgium
and
Department of Radiology, AZ Nikolaas, Moerlandstraat 1, 9100 Sint-Niklaas, Belgium
A. Van Campenhout, MD
Department of Orthopaedics, University Hospitals Leuven, Pellenberg, Weligerveld 1, 3212 Pellenberg, Belgium

Table 4.1. Indications for imaging in scoliosis

Routine use in monitoring the changes of the deformity that take place during growth
Determining the underlying etiology in non-idiopathic cases of scoliosis
Pre- and postoperative monitoring

KEY POINTS

- Scoliosis is defined as a deviation of the spine of ≥10° in the frontal plane
- Scoliosis may be either:
  - Congenital: most frequent congenital spinal deformity
  - Idiopathic: most frequent form (80%)
  - Associated with generalized diseases and syndromes
  - Traumatic
  - Degenerative: develops after age 50 years
- Classification:
  - Etiology
  - Curve location, according to the location of the apical (most lateral) vertebra or disc:
    - Cervical: C2–C6
    - Cervicothoracic: C7–T1
    - Thoracic: T2–T11
    - Thoracolumbar: T12–L1
    - Lumbar: L2–L4
    - Lumbosacral (L5 and below)
  - Age at onset:
    - Infantile: 0–3 years
    - Juvenile: 4–10 years
    - Adolescent: 11–17 years
    - Adult: ≥18 years
  - Curve type:
    - Primary vs secondary curves
    - Structural vs non-structural curves
    - Curve pattern: Lenke classification (see Fig. 4.5)
- Prevalence: 0.5–3% in the childhood and adolescent population, large curves (>30°) in <0.3%
- Clinical features:
  - Usually no discomfort in mild curves (<25°)
  - Cardiopulmonary complications in early onset (<5 years old)
- Congenital and juvenile idiopathic scoliosis are usually progressive
- Imaging
  - Screening: upright PA radiograph: minimize radiation thoroughly! No lateral film in screening
  - When surgical treatment is considered: PA, lateral, and lateral bend films
  - Measurements: Cobb angle
  - MRI is required in:
    - Infantile and juvenile idiopathic scoliosis
    - Congenital bony anomalies
    - Scoliosis associated with specific neurological or cutaneous abnormalities
    - In adolescent scoliosis with severe pain, a left thoracic curve, and/or an abnormal neurological examination
- Treatment:
  - Braces: in growing children with curves greater than 25–30° or progression of >5°/year
  - Surgery: curves >45° with remaining spinal growth

diatric problems; however, patients with scoliosis may present themselves directly to the radiology department through a primary health care physician, or they may be referred from the pediatric, neurology, or neurosurgery services. Many of these physicians look toward the radiologist as the spinal expert; therefore, radiologists should know the basics of scoliosis, how to perform the radiological examination, how to read these films correctly, and how to make a coherent and helpful interpretation.

4.2 Etiology

4.2.1 Congenital Scoliosis

Congenital scoliosis is the most frequent congenital spinal deformity (Fig. 4.1). It is present at birth as the result of embryological or intrauterine maldevelopment of vertebral elements; these may be caused by either failure of formation or failure of

Fig. 4.1. A 5-year-old boy with Klippel-Feil syndrome type 2. Klippel-Feil syndrome occurs in a heterogeneous group of patients unified only by the presence of a congenital defect in the formation or segmentation of the cervical spine (Tracy et al. 2004). Numerous associated abnormalities of other organ systems may be present. It is unclear whether Klippel-Feil syndrome is a discrete entity, or if it is one point on a spectrum of congenital spinal deformities. As a consequence of these fusion and segmentation anomalies, this boy has a congenital cervical and thoracic scoliosis. Klippel-Feil type 1 shows massive fusion of cervical and upper thoracic vertebrae. Type 2 shows fusion of a limited number of vertebrae and hemivertebrae. Occipitoatlantal fusion, as in this case (*long arrow*), and other lower thoracic anomalies, are present. Type 3 shows both cervical fusions and lower thoracic or lumbar fusions. C2–C3 fusion, also present in this case (*short arrow*), is the most common form of congenital fused cervical vertebrae and is probably dominant with variable expression. This boy furthermore shows hemivertebrae and unilateral fused vertebrae (*arrowheads*).

segmentation. They are commonly associated with cardiac or urological abnormalities that develop during the same period (before 48 days of gestation). Vertebral maldevelopment can be classified as defects of segmentation and/or defects of formation. Curve progression is strongly related to the type of vertebral abnormality with the poorest prognosis for unilateral unsegmented bars with contralateral hemivertebrae (up to 10°/year progression), a less severe progression in cases of hemivertebrae or double hemivertebrae (1–2.5 and 2–5°/year, respectively; Fig. 4.2) and a least severe progression in patients with block and wedge vertebrae (< 1°/year progression).

4.2.2 Idiopathic Scoliosis

Most frequently scoliosis is idiopathic (80%). Substantial research efforts have identified several factors contributing to the development of idiopathic scoliosis.

Genetic factors are a potential etiological component in the development of scoliosis. Studies suggest a multigene dominant inheritance pattern with variable phenotypic expression. Several candidate regions have been identified including on chromosomes 6p, distal 10q, 17p11, 18q and 19p13. Family members of affected individuals have an increased incidence of scoliosis. Studies in families with twins have identified 73–92% concordance in monozygotic

Fig. 4.2. Shaded-surface display (SSD) 3D reformation of a multirow detector CT (MDCT) in a patient with congenital thoracic scoliosis with wedge vertebrae and hemivertebrae. Curve progression is strongly related to the type of vertebral abnormality with the poorest prognosis for unilateral unsegmented bars with contralateral hemivertebrae (up to 10°/year progression), a less severe progression in cases of hemivertebrae or double hemivertebrae (1–2.5 and 2–5°/year, respectively), as in this case, and a least severe progression in patients with block and wedge vertebrae (< 1°/year progression). Associated rib anomalies are not infrequent.

twins and only 36–63% concordance in dizygotic twins. The prevalence of scoliosis increases seven times in individuals with affected siblings and three times in those with affected parents.

Tissue deficiencies in bone, muscle, ligament, and/or disc may lead to scoliosis. For example, adolescent idiopathic scoliosis may be related to osteopenia in some patients.

Vertebral growth anomalies may also be related to adolescent idiopathic scoliosis, as described in the following:

1. Differential growth rates between left and right sides of the spine may lead to asymmetry that could be accentuated by the so-called Heuter-Volkmann effect (suppression of growth on the concave side of the curve). When anterior spinal growth outpaces posterior growth in the adolescent, hypokyphosis is produced with subsequent buckling of the vertebral column.
2. Scoliotic spines in girls between 12 and 14 years have longer thoracic vertebral bodies, shorter pedicles, and a larger interpedicular distance compared with normal aged-matched spines (Guo et al. 2003). The differential growth between the anterior and posterior elements is not only significantly different in scoliosis vs normal spines, but is also correlated to the severity of scoliosis. This overgrowth in length occurs mainly by enchondral ossification, whereas circumferential growth is slower and happens by membranous ossification.
3. Compared with others, adolescents with scoliosis are taller, thinner, and have an increased level of growth hormone.
4. Finally, central nervous system disorders may result in scoliosis. Several factors have been identified that correlate with a higher incidence in scoliosis, such as equilibrium and vestibular dysfunction, melatonin deficiency, syringomyelia, Chiari malformation, and spinal tumors.

4.2.3 Scoliosis in Generalized Diseases and Syndromes

Neuromuscular disorders (e.g., cerebral palsy, muscular dystrophy) and some generalized diseases and syndromes (e.g., Marfan, neurofibromatosis, rheumatoid disease, or bone dysplasia) are associated with scoliosis (Fig. 4.3).

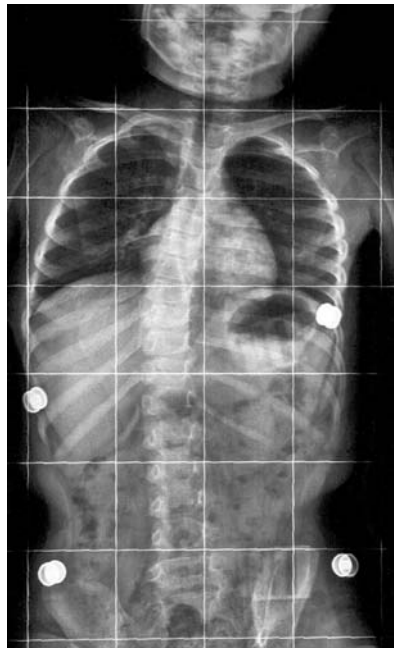

Fig. 4.3. Scoliosis is commonly associated with a variety of neuromuscular disorders including conditions affecting upper and lower motor neurons as well as myopathies. This 5-year-old boy with a neuromuscular dystrophy was unable to stand, and in these cases spinal imaging can be accomplished lying down or, preferably, sitting, as in this case.

4.2.4 Traumatic Scoliosis

Traumatic scoliosis can be caused either by bony lesions (fractures, dislocations) or by soft tissue lesions (e.g., burns, postempyema).

4.2.5 Degenerative Scoliosis

Degenerative lumbar scoliosis is a lateral deviation of the spine that typically develops after age 50 years (Tribus 2003). This is the type-1 adult scoliosis, a primary degenerative scoliosis, mostly on the basis of a disc and/or facet joint arthritis, affecting those structures asymmetrically. Type-2 adult scoliosis is the progression of adolescent scoliosis in adulthood, whereas type-3 adult scoliosis is a secondary scoliosis mostly on the basis of osteoporosis (Aebi 2005). Although the clinical presentation may vary, degenerative scoliosis is usually associated with loss of lordosis, axial rotation, lateral listhesis, and spon-

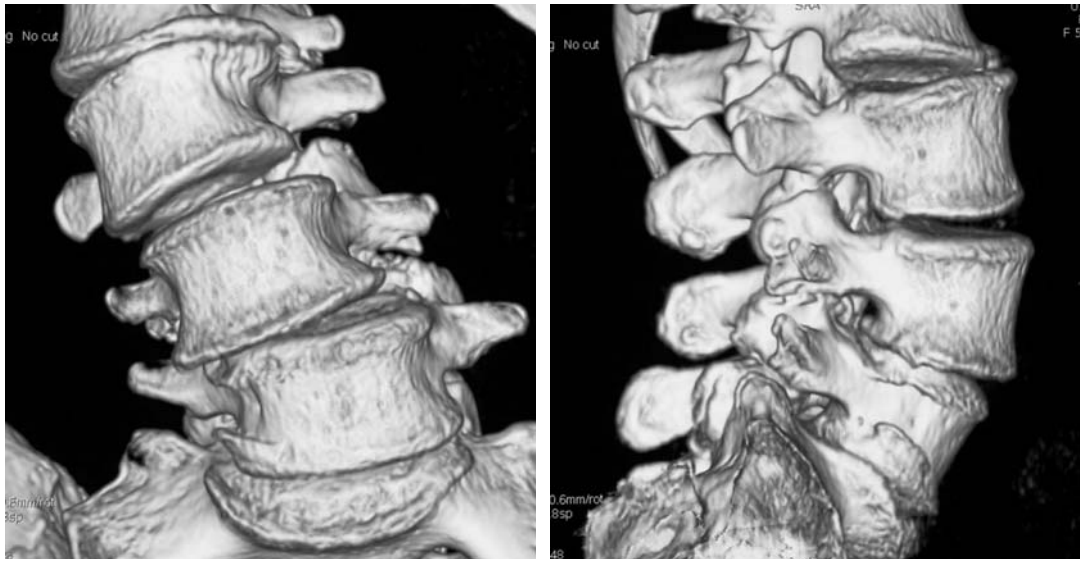

a b

Fig. 4.4a,b. Degenerative lumbar scoliosis is a lateral deviation of the spine that typically develops after age 50 years (Tribus 2003). It is also known as type-1 or primary adult scoliosis. It is usually associated with loss of lordosis, axial rotation, lateral listhesis, and spondylolisthesis (**a**). It is associated with degenerative disk and facet disease and hypertrophy of the ligamenta flava, typically leading to neurogenic claudication, foraminal narrowing (**b**), and back pain.

dylolisthesis (Fig. 4.4). It is associated with degenerative disk and facet disease and hypertrophy of the ligamenta flava, typically leading to neurogenic claudication and back pain. Rarely, sagittal or coronal imbalance may develop.

4.3 Classification

Scoliosis can be classified according to (a) etiology, (b) curve location, (c) age at onset, and (d) curve type.

Curve location is defined by its center, known as the apex, which is the most lateral disc or vertebra of the curve. Usually the apical vertebra is also the most horizontal. As such scoliosis can be classified as cervical (apex between C2 and C6), cervicothoracic (C7–T1), thoracic (T2–T11), thoracolumbar (T12–L1), lumbar (L2–L4), and/or lumbosacral (L5 and below).

Age at onset – or rather diagnosis – is used to classify scoliosis as follows: (a) infantile (0–3 years); (b) juvenile (4–10 years); (c) adolescent (11–17 years); and (d) adult (≥18 years).

Different classifications exist according to curve type:

1. Spinal asymmetry (< 10°), mild scoliosis (10–25°). and severe scoliosis (> 25°)
2. Primary curves are the first to develop. Secondary curves develop afterwards as a means to balance the head and trunk over the pelvis, not only in the frontal but also in the sagittal plane. At the time of diagnosis it is not always possible to differentiate primary curves from secondary curves.
3. Structural curves (as opposed to nonstructural curves) cannot be corrected with side bending or traction. Nonstructural curves can be secondary curves or functional curves (postural, secondary to short leg, muscle spasm, etc.).

The use of these classification schemes is important as a means of common communication between various scoliosis practitioners to have the ability to compare various treatments of similar curve patterns and as a method of recommending selective fusions of the spine when appropriate. The most widely used classification developed by Moe and reported by King et al. (1983), the King-Moe classification, was designed primarily to decide when to instrument the thoracic curve alone, and when to instrument both the thoracic and lumbar curves. This classification, however, is not comprehensive, and a more complete and reliable classification was proposed by Lenke et al. (2001; Fig. 4.5; Table 4.2). The Lenke classification considers three compo-

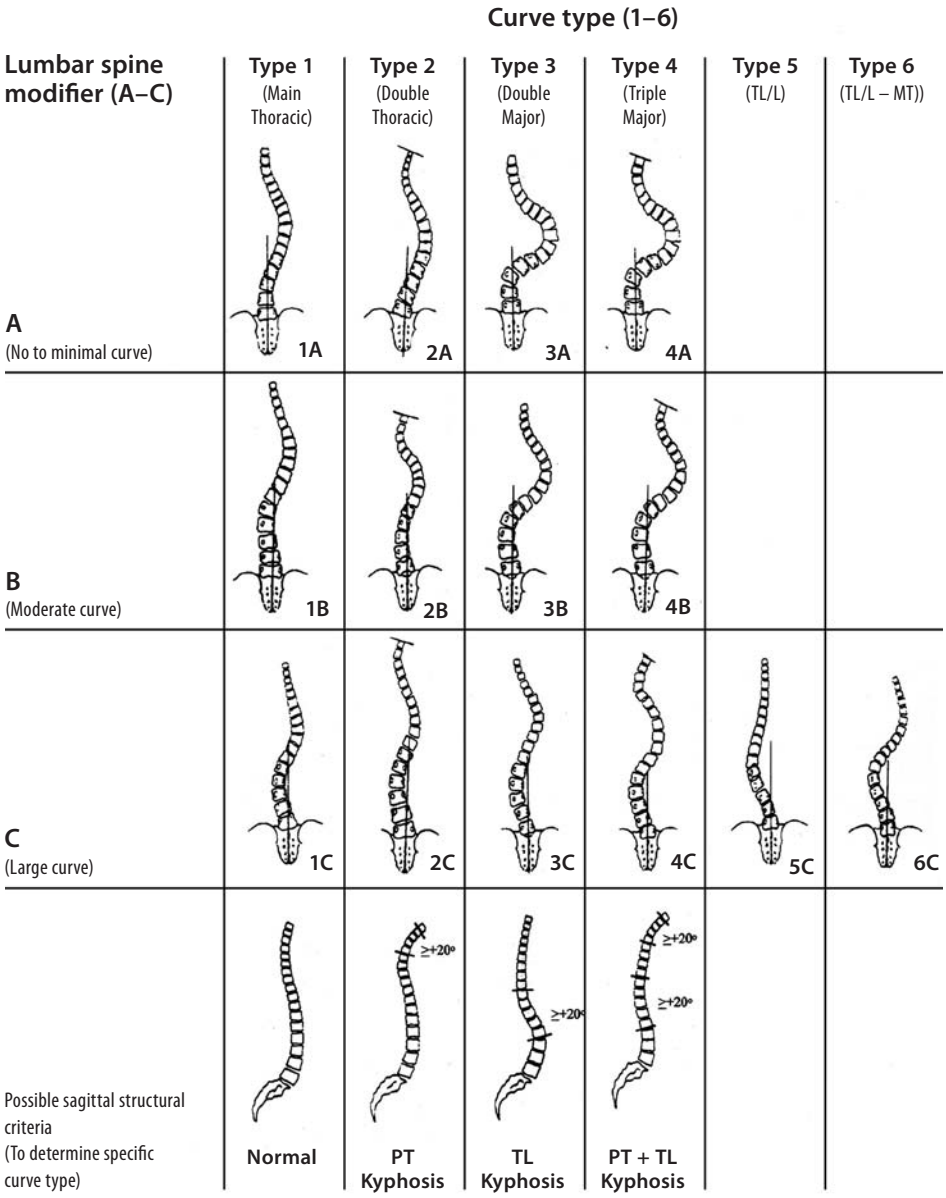

Fig. 4.5. Lenke classification of scoliosis. The Lenke classification considers three components: curve type (*1–6*), a lumbar spine modifier (*A*, *B*, or *C*), and a sagittal thoracic modifier (-, *N*, or +). The six curve types have specific characteristics, on frontal and sagittal radiographs, that differentiate structural and nonstructural curves in the proximal thoracic (*PT*), main thoracic (*MT*), and thoracolumbar/lumbar regions (*TL/L*). The major curve is the one with the largest Cobb measurement and will always be included in fusion surgery for idiopathic adolescent scoliosis. The minor curves are all other non-major curves present. One of the main debates in scoliosis surgery is whether to include those minor curves in the fusion or not; thus, six curve types are distinguished in this system based on whether the PT, MT, and TL/L regions are major, minor structural, or nonstructural including: type 1, MT; type 2, double thoracic; type 3, double major; type 4, triple major; type 5, TL/L; and type 6, TL/L-MT (Lenke et al. 2003). The lumbar spine modifier is based on the relationship of the center sacral vertical line to the apex of the lumbar curve, and the sagittal thoracic modifier is based on the sagittal curve measurement from the fifth to the twelfth thoracic level. A minus sign represents a curve of < 10°, *N* represents a curve of 10–40°, and a plus sign represents a curve of > 40°. (With permission from Lenke 2005)

Table 4.2. Classification of scoliosis according to Lenke et al. (2003). *PT* proximal thoracic, *MT* main thoracic, *TL/L* thoracolumbar/lumbar, *DM* double major, TM triple major

Curve type	PT	MT	TL/L	Description
1	NS	S	NS	MT
2	S	S	NS	DT
3	NS	S	S	DM
4	S	S	S	TM
5	NS	NS	S	TL/L
6	NS	S	S	TL/L – MT

Classification of curve types in adolescent idiopathic scoliosis according to Lenke et al. (2001): Curve types 1–6 are determined by the regional structural characteristics of the proximal thoracic (PT), main thoracic (MT), and thoracolumbar/lumbar (TL/L) regions

Type 1, main thoracic: The main thoracic curve is the major curve, and the proximal thoracic and thoracolumbar/lumbar curves are minor nonstructural curves

Type 2, double thoracic: The main thoracic curve is the major curve, whereas the proximal thoracic curve is minor and structural and the thoracolumbar/lumbar curve is minor and nonstructural.

Type 3, double major: The main thoracic and thoracolumbar/lumbar curves are structural, whereas the proximal thoracic curve is nonstructural. The main thoracic curve is the major curve and is greater than, equal to, or no more than 5° less than the Cobb measurement of the thoracolumbar/lumbar curve

Type 4, triple major: The proximal thoracic, main thoracic, and thoracolumbar/lumbar curves are all structural; either of the two latter curves may be the major curve

Type 5, thoracolumbar/lumbar: The thoracolumbar/lumbar curve is the major curve and is structural. The proximal thoracic and main thoracic curves are nonstructural

Type 6, thoracolumbar/lumbar-main thoracic: The thoracolumbar/lumbar curve is the major curve and measures at least 5° more than the main thoracic curve, which is structural. The proximal thoracic curve is nonstructural

nents: curve type (1–6); a lumbar spine modifier (A, B, or C); and a sagittal thoracic modifier (–, N, or +). The six curve types have specific characteristics, on frontal and sagittal radiographs, that differentiate structural and nonstructural curves in the proximal thoracic (PT), main thoracic (MT), and thoracolumbar/lumbar regions (TL/L). The major curve is the one with the largest Cobb measurement and will always be included in fusion surgery for idiopathic adolescent scoliosis. The minor curves are all other non-major curves present. One of the main debates in scoliosis surgery is whether to include those minor curves in the fusion or not; thus, six curve types are distinguished in this system based on whether the PT, MT, and TL/L regions are major, minor structural, or nonstructural including: type 1, MT; type 2, double thoracic (DT); type 3, double major (DM); type 4, triple major (TM); type 5, TL/L; and type 6, TL/L-MT (Lenke et al. 2003). The lumbar spine modifier is based on the relationship of the center sacral vertical line to the apex of the lumbar curve, and the sagittal thoracic modifier is based on the sagittal curve measurement from the fifth to the twelfth thoracic level. A minus sign represents a curve of less than 10°, N represents a curve of 10–40°, and a plus sign represents a curve of more than 40°.

4.4 Prevalence

The prevalence of scoliosis (≥10°) in the childhood and adolescent population is between 0.5 and 3.0%. Adolescent idiopathic scoliosis is present in 2–4% of children between 10 and 16 years of age. Larger curves (> 30°) are reported to be between 0.04 and 0.29%. In childhood scoliosis, 0.5% is reported in the infantile group, 10% in the juvenile group, and the remainder in the adolescent group.

4.5 Clinical Features

There is no difference in the prevalence of back pain or mortality between patients with untreated adolescent idiopathic scoliosis and the general population. Patients with mild idiopathic scoliosis (< 25°) usually have no or only very little discomfort. Cardiopulmonary complications are almost exclusively seen in early onset scoliosis (< 5 years old).

Patients presenting with severe pain, neurological symptoms, or rapidly progressing scoliosis require thorough further examination.

In North America and Europe a screening examination in school often leads to a first referral for scoliosis. The goal of school screening programs is to detect childhood scoliosis at a stage where surgical correction can be avoided.

Different specific clinical tests are available to assess scoliosis. The forward-bend test, or Adams test, is probably the best known. In this test the patient bends forward with the knees straight and the palms together. During this test the thoracic and lumbar regions should stay symmetric. An asymmetric rotational hump of 5–7° (angle of trunk rotation, ATR) is associated with a scoliosis of 15–20°. A referral and imaging is recommended when the ATR is > 7°. This is a sensitive, although not very specific test (2–3% referral).

4.6 Natural History

4.6.1 Congenital Scoliosis

Congenital scoliosis shows progression in 75% of cases. The poorest prognosis is that for thoracic curves and those with multiple hemivertebrae and a convex unilateral bar (failure of segmentation) opposite the hemivertebrae. Block and wedge vertebrae show progression < 1°/year, hemivertebrae show a mean progression of 1–2.5°/year, double hemivertebrae increase at a double rate, and unilateral unsegmented bars with contralateral vertebrae may progress up to 10°/year. The management of congenital scoliosis requires frequent clinical and radiographic follow-up to detect progression. Curve progression or severe vertebral anomalies known to cause curve progression require prompt treatment to prevent deformity and morbidity such as thoracic insufficiency syndrome (Kose and Campbell 2004).

4.6.2 Infantile Idiopathic Scoliosis

Infantile idiopathic scoliosis presents as a left thoracic curve in 90% of cases. The male:female ratio is 3:2. The vast majority of these curves are self-limiting. The few curves that do progress, usually double structural curves, can be difficult to manage. In cases where the rib vertebral angle difference (RVAD) is larger than 20°, progression is very likely. The RVAD is defined as the difference in angulation of the left and right ribs on the apical vertebra as measured on an anteroposterior (AP) radiograph.

4.6.3 Juvenile Idiopathic Scoliosis

The male:female ratio is 1:2 to 1:4, with boys being more affected between 3 and 6 years (1:1), and girls between 6 and 10 years (1:8). The number of right and left curves is equal in the younger group (< 6 years at presentation) and right curves predominate in the older group (80%). This type of scoliosis is often progressive (70%). Potential for trunk deformity with cardiac and pulmonary compromise exists especially in scoliosis with onset before 5 years of age. Curves of > 30° are almost always progressive, at a rate of 1–3°/year before age 10 years and at a rate of 4.5–11°/year after that age. If the scoliosis is in the thoracic region, surgery is required in > 95% of these cases.

4.6.4 Adolescent Idiopathic Scoliosis

For minor curves the male:female ratio is equal, but for larger curves the ratio is as high as 1:8. Approximately 2% of adolescents have scoliosis (> 10°), but only 5% of these have a progression of the curve to > 30°. Right thoracic curves are the most progressive. In the major left thoracic and lumbar scoliosis, initial minor curves progress faster than major curves. The progression of scoliosis is dependent on the growth velocity and the magnitude of the curve at the first visit. Progression is most notable with a growth velocity of > 2 cm/year, at ages between 9 and 13 years, bone ages between 9 and 14 years, Risser signs 0–1 (see also 4.7.3), and between 0.5–2 years before menarche (Ylikoski 2005).

4.6.5 Adult Idiopathic Scoliosis

Curves of < 30° usually show no progression. Curves measuring 30–50° at skeletal maturity progress an average of 10–15° during a normal lifetime. Curves between 50 and 75° show a continuing rate of nearly 1°/year. In untreated patients an increased mortality rate due to cardiopulmonary disorders is almost only seen in scoliosis of > 90°.

4.6.6 Risk Factors for Progression

The main risk factors for curve progression are a large curve magnitude, skeletal immaturity, and female gender. Skeletal immaturity or remaining skeletal growth is determined by age, menarchal status, and Risser sign (radiological) (see also 4.7.3) or Tanner staging (clinical). A Risser < 1 is associated with progression in 60–70% of patients, whereas Risser 3 has a risk for progression in < 10% of cases. Curve pattern has also been identified as an important variable for predicting the probability of progression. Primary thoracic curve scoliosis progresses more than primary lumbar curve scoliosis. The larger the curve, the more progression can be expected. Finally, in infantile scoliosis right-sided thoracic curves in females have a worse progression.

4.7 Imaging in Scoliosis

4.7.1 Plain Film Imaging Technique

The ideal imaging modality for screening in scoliosis is the upright posteroanterior (PA) radiograph of the entire spine. The head and pelvis should be on the same film. The patient must be standing, but in young patients or patients with severe neuromuscular disorders a sitting or even supine radiograph may be the only possibility (Fig. 4.3). In general, no attempt should be made to equalize differences in leg length. A lateral film is not required as a part of the screening examination.

Radiographic techniques should be used to minimize radiation of sensitive organs (breast, thyroid, ovaries, bone marrow, lens, etc.). It is imperative that radiation-lowering techniques be used judiciously to minimize the radiation burden. In a recent study of 5466 women, who received an average of 24.7 X-rays with a mean estimated cumulative radiation dose to the breast of 10.8 cGy (range 0–170), the risk of breast cancer was found to be 70% higher than in women in the general population (Morin et al. 2000). There were 77 breast cancer deaths among the patients, compared with 46 expected deaths based on U.S. mortality rates. Risk increased significantly with increasing number of radiograph exposures and with cumulative radiation dose. A posterior-to-anterior technique reduces radiation to the breast three to sevenfold compared with an anterior-to-posterior technique. If breast shielding is used, care should be taken so that automatic exposure systems do not increase the radiation dose accordingly.

A further decrease in radiation dose can be accomplished using the so-called air-gap technique. This technique was first described by Lindblom (1934). In clinical practice, it was soon superseded by the use of antiscatter grids; however, air gaps are still used in, for example, lung examinations, and compare favorably with the use of grids in pediatric radiology. Moreover, the introduction of digital radiography is likely to create a new interest in the air-gap technique (Persliden and Carlsson 1997). With air-gap and computed radiology techniques the mean effective dose can be reduced by a factor 10 (Hansen et al. 2003).

At least when surgical treatment is considered, lateral bend radiographs and a lateral film should be acquired (Fig. 4.6). Bend films aid in deciding what levels should be included in the instrumentation. Lateral bending is usually performed as a standing PA film, but in some institutions supine AP films are used. The Stagnara oblique view is taken perpendicularly to the rib prominence and shows a more accurate picture of large curves with a true magnitude of the scoliosis.

Several studies have used 3D techniques to evaluate idiopathic scoliosis. These studies have showed that although the deformity of the spine is three-dimensional, the regional deformity is almost always two-dimensional, but in a plane different from the standard frontal or sagittal views.

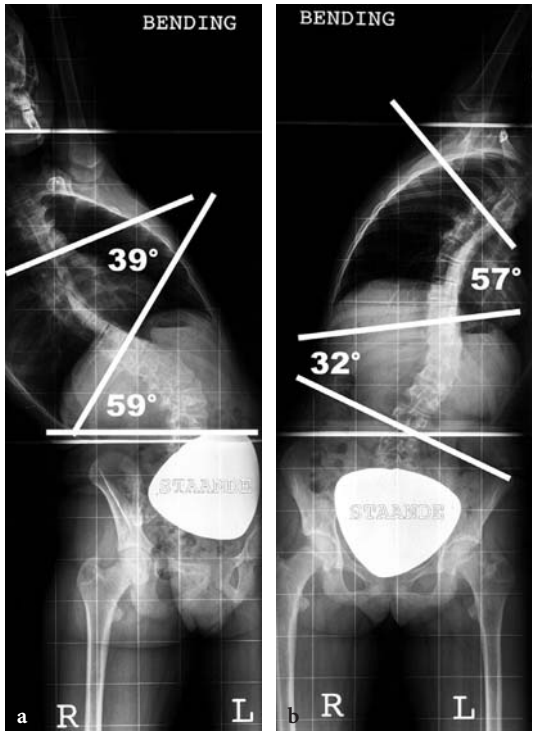

Fig. 4.6a,b. Lateral bend films in a young girl as a preoperative assessment. In this case lateral bending shows a reduced mobility at the level of the thoracic curve which consequently was instrumented

4.7.2 Imaging Interval

Follow-up is necessary in those patients with severe curves that are at risk for significant curve progression or require some form of treatment. Idiopathic curves of less than 25° should be monitored every 4–12 months, depending on the age and growth rate of the patient (Fig. 4.7). Curves of >30° should be monitored for progression after skeletal maturity every 5 years.

4.7.3 Measurements

Curve measurement is usually performed by the Cobb method (Fig. 4.8). The caudal and cranial end vertebrae of a scoliosis are the most tilted in a frontal plane. A line parallel to the superior end plate of the cranial end vertebra and a line parallel to the inferior end plate of the caudal end vertebra are drawn first (on film or digitally on a diagnostic workstation). Then perpendiculars to both these lines are drawn and the angle is measured where these lines cross. A Cobb angle is measured for each curve that

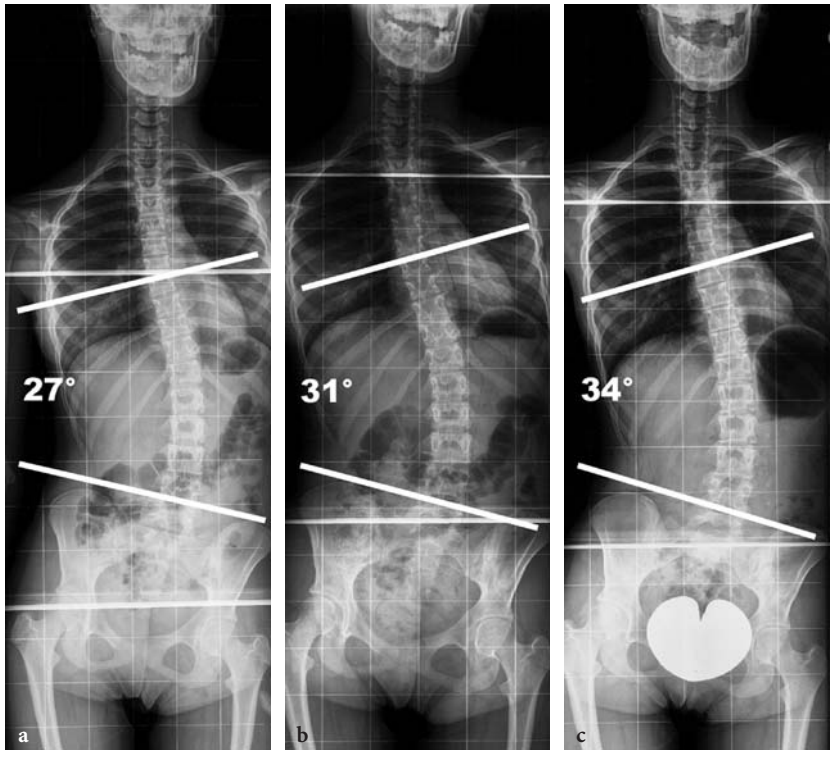

Fig. 4.7a–c. Three posteroanterior films in the same 12-year-old girl at 6-month intervals. This right thoracolumbar curve progresses by 3–4° every 6 months. Note that Cobb angles are measured from the same end vertebrae in each consecutive control

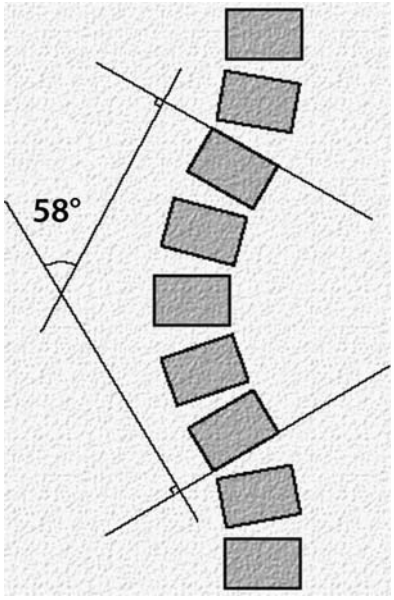

Fig. 4.8. Curve measurement is usually performed by the Cobb method. The caudal and cranial end vertebrae of a scoliosis are the most tilted in a frontal plane. A line parallel to the superior end plate of the cranial end vertebra and a line parallel to the inferior end plate of the caudal end vertebra are drawn first. Then perpendicular lines to both these lines are drawn and the angle is measured where these lines cross. A Cobb angle is measured for each curve that is present. When comparing different radiographs the end vertebrae usually remain the same, although corrections might be needed over time

is present. When comparing different radiographs the end vertebrae usually remain the same, although corrections can be needed over time. One should understand that there is a wide inter- and intra-observer variation with this technique, usually on the order of 5°.

Cobb angle measurements are done on AP radiographs; however, because of the associated vertebral rotation, these are not true AP views of the rotated spinal segment. Cobb angle measurements can increase by >20% when measured on these true-AP views (Gocen and Havitcioglu 2001); therefore, in the follow-up of scoliosis, consistent patient positioning is of utmost importance.

For surgeons it is important to recognize the important decrease of curves both in the frontal and sagittal plane due to prone positioning, anesthesia, and exposure during surgery. When patients resume their standing position a "spring-back" effect is noted in the sagittal plane with loss of correction (Delorme et al. 2000).

Alternatively, and much less frequently used compared with the Cobb angle measurement, the Ferguson method measures the angle between lines drawn from the centers of the end vertebrae to the center of the apical vertebra/disc.

As a result of the increased appreciation of the three-dimensional nature of scoliosis and modern spinal instrumentation's improved corrective capabilities, there has been renewed interest in the correction and measurement of vertebral rotation (Kuklo et al. 2005). Vertebral rotation is maximal at the apex of the curve and can be quantified by different methods, all of which are fairly inaccurate. Computed tomography is limited in its clinical utility owing to cost, radiation exposure, and the effects of postural changes on scoliosis curves and consequently vertebral rotation; therefore, and because of their simplicity, the Perdriolle (Perdriolle 1979) and Nash-Moe (Nash and Moe 1969) techniques remain the standard measurements for providing a reasonable estimate of pre- and postoperative vertebral rotation.

On lateral films sagittal balance can be assessed. Normal sagittal balance is the alignment of C7 to the posterior superior aspect of the sacrum. The sagittal plumb line, as drawn from center of C7, should be ±2 cm from the sacral promontory. Thoracic kyphosis depends mostly on the spinal deformity, whereas lumbar lordosis is influenced mainly by the pelvic configuration. The scoliotic curve type is not associated with a specific pattern of sagittal pelvic morphology and balance (Mac-Thiong et al. 2003). Positive sagittal balance, i.e., an anterior deviation of the C7 plumb line, is more significantly associated with pain and disability than curve magnitude, curve location, or coronal imbalance (Glassman et al. 2005).

Skeletal maturity is usually assessed using the Risser sign (Fig. 4.9). The lateral to medial ossification of the iliac crest occurs in a predictable fashion over an 18- to 24-month period. Risser 0 is the absence of ossification, stages 1–4 correspond to partial ossification, and Risser 5 indicates the fusion of the fully ossified apophysis to the ilium. Another useful landmark is the status of the triradiate cartilage of the acetabulum. This usually closes before Risser 0, at the stage of maximal spinal growth.

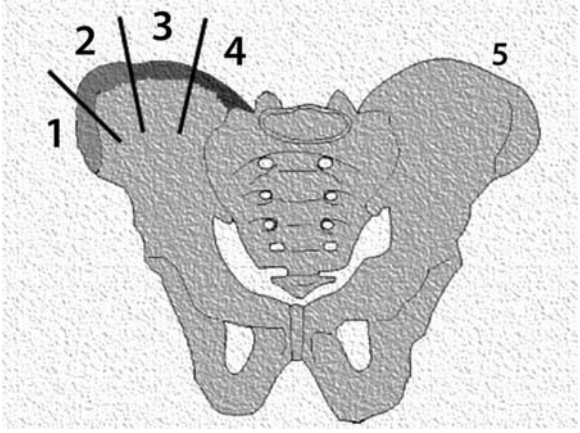

Fig. 4.9. The lateral to medial ossification of the iliac crest occurs in a predictable fashion over an 18- to 24-month period. Risser 0 is the absence of ossification, stages *1–4* correspond to partial ossification, and Risser *5* indicates the fusion of the fully ossified apophysis to the ilium

4.7.4 Specialized Imaging

Computed tomography (CT), especially multirow detector CT (MDCT), is the best method for visualization of complex scoliotic deformities. In general, it is used in cases of computer-assisted surgery (CAS), since it is known that the placement of pedicles screws on the concavity in the apical region of thoracic curves can be critical because of small endosteal pedicle width (Liljenqvist et al. 2000), where it can assist in pedicle screw placement. Computed tomography is also useful for defining abnormalities and for picking up previously unrecognized anomalies in patients with congenital scoliosis (Newton et al. 2002). The excision of hemivertebra is a technically challenging procedure and can be performed as an AP procedure or an isolated posterior procedure, and the use of CT is very helpful in the operative planning of these patients (Hedequist and Emans 2003). Most surgeons prefer MDCT with 3D reconstructions over planar CT in the pre-operative depiction of congenital scoliosis (Bush and Kalen 1999).

Magnetic resonance imaging (MRI) is required in: (a) infantile and juvenile idiopathic scoliosis; (b) congenital bony anomalies; and (c) scoliosis associated with specific neurological or cutaneous abnormalities.

The prevalence of neural axis abnormalities, both in infantile and juvenile idiopathic scoliosis with a curve of more than 20°, is approximately 20% (Dobbs et al. 2002). These abnormalities include Chiari malformations, syringomyelia, and, less frequently, spinal or brain tumors. In adolescent idiopathic scoliosis MRI should be considered in case any of the following warning signs are present (Reamy and Slakey 2001): (a) severe pain; (b) a left thoracic curve; or (c) an abnormal neurological examination.

A more recent study indicates that pain as a sole indicator is not a reliable for detecting pathology (Davids et al. 2004). Atypical curve pattern most frequently is the only indicator of abnormal MRI findings. This includes left thoracic curve, short segment scoliosis (four to six levels), decreased vertebral rotation, absence of thoracic apical segment lordosis, and rapid progression (Davids et al. 2004). Other curve patterns are also associated with an increased incidence of neural axis abnormalities, including left thoracic, double thoracic, triple, and a long right thoracic curve with end vertebra caudal to T12, and with a high or low apex and/or end vertebra, especially in males and patients with a normal to hyperkyphotic thoracic spine (Spiegel et al. 2003). Patients with severe curves despite skeletal immaturity and an abnormal neurological examination have a significant probability of neurogenic lesions (Morcuende et al. 2004) (Table 4.3).

Spinal cord abnormalities are seen in 3% of patients with adolescent idiopathic scoliosis and include mainly syringomyelia and, less frequently, Chiari malformations (Hausmann et al. 2003). Whether pre-operative MRI in all patients with adolescent idiopathic scoliosis is routinely indicated remains controversial (Do et al. 2001; Hausmann et al. 2003). The role of specialized imaging in extremely severe scoliosis remains unclear. The MR screening of all patients with scoliosis is not indicated.

Table 4.3. Curves associated with neurogenic lesions: indications for magnetic resonance imaging

Left thoracic curve
Double thoracic
Triple
Short-segment scoliosis (four to six levels)
Decreased vertebral rotation
Absence of thoracic apical segment lordosis
Rapid progression
Long right thoracic curve with end vertebra caudal to T12, and with a high or low apex and/or end vertebra
Severe curves despite skeletal immaturity

4.8 Treatment

4.8.1 Non-Operative Treatment (Braces)

In growing children a spinal orthosis (brace) is indicated when a curve progresses to 25–30°. Also lesser curves, but with an annual growth of more than 5°, are an indication for bracing. Only in patients with substantial remaining spinal growth (Risser 3 or less) are braces used. The upper limit of curves manageable with braces is 45°. Even in the most cooperative patients the final result of brace treatment is the maintenance of the curve degree at the level of the start of bracing. Braces should be used 23 h/day, usually for several years, until the curve is stabilized. Generally, the brace should be worn at night until skeletal maturity is reached (Risser 5 or no spinal growth for 18 months). Curve progression can be limited to $<5°$ in 75% of patients, compared with 35% in a comparable non-treated group.

4.8.2 Surgical Treatment

In general, curves $>45°$ in patients with remaining spinal growth should be corrected surgically. Corrective instrumentation (rods) in combination with arthrodesis (strength) is the best method for achieving long-term results.

The typical posterior spinal approach comprises the Harrington instrumentation. It consists of a distraction rod with hooks at either end and a threaded compression rod attached to the transverse processes on the convex side of the curve. This original concept corrected scoliosis at the cost of a decreased thoracic kyphosis. This system was subsequently modified with different systems.

The Cotrel-Dubousset system is more recent (1980s) and uses a multihook concept that allows distraction and compression on the same rod (Fig. 4.10). Many of these systems can be attached with hooks, wires, and/or pedicle screws.

Anterior spinal instrumentation is a newer technique with several systems on the market [Dwyer, Zielke, Texas Scottish Rite Hospital (TSRH), Kaneda, etc.]. Initially it was primarily used for the correction of lumbar or thoracolumbar scoliosis, but it is presently also utilized in the thoracic region. It can also be helpful in a combination anterior and posterior approach, especially for curves $>75°$, and also in younger patients.

The correct surgical technique depends on the curve pattern as explained previously. For example, in the idiopathic right thoracic curve pattern (Lenke type 1) posterior spinal instrumentation and fusion of the thoracic curve is common. The segment to be fused should be as short as possible, yet long enough to minimize residual imbalance or progression. The lowest hook is attached above the level where the central vertical sacral line bisects the spine. Shorter fusions are possible with anterior instrumentation, including all vertebrae in the measured Cobb angle. In a double thoracic curve (Lenke type 2) instrumentation is often extended up to T1 or T2. Different schemes exist for other patterns.

Although instrumentation generally achieves good to excellent improvement of the Cobb angle, there are conflicting reports on the long-term functional results such as low back pain. Complications

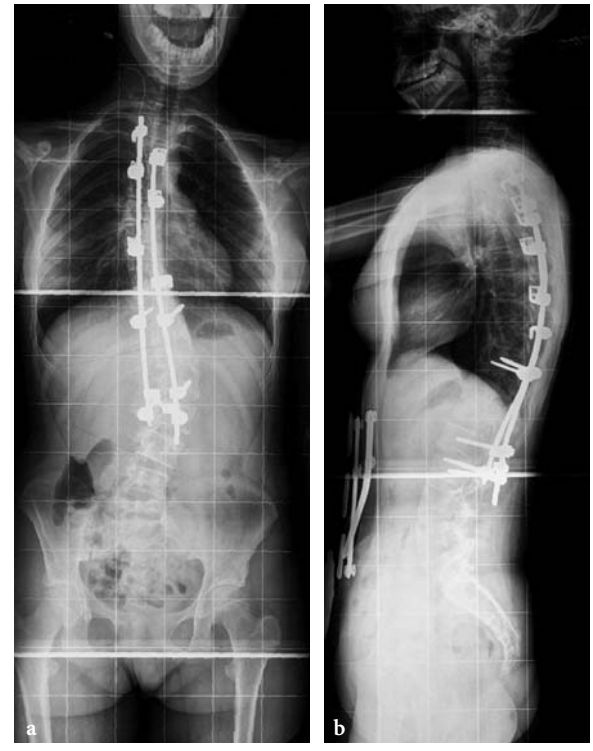

Fig. 4.10a,b. Same patient as in Figure 4.7. Instrumentation with a mix of rods with pedicle screws and hooks. This Cotrel-Dubousset system is fairly recent (1980s) and uses a multihook concept that allows distraction and compression on the same rod. Many of these systems can be attached with hooks, wires, and/or pedicle screws

range from blood loss over hardware failures to neurological injury.

In congenital scoliosis the curves tend to be short with little flexibility and do not show substantial response to brace treatment. Progressive congenital scoliosis is therefore generally treated with surgery.

References

Aebi M (2005) The adult scoliosis. Eur Spine J 14:925–948

Bush CH, Kalen V (1999) Three-dimensional computed tomography in the assessment of congenital scoliosis. Skeletal Radiol 28(11):632–637

Davids JR, Chamberlin E, Blackhurst DW (2004) Indications for magnetic resonance imaging in presumed adolescent idiopathic scoliosis. J Bone Joint Surg Am 86-A(10):2187–2195

Delorme S, Labelle H, Poitras B et al. (2000) Pre-, intra-, and postoperative three-dimensional evaluation of adolescent idiopathic scoliosis. J Spinal Disord 13(2):93–101

Do T, Fras C, Burke S et al. (2001) Clinical value of routine preoperative magnetic resonance imaging in adolescent idiopathic scoliosis. A prospective study of three hundred and twenty-seven patients. J Bone Joint Surg Am 83-A(4):577–579

Dobbs MB, Lenke LG, Szymanski DA et al. (2002) Prevalence of neural axis abnormalities in patients with infantile idiopathic scoliosis. J Bone Joint Surg Am. 84(12):2230–2234

Glassman SD, Bridwell K, Dimar JR (2005) The impact of positive sagittal balance in adult spinal deformity. Spine 15 30(18):2024–2029

Gocen S, Havitcioglu H (2001) Effect of rotation on frontal plane deformity in idiopathic scoliosis.Orthopedics 24(3):265–268

Guo X, Chau WW, Chan YL, Cheng JC (2003)Relative anterior spinal overgrowth in adolescent idiopathic scoliosis. Results of disproportionate endochondral-membranous bone growth. J Bone Joint Surg Br 85(7):1026–1031

Hansen J, Jurik AG, Fiirgaard B et al. (2003) Optimisation of scoliosis examinations in children. Pediatr Radiol 33:752–765

Hausmann ON, Boni T, Pfirrmann CW et al. (2003) Preoperative radiological and electrophysiological evaluation in 100 adolescent idiopathic scoliosis patients. Eur Spine J 2(5):501–506

Hedequist DJ, Emans JB (2003) The correlation of preoperative three-dimensional computed tomography reconstructions with operative findings in congenital scoliosis. Spine 15 28(22):2531–2534

King HA, Moe JH, Bradford DS, Winter RB (1983) The selection of fusion levels in thoracic idiopathic scoliosis. J Bone Joint Surg Am 65(9):1302–1313

Kose N, Campbell RM (2004) Congenital scoliosis. Med Sci Monit 10(5):104–110

Kuklo TR, Potter BK, Lenke LG (2005) Vertebral rotation and thoracic torsion in adolescent idiopathic scoliosis: What is the best radiographic correlate? J Spinal Disord Tech 18(2):139–147

Lenke LG (2005) Lenke classification system of adolescent idiopathic scoliosis: treatment recommendations. Instr Course Lect 54:537–542

Lenke L, Betz R, Harms J et al. (2001) Adolescent idiopathic scoliosis: a new classification to determine extent of spinal arthrodesis. J Bone Joint Surg Am 83A: 1169–1181

Lenke LG, Edwards CC 2nd, Bridwell KH (2003) The Lenke classification of adolescent idiopathic scoliosis: how it organizes curve patterns as a template to perform selective fusions of the spine. Spine 15 28(20):S199–S207

Liljenqvist UR, Link TM, Halm HF (2000) Morphometric analysis of thoracic and lumbar vertebrae in idiopathic scoliosis. Spine 15 25(10):1247–1253

Lindblom K (1934) Secondary screening by means of filtering. Acta Radiol 15 620–627

Mac-Thiong JM, Labelle H, Charlebois M et al. (2003) Sagittal plane analysis of the spine and pelvis in adolescent idiopathic scoliosis according to the coronal curve type. Spine 1 28(13):1404–1409

Morcuende JA, Dolan LA, Vazquez JD et al. (2004) A prognostic model for the presence of neurogenic lesions in atypical idiopathic scoliosis. Spine 1 29(1):51–58

Morin Doody M, Lonstein JE, Stovall M et al. (2000) Breast cancer mortality after diagnostic radiography: findings from the U.S. Scoliosis Cohort Study. Spine15 25(16):2052–2063

Nash C, Moe J (1969) A study of vertebral rotation. J Bone Joint Surg 51:223–229

Newton PO, Hahn GW, Fricka KB et al. (2002) Utility of three-dimensional and multiplanar reformatted computed tomography for evaluation of pediatric congenital spine abnormalities. Spine 15 27(8):844–850

Pedriolle R (1979) La Scoliose, Maloine. SA editeur Paris

Persliden J, Carlsson GA (1997) Scatter rejection by air gaps in diagnostic radiology. Calculations using a Monte Carlo collision density method and consideration of molecular interference in coherent scattering. Phys Med Biol 42 155–175

Reamy BV, Slakey JB (2001) Adolescent idiopathic scoliosis: review and current concepts. Am Fam Phys 1 64 (1):111–116

Spiegel DA, Flynn JM, Stasikelis PJ et al. (2003) Scoliotic curve patterns in patients with Chiari I malformation and/or syringomyelia. Spine 15 28(18):2139–2146

Tracy MR, Dormans JP, Kusumi K (2004) Klippel-Feil syndrome: clinical features and current understanding of etiology. Clin Orthop Relat Res (424):183–190

Tribus CB (2003) Degenerative lumbar scoliosis: evaluation and management. J Am Acad Orthop Surg 11(3):174–183

Ylikoski M (2005) Growth and progression of adolescent idiopathic scoliosis in girls. J Pediatr Orthop B 14(5):320–324

Degenerative Disease

Evidence-Based Medicine for Low Back Pain

5

Maurits van Tulder and Bart Koes

CONTENTS

5.1 Introduction

During the last decade, the importance of evidence-based medicine has steadily gained ground. Sackett, in his landmark book published in 1997, defined evidence-based medicine as 'conscientious, explicit and judicious use of current best evidence in making decisions about care of individual patients' (Sackett 1997). The evidence may refer to new or existing interventions and to preventive, diagnostic or therapeutic interventions. Sackett suggested five steps on how individual care providers can practice evidence-based medicine: (1) ask clinical questions that you can answer, (2) search for the best evidence, (3) critically appraise the evidence, (4) apply the evidence in care for your patient, and (5) self-evaluation (of the above steps). Although this seems very reasonable, it is probably impossible for individual care providers to search for and critically appraise the evidence. At present, there are more than 2 million new articles published every year. It will be impossible for individual care providers to find all relevant studies on a specific clinical topic and to critically appraise these studies. Most care providers will lack time to perform comprehensive literature searchers and lack adequate methodological skills to conduct the critical appraisal. Systematic reviews help care providers overcoming these problems. Reviews in which all available studies have been critically appraised and summarized in a systematic, transparent and reproducible way are probably the best available source of evidence. Clinical guidelines that have been based on such systematic reviews may further help in closing the gap between research and practice.

Many randomized controlled trials (RCTs) have been conducted and published on conservative and complementary treatments for non-specific low back pain. A substantial number of systematic reviews have also been published, in which the evidence from these trials have been summarized (van Tulder and Koes 2003a,b). Recently, the evidence from trials and reviews have formed the basis for clinical practice guidelines on the management of low back pain that have been developed in various countries around the world (Koes et al. 2001). This chapter on evidence-based medicine for low back pain provides an overview of the evidence on diagnosis and treatment of non-specific low back pain and summarizes how this evidence has been translated into guideline recommendations. The chapter will start with defining low back pain.

M. van Tulder, MD, PhD
Institute for Research in Extramural Medicine (EMGO), VU University Medical Center and Institute for Health Sciences, Faculty of Earth & Life Sciences, Van der Boechorststraat 7, 1081 BT Amsterdam, The Netherlands
B. Koes, PhD
Department of General Practice, Erasmus MC-University Medical Center Rotterdam, Burgemeester Oudlaan 50, 3062 PA Rotterdam, The Netherlands

KEY POINTS

- Evidence-based medicine (EBM)
  - Definition: 'conscientious, explicit and judicious use of current best evidence in making decisions about care of individual patients' (Sackett 1997)
  - Many randomized controlled trials (RCTs) exist on conservative and complementary treatments for non-specific low back pain (LBP)
  - Many systematic reviews have been published, in which the evidence from these trials has been summarized
  - The evidence from these trials and reviews has formed the basis for clinical practice guidelines on the management of LBP
- Low back pain (LBP)
  - Definition: pain, muscle tension, or stiffness localized below the costal margin and above the inferior gluteal folds, with or without leg pain (sciatica)
  - May be classified as:
    - 'Specific'
      - +/– 10% of the patients
      - Symptoms caused by a specific pathophysiologic mechanism (e.g., HNP, infection, fracture, etc.)
    - 'Non-specific'
      - Vast majority of patients (up to 90%)
      - Symptoms without clear specific cause
      - Good prognosis; patients usually recover within weeks
      - Weak correlation with imaging abnormalities; many people without symptoms also show these abnormalities
      - According to duration classified as acute, subacute, or chronic (different management strategies)
- "Red flags"
  - Diagnosis of non-specific LBP is made by excluding specific causes
  - Based on patient's age and history, standard history taking (distribution and severity of the pain, relation with time and posture, etc.), and a standard physical examination (including a neurological examination) patients are categorized into three groups, so-called diagnostic triage
    - Serious spinal pathology
    - Nerve root pain/radicular pain
    - Non-specific LBP
  - Initial examination also makes it possible to outline a specific management strategy that matches the magnitude of the problem and may serve as a basis for credible information to the patient regarding diagnosis, management, and prognosis and may help in reassuring the patient
- EBM and history taking:
  - Poor sensitivity and specificity for radiculopathy and ankylosing spondylitis
  - Relatively high diagnostic accuracy for the combination of history and erythrocyte sedimentation rate in vertebral cancer
- EBM and physical examination:
  - High sensitivity, but low specificity for straight leg raising in the diagnosis of nerve root pain
  - Studies do not enable a valid evaluation of diagnostic accuracy of the straight leg raising test
- EBM and diagnostic imaging:
  - X-ray findings (disc space narrowing, osteophytes, and sclerosis) are associated with non-specific LBP
  - Spondylolysis/listhesis, spina bifida, transitional vertebrae, spondylosis, and Scheuermann's disease did not appear to be associated with LBP
  - No evidence is found on the association between degenerative signs at the acute stage and the transition to chronic symptoms
  - Diagnostic imaging (radiography, CT, MRI, and isotope studies)
    - Does not improve treatment of LBP in adults younger than 50 years of age with no signs or symptoms of systemic disease
    - Plain radiography and simple laboratory tests can almost completely rule out underlying systemic diseases in patients 50 years of age and older or those whose findings suggest systemic disease
    - Advanced imaging should be reserved for patients who are considering surgery or those in whom systemic disease is strongly suspected

- Systemic review on conservative treatment for acute and subacute LBP:
  - Faster recovery when advised to stay active or visiting back schools
  - Faster return to work in a multidisciplinary treatment setting
  - Better short-term pain relief for muscle relaxants and spinal manipulation
- In patients with chronic LBP, systemic review on conservative treatment options demonstrated:
  - Better pain relief with the use of antidepressants and back schools
  - Moderate positive effect for behavioral therapy
- Clinical guidelines (on treatment of acute LBP)
  - Should ensure that patients are treated according to the best available evidence and should lead to optimal patient outcomes
  - May differ from one country to another (possibly related to differences in health care systems, differences in membership of guidelines committees, etc.)
  - Aims at:
    - Providing adequate information, reassuring the patient that LBP is usually not a serious disease and that rapid recovery is expected
    - Providing adequate symptom control, if necessary
    - Recommending staying as active as possible and returning to normal activities early, including work. Most guidelines do not recommend routine use of passive treatment modalities (bed rest, electrotherapy, and massage, etc.) as single treatment. Most guidelines also do not recommend referral to secondary health care and routine X-ray examination
  - "COST B13"
    - European guidelines for the prevention, diagnosis, and treatment of non-specific low back pain
    - Ensuring an evidence-based approach through the use of systematic reviews and existing clinical guidelines
    - Enabling a multidisciplinary approach; stimulating collaboration between primary health care providers and promoting consistency across providers and countries in Europe
    - Promoting implementation of these guidelines across Europe
    - European guidelines are available on www.backpaineurope.org for:
      - 1. Acute low back pain
      - 2. Chronic low back pain
      - 3. Prevention of low back pain
      - 4. Pelvic girdle pain

5.2 Low Back Pain

Low back pain is usually defined as pain, muscle tension, or stiffness localized below the costal margin and above the inferior gluteal folds, with or without leg pain (sciatica). Low back pain is typically classified as being 'specific' or 'non-specific'. Specific low back pain refers to symptoms caused by a specific patho-physiologic mechanism, such as hernia nucleus pulposus (HNP), infection, inflammation, osteoporosis, rheumatoid arthritis, fracture or tumor. Only in about 10% of the patients specific underlying diseases can be identified (Deyo et al. 1992). The vast majority of patients (up to 90%) are labeled as having non-specific low back pain, which is defined as symptoms without clear specific cause, i.e., low back pain of unknown origin. Spinal abnormalities on plain film and MR imaging are not strongly associated with non-specific low back pain, because many people without any symptoms also show these abnormalities (Jensen et al. 1994; van Tulder et al. 1997a).

Non-specific low back pain is usually classified according to duration as acute (less than 6 weeks), subacute (between 6 weeks and 3 months) or chronic (longer than 3 months) (Frymoyer 1988). In general, prognosis is good and most patients with an episode of non-specific low back pain will recover within a couple of weeks. However, back pain among primary care patients is often a recurrent problem

with fluctuating symptoms. The majority of back pain patients will have experienced a previous episode and acute exacerbations of chronic low back pain are common (von Korff and Saunders 1996). The management of acute, subacute and chronic low back pain differs.

5.3 Diagnosis

The diagnosis of non-specific low back pain is based on the exclusion of relevant specific causes. When searching for specific causes, the physician should first focus on features of serious spinal pathology (so called red flags, Table 5.1). Such pathology may be suspected primarily on the basis of history and physical examination and can be confirmed with additional diagnostic procedures. However, in most cases of acute low back pain it is not possible to arrive at a diagnosis based on detectable pathological changes. Several classification systems of diagnosis have been suggested, in which low back pain is categorized based on, for example, pain distribution, pain behavior, functional disability, and clinical signs. However, none of these systems of classification have been critically validated. A simple and practical classification, which has gained international acceptance, divides acute low back pain into three categories – the so-called diagnostic triage:

Table 5.1. 'Red flags': warning signs and symptoms indicating an increased likelihood of serious spinal pathology

• Age of onset <20 or >55 years
• Violent trauma
• Constant progressive, non mechanical pain (no relief with bed rest)
• Thoracic pain
• Past medical history of malignant tumor
• Prolonged use of corticosteroids
• Drug abuse, Immunosuppression, HIV
• Signs of systemic disease
• Unexplained weight loss
• Widespread neurology (including cauda equina syndrome)
• Structural deformity
• Fever

- Serious spinal pathology
- Nerve root pain/radicular pain
- Non-specific low back pain

The priority in the examination procedure follows this line of clinical reasoning. Firstly, the patient's age and history should be considered. Secondly, a standard history taking should include considering the distribution and severity of the pain and the relation with time and posture. Thirdly, a standard physical examination is conducted including inspection of posture and movement, and local anatomical derangements, assessment of spinal tenderness on percussion over the spinal processes, or axial pressure and palpation of the abdomen. In some patients nerve root disorders may be suspected on the basis of pain distribution and pattern. Then, provocation of pain on coughing, sneezing or straining, weakness, sensory loss and miction disturbance (decreased feeling during urinary passage, incontinence) should be asked for. Also, the diagnostic process should include a neurological examination looking for typical radiating pain in the leg during straight leg raising (SLR), and anteflexion, paresis (at least requesting the patient to walk on toes and heels), and reflex disturbance.

The initial examination also serves other important purposes besides reaching a 'diagnosis'. Through a thorough history taking and physical examination, it is possible to evaluate the degree of pain and functional disability. This enables the health care professional to outline a management strategy that matches the magnitude of the problem. Finally, the careful initial examination serves as a basis for credible information to the patient regarding diagnosis, management and prognosis and may help in reassuring the patient.

5.3.1 History Taking

One systematic review of nine studies evaluated the accuracy of history in diagnosing low back pain in general practice (van den Hoogen et al. 1995). The review found that history taking does not have a high sensitivity and high specificity for radiculopathy and ankylosing spondylitis. The combination of history and erythrocyte sedimentation rate had a relatively high diagnostic accuracy in vertebral cancer.

5.3.2 Physical Examination

One systematic review of 17 studies found that the pooled diagnostic Odds Ratio for SLR for nerve root pain was 3.74 (95% CI 1.2–11.4); sensitivity for nerve root pain was high (1.0–0.88), but specificity was low (0.44–0.11) (Deville et al. 2000). All included studies were surgical case series at non-primary care level. Most studies evaluated the diagnostic value of SLR for disc prolapse. The pooled diagnostic Odds Ratio for the crossed straight leg raising test was 4.39 (95% CI 0.74–25.9); with low sensitivity (0.44–0.23) and high specificity (0.95–0.86). The authors concluded that the studies do not enable a valid evaluation of diagnostic accuracy of the straight leg raising test (Deville et al. 2000).

5.3.3 Diagnostic Imaging

One systematic review was found that included 31 studies on the association between plain film abnormalities of the lumbar spine and non-specific low back pain (van Tulder et al. 1997a). The results showed that degeneration, defined by the presence of disc space narrowing, osteophytes and sclerosis, is consistently and positively associated with non-specific low back pain with Odds Ratios ranging from 1.2 (95% CI 0.7–2.2) to 3.3 (95% CI 1.8–6.0). Spondylolysis/listhesis, spina bifida, transitional vertebrae, spondylosis and Scheuermann's disease did not appear to be associated with low back pain. There is no evidence on the association between degenerative signs at the acute stage and the transition to chronic symptoms.

A recent review of the diagnostic imaging literature (magnetic resonance imaging, radionuclide scanning, computed tomography, radiography) concluded that for adults younger than 50 years of age with no signs or symptoms of systemic disease, diagnostic imaging does not improve treatment of low back pain. For patients 50 years of age and older or those whose findings suggest systemic disease, plain radiography and simple laboratory tests can almost completely rule out underlying systemic diseases. The authors concluded that advanced imaging should be reserved for patients who are considering surgery or those in whom systemic disease is strongly suspected (Jarvik and Deyo 2002).

A recent randomised controlled trial (RCT) of 380 patients aged 18 years or older whose primary physicians had ordered that their low back pain be evaluated by radiographs determined the clinical and economic consequences of replacing spine radiographs with rapid MRI (Jarvik et al. 2003). Although physicians and patients preferred the rapid MRI, there was no difference between rapid MRIs and radiographs in outcomes for primary care patients with low back pain. The authors concluded that substituting rapid MRI for radiographic evaluations in the primary care setting may offer little additional benefit to patients, and it may increase the costs of care because of the increased number of spine operations that patients are likely to undergo.

5.4 Treatment

Various health care providers may be involved in the treatment of low back pain in primary care. Although there may be some variations between countries, general practitioners, physiotherapists, manual therapists, chiropractors, exercise therapists, McKenzie therapists, orthopaedic surgeons, neurologists/neurosurgeons, rheumatologists and others, may all be involved. The primary care physician has a central role in the management of non-specific low back pain. The therapeutic management of specific spinal disorders is generally the domain of medical specialists. It is important that information and treatment are consistent across professions, and that health care providers closely collaborate with each other.

Within the framework of the Cochrane Back Review Group systematic reviews of RCTs on therapeutic interventions for back pain are promoted, conducted, and disseminated (Bombardier et al. 1997; Bouter et al. 2003). In 1997, the Cochrane Back Review Group developed and published method guidelines for systematic reviews in this field. These method guidelines have recently been updated (van Tulder et al. 2000a). The aim of these method guidelines is to improve the quality of reviews, to facilitate comparison across reviews, and to enhance consistency among reviewers. The evidence on treatment of acute and chronic low back pain is summarized below. Cochrane and other systematic reviews are used and a recent edition of *Clinical Evidence*, in which these reviews have

been updated with additional trials (van Tulder and Koes 2003b,c). The evidence from systematic reviews on acute and subacute low back pain is summarized in Table 5.1 and on chronic low back pain in Table 5.2. Due to the heterogeneity of trials with regard to population, intervention, comparison and outcomes included, most Cochrane reviews did not perform a meta-analysis. Consequently, overall estimates of the effect of each treatment modality are not provided. In general, effects are small.

Table 5.2. Effectiveness of systematic reviews on conservative treatment for acute and subacute low back pain

Systematic review[a]	No. of trials	Comparison	Results
Advise to stay active			
Waddell et al. 1997	2	Bed rest	Faster recovery
	7	Usual care	Faster recovery, less chronic disability, less health care use, faster return to work
Hilde et al. 2002	4	Bed rest	Inconsistent findings; small beneficial effects on functional status, sick leave
Analgesics			
Van Tulder et al. 1997b	0	Placebo	
	3	NSAIDs	No difference in pain intensity
Back exercises			
Van Tulder et al. 2000	8	Other treatment	No differences in pain intensity, functional status, overall improvement
	4	Inactive or no treatment	No differences in pain intensity, functional status
Back schools			
Van Tulder et al. 1999	2	'Placebo'/no treatment	Faster recovery, no difference in pain relief, better physical outcomes
	2	Other treatments	Not more effective
Bed rest			
Hagen et al. 2000	4	Advise to stay active	Inconsistent findings
	2	Short vs long bed rest	No differences
	2	Exercises	No differences in pain intensity, functional status
Behavioural therapy			
Van Tulder et al. 1997b	1	Usual care	Better on pain drawings, claimed impairment
Epidural steroid injections			
Koes et al. 1999	2	Lidocaine, bupivacaine	Inconsistent findings
	1	Saline	No difference in proportion of people improved
Massage			
Furlan et al. 2002	1	Spinal manipulation	No difference in pain
Multidisciplinary treatment			
Karjalainen et al. 2001	2	Usual care	Faster return to work, fewer sick leaves, alleviates disability
Muscle relaxants			
Van Tulder et al. 2003	1	Benzodiazepines vs. placebo	Better short-term pain relief and overall improvement *Note: more CNS side effects*
	8	Non-benzodiazepines vs. placebo	Better short-term pain relief and overall improvement *Note: more CNS side effects*
	2	Anti-spasticity drugs vs. placebo	Better short-term pain relief

Systematic review[a]	No. of trials	Comparison	Results
NSAIDs			
Van Tulder et al. 2000	9	Placebo	Inconsistent findings on pain relief; better global improvement; less analgesic use
	6	Other drugs	No differences
	3	Paracetamol/acetaminophen	Inconsistent findings on pain relief
Spinal manipulation			
Assendelft et al. 2003	1	Sham	Better short-term pain relief; no difference in function
	3	General practitioner care	No differences in pain, function
	5	Physical therapy or exercise	No differences in pain, function
	7	Ineffective therapies	Better short-term pain relief
	2	Back school	No differences in pain, function
Traction			
Van der Heijden et al. 1995	2	Placebo	No difference in global improvement
	2	Other treatment	Inconsistent findings

[a] Cochrane review if available, otherwise most recent systematic review; two reviews are included on advice to stay active, because the Cochrane review had defined advice to stay active as single treatment and Waddell et al. (1997) used a broader definition and consequently included more trials

5.4.1 Acute and Subacute Low Back Pain

- **Acupuncture: A Cochrane review did not find any** RCTs of acupuncture specifically in people with acute low back pain (van Tulder et al. 1999).
- **Advice to stay active:** Two systematic reviews (one Cochrane review) and two subsequent RCTs (total of eight RCTs) found that advice to stay active versus advice to rest in bed or bed rest significantly increased the rate of recovery, reduced pain, reduced disability, and reduced time spent off work (Hilde et al. 2003; Waddell et al. 1997; Hagen et al. 2000; Rozenberg et al. 2002).
- **Analgesics (paracetamol, opioids):** We found no placebo controlled RCTs. Systematic reviews of three RCTs have found no consistent difference with analgesics versus non-steroidal anti-inflammatory drugs in reducing pain (van Tulder et al. 1997b).
- **Back exercises: A Cochrane review and** two additional RCTs (total of 14 RCTs) have found either no significant difference with back exercises versus other conservative treatments (for example, manual therapy and analgesics) or inactive treatments (for example, detuned ultrasound) in pain or disability, or have found that back exercises increase pain or disability (Chok et al. 1999; Hides et al. 1996; van Tulder et al. 2000a).
- **Back schools: Back school techniques vary widely, but essentially consist of repeated sessions of instruction about anatomy and function of the back and isometric exercises to strengthen the back. A Cochrane** review of four RCTs found limited evidence that back schools versus placebo increased rates of recovery and reduced sick leave in the short term. The review found no significant difference in outcomes with back school versus physiotherapy, and found that a mini back school of one 45-min session versus McKenzie exercises increased pain and sick leave (Van Tulder et al. 2000b). McKenzie exercises use self-generated stresses and forces to centralize pain from the legs and buttocks to the lower back. This method emphasizes self care.
- **Bed rest: A Cochrane** review of eight RCTs have found that bed rest could be worse than no treatment, advice to stay active, back exercises, physiotherapy, spinal manipulation, or non-steroidal anti-inflammatory drugs (Hagen et al. 2003). Adverse effects of bed rest include joint stiffness, muscle wasting, loss of bone mineral density, pressure sores, and venous thromboembolism.
- **Behavioural therapy: A Cochrane review including one** RCT on acute low back pain, found that cognitive behavioral therapy versus analgesics and exercises reduces acute low back pain and disability (van Tulder 1997b). **One additional**

RCT showed better pain relief compared with electromyographic biofeedback **for patients with acute sciatica and a high risk for chronicity** (Hasenbring et al. 1999).

- **Epidural steroid injections: A systematic review included two RCTs on acute low back pain (Koes et al. 1999).** One RCT found that epidural steroids versus subcutaneous lidocaine (lignocaine) injections increased the proportion of people who were pain free after 3 months. A second RCT found no significant difference in the proportion of people cured or improved with epidural steroids versus epidural saline, epidural bupivacaine, or dry needling.
- **Massage:** A Cochrane review found insufficient evidence from one RCT about the effects of massage compared with spinal manipulation or electrical stimulation (Furlan et al. 2002).
- **Multidisciplinary treatment programs:** A Cochrane review in people with subacute low back pain found limited evidence that multidisciplinary treatment, including a workplace visit, versus usual care by the attending physician reduced sick leave (Karjalainen et al. 2001).
- **Muscle relaxants: A Cochrane** review of nine RCTs have found that muscle relaxants versus placebo improve symptoms (including pain and function), but found no significant difference in outcomes among muscle relaxants. Adverse effects in people using muscle relaxants were common and included dependency, drowsiness, and dizziness (van Tulder et al. 2003a–c).
- **Non-steroidal anti-inflammatory drugs:** A Cochrane review of 25 RCTs and two additional RCTs have found that non-steroidal anti-inflammatory drugs versus placebo significantly increase the proportion of people with overall improvement after 1 week and significantly reduce the proportion of people requiring additional analgesics. No significant difference was found in pain relief with non-steroidal anti-inflammatory drugs versus each other or versus other treatments (paracetamol, opioids, muscle relaxants, and non-drug treatments) (Laws 1994; Pohjalainen et al. 2000; van Tulder et al. 2000c).
- **Spinal manipulation: A** systematic review of 16 RCTs on acute and subacute low back pain found that spinal manipulation versus sham therapy significantly decreases pain but not function. Spinal manipulation was not more or less effective than general practitioner care, analgesics, physical therapy, exercises or back school (Assendelft 2003).
- **Traction: A systematic review of two RCTs** found conflicting evidence on the effects of traction (van der Heijden 1995).
- **Electromyographic biofeedback, lumbar supports, temperature treatments (short wave diathermy, ultrasound, ice, heat), transcutaneous electrical nerve stimulation:** We found neither systematic reviews nor randomised controlled trials on the effects of these interventions for acute low back pain.

5.4.2 Chronic Low Back Pain

- **Acupuncture:** We found conflicting evidence from two systematic reviews (one Cochrane review) and two subsequent RCTs about effects of acupuncture compared with placebo or no treatment (Carlsson and Sjölund 2001; Cherkin et al. 2001; Ernst and White 1998; van Tulder et al. 1999).
- **Analgesics:** One RCT found that tramadol versus placebo decreased pain and increased functional status. A second RCT found that paracetamol versus diflunisal increased the proportion of people who rated the treatment as good or excellent (van Tulder et al. 1997b).
- **Antidepressants:** One systematic review and six additional RCTs have found that antidepressants versus placebo provided significantly better pain relief, but have found no consistent difference in functioning or depression. Additional RCTs have found conflicting results on pain relief with antidepressants versus each other or versus analgesics (Atkinson et al. 1998, 1999; Dickens et al. 2000; Hameroff et al. 1982, 1984; Salerno et al. 2002; Treves et al. 1991).
- **Back schools:** A Cochrane review and one subsequent RCT have found that, in occupational settings, back schools versus no treatment improve short-term pain and reduce disability (van Tulder et al. 2000a; Dalichau et al. 1999). There were no long-term differences. There is conflicting evidence on the effects of back schools in primary or secondary care compared with waiting list controls.
- **Behavioural therapy: A Cochrane** review has found that behavioral therapy reduces pain and improves functional status and behavioral outcomes compared with no treatment, placebo, or waiting list control. The review found no significant difference in functional status, pain, or

behavioral outcomes between different types of behavioral therapy, and found conflicting results with behavioral therapy versus other treatments (van Tulder et al. 2000b).

- **Electromyographic biofeedback:** One systematic review has found no difference in pain relief or functional status between electromyographic biofeedback and placebo or waiting list control, but found conflicting results on the effects of electromyographic biofeedback compared with other treatments (van Tulder et al. 1997a–c).
- **Epidural steroid injections:** A Cochrane review has found no significant difference between epidural steroid injections and placebo nor between epidural steroid injections and saline injections in pain relief after 6 weeks or 6 months (Nelemans et al. 2002). Most of these trials included patients with sciatica.
- **Exercise: A Cochrane** review and nine additional RCTs have found that exercise improves pain and functional status compared with usual care by the general practitioner. RCTs have found conflicting evidence on the effects of different types of exercise, or exercise compared with inactive treatments (Bendix et al. 1995, 1998; Hildebrandt et al. 2000; Friedrich et al. 1998; Kankaanpaa et al. 1999; Kuukkanen and Malkia 2000; Mannion et al. 1999, 2001a,b; Soukup et al. 1999, 2001; O'Sullivan et al. 1997; van Tulder et al. 2000c).
- **Facet joint injections:** A Cochrane review found no significant difference in pain relief between facet joint injections and placebo or facet joint nerve blocks (Nelemans et al. 2002). Most of these trials included patients with sciatica.
- Functional restoration: A Cochrane review has found that functional restoration programs with a cognitive behavioural approach plus physical training for workers with back pain reduced sick days but not the risk of being off work at 12 months compared with usual general practitioner care or with other interventions (Schonstein et al. 2003).
- **Local injections:** A Cochrane review found that four out of five trials indicated that injection therapy was more effective than placebo injection, irrespective of the medication used. However, the meta-analysis showed that there was no significant difference in pain relief. Two trials did not show any differences between local injection with bupivacaine and lignocaine or bupivacaine and methylprednisolone (Nelemans et al. 2002). Most of these trials included patients with sciatica.
- **Lumbar supports:** We found insufficient evidence on the effects of lumbar supports (van Tulder et al. 2000d).
- **Massage:** A Cochrane review found that massage combined with exercises and education is more effective than soft tissue massage only, remedial exercises and education only, and sham laser therapy. The review found conflicting evidence about the effects of massage compared with other treatments (Furlan et al. 2002).
- **Multidisciplinary treatment programs:** A Cochrane review has found that intensive multidisciplinary biopsychosocial rehabilitation with functional restoration reduces pain and improves function compared with inpatient or outpatient non-multidisciplinary treatments or usual care. The review found no significant difference between less intensive multidisciplinary treatments and non-multidisciplinary treatment or usual care in pain or function (Guzman et al. 2001).
- **Muscle relaxants:** A Cochrane review found better short-term pain relief and overall improvement with muscle relaxants compared to placebo. One RCT found that adverse effects in people using muscle relaxants are common and include dependency, drowsiness, and dizziness (van Tulder et al. 2003a–c).
- **Non-steroidal anti-inflammatory drugs:** A Cochrane review and two additional RCTs have found no significant difference with non-steroidal anti-inflammatory drugs versus each other for symptom outcomes. One RCT found that naproxen versus placebo increased pain relief. Two RCTs found conflicting evidence on the effects of non-steroidal anti-inflammatory drugs versus other analgesics (Famaey et al. 1998; Veenema et al. 2000; van Tulder et al. 2000c).
- **Spinal manipulation: One** systematic review identified 16 comparisons in 13 RCTs. The review found that spinal manipulation versus placebo did not improve pain and function (Assendelft et al. 2003).
- **Traction:** One systematic review and two additional RCTs found no significant difference between traction and placebo or between traction plus massage and interferential treatment in pain relief or functional status (Beurskens et al. 1995; van der Heijden et al. 1995; Werners et al. 1999).
- **Transcutaneous electrical nerve stimulation:** A Cochrane review found no significant difference in pain relief and function between transcutaneous electrical nerve stimulation and sham stimulation (Milne et al. 2002).

Table 5.3. Effectiveness of systematic reviews on conservative treatment for chronic low back pain

Systematic review[a]	No. of trials	Comparison	Results
Acupuncture			
Van Tulder et al. 1999	3	No treatment	Conflicting evidence on pain relief and global improvement
	8	Placebo/sham treatment	Conflicting evidence on pain relief and global improvement
	2	Conventional treatment	Not more effective on pain relief and global improvement
Analgesics			
Van Tulder et al. 1997b	1	NSAID	No difference on pain intensity; fewer patients improved
Antidepressants			
Salerno et al. 2002	9	Placebo	Better pain relief; no difference in activities of daily living; more adverse effects
Back schools			
Van Tulder et al. 2000	5	Other treatments	Better short-term effects on pain and functional disability; no long-term effects
	6	Waiting list controls	Conflicting evidence on short-term effects; no long-term effects
Behavioural therapy			
Van Tulder et al. 2000	11	No treatment, waiting list controls	Moderate positive effect on pain intensity and small positive effects on generic functional status and behavioral outcomes
	2	Other treatments	Graded activity better return to work than usual care; no difference between behavioral treatment and exercise therapy
EMG biofeedback			
Van Tulder et al. 1997b	3	Placebo, waiting list controls	No difference in pain intensity and functional status. Note: very small sample sizes
Epidural steroid injections			
Nelemans et al. 2002	4	Placebo	No difference in pain relief
	6	Pragmatic trials	No difference in pain relief compared with saline injections
Exercise			
Van Tulder et al. 2000	6	Inactive treatment/placebo	Conflicting evidence on pain, functional status and overall improvement
	3	Conventional physiotherapy	No differences on pain intensity, functional status, overall improvement or return to work
	3	Usual care by general practitioner	Better pain relief, functional status and return to work
Facet joint injections			
Nelemans et al. 2002	2	Placebo	No difference in pain relief
	1	Pragmatic trial	No difference in pain relief between facet joint injections and facet blocks
Functional restoration			
Schonstein et al. 2003	6	Usual care	Reduction in duration of sick leave; no difference in proportion of patients off work at 12 months
	5	Other interventions	Reduction in duration of sick leave; no difference in function

Systematic review[a]	No. of trials	Comparison	Results
Local injections			
Nelemans et al. 2002	5	Placebo	No difference in pain relief
	2	Pragmatic trials	No difference in pain relief
Lumbar supports			Note: very small sample size and poor methodological quality
Van Tulder et al. 2000	1	Lumbar support plus corset vs. corset alone	Better subjective but not objective index after 4 and 8 weeks
Massage			
Furlan et al. 2002	1	Inert treatment	Better short-term pain; better short- and long-term function
	7	Other active treatment	Worse immediate improvement in function and pain relief compared with spinal manipulation; better short-term function than acupuncture, self-care education and exercise; no differences in pain and no long-term differences.
Multidisciplinary treatment			
Guzman 2002	10	Non-multidisciplinary treatment or usual care	Better improvement of pain and function; conflicting evidence on vocational outcomes
Muscle relaxants			
Van Tulder et al. 2003	3	Benzodiazepines vs. placebo	Better short-term pain relief and overall improvement
	3	Non-benzodiazepines vs. placebo	Better short-term overall improvement; conflicting evidence on pain relief
NSAIDs			
Van Tulder et al. 1999	1	Placebo	Better short-term pain relief. Note: small sample size; data in only graphs
	1	Paracetamol/acetaminophen	No difference in short-term pain relief; better overall improvement. Note: small sample size
Spinal manipulation			
Assendelft et al. 2003	3	Sham	No differences in pain, function
	4	General practitioner care	No differences in pain, function
	2	Physical therapy or exercise	No differences in pain, function
	4	Ineffective therapies	No differences in pain, function
	3	Back school	No differences in pain, function
TENS			
Milne 2001	5	Placebo	No differences in pain, function
Traction			Note: most studies had small sample sizes and methodological flaws in design and conduct which do not allow clear conclusions
Van der Heijden et al. 1995	1	Placebo	No difference in global improvement
	2	Conservative treatment	Better global improvement after 3–4 weeks

[a] Cochrane review if available, otherwise most recent systematic review.

5.5 Guidelines and Implementation

During the last decade, various clinical guidelines on the management of acute low back pain in primary care have been issued (Koes et al. 2001; van Tulder et al. 2004). At present, guidelines exist in at least 12 different countries: Australia, Denmark, Finland, Germany, Israel, the Netherlands, New Zealand, Norway, Sweden, Switzerland, the United Kingdom, and the United States. Since the available evidence is international, one would expect that each country's guidelines would give more or less similar recommendations regarding diagnosis and treatment. Comparison of clinical guidelines for the management of low back pain in primary care from 11 different countries showed that the content of the guidelines regarding the diagnostic classification (diagnostic triage) and the use of diagnostic and therapeutic interventions is quite similar. However, there were also some discrepancies in recommendations across guidelines (Koes et al. 2001). Differences in recommendations between guidelines may be due to incompleteness of the evidence, different levels of evidence, magnitude of effects, side effects and costs, differences in health care systems (organization/financial), or differences in membership of guidelines committees. More recent guidelines may have included more recently published trials and, therefore, may end up with slightly different recommendations. Also, guidelines may have been based on systematic reviews that included trials in different languages; the majority of existing reviews have considered only studies published in a few languages, and several, only those published in English. Recommendations in guidelines are not only based on scientific evidence, but also on consensus. Guideline committees may consider various arguments differently, such as the magnitude of the effects, potential side effects, cost-effectiveness, and current routine practice and available resources in their country. Especially as we know that effects in the field of low back pain, if any, are usually small and short-term effects only, interpretation of effects may vary among guideline committees. Also, guideline committees may differently weigh other aspects such as side effects and costs. The constitution of the guideline committee and the professional bodies they represent may introduce bias – either for or against a particular treatment. This does not necessarily mean that one guideline is better than the other or that one is right and the other is wrong. It merely shows that when translating the evidence into clinically relevant recommendations more aspects play a role, and that these aspects may vary locally or nationally.

The development of clinical guidelines should ensure that patients are treated according to the best available evidence and should lead to optimal patient outcomes.

In general, the recommendations in the international guidelines on acute low back pain are quite consistent. Treatment of acute low back pain aims at: (1) providing adequate information, reassuring the patient that low back pain is usually not a serious disease and that rapid recovery is expected in most patients; (2) providing adequate symptom control, if necessary; and (3) recommending to stay as active as possible and to return to normal activities early, including work. An active approach is the best treatment option for acute low back pain. Most guidelines do not recommend routine use of passive treatment modalities (for example bed rest, ultrasound, electrotherapy and massage) as single treatment, because they may increase the risk of illness behavior and chronicity. Most guidelines also do not recommend referral to secondary health care and routine plain film imaging.

To increase consistency in the management of non-specific low back pain across countries in Europe, the European Commission has approved a program for the development of European guidelines for the management of low back pain, called "COST B13". The main objectives of this COST action were:

- Developing European guidelines for the prevention, diagnosis and treatment of non-specific low back pain.
- Ensuring an evidence-based approach through the use of systematic reviews and existing clinical guidelines.
- Enabling a multidisciplinary approach; stimulating collaboration between primary health care providers and promoting consistency across providers and countries in Europe.
- Promoting implementation of these guidelines across Europe.

Representatives from 13 countries participated in this project conducted between 1999 and 2004. The experts represented all relevant health professions in the field of low back pain: anatomy, anaesthesiology, chiropractice, epidemiology, ergonomy, general

practice, occupational care, orthopaedic surgery, pathology, physiology, physiotherapy, psychology, public health care, rehabilitation, and rheumatology. Within this COST B13 project four European guidelines were developed on: (1) acute low back pain, (2) chronic low back pain, (3) prevention of low back pain, (4) pelvic girdle pain. The guidelines are available at www.backpaineurope.org.

Development and dissemination of guidelines does not automatically mean that health care providers will read, understand, and use the guidelines. Passive dissemination of information is generally ineffective and specific implementation strategies are necessary to establish changes in practice. Systematic reviews have shown that a clear and strong evidence base, clear messages, consistent messages across professions, clear sense of ownership, communication with all relevant stakeholders, charismatic leadership, continuity of care, continuous education, and continuous evaluation are successful ingredients for implementation of guidelines (Bero et al. 1998; Grol 1997; Grimshaw et al. 2001).

Guidelines should have a clear and strong evidence base and be based on systematic reviews. Guidelines that are not based on sound scientific evidence might effectively implement the wrong evidence. Also, there should be an explicit link between recommendations and evidence. Messages should be clear, specific, and unambiguous. Inconsistent recommendations across health professions may be confusing. Therefore, messages of the various health care providers involved in the management of low back pain should be consistent. Communication with all relevant stakeholders (patients, professional organizations, and policy makers) is also important for successful implementation. Guideline committees should include representatives of all relevant stakeholders. Additionally, stakeholders should all have the opportunity to comment on the guidelines before publication. In that way, stakeholders will have a clear sense of ownership of the guidelines. It is also important to realize that development, publication, dissemination, implementation, and evaluation of guidelines is a continuous process. Continuous evaluation of the evidence, the guidelines, and their implementation may result in improved implementation.

However, several barriers to implementation of guidelines have been identified. The practice behavior of health professionals may be influenced by a lack of knowledge, a shortage of time, disagreement with the guideline content, or reluctance from colleagues to adhere to the guideline. Furthermore, health professionals may get lost in the large number of different guidelines received. Priority in getting evidence into practice is identifying barriers to change behavior of health professionals. However, changing behavior is complex and difficult and interventions developed to change behavior of health professionals have shown only limited effects. Identifying efficient implementation strategies to increase the uptake of evidence-based guideline recommendations will be a major challenge for the future.

References

Andersson GBJ (1997) The epidemiology of spinal disorders. In: Frymoyer JW (ed) The adult spine: principles and practice. Lippincott-Raven, Philadelphia, pp 93–141

Assendelft WJJ, Morton SC, Yu EI, Suttorp MJ, Shekelle PG (2003) Spinal manipulative therapy for low back pain. A meta-analysis of effectiveness relative to other therapies. Ann Intern Med 138:871–81

Atkinson JH, Slater MA, Williams RA et al. (1998) A placebo-controlled randomized clinical trial of nortriptyline for chronic low back pain. Pain 76:287–296

Atkinson JH, Slater MA, Wahlgren DR et al. (1999) Effects of noradrenergic and serotonergic antidepressants on chronic low back pain intensity. Pain 83:137–145

Bendix AF, Bendix T, Ostenfeld S et al. (1995) Active treatment programs for patients with chronic low back pain: a prospective, randomized, observer-blinded study. Eur Spine J 4:148–52

Bendix AF, Bendix T, Labriola M et al. (1998) Functional restoration for chronic low back pain: two-year follow-up of two randomized clinical trials. Spine 23:717–725

Bero LA, Grilli R, Grimshaw JM, Harvey E, Oxman AD, Thomson MA (1998) Closing the gap between research and practice: an overview of systematic reviews of interventions to promote the implementation of research findings. The Cochrane Effective Practice and Organization of Care Review Group. BMJ 317:465–468

Beurskens AJ, de Vet HCW, Köke AJ et al. (1995) Efficacy of traction for non-specific low back pain: a randomised clinical trial. Lancet 346:1596–1600

Bombardier C, Esmail R, Nachemson AL (1997) Back Review Group Editorial Board. The Cochrane Collaboration Back Review Group for spinal disorders. Spine 22:837–840

Bouter LM, Pennick V, Bombardier C (2003) The Editorial Board of the Back Review Group. Cochrane Back Review Group. Spine 28:1215–1218

Browning R, Jackson JF, O'Malley PG (2001) Cyclobenzaprine and back pain. Arch Intern Med 161:1613–1620

Carlsson CPO, Sjölund BH (2001) Acupuncture for chronic low back pain: a randomized placebo-controlled study with long-term follow-up. Clin J Pain 17:296–305

Cherkin DC, Eisenberg D, Sherman KJ et al. (2001) Randomized trial comparing traditional Chinese medical acupuncture, therapeutic massage, and self-care education

for chronic low back pain. Arch Intern Med 161:1081–1088
Chok B, Lee R, Latimer J et al. (1999) Endurance training of the trunk extensor muscles in people with subacute low back pain. Phys Ther 79:1032–1042
Deville WL, van der Windt DA, Dzaferagic A, Bezemer PD, Bouter LM (2000) The test of Lasegue: systematic review of the accuracy in diagnosing herniated discs. Spine 25:1140–1147
Deyo RA, Rainville J, Kent DL (1992) What can the history and physical examination tell us about low back pain? JAMA 268:760–765
Dickens C, Jayson M, Sutton C et al. (2000) The relationship between pain and depression in a trial using paroxetine in sufferers of chronic low back pain. Psychosomatics 41:490–499
Ernst E, White AR (1998) Acupuncture for back pain. A meta-analysis of randomized controlled trials. Arch Intern Med 158:2235–2241
Famaey JP, Bruhwyler J, Vandekerckhove K et al. (1998) Open controlled randomised multicenter comparison of nimesulide and diclofenac in the treatment of subacute and chronic low back pain. J Drug Assess 1:349–368
Friedrich M, Gittler G, Halberstadt Y et al. (1998) Combined exercise and motivation program: effect on the compliance and level of disability of patients with chronic low back pain: a randomized controlled trial. Arch Phys Med Rehabil 79:475–487
Frymoyer JW (1988) Back pain and sciatica. N Eng J Med 318:291–300
Frymoyer JW, Cats-Baril W (1991) An overview of the incidences and costs of low back pain. Orthop Clin N Am 22:263–271
Furlan AD, Brosseau L, Imamura M, Irvin E (2002) Massage for low-back pain: a systematic review within the framework of the Cochrane Collaboration Back Review Group. Spine 27:1896–1910
Grimshaw J, Shirran L, Thomas R (2001) Changing provider behavior: an overview of systematic reviews of interventions. Medical Care 29:II2–II45
Grol R (1997) Beliefs and evidence in changing clinical practice. BMJ 315:418–421
Hagen EM, Eriksen HR, Ursin H (2000) Does early intervention with a light mobilization program reduce long-term sick leave for low back pain? Spine 25:1973–1976
Hagen KB, Hilde G, Jamtvedt G et al. (2003) Bed rest for acute low back pain and sciatica (Cochrane Review). In: The Cochrane Library, Issue 1, 2003. Oxford, Update Software
Hameroff SR, Cork RC, Scherer K et al. (1982) Doxepin effects on chronic pain, depression and plasma opioids. J Clin Psychiatry 43:22–27
Hameroff SR, Weiss JL, Lerman JC et al. (1984) Doxepin's effects on chronic pain and depression: a controlled study. J Clin Psychiatry 45:47–52
Hasenbring M, Ulrich HW, Hartmann M et al. (1999) The efficacy of a risk factor-based cognitive behavioral intervention and electromyographic biofeedback in patients with acute sciatic pain: an attempt to prevent chronicity. Spine 24:2525–2535
Hides JA, Richardson CA, Jull GA (1996) Multifidus muscle recovery is not automatic after resolution of acute first episode low back pain. Spine 21:2763–2769
Hilde G, Hagen KB, Jamtvedt G et al. (2003) Advice to stay active as a single treatment for low back pain and sciatica (Cochrane Review). In: The Cochrane Library, Issue 1, 2003. Oxford, Update Software
Hildebrandt VH, Proper KI, van den Berg R et al. (2000) Cesar therapy is temporarily more effective in patients with chronic low back pain than the standard treatment by family practitioner: randomized, controlled and blinded clinical trial with 1 year follow-up. [Dutch]. Ned Tijdschr Geneesk 144:2258–2264
Jarvik JG, Deyo RA (2002) Diagnostic evaluation of low back pain with emphasis on imaging. Ann Intern Med 137:586–597
Jarvik JG, Hollingworth W, Martin B, Emerson SS, Gray DT, Overman S, Robinson D, Staiger T, Wessbecher F, Sullivan SD, Kreuter W, Deyo RA (2003) Rapid magnetic resonance imaging vs radiographs for patients with low back pain: a randomized controlled trial. JAMA 289:2810–2818
Jensen MC, Brant-Zawadzki MN, Obuchowski N, Modic MT, Malkasian D, Ross JS (1994) Magnetic resonance imaging of the lumbar spine in people without back pain. N Engl J Med 331:69–73
Kankaanpaa M, Taimela S, Airaksinen O et al. (1999) The efficacy of active rehabilitation in chronic low back pain. Effect on pain intensity, self-experienced disability, and lumbar fatigability. Spine 24:1034–1042
Karjalainen K, Malmivaara A, van Tulder M, Roine R, Jauhiainen M, Hurri H, Koes B (2001) Multidisciplinary biopsychosocial rehabilitation for subacute low back pain in working-age adults. Spine 26:262–269
Koes BW, Scholten RJPM, Mens JMA et al. (1999) Epidural steroid injections for low back pain and sciatica: an updated systematic review of randomized clinical trials. Pain Digest 9:241–247
Koes BW, van Tulder MW, Ostelo R, Kim BA, Waddell G (2001) Clinical guidelines for the management of low back pain in primary care: an international comparison. Spine 26:2504–2513
Kuukkanen T, Malkia E (2000) Effects of a three-month therapeutic exercise programme on flexibility in subjects with low back pain. Physiother Res Int 5:46–61
Laws D (1994) Double blind parallel group investigation in general practice of the efficacy and tolerability of acemetacin, in comparison with diclofenac, in patients suffering with acute low back pain. Br J Clin Res 5:55–64
Mannion AF, Muntener M, Taimela S et al. (1999) A randomized clinical trial of three active therapies for chronic low back pain. Spine 24:2435–2448
Mannion AF, Muntener M, Taimela S et al. (2001) Comparison of three active therapies for chronic low back pain: results of a randomized clinical trial with one-year follow-up. Rheumatology 40:772–778
Mannion AF, Junge A, Taimela S et al. (2001) Active therapy for chronic low back pain: part 3. Factors influencing self-rated disability and its change following therapy. Spine 26:920–929
Mannion AF, Taimela S, Muntener M et al. (2001) Active therapy for chronic low back pain part 1. Effects on back muscle activation, fatigability, and strength. Spine 26:897–908
Nelemans PJ, de Bie RA, de Vet HCW et al. (2002) Injection therapy for subacute and chronic benign low back pain. In: The Cochrane Library, Issue 3

O'Sullivan PB, Twomey LT, Allison GT (1997) Evaluation of specific stabilizing exercise in the treatment of chronic low back pain with radiologic diagnosis of spondylolysis or spondylolisthesis. Spine 24:2959–2967

Pohjolainen T, Jekunen A, Autio L et al. (2000) Treatment of acute low back pain with the COX-2 selective anti-inflammatory drug nimesulide: results of a randomised, double-blind comparative trial versus ibuprofen. Spine 25:1579–1585

Rozenberg S, Delval C, Rezvani Y, Olivieri-Apicella N, Kuntz JL, Legrand E, Valat JP, Blotman F, Meadeb J, Rolland D, Hary S, Duplan B, Feldmann JL, Bourgeois P (2002) Bed rest or normal activity for patients with acute low back pain: a randomized controlled trial. Spine 27:1487–1493

Sackett D (1997) Evidence-based medicine. Churchill Livingstone, Chicago

Salerno SM, Browning R, Jackson JL (2002) The effect of antidepressant treatment in chronic back pain: a meta-analysis. Arch Intern Med 162:19–24

Schonstein E, Kenny DT, Keating J, Koes BW (2003) Work conditioning, work hardening and functional restoration for workers with back and neck pain (Cochrane Review). In: The Cochrane Library, Issue 1, 2003. Oxford, Update Software

Soukup MG, Glomsrod B, Lonn JH et al. (1999) The effect of a Mensendieck exercise program as secondary prophylaxis for recurrent low back pain. A randomized, controlled trial with 12-month follow-up. Spine 24:1585–1591

Soukup MG, Lonn J, Glomsrod B et al. (2001) Exercises and education as secondary prevention for recurrent low back pain. Physiother Res Int 6:27–39

Treves R, Montane de la Roque P, Dumond JJ et al. (1991) Prospective study of the analgesic action of clomipramine versus placebo in refractory low back pain and sciatica (68 cases). [French]. Rev Rhum Mal Osteoartic 58:549–552

Van den Hoogen HMM, Koes BW, van Eijk JThM, Bouter LM (1995) On the accuracy of history, physical examination and erythrocyte sedimentation rate in diagnosing low back pain in general practice. A criteria-based review of the literature. Spine 20:318–327

Van der Heijden GJMG, Beurskens AJHM, Koes BW, de Vet HCW, Bouter LM (1995) The efficacy of traction for back and neck pain: a systematic, blinded review of randomized clinical trial methods. Phys Ther 75:93–104

van Tulder MW, Koes BW, Bouter LM (1995) A cost-of-illness study of back pain in The Netherlands. Pain 62:233–240

van Tulder MW, Assendelft WJJ, Koes BW, Bouter LM (1997a) Spinal radiographic findings and nonspecific low back pain: a systematic review of observational studies. Spine 22:427–434

van Tulder MW, Koes BW, Bouter LM (1997b) Conservative treatment of acute and chronic non-specific low back pain: a systematic review of randomized controlled trials of the most common interventions. Spine 22:2128–2156

van Tulder MW, Cherkin DC, Berman B, Lao L, Koes BW (1999) The effectiveness of acupuncture in the treatment of acute and chronic low back pain: a systematic review within the framework of the Cochrane Collaboration Back Review Group. Spine 24:1113–1123

van Tulder MW, Esmail R, Bombardier C, Koes BW (2000a) Back schools for non-specific low back pain (Cochrane Review). In: The Cochrane Library, Issue 3. Oxford, Update Software

van Tulder MW, Ostelo RWJG, Vlaeyen JWS, Linton SJ, Morley SJ, Assendelft WJJ (2000b) Behavioral treatment for chronic low back pain: a systematic review within the framework of the Cochrane Collaboration. Spine 25:2688–2699

van Tulder MW, Malmivaara M, Esmail R, Koes BW (2000c) Exercise therapy for low back pain: a systematic review within the framework of the Cochrane Collaboration. Spine 25:2784–2796

van Tulder MW, Scholten RJPM, Koes BW, Deyo RA (2000d) Non-steroidal anti-inflammatory drugs for low back pain: a systematic review within the framework of the Cochrane Collaboration. Spine 25:2501–2513

van Tulder MW, Jellema P, Nachemson AL, van Poppel MNM, Bouter LM (2000e) Lumbar supports for prevention and treatment of low back pain (Cochrane Review). In: The Cochrane Library, Issue 3. Oxford: Update Software

van Tulder M, Furlan A, Bombardier C, Bouter L (2003a) The Editorial Board of the Cochrane Collaboration Back Review Group. Updated method guidelines for systematic reviews in the cochrane collaboration back review group. Spine 28:1290–1299

van Tulder MW, Koes BW (2003b) Acute low back pain and sciatica. Clin Evid 9:1245–1259

van Tulder MW, Koes BW (2003c) Chronic low back pain and sciatica. Clin Evid 9:1260–1276

Veenema KR, Leahey N, Schneider S (2000) Ketorolac versus meperidine: ED treatment of severe musculoskeletal low back pain. Am J Emerg Med 18:404–407

Von Korff M, Saunders K (1996) The course of back pain in primary care. Spine 21:2833–2837

Waddell G, Feder G, Lewis M (1997) Systematic reviews of bed rest and advice to stay active for acute low back pain. Br J Gen Pract 47:647–652

Watson PJ, Main CJ, Waddell G, Gales TF, Purcell-Jones G (1998) Medically certified work loss, recurrence and costs of wage compensation for back pain: a follow-up study of the working population of Jersey. Br J Rheumatol 37:82–86

Webster BS, Snook SH (1990) The cost of compensable low back pain. J Occup Med 32:13–15

Werners R, Pynsent PB, Bulstrode CJK (1999) Randomized trial comparing interferential therapy with motorized lumbar traction and massage in the management of low back pain in a primary care setting. Spine 24:1579–1584

Degenerative Disc Disease

6

Paul M. Parizel, Johan W. M. Van Goethem, Luc Van den Hauwe, and Maurits Voormolen

CONTENTS

6.1 Introduction

The spinal column is a complex anatomical structure which is composed of vertebrae, intervertebral discs, and ligaments. All components undergo degenerative changes and morphologic alterations during life (Prescher 1998). In this chapter we shall focus our attention on the intervertebral discs, which are also referred to as "intervertebral fibrocartilages"; the two terms can be used interchangeably (Warwick and Williams 1973). From the axis (C2) to the sacrum, the intervertebral discs are situated between the upper and lower endplates of adjacent vertebral bodies. They constitute the principal connections between the vertebrae, and have two main functions: to serve as shock absorbers, and to allow movement of the spinal column. Movement at a single disc level is limited, but all of the vertebrae and discs combined allow for a significant range of motion (Inoue and Takeda 1975). All together, the intervertebral discs constitute approximately one-quarter of the length of the spinal column, not including the first two vertebrae and the sacrum. The cervical and lumbar segments of the spine have, in proportion to their height, greater amounts of disc space width than the thoracic region; therefore, these parts of the spine are more flexible and allow a greater freedom of movement.

The intervertebral disc is a highly organized matrix structure (Roberts et al. 2006). It adheres to the thin layer of hyaline cartilage which covers the upper and lower endplates of the vertebral bodies. In the lower cervical spine, there are small joints lined by synovial membrane between the upper surfaces of the bodies and the margins of the fibrocartilages on either side ("uncovertebral joints"). The circumference of the intervertebral discs is closely connected to the anterior and posterior longitudinal ligaments. In the thoracic region they are joined laterally, by means of the interarticular ligaments, to the heads of those ribs that articulate with two vertebrae.

Intervertebral discs vary in shape, size, and thickness in different parts of the vertebral column. In *shape* and *size* they correspond with the surfaces of the bodies between which they are placed, except in the cervical region, where they are slightly smaller from side to side than the corresponding bodies. In *thickness* they vary not only in the different regions of the column, but in different parts of the same fibrocartilage; they are thicker in front than behind in the cervical and lumbar regions, and thus con-

P. M. Parizel, MD, PhD; J. W. M. Van Goethem, MD, PhD; L. Van den Hauwe, MD; M. Voormolen, MD, PhD
Department of Radiology, Antwerp University Hospital and University of Antwerp, Wilrijkstraat 10, 2650 Edegem, Belgium

KEY POINTS

- Plain X-ray films are of limited use in the assessment of degenerative disc disease, since early signs of degeneration cannot be seen.
- Multi-detector row computed tomography (MDCT) provides excellent anatomic detail for the detection of disc herniation and nerve root compression.
- Magnetic resonance imaging (MRI) is the method of choice to detect early signs of intervertebral disc degeneration.
- New functional MR imaging techniques improve our diagnostic potential and may show intervertebral disc degeneration in an early stage in patients with pain.
- A general classification system and comprehensive nomenclature has been proposed by the Combined Task Forces (Table 6.1).
- Annular tears (syn. annular fissures) are classified as concentric, transverse or radial.
- Complete radial tears predispose to extrusion.
- Annular tears are recognizable as areas of high signal intensity on T2-weighted images or as foci of annular enhancement on Gd-enhanced T1-weighted images.
- A bulging disc (also known as bulging annulus) is not a herniation.
- Bulges and protrusions are frequent in asymptomatic individuals, extrusions are not.
- Spontaneous regression of a herniated disc is common. Factors associated with a high probability of spontaneous regression are: free fragment herniation, high signal intensity on T2-weighted images, and herniations with peripheral contrast enhancement on T1-weighted images.
- Reactive changes involving the vertebral endplates and adjacent bone marrow are classified by Modic into 3 types: inflammatory (type 1), fatty (type 2) and osteosclerosis (type 3) (Table 6.2).

tribute to the lordotic curvature (anterior convexity) of these parts of the column; while they are of nearly uniform thickness in the thoracic region, the thoracic kyphotic curvature (anterior concavity) is almost entirely determined by the shape of the vertebral bodies (Warwick and Williams 1973).

6.1.1 Anatomical Structure of the Intervertebral Discs

The intervertebral disc is made up of two components: the annulus fibrosus and the nucleus pulposus. The central gelatinous *nucleus pulposus* is surrounded by the more collagenous annulus fibrosus and is located between the cartilage of the endplates superiorly and inferiorly (Roberts et al. 2006). Macroscopically, the nucleus pulposus is soft, pulpy, highly elastic, and of a yellowish color (Schiebler et al. 1991a). The nucleus pulposus is composed primarily of water, proteoglycans, and loose collagen fibers. The water content of the nucleus decreases with age from about 90% at birth to about 70% by the fifth decade (Schiebler et al. 1991b). Embryologically, the nucleus pulposus is formed by cells of the notochord. In humans, these notochordal cells are eventually lost, either through apoptosis or terminal differentiation, and are replaced by chondrocyte-like cells. However, there is some evidence that the notochordal cells may persist in at least some humans.

Under pressure, the highly elastic nucleus pulposus becomes flatter and broader and pushes the more resistant fibrous laminae of the annulus fibrosus outward in all directions. The *annulus fibrosus* constitutes the outer portion of the disc and is composed of multiple concentric layers (lamellae) of fibrocartilage (Schiebler et al. 1991b). The outer lamellae (Sharpey's fibers) continue into the longitudinal ligaments and vertebral bodies. The fibers of which each lamella is composed are directed obliquely from above downward (at 30° angles), with fibers of adjacent lamellae running in opposite directions. In this way, the fibers of one layer are directed across those of another (like a meshwork). This arrangement creates a structure that is exceptionally strong, yet facilitates movement and flexibility. In the outer half of the annulus the lamellae are closely approximated; near the center of the disc, the fibers are somewhat more widely separated.

6.1.2 Blood Supply to the Intervertebral Discs

At birth, and during (early) childhood, human intervertebral discs have some blood supply within both the cartilage endplates and the annulus fibrosus (Roberts et al. 2006). Beginning in the first decade of life, the nutritive blood vessels in the endplates recede, leaving the disc with little direct blood supply in the healthy adult. At this point, diffusion is the only source of nutrition to the discs (Rajasekaran et al. 2004). The process of diffusion from the vertebral body through the endplates to the disc can be shown by performing serial magnetic resonance imaging (MRI) studies after intravenous gadolinium chelate injection. Disturbances in diffusion of a contrast agent to the intervertebral disc are correlated with endplate cartilage damage. With age and/or disease, calcification of the vertebral endplates causes occlusion of the vascular openings in the osseous endplates, and a decreased size of the capillary buds. It has been suggested that the occlusion of endplate openings, which contain vascular sources for the disc, may limit the transport of nutrients, leading to disc degeneration (Benneker et al. 2005a). When the supply of nutrients recedes, the disc begins to degenerate. With increasing age, water is lost from the matrix (desiccation), and the proteoglycan content diminishes (Roberts et al. 2006). The disc, and particularly the nucleus, becomes less gelatinous and more fibrous, which leads to shrinking and loss of height. The spine's range of motion and shock-absorbing ability are decreased.

6.1.3 Imaging the Intervertebral Discs

There are many imaging modalities for assessing intervertebral discs (Herzog 1996). On *plain X-ray films* of the spine, degenerative disc disease is characterized by narrowing of the intervertebral space, endplate erosions with reactive osteosclerosis, formation of osteophytes (which often involve the spinal canal and foramina), intradiscal calcifications, and intradiscal gas ("vacuum phenomenon"). Due to its soft tissue nature, the normal intervertebral disc is not visualized on plain X-ray films (unless it contains foci of calcification or ossification). Therefore, it follows that plain X-ray films have a limited role in the assessment of disc degeneration, since early degenerative changes within the disc cannot be detected. Recent evidence however appears to indicate that three radiographic parameters (height loss, osteophytes and intradiscal calcifications) are significantly correlated with the morphological degree of degeneration of human lumbar discs harvested from cadavers (Benneker et al. 2005b).

In the evaluation of degenerative disc disease, *myelography and CT myelography* have been supplanted by MRI and CT, which have few associated side-effects or morbidity, and which are noninvasive (Jackson et al. 1989). It has been demonstrated in a controlled prospective blinded study that both CT and MRI are significantly more informative than myelography; therefore, CT or MRI should be the first-choice diagnostic procedures for patients with suspected lumbar disc herniation (Albeck et al. 1995).

Discography is a radiographic technique in which contrast medium is injected percutaneously into the central part of the intervertebral disc. The method allows evaluation of disc disease in two ways. *First*, the injection of contrast medium into the nucleus pulposus may provoke a pain sensation which reproduces (or aggravates) the original pain pattern experienced by the patient (Vanharanta et al. 1988a; Moneta et al. 1994; Tehranzadeh 1998). Pain provocation suggests disruption of the outer annulus fibrosus, and may provide the specificity missing from the purely morphologic information that CT and MR imaging provides (Jarvik and Deyo 2000). *Second*, the contrast medium injected into the nucleus pulposus can reveal the exact location of fissures and defects in the annulus fibrosus (Vanharanta et al. 1988b; Tehranzadeh 1998). Despite its merits, discography is an invasive and controversial procedure and its value remains under discussion (Bogduk and Modic 1996; Weishaupt et al. 2001). Proponents argue that discography is the only method that directly relates a radiographic image to the patient's pain, and that it is the only modality that can detect the internal disc disruption syndrome (Guyer and Ohnmeiss 1995; Guyer et al. 2003). Some investigators use discography as a preoperative diagnostic test to identify painful discs (Bini et al. 2002) or before performing intradiscal electrothermal annuloplasty (IDET) (Karasek and Bogduk 2000). On the other hand, many authors recommend the procedure to be limited to a strictly scientific and prospective evaluation, and argue that there is no basis for the performance of discography in clinical medicine (Nachemson 1989; Bogduk and Modic 1996). The specificity of discography is

far from clear (Jarvik and Deyo 2000). Abnormal discography examinations have been reported in normal asymptomatic subjects (Walsh et al. 1990; Carragee et al. 2006). Moreover, discography has many disadvantages: it is invasive and time-consuming; it includes a potential risk of infection; and it involves a moderate dose of radiation (especially when combined with CT). Subjects with significant emotional and chronic pain problems may have long-term back symptoms after discography, and these patients may present a false-positive pain provocation (Carragee and Alamin 2001). Discography is therefore not recommendable as a screening technique and the results should be interpreted with great caution.

CT allows physicians to complement their clinical diagnosis of low back pain with a detailed in vivo image of the structure and soft tissues of the spine. The importance of CT as a diagnostic tool in visualizing intervertebral discs has been further enhanced by the recent development of multi-detector row CT (MDCT) scanning. MDCT allows us to scan an entire "volume" of the vertebral column segment within seconds. The dataset can then be reformatted to provide images in axial, sagittal, coronal imaging planes, or any combination thereof. An important advantage of CT is the ability to distinguish soft tissues from bone changes (Modic et al. 1988a). However, due to the intrinsically limited soft tissue contrast resolution between various soft tissues, intradiscal structure can only be grossly evaluated and its sensitivity at the early phases of disc degeneration is poor. Intradiscal calcifications are easily recognized on CT (Fig. 6.1). Moreover, CT (and MRI for that matter) cannot reliably distinguish symptomatic from incidental findings (Haughton 2004). At present, CT is mainly applied to show nerve root compression caused by either intervertebral disc extrusion or spinal stenosis. MDCT is also useful to demonstrate reactive or secondary signs of degeneration, such as calcification, the vacuum phenomenon and sclerosis of the adjacent intervertebral body (Modic et al. 1988a). Advantages of CT over MRI include imaging of claustrophobic patients and patients with underlying contraindications to MRI (e.g. patients with pacemakers). An important drawback of this method is the relatively high dose of ionizing radiation.

MRI is the most sensitive imaging method for evaluating the intervertebral disc and has become the primary imaging modality for investigation of the spine (Parizel and Wilmink 1998). In addition to the noninvasive nature of this modality, MRI provides excellent anatomic detail of the spine thanks to its superb soft tissue contrast discrimination and multiplanar imaging capability (Parizel et al. 2003).

Many different pulse sequences have been applied to MRI of the spine (Georgy and Hesselink 1994). For the lumbar spine, our standard imaging protocol in degenerative disc disease consists of sagittal T1- and T2-weighted images, supplemented with axial T1- and T2-weighted images at selected levels (Morgan and Saifuddin 1999). Turbo spin echo (TSE) have supplanted conventional spin echo (SE) sequences, because of the improved image quality, superior spatial resolution, reduced motion artifacts and shorter acquisition times (Ross et al. 1993). For the cervical and thoracic spine regions we use sagittal TSE T1- and T2-weighted images, with axial TSE T2- or gradient echo T2*-weighted images. Saturation slabs and motion compensation techniques are helpful to reduce artifacts. The use of paramagnetic contrast agents improves the sensitivity and specificity of MRI of the spine (Jinkins and Runge 1995). Fat suppression techniques can be used in conjunction with gadolinium-based contrast material to improve visualization of annular tears, as well as inflammatory and neoplastic diseases. Gadolinium chelates are especially useful

Fig. 6.1. Intradiscal calcification of a mid-thoracic disc in a 40-year-old woman. Axial CT scan after myelography. A focal dense calcification is seen in the nucleus pulposus. Mild, incipient spondylotic changes are seen along the anterior margin of the intervertebral disc space

for distinguishing recurrent disc herniation from epidural scar tissue in the postoperative spine (Bradley 1999).

MRI yields exquisitely detailed images of disc herniation and root compression, but fails to distinguish clinically symptomatic findings from those that are incidental (Haughton 2004). This limitation has led to the development of newer MR-based techniques, such as:

- Serial post-gadolinium MRI scans to assess the diffusion characteristics of lumbar intervertebral discs (Rajasekaran et al. 2004). The status of the endplate influences diffusion of a contrast agent to the center of the disc. Endplate cartilage damage increases with age and produces considerable changes in diffusion.
- Diffusion-weighted imaging with calculation of apparent diffusion coefficient maps to evaluate disc disease in an early phase (Kerttula et al. 2000). Diffusion tensor microscopy imaging has been utilized to study the integrity of the fibers in the annulus fibrosus (Hsu and Setton 1999).
- Measuring changes in T2-relaxation values as a means to assess the water content and structure of intervertebral discs (Kerttula et al. 2001).
- Magnetic resonance spectroscopy (MRS) of intervertebral discs to detect lactic acid, which increases in degenerative disc disease (Haughton 2004).
- Dynamic imaging of the spine (e.g. during flexion-extension or by using axial loading) to increase the sensitivity of MRI. The application of axial compression can cause narrowing of the spinal canal or the neural foramina (Saifuddin et al. 2003a). High intensity zones have been shown to develop on axial-loaded images of the lumbar spine (Saifuddin et al. 2003b).
- Neurography. This term is used to describe signal intensity changes in spinal nerves and spinal nerve roots on T2-weighted images obtained with high-resolution phased array surface coils (Grant et al. 2004).

6.2 Nomenclature and Classification of Degenerative Disc Disease

Ever since the initial description in 1934 by Mixter and Barr of a "ruptured disc" with monoradiculopathy (Mixter and Barr 1934), the terminology to report and grade degenerative diseases of the spine has been surrounded by controversy and confusion (Milette 1997). In a recently published literature review study based on a Medline search, the authors found as many as 42 different grading systems for assessing cervical or lumbar disc and facet degeneration (Kettler and Wilke 2006). Different terminology is used by pathologists, neurosurgeons, orthopedic surgeons, radiologists, and neuroradiologists. The same terms are used with different definitions, which is highly confusing. Some nomenclature systems describe disc pathology based on the observed morphology of the disc contour, whereas others take into account anatomical, clinical and pathological findings. Definitions and concepts based on cross-sectional imaging studies are different from those based on discography or myelography (Bogduk and Modic 1996). The lack of standardization in terminology contributes to a substantial interobserver variability in the interpretation of imaging studies (Jarvik et al. 1996). In one study evaluating reader consistency in the interpretation of lumbar disc abnormalities, authors compared two different nomenclatures ("normal/bulge/herniation" *versus* "normal/bulge/protrusion/extrusion"); they commonly found disagreements for normal versus bulge and between bulge versus herniation or protrusion (Brant-Zawadzki et al. 1995). There is a dire need for a reliable and unambiguous terminology to describe normal and pathologic conditions of intervertebral discs.

In 2001, the Combined Task Forces of the North American Spine Society, American Society of Spine Radiology, and American Society of Neuroradiology proposed a new nomenclature and consistent classification system, intended for the reporting of imaging studies (Fardon and Milette 2001; Milette 2001). The focus of this document is on the lumbar spine, though certain terms and definitions can be extrapolated to the cervical and thoracic spine. The diagnostic categories and subcategories are based on pathology. The general classification of disc lesions is given in Table 6.1 (Milette 2000). There are, however, other classification systems in use which are based on the three-joint complex: the intervertebral disc (anterior column of the spine) and the two facet joints (posterior column) (Thalgott et al. 2004). In this chapter, we shall follow the general classification of disc lesions as proposed by the Combined Task Forces.

Table 6.1. General classification of disc lesions

- Normal (excluding aging changes)
- Congenital/developmental variant
- Degenerative/traumatic lesion
  - Anular tear
  - Herniation
    - Protrusion/extrusion
    - Intravertebral
  - Degeneration
    - Spondylosis deformans
    - Intervertebral osteochondrosis
- Inflammation/infection
- Neoplasia
- Morphologic variant of unknown significance

6.3 The Normal Intervertebral Disc, Including Age-Related Changes

In the Combined Task Forces nomenclature, the term "normal" is reserved for young discs that are morphologically normal, without signs of disease, trauma, or aging. The clinical context is not taken into account. This strict definition implies that many clinically asymptomatic normal people have morphologically abnormal discs.

However, the "normal" appearance of an intervertebral discs is age-related, because of the marked anatomical and biochemical changes which occur within the disc over time. This results in a variable appearance on MRI (Sether et al. 1990).

In *infants and young children*, the intervertebral disc is prominent relative to the volume of the adjacent vertebral bodies; with increasing age, its volume decreases. The transition between the nucleus pulposus and the annulus fibrosus is relatively sharp in a young disc and becomes less distinct with age (Yu et al. 1988).

In *young adults*, the normal intervertebral disc does not extend beyond the interspace on transverse CT or MRI scans. The disc contour coincides with the margin of the adjacent vertebral endplates. On MRI, the normal adult disc presents an intermediate to low signal intensity on T1-weighted images and a high signal intensity on T2-weighted images, when compared to the bone marrow in the adjacent vertebral bodies (Yu et al. 1988; Morgan and Saifuddin 1999). On T2-weighted MRI scans the normal bright nucleus pulposus and the inner annulus are indistinguishable (Schiebler et al. 1991b). Normal adult endplates and ligamentous structures as well as the outer annulus fibrosus have low signal intensities on both T1- and T2-weighted images. The outer annulus, which contains densely packed fibers, is hypointense on all pulse sequences and is optimally demonstrated on T2-weighted images (Morgan and Saifuddin 1999). In young adults, there are statistically significant diurnal T2 relaxation value changes in the normal lumbar intervertebral discs; after the age of 35 years the diurnal T2 value changes in the normal discs disappear and this is thought to be an aspect of aging, not caused by degeneration Karakida et al. 2003).

As early as in the third decade, a horizontal band of decreased signal intensity on T2-weighted sagittal images develops in the central part of the disc (Aguila et al. 1985). This is called the *intranuclear cleft*, and it represents a fibrous transformation of the gelatinous matrix of the nucleus pulposus (Schiebler et al. 1991a). Due to the development of the intranuclear cleft, the normal adult nucleus presents a bilocular appearance on sagittal T2-weighted scans, and this is considered a sign of normal maturation.

In *middle-aged and elderly subjects*, the bright signal intensity of the intervertebral discs on T2-weighted images gradually decreases, until the discs become hypointense (Modic and Herfkens 1990). T2-weighted scans are best suited for detecting degenerative discs. There is a significant correlation between the decrease in signal intensity and age (Sether et al. 1990). The loss of signal intensity is concomitant with a decrease in water and proteoglycan content, and an increase in collagen in the disc (Sether et al. 1990). With aging, the disc undergoes a process of desiccation: the nucleus pulposus dries, becomes less elastic, and the amount of collagen in the disc increases. The T2-signal intensity of the intervertebral disc is highly significantly correlated with the water and proteoglycan content (Benneker et al. 2005b). Though the decrease in T2-signal intensity is an age-related physiologic phenomenon, it predisposes the discs to degenerative changes, such as loss of disc height, annular tears and disc herniation (Fig. 6.2). Calculated T2 relaxation times can be used as a continuous measure of intervertebral disc degeneration (Perry et al. 2006). Within the disc, there are variations in T2 relaxation times: the highest T2 values are found in the nucleus pulposus near the vertebral endplates and lower T2 values are encountered in the intranuclear cleft region and peripheral annulus fibrosus, reflecting the fibrous nature of these structures.

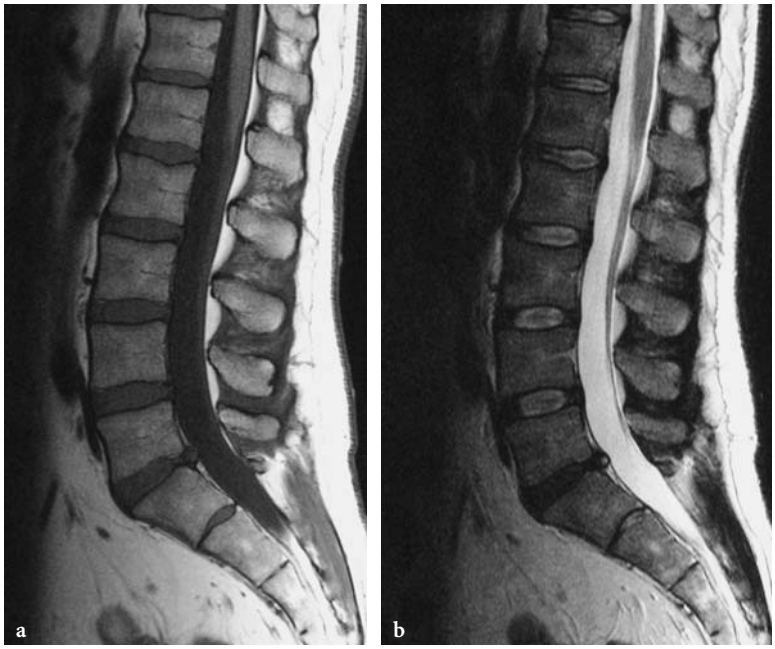

Fig. 6.2a,b. Loss of T2-signal intensity at L5-S1 ("black disc") in a 38-year-old man. **a** Sagittal T1-weighted and **b** T2-weighted scans. Decrease in T2-signal intensity predisposes the disc to degenerative changes, such as disc protrusion as seen in this patient

There remains, however, considerable confusion regarding what constitutes normal versus abnormal aging. As a general rule, in normal aging disc height is preserved, disc margins remain regular, and radial annular tears are not a usual consequence of aging. Some authors believe that the MRI signal characteristics of discs allow differentiation of the normal aging process from true pathologic degeneration (Sether et al. 1990); other investigators consider this distinction impossible (Modic and Herfkens 1990); still others consider that pathologic degeneration is just an acceleration of the normal aging process (Czervionke 1993). On the basis of serial post-contrast MRI studies of lumbar discs, normal aging and degeneration have been shown to be two separate processes by documenting clear-cut differences in diffusion (Rajasekaran et al. 2004).

According to Resnick and Nywayama, the intervertebral disc is affected by two different degenerative processes, one involving the annulus fibrosus and adjacent ring apophyses ("spondylosis deformans") and the other affecting mainly the nucleus pulposus and vertebral body endplates ("intervertebral osteochondrosis") (Fig. 6.3) (Resnick and Niwayama 1995). With this concept in mind, one could consider that what is referred to as "spondylosis deformans" reflects the normal aging process, while "intervertebral osteochondrosis" corresponds to real pathologic deterioration and collapse of the disc, associated with bone erosion and reactive osteosclerosis (Twomey and Taylor 1987; Milette 1997). In the cervical spine, this process may result in spinal stenosis and compression of the spinal cord (Fig. 6.4).

Small amounts of gas are often seen on plain X-rays or CT scans in elderly individuals near the apophyseal enthesis: they are probably located in transverse annular tears and should be considered as spondylosis deformans. Large amounts of gas in the central disc space indicate degeneration of the nucleus pulposus and are indicative of pathologic intervertebral osteochondrosis (Fig. 6.5). Anterior and lateral marginal osteophytes are consequences of normal aging. Endplate erosions and reactive bone marrow changes are pathologic.

6.4 Congenital Abnormalities and Developmental Variations

Congenital abnormalities and developmental variations of the spine are common. Intervertebral discs between anomalous segments undergo morphological changes which can be observed on T2-weighted images (Desmond and Buirski 1993). Transitional discs (partial fusion of the adjacent bony segments), or rudimentary discs (complete fusion of the two

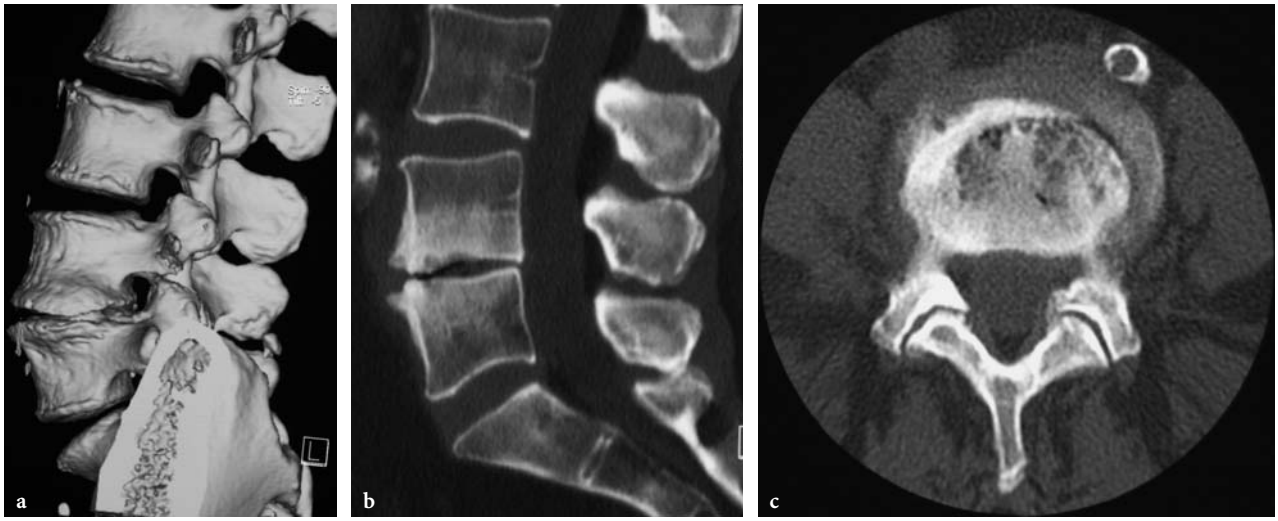

Fig. 6.3a–c. Spondylosis deformans ("normal aging") versus intervertebral osteochondrosis ("abnormal aging") in a 62-year-old woman. MDCT scan with lateral volume rendering view (**a**), sagittal multi-planar reformation (**b**) and axial scan at L4–L5 (**c**). The L4–L5 intervertebral disc is narrowed, with irregular endplates, vacuum phenomenon and concentric protrusion of the disc. At the other levels, mild spondylotic changes are seen at the adjacent ring apophyses, indicating normal aging

Fig. 6.4a,b. Normal versus abnormal aging of the cervical spine. Sagittal T2-weighted scans in two different patients. **a** The patient is a 76-year-old man with mild age-related degenerative changes, without impingement on the dural sac or the spinal cord. **b** The patient is a 40-year-old woman with severe degenerative disease at C5–C6 and C6–C7, resulting in spinal stenosis, cord compression and focal myelomalacia

Fig. 6.5a–c. Vacuum phenomenon in a 79-year-old woman. The axial CT scan (**a**), as well as the coronal (**b**) and sagittal (**c**) reformatted images show intradiscal gas at the L4–L5 and L5–S1 levels. This so-called vacuum phenomenon is a sign of advanced degeneration

adjacent vertebral bodies) usually present a normal signal intensity, but lack an intranuclear cleft and are smaller than adjacent, normal, mobile disc segments (Fig. 6.6). In the presence of a lumbosacral transitional vertebra, degenerative disc changes are much more common at the interspace immediately above than at any other level (Fig. 6.7) (Elster 1989; Vergauwen et al. 1997). Discs from patients with spinal deformities such as scoliosis are more prone to early degeneration (Fig. 6.8). They may contain ectopic calcifications in the cartilage endplate and sometimes in the disc itself (Roberts et al. 2006). Accelerated degenerative intervertebral disc changes are also associated with conditions such as spondylolisthesis (Fig. 6.9) (Rauch and Jinkins 1993; Bertram et al. 2006).

6.5 Degenerative Disc Disease

The degenerative disc process is related to aging, and the prevalence of degenerative discs increases linearly with age. It is likely that many other factors (e.g. autoimmune, genetic quality of collagen and proteoglycan, reabsorption, and biomechanical) are also implicated. The concept of degeneration encompasses changes involving the disc (desiccation, fibrosis, annular tears, mucinous degeneration of the annulus, loss of height), as well as the endplates (defects, sclerosis, osteophytic spurring at the apophyses, Modic changes).

Intervertebral disc degeneration begins early in life (Erkintalo et al. 1995). However, the relation between abnormalities found in the lumbar spine and low back pain is controversial, since abnormal findings are frequently reported in asymptomatic subjects on plain radiographs (Torgerson and Dotter 1976; Frymoyer et al. 1984; Witt et al. 1984), myelograms (Hitselberger and Witten 1968), discograms (Walsh et al. 1990), CT scans (Wiesel et al. 1984) and MRI scans (Weinreb et al. 1989; Boden et al. 1990). Disc degeneration is already present in over one-third of normal healthy subjects aged 21–40 years (Powell et al. 1986). In a study where MRI of the lumbar spine was performed in 98 asymptomatic people; only 36% had normal lumbar discs at all levels, with almost two-thirds of the sub-

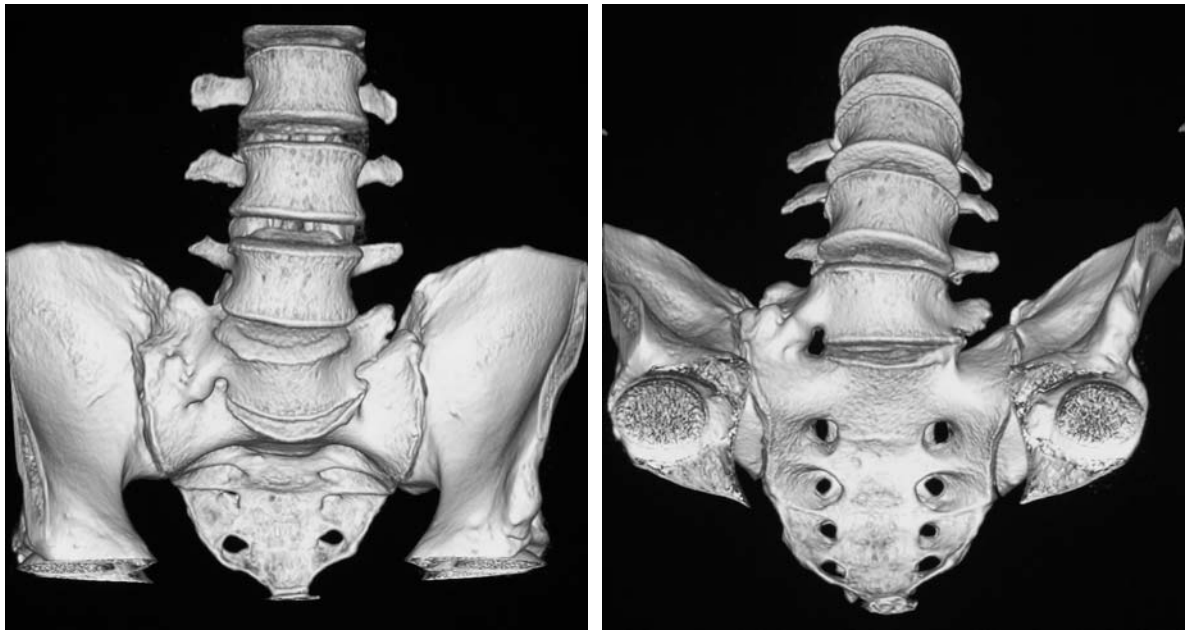

Fig. 6.6a,b. Lumbosacral transitional vertebra (right-sided hemisacralisation of L5). Multi-detector row CT scan with volume rendered reconstructions (**a**,**b**). The transitional disc is narrower than the normal, mobile disc segments. There are degenerative disc changes involving both the transitional disc and the interspace immediately above it

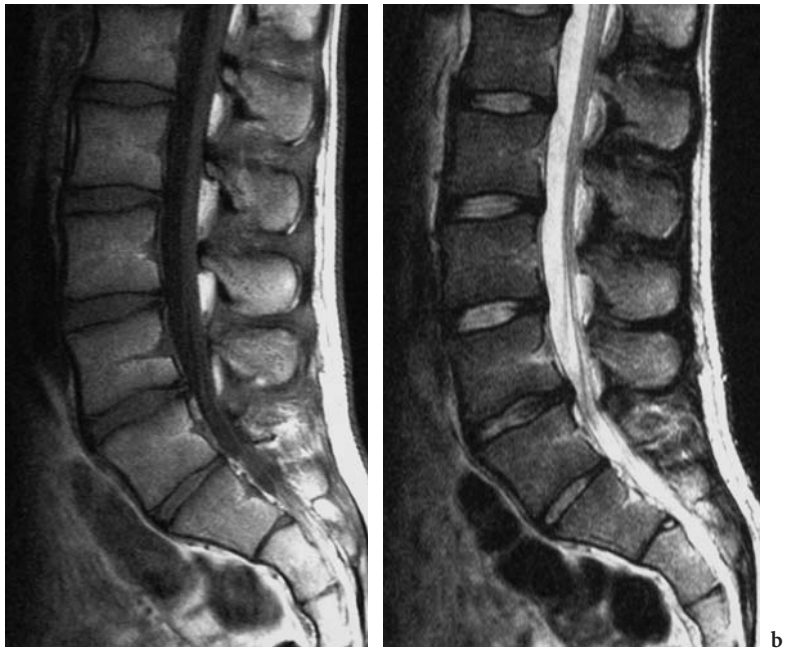

Fig. 6.7a,b. Transitional disc in a 17-year-old boy. Sagittal T1-weighted (**a**) and T2-weighted (**b**) scans. The transitional disc is narrower and presents a normal signal intensity. There is some degeneration of the disc level above the transitional vertebra, as characterized by a decreased signal intensity on T2-weighted scans in the posterior portion of the disc

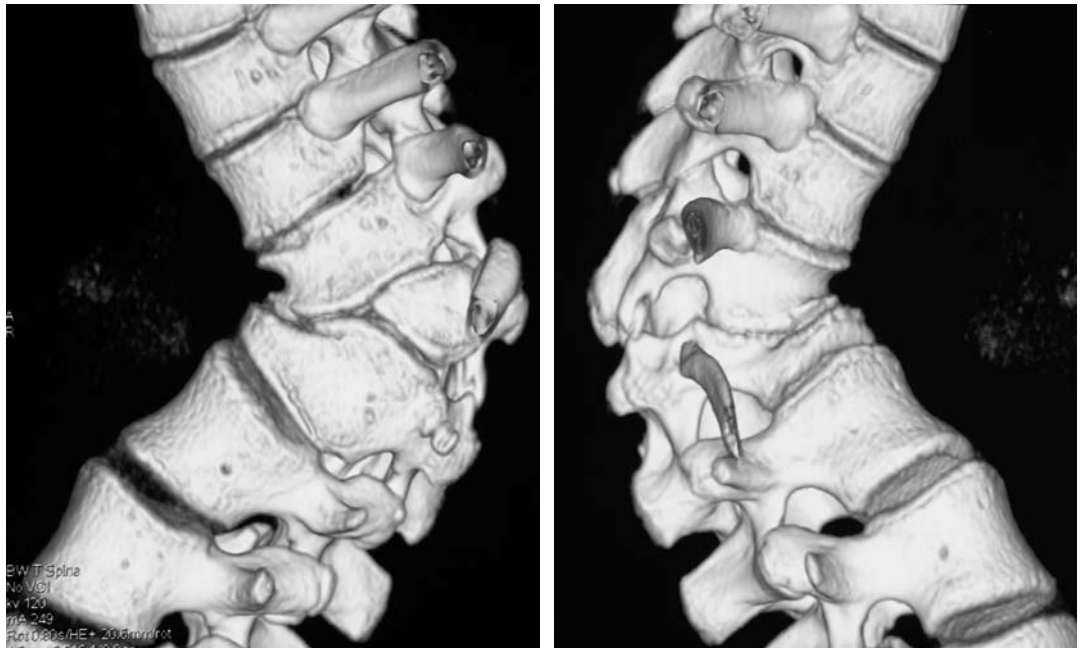

a b

Fig. 6.8a,b. Accelerated disc degeneration in a 14-year-old boy with a complex congenital spinal deformity, characterized by a hemivertebra. CT scan with volume rendered reconstructions (**a**, **b**). Despite the young age of the patient, there are already degenerative changes at the level of maximum scoliotic deformity

a b

Fig. 6.9a,b. Accelerated disc degeneration in a 73-year old man with an L4–L5 spondylolisthesis due to a bilateral spondylolysis (pars interarticularis defect). Sagittal T1-weighted (**a**) and T2-weighted (**b**) images. The L4–L5 disc is markedly narrowed and contains a vacuum cleft. The adjacent intervertebral discs present a normal appearance for the age of the patient

jects having an abnormality at one or more lumbar intervertebral discs (Jensen et al. 1994). The high prevalence of symptomless disc degeneration must be taken into account when MRI is used for assessment of spinal symptoms. The discovery by MRI of bulges or protrusions in people with low back pain is frequently coincidental.

Signal loss on T2-weighted scans is an early indicator of intervertebral disc degeneration on MRI (Modic and Herfkens 1990; Sether et al. 1990). The decrease in signal intensity is caused by the increase in fibrous tissue (collagen), which replaces the mucoid matrix of the nucleus pulposus. In the process of normal aging, the decrease in central disc signal intensity on T2-weighted MRI scans should be uniformly distributed among all the discs of the individual. If the signal loss affects only one or two discs, it should be considered abnormal. This finding is sometimes reported as a "black disc" in the neurosurgical and orthopedic literature (Fig. 6.2); and the term "black disc disease" has been applied to describe a discogenic pain syndrome (Rengachary and Balabhadra 2002). The degenerative process typically starts at the intervertebral discs that are subjected to the greatest mechanical stress in terms of weight-bearing or motion. In the lumbar spine L5–S1 and L4–L5 are most commonly affected. In the cervical spine, the C5–C6 and C6–C7 discs are most frequently involved (these segments bear the brunt of cervical spine motion).

Loss of height of the intervertebral disc is the earliest sign of disc degeneration to be seen on plain X-ray films. This finding indicates late shrinkage of the disc matrix and is only an indirect sign of disc degeneration (Brinckmann and Grootenboer 1991). Measuring disc height is a poor method for detecting early, painful degeneration changes (Vanharanta et al. 1988a). Loss of disc height has been reported on plain radiographs in asymptomatic subjects, indicating that there is no direct relationship between the imaging findings and the clinical symptoms. When assessing disc height, the position of the patient (standing or lying down) during the examination should be taken into account. Overall, the validity of disc height as an indicator of early disc degeneration is questionable (Luoma et al. 2001). Other signs, such as osteochondrotic changes, including sclerosis of the vertebral endplates with osteophytes, calcification and the vacuum disc phenomenon, are more reliable, though they indicate secondary or late stages of degenerative changes (Resnick 1985).

6.6 Annular Tears

With increasing age the water and proteoglycan content of intervertebral disc decreases, especially in the nucleus pulposus (Roberts et al. 2006). The degenerative process is accelerated when the structural integrity of the posterior annulus fibrosus becomes damaged by overload, usually due to a combination of flexion, rotation, and compressive loading forces (Southern et al. 2000). The intervertebral disc becomes less elastic and more fibrous. Eventually this leads to the formation of cracks and fissures in the annulus fibrosus, which are known as "annular tears".

It has been suggested that the terminology "annular fissure" is preferable to "annular tear" since the former does not imply a traumatic etiology, as the latter seems to do. However, in the international literature "annular tear" is most widely used, and this is also the terminology accepted by the Combined Task Forces of the North American Spine Society, American Society of Spine Radiology, and American Society of Neuroradiology (Fardon and Milette 2001; Milette 2001). Both concepts, annular fissure and annular tear, can be used synonymously, but it is important to remember that neither term articulates any knowledge of etiology, symptomatology, or need for treatment.

Annular tears can be classified as concentric, transverse or radial (Osti et al. 1992).

- *Concentric tears* are circumferential lesions which are found in the outer layers of the annular wall (Martin et al. 2002). They represent splitting between adjacent lamellae of the annulus, like onion rings. Concentric tears are most commonly encountered in the outer annulus fibrosus, and are believed to be of traumatic origin especially from torsion overload injuries.
- *Transverse tears*, also known as "peripheral tears" or "rim lesions," are horizontal ruptures of Sharpey's fibers, near the insertion in the bony ring apophysis. Their clinical significance remains unclear. Transverse tears are believed to be traumatically induced and are often associated with small osteophytes. According to some investigators transverse tears influence and accelerate the degeneration of the intervertebral disc and play a part in producing discogenic pain (Osti et al. 1992). Other authors assume transverse tears to be clinically insignificant (Morgan and Saifuddin 1999).

- *Radial tears* are characterized by an annular tear which permeates from the deep central part of the disc (nucleus pulposus) and extends outward toward the annulus, in either a transverse or cranial-caudal plane (Fig. 6.10). Most radial tears extend only partially into the annulus and do not reach the pain-sensitive outer rim of the annulus. The term "full thickness radial tear" is reserved for a tear that extends completely through the annulus fibrosus and reaches the outer rim. Radial annular tears are strongly associated with disc degeneration (Osti et al. 1992). The formation of a complete radial annular tear appears to be the necessary condition for the progressive deterioration of a disc (Herzog 1996).

In the thoracic spine, herniated discs are frequently associated with abnormal straight or curvilinear densities on CT; this finding is known as the "nuclear trail sign" (Awwad et al. 1992). On MRI, this may be associated with a comet-tail configuration in the axial plane (Fig. 6.11). This state of biomechanical disc failure indicates advanced disc disruption and degeneration; it must be distinguished from an aging disc that has not failed.

The clinical significance of annular tears is not yet fully understood. Some annular tears cause low back pain, even without modification of the disc contour. This concept is known as "discogenic pain" and is likely mediated by nociceptors in the external part of the annulus fibrosus (Southern et al. 2000). On the other hand, annular tears (and even nonfocal disc protrusions) are often found on MRI scans in asymptomatic subjects and can be considered as insignificant components of the aging process (Stadnik et al. 1998; Boos et al. 2002). Why are some annular tears painful and others not? One hypothesis states that, when nuclear material migrates through the tear into the external part of the annulus, which is well innervated with pain-sensitive nerve fibers, a chemical irritation and inflammation process occurs and causes "discogenic pain" (Crock 1986). This mechanism may also cause pain radiating to an extremity, even in the absence of any direct contact between extruding disc material and a nerve root (Milette et al. 1995). Another theory is that the degenerated and damaged nucleus no longer supports its share of the axial load of the body.

Annular tears can be recognized in two ways on MRI: as areas of high signal intensity on T2-weighted

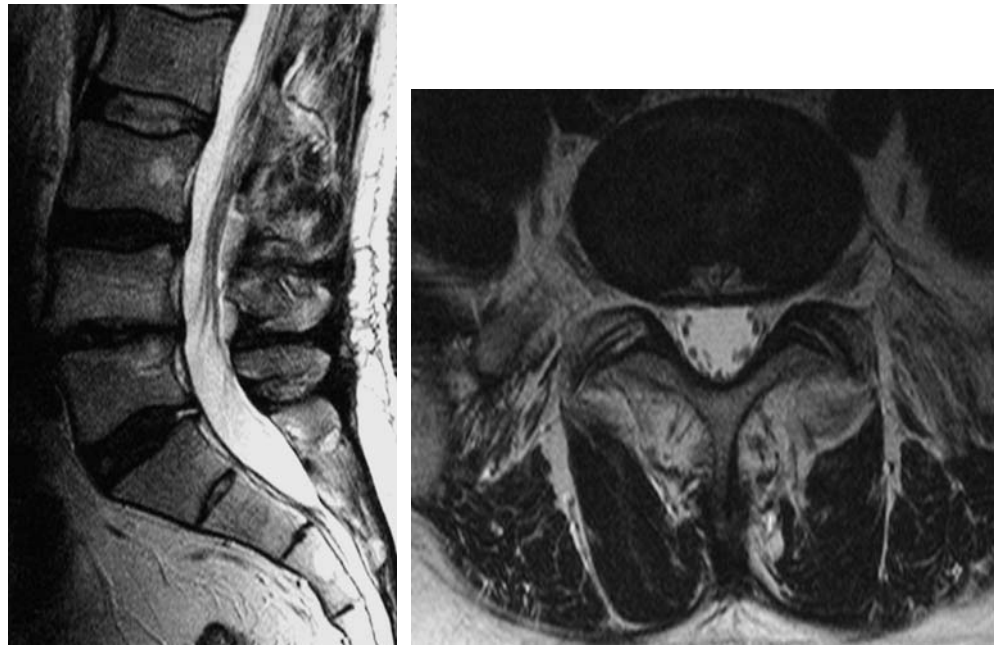

a b

Fig. 6.10a,b. Radial and concentric annular tear at L5–S1. Sagittal (**a**) and axial (**b**) T2-weighted images. The radial tear extends to the outer rim of the annulus fibrosus (**a**). The axial image (**b**) shows that, in addition, there is a concentric tear involving the outer circumference of the annulus fibrosus. There is marked degenerative narrowing of the L4–L5 intervertebral disc space. Note the T2-signal loss involving the lower intervertebral discs

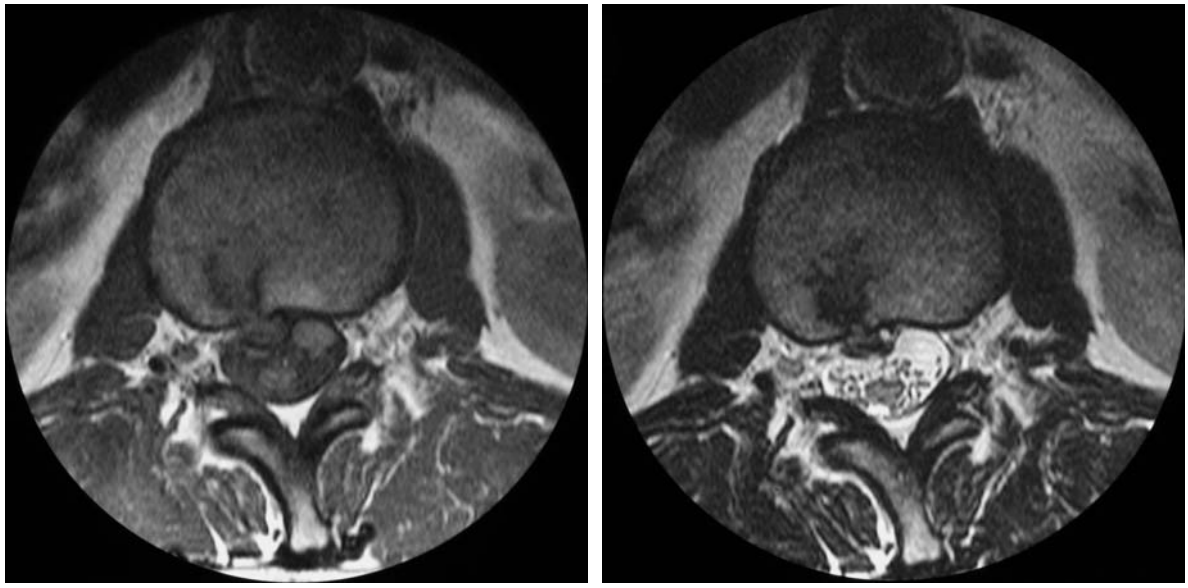

Fig. 6.11a, b. Complete radial annular tear with extruded disc at T12–L1 in a 58-year-old man. Axial T1-weighted (**a**) and T2-weighted (**b**) images. The trajectory of nuclear material through a complete radial annular tear presents a "comet tail" appearance. The extruded disc material in the spinal canal constitutes the head of the comet

images or as foci of annular enhancement on Gd-enhanced T1-weighted images (Ross et al. 1989). With repetitive microtrauma, annular tears may enlarge and become inflamed. The inflammatory response can be seen as an area of increased signal intensity in the posterior annulus fibrosus. This phenomenon, which is known in the lumbar spine as the high-intensity zone (HIZ), can be observed on T2-weighted MRI scans (Aprill and Bogduk 1992; Schellhas et al. 1996). On T2-weighted scans, the HIZ appears almost as hyperintense as the adjacent cerebrospinal fluid in the dural sac. The HIZ is believed to be a combination of a concentric and a radial annular tear, merged within the periphery of the disc (Aprill and Bogduk 1992). The presence of a HIZ has been suggested to correlate closely with painful outer annular disruption (Schellhas et al. 1996; Peng et al. 2006). However, the role of the HIZ in discogenic pain remains highly controversial, because it has been found in asymptomatic subjects as well (Stadnik et al. 1998; Weishaupt et al. 1998). The HIZ is considered to be a marker of a painful posterior annular tear, but the usefulness of this sign is limited by its poor sensitivity and limited positive predictive value (Saifuddin et al. 1998; Carragee et al. 2000; Weishaupt et al. 2001). In the cervical spine, histological features such as annular tears, rim lesions and prolapsed disc material are poorly recognized by MRI, even in severely degraded discs (Christe et al. 2005).

Annular tears tend to enhance strongly with gadolinium (Fig. 6.12) (Ross et al. 1989; Stadnik et al. 1998). The enhancement of annular tears corresponds with the microscopically confirmed presence of vascularization (newly formed blood vessels grow into the disc from the outer areas of the annulus) and granulation tissue (scar tissue formation) (Roberts et al. 2006). In association with an annular tear, extradural inflammation tissue is commonly found, suggesting a chemical inflammation due to an annular leak from a degenerating disc (Saifuddin et al. 1999). On pre-contrast T1-weighted images, extradural inflammation is seen as a region of intermediate signal intensity replacing the fat between the posterior disc margin and the dural sac; on post-contrast scans, it enhances intensely with gadolinium. Enhancement of a nerve root can also be observed, indicating the possibility of a "chemical radiculopathy" in the absence of mechanical root compression.

6.7 Disc Herniation

Degenerative disc disease leads to a loss of turgor of the nucleus pulposus and a diminished elasticity

of the annulus fibrosus. As a result, the disc bulges outward. *Herniation* is defined as a localized displacement of disc material (nucleus, cartilage, fragmented apophyseal bone, fragmented annular tissue) beyond the limits of the intervertebral disc space (Fardon and Milette 2001). The intervertebral disc space is the three-dimensional volume defined by the adjacent vertebral body endplates and by the outer edges of the vertebral ring apophyses, exclusive of osteophytes. Displacement of disc material can thus only occur when there is a disruption of the annulus fibrosus, or a break in the vertebral body endplate.

Herniated discs in the cranio-caudal (vertical) direction through a break in one or both of the vertebral body endplates are referred to as "*intravertebral herniations*" (also known as Schmorl's nodes). They are often surrounded by reactive bone marrow changes (Fig. 6.13). One hypothesis regarding the formation of intravertebral herniations is that the regression of the nutrient vascular canals may leave scars in the endplates, which are weak spots representing a route for the early formation of intrabody nuclear herniations (Chandraraj et al. 1998).

In young individuals, intrabody herniation of disc material can instigate the formation of a "*lim-*

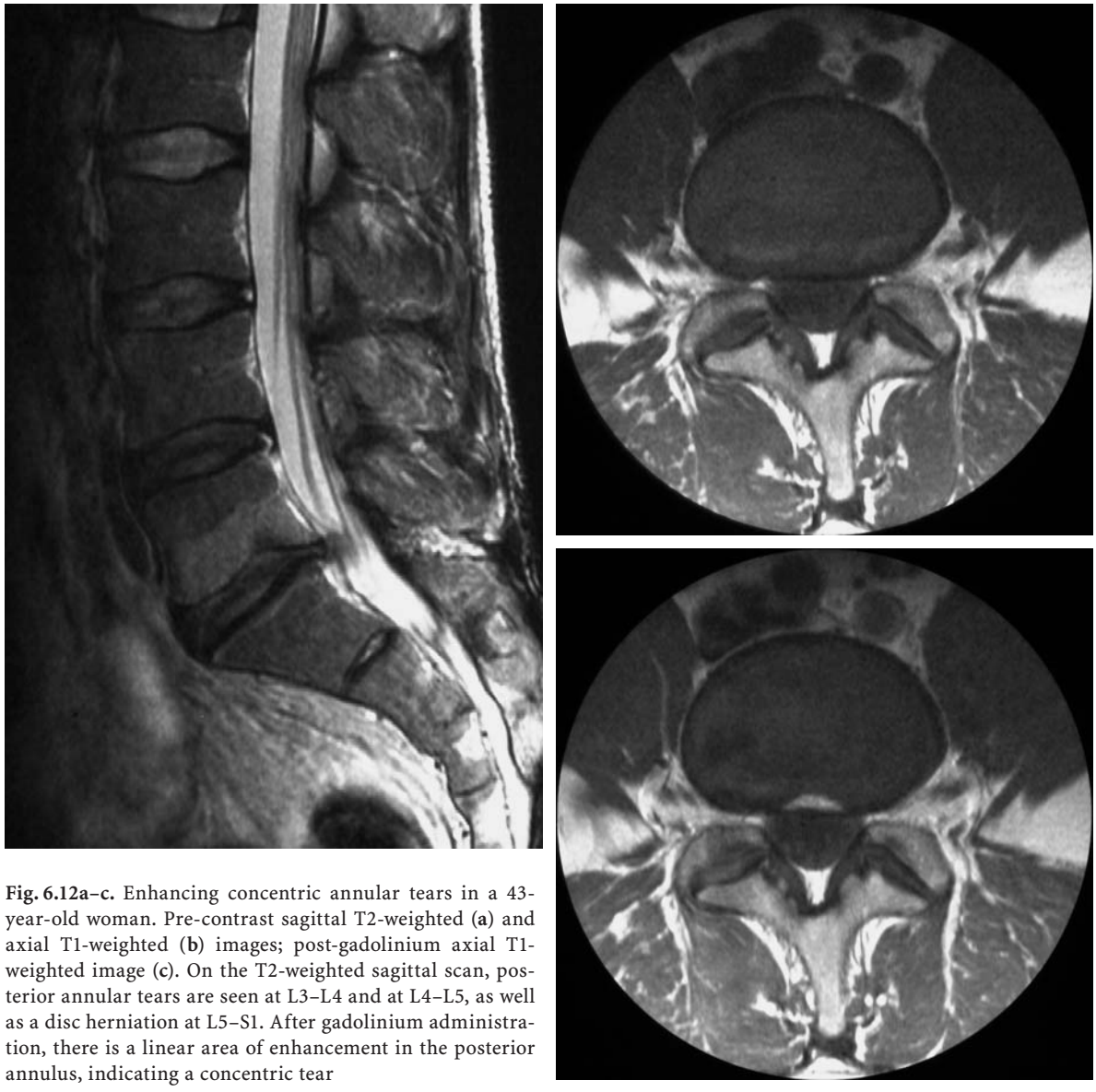

Fig. 6.12a–c. Enhancing concentric annular tears in a 43-year-old woman. Pre-contrast sagittal T2-weighted (**a**) and axial T1-weighted (**b**) images; post-gadolinium axial T1-weighted image (**c**). On the T2-weighted sagittal scan, posterior annular tears are seen at L3–L4 and at L4–L5, as well as a disc herniation at L5–S1. After gadolinium administration, there is a linear area of enhancement in the posterior annulus, indicating a concentric tear

bus vertebra". When herniation of the nucleus pulposus occurs through the ring apophysis prior to bony fusion, a small segment of the vertebral rim may become isolated (Mupparapu et al. 2002). Limbus vertebrae are most commonly found in the mid-lumbar region, and less commonly in the mid-cervical region. They are characterized by a defect in the anterior margin of the vertebral body usually at the anterior superior margin in the lumbar spine, and the anterior inferior margin in the cervical spine.

Generalized or circumferential disc displacement (involving 50% to 100% of the disc circumference) is known as "*bulging*", and is *not* considered a form of herniation. Bulging can be symmetrical (displacement of disc material is equal in all directions) or asymmetrical (frequently associated with scoliosis) (Fig. 6.14). The term bulge refers to a morphologic characteristic and is not correlated with etiology or symptomatology. Bulging can be physiologic (e.g. in the mid-cervical spine and at L5–S1), can reflect advanced degenerative disc disease, can be associated with bone remodeling (as in advanced osteoporosis), occur with ligamentous laxity, or can be a "pseudo-image" due to partial volume averaging (Fardon and Milette 2001).

Herniated discs can be more specifically classified as protrusion or extrusion, on the basis of the shape of the displaced material (Fig. 6.15). The terminology "*protruded disc*" is used when the base of the disc is broader than any other diameter of the displaced material. Based on a two-dimensional assessment of the disc contour in the transverse plane, a protruded disc can be focal (involving <25% of the disc circumference) or broad-based (involving 25%–50% of the disc circumference). The terminology "*extruded disc*" is used for a focal disc extension of which the base against the parent disc is narrower than the diameter of the extruded disc material, measured in the same plane (Figs. 6.16–6.18). Extrusion is also used when there is no continuity between the herniated disc material beyond the disc space and that within the disc space. If the displaced disc material has no connection with the parent disc, it is called a "*sequestrated fragment*" (Fig. 6.19). This is synonymous with a "*free fragment*". On imaging studies it is often impossible to determine if continuity exists between the extruded disc material and the parent disc. Therefore, it is sometimes more practical to use the term "*migration*", which signifies displacement of disc material away from the site of the extrusion, regardless of whether it is sequestrated or not (Fig. 6.20). The term migrated only refers to position and not to continuity.

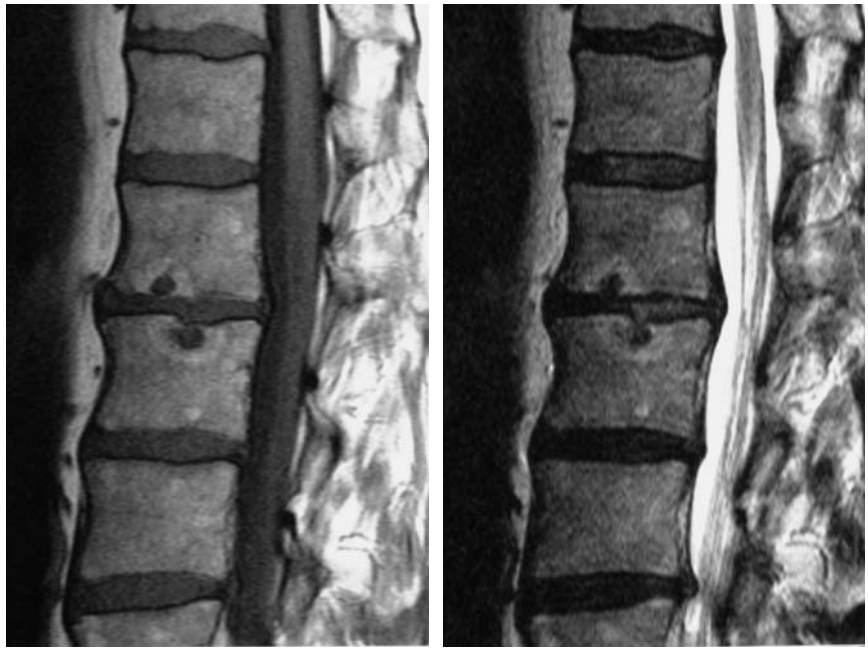

a b

Fig. 6.13a,b. Intravertebral herniations at L1–L2. Sagittal T1-weighted (**a**) and T2-weighted (**b**) scans. The intravertebral herniations are located in the lower endplate of L1 and the upper endplate of L2. They are surrounded by reactive bone marrow changes, which are hyperintense both on T1-and T2-weighted images (Modic type II changes)

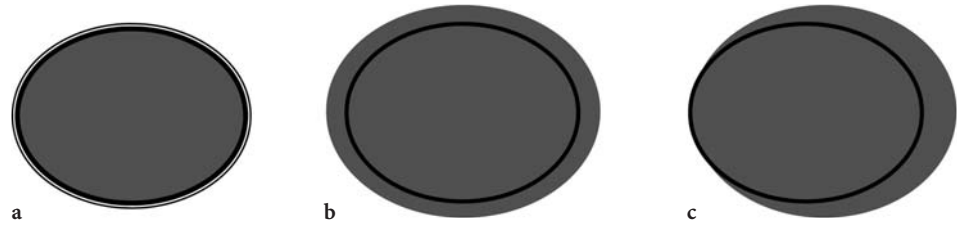

Fig. 6.14a–c. Symmetrical and asymmetrical bulging disc on transverse CT or MRI scans. **a** Normally the intervertebral disc (*gray*) does not extend beyond the edges of the ring apophyses (*black line*). **b** In a symmetrically bulging disc, the disc tissue extends concentrically beyond the edges of the ring apophyses (50%–100% of disc circumference). **c** An asymmetrical bulging disc can be associated with scoliosis. Bulging discs are not considered a form of herniation

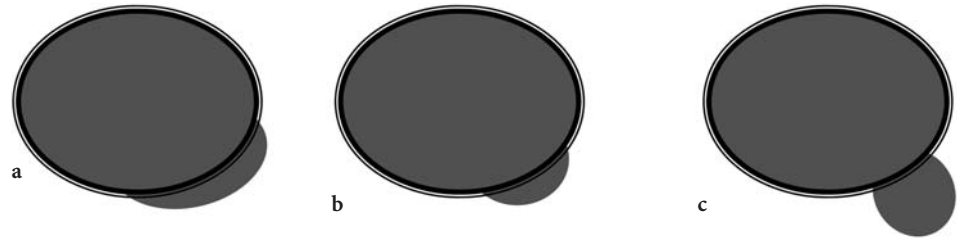

Fig. 6.15a–c. Types of disc herniation as seen on transverse CT or MRI scans. **a**, **b** Protrusions: the base of the herniated disc material is broader than the apex. Protrusions can be broad-based (**a**) or focal (**b**). **c** Extrusion: the base of the herniation is narrower than the apex (toothpaste sign)

It has been suggested to simplify the terminology by using the word herniation to designate both protrusions and extrusions as a group (Czervionke 1993). The Combined Task Forces have maintained the distinction, which is useful because extrusions are rare in asymptomatic patients, as opposed to bulges and protrusions (Brant-Zawadzki et al. 1995). Furthermore, the term extruded disc is more acceptable to patients because it is less emotionally laden and has fewer histologic, traumatic and clinical connotations than the word herniation (Deyo et al. 1990).

The term "*contained*" refers to displaced disc material which is covered by the outer annulus. If this covering is absent, the herniation is "*uncontained*". With cross-sectional imaging techniques such as CT or MRI it is usually not possible to distinguish a contained from an uncontained disc herniation. With discography, it is possible to separate a "leaking" from "nonleaking" disc, depending on the displacement of the injected contrast agent.

Reliable communication with clinicians requires an accurate and simple system to classify the position of disc fragments that have migrated horizontally or vertically. An elegant and useful alpha-numerical classification system, based on imaging findings, has been reported in the European literature (Bonneville 1990). Instead, the Combined Task Forces have opted for a classification based on anatomic boundaries frequently used by surgeons (Wiltse et al. 1997). In the transverse (axial) plane, the following zones are recognized:

- Central (posterior midline) (Fig. 6.21)
- Right/left central (also known as paracentral) (Fig. 6.22)
- Right/left subarticular (lateral recess)
- Right/left foraminal (neural foramen) (Fig. 6.23)
- Right/left extraforaminal (outside the neural foramen, also known as far lateral)
- anterior zone (anterior and anterolateral regions) (Fig. 6.24).

In the vertical plane, three levels are defined (from top to bottom):

- Pedicle level
- Infrapedicle level
- Disc level (Fig. 6.25)
- Suprapedicle level

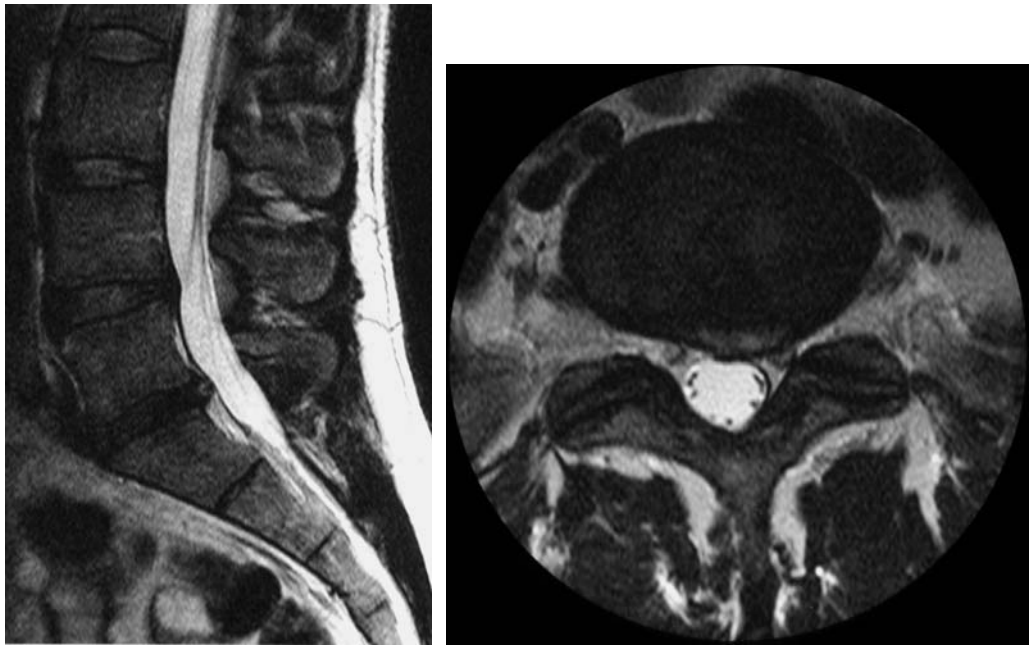

Fig. 6.16a,b. Broad-based lumbar disc protrusion at L5–S1 in a 44-year-old man. Sagittal (**a**) and axial (**b**) T2-weighted images. The protruding disc presents an increased signal intensity on these T2-weighted images, indicating an area of myxoid degeneration. The left lateral recess is narrowed, and the left S1 nerve root is displaced

Fig. 6.17a,b. Cervical disc extrusion at C6–C7 in a 43-year-old woman. Sagittal T2-weighted (**a**) and axial (**b**) T2*-weighted images. The extruded disc extends into the left lateral recess and the left intervertebral foramen. There is asymmetric deformation of the thecal sac

Fig. 6.18a–d. Massive lumbar disc extrusion at L5–S1 in a 44-year-old man. Sagittal (**a**) and axial (**b**) T1-weighted images; sagittal (**c**) and axial (**d**) T2-weighted images. The extruded disc compresses and displaces the right S1 nerve root. On the sagittal T1-weighted image, the continuity between the extruding portion and the parent disc can clearly be identified

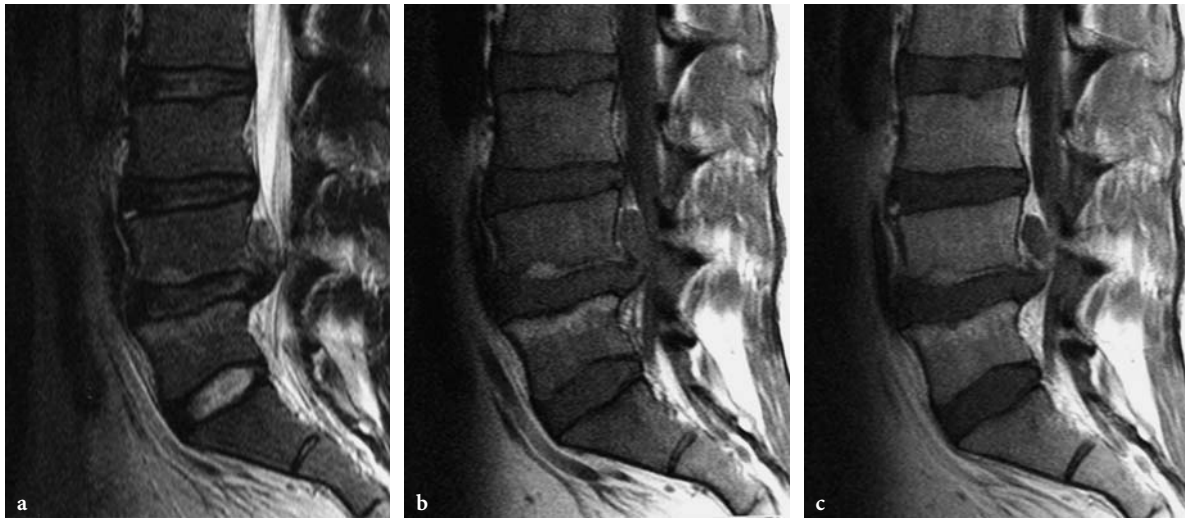

Fig. 6.19a–c. Upwardly migrated (ascending) disc herniation at L4–L5 in a 34-year old man. Pre-contrast sagittal T2-weighted (**a**) and T1-weighted (**b**) images; post-gadolinium sagittal T1-weighted image (**c**). The ascending fragment originates from the L4–L5 disc. After gadolinium injection, the disc fragment does not enhance; it is surrounded by enhancing structures (PLL, epidural veins)

Fig. 6.20a–d. Downwardly migrated (descending) disc herniation at L4–L5 in a 34-year-old man. Sagittal (**a**) and axial (**b**) T1-weighted images; sagittal (**c**) and axial (**d**) T2-weighted images. A very large disc fragment descends into the left lateral recess behind the L5 vertebral body. The disc is hypointense on T2-weighted scans indicating a fibrous nature

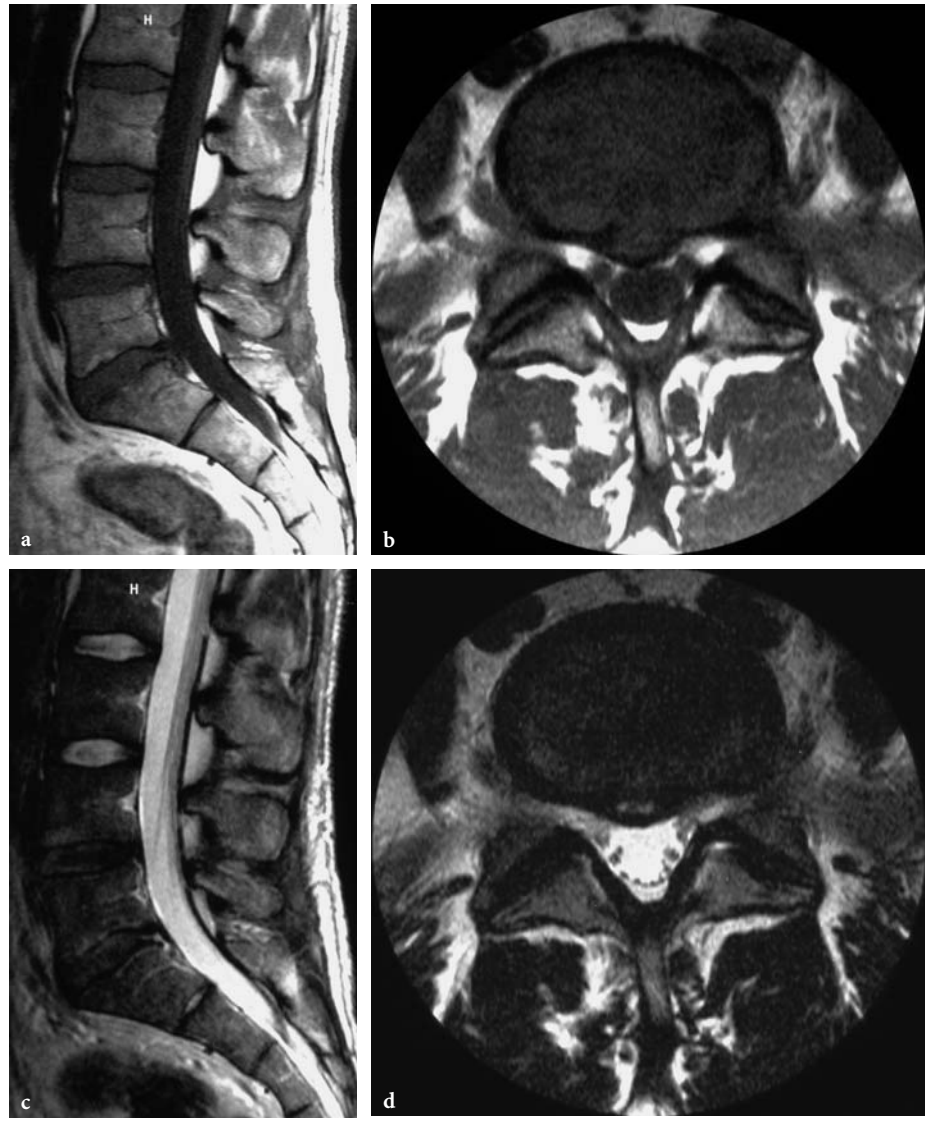

Fig. 6.21a–d. Central disc extrusion at L5–S1 in a 35-year-old man. Sagittal (**a**) and axial (**b**) T1-weighted images; sagittal (**c**) and axial (**d**) T2-weighted images. The herniated disc is located in the midline, in the anterior epidural space between the S1 nerve roots. There is an associated radial tear of the disc, as can be seen on the sagittal T2-weighted scan

6.8 Spontaneous Regression of Disc Herniation

Spontaneous regression of a lumbar disc herniation is a well-established and common finding in patients who do not undergo surgery or interventional therapy (Bozzao et al. 1992; Splendiani et al. 2004). The regression can imply a decrease in size or even complete disappearance of the herniated disc.

The exact underlying mechanism of spontaneous disc regression remains largely unknown, though several hypotheses have been proposed: retraction of disc material into the intervertebral space, dehydration or shrinkage of the disc, and resorption due to an inflammatory reaction (phagocytosis by macrophages) (Slavin et al. 2001). Factors which are associated with a high probability of spontaneous regression are: free fragment herniation,

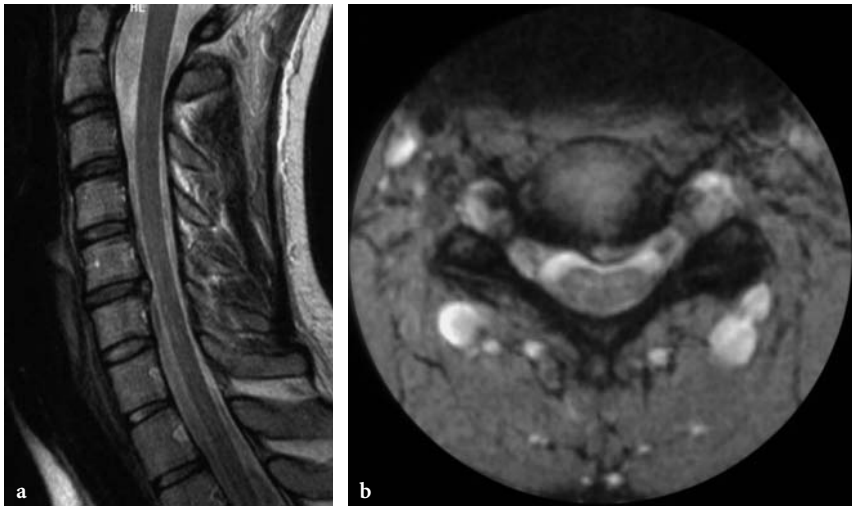

Fig. 6.22a,b. Left central disc protrusion at C5–C6 in a 26-year-old woman. Sagittal (**a**) and axial (**b**) T2-weighted images. The protruding disc is broad-based and impinges on the dural sac. It is slightly eccentric to the *left*. There is no radicular compression

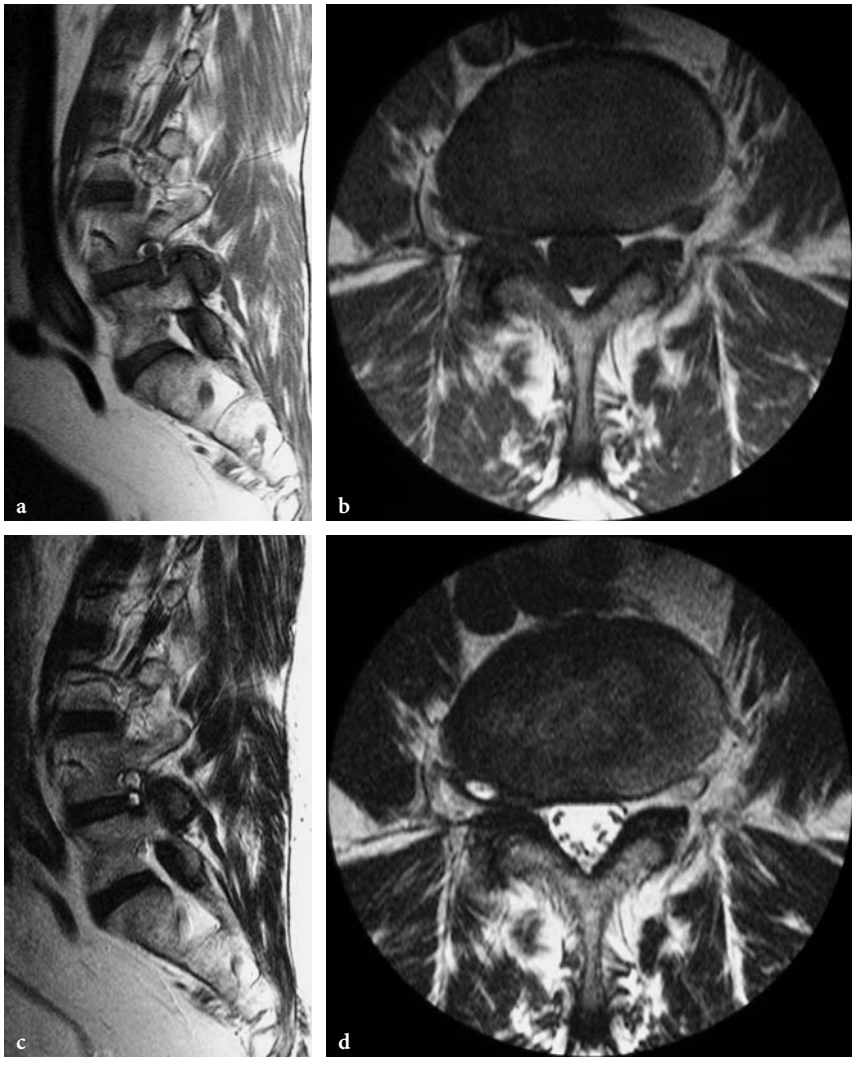

Fig. 6.23a–d. Right foraminal disc extrusion at L4–L5 in a 51-year-old man. Sagittal (**a**) and axial (**b**) T1-weighted images; sagittal (**c**) and axial (**d**) T2-weighted images. A broad-based disc extrusion extends into and beyond the right neural foramen. The herniated disc material contains a focal T2-hyperintense component, likely representing a fluid-filled disc cyst

Fig. 6.24a,b. Anterior zone disc extrusion at L2–L3 in a 38-year-old man. Sagittal (**a**) and axial (**b**) T1-weighted images. The L2–L3 disc space shows height loss, decreased signal intensity on T2, and there is an anterior zone disc extrusion with associated osteophytic spur formation

Fig. 6.25. Right foraminal herniation at the disc level in a 56-year-old man. Sagittal T1-weighted image. The disc extrudes into the neural foramen, and displaces the right L4 nerve root

high signal intensity on T2-weighted images, and herniations with peripheral contrast enhancement on T1-weighted images (Splendiani et al. 2004) (Fig. 6.26). Extruded disc material which is exposed to the epidural space (as in a free fragment) appears to be resolved more quickly than subligamentous disc material. Exposure to vascular supply probably plays an important role in the process of spontaneous resorption (Komori et al. 1996). Contrast enhancement of the posterior longitudinal ligament indicates an inflammatory response (Fig. 6.27). Areas of contrast uptake in the epidural space above and below the herniated disc reflect dilated and congested epidural veins (Fig. 6.28) (Parizel et al. 1989). A high rate of contrast enhancement is also correlated with invasion of granulation tissue; this indicates an ongoing absorption process and can be used to predict spontaneous reabsorption of a disc herniation (Kawaji et al. 2001).

The phenomenon of spontaneous regression of disc herniations has also been reported to occur in the cervical spine and rarely in the thoracic spine (Mochida et al. 1998). In the cervical spine, soft disc herniations are more likely to regress spontaneously if they are median or diffuse, while focal type herniations show less tendency to spontaneous regression (Matsumoto et al. 2001).

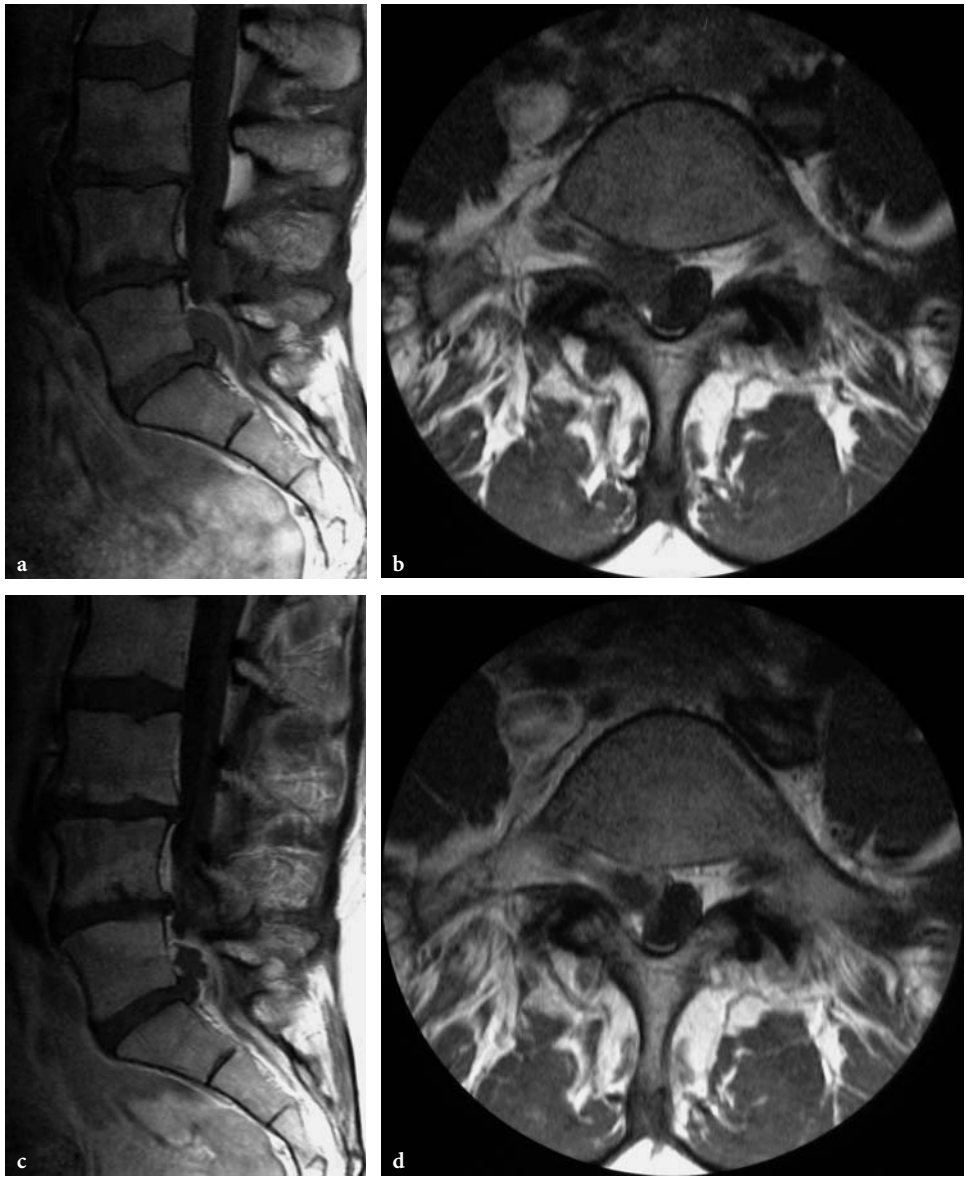

Fig. 6.26a–d. Sequestrated disc fragment at L5–S1 in a 48-year old woman. Pre-contrast sagittal (**a**) and axial (**b**) T1-weighted images; post-gadolinium sagittal (**c**) and axial (**d**) T1-weighted images. There is peripheral contrast enhancement on T1-weighted images (**c** and **d**). Peripheral contrast enhancement is associated with a high probability of spontaneous regression.

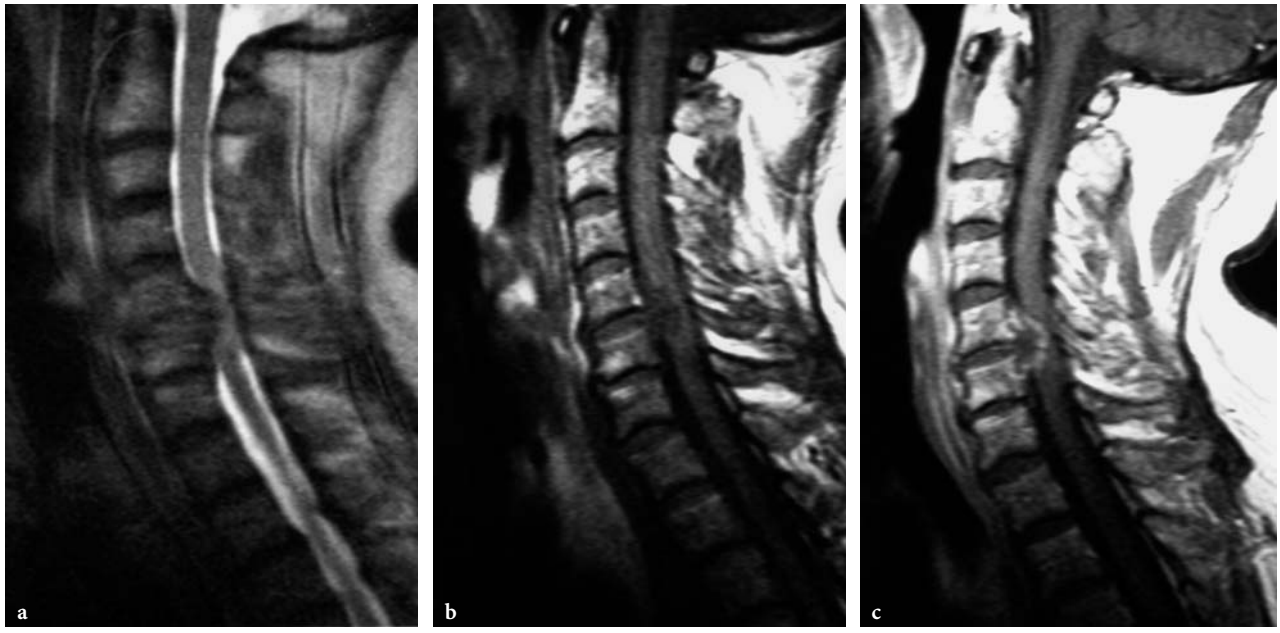

Fig. 6.27a–c. Enhancement surrounding a large C5–C6 disc extrusion indicates an inflammatory response. The patient is a 47-year-old woman. Pre-contrast sagittal T2-weighted (**a**) and T1-weighted (**b**) images; post-gadolinium sagittal T1-weighted image (**c**). After gadolinium injection, the extruded disc is surrounded by the enhancing posterior longitudinal ligament, indicating an inflammatory response

Fig. 6.28a–c. Thoracic disc extrusion in a 32-year-old woman. Pre-contrast sagittal T2-weighted (**a**) and T1-weighted (**b**) images; post-gadolinium sagittal T1-weighted image (**c**). After gadolinium injection, the extruded disc is surrounded by the enhancing posterior longitudinal ligament, which indicates an inflammatory response. Focal areas of contrast uptake in the epidural space above and below the herniated disc reflect dilated and congested epidural veins

6.9 Vertebral Endplates and Bone Marrow Changes

With aging, reactive degenerative changes frequently occur in the vertebral endplates and vertebral bodies (Karchevsky et al. 2005). In 1988, Modic and colleagues described three degenerative stages of vertebral endplates and subchondral bone (Modic et al. 1988a,b) (Table 6.2).

- Type 1 changes (decreased signal intensity on T1-weighted images and increased signal intensity on T2-weighted images) indicate bone marrow edema associated with acute or subacute inflammation (Fig. 6.29). Histopathologically, Modic type 1 changes correspond to disruption and fissuring of the endplates and vascularized fibrous tissue with bone marrow edema.
- Type 2 changes (increased signal intensity on T1-weighted images and isointense or increased signal intensity on T2-weighted images) indicate replacement of normal bone marrow by fat (Fig. 6.30).
- Type 3 changes (decreased signal intensity on both T1- and T2-weighted images) indicates reactive osteosclerosis. Overall, Modic type 2 changes (fatty pattern) are the most common, with Modic type 3 changes (sclerotic pattern) being rare (Karchevsky et al. 2005).

The Modic classification has the advantage of being reliable and reproducible, even for observers of varying clinical experience (Jones et al. 2005).

Modic signal intensity changes in the bone marrow adjacent to the vertebral endplates are a common observation on MRI. They occur more frequently with aging, and are correlated with weight and male gender (Karchevsky et al. 2005). Endplate degeneration may affect the whole of both endplates,

Table 6.2. Signal intensity changes in vertebral bone marrow adjacent to endplates of degenerative discs. (*SI* Signal intensity, *wi* weighted image)

Type I	↓ SI on T1 wi ↑ SI on T2 wi	Inflammatory stage (bone marrow edema)
Type II	↑ SI on T1 wi ↑ (or ≅) SI on T2 wi	Fatty stage (local fatty replacement of bone marrow)
Type III	↓ SI on T1 wi ↓ SI on T2 wi	Reactive osteosclerosis adjacent to the endplates

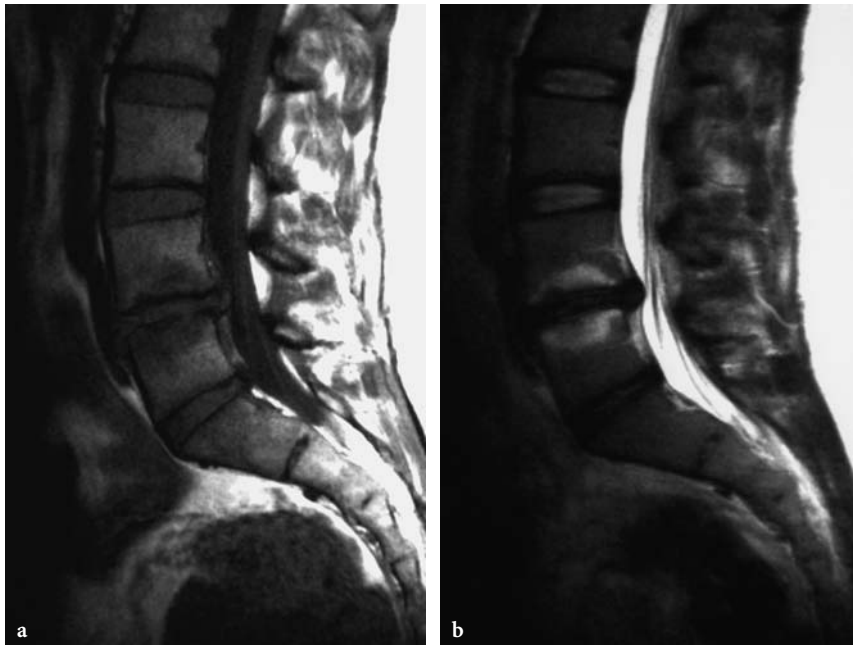

Fig. 6.29a, b. Modic type 1 changes at L4–L5 in a 29-year-old woman. Sagittal (**a**) T1-weighted (**a**) and sagittal T2-weighted (**b**) images. There is decreased signal intensity on T1-weighted images and increased signal intensity on T2-weighted images, indicating bone marrow edema associated with acute or subacute inflammation. The patient also has a right central disc protrusion

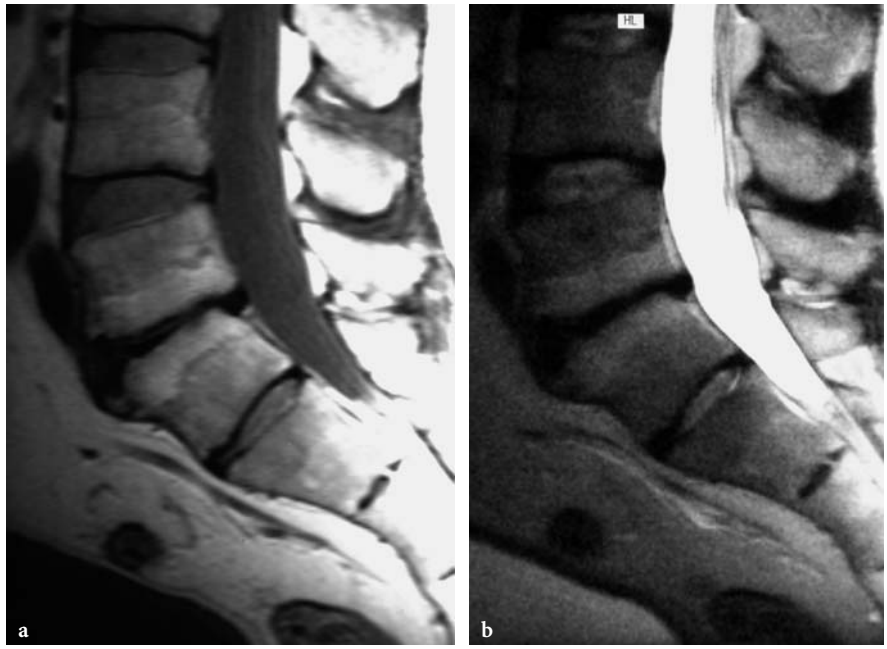

Fig. 6.30a, b. Modic type 2 changes at L4–L5 in a 51-year-old woman. Sagittal T1-weighted (**a**) and sagittal T2-weighted (**b**) images. There is increased signal intensity on T1-weighted images and mildly increased signal intensity on T2-weighted images, indicating replacement of normal bone marrow by fat. The patient has a rudimentary L5–S1 disc, with accelerated degeneration at L4–L5

although involvement of just one endplate, or even a segment thereof, can occur. In the lower lumbar spine, the anterior aspect of the endplates is most commonly involved.

Modic type 1 changes reflect an acute inflammatory stage, and can be associated with substantial functional disability. In a large majority of cases, Modic type 1 lesions naturally transform into type 2 lesions (Mitra et al. 2004). The transformation usually takes place over a time course of 1–2 years, and can relate to a change in patient's symptoms. In patients with painful lumbar instability, Modic type 1 lesions are frequently found (Parizel et al. 1999). The evolution of type 1 into type 2 lesions is accelerated after osteosynthesis, probably by correcting mechanical instability (Vital et al. 2003). Types 2 and 3 indicate chronic changes, and tend to remain stable over many years.

References

Aguila LA, Piraino DW, Modic MT, Dudley AW, Duchesneau PM, Weinstein MA (1985) The intranuclear cleft of the intervertebral disk: magnetic resonance imaging. Radiology 155:155–158

Albeck MJ, Hilden J, Kjaer L, Holtas S, Praestholm J, Henriksen O, Gjerris F (1995) A controlled comparison of myelography, computed tomography, and magnetic resonance imaging in clinically suspected lumbar disc herniation. Spine 20:443–448

Aprill C, Bogduk N (1992) High intensity zone: a diagnostic sign of painful lumbar disc on magnetic resonance imaging. Br J Radiol 65:361–369

Awwad EE, Martin DS, Smith KR Jr (1992) The nuclear trial sign in thoracic herniated disks. AJNR Am J Neuroradiol 13:137–143

Benneker LM, Heini PF, Alini M, Anderson SE, Ito K (2005a) 2004 Young Investigator Award Winner: vertebral endplate marrow contact channel occlusions and intervertebral disc degeneration. Spine 30:167–173

Benneker LM, Heini PF, Anderson SE, Alini M, Ito K (2005b) Correlation of radiographic and MRI parameters to morphological and biochemical assessment of intervertebral disc degeneration. Eur Spine J 14:27–35

Bertram H, Steck E, Zimmerman G, Chen B, Carstens C, Nerlich A, Richter W (2006) Accelerated intervertebral disc degeneration in scoliosis versus physiological ageing develops against a background of enhanced anabolic gene expression. Biochem Biophys Res Commun 342:963–972

Bini W, Yeung AT, Calatayud V, Chaaban A, Seferlis T (2002) The role of provocative discography in minimally invasive selective endoscopic discectomy. Neurocirugia (Astur) 13:27–31

Boden SD, Davis DO, Dina TS, Patronas NJ, Wiesel SW (1990) Abnormal magnetic-resonance scans of the lumbar spine

in asymptomatic subjects. J Bone Joint Surg Am 72:403–408
Bogduk N, Modic MT (1996) Lumbar discography. Spine 21:402–404
Bonneville JF (1990) Plaidoyer pour une classification par l'image des hernies discales lombaires: la carte-image. Rev Im Med 2:557–560
Boos N, Weissbach S, Rohrbach H, Weiler C, Spratt KF, Nerlich AG (2002) Classification of age-related changes in lumbar intervertebral discs: 2002 Volvo award in basic science. Spine 27:2631–2644
Bozzao A, Gallucci M, Masciocchi C, Aprile I, Barile A, Passariello R (1992) Lumbar disk herniation: MR imaging assessment of natural history in patients treated without surgery. Radiology 185:135–141
Bradley WG (1999) Use of contrast in MR imaging of the lumbar spine. Magn Reson Imaging Clin N Am 7:439–457
Brant-Zawadzki MN, Jensen MC, Obuchowski N, Ross JS, Modic MT (1995) Interobserver and intraobserver variability in interpretation of lumbar disc abnormalities. A comparison of two nomenclatures. Spine 20:1257–1263
Brinckmann P, Grootenboer H (1991) Change of disc height, radial disc bulge, and intradiscal pressure from discectomy. An in vitro investigation on human lumbar discs. Spine 16:641–646
Carragee EJ, Alamin TF (2001) Discography: a review. Spine J 1:364–372
Carragee EJ, Paragioudakis SJ, Khurana S (2000) 2000 Volvo Award winner in clinical studies: lumbar high-intensity zone and discography in subjects without low back problems. Spine 25:2987–2992
Carragee EJ, Alamin TF, Carragee JM (2006) Low-pressure positive discography in subjects asymptomatic of significant low back pain illness. Spine 31:505–509
Chandraraj S, Briggs CA, Opeskin K (1998) Disc herniations in the young and end-plate vascularity. Clin Anat 11:171–176
Christe A, Laubli R, Guzman R, Berlemann U, Moore RJ, Schroth G, Vock P, Lovblad KO (2005) Degeneration of the cervical disc: histology compared with radiography and magnetic resonance imaging. Neuroradiology 47:721–729
Crock HV (1986) Internal disc disruption. A challenge to disc prolapse fifty years on. Spine 11:650–653
Czervionke LF (1993) Lumbar intervertebral disc disease. Neuroimaging Clin N Am 3:465–485
Desmond PM, Buirski G (1993) Magnetic resonance appearances of developmental disc anomalies in the lumbar spine. Australas Radiol 37:26–29
Deyo RA, Loeser JD, Bigos SJ (1990) Herniated lumbar intervertebral disk. Ann Intern Med 112:598–603
Elster AD (1989) Bertolotti's syndrome revisited. Transitional vertebrae of the lumbar spine. Spine 14:1373–1377
Erkintalo MO, Salminen JJ, Alanen AM, Paajanen HEK, Kormano MJ (1995) Development of degenerative changes in the lumbar intervertebral disk: results of a prospective MR imaging study in adolescents with and without low-back pain. Radiology 196:529–533
Fardon DF, Milette PC, Combined Task Forces of the North American Spine Society, American Society of Spine Radiology, and American Society of Neuroradiology (2001) Nomenclature and classification of lumbar disc pathology. Recommendations of the Combined Task Forces of the North American Spine Society, American Society of Spine Radiology, and American Society of Neuroradiology. Spine 26:E93–E113
Frymoyer JW, Newberg A, Pope MH, Wilder DG, Clements J, MacPherson B (1984) Spine radiographs in patients with low-back pain. J Bone Joint Surg Am 66:1048–1055
Georgy BA, Hesselink JR (1994) MR imaging of the spine: recent advances in pulse sequences and special techniques. AJR Am J Roentgenol 162:923–934
Grant GA, Goodkin R, Maravilla KR, Kliot M (2004) MR neurography: diagnostic utility in the surgical treatment of peripheral nerve disorders. Neuroimaging Clin N Am 14:115–133
Guyer RD, Ohnmeiss DD (1995) Lumbar discography. Position statement from the North American Spine Society Diagnostic and Therapeutic Committee. Spine 20:2048–2059
Guyer RD, Ohnmeiss DD; NASS (2003) Lumbar discography. Spine J 3 (Suppl):11S–27S
Haughton V (2004) Medical imaging of intervertebral disc degeneration. Spine 29:2751–2756
Herzog RJ (1996) The radiologic assessment for a lumbar disc herniation. Spine 21:19S–38S
Hitselberger WE, Witten RM (1968) Abnormal myelograms in asymptomatic patients. J Neurosurg 28:204–206
Hsu EW, Setton LA (1999) Diffusion tensor microscopy of the intervertebral disc anulus fibrosus. Magn Reson Med 41:992–999
Inoue H, Takeda T (1975) Three-dimensional observation of collagen framework of lumbar intervertebral discs. Acta Orthop Scand 46:949–956
Jackson RP, Cain JE Jr, Jacobs RR, Cooper BR, McManus GE (1989) The neuroradiographic diagnosis of lumbar herniated nucleus pulposus: II. A comparison of computed tomography (CT), myelography, CT-myelography, and magnetic resonance imaging. Spine 14:1362–1367
Jarvik JG, Deyo RA (2000) Imaging of lumbar intervertebral disk degeneration and aging, excluding disk herniations. Radiol Clin North Am 38:1255–1266
Jarvik JG, Haynor DR, Koepsell TD, Bronstein A, Ashley D, Deyo RA (1996) Interreader reliability for a new classification of lumbar disk disease. Acad Radiol 3:537–544
Jensen MC, Brant-Zawadzki MN, Obuchowski N, Modic MT, Malkasian D, Ross JS (1994) Magnetic resonance imaging of the lumbar spine in people without back pain. N Engl J Med 331:69–73
Jinkins JR, Runge VM (1995) The use of MR contrast agents in the evaluation of disease of the spine. Top Magn Reson Imaging 7:168–180
Jones A, Clarke A, Freeman BJ, Lam KS, Grevitt MP (2005) The Modic classification: inter- and intraobserver error in clinical practice. Spine 30:1867–1869
Karakida O, Ueda H, Ueda M, Miyasaka T (2003) Diurnal T2 value changes in the lumbar intervertebral discs. Clin Radiol 58:389–392
Karasek M, Bogduk N (2000) Twelve-month follow-up of a controlled trial of intradiscal thermal anuloplasty for back pain due to internal disc disruption. Spine 25:2601–2607
Karchevsky M, Schweitzer ME, Carrino JA, Zoga A, Montgomery D, Parker L (2005) Reactive endplate marrow changes: a systematic morphologic and epidemiologic evaluation. Skeletal Radiol 34:125–129

Kawaji Y, Uchiyama S, Yagi E (2001) Three-dimensional evaluation of lumbar disc hernia and prediction of absorption by enhanced MRI. J Orthop Sci 6:498–502
Kerttula LI, Jauhiainen JP, Tervonen O, Suramo IJ, Koivula A, Oikarinen JT (2000) Apparent diffusion coefficient in thoracolumbar intervertebral discs of healthy young volunteers. J Magn Reson Imaging 12:255–260
Kerttula L, Kurunlahti M, Jauhiainen J, Koivula A, Oikarinen J, Tervonen O (2001) Apparent diffusion coefficients and T2 relaxation time measurements to evaluate disc degeneration. A quantitative MR study of young patients with previous vertebral fracture. Acta Radiol 42:585–591
Kettler A, Wilke HJ (2006) Review of existing grading systems for cervical or lumbar disc and facet joint degeneration. Eur Spine J 15:705–718
Komori H, Shinomiya K, Nakai O, Yamaura I, Takeda S, Furuya K (1996) The natural history of herniated nucleus pulposus with radiculopathy. Spine 21:225–229
Luoma K, Vehmas T, Riihimaki H, Raininko R (2001) Disc height and signal intensity of the nucleus pulposus on magnetic resonance imaging as indicators of lumbar disc degeneration. Spine 26:680–686
Martin MD, Boxell CM, Malone DG (2002) Pathophysiology of lumbar disc degeneration: a review of the literature. Neurosurg Focus 13:E1–E5
Matsumoto M, Chiba K, Ishikawa M, Maruiwa H, Fujimura Y, Toyama Y (2001) Relationships between outcomes of conservative treatment and magnetic resonance imaging findings in patients with mild cervical myelopathy caused by soft disc herniations. Spine 26:1592–1598
Milette PC (1997) The proper terminology for reporting lumbar intervertebral disk disorders. AJNR Am J Neuroradiol 18:1859–1866
Milette PC (2000) Classification, diagnostic imaging, and imaging characterization of a lumbar herniated disc. Radiol Clin North Am 38:1267–1292
Milette PC (2001) Reporting lumbar disk abnormalities: at last, consensus! AJNR Am J Neuroradiol 22:428–429
Milette PC, Fontaine S, Lepanto L, Breton G (1995) Radiating pain to the lower extremities caused by lumbar disk rupture without spinal nerve root involvement. AJNR Am J Neuroradiol 16:1605–1613
Mitra D, Cassar-Pullicino VN, McCall IW (2004) Longitudinal study of vertebral type-1 end-plate changes on MR of the lumbar spine. Eur Radiol 14:1574–1581
Mixter WJ, Barr JS (1934) Rupture of the intervertebral disc with involvement of the spinal canal. N Engl J Med 211:210 –214
Mochida K, Komori H, Okawa A, Muneta T, Haro H, Shinomiya K (1998) Regression of cervical disc herniation observed on magnetic resonance images. Spine 23:990–995
Modic MT, Herfkens RJ (1990) Devil's advocate: normal age-related changes in MR signal intensity. Radiology 177:332–334
Modic MT, Masaryk TJ, Ross JS, Carter JR (1988a) Imaging of degenerative disk disease. Radiology 168:177–186
Modic MT, Steinberg PM, Ross JS, Masaryk TJ, Carter JR (1988b) Degenerative disk disease: assessment of changes in vertebral body marrow with MR imaging. Radiology 166:193–199
Moneta GB, Videman T, Kaivanto K, Aprill C, Spivey M, Vanharanta H, Sachs BL, Guyer RD, Hochschuler SH, Raschbaum RF (1994) Reported pain during lumbar discography as a function of anular ruptures and disc degeneration. A re-analysis of 833 discograms. Spine 19:1968–1974
Morgan S, Saifuddin A (1999) MRI of the lumbar intervertebral disc. Clin Radiol 54:703–723
Mupparapu M, Vuppalapati A, Mozaffari E (2002) Radiographic diagnosis of Limbus vertebra on a lateral cephalometric film. Dentomaxillofac Radiol 31:328–330
Nachemson A (1989) Lumbar discography – where are we today? Spine 14:555–557
Osti OL, Vernon-Roberts B, Moore R, Fraser RD (1992) Annular tears and disc degeneration in the lumbar spine. A post-mortem study of 135 discs. J Bone Joint Surg Br 74:678–682
Parizel PM, Wilmink JT (1998) Imaging of the spine: techniques and indications. In: Algra PR, Valk J, Heimans JJ (eds) Diagnosis and therapy of spinal tumors (Medical Radiology – Diagnostic Imaging and Radiation Oncology). Springer-Verlag, Berlin Heidelberg New York, pp 15–48
Parizel PM, Rodesch G, Baleriaux D, Zegers de Beyl D, D'Haens J, Noterman J, Segebarth C (1989) Gd-DTPA-enhanced MR in thoracic disc herniations. Neuroradiology 31:75–79
Parizel PM, Özsarlak Ö, Van Goethem JWM, van den Hauwe L, De Schepper AMA (1999) The use of magnetic resonance imaging in lumbar instability (Chapter 13). In: Szpalski M, Gunzburg R, Pope MH (eds) Lumbar segmental instability. Lippincott Williams and Wilkins, Philadelphia, pp 123–138
Parizel PM, Van Goethem JW, Ozsarlak O, De Schepper AM (2003) Pattern recognition of degenerative disorders in the lumbar spine. Guidelines to MR image interpretation. JBR-BTR 86:222–226
Peng B, Hou S, Wu W, Zhang C, Yang Y (2006) The pathogenesis and clinical significance of a high-intensity zone (HIZ) of lumbar intervertebral disc on MR imaging in the patient with discogenic low back pain. Eur Spine J 15:583–587
Perry J, Haughton V, Anderson PA, Wu Y, Fine J, Mistretta C (2006) The value of T2 relaxation times to characterize lumbar intervertebral disks: preliminary results. AJNR Am J Neuroradiol 27:337–342
Powell MC, Wilson M, Szypryt P, Szypryt P, Symonds EM, Worthington BS (1986) Prevalence of lumbar disc degeneration observed by magnetic resonance in symptomless women. Lancet 2(8520):1366–1367
Prescher A (1998) Anatomy and pathology of the aging spine. Eur J Radiol 27:181–195
Rajasekaran S, Babu JN, Arun R, Armstrong BR, Shetty AP, Murugan S (2004) ISSLS prize winner: a study of diffusion in human lumbar discs: a serial magnetic resonance imaging study documenting the influence of the end-plate on diffusion in normal and degenerate discs. Spine 29:2654–2667
Rauch RA, Jinkins JR (1993) Lumbosacral spondylolisthesis associated with spondylolysis. Neuroimaging Clin North Am 3:543–555
Rengachary SS, Balabhadra RS (2002) Black disc disease: a commentary. Neurosurg Focus 13:1–4
Resnick D (1985) Degenerative diseases of the vertebral column. Radiology 156:3–14
Resnick D, Niwayama G (1995) Degenerative disease of the spine. In: Resnick D, (ed) Diagnosis of bone and joint

disorders, 3rd edn. Saunders, Philadelphia, Pa, pp 1372–1462

Roberts S, Evans H, Trivedi J, Menage J (2006) Histology and pathology of the human intervertebral disc. J Bone Joint Surg Am 88 (Suppl 2):10–14

Ross JS, Modic MT, Masaryk TJ (1989) Tears of the anulus fibrosus: assessment with Gd-DTPA-enhanced MR imaging. AJNR Am J Neuroradiol 10:1251–1254

Ross JS, Ruggieri P, Tkach J, Obuchowski N, Dillinger J, Masaryk TJ, Modic MT (1993) Lumbar degenerative disk disease: prospective comparison of conventional T2-weighted spin-echo imaging and T2-weighted rapid acquisition relaxation-enhanced imaging. AJNR Am J Neuroradiol 14:1215–1223

Saifuddin A, Braithwaite I, White J, Taylor BA, Renton P (1998) The value of lumbar spine magnetic resonance imaging in the demonstration of anular tears. Spine 23:453–457

Saifuddin A, Mitchell R, Taylor BA (1999) Extradural inflammation associated with annular tears: demonstration with gadolinium-enhanced lumbar spine MRI. Eur Spine J 8:34–39

Saifuddin A, Blease S, MacSweeney E (2003a) Axial loaded MRI of the lumbar spine. Clin Radiol 58:661–671

Saifuddin A, McSweeney E, Lehovsky J (2003b) Development of lumbar high intensity zone on axial loaded magnetic resonance imaging. Spine 28:E449–E451

Schellhas KP, Pollei SR, Gundry CR, Heithoff KB (1996) Lumbar disc high-intensity zone. Correlation of magnetic resonance imaging and discography. Spine 21:79–86

Schiebler ML, Camerino VJ, Fallon MD, Zlatkin MB, Grenier N, Kressel HY (1991a) In vivo and ex vivo magnetic resonance imaging evaluation of early disc degeneration with histopathologic correlation. Spine 16:635–640

Schiebler ML, Grenier N, Fallon M, Camerino V, Zlatkin M, Kressel HY (1991b) Normal and degenerated intervertebral disk: in vivo and in vitro MR imaging with histopathologic correlation. AJR Am J Roentgenol 157:93–97

Sether LA, Yu S, Haughton VM, Fischer ME (1990) Intervertebral disk: normal age-related changes in MR signal intensity. Radiology 177:385–388

Slavin KV, Raja A, Thornton J, Wagner FC Jr (2001) Spontaneous regression of a large lumbar disc herniation: report of an illustrative case. Surg Neurol 56:333–336

Southern EP, Fye MA, Panjabi MM, Patel TC, Cholewicki J (2000) Disc degeneration: a human cadaveric study correlating magnetic resonance imaging and quantitative discomanometry. Spine 25:2171–2175

Splendiani A, Puglielli E, De Amicis R, Barile A, Masciocchi C, Gallucci M (2004) Spontaneous resolution of lumbar disk herniation: predictive signs for prognostic evaluation. Neuroradiology 46:916–922

Stadnik TW, Lee RR, Coen HL, Neirynck EC, Buisseret TS, Osteaux MJ (1998) Annular tears and disk herniation: prevalence and contrast enhancement on MR images in the absence of low back pain or sciatica. Radiology 206:49–55

Tehranzadeh J (1998) Discography 2000. Radiol Clin North Am 36(3):463–495

Thalgott JS, Albert TJ, Vaccaro AR, Aprill CN, Giuffre JM, Drake JS, Henke JP (2004) A new classification system for degenerative disc disease of the lumbar spine based on magnetic resonance imaging, provocative discography, plain radiographs and anatomic considerations. Spine J 4(Suppl):167S–172S

Torgerson WR, Dotter WF (1976) Comparative roentgenographic study of the asymptomatic and symptomatic lumbar spine. J Bone Joint Surg Am 58:850–853

Twomey LT, Taylor JR (1987) Age changes in lumbar vertebrae and intervertebral discs. Clin Orthop 224:97–104

Vanharanta H, Guyer RD, Ohnmeiss DD, Stith WJ, Sachs BL, Aprill C, Spivey M, Rashbaum RF, Hochschuler SH, Videman T (1988a) Disc deterioration in low-back syndromes. A prospective, multi-center CT/discography study. Spine 13:1349–1351

Vanharanta H, Sachs BL, Spivey M, Hochschuler SH, Guyer RD, Rashbaum RF, Ohnmeiss DD, Mooney V (1988b) A comparison of CT/discography, pain response and radiographic disc height. Spine 13:321–324

Vergauwen S, Parizel PM, van Breusegem L, Van Goethem JW, Nackaerts Y, van den Hauwe L, De Schepper AM (1997) Distribution and incidence of degenerative spine changes in patients with a lumbo-sacral transitional vertebra. Eur Spine J 6:168–172

Vital JM, Gille O, Pointillart V, Pedram M, Bacon P, Razanabola F, Schaelderle C, Azzouz S (2003) Course of Modic 1 six months after lumbar posterior osteosynthesis. Spine 28:715–720

Walsh TR, Weinstein JN, Spratt KF, Lehmann TR, Aprill C, Sayre H (1990) Lumbar discography in normal subjects. J Bone Joint Surg Am 72:1081–1088

Warwick R, Williams PL (1973) Gray's anatomy, 35th edn. Longman Group, Edinburgh

Weinreb JC, Wolbarsht LB, Cohen JM, Brown CEL, Maravilla KR (1989) Prevalence of lumbosacral intervertebral disk abnormalities on MR images in pregnant and asymptomatic nonpregnant women. Radiology 170:125–128

Weishaupt D, Zanetti M, Hodler J, Boos N (1998) MR imaging of the lumbar spine: prevalence of intervertebral disk extrusion and sequestration, nerve root compression, end plate abnormalities, and osteoarthritis of the facet joints in asymptomatic volunteers. Radiology 209:661–666

Weishaupt D, Zanetti M, Hodler J, Min K, Fuchs B, Pfirrmann CW, Boos N (2001) Painful lumbar disk derangement: relevance of endplate abnormalities at MR imaging. Radiology 218:420–427

Wiesel SW, Tsourmas N, Feffer HL, Citrin CM, Patronas N (1984) A study of computed-assisted tomography. I. The incidence of positive CAT scans in an asymptomatic group of patients. Spine 9:549–551

Wiltse LL, Berger PE, McCulloch JA (1997) A system for reporting the size and location of lesions of the spine. Spine 22:1534–1537

Witt I, Vestergaard A, Rosenklint A (1984) A comparative analysis of X-ray findings of the lumbar spine in patients with and without lumbar pain. Spine 9:298–300

Yu S, Haughton VM, Sether LA, Wagner MI (1988) Annulus fibrosus in bulging intervertebral disks. Radiology 169:761–763

Pathology of the Posterior Elements

7

Luc van den Hauwe

CONTENTS

L. van den Hauwe, MD
Department of Radiology, University Hospital Antwerpen, Wilrijkstraat 10, 2650 Edegem, Belgium
and Department of Radiology, AZ KLINA, Augustijnslei 100, 2930 Brasschaat, Belgium

7.1 Introduction

Facet joints are a major source of neck and low-back pain. Facet joint syndrome is defined as a constellation of symptoms that result in diffuse pain that does not fit a clear nerve root pattern (e.g. not sciatica). Both cervical and lumbar facet syndromes have been described (Cavanaugh et al. 2006).

In the early years of the previous century, the facet joints were the focus of intense research and speculation with regard to their role in the production of back pain and sciatica. When Mixter and Barr in 1934 first emphasized that herniation of disc material (nucleus pulposus) through the annulus fibrosus caused low-back pain and sciatica, discussion, research and therapy shifted to the herniated nucleus pulposus (Schellinger et al. 1987). Ever since then, the role of the facet joints when evaluating patients with low-back pain and sciatica has been underestimated (Carrera 1980). Synovial linings and joint capsules of the facet joints are richly innervated and can be an important source of pain (Schellinger et al. 1987).

7.2 Normal Anatomy

The spine has a segmental organization. Each segment is composed of a vertebral body (corpus vertebrae) anteriorly and a vertebral or neural arch (arcus posterior) posteriorly (Fig. 7.1). Together they enclose the vertebral foramen (spinal canal). From each neural arch a spinous process protrudes posteriorly, and transverse processes extend from the lateral edges of each arch. These bony processes serve as important sites of attachment of deep back muscles. They also divide the neural arch into different parts. The neural arch between the spinous

KEY POINTS

- Because of their rich innervation, facet joints are an important source of pain. Their role in evaluating patients with low-back pain and sciatica is often underestimated.
- Radicular symptoms are the result of direct nerve compression. This is not exclusively caused by disc herniation; facet joint abnormalities (osteophytes, hypertrophy, joint effusion) may also cause neural compression.
- The intervertebral disc and the facet joints function as a three-joint complex; degenerative changes of the intervertebral disc will affect the normal anatomy and function of the facet joints.
- Degenerative changes observed in facet joint osteoarthritis are similar to those observed in peripheral joints (osteophytes, hypertrophy, osteosclerosis, subchondral bone erosions, cartilage abnormalities).
- Although both CT and MR imaging can be used in the evaluation of facet joint osteoarthritis, CT is the imaging modality of choice to demonstrate subtle changes (e.g. subchondral lesions). Axial images are chosen to do so.
- In the evaluation of the intervertebral foramina, sagittal MR and (reconstructed) CT images are preferred. They easily allow identification of the affected levels and measurement of the sagittal diameter of the spinal canal.
- Associated soft tissue changes include facet joint synovial or ganglion cysts, ligamentum flavum hypertrophy and ligamentum flavum cysts. These cysts must be differentiated from other lesions causing low-back pain and radicular symptoms.
- Other degenerative changes of the neural arch include neural arch intervertebral neoarthrosis, spinous process abnormalities (Baastrup's disease) and associated ligamentous changes.
- Facet joint osteoarthritis is a frequent cause of central, lateral and foraminal stenosis.
- Spondylolisthesis is defined as an anterior displacement of a vertebra relative to the vertebra below. Most frequently encountered causes of spondylolisthesis that have to be discriminated are isthmic spondylolisthesis (spondylolysis) and degenerative spondylolisthesis. Plain film radiography oblique views are useful for visualizing the pars defect, but CT and MR imaging are preferred to demonstrate associated disc abnormalities and to evaluate the intervertebral foramina.
- Isthmic spondylolisthesis is the result of a bilateral defect in the pars interarticularis. Nerve root compression typically occurs at the level of the intervertebral foramina. In addition, the spinal canal is usually widened.
- Degenerative spondylolisthesis, as a result of facet joint osteoarthritis, is more frequently observed when the facet joints have a more sagittal orientation. Narrowing of the central canal, lateral recess and intervertebral foramina is a typical finding.

and transverse processes is the lamina and the part of the arch between the transverse process and the vertebral body is the pedicle. The pedicle of each vertebra is notched at its superior and inferior edges. Together, the notches from two contiguous vertebrae form an opening, the intervertebral foramen, through which the spinal nerves pass (Gray 1918).

The functional unit of the vertebral column consists of two adjacent vertebral bodies, an intervertebral disc and two facet joints. This unit is called the motion segment. It constitutes a three-joint complex which forms a universal joint. Six types of motion are possible, i.e. axial rotation and translation along the three coordinate (x, y, z) axes. The shape and orientation of the facet joints determines the range of motion (Schellinger et al. 1987).

The facet joints (also known as zygoapophyseal joints) are diarthrodial synovial joints between the superior and inferior articular processes of adjacent neural arches. These articular processes arise from the articular pillars, which include the bone at the junction of the laminae and the pedicles. The inferior articular process faces anteriorly and is posterior relative to the superior articular process. The joint surfaces are oriented in an oblique plane halfway between the sagittal and coronal planes (i.e. 45°); the

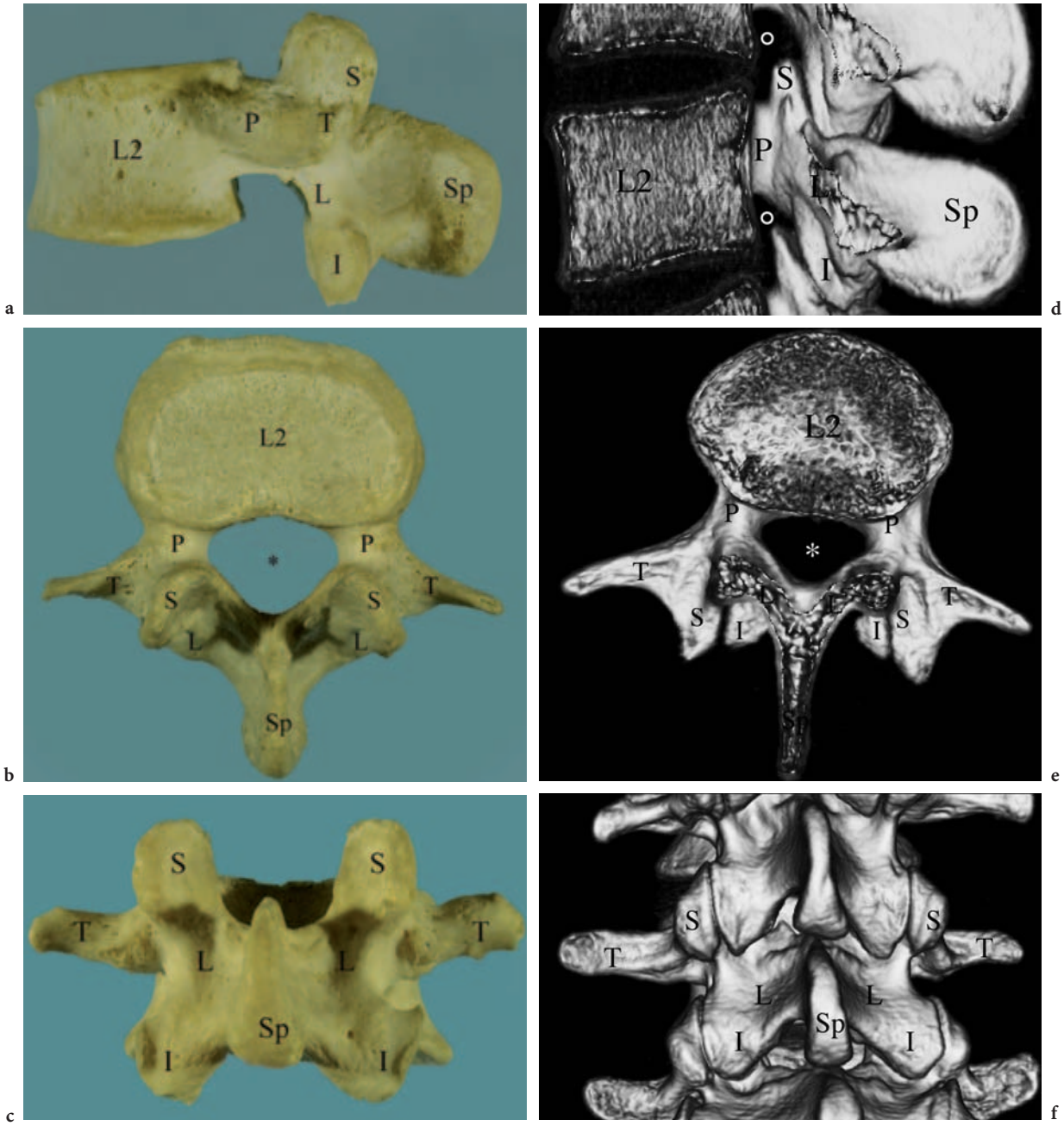

Fig. 7.1a–f. Anatomy of the posterior arch of a lumbar vertebra. Anatomical specimen (**a–c**) and CT volume rendering (VR) (**d–f**) illustrating posterior arch anatomy. Left sagittal view (**a**,**d**), superior view (**b**,**e**), and posterior view (**c**,**f**). Each vertebra is composed of a vertebral body anteriorly and a posterior arch. Together they enclose the vertebral foramen (*). From each neural arch a spinous process (*Sp*) is protruding posteriorly, and transverse processes (*T*) are extending from the lateral edges of each arch . These bony processes serve as important sites of attachment of deep back muscles. They also divide the neural arch into different parts. The neural arch between the spinous and transverse process is the lamina (*L*) and the part of the arch between the transverse process and the vertebral body is the pedicle (*P*). The pedicle of each vertebra is notched at its superior and inferior edges. Together the notches from two contiguous vertebra form an opening, the intervertebral foramen (°), through which the spinal nerves pass. Superior (*S*) and inferior (*I*) articular processes arise from the articular pillars, which include the bone at the junction of the laminae and the pedicles. The inferior articular process faces anteriorly and is posterior relative to the superior articular process

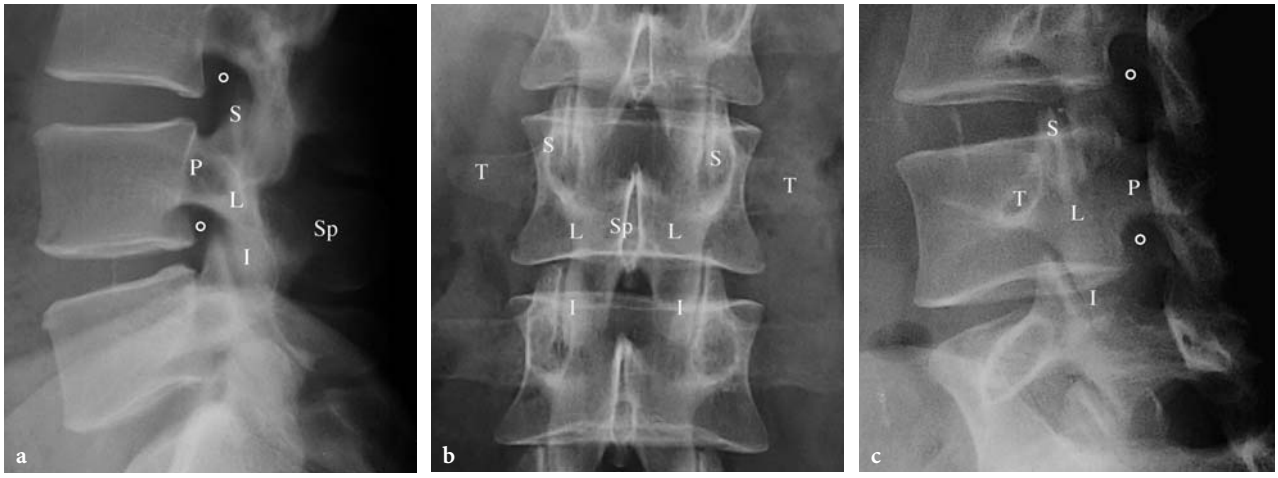

Fig. 7.2a–c. Normal imaging anatomy of the posterior arch of the lumbar spine on plain film radiography. Lateral (**a**), anteroposterior (**b**) and oblique (**c**) views. *P* = pedicle, *L* = lamina, *I* = inferior articular process, *S* = superior articular process, *Sp* = spinous process, *T* = transverse process, ° = intervertebral foramen

orientation is almost parasagittal in the upper lumbar spine, whereas they are oriented in a more coronal plane in the lower lumbar region. In the thoracic spine, the orientation is nearly in the coronal plane (Grenier et al. 1987).

The joint surfaces are smooth and are slightly curved, the superior facets having a concave surface and the inferior facets a convex surface. They are lined by articular hyaline cartilage. The cartilage is thickest toward the center of the joint, which provides a perfect match of the joint surfaces. The distance between the bony articular processes on radiography measures 2–4 mm, corresponding to the articular lining and interposed joint space (Schellinger et al. 1987).

A tough fibrous capsule is present on the posterolateral aspect of the lumbar facet joint. It is composed of several layers of fibrous tissue and a synovial membrane, separated by a layer of loose areolar tissue. On the ventral aspect of the joint, there is no fibrous capsule; the ligamentum flavum and synovial membrane are the only barriers between the facet joint space and the spinal canal (Xu et al. 1990). The capsule has two recesses (superior and inferior) containing fat pads, from which fat-filled synovial folds project between the articular surfaces for a distance of 2–4 mm. Their function is twofold: they act as a movement-compensating mechanism, pushed by the facet when it slides into the recess area; and, because they are partially covered with synovial tissue, they provide lubrication for the joint (Grenier et al. 1987).

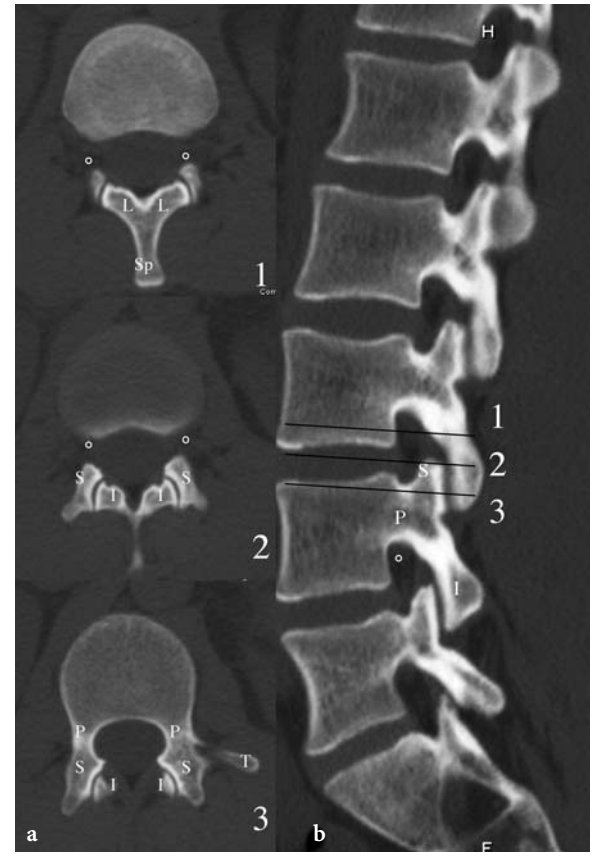

Fig. 7.3a,b. Normal imaging anatomy of the posterior arch of the lumbar spine on CT. Axial (**a**) and sagittal reformatted (**b**) CT images. *P* = pedicle, *L* = lamina, *I* = inferior articular process, *S* = superior articular process, *Sp* = spinous process, *T* = transverse process, ° = intervertebral foramen

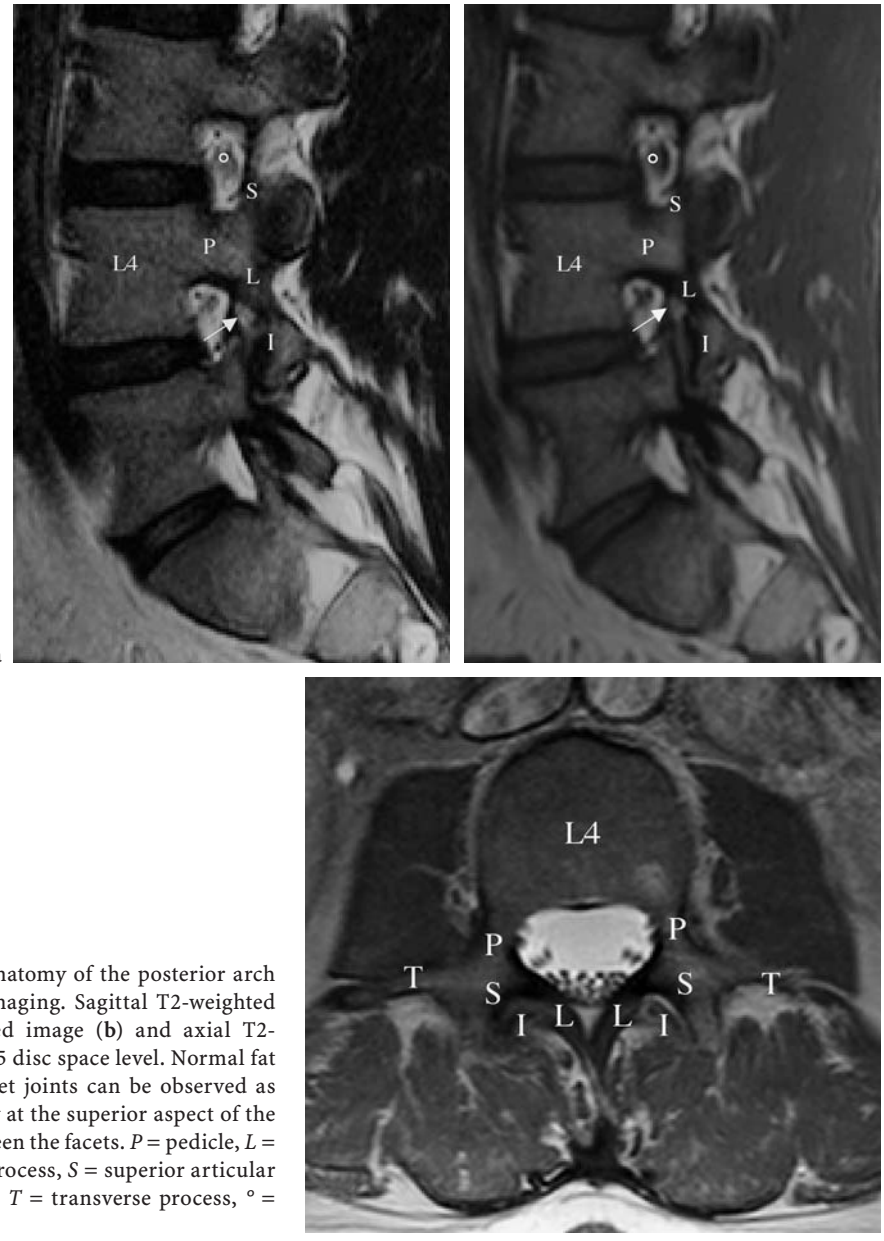

Fig. 7.4a–c. Normal imaging anatomy of the posterior arch of the lumbar spine on MR imaging. Sagittal T2-weighted image (**a**), sagittal T1-weighted image (**b**) and axial T2-weighted image (**c**) at the L4–L5 disc space level. Normal fat pads (*white arrows*) in the facet joints can be observed as an area of high signal intensity at the superior aspect of the joint extending inferiorly between the facets. *P* = pedicle, *L* = lamina, *I* = inferior articular process, *S* = superior articular process, *Sp* = spinous process, *T* = transverse process, ° = intervertebral foramen

The ligamenta flava (yellow ligaments) are paired structures, one on each side, connecting the spinal laminae, and forming part of the posterior wall of the vertebral canal. Laterally, these ligaments fuse with the articular capsules and form one boundary of the intervertebral foramina (Mahalatti et al. 1999). On imaging studies, they are indistinguishable from each other. The ligamenta flava limit flexion and provide a static elastic force to aid the return to a neutral position after spinal flexion/extension. They also help to maintain a smooth posterior lining of the central spinal canal (Xiong et al. 2001).

The facet joints are extensively reinforced by different ligaments. These ligaments connect the tips of the spinous processes (supraspinous ligaments), the base of the spinous processes (interspinous ligaments), and the transverse processes (intertransverse ligaments). In addition the laminae of adjacent vertebrae are bound together by the ligamentum flavum. The anterior and posterior longitudinal ligaments connect the vertebral bodies anteriorly and posteriorly and thereby support the spinal column.

7.3 The Role of Facet Joints in Spinal Pain

Radicular pain is the result of direct compression of major nerve roots within the spinal canal, along their exit zones, or outside the intervertebral foramen. Disc herniation, osteophytes, facet joint hypertrophy, rostrocaudal subluxation of facets and expansion of the facet joint capsule secondary to joint effusion may all cause neural compression. Also, inflammatory processes emanating from the facet joint complexes can spread through the myofascial areas and involve several nearby nerve roots (Schellinger et al. 1987).

Pain may also arise from direct irritation of local pain fibers in the spine. This pain can be referred to the extremities and become indistinguishable from radicular pain (so-called pseudo-radicular pain) (Schellinger et al. 1987).

The synovial linings and joint capsules are richly innervated. Therefore, facet joints can be an important source of pain. Each facet joint is innervated by the medial branch, a section of the dorsal ramus. The medial branch is one of three branches of the dorsal ramus, with the other two being the lateral branch (which does not exist for the L5 dorsal ramus) and the intermediate branch. The lateral branch innervates the iliocostalis muscle, and the intermediate branch innervates the longissimus muscle. The medial branch innervates many structures, including the facet joint, but it also innervates the multifidus, interspinales, and intertransversii mediales muscles, the interspinous ligament, and, possibly, the ligamentum flavum. After the medial branch splits off from the dorsal ramus, it courses caudally around the base of the superior articular process of the level below toward that level's facet joint (e.g. the L4 medial branch wraps around the L5 superior articular process to approach the L4–L5 facet joint). It then continues in a groove between the superior articular process and the transverse process (or, in the case of the L5 medial branch, between the superior articular process of S1 and the sacral ala of S1, which is the homologous structure to the transverse processes of the lumbar vertebrae). The medial branch of the dorsal ramus gives off two branches to nearby facet joints. One branch innervates the facet joint of that level, and the second branch descends caudally to the level below. Therefore, each medial branch of the dorsal ramus innervates two joints – that level and the level below (e.g. the L4 medial branch innervates the L4–L5 and L5–S1 facet joints). Similarly, each facet joint is innervated by the two most cephalad medial branches (e.g. the L4–L5 facet joint is innervated by the L3 and L4 medial branches) (Malanga et al. 2006).

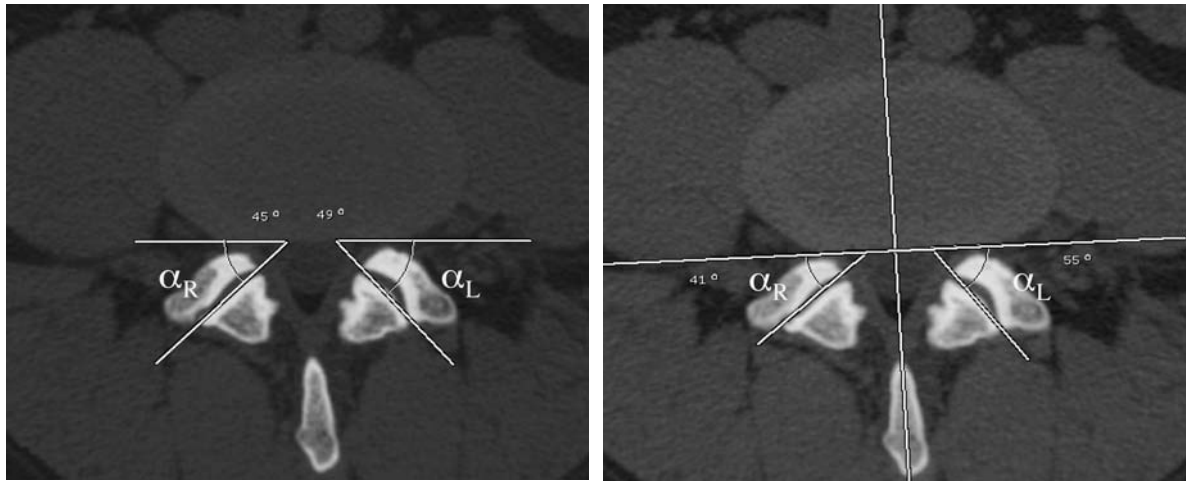

a b

Fig. 7.5a,b. Measuring facet joint angles. Axial CT image of the lumbar spine at the L4–L5 disc level. **a** The coronal reference plane is defined using the posterior aspect of the intervertebral disc. **b** An alternative is using a line through two points in the midline and tip of the spinous process - representing the midsagittal plane - and to draw a line perpendicular to it to define the coronal plane. A line through the anteromedial and posterolateral margins of each facet joint is used to calculate the angle relative to the coronal (**a**) or sagittal plane. Normal, almost symmetrical, orientation of the facet joint surfaces in an oblique plane halfway between the axial and coronal planes (i.e. 45°) is seen in **a**. Moderate tropism (difference of 7° to 15° between the two angles) is observed in **b**

Fig. 7.6. Association between sagittal orientation and osteoarthritis of the facet joints. Axial CT clearly demonstrates facet joint tropism in this patient; the right facet joint has a more sagittal orientation when compared to the left side. Associated osteoarthritis of the right facet joint with joint space narrowing, osteophytosis and osteosclerosis is observed

7.4 Degenerative Changes of the Posterior Elements

Both disc degeneration and facet joint osteoarthritis increase with age. Degeneration of the lumbar spine occurs from age 30 and is almost invariably present after 60 years (Wybier 2001).

Since the intervertebral disc and the facet joints function as a three-joint complex, degenerative changes of the intervertebral disc will affect the normal anatomy and function of the posterior elements (and possibly also vice versa). Disc degeneration sometimes occurs without the presence of facet joint osteoarthritis; on the other hand, facet joint osteoarthritis mostly occurs in the presence of disc degeneration. Therefore, it was postulated that disc degeneration occurs before facet joint osteoarthritis, which may be secondary to mechanical changes in the loading of the facet joints (Butler et al. 1990). Other factors contributing to facet joint degeneration include weight, scoliosis and lordosis (Grogan et al. 1997).

Conflicting results have been reported concerning a possible association between facet joint tropism and disc degeneration (Farfan et al. 1972; Van Schaik et al. 1984; Hagg and Wallner 1990; Cassidy et al. 1992; Grogan et al. 1997) and between the association of sagittal-oriented facet joints and facet joint osteoarthritis and/or degenerative spondylolisthesis (Sato et al. 1989; Grobler et al. 1993; Fujiwara et al. 2001a; Karacan et al. 2004; Boden et al. 2005). Facet joint tropism is defined as asymmetry between the left and right facet joint angles, with one joint having a more sagittal orientation than the other (Boden et al. 2005).

In a study of asymptomatic volunteers, Boden et al. observed that more sagittally oriented facet joints at the level of the fourth and fifth lumbar vertebrae were highly associated with herniated discs and degenerative spondylolisthesis (Boden et al. 2005). A significant association was found between sagittal orientation and osteoarthritis of the lumbar facet joints, even in patients without degenerative spondylolisthesis (Fujiwara et al. 2001a).

7.4.1 Osteoarthritis of the Facet Joints

Degenerative changes of the facet joints most frequently involve the lordotic segments of the spine: cervical and lumbar. These changes may play an important role in the development of acquired spinal stenosis.

Degenerative changes are similar to those observed in peripheral joints and they include osteophyte formation, hypertrophy of the articular processes, osteosclerosis, thinning of the articular cartilage with erosions and subchondral cyst formation, vacuum joint phenomenon or joint effusion, hypertrophy and/or calcification of the joint capsule and ligamentum flavum (Carrera et al. 1980).

Osteophyte formation is defined as excrescent new bone formation, lacking a medullary space, arising from the margin of the joint. Osteophytes protruding ventrally from the anteromedial aspect of the facet joints may narrow the lateral recesses and intervertebral foramina causing central or lateral spinal canal stenosis (Wybier 2001).

Hypertrophy was defined as enlargement of an articular process with normal proportions of its medullary cavity and cortex (Carrera et al. 1980). Hypertrophy of the facet joints causes distortion of the articular surfaces which may be responsible for

pain, abnormal mechanical stress, and nerve root compression (Carrera et al. 1980).

Fibrillation and later fissuring and ulceration of articular cartilage will develop, progressing from the superficial to the deep cartilage layers (Weishaupt et al. 1999). Osteochondral fragments that break off from the joint surface can act as joint mice. In advanced disease, the joints become denuded from their articular cartilage and subchondral bone sclerosis with degenerative cysts will appear (Schellinger et al. 1987).

The joint space may be preserved despite the presence of osteophytes and degenerative subchondral bone erosions. Narrowing of the joint space is frequently observed and may be advanced in patients with facet joint erosive osteoarthritis and facet joint subluxation. Also widening of the facet joint space may be observed in advanced facet joint degeneration with retrolisthesis due to facet joint posterior subluxation (Wybier 2001).

Pathria et al. (1987) used a four-point scale to grade facet joint osteoarthritis on oblique radiographs and CT scans. These criteria were refined by Weishaupt et al. (1999) who used these criteria for grading osteoarthritis of the facet joints on CT and MR imaging. They are listed in Table 7.1.

The imaging techniques used for the evaluation of facet joint degeneration are standard radiographs, CT and MR imaging. Standard radiographs, especially without oblique views, are of limited value (Weishaupt et al. 1999). The double obliquity of the facet joints in transverse and sagittal planes, and the curvature of the articular surfaces makes plain films less suited to the evaluation of facet joint degeneration (Grenier et al. 1987). Only the portion of each joint that is oriented parallel to the X-ray beam is visible. Although it is a moderately insensitive technique compared to CT, it may be valuable in screening for facet joint osteoarthritis (Pathria et al. 1987). Osteophytes, hyperostosis and facet joint narrowing may be observed on plain film; also concomitant spondylolisthesis may be demonstrated by standard radio-

Table 7.1. Criteria for grading osteoarthritis of the facet joints (after Weishaupt et al. 1999)

Grade	Criteria
0	Normal facet joint space (2–4 mm width)
1	Narrowing of the facet joint space (<2 mm) and/or small osteophytes and/or mild hypertrophy of the articular processes
2	Narrowing of the facet joint space and/or moderate osteophytes and/or moderate hypertrophy of the articular processes and/or mild subarticular bone erosions
3	Narrowing of the facet joint space and/or large osteophytes and/or severe hypertrophy of the articular processes and/or severe subarticular bone erosions and/or subchondral cysts

Fig. 7.7a,b. Osteophytosis of the superior articular processes. Sagittal T2-weighted image (**a**) and sagittal reformatted CT scan (**b**) of the lower lumbar spine demonstrate upward projection of an osteophytic spur arising from the superior articular process of L5 and S1 toward the L4–L5 and L5–S1 intervertebral foramen respectively. This results in foraminal narrowing and nerve root compression. Mild fluid accumulation (**a**) and vacuum phenomenon (**b**) of the facet joint and associated disc degeneration is observed

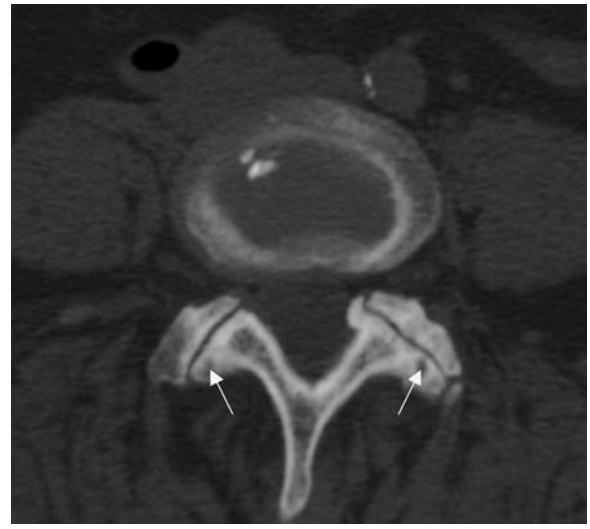

Fig. 7.8. Facet joint subchondral bone changes. Axial CT image at the L4–L5 level shows degenerative changes of both facet joints, which is more pronounced at the left side. Hypertrophy and osteosclerosis, joint space narrowing, osteophytes and subarticular bone erosions (*white arrows*) are present

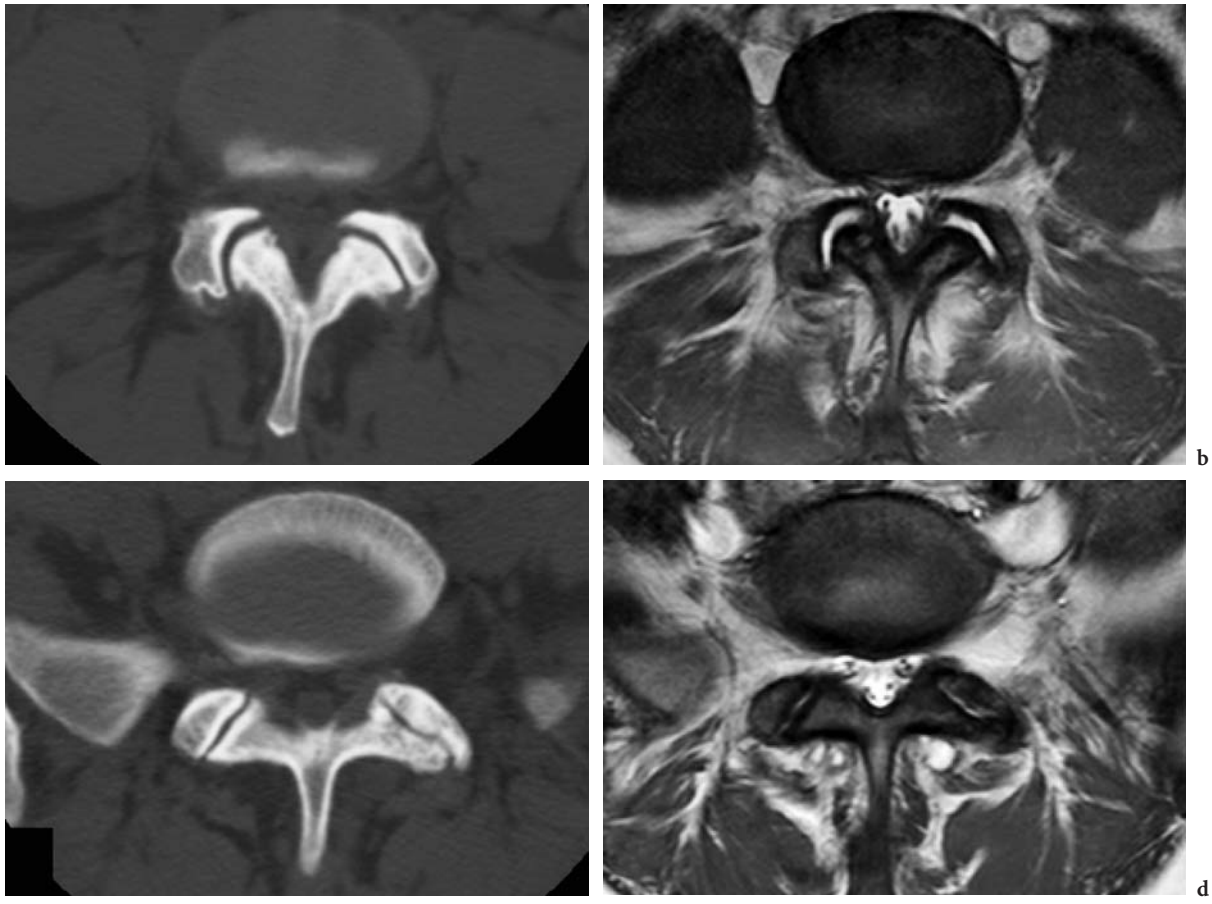

Fig. 7.9a–d. Joint space changes in facet joint osteoarthritis. Axial CT and axial MR T2-weighted image at the L4–L5 (**a**,**b**) and L5–S1 (**c**,**d**) levels in the same patient demonstrate facet joint degeneration. Osteophytes at the L4–L5 level can be better appreciated on CT (**a**), whereas fluid accumulation in the facet joints is better seen on MR (**b**). Joint space narrowing of the left L5–S1 facet joint is observed on both modalities (**c**,**d**). Associated disc degeneration with an annular tear in the L4–L5 intervertebral disc is seen (**b**)

Fig. 7.10. Vacuum joint phenomenon in facet joint osteoarthritis. Axial CT shows the presence of gas within the L4–L5 facet joints, which may be explained as a result of uneven apposition of the joint surfaces. Associated hypertrophy and juxta-articular calcifications and osteophytes are present

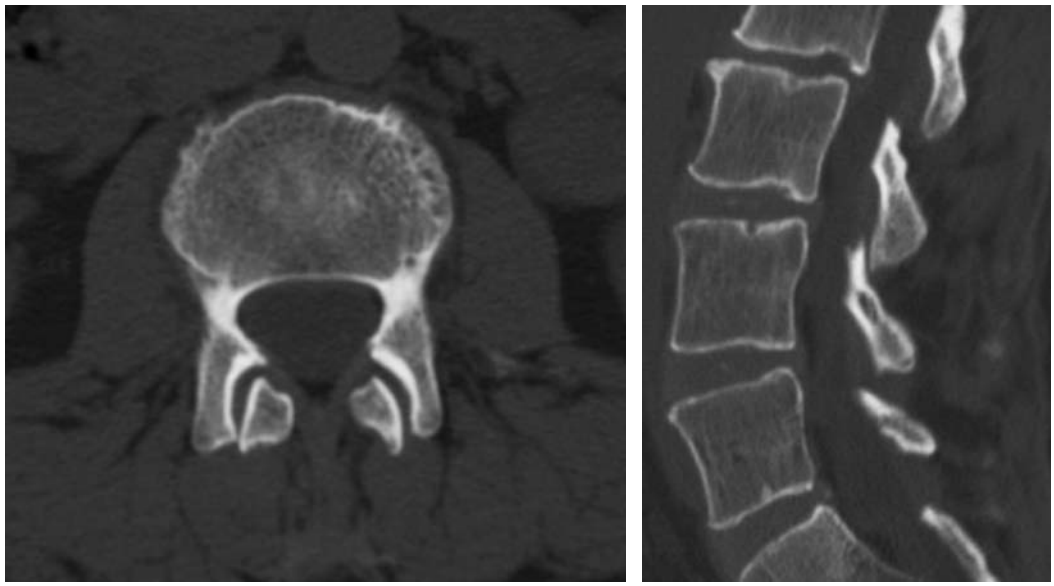

a b

Fig. 7.11a,b. Facet joint subluxation due to the sagittal orientation of the facet joints. Axial (**a**) and sagittal reformatted CT (**b**). Axial CT shows loss of the normal coincidence of the facet joints (**a**). This is the result of the sagittal orientation of the facet joints and associated retrolisthesis L2–L3 can be observed (**b**)

graphs. More subtle changes, e.g. cartilage changes, and subchondral erosions can be better analyzed on axial CT and MR imaging. Both techniques have intrinsic high spatial and contrast resolution. In general there is moderate to good agreement between MR imaging and CT in the assessment of facet joint osteoarthritis. Therefore, in the presence of an MR examination, CT is not required for the evaluation of facet joint degeneration. Conversely, it was demonstrated that CT was superior to MR imaging in the depiction of joint space narrowing and subchondral sclerosis (Weishaupt et al. 1999).

Using MR imaging, sagittal views are preferred for identifying the pathological level(s), measuring the sagittal diameter of the spinal canal, and for grading foraminal stenosis. Axial images at appropriate levels are preferred for a more precise analysis of the facet joints (cartilage, osteophytes), analysis

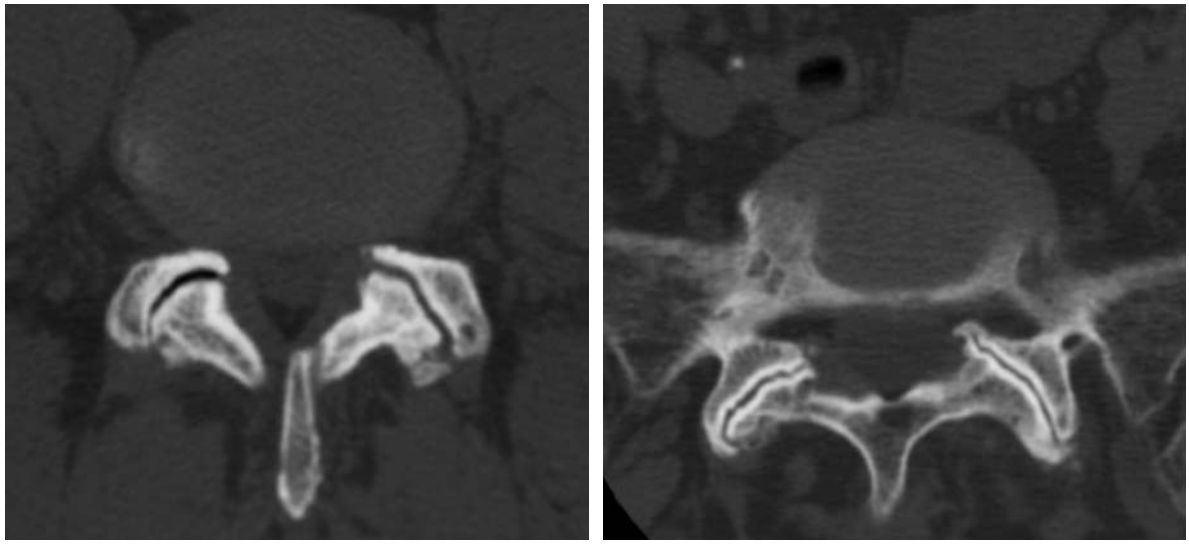

Fig. 7.12a,b. Grading facet joint osteoarthritis. Axial CT at the L4–L5 (**a**) and L5–S1 (**b**) level in a patient with multilevel facet joint degeneration. Grade 1 osteoarthritis of the right facet joint (mild hypertrophy) and grade 2 osteoarthritis of the left facet joint (narrowing of the joint space, moderate hypertrophy and osteophytes, mild subarticular erosions) is seen at the L4–L5 level (**a**). Grade 3 osteoarthritis of the L5–S1 facet joints. Severe degeneration of the facet joints with joint space narrowing, hypertrophy of the articular processes, large osteophytes and subarticular bone erosions can be noticed (**b**)

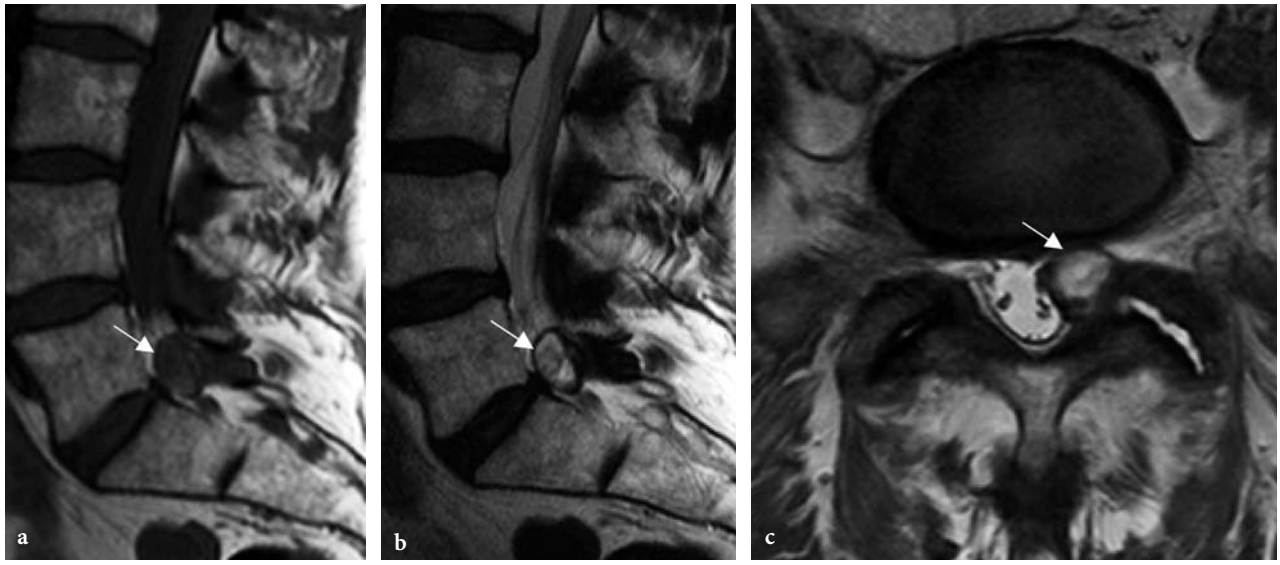

Fig. 7.13a–c. Juxtafacet (ganglion) cyst arising from the left facet joint. Sagittal T1-weighted image (**a**), sagittal T2-weighted image (**b**), and axial T2-weighted image (**c**) show a cystic lesion arising from the anteromedial aspect of the left facet joint. The content from the cyst appears mildly hyperintense on T2-weighted image and is of intermediate signal intensity on T1-weighted image (**a**). A low signal intensity rim is observed on T2-weighted images (**b**,**c**). Facet joint degeneration with joint space narrowing at the right side and joint effusion at the left side is noted (**c**). The cyst causes compression of the thecal sac and obliteration of the left lateral recess is seen. Resection of the cyst was performed and pathology revealed the diagnosis of ganglion cyst

of posterior soft tissue elements (i.e. ligamentum flavum) and measurement of the transverse diameter of the spinal canal (Grenier et al. 1987).

With the introduction of multirow-detector CT (MDCT), high-resolution reformats in the sagittal and coronal planes have now become routinely available. The role of this technique in the evaluation of spinal trauma patients has been validated (Van Goethem et al. 2005). It may replace plain radiographic clearance of the cervical spine in trauma situations, eliminate MRI in some degenerative diseases, and allow dynamic studies such as flexion-extension or rotational movements (Anderson 2003). To the best of our knowledge, no studies have been published yet to demonstrate the added value of MDCT with sagittal reformats in the analysis of facet joint osteoarthritis.

7.4.2 Associated Soft Tissue Changes

Soft tissue changes associated with facet joint degeneration include: degenerative cysts arising from the facet joints (so-called juxtafacet cysts), ligamentum flavum cysts, and hypertrophy and/or calcification of the ligamentum flavum.

7.4.2.1 Degenerative Cysts Arising from the Facet Joints: Juxtafacet Cysts

Spinal synovial cysts are grouped with ganglion cysts under the heading "juxtafacet" or "juxta-articular" cysts. This term reflects the close anatomic relationship between the cyst and the spinal facet joint capsule (Paolini et al. 2002).

Synovial cysts are periarticular cysts of the synovial membrane, with a membrane attached to the joint capsule. They contain clear or yellow mucinous fluid or gas. The walls are of loose myxoid connective or fibrocollagenous tissue with a synovial lining. In contrast, ganglion cysts have no connection to the joint and no synovial lining. They contain myxoid material. The consistency of fluid within the cysts varies greatly because of hemorrhage and inflammation (Stoodley et al. 2000).

Juxtafacet cysts are not evenly distributed in the spine. The lumbar spine is by far the predominant site of symptomatic cysts and most cysts are observed at the L4–L5 level, which generally has the most motion within the lumbar spine. Lumbar juxtafacet cysts are increasingly being reported, probably related to the increased number of MR examinations (Apostolaki et al. 2000). In the cervical and thoracic spine, only a handful of cases have been reported in the literature (Song et al. 2006). Those occurring in the cervical spine may not only arise from the facet joint, but in approximately half of cases they arise from the cruciate ligament of the atlas (Stoodley et al. 2000).

Synovial cysts of the facet joints are almost invariably associated with osteoarthritis of the facet joints. The most accepted explanation for their pathogenesis is increased motion of the facet joint. This instability could predispose to herniation of the synovium through tears in the facet joint capsule (Apostolaki et al. 2000). An association of juxtafacet cysts with trauma (Paolini et al. 2002), rheumatoid arthritis, spondylolysis, chondrocalcinosis (Gadgil et al. 2002), and Baastrup's disease (Chen et al. 2004) has also been reported.

In a large retrospective study, Doyle and Merrilees (2004) observed posterior cysts, external to the vertebral canal, four times as often as anterior cysts. Anterior cysts, projecting into the vertebral canal, had a prevalence of 2.3%; posterior cysts a prevalence of 7.3%.

In the lumbar spine, these cysts may cause low-back pain and radicular symptoms by direct compression of the thecal sac and/or nerve roots in the lateral recesses. Also an inflammatory response around the cyst may cause sciatica (Apostolaki et al. 2000). Depending on the size and location of the cyst, neurogenic claudication may be the presenting complaint. Spinal stenosis may be observed on imaging studies. It is extremely rare for facet joint cysts to cause symptomatic cauda equina compression (Shaw and Birch 2004). Radiculopathy is an unusual presentation in cervical cysts (Stoodley et al. 2006).

The natural history of these lesions is unclear; although they may resolve spontaneously, this is very rare (Swartz and Murtagh 2003). Juxtafacet cysts may occasionally enlarge and cause severe symptoms within months. Hemorrhage is a well-known cause of rapid or even dramatic cyst enlargement (Paolini et al. 2002).

Symptomatic radiculopathy and myelopathy are indications for surgical treatment. Often there is an associated spondylotic spinal stenosis that is an indication for generous laminectomy and decompression in addition to cyst removal. If there is no associated canal stenosis, excision of the cyst with minimal exposure can be performed (Stoodley et al. 2000).

Various imaging techniques including MR imaging, CT, myelography, CT myelography, facet

Fig. 7.14a,b. CT aspect of a juxtafacet cyst arising from the right facet joint. Axial (**a**) and sagittal (**b**) reformatted CT images show a juxtafacet cyst arising from the right facet joint. Gas inside the cyst is observed (*white arrows*). Associated facet joint degeneration (joint space narrowing), is demonstrated. There is obliteration of the right

arthrography and CT facet arthrography have been used to identify intraspinal facet joint cysts (Apostolaki et al. 2000).

MR imaging is the diagnostic imaging technique of choice due to its high sensitivity (Hagen et al. 2001). On MR imaging, intraspinal synovial cysts are depicted as sharply marginated epidural masses near the facet joint. In some cases, MR imaging may demonstrate the communication with the facet joint.

The signal intensity of the cysts is equal to or slightly greater than that of cerebrospinal fluid (CSF) on both T1- and T2-weighted images. Synovial cysts with high signal on T1- and T2-weighted images indicate the presence of subacute breakdown products of blood. All synovial cysts have a low signal intensity rim at the periphery that is accentuated on long TR/TE sequences. After administration of gadolinium these cysts show rim enhancement (Tillich et al. 2001).

The differential diagnosis of a well-defined, round, T2-hyperintense epidural lesion in the posterior or lateral spinal canal is broad, and includes juxtafacet cyst, ligamentum flavum cyst, disc cyst, sequestered disc fragment, infectious (e.g. cysticercosis or hydatid) cyst, arachnoid cyst (rare in the lumbar spine), and neoplasm (cystic degeneration in a neurofibroma or schwannoma) (Mahallati et al. 1999; Apostolaki et al. 2000). It may be difficult to differentiate juxtafacet cysts from ligamentum flavum hematoma in post-trauma cases (Hirakawa et al. 2000).

The typical appearance on CT is of a rounded mass of low attenuation adjacent to the facet joint. CT may show egg-shell calcifications of the wall of the cyst (Lunardi et al. 1999) and gas inside the cyst (Stoodley et al. 2000).

Facet joint arthrography and CT arthrography can be performed in cases with a difficult differential diagnosis to determine whether a communication exists between the cyst and the facet joint (Schmid et al. 2002). Subsequent injection of long-acting steroids and local anesthetics may be a useful alternative to surgical removal in some cases (Sarazin et al. 1999; Sauvage et al. 2000).

In patients with radicular pain, nonsurgical management does not appear to be as successful as surgery (Shah and Lutz. 2003). Surgical removal of the cyst is a safe and effective treatment for symptomatic relief in patients with lumbar synovial cysts (Hsu et al. 1995). A concomitant fusion procedure may be performed in selected cases (spinal instability, spondylolisthesis) (Lyons et al. 2000).

7.4.2.2 Cysts of the Ligamentum Flavum

Ligamentum flavum cysts are rare (Terada et al. 2001). They are different from synovial and ganglion cysts in that they arise from, or are partially embedded in, the ligamentum flavum rather than

being closely related to the facet joint. The development of these cysts may be related to necrosis or myxoid degeneration occurring in a hypertrophied ligamentum flavum (Cakir et al. 2004). On histology, myxoid degeneration with reactive hypervascularity is found; a synovial lining is not identified (Mahalatti et al. 1999). Chronic degenerative changes in the ligamentum flavum, followed by (repeated) hemorrhage gives rise to small degenerative cysts which enlarge and coalesce to form a large cyst (Cakir et al. 2004).

As with juxtafacet cysts, they are typically located at the L4–L5 level. Usually they are associated with degenerative changes, but they can be found in the absence of facet joint degeneration, which may be helpful in the differential diagnosis (Terada et al. 2001).

Although ligamentum flavum cysts may have similar imaging characteristics as juxtafacet cysts, such a differentiation may be helpful to the surgeon, as the former are easier to resect by means of a standard laminectomy.

On imaging, an intraspinal, extradural mass adjacent to the ligamentum flavum is found. On CT, the lesion has a low density attenuation. Unlike in synovial or ganglion cysts, rim calcification has not been reported (Terada et al. 2001). On MRI, a well-defined, round to ovoid cystic mass lesion is observed. It has a high signal intensity on T2-weighted images with a low signal intensity rim. Thick peripheral enhancement after gadolinium injection is seen (Mahalatti et al. 1999).

7.4.2.3 Ligamentum Flavum Hypertrophy

Symmetrical thickening of the ligamenta flava is a frequently observed finding in facet joint arthropathy. It results from joint effusion, progressive ligamentous fibrosis, calcification and/or ossification (Wybier 2001).

Calcifications of the ligamenta flava have been observed in patients with diffuse idiopathic skeletal hyperostosis (DISH) and ankylosing spondylitis. Calcifications are also associated with metabolic diseases such as renal failure, hypercalcemia, hyperparathyroidism, hemochromatosis, and pseudogout. At the periarticular level, however, it is generally considered a sign of degenerative disease, whereas at the levels of insertions, it is considered a normal variant related to traction (Ruiz Santiago et al. 1997).

Degenerative changes, mainly at the level of the facet joints, are strongly associated with ligamentum flavum and posterior capsule calcifications. These degenerative changes have a higher incidence with age (Ruiz Santiago et al. 1997).

Calcification of spinal ligaments, the ligamentum flavum and especially the posterior longitudinal ligament, is a well-known cause of compressive myelopathy and radiculopathy at the cervical and thoracic levels. Calcification and/or ossification of the thoracic ligamenta flava (OLF) is a rare disease that mainly has been reported in the Japanese-Asian literature and is very rare in the Caucasian population. It may cause spinal stenosis in the thoracic region with compressive myelopathy with or without radiculopathy (Xiong et al. 2001). In the literature, OLF predominantly affects males younger than 50 years. The most common clinical picture consists of progressive thoracic myelopathy, resulting in spastic paraparesis (Pascal-Moussellard et al. 2005). The lower one-third of the thoracic spine (T9–T12) is the most common location, and the cervical spine is rarely affected. The pathogenesis of OLF is poorly understood; developmental, mechanical and/or degenerative changes are thought to be involved (Xiong et al. 2001).

Histopathological examination of OLF typically shows mature bone. The ligamentum flavum is progressively replaced by lamellar bone through a process of endochondral ossification. This process appears to begin near the facet joint, at the junction between the joint capsule and the ligamentum flavum, where a proliferation of cartilaginous tissue triggers the ossification (Pascal-Moussellard et al. 2005).

CT and MR imaging are preferred over plain radiography and myelography to demonstrate the shape, location, distribution, and level(s) of the OLF as well as the relative degree of spinal stenosis (Xiong et al. 2001). CT is the imaging modality of choice, revealing the pathognomonic intensely radiodense lines highlighting laminae, bilaterally in most cases of OLF. The latter tend to develop from the medial aspect of the pedicles near the insertion of the ligamentum flavum in the joint capsule and progress toward the midline, creating a characteristic V-shape with anterior concavity situated in the epidural space (Pascal-Moussellard et al. 2005). Sagittal CT reconstructions are useful for distinguishing OLF from calcification of the ligamenta flava, which is the only differential diagnosis of OLF. MR imaging has the advantage over CT that it directly shows the effects of spinal cord compression when present (Yamashita et al. 1990; Hirai et al. 2001).

Ossification of the posterior longitudinal ligament (OPLL), which is most frequently observed in the

Fig. 7.15a–d. Spinal stenosis due to an enlarging juxtafacet cyst. Sagittal (**a**,**c**) and axial (**b**,**d**) T2-weighted images of the lumbar spine in a 70-year-old women suffering from low back pain, presents now with left-sided sciatica. MR examination (**a**,**b**) demonstrates multi-level degenerative changes; degenerative spondylolisthesis at the L5-S1 level and a L4-L5 disc protrusion with associated facet joint osteoarthritis is seen. A small juxtafacet cyst may be observed obliterating the left lateral recess (**b**). A repeat MR study, performed one year later (**c**,**d**), shows a remarkable enlargement of the cyst with thecal sac compression and lateral canal stenosis. Direct communication with the left facet joint (white arrow) is demonstrated on the axial image (**d**). The cyst was removed surgically and diagnosis of synovial cyst of the facet joint was made

cervical and more rarely in the thoracic and lumbar region, may be an associated finding. Also thoracic disc herniations may be observed in these patients (Yamashita et al. 1990); they also show a tendency to calcify and ossify (van den Hauwe et al. 1993).

Spinal involvement with calcification of the ligamenta flava due to calcium pyrophosphate dihydrate (CPPD) deposition disease, also known as pseudogout, is rare, but may also lead to spinal stenosis and spinal cord compression. When involved, the cervical and lumbar regions are commonly affected (Muthukumar et al. 2000). CPPD deposition may be associated with hyperparathyroidism and haemochromatosis (Brown et al. 1991).

7.4.3 Other Degenerative Changes of the Neural Arch

7.4.3.1 Neural Arch Intervertebral Neoarthrosis

Excessive lumbar lordosis is frequently associated with spine degeneration, especially in women after menopause. Approximation of adjacent vertebral neural arches may result in abnormal bony contacts in different areas and may even result in a neoarthrosis (Wybier 2001). Associated remodelling or bony sclerosis of the pedicles and laminae may occur in these patients.

7.4.3.2 Spinous Process Abnormalities (Baastrup's Disease) and Associated Ligamentous Changes

Baastrup's disease, also known as kissing spine, has been described as a cause of low-back pain. It is characterized by close approximation and contact of adjacent spinous processes with resultant enlargement, flattening and reactive sclerosis of the apposing interspinous surfaces (Chen et al. 2004). Neoarthrosis between the spinous processes has been described. Patients with Baastrup's disease may experience pain owing to irritation of the periosteum or adventitial bursae between abutting spinous processes (Pinto et al. 2004). Interspinous bursitis may communicate with the facet joints at the same intervertebral level. They may be treated with steroid injections (Wybier 2001).

Extension of the synovial cavity to the intraspinal space may result in cyst formation. The cyst can enter the epidural space through the midline cleft of the ligamentum flavum to result in extradural compression (Rajasekaran and Pithwa 2003; Chen et al. 2004).

On imaging, profound fatty replacement of the paraspinal musculature is frequently observed in Baastrup's disease (Haig et al. 2001).

7.4.4 Foraminal Stenosis

Facet joint osteoarthritis has been recognized as an important cause of acquired lumbar spinal stenosis. It can produce central, lateral and foraminal stenosis (Schellinger et al. 1987). Although the topic of spinal stenosis is covered in detail in Chapter 8, acquired foraminal stenosis as a result of facet joint osteoarthritis will be discussed briefly.

The normal intervertebral foramen is shaped like an inverted teardrop, and its height and cross-sectional area vary from 11 to 19 mm and from 40 to 160 mm^2, respectively. The intervertebral foramen of the lumbar spine changes significantly not only on flexion-extension but also on lateral bending and axial rotation (Fujiwara et al. 2001b). Foraminal height ranges between 19 mm and 21 mm and the superior and inferior sagittal diameter of the foramen ranges between 7 mm and 8 mm and between 5 mm and 6 mm, respectively (Cinotti et al. 2002).

Instead of measuring the dimensions of the intervertebral foramen, a qualitative scoring system (Table 7.2) introduced by Wildermuth et al. (1998) can be used to determine foraminal narrowing.

Disc narrowing significantly reduces the foraminal height at each intervertebral level but has little effect on the sagittal dimensions of the intervertebral foramen. This is due to the peculiar morphology of the lower lumbar vertebrae, which reduces the risk of intraforaminal nerve root compression in patients with marked disc degeneration and subluxation of the superior facet joint (Cinotti et al. 2002). The foraminal width was found to be related to the dimensions of the spinal canal and pedicle length (Cinotti et al. 2002).

Foraminal stenosis with compression of the spinal nerve within the intervertebral foramen is a distinct feature of lateral spinal stenosis, although lateral recess stenosis may be more com-

Table 7.2. Criteria for grading foraminal of the facet joints (after Wildermuth et al. 1998)

Grade	Criteria
0	Normal intervertebral foramina; normal dorsolateral border of the intervertebral disc and normal form at the foraminal epidural fat (oval or inverted pear shape)
1	Slight foraminal stenosis and deformity of the epidural fat, with the remaining fat still completely surrounding the exiting nerve root
2	Marked foraminal stenosis, with epidural fat only partially surrounding the nerve root
3	Advanced stenosis with obliteration of the epidural fat

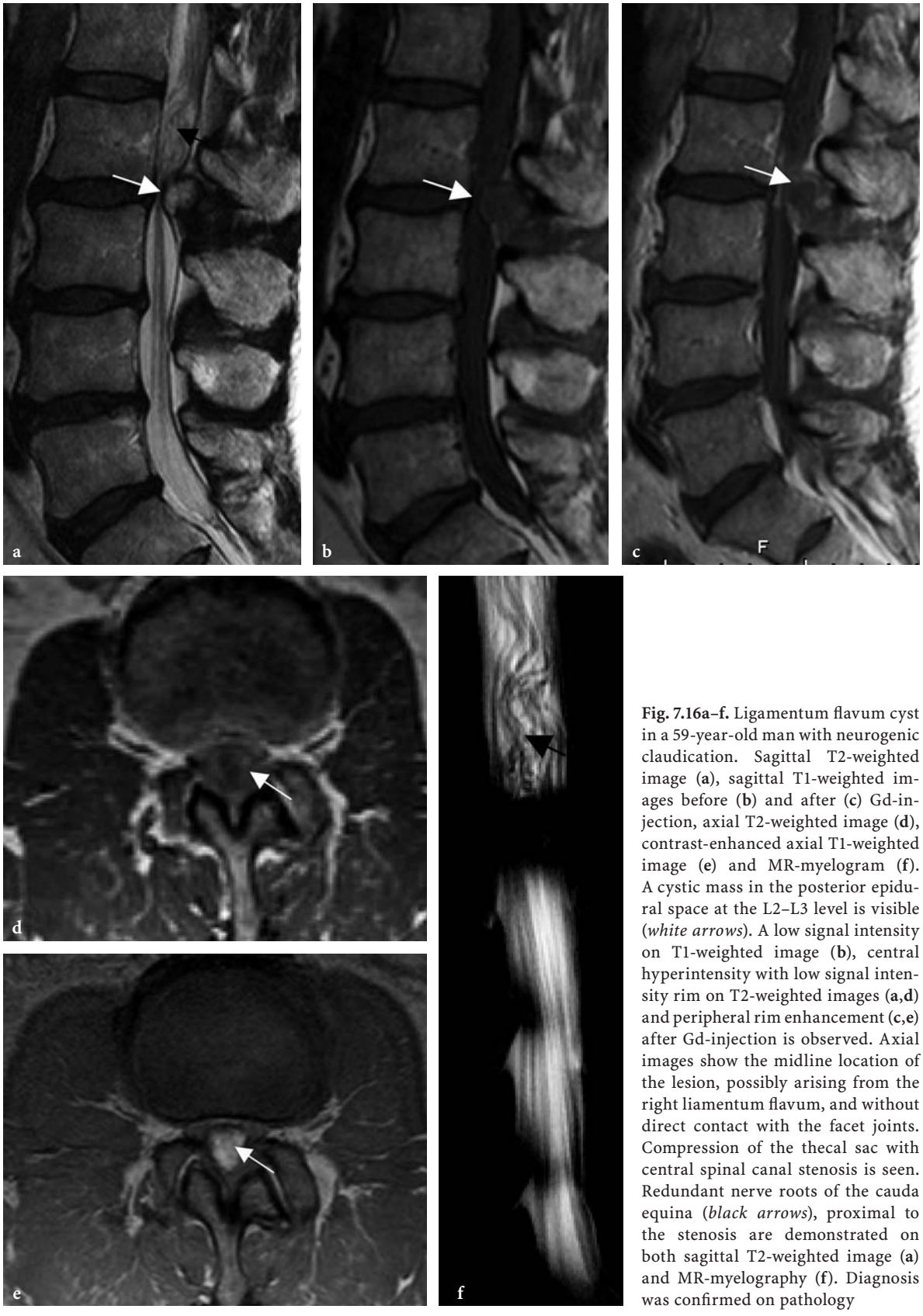

Fig. 7.16a–f. Ligamentum flavum cyst in a 59-year-old man with neurogenic claudication. Sagittal T2-weighted image (**a**), sagittal T1-weighted images before (**b**) and after (**c**) Gd-injection, axial T2-weighted image (**d**), contrast-enhanced axial T1-weighted image (**e**) and MR-myelogram (**f**). A cystic mass in the posterior epidural space at the L2–L3 level is visible (*white arrows*). A low signal intensity on T1-weighted image (**b**), central hyperintensity with low signal intensity rim on T2-weighted images (**a**,**d**) and peripheral rim enhancement (**c**,**e**) after Gd-injection is observed. Axial images show the midline location of the lesion, possibly arising from the right liamentum flavum, and without direct contact with the facet joints. Compression of the thecal sac with central spinal canal stenosis is seen. Redundant nerve roots of the cauda equina (*black arrows*), proximal to the stenosis are demonstrated on both sagittal T2-weighted image (**a**) and MR-myelography (**f**). Diagnosis was confirmed on pathology

a b

Fig. 7.17a,b. Ligamentum flavum hypertrophy and calcification. Axial (**a**) and sagittal reformatted CT (**b**) images show degenerative spondylolisthesis, as a result of sagittal oriented facet joints with osteoarthritic changes and subluxation of the facet joints. Associated hypertrophy and calcifications (*white arrows*) of the ligamentum flavum is seen. All these degenerative changes result in spinal stenosis. Protruded discs at the L4–L5 and L5–S1 level may be observed as well

Fig. 7.18. Ligamentum flavum calcification in pseudogout (CPPD). Axial CT shows bilateral ligamentum flavum calcifications (*white arrows*) in a patient known with pseudogout. Pseudogout is a crystal-induced arthropathy, which is a debilitating illness in which pain and joint inflammation are caused by the formation of calcium pyrophosphate (CPP) crystals within the joint space. It is sometimes referred to as calcium pyrophosphate disease (CPPD). Important associated facet joint degeneration is observed. (Courtesy: F. Vanhoenacker, Belgium)

mon than foraminal stenosis (Fujiwara et al. 2001a). The emerging and exiting nerve root may be compressed at various levels along its descent. Compression of the nerve may be the result of an enlarged superior articular facet or by focal osteophytic spurs. Rostrocaudal subluxation of the facet joints will constrict the upper part of the intervertebral foramen and present an obstacle to the nerve root (Schellinger et al. 1987).

In degenerative spondylolisthesis, the anterior slipping of the inferior articular processes may cause lateral or central stenosis but not foraminal stenosis, whereas both retrolisthesis and isthmic spondylolisthesis may cause a foraminal stenosis (Cinotti et al. 2002).

In patients with combined developmental and degenerative stenosis, a marked disc narrowing may further reduce the foraminal width because bulging of a hypertrophic ligamentum flavum is frequent in these patients (Cinotti et al. 2002).

Positional pain differences may be related to position-dependent changes in foraminal size and may therefore only be demonstrated using positional MR imaging. This technique may demonstrate minor forms of neural compromise in these patients, which may remain non-visible with conventional MR imaging. (Weishaupt et al. 2000).

7.5 Spondylolisthesis-Spondylolysis

Spondylolisthesis (also known as anterolisthesis) is defined as an anterior displacement of a vertebra relative to the vertebra below, whereas the reverse, i.e. when the superior vertebra slips posterior to that below, is called retrolisthesis (Butt and Saifuddin 2005). Based on etiology, spondylolisthesis has been classified by Wiltse et al. (1976). A revised version of this classification is shown in Table 7.3. Only type 2, isthmic spondylolisthesis, and type 3, degenerative spondylolisthesis, will be discussed in this chapter, since Chapters 8 and 9 also deal with spondylolisthesis.

Table 7.3. Etiology of lumbar spondylolisthesis (after Wiltse et al. 1976)

Type	Cause
1. Dysplastic	Congenital dysplasia of the articular processes
2. Isthmic	Defect in the pars articularis
3. Degenerative	Degenerative changes in the facet joints
4. Traumatic	Fracture of the neural arch other than the pars articularis
5. Pathological	Weakening of the neural arch due to disorders of the bone
6. Iatrogenic	Excessive removal of bone following spinal decompression

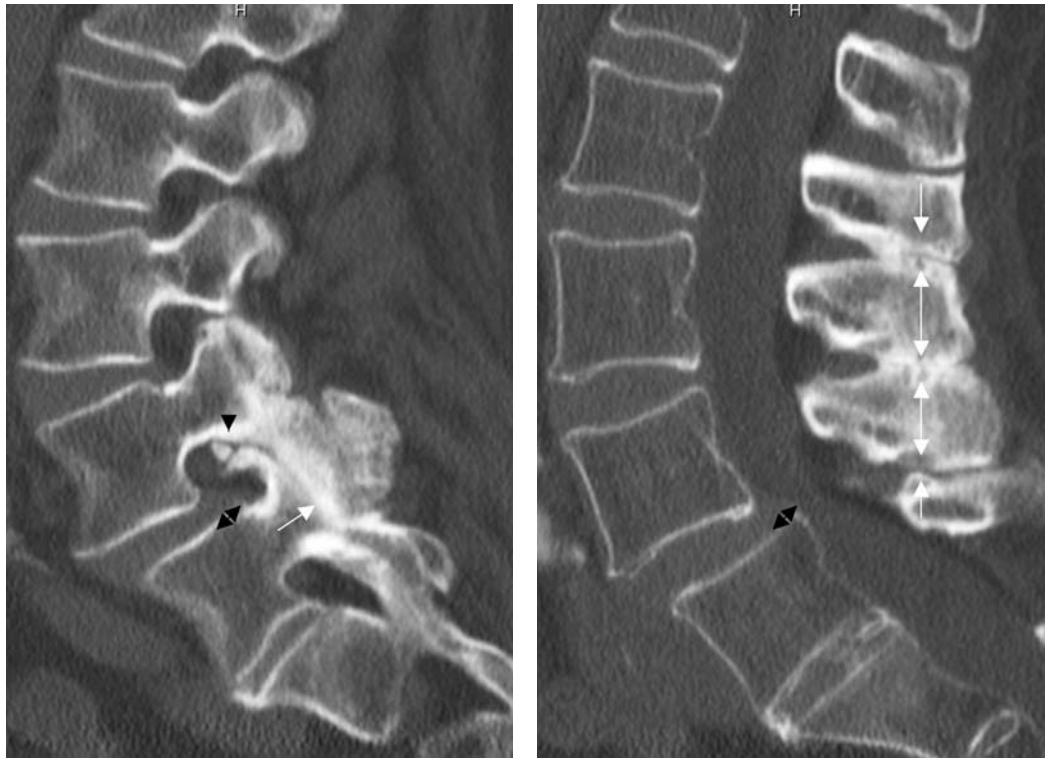

a b

Fig. 7.19a,b. Neural arch intervertebral neoarthrosis. Sagittal reformatted CT images at the level of the facet joints (**a**) and in the midsagittal plane (**b**). Grade 1 degenerative spondylolisthesis at the L4–L5 level (*double arrows*). Curved remodeling associated with osteophytic overgrowth and fragmentation of the apex of the L5 superior articular process (*black arrowhead*) and abnormal bony contact and neoarthrosis formation with the inferior aspect of the L4 pedicle (**a**). Concomitantly, a neoarthrosis is formed between the apex of the L4 inferior articular process and the posterior aspect of the L5 pars interarticularis (*white arrow*, **a**). In the midsagittal plane (**b**), spinous process collision of adjacent vertebrae (*white arrows*) with progressive interspinous degenerative changes (Baastrup's phenomenon). Bulging of the posterior epidural fat with impressions on the posterior aspect of the thecal sac

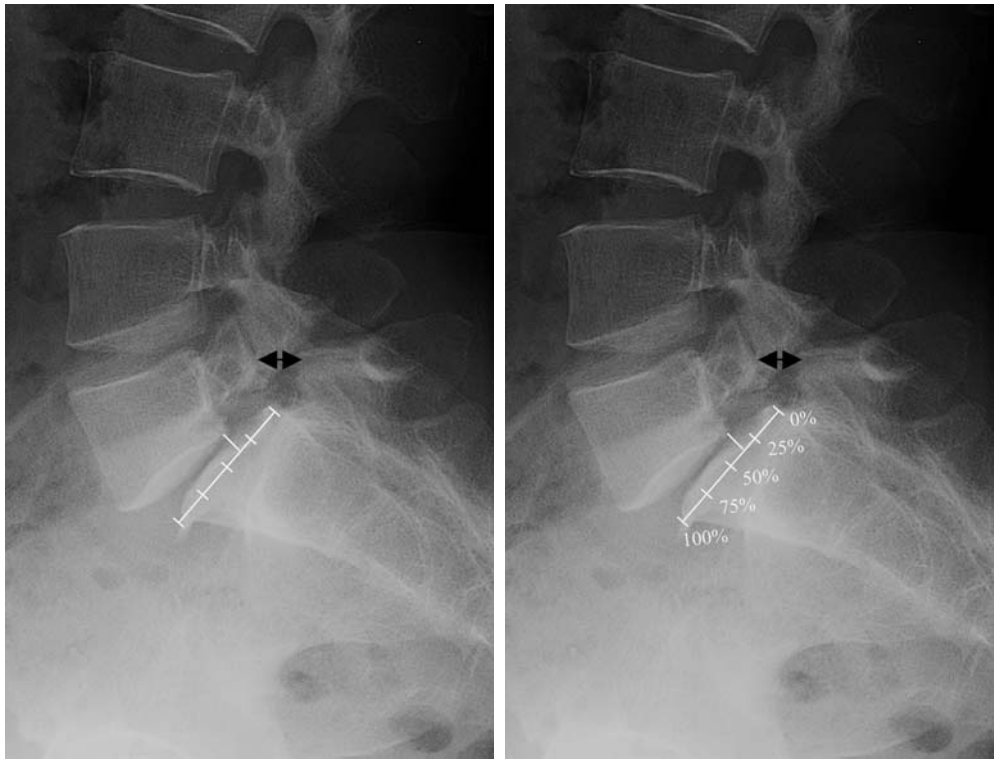

a b

Fig. 7.20a,b. Methods of grading lumbar spondylolisthesis. The method of Meyerding (**a**): lateral radiograph of the lumbar spine in type 2b isthmic spondylolisthesis (double arrows) shows a grade II slip. The method of Taillard (**b**) in the same patient shows an approximately 35% slip

7.5.1 Grading of Lumbar Spondylolisthesis

The forward slip of the upper vertebra is measured using the method of Meyerding, or the method described by Taillard. Using the method of Meyerding, the anteroposterior (AP) diameter of the superior surface of the lower vertebra is divided into quarters and a grade of I– IV is assigned to slips of one, two, three or four quarters of the superior vertebra, respectively. The other method, described by Taillard, expresses the degree of slip as a percentage of the AP diameter of the top of the lower vertebra (Butt and Saifuddin 2005).

7.5.2 Type 2, Isthmic Spondylolisthesis: Spondylolysis

Isthmic spondylolisthesis occurs when a bilateral defect in the pars interarticularis is present. The pars interarticularis (also known as the isthmus) is the part of the neural arch that joins the superior and inferior articular processes. A defect at this point functionally separates the vertebral body, pedicle, and superior articular process from the inferior articular process and remainder of the vertebra. Thus, the defect cleaves the vertebra into two parts. The portion of the vertebra posterior to the defect remains fixed, and the anterior portion has the potential to slip forward relative to the posterior structures and the spine below. Isthmic spondylolisthesis can be further categorized into three subtypes (Wiltse et al. 1976).

In type 2a, a lytic pars defect is present, due to a congenital weakness in the bone and/or repeated mechanical strain. Under the age of 50, it is the commonest cause of lumbar spondylolisthesis. Most defects are believed to begin as a stress fracture that most likely persists because of continued motion (especially extension movements of gymnasts, which have been implicated in causing the fractures in the first place), which usually impairs bone healing. The incidence in men is twice that in women. The L5–S1 segment is the most commonly affected segment (Butt and Saifuddin 2005).

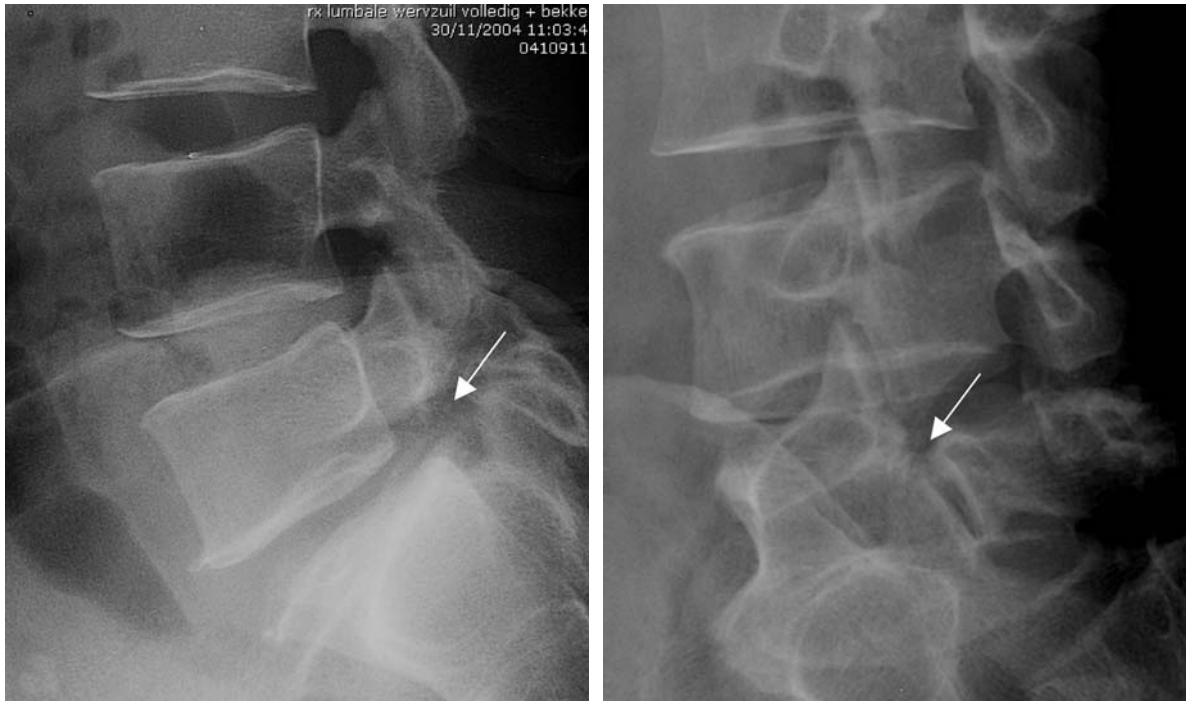

a b

Fig. 7.21a,b. Type 2b isthmic spondylolisthesis. Lateral (**a**) and oblique radiograph (**b**) of the lumbar spine demonstrate bilateral L5 pars defects (*white arrows*) with associated grade I L5–S1 isthmic spondylolisthesis. The pars defect has the typical appearance of a Scottie dog with a collar on oblique radiographs (**b**). Associated L5–S1 disc degeneration is observed

In type 2b, the elongated pars is a true stress fracture of the pars. Repeated trauma results in microfractures, which may heal over time, and the elongated pars is no longer able to check the forward movement of the vertebrae. In contrast with type 2a, this condition is very rare (Butt and Saifuddin 2005).

In type 2c, the pars fractures as a result of direct trauma.

Nerve root compression in isthmic (lytic) spondylolisthesis typically occurs at the level of the intervertebral foramen, due to a combination of reduced foraminal height, caused by the more horizontal oriented (elongated) aspect of the foramen, and the associated (pseudo-)bulging/protrusion of the intervertebral disc into the foramen, which compresses the exiting nerve root against the undersurface of the pedicle (Butt and Saifuddin 2005). In addition, the spinal canal is widened.

Imaging of spondylolisthesis and spondylolysis can be done using plain film radiography, CT and/or MR imaging. A lateral view will demonstrate spondylolisthesis and the grade of listhesis can be measured. The pars defect may or may not be visualized on the lateral view, and oblique views are especially useful for visualizing the pars defect, which has the appearance of a Scottie dog with a collar. An elongated pars may also be observed.

Both sagittal CT reformats and sagittal MR images demonstrate the levels involved and the grade of spondylolisthesis can be evaluated. CT will better demonstrate the pars defect in detail. Associated disc degeneration and disc bulging/protrusion may be observed. Foraminal height reduction with compression of the exiting nerve root between the bulging disc and the undersurface of the pedicle is obviously demonstrated on both techniques (Butt and Saifuddin 2005). The increased AP canal dimension identified on mid-sagittal MR images or reformatted CT allows for the differentiation between isthmic and degenerative spondylolisthesis to be made with a high degree of accuracy (Ulmer et al. 1994).

Scintigraphy can be used to detect pars microfractures in the absence of a lytic defect (type 2b) and to determine the process of healing of these fatigue fractures (Sys et al. 2001). In young patients, MR imaging should be the first and only imaging modality with low-back pain during and after ex-

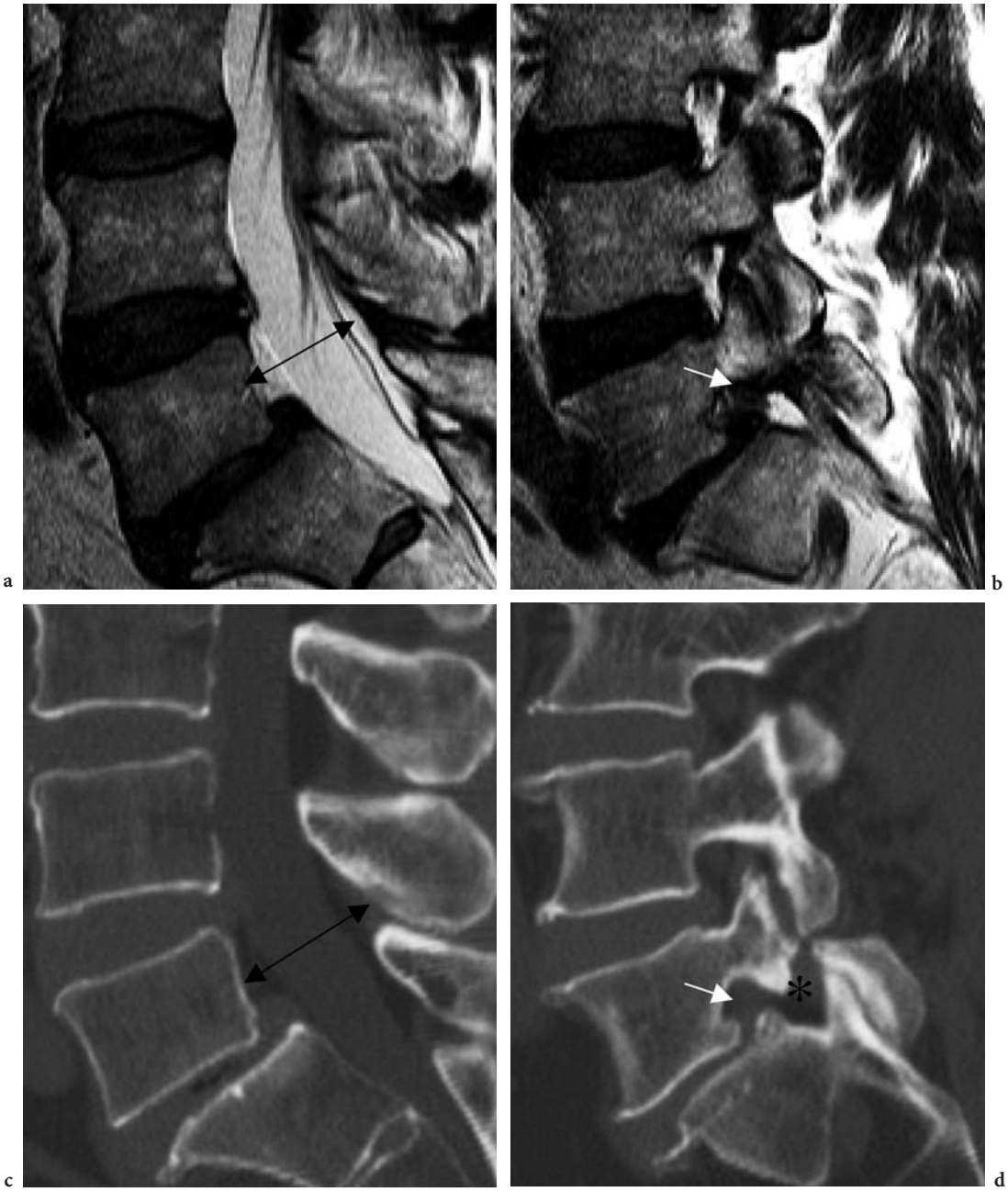

Fig. 7.22a-d. CT and MR imaging in type 2b isthmic spondylolisthesis. Sagittal T2-weighted images (**a**,**b**) and sagittal reformatted CT images (**c**,**d**) show grade I isthmic spondylolisthesis with associated protrusion of the disc. Both CT and MR images demonstrate foraminal height reduction with compression of the exiting nerve root (*white arrows*) between the protruding disc and the undersurface of the pedicle (**b**,**d**). CT better demonstrates the pars defect (*asterisk*) in detail (**d**). The increased AP canal dimension (*black double arrows*) identified on mid-sagittal MR images (**a**) or reformatted CT (**b**) may help in differentiating between isthmic and degenerative spondylolisthesis

Fig. 7.23a,b. Malalignment of the spinous processes in type 3 degenerative spondylolisthesis. Lateral radiographs (**a**,**b**) of the lumbar spine show grade I degenerative L4–L5 and grade II L5–S1 spondylolisthesis. Malalignment of the spinous processes (*white arrows*) with anterior slip of the L4 spinous process relative to L5 allows differentiation from isthmic spondylolisthesis (**b**). Associated disc space narrowing at the L3-L4, L4-L5 and L5-S1 levels is seen

ercise and pain with hyperextension. High signal intensity in the pars interarticularis and pedicle on fat-suppressed T2-weighted images indicating bone marrow edema is frequently observed. Bone scans and CT should be avoided due to irradiation (Stäbler et al. 2000).

7.5.3 Type 3, Degenerative Spondylolisthesis

This is the commonest cause of lumbar spondylolisthesis above the age of 50. Degenerative changes of the facet joints and associated disc degeneration are responsible for the anterior slip, which is usually mild. A more sagittal orientation of the facet joints is typically observed in these patients (Boden et al. 1996; Fujiwara et al. 2001). As the neural arch is intact, even a small progression in the slip may cause cauda equina syndrome. Women are four times more affected than men. Most commonly, the L4–L5 level is involved and its incidence increases four times if there is a sacralized L5. Clinical symptoms include low-back pain and leg pain as a result of disc and facet joint degeneration, lateral recess and foraminal stenosis leading to nerve root compression. With progression of the spondylolisthesis, the symptoms may change from low-back pain to neurogenic claudication due to central canal stenosis (Butt and Saifuddin 2005).

Lateral plain film shows anterolisthesis, degenerative changes of the facet joints, and disc space narrowing. Malalignment of the spinous processes with anterior slip of the spinous process relative to the spinous process of the lower vertebra allows differentiation from isthmic spondylolisthesis (Butt and Saifuddin 2005).

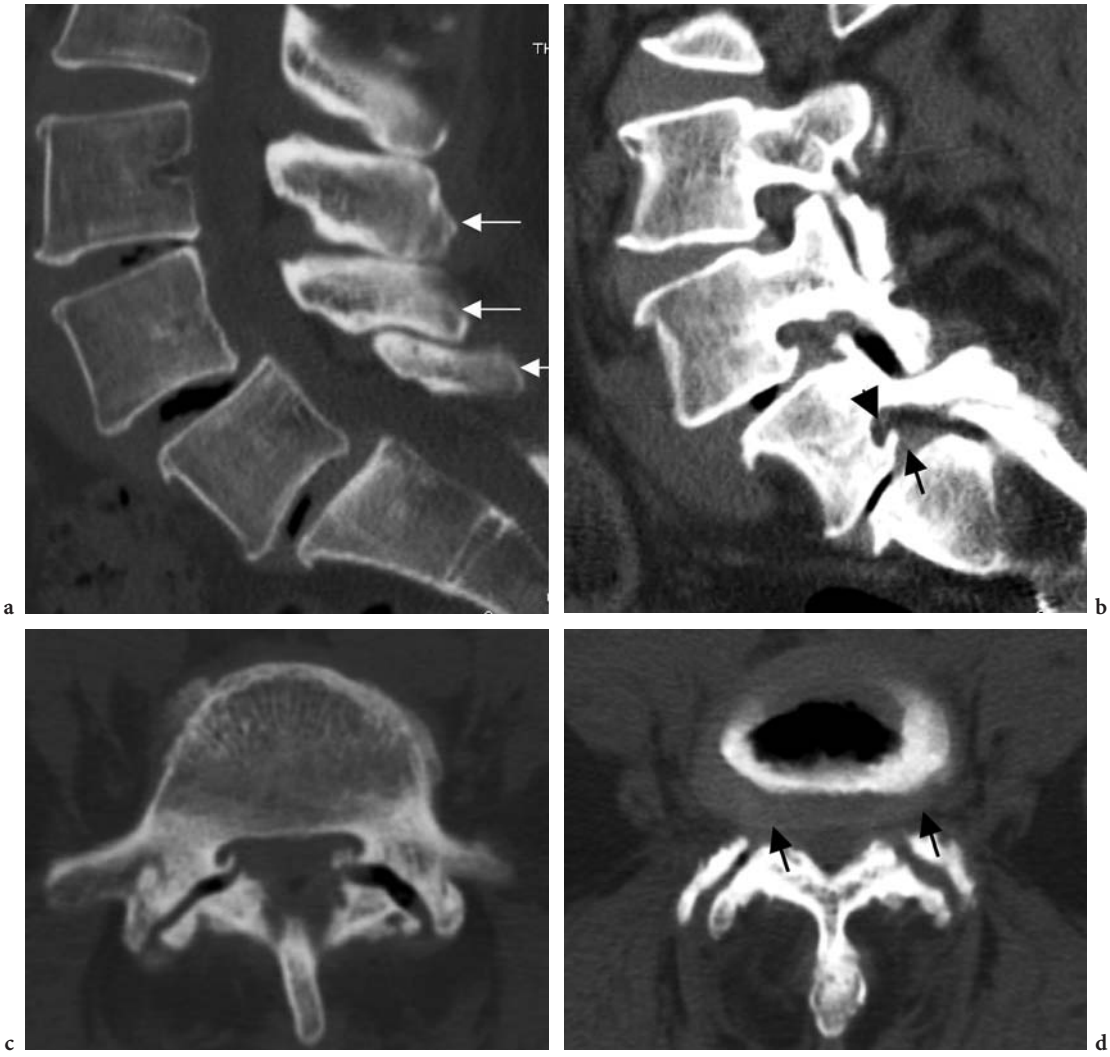

Fig. 7.24a–d. Value of MDCT in type 3 degenerative spondylolisthesis. MDCT of the lumbar spine (same patient as in Fig. 7.23) with sagittal (**a**,**b**) and axial (**c**,**d**) reformats shows grade I degenerative spondylolisthesis at the L4–L5 and L5–S1 levels. Associated degenerative disc disease with disc space narrowing, vacuum phenomenon in the intervertebral discs and disc protrusion (*black arrows*) is seen (**a**,**b** and **d**). Malalignment of the spinous processes (*white arrows*) with anterior slip of the L4 spinous process relative to L5 is typical for degenerative spondylolisthesis (**a**). Extensive facet joint osteoarthritis, narrowing of the L4-L5 and L5-S1 intervertebral foramina with nerve root compression (*black arrowhead*) is observed (**b**,**d**)

CT and MR imaging demonstrate degeneration of the facet joints and associated spondylolisthesis. The sagittal orientation of the facet joints can be evaluated. Both techniques allow for direct visualization of disc degeneration and disc bulging. Sagittal images demonstrate narrowing of the central canal, lateral recess and intervertebral foramina with associated compression of the cauda equina and exiting nerve roots. Thickening of the ligamenta flava may add to central canal and lateral recess stenosis. Anterior slip of the inferior articular process will narrow the inferior aspect of the lateral recess and the intervertebral foramen (Butt and Saifuddin 2005).

Bone marrow signal intensity changes in the pedicle are not a specific sign of spondylolysis; they are commonly observed in patients with degenerative facet joint disease. These bone marrow changes are probably a response to abnormal stresses related to abnormal motion or loading caused by the degenerative changes in the spinal segment. (Morrison et al. 2000).

a b

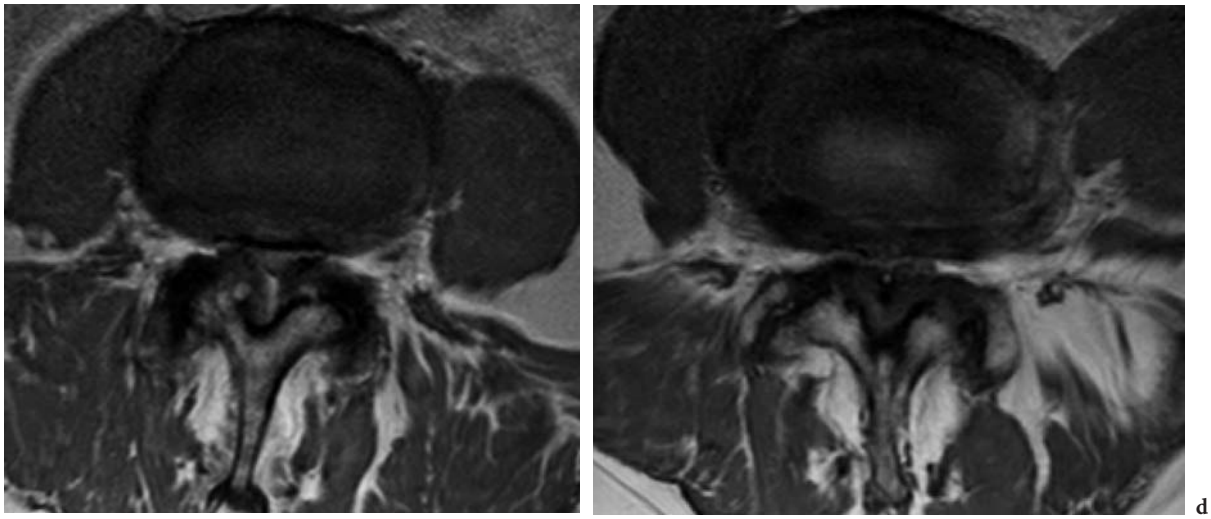

c d

Fig. 7.25a–d. MR imaging in type 3 degenerative spondylolisthesis. Sagittal T2-weighted image (**a**), sagittal T1-weighted image (**b**) of the lumbar spine and axial T2-weighted image at the L3–L4 (**c**) and the L4–L5 level (**d**) show a grade I degenerative spondylolisthesis at both levels. Disc degeneration with disc space narrowing, signal loss and bulging of the intervertebral disc is observed. Facet joint osteoarthritis with joint space narrowing, hypertrophy and marked thickening of the ligamentum flavum is observed. These degenerative changes result in spinal stenosis

References

Anderson PA (2003) The Future of the Cervical Spine: Presidential Address to the Cervical Spine Research Society. Spine 28:2643–2647

Apostolaki E, Davies AM, Evans N, Cassar-Pullicino (2000) MR imaging of lumbar facet joint synovial cysts. Eur Radiol 10:615–623

Barry M, Livesly P (1997) Facet joint hypertrophy: the cross-sectional area of the superior articular process of L4 and L5. Eur Spine J 6:121–124

Boden SD, Riew KD, Yamaguchi K, Branch TP, Schellinger D, Wiesel SW (1996) Orientation of the lumbar facet joints: association with degenerative disc disease. J Bone Joint Surg Am 78:403–411

Brown TR, Quinn SF, D'Agostino AN (1991) Deposition of calcium pyrophosphate dihydrate crystals in the ligamentum flavum: evaluation with MR imaging and CT. Radiology 178:871–873

Butler D, Trafimow JH, Andersson GB, McNeill TW, Huckman MS (1990) Discs degenerate before facets. Spine 15:111–113

Butt S, Saifuddin A (2005) The imaging of lumbar spondylolisthesis. Clin Radiol 60:533–546

Cakir E, Kuzeyli K, Usul H, Peksoylu B, Yazar U, Reis A, Karaarslan G (2004) Ligamentum flavum cyst. J Clin Neurosci 11:67–69

Carrera GF (1980) Lumbar facet joint injection in low back pain and sciatica. Radiology 137:661–664

Carrera GF, Haughton VM, Syvertsen A, Williams AL (1980) Computed tomography of the lumbar facet joints. Radiology 134:145–158

Cassidy JD, Loback D, Yong-Hink K, Tchang S (1992) Lumbar facet joint asymmetry. Intervertebral disc herniation. Spine 17:570-574

Cavanaugh JM, Lu Y, Chen C, Kallakuri S (2006) Pain generation in lumbar and cervical facet joints. J Bone Joint Surg Am 88 [Suppl 2]:63–67

Chen CKH, Yeh LR, Resnick D, Lai HL, Liang HL, Pan HB, Yang CF (2004) Intraspinal posterior epidural cysts associated with Baastrup's disease: report of 10 patients. AJR Am J Roentgenol 182:191–194

Chen HC, Hsu PW, Lin CY, Tzaan WC (2005) Symptomatic hematoma of cervical ligamentum flavum. Spine 30: E489–E491

Chiba K, Toyama Y, Matsumoto M, Maruiwa H, Watanabe M, Nishizawa T (2001) Intraspinal cyst communicating with the intervertebral disc in the lumbar spine: discal cyst. Spine 26:2112–2118

Cinotti G, De Santis P, Nofroni I, Postacchini F (2002) Stenosis of lumbar intervertebral foramen: anatomic study on predisposing factors. Spine 27:223-229

Demondion X, Vidal C, Glaude E, Subocz L, Francke JP, Cotton A (2005) The posterior lumbar ramus: CT correlation and propositions of new sites of infiltration. AJNR Am J Neuroradiol 26:706–710

Doyle AJ, Merrilees M (2004) Synovial cysts of the lumbar facet joints in a symptomatic population. Prevalence on magnetic resonance imaging. Spine 29:874–878

Farfan HF, Huberdeau RM, Dubow HI (1972) Lumbar intervertebral disc degeneration: the influence of geometrical features on the pattern of disc degeneration: a post mortem study. J Bone Joint Surg Am 54:492–510

Fujiwara A, Lim TH, An HS, Tanaka N, Jeon CH, Andersson GBJ, Haughton VM (2000) The effect of disc degeneration and facet joint osteoarthritis on the segmental flexibility of the lumbar spine. Spine 25:3036–3044

Fujiwara A, Tamai K, An HS, Lim TH, Yoshida H, Kurihashi A, Saotome K (2001a) Orientation and osteoarthritis of the lumbar facet joint. Clin Orthopaed Rel Res 385:88–94

Fujiwara A, An HS, Lim TH, Haughton VM (2001b) Morphologic changes in the lumbar intervertebral foramen due to flexion-extension, lateral bending, and axial rotation: an in vitro anatomic and biomechanical study. Spine 26:876–882

Gadgil AA, Eisenstein SM, Darby A, Cassar-Pullicino V (2002) Bilateral symptomatic synovial cysts of the lumbar spine caused by calcium pyrophosphate deposition disease: a case report. Spine 27:E428–E431

Gray H (1918) Anatomy of the human body. Lea and Febiger, Philadelphia; available online at http://Bartleby.com/107/

Grenier N, Kressel HY, Schiebler ML, Grossman RI, Dalinka MK (1987) Normal and degenerative posterior spinal structures: MR imaging. Radiology 165:517–525

Grobler LJ, Robertson PA, Novotny JE, Pope MH (1993) Etiology of spondylolisthesis. Assessment of the role played by lumbar facet joint morphology. Spine 18:80–91

Grogan J, Nowicki BH, Schmidt TA, Haughton VM (1997) Lumbar facet joint tropism does not accelerate degeneration of the facet joints. AJNR Am J Neuroradiol 18:1325–1329

Hagen T, Daschner H, Lensch T (2001) Juxtafacettenzysten: Magnetresonanztomographische Diagnostik (Juxta-facet cysts: MR imaging). Radiologe 41:1056–1062

Hagg O, Wallner A (1990) Facet joint asymmetry and protrusion of the intervertebral disc. Spine 15:356-359

Haig AJ, Harris A, Quint DJ (2001) Baastrup's disease correlating with diffuse lumbar paraspinal atrophy: a case report. Arch Phys Med Rehabil 82:250–252

Hasegawa T, An HS, Haughton VM, Nowicki BH (1995) Lumbar foraminal stenosis: critical heights of the intervertebral discs and foramina. J Bone Joint Surg Am 77:32–38

Hirai T, Korogi Y, Takahashi M, Shimomura O (2001) Ossification of the posterior longitudinal ligament and ligamentum flavum: imaging features. Semin Musculoskelet Radiol 5:83–88

Hirakawa K, Hanakita J, Suwa H, Matsuoka N, Oda M, Muro H, Fukushima T (2000) A post-traumatic ligamentum flavum progressive hematoma. Spine 25:1182–1184

Hollenberg GM, Beattie PF, Meyers SP, Weinberg EP, Adams MJ (2002) Stress reactions of the lumbar pars interarticularis: the development of a new MRI classification system. Spine 27:181–186

Hsu KY, Zucherman JF, Shea WJ, Jeffry RA (1995) Lumbar intraspinal synovial and ganglion cysts (facet cysts). Ten-year experience in evaluation and treatment. Spine 20:80–89

Jenis LG, An HS (2000) Spine update. Lumbar foraminal stenosis. Spine 25:389–394

Jinkins JR (2001) Acquired degenerative changes of the intervertebral segments at and supradjacent to the lumbosacral junction. A radioanatomic analysis of the nondiskal structures of the spinal column and perispinal soft tissues. Rad Clinics North Am 39:73–99

Karacan I, Aydin T, Sahin Z, Cidem M, Koyuncu H, Aktas I, Uludag M (2004) Facet angles in lumbar disc herniation: their relation to anthropometric features. Spine 29:1132-1136

Kono K, Nakamura H, Inoue Y, Shakudo M, Yamada R (1999) Intraspinal extradural cysts communicating with adjacent herniated disks: imaging characteristics and possible pathogenesis. AJNR Am J Neuroradiol 20:1373–7

Lunardi P, Acqui M, Ricci G, Agrillo A, Ferrante L (1999) Cervical synovial cysts: case report and review of the literature. Eur Spine J 8:232–237

Lyons MK, Atkinson JL, Wharen RE, Deen HG, Zimmerman RS, Lemens SM (2000) Surgical evaluation and management of lumbar synovial cysts: the Mayo Clinic experience. J Neurosurg 93(1 Suppl):53–57

Mahalatti H, Wallace CJ, Hunter KM, Bilbao JM, Clark AW (1999) MR imaging of a hemorrhagic and granulomatous cyst of the ligamentum flavum with pathologic correlation. AJNR Am J Neuroradiol 20:1166–1168

Malanga GA, Chimes GP, Memmo P (2006) Lumbrosacral facet syndrome. eMedicine, Stedman's Health Professions and Nursing Dictionary. Lippincott Williams and Wilkins, Baltimore

Manchikanti L, Pampati V, Fellows B, Baha AG (2000) The inability of the clinical picture to characterize pain from facet joints. Pain Physician 3:158–166

Manchikanti L, Singh V, Pampati V, Damron KS, Beyer CD, Barnhill RC (2002) Is there correlation of facet joint pain in lumbar and cervical spine? An evaluation of prevalence in combined chronic low back and neck pain. Pain Physician 5:365–371

Manchikanti L, Boswell MV, Singh V, Pampati V, Damron KS, Beyer CD (2004) Prevalence of facet joint pain in chronic spinal pain of cervical, thoracic, and lumbar regions. BMC Musculoskeletal Disord 5:15–22

Miyasaka K, Kaneda K, Sato S, Iwasaki Y, Abe S, Takei H, Tsuru M, Tashira K, Abe H, Fujioka Y (1983) Myelopathy due to ossification or calcification of the ligamentum flavum: radiologic and histologic evaluations. AJNR Am J Neuroradiol 4:629–632

Morrison JL, Kaplan PA, Dussault RG, Anderson MW (2000) Pedicle marrow signal intensity changes in the lumbar spine: a manifestation of facet degenerative joint disease. Skeletal Radiol 29:703–707

Muthukumar N, Karuppaswamy U, Sankarasubbu B (2000) Calcium pyrophosphate dihydrate deposition disease causing thoracic cord compression: case report. Neurosurgery 46:222–225

Nowicki BH, Haughton VM, Schmidt TA, Lim TH, An HS, Riley LH III, Yu L, Hong JW (1996) Occult lumbar lateral spinal stenosis in neural foramina subjected to physiologic loading. AJNR Am J Neuroradiol 17:1605–1614

Oertel MF, Ryang YM, Gilsbach JM, Rohde V (2006) Lumbar foraminal and far lateral juxtafacet cyst of intraspinal origin. Surg Neurol 66:197–199

Palmieri F, Cassar-Pullicino VN, Lalam RK, Tins BJ, Tyrrell PN, McCall IW (2006) Migrating lumbar facet joint cysts. Skeletal Radiol 35:220–226

Paolini S, Ciapetta P, Santoro A, Ramieri A (2002) Rapid, symptomatic enlargement of a lumbar juxtafacet cyst. Spine 27:E281–E283

Park JB, Chang H, Kim KW, Park SJ (2001) Facet tropism. A comparison between far lateral and posterolateral lumbar disc herniations. Spine 26:677–679

Pascal-Moussellard H, Cabre P, Smadja D, Catonne Y (2005) Symptomatic ossification of the ligamentum flavum: a clinical series from the French Antilles. Spine 30:E400–E405

Pathria M, Sartoris DJ, Resnick D (1987) Osteoarthritis of the facet joints: accuracy of oblique radiographic assesment: Radiology 164:227-230

Pinto PS, Boutin RD, Resnick D (2004) Spinous process fractures associated with Baastrup disease. Clin Imaging 28:219–222

Rajasekaran S, Pithwa YK (2003) Baastrup's disease as a cause of neurogenic claudication: a case report. Spine 28:E273–E275

Ruiz Santiago F, Alcazar Romero PP, Lopez Machado E, Garcia Espona MA (1997) Calcification of lumbar ligamentum flavum and facet joints capsule. Spine 22:1730–1734

Sarazin L, Chevrot A, Pessis E, Minoui A, Drape JL, Chemla N, Godefroy D (1999) Titel facet joint arthrography posterior approach. Radiographics 19:93–104

Sato K, Wakamatsu E, Yoshizumi A, Watanabe N, Irei O (1989) The configuration of the laminas and facet joints in degenerative spondylolisthesis. A clinicoradiologic study. Spine 14:1265–1271

Sauvage P, Grimault L, Ben Salem D, Roussin I, Huguenin M, Falconnet M (2000) Lumbar intraspinal synovial cysts: imaging and treatment by percutaneous injection. Report of thirteen cases. J Radiol 81:33–38

Schellinger D, Wener L, Ragsdale BD, Patronas NJ (1987) Facet joint disorders and their role in the production of back pain and sciatica. RadioGraphics 7:923–944

Schmid G, Willburger R, Jergas M, Pennekamp W, Bickert U, Koster O (2002) Lumbar intraspinal juxtafacet cysts: MR imaging and CT-arthrography. Rofo 174:1247–52.

Shah RV, Lutz GE (2003) Lumbar intraspinal synovial cysts: conservative management and review of the world's literature. Spine J 3:479–488

Shaw M, Birch N (2004) Facet joint cysts causing cauda equina compression. J Spinal Disord Tech 17:442–445

Sherif H, Mahfouz AE (2004) Epidural fat interposition between dura mater and spinous process: a new sign for the diagnosis of spondylolysis on MR imaging of the lumbar spine. Eur Radiol 14:970–973

Silbergleit R, Mehta BA, Sanders WP, Talati SJ (2001) Imaging-guided injection techniques with fluoroscopy and CT for spinal pain management Radiographics 21:927–939

Song JK, Musleh W, Christie SD, Fessler RG (2006) Cervical juxtafacet cysts: case report and literature review. Spine J 6:279–281

Stäbler A, Paulus R, Steinborn M, Bosch R, Matzko M, Reiser M (2000) Spondylolysis in adolescents: the diagnostic value of MRI. Fortschr Röntgenstr 172:33–37

Stoodley MA, Jones NR, Scott G (2000) Cervical and thoracic juxtafacet cysts causing neurologic deficits. Spine 25:970–973

Swartz PG, Murtagh FR (2003) Spontaneous resolution of an intraspinal synovial cyst. AJNR Am J Neuroradiol 24:1261–1263

Sys J, Michielsen J, Bracke P, Martens M, Verstreken J (2001) Nonoperative treatment of active spondylolysis in elite athletes with normal X-ray findings: literature review and results of conservative treatment. Eur Spine J 10:498–504

Taylor JR, McCormick CC (1991) Lumbar facet joint fat pads: their normal anatomy and their appearance when enlarged. Neuroradiology 33:38–42

Terada H, Yokoyama Y, Kamata N, Hozumi T, Kondo T (2001) Cyst of the ligamentum flavum. Neuroradiology. 43:49–51

Thalgott JS, Albert TJ, Vaccaro AR, Aprill CN, Giuffre JM, Drake JS, Henke JP (2004) A new classification system for degenerative disc disease of the lumbar spine based on magnetic resonance imaging, provocative discography, plain radiographs and anatomic considerations. Spine J 4:167S–172S

Tillich M, Trummer M, Lindbichler F, Flaschka G (2001) Symptomatic intraspinal synovial cysts of the lumbar spine: correlation of MR and surgical findings. Neuroradiology 43:1070-1075

Ulmer JL, Elster AD, Mathews VP, King JC (1994) Distinction between degenerative and isthmic spondylolisthesis on sagittal MR images: importance of increased anteroposterior diameter of the spinal canal ("wide canal sign"). AJR Am J Roentgenol 163:411–416

Ulmer JL, Mathews VP, Elster AD, King JC (1995a) Lumbar spondylolysis without spondylolisthesis: recognition of isolated posterior element subluxation on sagittal MR. AJNR Am J Neuroradiol 16:1393–1398

Ulmer JL, Elster AD, Mathews VP, Allen AM (1995b) Lumbar spondylolysis: reactive marrow changes seen in adjacent pedicles on MR images. AJR Am J Roentgenol 164:429–433

Ulmer JL, Mathews VP, Elster AD, Mark LP, Daniels DL, Mueller W (1997) MR imaging of lumbar spondylolysis: the importance of ancillary observations. AJR Am J Roentgenol 169:233–239

van den Hauwe L, Van Goethem JW, Parizel PM, De Schepper AM (1993) Magnetic resonance imaging of calcified thoracic disk herniation. Eur J Radiol 17:148–149

Van Goethem JW, Maes M, Ozsarlak O, van den Hauwe L, Parizel PM (2005) Imaging in spinal trauma. Eur Radiol 15:582–590

Van Schaik JP, Verbiest H, Van Schaik FD (1984) The orientation and shape of the lower lumbar facet joints: a computed tomographic study of their variation in 100 patients with low back pain and a discussion of their possible clinical implications. In: Post MJ (ed) Computed tomography of the spine Williams and Wilkins, Baltimore, pp 495–505

Weishaupt D, Zanetti M, Boos N, Hodler J (1999) MR imaging and CT in osteoarthritis of the lumbar facet joints. Skeletal Radiol 28:215–219

Weishaupt D, Schmid MR, Zanetti M, Boos N, Romanowski B, Kissling RO, Dvorak J, Hodler J (2000) Positional MR imaging of the lumbar spine: does it demonstrate nerve root compromise not visible at conventional MR imaging? Radiology 215:247–253

Wildermuth S, Zanetti M, Duewell, S, Schmid MR, Romanowski B, Benini A, Böni T, Hodler J (1998) Lumbar spine: quantitative and qualitative assessment of positional (upright and extension) MR and myelography. Radiology 207:391–398

Wiltse LL, Newman PH, Macnab I (1976) Classification of spondylolysis and spondylolisthesis. Clin Orthop 117:23–29

Wybier M (2001) Imaging of lumbar degenerative changes involving structures other than disk space. Radiol Clin North Am 39:101–114

Xiong L, Zeng QY, Jinkins JR (2001) CT and MRI characteristics of ossification of the ligamnta flava in the toracic spine. Eur Radiol 11:1798-1802

Xu GL, Haughton VM, Carrera GF (1990) Lumbar facet joint capsule: appearance at MR imaging and CT. Radiology 177:415–420

Yamashita Y, Takahashi M, Matsuno Y, Sakamoto Y, Yoshizumi K, Oguni T, Kojima R (1990) Spinal cord compression due to ossification of ligaments: MR imaging. Radiology 175:843–848

Spinal Stenosis

8

Massimo Gallucci, Silvia Capoccia, and Mauro Colajacomo

CONTENTS

M. Gallucci, MD
Department of Radiology, University of L'Aquila, Ospedale Nuovo S. Salvatore, Località Coppito, 67100 L'Aquila, Italy
S. Capoccia, MD
Department of Radiology, Hospital "S. Maria della Stella", Orvieto, Italy
M. Colajacomo, MD
Department of Radiology, Pediatric Hospital "Bambino Gesù" Palidoro, Via Torre di Palidoro, Passoscuro (Fiumicino) Rome, Italy

8.1 Introduction

Spinal stenosis is defined as a reduction of the diameters of the spinal canal. The size of the spinal canal varies according to location and several corresponding diameters are recognized (sagittal, interpeduncular, interarticular, depth of lateral recesses). Spinal stenosis may lead to neurological disorders associated with compression of the nervous structures contained in this canal (spinal cord, conus medullaris, cauda equina, nerve roots, meninges).

According to epidemiological data, the incidence of congenital stenosis is low and the incidence of degenerative stenosis, the main cause of stenosis with regard to both disco-somatic and ligamentous components, increases with age, starting at 30 to 40 years. It consequently leads to considerable socio-economic repercussions and both conservative and surgical treatment.

For a long time, if spinal stenosis was suspected, the spine was studied only with plain film myelography. Later, the use of computed tomography (CT) and magnetic resonance imaging (MR imaging), both non-invasive techniques, allowed a better evaluation of the spinal canal and, in particular, of the lateral recesses and intervertebral foramina.

While MR imaging has been considered useful for the study of soft tissues and for an overview of the spine and its content, CT is important for the study of bony structures. Although it is invasive and was mostly replaced by MR imaging, conventional dynamic myelography until recently remained the only examination technique capable of evaluating changes in the vertebral canal's caliber and in spinal cord or radicular conflicts, during physiological loading.

In general, MR-examinations are limited to the supine position, which cannot always give a clear answer to some clinical conditions. More recently, stand-up MR equipment has allowed the implemen-

KEY-POINTS

- Definition:
  - Spinal stenosis is a clinical condition in which the dimensions of the spinal canal have reached a critical value with neurological symptoms, related to direct compression of its' contents (i.e. dural sac, spinal cord and nerves).

- Spinal stenosis may be classified:
  - according to etiology: congenital, acquired or combined
  - according to location: central, lateral, foraminal and/or concentric
  - and graded as: slight, moderate, severe

- Etiology:
  - congenital: most frequent in the lumbar spine and idiopathic (racial and regional differences)
    - prenatal factors (e.g. IUGR, gestation duration, …)
    - anomalies in vertebral development
    - congenital spondylolisthesis
    - metabolic disorders: e.g. mucopolysaccharidosis
    - skeletal dysplasia: achondroplasia, Gorlin's syndrome, …
  - acquired: most frequent cause of spinal stenosis, both in lumbar and cervical region
    - degenerative pathology (discovertebral, facet joints, ligamentous)
    - rheumatic diseases, crystal deposition diseases, metabolic and endocrine diseases, osteodystrophy
    - traumatic disease (especially at the cervical and thoracolumbar region)
    - epidural lipomatosis

- Clinical picture:
  - varies according to
  - neurogenic claudication: pathognomonic for lumbar spinal stenosis
  - cauda equina syndrome
  - para- and tetraparesis

- Imaging modalities
  - plain film
    - AP and LL projections
    - dynamic imaging (flexion-extension) to look for spinal instability
    - Torg ratio (ratio between the sagittal diameter of the spinal canal and that of the vertebral body)
  - MR imaging
    - sagittal and transverse dimensions
    - SAC: space available for the cord
  - myelography/CT myelography
  - discrepancy between imaging modalities:
    - myelography: prone position/standing
    - CT myelography and MR imaging: supine position: underestimate spinal stenosis

- Therapy
  - conservative versus surgical treatment
    - the choice should be based on the disability and not on the degree of stenosis
    - the choice also depends on the patient's comorbidity, cardiovascular, living and socioeconomic conditions
  - conservative treatment:
    - NSAID, myorelaxing drugs, facet joints or epidural steroid infiltrations, …
    - may have good results even for many years
    - if medical therapy fails, then the results obtained when the patient switches to the surgical treatment are the same as those obtained by patients that had chosen the surgical treatment from the very start
  - surgical treatment:
    - no scientific evidence has shown that surgery is actually effective in vertebral canal stenosis and surgical therapy is not always necessary
    - surgery should be reserved for patients with severe stenosis, important clinical symptoms, degenerative spondolisthesis, and those who tend to worsen with time

tation of studies in orthostatic position; however, these devices have been scarcely used, above all for their high cost. Alternatively, devices have been developed which can simulate the axial load during MR imaging or CT using an axial-loading compressor (Fig. 8.1).

Although these devices are useful, they cannot always adequately reproduce the static and dynamic loads on the spine and spinal cord with various positions.

In this context, plain film conventional dynamic myelography can still have a role. Since it is obtained in upright, prone, and in squatting position, it is able to demonstrate central or lateral narrowing of the canal with different dynamic postures (Fig. 8.2).

For standard and dynamic projections, plain film examination remains the technique of choice and allows the evaluation of the presence of anomalies and skeletal degenerative alterations.

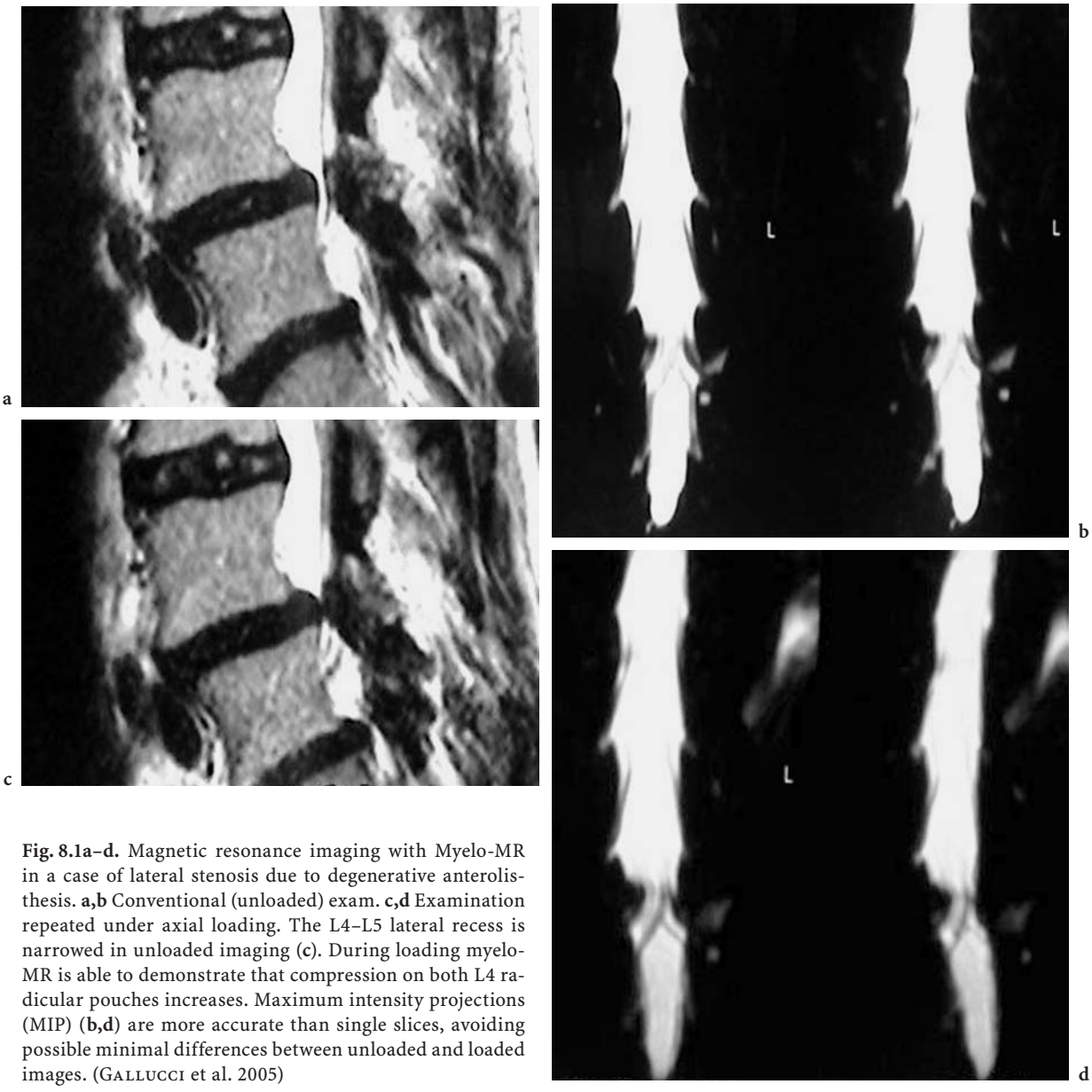

Fig. 8.1a–d. Magnetic resonance imaging with Myelo-MR in a case of lateral stenosis due to degenerative anterolisthesis. **a,b** Conventional (unloaded) exam. **c,d** Examination repeated under axial loading. The L4–L5 lateral recess is narrowed in unloaded imaging (**c**). During loading myelo-MR is able to demonstrate that compression on both L4 radicular pouches increases. Maximum intensity projections (MIP) (**b,d**) are more accurate than single slices, avoiding possible minimal differences between unloaded and loaded images. (Gallucci et al. 2005)

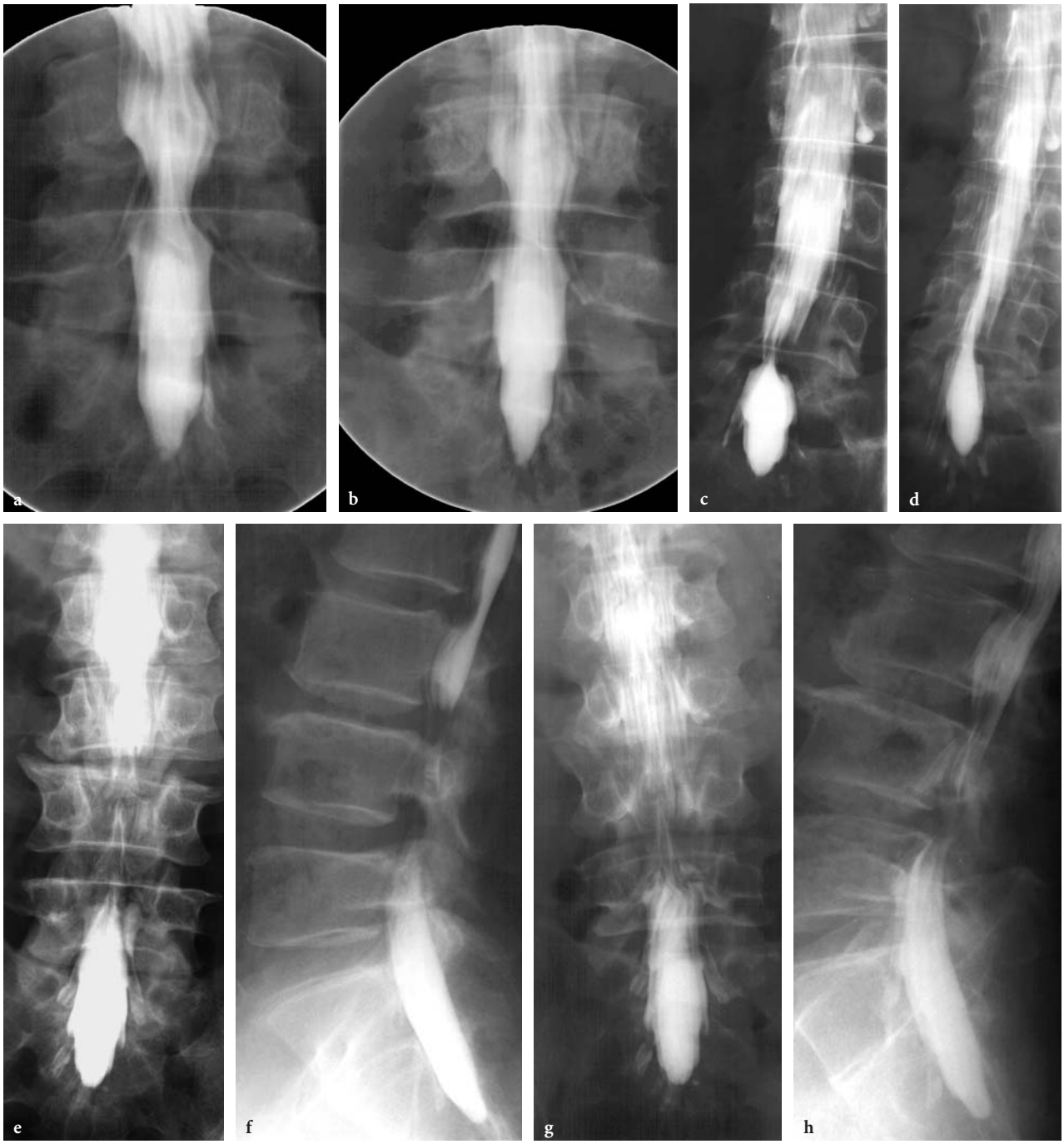

Fig. 8.2a–h. Three different cases of dynamic myelography. **a,b** In case 1 myelograms are obtained in anteroposterior (AP) projections, in prone position (**a**) and in squatting position (**b**). **b** The squatting position reduces compression on L4 radicular pouches, by distension of the flava ligaments and widening of intervertebral distance. **c,d** In case 2 similarly to the previous case, squatting (**d**) strongly reduces the compression evident in prone AP projection. **e-h** Case 3. In prone position contrast medium has two blocks, L3–L4 and L4–L5, thus suggesting two levels of disease (**e** AP, **f** left lateral projection). In upright position (**g,h**) radiograms the compromise involves only the L4–L5 level, with a minor degree of stenosis at L3–L4

8.2 Classification

From an etiopathological point of view, stenosis can be divided into congenital (Table 8.1) (abnormal development of the bony elements constituting the spinal canal), acquired (Table 8.2) (normal dimensions of the spinal canal, but degenerative changes modify the normal morphology and structure of its osteo-ligamentous formations), and mixed (degenerative changes superimposed on a pre-existing congenital stenosis).

According to the severity of narrowing its location, stenosis can be divided into four subgroups: central (reduction of the sagittal diameter); lateral (reduction of the recess diameter); foraminal (reduction of the neural foramen's caliber); and concentric (reduction of all canal's diameters). According to the severity of narrowing, spinal stenosis can be graded as slight, moderate, or severe (see later).

In Tables 8.1 and 8.2 an etiological classification of spinal stenosis is proposed according to location (cervical, thoracic or lumbar).

Table 8.1. Classifications of Congenital Spinal Stenosis

	Classification of Congenital Spinal Stenosis		
	Cervical	**Thoracic**	**Lumbosacral**
Idiopathic	Central - concentric	Central - concentric	Central - concentric
Hypoplasia of the pedicles, posterior arch/lamina	Central	Central	Central
Anterolisthesis	Lateral - foraminal		
Retrolisthesis	Central		Central
Achondroplasia		Concentric	Concentric
Acromegaly			Central - lateral
Brachyolmia	Central	Central	Central
Chondrodysplasia punctata	Central		
Craniodiaphyseal dysplasia (Gorlin's disease)	Concentric		
Down's syndrome	Central		
Ehlers-Danlos syndrome		Lateral - foraminal	Lateral - foraminal
Fibrous Dysplasia			Central
Hypophosphatemic X-linked rickets		Central	
Klippel-Feil deformity	Central		
Marfan's syndrome	Central	Lateral - foraminal	
Mucopolysaccharidosis type IV (Morquio Syndrome) and type VI (Maroteaux-Lamy Syndrome)	Central	Central	
Osteochondrodysplasias - congenital spondyloepi physeal dysplasia - Dyggve-Melchior-Clausen dysplasia	Central		
Progressive myositis ossificans	Central - lateral - foraminal - concentric	Central - lateral - foraminal - concentric	Central - lateral - foraminal - concentric
Scoliosis (fusion and segmentation anomalies)		Lateral - foraminal	Lateral - foraminal
Spinal epidural lipomatosis			Concentric
Sternocostoclavicular hyperostosis	Central - lateral - foraminal		

Table 8.2. Classifications of Acquired Spinal Stenosis

	Classification of Acquired Spinal Stenosis		
	Cervical	Thoracic	Lumbosacral
Degenerative (osteophytes, listhesis, disc herniation, synovial cyst)	Central - lateral - foraminal	Central - lateral - foraminal	Central - lateral - foraminal
PLL (or tectorial membrane) hypertrophy and/or calcification, ossification	Central	Central	Central
Yellow ligament hypertrophy and/or calcification, ossification	Central - lateral - foraminal	Central - lateral - foraminal	Central - lateral - foraminal
Scoliosis		Lateral - foraminal	Lateral - foraminal
Spinal eidural lipomatosis			Concentric
Rheumatoid arthritis - ankylosing spondylitis	Central - lateral - foraminal - concentric	Central - lateral - foraminal	Central - lateral - foraminal
CPPD - hyperparathyroidism	Central - lateral - foraminal		Central - lateral - foraminal
DISH - pseudogout	Central - lateral - foraminal		
Still's disease - chronic arthritis in childhood	Central - lateral - foraminal - concentric		
Paget's disease	Central - lateral - foraminal - concentric	Concentric	
Steroids		Central	Central
Hypervitaminose D	Lateral - foraminal	Central - lateral - foraminal	Central - lateral - foraminal
Fluorosis	Central		
Amyloidosis	Concentric	Concentric	Concentric
Infectious (spondyl(odisc)itis)	Central - lateral - foraminal	Central - lateral - foraminal	Central - lateral - foraminal
Neoplastic	Central - lateral - foraminal	Central - lateral - foraminal	Central - lateral - foraminal
Traumatic (luxation, herniation, listhesis, fracture, hematoma)	Central - lateral - foraminal	Central - lateral - foraminal	Central - lateral - foraminal
Iatrogenic (redundant fibrous tissue, graft hypertrophy, pseudocyst, inflammatory granuloma)	Central - lateral - foraminal	Central - lateral - foraminal	Central - lateral - foraminal

8.3 Etiology

8.3.1 Congenital Stenosis

Congenital stenosis of the spinal canal is more frequent in the lumbar region and is idiopathic in most cases (Fig. 8.3). Genetic factors are important, because they control the different dimensions of the spinal canal between different races and different populations of the same race (Jeffrey et al. 2003).

According to some recent studies, also prenatal factors influence the growth of the spinal canal.

8.3.1.1 Prenatal Factors

Among prenatal factors, including intrauterine fetal growth retardation, standardized birthweight score (SBS), placenta weight, gestation duration, number of previous pregnancies, mother's weight and age,

a

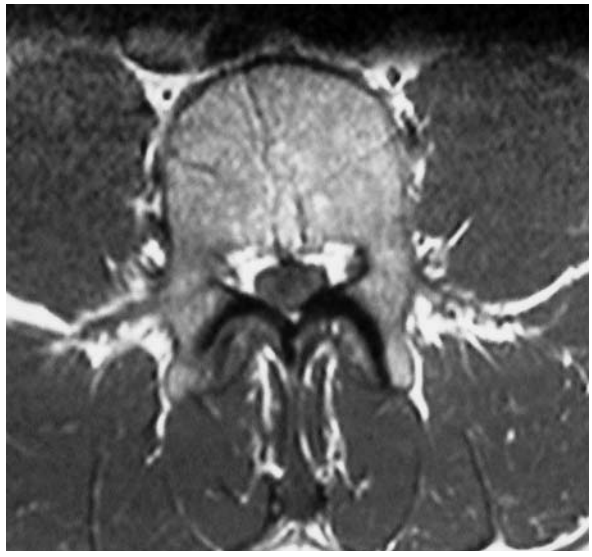

b

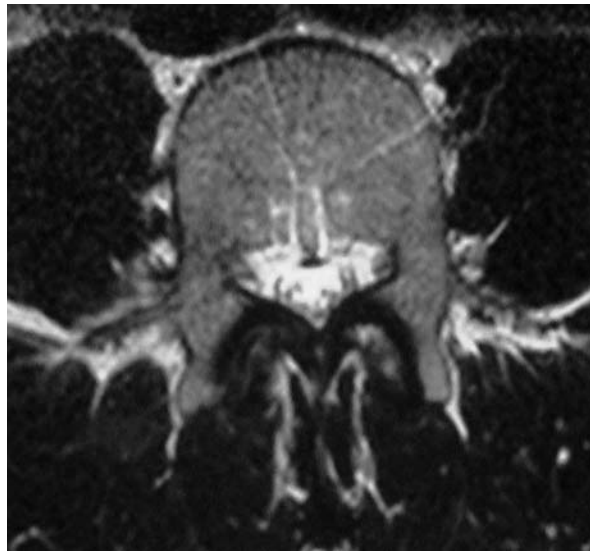

c

Fig. 8.3a–c. The MR appearance of a congenital idiopathic lumbar stenosis due to short pedicles

socio-economic class, mother's smoking habit and the mother's hypertensive, and infective pathology, the SBS, the unborn child's sex and the duration of gestation, seem to be the most significant factors determining the canal's dimensions. The sagittal diameter of the lumbar spinal canal in particular is determined by prenatal factors because it has its maximum development between the 12th and 32nd week of intrauterine life and at birth has already reached 70% of its normal grown-up dimensions at the L1-L4 level.

Therefore, if during intrauterine life the normal development of the spinal canal is disturbed, mostly the L1-L4 levels will be affected. After birth, it is less likely that complete growth throughout further development will be reached.

At the L5 level however, the spinal canal only reaches 50% of its final size at birth and continues to grow until 5 years of age. It has been shown that children with equal or, on average, lower SBS have smaller canal diameters from L1 to L5 than children with, on average, higher SBS. The same is true for children with low placenta weight or those who belong to lower socio-economic classes or whose mothers are smokers (in the latter situation, especially at the L3-L5 level).

Vertebrae will continue to grow proportionally to the height during the whole childhood (Jeffrey et al. 2003).

8.3.1.2 Anomalies in Vertebral Development

Generally, congenital stenosis is caused by an anomaly in the vertebral arch. These malformations can lead to an abnormal orientation of the facet joints, hypoplasia of the laminae or pedicles with possible central, lateral, or foraminal stenosis, and obliteration of the epidural fat, defensive barrier of the dural sac (Osborn 1994).

Atlantal stenosis is rare and up to now has been noted only in the pediatric age group. It can be associated with achondroplasia or anomalies in the vertebral arch (Liliang et al. 2002).

8.3.1.3 Spondylolisthesis

Congenital spondylolisthesis mostly affects the lumbar spine and in 95% of cases the fifth lumbar metamer. This is because the intervertebral disc L5-S1 is more vertically oriented and, does not succeed in cushioning the load pressure of the vertebral column. Therefore, the load rests on the anterior third of the vertebral body. Considering this, the facet joints are the point of least resistance and eventually the vertebra divides itself into anterosuperior (body, pedicles, upper facet joints, transverse processes) and posteroinferior parts (lower facet joints, laminae, spinous processes) which align with the posterior elements of the vertebra below.

Kornblum and co-workers distinguished spondylolisthesis associated with a bilateral lysis of the pars interarticularis (Kornblum et al. 2004), congenital spondylolisthesis (for anomalous orientation of the interapophyseal joints), dysplastic spondylolisthesis (secondary to hypoplasia or agenesis of the articular apophysis in S1 and posterior arch in L5), and secondary spondylolisthesis (degenerative, post-traumatic, iatrogenic, associated with bone alterations as in Paget's disease or neoplasms) (Osborn 1994). An anterior slipping of a vertebral body on the one below causes an increased anteroposterior diameter of the spinal canal, but narrows the neural foramen because of a downward and forward slipping of the upper isthmic segment (Osborn 1994). The neural foramen appears bilobate and the periradicular fat is not clearly visible (Fig. 8.4). At this level the disc height seems reduced and degenerated with a posterior pseudobulging. This is the result of stretching of Sharpey's fibers secondary to misalignment of the vertebral bodies with consecutive and consequent distortion of the annulus fibrous.

In retrolisthesis, which is more rare, the longitudinal diameter of the neural foramen is reduced.

8.3.1.4 Metabolic Disorders

Spinal stenosis is seen in metabolic disorders and severe skeletal dysplasias. Mucopolysaccharidosis represents a group of metabolic disorders with a deficit of lysosomal enzymes leading to an intracellular accumulation of partially degraded glycosaminoglycans (GAG) and ubiquitous elements of the connective tissue.

In mucopolysaccharidosis type VI (Maroteaux-Lamy syndrome), a pronounced skeletal dysplasia and severe growth retardation are associated with facial dysmorphism, obstruction of the upper airways, cardiomyopathy, and organomegaly. Spinal cord compression in mucopolysaccharidosis type

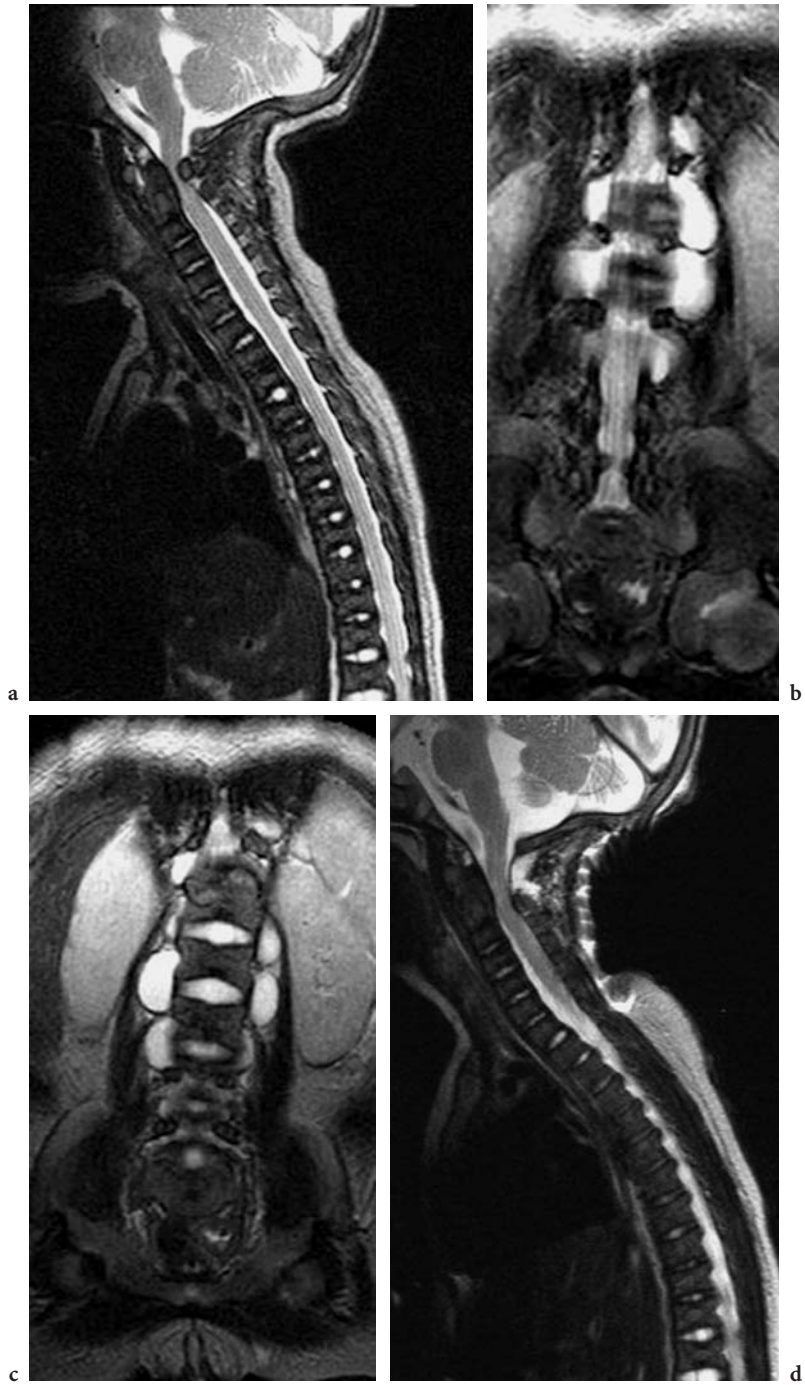

Fig. 8.4a–d. Spinal MR in a 5-month-old baby affected by achondroplasia shows high degree of stenosis at atlanto-axial level (**a**). The cord is impinged and several periradicular dural ectasias are evident (**b,c**) at thoracic and lumbar levels, probably secondary to altered cerebrospinal fluid dynamics caused by the stenosis. **d** Postoperative control after surgical decompression

VI can be caused by atlanto-axial subluxation associated with spinal stenosis but more commonly from a thickened posterior longitudinal ligament (PLL). Dural thickening as a result of GAG deposition is observed, as well as occipito-cervical instability. Kyphosis secondary to retrolisthesis can be noticed at the thoracolumbar junction.

Dysplasia of the odontoid process with hypertrophied posterior longitudinal ligaments may be observed in patients suffering from mucopolysaccharidosis type IV (Morquio syndrome). Occipito-cervical instability is more significant and kyphosis more frequent than in patients suffering from mucopolysaccharidosis type VI (Thorne et al. 2001).

8.3.1.5 Skeletal Dysplasias

Skeletal dysplasias often involve the spinal canal (Naique and Laheri 2001; Mukamel et al. 2003; Eash et al. 2003; Thomeer and van Dijk 2002).

In **achondroplasia** lumbar stenosis seems to result from a difference between spinal anatomic dimensions and its neural contents (Fig. 8.4). Short pedicles, combined with hypertrophied interapophyseal joints and thickened laminae, caused a reduced spinal canal in all its dimensions. The vertebral disproportion is caused by a premature fusion of the vertebral body's chondrification centers with those of the vertebral arch, during the embryo's development. This results in a reduced bony spinal diameter in comparison with the normally developed neural structures. The upper lumbar region is most frequently involved. It may be associated with multilevel compression of the dural sac, and redundant nerve roots of the cauda equina (Thomeer and van Dijk 2002).

Craniodiaphyseal dysplasia, or Gorlin's syndrome, is a rare bone disorder characterized by a significant systematized spinal sclerosis, generalized hyperostosis and progressive craniofacial deformity. The pathogenesis of the spinal stenosis, a delayed complication, seems to be correlated to an inexorable hyperostosis and insufficient enlargement and remodeling, resulting in a concentric spinal stenosis predominantly of the cervical canal at the C2-C6 level. The sclerotic process does not involve the soft tissues, as demonstrated by the absence of ossified yellow ligaments (Naique and Laheri 2001).

Brachyolmia is a rare bone dysplasia characterized by short stature and generalized platyspondyly. Various types have been described according to their relevant clinical and radiological characteristics. Spinal stenosis is a common complication of Hobaek-type brachyolmia, which shows a platyspondyly of cervical, thoracic, and lumbar metamers. It is more obvious at the thoracic level, where the metamers are rectangular, anteriorly rounded, and have irregular somatic limits and narrow intervertebral spaces. Multiple disc bulgings can co-exist and produce minimal pressure on the dural sac.

In the **Maroteaux syndrome**, the vertebral bodies possess an anterior and posterior roundish aspect (Mukamel et al. 2003).

Chondrodysplasia punctata (CDP) indicates a heterogenic group of dysplasias associated with spinal stenosis with atlanto-axial instability and cervical kyphosis, resulting from an abnormal ossification of the vertebral bodies (Eash et al. 2003).

8.3.2 Acquired Stenosis

Acquired stenosis is the most frequent form of spinal stenosis at the lumbar and cervical level. It is less frequent at the thoracic level.

8.3.2.1 Degenerative Pathology

Degeneration of the vertebral bodies and interapophyseal joints can be associated with degenerative changes of the ligamentous system (thickening, calcification) and herniated discs.

There is no sexual predominance, except for spondylolisthesis, which is more frequent in women (M:F ratio 1:4) (Tan 2003).

Posterior and central marginal osteophytosis may reduce the spinal canal diameter at the central level, with cord compression and in case of multilevel disease a dural sac similar to a "string of pearls" (Fig. 8.5). It may also cause lateral radicular compression with a so-called upper facet syndrome, radicular entrapment in the spinal lateral recess, which is more frequent at the lumbar level (Fig. 8.6), generated by a bony protrusion at the base of the facet joint. The herniated disc can be associated with radicular entrapment (Kanamiya et al. 2002). Osteophytes, which reach the neural foramen, can obstruct the foramen at its lower portion, without touching the nerve root. When associated with a foraminal disc herniation, it may cause total obliteration of the neural foramen and radicular compression against the vertebral pedicle (Osborn 1994).

The compressed nerve root sometimes appears edematous, due to venous congestion and alterations in the blood-nerve barrier. According to recent studies, nerve root compression may induce an inflammatory reaction by proteoglycans released by the involved disc. Other theories suppose an autoimmune response, others an increased lactic acid with consequently a reduced pH around the nerve root, while other theories state that inflammatory phenomena are caused by the enzymatic activity of A2 phospholipase released by the herniated disc (Orendacova et al. 2001).

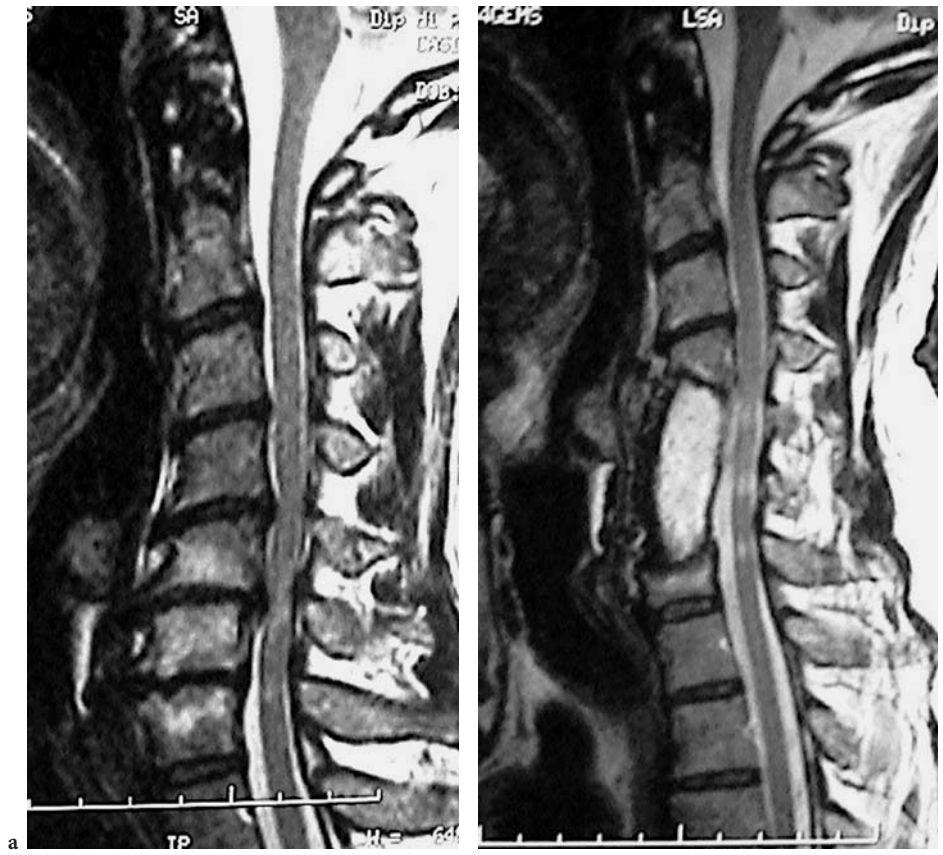

a b

Fig. 8.5a,b. a Spondylotic acquired stenosis with spondylotic myelopathy, as demonstrated by the high signal of the spinal cord. **b** Early postoperative control. Altered signal in the spinal cord is still present, confirming post-stenotic damage

Posterior and central marginal osteophytosis, with or without a herniated disc can lead to the development of a cauda equina syndrome (CES). Compression of the dural sac leads to a reduced space necessary for the nerve roots of the cauda equina, averaging 77±13 mm^2 at the L3 level. This is the critical value, below which the subarachnoid fluid pressure tends to increase among the cauda equina nerve roots (e.g., a reduced space of 63±13 mm^2 leads to an increased pressure of 50 mmHg among the nerve roots). When the intrathecal pressure of the subarachnoid fluid increases, there is an alteration in the venous drainage causing perineural venous congestion, and consequently ischemic damage. Because of its vascular anatomy, the nerve roots of the cauda equina have a higher ischemic risk if compression is at more than one level. Predominantly the motor roots of L4, L5, and S1 are affected because of their anterolateral position in the dural sac at the L2-S1 level (Kanamiya et al. 2002). In contrast-enhanced MR imaging, the roots show contrast enhancement due to breakdown of the blood-nerve barrier, inflammatory reaction, and venous congestion.

Degenerative changes of the facet joints may cause stenosis of the central spinal canal and lateral and foraminal recesses. The articular masses are hypertrophic and dysmorphic with widened articular spaces filled with fluid and/or gas. This is seen more frequently at the lumbar level and is generally associated with disc degeneration.

At the lumbar level, in 75% of cases degenerative facet joins are associated with uni- or bilateral synovial cysts, most commonly extradural with liquid and/or myxoid contents (Epstein 2004; Jeong and Bendo). In 50% of the cases they are seen at the L4-L5 level. They are located posterior or posterolateral to the dural sac in direct communication with the facet joint and also associated with degenerative spondylolisthesis. Sometimes bony erosion

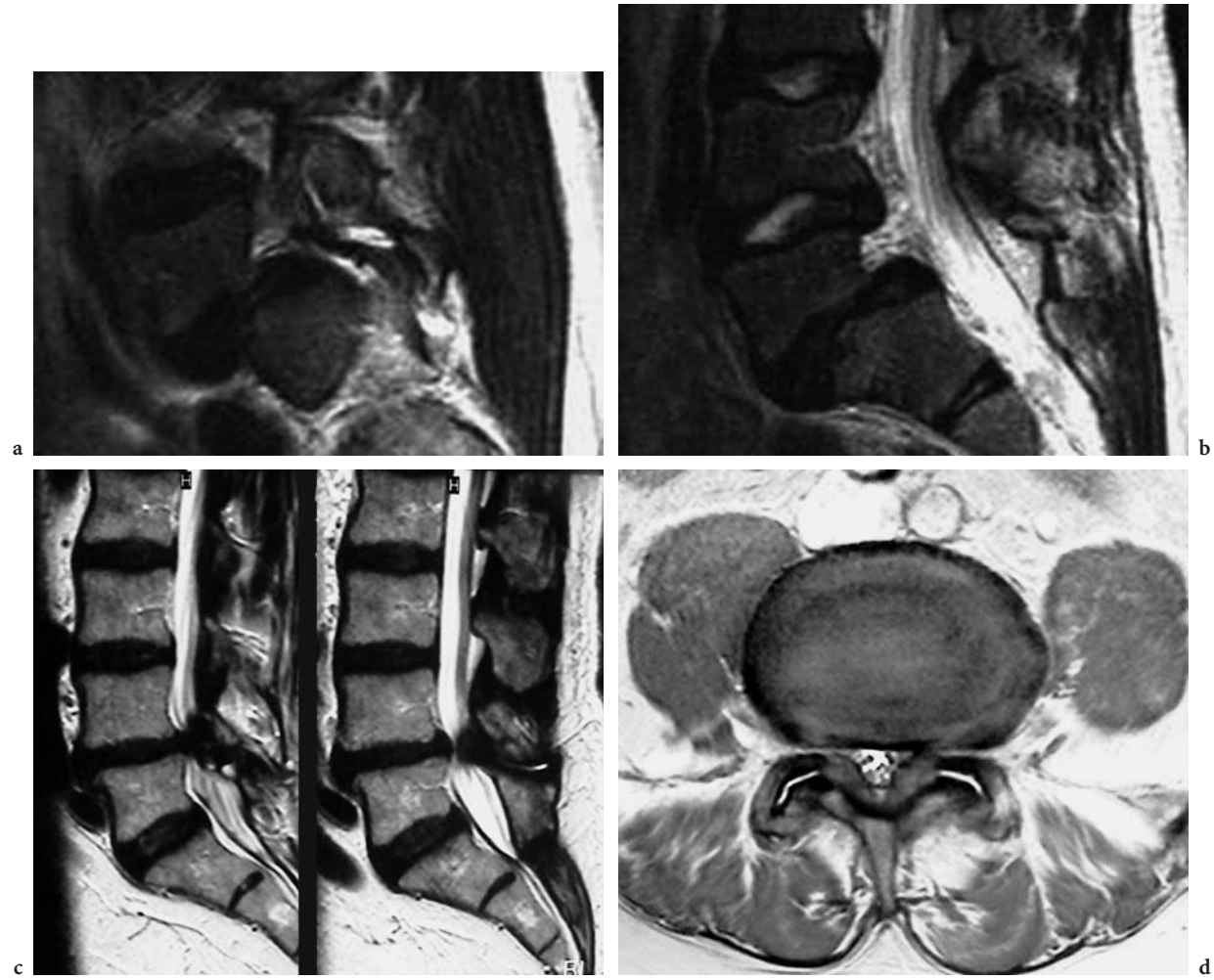

Fig. 8.6a–d. Two cases of lateral and concentric stenosis. In the first one (**a,b**) lateral stenosis is evident, as a result of anterolisthesis and bilateral isthmic lysis. **a** T2-weighted sagittal image showing the "8"-shaped narrow foramen with root compression. High signal within the isthmus represents lytic changes. **b** Mid-sagittal T2-weighted image shows anterolisthesis and disc pseudo-bulging. **c,d** A case of concentric stenosis due to yellow ligament thickening and cysts, disc bulging, and minor intervertebral instability, as demonstrated by widening of the facet joints with intra-articular fluid (**d**). **c** Interspinous changes, characterized by high signal on T2-WI with fluid inside, representing interspinous neoarthrosis (Baastrup's disease)

is noted (Osborn 1994). At the level of the synovial cyst, segmental instability may be observed. Its characteristic location allows it to be distinguished from herniated discs and perineural cysts. In contrast-enhanced MR imaging, facet joint cysts may show peripheral enhancement.

The most frequently degenerated ligaments, are the yellow ligaments and the posterior longitudinal ligament (PLL).

The PLL can be affected by hypertrophy, calcification, and ossification predominantly at the cervical and thoracic level. It may be associated with a herniated disc, causing a central and lateral stenosis with loss of epidural adipose tissue (Matsumoto et al. 2001; Matsunaga et al. 2004).

Calcified or ossified yellow ligaments are rare. Ossified yellow ligaments are usually localized at the lower half of the thoracic spine whereas calcified yellow ligaments are more frequent in elderly women at the cervical level. At this level the association with a herniated disc can generate a lateral and intraforaminal acute cervical stenosis with consequent myelopathy and/or radiculopathy (Fig. 8.7). According to some studies, hypertro-

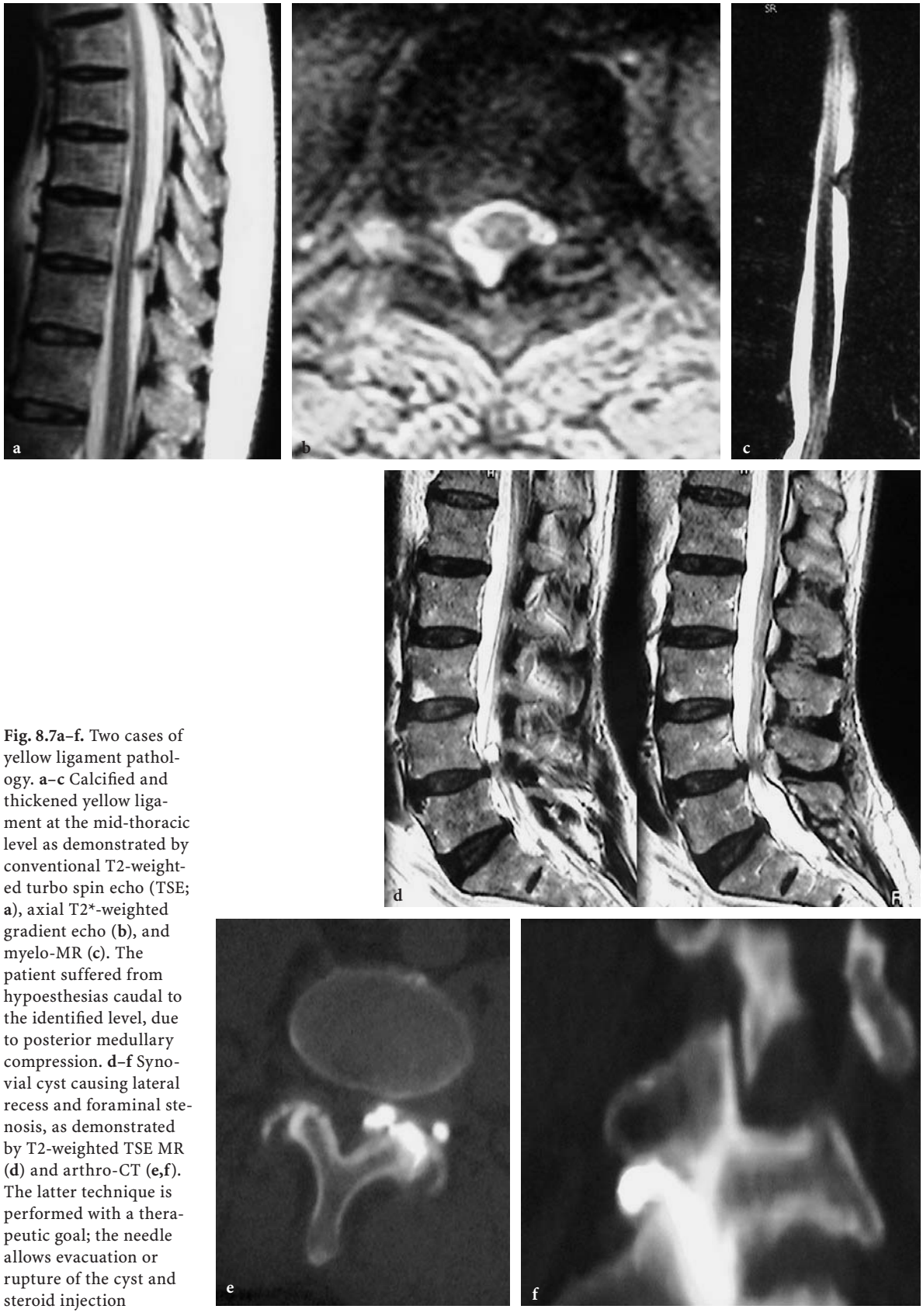

Fig. 8.7a–f. Two cases of yellow ligament pathology. **a–c** Calcified and thickened yellow ligament at the mid-thoracic level as demonstrated by conventional T2-weighted turbo spin echo (TSE; **a**), axial T2*-weighted gradient echo (**b**), and myelo-MR (**c**). The patient suffered from hypoesthesias caudal to the identified level, due to posterior medullary compression. **d–f** Synovial cyst causing lateral recess and foraminal stenosis, as demonstrated by T2-weighted TSE MR (**d**) and arthro-CT (**e,f**). The latter technique is performed with a therapeutic goal; the needle allows evacuation or rupture of the cyst and steroid injection

phied and calcified cervical yellow ligaments are caused by the high mobility of the C3-C7 segment, and sometimes a calcified dura mater has been observed, separated by a cleavage plane from the involved yellow ligament (Fernando Ugarriza et al. 2001).

Degenerative spondylolisthesis, first described by Newman (Newman 1955), most frequently is found at the lumbar and cervical level. In contrast to what happens in isthmic spondylolisthesis, particularly if bilateral, there is a spinal canal stenosis due to arthritic facet joints and hypertrophic yellow ligaments with associated narrowing of the neural foramen and the lateral recess (Fig. 8.8). Obliterated anterior fat tissue, lost periradicular tissue, and compression of the dural sac are observed. If unilateral, the side of the degenerated facet joints is mostly stressed (Osborn 1994).

Fig. 8.8a–d. Degenerative concentric stenosis as demonstrated by axial CT (**a,b**) and sagittal reformatted images (**c,d**). Disc and facet joint degeneration causes degenerative anterolisthesis and lateral canal narrowing. Lateral recess and foraminal canals are stenosis due to cotton-like calcifications of yellow ligaments. Thickening of the ligaments and disc bulging also cause central canal narrowing

Degenerative lumbar spinal stenosis can be associated with a thoracolumbosacral scoliosis. In these cases, lateral and foraminal stenosis occurs more frequently. Some recent studies show that there is no significant difference between radicular compression at the scoliosis' concave or convex side, and that the L3 and L4 root is more frequently compressed at the concave side at the foraminal and extraforaminal level, whereas the L5 and S1 roots are the most compressed ones on the convex side, at the level of the lateral recesses (Liu et al. 2003).

8.3.2.2 Rheumatic Diseases, Crystal Deposition Diseases, Metabolic and Endocrine Diseases, and Osteodystrophy

Rheumatoid arthritis, ankylosing spondylitis, psoriatic arthritis, calcium pyrophosphate dihydrate crystal deposition disease (CPPD), DISH, gout, hyperparathyroidism, and Paget's osteodystrophy may not only cause central, but also lateral, foraminal, and concentric stenosis, predominantly at the cervical level.

In **CPPD** compressive cervical myelopathy has been reported secondary to nodular depositions of crystals in the yellow and atlanto-occipital ligaments without involvement of the intervertebral elements. Facet joints are less frequently involved in CPPD. These depositions can either be individual or multiple (Fujishiro et al. 2002). In the differential diagnosis bacterial and fungal infections should be included. In the latter case, posterior vertebral elements are rarely affected, whereas the intervertebral disc is frequently involved (Fig. 8.9) (Ha and Kim).

Posterior longitudinal ligament ossification may be associated with DISH. DISH is found in 14-30% of Paget's osteodystrophy cases. Paget's tissue may invade the hyperostosis of DISH and transform it into Paget's exostosis (Hadjipavlou et al. 2002).

Moreover, **Paget's** osteodystrophy seems to be associated with an increased incidence of gout and pseudogout. The spine is affected in 15% of patients with Paget's disease. In Paget's disease, the bone tends to expand in all directions with ensuing hypertrophy of facet joints and spinal stenosis (Fig. 8.9). It is mainly seen at the cervical and thoracic spine and is caused by an excessive bone growth associated with an anomalous remodeling due to the lack of balance between the osteoblastic and osteoclastic activity and ossification of epidural fat. The disc may be affected as well. Spinal stenosis in Paget's disease is mainly of the concentric type and can be asymptomatic. This suggests the adaptability of the dural sac and its neural elements with no significant alteration of nervous function. Moreover, it was shown that myelopathy is actually caused by the compression exerted on the arteries by the expanded bone, as well as by vascular alterations such as arterial steal syndrome, which is common in Paget's disease (Hadjipavlou et al. 2002).

The pathological changes of the cervical spine in patients affected by **rheumatoid arthritis** are caused by alterations of the bone structures induced by the synovial pannus (Fig. 8.9). The synovial pannus causes secondary destruction of bone, cartilage, and ligamentous structures, and consequently instability and deformation. In the upper cervical spine, atlanto-axial horizontal transverse instability is caused by insufficiency of the ligaments and destruction of the lateral masses of the atlas with ensuing vertical instability. The odontoid process of the axis can migrate in the skull base, thus reducing the distance between the atlanto-axial joint and the base of the skull. Upward migration may cause compression of the medulla oblongata. At the lower cervical level, kyphosis deformity and anterior mono- or multisegmental vertebral instability are caused by alterations of the disc, destruction of bone, and ligament insufficiency (Grob et al. 1999).

8.3.2.3 Trauma

Traumatic injury of the vertebrae, ligaments, and intervertebral discs may cause compression and stenosis, mainly at the cervical level. This is because of its higher degree of mobility compared with the thoracic and lumbar levels, the position of the vertebral joints, and also because the osteo-disc-ligamentous apparatus and the paravertebral musculature are less developed here and thus offer less resistance to traumas. Another level where stenosis and posttraumatic cord compression is frequently found is T11-L3 , owing to the transition from a thoracic rigid kyphosis to a mobile lumbar lordosis (Osborn 1994).

Nevertheless, both congenital and secondary stenosis is by itself a condition that predisposes to post-traumatic spinal cord injuries at any spinal level. In particular, in hyperextension trauma, 30% of the sagittal diameter of the vertebral canal is com-

Fig. 8.9a–h. Acquired stenosis from different causes. **a–c** Idiopathic calcification and thickening of the posterior longitudinal ligament at thoracic level, as demonstrated by CT (**a**) and MR (**b** and **c**). **d** Computed tomography of the cervical spine in a case of Paget's disease in which the left foramen is narrowed with consequent left cervico-brachial pain. **e,f** T1-weighted (**e**) and T2-weighted (**f**) MR in a typical case of foramen magnum stenosis due to rheumatoid arthritis. The odontoid process is ▷▷

promised by the yellow and the intralaminar ligaments and, by means of an "anchoring mechanism" described by Penning (Penning 1962), the spinal cord is anchored between the lower part of the upper vertebral body and the portion that is closest to the spinolaminar line of the lower metamer (Boockvar et al. 2001).

8.3.2.4 Epidural Lipomatosis

Spinal epidural lipomatosis (SEDL) is mainly seen at the lumbar level. It is caused by hypertrophy of the epidural fatty tissue, with narrowing of the spinal canal. This may occasionally cause progressive

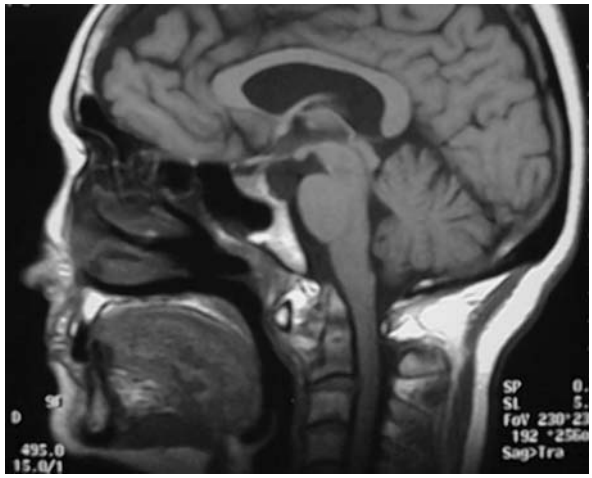

e

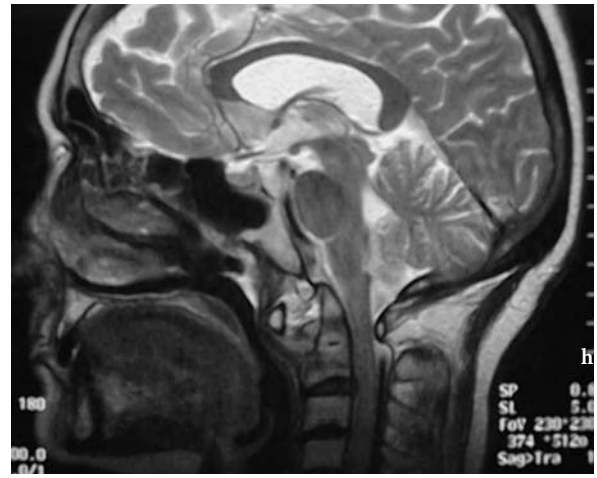

f

g

h

thinner, flattened in its anterior aspect, thickening of the anterior synovial compartment is clearly evident, the atlanto-axial transverse distance is increased, and the central canal is narrowed. **g,h** Sagittal T2-weighted (**g**) and Gd-enhanced T1-weighted (**h**) MR images from a patient affected by sarcoidosis. Peridural enhancing tissue determines reduction of diameters of the vertebral canal

myelopathy, radiculopathy, and/or cauda equina syndrome (Clancey 2004; Christopoulos et al. 1982; Lisai et al. 2001). It is a fairly frequent side effect in patients been taking corticosteroids for a long time, but it has also been observed in patients affected by diseases that cause an excessive production of steroids (Cushing's syndrome), in obese patients, and in those using anabolic steroids. Idiopathic SEDL is uncommon (Fassett and Schmidt 2004).

On MR imaging mild, moderate and severe grading has been proposed to classify lipomatosis, taking into consideration parameters such as the anteroposterior diameter of the dural sac, the an-

teroposterior diameter of the epidural lipomatosis both ventrally and dorsally, and the anteroposterior diameter of the spinal canal, measured at the level of the superior endplate of S1 (Borre et al. 2003).

Both CT and MR imaging show a concentric increase in the epidural fat with a typical polygonal form of the dural sac caused by the meningo-vertebral ligaments (Fig. 8.10). Such ligaments are found on the midline, paramedian, and lateral, both on the front and the back of the epidural space, and secure the external surface of the dura mater to the spinal canal (Geers et al. 2003).

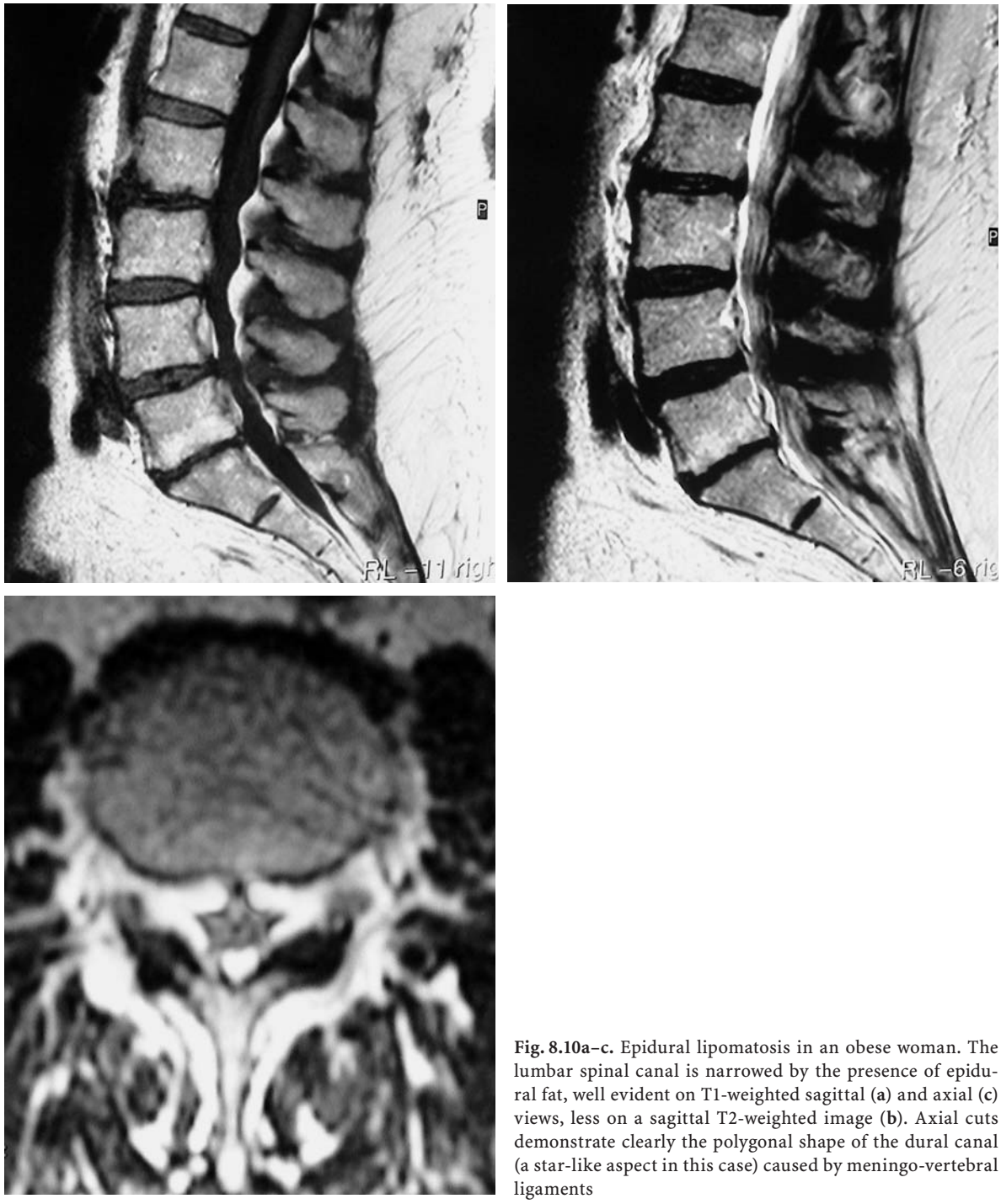

Fig. 8.10a–c. Epidural lipomatosis in an obese woman. The lumbar spinal canal is narrowed by the presence of epidural fat, well evident on T1-weighted sagittal (**a**) and axial (**c**) views, less on a sagittal T2-weighted image (**b**). Axial cuts demonstrate clearly the polygonal shape of the dural canal (a star-like aspect in this case) caused by meningo-vertebral ligaments

8.4 Clinical Picture

The clinical picture of spinal stenosis varies greatly with the level of stenosis. Patients often may remain asymptomatic for a long time, until an acute event. Symptoms may misleading and therefore the diagnosis is often not straightforward (Coulier et al. 2003). The clinical course of the disease can be influenced by age, sex, socio-economic situation, site, and degree of stenosis (Benoist 2002).

Acute and/or chronic limb pain (not relieved when the patient is supine), and paresthesias are typical signs of lateral and foraminal radicular entrapment syndrome (Benoist 2002). Pain, sensory deficits (generally paresthesia) and motor deficits of the upper limbs can have an aspecific irradiation not only seen in nerve root compression but also in other pathologies (degenerative shoulder arthropathy, ulnar nerve syndrome, carpal tunnel syndrome).

Sensory and motor deficits associated with lower limb pain during walking and in upright position are pathognomonic of lumbar canal stenosis (neurogenic claudication). With regard to claudication, vascular problems should be ruled out, even though they may coexist, and also the presence of degenerative hip and/or knee disease should be excluded. In general, walking, the sitting position, intensify the symptoms. On the other hand, forward-bending and supine position relieves the symptoms. This can be explained by the increase in size of the spinal canal in bending and a reduction during extension and under load.

In patients with lumbar stenosis, a neurogenic bladder can be observed due to direct mechanic direct compreaaion of the S2-S4 nerve roots which are located in the posteromedian area of the spinal canal (Inui et al. 2004). The combination of a disc herniation and spinal stenosis more frequently causes symptoms at the lower urinary tract.

Urodynamic testing will help to make a distinction between an urological disorder caused by spinal stenosis and one that is related to diseases of the urinary tract (obstructive injury including prostatic hypertrophy, urethral stenosis and spasms of cervix vesicae).

Spinal stenosis and diabetic neuropathy may present with the same symptoms. Flexion of the lumbar spine increase with the diameters of the central spinal canal and the lateral recesses, and may induce or eliminate the symptoms related to spinal stenosis. The presence of neurological symptoms at the lower limbs during night, when the position of the lumbosacral spine is changed, suggests a spinal etiology.

Diabetic neuropathy is a clinical diagnosis. It is characterized by hypoesthesia at the level of the foot, with or without neurological symptoms. However, it has been observed that the frequency of spinal stenosis is higher in patients affected by diabetic neuropathy than in healthy subjects.

The clinical presentation of the cauda equina syndrome (CES) may differ from patient to patient. In a fully developed cauda equina syndrome, multiple signs of sensory disorders may appear. These disorders include low-back pain, saddle anesthesia, bilateral sciatica, then motor weakness of the lower extremities or chronic paraplegia, impotence and bladder dysfunction. Compression of the epiconus and conus medullaris determines these symptoms, but their onset is often asymmetrical (Orendacova et al. 2001).

The involvement of sphincters is central; therefore, in general, a bladder disorder of the "reflex neurogenic bladder type" appears and is characterized by small bladder and automatic urinary reflex. On the contrary, the involvement of the bladder in cauda compressions is peripheral, with an atonic, globular bladder that passively fills up with urine.

The involvement of L5 and S1 roots can lead to calf hypertrophy by denervation (Swartz et al. 2002). Other factors that lead to an increase in the muscle size include muscular dystrophy, maltase deficiency, hypothyroidism, inflammatory myopathies, tendon rupture, muscular infiltration in case of neoplasm, amyloidosis (Niwa 2001; Bellotti et al. 2001), sarcoidosis, and parasitic diseases.

If stenosis and myelopathy worsen, they can lead to paraparesis and tetraparesis. The degree of the injury may lead to the following:

- In case of atlantal stenosis, hypotension and respiratory disorders may appear (Liliang et al. 2000)
- Spastic tetraparesis if the level is above C5
- Spastic paraparesis with flaccid paresis of upper limbs if the injury is located between C5 and C7
- Paraparesis with regular tone of upper limbs if the lesion is located between C7 and L3
- Flaccid paraparesis, if the injury is caudal to L3

8.5 Imaging

Plain film is the primary imaging technique used to study spinal stenosis. Standard anteroposterior (AP) and left lateral (LL) projections allow the assessment of possible degenerative pathology.

With the LL projections in flexion-extension, it is possible to assess the presence of instability, and with AP dynamic projections, lateral vertebral slipping.

The LL projection of the cervical spine is also used to measure the sagittal diameter of the vertebral canal. The sagittal diameter is measured from the middle of the posterior wall of the vertebral body to the spinolaminar line.

In order to avoid significant variation in this measurement, the Torg ratio has recently been used in the cervical spine (Fig. 8.11). This produces greater uniformity in the values of the sagittal diameter. The Torg ratio is the ratio between the sagittal diameter of the spinal canal and that of the vertebral body measured by plain film in the LL projection. This ratio proved reliable in assessing cervical canal stenosis. A ratio >1 indicates a normal diameter; a ratio <0.82 indicates absolute stenosis (Prasad et al. 2003).

Nevertheless, even though cervical canal stenosis affects mainly the sagittal diameter, the lateral diameter and area of the spinal canal can also be important.

False positives can be found in athletes, who have bigger vertebral bodies (Tierney et al. 2002). Furthermore, a wide variability of the sagittal diameter values was observed in the normal population.

For these reasons another parameter, the space available for the cord (SAC), was taken into consideration. Such a parameter is determined in MR imaging by subtracting the sagittal diameter of the spinal cord from the sagittal diameter of the spinal canal, measured with the patient's head is in neutral position, i.e. with the orbitomeatal line perpendicular to the horizontal plane (Tierney et al. 2002). It was observed that the SAC is smaller at C3 and C5, due to an increase in size of the spinal cord at those levels (cervical enlargement).

Measuring the SAC seems to be more accurate than using the Torg ratio, since the former does not depend on the size of the vertebral body.

In general, on plain film the sagittal diameter of the cervical spinal canal is constant from C4 to C7 (range 15-25 mm, average 17 mm) and below 14 mm it is considered critical. The diameter of the vertebral body gradually enlarges from C4 to C7.

Fig. 8.11a,b. Normal left lateral cervical radiograph with Torg ratio measures. Torg ratio is the ratio between the sagittal diameter of the spinal canal (blue line) and that of the vertebral body (red line). The sagittal diameter is measured from half the height of the posterior wall of the vertebral body, taken from the upper to the lower endplates (*black lines*), up to the spinolaminar line

The spinal cord sagittal diameter is, on average, 6.9 mm at the cervical levels (Prasad et al. 2003).

MR imaging also allows assessment of the transverse diameter of the spinal canal. This measurement is highly variable from person to person and is not correlated with central stenosis or lateral recess stenosis at the foraminal level (Speciale

et al. 2002). The sagittal diameter is less reliable, because on MR imaging it can be difficult to distinguish the cortical bone on the one hand and the PLL and dura mater on the other hand, since all have low signal.

In this regard, it can be more useful to assess the perimedullary CSF-space compared to the sagittal diameter of the spinal cord. If an approximate assessment is made, it can be easily seen if the CSF-fluid space is preserved. If no perimedullary CSF is visible, stenosis is present.

CT scans have also been used to assess the spinal canal size. These measures are not generally accepted, because these ligamentous structures can be assessed only when they show signs of calcification and/or ossification.

Whereas these are the most common, non-invasive techniques in the assessment of stenosis, myelography and CT myelography are still, but rarely, performed.

When comparing myelography, CT myelography, and MR imaging, a discrepancy is observed with regard to the measurement of the degree of stenosis, both in symptomatic and healthy patients. This can be explained by the patient's position during the scan: in supine position for MR imaging and CT myelography, and in prone position for myelography (Fig. 8.12) (Blease Graham 2001). Using dynamic MR imaging in cervical flexion-extension and relying on the assessment of the sagittal diameter, it was possible to prove that cervical stenosis and cord compression increases in extension. Further changes were observed when the size of the sagittal diameter was acquired by CT myelography at the level of the pedicles and intervertebral discs.

Results showed that cervical spinal canal stenosis worsens in prone position with the sagittal diameter measured at the level of the pedicles, and in supine position in extension.

Myelography has played a pivotal role, especially at the lumbar level, in the assessment of the degree of stenosis, because it relies on the measurement of the anteroposterior diameter of the dural sac. A classification of stenosis was derived from this: severe stenosis (<10 mm), moderate stenosis (between 10 and 12 mm) and mild stenosis (between 12 and 14 mm) (Benoist 2002). In MR imaging severe stenosis is associated with an almost total absence of epidural fat.

At the lumbar level MR imaging in the supine position risks to underestimate stenosis. In fact, it was observed that myelography in prone position shows an increase in the deformity of the dural sac (Fig. 8.12; Blease Graham 2001).

Nevertheless, the size, causes, and level of stenosis relative to a supine or prone patient are assessed without considering the forces that act on the spine in orthostatism, i.e., under loading. In fact, mild or moderate stenosis found in a supine or prone patient may become severe under load (Fig. 8.2).

From this viewpoint, an AP or LL plain film in standing position allows to assess stenosis, especially if it is performed in flexion-extension (e.g., instability, synostosis) and completed with oblique projections (for instance a reduction in size of the neural foramens in the presence of osteophytes).

Axial loaded MR imaging (Gallucci et al. 2005) may show instability in degenerative pathology, and sometimes associated with an increase in spinal stenosis (Fig. 8.1). MR imaging can assess the presence of redundant nerve roots and signal alterations at the level of stenosis, by slowed and disorderly cerebrospinal fluid flow due to the reduction of the space available for its circulation (Fig. 8.13).

In general, MR imaging will demonstrate the cause of spinal stenosis (hypertrophy of the yellow ligaments, facet degeneration, etc.) and as such can help to direct a surgical treatment.

Magnetic resonance myelography does not generally provide significant and/or more information compared with a traditional MR (Gallucci et al. 2005; Micheli et al. 1999).

Computed tomographic myelography cannot always be performed on a prone patient, owing to the patient's inadequate compliance, because of age and physical condition which do not always allow for the neck to be well positioned.

Furthermore, both in MR and CT imaging performed on a prone patient, artifacts due to respiratory movements should not be underestimated.

Table 8.3 gives an overview of the MR technique that is most frequently used when stenosis is suspected.

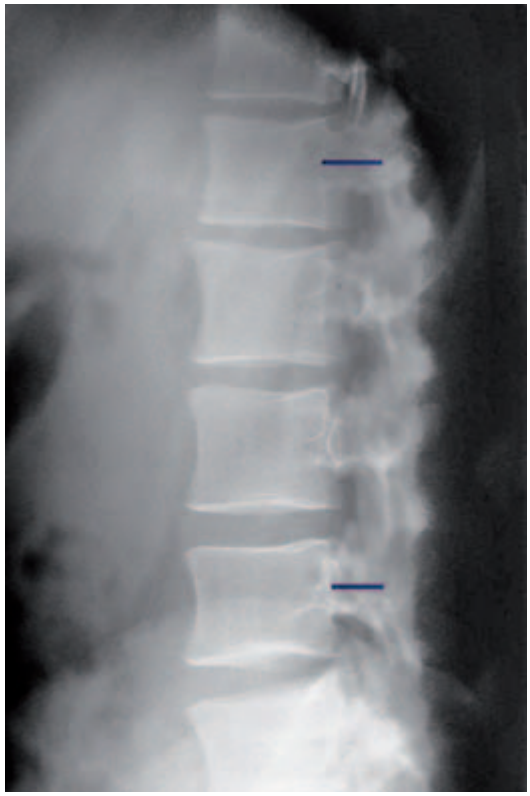

a

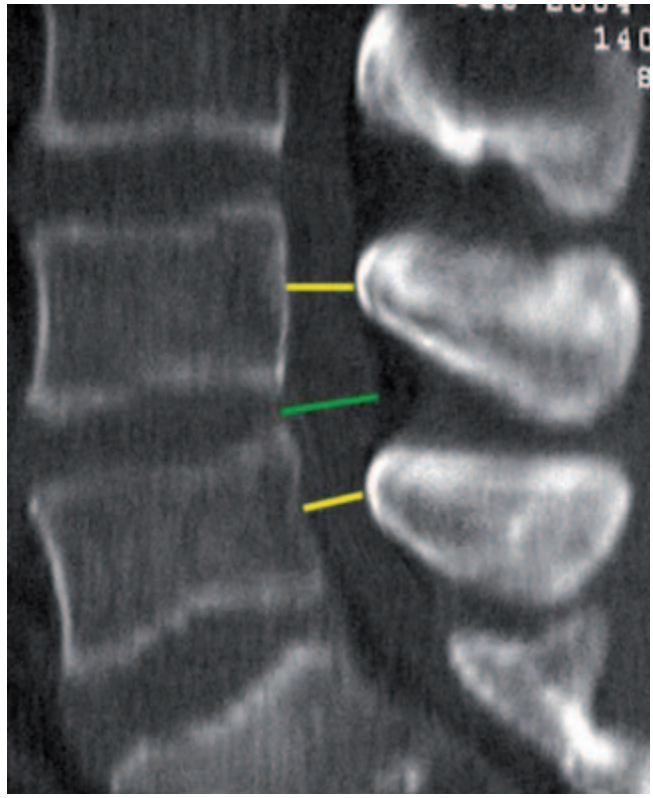

b

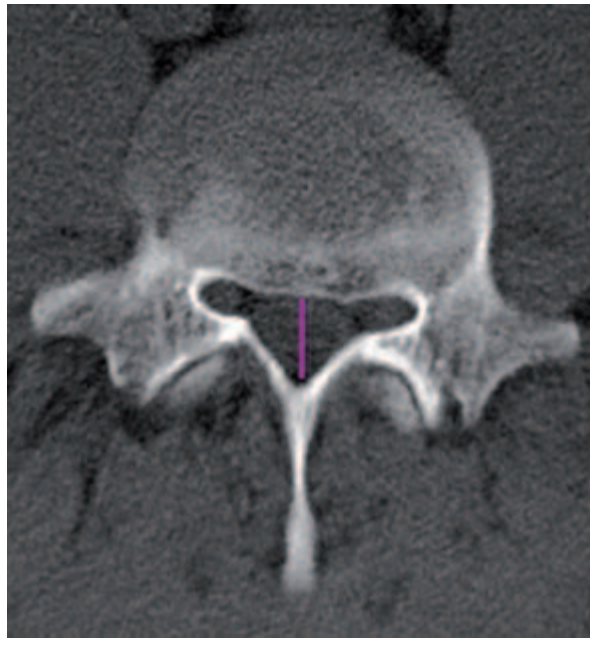

c

Fig. 8.12a–c. Left lateral radiograph (**a**), sagittal mid-reformatted CT (**b**), and axial CT scan in a case of lumbar stenosis. **a** Lateral radiograph of the lumbar spine: the sagittal diameter of the spinal canal is measured from half the height taken from the upper to the lower endplates (*blue lines*) of the posterior wall of the vertebral body up to the spinolaminar line on the same plane. **b** A CT mid-sagittal reformatted image. Sagittal diameter of the lumbar spine measured at the level of the pedicle (*yellow lines*) and the disc (*green line*). The SI value is usually larger than *S* in congenital stenosis. **c** Axial CT. Sagittal diameter (*magenta line*) of the lumbar spine is measured from the posterior wall of the vertebral body up to the spinolaminar line on the same plane

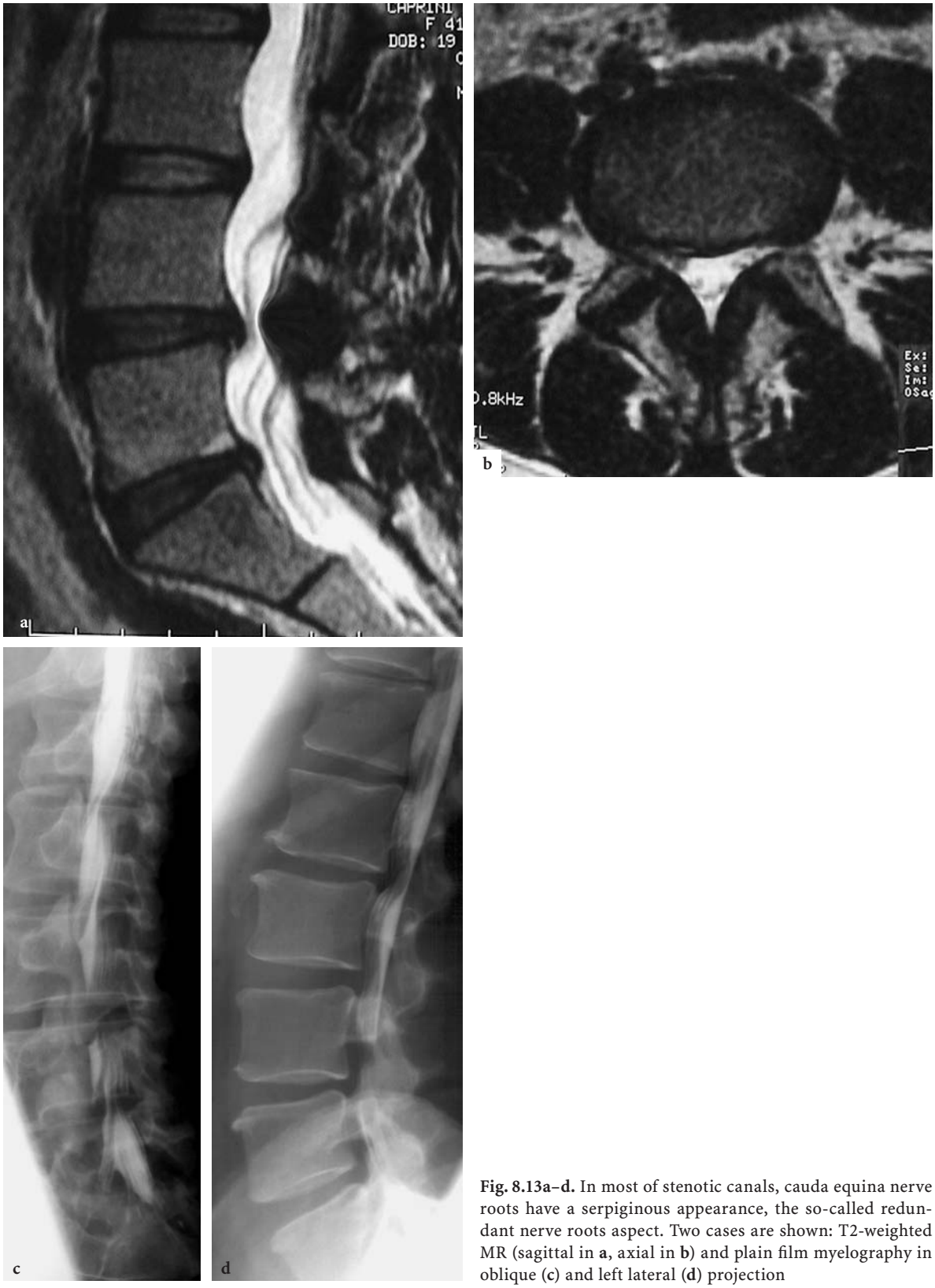

Fig. 8.13a–d. In most of stenotic canals, cauda equina nerve roots have a serpiginous appearance, the so-called redundant nerve roots aspect. Two cases are shown: T2-weighted MR (sagittal in **a**, axial in **b**) and plain film myelography in oblique (**c**) and left lateral (**d**) projection

Table 8.3. MR imaging technique. *SE* spin echo, *TSE* turbo spin echo, *GRE* gradient-recalled echo

Cervical spine			Thoracic spine			Lumbosacral spine		
Scan acquisition plane	Sequence	Thickness	Scan acquisition plane	Sequence	Thickness	Scan acquisition plane	Sequence	Thickness
Sagittal	SE T1 TSE T2 GRE T2	4mm	Sagittal	SE T1 TSE T2 GRE T2	4mm	Sagittal	SE T1 TSE T2 GRE T2	4mm
Axial	GRE T2	3mm	Axial	GRE T2	3mm	Axial	SE or TSE T2	4mm
Coronal	TSE T2	4mm				Coronal	SE or TSE T2	4mm

8.6 Therapy

Conservative treatment in spinal stenosis includes anti-inflammatory non-steroid drugs, pain killers, myorelaxing drugs, injections at the level of facet joints, or epidural steroids (Tan 2003). Alternatively, surgical treatment can be chosen. This choice should be made according to the degree of disability and not according to the degree of stenosis.

At present, there is no scientific evidence that surgery is actually effective in treating spinal stenosis, and surgery is not always necessary considering that conservative treatment can give good results, even for many years. But in cases where conservative therapy fails, the results obtained by surgical treatment are the same as those obtained by patients who had chosen surgical treatment from the very start (Matsunaga et al. 2004). Surgical treatment should be reserved for patients suffering from severe stenosis accompanied by major symptoms, degenerative spondylolisthesis, and for those who tend to worsen with time.

The choice also depends on the patient's comorbidity, cardiovascular, living, and socio-economic conditions.

Contraindications for surgical therapy are old age, comorbidity, instability at various levels, association with scoliosis, and presence of symptoms for a long time (Tan 2003).

At times, following the surgical treatment, symptoms and neurological problems may worsen, due to alteration of the nerve root component vascularization, stretch of the neural elements, or direct trauma (Dezawa et al. 2002).

Therefore, patients affected by myelopathy can choose either surgical or conservative treatment. In patients without myelopathy, conservative therapy should be preferred.

References

Bellotti V, Gallieni M, Giorgetti S, Brancaccio D (2001) Dynamic of beta 2-microglobulin fibril formation and reabsorption: the role of proteolysis. Semin Dial 14:117–122

Benoist M (2002) The natural history of lumbar degenerative spinal stenosis. Joint Bone Spine 69:450–457

Blease Graham III C, Wippold II FJ, Bae KT, Pilgram TK, Shaibani A, Kido DK (2001) Comparison of CT myelography performed in the prone and supine positions in the detection of cervical spinal stenosis. Clin Radiol 56:35–39

Boockvar JA, Durham SR, Sun PP (2001) Cervical spinal stenosis and sports-related cervical cord neurapraxia in children. Spine 26:2709–2713

Borre DG, Borre GE, Aude F, Palmieri GN (2003) Lumbosacral epidural lipomatosis: MRI grading. Eur Radiol 13:1709–1721

Christopoulos S, Minuk J, Assimakopoulos P, Kahn SR (1982) Clinical picture: epidural lipomatosis. Lancet 2001:358 (9297)

Clancey JK (2004) Spinal epidural lipomatosis: a case study. J Neurosci Nurs 36:208–209, 213

Coulier B, Devyver B, Ghosez JP (2003) Severe underestimation of lumbar spinal stenosis by supine imaging. Clin Radiol. 2003 Feb;58(2):167-169

Dezawa A, Unno K, Yamane T, Miki H (2002) Changes in the microhemodynamics of nerve root retraction in patients with lumbar spinal canal stenosis. Spine 27:2844–2849

Eash DD, Weaver DD, Brunetti-Pierri N (2003) Cervical spine stenosis and possible vitamin K deficiency embryopathy in an unusual case of chondrodysplasia punctata and an updated classification system. Am J Med Genet 122A:70–75

Epstein NE (2004) Lumbar laminectomy for the resection of synovial cysts and coexisting lumbar spinal stenosis or degenerative spondylolisthesis. Spine 29:1049–1056

Fassett DR, Schmidt MH (2004) Spinal epidural lipomatosis: a review of its causes and recommendation treatment. Neurosurg Focus 16:E11

Fernando Ugarriza L, Cabezudo JM, Porras LF, Rodrìguez-Sànchez JA (2001) Cord compression secondary to cervical disc herniation associated with calcification of the ligamentum flavum: case report. Neurosurgery 48(3): 673-676

Fujishiro T, Nabeshima YM, Yasui S, Fujita I, Yoshiya S, Fujii

H (2002) Pseudogout attack of the lumbar facet joint: a case report. Spine 27:E396–E398
Gallucci M, Puglielli E, Splendiani A, Pistoia F, Spacca G (2005) Degenerative disorders of the spine. Eur Radiol 15(3):591-598
Geers C, Lecouvet FE, Behets C, Malghem J, Cosnard G, Lengele BG (2003) Polygonal deformation of the dural sac in lumbar epidural lipomatosis explanation by the presence of meningovertebral ligaments. Am J Neuroradiol 24:1276–1282
Goldman SM (2004) Diabetic peripheral neuropathy and spinal stenosis: prevalence of overlap and misdiagnosis. An introduction report. 2004 Diabetes UK. Diabet Med 21:393–399
Grob D, Schutz U, Plotz G (1999) Occipitocervical fusion in patients with rheumatoid arthritis. Clin Orthop Relat Res 366:46–53
Ha K-Y, Kim Y-H (2003) Chronic inflammatory granuloma mimics clinical manifestations of lumbar spinal stenosis after acupuncture: a case report. Spine 28:E217–E220
Hadjipavlou AG, Gaitanis IN, Kontakis GM (2002) Paget's disease of the bone and its management. J Bone Joint Surg 84-B:160-169
Inui Y, Doita M, Ouchi K, Tsukuda M, Fujita N, Kurosaka M (2004) Clinical and radiologic features of lumbar spinal stenosis and disc herniation with neuropathic bladder. Spine 29:869–873
Jeffrey JE, Campbell D, Golden MHN, Smith FW, Porter RW (2003) Antenatal factors in the development of the lumbar vertebral canal. Spine 28:1418–1423
Jeong GK, Bendo JA (2003) Lumbar intervertebral disc cyst as a cause of radiculopathy. Spine J 3:242–246
Kanamiya T, Kida H, Seki M, Aizawa T, Tabata S (2002) Effect of lumbar disc herniation on clinical symptoms in lateral recess syndrome. Clinical orthopaedics and related research 398:131–135
Kornblum MB, Fishgrund JS, Herkowitz HN, Abraham DA, Berkower DL, Ditkoff JS (2004) Degenerative lumbar spondylolisthesis with spinal stenosis. Spine 29:726–734
Liliang P-C, Lui C-C, Cheng M-H, Shih T-Y (2000) Atlantal stenosis: a rare cause of quadriparesis in a child. J Neurosurg 92:211–213
Lisai P, Doria C, Crissantu L, Meloni GB, Conti M, Achene A (2001) Cauda equina sindrome secondary to idiopathic spinal epidural lipomatosis. Spine 26:307–309
Liu H, Ishihara H, Kanamori M, Kawaguchi Y, Ohmori K, Kimura T (2003) Characteristics of nerve root compression caused by degenerative lumbar spinal stenosis with scoliosis. Spine J 3:524–529
Matsumoto T, Yoshida M, Yamada H, Kurimoto K, Tamaki T (2001) Lumbar canal stenosis caused by hypertrophy of the posterior longitudinal ligament. Spine 26:E576–E579
Matsunaga S, Sakou T, Taketomi E, Komiya S (2004) Clinical course of patients with ossification of the posterior longitudinal ligament: a minimum 10-year cohort study. J Neurosurg 100:245–248
Micheli C, Gallucci M, Cardone G, Gagliardo O, Minio Paluello GB, Castrucci M (1999) Magnetic resonance myelography at 0.5 T. Riv Neuroradiol 12:451–461
Mukamel M, Karmazyn B, de Vries L, Horev G, Shohat M (2003) Brachyolmia and spinal stenosis. Am J Med Genet 120A:272–275
Naique S, Laheri VJ (2001) Stenosis of the cervical canal in craniodiaphyseal dysplasia. J Bone Joint Surg 83-B:328-331
Newman (1955) Degenerative Spondylolisthesis. Ann R Coll Surg Engl 16:305-323
Niwa T (2001) Dialysis-related amyloidosis: pathogenesis focusing on AGE modification. Semin Dial 14:123–126
Orendacova J, Cizkova D, Kafka J, Lukacova N, Marsala M, Sulla I, Marsala J, Katsube N (2001) Cauda equina syndrome. Prog Neurobiol 64:613–637
Osborn AG (1994) Diagnostic neuroradiology. Mosby, St. Louis, pp 840–849
Penning L (1962) Some aspects of plain radiography of the cervical spine in chronic myelopathy. Neurology 12:513-519
Prasad SS, O'Malley M, Caplan M, Shackleford IM, Pydisetty RK (2003) MRI measurements of the cervical spine and their correlation to Pavlov's ratio. Spine 28:1263–1268
Speciale AC, Pietrobon R, Urban CW, Richardson WJ, Helms CA, Major N, Enterline D, Hey L, Haglund M, Turner DA (2002) Observer variability in assessing lumbar spinal stenosis severity on magnetic resonance imaging and its relation to cross-sectional spinal canal area. Spine 27:1082–1086
Swartz KR, Fee DB, Trost GR, Waclawik AJ (2002) Unilateral calf hypertrophy seen in lumbosacral stenosis. Spine 27: E406–E409
Tan SB (2003) Spinal canal stenosis. Singapore Med J 168:44
Thomeer RTWM, van Dijk JMC (2002) Surgical treatment of lumbar stenosis in achondroplasia. J Neurosurg 96:292–297
Thorne JA, Javadpour M, Hughes DG, Wraith E, Cowie RA (2001) Craniovertebral abnormalities in type VI mucopolysaccharidosis (Maroteaux-Lamy syndrome). Neurosurgery 48:849-852
Tierney RT, Maldjian C, Mattacola CG, Straub SJ, Sitler MR (2002) Cervical spine stenosis measures in normal subjects. J Athlet Training 37:190–193

Spinal Instability – Axial Loaded Imaging of the Spine

9

Luigi Manfrè, Roberto Cartolari, Guido Trasimeni, and Concetto Cristaudo

CONTENTS

L. Manfrè, MD
Department of Neuroradiology, Hospital Cannizzaro, via Messina 829, 95127 Catania, Italy
Roberto Cartolari, MD
Department of Neuroradiology, Hospital Belcolle, Via R. Capozzi 13, 01100 Viterbo, Italy
Guido Trasimeni, MD
Department of Neuroradiology, Hospital Sant'Andrea, University La Sapienza Rome, Via di Grottarossa 1035, 00189 Rome, Italy
Concetto Cristaudo, MD
Director of Neuroradiology, Department of Neuroradiology, Hospital Cannizzaro, Via Messina 829, 95127 Catania, Italy

9.1 Introduction

In the last 15 years, understanding of spinal instability and diagnostic criteria to establish spinal instability have improved dramatically. This has also lead to improved therapy for spinal instability. Often, spine surgery has changed from simple disc ablation to disc function substitution, using different kinds of spinal devices.

The diagnosis of spinal instability may be hard to establish from a clinical-radiological point of view. Frequently, a radiologically abnormal segmental movement can be incidentally discovered in asymptomatic patients. On the other hand, normal radiological findings are found in patients with spinal instability symptoms.

A keynote element in the diagnosis of "spinal instability" is the loss of functional spine units – FSU (vertebra, ligaments and muscular complex) stability. This may result in reduced elasticity, increased mobility and abnormal motion. According to Panjabi and White (1990), this concept can be extrapolated from the American Academy of Orthopaedic Surgeons, considering spinal instability as "The loss of spine's ability to maintain its pattern of displacement under physiologic loads". Several experimental data have demonstrated the reduced capability of the unstable spine in loading. Where a normal spine can resist up to 12000 N compressive load, an unstable spine only can bear 100 N (Granata and Marras 2000).

Although the first clinical studies on spinal instability were performed more than 50 years ago (American Academy of Orthopaedic Surgeons 1981), it seems that the radiological diagnosis has not seen much progress in recent decades (Nachemson 1991). This apparent gap in modern neuroradiology is related to the fact that functional evaluation of the lumbar spine is a difficult task using conventional CT and MR examinations. Patients are examined in a supine position, whereas the pain in patients with

KEY POINTS

- Keynote element in the diagnosis of "spinal instability" is the loss of functional spine unit (vertebra, ligaments and muscular complex) stability, which may result in reduced elasticity, increased mobility and abnormal motion.
- Functional evaluation of the lumbar spine is a difficult task using conventional CT and MR examinations. Patients are examined in a supine position, whereas the pain in patients with spinal instability is generally elicited in the upright position. Therefore, several devices have been developed in an attempt to reproduce the physiological spinal loading during CT or MR examination.
- A typical functional study of the spine consists of two sets of similar images of the same lumbar spine volume at rest and during axial loading. From the CT dataset, sagittal reformats and surface shading display images are reconstructed. Matching images are organized in two-frame cine-loops (cine-AL studies). Using MRI, T2-weighted images are performed and fast sequences are generally preferred.
- The advantages of AL-MRI are the absence of radiation exposure, larger field-of-view, direct sagittal acquisition and consequently no time-consuming post-processing. The main drawback is the 2D acquisition, usually in the axial and sagittal plane with poor visualization of the 3D dynamics of the posterior arches.
- A lumbar spine can be considered as "normal" when, at rest, vertebrae are well aligned and lumbar lordosis, disc spaces and interspinous spaces are preserved. A slight increase in lordosis, with minimal disc circumferential bulging, leads to a more pronounced posterior wedged shaping of discs, particularly at the L5–S1 level. No significant changes are expected in the interspinous and interarticular relationships. This normal motion pattern is referred to as "complex dynamic modification type 0" (CDM-0).
- Compared to standard imaging, AL scans may demonstrate more and often co-existing abnormalities. These abnormalities can be classified as elementary dynamic modifications (EDMs). These EDMs include changes in: disc morphology, intersomatic relationships, facet joints, flaval ligaments, interspinous spaces, spinous processes mobility, and foraminal shape.
- The most frequently observed modification during AL is the increase in spinal stenosis, already present on pre-load MR studies. Increased spinal stenosis is secondary to increased disk protrusion, thickening of the ligamenta flava, the presence of a synovial cyst, or increased listhesis.
- Associations of EDMs could represent definite motion patterns, that were named complex dynamic modifications (CDMs) types 1–3. Pattern 4 is observed in patients with isthmic lysis.
- Lumbar segmental instabilities usually have etiological or morphological classifications, which do not take into account a possible common mechanism. The use of CDMs (particularly of CDM1) could lead to a more generally accepted classification of chronic segmental instability.
- The conversion from CDM0 to CDM1 identifies L4 as the possible fulcrum of the lumbar spine system and suggests the presence of at least three functional levels and four functional columns in the lumbar spine. As one of the components of the columns fails for any reason, a stereotyped series of actions occur which lead to a cascade series of alterations in a sort of "domino effect".
- The functional fulcrum of the lumbar spine is L4 and L4–L5 disc insufficiency is the most frequent cause of segmental instability. L4–L5 dysfunction has effects particularly on L4–L5 and L5–S1 levels. With the exception of acute episodes (i.e disc herniation with acute nerve root compression) the disease is usually chronic and with time progressive deformation of the spine occurs. Where the transition from CDM0 to CDM1 could even be subacute, the conversion from CDM1 to CDM3 could take many years.
- The diagnostic goals of evaluating an instrumented spine include: evaluation of the stability of the fixed segment(s), analysis of the "internal" stability of the implant, assessment of the stability of the levels adjacent to the spondylodesis, and assessment of the correction of the preoperative instability/deformity.

spinal instability is generally elicited in the upright position.

Although a report on the use of CT during forced axial rotatory stresses has been published (Kirkaldy-Willis and Farfan 1982), it is difficult to superimpose a reproducible physiological functional load on a patient lying in supine position. More accessible diagnostic tools such as dynamic plain film and/or myelography can only evaluate certain spinal components, such as bone, and therefore are of no use for a global evaluation of spinal instability.

Many in vivo (Brickmann 1986; Graf 1992; Ito et al. 1993; Knutsson 1944; Nachemson and Elfstrom 1970; Olsson et al. 1977; Stockes et al. 1981; Wood et al. 1994) and in vitro (Lin 1978; Nachemson 1960; Nachemson et al. 1979; Nowiki et al. 1990; Panjabi et al. 1981; Smith 1991; Yang and King 1984) studies on spinal kinetics have shown that it is impossible for a single diagnostic examination to display all the different components of the FSU. As a consequence, a global view of the different patterns of spine dynamics is difficult to obtain with conventional studies.

9.2 Axial Loaded Imaging

From physiology we know that the spine also has to obey Newton's third law of preservation of momentum (Krag et al. 1987; Smith and Fernie 1991), that is "to every axial vector acting on a FSU corresponds a second vector of equal intensity and of opposite direction, that counterbalances the first one and brings all the structures to a dynamic equilibrium".

Several devices have been developed in an attempt to reproduce physiological spinal loading during CT or MR examination where the patient is examined in a recumbent position. Cartolari et al. (1993) designed a dedicated device known as the "axial loader" (AL) (Mikai Manufacturing srl, Padova, Italy). It is able to develop a variable and reproducible axial load, mimicking the orthostatic load, with the patient in supine position.

An AL is a non-ferromagnetic (MRI compatible), X-ray transparent (CT compatible) cradle with double blocking rests for shoulders and feet, that can be easily placed on the CT or MRI table (Fig. 9.1). The upper block (at the level of the shoulders) is fixed, while the inferior one consists of a wide, flat platform moving longitudinally thanks to a micrometric electromechanical pump, which is controlled by an external workstation. Before CT or MRI is performed, a value corresponding to 65% of the total patient weight is set in the AL computer, mimicking the physiological weight of the head and the trunk at the lumbar level in an orthostatic position. A dynamometer placed between the inferior platform and patient's feet can measure the load applied. This allows a functional study of the spine with CT and MRI which is easy to reproduce.

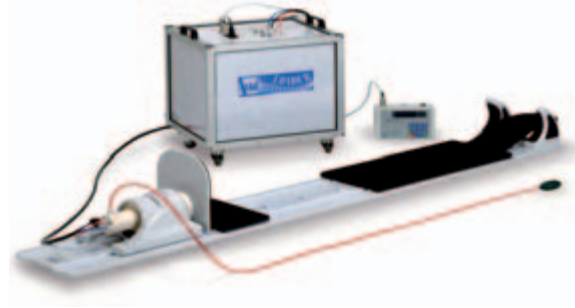

Fig. 9.1. The axial loader

A typical functional study of the spine consists of two sets of similar images of the same lumbar spine volume at rest and during axial loading. From the CT dataset, sagittal two dimensional (2D) reformats and three dimensional (3D) surface shading display (3D-SSD) images are reconstructed. Matching images are organized in two-frame cine-loops; this dynamic linkage mimicking a virtual motion is called cine-AL studies (Cartolari et al. 1996; Cartolari 1997).

Using MRI, T2-weighted images are performed because of their high contrast-to-noise ratio. To minimize artifacts from unintentional movements (the AL maneuver may provoke pain similar to that experienced by the patient in an up-right position), fast sequences are generally preferred.

9.2.1 Normal Motion Pattern

Before describing pathological findings in AL studies, it is necessary to first analyze the normal pattern of lumbar spine motion.

A lumbar spine can be considered as "normal" when, at rest, vertebrae are well aligned and lumbar lordosis, disc spaces and interspinous spaces are preserved (Fig. 9.2a).

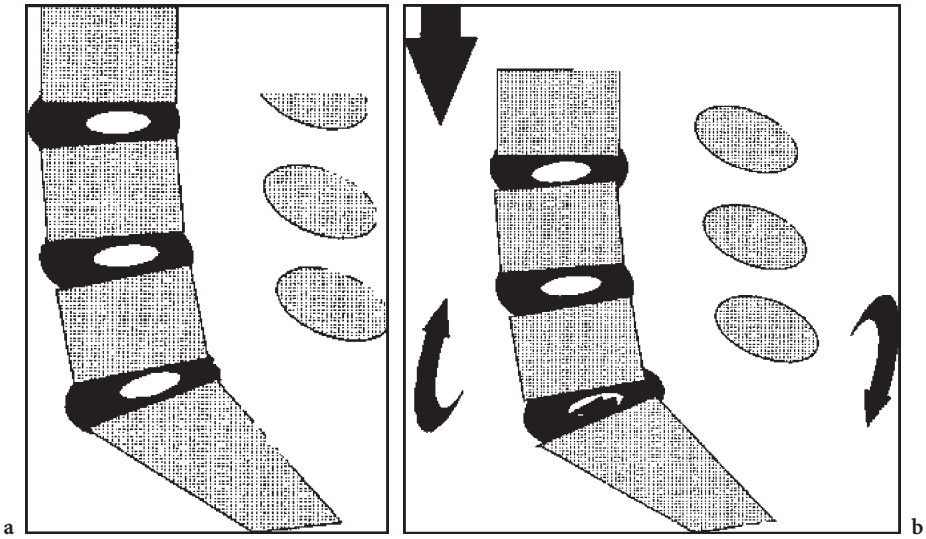

Fig. 9.2a,b. Normal motion pattern during loading. **a** Scheme of the normal discosomatic relationships in the lumbar spine. **b** Discosomatic response of a normal lumbar spine during axial loading (AL) [complex dynamic modification type 0 (CDM0)]

The inferior edge of the inferior facet is always in a more cranial plane with respect to the inferior edge of the superior facet of the lower vertebra.

A standing position is the easiest work for the spine to do; in this situation the normal spine subsides only minimally due to creep and stiffness of the system (Boden and Frymoyer 1997). A slight increase in lordosis, with minimal disc circumferential bulging, leads to a more pronounced posterior wedged shaping of discs, particularly at the L5–S1 level (Fig. 9.2b).

This means that the greatest part of a purely axial load is distributed and dissipated by the disc through the specific functions of the nucleus pulposus and of the annulus fibrosus. In a normal disc, the nucleus pulposus moves anteriorly and the annulus fibrosus mildly protrudes posteriorly. No significant changes are expected in the interspinous and interarticular relationships.

This normal motion pattern will be further referred to as "complex dynamic modification type 0" (CDM-0); any changes from this type will be considered as abnormal.

9.2.2 Axial Loaded Imaging of the Degenerative Spine

Compared to standard imaging, AL scans may demonstrate more and often co-existing abnormalities. These abnormalities can be classified as elementary dynamic modifications (EDMs) and are summarized in Table 9.1.

9.2.2.1 Disc Modifications

The appearance or increase of disc bulging, causing compression on the dural sac or nerve roots (Fig. 9.3) as a finding is generally associated with pain recurrence. It has the same meaning as disc compression on the dural sac during dynamic myelography.

The disappearance (vacuum sign) or appearance of disc vacuum (inverted vacuum sign) (Fig. 9.4) as a finding, always associated with narrowing or disappearance of the corresponding disc space (i.e. hypermobility), suggests that gas like nitrogen, as a sign of heavy disc degeneration (Burgener and Kormano 1987), is produced by an aspiration mechanism, due to the loss of axial load, in resting positions. It is usually associated with underslipping of facet joints and narrowing of the corresponding interspinous space (see below) at pre-load study, and with longitudinal hypermobility of facet joints during AL studies. In some cases, the axial loading can produce an increase in disc space due to complex alterations of normal spine mechanics, with the appearance of the vacuum phenomenon during axial loading (inverted vacuum sign). This finding seems to correspond to the appearance of vacuum phenomenon during extension in dynamic plain films.

Table 9.1. Elementary dynamic modifications observed on axial loaded imaging

Disc modifications	• Volumetric increase or appearance of disc protrusions and herniations (Figs. 9.3 and 9.4) • Disappearance of vacuum phenomenon (vacuum sign) (Fig. 9.4) • Appearance of vacuum phenomenon (inverted vacuum sign)
Intersomatic relationships	• Appearance or increment to various degrees of listhesis (and widening of the coexisting lysis when present), degenerative or associated to isthmic lysis (Fig. 9.4) • Narrowing or disappearance of one or more disc spaces (Fig. 9.4) • Widening of L5-S1 disc spaces (paradoxical motion) (Fig. 9.5) • Rotational movements on "Z" axis (Fig. 9.6) • Posterior translation of vertebral body
Facet joints	• Appearance or increasing of facets longitudinal underslipping and facets hypermobility (Fig. 9.5) • Disappearance of intra-articular vacuum (Fig. 9.4) • Upperslipping (paradoxical motion) of L5 facets (Figs. 9.5 and 9.7)
Foraminal narrowing	
Thickening of the ligamenta flava	
Narrowing of the interspinous spaces and hypermobility of the spinous processes	

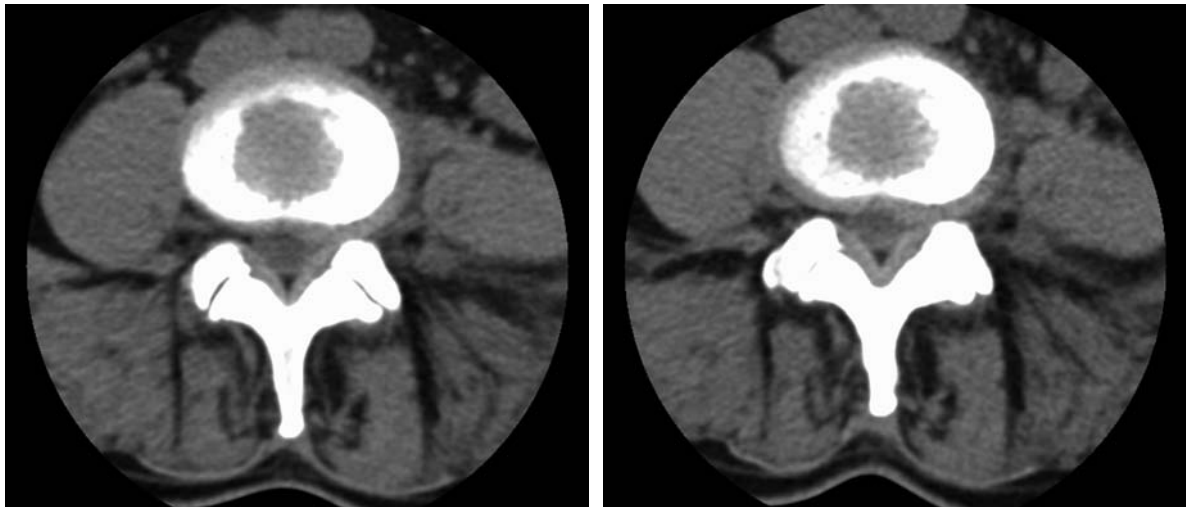

a b

Fig. 9.3a,b. Disc bulging supine-unloaded and during loading. **a** Bulging disc on supine-unloaded CT. **b** During AL one can appreciate increased disc bulging (in particular posterolateral on the left and intraforaminal) and thickening of the yellow ligaments. Together these cause a central spinal stenosis

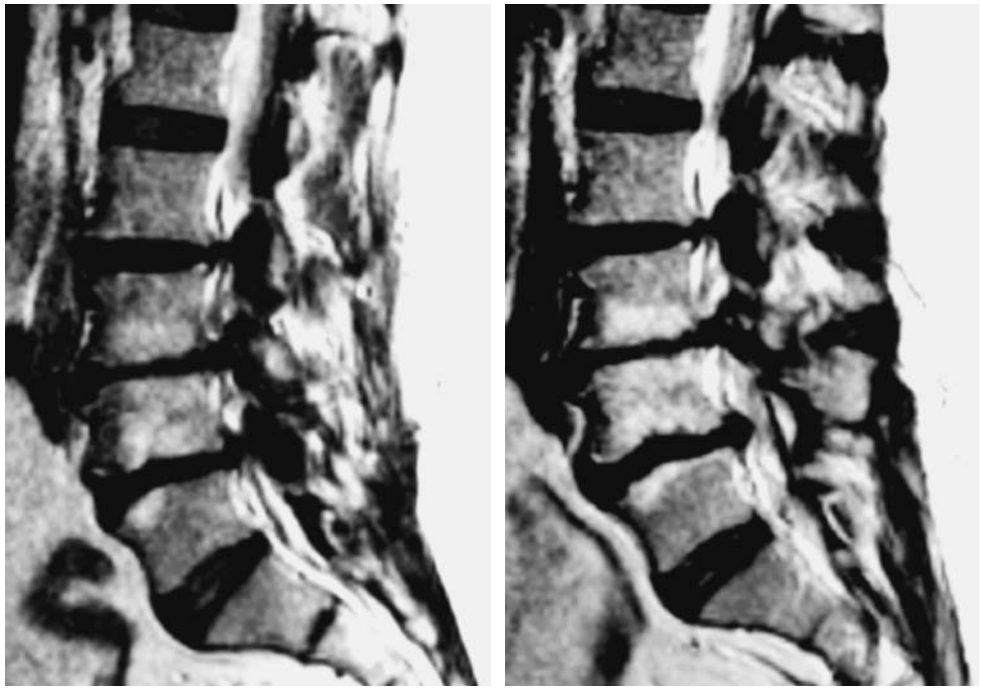

a b

Fig. 9.4a,b. Paradoxical motion during loading. **a** Supine-unloaded MRI: multiple discopaties with disc protrusion in L2–L3, L3–L4, L4–L5. Yellow ligaments are thickened with central stenosis at the same levels. **b** During AL-MRI: paradoxical motion of L5. All disc protrusions increase, in particular at L4–L5

9.2.2.2 Intersomatic Changes

9.2.2.2.1 Appearance or Increase in Listhesis (Fig. 9.4)

In all patients with isthmic lysis and degenerative listhesis, the axial load increases listhesis (known or unknown) to a varying degree, and AL study is more sensitive than dynamic film in demonstrating this finding.

9.2.2.2.2 Narrowing of Disc Spaces (Fig. 9.4)

This finding is always associated with articular facet underslipping (at basal CT) and usually facets (and spinous processes) demonstrate longitudinal hypermobility during axial loading. In some patients it can be associated with slight anterior translation of L4.

This finding seems to be related to a functional insufficiency of FSUs (mainly to disc insufficiency), and its significance seems to be similar to the vacuum sign.

9.2.2.2.3 Increase in Disc Space (Fig. 9.5)

Posterior widening of the L5–S1 disc space, with reduction of its posterior-wedged shape, can be observed, usually in patients with previous L4–L5 disc surgery. These patients show slight anterior translation of L4 during AL. The widening of the L5–S1 disc space during AL studies, in contrast to what one expects to see during an orthostatic load, has been named paradoxical motion (PM). PM is related to the upward movement of the neural arch with (paradoxical) upperslipping of the articular facets and raising of the corresponding spinous process (see below).

9.2.2.2.4 Rotational Movements on "Z" Axis (Fig. 9.6)

Somatic rotation on "Z" axis – clockwise (CW) or counterclockwise (CCW) – can be discovered and is usually associated with asymmetrical facet hypermobility (see below). This finding may be related to disc degeneration, with asymmetrical nucleus pulposus distribution in disc space, since it is usually observed

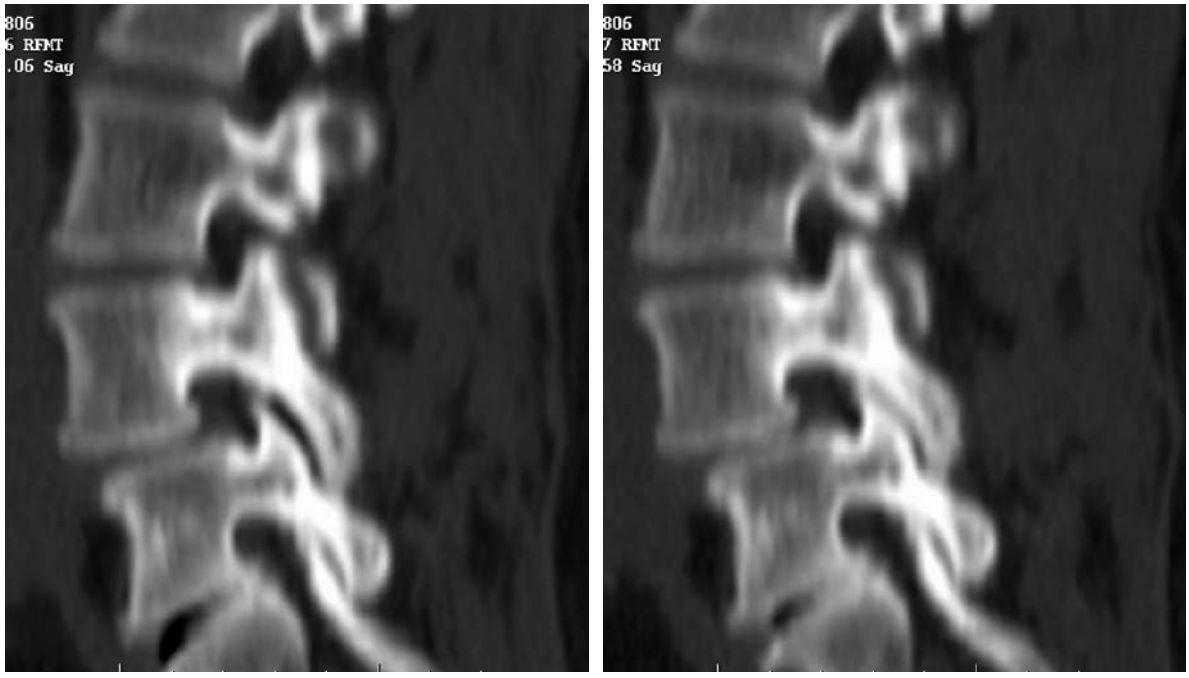

a b

Fig. 9.5a,b. Vacuum-sign supine-unloaded and during loading. **a** Supine-unloaded CT, sagittal reconstruction: vacuum-sign is present in the L5–S1 disc and in the articular space. Degenerative listhesis of L4 on L5 (3 mm). **b** During AL-CT disappearance of articular vacuum; reduction of disc vacuum, with narrowing of disc space and increased listhesis

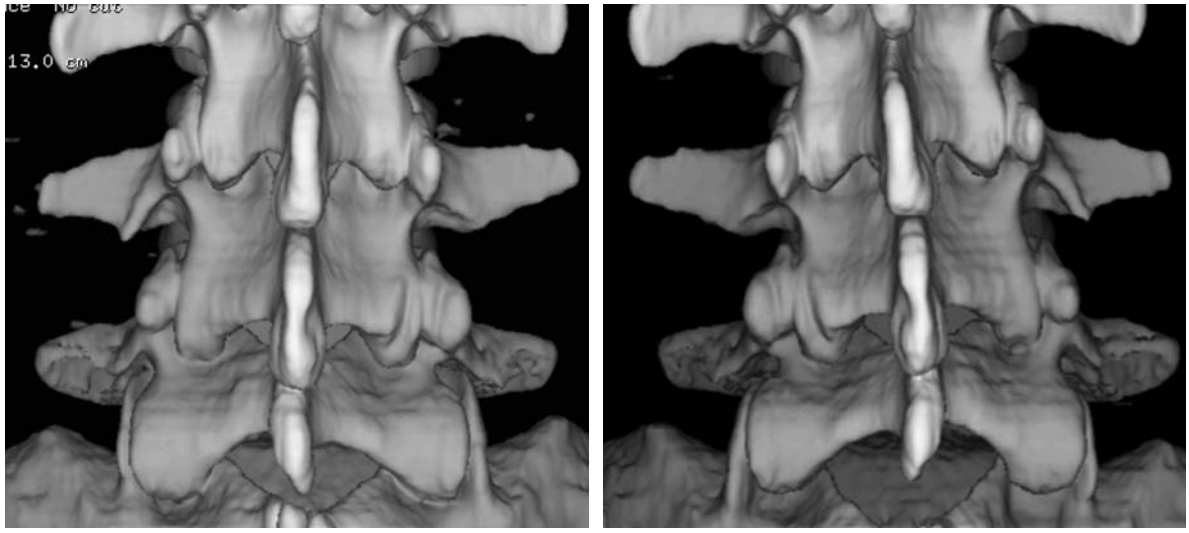

a b

Fig. 9.6a,b. Underslipping of facet joints during loading. **a** Supine-unloaded CT: underslipping of articular processes (++ in L4–L5) with narrow interspinous spaces. **b** During AL-CT: paradoxical motion of L5, with opening of the interspinous space L4–L5 and L5–S1; further underslipping of the other articular processes

in patients previously operated or with a pre-load CT and MRI study showing disc degeneration.

9.2.2.2.5
Posterior Translation of Vertebral Body

Posterior body translation – posterior vertebral translation (usually of L5 or L4 in patients with L5 isthmic lysis and listhesis) usually increases during AL studies, with narrowing of the corresponding disc space.

9.2.2.3
Articular Facet Modifications

9.2.2.3.1
Appearance or Increase of Articular Facet Underslipping (Fig. 9.5)

In a "normal" spine, the AL is maximally supported by the disc. If flexion-extension and/or rotational movements are not superimposed, the posterior arch, and particularly the facets, usually support only a minimal part of this load (Kramer 1990).

In many patients (usually those previously having undergone disc surgery) this facet underslipping is detected on conventional CT or MRI study. This finding is more frequently at the L4–L5 level. The association with facet degeneration is very common, as the narrowing of the corresponding interspinous space. A constant association is found between facet underslipping and disc and articular vacuum phenomenon. The disc's inability to support the axial load can cause posterior load transfer, primarily to the facets and then to the spinous processes.

During AL studies the appearance or further underslipping of facets, sometimes asymmetrically, can be detected. This finding is particularly well seen with cine-AL studies, even in the presence of minor modifications. Using sagittal 2D reformations with bone windowing, this hypermobility often seems to demonstrate a traumatic action of the inferior facet of a vertebra on the isthmus of the vertebra below (Danielson et al. 1998). According to the physiological lordosis of the lumbar spine, this finding is usually visible in L4–L5.

This mechanism could explain the typical low back pain most of these patients experienced as the main symptom. Chronic stress on the isthmus could possibly lead to an isthmic "stress fracture" (Marchetti and Bartolozzi 1986) with isthmic lysis (adult type).

9.2.2.3.2
Disappearance of Intra-articular Vacuum (Fig. 9.4)

Gas inside the articular space of patients with severe degenerative phenomena of the articular facets is not an uncommon finding. During AL, reduction and disappearance of this finding associated with reduction or disappearance of the disc vacuum can be found. The association with facet hypermobility and narrowing of the articular space is relatively common.

This finding is known as articular vacuum sign, having the same meaning as the disc vacuum sign.

9.2.2.3.3
Upperslipping (Paradoxical Motion) of the Articular Facets (Figs. 9.5 and 9.7)

An upward movement of the neural arch of L5 can be detected in young patients during AL; this finding is always associated with underslipping and hypermobility of the L4 inferior facets and with posterior widening of the L5-S1 disc space. This upward movement of L5 could increase the impact of the L4 inferior facets on the L5 isthmi, responsible for local osteolysis and/or sclerotic phenomena.

9.2.2.4
Foraminal Narrowing

Foraminal narrowing is often caused by longitudinal hypermobility of the hypertrophic articular facets. In patients with isthmic lysis, an increase in listhesis causes a narrowing of foramina by the superior spur of the lysis with compression of the nearby nerve root.

9.2.2.5
Thickening of the Ligamenta Flava

Some thickening of the yellow ligaments can be observed in patients with facet underslipping on preload studies. During AL, patients with longitudinal hypermobility of the posterior arch may have a shortening of the ligamenta flava and hence further thickening due to their elastic properties on sagittal reformations.

In contrast, a widening of the spaces between the posterior arches (i.e. a paradoxical motion) causes elongation and thinning of the ligamenta flava. In most patients with facet hypermobility, pronounced calcification of the proximal insertion of the liga-

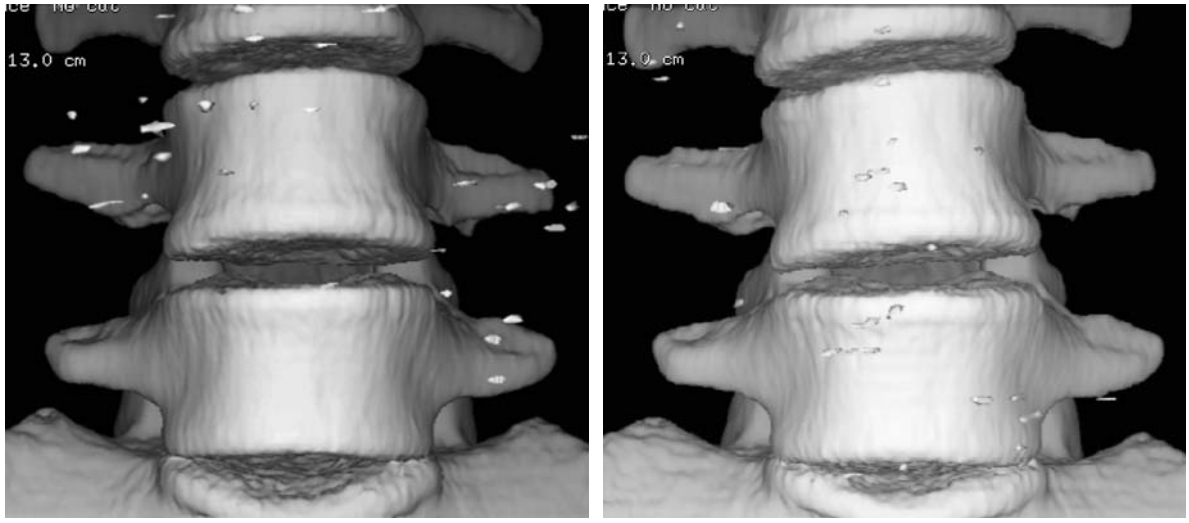

a b

Fig. 9.7a,b. Rotation around the Z-axis during loading (same patient as in Fig. 9.6). **a** Supine-unloaded CT: the lumbar spine is parallel to the sagittal plane. **b** During AL-CT: CCW rotation of L4 along the "Z" axis

ments – considered an indirect sign of segmental instability – can be appreciated on pre-load scans.

9.2.2.6 Modifications in the Relationship Between Spinous Processes

The narrowing of the interspinous space, particularly at the L4–L5 level, is a common finding on plain films and may be particularly well be appreciated on CT 3D reformations. This finding is quite frequently associated with degenerative signs and underslipping of the corresponding articular facets. In all patients with facet hypermobility, associated hypermobility of the spinous processes with both further narrowing of the interspinous spaces or widening of the spaces when a paradoxical motion was present is observed.

9.2.3 AL-CT Versus AL-MRI

The EDMs previously described can be found in almost all AL-MRI studies. The advantages of AL-MRI are the absence of radiation exposure, larger field-of-view (usually the whole lumbar spine and lower thoracic spine), direct sagittal acquisition and consequently no time-consuming post-processing. The main drawback is the 2D acquisition, usually in the axial and sagittal plane (while AL-CT can generate 3D imaging of the spine), with poor visualization of the 3D dynamics of the posterior arches (i.e. articular and spinous processes). The same observations described on AL-CT can be found on AL-MRI studies except for the so-called vacuum sign, which can be hard to detect. On the other hand, MRI has a higher sensitivity in demonstrating fluid collections inside articular spaces (Fig. 9.8). They are probably the counterpart of the vacuum sign in AL-CT. Moreover, fluid dynamics during axial loading are better seen with MRI (Fig. 9.9).

The most frequently observed modification is the increase in spinal stenosis, present on pre-load MR studies (Fig. 9.10). Increased spinal stenosis is secondary to increased disk protrusion, thickening of the ligamenta flava, the presence of a synovial cyst (Fig. 9.9), or increased listhesis. There is agreement in the literature that patients with clinical symptoms of lumbar spinal stenosis should undergo AL studies to optimally evaluate spinal canal dimensions (Danielson et al. 1998; Hiwatashi et al. 2004; Trasimeni et al. 2001). In selected patients with lumbar spinal stenosis symptomatology and narrowing of the spinal canal on AL-MRI, this information may influence treatment options (Hiwatashi et al. 2004). In some cases, stenosis may appear only after AL and it is secondary to microinstability, usually undetected on conventional MRI scans in a neutral position. In these cases, standard MRI only shows an increase in intra-articular space fluid with further normal vertebral relationships on the sagittal images. After loading, anterior displacement of the

a

b

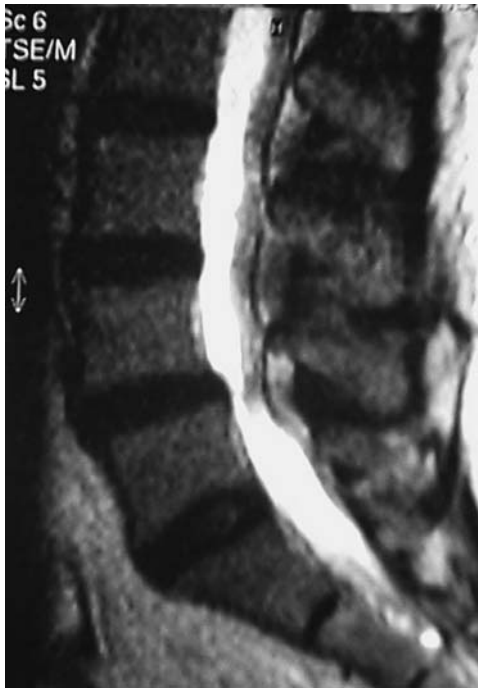

c

Fig. 9.8a–c. Anterolisthesis during loading. Axial (**a**) and sagittal (**b**) supine-unloaded MRI: degenerative facet joints with increased intra-articular fluid and widened joint spaces at the L4–L5 level. Normal alignment of L4–L5. **c** During AL-MRI: mild anterior displacement of L4 on L5

superior vertebra and increase in spinal stenosis can be observed. Conventional X-ray studies in a standing position will show a spondylolisthesis. Conventional MR studies may underestimate the degree of spinal stenosis compared to AL-MRI scans.

Advantages of AL-CT over AL-MRI include better bony detail appraisal, better analysis of complex spatial instabilities and easier evaluation of articular "micro-movements" in a shorter acquisition time. This makes it a very valuable technique in older patients, in patients previously having undergone spinal surgery (complex instability patterns) and in late stages of instability, where reciprocal movements are usually less pronounced. AL-MRI is indicated in younger patients and in early stages of spinal instability. MRI better depicts small fluid collections in interarticular spaces and fluid modifications after loading, as well as better evaluation of soft tissue

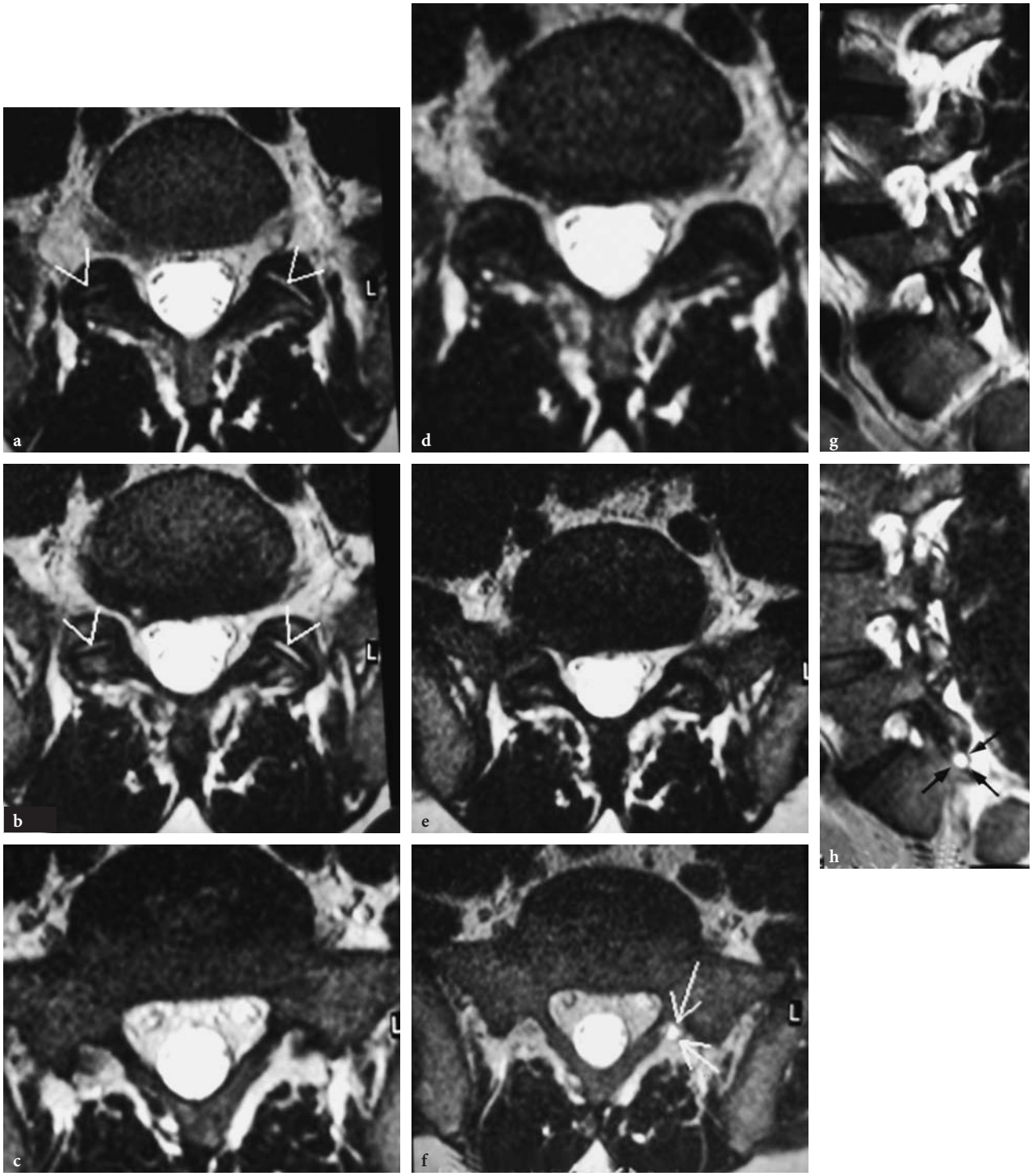

Fig. 9.9a–h. Facet joint fluid redistribution during loading. Axial T2-WI in supine-unloaded MRI (**a–c**) and during AL-MRI (**d–f**) at the L5–S1 level in a patient with LBP. Sagittal T2-WI in supine-unloaded (**g**) and during AL-MRI (**h**). On supine-unloaded MR images there is fluid in the joint space (*arrowheads* in **a** and **c**). On AL-MRI, intra-articular fluid motion is observed with appearance of a small synovial extra-articular cyst on the left side (*arrows* in **f** and **h**)

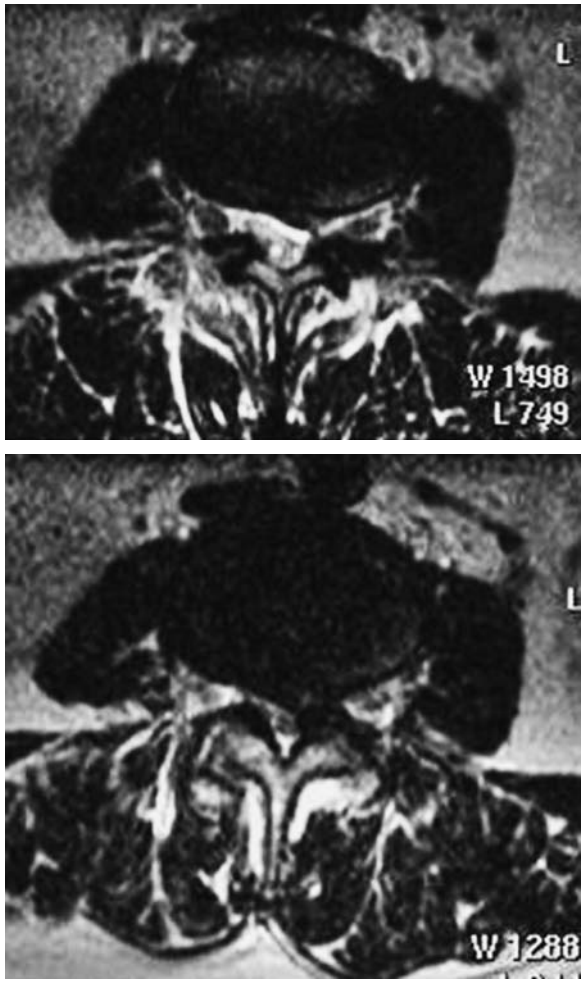

a

b

Fig. 9.10a,b. Spinal stenosis during loading. **a** Supine-unloaded MRI. **b** During AL-MRI. Increased spinal stenosis secondary to increased disc herniation and abnormal motion of the articular processes and thickening of the yellow ligaments

structures involved in spinal stenosis such as the ligamenta flava, vertebral disc, etc. Small synovial cysts and soft tissues appearing during loading are better demonstrated by MRI.

9.2.4 Loading of the Degenerative Spine: Classification of Changes

EDMs described above may be observed alone or may coexist in various combinations, sometimes apparently conflicting with each other. In a series of 300 patients (Cartolari 1997) we were able to identify four patterns. The associations of EDMs found in our patients could represent definite motion patterns, that we named complex dynamic modifications (CDMs) types 1–3. Pattern 4 was observed in patients with isthmic lysis.

9.2.4.1 CDM1

The observations made during AL studies are listed in Table 9.2 and illustrated in Fig. 9.11.

A possible explanation of CDM1 is a modification of the mechanisms of load and motion transmission at the L4 level. This usually happens because of disc insufficiency (disc changes observed on basal CT should be considered a predictive sign). Part of the axial load is transferred to the posterior arch, as suggested by the facet underslipping and narrowing of the L4–L5 interspinous space.

A second hypothesis is the development of a lumbar spine sagittal imbalance, usually secondary to degenerative disc disease (Depuis et al. 1985). Both mechanisms can even co-exist at the same time.

In the case of a normal or early degenerative L5–S1 disc (as suggested by the younger age of these patients), the axial loading causes an anterior translation of the L4 body, while the normal L5–S1 nucleus pulposus acts as a fulcrum and causes the paradoxical motion of L5. This could produce a posterior migration of the nucleus itself (instead of an anterior migration).

In practical terms, L4–L5 and L5–S1 discs work "in flexion" instead of working "in extension" (to increment lordosis), as we expect, with an inversion of the normal disco-articular mechanics.

This modification of the motion pattern may be very early, causing an impairment in normal disco-articular mechanics, prodromic to a series of cascade effects, at least on L4–L5 and L5–S1 levels (see below).

The modifications of load distribution due to L4–L5 impairment seem to be responsible for low back pain.

9.2.4.2 CDM2

As a CDM1 develops, we can presume that at least the FSUs between L3 and S1 undergo impaired function. Early aging is probably more pronounced on lower FSUs (L4–L5 and especially L5–S1), as documented by disc space narrowing and degenerative disc and articular signs (e.g. vacuum sign).

Table 9.2

Pattern 1: complex dynamic modifications, type 1 (CDM1)	
Standard CT	**AL-CT**
• L4 facet underslipping • L4–L5 disc space narrowing • Interspinous space narrowing	• Further L4 facet underslipping • Further narrowing of the L4–L5 disc space • Anterior translation of L4 on L5 • Paradoxical motion of L5, with posterior widening of L5–S1 disc space, upperslipping of articular facets and hyper-mobility of the spinous processes
In all cases, abnormal movements were of clearly evident ranging from 1 to 3 mm All patients had low back pain as the main symptom and about half of them had previously undergone L4–L5 disc surgery, with a percutaneous or micro-surgical approach	

Pattern 2: complex dynamic modifications, type 2 (CDM2)	
Standard CT	**AL-CT**
• L4 and L5 facet underslipping • Narrowing of L4–L5 and L5–S1 disc spaces, sometimes with degenerative signs (vacuum sign) • Facet degeneration and underslipping • Narrowing of interspinous spaces	• Further narrowing of disc spaces (sometimes with paradoxical motion) with vacuum reduction / disappearance when present and sometimes appearance of rotational movements • Sometimes paradoxical motion; usually further facet underslipping, sometimes asymmetrical (if body rotational movements were present) • Further narrowing of interspinous spaces. further L4 facet underslipping
In these patients, abnormal facet and spinous movements were usually limited (about 1 mm) where the most important EDMs regarded disc spaces About one third of these patients had previously undergone disc surgery, usually with a microsurgical approach at the L4–L5, L5–S1, or at both these levels Relatively consistently, L4 showed an anterior translation on L5, but always < 3 mm	

Pattern 3: complex dynamic modifications, type 3 (CDM3)	
Standard CT	**AL-CT**
• L4 and L5 facet underslipping • Narrowing of L4–L5 and L5–S1 disc spaces, sometimes with degenerative signs (vacuum sign) • Facet degeneration and underslipping • Narrowing of interspinous spaces	• Reduction or disappearance of vacuum sign (both discal and articular) • Further disc space narrowing • Increment of listhesis
Basal CT findings were similar when compared to patients with a pattern 2, but disc and articular degeneration was more frequent (often with vacuum). All the patients had degenerative listhesis (usually L4–L5) Articular and spinous movement were usually less than 1 mm	

Pattern 4: patients with isthmic lysis (mostly at L5-S1, some at L4-L5 level)	
Standard CT	**AL-CT**
• Listhesis of L5 (L4) on S1 (L5) at various degrees • Underslipping of L4 inferior facets • Narrowing of interspinous spaces	• Increment of listhesis and widening of lysis • Further underslipping of L4 inferior facets, that wedge into the lysis • Further narrowing of interspinous spaces • Conserved L5–S1 disc space

As the L5–S1 disc ages, the same posterior redistribution of axial loads (hypothesized in L4–L5) probably occurs (Fig. 9.12) with L5–S1 facet underslipping. This posterior redistribution of loads is favoured by the down-projection of the L4 neural arch that leans on the posterior arch of L5. In this way, the L5-S1 disc tends to resume a normal (even if narrowed) shape in response to loading. According to the mean age of the patients, the CDM2 could be the second step in the progression of a chronic lumbar spine instability.

The degenerative changes of articular facet joints are more evident, which could explain why the EDMs seen during cine-AL studies are of minor extent.

9.2.4.3 CDM3

As alterations in the spine load distribution persist, the spine undergoes progressive changes, with evidence of modification and deformation of vertebral shape. Over the years, a progressive anterior translation of a vertebral body (usually L4) occurs (Fig. 9.13).

This anterior translation probably originates from changes in force distribution due to disc degeneration. This is probably then maintained and incremented by the down projection of the neural arch. The spinous processes could have, in the early

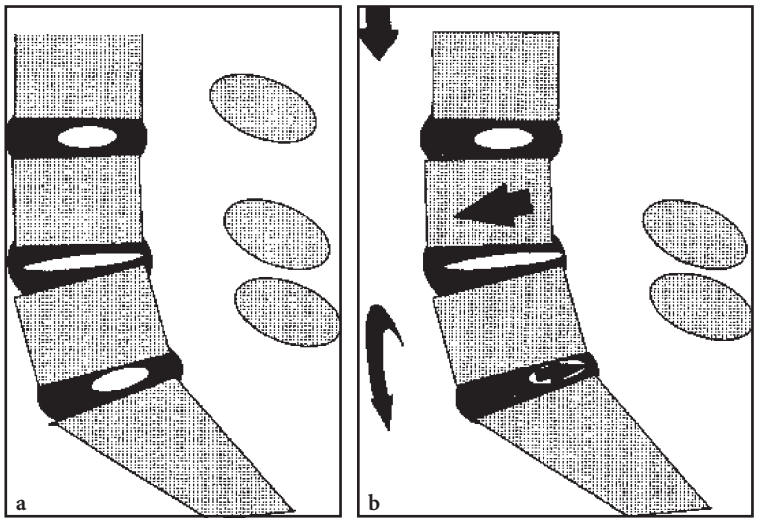

Fig. 9.11a,b. Scheme of CDM1. CDM1 consists of: (1) further L4 facet underslipping, (2) further narrowing of the L4-L5 disc space, (3) anterior translation of L4 on L5, (4) paradoxical motion of L5, with posterior widening of L5-S1 disc space and (5) upperslipping of articular facets and hypermobility of the spinous processes

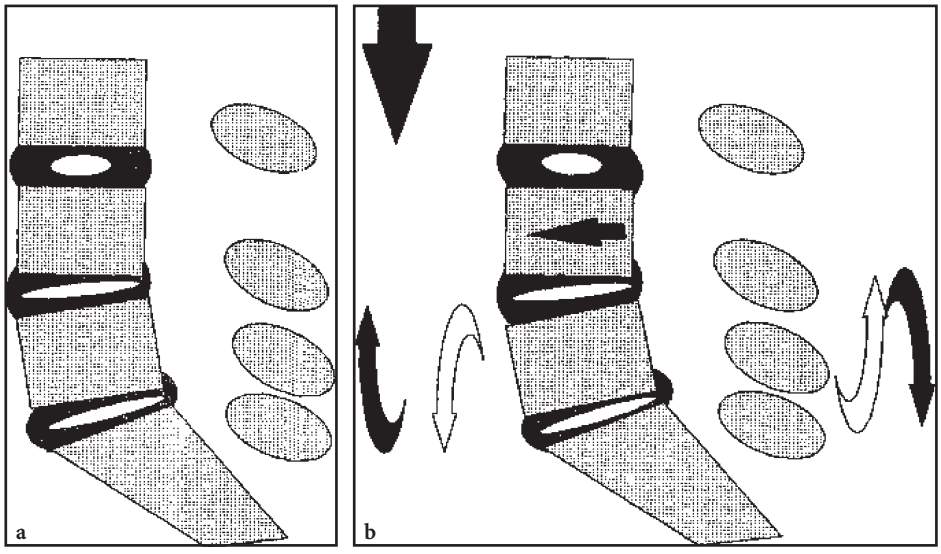

Fig. 9.12a,b. Scheme of CDM2. Unloaded (**a**) and loaded (**b**) motion segment. L5 paradoxical motion (*white curved arrows*) reduces, with normalization of L5–S1 motion (*black curved arrows*) and disc shape (even if narrowed)

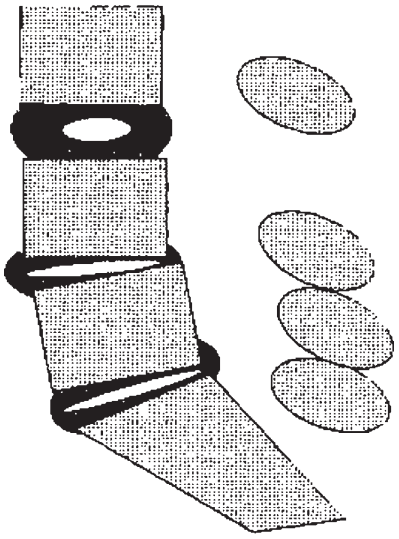

Fig. 9.13. Scheme of CDM3. As alterations in the spine load distribution persist, the spine undergoes progressive changes, with evidence of modification and deformation of vertebral shape. Over the years, a progressive anterior translation of a vertebral body (usually L4) occurs

stages, a dynamic supportive function to articular facets and disc.

This could represent a fourth (extreme) posterior functional column (Hazlett and Kinnard 1982), that prevents excessive facet underslipping and further body anterior translation (see Fig. 9.11). With time, as the L4 posterior arch down-projection progresses, the spinous process encroaches the L5 spinous process and stops.

At this point, the posterior arch is quite blocked. Since the vector's sum must be constant, as an axial vector acts on the lumbar spine, the anteriorly directed vector increases and the vertebra moves anteriorly.

If anatomical variations exist (e.g. hypoplastic S1 neural arch or isthmic lysis of L5), the spinous processes do not block their down projection and this could lead to posterior translation of the upper vertebra. This often happens at the L5–S1 or L4–L5 level in patients with young-type L5 isthmic lysis.

When anterior translation progresses, degenerative listhesis (i.e. an anterior translation of at least 3 mm) often occurs together with the appearance of bony spurs and obvious signs of disc and articular degeneration (e.g. vacuum phenomenon) on basal CT. These patients often show disc and articular vacuum signs during AL studies. Sometimes, an inverted vacuum sign may be observed as a major sign of pathological load transmission.

Usually, articular and spinous EDMs are very small (1 mm or less) and best, or only, appreciated on 3D cine-AL studies. In most cases, AL studies were able to show some increment in listhesis, with more sensitivity and specificity than conventional dynamic plain film (Cartolari et al. 1996; Cartolari 1997). Since the mean age of patients is highest among this group, we believe that CDM3 is the third step in the progression of chronic lumbar spine instability.

As mentioned earlier, all definitions of lumbar spine instability are vague. Segmental instability is an abnormal response to applied loads, characterized by motion in motion segments beyond normal constraints (American Academy of Orthopaedic Surgeons 1981). There is no an acute disruption of spinal structures. In contrast, we have the slow evolution of an unstable condition which is most likely the result of subacute, chronic and repetitive mechanical overloads (American Academy of Orthopaedic Surgeons 1981).

We agree with Boden and Frymoyer's definition that segmental instability is a loss of spinal motion segment stiffness, such that force application to that motion segment produces greater displacement than would be seen in a normal structure, resulting in a painful condition, the potential for progressive deformity and neurological structures at risk (Boden and Frymoyer 1997).

In our opinion, the term spine "dystability" should be preferred to indicate a different, lower energetic state of the spine which is the result of disc and/or ligament and/or bone problems at any level.

Lumbar segmental instabilities usually have etiological or morphological classifications that do not take into account a possible common mechanism. Some of these classifications are reported in Tables 9.3 and 9.4.

In our opinion, the use of CDMs (particularly of CDM1) could lead to a universally accepted classification of chronic segmental instability.

First of all, the conversion from CDM0 to CDM1 identifies L4 as the possible fulcrum of the lumbar spine system and suggests the presence of at least three functional levels and four functional columns in the lumbar spine (Fig. 9.14).

As one of the components of the columns fails for any reason (infection, trauma, degenerative changes, etc.), a stereotyped series of actions occurs which lead to a cascade of alterations in a sort of "domino effect" (Fig. 9.15).

In our opinion, the functional fulcrum of the lumbar spine is L4 and L4–L5 disc insufficiency is the

Table 9.3. Lumbar segmental instabilities

1. Fractures and fracture dislocations
2. Infections involving the anterior columns
a. With progressive loss of vertebral body height and deformity despite treatment with antibiotics
b. With progressing neurologic symptoms despite treatment with antibiotics, if accompanied by progressive loss of vertebral body height and deformity
3. Primary and metastatic neoplasms
a. With progressive loss of vertebral body height and deformity
b. With progressing neurologic symptoms not resulting from direct tumor involvement of the spinal cord, cauda equina, or nerve roots
c. Postsurgical (after resection of the neoplasm)
4. Spondylolisthesis
a. Isthmic spondylolisthesis
I. L5–S1 progressive deformity in a child (rarely unstable in adults)
II. L4–L5 deformity
5. Degenerative instabilities
6. Scoliosis

Table 9.4. Degenerative segmental instabilities

Primary instabilities
1. Axial rotational
2. Translational
3. Retrolisthetic
4. Progressing degenerative scoliosis
5. Disc disruption syndrome
Secondary instabilities
1. Post-discectomy – Subclassified as for primary instabilities
2. Post-decompressive laminectomy
a. Accentuation of preexistent deformity
b. New deformity
3. Post-spinal fusion
a. Above or below a spinal fusion – Subclassified as for primary instabilities
b. Pseudoarthrosis
4. Post-chemionucleolysis

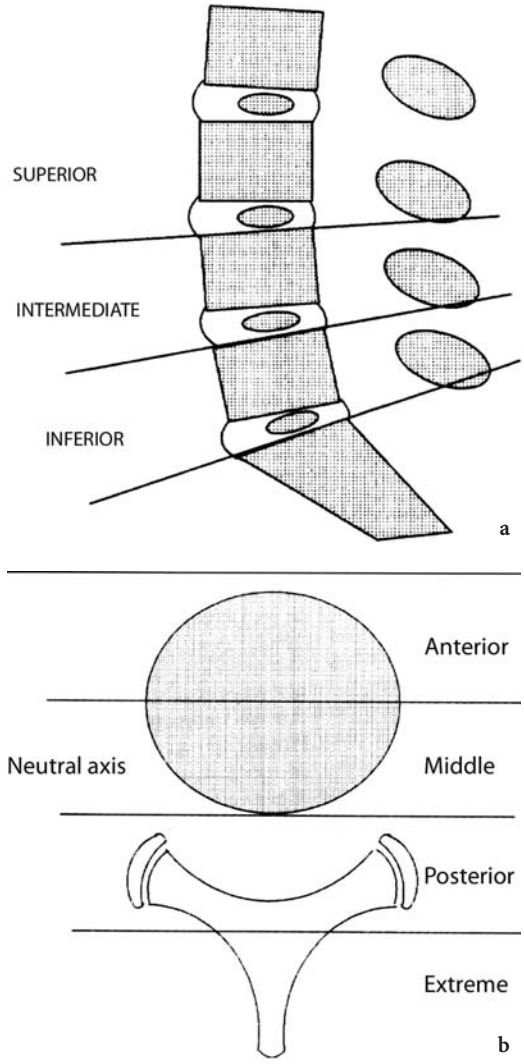

Fig. 9.14a,b. Functional model of the lumbar spine. The proposed functional model, with three horizontal levels (**a**) and four functional columns (**b**). In this model the L4-L5 level is the possible functional fulcrum of the lumbar spine

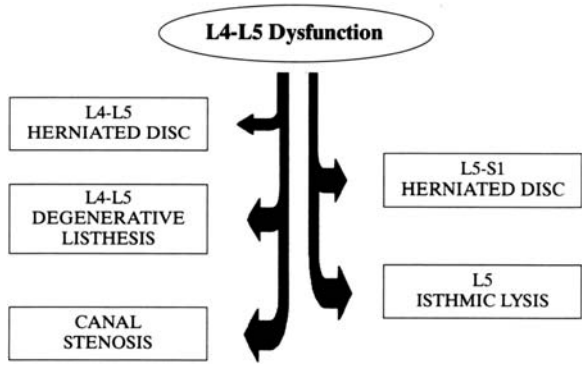

Fig. 9.15. "Domino effect" of L4–L5 dysfunction

most frequent cause of segmental instability. L4–L5 dysfunction has effects particularly on L4–L5 and L5–S1 levels. With the exception of acute episodes (i.e. disc herniation with acute nerve root compression), the disease is usually chronic and with time progressive deformation of the spine occurs. Where the transition from CDM0 to CDM1 could even be subacute, the conversion from CDM1 to CDM3 could take many years.

This common view not only explains the progression of the disease, but also agrees with the hypothesis of Kirkaldy-Willis and Farfan (1982) that degenerative processes occur in three sequential phases: dysfunction, instability and restabilization.

If a segmental dysfunction exists (e.g. L4–L5 disc insufficiency), we could have the conversion from CDM0 to CDM1, which includes instability. With time, the whole system tends to restabilize and we could find CDM2.

This lower level stabilization (dystability) transmits a dysfunction wave to the nearby structures, with progressive sequences of microinstability and restabilization. The end of the process is CDM3 (degenerative listhesis).

Since the whole sequence seems to be stereotyped, every CDM could correspond to a different degree of segmental instability in a grading system from grade 0 to grade 3. On the other hand, every CDM corresponds to a typical basal CT and plain film pattern. In the presence of the findings described above, a grade 1–3 segmental instability can be highly suspected (Table 9.5); confirmation can be obtained with AL studies and cine-AL studies.

Patients with isthmic lysis and listhesis present a different functional problem. In fact, this entity usually occurs in younger people at the L5–Sl level, and this for developmental reasons (Kaech 1995). In these patients, the whole lumbar spine undergoes a functional rearrangement, bringing the structure into a low-unstable equilibrium.

In some adult patients, it can be hypothesized that a CDM1, with L4 facet underslipping, can result in a fatigue fracture of the L5 isthmus in an otherwise normal neural arch.

This kind of lumbar instability could be named Grade 4 instability, with subtypes A (developmental spondylolisthesis) and B (acquired spondylolisthesis) (Table 9.5).

9.2.5 Axial Loaded Imaging of the Postoperative Spine

If the examination of the "unstable" spine is difficult, the diagnostic evaluation of a postoperative, instrumented spine is even more difficult. This is not only because of the possible interference of surgical devices with CT or MRI, but also because the same difficulties encountered in the analysis of possible hypermobile instability of the non-operated spine are also present (and generally greater) when trying to assess the stability of the operated spine.

We believe it is feasible to evaluate the surgically instrumented segments. Cages, Dynesis or DIAM (Device for Intervertebral Assisted Motion) spinal stabilization systems (Medtronic) do not produce artifacts severe enough to significantly compromise the image quality (Figs. 9.16–9.19). Sagittal and 3D images allow a global visualization of the lumbar

Table 9.5 The proposed instability grading system

CDMs	Basal studies plain films	AL studies	Instability grade
CDM1	- L4 facet underslipping - Narrowing L4-L5 (disc) interspinous space - Conserved L5-S1 disc space	- Further L4 facet underslipping - Further narrowing L4-L5 space - Anterior L4 translation - L5 paradoxical motion	*Grade 1*
CDM2	- L4, L5 facet underslipping - Narrowing of L4-L5 and L5-S1 and spinous spaces	- Further facet underslipping - Further disc and spinous spaces narrowing - Anterior translation of L4 (<3 mm)	*Grade 2*
CDM3	- As CDM2, plus: - Degenerative listhesis (>3 mm) - often disc and articular vacuum phenomenon	- Further disc space narrowing - Increment of listhesis - vacuum disappearing (Vacuum Sign)	*Grade 3*
CDM4	- Lysis and listhesis of L5 (L4) - Underslipping of L4 inferior facets - Narrowing of interspinous spaces	- Widening of lysis and increment of listhesis - Wedging of L4 inferior facets into the lysis	*Grade 4A* *Grade 4B*

spine before and after instrumentation. Posterior stainless steel screws may yield some CT artifacts (beam hardening artifacts), primarily seen on the axial source images. Even in these cases, sagittal reformations and 3D images with transparencies allow a good overview of the spine (Figs. 9.20 and 9.21).

The cine-AL-CT frames allow for an evaluation of the spondylodesis (surgically instrumented segments), as well as the adjacent levels.

The diagnostic goals of evaluating an instrumented spine include: evaluation of the stability of the fixed segment(s), analysis of the "internal" stability of the implant, assessment of the stability of the levels adjacent to the spondylodesis and assessment of the correction of the preoperative instability/deformity.

AL-CT in non-operated spines has been shown to be able to depict even minimal alterations in intersegmental spatial relationships. In the same way, we have been able to observe the response of the surgically instrumented spine to axial loading. In the literature, reports indicate that no residual intersegmental movement should be found to confirm the presence of complete intersegmental fusion (Kaech 1995). In our opinion, AL-CT has higher sensitivity than conventional radiographs since movements are

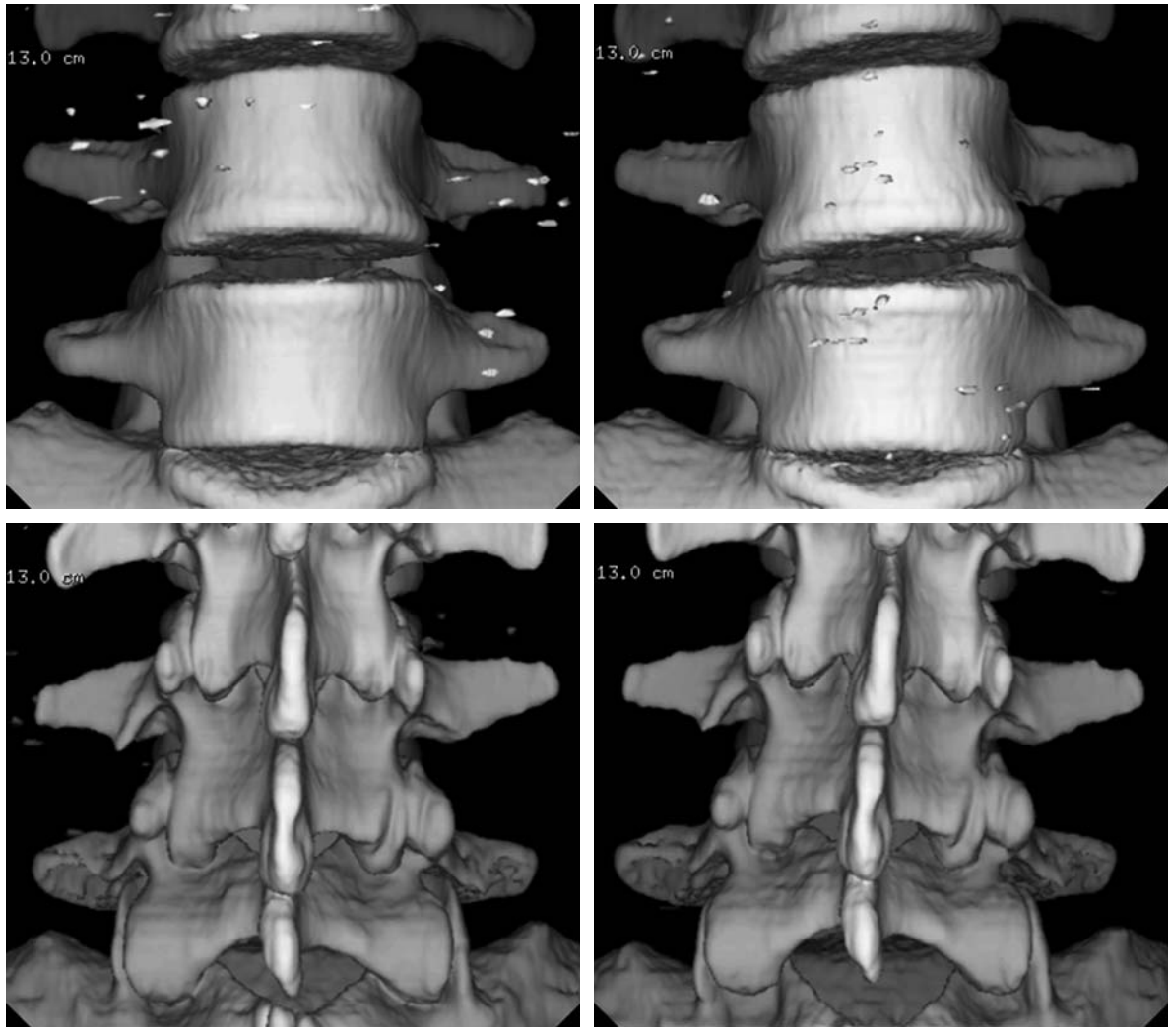

Fig. 9.16. a Basal CT, 3D anterior view. Young female (33 years old) with low back pain especially in orthostatism; the lumbar spine has correct sagittal alignment. **b** AL-CT, 3D anterior view. Comparison of mild right-convex scoliosis; anterior reduction of L5–S1 disc space (paradoxical motion). The patient refers the comparison of low back pain during axial loading. **c** Basal CT, 3D posterior view. Same patient; note the articular underslipping and the loss of interspinous spaces. **d** AL-CT, 3D posterior view. Mild right-convex scoliosis; superior translation of L5-S1 posterior arch (paradoxical motion) and further underslipping of L3 and L4 inferior articular processes

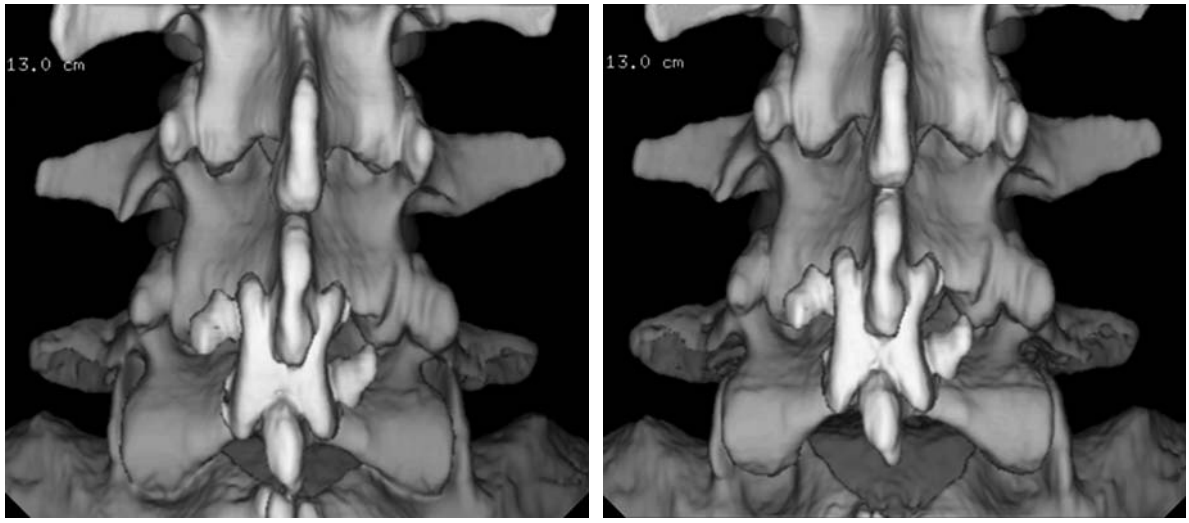

a b

Fig. 9.17. a Same Patient as in Fig. 9.16. Basal CT, 3D posterior view. In L4–L5 a DIAM has been positioned. The spine has right sagittal assessment; partial recovery of correct articular and spinous processes spatial situation. The patient reports only partial reduction of her symptoms in orthostatism. **b** Same patient; AL-CT, 3D posterior view. The spine still has right sagittal assessment; superior translation of L5–S1 posterior arch (paradoxical motion) is still present. The orthostatic low back pain appeared during axial loading

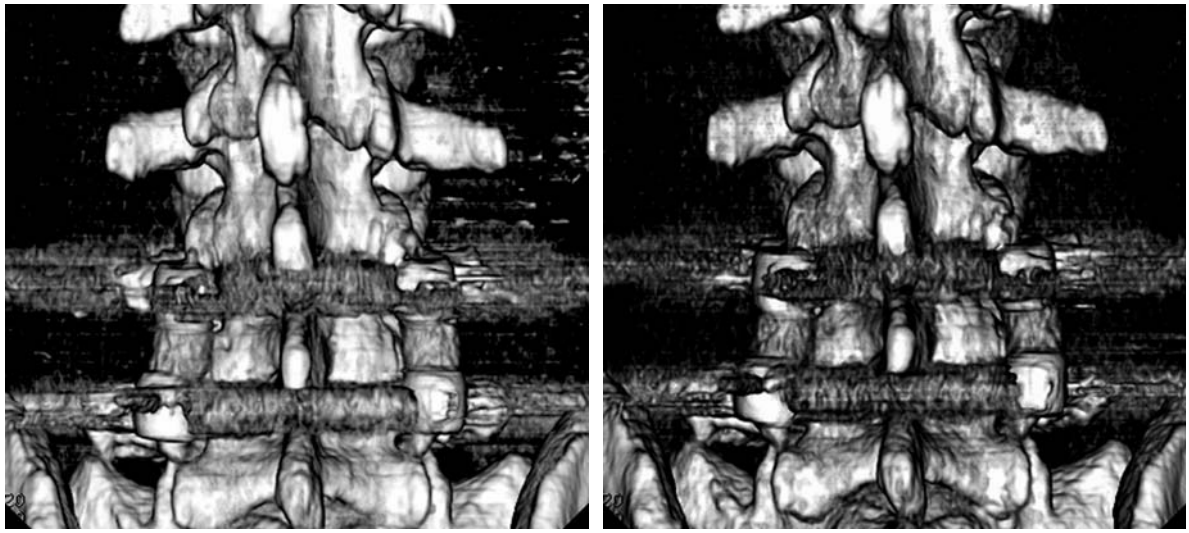

a b

Fig. 9.18. a Basal CT, 3D posterior view. Presence of DYNESYS in L4–L5. Even in the presence of some Hounsfield artefacts, we can well evaluate that the spine has right sagittal balance and that the anatomical relationships between spinous and articular processes are correct. The patient is actually symptoms-free. **b** Same patient, AL-CT. No changes in the spatial situation of the spine; a slight longitudinal size reduction, with minimal shape deformation, is present in the spacers of the DYNESYS system in L4–L5, due to the work the system performs during axial loading. No pain appeared during axial loading

typically within a range of millimeters. In patients with cages, we found the persistence of some interbody movement, even of 1 mm or less motion in the craniocaudal dimension. This probably means that incomplete fusion may be present even when the patients are asymptomatic at the time of the AL-CT (Danielson and Willen 2001).

In patients with prior posterior fusion procedures, we believe that some interbody movement may always be possible in the subacute stages of bony interbody fusion (Figs. 9.20 and 9.21). This may be due to the elastic properties of the devices used, as well as that of the immature bony interbody fusion mass. In all cases we could observe some re-

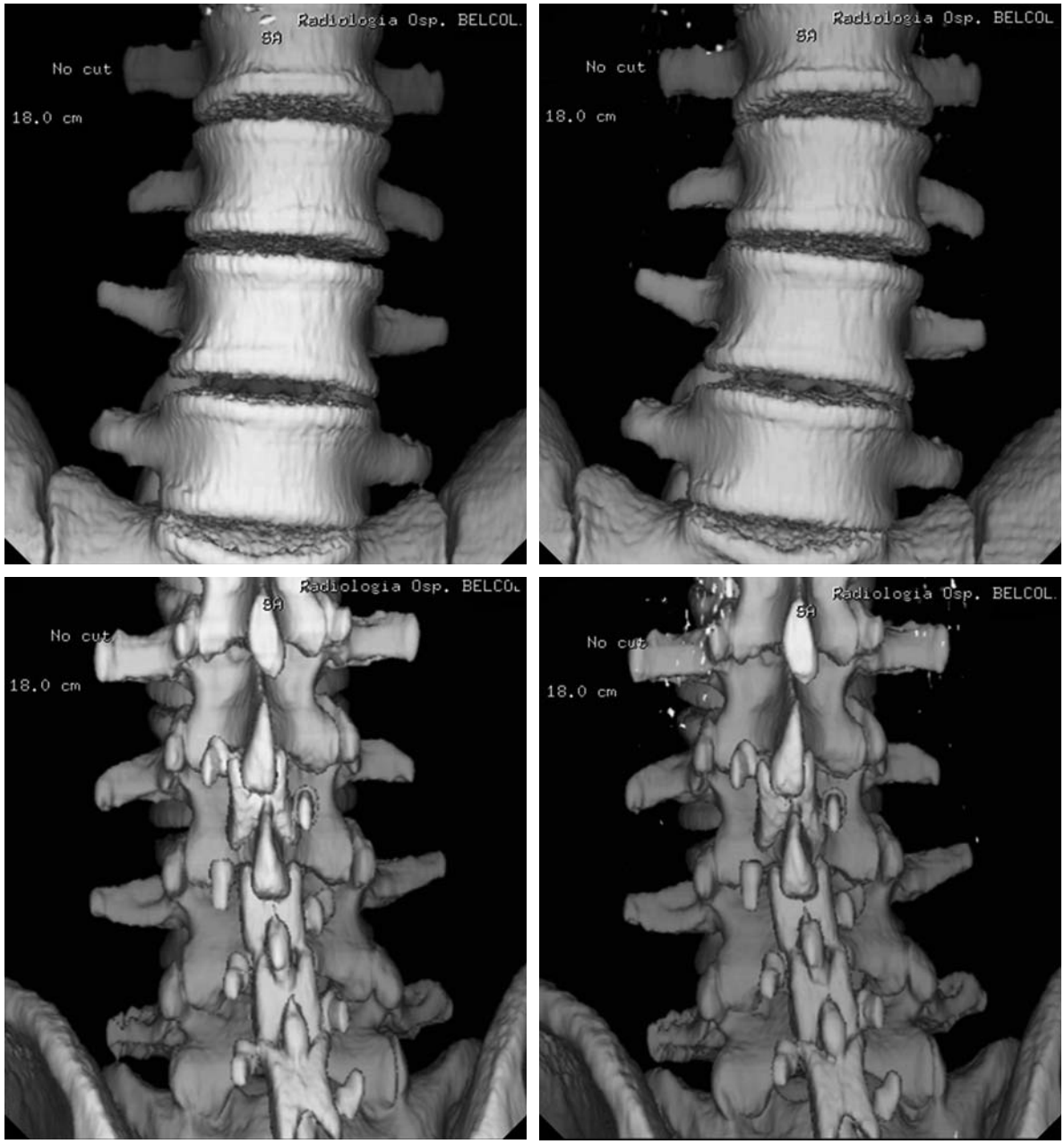

Fig. 9.19. a Basal CT, 3D anterior view. Young male (29 years old) after positioning of four DIAM. Mild left-convex scoliosis. The patient still has low back pain in orthostatism. **b** AL-CT. Same patient; during loading further left-convex scoliosis, with CCW rotation of L2 and L3 bodies and CW rotation of L4 and L5 bodies. On "Z" axis. Deformation of L3–L4 disc space and anterior reduction of L5–S1 disc space (paradoxical motion). Pain during axial loading. **c** Basal CT, 3D posterior view. Young male (29 years old) after positioning of four DIAM. Mild left-convex scoliosis. **d** AL-CT. Same patient; during loading further left-convex scoliosis, with CCW rotation of L2 and L3 bodies and CW rotation of L4 and L5 bodies. On "Z" axis. Minimal superior translation of L5 neural arch (paradoxical motion). It is possible to evaluate the deformation of the interspinous devices due to the work the devices perform during axial loading

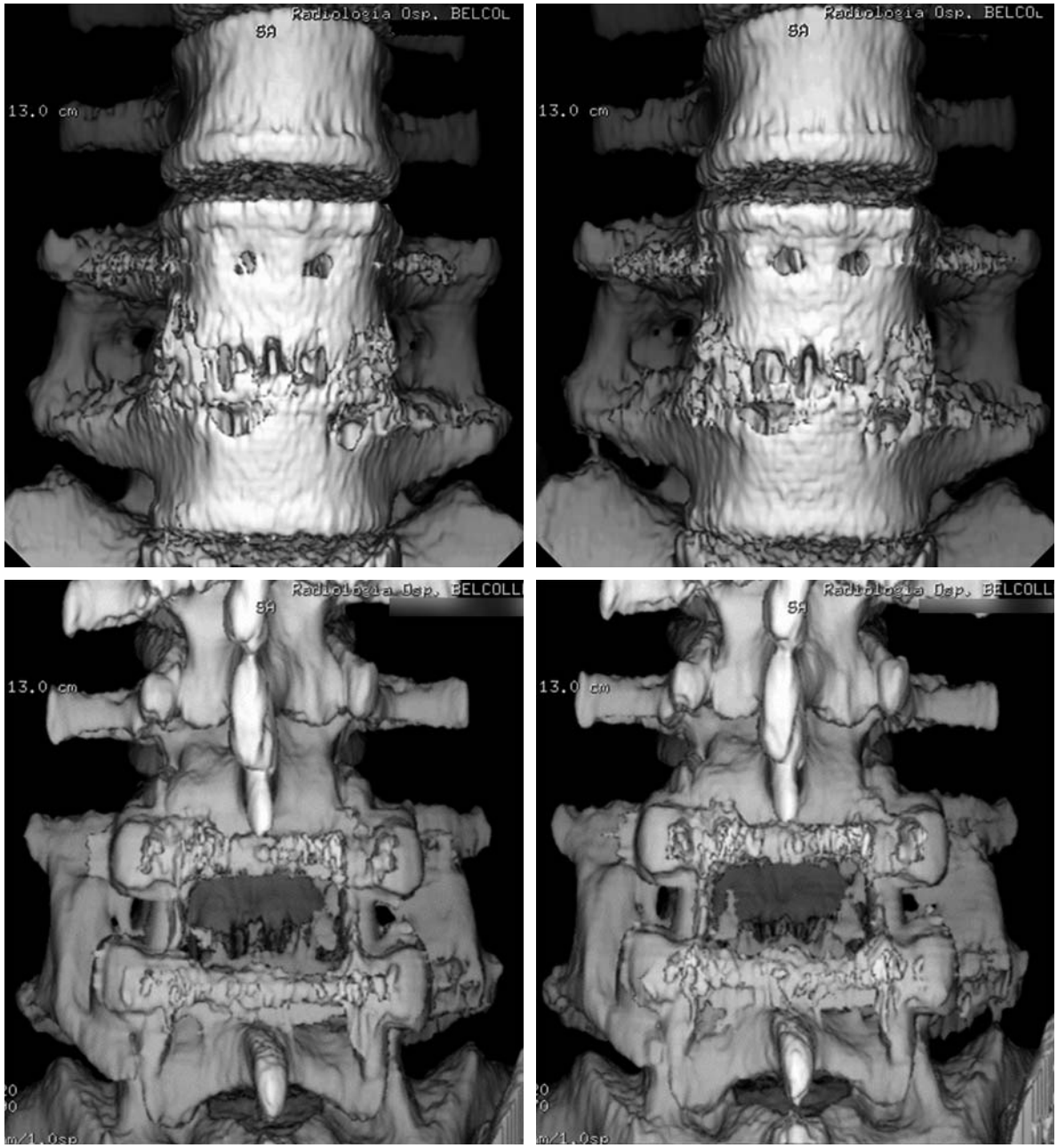

a b c d

Fig. 9.20a-d. Basal CT, 3D anterior view. Male (53 years old), underwent complex surgery in L4-L5 some years previously: intersomatic cages, posterior fusion with screws and bone fusion of the transverse processes. Actually has increasing low back pain in orthostatism without leg pain. The lumbar spine has correct sagittal alignment. **b** AL-CT, 3D anterior view. Same patient; CCW rotation on L3 body on "Z" axis. **c** Basal CT, 3D posterior view. Same patient. The results of surgery in L4–L5 with intersomatic cages, posterior fusion with screws and bone fusion of the transverse processes are evident. **d** AL-CT, posterior 3D view. The CCW rotation on L3 body on "Z" axis is visible and so the change in articular process relationships at the same level: hypermobile instability proximally to the fusion

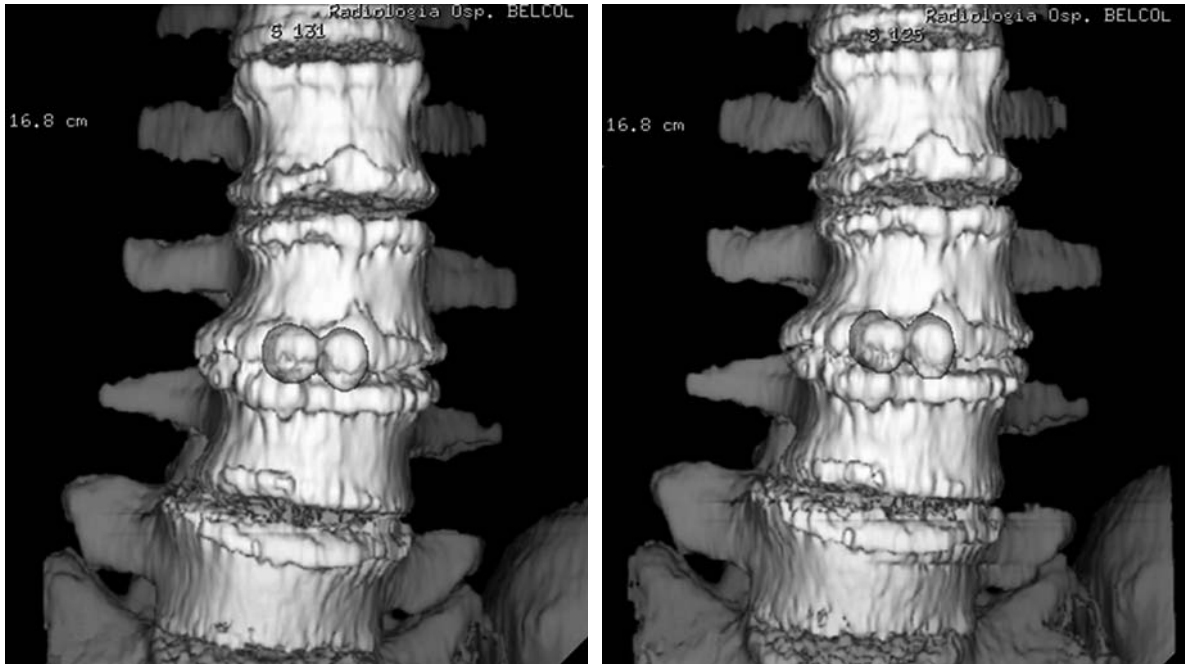

a b

Fig. 9.21. a Basal CT, 3D anterior view. This elderly woman (78 years old) underwent an examination for intersomatic fusion with L3–L4 cages (seen in transparency) 2 years previously. A left-convex lumbar scoliosis is present as well as spondylosis phenomena at the same level. The patient is relatively asymptomatic. **b** AL-CT anterior view. Same patient. Only some minimal change is visible in L3–L4, sign of still incomplete intersomatic fusion. No internal instability of the inserted devices

sidual interbody movement up to 2 years after the surgical spondylodesis, which should probably be considered as normal in asymptomatic patients.

On the other hand, the persistence of some degree of motion is normal when considering some of the "elastic" intersegmental instrumentation devices such as the Dynesis and DIAM spinal stabilization systems. In patients with both such devices, we observed the way the device dissipated the axial load through the instrumentation system mainly on the 3D images (Fig. 9.19).

With "internal" stability of the implant, we mean several types of movements intrinsic to the device used. For example, the approximation of the two cages within the disc space, or some movement occurring between the screws and the attached posterior fixation device. We did not observe such findings in our patients.

Reports in the literature describe the presence of increased motion at levels adjacent to correctly fused spondylodeses. As expected, we were able to observe this adjacent intersegment motion clearly in cases of "rigid" corrections of intersegmental instability (e.g. posterior fixation instrumentation, disc cages). However, almost no movement is observed intersegmentally at levels adjacent to intersegmental instrumentation utilizing the "elastic stabilization" devices (e.g. Dynesis instrumentation, DIAM spinal stabilization systems).

The correction of instability is generally achieved given the specifications and limitations of the systems used. The more rigid systems may have engendered some incremental, new hypermobility in the levels adjacent to the instrumented segments (typically superiorly). In one case of DIAM instrumentation, we observed the persistence of the "paradoxical" motion at L5–S1, caudal to the instrumented level (i.e. placed at the L4–L5 level) (Figs. 9.16 and 9.17).

In our experience, AL-CT seems to be able to image clearly the surgically instrumented spine, allowing the observation of even minimal residual normal and abnormal intersegmental movements at and adjacent to the instrumented level. Even in the presence of large stainless steel metallic implants, sagittal reformations and 3D images enable a sufficiently clear analysis of the spine, while the functional aspects of the examination (i.e. axial loading) enable excellent evaluation of the postsurgical load transmission patterns and an analysis of the way in which the instrumentation works. AL-CT can yield important and potentially useful functional information and seems to be the reference approach to the post-surgical evaluation of the lumbar spine.

References

American Academy of Orthopaedic Surgeons (1981) A glossary on spinal terminology. American Academy of Orthopaedic Surgeons, Chicago, p 34

Boden SD, Frymoyer JW (1997) Segmental stability overview and classification. In: Frymoyer JW (ed) The adult spine: principles and practice, 2nd ed. Lippincott-Raven Publishers, Philadelphia, pp 2137–2155

Brickmann P (1986) Injury of the annulus fibrosus and disc protrusion: an in vitro investigation oh human lumbar disc. Spine 11:149–153

Burgener FA, Kormano M (1987) Differential diagnosis in conventional radiology. Georg Thieme Verlag, Stuttgart

Cartolari R (1997) Functional evaluation of the lumbar spine with axial loaded computed tomography (AL studies) and cine AL studies. Rivista di Neuroradiologia 10:569–584

Cartolari R, Boni S et al. (1993) La tomografia computerizzata con carico assiale della colonna lombare. Osservazioni preliminari. In: Salvolini U, Leonardi M (eds) Neuroradiologia 1993. Ed. del Centauro, Udine, pp 95–100

Cartolari R, Scarfi GB, Boni S (1996) La TC con carico assiale nella instabilita del rachide lombo-sacrale. Rivista di Neuroradiologia 9:147–155

Danielson B, Willen J (2001) Axially loaded magnetic resonance imaging of the lumbar spine in asymptomatic individuals. Spine 26:2601–2601

Danielson BI, Willen J, Gaulitz A et al. (1998) Axial loading of the spine during CT and MR in patients with suspected lumbar spinal stenosis. Acta Radiol 39:604–611

Depuis PR, Yung-Hing K et al. (1985) Radiologic diagnosis of degenerative lumbar spine instability. Spine 10:262–276

Graf H (1992) Instabilite vertebrale lombaire: diagnostic, nouvelle tecnique de traitment par stabilisation souple. La Revue de Medecine Orthopedique 28:15–19

Granata KP, Marras WS (2000) Cost-Benefit of muscle cocontraction in protecting against spinal instability. Spine 25:1398-14042001; 28 (5) 513–518

Hazlett JW, Kinnard P (1982) Lumbar apophyseal process excisions and spinal instability. Spine 7:171–176

Hiwatashi A, Danielson B, Moritani T et al. (2004) Axial loading during MR imaging can influence treatment decision for symptomatic spinal stenosis. Am J Neuroradiol 25:170–174

Ishihara H, Matsui H, Osada R et al. (1997) Facet joint asymmetry as a radiologic feature of lumbar intervertebral disc herniation in children and adolescents. Spine 22:2001–2004

Ito M, Tadano S, Kaneda K (1993) A biomechanical definition of spinal segmental instability taking personal and disc level differences into account. Spine 15: 2295–2304

Kaech DL (1995) Lumbar disc herniation, spinal stenosis and segmental instability: role of diagnostic imaging. Rivista di Neuroradiologia 8[Suppl 1]:99–109

Kirkaldy-Willis WH, Farfan HF (1982) Instability of the lumbar spine. Clin Orthop 165:110–123

Knutsson F (1944) The instability associated with disk degeneration in the lumbar spine. Acta Radiol 25:593–609

Krag M, Seroussi RE et al. (1987) Internal displacement distribution from in vitro loading ofd human thoracic and lumbar spine motion segments: experimental results and theoretical predictions. Spine 12:1001–1007

Kramer J (1990) Intervertebral disc desease. Georg Thieme Verlag, Stuttgart

Lin HS (1978) Mechanical response of lumbar intervertebral joint under physiological (complex) loading. J Bone Joint Surg 60:41–55

Marchetti PG, Bartolozzi P (1986) Spondylolisthesis: classification and etiopathogenesis. In: Progress in spinal pathology: spondylolisthesis II. Italian Scoliosis Research Group, Bologna

Nachemson A (1960) Lumbar intradiscal pressure: experimental studies on post-mortem material. Acta Orthop Scand Suppl 43:1–104

Nachemson AL (1991) Instability of the lumbar spine: pathology, treatment, and clinical evaluation. Neurosurg Clin North Am 2:785–790

Nachemson A, Elfstrom G (1970) Intravital dynamic pressure measurements in lumbar discs. A study of common movements, maneuvers and exercises. Scan J Rehab Med 1:1–40

Nachemson AL, Schultz AB, Berkson MH (1979) Mechanical properties of human lumbar spine motion segments: influence of age, sex, disc level and generation. Spine 4:1–8

Nowiki BH, Shiwei Y et al. (1990) Effect of axial loading on neural foramina and nerve roots in the lumbar spine. Radiology 176:433–437

Olsson TH, Selvik G, Wilner S (1977) Mobility in the lumbosacral spine after fusion with the aid of Roentgen stereophotogrammetry. Clin Orthop 129:181–190

Panjabi MM, White AA (1990) Clinical biomechanics of the spine,, 2nd ed. Lippincott, Philadelphia, 1990

Panjabi MM, Krag MH, Goel VK (1981) A technique for measurement and description of three dimensional six degree of freedom of a body joint with an application to the human spine. J Biomech 14:447–460

Smith TJ (1991) In vitro spinal biomechanics. Experimental methods and apparatus. Spine 10:1204–1210

Smith TJ, Fernie GR (1991) Functional biomechanics of the spine. Spine 10:1197–1203

Stockes IA, Wilder DG et al. (1981) Assessment of patients with low back pain by biplanar radiographic measurement of intervertebral motion. 1980 Volvo award for spine research. Spine 6:233–240

Trasimeni G, Di Biasi C, Melone A et al. (2001) Utilizzo dell'axial loader nello studio della colonna lombosacrale: osservazioni preliminari. Rivista di Neuroradiologia 14:216–221

Wood KB, Popp CA et al. (1994) Radiographic evaluation of instability in spondylolisthesis. Spine 19:3–10

Yang KH, King AL (1984) Mechanism of facet load transmission as an hypothesis of low back pain. Spine 9:557–565

Osteoporosis – Insufficiency Fractures

10

Menno Maes

CONTENTS

10.1 Introduction

Osteoporosis, or literally translated "bone (osteo) that is porous (porosis)", is defined as "a systemic skeletal disorder characterized by compromised bone strength predisposing to an increased risk of fracture" (NIH 2000).

M. Maes, MD
Department of Radiology, Sint-Vincentius Hospital, Sint-Vincentiusstraat 20, 2018 Antwerp, Belgium

Osteoporosis is increasingly recognised as a major healthcare problem. Since it is mainly a disease of the elderly, and given the continuous aging of the population, it will affect the lives of a growing number of individuals. This is not so much because of the disease itself but above all because of the complications involved. Fractures of osteoporotic bones, especially femoral neck fractures and vertebral body insufficiency fractures, are a cause of increased mortality, increased morbidity, decreased mobility and a reduced quality of life. In addition to this personal detriment there is also a socioeconomic impact (increased healthcare cost).

Therefore, there is need for diagnostic modalities for screening and early detection of osteoporosis, assessment of complication risk, detection of complications and monitoring treatment. Diagnostic imaging plays an important role here.

10.2 Bone Anatomy and Physiology

10.2.1 Bone Structure

Bones are the hardest structures of the human body and provide the framework that supports the body. On sectional examination any bone is composed of two kinds of tissue. The exterior layer is dense in texture, like ivory, and is termed compact bone or cortical bone. The interior consists of slender fibres and lamellae, which join to form a reticular structure. This is called cancellous, spongy or trabecular bone. These two types of bone differ in porosity and microstructure. Cortical bone is much denser with a porosity ranging between 5% and 10%. Trabecular bone is much more porous with porosity ranging anywhere from 50% to 90%.

KEY-POINTS

- Definition of osteoporosis:
  - Systemic skeletal disorder characterized by compromised bone strength, predisposing to increased risk of fracture
- Radiography: insensitive in early stage
  - Radiolucency
  - Cortical thinning
  - Deformation of the vertebral bodies. However, conventional spine of osteoporosis
- Dual-energy X-ray absorptiometry (DEXA):
  - Best method for assessing bone mineral density (BMD)
  - Used for determining when therapy is indicated
  - Used for monitoring if an agent is therapeutically effective or not
  - T-score between -1 and -2.5 is consistent with osteopenia, and a T-score lower than -2.5 is classified as osteoporosis
  - Z-score < –1 means that an individual has a substantially increased risk of sustaining an osteoporotic fracture
- Vertebral insufficiency fractures:
  - Frequent complication in patients with low BMD/osteoporosis
  - Routine spine X-rays have a high false-negative rate
  - Semi-quantitative method (Genant):
    - *classified* as wedge, biconcave, or crush, depending on whether the height reduction is most in the anterior, middle, or posterior part of the vertebral body
    - *graded* as mild, moderate or severe
  - MDCT: sagittal reformats
    - cortical disruption, bone impaction and a retropulsed bony fragment at the superoposterior edge of the vertebral body favour the diagnosis of an acute insufficiency fracture
  - Additional imaging studies:
    - to determine the age of the fracture (MRI and/or bone scintigraphy)
    - to differentiate osteoporotic (benign) insufficiency fractures from malignant fractures, especially in the acute and subacute stage (MRI)
    - FDG-PET may have potential value for differentiation between osteoporotic and pathological vertebral fractures
  - CT-guided biopsy if findings on other imaging techniques are equivocal

Compact bone consists of closely packed osteons or haversian systems. The osteon consists of a central canal called the Haversian (osteonic) canal, which is surrounded by concentric rings (lamellae) of matrices. Between the rings of matrices, the bone cells (osteocytes) are located in spaces called lacunae. Small channels (canaliculi) radiate from the lacunae to the Haversian canal to provide passageways through the hard matrix. In compact bone, the Haversian systems are packed tightly together to form what appears to be a solid mass. The Haversian canals contain blood vessels that are parallel to the long axis of the bone. These blood vessels interconnect, by way of perforating canals (Volkmann's canals), with vessels on the surface of the bone. Haversian canals are important for nutrition, growth and repair of bone.

Trabecular bone is built almost entirely of extracellular substances (the matrices), consisting of calcium and phosphorus (which form the mineral salt hydroxyapatite) and the protein collagen. Osteoblasts deposit the matrices in the form of thin sheets which are called lamellae and that form a mesh-like structure. The spaces of this mesh-like structure contain blood vessels and bone marrow. Blood vessels interconnect via small canaliculi. Trabecular bone is made of primary and secondary trabeculae. The primary trabeculae are also known as stress trabeculae and are found along lines of stress. Secondary trabeculae are found perpendicular or oblique to the primary or stress trabeculae.

10.2.2 Bone Turnover

Bone is tissue that is constantly being renewed and remodelled through the bone turnover cycle, which is carried out by the bone cells.

Cortical bone represents 75% of the bone mass in the body, trabecular the remaining 25%. The surface-to-volume ratio is much higher in trabecular than cortical bone and accordingly bone remodelling has a greater effect on trabecular bone. Thus, bone remodelling has an annual turnover rate of about 25% in trabecular and 2%–3% in cortical bone. Adults renew their entire skeleton every 7–10 years.

There are two different types of bone cells (osteocytes) responsible for this bone remodelling; the osteoblasts which are responsible for bone formation and the osteoclasts which are responsible for bone resorption. The osteoclasts remove the mineral compound and protein matrix from the bone, in a one stage process, assisting in the breakdown. The resulting cavity on the surface is then refilled by the action of the osteoblasts which assist bone formation. This occurs in two stages. Firstly the osteoblasts produce collagen fibres and other components of the matrix, which becomes the osteoid, and secondly they harden the matrix by encouraging the deposition of minerals on to the protein framework to form new bone.

As a consequence of the bone turnover cycle, bones are vulnerable to disease, the most prevalent disease being osteoporosis. Moreover, the actions of osteocytes are under hormonal control. The hormones involved include growth hormone, oestrogen, testosterone, adrenal hormone, parathyroid hormone, thyroid hormone, and thyrocalcitonin. This has great significance when considering the risk factors and treatments for osteoporosis.

10.3 Epidemiology and Aetiology

With aging of the population there are an increasing number of people suffering from osteoporosis. It is estimated that 10 million individuals already have osteoporosis in the US, and 18 million more have a low bone mass, placing them at increased risk for this disorder (NIH 2000). For women it has been estimated that approximately 20% will have osteoporosis at the age of 50, 30% at the age of 70 and 40% at the age of 80 (Kanis et al. 1994).

Although generally considered a disease affecting only females, new insights show that osteoporosis should no longer be considered age- or gender-dependent (NIH 2000).

Osteoporosis can be characterised as either primary or secondary, depending on the absence or presence of an underlying disease as a cause of bone resorption.

Primary osteoporosis is the result of bone loss occurring during aging, or of sub-optimal bone growth during childhood and adolescence (NIH 2000). So, individuals can develop osteoporosis without accelerated bone loss, if at skeletal maturity (which occurs between the ages of 25 and 35) the peak bone mass does not reach the level of the normal population.

Primary osteoporosis is usually generalized and thus affects the entire skeleton. Primary osteoporosis due to aging is often referred to as "senile osteoporosis". The cause of senile osteoporosis is multifactorial with an important role played by hormonal influences. It is often seen in postmenopausal woman (hence "postmenopausal osteoporosis") due to deprivation of oestrogen. Because of this, women show an earlier onset and more profound manifestation of the disorder than men. Primary osteoporosis can be encountered in women as young as 45 years, but is rarely seen in men below 65 years (Quek and Peh 2002). Other contributing factors include: genetic predisposition, environmental factors such as calcium intake during childhood, physical activity and patient constitution. Thin individuals generally have lower bone mineral density than heavier individuals (Liggett and Reid 2000). In women 70% of all osteoporosis is considered to be primary, with the vast majority of this due to postmenopausal oestrogen deficiency (Caplan et al. 1994). In men, however, only 46% of osteoporosis sufferers have no known predisposing illness (Baillie et al. 1992).

Many clinical conditions have been associated with osteoporosis (Table 10.1). As mentioned, osteoporosis secondary to an underlying disease is referred to as secondary osteoporosis.

10.4 Imaging of Osteoporosis

10.4.1 Conventional Radiography

Irrespective of aetiology, the main radiographic features of osteoporosis of the spine are: (1) increased radiolucency of vertebrae, (2) cortical thinning and

Table 10.1. Risk factors for osteoporosis

Strongest risk factors	Female sex Age >60 years Family history of osteoporosis
Other risk factors	Caucasian origin Early menopause Low BMI Smoking Sedentary lifestyle Long term corticosteroid usage Underlying diseases Anorexia nervosa Chronic liver disease Celiac disease Hyperparathyroidism Inflammatory bowel disease Male hypogonadism Renal disease Rheumatoid arthritis Vitamin D deficiency Prostate carcinoma Breast carcinoma

(3) deformation of vertebral bodies (Figs. 10.1 and 10.2) (Quek and Peh 2002).

Increased radiolucency, or so-called osteopenia, is the result of resorption of bone trabeculae, a process in which secondary (horizontal) trabeculae are affected earlier than primary (vertical) trabeculae in the course of the disease. Therefore, vertical striations can be seen in the vertebral bodies.

Cortical thinning is due to osseous resorption of the cortex, mainly occurring at the endosteal side, with concomitant scalloping of the inner cortical margin. Because of the loss of adjacent bone trabeculae the cortex remains clearly visible. At the vertebral bodies this feature is referred to as "picture-framing".

Deformation of vertebrae can be recognized as concavity of the vertebral end plates (so-called fish vertebrae), loss of parallelism of endplates, or as height reduction of vertebral bodies due to insufficiency fractures.

Conventional spine radiography is relatively insensitive in detecting early-stage osteoporosis, because a substantial bone loss (approximately 30%) must have already occurred before radiographic detection is possible (Harris and Heaney 1969). Moreover, radiographic assessment of bone density is subjective and made difficult by overlying soft tissues and technical factors (image penetration). For more advanced stages of the disease, however, conventional radiography can provide a rough estimation of bone loss, and correlation with dual energy X-ray absorptiometry is the best if looked at at the level of the third lumbar vertebra (Yuan et al. 1998).

10.4.2 Dual-Energy X-Ray Absorptiometry (DEXA)

Dual-energy X-ray absorptiometry (DEXA) is currently still considered the best method for assessing bone mineral density (BMD), and hence for diagnosing osteoporosis. The technique is simple and non-invasive, equipment is widely available and radiation exposure is limited (Njeh et al. 1999).

The fundamental principle behind DEXA is the measurement of the transmission through the body of X-rays of two different photon energies. Because the attenuation coefficient differs with atomic number and photon energy, measurement of the transmission factors at two energies enables the areal density (mass per unit projected area in g/cm^2) of

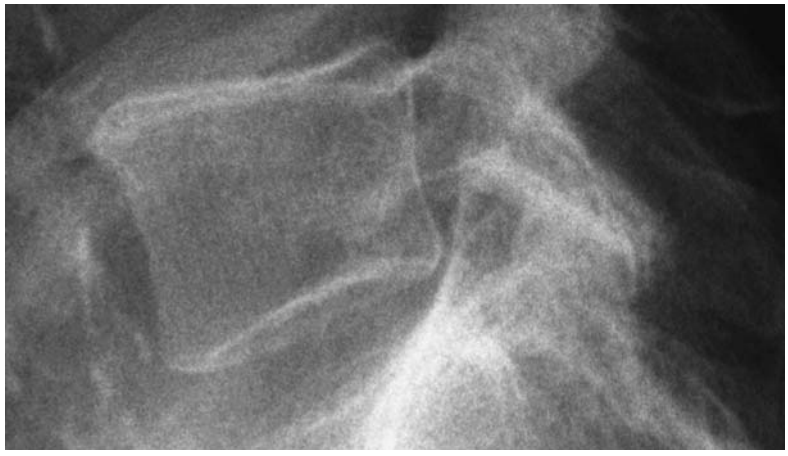

Fig. 10.1. Lateral X-ray of the 5th vertebra shows increased lucency, cortical thinning and vertical striations at the vertebral body. These findings are suggestive for osteoporosis

Fig. 10.2. Lateral X-ray of the lumbar spine shows increased lucency, cortical thinning and vertical striations at the vertebral bodies. The vertebral endplates have lost their parallelism

two different types of tissue to be inferred, namely bone mineral and soft tissue.

According to the recommendations of the World Health Organisation (WHO 1994) the diagnosis of osteoporosis based on BMD can be made using a so-called T-score (Table 10.2), that is calculated by taking the difference of a patient's measured BMD and the mean BMD in healthy young adults, relative to the young adult population standard deviation (SD). These numbers are matched for gender and ethnic group.

T-score = (measured BMD – young adult mean BMD) / young adult SD

Such a T-score indicates the difference between the patient's measured BMD and the ideal peak bone mass achieved by a young adult (Heaney et al. 2000). A negative T-score means that either the patient failed to achieve the optimum young adult BMD or has subsequently lost bone mass due to the effects of ageing or disease (Blake and Fogelman 2002). A T-score between –1 and -2.5 is consistent with osteopenia (Fig. 10.3), and a T-score lower than –2.5 is classified as osteoporosis (Fig. 10.4).

Alongside the T-score, another useful way of expressing BMD measurements is by using Z-scores.

Z-score = (measured BMD – age matched mean BMD) / age matched SD

Like the T-score, the Z-score is expressed in units relative to the population's SD. However, instead of comparing the patient's BMD with the young adult mean, it is compared with the mean BMD expected for the patient's peers (e.g., for a healthy normal subject matched for age, gender and ethnic origin) (Blake and Fogelman 2002).

A Z-score is not useful to diagnose osteoporosis, but it expresses the patient's fracture risk compared to its peers (the lower the score, the higher the risk). A Z-score < –1 means that an individual has a substantially increased risk of sustaining an osteoporotic fracture (Blake and Fogelman 2002).

DEXA measurements can be carried out at the peripheral skeleton (forearm, hand or heel). This is referred to as peripheral DEXA (pDEXA). Clinically more important, however, are DEXA measurements of the axial skeleton (spine, hip), because fractures at these sites can cause a substantial impairment of quality of life, morbidity and mortality (Blake and Fogelman 2002). Hip BMD measurements have been shown to be the most reliable way of evaluating the risk of hip fracture, and the spine is regarded as the optimum site for monitoring treatment response (Cummings et al. 1993, Eastell 1998).

10.4.3 Computer Tomography

CT features of spine osteoporosis are similar to those seen on conventional radiology (Fig. 10.5). First of all there is an overall decrease in the density of trabecular bone. The lower density of trabecular bone is in stark contrast to the higher density of cortical bone. This is best appreciated at the vertebral bodies. Secondly, vertical striations can be seen in the vertebral body, similar to the vertical striations seen on conventional radiographs. Thirdly, in osteoporosis there is thinning of the vertebral cortex throughout the whole spine (Ritzel et al. 1998). Moreover, deformity of endplates as the result of insufficiency fractures is easily detected on sagittal reformations of a multislice CT dataset.

Table 10.2. WHO recommendations for the definitions of osteoporosis and osteopenia

Terminology	T-score definition
Normal	T ≥ –1.0
Osteopenia	–2.5 < T < –1.0
Osteoporosis	T ≤ –2.5
Established osteoporosis	T ≤ –2.5 in the presence of one or more insufficiency fractures

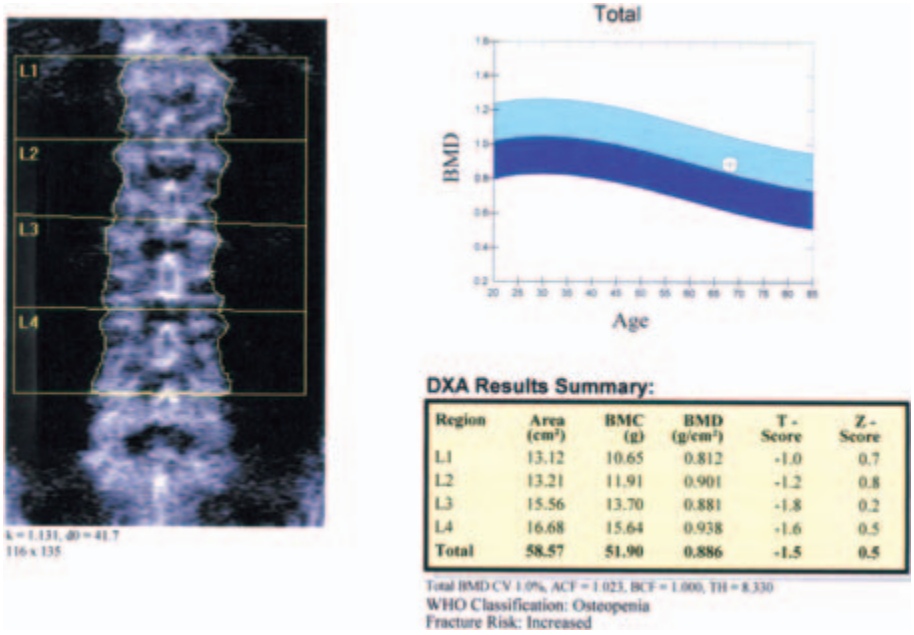

Fig. 10.3. DEXA examination of the lumbar spine. Mean T-score is –1.5. Diagnosis: osteopenia

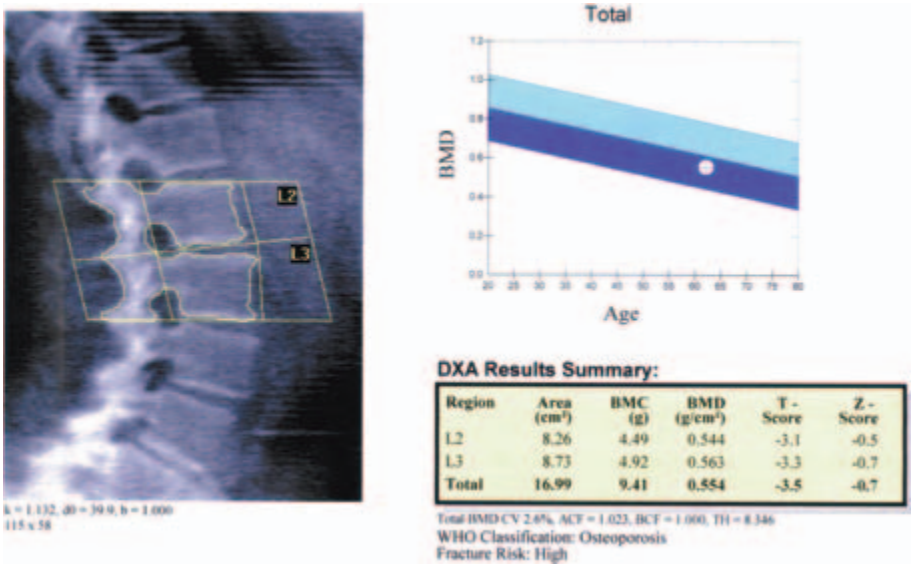

Fig. 10.4. DEXA examination of the lumbar spine. Mean T-score is –3.5. Diagnosis: osteoporo-

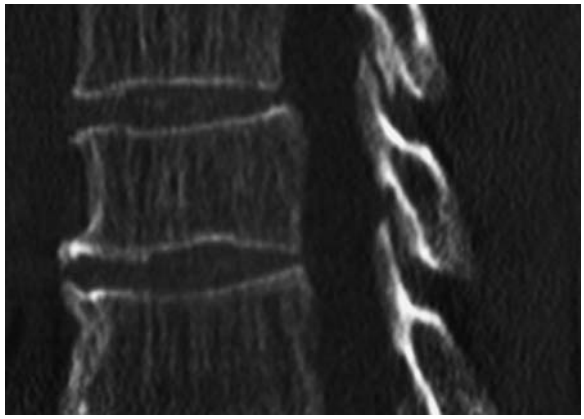

Fig. 10.5. Sagittal reformation of a multislice CT dataset showing decreased bone density, cortical thinning and vertical striations at the vertebral bodies

By using special software, conventional CT scanners can be used for BMD measurement. This is referred to as quantitative computed tomography (QCT). QCT is particularly useful to measure BMD at the spine. Correlation with BMD values obtained with DEXA is high and significant (Sosa et al. 1998). The main advantage of QCT is that it can measure cortical and trabecular bone separately. Indeed, cortical BMD is a better predictor for fracture risk than is trabecular BMD (Andresen et al. 1999). Disadvantages are the relatively high radiation dose involved (Njeh et al. 1999) and the high cost of CT scanning equipment.

10.4.4 Magnetic Resonance Imaging

The diagnosis of non-complicated osteoporosis can not be made based upon the appearance of bone marrow on standard T1- and T2-weighted images. Signal intensities on T1 and T2 are mainly the reflection of bone marrow quality (cellular marrow versus fatty marrow), which can be altered by age or the presence of an underlying haematopoietic disorder. On the other hand osteoporosis is a disease generally affecting the elderly, so most osteoporotic spines will present with diffuse high signal intensity of bone marrow on T1- and T2-weighted images as the result of age-related fatty degeneration of bone marrow (Ricci et al. 1990). In cases of complicated (established) osteoporosis with deformed and collapsed vertebral endplates, the diagnosis of osteoporosis is more obvious.

Although still experimental, Lin et al. (2000) reported that MR spectroscopy of spine vertebra could be helpful in the diagnosis of osteoporosis, by showing an increase in the lipid-to-water ratio. Shih et al. (2004) reported a decrease in marrow perfusion on perfusion MR imaging, with significant correlation between the peak enhancement ratio of vertebral bone marrow and BMD.

Furthermore, on diffusion weighted imaging accumulation of fatty bone marrow associated with osteoporosis has been reported to be reflected by a decrease in extravascular diffusion and apparent diffusion coefficient (Yeung et al. 2004).

Further investigation is needed to determine whether these bone marrow changes on MR spectroscopy, perfusion MR imaging and diffusion MR imaging are truly due to osteoporosis and not age related phenomena.

In literature some reports focus on the use of quantitative MR for measuring BMD, using the MR relaxation time T2 of protons (Majumdar and Genant 1995; Machann et al. 2001). The value of this technique in clinical practice, however, is still unclear.

10.4.5 Scintigraphy

There is no role for bone scintigraphy in the diagnosis of osteoporosis itself, but it can provide useful information in cases of complicated osteoporosis by confirming whether a fracture has occurred, determining the age of the fracture or identifying unsuspected fractures (Hain and Fogelman 2002).

10.5 Complications

10.5.1 Insufficiency Fractures

10.5.1.1 Prevalence

Vertebral insufficiency fractures are a frequent complication of osteoporosis. It is estimated that in the US vertebral insufficiency fractures occur in about 25% of Caucasian females over age 50, and in Europe in 20% (Melton et al. 1993; O'Neill et al. 1996).

Moreover, the proportion of females with fractures is increasing with age. By the age of 75 more than one in three Caucasian females has at least one fracture (Melton et al. 1993).

In other ethnic groups the prevalence of vertebral insufficiency fractures is lower. They are found in only 10% of Hispanic-American and Japanese-American females over the age of 50 (Bauer and Deyo 1987; Ross et al. 1991), and estimates suggest that vertebral fractures are even less common for African-American men and women, with a prevalence of only a few percent (Jacobsen et al. 1992).

10.5.1.2 Fracture Risk

It is well known that the risk for a future osteoporotic fracture is increased for patients with low BMD.

In addition, the existence of an earlier vertebral fracture increases the risk of subsequent fractures due to osteoporosis, irrespective of a person's BMD (see Table 10.1). This has been well established by several authors (Ross et al. 1991, 1993; Davis et al. 1999; Melton et al. 1999). Not surprisingly, the presence of multiple vertebral fractures is associated with even higher risk. A patient with low BMD and two or more fractures has 75 times the risk of a patient with high BMD and no fractures.

10.5.1.3 Imaging of Vertebral Insufficiency Fractures

10.5.1.3.1 Conventional Radiography

The diagnosis of a vertebral fracture is often difficult to make on clinical grounds only. Therefore, suspected patients are often referred to the radiology department for spine X-rays, despite the high false-negative rate (27%–45%) (Delmas et al. 2001) of this imaging technique. To improve sensitivity of the examination and uniformity of radiology reports, in the past several quantitative and semi-quantitative techniques have been developed, of which the method proposed by Genant et al. (1993) is the most applicable in general practice.

When evaluating imaging studies in which the vertebrae are included (not just spine radiography but also lateral chest radiography), the following questions should be resolved (Lenchik et al. 2004):

- Is there a fracture?
- What is the age of the fracture?
- Can it be a pathologic fracture?

A vertebral fracture should be diagnosed when there is loss of height of more than 20% of the anterior, middle, or posterior dimension of the vertebral body. Vertebral fractures can be classified and graded according to the semi-quantitative method as proposed by Genant et al. (1993) (Figs. 10.6 and 10.7a). Following this method vertebral fractures are classified as wedge, biconcave, or crush fractures, depending on whether the height reduction is most in the anterior, middle, or posterior part of the vertebral body.

Moreover, following the same method, vertebral body fractures can be graded as mild (grade 1, 20%–25% height reduction), moderate (grade 2, 26%–40% height reduction) or severe (grade 3, >40% height reduction).

On conventional radiographs alone, it is often difficult to determine the age of the fracture, unless previous radiographs are available for comparison. Acute fractures present with cortical disruption or impaction of the trabeculae (Fig. 10.7b). When cortical disruption is not present and the vertebra appears equal in density to the neighbouring vertebrae, the fracture is probably of older age. In many

Fig. 10.6. X-ray of the thoracolumbar region: old grade II biconcave fracture of the 12th thoracic vertebra and old grade III wedge fracture of the 11th thoracic vertebra

a

b

Fig. 10.7a,b. X-ray of the lumbar spine. **a** Acute grade II wedge fracture of the 3rd lumbar vertebra. **b** Magnification showing trabecular impaction and cortical disruption

instances, however, additional imaging studies, such as MDCT, MRI or bone scintigraphy, are necessary to determine the age of the fracture. In any case, all fractures, even old ones, should be reported, because they increase the risk of subsequent fractures.

It is important to acknowledge the fact that not all vertebral fractures are due to osteoporosis. In particular, previous trauma, infection, and an underlying tumour must be excluded. The presence of sclerotic or osteolytic bone lesions suggests a malignant aetiology. An intravertebral vacuum cleft in a collapsed vertebra is indicative of avascular necrosis and suggests a benign aetiology (Malghem et al. 1993). If a tumour is suspected, further work-up with CT and/or MRI is mandatory.

It is also important to realise that not every deformed vertebra is a vertebral fracture caused by osteoporosis. As a radiologist you should become familiar with diagnostic pitfalls. Poor technique in which the lateral projection is really an oblique projection may lead to the vertebrae appearing fractured. Similar pseudo fractures may be seen on lateral projections in patients with scoliosis. Fractures can also be mimicked by other abnormalities in vertebral shape, e.g. Cupid's bow deformity, limbus vertebra, Schmorl's nodes (Scheuermann's disease) and H-shaped vertebrae (sickle cell disease or Gaucher's disease) (Lenchik et al. 2004).

10.5.1.3.2 Magnetic Resonance Imaging

When a vertebral fracture is suspected, the main purpose of MR is to differentiate osteoporotic (benign) insufficiency fractures from malignant fractures, especially in the acute and subacute stage, when bone scintigraphy is unable to do so. The performed MR examination should help the radiologist answer the following questions:

- Is there a fracture (or more than one fracture)?
- What is the cause of the fracture (benign vs. malignant fracture)?
- Is the fracture old or acute/subacute?
- Is there an immediate risk for nearby structures (nerves, myelum, etc.)

The imaging protocol used (Table 10.4) should therefore contain sequences that deliver good anatomical detail and sequences that are sensitive for bone marrow changes (particularly oedema). Imaging should be performed in at least two planar directions, and if a tumour is suspected gadolinium

Table 10.3. Increase in risk for subsequent fractures in case of existing vertebral fractures (Ross et al. 1991, 1993; Davis et al. 1999; Melton et al. 1999)

Site of subsequent fracture	Increase in risk due to preceding vertebral fracture
Spine	4–5 x
Hip	2 x
Any	3 x

enhanced images should be obtained to determine tumour extension.

Osteoporotic Compression Fractures

First of all, it is very important to be aware that the presence of multiple collapsed vertebrae in a patient suggests neither a benign nor a malignant aetiology (Rupp et al. 1995). Not infrequently are both benign and malignant compression fractures present in the same patient. Therefore, the morphological and signal intensity criteria described in this chapter should be applied to each collapsed vertebra separately. MR features of osteoporotic and malignant fractures are resumed in Table 10.5.

The signal intensity of vertebral bone marrow in a benign compression fracture differs in accordance with the age of the fracture.

In the acute stage (Figs. 10.8 and 10.9) osteoporotic fractures (<2 months old) usually present with a focal band-like area of low signal intensity bordering the fractured endplate on T1-weighted images. Near the opposite endplate there is generally an area of normal signal intensity of variable shape (Cuenod et al. 1996; Jung et al. 2003). The size of the low signal intensity area seen on T1-weighted images in acute compression fractures remains unchanged for 2–4 months and then gradually returns to normal. The time to complete normalisation of the marrow signal is variable (Yuh et al. 1989; Yamato et al. 1997).

Normal marrow preservation of the compressed vertebral body on T1 imaging is consistent with an old osteoporotic fracture (Rupp et al. 1995).

On T2-weighted images, a collapsed vertebra is isointense compared to neighbouring non-collapsed vertebrae (Cuenod et al. 1996). An area of low signal corresponding to the fracture line or trabecular impaction can also be seen on T2-weighted images (Palmer et al. 1999).

On STIR images, the presence of focal, linear or triangular areas of high signal intensity, equal to the signal of CSF, adjacent to the fractured vertebral endplate ("fluid sign") (Fig. 10.8) is an additional feature of acute and subacute osteoporotic fractures and is not often seen in metastatic fractures (Baur et al. 2002).

On contrast-enhanced T1-weighted images, there is partial or complete equalization of the marrow signal of the acutely collapsed vertebra with that of neighbouring non-collapsed vertebrae. This is called "return to normal signal intensity" (Cuenod et al. 1996).

Morphologically, an insufficiency fracture has the same features as encountered on conventional radiographs: height reduction of the vertebral body, loss of parallelism of endplates and deformity of

Table 10.4. Proposed MR imaging protocol

	Plane	Sequence
Before gadolinium administration	Sagittal	TSE T1
	Sagittal	TSE T2
	Sagittal	STIR
	Axial	GRE T2* or TSE T2
After gadolinium administration	Sagittal	TSE T1
	Axial	TSE T1 (+/– fat sat)
Optional	Sagittal	GRE out-of-phase
	Sagittal	Subtraction images
	Sagittal	Diffusion weighted images
	Sagittal	Perfusion images

Table 10.5. Differential diagnosis of osteoporotic and malignant fractures

Feature	Old benign fracture	Acute/subacute benign fracture	Malignant fracture
SI on T1	Iso	Low signal intensity band	Low
SI on T2	Iso	Iso/high	Iso/high
SI on STIR	Low	High Fluid sign	High No fluid sign
Deformation of posterior wall	Posterosuperiorly located	Posterosuperiorly located	Whole posterior wall
Involvement of pedicles/posterior elements	No	Usually not	Often
Soft tissue mass	No	Usually not	Often
Abnormal enhancement	No	Usually not	Usually
Diffusion	Normal	Normal/increased	Restricted
Perfusion	Low peak	High peak Rapid wash in Second slower-rising slope	High peak Rapid wash in Early wash out

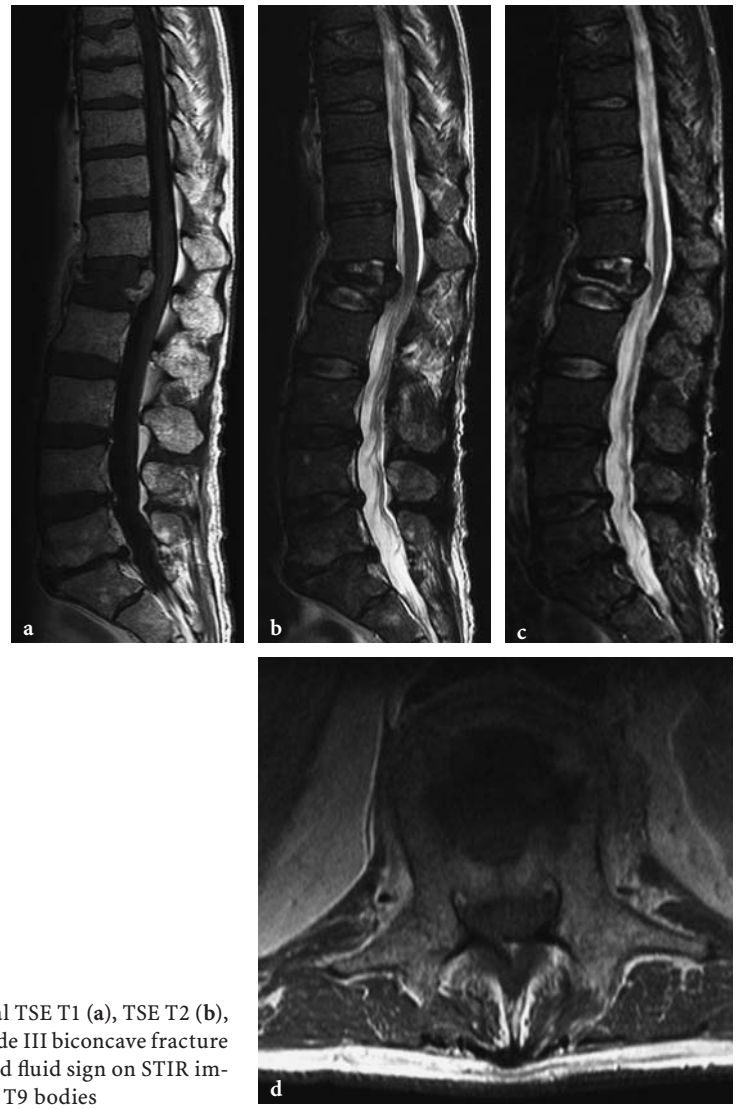

Fig. 10.8a–d. MRI thoracolumbar spine: sagittal TSE T1 (**a**), TSE T2 (**b**), STIR (**c**) and axial TSE T1 images (**d**). Acute grade III biconcave fracture of L1 with retropulsion of the posterior wall and fluid sign on STIR images. Note also the old fractures of the T8 and T9 bodies

endplates. The lumbar pedicles and posterior elements are usually not affected. One morphological feature that is highly specific for a benign fracture is the presence of a retropulsed fragment at the posterior wall of the affected vertebral body (usually posteriorly and superiorly located), that bulges into the spinal canal (Figs. 10.8 and 10.10). This finding is highly specific (100%) but has an extremely low sensitivity (16%) (Cuenod et al. 1996; Jung et al. 2003).

Malignant Compression Fractures

On T1-weighted images a malignant compression fracture shows replacement of bone marrow with low signal intensity (Rupp et al. 1995; Cuenod et al. 1996). On T2-weighted images signal intensity in the collapsed vertebra is either normal or high. Marrow oedema is most easily detected on STIR images. Bone marrow displacement in malignant fractures is usually diffuse and less commonly nodular or multifocal. Gradient echo out-of-phase images are very sensitive in detecting focal bone lesions.

On contrast-enhanced images abnormal enhancement is seen in the affected vertebra(e). The enhancement effect is mostly marked and inhomogeneous with diffuse or patchy distribution (Cuenod et al. 1996; Shih et al. 1999).

Morphological features suggestive of malignancy include a convex bulge involving the whole of the posterior cortex of the vertebral body, involvement of the pedicles and the presence of an epidural and/or paraspinal soft tissue mass (Fig. 10.11) (Yuh et al. 1989; An et al. 1995; Rupp et al. 1995; Cuenod et al. 1996; Baker et al. 1990; Shih et al. 1999).

The presence of an epidural mass is sensitive (80%) and highly specific (100%) for a malignant fracture. Convexity of the whole posterior cortex of the vertebra and pedicular involvement have respective sensitivities and specificities of 70% and 94%, and 80% and 94% (Cuenod et al. 1996).

If findings on routine images are not completely conclusive for distinction between an acute benign or pathologic vertebral compression fracture, then

Fig. 10.9a–c. MRI lumbar spine: sagittal TSE T1 (**a**), TSE T2 (**b**) and STIR (**c**) images revealing an old grade I wedge fracture of L4 and an acute grade III biconcave fracture of L1. The signal intensities of bone marrow in the L4 body are similar to that of the neighbouring vertebrae. This is in contrast to the band-like area of low signal intensity (T1) and the edema in the body of L1 (STIR)

Fig. 10.10a–e. Lateral Spine X-ray (**a**) and MRI of the lumbar spine: sagittal TSE T1 (**b**), TSE T2 (**c**), STIR (**d**) and GRE out-of- phase (**e**) images. The X-ray shows four osteoporotic fractures. The cortical disruption at the lower endplate of L3, and sclerosis of the upper end plate of L2 and lower endplate of L1 suggest acute fractures. This is confirmed by MRI (low signal bands on T1 in the L1, L2 and L3 bodies; fluid sign on T2 and STIR in the L1 and L3 bodies). GRE out-of-phase images show no focal bone lesions. Note the retropulsed bony fragment at the superior edge of the posterior wall of L2 and L5

Fig. 10.11a–f. MRI lumbar spine: sagittal TSE T1 (**a**), TSE T2 (**b**), STIR (**c**), GRE out-of-phase (**d**), and axial TSE T2 images (**e, f**). Multiple myeloma with tumoral masses at the T9 and L1 bodies and para spinal soft tissues, involvement of the L1 pedicles and pathologic fracturing of L1

diffusion-weighted imaging of the spine might be helpful. Diffusion restriction is indicative for a pathologic fracture, whereas normal or increased diffusion is suggestive for an osteoporotic fracture (Baur et al. 2001; Herneth et al. 2002).

A recent report from Chen et al. (2002) states that perfusion MR imaging is also valuable in the differentiation of benign and malignant vertebral lesions. According to the authors, a time-intensity curve showing rapid contrast wash-in followed by early wash-out has a high positive predictive value (100%) for malignancy, whereas a rapid contrast wash-in with a second slower-rising slope has a high positive predictive value (85.7%) for benign compression fractures. Moreover, metastatic vertebral lesions with or without fracture had a higher peak enhancement percentage and steeper enhancement slope than those of chronic compression fractures, but these parameters were not different as compared to acute compression fractures.

10.5.1.3.3 Computer Tomography

Of all imaging modalities CT is the one best suited for evaluating bone structure (Figs. 10.12–10.14).

A malignant compression fracture on CT frequently shows destruction of the anterolateral or posterior cortical bone, cancellous bone and/or pedicle (Laredo et al. 1995). On the contrary, bone destruction is rare in insufficiency fractures. Cortical disruption and bone impaction occurring with an acute insufficiency fracture, or a retropulsed bony fragment at the superoposterior edge of the vertebral body, favouring the diagnosis of an insufficiency fracture, are easily detected on sagittal reformations of a multislice CT dataset. Paraspinal and epidural masses, which are highly suggestive for malignant fractures, are well depicted on CT.

Additionally, CT-guided biopsy can be useful if findings on other imaging techniques (especially MR) are equivocal.

10.5.1.3.4 Nuclear Imaging

In symptomatic osteoporotic patients bone scintigraphy with Tc-99m HDP may be helpful in elucidating the aetiology of back pain and can have an impact on patient management (Cook et al. 2002). A negative bone scintigraphy rules out a recently occurred osteoporotic fracture, so further examinations can be directed in finding other causes for back pain. If bone scintigraphy shows a hot spot, however, further imaging is necessary to differentiate between for example osteoarthritis, an insufficiency fracture and malignancy.

Preliminary results of a German study showed that positron emission tomography with fluorine-18 deoxyglucose (FDG-PET) may have potential value for differentiation between osteoporotic and pathological vertebral fractures, since a high FDG uptake is characteristic for malignant and inflammatory processes (Schmitz et al. 2002).

10.5.2 Spinal Cord Injury

Although vertebral fractures occur frequently in osteoporosis, there is only seldom an associated spinal cord injury. When neurological injury occurs it has in general a gradual, delayed onset and spontaneous recovery can be expected (O'Connor et al. 2002). Most reports in the literature describe delayed-onset paraplegia after vertebral collapse, but sudden and catastrophic spinal cord injury can occur (O'Connor et al. 2002). Neurological injury is usually the result of deformation of the posterior wall of the fractured body with narrowing of the spinal canal, or due to spinal cord compression by a retropulsed bony fragment (Kaplan et al. 1987).

The risk of spinal cord compression is increased in patients suffering from pre-existing epidural lipomatosis, for example after long term steroid therapy (Andress et al. 2000).

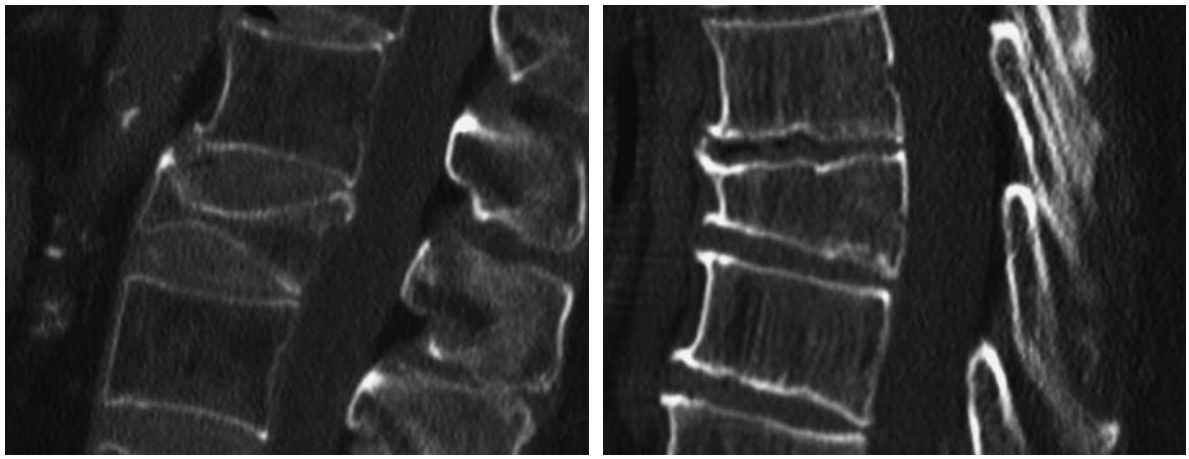

a b

Fig. 10.12a,b. Sagittal reformations of multislice CT datasets: old insufficiency fractures. **a** Old grade III biconcave fracture. **b** Old grade III wedge fracture. For both affected vertebrae cancellous bone structure is similar to that of neighbouring vertebral bodies

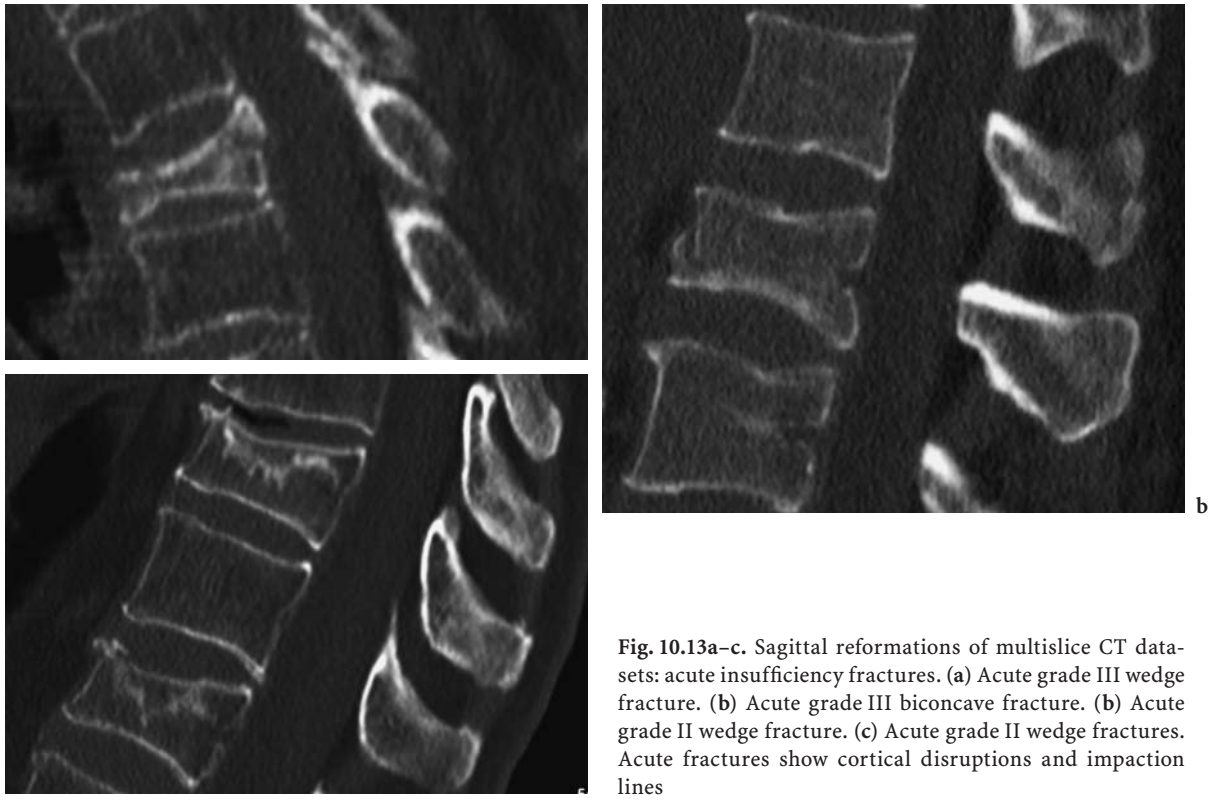

Fig. 10.13a–c. Sagittal reformations of multislice CT datasets: acute insufficiency fractures. (**a**) Acute grade III wedge fracture. (**b**) Acute grade III biconcave fracture. (**b**) Acute grade II wedge fracture. (**c**) Acute grade II wedge fractures. Acute fractures show cortical disruptions and impaction lines

Fig. 10.14. Sagittal reformation of a multislice CT datasets: subacute insufficiency fracture. Sclerosis near the deformed upper endplate indicates fracture healing

10.5.3 Kyphosis and Scoliosis

Multiple vertebral fractures, particularly at the thoracic spine, can result in severe postural deformity due to kyphosis and/or scoliosis. Spinal deformity is associated with decreased mobility and diminished function, especially concerning mobility tasks, like walking, reaching and performing heavy housework (Ryan and Fried 1997). Reduced spinal mobility has a strong negative effect on quality of life (Miyakoshi et al. 2003).

In addition, kyphosis due to osteoporotic fractures is associated with diminished pulmonary function, dyspnoea and ventilatory dysfunction of a restrictive and obstructive type (Di Bari et al. 2004). Reduction of pulmonary function is correlated significantly with clinical and radiological measures of severity of spinal deformation due to osteoporotic fractures (Schlaich et al. 1998). As possible causes of pulmonary dysfunction Culham et al. (1994) mention reduced lung volumes and impaired rib mobility due to thoracic kyphosis.

10.6 Treatment of Osteoporosis and Treatment Monitoring

10.6.1 Medical Treatment

Early recognition and medical treatment of osteoporosis is important, since effective treatment can reduce future fracture risk. Calcium and vitamin D in combination is the accepted baseline treatment for osteoporosis and is also used as a preventive measure (Akesson 2003), particularly because of the low cost of this treatment.

Several additional, more expensive drugs are commercially available, of which the bisphosphonates (risedronate and alendronate) are most effective in reducing the risk of vertebral and non-vertebral fractures. Risedronate has been shown to reduce fracture risk within 1 year in postmenopausal women with osteoporosis and in patients with glucocorticoid-induced osteoporosis. Hormone therapy reduces fracture risk, but the benefits may not outweigh the reported risks. Teriparatide, a recombinant human parathyroid hormone, reduces the risk of new fractures and is indicated for use in patients with severe osteoporosis. Raloxifene has been shown to lower the incidence of vertebral fractures in women with osteoporosis. Calcitonin is reserved for use in patients who cannot tolerate bisphosphonates or hormone therapy (Zizic 2004).

10.6.2 Treatment Monitoring

DEXA is a good method of measuring changes in BMD if performed at 1- to 2-year time intervals. It can be used for determining when therapy is indicated, and if an agent is therapeutically effective or not (i.e., when bone loss occurs despite treatment). The preferred anatomic site for monitoring is the PA spine. The total hip can be used when the spine study is technically invalid (Lenchik et al. 2002).

10.6.3 Surgical and Radiological Treatment

In cases of complicated osteoporosis surgical or radiological treatment (spondylodesis, decompression, vertebroplasty) might be justified.

References

Akesson K (2003) New approaches to pharmacological treatment of osteoporosis. Bulletin of the World Health Organization 81:657–663

An HS, Andreshak TG, Nguyen C, Williams A, Daniels D (1995) Can we distinguish between benign versus malignant compression fractures of the spine by magnetic resonance imaging? Spine 20:1776–1782

Andresen R, Haidekker MA, Radmer S, Banzer D (1999) CT determination of bone mineral density and structural investigations on the axial skeleton for estimating the osteoporosis-related fracture risk by means of a risk score. Br J Radiol 72:569–578

Andress HJ, Schurmann M, Heuck A, Schmand J, Lob G (2000) A rare case of osteoporotic spine fracture associated with epidural lipomatosis causing paraplegia following long-term cortisone therapy. Arch Orthop Trauma Surg 120:484–486

Baillie SP, Davison CE, Johnson FJ, Francis RM (1992) Pathogenesis of vertebral crush fractures in men. Age Ageing 21:139–141

Baker LL, Goodman SB, Perkash I, Lane B, Enzmann DR (1990) Benign versus pathological compression fractures of vertebral bodies: assessment with conventional spin-echo, chemical-shift, and STIR MR imaging. Radiology 174:495–502

Bauer RL, Deyo RA (1987) Low risk of vertebral fracture in Mexican American women. Arch Intern Med 147:1437–1439

Baur A, Huber A, Ertl-Wagner B, Durr R, Zysk S, Arbogast S, Deimling M, Reiser M (2001) Diagnostic value of increased diffusion weighting of a steady-state free precession sequence for differentiating acute benign osteoporotic fractures from pathologic vertebral compression fractures. Am J Neuroradiol 22:366–372

Baur A, Stabler A, Arbogast S, Duerr HR, Bartl R, Reiser M (2002) Acute osteoporotic and neoplastic vertebral compression fractures: fluid sign at MR imaging. Radiology 225:730–735

Blake GM, Fogelman I (2002) Dual energy X-ray absorptiometry and its clinical applications. Semin Musculoskelet Radiol 6:207–217

Caplan GA, Scane AC, Francis RM (1994) Pathogenesis of vertebral crush fractures in women. J R Soc Med 87:200–202

Chen WT, Shih TT, Chen RC, Lo HY, Chou CT, Lee JM, Tu HY (2002) Blood perfusion of vertebral lesions evaluated with gadolinium-enhanced dynamic MRI: in comparison with compression fracture and metastasis. J Magn Reson Imaging 15:308–314

Cook GJ, Hannaford E, See M, Clarke SE, Fogelman I (2002) The value of bone scintigraphy in the evaluation of osteoporotic patients with back pain. Scand J Rheumatol 31:245–248

Cuenod CA, Laredo JD, Chevret S, Hamze B, Naouri JF, Chapaux X, Bondeville JM, Tubiana JM (1996) Acute vertebral collapse due to osteoporosis or malignancy: appearance on unenhanced and gadolinium-enhanced MR images. Radiology 199:541–549

Culham EG, Jimenez HA, King CE (1994) Thoracic kyphosis, rib mobility, and lung volumes in normal women and women with osteoporosis. Spine 19:1250–1255

Cummings SR, Black DM, Nevitt MC, Browner W, Cauley J, Ensrud K, Genant HK, Palermo L, Scott J, Vogt TM (1993) Bone density at various sites for prediction of hip fractures. The Study of Osteoporotic Fractures Research Group. Lancet 341:72–75

Davis JW, Grove JS, Wasnich RD, Ross PD (1999) Spatial relationships between prevalent and incident spine fractures. Bone 24:261–264

Delmas PD, Watts N, Eastell R (2001) Underdiagnosis of vertebral fractures is a worldwide problem. J Bone Miner Res 16[Suppl]:S139

Di Bari M, Chiarlone M, Matteuzzi D, Zacchei S, Pozzi C, Bellia V, Tarantini F, Pini R, Masotti G, Marchionni N (2004) Thoracic kyphosis and ventilatory dysfunction in unselected older persons: an epidemiological study in Dicomano, Italy. J Am Geriatr Soc 52:909–915

Eastell R (1998) Treatment of postmenopausal osteoporosis. N Engl J Med 338:736–746

Genant HK, Wu CY, van Kuijk C, Nevitt MC (1993) Vertebral fracture assessment using a semiquantitative technique. J Bone Miner Res 8:1137–1148

Guyton A (1985) Anatomy and physiology. Saunders College Publishing, Philadelphia

Hain SF, Fogelman I (2002) Nuclear medicine studies in metabolic bone disease. Semin Musculoskelet Radiol 6:323–329

Harris WH, Heaney RP (1969) Skeletal renewal and metabolic bone disease. N Engl J Med 280:303–311

Heaney RP, Abrams S, Dawson-Hughes B, Looker A, Marcus R, Matkovic V, Weaver C (2000) Peak bone mass. Osteoporosis Int 11:985–1009

Herneth AM, Philipp MO, Naude J, Funovics M, Beichel RR, Bammer R, Imhof H (2002) Vertebral metastases: assessment with apparent diffusion coefficient. Radiology 225:889–894

Jacobsen SJ, Cooper C, Gottlieb MS, Goldberg J, Yahnke DP, Melton LJ 3rd (1992) Hospitalization with vertebral fracture among the aged: a national population-based study, 1986–1989. Epidemiology 3:515–518

Jung HS, Jee WH, McCauley TR, Ha KY, Choi KH (2003) Discrimination of metastatic from acute osteoporotic compression spinal fractures with MR imaging. Radiographics 23:179–187

Kanis JA, Melton LJ, Christiansen C, Johnston CC, Khaltaev N (1994) The diagnosis of osteoporosis. J Bone Min Res 9:1137–1141

Kaplan PA, Orton DF, Asleson RJ (1987) Osteoporosis with vertebral compression fractures, retropulsed fragments, and neurologic compromise. Radiology 165:533–535

Laredo JD, Lakhdari K, Bellaiche L, Hamze B, Janklewicz P, Tubianna JM (1995) Acute vertebral collapse: CT findings in benign and malignant non-traumatic cases. Radiology 194:41–48

Lenchik L, Kiebzak GM, Blunt BA (2002) What is the role of serial bone mineral density measurements in patient management? J Clin Densitom 5[Suppl]:29–38

Lenchik L, Rogers LF, Delmas PD, Genant HK (2004) Diagnosis of osteoporotic vertebral fractures: importance of recognition and description by radiologists. AJR Am J Roentgenol 183:949–958

Liggett NW, Reid DM (2000) The incidence, epidemiology and aetiology of osteoporosis. Hospital Pharmacist 7:62–68

Lin CS, Fertikh D, Davis B, Lauerman WC, Henderson F, Schellinger D (2000) 2D CSI proton MR spectroscopy of human spinal vertebra: feasibility studies. J Magn Reson Imaging 11:287–293

Machann J, Raible A, Schnatterbeck P, Lutz O, Claussen CD, Schick F (2001) Osteodensitometry of human heel bones by MR spin-echo imaging: comparison with MR gradient-echo imaging and quantitative computed tomography. J Magn Reson Imaging 14:147–155

Majumdar S, Genant HK (1995) A review of the recent advances in magnetic resonance imaging in the assessment of osteoporosis. Osteoporos Int 5:79–92

Malghem J, Maldague B, Labaisse MA, Dooms G, Duprez T, Devogelaer JP, Vande Berg B (1993) Intravertebral vacuum cleft: changes in content after supine positioning. Radiology 187:483–487

Melton LJ 3rd, Atkinson EJ, Cooper C, O'Fallon WM, Riggs BL (1999) Vertebral Fractures Predict Subsequent Fractures. Osteoporos Int 10:214–221

Melton LJ 3rd, Lane AW, Cooper C, Eastell R, O'Fallon WM, Riggs BL (1993) Prevalence and incidence of vertebral fractures. Osteoporosis Int 3:113–119

Miyakoshi N, Itoi E, Kobayashi M, Kodama H (2003) Impact of postural deformities and spinal mobility on quality of life in postmenopausal osteoporosis. Osteoporos Int 14:1007–1012

NIH [no authors listed] (2000) Osteoporosis prevention, diagnosis, and therapy. NIH Consensus Statement 17:1–45

Njeh CF, Fuerst T, Hans D, Blake GM, Genant HK (1999) Radiation exposure in bone mineral density assessment. Appl Radiat Isot 50:215–236

O'Connor PA, Eustace S, O'Byrne J (2002) Spinal cord injury following osteoporotic vertebral fracture: case report. Spine 27:E413–415

O'Neill TW, Felsenberg D, Varlow J, Cooper C, Kanis JA, Silman AJ (1996) The prevalence of vertebral fracture in European men and women: the European Vertebral Osteoporosis Study. J Bone Miner Res 11:1010–1018

Palmer WE, Suri R, Kattapuram SV (1999) Benign versus malignant vertebral collapse: value of a fracture line on MR images. Radiology 213[Suppl. P]:293

Quek S, Peh WCG (2002) Radiology of osteoporosis. Semin Musculoskelet Radiol 6:197–206

Ricci C, Cova M, Kang YS, Yang A, Rahmouni A, Scott WW Jr, Zerhouni EA (1990) Normal age-related patterns of cellular and fatty bone marrow distribution in the axial skeleton: MR imaging study. Radiology 177:83–88

Ritzel H, Amling M, Hahn M, Maas R, Delling G (1998) Quantitative morphology of vertebral body cortical bone. Building block for noninvasive calculation of fracture threshold in osteoporosis. Radiologe 38:315–320

Ross PD, Davis JW, Epstein RS, Wasnich RD (1991) Pre-existing fractures and bone mass predict vertebral fracture incidence in women. Ann Intern Med 114:919–923

Ross PD, Genant HK, Davis JW, Miller PD, Wasnich RD (1993) Predicting vertebral fracture incidence from prevalent fractures and bone density among non-black, osteoporotic women. Osteoporos Int 3:120–126

Rupp RE, Ebraheim NA, Coombs RJ (1995) Magnetic resonance imaging differentiation of compression spine fractures or vertebral lesions caused by osteoporosis or tumor. Spine 20:2499–2504

Ryan SD, Fried LP (1997) The impact of kyphosis on daily functioning. J Am Geriatr Soc 45:1479–1486

Schlaich C, Minne HW, Bruckner T, Wagner G, Gebest HJ, Grunze M, Ziegler R, Leidig-Bruckner G (1998) Reduced pulmonary function in patients with spinal osteoporotic fractures. Osteoporos Int 8:261–267

Schmitz A, Risse JH, Textor J, Zander D, Biersack HJ, Schmitt O, Palmedo H (2002) FDG-PET findings of vertebral compression fractures in osteoporosis: preliminary results. Osteoporos Int 13:755–761

Shih TT, Huang KM, Li YW (1999) Solitary vertebral collapse: distinction between benign and malignant causes using MR patterns. J Magn Reson Imaging 9:635–642

Shih TT, Liu HC, Chang CJ, Wei SY, Shen LC, Yang PC (2004) Correlation of MR lumbar spine bone marrow perfusion with bone mineral density in female subjects. Radiology 233:121–128

Sosa M, Hernandez D, Estevez S, Rodriguez M, Liminana JM, Saavedra P, Lainez P, Diaz P, Betancor P (1998) The range of bone mineral density in healthy Canarian women by dual X-ray absorptiometry radiography and quantitative computer tomography. J Clin Densitom 1:385–394

WHO [no authors listed] (1994) Assessment of fracture risk and its application to screening for postmenopausal osteoporosis. WHO Technical Report Series 843

Yamato M, Nishimura G, Kuramochi E, Saiki N, Fujioka M (1997) MR appearance of different ages of osteoporotic compression fractures of the vertebra. Radiat Med 16:329–334

Yeung DK, Wong SY, Griffith JF, Lau EM (2004) Bone marrow diffusion in osteoporosis: evaluation with quantitative MR diffusion imaging. J Magn Reson Imaging 19:222–228

Yuan X, Takahashi N, Terashita T, Nakatani M, Mizuno K (1998) Which vertebrae should be assessed in diagnosing osteoporosis by plain radiography? Comparative study of radiographic findings and bone mineral density measured by dual energy X-ray absorptiometry. J Orthop Sci 3:252–256

Yuh WTC, Zachar CK, Barloon TJ, Sato Y, Sickels WJ, Hawes DR (1989) Vertebral compression fractures: distinction between benign and malignant causes with MR imaging. Radiology 172:215–218

Zizic TM (2004) Pharmacologic prevention of osteoporotic fractures. Am Fam Physician 70:1293–300

Trauma

Whiplash Injuries

11

Jostein Kråkenes

CONTENTS

J. Kråkenes, MD, PhD
Head of Section of Neuroradiology, Department of Radiology, Haukeland University Hospital, 5021 Bergen, Norway

11.1 Introduction

11.1.1 The Term "Whiplash"

Crowe (1928) first introduced the term "whiplash" to describe the manner in which the head is moved suddenly to produce a neck sprain. Gay and Abbot (1953) used it first in a medical journal. Since then, more than 10,000 papers have been published, and still there is a great focus on whiplash in the medical literature as well as in the newspapers. Whiplash presently has a much wider usage than only to describe an injury mechanism. It is used to describe the injury itself – whiplash injury; to describe the clinical manifestations of the injury – whiplash symptoms or syndrome; and even to name patients – whiplash patients.

11.1.2 Definition and Incidence

Soft tissue injuries of the cervical spine have been described by terms such as neck sprain, neck strain, neck distortion, neck soft tissue injury, and acceleration–deceleration injury (Lovell and Galasko 2002). A review of the whiplash literature shows that there is a striking heterogeneity concerning results and conclusions drawn from different studies (Schrader et al. 1996; Bunketorp et al. 2002). Among the reasons for this could be different patient selection and inconsistent definitions of the condition. To obtain a common understanding of the whiplash injury, a summit was held in Quebec, Canada, namely the Quebec Task Force, which introduced whiplash-associated disorders (WAD) as a convenient term because the symptoms are not always confined to the neck (Spitzer et al. 1995). The Task Force defined the whiplash injury as follows:

KEY-POINTS

- Whiplash is an acceleration–deceleration mechanism of energy transfer to the neck that may result in bony or soft tissue injuries, which in turn may lead to a variety of clinical manifestations known as whiplash-associated disorders (WAD).
- Whiplash can result from rear-end vehicle collisions but is also seen in side-impact and front-impact collisions, and can also occur in other mishaps.
- Whiplash-type neck distortions are quite common, with an annual incidence between 1 and 4 per 1000 inhabitants.
- Rear-impact collisions result in complex biphasic kinematics of the cervical spine.
- WAD is a clinical diagnosis. The main symptoms include:
  - Neck pain, immediately or within 24 h after trauma is the cardinal manifestation.
  - Neck stiffness
  - Headache
  - Dizziness, vertigo, auditory symptoms, visual disturbances
  - Concentration and memory problems
  - Psychological problems
- Imaging
  - Plain film
    - To exclude fractures, adds little to the diagnosis
    - 10% of patients with normal initial plain films develop new degenerative changes. Degenerative changes are more frequent and pre-existing spondylosis is associated with an increased risk for chronic complaints
  - CT
    - Initial work-up of severely traumatized patients
    - Rotatory instability: asymmetrical pathological increased rotation at C0–C1 and/or C1/C2 in up to 36% of patients after whiplash injury
  - MRI
    - Disc herniations
    - Ligamentous lesions at the craniovertebral junction, especially the alar ligaments and transverse ligament
- Post-mortem studies
  - Facet joint, yellow ligament, uncovertebral and, to a lesser extent, disc lesions/endplate lesions
  - Dorsal root ganglion lesions
  - Craniovertebral ligament lesions

"Whiplash is an acceleration–deceleration mechanism of energy transfer to the neck. It can result from rear-end or side-impact motor vehicle collisions, but can also occur during diving or other mishaps. The impact may result in bony or soft tissue injuries (whiplash injury), which in turn may lead to a variety of clinical manifestations (Whiplash-Associated Disorders–WAD)".

Approximately 30% of all traffic accidents are whiplash-type neck distortions, and the frequency of such injuries has increased significantly over the past two decades (Galasko et al. 1993; Richter et al. 2000). An American estimate from the year 2000 indicates an incidence of approximately 900,000 such injuries annually, which is approximately 3 per 1000 inhabitants (Quinlan et al. 2004). Other authors report an annual incidence of 1–4 per 1000 inhabitants (Barnsley et al 1994; Herrstrom et al 2000; Sterner et al. 2003).

11.1.3 Injury Mechanism

Whiplash injuries are traditionally associated with rear-end impacts. Several biomechanical studies have been performed to understand why rear-end collisions are less tolerable than other impact types. Croft et al. (2002) showed that rear-impact crashes resulted in biphasic, complex kinematics compared with the monophasic, less complex frontal crashes. Externally, the head and neck do not exceed normal physiological limits; however, the cervical spine undergoes a sigmoid deformation very early after impact. During this deformation, lower cervical segments undergo posterior rotation around an abnormally high axis of rotation, resulting in abnormal separation of the anterior elements of the cervical spine, and impaction of the zygapophysial joints (Bogduk and Yoganandan 2001). Head linear ac-

celeration can be three times greater in rear-end than in frontal crashes; however, several authors have also reported a classical whiplash syndrome after lateral and frontal impacts as well. The set of symptoms in these trauma types is indistinguishable from those of rear-end impacts (Minton et al. 2000; Jakobsson et al 2004). Although whiplash injuries may be more likely to occur in rear-end than in frontal collisions, there is no doubt that frontal collisions are also responsible for a considerable number of lesions (Kullgren et al. 2000). Furthermore, the definition of whiplash injuries, as proposed by the Quebec Task Force, recognises that these injuries are not exclusively caused by traffic accidents. Whiplash-like syndromes can be seen after a variety of injury mechanisms such as falls, violence, or other types of head/neck distortion.

11.2 Clinical Diagnosis

11.2.1 Symptoms

The diagnosis of WAD remains clinical. No imaging, physiological, or psychological study can provide specific diagnostic criteria. Neck pain is the cardinal manifestation of a whiplash injury (Hildingsson and Toolanen 1990). The pain can appear immediately or usually within 24 h after trauma. It is typically located over the back of the neck, and may radiate to the head, shoulders, arm or interscapular region (Ronnen et al. 1996). The pain frequently shows exacerbation on movement, and is typically associated with neck stiffness (Kasch et al. 2001). Besides neck pain, headache is the most frequent complaint. Usually it is located in the occipital or suboccipital region, and radiates toward the orbital and temporal region (Maimaris et al. 1988). The headache may be tension-like, migraine-like, cervicogenic or unspecific (Radanov et al. 2001). Dizziness, often in combination with vertigo or auditory symptoms, is also frequently reported (Tjell and Rosenhall 1998; Tjell et al. 1999). Visual disturbances, especially reading difficulties, are sometimes reported. Accommodation errors and diverging eye movements are found in these patients (Gimse et al. 1997; Wenngren et al. 2002). Oculomotor dysfunction after neck trauma might be related to cervical afferent input disturbances (Heikkila and Wenngren 1998). Concentration and memory problems are frequent complaints. The etiology of these symptoms is controversial (Di Stefano and Radanov 1995; Kessels et al. 2000). Weakness may have a myotomal distribution, but far more common is a subjective sensation of fatigue and heaviness in the upper limbs without any clinical findings (Berglund et al. 2001; Hartling et al. 2002). Paresthesia, sensation of numbness and tingling in the arms or hands is common (Ronnen et al. 1996). These symptoms could be attributed to nerve root compression or a direct lesion of the root ganglia (Taylor et al. 1998). Many series report psychological symptoms in whiplash patients (Mayou et al. 1993; Sterling al. 2003). The relationship between such symptoms and the whiplash injury is disputed (see section 11.2.3). Other symptoms occasionally reported are dysphagia and temporomandibular pain.

11.2.2 Injury Grading

Norris and Watt introduced for the first time a grading system of whiplash injuries based upon symptoms and physical signs (Norris and Watt 1983). The Quebec Task Force classification used presently is based on their work, together with the work of Hirsch et al. (1988). Only neck complaints, musculoskeletal signs and neurological signs are considered in this grading system (Spitzer et al. 1995). Other symptoms and disorders, such as headache, dizziness, memory loss, tinnitus, deafness, visual disorders and joint pain, can manifest in all grades. In clinical practice a whiplash injury typically is confined to grades 1–3 (Table 11.1). A more precise grading system should provide a more reliable basis for prognosis.

Table 11.1. Clinical grading of whiplash injuries according to the Quebec Task Force of whiplash-associated disorders

Grade	Symptoms and signs
0	No complaint about the neck. No physical sign(s)
1	Neck complaint of pain, stiffness, or tenderness only. No physical sign(s)
2	Neck complaint and musculoskeletal sign(s)[a]
3	Neck complaint and neurological sign(s)[b]
4	Neck complaint and fracture or dislocation

[a] Signs include decreased range of motion and point tenderness
[b] Signs include decreased or absent deep tendon reflexes, weakness, and sensory deficits

11.2.3 Outcome

The whiplash injury has been one of the more frequently disputed conditions in the medical literature in recent decades (Jaspers 1998; Freeman et al. 1999; Ferrari and Schrader 2001; Kwan and Friel 2003). Although there is no doubt that WAD occurs, it is its chronicity that has been questioned. Most authors who have studied the natural history of whiplash patients have found that between 24 and 70% have long-term symptoms, whereas 12–16% are severely impaired many years after the accident (Radanov et al. 1994; Borchgrevink et al. 1996; Bunketorp et al. 2002; Squires et al. 1996). Some investigators report a lower frequency of chronic impairment (Drottning et al. 2002; Miettinen et al. 2002), probably due to different inclusion criteria and perhaps also different thresholds for registration of pain and impairment. A gradual recovery is reported for the first years after the accident. Parmar and Raymackers (1993) investigated 100 WAD patients who had originally been seen for medicolegal reports. Fifty percent of patients had significant pain at 8 months, 44% at 1 year, 22% at 2 years, and 18% at 3 years. At the final review after 8 years, 14% still had significant pain.

The validity of the whiplash syndrome is a key issue in litigation cases. Some authors conclude that in countries with low insurance coverage for car drivers and little awareness of potentially disabling consequences of the whiplash injury in the general population, neck injuries cause only moderate symptoms and for a brief period only (Schrader et al. 1996). To explain geographic variability some authors have proposed a biopsychosocial model of whiplash (Ferrari and Schrader 2001). Several authors have examined the relationship between premorbid personality traits and outcome after neck sprain. Psychological functioning did not differ significantly between the group with complaints compared with the group without complaints (Radanov et al. 1994; Turner et al. 2003; Versteegen et al. 2003); others conclude that psychiatric morbidity may be a risk factor for chronic symptoms after a whiplash injury (Joslin et al. 2004; Kivioja et al. 2004). Although psychological factors may play a role, there is no doubt that the chronic whiplash syndrome is real. In all studies a part of the patient is left with significant disability that interferes with their job and everyday activities. Most studies show that WAD is not necessarily a benign condition, whatever the cause of the residual symptoms may be.

11.3 Imaging in Whiplash Injury

The role of imaging in the work-up of whiplash injuries is under evaluation (Van Goethem et al 1996). Several studies conclude that routine spine imaging in blunt head and neck trauma is unnecessary for patients who are fully orientated and co-operative, non-intoxicated, exhibit no neurological deficits and who do not have neck pain or tenderness by palpation (Ersoy et al. 1995; Edwards et al. 2001).

11.3.1 Plain Radiography

Traditionally, X-ray examination of the neck with or without flexion and extension views is widely used in the acute work-up of neck injuries. The value of flexion and extension views after whiplash trauma has been evaluated in several reports. Dvorak et al. (1993) found slight hypermobility in the upper and middle cervical levels in the late stage of WAD compared with a healthy population. Griffiths et al. (1995) showed localised angulation greater than 10° and fanning greater than 12 mm between spinous processes in the follow-up of whiplash injured compared with uninjured individuals. They concluded that flexion and extension views are essential in the distinction of whiplash injuries from other ligamentous injuries. Ovadia et al. (2002) evaluated long-term findings 32 months post-trauma in 860 WAD patients. Ten percent of the patients with normal radiographic findings in the acute stage developed new degenerative changes at follow-up. Watkinson et al (1991) showed that degenerative changes of the cervical spine were present in 68% of whiplash-injured patients, of whom 87% were symptomatic. Of those with normal radiographs, 80% were symptom free. Degenerative changes occurred significantly more frequently in patients who had sustained soft tissue injuries than in a control population. Several studies show that pre-existing spondylosis is associated with increased risk of late chronic impairment in whiplash patients, probably due to increased neck stiffness (Radanov et al. 1994; Borchgrevink et al. 1995). Even though statistical differences between whiplash patients and controls are shown, plain radiography adds little to the diagnosis in the individual patient, except for excluding fractures.

11.3.2 Scintigraphy

One study evaluated scintigraphy after whiplash trauma. It included 35 patients with a whiplash injury and found a normal scintigraphy in 31 of the patients, whereas 4 patients had either a focal or multifocal increase in activity. Plain radiography revealed skeletal changes secondary to spondylosis in 3 of these patients and a localised bony spur with avulsion in 1 patient. The authors concluded that scintigraphy gave no new and significant information and is not indicated for screening purposes in whiplash-injured patients (Hildingsson et al. 1989).

11.3.3 Computed Tomography

Computed tomography (CT) has become the modality of choice in evaluating neck injuries in severely traumatised patients, and is superior to plain radiography (Barba et al. 2001; Griffen et al. 2003). In hyperextension–hyperflexion injuries CT has been used to estimate range of rotation in the craniovertebral junction. Mainly the alar ligaments (Dvorak et al. 1987a) restrict axial rotation in the upper cervical spine. Increased rotation towards one side is taken as a sign of insufficiency of the opposite side alar ligament. In a study of 43 patients with clinically suspected rotatory instability after traffic accidents, 26 showed increased rotation at C0–C1 and at C1–C2, strongly suggesting alar ligament insufficiency (Dvorak et al. 1987b). The same authors obtained functional CT of 35 healthy adults and 137 whiplash-injured individuals with therapy-resistant neck pain. A rotation at C0–C1 of more than 7°, and at C1–C2 more than 54°, was regarded as pathological. Thirty-three percent of the whiplash group showed signs of increased rotation between these segments (Dvorak et al. 1988a). Antinnes et al. (1994) examined 423 whiplash patients to determine the diagnostic value of functional rotatory CT in cervical soft tissue injury. They found that asymmetric rotation reached pathological values in 36% of this whiplash population at the level of C0–C1. A higher percentage of pathological values for hypermobile rotation was found at the level of C0–C1 than at C1–C2. The authors postulate that alar ligament lesions cause such instability, and conclude that their findings legitimate the use of functional CT in the evaluation of soft tissue damage of the upper cervical spine in whiplash injury; however, other authors have not been able to reproduce their findings (Patijn et al. 2001). The reason could be that functional CT is difficult to standardise. The method depends on the patient's ability to relax, which is difficult because rotation of the head beyond its normal range causes pain and dizziness. In general, except for excluding fractures and/or dislocations in severe injuries, CT is not accepted as a reliable diagnostic tool in WAD.

11.3.4 Magnetic Resonance Imaging

Magnetic resonance imaging (MRI) has become an important supplement to conventional radiography and CT for the detection of a wide spectrum of cervical injuries, especially disk herniation, disk degeneration, ligament disruption and cord injury (D'Alise et al. 1999). Several authors have evaluated the benefit of MRI in hyperextension–hyperflexion neck injuries. Davis et al. (1991) found two of nine patients with disk separation from the vertebral endplate, still evident as late as 9 months after injury. The authors state "that these MR changes are likely to be seen among severe whiplash injuries, representing a small minority of such injuries".

In a prospective study of 39 patients, Pettersson et al. (1997) found 25% of patients with persistent disc herniation over a 2-year follow-up period. There was no correlation between clinical signs/symptoms and MR findings. No ligament injuries were diagnosed. Jonsson et al. (1994) demonstrated that 20% of whiplash patients had severe disc herniations that correlated with radicular symptoms. Surgically, these discoligamentous lesions were confirmed as "fresh" disc herniations. Discectomy and fusion alleviated pain in these patients, whereas symptoms largely persisted in the conservatively treated patients. Another study also demonstrated disc herniations and cartilaginous endplate injuries in whiplash patients (Davis et al. 1991). Bonucelli et al. (1999) showed that whiplash patients with spondylosis ended up with worse clinical state than those without such changes, even though the spondylosis was not caused by the neck injury. Ronnen et al. (1996) examined 100 patients within 3 weeks after a whiplash trauma; only one had prevertebral edema related to the trauma. In 17 patients, functional images showed a kyphotic angle but no evidence of soft tissue lesions. They concluded that there is no role for MR imaging in the routine work-up of patients with acute whiplash injury who have normal X-ray examination and no evidence of a

neurological deficit. Other authors share this opinion (Borchgrevink et al. 1995). Image parameters used in these studies were sagittal T1 and T2, short echo time inversion recovery (STIR), and axial T1 or T2. Slice thickness was 3–5 mm.

Several investigators have studied the alar ligaments. Willauschus et al. (1995) conducted MR studies of eight healthy volunteers and seven patients with chronic upper neck injury, in whom manual examination suggested craniovertebral instability. The MR findings in the patient group were identical to those in the volunteers. Wilmink and Patijn (2001) examined the alar ligaments in 12 patients with chronic whiplash syndrome and six controls. The ligaments could be identified in all cases, but they concluded that with the MRI technique employed, alar ligament damage, as a causative factor in WAD, could not be proven. To diagnose instability in the craniovertebral junction, Volle and Montazem (2001, 2003) performed functional MR studies with tilting of the upper cervical spine to the right and to the left in small steps, and then axial rotation to the right and to the left, also in small steps. The images were studied in a video loop to evaluate functional disturbances regarding lateral bending and rotation. They studied a population of 420 patients and found complete alar ligament rupture in 4.8% and partial rupture in 12.4%, all accompanied by instability. Based on their findings, craniocervical fixation was undertaken in 42 patients (10%), and almost all symptoms reportedly disappeared 5 days after surgery; however, rupture criteria or criteria for instability were imprecisely described, and they had no control group.

Looking for structural alterations in normal alar ligaments, Pfirrmann et al. (2001) studied 50 asymptomatic individuals. Their MRI protocol included T1- and T2-weighted coronal and axial sections with a slice thickness of 3–4 mm. Only 80% of the alar ligaments could be visualised, and they found asymmetric high signal intensity in the majority of cases. Since such alterations frequently were found in a non-injured population, they concluded that the clinical relevance of structural alterations in these ligaments is limited. These authors also examined segmental motion in the upper cervical spine in the same 50 asymptomatic individuals. They found a wide variation in rotation, and concluded that measurements of segmental rotation are unsuitable in the diagnosis of soft tissue lesions after whiplash injury (Pfirrmann et al. 2000). (The author's own MR studies of the craniovertebral junction are presented in section 11.6.)

11.4 Structural Correlate to the Whiplash Syndrome

11.4.1 Post-Mortem Studies

Several soft tissue structures are vulnerable in whiplash injuries. Dissecting 22 cervical spines from traffic victims after craniocervical injuries, Jonsson et al. (1991) found 77 facet joint and ligamentum flavum lesions, 77 uncovertebral, and 22 disc lesions. In two adolescents, eight cartilaginous endplate avulsions of the discs were found. Taylor et al. (1998) found 44 examples of interstitial haemorrhage into a dorsal root ganglion in 15 of 109 individuals who had died after blunt head trauma. This was sometimes accompanied by neural tissue disruption, visible only at histological examination. In a study of 16 subjects who died of major trauma these authors showed clefts in the cartilage endplates in six of them, blood in the annulus in ten discs, and hemarthrosis in 22 facet joints (Taylor and Finch 1993). Similar changes are yet to be demonstrated in invivo examinations; however, there is reason to believe that the great forces involved in a car collision can strain several soft tissue structures in the cervical spine.

Post-mortem studies of fatal head/neck injuries document that craniovertebral ligaments are vulnerable to trauma. Saternus and Thrun (1987) reported alar ligament lesions in 11 of a total of 30 such cases. Another post-mortem study of 21 non-dislocated head/neck injuries showed either laceration or sprain of the alar ligaments in 20 cases; 13 had injury of the dura mater and the tectorial membrane as well, either lacerations or loosening from the clivus or from the C2 body, one had total and one had partial laceration of the transverse ligament (Adams 1993).

11.4.2 Clinical Studies

The facet joints, as an anatomical source of chronic pain after whiplash trauma, have been investigated in several reports (Lord et al. 1995; Barnsley et al. 1995). The prevalence of such pain was studied in 68 consecutive patients referred for chronic neck pain after whiplash in a placebo-controlled study with local anaesthetic blocks. The joints were blocked ei-

ther with lignocaine (short-acting local anaesthetic) or bupivacaine (long-acting local anaesthetic) in a random order. A positive diagnosis of joint pain was made only if both blocks relieved the patient's pain and bupivacaine provided longer relief. Among patients with headache, the prevalence of C2–C3 facet joint pain was 50%. Overall, the prevalence of cervical facet joint pain (C2–C3 or below) was 60% (Lord et al. 1996). The morphological correlate to such pain is not known.

Some study results suggest that whiplash injury causes structural changes predisposing to premature degenerative disc disease (Hamer et al. 1993). Many studies focus on a central neurological cause for chronic pain and complaints in whiplash-injured patients. Central hypersensitivity may explain exaggerated pain in the presence of minimal nociceptive input arising from minimally damaged tissues. This could account for pain and disability in the absence of objective signs of tissue damage in patients with whiplash. Central hypersensitivity may provide a common neurobiological framework for the integration of peripheral and supraspinal mechanisms in the pathophysiology of chronic pain after whiplash (Curatolo et al. 2004). Other authors state that chronic post-traumatic neck and head pain is rarely either organic or psychogenic. Instead, physiological, social, and cultural factors play major roles in modulating pain and either perpetuate or ameliorate these chronic pain conditions (Solomon 2005).

Both SPECT and PET studies have shown parieto-occipital hypometabolism in the late whiplash syndrome, maybe caused by activation of nociceptive afferences from the upper cervical spine. These tests could be used in the objective proof of post-traumatic symptoms (Otte 2001).

11.4.3 Whiplash Simulation Models

Biomechanical studies have determined that after rear-impact, C6 is rotated back into extension before movement of the upper cervical vertebrae; thus, the lower cervical vertebrae were in extension while the upper vertebrae were in a position of relative flexion, producing an S shape in the cervical spine. It is believed that this abnormal motion pattern might play a role in the development of whiplash injuries. During this motion, at approximately 100 ms after impact, the lower cervical vertebrae undergo extension but without translation. This motion causes the vertebral bodies to separate anteriorly and the zygapophysial joints to impact posteriorly. The lesions likely to result from such motion are tears of the anterior anulus fibrosus and fractures or contusions of the zygapophysial joints (Bogduk and Teasell 2000).

Panjabi et al (2004) noted exceeding of sagittal physiological levels during simulated whiplash. Peak disc shear strain was greatest at the posterior region of C5–C6. They concluded that the cervical intervertebral discs may be at risk for injury during whiplash because of excessive fiber strain, disc shear strain, and anterior axial deformation. The same group also described facet joint compression especially at C4–C5. In general, peak facet joint sliding and capsular ligament strains were largest in the lower cervical spine and increased with impact acceleration. They concluded that facet joint components may be at risk for injury due to facet joint compression during rear-impact accelerations. Capsular ligaments are at risk for injury at higher accelerations (Pearson et al. 2004).

Other simulations showed that abnormal curvatures (straight or kyphotic) of the cervical column affect spinal kinematics during whiplash loading and enhance the likelihood of whiplash injury and may have long-term clinical and biomechanical implications (Stemper et al. 2005)

11.5 Anatomy of the Craniovertebral Articulation

11.5.1 Joints

The craniovertebral junction is a three-unit articulation (C0–C2) with six separate joints. The atlanto-occipital joint consists of two crescent-shaped, reciprocally curved surfaces, one on each occipital condyle and the other on the lateral masses of the atlas. The atlantal facets are concave and tilted medially.

The atlanto-axial joints comprise a lateral and a median articulation. The lateral articulations consist of the inferior facets of the atlas and the superior facets of the axis. Both the superior and the inferior surfaces are slightly convex and they are tilted laterally. The median joint consists of a pivot articulation

with the dens axis rotating in the anterior atlantal ring, which is formed by the anterior atlantal arch and the transverse ligament. The facets of the median articulation are (a) the anterior facet of the dens and the fovea dentis on the anterior arch, and (b) the transverse ligament and the posterior dens surface.

11.5.2 Ligaments

The apical ligament of the dens axis extends from the tip of the dens to the basion. It is rudimentary and regarded to be of little significance.

The transverse ligament of the atlas is a flattened band crossing the anterior atlantal ring that acts as a sling holding the dens against the anterior atlantal arch. It is stabilised by two longitudinal bands, one upward extension to the basion, and one downward extension to the base of the axis. The transverse ligament together with these two bands forms the cruciform ligament of the atlas (Fig. 11.1).

The alar ligaments are paired rounded cords, which arise on the upper posterior part of the dens axis. They are inserted into the fovea on the medial side of the condyles of the occipital bone. From the posterior tip of the dens they pass laterally, slightly upwards and backwards (Fig. 11.1).

The tectorial membrane is a broad, strong band that covers the dens axis and its ligaments posteriorly, and appears to be a prolongation upwards of the posterior longitudinal ligament of the vertebral column. It is fixed, below to the posterior surface of the axis body, and expanding as it ascends, it is attached to the basilar groove of the occipital bone in front of the foramen magnum. Its anterior surface is in contact with the transverse and the alar ligaments, and its posterior surface blends with the dura mater of the upper spinal canal (Fig. 11.2).

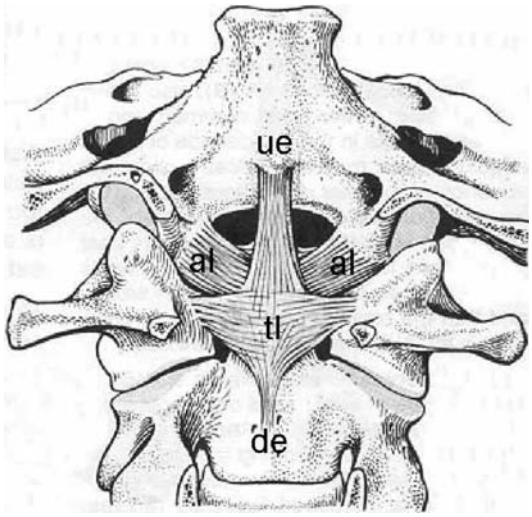

Fig. 11.1. Posterior view of the transverse ligament (*tl*) with its upward extension (*ue*) and downward extension (*de*) constituting the cruciform ligament. The alar ligaments (*al*) are partially covered by the cruciform ligament (From Platzer 1986)

The anterior atlanto-occipital membrane is composed of densely woven fibres, that stretch between the anterior margin of the foramen magnum above, and the upper border of the anterior arch of the atlas below (Fig. 11.2).

The anterior atlanto-axial ligament is a strong membrane, fixed above to the lower border of the anterior arch and below to the front of the axis body. It is strengthened in the midline by a rounded cord, which connects the tubercle on the anterior atlantal arch of the atlas to the body of the axis, and is a continuation upward of the anterior longitudinal ligament (Fig. 11.2).

The posterior atlanto-occipital membrane represents the continuation of the flavum ligaments of the posterior spinal canal. It is connected above to the posterior margin of the foramen magnum and below to the upper border of the posterior arch of the atlas. Either side of this membrane has an opening for the entrance of the vertebral artery and the exit of the suboccipital nerve. The membrane is in front intimately adherent to the dura mater of the vertebral canal (Fig. 11.2).

The posterior atlanto-axial membrane is a broad, thin and elastic membrane that passes from the lower border of the posterior arch of the atlas to the upper edges of the lamina of the axis (Fig. 11.2).

The nuchal ligament extends from the external occipital protuberance to the spinous process of the seventh cervical vertebra. In man it is merely the rudiment of an elastic ligament which, in some of the lower animals, serves to sustain the weight of the head.

11.5.3 Functional Anatomy

The occipito-atlanto-axial articulation is the most complex joint in the axial skeleton, both anatomically and kinematically. The atlanto-occipital joints are cup-shaped both in the coronal and in the sagittal planes. The atlanto-axial joint, however, has a

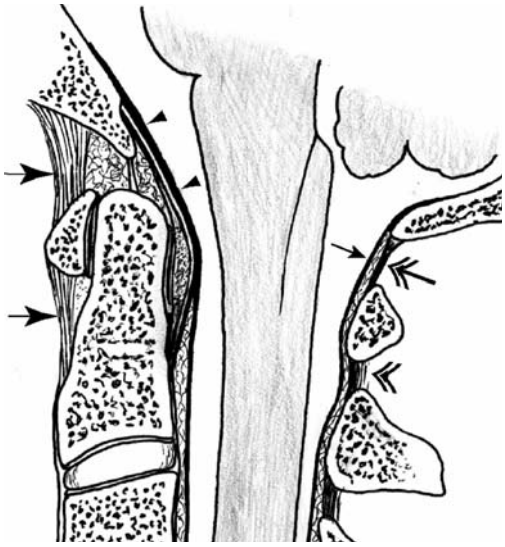

Fig. 11.2. Mid-sagittal section of the upper cervical spine shows the tectorial membrane (*arrowheads*), the anterior atlanto-occipital membrane (*long arrow*), the anterior atlanto-axial ligament (*short arrow*), the posterior atlanto-occipital membrane (*double arrow*), with the adjoining dura mater (*small arrow*), and the atlanto-axial membrane (*double arrowhead*)

convex configuration of both joint surfaces, superior and inferior, in the sagittal plane. This anatomic design allows large mobility. During flexion–extension, the joints C0–C1 and C1–C2 participate equally. The total range of motion is approximately 25° (Frobin et al. 2002). The craniovertebral rotation takes place mainly between C1 and C2. Previously, it was assumed that there is very little or no rotation between the occiput and the atlas. Dvorak et al. (1987b) found an average axial rotation of C0–C1 on CT of 4.3°, both to the right and to the left, and of C1–C2, of 41.5°. They concluded that a rotation at C0–C1 >8° and at C1–C2 >56° indicates hypermobility. A right–left difference at C0–C1 >5° and at C1–C2 >8° indicates one-sided hypermobility. Other authors have found a mean rotation of only 1° between C0 and C1 (Penning and Wilmink 1987; Patijn et al. 2001).

The alar and transverse ligaments provide much of the stability of the healthy craniocervical junction. The alar ligaments restrain rotation (Dvorak 1987a), whereas the transverse ligament restricts flexion as well as anterior displacement of the atlas. The alar ligaments have an average in vitro strength of 200 N, and the transverse ligaments of 350 N. Histological analysis revealed a collagenous nature for both (Dvorak et al. 1988). In an anatomical study using fresh human cadaver spines, Harris et al. (1993) examined the instability after sequential incision of the craniovertebral membranes. Their study demonstrated the essential role of the tectorial membrane in maintaining upper cervical spine stability, whereas the atlanto-occipital membranes played a minor role in the preservation of stability in flexion–extension.

11.6 High-Resolution MRI of the Craniovertebral Junction

11.6.1 Imaging Protocol

Based on the hypothesis of craniovertebral hypermobility after whiplash trauma (Dvorak et al. 1987b), we developed an imaging protocol to visualise ligaments and membranes in the upper cervical spine (Krakenes et al. 2001).

We obtained 2-mm-thick, interleaved, contiguous proton-density-weighted sections in three orthogonal planes with the head in a neutral position, using a head coil. Axial sections covered the volume from the foramen magnum to the base of the dens (Fig. 11.3), coronal sections from the anterior arch of the atlas and halfway through the spinal canal (Fig. 11.4), and sagittal sections from the right to the left occipital condyle (Fig. 11.5). Repetition time/echo time (TR/TE) was 2200/15 ms, matrix size 224×512 and field of view (FOV) 127×203 mm for the axial and the coronal series, and TR/TE 2660/15, matrix size 322×512 and FOV 184×210 mm for the sagittal series. Echo-train length was seven, four signals were acquired, and receiver bandwidth was 130 Hz/pixel. We applied saturation pulses superior and inferior to the axial and coronal slabs and for the sagittal series also, anterior to the slab. Pixel size was 0.57×0.40 mm in all three planes, and voxel size was 0.46 mm3.

11.6.2 Study Population

Individuals sustaining a frontal or rear-end collision and diagnosed as having a WAD grade 2, were prospectively registered (Krakenes and Kaale 2006). Neck radiographs with extension and flexion

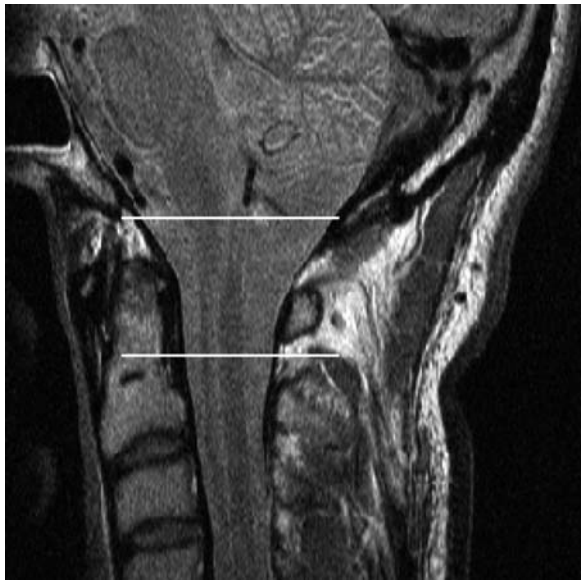

Fig. 11.3. Sagittal image with locator lines for axial sections

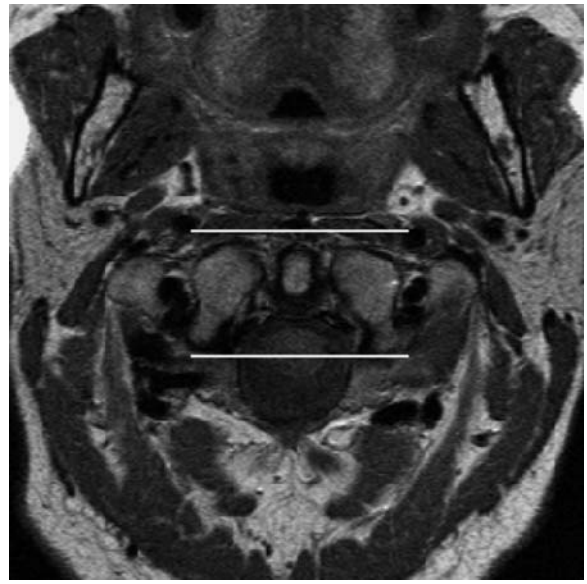

Fig. 11.4. Axial image with locator lines for coronal sections

Fig. 11.5. Coronal image with locator lines for sagittal sections

views in the acute phase were normal in all patients. All patients were re-evaluated 12–16 weeks after the injury, and only those who still met the criteria of WAD grade 2 at that time were included. One hundred patients were invited to participate. All patients were interviewed prior to MRI to exclude those with a new neck injury occurring between the whiplash injury and the MRI. Those patients with other neck injuries of any kind were excluded; 92 patients, 33 males and 59 females with a mean age of 40 years (age range 14–61 years) underwent MRI, 2–9 years (mean 6 years) after the whiplash injury, the only known injury in the study group (Krakenes and Kaale 2006).

Fifty individuals matched for age and gender with no history of head or neck trauma were invited as a control group; 12 did not respond and 8 did not show up on the examination day, ending up with 11 men and 19 women, with a mean age of 46 years (age range 28–66 years), slightly older than the patient group (Krakenes et al. 2002, 2003a,b).

11.6.3 Image Interpretation and Grading Criteria

The whiplash group and the control group were mixed in random order and images were read twice at 3-month intervals by three radiologists, blinded to all clinical information. Grading criteria were based on high signal intensity within the substance of the ligaments and the membranes. Normal ligaments show low signal intensity (Erickson 1997), whereas increased signal intensity is regarded as a sign of ligament injury (Chen et al. 2002; Nomura et al. 2002).

For the alar ligaments we based our grading on the ratio between any high-signal part and the total cross-sectional area in sagittal sections as shown in Table 11.2 (Krakenes et al. 2002). A lesion should always be seen on coronal images as well. Axial images were of little importance. Normal ligaments showed low signal intensity both on coronal and sagittal images (Fig. 11.6), whereas high signal intensity in a ligament was regarded as a trauma-induced lesion (Fig. 11.7). Alar ligament lesions could either be symmetrical or asymmetrical (Fig. 11.8).

Grading criteria for the transverse ligament were based on the same principles as those for the alar ligaments (Table 11.3; Krakenes 2003a). A normal transverse ligament is dark and well defined both in axial and coronal sections (Fig. 11.9). A lesion could be unilateral, usually near the atlantal tubercle (Fig. 11.10), or it could include the entire

Table 11.2. Criteria for classification of structural changes in the alar ligaments

Grade	Criteria
0	Low signal intensity throughout the entire cross section
1	High signal intensity in one-third or less of cross section
2	High signal intensity in one-third to two-thirds of cross section
3	High signal intensity in two-thirds or more of cross section

Fig. 11.6a–c. Coronal image (**a**) with locator lines for sagittal view of right (**b**) and left (**c**) alar ligament (*arrows*). Normal ligaments show low signal intensity, appearing dark

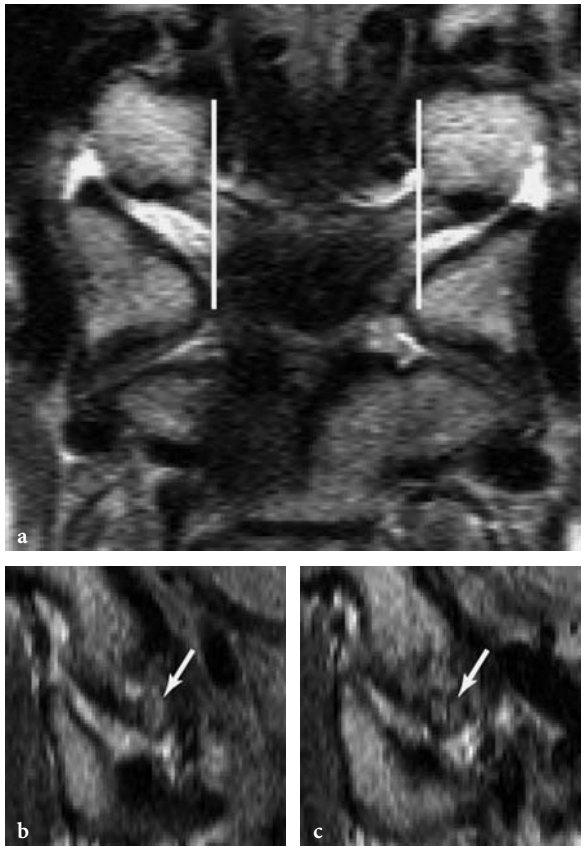

Fig. 11.7a–c. Coronal image (**a**) with locator lines for sagittal view of right (**b**) and left (**c**) alar ligament (*arrows*). Both ligaments show high signal intensity except for a dark lining in the periphery

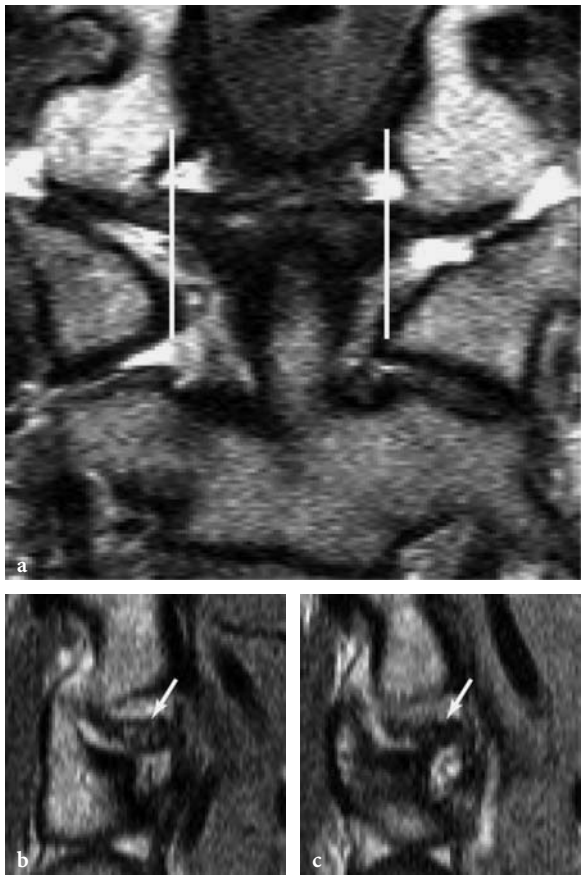

Fig. 11.8a–c. Coronal image (**a**) with locator lines for sagittal view of right (**b**) and left (**c**) alar ligament (*arrows*). Both ligaments are wing shaped in cross section. On the right side there are *spots* of high signals, classified as grade 2, whereas the left side has normal signal intensity

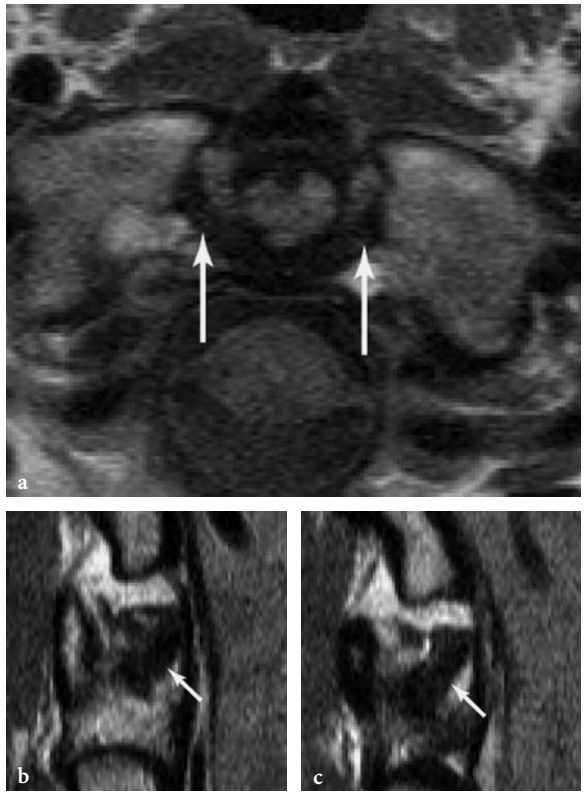

Fig. 11.9a–c. Axial image (**a**) of a normal transverse ligament. Sagittal views near the insertion area (along the *arrows*) show low signal intensity in cross-section area both on the right (**b**) and the left (**c**) side (*arrows*)

Table 11.3. Criteria for classification of structural changes in the transverse ligament

Grade	Criteria
0	Ligament with low signal intensity, appearing dark
1	High signal intensity in one-third or less of cross section, well-defined or slightly diffuse margins
2	High signal intensity in one-third to two-thirds of cross section, with or without diffuse margins
3	High signal intensity in two-thirds or more of cross section, usually with ill-defined margins

ligament (Fig. 11.11). A lesion should be seen in at least two imaging planes. Depending on the sharpness of the ligament curve, the cross-sectional area was assessed either in coronal or sagittal sections. Decreased signal intensity in the anterior atlantal space, obscuring the ligament, was found both in the whiplash group and in the control group, regarded either as a normal variant or as degenerative changes (Fig. 11.12).

The major challenge in grading these ligaments was intermediate signal increase: grey ligaments, often combined with increased thickness (Figs. 11.13, 14). Ligaments with intermediate signal intensity did not fit into our grading system. Such changes could be due to fibrous scarring (Farooki and Seeger 1999).

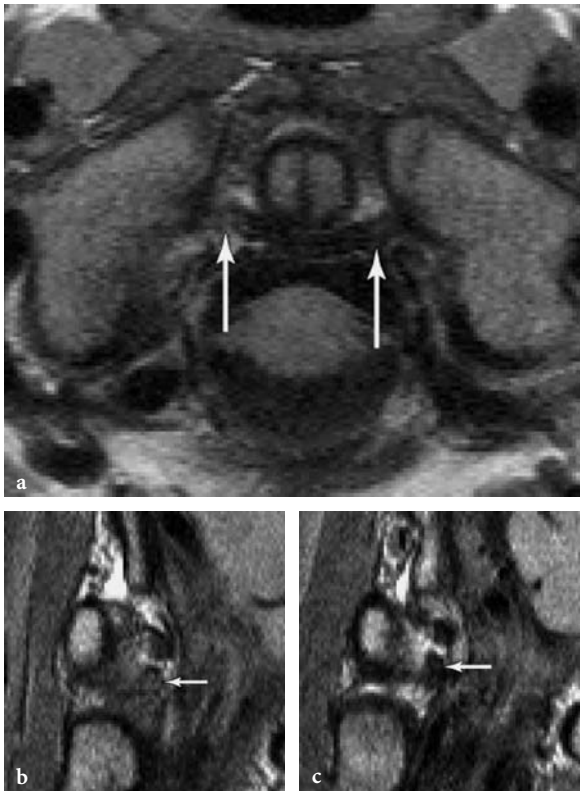

Fig. 11.10a–c. Axial image (**a**) of a transverse ligament with a right-side lesion. Sagittal views near the insertion area (along the *arrows*) show high signal intensity in cross-sectional area on the right side (**b**; *arrow*) indicating a grade-3 lesion, and low signal intensity on the left side (**c**; *arrow*)

Fig. 11.11a,b. Axial image (**a**) of a transverse ligament with generally increased signal intensity. Coronal view near the insertion area (along the *arrows*) show high signal intensity in cross-sectional area on both sides (**b**) indicating a grade-3 lesion (*arrows*)

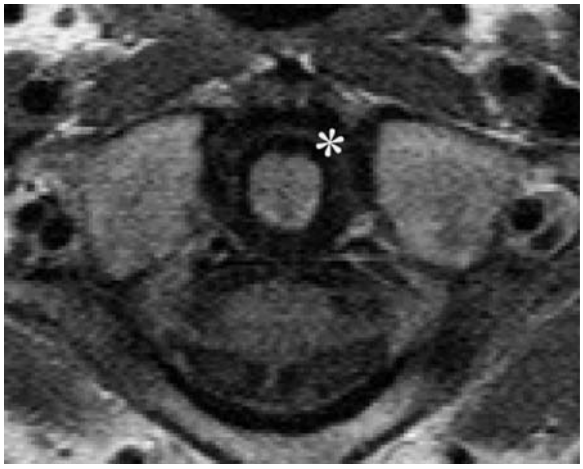

Fig. 11.12. Axial image of a transverse ligament coalesced with soft tissue in anterior atlantal space (*asterisk*), probably a normal variant

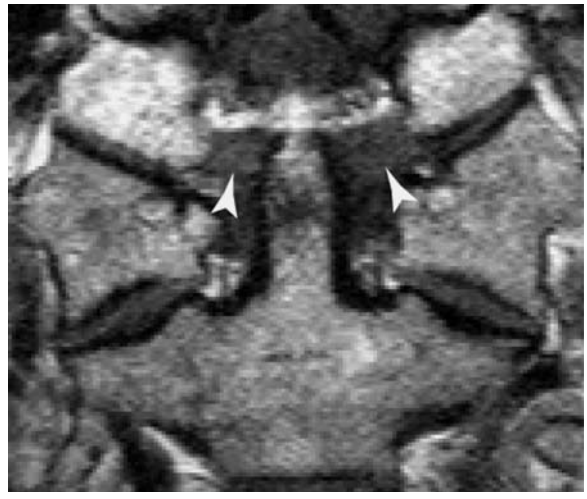

Fig. 11.13. Coronal image of thick alar ligaments with intermediate signal intensity (*arrowheads*)

Fig. 11.14. Axial image of an apparently swollen transverse ligament with generally increased signal intensity (*arrowheads*)

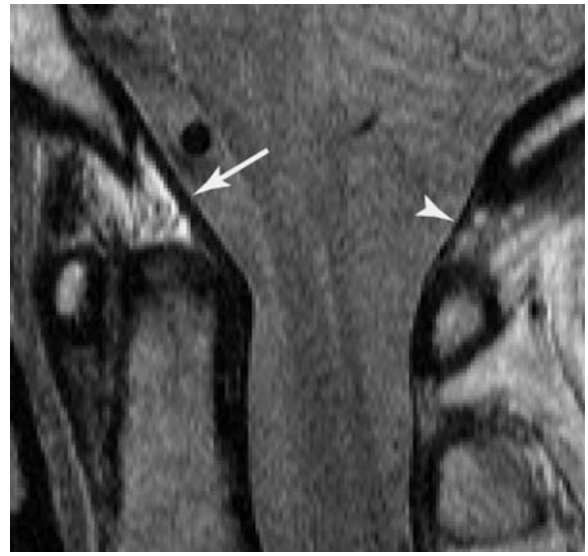

Fig. 11.15. Sagittal image of normal tectorial- (*arrow*) and atlanto-occipital (*arrowhead*) membranes. Both membranes are fused with the dura mater

The tectorial- and the posterior atlanto-occipital membranes were evaluated on sagittal sections. The cranial part of the tectorial membrane, the segment between the dens and the clivus, is adherent to, and indistinguishable from, the dura. A normal membrane/dura complex was seen as a dark band with a mean thickness of 1.4 mm (Fig. 11.15). A membrane/dura complex with reduced thickness, similar to that of the dura alone, was regarded as a membrane rupture. Such membrane defects could either involve a short portion (Fig. 11.16) or the entire segment (Fig. 11.17). Grading criteria were based on the fraction of the total transverse width with such reduced thickness (Table 11.4).

The posterior atlanto-occipital membrane either appeared as a dark band fused with the dura (Fig. 11.15), or it was separated from the dura by a connective tissue layer (Fig. 11.16). We based our grading of the membrane/dura complex on structural changes of the adjoined dura: dural hump (Fig. 11.18), thinning (Fig. 11.19), discontinuity, and/or flap (Fig. 11.20). Dural hump and thinning were interpreted as an elongation of the dura and were regarded as signs of minor sprain, whereas discontinuity or dural flap were regarded as rupture and thus as a more severe lesion. Grading criteria were based on the extent of these changes (Table 11.4; Krakenes 2003b).

Table 11.4. Criteria for classification of structural changes in the tectorial and the posterior atlanto-occipital membranes

Grades	Criteria
Tectorial membrane	
0	A membrane/dura complex thicker than the dura alone in all sagittal sections
1	Only dura left in less than one-third of transverse width
2	Only dura left in one-third to two-thirds of transverse width
3	Only dura left in more than two-thirds of transverse width
Posterior atlanto-occipital membrane	
0	Smooth and well-defined membrane/dura complex
1	Thinning, minor discontinuity or a dural hump in less than one-third of transverse width
2	Thinning, minor discontinuity or a dural hump affecting one-third to two-thirds of transverse width
3	Discontinuity with or without a dural flap in more than two-thirds of transverse width

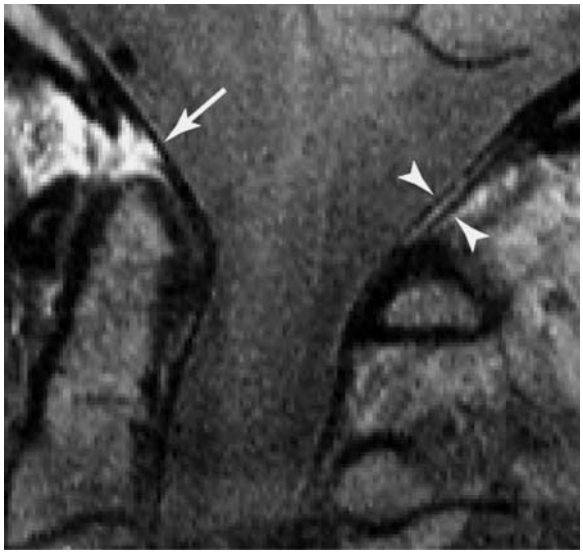

Fig. 11.16. Sagittal image of a tectorial membrane with a marked defect in the mid-part (*arrow*). The atlanto-occipital membrane and the dura mater are separated, which is a normal variant (*arrowheads*)

Fig. 11.17. Sagittal image of the tectorial membrane. Most of the segment between the dens and the clivus is absent; only the dura mater is shown (*arrow*)

Fig. 11.18. Sagittal image of an atlanto-occipital membrane with a dural hump (*arrowhead*)

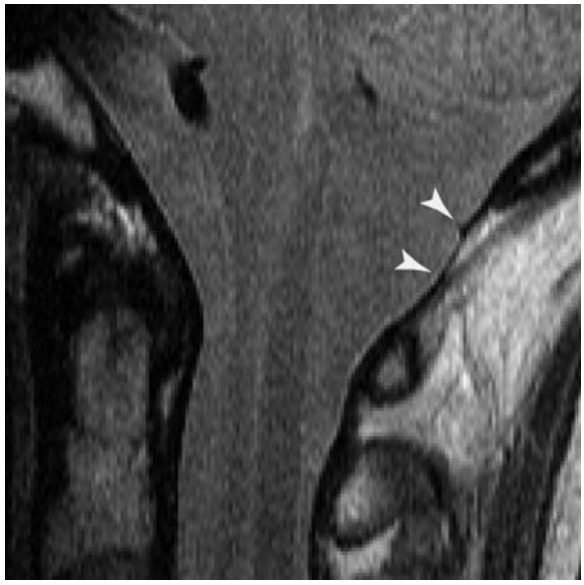

Fig. 11.19. Sagittal image of an atlanto-occipital membrane with a thinning in the mid-part (between the *arrowheads*). Normal thickness above and below

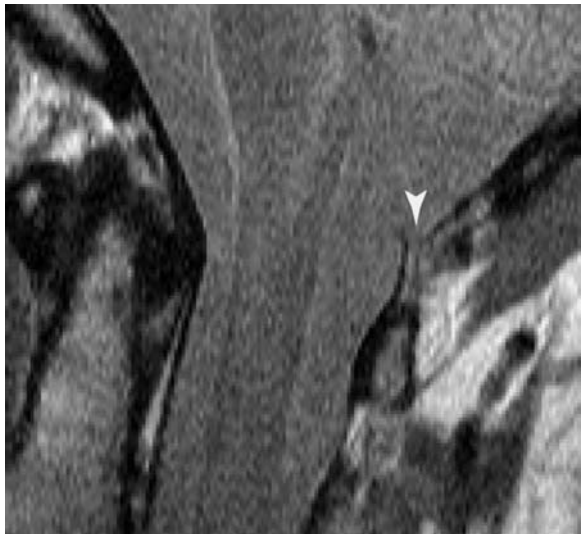

Fig. 11.20. Sagittal image of an atlanto-occipital membrane with dural flap indicating a rupture (*arrowhead*)

To reduce flow artefacts from the cerebrospinal fluid, we used head–feet as phase-encoding direction. Due to chemical shift artefacts in the anterior–posterior direction, these membranes decrease or increase in thickness depending on the polarity of the readout gradient. Chemical shift is the major difficulty in the evaluation of both these membranes, and should be taken into consideration in the interpretation of both the tectorial- and the atlanto-occipital membranes.

11.6.4 Observer Variation

Reliability of a diagnostic test generally means consistency of the interpretation. We used the kappa statistic to measure the ability of different observers to classify the ligaments into one of several groups. Weighted kappa allows weighting for the magnitude or importance of individual discrepancies (Landis and Koch 1977). A one-step difference in grading does not necessarily mean real disagreement; therefore, we used weighted kappa, which may be more appropriate than ordinary kappa in this kind of task.

In this study, the consistency in grading varied considerably, both between observers and for the different structures evaluated. Generally, we found better intraobserver- than interobserver agreement. Good agreement was obtained for the posterior atlanto-occipital membrane, and moderate to good agreement for the alar ligaments and for the tectorial membrane. The least agreement was found for the transverse ligament.

11.6.5 MRI Findings: Whiplash Group vs Control Group

The number of high-grade changes (2 and 3) in the whiplash group and in the control group is given in Table 11.5. Figures are based on agreement in grading between at least two observers. Ligaments graded differently by all observers are excluded (13.6% of all). In the whiplash group we found 117 high-grade changes among 394 ligaments/membranes evaluated (29.7%). Only seven grade-2 changes, and no grade-3 changes, were found among 133 ligaments/membranes in the control group (5.3%).

11.6.6 Neck Disability and MRI Findings

Ninety-two WAD patients and 30 control persons completed the neck disability index (NDI) score, a modification of the Oswestry Low Back Pain Index, comprising ten items related to activity of daily living. The score reflected either degree of neck pain or difficulties performing certain activities due to neck pain (Kaale et al. 2005a).

Table 11.5. Number of high-grade lesions (grades 2 and 3) in 92 individuals with a whiplash trauma and 30 controls

Grade	Alar ligament (n=158/56)[a]	Transverse ligament (n=71/28)[a]	Posterior atlanto-occipital membranes (n=88/26)[a]	Tectorial membrane (n=77/23)[a]
2	29/0	19/3	9/1	19/3
3	23/0	5/0	11/0	12/0
Total	52/0	24/3	20/1	21/3

[a] Only cases in which at least two observers agreed on grading are included (number of WAD-patients/number of controls)

We found a significantly higher NDI score in the WAD group than in the control group, particularly for neck pain, reading abilities, concentration, car driving, and general activity level. In the WAD group NDI increased significantly with increasing MRI grading of the alar ligaments (p=0.002). Disability tended to increase with increasing MRI grading for the transverse ligament as well (p=0.059). No consistent pattern was found for the membranes.

Lesions in the alar ligaments only were associated with a higher score than lesions in the transverse ligament only. Lesions in the atlanto-occipital membrane showed only the same score as those with abnormal alar ligaments. Analysis with mutual adjustment for all four structures showed that abnormal alar ligaments were the strongest predictor for severity of symptoms. Finally, we found a highly significant increase in NDI score with increasing number of high-grade lesions (p=0.003).

11.6.7 Injury Mechanism and MRI Findings

Fifty-four of the 92 WAD patients sustained a frontal collision and 38 a rear-end collision, 45 had neutral head position and 47 had rotated head position at the moment of impact (Kaale et al. 2005b).

We found a significantly higher frequency of high-grade (2 and 3) alar ligament lesions among those with rotated head position at the moment of collision (61.7%) than among those with neutral head position (4.4%; p<0.001). The association between rotated head position and high-grade lesions was more pronounced after rear-end collision than after frontal collision (93.8 vs 31.8%; p<0.001). Also for the transverse ligament we found significantly more high-grade lesions among those with rotated head position than among those with neutral head position (p=0.040).

High-grade MRI findings in the transverse ligament and in the atlanto-occipital membrane were significantly more common in frontal collision than in rear-end collision (p<0.001). There was no such difference for the alar ligaments or the tectorial membrane.

Our study confirms the hypothesis that the alar ligaments are vulnerable to neck trauma, in particular when the head is rotated at the moment of impact (Dvorak 1987a). The transverse ligament and the atlanto-occipital membrane, which restrict anterior translation and hyperflexion of the head/neck, are more vulnerable in frontal than in rear-end collision.

11.7 Conclusion

Whiplash-associated disorders account for a large proportion of the overall impairment and disability caused by traffic injuries or even trauma in general. Many theories regarding the etiology of WAD exist, and several trauma mechanisms, possibly causing different injuries, have been described. Imaging only rarely demonstrates a definite injury in the acute (or chronic) phase. Primary disc lesions and/or secondary accelerated disc degeneration and/or lesions to the craniovertebral ligaments may cause WAD and can be detected on high-resolution MRI studies (Fig. 11.21).

Variables such as pain intensity, restricted motion, neurological symptoms and signs, together with central nervous system symptoms can predict an increased risk of chronic complaints. Persistent/chronic pain is not merely acute pain that persists over time; changes occur at different levels of the pain transmission system. Chronic WAD is associated with problems concerning social functioning, daily anxieties and dissatisfaction with different aspects of life. Early multidisciplinary rehabilitation focusing on cognitive–behavioural changes might be of value. To develop specific treatment and rehabilitation, it is important to identify homogeneous subgroups (Sterner and Gerdle 2004).

The proposed MR protocol allows a detailed assessment of the craniovertebral articulation. We have shown that whiplash injuries cause substantial signal changes in craniovertebral ligaments and membranes. Such lesions, especially in the alar- and transverse ligament, are associated with pain and disability. We have also shown that specific injury mechanisms cause specific lesions. To obtain a histological correlate to MRI findings, patients with fatal head/neck injuries can be examined with MRI prior to post-mortem examination; thus, MRI grading can be compared with pathological anatomy.

Magnetic resonance imaging, and especially high-resolution MRI of the upper cervical spine, may become an important tool in the assessment of whiplash and other trauma-induced neck disorders in the future.

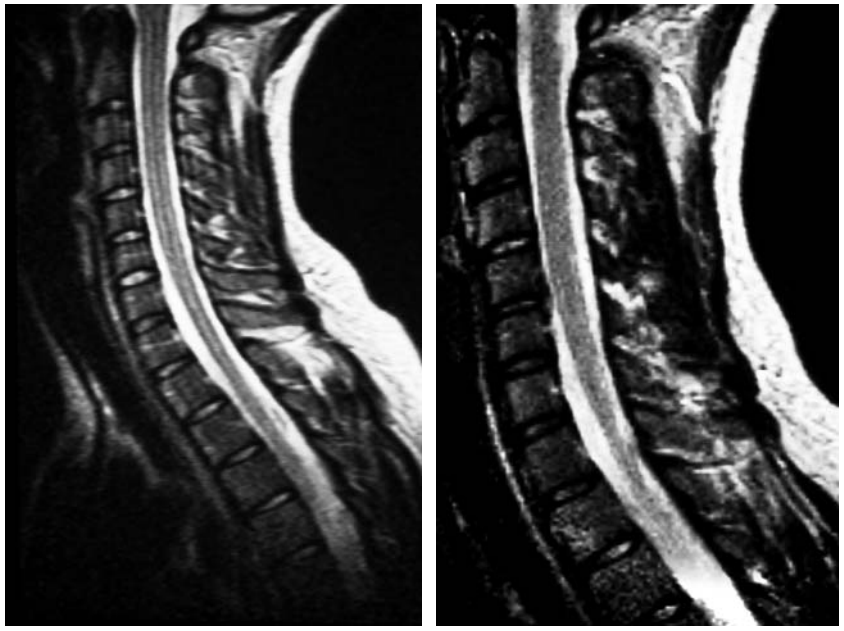

a b

Fig. 11.21a,b. Sagittal T2-weighted images in a young woman after whiplash injury. The first MR examination (**a**) was performed 3 days after the injury and showed no abnormalities. The second examination (**b**) was done 6 months later because of persistent whiplash-associated disorders. At that time, MR showed signal loss in the C5–C6 disc with an associated disc protrusion. This was interpreted as an accelerated post-whiplash disc degeneration

References

Adams VI (1993) Neck injuries: III. Ligamentous injuries of the craniocervical articulation without occipito-atlantal or atlanto-axial facet dislocation. A pathologic study of 21 traffic fatalities. J Forensic Sci 38:1097–1104

Antinnes JA, Dvorak J, Hayek J et al. (1994) The value of functional computed tomography in the evaluation of soft-tissue injury in the upper cervical spine. Eur Spine J 3:98–101

Barba CA, Taggert J, Morgan AS et al. (2001) A new cervical spine clearance protocol using computed tomography. J Trauma 51:652–656

Barnsley L, Lord S, Bogduk N (1994) Whiplash injury. Pain 58:283–307

Barnsley L, Lord SM, Wallis BJ et al. (1995) The prevalence of chronic cervical zygapophysial joint pain after whiplash. Spine 20:20–25

Berglund A, Alfredsson L, Jensen I et al. (2001) The association between exposure to a rear-end collision and future health complaints. J Clin Epidemiol 54:851–856

Bogduk N, Teasell R (2000) Whiplash: the evidence for an organic etiology. Arch Neurol 4:590–591

Bogduk N, Yoganandan N (2001) Biomechanics of the cervical spine, part 3: minor injuries. Clin Biomech 4:267–275

Bonucelli U, Pavese N, Lucetti C et al. (1999) Late whiplash syndrome: a clinical and magnetic resonance imaging study. Funct Neurol 14:219–225

Borchgrevink GE, Smevik O, Nordby A et al. (1995) MR imaging and radiography of patients with cervical hyperextension-flexion injuries after car accidents. Acta Radiol 36:425–428

Borchgrevink GE, Lereim I, Royneland L et al. (1996) National health insurance consumption and chronic symptoms following mild neck sprain injuries in car collisions. Scand J Soc Med 24:264–271

Bunketorp L, Nordholm L, Carlsson J (2002) A descriptive analysis of disorders in patients 17 years following motor vehicle accidents. Eur Spine J 11:227–234

Chen WT, Shih TT, Tu HY et al. (2002) Partial and complete tear of the anterior cruciate ligament. Acta Radiol 43:511–516

Croft AC, Haneline MT, Freeman MD (2002) Low speed frontal crashes and low speed rear crashes: Is there a differential risk for injury? Annu Proc Assoc Adv Automot Med 46:79–91

Crowe HE (1928) Injuries to the cervical spine. Presented at the meeting of the Western Orthopaedic Association, San Fransisco, Calif. Ref type: Hearing

Curatolo M, Arendt-Nielsen L, Petersen-Felix S (2004) Evidence, mechanisms, and clinical implications of central hypersensitivity in chronic pain after whiplash injury. Clin J Pain 20:469–476

D'Alise MD, Benzel EC, Hart BL (1999) Magnetic resonance imaging evaluation of the cervical spine in the comatose or obtunded trauma patient. J Neurosurg 91:4–59

Davis SJ, Teresi LM, Bradley WG Jr et al. (1991) Cervical spine hyperextension injuries: MR findings. Radiology 180:245–251

Drottning M, Staff PH, Sjaastad O (2002) Cervicogenic head-

ache (CEH) after whiplash injury. Cephalalgia 22:165–171
Dvorak J, Panjabi M, Gerber M et al. (1987a) CT-functional diagnostics of the rotatory instability of upper cervical spine. Part 1. An experimental study on cadavers. Spine 12:197–205
Dvorak J, Hayek J, Zehnder R (1987b) CT-functional diagnostics of the rotatory instability of the upper cervical spine. Part 2. An evaluation on healthy adults and patients with suspected instability. Spine 12:726–731
Dvorak J, Penning L, Hayek J et al. (1988a) Functional diagnostics of the cervical spine using computer tomography. Neuroradiology 30:132–137
Dvorak J, Schneider E, Saldinger P et al. (1988b) Biomechanics of the craniocervical region: the alar and transverse ligaments. J Orthop Res 6:452–461
Dvorak J, Panjabi MM, Grob D et al. (1993) Clinical validation of functional flexion/extension radiographs of the cervical spine. Spine 18:120–127
Edwards MJ, Frankema SP, Kruit MC et al. (2001) Routine cervical spine radiography for trauma victims: Does everybody need it? J Trauma 50:529–534
Erickson SJ (1997) High-resolution imaging of the musculoskeletal system. Radiology 205:593–618
Ersoy G, Karcioglu O, Enginbas Y et al. (1995) Are cervical spine X-rays mandatory in all blunt trauma patients? Eur J Emerg Med 2:191–195
Farooki S, Seeger LL (1999) Magnetic resonance imaging in the evaluation of ligament injuries. Skeletal Radiol 28:61–74
Ferrari R, Schrader H (2001) The late whiplash syndrome: a biopsychosocial approach. J Neurol Neurosurg Psychiatry 70:722–726
Freeman MD, Croft AC, Rossignol AM et al. (1999) A review and methodologic critique of the literature refuting whiplash syndrome. Spine 24:86–96
Frobin W, Leivseth G, Biggemann M et al. (2002) Sagittal plane segmental motion of the cervical spine. A new precision measurement protocol and normal motion data of healthy adults. Clin Biomech 17:21–31
Galasko CS, Murray PM, Pitcher M et al. (1993) Neck sprains after road traffic accidents: a modern epidemic. Injury 24:155–157
Gay JR, Abbot KH (1953) Common whiplash injuries of the neck. J Am Med Assoc 152:1698–1704
Gimse R, Bjorgen IA, Tjell C et al. (1997) Reduced cognitive functions in a group of whiplash patients with demonstrated disturbances in the posture control system. J Clin Exp Neuropsychol 19:838–849
Griffen MM, Frykberg ER, Kerwin AJ et al. (2003) Radiographic clearance of blunt cervical spine injury: plain radiograph or computed tomography scan? J Trauma 55:222–226
Griffiths HJ, Olson PN, Everson LI et al. (1995) Hyperextension strain or "whiplash" injuries to the cervical spine. Skeletal Radiol 24:263–266
Hamer AJ, Gargan MF, Bannister GC et al. (1993) Whiplash injury and surgically treated cervical disc disease. Injury 24:549–550
Harris MB, Duval MJ, Davis JA Jr et al. (1993) Anatomical and roentgenographic features of atlantooccipital instability. J Spinal Disord 6:5–10
Hartling L, Pickett W, Brison RJ (2002) Derivation of a clinical decision rule for whiplash associated disorders among individuals involved in rear-end collisions. Accid Anal Prev 34:531–539
Heikkila HV, Wenngren BI (1998) Cervicocephalic kinesthetic sensibility, active range of cervical motion, and oculomotor function in patients with whiplash injury. Arch Phys Med Rehabil 79:1089–1094
Herrstrom P, Lannerbro-Geijer G, Hogstedt B (2000) Whiplash injuries from car accidents in a Swedish middle-sized town during 1993–1995. Scand J Prim Health Care 18:154–158
Hildingsson C, Toolanen G (1990) Outcome after soft-tissue injury of the cervical spine. A prospective study of 93 car-accident victims. Acta Orthop Scand 61:357–359
Hildingsson C, Hietala SO, Toolanen G (1989) Scintigraphic findings in acute whiplash injury of the cervical spine. Injury 20:265–266
Hirsch SA, Hirsch PJ, Hiramoto H et al. (1988) Whiplash syndrome. Fact or fiction? Orthop Clin North Am 19:791–795
Jakobsson L, Norin H, Svensson MY (2004) Parameters influencing AIS 1 neck injury outcome in frontal impacts. Traffic Inj Prev 5:156–163
Jaspers JP (1998) Whiplash and post-traumatic stress disorder. Disabil Rehabil 20:397–404
Jonsson H Jr, Bring G, Rauschning W et al. (1991) Hidden cervical spine injuries in traffic accident victims with skull fractures. J Spinal Disord 4:251–263
Jonsson H Jr, Cesarini K, Sahlstedt B (1994) Findings and outcome in whiplash-type neck distortions. Spine 19:2733–2743
Joslin CC, Khan SN, Bannister GC (2004) Long-term disability after neck injury: a comparative study. J Bone Joint Surg Br 86:1032–1034
Kaale BR, Krakenes J, Albrektsen G et al. (2005a) Whiplash-associated disorders impairment rating: neck disability index score according to severity of MRI findings of ligaments and membranes in the upper cervical spine. J Neurotrauma 22:466–475
Kaale BR, Krakenes J, Albrektsen G et al. (2005b) Head position and impact direction in whiplash injuries: associations with MRI verified lesions of ligaments and membranes in the upper cervical spine. J Neurotrauma
Kasch H, Stengaard-Pedersen K, Arendt-Nielsen L et al. (2001) Headache, neck pain, and neck mobility after acute whiplash injury: a prospective study. Spine 26:1246–1251
Kessels RP, Aleman A, Verhagen WI et al. (2000) Cognitive functioning after whiplash injury: a meta-analysis. J Int Neuropsychol Soc 6:271–278
Kivioja J, Sjalin M, Lindgren U (2004) Psychiatric morbidity in patients with chronic whiplash-associated disorder. Spine 29:1235–1239
Krakenes J, Kaale BR, Rorvik J et al. (2001) MRI assessment of normal ligamentous structures in the craniovertebral junction. Neuroradiology 43:1089–1097
Krakenes J, Kaale BR, Moen G et al. (2002) MRI assessment of the alar ligaments in the late stage of whiplash injury: a study of structural abnormalities and observer agreement. Neuroradiology 44:617–624
Krakenes J, Kaale BR, Moen G et al. (2003a) MRI of the tectorial and posterior atlanto-occipital membranes in the late stage of whiplash injury. Neuroradiology 45:585–591
Krakenes J, Kaale BR, Nordli H et al. (2003b) MR analysis

of the transverse ligament in the late stage of whiplash injury. Acta Radiol 44:637–644
Krakenes J, Kaale B (2006) Magnetic Resonance Imaging Assessment of Craniovertebral Ligaments and Membranes After Whiplash Trauma. Spine 31:2820–2826
Kullgren A, Krafft M, Nygren A et al. (2000) Neck injuries in frontal impacts: influence of crash pulse characteristics on injury risk. Accid Anal Prev 32:197–205
Kwan O, Friel J (2003) A review and methodologic critique of the literature supporting "chronic whiplash injury". Part I: research articles. Med Sci Monit 9:RA203–RA215
Landis JR, Koch GG (1977) The measurement of observer agreement for categorical data. Biometrics 33:159–174
Lord SM, Barnsley L, Bogduk N (1995) The utility of comparative local anesthetic blocks versus placebo-controlled blocks for the diagnosis of cervical zygapophysial joint pain. Clin J Pain 11:208–213
Lord SM, Barnsley L, Wallis BJ et al. (1996) Chronic cervical zygapophysial joint pain after whiplash. A placebo-controlled prevalence study. Spine 21:1737–1744
Lovell ME, Galasko CS (2002) Whiplash disorders: a review. Injury 33:97–101
Maimaris C, Barnes MR, Allen MJ (1988) "Whiplash injuries" of the neck: a retrospective study. Injury 19:393–396
Mayou R, Bryant B, Duthie R (1993) Psychiatric consequences of road traffic accidents. Br Med J 307:647–651
Miettinen T, Lindgren KA, Airaksinen O et al. (2002) Whiplash injuries in Finland: a prospective 1-year follow-up study. Clin Exp Rheumatol 20:399–402
Minton R, Murray P, Stephenson W et al. (2000) Whiplash injury: Are current head restraints doing their job? Accid Anal Prev 32:177–185
Nomura E, Horiuchi Y, Inoue M (2002) Correlation of MR imaging findings and open exploration of medial patellofemoral ligament injuries in acute patellar dislocations. Knee 9:139–143
Norris SH, Watt I (1983) The prognosis of neck injuries resulting from rear-end vehicle collisions. J Bone Joint Surg Br 65:608–611
Otte A (2001) The "railway spine": a precursor for the "whiplash syndrome"? Med Sci Monit 7:1064–1065
Ovadia D, Steinberg EL, Nissan MN et al. (2002) Whiplash injury: a retrospective study on patients seeking compensation. Injury 33:569–573
Panjabi MM, Ito S, Pearson AM et al. (2004) Injury mechanisms of the cervical intervertebral disc during simulated whiplash. Spine 29:1217–1225
Parmar HV, Raymakers R (1993) Neck injuries from rear impact road traffic accidents: prognosis in persons seeking compensation. Injury 24:75–78
Patijn J, Wilmink J, ter Linden FH et al. (2001) CT study of craniovertebral rotation in whiplash injury. Eur Spine J 10:38–43
Pearson AM, Ivancic PC, Ito S (2004) Facet joint kinematics and injury mechanisms during simulated whiplash. Spine 29:390–397
Penning L, Wilmink JT (1987) Rotation of the cervical spine. A CT study in normal subjects. Spine 12:732–738
Pettersson K, Hildingsson C, Toolanen G et al. (1997) Disc pathology after whiplash injury. A prospective magnetic resonance imaging and clinical investigation. Spine 22:283–287
Pfirrmann CW, Binkert CA, Zanetti M et al. (2000) Functional MR imaging of the craniocervical junction. Correlation with alar ligaments and occipito-atlantoaxial joint morphology: a study in 50 asymptomatic subjects. Schweiz Med Wochenschr 130:645–651
Pfirrmann CW, Binkert CA, Zanetti M et al. (2001) MR morphology of alar ligaments and occipitoatlantoaxial joints: study in 50 asymptomatic subjects. Radiology 218:133–137
Platzer W (1986) Color atlas and textbook of human anatomy, vol 3. Locomotor system. Thieme, Stuttgart
Quinlan KP, Annest JL, Myers B et al. (2004) Neck strains and sprains among motor vehicle occupants: United States, 2000. Accid Anal Prev 36:21–27
Radanov BP, Sturzenegger M, De Stefano G et al. (1994) Relationship between early somatic, radiological, cognitive and psychosocial findings and outcome during a one-year follow-up in 117 patients suffering from common whiplash. Br J Rheumatol 33:442–448
Radanov BP, Stefano G di, Augustiny KF (2001) Symptomatic approach to posttraumatic headache and its possible implications for treatment. Eur Spine J 10:403–407
Richter M, Otte D, Pohlemann T et al. (2000) Whiplash-type neck distortion in restrained car drivers: frequency, causes and long-term results. Eur Spine J 9:109–117
Ronnen HR, de Korte PJ, Brink PR et al. (1996) Acute whiplash injury: Is there a role for MR imaging? A prospective study of 100 patients. Radiology 201:93–96
Saternus KS, Thrun C (1987) Traumatology of the alar ligaments. Aktuelle Traumatol 17:214–218 [in German]
Schrader H, Obelieniene D, Bovim G et al. (1996) Natural evolution of late whiplash syndrome outside the medicolegal context. Lancet 347:1207–1211
Solomon S (2005) Chronic post-traumatic neck and head pain. Headache 45:53–67
Spitzer WO, Skovron ML, Salmi LR et al. (1995) Scientific monograph of the Quebec Task Force on Whiplash-Associated Disorders: redefining "whiplash" and its management. Spine 20:1S–73S
Squires B, Gargan MF, Bannister GC (1996) Soft-tissue injuries of the cervical spine: 15-year follow-up. J Bone Joint Surg Br 78:955–957
Stemper BD, Yoganandan N, Pintar FA (2005) Effects of abnormal posture on capsular ligament elongations in a computational model subjected to whiplash loading. J Biomech 38:1313–1323
Stefano G di, Radanov BP (1995) Course of attention and memory after common whiplash: a two-year prospective study with age, education and gender pair-matched patients. Acta Neurol Scand 91:346–352
Sterling M, Kenardy J, Jull G et al. (2003) The development of psychological changes following whiplash injury. Pain 106:481–489
Sterner Y, Toolanen G, Gerdle B et al. (2003) The incidence of whiplash trauma and the effects of different factors on recovery. J Spinal Disord Tech 16:195–199
Sterner Y, Gerdle B (2004) Acute and chronic whiplash disorders: a review. J Rehabil Med 36:193–209
Taylor JR, Finch P (1993) Acute injury of the neck: anatomical and pathological basis of pain. Ann Acad Med Singapore 22:187–192
Taylor JR, Twomey LT, Kakulas BA (1998) Dorsal root ganglion injuries in 109 blunt trauma fatalities. Injury 29:335–339

Tjell C, Rosenhall U (1998) Smooth pursuit neck torsion test: a specific test for cervical dizziness. Am J Otol 19:76–81
Tjell C, Tenenbaum A, Rosenhall U (1999) Auditory function in whiplash-associated disorders. Scand Audiol 28:203–209
Turner MA, Taylor PJ, Neal LA (2003) Physical and psychiatric predictors of late whiplash syndrome. Injury 34:434–437
Van Goethem JW, Biltjes IG, van den Hauwe L et al. (1996) Whiplash injuries: Is there a role for imaging? Eur J Radiol 22:30–37
Versteegen GJ, Dijkstra PU, Jaspers JP et al. (2003) Sprain of the neck: quality of life and psychological functioning. A 4-year retrospective study. Qual Life Res 12:335–343
Volle E, Montazem A (2001) MRI video diagnosis and surgical therapy of soft tissue trauma to the craniocervical junction. Ear Nose Throat J 80:41–48
Volle E, Montazem A (2003) Strukturdefekte der Ligamenta alaria in der offenen Fuktionskernspintomographie. Manuelle Medizin 35:188–193
Watkinson A, Gargan MF, Bannister GC (1991) Prognostic factors in soft tissue injuries of the cervical spine. Injury 22:307–309
Wenngren BI, Pettersson K, Lowenhielm G et al. (2002) Eye motility and auditory brainstem response dysfunction after whiplash injury. Acta Otolaryngol 122:276–283
Willauschus WG, Kladny B, Beyer WF et al. (1995) Lesions of the alar ligaments. In vivo and in vitro studies with magnetic resonance imaging. Spine 20:2493–2498
Wilmink JT, Patijn J (2001) MR imaging of alar ligament in whiplash-associated disorders: an observer study. Neuroradiology 43:859–863

Cervical Trauma

12

Özkan Özsarlak

CONTENTS

Ö. Özsarlak, MD
Department of Radiology, University Hospital Antwerp, Wilrijkstraat 10, 2650 Edegem-Antwerp, Belgium

12.1 Injury-Related Anatomy of the Cervicocranium and Cervical Spine

The cervicocranium extends from the skull base to the C2–C3 disk space. Characteristics of the cervicocranium related to the normal development during childhood or later should not be misinterpreted as signs of trauma. Examples of these include the ter-

KEY-POINTS

- Acute cervical spine injury:
  - 1.9%–4.6% of all patients with blunt trauma in emergency room
  - 6000 deaths and 5000 Quadriplegia/year in US
  - 4:1 male:female ratio
  - Motor vehicle accident (40%), falls (20%), violence (14%)
- Cervical fractures:
  - 1/3 at C2
  - 1/2 at C6 and/or C7
  - Older patients especially C2, younger patients more lower cervical spine
- Classification according to:
  - Level
  - Mechanism
    - Flexion (46%–79%)
    - Extension (20%–38%)
    - Flexion-rotation (12%)
    - Vertical compression (12%)
    - Hyperextension-rotation (4%–6%)
  - Morphology
  - Stability/instability
    - Three-column model: anterior – middle – posterior. Injury to ≥2 columns results in instability
- Imaging necessary if any of the following applies:
  - High-risk factor present:
    - Age ≥65 years
    - Dangerous mechanism:
      - Fall from elevation ≥3 ft/5 stairs
      - Axial load to the head
      - >100 km/h MVA, rollover or ejection MVA
      - Motorized recreational vehicles
      - Bicycle collision
    - Paresthesias in extremities
  - No low-risk factor present:
    - Simple rear-end MVA, excluding:
      - Into oncoming traffic
      - Hit by bus or large truck
      - Rollover
      - Hit by high speed vehicle
    - Sitting position in ED
    - Ambulatory at any time since injury
    - Delayed onset of neck pain
    - No midline tenderness
  - Unable to actively rotate the neck 45° to the left and right
- CT as the initial imaging examination if any of these:
  - High-speed MVA (>50 km/h)
  - MVA with death at scene
  - Fall from >3 m
  - Significant head injury (intracranial hemorrhage, unconscious in emergency room)
  - Neurologic symptoms referred to the C-spine
  - Pelvic or multiple extremity fractures
- Plain film for cervical trauma should include at least:
  - Lateral
  - AP
  - Open-mouth odontoid

minal ossification center of the dens, vertical cleft in the anterior arch of C1 and the non-ossified vertical cleft of the dens (Figs. 12.1 and 12.2). The smooth sclerotic margins distinguish these ossicles or clefts from acute traumatic lesions. Another normal developmental variant in childhood is the physiologic pseudosubluxation at C2–C3, or C3–C4 levels, which is found in up to 25% of children (Lustrin et al. 1994). Normal appearing apophyseal joints and a smoothly delineated spinolaminar line exclude a true subluxation. The cervicocranium includes the atlanto-occipital, atlanto-axial, and the intervertebral cervical joints. The atlanto-occipital joint provides the "yes" movement (flexion-extension of the neck), and the atlanto-axial joint the "no" movement (lateral rotation of atlas on axis). The external and the internal ligaments stabilize the cervicocranium, protect the spinal cord, and prevent excessive neck movements.

The external ligaments include:

1. Posterior atlanto-occipital membrane, and atlanto-axial ligament (Figs. 12.3, 12.4): These structures are the superior extension of the ligamenta flava, which ends at the C2 level.
2. Anterior atlanto-occipital membrane, and atlanto-axial ligament (Figs. 12.3, 12.4): These structures are the upward continuation of the anterior longitudinal ligament.
3. Anterior longitudinal ligament (Figs. 12.3, 12.4): This ligament is a thick band of fibrous tissue that runs along the anterior surfaces of the vertebral bodies. It extends from the anterior tubercle of the atlas over the full length of the spinal column to

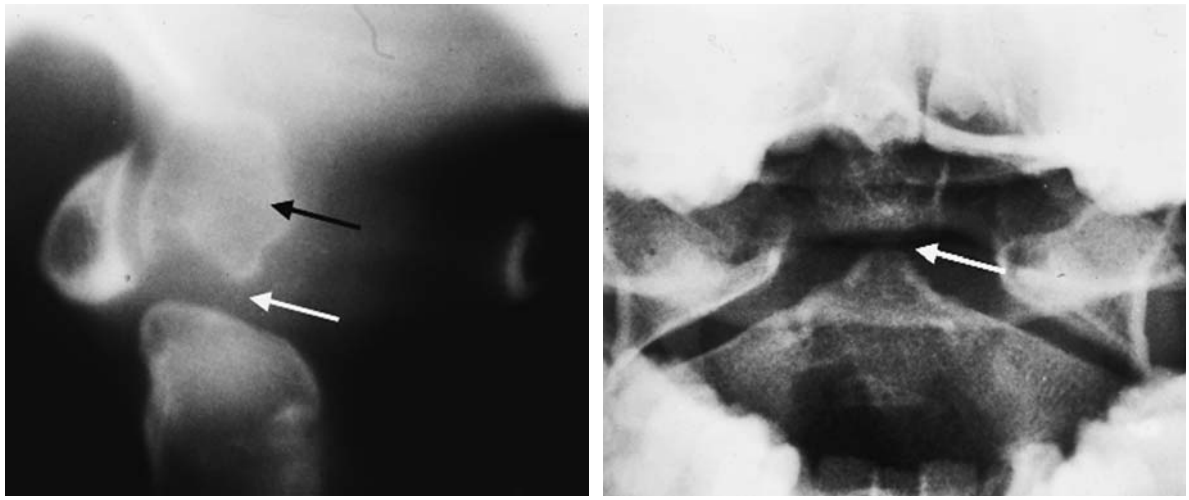

a b

Fig. 12.1a,b. Os odontoideum. Lateral view radiograph. Terminal ossification of dens (os odontoideum) (*black arrow*), non-ossified cartilage (*white arrows*), and body of the dens

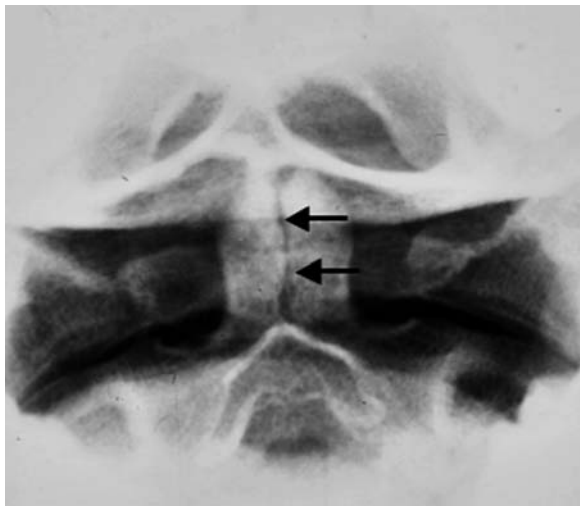

Fig. 12.2. Vertical cleft of the dens axis. Open-mouth odontoid view radiograph. Non-ossified physiologic vertical cleft within the dens (*arrows*)

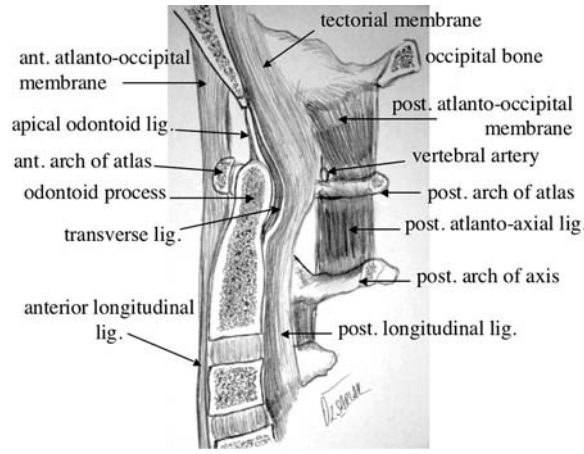

Fig. 12.3. Cervicocranium, medial view. Cervicocranium, median sagittal section, medial view

fuse with the upper, pelvic surface of the sacrum. It blends with the periosteum of each vertebra, but is less firmly attached to the intervertebral discs.

4. Ligamentum nuchae (Fig. 12.4): The ligamentum nuchae runs from the external occipital protuberance along the tips of the spinous processes of the cervical vertebrae, to the tip of the spinous process of the vertebra prominens (usually C7).

The internal ligaments include:

1. Cruciate ligament (Figs. 12.3–12.6): This ligament is composed of the transverse ligament of the atlas and two small bands. The transverse ligament is a thick and strong band that bridges horizontally across the ring of the atlas. It is broader and thicker in the middle, and is firmly attached on either side to the lateral mass of the atlas. As it crosses the odontoid process, a small band (crus superius) is prolonged upward attaching the occipital bone, and another (crus inferius) extending downward along the posterior surface of the body of the axis. The transverse ligament divides the spinal canal into two unequal parts: the larger posterior part includes the medulla, while the anterior and smaller part contains the odontoid process. The transverse ligament holds the odontoid against

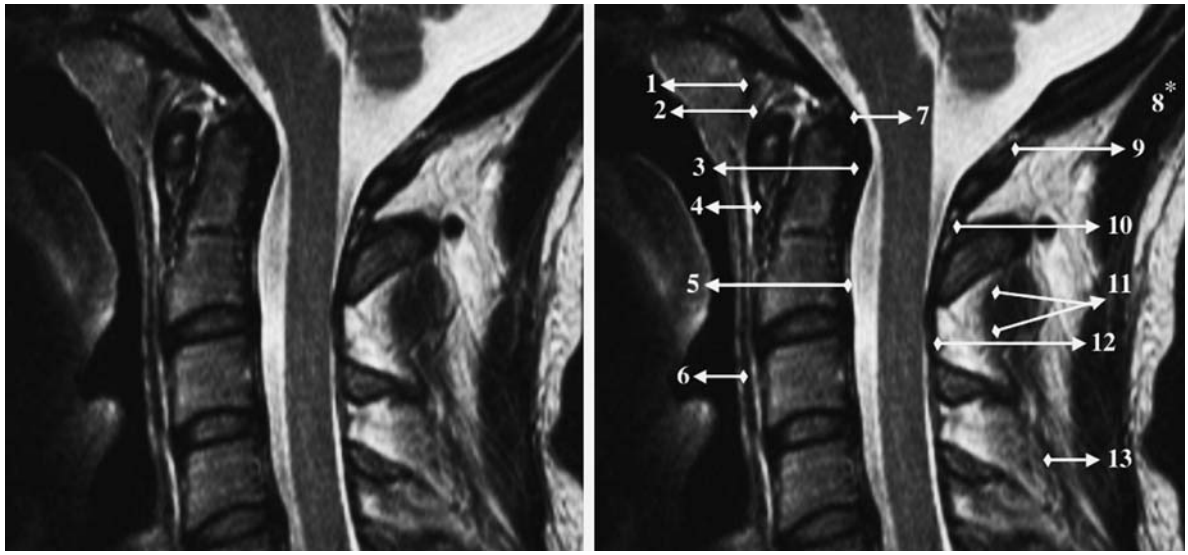

Fig. 12.4. Normal ligamentous MR anatomy. Sagittal T2-weighted MR image obtained on 1.5-T. *1*, Anterior atlanto-occipital membrane; *2*, apical odontoid ligament; *3*, transverse (cruciform) ligament; *4*, anterior atlanto-axial ligament; *5*, posterior longitudinal ligament; *6*, anterior longitudinal ligament; *7*, tectorial membrane; *8*, nuchal ligament; *9*, posterior atlanto-occipital membrane; *10*, posterior atlanto-axial ligament; *11*, interspinous ligaments; *12*, flaval ligaments; *13*, supraspinous ligament

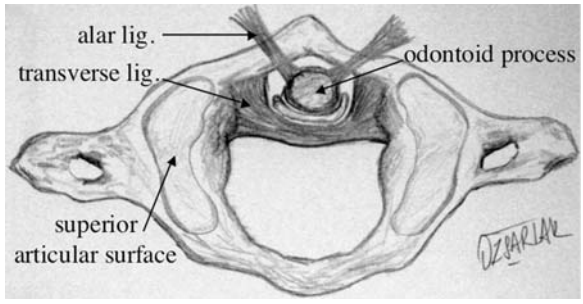

Fig. 12.5. Atlas, view from above. First cervical vertebra

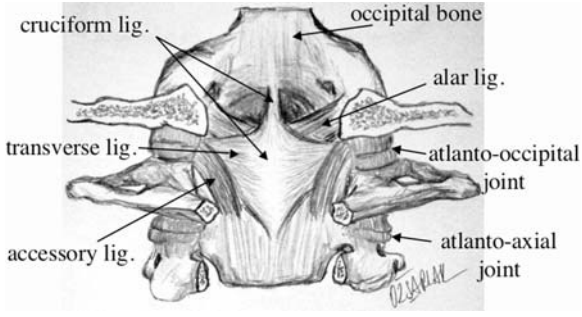

Fig. 12.6. Cervicocranium, posterior view, coronal section after removal of the tectorial membrane. The posterior of the occipital bone, the anterior arcs of the foramen magnum (basion), C1 (atlas), and C2 (axis), and the intervertebral articulations

the atlas, and prevents anterior subluxation of C1 on C2. The cruciate ligament limits both flexion at the craniovertebral junction and anterior displacement of the atlas. If the cruciate ligament ruptures, anterior luxation of the atlas may compress the spinal cord, which can result in quadriplegia, or even death.

2. Accessory ligaments (Fig. 12.6): These paired ligaments arise posterior to and in conjunction with the transverse ligament above the lateral mass of the atlas and insert below into the body of the axis near the base of the odontoid process.
3. Apical odontoid ligament (Figs. 12.3, 12.4): This ligament originates from the anterior rim of the foramen magnum (basion) and inserts into the tip of the odontoid. It anchors the odontoid to the basion.
4. Alar ligaments (Figs. 12.5, 12.6): These paired ligaments extend laterally from the tip of the dens to the occipital condyles, and prevent excessive rotation of head.
5. Posterior longitudinal ligament (Figs. 12.3, 12.4): This ligament runs along the posterior surfaces of vertebral bodies. The tectorial membrane is a superior extension of the posterior longitudinal ligament and continues along the anterior margin of the foramen magnum. It limits extension, flexion, and vertical translation.

The major stabilizers of the cervicocranium are the tectorial membrane, the alar ligaments, and the cruciate ligament, particularly the transverse ligament. The tectorial membrane and transverse ligament are routinely seen on MR imaging, whereas the normal alar ligaments can be more difficult to visualize because of lack of contrast compared to adjacent tissues (Ellis et al. 1991; Schweitzer et al. 1992). In trauma, blood or edema adjacent to the alar ligaments improve the visualization of these ligaments (Katzberg et al. 1999).

12.2 Cervical Trauma

12.2.1 Incidence, Mortality, and Morbidity

- Incidence: The incidence of acute cervical spine injury ranges from 1.9% to 4.6% of patients with blunt trauma. The incidence increases up to 5.9% in multiple-injured patients (McNamara et al. 1990; Nunez et al. 1996). In infants and children, the reported incidence of blunt cervical spine injury is less than 1% (John 1999).
- Level of injury: Cervical spine fractures occur predominantly at two levels. One third of cervical vertebral fractures occur at the level of C2, and one half of injuries occur at the level of C6 or C7. The most frequent level of spinal cord injury is C5 (Prasad et al. 1999). Most fatal cervical spine injuries occur at the upper cervical levels, either at the craniocervical junction, C1, or C2. The atlas is involved in 3%–13% of cases. C3 is involved in less than 5% of cases. The location of the cervical injury by decreasing frequency is (Hahn 2004): C2, C6 > C5, C7 > C3, C4 > C1.
- Mortality, morbidity, and neurologic deficit: Cervical spine injuries cause an estimated 6000 deaths and 5000 new cases of quadriplegia in the US each year. A total of 20% of deaths from traffic accidents are attributed to or caused by severe cervical spinal cord injury, and the majority of those involve the upper cervical spine (occiput to C3). In traumas isolated to the cervical spine, the mortality rate decreases to 7% (Burney et al. 1993). Most deaths associated with spinal cord injury occur during the first 24 h after hospitalization. Injuries to the cervical spine can result in neurologic damage in up to 40%–50% of patients (Borock et al. 1991). In all, 25% of patients with a cervical spine fracture suffer a secondary neurological deficit (quadriplegia, incomplete spinal cord injuries, or radiculopathies) (Colterjohn and Bednar 1995).

12.2.2 Sex and Age

Cervical spine injuries are more common in males than females (M:F ratio 4:1), and are less frequent in people older than 65 year (Jackson et al. 2004). The age distribution of patients presenting with lower cervical spine and spinal cord injuries is bimodal. According to US statistics, 63% of spinal cord injury victims are between 16 and 30 years old, and 1%–3% between 0 and 15 years old (Braakman and Braakman 1987). Most patients with a cervical spine injury lead active lifestyles prior to the injury. Injuries in persons between 15 and 24 years of age are usually the result of a high-energy trauma, such as motor vehicle accidents, accidents resulting from sporting activities, or acts of violence. Injury patterns in elderly patients may differ from those of younger patients because of differences in bone density, injury mechanism, and presence of degenerative changes affecting biomechanics (Lomoschitz et al. 2002). The associated degenerative changes influence the site of injury by narrowing the spinal canal and as such predisposing to a cervical cord injury. Injuries in persons older than 55 years usually result from low-energy trauma, such as falling from standing or seated height (Regenbogen et al. 1986). The prevalence of spinal fractures increases with increasing age. In the younger ages, the most mobile segments are C4 to C7, and most fractures in younger patients occur at these levels (Hu et al. 1996; Blackmore et al. 1999a). With degenerative changes, these segments become less mobile, and the C1–C2 motion segment becomes the most mobile portion. The higher incidence of upper cervical injury in the elderly population may be due to this stiffening effect of aging on the vertebral column (Weller et al. 1997; Spivak et al. 1994).

12.2.3 Patient's History and Clinical Findings

In patients arriving at the emergency department with a history of motor vehicle accident, blunt head or facial trauma, neurologic deficit, and/or neck pain, a cervical

spine injury should be considered present until proven otherwise. Central nervous system evaluation has the highest priority following the emergency assessment of the airways and hemodynamic stability. Alarming findings include posterior neck pain on palpitation, limited range of motion, weakness, numbness, and/or paresthesias along the affected nerve roots. However, the ability to predict cervical injury on the basis of a clinical examination alone is limited. Because of these limitations, most patients who are at high risk for cervical spine injury and those patients that cannot be assessed due to obtundation undergo radiographic evaluation to clear the cervical spine (Ross et al. 1987). Factors that help identify those at a higher risk for cervical spine injury have been described in the literature and include both clinical criteria; Glasgow Coma Score less than 14, neck tenderness, loss of consciousness, neurologic deficit, drug ingestion, and specific mechanisms of injury (motor vehicle accident, fall from a height greater than 3 m) (Schleehauf et al. 1989; Ross et al. 1987; Cadoux et al. 1987; Nunez and Quencer 1998). Due to more effective and successful first aid during the "golden hour" on the trauma site and during transportation to hospital, the number of more seriously injured trauma patients surviving at least until admission to the emergency room has increased during the past decades (Lali and Fehlings 2001; Blackmore et al. 2000).

12.2.4 Etiology

The cause of the cervical spine injuries in decreasing order is motor vehicle accidents (40%), falls (20%), violence such as gunshot wounds (14%), and sports-related activities (14%) (Burney et al. 1993). Though motor vehicle accidents and sports-related injuries are common in younger ages, falls are the most common injury mechanism in elderly patients. Almost 2/3 of isolated spinal cord trauma injuries are at the level of the cervical spine, and complete spinal cord injury (total sensory and motor function loss distal to the injury) occurs in 43%–46% of these cases.

12.2.5 Pathophysiology, Classification, and Biomechanical Instability

Cervical spine injuries can be classified according to the level of injury, the mechanism of the trauma, morphology, or instability of the fracture (Bohlman 1979; Allen et al. 1982; Harris 1986). The exact trauma mechanism in a cervical spine injury often remains uncertain and the complexity of some injuries indicates the presence of several different injury mechanisms in a single trauma (Cusick et al. 1996). Assessment of spinal stability or instability are essential in deciding the correct choice of treatment in each specific type of cervical spine injury. The anatomical and biomechanical properties of the two uppermost cervical vertebrae significantly differ from those in the third to seventh vertebra. A combination of several classification methods, such as level and trauma mechanism followed by a morphological description of the injury and assessment of stability, is used in most studies. Table 12.1 summarizes the craniocervical injuries classified by trauma mechanism, level of injury, and the stability.

The most frequent mechanism of injury is flexion (46%–79%), followed by extension (20%–38%), flexion-rotation (12%), vertical compression (12%), and hyperextension/lateral rotation (4%–6%), respectively. Although the anatomy of the cervical spine permits motion in all planes, the dominant motion is flexion-extension. The position of the head and neck at the time of impact and the direction of the forces causing the injury play an important role in the mechanism of injury. Regardless of the mechanism, cervical spine fractures are serious injuries, and they may cause spinal cord damage, which may result in partial or complete paralysis or even death.

Stability is provided by intact osseous and ligamentous structures (see also Sect. 12.1). To assess the stability of the cervical spine it is divided into three coronal columns (Fig. 12.7); the anterior column includes the anterior two thirds of vertebral bodies, the annulus fibrosus, intervertebral discs, and the anterior longitudinal ligament. The middle column is composed of the posterior one third of the vertebral bodies, the posterior annulus fibrosus, intervertebral discs, and the posterior longitudinal ligament. Hyperextension can result in injury to the anterior column or to both the anterior and middle columns (Katzberg et al. 1999; Benedetti et al. 2000). The posterior column contains all of the remaining posterior elements of the spine formed by the pedicles, transverse processes, articulating facets, laminae, spinous processes, and posterior ligaments (ligamenta flava, interspinous ligaments, supraspinous ligaments, and facet joint capsules). The anterior and posterior longitudinal ligaments

Table 12.1. Classification of craniocervical injuries

Mechanism	Type	Level	Stability
Flexion injury	Simple wedge fracture	Any level	Stable
	Flexion teardrop fracture	Any level	Unstable
	Anterior subluxation	Any level	Stable
	Bilateral facet dislocation	Any level	Unstable
	Clay shoveler's fracture	Lower cervical	Stable
Flexion-rotation injury	Unilateral facet dislocation	Any level	Stable
	Rotatory atlanto-axial dislocation	C1–C2	Unstable
Extension injury	Hyperextension dislocation	Any level	Unstable
	Hangman's fracture	C2	Stable/unstable
	Extension teardrop fracture	Any level	Stable/unstable
	Isolated posterior arch fracture	Any level, usually C1	Stable
	Anterior arch avulsion fracture	C1	Stable
	Laminar fracture	Any level	Stable
Hyperextension-lateral rotation injury	Pillar fracture	Any level	Stable
	Pedicolaminar fracture – separation types I, II, III	Any level	Stable
	Pedicolaminar fracture – separation types IV	Any level	Unstable
Vertical compression injury	Jefferson's fracture	C1	Unstable
	Burst fracture of vertebral body	Lower cervical	Stable/unstable
Craniocervical injury	Atlas fractures types I, II, IV	C1	Stable
	Atlas fractures type III	C1	Stable/unstable
	Atlas fractures types V (Jefferson's fracture)	C1	Unstable
	Atlanto-axial subluxation-distraction	C1	Unstable
	Atlanto-occipital dislocation-distraction	C1	Unstable
	Odontoid process fracture types I, III	C2	Stable
	Odontoid process fracture types II, IIA	C2	Unstable
	Occipital condyle fracture types I, II	Occipital bone	Stable
	Occipital condyle fracture type III	Occipital bone	Unstable

maintain the structural integrity of the anterior and middle columns. The posterior column is held in alignment by a complex ligamentous system, including the nuchal ligament complex, capsular ligaments, and ligamenta flava. If one column is disrupted, other columns may provide sufficient stability to prevent spinal cord injury. Injury to any two adjacent columns will result in instability, and the spine may move as two separate units, increasing the likelihood of spinal cord injury (Denis 1983).

Most sports-related fractures and dislocations of the cervical spine occur in the lower cervical segment, C4 to C7, with axial loading of the neck in flexion, and most of the severe injuries involve fractures of the vertebral body with varying degrees of compression, subluxation, or dislocation (Torg and Ramsey-Emrhein 1997). The degree of instability depends on several factors that may translate into neurologic disability, secondary to spinal cord compression. The risk of neurologic injury, secondary to spinal injury, increases with degenerative changes related to aging, arthritic conditions (rheumatoid arthritis, ankylosing spondylitis) (Fig. 12.8), spinal stenosis, spina bifida, as well as the specific mechanism and location of the injury (Torg and Ramsey-Emrhein 1997; Dvorak et al. 1989).

Fig. 12.7. Imaginary coronal columns of cervical spine, lateral view. *1*, Anterior column including the anterior 2/3 of vertebral bodies, annulus fibrosus, intervertebral discs, and anterior longitudinal ligament. *2*, Middle column including posterior 1/3 of vertebral bodies, annulus fibrosus, intervertebral discs, and posterior longitudinal ligament. *3*, Posterior column including pedicles, transverse processes, and posterior ligaments

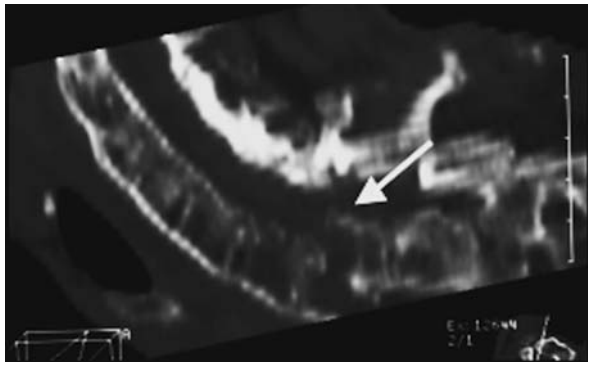

a

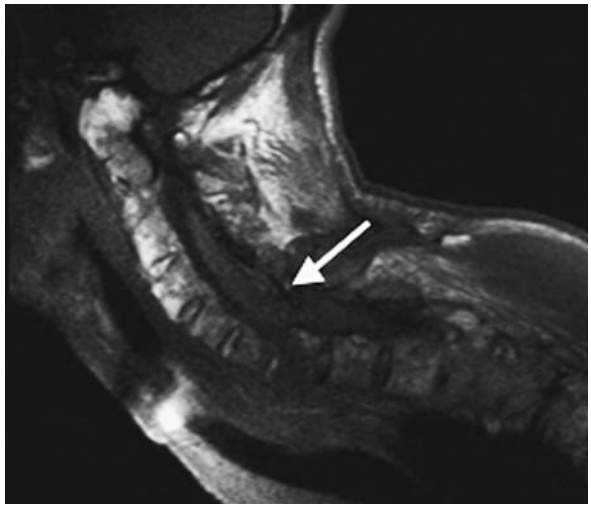

b

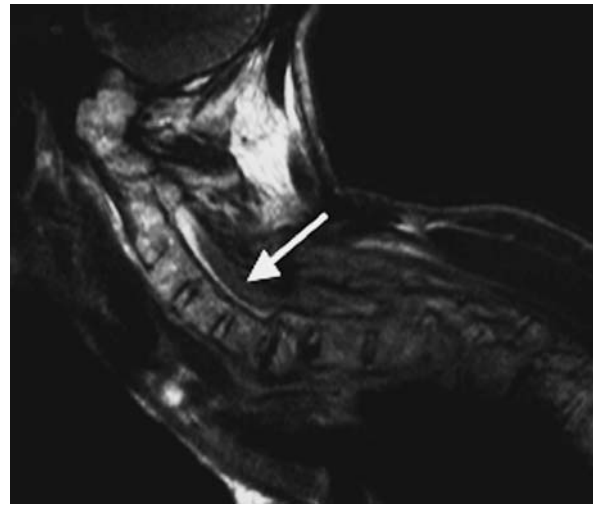

c

Fig. 12.8a–c. Ankylosing spondylitis. Cervical fusion due to ankylosing spondylitis in a 72-year-old male patient, complicated by a C7 fracture and anterior dislocation of the C6 vertebral body. **a** Sagittal CT reformation showing a burst fracture of the C7 vertebral body (*white arrow*), anterior dislocation of the C6 vertebral body, and spinal canal stenosis at the level of C7. **b** Sagittal T1-weighted MR image showing a step at the posterior spinal contour with compression of the cervical myelum, more pronounced due to a posterior bony spur (*arrow*). **c** Sagittal T2-weighted MR image showing an increased medullary T2 signal due to cord edema (*arrow*)

12.3 Imaging Studies

According to the NEXUS study (National Emergency X-Radiography Utilization Study) for low-risk criteria, cervical spine radiography is indicated for trauma patients unless they exhibit all of the following criteria: no posterior midline cervical spine tenderness, no evidence of intoxication, normal level of alertness, no focal neurological deficit, and no painful distracting injuries. These criteria are highly accurate and in most patients they can rule out virtually any unstable cervical spine injury. Patients who meet all five criteria have a very low risk for cervical spine injury (99.8% negative predictive value). The sensitivity of the decision rule is high (99.0%), but due to its low specificity (12.9%), its positive predictive value is low (2.7%) (Hoffman et al. 2000). The Canadian C-Spine Rule based on 20 clinical variables is a more accurate tool in alert and stable trauma patients, with a specificity of 42.5% (Stiell et al. 2003) (Table 12.2). Use of these criteria reduces the number of radiographic examinations of the cervical spine by 20%–42% in alert and stable patients (Stiell et al. 2001; Touger et al. 2002). All patients with blunt spinal trauma who do not meet the clinical low-risk criteria require spinal imaging.

While the discussion is still ongoing regarding what constitutes an adequate radiographic examination, and how many radiographic views are necessary to rule out any cervical spine injury, there is broad acceptance that the adequate cervical spine series must include at least three views: a true lateral view, an anteroposterior view, and an open-mouth odontoid view (Streitwieser et al. 1983; Freemyer et al. 1989; MacDonald et al. 1990). Although missed cervical fractures, subluxations, and dislocations can be the result of image misinterpretation, the most frequent cause of an overlooked injury is an inadequate film series (Davis et al. 1993). A lateral view alone is inadequate and will miss up to 15% of cervical spine injuries (Ross et al. 1987). When combined with standard AP, and odontoid views, 5%–8% of patients with fractures may still have normal radiographs (Woodring and Lee 1993; Ringenberg et al. 1988). In addition, difficulty in positioning polytraumatized patients may lead to a larger number of inadequate radiographic examinations. Some authors also suggest adding two lateral oblique views to detect fractures or subluxations that are not identified with a standard three-view series (Turetsky et al.

Table 12.2. Canadian C-Spine rule for indications of radiography in patients with cervical trauma (Stiell et al. 2001)

Risk factors		Imaging

High-risk factor:
• Age > 65 years
• Dangerous mechanism
  • Fall from elevation ≥3 ft/5 stairs
  • Axial load to the head
  • >100 km/h MVA, rollover or ejection MVA
  • Motorized recreational vehicles
  • Bicycle collision
• Paresthesias in extremities
	Present	Required

Low-risk factors:	Not present	Required

• Simple rear-end motor vehicle accident, excluding:
  • Into oncoming traffic
  • Hit by bus or large truck
  • Rollover
	Present but unable to rotate neck actively (45° left and right)	Required

• Hit by high speed vehicle • Sitting position in emergency department • Ambulatory at any time • Delayed or not immediate onset of neck pain • Absence of midline cervical spine tenderness	Present and able to rotate neck actively (45° left and right)	Not required

1993; Doris and Wilson 1985). However, repeated attempts to improve on the quality of plain films are usually unsuccessful and a waste of valuable time. A CT scan with sagittal and coronal reconstructions is indicated to evaluate possible spinal injury at any level or through the lower cervical spine if this area cannot be visualized on conventional radiographs (Nunez et al. 1996; Jelly et al. 2000). Borock et al. (1991) report that CT alone shows 98% of cervical spine injuries, and when combined with plain radiography, 100% of injuries were detected. For cases in which the plain film and CT findings are normal, lateral radiographs in flexion and extension can then be obtained to assess possible ligamentous injury (Borock et al. 1991). MR imaging may play a role to evaluate the presence of hemorrhagic or non-hemorrhagic cord contusion; however, MR imaging in patients with cervical spine injury is still controversial, because its influence on the patient's outcome has not been fully established (Flanders et al. 1996; Bondurant et al. 1990). Nevertheless, the detection of a cord injury may have therapeutic implications in the decision making for immediate decompressive surgery. Table 12.3 summarizes the checkpoints of conventional radiography, CT, and MRI in the assessment of cervicocranial injuries.

12.3.1 Cross-Table Lateral View

Approximately 85%–90% of cervical spine injuries can be detected on a lateral view plain film (Graber and Kathol 1999). A lateral view of the cervical spine should show all seven vertebral bodies, and the cervicothoracic junction. Normal measures have been determined for many of the osseous relationships and soft-tissue contours at the craniocervical junction using a lateral radiogram and are valuable for excluding upper cervical spine injury (Table 12.4). To avoid missing significant abnormalities, interpretation should be methodical.

Table 12.3. Imaging assessment guidelines in cervicocranial injury

Lateral view radiograph	AP view radiograph	CT	MR
Posterior vertebral line	Lateral atlanto-dens interval	Occipital condyles, C1, C2, foramen magnum	Bone marrow signal intensity
Anterior vertebral line	Atlanto-occipital joint	Atlanto-occipital joint	Atlanto-occipital joint
Spinolaminar line	Atlanto-axial joint	Atlanto-axial joint	Atlanto-axial joint
Basion-dens interval	C1–C2 overhanging	Prevertebral soft tissues	Prevertebral soft tissues
Prevertebral soft tissues	Occipital condyles	Presence of SAH or EDH	Presence of EDH
Osseous integrity	C1, C2, dens		Nuchal ligament signal intensity
Clivus, C1, C2			Interspinous ligament
Interpedicular distance			Tectorial membrane
Anterior atlanto-dens interval			Spinal cord

SAH, subarachnoid hemorrhage; *EDH*, epidural hemorrhage

Table 12.4. Normal values

Parameters	Adults	Children
Predental space	<3 mm	<4–5 mm
C2–C3 pseudosubluxation	<3 mm	<4–5 mm
Prevertebral (retropharyngeal) space	<7 mm at C2	1/2 to 2/3 vertebral body distance anteroposteriorly
	<5 mm at C3–C4	
	<22 mm at C6	<14 mm at C6
Angulation of two adjacent vertebrae	<11°	<11°
Spinal cord dimension	>13 mm	Adult size by 6 years of age
Basion-dens interval	<12 mm	

1. Check alignment of the cervical spine by following three imaginary contour lines (Fig. 12.9). The disruption of the normally smooth lordotic curve of these lines may be caused by bony or ligamentous injury.
   - Anterior contour line: the anterior margins of all vertebrae
   - Posterior contour line: the posterior aspect of all vertebrae
   - Spinolaminar contour line: through the bases of the spinous processes

   There are two exceptions to this rule, where these contours may have a physiologic misalignment or "pseudosubluxation": in young children because of immature muscular development, and in adults with a "physiologic benign pseudosubluxation" due to ligamentous laxity. This is mostly seen at the C2–C3 level and, less commonly, at the C3–C4 level. Pseudosubluxation should disappear on an extension view. However, flexion-extension views should not be obtained until the entire cervical spine is otherwise cleared radiographically.
2. Check each vertebra individually for obvious fracture or bone density changes.

Fig. 12.9. Alignment of the cervical spine. Lateral view radiograph. *1*, Anterior contour line through the anterior margins of all vertebrae. *2*, Posterior contour line through the posterior margins of all vertebrae. *3*, Spinolaminar contour line through the bases of the spinous processes

3. Check soft tissue changes in the predental and prevertebral spaces.
   - Predental space (anterior atlanto-dens interval): the distance between the anterior aspect of the odontoid and the posterior aspect of the anterior arch of C1. This space should be no more than 3 mm in an adult and 5 mm in a child. Suspect transverse ligament disruption if these limits are exceeded (Harris et al. 1994). An increase in this space is presumptive evidence of a fracture of C1 or of the odontoid process.
   - Prevertebral space (retropharyngeal space): extends between the anterior border of the vertebrae to the posterior wall of the pharynx in the upper vertebral level (C2–C4) or to the trachea at the lower vertebral level (C6) (Lee et al. 1997; Harris et al. 1994).
     - At the level of C2 the prevertebral space should not exceed 7 mm.
     - iAt the level of C3 and C4, it should not exceed 5 mm
     - At the level of C6 the prevertebral space is widened by the presence of the esophagus and cricopharyngeal muscle. At this level, the space should be no more than 22 mm in adults or 14 mm in children younger than 15 years.

   Children younger than 24 months may exhibit a physiologic widening of the prevertebral space during expiration; therefore, one should obtain images in small children during inspiration to assess the prevertebral space adequately. If the prevertebral space is widened at any level, a hematoma secondary to a fracture should be assumed.
4. Check for widening of the space between the two spinous process tips. If widening is present, a posterior ligamentous injury or fracture should be considered.
5. Check for an abrupt change in angulation of greater than 11 degrees at any level of the cervical spine, a ligamentous injury or fracture should be ruled out.
6. The spinal canal should be more than 13 mm wide on the lateral view. Anything less than this suggests that spinal cord compromise may be impending.
7. The basion–dens interval (tip of the dens to the basion) and the basion–posterior axial line interval (vertical line drawn along the posterior aspect of the subdental body of C2) are the indicators of an injury to the alar ligaments or tectorial membrane, and should not exceed 12 mm (Harris et al. 1994).

12.3.1.1 Limitations of the Lateral View

Fractures of the occipital condyles and of the lateral masses of C1 are usually not visible on the lateral radiograph because of the inherent anatomic relationships of the occipitoatlantal articulations, the bilateral superimposition of the lateral masses of C1 and the occipital condyles, and the superimposition of the mastoid processes on the occipitoatlantal articulations. Fractures of the anterior arch of C1 can also go undetected by superposition of the posterior obliquity of the anterior arch of C1 between the anterior tubercle and lateral masses of C1.

12.3.2 Open-Mouth Odontoid View

The open-mouth view should include the inferior aspect of the occipital condyles in addition to the entire odontoid process, the lateral masses of C1, the lateral atlanto-dental intervals, the axis body, and the lateral atlanto-axial articulations. The spinous process of C2 should be on the midline. In the unconscious, intubated patient, the open mouth view is inadequate and should be replaced by a CT scan.

1) Check the symmetric alignment of the lateral masses of C1 with respect to the odontoid process. Asymmetry or misalignment is suggestive of a fracture or lateral displacement, but only in cases where the view was taken absolutely straight and without rotation of the head.
2) Assess the symmetry of the lateral aspects and interspace between C1 and C2.
3) Check for fractures of the dens. Radiographic lines caused by the teeth or soft-tissues either longitudinal or horizontal through the dens may simulate a fracture. If there is any doubt of a fracture, the view should be repeated. If it is not possible to exclude a fracture of the dens, CT scan is indicated.

12.3.2.1 Limitations of the Open-Mouth View

Frequent limitations include partial or complete masking of the occipital condyles by the maxillary premolar and/or molar teeth, covering of the lateral masses of C1 by the occipital bone, superimposition of maxillary incisor teeth on the dens, and the presence of an endotracheal and/or nasogastric tube. In addition, it is impossible to obtain an open-mouth view in patients who are unconscious, or who have sustained major midfacial or mandibular fractures.

12.3.3 Anteroposterior (AP) View

The structures recognized on the AP radiograph of the cervical spine include the lower cervical vertebral bodies including superior and inferior endplates, disk spaces, uncinate processes, uncovertebral joints of Luschka, lateral masses forming the lateral columns, and the tracheal air column. The anteroposterior view must include the spinous processes of all the cervical vertebrae from C2 to T1.

The spinous processes should be on the midline and in a straight line. If this is not the case, one should consider a rotation injury (e.g. unilateral facet dislocation) (Graber and Kathol 1999). If a spinous process appears vertically split, also consider a clay shoveler fracture. The height of all cervical vertebral bodies should be approximately equal on the AP view.

12.3.4 Swimmer's View

Sometimes it is not possible to fully visualize all seven cervical vertebrae, particularly those of the cervicothoracic junction on a lateral view. In cases where there is no injury to the upper limbs or shoulder girdle, "a swimmer's view" or transaxillary lateral view with traction on the arms may allow adequate visualization of the lower cervical spine and cervicothoracic junction. Disadvantages of the swimmer's view include the inability of the patient to cooperate for the required positioning and superposition of the clavicles, upper ribs, and/or shoulder joints.

12.3.5 Supine Oblique Views

These views can provide visualization of the posterior elements or laminae of the cervical spine and give more information than the AP view. Therefore, it replaces the routine AP view in trauma patients in some centers. The normal structural appearance of the laminae is described as shingles on a roof, forming a regular elliptical curve with equal interlami-

nar spaces. If the interlaminar space between two continuous laminae is increased, subluxation of the involved vertebrae should be suspected. Similarly, if the expected tiling of shingles is disrupted, suspect a unilateral facet dislocation. A posterior laminar fracture should be evident as disruption of the body of a single shingle.

12.3.6 Flexion-Extension Radiographs

Literature regarding the use of flexion-extension radiographs in cervical spine trauma is controversial (Dwek and Chung 2000; Fazl et al. 1990). If there is a question of ligamentous injury in a patient with focal neck pain, minimal misalignment on the lateral view and no evidence of instability or fracture, flexion-extension views can be obtained (Lewis et al. 1991). These radiographs should only be obtained in conscious patients who are able to cooperate. Only active motion should be allowed. Under no circumstance should cervical spine flexion and extension be forced, since force may result in cord injury.

12.3.7 CT

Although cervical spine radiographs are considered to be adequate to rule out fractures, plain films have limitations. Some studies report up to 66% percent missed fractures on plain radiographs (Woodring and Lee 1993). The ideal imaging strategy depends on the individual characteristics of an injury. Blackmore et al. (1999b) studied a large group of patients with several injury mechanisms and clinical parameters. They proposed a clinical decision rule that is designed to select adult patients with blunt trauma who are at greater than 5% risk for cervical spine fracture to undergo screening helical CT (Blackmore 1999b; Hanson et al. 2000). The clinical decision rule to select high-risk patients to undergo CT of the cervical spine is summarized in Table 12.5 (Nunez and Quencer 1998).

Trauma patients need to be evaluated promptly so that critical injuries can be detected promptly and treated adequately. Anything that delays treatment, such as prolonged imaging times, can adversely affect the outcome. Daffner (2000) reported that the average time needed to perform a six-view radiographic evaluation in a group of trauma patients was 22 min and 45%–79% of their patients required one or more repeated radiographs for a satisfactory examination (Daffner 2000). CT is used as an adjunct to conventional radiography at many institutions, some of which even suggest obtaining CT as the primary imaging modality in severely traumatized patients due to its higher diagnostic yield and cost-effectiveness (Blackmore et al. 1999b; Berne et al. 1999; Hanson et al. 2000; Nunez et al. 1996; Jelly et al. 2000). CT may also reveal minimally symptomatic or asymptomatic non-displaced spinous and transverse process fractures that have been previously overlooked on conventional radiographic series. Although there may be no risk of neurologic injury, their presence reflects substantial absorbed energy, and it may be important to detect them as markers for more severe ligamentous, disk, brachial plexus, or vertebral artery injuries (Woodring et al. 1993). Moreover, spinal CT can be performed simultaneously with head, thoracic, and/or abdominal CT, even using the same raw data, in the polytraumatized patient, therefore further reducing imaging time and patient manipulation (Linsenmaier et al. 2002). Multi-row detector CT (MDCT) can overcome the limitations that were experienced with axial or single slice spiral CT, such as the evaluation of intervertebral distances, abnormal angulation, rotation, subluxation and/or dislocations (Van Goethem et al. 2005). Due to technical breakthroughs, MDCT is faster and has better temporal, spatial, and contrast resolution due to smaller isotropic voxels compared with conventional helical CT

Table 12.5. Clinical decision rule to select high-risk patients[a]. These should have helical CT as their initial imaging examination of the cervical spine (Nunez and Quencer 1998)

Injury mechanism parameters:
1. High-speed motor vehicle accident (>50 km/h)
2. Motor vehicle accident with death at scene
3. Fall from height (>3 m)
Clinical parameters:
4. Significant closed head injury (intracranial hemorrhage, unconscious in ED)
5. Neurologic symptoms or signs referred to the cervical spine
6. Pelvic or multiple extremity fractures

[a] The presence of at least one parameter places the patient in the high risk category (>5% risk of cervical spine fracture) and indicates that the patient requires CT as the initial examination.

(Van Goethem et al. 2005; Bensch et al. 2004). CT can reduce the time required for the examination by as much as half when compared with a complete radiographic examination. Further reduction in examination time is also observed with the introduction of newer and faster MDCT. However, the occupied scanner room time per patient will not significantly decrease in the future, as the actual scanning time takes up only a minor part of the occupied scanner room time. The greater part of the occupied scanner room time is spent on patient preparation, injector setup, and the programming of the scanner. This is especially the case in seriously injured trauma patients, whose vital signs are continuously being monitored by emergency room staff and, if necessary, life-saving therapies are administered while the patient is in the CT scanner room (Bensch et al. 2004). On the other hand, MDCT produces a large number of images, and, therefore, in emergency trauma cases, the radiologist should interpret these images using advanced post-processing techniques available on-line on the scanner console, or on the additional workstations or PACS (Bensch et al. 2004; Blackmore et al. 2000). Routine coronal and sagittal reformations are particularly helpful in the evaluation of odontoid fractures and endplate fractures (Van Goethem et al. 2003). The advent of advanced post-processing methods such as two-dimensional (2D) multiplanar reformation (MPR), maximal intensity projection (MIP), and three-dimensional (3D) volume rendering (VR) may give additional information, and has improved the diagnostic interpretation of injuries. Multiplanar and 3D reformations can provide an excellent display of displaced fractures, dislocations, and fracture-dislocations (Fig. 12.10). In addition, MDCT is also able to show soft-tissue abnormalities such as disc herniations, soft tissue hematomas, and sometimes ligamentous ruptures (Van Goethem et al. 2003). Evidence-based approaches have shown that the appropriate use of CT, particularly MDCT, not only improves outcome but also saves money in the diagnosis and treatment planning of the acutely injured

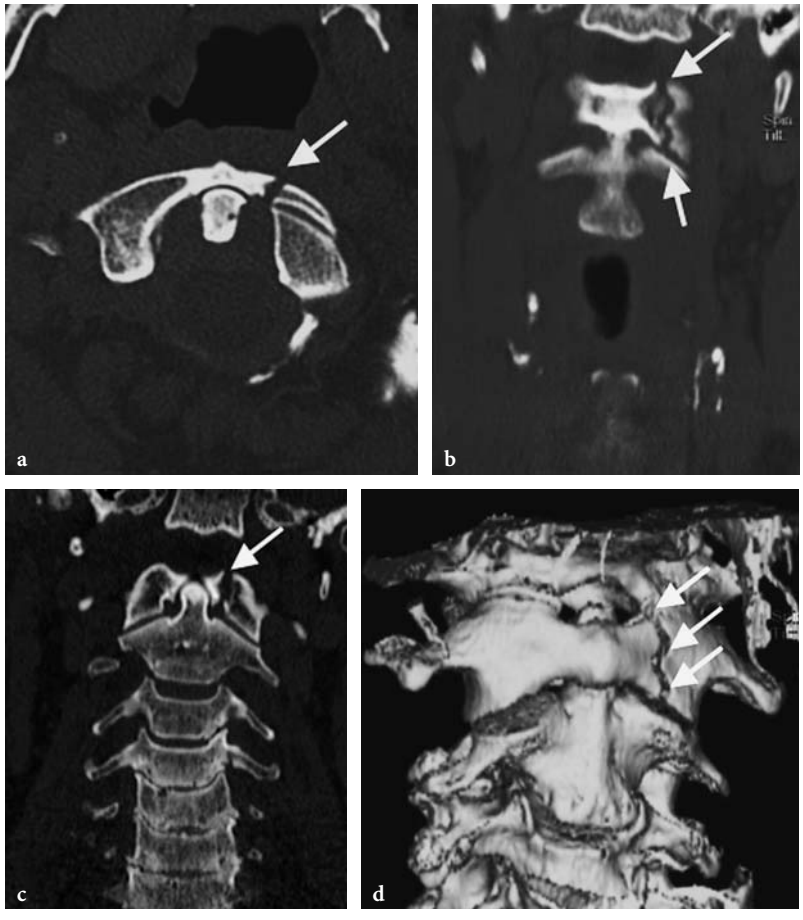

Fig. 12.10a–d. Advantages of multidetector CT (MDCT). Fracture of the anterior arch of C1 (atlas). **a** Axial CT shows a fracture through the anterior arch of C1 (*arrow*). **b**,**c** Coronal reformations through the anterior arch of C1 (*arrows*). **d** Surface shaded display of the cervicocranium showing the exact extension of the fracture (*arrows*)

cervical spine (Mann et al. 2003; Van Goethem et al. 2005). Many institutions now recognize MDCT as the preferred initial imaging procedure in acute (blunt) spinal trauma patients (Obenauer et al. 2002; Van Goethem et al. 2005).

12.3.8 MRI

MRI is superior to either CT or conventional radiography in the evaluation of neural elements such as cord compression, cord edema or hemorrhage, and soft-tissue structures such as ligamentous injury, prevertebral hemorrhage, and traumatic disk herniation (Van Goethem et al. 2005; Katzberg et al. 1999). It is the only method of directly visualizing and differentiating spinal cord hemorrhage and edema, which can have a significant prognostic significance (Schaefer et al. 1992). Additionally, MRI is also able to show the secondary traumatic bony changes such as bone marrow edema. The indications of MRI after stabilizing the patient's life-threatening injury include (Van Goethem et al. 2005; Brohi and Wilson-Macdonald 2000; Geck et al. 2001):

1. Unexpected level of neurologic signs above the level of radiographically seen injury
2. Presence of instability or progressive neurologic deficit
3. Signs of radiculopathy, myelopathy, or cord injury
4. Patients with negative radiographs and suspected cervical ligamentous injury
5. Widening, slippage, or rotational abnormalities of the cervical vertebrae suggesting soft tissue injury

A typical MR imaging protocol for spinal trauma should include sagittal T1- and T2-weighted fast spin-echo images, short TI inversion-recovery (STIR) sagittal images, and axial gradient-echo or T2-weighted images. T1-weighted images provide the best anatomic detail. Ligamentous integrity is usually best seen on gradient-echo and T2-weighted sequences, as well as the detection of blood products within the spinal cord (Warner et al. 1996). T2-weighted and STIR sequences are most sensitive for bone marrow edema, spinal cord injury, and soft-tissue edema (Benedetti et al. 2000; Gunzburg et al. 2003). Spinal cord injury has been classified into three groups according to MRI pattern and patient outcome. The first pattern includes cord edema due to contusion, which has a more favorable prognosis with potential reversibility. The second pattern is hemorrhage, which has much less potential for reversibility. The third pattern is a mixed pattern of blood and edema, which has an intermediate prognosis with some potential for recovery (Kulkarni et al. 1988). The craniocaudal length of the area of abnormal signal intensity of the cord contusion has also been correlated with prognosis. Schaefer et al. (1992) reported that if cord contusion is greater than one vertebral level in length, the prognosis is less favorable. It is also reported that there is a significant association between the occurrence of a cord injury in patients with spondylosis, central canal stenosis, or acute vertebral fractures (Fig. 12.8) (Katzberg et al. 1999; Torg and Ramsey-Emrhein 1997a). Traumatic disk herniation can also be demonstrated on MRI. Secondary findings of cervical disc damage include increased signal intensity of the injured disk on the T2-weighted images representing edematous changes and the presence of associated paraspinal soft tissue injuries (Flanders et al. 1990; Katzberg et al. 1999).

12.4 Flexion Injuries

12.4.1 Simple Wedge Fracture

With a pure flexion injury, the anterior vertebral body bears most of the force and hits against the superior endplate of the subjacent vertebra. This results in an anterior simple wedge compression. The posterior column remains intact. This neurologically stable fracture only requires the use of a cervical orthosis for treatment. Radiographic findings on the lateral film are the loss of anterior vertebral body height, "wedge" configuration, increased concavity, increased density of the endplate due to bony impaction, and loss of definition of the superior endplate (Fig. 12.11) (Campbell et al. 1995). An AP view has limited value, and may show increased interspinous distance and/or loss of definition of the superior endplate. Additional CT or MRI is not indicated, unless there is evidence of potential instability on plain films (Leferink et al. 2002). The characteristics of a simple wedge fracture are summarized in Table 12.6.

Fig. 12.11. Simple wedge fracture. Lateral radiograph. Loss of superior endplate delineation, loss of concavity of the superior aspect of the anterior vertebral body edge and diminished anterior vertical height of C5 vertebral body (*white arrow*)

Table 12.6. Flexion injury: simple wedge fracture

Mechanism	Flexion
Definition	Simple wedge fracture
Spine level	Any level
Stability	Stable
Associated lesions	Swelling of the paravertebral soft tissues
Radiographic findings	Diminished height of the anterior body, increased concavity
Management	Cervical orthosis

12.4.2 Flexion Teardrop Fracture

A flexion teardrop fracture occurs with extreme hyperflexion and vertical axial compression causing a fracture of the anteroinferior aspect of the vertebral body. The typical triangular shaped bony fragment is displaced anteriorly and resembles a teardrop. This is an extremely unstable injury disrupting all three columns, the posterior ligament complex, posterior longitudinal ligament, the anterior longitudinal ligament, and the intervertebral disk (Signoret et al. 1999). It is also a frequently associated injury to the spinal cord (Scher 1982). The latter presents clinically as an acute cervical cord syndrome with quadriplegia, loss of touch, pain, and temperature sensations. Radiographic signs on the AP view include increased interspinous distance, disruption of the lateral columns, disruption of the endplates and disk spaces, distorted facet joints, and/or fracture of the vertebral bodies. The findings on lateral view are hyperkyphosis and severe displacement of the involved vertebral body segment, teardrop fracture fragment, apophyseal joint distraction, and diffuse prevertebral soft tissue swelling (Fig. 12.12). CT helps to determine the extent of the fracture of the involved vertebra, the displacement of the fragment into the spinal canal, and to assess the adjacent vertebrae (Signoret et al. 1999). MRI determines the extent and type of spinal cord injury, and can assess ligamentous and/or disk injury. The initial management is traction. The characteristics of flexion teardrop fracture are summarized in Table 12.7.

Fig. 12.12. Flexion teardrop fracture. Lateral radiograph. Typical triangular fragment anteriorly (*white arrow*), increased interspinous distance (*dashed arrow*), hyperkyphosis and displacement of the C5 vertebral body

Table 12.7. Flexion injury: flexion teardrop fracture

Mechanism	Sudden and forceful flexion
Definition	Avulsion of the anteroinferior corner of a vertebral body
Spine level	Any level
Stability	Unstable
Associated lesions	Anterior and posterior ligamentous disruption, distorted facet joints, spinal cord injury, quadriplegia
Radiographic findings	Teardrop fracture dislocation of the anteroinferior corner of a vertebral body, alignment abnormalities due to ligamentous instability
Management	Traction with cervical tongs

12.4.3 Anterior Subluxation

Anterior subluxation or hyperflexion sprain refers to an incomplete dislocation of the facet joints in an anterior direction and disruption of the posterior ligament complex, without bony injury (see also Sects. 12.9.2 and 12.11.2). The posterior ligament complex consists of the nuchal ligament, the capsular ligaments, the ligamenta flava, and the posterior longitudinal ligament. The anterior longitudinal ligament remains intact. Initially, anterior subluxation is mechanically and neurologically stable, since the anterior columns remain intact. Nevertheless, delayed instability with significant displacement may occur in flexion, especially in patients with unrecognized and untreated anterior subluxation. The radiographic signs include a hyperkyphotic angulation at the level of injury, anterior rotation, or displacement of the subluxed vertebra, widening of the interspinous space ("fanning"), disruption of the anterior and posterior contour lines in flexion views, anterior narrowing and posterior widening of the disc space, increased distance between the vertebral bodies of the involved level and the subjacent superior articular process, and partial uncovering of the facets of the subluxated apophyseal joints (Green et al. 1981) (Fig. 12.13). The combination of an adequate lateral film and CT scanning is reliable in diagnosing these injuries (Demetriades et al. 2000). The characteristics of anterior subluxation injury are summarized in Table 12.8.

Fig. 12.13. Anterior subluxation. Lateral radiograph. Widening of the interspinous distance (*double-headed arrow*), partially uncovered facet surface (*black arrow*), anterior displacement of the vertebral body of C2, hyperkyphotic angulation at the C2–C3 level

Table 12.8. Flexion injury: anterior subluxation

Mechanism	Rupture of the posterior ligamentous complex in flexion
Definition	Anterior subluxation of the interfacetal joints
Spine level	Any level
Stability	Can be unstable in flexion
Associated lesions	No bone injury, rarely neurologic deficit
Radiographic findings	Hyperkyphosis, fanning, displacement of subluxed vertebra, anterior and posterior contour malalignment in flexion
Management	Cervical tongs, approach this potentially unstable because of the significant displacement that can occur with flexion

12.4.4 Bilateral Facet Dislocation

Bilateral facet dislocation occurs in extreme flexion and anterior subluxation. Pathologically, this injury includes a tear of the posterior ligamentous complex, the anterior longitudinal ligament, the annulus fibrosus, disk herniation, and complete dislocation of both facet joints at the level of injury (Vaccaro et al. 2001). This injury is extremely unstable and is associated with a high prevalence of spinal cord injuries. Initial management is closed reduction and traction.

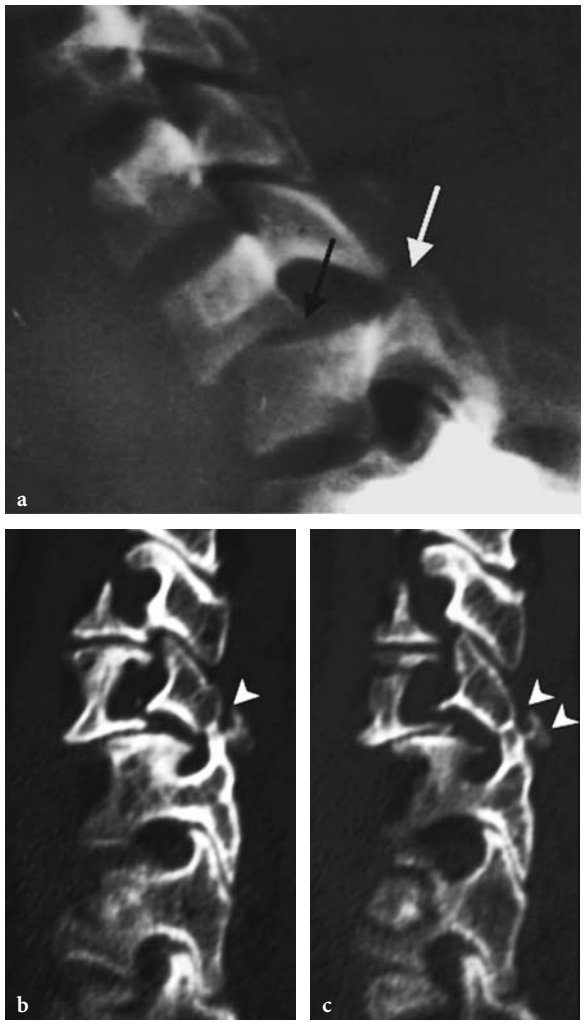

Fig. 12.14a–c. Bilateral facet dislocation. Two different patients. Lateral view radiograph (**a**) demonstrates 50% anterior slippage of the C5 vertebral body (*black arrow*), and anterior dislocation of both articular masses of C5 (*white arrow*). CT sagittal reformations (**b**,**c**) through the neural foramina showing anterior dislocated inferior articular processes of C5 (*arrowheads*)

Radiographically, on the lateral projection there is at least 50% anterior translation of the injured vertebral body and an anterior dislocation of articular masses (Ebraheim et al. 1997) (Fig. 12.14). On the AP view, the only abnormal finding is a widened interspinous distance at the level of injury. MDCT shows the body of the dislocated vertebra anterior to the uncinate processes and body of the subjacent vertebra and the dislocated articular masses anterior to the subjacent masses. MRI is indicated in all cases to determine the type and extent of the cord injury and to assess for other intraspinal injuries (Vaccaro et al. 2001; Leite et al. 1997). The characteristics of bilateral facet dislocation are summarized in Table 12.9.

Table 12.9. Flexion injury: bilateral facet dislocation

Mechanism	Hyperflexion and anterior subluxation
Definition	Extreme form of anterior subluxation
Spine level	Any level
Stability	Unstable
Associated lesions	Spinal cord injury, disk herniation
Radiographic findings	Anterior displacement of 50% or more of one cervical vertebra
Management	Closed reduction and traction with cervical tongs

12.4.5 Clay Shoveler's Fracture

The name of this cervical spine fracture is derived from an injury occurring in Australian clay miners whereby the head and neck are abruptly pulled in hyperflexion when attempting to throw a shovel full of clay from the mine floor. Clay shoveler's fracture is an oblique fracture of the base of the spinous process, caused by abrupt flexion of the neck or a direct blow to the spinous process or to the occiput, combined with a heavy upper body and lower neck muscular contraction. Since this injury involves only the spinous process, this fracture is considered stable, and it is not associated with neurologic impairment. Management involves only cervical immobilization with an orthotic device. Radiographically, this injury is commonly observed on the lateral view as an avulsed bony fragment of the spinous process,

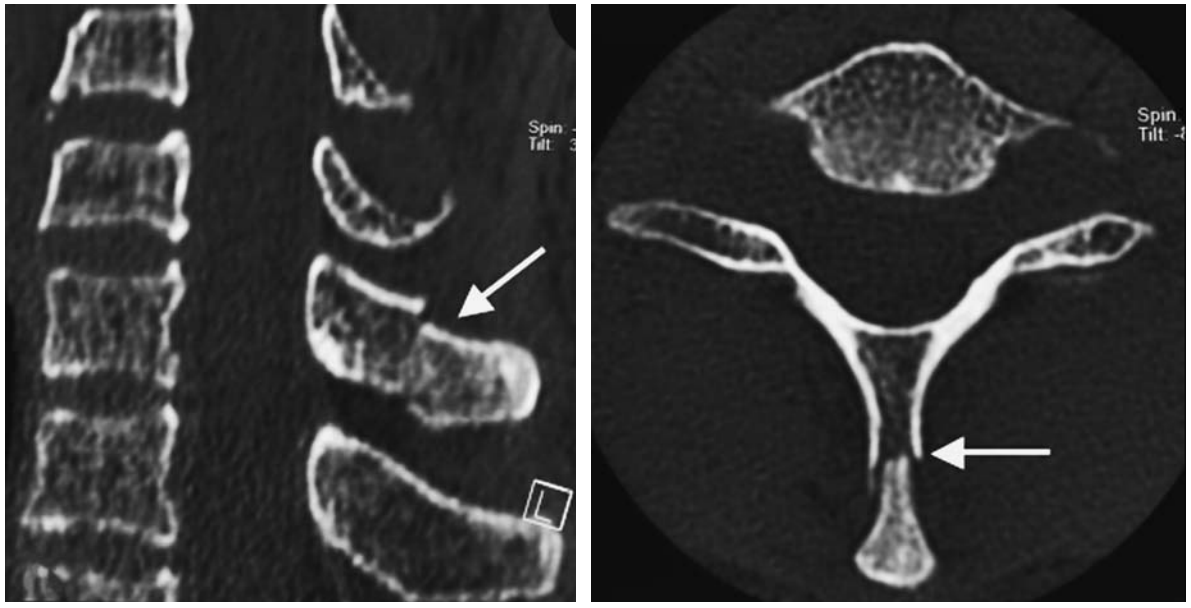

Fig. 12.15a,b. Clay shoveler's fracture. **a** Sagittal MDCT reformation. **b** Axial MDCT reformation. Oblique fracture of the base of the spinous process of C6 (*arrows*)

particularly at the lower cervical levels (Fig. 12.15). An AP view is usually of little value, but may occasionally show the fracture line or displaced bony fragment. CT is sometimes warranted to exclude skeletal injury in the lower cervical spine, since in some trauma patients the lower cervical spine is not optimally visualized on routine lateral views, thus avoiding delay in the patient's workup and unnecessary hospitalization (Tehranzadeh et al. 1994; Lin et al. 2003). The characteristics of a clay shoveler's fracture are summarized in Table 12.10.

Table 12.10. Flexion injury: clay shoveler's fracture

Mechanism	Abrupt hyperflexion with lower neck muscular contraction or direct trauma
Definition	Base of the spinous process fracture
Spine level	Lower cervical or upper thoracic
Stability	Stable
Associated lesions	No neurologic impairment
Radiographic findings	Avulsion of posterior aspect of spinous process
Management	Cervical immobilization with orthosis

12.5 Flexion-Rotation Injuries

12.5.1 Unilateral Facet Dislocation

A unilateral facet dislocation occurs with hyperflexion in combination with rotation. One inferior articular facet of an upper vertebra passes above and anterior to the superior articular facet of a lower vertebra (so-called "jumped facet"). Although the posterior ligaments may be disrupted, this injury is mechanically and neurologically stable due to the so-called "locked" vertebra: the dislocated inferior articular mass is fixed in the inferior part of the intervertebral foramen between the body and superior articular process of the underlying vertebra. Depending on the relation of this dislocated inferior articular mass to the cervical root in the intervertebral foramen, radicular compression is possible. Initial management includes cervical traction to attempt a closed reduction (Shapiro 1993). Radiographically, on the lateral view there is an anterior displacement over less than one half the diameter of the vertebral body. The AP view may show a disruption of the line connecting the spinous processes. The oblique view shows a typical disruption of the "shingles on a roof"

appearance at the level of the involved vertebra. The dislocated inferior facet of the upper vertebra is seen projecting within the neural foramina (Fig. 12.16). This abnormal relationship is best shown on CT (Shapiro et al. 1999). Small marginal impaction fractures of the articular facet are common, and clinically insignificant (Fig. 12.16). MRI may assess the posterior longitudinal ligament and disk abnormalities at the level of the injury (Halliday et al. 1997). The characteristics of a unilateral facet dislocation are summarized in Table 12.11.

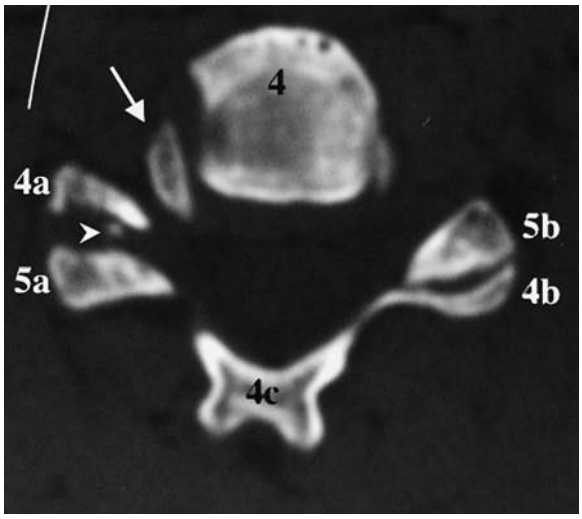

Fig. 12.16. Unilateral facet dislocation. Axial CT image. The right inferior articular facet process of C4 (*4a*) is dislocated into the neural foramen, in front of the superior articular process of C5 (*5a*). The uncinate process of C5 (*white arrow*) is also projecting within the neural foramen. Small articular process fracture (*arrowhead*). Dislocated C4 vertebral body (*4*) and spinous process of C4 (*4c*). The normal facet joint on the left side (*4b*, *5b*)

Table 12.11. Flexion-rotation injury: unilateral facet dislocation

Mechanism	Flexion with rotation
Definition	Posterior ligament disruption and unilateral facet dislocation
Spine level	Any level
Stability	Stable due to locked-in-place vertebra
Associated lesions	No neurologic impairment
Radiographic findings	Anterior displacement of less than 50% of one cervical vertebra, rotation of the affected vertebra, lateral displacement of spinous process
Management	Cervical traction

12.5.2 Rotatory Atlanto-axial Dislocation

Rotatory atlanto-axial injury is a specific type of unilateral facet dislocation (see also Sect. 12.9.2.). This injury is rare in adults and more common in children and adolescents (Pang and Li 2004). Sports and motor vehicle accidents are the two most common causes. Radiographically, the odontoid view shows an asymmetry of the lateral masses of C1. However, since the atlanto-axial joint permits flexion, extension, rotation, and lateral bending, radiographic asymmetry may also be produced in healthy individuals with asymmetric positioning of the head (Tucker and Taylor 1998). To confirm true dislocation the basilar skull structures should appear perfectly symmetric in the presence of the findings described above. The AP view shows broadening of the lateral mass of the atlas on the side that is rotated forward, projecting closer to the midline while the opposite lateral mass becomes narrower and turns away from the midline. The spinous process of the axis is usually tilted in one and rotated in the opposite direction. This injury is unstable because of its location. CT may easily demonstrate the displaced and rotated atlanto-axial articulation with the use of more advanced post-processing techniques such as MIP (Fig. 12.17). Associated rupture of the transverse ligament or alar ligaments increases the risk of a neurologic injury because the spinal canal can be further compromised (Niibayashi 1998; Pang and Li 2004). Rotation of 30 ° of more causes an angulation of the contralateral vertebral artery. Beyond 45 °, the artery may become occluded. The characteristics of rotatory atlanto-axial dislocation are summarized in Table 12.12.

Table 12.12. Flexion-rotation injury: rotatory atlanto-axial dislocation

Mechanism	Flexion along with rotation of C1
Definition	Specific type of unilateral atlanto-axial facet dislocation
Spine level	Atlanto-axial joint, C1–C2
Stability	Unstable
Radiographic findings	Asymmetry of the lateral masses of C1 with unilateral magnification of a lateral mass on odontoid view
Management	Cervical traction

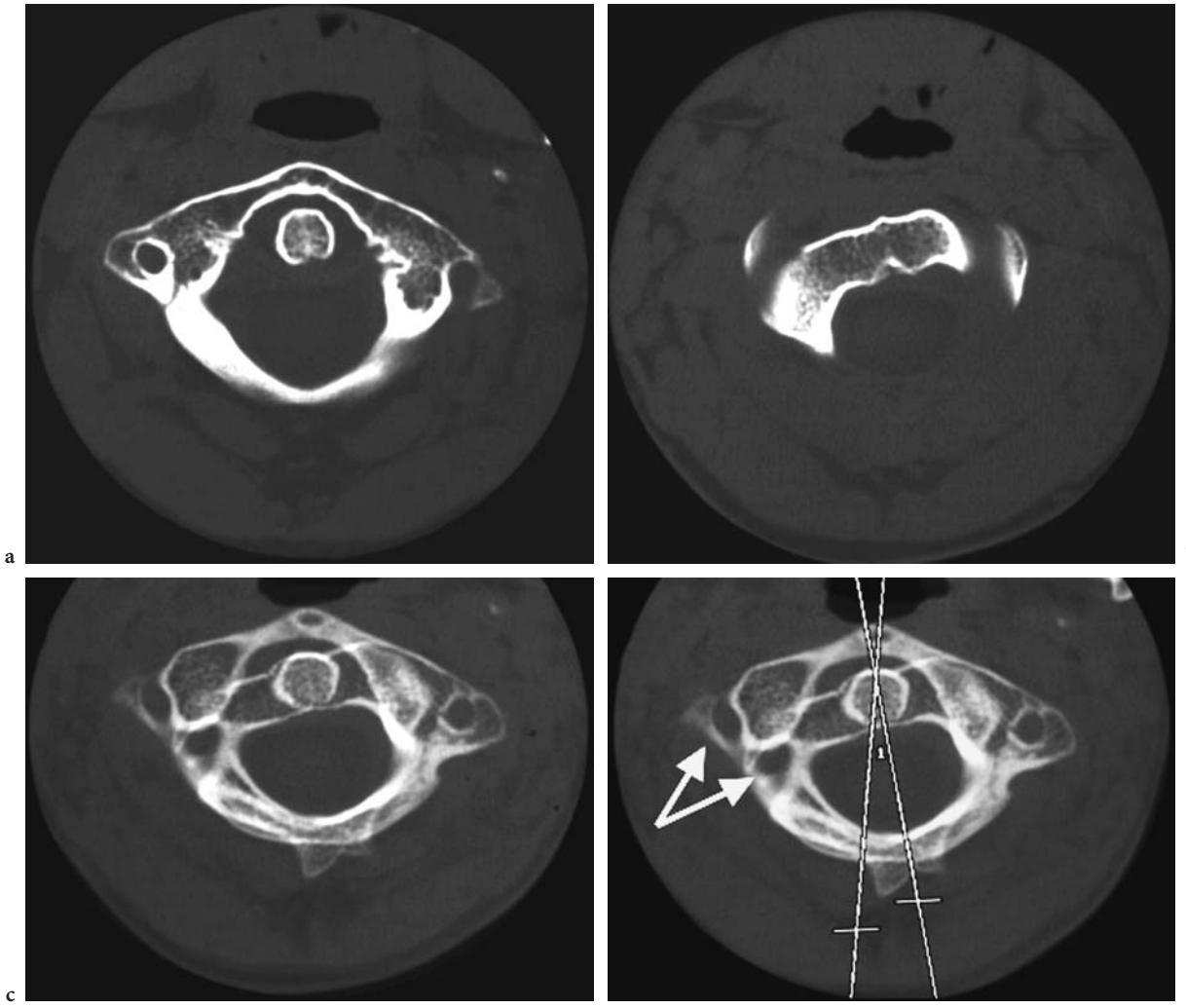

Fig. 12.17a–d. Rotatory atlanto-axial dislocation. **a** Axial CT image through the atlanto-dental articulation. **b** Axial CT image through the rotated vertebral body of C2 and the lateral masses of the atlas. **c** Thick MIP axial projection of C1 and C2 vertebral bodies. **d** 14° Rotation of axis. Note the posterior projection of the C2 vertebral foramen (*arrows*)

12.6 Extension Injuries

12.6.1 Hyperextension Dislocation

Although this injury is called hyperextension dislocation, there is no dislocation on the lateral radiograph. There is a predominant soft tissue injury with a characteristic avulsion fracture of the anterior aspect of the inferior endplate of the suprajacent vertebra. Mechanically, the impacting force is applied directly to the face moving the head and neck in a straight posterior direction without rotation. At the time of impact, the involved cervical segment is posteriorly dislocated compressing the spinal cord, possibly with central hemorrhage leading to an acute central cervical cord syndrome. There is a disruption of the anterior longitudinal ligament, posterior longitudinal ligament, and the ligamentum flavum, and a horizontal disruption of the annulus and disk (Kiwerski 1993). On the lateral view, a diffuse prevertebral soft tissue swelling with normally aligned vertebra and a characteristic triangular avulsion fracture fragment are seen. The transverse length of the fracture fragment usually exceeds its vertical height (Fig. 12.18).

Although MDCT shows the extent of the prevertebral soft tissue swelling and the fracture com-

ponents and its relation to the adjacent vertebrae, MRI is superior in determining the extension of the spinal cord injury, and the associated ligamentous disruption (Harris and Yeakley 1992). This injury is mechanically and neurologically unstable. The characteristics of a hyperextension dislocation are summarized in Table 12.13.

Fig. 12.18. Hyperextension dislocation. Lateral view radiograph. A triangular shaped fracture (*white arrow*) at the anteroinferior edge of the C6 vertebral body, with a greater transverse length than height. The C6 vertebral body is dislocated posteriorly (*black arrow*)

Table 12.13. Extension injury: hyperextension dislocation

Mechanism	Hyperextension with face trauma
Definition	Avulsion fracture of the anterior aspect of the inferior end-plate, cord injury
Spine level	Any level
Stability	Unstable
Associated lesions	
Radiographic findings	Prevertebral soft tissue swelling. Triangular anterior avulsion fracture, spinal cord injury, hemorrhage, and ligamentous injury
Management	Cervical traction

12.6.2 Hangman's Fracture (Traumatic Spondylolisthesis of C2)

Although the name of this injury is derived from the typical fracture that occurs after hangings, it is commonly caused by motor vehicle accidents, diving accidents, and falls. It consists of bilateral fractures through the pedicles of C2 due to a combination of axial loading and hyperextension forces (Fielding et al. 1989). This injury is the second most common fracture of C2 (after odontoid fractures) and it is usually bilateral, but rarely symmetrical. Hangman's fractures are classified into three types (Effendi et al. 1981). The pathology in all three types involves fracture of the pars interarticularis (pedicle) of C2, with variable C2 on C3 displacement. Radiographically, the AP view has limited value. On the lateral radiograms; type-I injuries show bilateral C2 pedicle fractures with minimal displacement of the body of C2. Besides the anteriorly displaced body of C2, type-II injuries show signs of a disrupted C2–C3 disk, and more than 3 mm displacement of C2. Additionally, there is an angulation of the odontoid process. Type-III injuries show all signs of type-II injuries and additionally bilateral C2–C3 interfacetal dislocation due to rebound flexion. The angulation is also much more severe in type-III fractures. In type-I and type-II, CT helps to confirm the fractures, and detects possible associated cervicocranial fractures (Fig. 12.19). In type-III injuries CT demonstrates the bony fragments within the spinal canal, the facet dislocation, and the interfacetal relations by use of 3D reconstructions (Mirvis et al. 1987). Since all types of Hangman's fractures may be associated with a prevertebral hematoma and ligamentous or muscle injury, MRI is helpful in detecting such soft-tissue injuries, as well as possible spinal cord injury (Forsberg et al. 1990). Since the AP diameter of the spinal canal is at its largest at the level of C2, and since the fractured pedicles allow "auto-decompression" type-I and type-II injuries are neurologically stable, with sparing of the spinal cord, and both can be managed with a cervical orthosis. A type-II injury, however, is mechanically unstable, because of the C2–C3 disk lesion. A type-II injury, because it is associated with unilateral or bilateral facet dislocation, is neurologically unstable and requires cervical traction, arthrodesis, and/or pedicle screw fixation (Greene et al. 1997). The characteristics of hangman's fractures are summarized in Table 12.14.

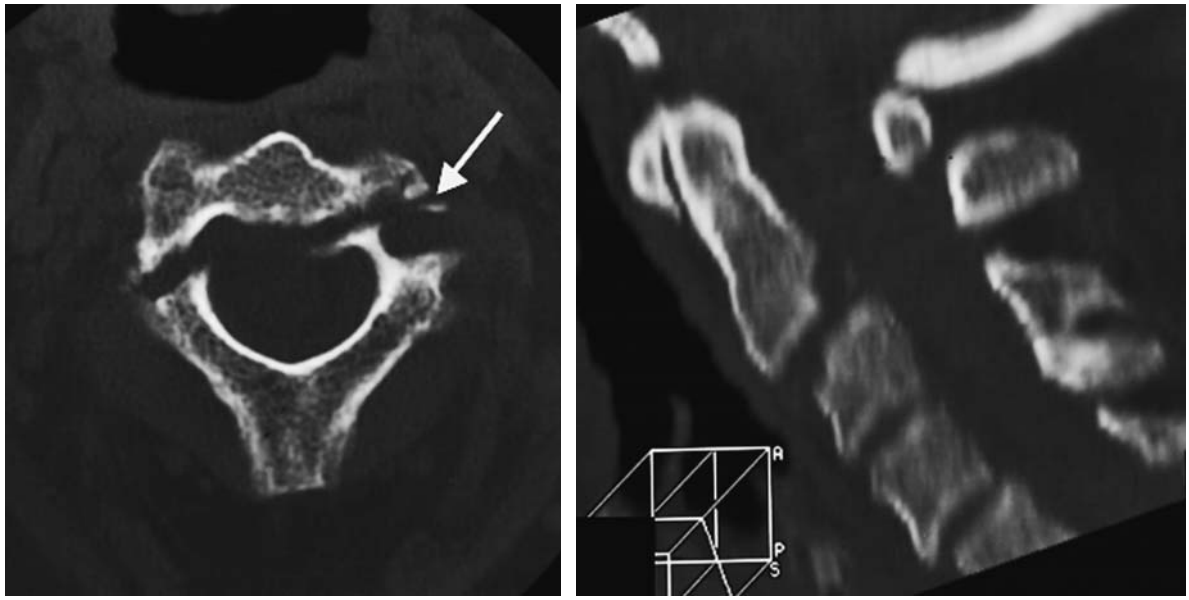

a b

Fig. 12.19a,b. Hangman fracture, type II. **a** Axial CT images through C2. Fracture lines through both pedicles. There is an extension of the fracture line through the left foramen transversarium (*arrow*). **b** Sagittal CT reformation. Slight anterior displacement and angulation of the body of the axis

Table 12.14. Extension injury: hangman's fracture (traumatic spondylolisthesis of C2)

Mechanism	Axial loading with hyperextension in type I, additionally rebound flexion in type II, primary flexion with rebound extension in type III
Definition	Bilateral fractures through the pedicles of C2 in all three types, minimal displacement (<3 mm) and no angulation in type I, more (>3 mm) displacement and angulation in type II, and associated facet dislocation in type III
Spine level	C2
Stability	Stable unless associated with unilateral or bilateral facet dislocation
Associated lesions	Neurological complications if associated with facet dislocation or spinal cord injury
Radiographic findings	Bilateral pedicle fractures of C2 with or without anterior subluxation, disk lesions, unilateral or bilateral facet dislocation
Management	Cervical orthotic device if no facet dislocation, otherwise traction

12.6.3 Extension Teardrop Fracture

As with flexion teardrop fractures, this injury also presents with a bony fragment displaced anteroinferior of the vertebral body (Stabler et al. 2001). In a hyperextension teardrop fracture, the fragment is a true avulsion due to the rupture of the anterior longitudinal ligament, in contrast to the flexion teardrop fracture in which the fragment is produced by vertebral compression. The fracture is commonly associated with diving accidents and can occur at any level, but is usually seen at the lower cervical vertebrae, associated with a hyperextension dislocation. Most patients have no neurologic impairment. Radiographically, the AP view has limited value. Lateral radiograms show a triangular bony fragment at the anteroinferior aspect of the vertebra. CT is usually not required, except in cases of massive prevertebral hematoma (Fig. 12.20). The differentiation of this fracture from the hyperextension dislocation is based on the dimensions of the triangular bony fragment. In extension teardrop fractures, the transverse axis of the avulsed bony fragment is equal to its height. MRI is necessary in young adults to exclude spinal cord injury. The injury is normally mechanically and neurologically stable in elderly patients. In

young adults, extension teardrop injuries may be mechanically unstable in the lower cervical spine, but 80% are neurologically unstable (Lee et al. 1997). The characteristics of extension teardrop fractures are summarized in Table 12.15.

Fig. 12.20. Extension teardrop fracture. Sagittal CT reconstruction. A triangular bony fragment at the anteroinferior edge of the C2 vertebral body (*arrow*). Vertical height and transverse axis are equal. Note the extensive prevertebral hematoma (*arrowheads*)

Table 12.15. Extension injury: extension teardrop fracture

Mechanism	Sudden hyperextension, diving accidents
Definition	Displaced bony fragment from the anteroinferior aspect of the vertebra
Spine level	Any level, usually lower cervical
Stability	Stable in elderly and neurologically unstable in young adults
Associated lesions	Central cord injury due to buckling of the ligamenta flava into spinal canal in young adults
Radiographic findings	Displaced anteroinferior bony fragment
Management	Cervical traction, avoid iatrogenic extension

12.6.4 Fracture of the Posterior Arch of C1 (Posterior Neural Arch Fracture)

This fracture occurs when the head is hyperextended and the posterior neural arch of C1 is compressed between the occipital bone and the spinous process of C2. The transverse ligament and the anterior arch of C1 are not involved, making this fracture stable, and management with a cervical orthosis is sufficient (Lee et al. 1998). Radiographically, the lateral view shows a fracture line through the posterior neural arch. Initial management involves the differentiation of this benign fracture from a Jefferson fracture (Fowler et al. 1990). The odontoid view fails to show any displacement of the lateral masses of C1, a finding that distinguishes this fracture from a Jefferson fracture. MDCT can easily distinguish this fracture from a Jefferson fracture (Fig. 12.25) and MRI is usually not necessary. Patients with a posterior arch fracture of C1 are usually elderly and have degenerative changes in the lower cervical spine. They are usually associated with fractures elsewhere in the cervical spine (Fowler et al. 1990). Congenital developmental anomalies of the posterior neural arch may mimic a fracture (Currarino et al. 1994). The characteristics of the posterior arch fracture of C1 are summarized in Table 12.16.

Table 12.16. Extension injury: fracture of the posterior arch of C1

Mechanism	Hyperextension and compression of the posterior arch of C1
Definition	Posterior arch of C1 fracture
Spine level	C1
Stability	Stable
Associated lesions	No ligamentous involvement (in contrast to Jefferson's fracture)
Radiographic findings	Fracture line through the posterior arch on lateral view, no associated displacement of the lateral masses of C1 on odontoid view
Management	Cervical orthosis

12.6.5 Avulsion Fracture of the Anterior Arch of C1

The anterior arch of C1 fracture is caused by hyperextension resulting in forces on the anterior atlantodental ligament, which inserts on the inferior edge of the anterior arch. When isolated these anterior arch fractures are avulsion fractures of the anterior portion of the ring and have a low morbidity rate (Fowler et al. 1990). This injury is mechanically and neurologically stable (Lee et al. 1998). Radiographically, on the lateral view a fracture line may be seen (Fig. 12.21). The normal developmental anomalies and synchondroses of C1 should not be misdiagnosed as a fracture (Lustrin et al. 2003). The C1 vertebra is formed from three primary ossification centers: the anterior arch and the two neural arches. The anterior arch ossifies by 1 year of age. The neural arches, which form the posterior ring when fused, appear around the 7th fetal week and fuse with the anterior arch by age 7.

12.6.6 Laminar Fracture

Isolated laminar fractures of the cervical spine are uncommon and usually occur after a hyperextension injury due to a direct trauma such as a gunshot (Makan 1999). They may also be associated with flexion teardrop fractures and occur predominantly at the level of C5 (Kim et al. 1989). Radiographically, the AP view has limited value. The lateral radiogram shows a simple or comminuted fracture of one or both laminae (Fig. 12.22) (Makan 1999). MDCT is necessary to evaluate the extension of the fracture and the relation of the fragments to the spinal canal. MRI is only indicated with fragments in the spinal canal or in cases of neurologic deficit (Fig. 12.23). This injury is mechanically stable, but neurologic stability depends on the location of bony fragments in the spinal canal.

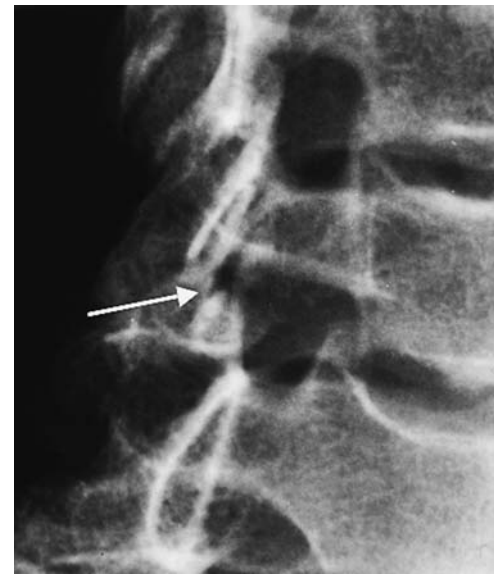

Fig. 12.22. Laminar fracture. Oblique view radiograph. The fracture line (*arrow*) is confined to the lamina

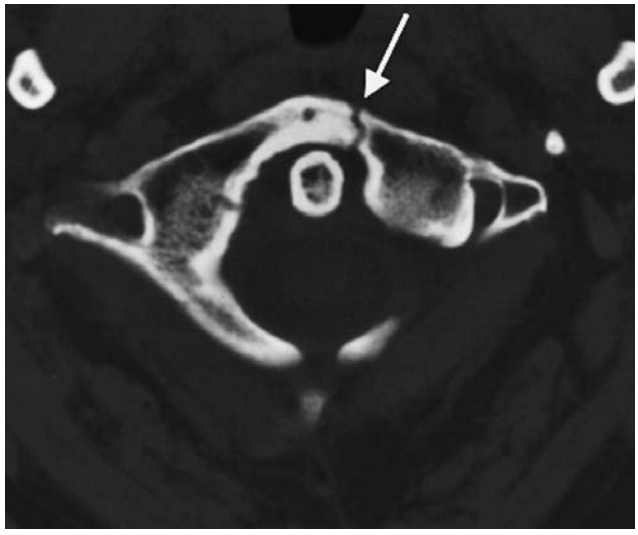

Fig. 12.21. Isolated anterior arch fracture of C1. Axial CT image showing a fracture through the anterior arch of C1 (*arrow*)

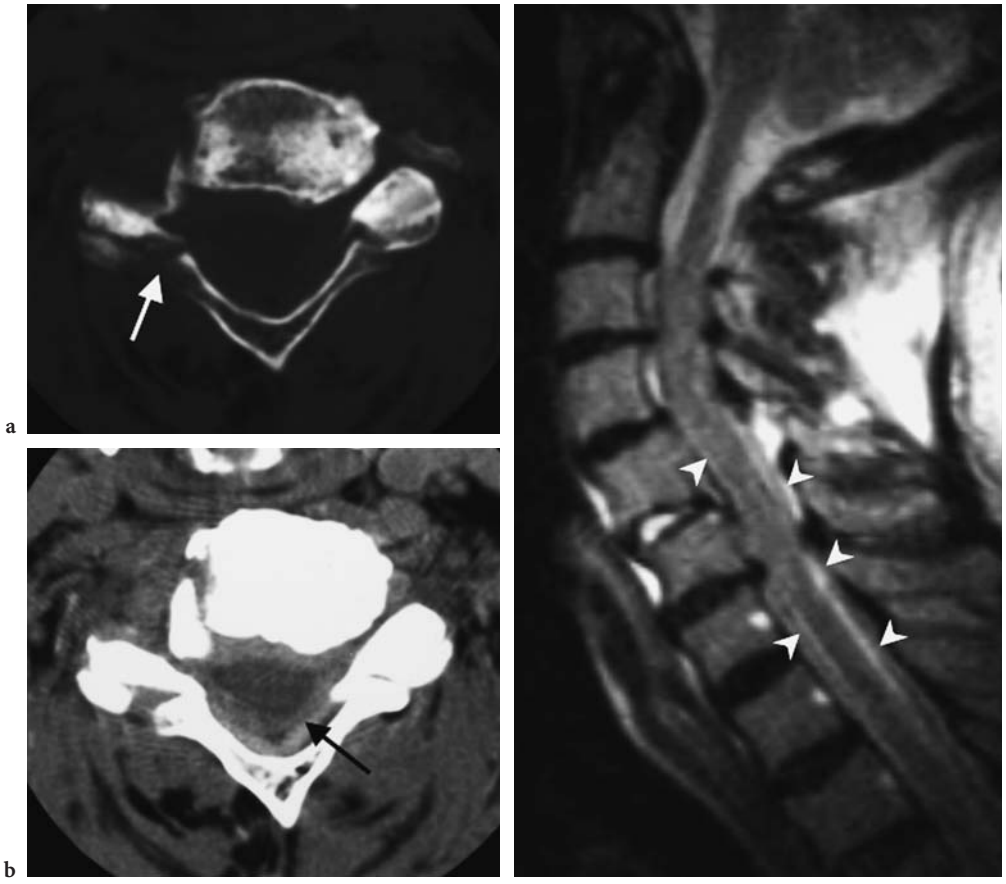

Fig. 12.23a–c. Laminar fracture. **a** Axial CT, bone window. The fracture line (*white arrow*) is confined to the lamina and the articular mass. **b** Axial CT image, soft-tissue window. Epidural hemorrhage compressing the dural sac (*black arrow*). **c** Sagittal T2-weighted MR image. Extensive epidural hemorrhage with secondary medullary compression (*arrowheads*)

12.7 Hyperextension and Lateral Rotation Injuries

12.7.1 Pillar Fracture

Pillar fractures are vertical fractures limited to one articular mass and mostly caused by simultaneous hyperextension and lateral rotation (Shanmuganathan et al. 1996). Less frequently they may caused by hyperextension and distraction. Pillar fractures are difficult to visualize on AP and lateral views, unless they are displaced. An AP view may show the disruption of the lateral column due to the lateral displacement of a fragment, and the vertical or oblique fracture line may also be visible. CT, particularly with the use of 3D reconstructions,

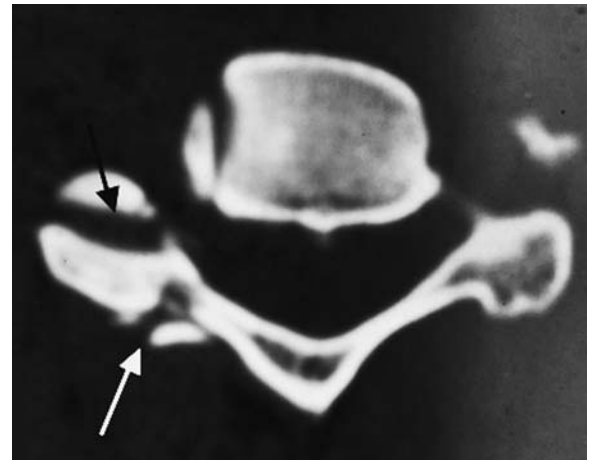

Fig. 12.24. Pillar fracture. Axial CT image. The fracture line (*white arrow*) is confined to the articular mass. Note the unilateral facet subluxation (*black arrow*)

confirms the diagnosis (Fig. 12.24). Patients may show a neurologic deficit including spinal cord injury or radiculopathy. MRI may be used to evaluate the integrity of the facet region, interspinous ligament, anterior longitudinal ligament, and posterior longitudinal ligament (Halliday et al. 1997).

12.7.2 Pediculolaminar Fracture–Separation

Pedicolaminar fracture–separation is a combination of a ligamentous and osseous injury, caused by hyperextension in rotation. This mechanism probably results in a fracture of the subjacent inferior articular mass hit by the articular mass of the vertebra above, and finally ending with separation of the fractured component (Argenson et al. 1988). The AP view may show lateral displacement of the fractured articular mass. The lateral radiogram classically shows the "double line appearance" produced by the two articular processes, and the fracture component. The involved articular mass becomes a separate fragment rotated anteriorly and displaced posteriorly. MDCT is necessary to confirm the diagnosis and further evaluate the fracture components. MRI is only indicated when neurologic signs are present. In 40% of cases, the fracture–separation of the articular complex is associated with neurological deficits (Argenson et al. 1988).

12.8 Vertical (Axial Load) Compression Injuries

12.8.1 Jefferson's Fracture (Burst Fracture of the Ring of C1)

As originally described by Jefferson, this fracture is caused by vertical compression transmitted through the occipital condyles to the lateral masses of C1 resulting in bilateral fractures of both the anterior and posterior arches of C1 (Guiot and Fessler 1999). The combination of one or more fractures of both the anterior and posterior arch of C1 can be classified as a Jefferson fracture (Hays and Alker 1988). Displacement of the lateral masses may result in either disruption of the transverse ligament or an avulsion fracture of one of the lateral masses of C1. More than 6.9 mm displacement of the lateral mass of C1 over C2 on AP view indicates a transverse atlantal ligament rupture and requires more rigid immobilization (Hadley et al. 1988a). Radiographically, the open-mouth view shows unilateral or bilateral displacement of the lateral articular masses of C1 with respect to the articular pillars of C2. There is a widening of the lateral atlanto-dental intervals. This finding differentiates it from a simple fracture of the posterior arch of C1. The lateral radiogram shows a bilateral fracture of the posterior arch of C1 and the paravertebral soft tissue edema (Fig. 12.25)

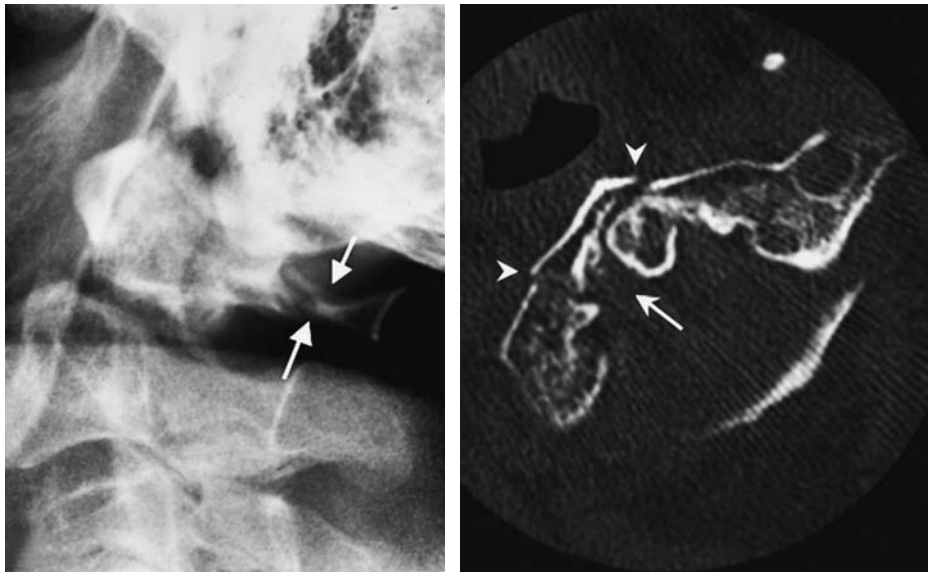

a b

Fig. 12.25a,b. Jefferson's fracture. **a** Lateral view radiograph. Bilateral posterior arch C1 fractures (*white arrows*), posterior displacement of C1, and type-II dens fracture. **b** Axial CT image. Bilateral anterior arch of C1 fracture (*arrowheads*), displacement of the C1 lateral mass and widened lateral atlantodental interval (*white arrow*)

(Kesterson et al. 1991). MDCT is necessary to detect an anterior arch fracture and possible avulsion fracture of the lateral masses (Fig. 12.25) (Koivikko et al. 2004a). MRI can be helpful to detect a possible ligamentous injury. This injury is mechanically unstable. The characteristics of a Jefferson's fracture are summarized in Table 12.17.

Table 12.17. Vertical compression injury: Jefferson's fracture

Mechanism	Vertical compression transmitted through the occipital condyles to the lateral masses of C1
Definition	Bilateral burst fracture of the anterior and posterior neural arches of C1 and transverse ligament disruption
Spine level	C1
Stability	Unstable
Associated lesions	Paravertebral soft tissue edema, neurologic injury when complete disruption of transverse ligament
Radiographic findings	Displaced lateral masses of C1 on odontoid view, predental space more than 3 mm
Management	Immediate cervical traction

12.8.2 Burst Fracture of the Vertebral Body

During vertical downward compression an abrupt increase in pressure within the disk space may cause explosive shift of the nucleus pulposus into the vertebral body through the endplates. This will result in bursting of the vertebral body (Bozic et al. 1994). The bony fragments may impinge on the spinal canal and cause anterior cord compression. Radiographically, the AP view may show a vertical fracture line of the endplates and the lateral view shows a biconcave vertebral body due to fractures of the endplate, (Fig. 12.26) (Clark et al. 1988). A prevertebral soft tissue swelling is common. CT and MRI are required to document the exact displacement of the fractured bony components, retropulsed fragments, and their relationship to the spinal cord, as well as any spinal cord lesions (Fig. 12.26) (Bensch et al. 2004). This injury is mechanically unstable and neurologically stable unless in the presence of cord symptoms. More than 25% loss of vertebral height, retropulsion, and neurologic deficit require cervical traction and fixation. The characteristics of burst fractures of the vertebral body are summarized in Table 12.18.

Table 12.18. Vertical compression injury: burst fracture of the vertebral body

Mechanism	Vertical compression force transmitted to lower levels in the cervical spine
Definition	Disruption of vertebral body
Spine level	Lower cervical
Stability	Usually stable, unstable if associated lesions occur
Associated lesions	Loss in height of more than 25%, retropulsion, or neurologic deficit
Radiographic findings	Vertical fracture line in AP view, protrusion or retropulsion of the vertebral body, required CT or MR
Management	Cervical traction when unstable

12.9 Craniocervical Injuries

Injury to the upper cervical spine (occipital bone to C2) occurs frequently in fatal motor vehicle accidents, particularly among pedestrians and motorcyclists (Tepper et al. 1990). Likely mechanisms include violent distractive hyperflexion or hyperextension with or without associated rotation. These injuries are considered unstable because of their location. Nevertheless, since the diameter of the spinal canal is greatest at the level of C2, spinal cord injury from compression is not frequent. Common injuries include fracture of the atlas, atlanto-axial subluxation, odontoid fracture, and hangman's fracture. Less common injuries include occipital condyle fracture, atlanto-occipital dislocation, atlanto-axial rotary subluxation, and C2 lateral mass fracture. Some of these injuries are already discussed earlier in this chapter. In this section, we will discuss the craniocervical injuries related rather to their anatomical location than the mechanism of injury. Table 12.19 summarizes the criteria for suspecting cervicocranial junction instability on the basis of the imaging findings (radiography, CT, or MRI) (Tuli et al. 1997).

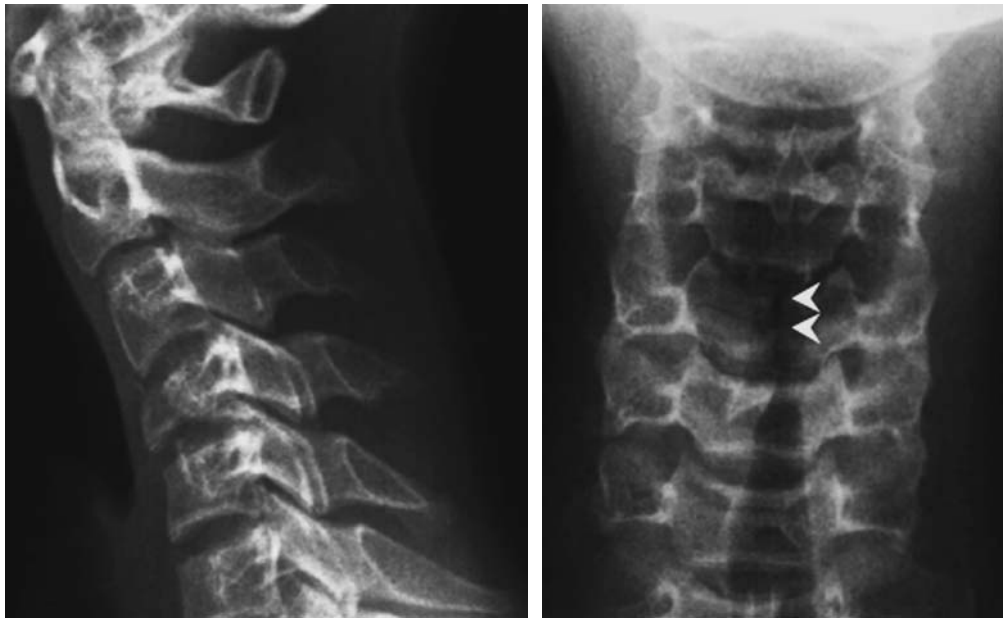

a b

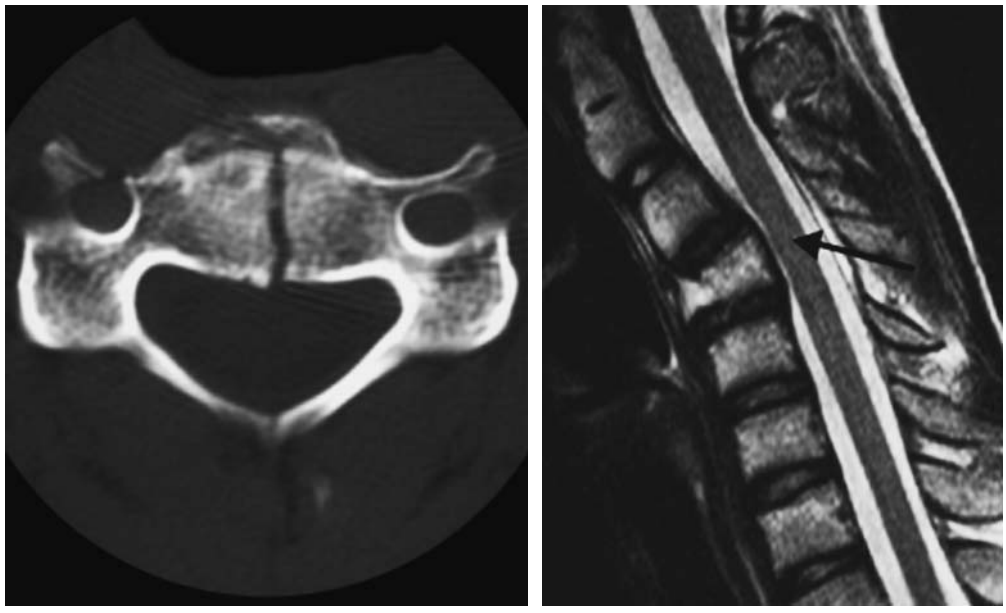

c d

Fig. 12.26a–d. Burst fracture of the vertebral body. **a** Lateral view radiograph. **b** AP view radiograph. **c** Axial CT image. **d** Sagittal T2-weighted MR image. Vertical fracture line of the C4 vertebral body on the AP view (*arrowheads*). Slight medullary signal increase on T2-weighted image corresponding to spinal cord edema (*arrow*)

Table 12.19. The criteria for craniocervical junction instability based on imaging findings

1) >8° Axial rotation of the atlanto-occipital joint
2) >45° Axial rotation of the atlanto-axial joint
3) >6 mm Displacement of the basion-dens interval
4) >6 mm Overhanging of the atlas on the axis
5) >4 mm Predental space
6) >3 mm Distance between the posterior contour of the dens and the anterior contour of the posterior arch of the atlas
7) MR evidence of disruption of the transverse ligament of the atlas

12.9.1 Atlas (C1) Fractures

Fractures of the atlas are classified into five types (Levine and Edwards 1991):

- Type I: Isolated bony apophysis fracture (extra-articular transverse process fracture)
- Type II: Isolated posterior arch fracture (see Sect. 12.6.4)
- Type III: Isolated anterior arch fracture (see Sect. 12.6.5)
- Type IV: Comminuted lateral mass fracture (Fig. 12.27)
- Type V: Jefferson burst fracture (see Sect. 12.8.1)

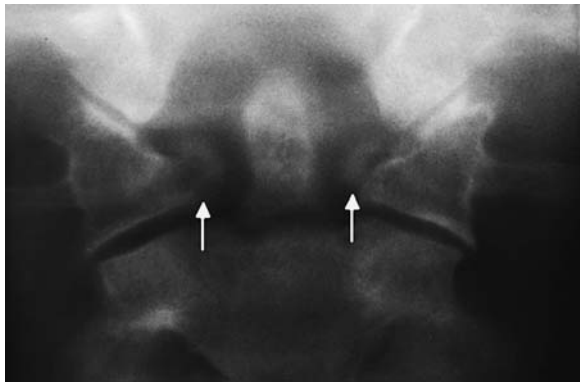

Fig. 12.27. Bilateral comminuted lateral mass fractures of C1. Open-mouth odontoid view showing bilateral lateral mass fractures (*arrows*)

Atlas fractures are already discussed in previous sections: extension injuries (anterior and posterior arch fractures of C1), and vertical (axial load) compression injuries (Jefferson fracture). The incidence of atlas fractures is 2%–13% of all acute cervical spine fractures (Hadley et al. 1988b; Levine and Edwards 1991). Combined fractures of C1 and C2 account for 4%–15% of all cervical fractures (Greene et al. 1997; Gleizes et al. 2000; Ryan and Henderson 1992). In comminuted lateral mass fractures, radiographically, asymmetric displacement of the lateral mass from the rest of the vertebra is seen in the odontoid view (Fig. 12.27). This fracture has a low morbidity rate and has only little clinical significance. Neurological injury following isolated atlas fractures is very rare. The characteristics of atlas fractures are summarized in Table 12.20.

Table 12.20. Craniocervical injury: atlas (C1) fractures

Mechanism	Impaction of the occipital condyles on the atlas
Definition	Single or multiple fractures around the ring of C1
Spine level	C1
Stability	Types I, II, IV stable, type III unstable if displaced, type-V (Jefferson fracture) unstable if transverse ligament disruption
Associated lesions	Neurologic impairment with type IV fracture, C2 and additional non-contiguous cervical fractures
Management	Cervical orthosis for stable fractures and cervical traction when unstable

12.9.2 Anterior Atlanto-axial Subluxation

There are two types of atlanto-axial subluxation: rotatory atlanto-axial subluxation (Sect. 12.5.2.) and anterior dislocation of C1.

12.9.2.1 Anterior Dislocation of C1

Under normal circumstances, hyperflexion is limited by the tectorial membrane and hyperextension by the anterior arch of C1 hitting against the odontoid process. The alar ligaments limit excessive rotational movement. When flexion occurs without a lateral or rotatory component at the upper cervical level, it may cause an anterior dislocation

of the atlanto-axial joint if the transverse ligament is disrupted (Carroll et al. 2001; Deliganis et al. 2000), as is seen in cases of acceleration-deceleration injuries where the skull grinds the C1–C2 complex in flexion. The atlas-dens distance is defined as the distance between the posterior edge of the anterior arch of C1 and the anterior edge of the odontoid process. The maximal normal distance between the atlas and the dens is 3.5 mm in adults and 4.5 mm in children. This should be measured on a lateral view (Fig. 12.28). The transverse ligament limits anterior translation of C1 on C2. When the transverse ligament ruptures, and the alar ligaments are intact, there will usually be less than 5 mm of movement. When both alar and transverse ligaments are ruptured, the anterior translation can be more than 5 mm. In some pathologies, such as Down syndrome, congenital skeletal dysplasias, Marfan syndrome, and chronic inflammatory disease (rheumatoid arthritis), there is a higher theoretical risk of subluxation due to increased atlanto-axial laxity. Since the transverse ligament is the main stabilizing element of the atlanto-axial joint, this injury is unstable. Neurologic injury may occur from cord compression between the odontoid and the posterior arch of C1. CT should be used to confirm the diagnosis, and to further define injuries to the bony elements. MRI findings include prevertebral soft tissue swelling, interspinous or nuchal ligament edema, facet effusion, or facet displacement. If the luxation is less than 5 mm, cervical orthosis is sufficient to allow for reasonable ligamentous reconstitution. If it is 6 mm or more, posterior fixation of C1 and C2 is needed. The characteristics of atlanto-axial subluxation are summarized in Table 12.21.

Fig. 12.28. Anterior atlanto-axial subluxation. Lateral view radiograph shows an increased atlanto-dens interval

Table 12.21. Craniocervical injury: anterior atlanto-axial subluxation

Mechanism	Flexion without lateral or rotatory component at the upper cervical level, frequently occurs in patients with Down syndrome, rheumatoid arthritis
Definition	Anterior atlanto-axial joint dislocation, transverse ligament disruption
Spine level	C1
Stability	Unstable
Associated lesions	Cord compression
Radiographic findings	Asymmetric lateral bodies on odontoid view, increased predental space, requires CT
Management	Fusion of C1 and C2 when significant dislocation

12.9.3 Atlanto-axial Distraction

Atlanto-axial distraction is a severe form of atlanto-axial dislocation resulting from extension and distraction forces. This injury is characterized by disruption of the articular capsules, alar ligaments, transverse ligament, tectorial membrane between C1 and C2, and a type-I odontoid process fracture (Adams 1992). Radiographically, prevertebral soft tissue swelling, C1–C2 dislocation or subluxation, and widening of the C1–C2 apophyseal joints can be observed on conventional radiograms, as well as on CT. MRI findings include prevertebral and interspinous ligamentous edema, apophyseal joint edema and widening, possible epidural hematoma, and spinal cord edema (Deliganis et al. 2000). Although most distraction injuries of the cervical spine are at the level of C1–C2, these can also be encountered at the lower cervical levels (Fig. 12.29).

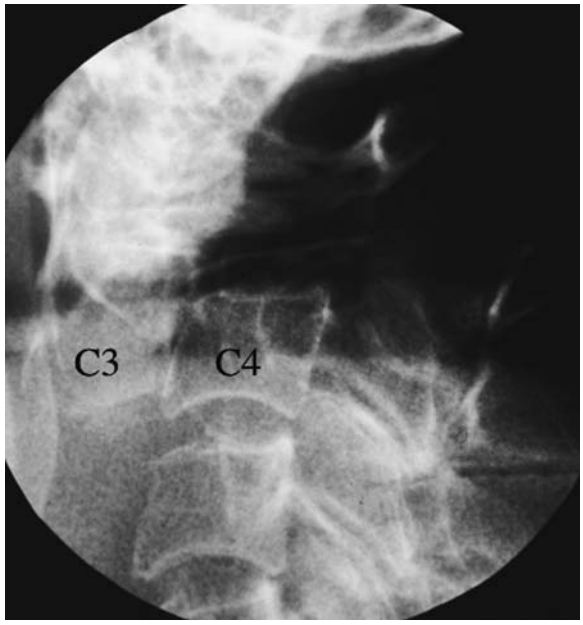

Fig. 12.29. Cervical distraction injury. Lateral view radiograph

12.9.4 Atlanto-occipital Dislocation and Distraction

Flexion of the atlanto-occipital joint is limited by contact between the anterior lip of the foramen magnum and the odontoid process. The tectorial membrane limits extension, while the alar ligaments limit lateral flexion. Atlanto-occipital dislocation is characterized by complete disruption of all ligamentous relationships between the occiput and the atlas with severe flexion or extension (Deliganis et al. 2000). Death usually occurs immediately due to stretching of the brainstem. In fatal cases of atlanto-occipital distraction, the most common spinocerebral injuries include lacerations of the pontomedullary junction, contusion or laceration of the caudal medulla and rostral spinal cord, and stretching or laceration of the midbrain. Subarachnoid hemorrhage is common but may be minimal. Subdural hemorrhage may also be seen (Adams 1992). Vasospasm and dissection of the internal carotid and vertebral arteries have been documented at angiography in several survivors of atlanto-occipital distraction who did not have significant injuries to the spinal cord or brainstem (Lee et al. 1991). Radiographically, disassociation between the base of the occiput and the arch of C1 is observed. The displacement of the cranium with respect to the atlas may be anterior, posterior, or longitudinal. CT is usually not necessary since the lesion is obvious on lateral radiograms as a separation of the atlas from the occipital condyles. MRI is required to assess soft tissue lesions and to evaluate the brainstem and/or spinal cord injury. Vascular injuries can be evaluated on CT or MR angiography (Weller et al. 1999). A traumatic atlanto-occipital dislocation is extremely unstable mechanically, as well as neurologically, and is usually fatal at the accident scene. In patients with these injuries, cervical traction is contraindicated, since further stretching of the brainstem may occur. Halo immobilization is required for 10–12 weeks. If instability persists, internal fixation with posterior occipito-cervical fusion is required. The characteristics of atlanto-occipital dislocation and distraction are summarized in Table 12.22.

Table 12.22. Craniocervical injury: atlanto-occipital dislocation and distraction

Mechanism	Severe flexion or extension at the upper cervical spine
Definition	Disruption of all ligamentous relationships between the occiput and C1
Spine level	C1
Stability	Unstable
Associated lesions	Stretching brainstem, respiratory arrest
Radiographic findings	Dissociation between the base of the occiput and the arch of C1
Management	Cervical traction is contraindicated, halo immobilization or fusion required

12.9.5 Odontoid Process Fractures

Odontoid fractures are the most common fractures of C2, and account for about 75% of all cervical spine fractures in children (Hadley et al. 1985). It is more common in males and is mostly seen in individuals less than 40 years of age. A total of 40% are associated with head injuries and 15%–20% with additional cervical spine injuries. Severe flexion, extension, and rotational forces can cause odontoid fractures. Most are due to hyperflexion, producing anterior displacement (Kokkino et al. 1996). Many of the signs and symptoms are non-specific, includ-

ing poorly localized pain posterior and superior in the neck region, headaches, and neck stiffness. Occipital neuralgia can occur. Traditionally, fractures of the dens have been classified according to the scheme proposed by Anderson and D'Alonzo (2004) (Hadley et al. 1988a):

- Type I: Avulsion fracture of the tip of the dens at the insertion site of the alar ligaments (Fig. 12.30). Although this injury is mechanically stable, plain films and/or CT are used to rule out or confirm associated atlanto-occipital dislocation.
- Type II: A fracture at the junction between the odontoid process and the body of the axis (Fig. 12.31). This is the most common type of odontoid fracture and is associated with a high prevalence of non-union due to limited vascular supply. Therefore, this lesion is unstable.
- Type IIA: Similar to type II but with fragments of bone present at the fracture site (Fig. 12.32).
- Type III: A fracture that extends down into the body of the axis (Fig. 12.33). This fracture is also stable.

Radiographically, AP, open-mouth odontoid view, and lateral radiograms are needed. Plain radiography is important for demonstrating indirect signs rather than the fracture itself (Ehara et al. 1992). The use of CT may be helpful in demonstrating the plane of the fracture line, as well as the degree of comminution. Both sagittal and coronal CT reconstructions often delineate the fractures more precisely than plain radiographs. MRI has a limited role in evaluating patients with odontoid fractures without neurological injuries. However, evaluation of the integrity of the ligaments, particularly the transverse ligament, associated soft tissue lesions, and assessment of the brainstem and spinal cord is done using MRI. Generally, the interval between the dens and the anterior arch of C1 is preserved in all dens fractures. Several anatomic variants such as an os odontoideum, an ossiculum terminale, hypoplasia or aplasia of dens, congenital non-union, or non-union of a previous fracture can mimic an acute fracture of the odontoid process (Fig. 12.1). In management, types I and III usually do not require fusion, and cervical orthosis can achieve the reduction. In type-II lesions, several factors are important in the surgical decision-making, such as patient age, bone fragment displacement, and the age of the fracture. The following absolute indications are recommended for surgery: age older than 7 years, displacement of more than 6 mm, instability in halo immobilization, and non-union (Koivikko et al. 2004b). The characteristics of odontoid process fractures are summarized in Table 12.23.

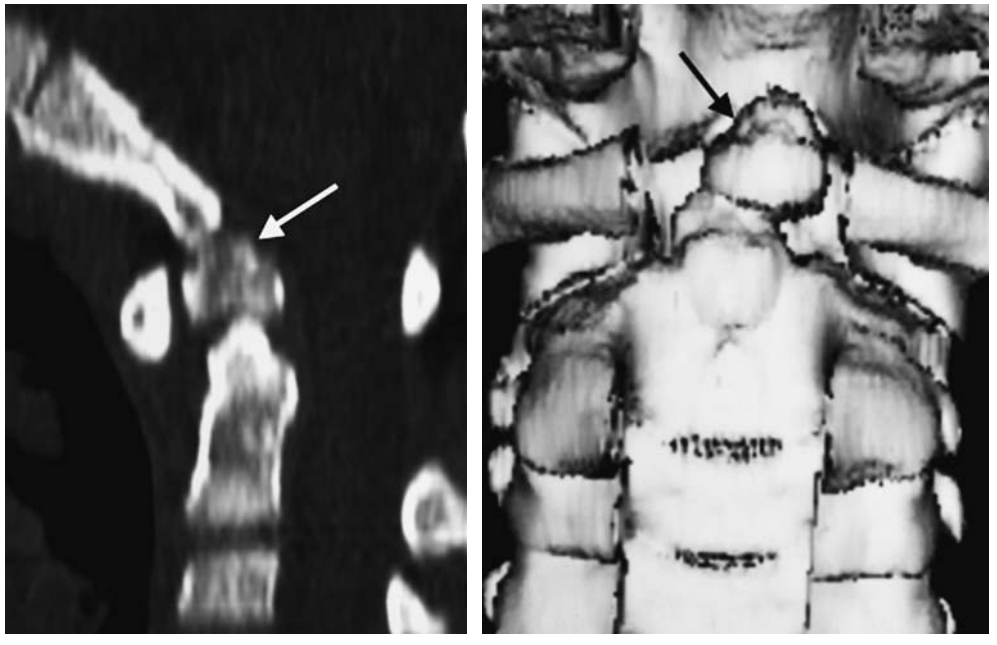

a b

Fig. 12.30a,b. Odontoid fracture: type I. **a** Sagittal CT reformation. **b** CT, shaded surface display. Coronal, posterior view after removal of the posterior arches

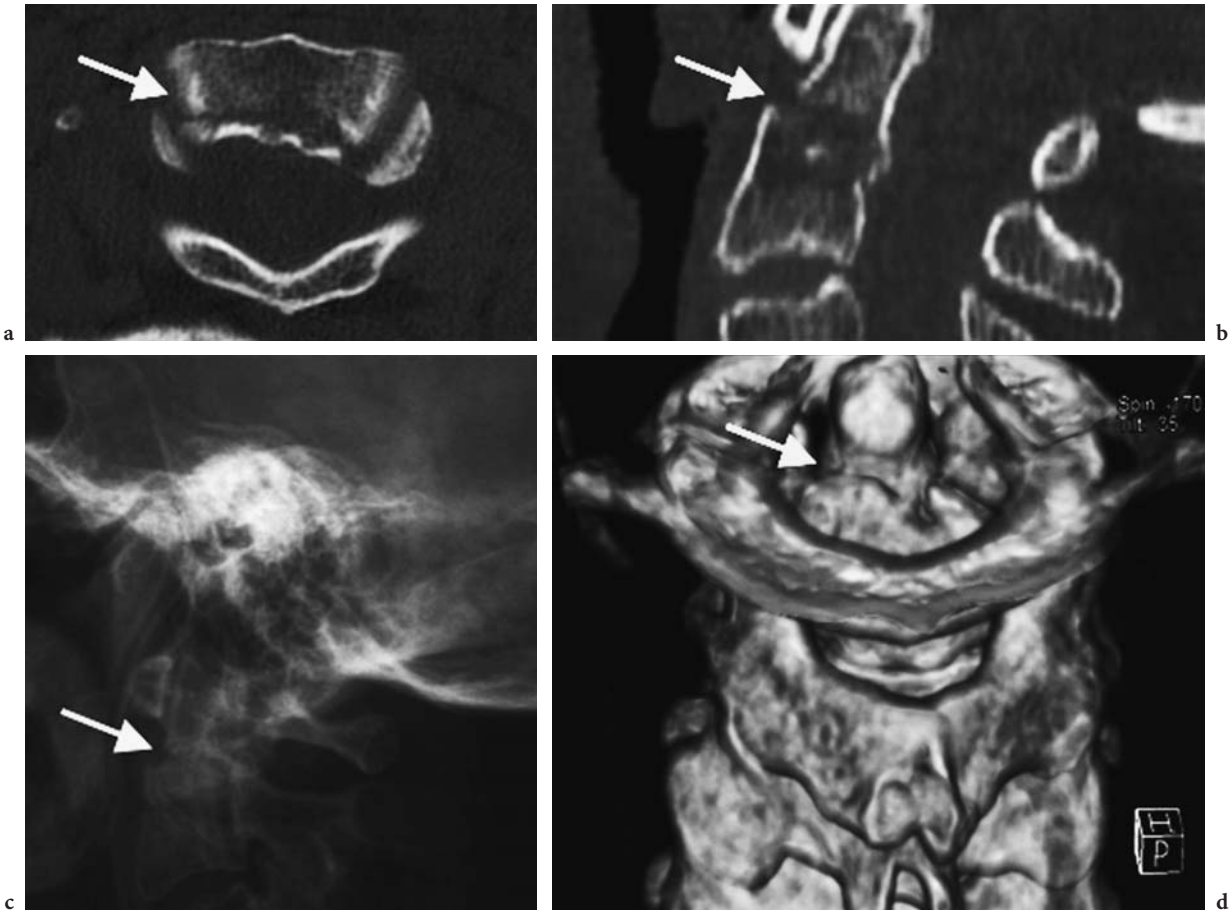

Fig. 12.31a–d. Odontoid fracture: type II. **a** Axial CT image. **b** Sagittal CT reformation. **c** Lateral view radiograph. **d** CT, volume rendering. Coronal, posterior view

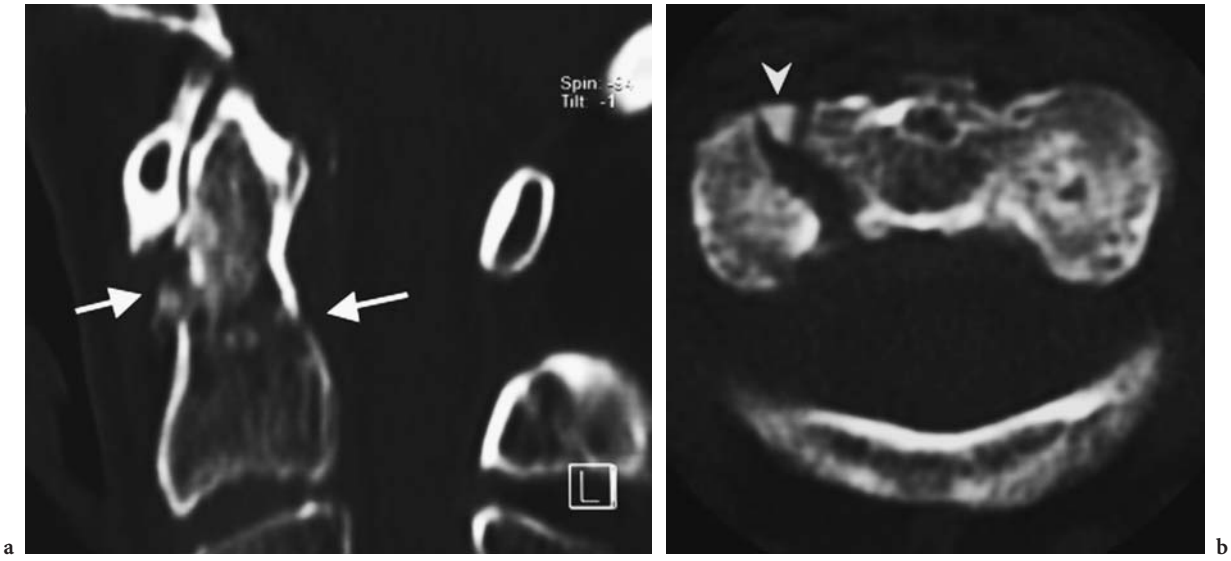

Fig. 12.32a,b. Odontoid fracture: type IIa. **a** Sagittal CT reformation. **b** Axial CT image. Fracture at the base of the odontoid process (*arrows*) with small bony fragments (*arrowhead*)

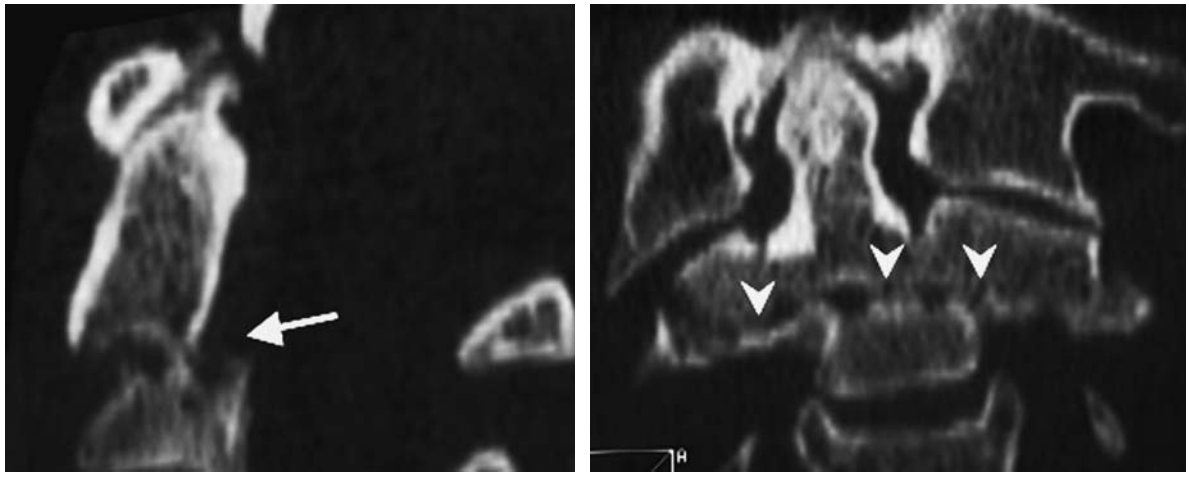

Fig. 12.33a,b. Odontoid fracture: type III. **a** Sagittal CT reformation. **b** Coronal CT reformation. Fracture extending into the body of C2 (*arrow* and *arrowheads*)

Table 12.23. Craniocervical injury: odontoid process fractures

Mechanism	Hyperflexion, hyperextension, and rotational forces
Definition	Type I: avulsion of the tip of the dens (5%–8%)
	Type II: fracture at the base of the dens (54%–67%)
	Type III: fracture extending into the body of the axis (30%–33%)
Spine level	C2
Stability	Type I and III are usually stable, and type II highly unstable
Associated lesions	Nonunion in type II, cord injury when fracture displaced
Radiographic findings	Type I is difficult to see on plain films, may require CT if high clinical suspicion
Management	Cervical orthosis for type I and III, and cervical traction for type II

12.9.6 Occipital Condyle Fractures

The occipital condyles are the prominences of the paired lateral occipital segments of the occipital bone. The occipital condyles, together with the basioccipital segment anteriorly and the squamosal segment posteriorly, form the foramen magnum (Lustrin et al. 1994). The occipital condyles are in close proximity to the medulla oblongata, the vertebral arteries, the jugular foramen, and the lower cranial nerves (Lustrin et al. 1994; Weber and McKenna 1994). Within the base of each occipital condyle lie the hypoglossal canals through which pass the hypoglossal nerve, a meningeal branch of the ascending pharyngeal artery, and an emissary vein. A displaced fragment due to a condylar fracture may involve the hypoglossal canal, the medulla oblongata, and/or vascular structures. Cranial nerve palsy may not be present immediately but may manifest months after trauma, possibly as a result of fragment migration or callus formation (Orbay et al. 1989; Demisch et al. 1998) (Fig. 12.34). The two most important ligamentous structures for the stability of this region are the tectorial membrane and the alar ligaments. Occipital condyle fractures are caused by a combination of vertical compression and lateral bending. Occipital condyle fractures may be classified as impaction fractures, extensions of occipital skull fractures, or avulsion fractures at the insertion of the alar ligaments (Anderson and Montesano 1988). The latter are potentially unstable fractures, particularly if displaced (Tuli et al. 1997) and when associated with tectorial membrane injury can result in gross atlanto-occipital discontinuity. Occipital condyle fractures may be unilateral or bilateral, may extend in a ring-like pattern around the foramen magnum, and are extremely difficult to identify on conventional radiographs (Bloom et al. 1997).

The most widely used classification system for condylar fractures recognizes three types, depending on the morphology of the fracture and mechanism of injury (Anderson and Montesano 1988).

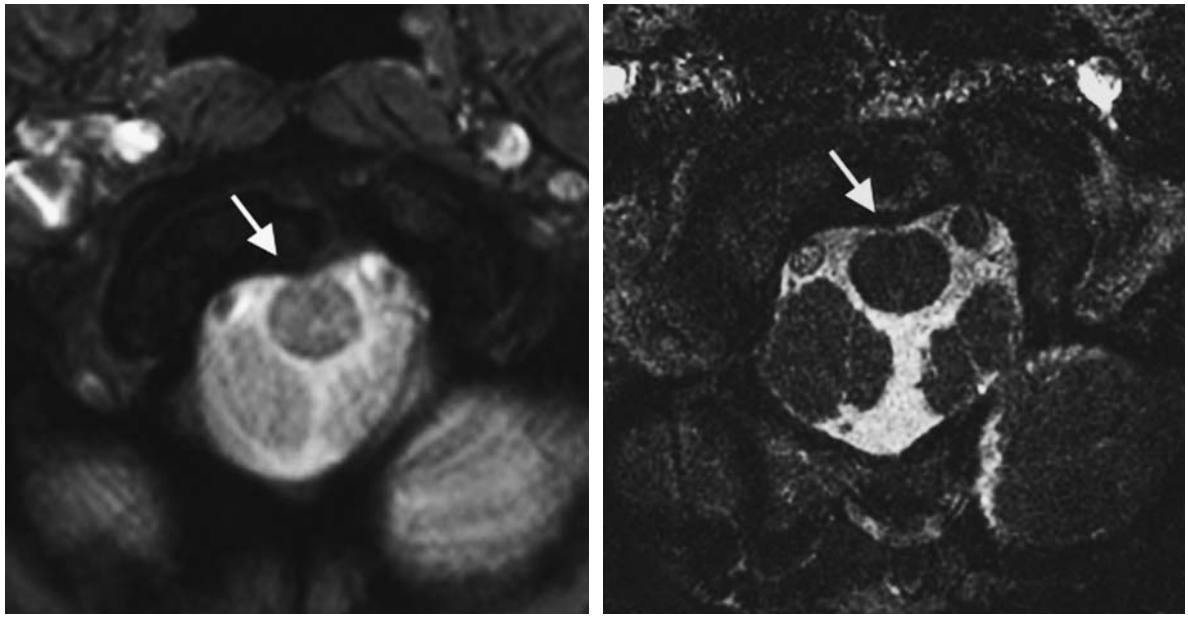

Fig. 12.34a,b. Condylar fracture, callus forming. **a** Axial T2-weighted MR image. **b** Axial 3D T2-weighted CISS image. Slight compression of the medulla oblongata due to a fracture of the condylar process with secondary callus formation (*arrows*)

- Type I: This is an impaction fracture resulting in a comminution of the occipital condyle, with possible minimal fragment displacement (Fig. 12.35). The mechanism of injury is usually an axial loading of the skull onto the atlas, similar to a Jefferson fracture of the atlas, with or without lateral bending. It is considered a stable entity because the tectorial membrane and the contralateral alar ligament are intact (Bloom et al. 1997).
- Type II: This type is a more extensive basilar skull fracture, involving one or both occipital condyles (Fig. 12.36). The mechanism of injury is a direct blow to the skull. An intact tectorial membrane and alar ligaments preserve stability.
- Type III: This is an unstable avulsion fracture near the alar ligament attachment resulting in medial displacement of the occipital condyle bone fragment into the foramen magnum (Mann and Cohen 1994). The mechanism of this injury is forced rotation, usually combined with lateral bending, causing a partial or complete tear of the contralateral alar ligament and tectorial membrane (Dickman et al. 1991). The inferior portion of the clivus may also be disrupted (Jones et al. 1990) (Fig. 12.37).

Radiographically, these lesions are difficult to delineate and both AP and lateral radiograms may fail to demonstrate occipital condyle lesions because of the bony superimposition. CT is the method of choice

Fig. 12.35. Condylar fracture: type I, minimal displacement type. Axial CT image. Condylar fracture with minimal displacement of the fragment (*arrow*)

for the diagnosis of condylar fractures. Cranial CT including the cervicocranium should be performed (Cornelius and Leach 1995). MDCT with two-dimensional multiplanar reformations are strongly recommended for the most accurate assessment of this type of fracture and the degree of craniocervical displacement (Wasserberg and Barlett 1995). MR imaging does not show additional diagnostic

information concerning the fracture or dislocation, but is recommended to evaluate associated soft tissue injuries. The application of MR imaging in the assessment of ligamentous structures is well established and continually increasing (Schweitzer et al. 1992; Dickman et al. 1996). MR imaging is extremely valuable for the evaluation of the fractured segment in relation to the surrounding structures, such as cerebrospinal fluid spaces, brainstem, and neurovascular structures. Type-I and -II condylar fractures are considered stable injuries, because the tectorial membrane and the contralateral alar ligament are not disrupted (Anderson and Montesano 1988; Young et al. 1994). Therefore, these injuries are typically treated conservatively, by orthotic immobilization alone, and most heal uneventfully. Due to ligamentous disruption, type-III injuries are potentially unstable, and may require rigid cervical orthosis to prevent neurologic compromise (Young et al. 1994). The need for surgical therapy is controversial. Most believe surgery may be indicated for neurovascular decompression and/or stabilization (Bozboga et al. 1992; Young et al. 1994; Leventhal et al. 1992). The characteristics of condylar fractures are summarized in Table 12.24.

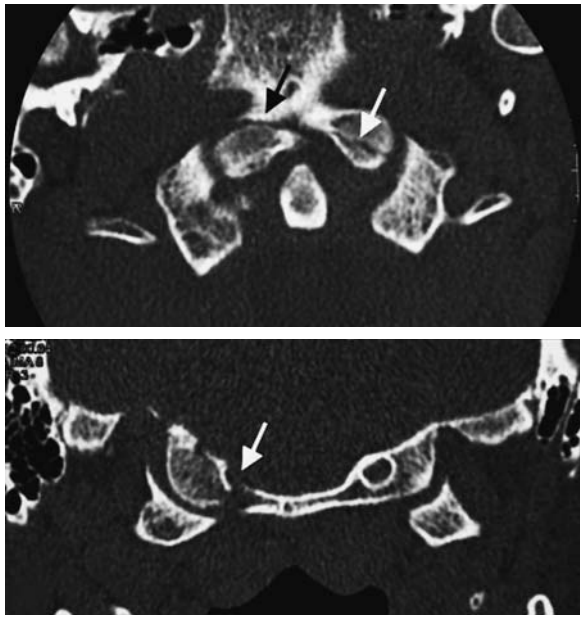

Fig. 12.36a,b. Condylar fracture: type II, extensive type. **a** Axial CT image. **b** Coronal CT reformation. Bilateral condylar fractures (*white arrows*) extending into the basion (*black arrow*)

Table 12.24. Craniocervical injury: occipital condyle fractures

Mechanism	Combination of axial loading, rotation, and lateral bending
Definition	A comminuted compression fracture or an avulsion of the occipital condyle
Spine level	Occipital condyles
Stability	Type I, II stable, type III unstable
Associated lesions	Head trauma, cranial nerve deficits, medulla oblongata injury
Radiographic findings	Difficult to see on plain film, CT and MRI required

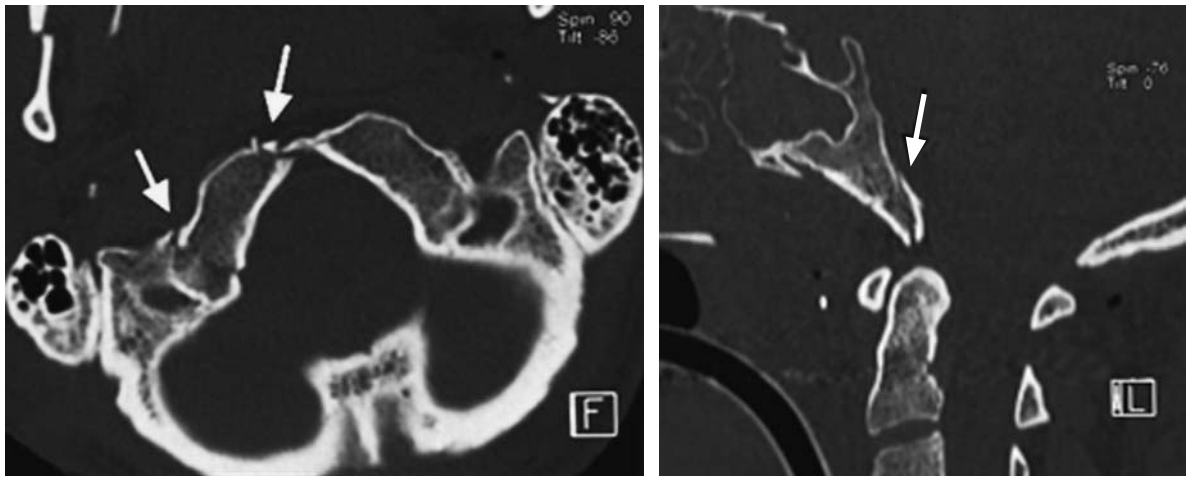

Fig. 12.37a,b. Condylar fracture: type III, unstable type. **a** Axial CT image. **b** Sagittal CT reformation. Multiple condylar fractures (*arrows*) extending to the clivus (*arrow*)

12.10 Spinal Cord Injury and Penetrating Injury

12.10.1 Spinal Cord Injury

Spinal cord injury can be caused by different mechanisms, such as destruction from direct trauma, compression by displaced bony fragments, hematoma or disk material, or ischemia from damage or impingement on the spinal arteries. Another form of spinal cord injury is SCIWORA (spinal cord injury without radiologic abnormality), which is caused by longitudinal distraction of the spinal cord and which is usually encountered in children (Pang and Wilberger 1982). Spinal cord injuries may be complete or incomplete. A complete cord syndrome is characterized by complete loss of motor and sensory functions below the level of injury. Incomplete cord syndromes include three syndromes (Maynard et al. 1997; Mirvis et al. 1988):

1. Anterior cord syndrome: This is usually seen as a result of arterial compression along the anterior face of the spinal cord with variable loss of motor function, pain and temperature sensation, and preserved proprioception. The compression may be from bone fragments or a large disc herniation.
2. Brown-Séquard syndrome: This syndrome is due to a hemisection of the cord, such as stab wounds, hematoma, or disc herniations resulting in ipsilateral loss of proprioception and motor function, and contralateral loss of pain, and temperature sensation.
3. Central cord syndrome: This is usually associated with extension injury, and frequently seen in the elderly with greater motor weakness in the upper limbs, variable sensory loss, and sacral sensory sparing.

The most common causes of spinal cord injury include motor vehicle accidents (50%), falls (21%), violence (14%), and sports injuries (14%) (De Vivo et al. 1992). Approximately 2.6% of trauma patients suffer from a spinal cord trauma. Patients with a complete cord injury have a less than 5% chance of recovery. Most deaths associated with spinal cord injury occur during the first 24 h of hospitalization. The prognosis is much better for incomplete cord syndromes.

The exact location, extent, and severity of a traumatic cervical spinal cord injury can be made with MRI, which also reflects accompanying changes, such as edema or hemorrhage (Ohsio et al. 1993). MR imaging allows direct visualization of the soft tissues, including the ligaments, intervertebral disk, and the spinal cord. Three different MR signal intensity patterns are described in acute spinal cord injury (Shimada and Tokioka 1999; Silberstein et al. 1992; Hackney 1990; Flanders et al. 1996). The first pattern is a blurred high-intensity area on T2-weighted images corresponding to edema within the spinal cord due to a contusion. This pattern has a more favorable prognosis (Fig. 12.38). The second pattern is a hemorrhage lesion indicating neuronal damage with less potential for reversibility. The third pattern is the combination of edema and hemorrhage and has the worst prognosis (Fig. 12.39). Schaefer et al. (1992) described a correlation between lesion length and prognosis. In a cord lesion greater than a vertebral body length the prognosis is less favorable (Schaefer et al. 1992). Other pa-

Fig. 12.38. Spinal cord injury, type I: cord edema. Sagittal T2-weighted MR image showing a central blurred increased signal intensity corresponding to diffuse post-traumatic edema (*arrowheads*)

rameters influencing the prognosis are underlying conditions, such as spondylosis, and central canal stenosis (Regenbogen et al. 1986). The critical issue in patients with cervical trauma is the presence or absence of cord compression by bone, disk, or hematoma, which influences the immediate surgical decision (Quencer et al. 1997; Blacksin and Lee 1995). In patients with acute cord compression, immediate spinal decompression is recommended. Therefore, expediting the MR examination is crucial in patients with a suspected spinal cord injury. The use of both spin-echo T1- and T2- weighted images in axial and sagittal planes, and additional gradient-echo sagittal T2*-weighted images are useful to exclude or detect cord edema and/or hemorrhage. Although controversy surrounds the use of CT and MR imaging in cases of cervical spine trauma, performing an immediate CT in all suspected cases is recommended unless the patient's neurological condition is stable. In these stable cases, MR is the method of choice to evaluate the spinal cord injury (Quencer et al. 1997; Link et al. 1995; Nunez et al. 1996).

12.10.2 Penetrating Injuries

Patients with penetrating injuries to the cervical spine and spinal cord with definite signs of vascular injury do not need imaging procedures because of hemodynamic instability (Kendall et al. 1998). For stable patients, the diagnostic evaluation is challenging because of the close proximity of the vital structures in this area. MDCT is the method of choice in penetrating injuries caused by metallic objects, such as industrial nails and bullets fragments (Fig. 12.40). Three-dimensional reformation techniques are able to demonstrate the trajectory of the injury, the location of the objects, and the associated bony fractures.

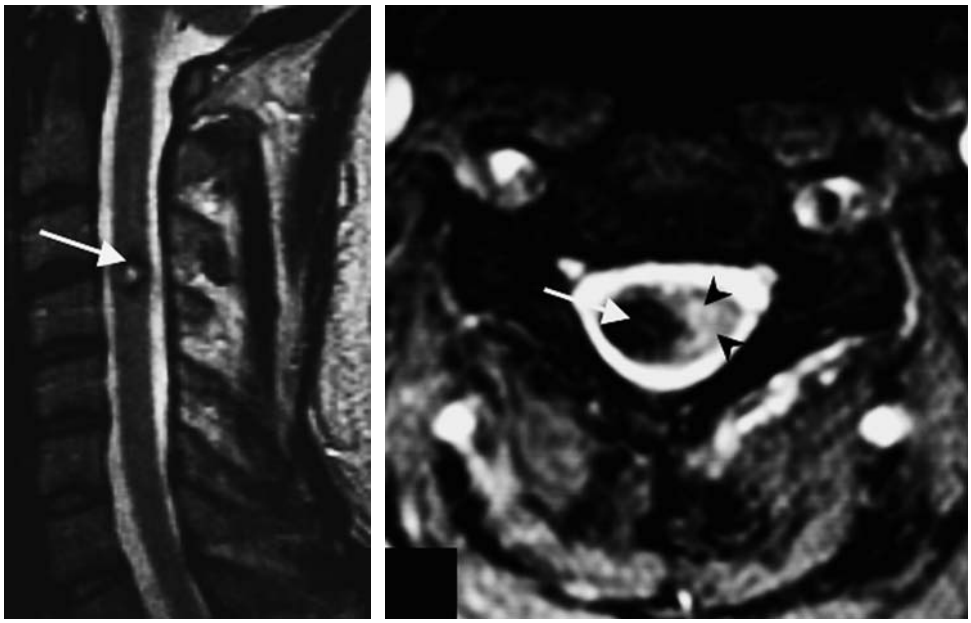

a b

Fig. 12.39a,b. Spinal cord injury, type III: cord hemorrhage and edema. **a** Sagittal T2-weighted MR image. **b** Axial T2-weighted MR image. Subacute cord hemorrhage with peripheral hemosiderin rim (*white arrows*) and associated cord edema (*black arrowheads*)

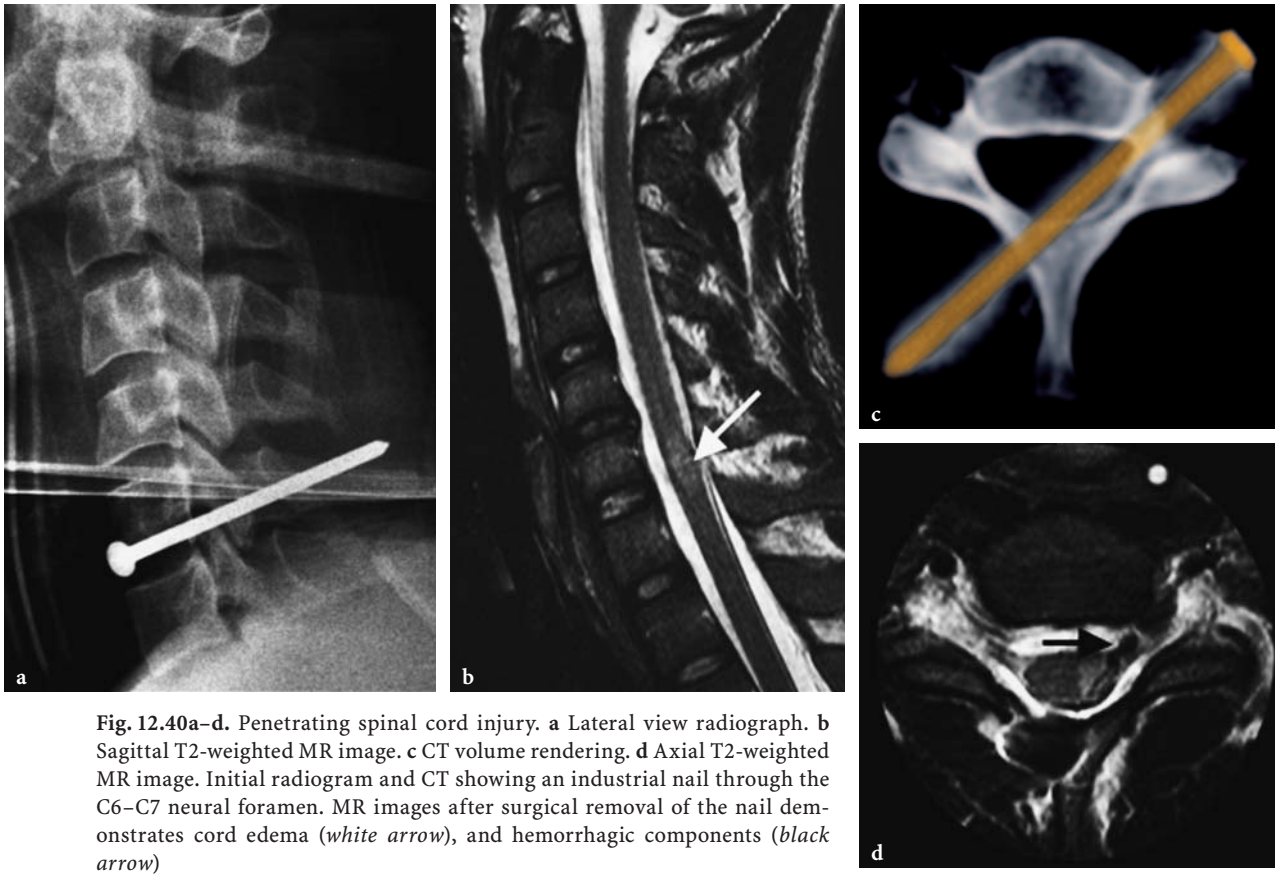

Fig. 12.40a–d. Penetrating spinal cord injury. **a** Lateral view radiograph. **b** Sagittal T2-weighted MR image. **c** CT volume rendering. **d** Axial T2-weighted MR image. Initial radiogram and CT showing an industrial nail through the C6–C7 neural foramen. MR images after surgical removal of the nail demonstrates cord edema (*white arrow*), and hemorrhagic components (*black arrow*)

12.11 Cervical Spine Sprains and Disc Injuries

Some of the pathology of cervical spine sprains, namely whiplash injury, is discussed in chapter 11. Among all cervical trauma cases, 80% are soft tissue injuries (Stabler et al. 2001). Cervical spine sprains include injuries of the ligaments and the intervertebral discs. These sprains may be caused by trauma to the cervicocranium, or cervical spine by several mechanisms, such as flexion, extension, or in a pattern where flexion follows extension (whiplash injury). Depending on the grade of severity, the sprains may be classified as benign or severe.

12.11.1 Benign Sprains

In benign sprains, there is stretching or a limited tear of the ligaments. A flexion sprain involves the posterior spinal ligamentous complex (supraspinous ligaments, interspinous ligaments, ligamenta flava, facet joint capsules) (Fig. 12.41), and an extension sprain involves the anterior longitudinal ligament. Since the posterior longitudinal ligament remains intact, these injuries are stable. Benign sprains mostly occur in motor vehicle accidents, but may also be encountered in sports or falls. Conventional radiographs are used to rule out fractures and/or dislocations. MR imaging has proved to be more accurate than conventional radiography in the depiction of a wide spectrum of ligamentous lesions (Katzberg et al. 1999). Treatment includes cervical immobilization with a soft collar and the use of analgesics. If the symptoms do not improve, a more severe sprain should be suspected, and the further radiologic investigation is warranted.

12.11.2 Severe Sprains

In a severe sprain, there is subluxation of a vertebra due to ligamentous rupture, without primary bone

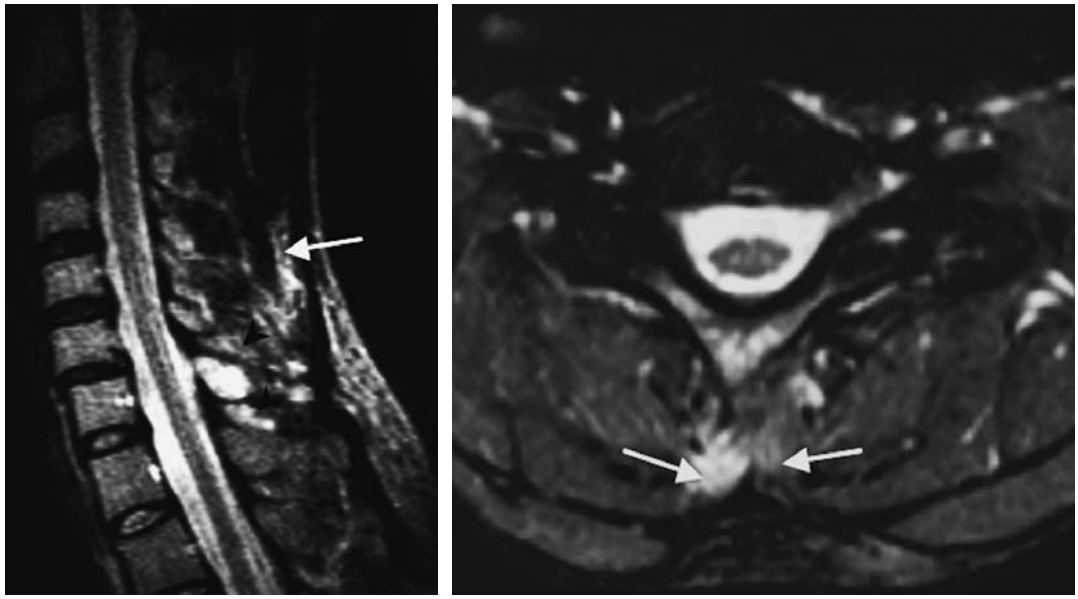

Fig. 12.41a,b. Benign cervical sprain involving the posterior ligamentous complex. **a** Sagittal fat-suppressed T2-weighted MR image. **b** Axial fat-suppressed T2-weighted MR image. Edema through the interspinous (*black arrowheads*) and supraspinous (*arrows*) ligaments. No associated fracture or rupture of the posterior longitudinal ligament. Slight bone edema at the spinous process and the posterior neural arch

fractures. This lesion mainly involves the middle cervical column (see Sect. 12.2.5). In flexion sprains, the direction of the injury is posterior-anterior, and the first structure to be torn is the posterior spinal ligamentous complex as observed in benign sprains. In severe sprains, however, further rupture of the posterior longitudinal ligament and the posterior annulus fibrosis will be observed which makes this injury unstable. The only associated bone lesions are avulsion fractures of the spinous process and secondary compression fractures of the vertebral body. The fracture of a spinous process should be differentiated from a clay shoveler's fracture where there are no associated ligamentous lesions (see Section 12.4.5) (Harris 1986). In an extension trauma, the direction of the force is anteroposterior and the first to tear will be the anterior column structures, such as anterior longitudinal ligament, anterior annulus fibrosis, followed by the middle column ligaments. Severe sprains account for 7% of all severe injuries of the lower cervical spine (Allen et al. 1982), and only 0.5% of all cases with cervical spine injuries (Wilberger and Maroon 1990). Although they are rare, if these sprains are missed, they may result in progressive vertebral luxation and subsequent myelopathy (Braakman and Braakman 1987). Clinical presentation includes non-specific neck pain and cervical radiculopathy in those cases where there is an associated disc herniation. The radiological diagnosis is based on a lateral radiogram in neutral position or in flexion-extension. Even in the presence of a severe sprain, the initial lateral radiogram may be normal. Therefore, serial radiograms with dynamic views are recommended. Some authors have suggested that the lateral and dynamic views should always be repeated after a certain period of time, from 5 to 21 days (Laporte et al. 1999). On lateral radiograms, severe extension sprains show a hyperlordotic cervical spine curve, together with widening of the anterior disc space, backward sagittal displacement, and slipping of the facet surfaces. Radiologic features of a severe sprain are illustrated in Figure 12.42 (Wilberger and Maroon 1990; Jonsson et al. 1994). On MRI, the disruption of the posterior ligamentous complex may be seen on T2-weighted images, as an increased signal intensity area between the two adjacent spinous processes. MRI may also directly visualize the rupture of the posterior or anterior longitudinal ligaments (Emery et al. 1989). Severe sprains should be treated surgically with the use of fixation through a posterior approach, or in case of an associated disc herniation with anterior fixation and discectomy.

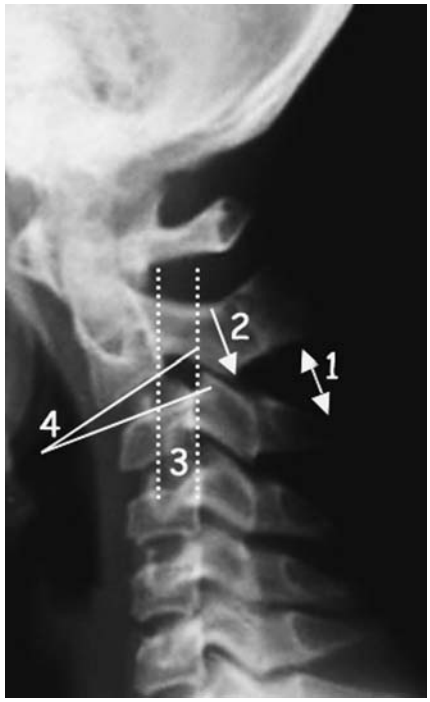

Fig. 12.42. Severe cervical sprain. Lateral view radiograph. Radiologic features include one of more of the following findings: *1*, widening of interspinous distance ("fanning"); *2*, loss of parallelism between facet joints; *3*, sagittal displacement of a vertebral body >3.5 mm. *4*, angular displacement (sagittal plane rotation) >11° compared with the adjacent interspaces

12.11.3 Intervertebral Disc Injuries

Post-traumatic disc injuries include annular tears with/or without disc extrusion, and usually occur secondary to axial loading forces to the cervical spine. The most common location is the lower cervical segment. Cervical disc extrusion may result in transient quadriplegia due to anterior cord syndrome (see Sect. 12.10). If congenital or spondylotic spinal stenosis exists, the neurologic deficit may be greater (Torg et al. 1997a,b). Conventional radiography is not able to detect a traumatic disc herniation. CT, particularly MDCT, is able to show the extruded disc with the use of axial and sagittal reformations; however, CT is not able to show the post-traumatic secondary cord changes (Fig. 12.43). Secondary findings of a cervical disk injury include increased T2 signal intensity of the injured disk, and possible edematous changes of the spinal cord at the same level (Katzberg et al. 1999; Flanders et al. 1990) (Fig. 12.44). The treatment is surgical and includes anterior decompression, laminectomy, and fusion.

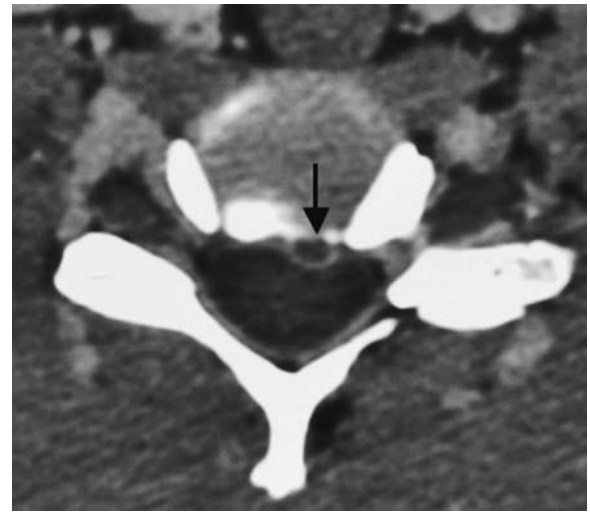

Fig. 12.43. Traumatic disc injury. Axial CT image

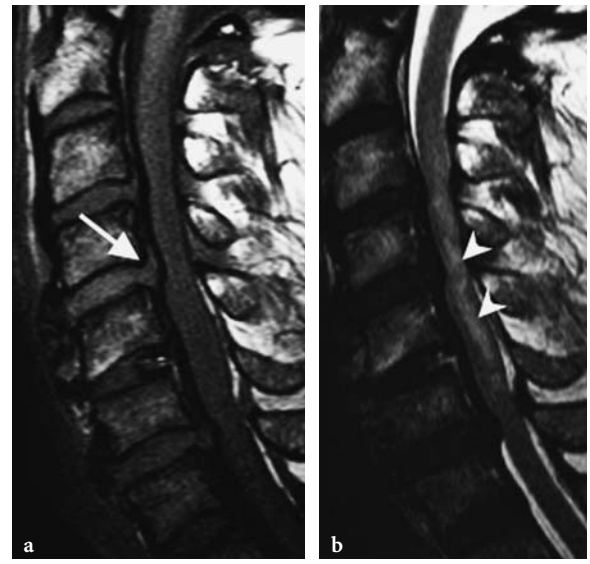

Fig. 12.44a,b. Traumatic disc injury. **a** Sagittal T1-weighted MR image. **b** Sagittal T2-weighted MR image. Traumatic disk herniation (*arrow*) with spinal cord compression, and cord edema (*arrowheads*)

References

Adams VI (1992) Neck injuries. II. Atlantoaxial dislocation: a pathologic study of 14 traffic fatalities. J Forensic Sci 37:565–573

Allen BL Jr, Ferguson RL, Lehmann TR, O'Brien RP (1982) A mechanistic classification of closed, indirect fractures and dislocations of the lower cervical spine. Spine 7:1–27

Anderson LD, D'Alonza RT (2004) Fractures of the odontoid process of the axis. 1974. J Bone Joint Surg Am 86:2081

Anderson PA, Montesano PX (1988) Morphology and treatment of occipital condyle fractures. Spine 13:731-736
Argenson C, Lovet J, Sanouiller JL, de Peretti F (1988) Traumatic rotatory displacement of the lower cervical spine. Spine 13:767–773
Benedetti PF, Fahr LM, Kuhns LR, Hayman LA (2000) MR imaging findings in spinal ligamentous injury. AJR Am J Roentgenol 175:661–665
Bensch FV, Kiuru MJ, Koivikko MP, Koskinen SK (2004) Spine fractures in falling accidents: analysis of multidetector CT findings. Eur Radiol 14:618–624
Berne JD, Velmahos GC, El-Tawil Q et al. (1999) Value of complete cervical helical computed tomographic scanning in identifying cervical spine injury in the unevaluable blunt trauma patient with multiple injuries: a prospective study. J Trauma 47:896–903
Blackmore CC, Emerson SS, Mann FA, Koepsell TD (1999a) Cervical spine imaging in patients with trauma: determination of fracture risk to optimize use. Radiology 211:759–765
Blackmore CC, Ramsey SD, Mann FA, Deyo RA (1999b) Cervical spine screening with computed tomography in trauma patients: a cost-effectiveness analysis. Radiology 212:117–125
Blackmore CC, Mann FA, Wilson AJ (2000) Helical CT in the primary trauma evaluation of the cervical spine: an evidence-based approach. Skeletal Radiol 29:632–639
Blacksin MF, Lee HJ (1995) Frequency and significance of fractures of the upper cervical spine detected by CT in patients with severe neck trauma. AJR Am J Roentgenol 196:741–745
Bloom AI, Neeman Z, Slasky S, Floman Y, Milgrom M, Rivkind A, Bar-Ziv J (1997) Fracture of the occipital condyles and associated craniocervical ligament injury: incidence, CT imaging and implications. Clin Radiol 42:198–202
Bohlman HH (1979) Acute fractures and dislocations of the cervical spine. An analysis of three hundred hospitalized patients and review of the literature. J Bone Joint Surg Am 61:1119–1142
Bondurant FJ, Cotler HB, Kulkarni MV, McArdle CB, Harris JH Jr (1990) Acute spinal cord injury. A study using physical examination and magnetic resonance imaging. Spine 15:161–168
Borock EC, Gabram SG, Jacobs LM, Murphy MA (1991) A prospective analysis of a two-year experience using computed tomography as an adjunct for cervical spine clearance. J Trauma 31:1001–1006
Bozboga M, Unal F, Hepgul K, Izgi N, Turantan I, Turker K (1992) Fracture of the occipital condyle. Spine 17:1119–1121
Bozic KJ, Keyak JH, Skinner HB, Bueff HU, Bradford DS (1994) Three-dimensional finite element modeling of a cervical vertebra: an investigation of burst fracture mechanism. J Spinal Disord 7:102–110
Braakman M, Braakman R (1987) Hyperflexion sprain of the cervical spine. Follow-up of 45 cases. Acta Orthop Scand 58:388–393
Brohi K, Wilson-Macdonald J (2000) Evaluation of unstable cervical spine injury: a 6-year experience. J Trauma 49:76–80
Burney RE, Maio RF, Maynard F, Karunas R (1993) Incidence, characteristics, and outcome of spinal cord injury at trauma centers in North America. Arch Surg 128:596–9
Cadoux CG, White JD, Hedberg MC et al. (1987) Highyield roentgenographic criteria for cervical spine injuries. Ann Emerg Med 16:738–742
Campbell SE, Phillips CD, Dubovsky E, Cail WS, Omary RA (1995) The value of CT in determining potential instability of simple wedge-compression fractures of the lumbar spine. Am J Neuroradiol 16:1385–1392
Carroll EA, Gordon B, Sweeney CA, Joy S, Connolly PJ (2001) Traumatic atlantoaxial distraction injury: a case report. Spine 26:454–457
Clark CR, Igram CM, el-Khoury GY, Ehara S (1988) Radiographic evaluation of cervical spine injuries. Spine 13:742–747
Colterjohn NR, Bednar DA (1995) Identifiable risk factors for secondary neurologic deterioration in the cervical spine-injured patient. Spine 20:2293–2297
Cornelius RS, Leach JL (1995) Imaging evaluation of cervical spine trauma. Neuroimaging Clin N Am 5:451–463
Currarino G, Rollins N, Diehl JT (1994) Congenital defects of the posterior arch of the atlas: a report of seven cases including an affected mother and son. Am J Neuroradiol 15:249–254
Cusick JF, Yoganandan N, Pintar F, Gardon M (1996) Cervical spine injuries from high-velocity forces: a pathoanatomic and radiologic study. J Spinal Disord 9:1–7
Daffner RH (2000) Cervical radiography for trauma patients: a time effective technique? AJR Am J Roentgenol 175:1309–1311
Davis JW, Phreaner DL, Hoyt DB, Mackersie RC (1993) The etiology of missed cervical spine injuries. J Trauma 34:342–346
Deliganis AV, Baxter AB, Hanson JA, Fisher DJ, Cohen WA, Wilson AJ, Mann FA (2000) Radiologic spectrum of craniocervical distraction injuries. Radiographics 20:S237–S50
Demetriades D, Charalambides K, Chahwan S, Hanpeter D, Alo K, Velmahos G, Murray J, Asensio J (2000) Nonskeletal cervical spine injuries: epidemiology and diagnostic pitfalls. J Trauma 48:724–727
Demisch S, Lindner A, Beck R, Zierz S (1998) The forgotten condyle: delayed hypoglossal nerve palsy caused by fracture of the occipital condyle. Clin Neurol Neurosurg 100:44–45
Denis F (1983) The three column spine and its significance in the classification of acute thoracolumbar spinal injuries. Spine 8:817–831
DeVivo MJ, Rutt RD, Black KJ, Go BK, Stover SL (1992) Trends in spinal cord injury demographics and treatment outcomes between 1973 and 1986. Arch Phys Med Rehabil 73:424–430
Dickman CA, Mamourian A, Sonntag VKH, Drayer BP (1991) Magnetic resonance imaging of the transverse atlantal ligament for the evaluation of atlantoaxial instability. J Neurosurg 75:221–227
Dickman CA, Greene KA, Sonntag VK (1996) Injuries involving the transverse atlantal ligament: classification and treatment guidelines based upon experience with 39 injuries. Neurosurgery 38:44–50
Doris PE, Wilson RA (1985) The next logical step in the emergency radiographic evaluation of cervical spine trauma: the five view trauma series. J Emerg Med 3:371–385
Dvorak J, Grob D, Baumgartner H, Gschwend N, Grauer W, Larsson S (1989) Functional evaluation of the spinal cord by magnetic resonance imaging in patients with rheumatoid arthritis and instability of upper cervical spine. Spine 14:1057–1064
Dwek JR, Chung CB (2000) Radiography of cervical spine injury in children: are flexion-extension radiographs useful for acute trauma? AJR Am J Roentgenol 174:1617–1619

Ebraheim NA, Xu R, Ahmad M, Heck B, Yeasting RA (1997) The effect of anterior translation of the vertebra on the canal size in the lower cervical spine: a computer-assisted anatomic study. J Spinal Disord 10:162–166

Effendi B, Roy D, Cornish B, Dussault RG, Laurin CA (1981) Fractures of the ring of the axis. A classification based on the analysis of 131 cases. J Bone Joint Surg Br 63:319–327

Ehara S, El-Khoury GY, Clark CR (1992) Radiologic evaluation of dens fracture: role of plain radiography and tomography. Spine 17:475–479

Ellis JH, Martel W, Lillie JH, Aisen AM (1991) Magnetic resonance imaging of the normal craniovertebral junction. Spine 16:105–111

Emery SE, Pathria MN, Wilber RG, Masaryk T, Bohlman HH (1989) Magnetic resonance imaging of posttraumatic spinal ligament injury. J Spinal Dis 2:229–233

Fazl M, LaFebvre J, Willinsky RA, Gertzbein S (1990) Posttraumatic ligamentous disruption of the cervical spine, an easily overlooked diagnosis: presentation of three cases. Neurosurgery 26:674–678

Fielding JW, Francis WR, Hawkins RJ, Pepin J, Hensinger R (1989) Traumatic spondylolisthesis of the axis. Clin Orthop 239:47–52

Flanders AE, Schaefer DM, Doan HT, Mishkin MM, Gonzalez CF, Northrup BE (1990) Acute cervical spine trauma: correlation of MR imaging findings with degree of neurologic deficit. Radiology 177:25–33

Flanders AE, Spettell CM, Tartaglino CM, Friedman DP, Herbison GJ (1996) Forecasting motor recovery after cervical spinal cord injury: value of MR imaging. Radiology 201:649–655

Forsberg DA, Martinez S, Vogler JB 3rd, Wiener MD (1990) Cervical spondylolysis: imaging findings in 12 patients. AJR Am J Roentgenol 154:751–755

Fowler JL, Sandhu A, Fraser RD (1990) A review of fractures of the atlas vertebra. J Spinal Disord 3:19–24

Freemyer B, Knopp R, Piche J, Wales L, Williams J (1989) Comparison of five-view and three-view cervical spine series in the evaluation of patients with cervical trauma. Ann Emerg Med 18:818–821

Geck MJ, Yoo S, Wang JC (2001) Assessment of cervical ligamentous injury in trauma patients using MRI. J Spinal Disord 14:371–377

Gleizes V, Jacquot FP, Signoret F, Feron JM (2000) Combined injuries in the upper cervical spine: clinical and epidemiological data over a 14-year period. Eur Spine J 9:386–392

Graber MA, Kathol M (1999) Cervical spine radiographs in the trauma patient. Am Fam Physician 59:331–342

Green JD, Harle TS, Harris JH Jr (1981) Anterior subluxation of the cervical spine: hyperflexion sprain. Am J Neuroradiol 2:243–250

Greene KA, Dickman CA, Marciano FF, Drabier JB, Hadley MN, Sonntag VK (1997) Acute axis fractures. Analysis of management and outcome in 340 consecutive cases. Spine 22:1843–1852

Guiot B, Fessler RG (1999) Complex atlantoaxial fractures. J Neurosurg 91:139–143

Gunzburg R, Szpalski M, Van Goethem J (2003) Initial assessment of whiplash patients. Pain Res Manag 8:24–27

Hackney DB (1990) Denominators of spinal cord injury. Radiology 177:18–20

Hadley MN, Browner C, Sonntag VKH (1985) Axis fractures: a comprehensive review of management and treatment in 107 cases. Neurosurgery 17:281–289

Hadley MN, Browner CM, Liu SS, Sonntag VK (1988a) New subtype of acute odontoid fractures (type IIA). Neurosurgery 22:67–71

Hadley MN, Dickman CA, Browner CM, Sonntag VK (1988b) Acute traumatic atlas fractures: management and long term outcome. Neurosurgery 23:31–35

Hahn YH (2004) Cervical spine fractures. http://chorus.rad.mcw.edu/doc/00907.html

Halliday AL, Henderson BR, Hart BL, Benzel EC (1997) The management of unilateral lateral mass/facet fractures of the subaxial cervical spine: the use of magnetic resonance imaging to predict instability. Spine 22:2614–2621

Hanson JA, Blackmore CC, Mann FA, Wilson AJ (2000) Cervical spine injury: A clinical decision rule to identify high-risk patients for helical CT screening. AJR Am J Roentgenol 174:713–717

Harris JH Jr (1986) Radiographic evaluation of spinal trauma. Orthop Clin North Am 17:75–86

Harris JH, Yeakley JW (1992) Hyperextension-dislocation of the cervical spine. Ligament injuries demonstrated by magnetic resonance imaging. J Bone Joint Surg Br 74:567–567

Harris JH, Carson GC, Wagner LK (1994) Radiologic diagnosis of traumatic occipitovertebral dissociation. 1. Normal occipitovertebral relationships on lateral radiographs of supine subjects. AJR Am J Roentgenol 162:881–886

Hays MB, Alker GJ Jr (1988) Fractures of the atlas vertebra. The two-part burst fracture of Jefferson. Spine 13:601–603

Hoffman JR, Mower WR, Wolfson AB, Todd KH, Zucker MI (2000) Validity of a set of clinical criteria to rule out injury to the cervical spine in patients with blunt trauma. National Emergency X-Radiography Utilization Study Group. N Engl J Med 343:138–140

Hu R, Mustard CA, Burns C (1996) Epidemiology of incident spinal fracture in a complete population. Spine 21:492–499

Jackson AB, Dijkers M, DeVivo M, Poczatek RB (2004) A demographic profile of new traumatic spinal cord injuries: change and stability over 30 years. Arch Phys Med Rehabil 85:1740–1748

Jelly LM, Evans DR, Easty MJ, Coats TJ, Chan O (2000) Radiography versus spiral CT in the evaluation of cervicothoracic junction injuries in polytrauma patients who have undergone intubation. Radiographics 20:251–259

John SD (1999) Trends in pediatric emergency imaging. Radiol Clin North Am 37:995–1034

Jones DN, Knox AM, Sage MR (1990) Traumatic avulsion fracture of the occipital condyles and clivus with associated unilateral atlantooccipital distraction. Am J Neuroradiol 11:1181–1183

Jonsson H, Cesarini K, Sahlstedt B, Rauschning W (1994) Findings and outcome in whiplash-type neck distortions. Spine 19:2733–2743

Katzberg RW, Benedetti PF, Drake CM, Ivanovic M, Levine RA, Beatty CS, Nemzek WR, McFall RA, Ontell FK, Bishop DM, Poirier VC, Chong BW (1999) Acute cervical spine injuries: prospective MR imaging assessment at a level 1 trauma center. Radiology 213:203–211

Kendall JL, Anglin D, Demetriades D (1998) Penetrating neck trauma. Emerg Med Clin North Am 16:85–105

Kesterson L, Benzel E, Orrison W, Coleman J (1991) Evaluation and treatment of atlas burst fractures (Jefferson fractures). J Neurosurg 75:213–220

Kim KS, Chen HH, Russell EJ, Rogers LF (1989) Flexion teardrop fracture of the cervical spine: radiographic characteristics. AJR Am J Roentgenol 152:319–326
Kiwerski J (1993) Hyperextension-dislocation injuries of the cervical spine. Injury 24:674–677
Koivikko MP, Kiuru MJ, Koskinen SK (2004a) Multidetector computed tomography of cervical spine fractures in ankylosing spondylitis. Acta Radiol 45:751–759
Koivikko MP, Kiuru MJ, Koskinen SK, Myllynen P, Santavirta S, Kivisaari L (2004b) Factors associated with nonunion in conservatively-treated type-II fractures of the odontoid process. J Bone Joint Surg Br 86:1146–1151
Kokkino AJ, Lazio BE, Perin NI (1996) Vertical fracture of the odontoid process: case report. Neurosurgery 38:200–202
Kulkarni MV, Bondurant FJ, Rose SL, Narayana PA (1988) 1.5 Tesla magnetic resonance imaging of acute spinal trauma. Radiographics 8:1059–1082
Lali HS, Fehlings MG (2001) Epidemiology, demographics, and pathophysiology of acute spinal cord injury. Spine 26:2–12
Laporte C, Laville C, Lazennec JY, Rolland E, Ramare S, Saillant G (1999) Severe hyperflexion sprains of the lower cervical spine in adults. Clin Orthop Relat Res 363:126–134
Lee C, Woodring JH, Walsh JW (1991) Carotid and vertebral artery injury in survivors of atlanto-occipital dislocation: case reports and literature review. J Trauma 31:401–407
Lee JS, Harris JH Jr, Mueller CF (1997) The significance of prevertebral soft tissue swelling in extension teardrop fracture of the cervical spine. Emerg Radiol 4:132–139
Lee TT, Green BA, Petrin DR (1998) Treatment of stable burst fracture of the atlas (Jefferson fracture) with rigid cervical collar. Spine 23:1963–1967
Leferink VJ, Veldhuis EF, Zimmerman KW, ten Vergert EM, ten Duis HJ (2002) Classificational problems in ligamentary distraction type vertebral fractures: 30% of all B-type fractures are initially unrecognised. Eur Spine J 11:246–50
Leite CC, Escobar BE, Bazan C 3rd, Jinkins JR (1997) MRI of cervical facet dislocation. Neuroradiology 39:583–538
Leventhal MR, Boydston WR, Sebes JI, Pinstein, ML, Watridge CB, Lowrey R (1992) The diagnosis and treatment of fractures of the occipital condyle. Orthopedics 15:944–947
Levine AM, Edwards CC (1991) Fractures of the atlas. J Bone Joint Surg Am 73:680–691
Lewis LM, Docherty M, Ruoff BE, Fortney JP, Keltner RA Jr, Britton P (1991) Flexion-extension views in the evaluation of cervical-spine injuries. Ann Emerg Med 20:117–121
Lin JT, Lee JL, Lee ST (2003) Evaluation of occult cervical spine fractures on radiographs and CT. Emerg Radiol 10:128–123
Link TM, Schuierer G, Hefendiek A. Horch C, Peters PE (1995) Substantial head trauma: value of routine CT examination of the cervicocranium. Radiology 196:741–745
Linsenmaier U, Krotz M, Hauser H, Rock C, Rieger J, Bohndorf K, Pfeifer KJ, Reiser M (2002) Wholebody computed tomography in polytrauma: techniques and management. Eur Radiol 12:1728–1740
Lomoschitz FM, Blackmore CC, Mirza SK, Mann FA (2002) Cervical spine injuries in patients 65 years old and older: epidemiologic analysis regarding the effects of age and injury mechanism on distribution, type, and stability of injuries. AJR Am J Roentgenol 178:573–577
Lustrin ES, Robertson RL, Tilak S (1994) Normal anatomy of the skull base. Neuroimaging Clin N Am 4:465–478
Lustrin ES, Karakas SP, Ortiz AO, Cinnamon J, Castillo M, Vaheesan K, Brown JH, Diamond AS, Black K, Singh S (2003) Pediatric cervical spine: normal anatomy, variants, and trauma. Radiographics 23:539–560
MacDonald RL, Schwartz ML, Mirich D, Sharkey PW, Nelson WR (1990) Diagnosis of cervical spine injury in motor vehicle crash victims: how many X-rays are enough? J Trauma 30:392–397
Makan P (1999) Neurologic compromise after an isolated laminar fracture of the cervical spine. Spine 24:1144–1147
Mann FA, Cohen W (1994) Occipital condyle fracture: significance in the assessment of occipitoatlantal stability. AJR Am J Roentgenol 163:193–194
Mann FA, Cohen WA, Linnau KF, Hallam DK, Blackmore CC (2003) Evidence-based approach to using CT in spinal trauma. Eur J Radiol 48:39–48
Maynard FM Jr, Bracken MB, Creasey G, Ditunno JF Jr, Donovan WH, Ducker TB (1997) International standards for neurological and functional classification of spinal cord injury. Spinal Cord 35:266–274
McNamara RM, Heine E, Esposito B (1990) Cervical spine injury and radiography in alert, high-risk patients. J Emerg Med 8:177–182
Mirvis SE, Young JW, Lim C, Greenberg J (1987) Hangman's fracture: radiologic assessment in 27 cases. Radiology 163:713–717
Mirvis SE, Geisler FH, Jelinek JJ, Joslyn JN, Gellad F (1988) Acute cervical spine trauma: evaluation with 1.5-T MR imaging. Radiology 166:807–816
Niibayashi H (1998) Atlantoaxial rotatory dislocation. A case report. Spine 23:1494–1496
Nunez DB, Quencer RM (1998) The role of helical CT in the assessment of cervical spine injuries. AJR Am J Roentgenol 171:951–957
Nunez DB Jr, Zuluaga A, Fuentes-Bernardo DA, Rivas LA, Becerra JL (1996) Cervical spine trauma: how much more do we learn by routinely using helical CT? Radiographics 16:1307–1318
Obenauer S, Alamo L, Herold T, Funke M, Kopka L, Grabbe E (2002) Imaging skeletal anatomy of injured cervical spine specimens: comparison of singleslice vs multi-slice helical CT. Eur Radiol 12:2107–2111
Ohshio I, Hatayama A, Kaneda K, Takahara M, Nagashima K (1993) Correlation between histopathologic features and magnetic resonance images of spinal cord lesions. Spine 18:1140–1149
Orbay T, Aykol S, Seckai Z, Ergun R (1989) Late hypoglossal nerve palsy following fracture of the occipital condyle. Surg Neurol 31:402–404
Pang D, Wilberger JE Jr (1982) Spinal cord injury without radiographic abnormalities in children. J Neurosurg 57:114–129
Pang D, Li V (2004) Atlantoaxial rotatory fixation: Part 1-Biomechanics of normal rotation at the atlantoaxial joint in children. Neurosurgery 55:614–625
Prasad VS, Schwartz A, Bhutani R, Sharkey PW, Schwartz ML (1999) Characteristics of injuries to the cervical spine and spinal cord in polytrauma patient population: experience from a regional trauma unit. Spinal Cord 37:560–568
Quencer RM, Nunez D, Green BA (1997) Controversies in imaging acute cervical spine trauma. AJNR Am J Neuroradiol 18:1866–1868

Regenbogen VS, Rogers LF, Atlas SW, Kim KS (1986) Cervical spinal cord injuries in patients with cervical spondylosis. AJR Am J Roentgenol 146:277–284

Ringenberg BJ, Fisher AK, Urdaneta LF, Midthun MA (1988) Rational ordering of cervical spine radiographs following trauma. Ann Emerg Med 17:792–796

Ross SE, Schwab CW, David ET, Delong WG, Born CT (1987) Clearing the cervical spine: initial radiologic evaluation. J Trauma 27:1055–1060

Ryan MD, Henderson JJ (1992) The epidemiology of fractures and fracture-dislocations of the cervical spine. Injury 23:38–40

Schaefer D, Flanders A, Northrup B et al. (1992) Prognostic significance of magnetic resonance imaging in the acute phase of cervical spine injury. J Trauma 76:218

Scher AT (1982) ‚Tear-drop' fractures of the cervical spine – radiological features. S Afr Med J 61:355–356

Schleehauf K, Ross SE, Civil ID, Schwab CW (1989) Computed tomography in the initial evaluation of the cervical spine. Ann Emerg Med 18:815–817

Schweitzer ME, Hodler J, Cervilla V, Resnick D (1992) Craniovertebral junction: normal anatomy with MR correlation. AJR Am J Roentgenol 158:1087–1090

Shanmuganathan K, Mirvis SE, Dowe M, Levine AM (1996) Traumatic isolation of the cervical articular pillar: imaging observations in 21 patients. AJR Am J Roentgenol 166:897–890

Shapiro SA (1993) Management of unilateral locked facet of the cervical spine. Neurosurgery 33:832–837

Shapiro S, Snyder W, Kaufman K, Abel T (1999) Outcome of 51 cases of unilateral locked cervical facets: interspinous braided cable for lateral mass plate fusion compared with interspinous wire and facet wiring with iliac crest. J Neurosurg 91:19–24

Shimada K, Tokioka T (1999) Sequential MR studies of cervical cord injury: correlation with neurological damage and clinical outcome. Spinal Cord 37:410–415

Signoret F, Jacquot FP, Feron JM (1999) Reducing the cervical flexion tear-drop fracture with a posterior approach and plating technique: an original method. Eur Spine J 8:110–116

Silberstein M, Tress BM, Hennessy O (1992) Prediction of neurologic outcome in acute spinal cord injury: the role of CT and MR. AJNR Am J Neuroradiol 13:1597–1608

Spivak JM, Weiss MA, Cotler JM, Call M (1994) Cervical spine injuries in patients 65 and older. Spine 19:2302–2306

Stabler A, Eck J, Penning R, Milz SP, Bartl R, Resnick D, Reiser M (2001) Cervical spine: postmortem assessment of accident injuries – comparison of radiographic, MR imaging, anatomic, and pathologic findings. Radiology 221:340–346

Stiell IG, Wells GA, Vandemheen KL, Clement CM, Lesiuk H, De Maio VJ, Laupacis A, Schull M, McKnight RD, Verbeek R, Brison R, Cass D, Dreyer J, Eisenhauer MA, Greenberg GH, MacPhail I, Morrison L, Reardon M, Worthington J (2001) The Canadian C-spine rule for radiography in alert and stable trauma patients. JAMA 286:1841–1848

Stiell IG, Clement CM, McKnight RD, Brison R, Schull MJ, Rowe BH, Worthington JR, Eisenhauer MA, Cass D, Greenberg G, MacPhail I, Dreyer J, Lee JS, Bandiera G, Reardon M, Holroyd B, Lesiuk H, Wells GA (2003) The Canadian C-spine rule versus the NEXUS low-risk criteria in patients with trauma. N Engl J Med 349:2510–2518

Streitwieser DR, Knopp R, Wales LR, Williams JL, Tonnemacher K (1983) Accuracy of standard radiographic views in detecting cervical spine fractures. Ann Emerg Med 12:538–542

Tehranzadeh J, Bonk RT, Ansari A, Mesgarzadeh M (1994) Efficacy of limited CT for nonvisualized lower cervical spine in patients with blunt trauma. Skeletal Radiol 23:349–345

Tepper SL, Fligner CL, Reay DT (1990) Atlanto-occipital disarticulation: accident characteristics. Am J Forensic Med Pathol 11:193–197

Torg JS, Ramsey-Emrhein JA (1997a) Management guidelines for participation in collision activities with congenital, developmental, or postinjury lesions involving the cervical spine. Clin J Sport Med 7:273–291

Torg JS, Corcoran TA, Thibault LE, Pavlov H, Sennett BJ, Naranja RJ Jr, Priano S (1997b) Cervical cord neurapraxia: classification, pathomechanics, morbidity, and management guidelines. J Neurosurg 87:843–850

Touger M, Gennis P, Nathanson N, Lowery DW, Pollack CV Jr, Hoffman JR, Mower WR (2002) Validity of a decision rule to reduce cervical spine radiography in elderly patients with blunt trauma. Ann Emerg Med 40:287–293

Tucker SK, Taylor BA (1998) Spinal canal capacity in simulated displacements of the atlantoaxial segment: a skeletal study. J Bone Joint Surg Br 80:1073–1078

Tuli S, Tator CH, Fehlings MG, Mackay M (1997) Occipital condyle fractures. Neurosurgery 41:368–376

Turetsky DB, Vines FS, Clayman DA, Northup HM (1993) Technique and use of supine oblique views in acute cervical spine trauma. Ann Emerg Med 22:685–689

Vaccaro AR, Madigan L, Schweitzer ME, Flanders AE, Hilibrand AS, Albert TJ (2001) Magnetic resonance imaging analysis of soft tissue disruption after flexion-distraction injuries of the subaxial cervical spine. Spine 26:1866–1872

Van Goethem JW, Ozsarlak O, Parizel PM (2003) Cervical spine fractures and soft tissue injuries. JBR-BTR 86:230–234

Van Goethem JW, Maes M, Ozsarlak O, van den Hauwe L, Parizel PM (2005) Imaging in spinal trauma. Eur Radiol 15:582–590

Warner J, Shanmuganathan K, Mirvis SE, Cerva D (1996) Magnetic resonance imaging of ligamentous injury of the cervical spine. Emerg Radiol 3:9–15

Wasserberg J, Bartlett RJ (1995) Occipital condyle fractures diagnosed by high-definition CT and coronal reconstructions. Neuroradiology 37:370–373

Weber AL, McKenna MJ (1994) Radiologic evaluation of the jugular foramen: anatomy, vascular variants, anomalies, and tumors. Neuroimaging Clin N Am 4:579–598

Weller SJ, Malek AM, Rossitch E (1997) Cervical spine fractures in the elderly. Surg Neurol 47:274–281

Weller SJ, Rossitch E, Malek AM (1999) Detection of vertebral artery injury after cervical spine trauma using magnetic resonance angiography. J Trauma 46:660–666

Wilberger JE, Maroon JC (1990) Occult posttraumatic cervical ligamentous instability. J Spinal Disord 3:156–161

Woodring JH, Lee C (1993) Limitations of cervical radiography in the evaluation of acute cervical trauma. J Trauma 34:32–39

Woodring JH, Lee C, Duncan V (1993) Transverse process fractures of the cervical vertebrae: are they significant? J Trauma 34:797–802

Young WF, Rosenwasser RH, Getch C, Jallo J (1994) Diagnosis and management of occipital condyle fractures. Neurosurgery 34:257–260

Thoracolumbar Spine Trauma

13

Rita G. Bhatia and Brian C. Bowen

CONTENTS

13.1 Introduction

The thoracolumbar spine refers to the region encompassing the thoracic (T1–T12) and lumbar (L1–L5) spinal segments. The most commonly injured region of the spine is the thoracolumbar junction (T10–L2). About 16% of thoracolumbar injuries occur between T1 and T10, 52% between T11 and L1, and 32% between L1 and L5 (Burgos et al. 1988; Carpenter 1991; Kraus et al. 1975). Typically, the injuries are sustained by middle-aged and younger individuals and are caused by high energy trauma such as motor vehicle accidents. Less often, the injuries are due to a fall from a height or industrial accidents (Burgos et al. 1988; Carpenter 1991). Males have a four-fold higher risk than females. Injuries due to sports and recreational activities are more common in children and adolescents (Hubbard 1974; Keene 1987). Low energy injuries resulting in osteoporotic compression fractures are more common in elderly individuals.

In 5%–20% of patients with a spinal injury, contiguous and non-contiguous spinal injuries are also present (Post and Green 1983; Henderson et al. 1991). Mid and upper thoracic spine fractures are commonly associated with a second fracture at the thoracolumbar junction or in the cervical spine (Hubbard 1974). Fractures at the thoracolumbar junction may be associated with a second injury at L4–L5 (Calenoff 1978). Failure to detect non-contiguous concomitant injuries can lead to delayed instability and additional neurologic deterioration (Calenoff 1978). Thus, in a patient with a thoracic fracture, a careful search should be made to exclude secondary injuries. In such cases, imaging of the entire spine may be necessary. In children, the majority of thoracolumbar fractures occur at the T4, T5, and L2 levels. Contiguous fractures are more common in children than in adults.

Depending on the type of thoracolumbar fracture, associated spinal and non-spinal injuries occur in up to 50% of patients (Cotler et al. 1986; Gertzbein and Court-Brown 1988; Gumley et al. 1982; Saboe et al. 1991; Weinstein et al. 1988). Intrathoracic injuries such as pulmonary contusions, hemothorax or pneumothorax, diaphragmatic rupture, and major vessel disruption occur in approximately 20% of patients while intraabdominal bleeding secondary to liver or splenic injury occurs in about 10%. Associated skeletal injuries are present in up to 20% of cases. The most common of these are calcaneal fractures and vertical

R. G. Bhatia, MD; B. C. Bowen, MD, PhD
Department of Radiology, Neuroradiology Section, Jackson Memorial Hospital/Miller School of Medicine, 1611 NW 12th Avenue, Miami, FL 33136, USA

KEY-POINTS

- T10–L2 most commonly injured
  - T1–T10: 16%
  - T11–L1: 52%
  - L2–L5: 32%
- Typically:
  - Young and middle-aged
  - M:F is 4:1
  - High energy trauma: MVA, less often falls or industrial accident
- Associated injuries:
  - 20% Intrathoracic
  - 10% Intraabdominal
  - 20% Other skeletal, most common calcaneal and pelvis
- Imaging
  - **Conventional radiography**: initial screening method in most hospitals, *but*:
  - **MDCT**, when available:
    - preferred as initial screening in the severely or polytraumatized patient
    - most commonly used in the imaging assessment of thoracolumbar fractures
    - assess spinal stability
    - guide patient management
  - **MR**: evaluation of spinal cord injury
- Stability: Denis's three-column theory:
  - **anterior**: anterior two thirds of vertebral body, adjacent annulus and disc and ALL
  - **middle**: posterior one third of vertebral body, posterior third of disc and annulus and PLL
  - **posterior**: neural arch, facets, and posterior ligamentous complex
  - **Stable:**
    - fractures involving only anterior column
  - **Unstable:**
    - fractures involving the anterior and middle column
    - fractures involving all three columns
    - disruption of middle column
- Classification:
  - **Minor injuries** (>15%): rarely result in significant neurologic injury or progressive deformity, are considered stable and include among others fractures of the:
    - transverse processes
    - spinous processes
    - articular processes
    - facet articulations and the pars interarticularis
  - **Major injuries**
    - hyperflexion compression - wedge (48%)
    - burst fractures (14%)
    - flexion-distraction (Chance type fractures) (5%)
    - fracture-dislocation (15%)
- Spinal conditions predisposing to traumatic lesions:
  - Ankylosing spondylitis
    - serious spinal injury even after minor trauma
    - horizontal fractures
  - Diffuse idiopathic skeletal hyperostosis

shear fractures of the pelvis in association with crush fractures of the spine (Holdsworth 1970). The incidence of bowel rupture in pediatric lumbar Chance fractures is 65%.

The anatomic characteristics of the thoracic and lumbar spine, the magnitude and direction of the impact of the force, and the patient's postural alignment all determine the severity of a spinal injury. Diagnostic imaging of the spine in trauma patients requires thorough knowledge of the regional anatomy, the pathological changes and the mechanisms of injury that determine the final radiographic picture. This knowledge is necessary for optimal management of spinal injuries and the avoidance of surgical complications.

13.2 Anatomical and Biomechanical Considerations

13.2.1 Thoracic Spine

Fractures of the thoracic spine are less common than those involving the cervical or lumbar spine or the thoracolumbar junction. Thoracic spine fractures account for 20% of all spinal fractures. The thoracic spine is more rigid than its cervical or lumbar counterparts because of the structural stability supplied

Table 13.1. Fracture-dislocations of the thoracolumbar spine

		Mechanism	Vertebral body	Neural arch ring	Fracture of superior facet of level below
Flexion-rotation		Rotation posterior to ALL	Compressed	Intact	Common
Shear fractures	PA	Horizontal shear, segment above forwards	Intact	Fractured at several levels	Yes
	AP	Horizontal shear, segment above backwards	Intact	Intact	Rare
Flexion-distraction		Flexion and distraction	Intact	Intact	Intact

by the upper nine rib articulations, the coronal orientation of the facet joints, and the vertebral body configurations. Most fractures involve the kyphotic apex around T6–T8 (Hanley and Eskay 1989; Magerl et al. 1994). Because of the strength and stability provided by the ribs, injuries that result in a fracture are of higher energy than in the cervical and lumbar regions. Thus, these fractures are frequently associated with a high degree of concomitant injuries to the chest, head, and cervical spine.

A total of 50% of patients with thoracic spine fractures have accompanying neurologic findings (Hanley and Eskay 1989). The small thoracic spinal canal relative to the cord diameter may in part explain why thoracic fractures have a higher frequency of neurological injury. Another contributing factor may be the relatively sparse blood supply to the mid and upper thoracic cord, which allows ischemic cord injury to occur with less severe compression than in the lumbar spine (Bohlman et al. 1982; King 1986; White et al. 1981).

A knowledge of the biomechanics of the thoracic spine is critical to understanding the various forces and mechanisms that determine spinal structure in both the normal and pathologic states (Resnick et al. 1997) and in understanding the concept of instability of the spine. The forces acting on the spine can be represented as vectors that produce rotation and/or linear displacements. Rotational forces result in flexion and rotation, lateral bending, and torsional motion. Linear forces result in compression, distraction, and translation. These forces act in isolation or in combination and produce various types of injuries.

The stability of the thoracic spine is imparted by the interaction of the bone and soft tissue elements including ligaments, discs, and muscles. The rib cage significantly increases the stability and immobility of the thoracic spine, about 70% in extension and about 30% in flexion. The tensile strength of the anterior and posterior longitudinal ligaments, paraspinal muscle insertions, and facet articulations also contribute to the stability of the thoracic spine.

The thoracic spine normally assumes a kyphotic posture. Proceeding caudally, the thoracic vertebral bodies increase in all dimensions. The anterior height of a vertebral body is 2–3 mm less than the posterior height. This difference results in an overall kyphosis from T1–T10 and shifts the axis of rotation forward. Deformation or rotation caused by this bending moment is resisted by two elements: the ventral aspects of the vertebral bodies which serve as a buttress and the dorsal elements which function predominantly as a tension band. Vertical loading causes a disproportionate amount of force to be borne by the anterior vertebral body and this explains the occurrence of simple wedge compression fractures in the thoracic spine (Resnick et al. 1997). The thoracic spine is relatively mobile in rotation and lateral bending but is limited in flexion and extension compared to the lumbar spine.

Extension of the thoracic spine is resisted by an intact rib cage, anterior longitudinal ligament, and the orientation of the facet joints and lamina. Flexion is limited by the posterior tension band, consisting of the interspinous and supraspinous ligaments, posterior longitudinal ligaments, and the ligamenta flava. Rotational stability is provided by the anterior and posterior longitudinal ligaments, rib cage, and facet joints, especially in the lower thoracic spine (Resnick et al. 1997). Translational or shear forces are countered by the anterior and posterior longitudinal ligaments, the annulus fibrosis, facets, and ligamentous attachments (Fessler and Masson 1996).

A horizontal displacement of up to 1 mm between the thoracic vertebra is normal. Greater than 2.5 mm of horizontal displacement of one vertebral body relative to another and greater than 5° of angular motion or greater is indicative of instability (Panjabi et al. 1981; Denis 1983).

The criteria for instability in thoracic spine trauma are not clearly defined, but most surgeons are inclined to surgically stabilize injuries associated with one of more of the following findings: fracture dislocations, posttraumatic kyphosis greater than 40°, spinal injuries associated with a sternal fracture, and concomitant rib fractures and/or costovertebral dislocations (El-Khoury and Whitten 1993). It is important to note any signs of delayed instability. If unrecognized and untreated, progressive kyphosis and neurologic deficit can result.

Most thoracic spine injuries occur during flexion and axial loading. This is because the rib cage allows very little rotation in the upper thoracic spine . As a result, fracture dislocations are more common than compression fractures and burst fractures.

13.2.2 Thoracolumbar Junction

The thoracolumbar junction is usually defined as the spinal region extending from T10 through L2. This is a transitional area of the spine between the less mobile thoracic spine and the more flexible lumbar spine. This region represents an abrupt change in the anatomy and kinematics. The three anatomic reasons for the thoracolumbar junction's increased vulnerability to injury are the loss of the stabilizing effects of the ribs and thoracic musculature, the change from the kyphotic curve to the lumbar lordotic curve, and the change in orientation of the facet joints. The change in facet orientation at the thoracolumbar junction from the coronal plane (thoracic) to the sagittal plane (lumbar) is thought to alter the stress distribution of loads applied to the spine and renders this area more susceptible to fractures than either the thoracic or lumbar region alone. At the thoracolumbar junction, the vertebral bodies have not yet assumed the massive size of the lower lumbar vertebral bodies, and they are less able to resist deformity following specific load application.

13.2.3 Lumbar Spine

There are typically five lumbar-type vertebrae, but many variations can exist at the thoracolumbar and lumbosacral junctions, respectively. The lumbar spine is more mobile than the thoracic spine, due to the changing orientation of the facet joints and the absence of ribs as noted above. In the upper lumbar spine, facets assume an oblique orientation compared to a near sagittal orientation at the lumbosacral junction. The lumbar lordosis and well developed paraspinal musculature protect the lower lumbar vertebrae (which are mechanically stronger than the upper lumbar vertebrae) from high direct compressive forces. The exaggerated lumbar lordosis at L5–S1 and near vertical orientation of the L5–S1 facet joint predisposes this area to a translational deformity, i.e., spondylolisthesis. The lumbar lordosis permits transmission of axial loads to the neutral axis of the spine, unlike the ventral bending moment caused by the thoracic kyphosis. This results in the more common burst fracture in the lumbar spine rather than a wedge compression fracture.

13.3 Spinal Stability

Spinal stability is best defined as the ability of the spine to withstand physiologic loading without mechanical deformity or progressive neurologic symptoms. White and Panjabi (1990) described two manifestations of instability, acute and chronic. Acute instability is apparent at or soon after the time of injury. Chronic instability is associated with delayed manifestations of pain and deformity with or without a neurological deficit. An unstable fracture undergoes progressive deformity and/or develops progressive neurologic symptoms. Stability depends on the integrity of both the bone and the soft tissues.

Numerous classification schemes have been proposed for evaluating spinal stability. The most widely accepted system is that of Denis who used the functional three-column anatomical model (Denis 1983, 1984). In the early 1960s, Holdsworth suggested a two column concept of the spine, and stability was determined by the state of the posterior column. Other investigators (McAfee et al. 1983; Ferguson and Allen 1984) agreed with the Denis three-column concept but presented some differences in their interpretation of injury mechanisms and patterns of tissue failure. Presently, Denis's three-column theory of the spine is the most workable classification. Denis defined the anterior column of the spine as the anterior two thirds of the vertebral body, the adjacent annulus and disc and the anterior longitudinal ligament. The middle column is composed of the posterior one third

of the vertebral body, posterior third of the disc and annulus, and the posterior longitudinal ligament. The posterior column includes the neural arch, facets, and posterior ligamentous complex. The posterior ligamentous complex is composed of the supraspinous and interspinous ligaments, ligamenta flava, and the capsular ligaments of the articular pillars.

Fractures involving the anterior column are considered stable whereas fractures involving the anterior and middle column or all three columns are considered unstable. Disruption of the middle column makes the injury unstable.

13.4 Imaging

13.4.1 Conventional Radiography

In a patient with thoracolumbar trauma, spinal precautions are maintained until injury is excluded by reliable examination comprising either a physical examination and/or imaging studies. The radiologic evaluation begins with anteroposterior (AP) and lateral radiographs of the entire spine. The lateral view is replaced with a cross table lateral view in the severely injured patient in order to decrease patient movement.

The plain films must be scrutinized for subtle abnormalities that may indicate more extensive injuries than suspected clinically. Cortical buckling, disruption of anterior and posterior vertebral cortices, anterior wedging, and fractures depict loss of bone integrity. A discrepancy of greater than 2 mm between the anterior and posterior height of the vertebral body usually indicates a fracture, except at T12–L1 where this height difference may be normal.

On the lateral radiograph, disruption of the posterior vertebral body line (Daffner et al. 1990) is a sign of a retropulsed fragment into the canal (Fig. 13.1). This line is normally mildly convex anteriorly. Widened distance between the spinous processes, disc spaces, and facet joints indicate joint space abnormality. Anterior vertebral body height loss with preservation of the height of the posterior body is observed with a compression-type fracture (Fig. 13.2a).

The AP radiograph is used to assess vertebral alignment and vertebral body cortical disruption. The interpediculate distance, for example, is an important clue to the severity of a fracture. Widening of this distance relative to the interpediculate distance of the vertebrae above and below the affected level is indicative of posterior column disruption and instability (Fig. 13.2b). Increased distance between the spinous processes will also be present on the AP radiograph as a result of distraction of the posterior column (Fig. 13.3).

Soft tissue disruption associated with thoracolumbar spine injury include loss of the psoas stripe, paraspinal soft tissue widening, hemothorax, and

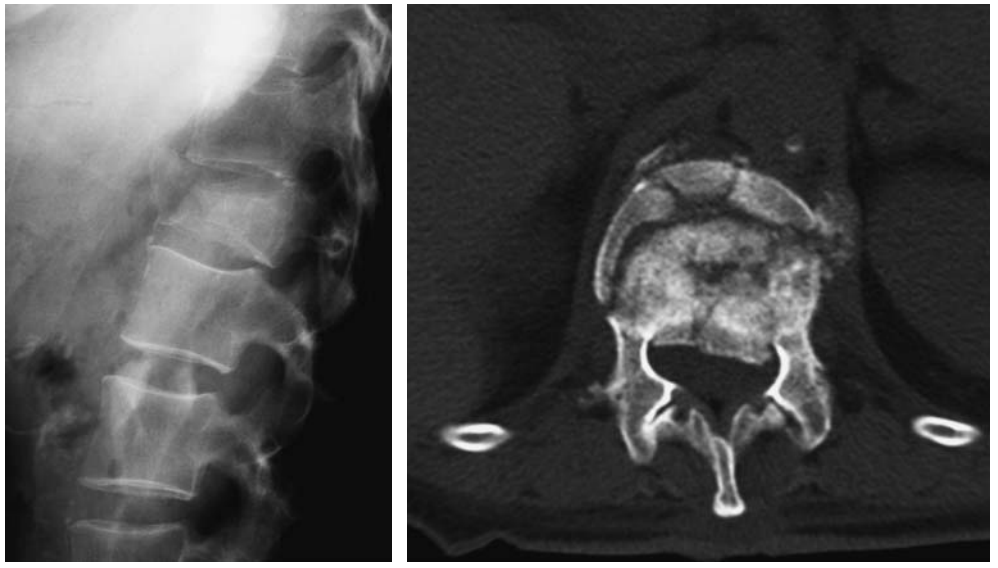

a b

Fig. 13.1a,b. Burst fracture. **a** Lateral radiograph shows disruption of the posterior vertebral body line indicating retropulsion of the fracture fragments. **b.** Axial CT confirms the retropulsed fracture fragments and associated canal compromise

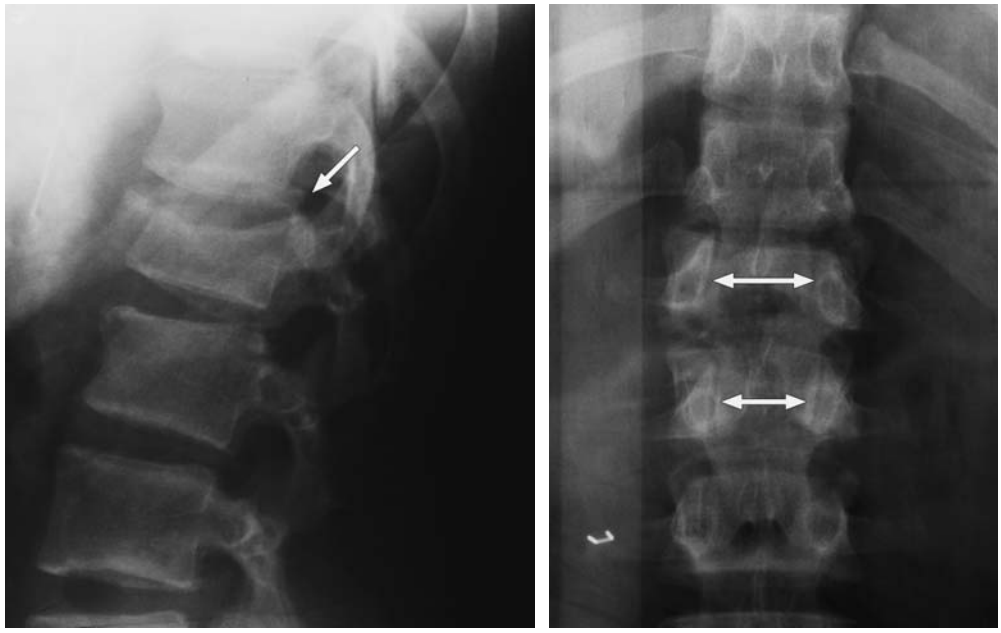

Fig. 13.2a,b. Contiguous fractures. Burst fracture of L1 and compression fracture of L2. **a**) Lateral radiograph demonstrates a comminuted fracture of the superior endplate of L1. The posterosuperior corner of the vertebral body is retropulsed into the spinal canal (*arrow*). An anterior compression fracture of L2 without posterior element involvement is also noted. **b** The AP radiograph shows loss of height of L1 with a widened interpediculate distance (*upper double arrow*) indicative of posterior element involvement. Compression fracture of L2 with a normal interpediculate distance (*lower double arrow*)

pneumothorax. Sternal and rib fractures, deviation of the airway within the upper thoracic region, left apical capping, vacuum disc, and pleural fluid are other ancillary findings. Sternal and rib fractures with or without associated costovertebral dislocation are not only indirect signs of thoracic spine injury but also indicators of instability (Fig. 13.4).

13.4.2 Computed Tomography

CT is a valuable tool in the assessment of spinal trauma. In cases where conventional radiographic findings are subtle, CT can frequently provide important diagnostic information. If a fracture is detected on plain radiographic studies, CT should be obtained to further evaluate and characterize the fracture. CT is also indicated if there is a discrepancy between radiographic findings and neurologic status. With new multidetector scanners, axial images thinner than 1 mm can be obtained through the region of interest, determined from the initial radiographs. Axial images should be reformatted routinely into sagittal and coronal images. The midsagittal and transverse dimension of the canal should be measured at the level of injury as well as levels immediately cephalad and caudal to it. Vacaro et al. (2001) have reported that the most clinically useful measurement is the ratio of the mid-sagittal to the transverse dimension of the canal. They found that the ratio correlated inversely with the risk of neurological deficit. Thus, a patient with a widened interpediculate distance and a relatively low ratio would be at increased risk for neurological deficits.

Advantages of CT over conventional radiography include the following: (1) a more detailed assessment of vertebral as well as associated soft tissue and visceral injuries; (2) a more accurate assessment of specific column involvement in order to determine stability; and (3) the ability to perform thin sagittal and coronal reconstructed images (Fig. 13.5). Subtle signs of posterior interspinous widening may be detected on the sagittal images. Fractures that are in the horizontal plane, parallel to the X-ray beam, such as Chance fractures may be missed on axial imaging. Reconstructed images are therefore the key to a correct diagnosis. CT is also preferable to radiography for assessing hardware placement and fracture reduction postoperatively. Although CT is secondary to MR in evaluating disc herniations, it can be used when MR is unavailable or contraindicated.

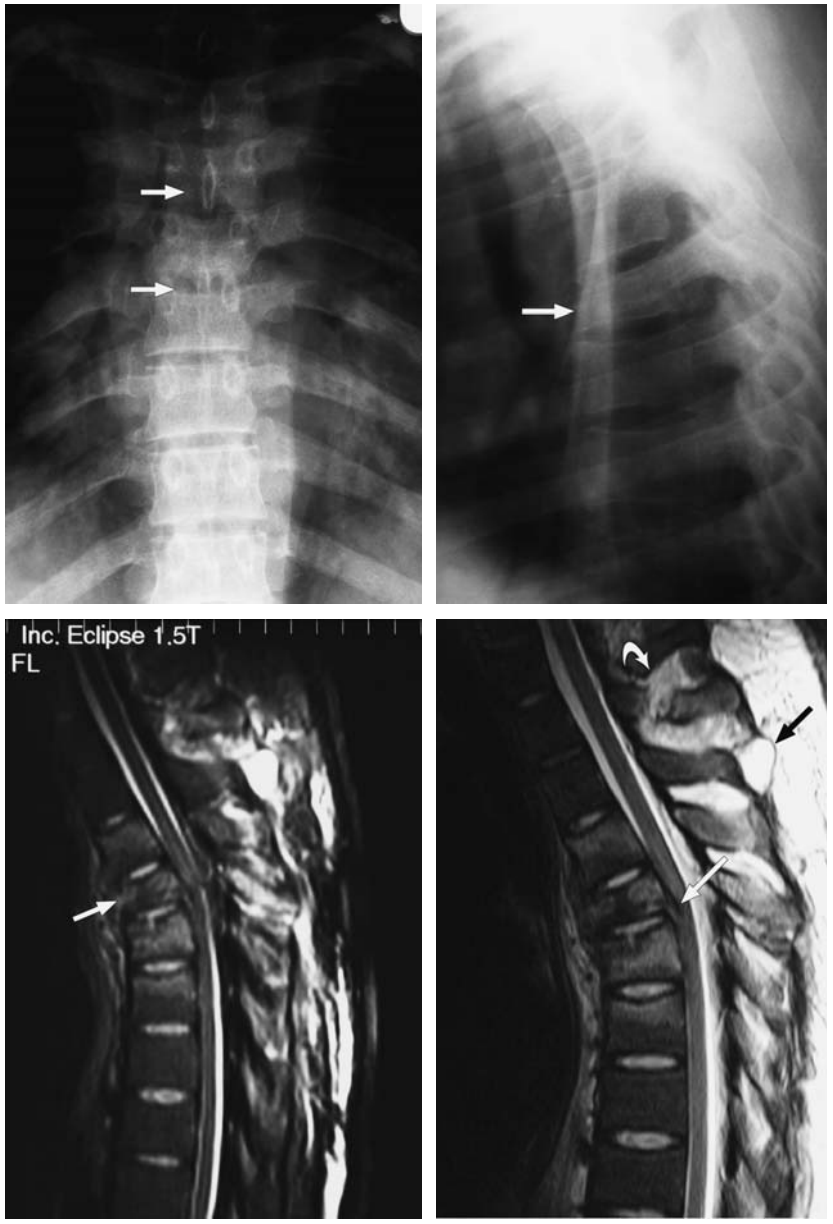

Fig. 13.3a–d. Fracture dislocation. **a** AP radiograph demonstrates increased distance between the spinous processes (*arrows*) implying distraction of the posterior elements. **b** Lateral radiograph shows the burst fracture and no subluxation (*arrow*). Plain radiographs are not accurate in determining involvement of the posterior wall of the vertebral body and subtle malalignment can be overlooked. **c,d** Sagittal STIR and FSE T2-weighted images show multiple fractures not detected on the plain radiographs, and ligamentous injury of the anterior and posterior longitudinal ligaments (*long white arrows*), interspinous (*curved arrow*) and supraspinous ligaments (*black arrow*). Findings of an unstable injury. The STIR sequence is more sensitive in depicting bony marrow edema and ligamentous injury than the FSE T2-weighted images

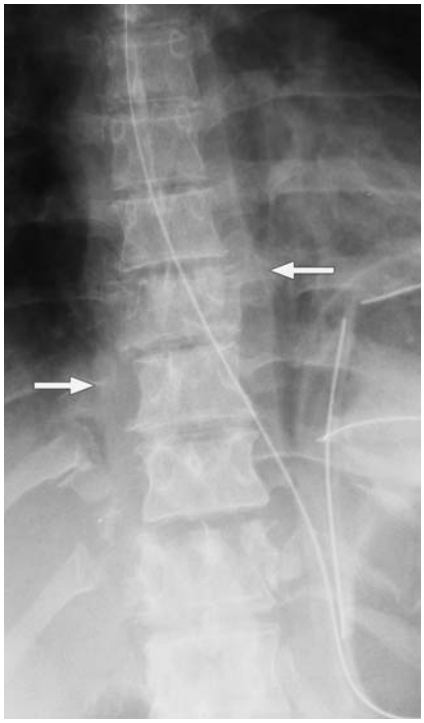

Fig. 13.4. AP radiograph showing paraspinal soft tissue mass indicating hematoma (*arrows*) associated with fractures of T9 and T12, rib fractures, and costovertebral dislocation

13.4.3 Magnetic Resonance Imaging

13.4.3.1 Technique

MR with its multiplanar capability, its high spatial resolution and high soft tissue contrast, and its non-invasive nature is clearly superior to all other imaging modalities in demonstrating ligamentous ruptures, posttraumatic disc herniations, epidural hemorrhage and spinal cord injuries. MR has revolutionized the evaluation and treatment of ligamentous injuries. It is a very useful adjunctive technique to conventional radiographs and CT, particularly in patients with a neurologic deficit.

MR imaging is recommended for trauma patients for the following reasons: (1) to explain new neurologic deficits, especially those not adequately explained by CT; (2) to evaluate the integrity of the spinal cord and; (3) to detect cord compression. MR has been found useful in assessing stability of the thoracolumbar spine because it sensitively detects ligamentous injury. MR has also been found useful in estimating the acuteness of osteoporotic fractures.

In spinal MR imaging, a dedicated phase-array coil is used to achieve a high signal-to-noise ratio (SNR) which allows for improved spatial resolution. Both T1- and T2-weighted axial and sagittal images should be obtained. Other types of images include gradient echo T2*-weighted images to evaluate for the presence of cord hemorrhage, disc herniations and fractures, and short tau inversion recovery (STIR) images (sagittal plane) to assess ligamentous injury, with hemorrhage and edema in the soft tissues, as well as spinal cord injury.

Disadvantages of MR imaging include its contraindications (pacemakers, cerebral aneurysm clips, incompatible life support systems, halo devices) and inconveniences (more time consuming, and sometimes less well tolerated by the patient). External fixation devices that are composed of ferromagnetic alloys may disrupt the static magnetic field close to the region of interest, resulting in image degradation. MR compatible titanium devices and other new materials, however, cause fewer MR artifacts, resulting in a higher percentage of diagnostic MR studies. For example, MR-compatible halo vests which are composed of a graphite composite, titanium, aluminum, and plastic are devoid of disruptive stainless steel components (Sharafuddin et al. 1990; Shellock 2002).

MR evaluation of the spine following penetrating trauma requires special consideration for two reasons: retained metallic fragments within the spinal canal can produce image degradation but can also be a potential safety hazard to the patient. Most firearm projectiles are non-ferrous and will not move or orient in the static magnetic field (Teitelbaum et al. 1990). A ferrous fragment could migrate and/or could produce thermal injury when exposed to a strong static and oscillating magnetic field potentially producing neurologic damage (Smugar et al. 1999). Thus, the MR examination should be performed at the discretion of the radiologist after a review of the radiographs and/or the CT of the fragment containing region. The potential risk of movement of the fragment is diminished in mature scar tissue. Myelography and CT myelography are alternative examinations for patients in whom MR is contraindicated or poses a high risk of complications.

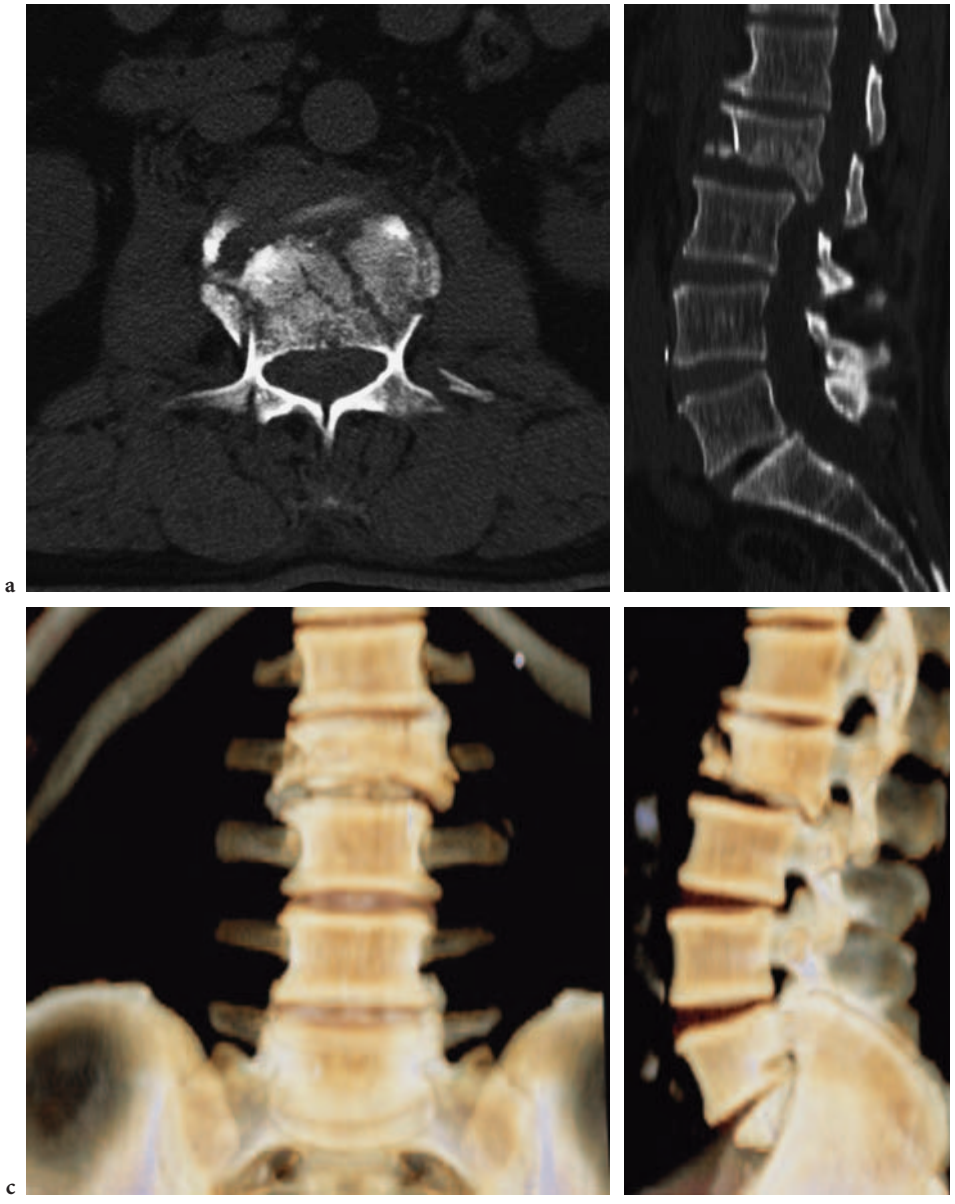

Fig. 13.5a–d. Unstable burst fracture. **a** Axial CT demonstrating fracture fragment involvement of all three columns. **b** Sagittal reconstruction from CT scan shows the degree of canal narrowing by the retropulsed fragment. **c**,**d** Anterior and lateral volume-rendered images show the full extent of bony involvement and relationship of fracture fragments

13.4.3.2 Findings

13.4.3.2.1 Osseous Injuries

Traumatic osseous injuries are divided into subluxations, fracture deformities, and compressive injuries. MR is probably more sensitive in detecting anterior subluxation than conventional lateral radiographs, whenever the area of interest may be obscured by overlying bone such as in the cervicothoracic region. Non-displaced fracture lines through the vertebral bodies and posterior elements are poorly demonstrated on MR (Flanders et al. 1992; Kerlaske et al. 1991). It may be difficult to distinguish an avulsed cortical bone fragment from an injured ligament on MR as both structures exhibit low signal intensity on all imaging sequences. Displaced fractures, on the other hand, are well shown on MR images.

MR is unique in its ability to detect compressive injury of the vertebral body marrow elements without a fracture deformity or cortical disruption. The signal alterations result from microfractures within the medullary bone plus hemorrhage. The vertebral bodies appear hypointense on T1-weighted and hyperintense on T2-weighted images, especially fat-saturated T2-weighted images such as STIR. The STIR sequence is the most sensitive of the three sequences for detecting bone marrow edema caused by fracture or trabecular contusion (Fig. 13.6).

13.4.3.2.2 Ligamentous and Joint Disruption

MR is the only imaging modality available that directly visualizes spinal ligaments. The ligaments routinely visualized on sagittal MR are the anterior longitudinal ligament (ALL), posterior longitudinal ligament (PLL), ligamentum flavum (LF), interspinous ligaments (ISP) and supraspinous ligament. These are composed of strong fibroelastic tissue and appear hypointense on all conventional MR pulse sequences.

Direct signs of disruption include visualization of the torn margins and discontinuity or absence of the ligament. Hemorrhage into the interspinous soft tissues is an indicator of interspinous or supraspinous ligament disruption. Secondary signs of disruption are similar to the radiographic signs of disruption. Thin section T1-weighted images are preferred for assessing ligament integrity, and STIR images are preferred for detecting interspinous hemorrhage in patients with posterior ligamentous disruption. STIR sequences show hyperintensity in and around a ruptured ligament, with a focal discontinuity indicating complete rupture (Fig. 13.7).

The MR assessment of spinal ligaments may help to further determine whether a fracture is stable or unstable when plain film findings are subtle. (Fig. 13.3c,d) (Petersilge et al. 1995; Brightman et al. 1992; Saifuddin et al. 1996). Disruption of the supraspinous ligament contributes significantly to instability of thoracolumbar burst fractures. The PLL is not significant in the determination of spinal stability. Disruption of the ALL indicates some rotational component to the injury (Petersilge et al. 1995).

Fractures of the facet joint complex are better detected with plain radiographs and CT (Fig. 13.8a), but subtle damage to the joint capsule is best appreciated with MR. Widening of the facet joint is evidence of a distraction injury which can show hyperintensity on T2-weighted images due to increased fluid within the joint space (Fig. 13.8b,c). This finding of hyperintensity may also be seen with degenerative facet disease and therefore should be interpreted cautiously.

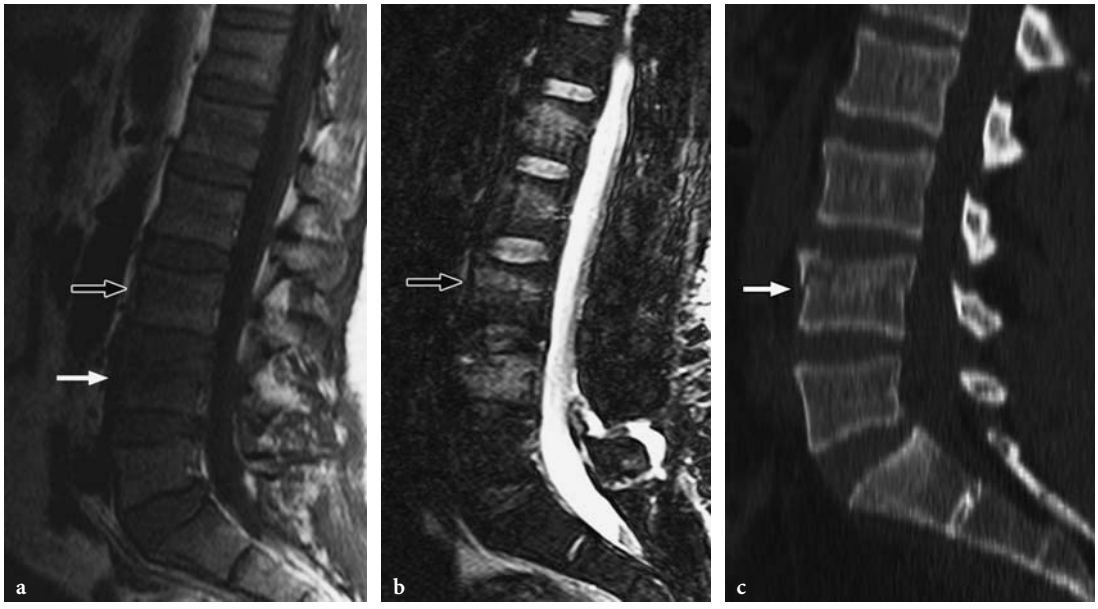

Fig. 13.6a–c. Multiple contiguous bony injury to the lumbar spine. **a**,**b** Sagittal T1-weighted and STIR images demonstrate loss of height of L4 (*white arrow*) and subtle marrow edema within the rest of the lumbar spine (*black arrows*). The STIR sequence is more sensitive in depicting marrow edema in the absence of a fracture deformity. **c** Sagittal CT reconstruction shows fracture of only L4 (*arrow*)

Fig. 13.7a,b. Fracture dislocation. **a,b** Sagittal GE and STIR images show a rotatory fracture dislocation and the associated soft tissue components to this injury. The anterior and posterior longitudinal ligaments (ALL and PLL) are disrupted and there is complete cord transection. The PLL is also elevated by a combination of bony fragments and hematoma (*arrow*). High T2 signal intensity seen within the interspinous ligaments indicates rupture (*white arrow*)

Fig. 13.8a–c. Facet distraction injury. **a** Axial CT demonstrates distraction of the left facet joint. **b,c** Axial FSE T2- and T1-weighted images demonstrate widening of the joint space, better appreciated on the T2-weighted sequences as high signal intensity representing fluid within the joint space (*arrow*)

13.4.3.2.3 Epidural Hematoma and Disc and Nerve Root Injury

Spinal epidural hematomas occur as the result of tearing of part of the epidural venous plexus with focal extravasation of blood into the anterior epidural space. The imaging characteristics are variable and depend on the oxidative state of the hemorrhage and the effects of clot retraction. In the acute phase, the epidural hematoma is isointense with spinal cord parenchyma on T1-weighted images and isointense with CSF on T2-weighted images (Fig. 13.9). The hypointense dura helps to differentiate the epidural compartment from the subarachnoid space (Fig. 13.10).

Traumatic disc herniations are rarer in the thoracic spine than in the cervical spine. When they occur, they are usually associated with significant neurologic damage. Unrecognized disc herniation is a cause of neurologic deterioration after stabilization (Pratt et al. 1990). An acute posttraumatic disc herniation may have a similar MR appearance to a nontraumatic disc herniation. However, hemorrhage is present, the ruptured disc has a higher signal intensity than normal disc material on T2-weighted images. The disc height of the injured disc may be either reduced or widened (Fig. 13.9a,b)

MR has not been successful in reliably demonstrating traumatic nerve root avulsions. Posttraumatic root pouch cysts (pseudomeningoceles) can be identified with high sensitivity, and these are frequently associated with nerve root avulsions. CT myelography has been the diagnostic method of choice for demonstrating the empty nerve root sheath and periradicular cavities in the cervical spine (Nussbaum et al. 1992; Volle et al. 1992); however, recent studies have reported similar sensitivity (92.9%) for detection of cervical root avulsion by MR imaging and CT myelography (Doi et al. 2002).

13.4.3.2.4 Spinal Cord Injuries

The narrow thoracic spinal canal predisposes to a higher frequency of complete spinal cord injury associated with (especially upper) thoracic fractures than cervical or lumbar spine fractures (Brandser and El-Khoury 1997; Meyer 1989). A total of 62% of patients with thoracic spine fracture-dislocations have complete neurological deficit, whereas 2% of patients with lumbar spine and 32% of patients with cervical spine fracture-dislocations have a complete neurological deficit (El-Khoury and Whitten 1993). Most of these fractures occur by hyperflexion mechanisms. When associated with posterior element fractures, the spinal cord may escape damage due to autodecompression of the spine.

Three patterns of acute cord injury are noted on MR images: (1) edema, (2) hemorrhage, and (3) mixed central hemorrhage and edema. The MR identification of hemorrhage in the spinal cord has significant clinical implications. The presence of hemorrhage implies a poor potential for neurologic recovery (Kulkarni et al. 1987; Hackney et al. 1986). The evolution of the signal intensity of blood products on MR follows the same sequence as in the brain; however, conversion from deoxyhemoglobin to intracellular methemoglobin may be delayed for up to 8 days in the spinal cord following injury, unlike the brain. The delay is attributed to local hypoxia (Kulkarni et al. 1987; Hackney et al. 1986). Acute hemorrhage is seen as a central cord hypointensity on T1- and T2-weighted spin-echo and gradient-echo sequences. This is surrounded by a halo of edema that extends both rostrally and caudally from the central hemorrhage (Fig. 13.11). The edema is hyperintense on T2-weighted images and hypointense on T1-weighted images and reflects accumulation of intracellular/interstitial fluid in response to injury. The edema involves a variable length of spinal cord above and below the level of injury. Cord edema alone denotes a more favorable prognosis than cord hemorrhage (Kulkarni et al. 1987). Posttraumatic cord hemorrhage always coexists with spinal cord edema; however, cord edema may occur without or with cord hemorrhage. Complete cord transection is delineated by transverse hemorrhage between segments with or without cord enlargement (Fig. 13.7b).

MR may be helpful in predicting the recovery of neurologic function after acute spinal cord injury. In chronic spinal cord injury, some patients may experience progressive neurologic symptoms after many years of a stable deficit. Progressive deficits may be due to progression of an unstable fracture or to abnormalities of the spinal cord itself. Cord abnormalities that are associated with onset of progressive neurologic deficits in patients with prior fracture are intramedullary cysts and posttraumatic myelomalacia. MR is the diagnostic modality of choice for the detection of these abnormalities (Fig. 13.12). Occasionally, MR also demonstrates evidence of Wallerian degeneration in the dorsal columns above the level of injury. Accurate diagnosis of a posttraumatic intramedullary cyst is important because these pa-

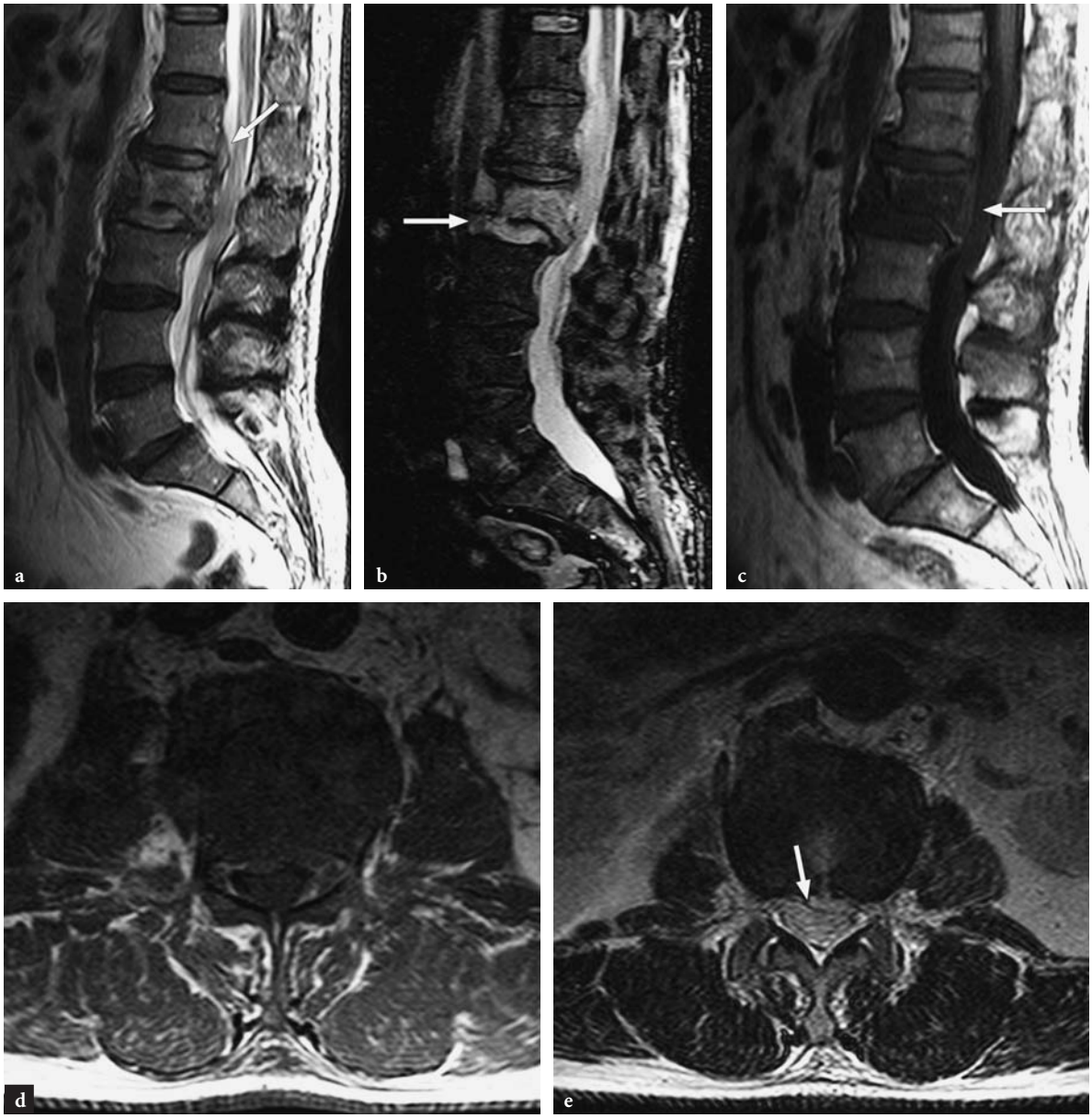

Fig. 13.9a–e. Burst fracture with traumatic injury to the disc. **a**,**b** Sagittal FSE T2-weighted and STIR images demonstrate a burst fracture of L2 and high T2 signal intensity and a widened disc suggestive of disc injury/hemorrhage (*arrow*). Anterior epidural hematoma is noted at L1–2 (*arrow*). **c–e** Sagittal T1, axial T1 and axial FSE T2-weighted images show an isointense T1 and hyperintense T2 epidural collection consistent with an acute epidural hematoma. The ALL is disrupted and the PLL is elevated as seen on the sagittal view. The hypointense signal intensity of the dura (*arrow*) separates the anterior epidural hematoma from the thecal sac best seen on the axial FSE T2 image

Fig. 13.10a,b. Burst fracture, large epidural hematoma and conus medullaris syndrome. **a** Sagittal T1-weighted image demonstrates a long segment isointense epidural hematoma that extends caudally from a bony injury and is compressing the conus medullaris. The hypointense band represents the ventral dural margin (*black double arrow*). **b** Sagittal FSE T2-weighted image demonstrates the mixed intensity epidural hematoma (*arrow*) and the posteriorly located retropulsed fragment elevates the posterior longitudinal ligament (PLL). Associated injury to the spinal cord manifests as an area of intramedullary high signal intensity. Marrow edema in the lumbar vertebra appears as linear bands of high signal intensity in the vertebral bodies

Fig. 13.11a,b. Acute spinal cord injury. **a,b** Sagittal GRE and sagittal STIR images demonstrate areas of low signal intensity consistent with acute cord hemorrhage (*arrow*) and associated cord edema proximal and distal to the level of injury (*arrow heads*). Hyperintense T2 signal intensity in the disc with mild disc space widening suggestive of disc injury/hemorrhage and posterior ligamentous injury are also features in this hyperextension injury

Fig. 13.12a,b. Progressive gait instability with spinal cord tethering and intramedullary cord cyst. **a**,**b** Sagittal T1-weighted and sagittal FSE T2-weighted images show an old fracture of T9 and splaying of the spinous processes (*arrow*) secondary to disruption of the interspinous ligament complex. The dorsal aspect of the injured cord is adherent to the posterior thecal sac (*arrow*) and rostral and caudal cord cysts are noted

tients may have a return of neurologic function with shunting or decompression of the cyst and lysis of adhesions. Patients with posttraumatic myelomalacia and cord atrophy, however, do not benefit from surgical intervention.

13.5 Fractures

13.5.1 Classification

Fractures of the spine can be divided into two groups. Minor injuries, which account for more than 15% of the fractures, include isolated fractures of transverse processes, spinous processes, articular processes, facet articulations, and of the pars interarticularis. The minor injuries rarely result in significant neurologic injury or progressive deformity and are considered stable. The major injuries have been classified by Denis into hyperflexion compression fractures, burst fractures, flexion-distraction (Chance type fractures) and fracture-dislocation.

13.5.1.1 Hyperflexion Compression Fractures

Wedge compression fractures account for the vast majority (48%) of thoracic and lumbar spine fractures (Denis 1984).The injury mechanism involves a combination of forward flexion and axial compression loading, producing the characteristic wedge-shaped vertebral deformity. The vertebral body fails under a compressive load and its anterior portion becomes compressed while the middle column remains intact. This fracture is rarely associated with a neurological injury and is considered stable unless multiple adjacent vertebral bodies are compressed. In simple hyperflexion compression, the fracture usually involves the superior endplate.

While the thoracolumbar spine is the most frequently involved area in compression injuries, certain injuries have a predilection for specific levels. Osteoporotic compression fractures usually occur from T12 to L4. Aircraft ejections involve the mid-

thoracic level and parachute landings result in L1 vertebral body fractures.

13.5.1.1.1 Imaging

Radiographically, the wedge deformity is best seen on the lateral view. This shows loss of height of the anterior aspect of the body which is usually less than 50% and the preservation of the height of the posterior aspect of the vertebral body (Fig. 13.2a). The anteroposterior radiograph often shows loss of definition of the superior endplate of the fractured vertebra and a normal interpediculate distance (Fig. 13.2b).

These fractures may be difficult to demonstrate on axial CT scans as the fracture lines nearly parallel the imaging plane. Subtle changes in the trabecular pattern and alterations in density may be detected on CT (Fig. 13.13a,b). This problem does not exist with MDCT, where high quality sagittal reformations perfectly demonstrate these lesions.

MR is more sensitive in depicting bone marrow edema (Fig. 13.13c–e), ligamentous disruption, and soft tissue hemorrhage within the anterior and posterior soft tissues.

If the compression and hyperflexion forces are great, loss of more than 50% of the anterior body height may occur and it may be associated with subluxation or dislocation of the facet joints secondary to posterior ligamentous failure. Axial CT images with sagittal reformatted images are required in order to exclude a more serious injury such as a burst fracture and to assess for canal compromise.

13.5.1.2 Burst Fractures

Burst fractures account for 14% of spinal fractures and 17% of all major spinal injuries (Denis 1983). They are thought to result from high energy axial loads to the spine that results in compression failure of the anterior and middle columns. A burst fracture may be stable or unstable depending on the integrity of the posterior elements. A stable burst fracture is one in which the anterior and middle columns fail because of a compressive load and the posterior elements are intact. An unstable burst fracture on the other hand, is one in which the anterior and middle columns fail in compression and the posterior column is disrupted. The sudden application of the axial load results in vertebral endplate fracture and herniation of the nucleus pulposus into the vertebral body, ultimately leading to bursting of the vertebral body and outward displacement of the bony fragments (Atlas et al. 1986). The presence of retropulsed fracture fragments is almost always pathognomonic of an axial loading injury.

Burst fractures occur more commonly from T4 to L5, with 50% occurring at L1 (Daffner et al. 1990). Evaluation of the entire spine is important because 5%–20% of all spinal injuries are multiple (Post and Green 1983; Henderson et al. 1991). Because burst fractures have the potential for severe neurologic sequelae in about 50% of cases, they are important to diagnose and should be considered unstable during the initial emergency department evaluation.

It should be noted that there is no direct correlation between the percentage of canal narrowing and neurologic damage (Shuman et al. 1985; Kilcoyne et al. 1983). In the thoracolumbar junction, however, burst fractures with a 50% decrease in midsagittal diameter secondary to retropulsed fragments or fractures of the lamina had a significant risk of neurologic damage (Trafton and Boyd 1984).

13.5.1.2.1 Imaging

Conventional radiographs have been reported to underdiagnose burst fractures in 25% of cases because of the failure to recognize involvement of the posterior aspect of the body (Ballock et al. 1992) and may underestimate the displacement of fragments into the spinal canal (Brant-Zawadski et al. 1982).

Conventional radiographic findings include anterior wedging and posterior body height loss. These comminuted fractures involve the superior, inferior (commonly the superior), or both endplates and result in additional findings such as disruption of the posterior vertebral body line, loss of the posterior vertebral body height, and retropulsion of fracture fragments. The retropulsed fragment is typically rotated into the spinal canal and may be associated with superior migration (Fig. 13.1a) (Guerra et al. 1984; Jelsma et al. 1982).

The interpediculate distance is unchanged in stable burst fractures and widened in unstable burst fractures when the pedicles are splayed apart by the bursting body indicating posterior column injury (Fig. 13.2b). CT can also detect posterior column fractures that may have been missed on the plain radiographs. The posterior column is intact in a stable burst fracture (Fig. 13.14).

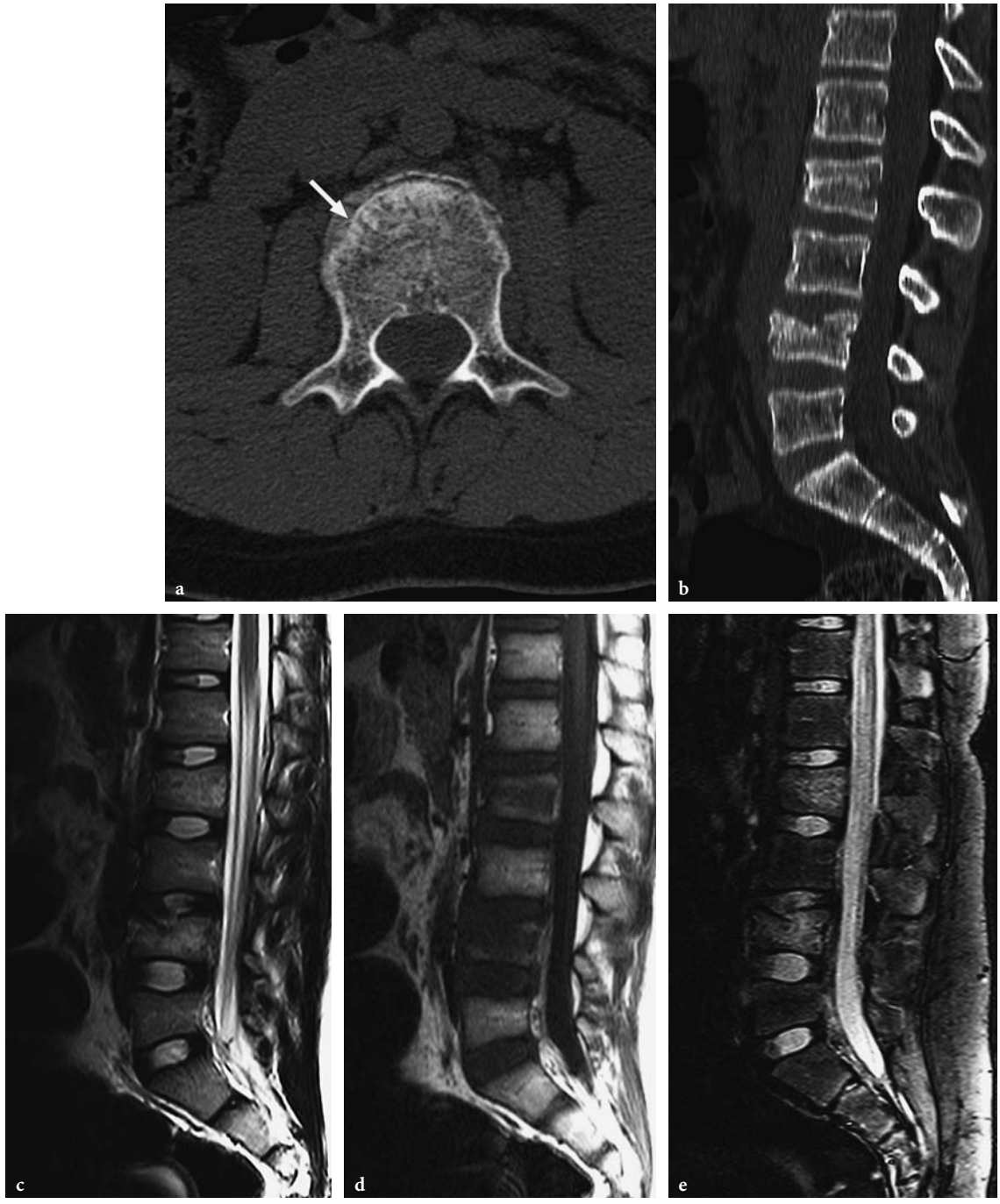

Fig. 13.13a–e. Non-contiguous fractures. Compression fracture of L2 and stable burst fracture of L4. **a** Axial CT demonstrates subtle alteration in trabecular pattern of L2 which can be easily missed as the fracture lines run parallel to the axial imaging plane. **b** Sagittal reconstructed image clearly shows the compression fracture of L2. **c–e** FSE T2-weighted, sagittal T1-weighted, and STIR images demonstrate the fractures in addition to the epidural hematoma posterior to the body of L4. STIR sequence is most sensitive for depicting marrow edema

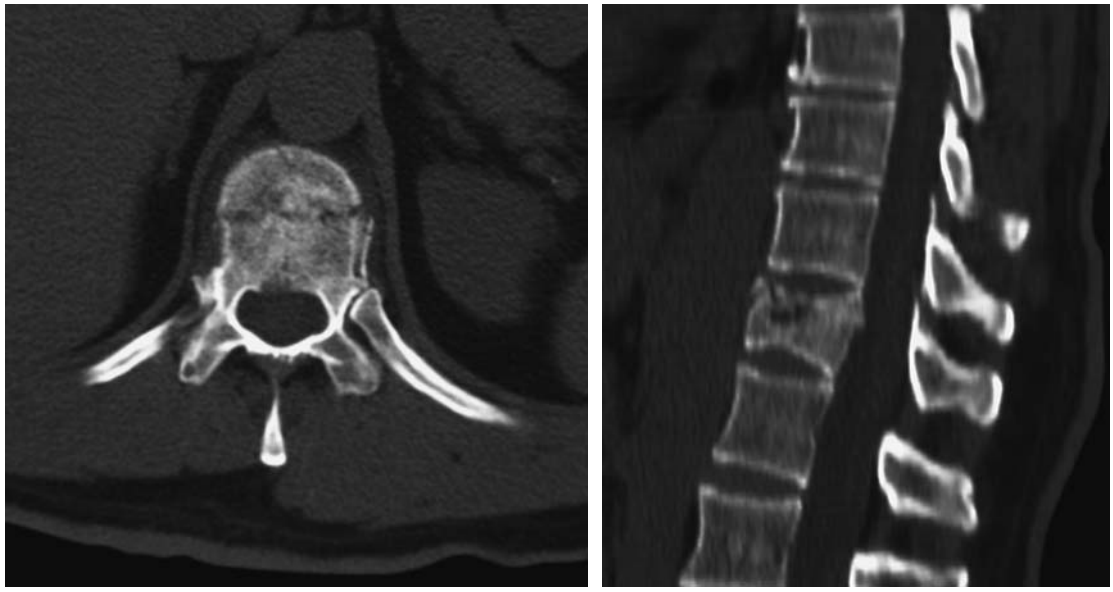

a b

Fig. 13.14a,b. Stable burst fracture. **a**,**b** Axial CT and sagittal reconstructed image show that the fracture only involves the anterior half of the vertebral body and the posterior elements are spared. This indicates a stable burst fracture. This distinction may be difficult on plain radiographs

Radiographic manifestations of the unstable fracture include widening of the interspinous or interlaminar distance, kyphosis greater than 20°, translation of more than 2 mm, a height loss of more than 50%, or articular process fractures (Atlas et al. 1986; Daffner et al. 1990; Holdsworth 1970; McAfee et al. 1982; Nagle et al. 1981).

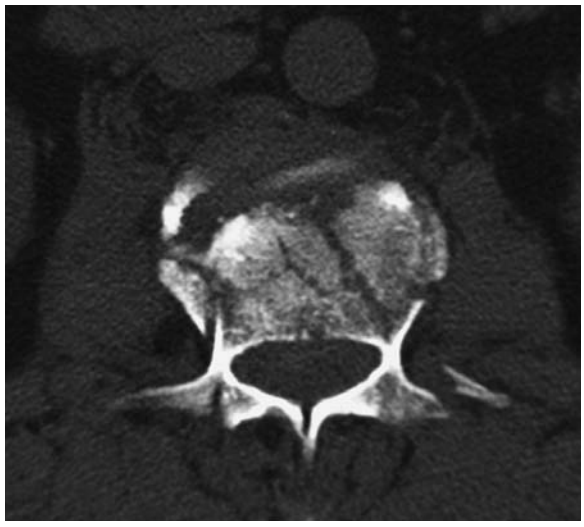

Fig. 13.15. Burst fracture. Axial CT demonstrates the comminuted fracture fragments without retropulsion into the canal, transverse process fractures, and the typical green stick laminar fracture

Laminar fractures and facet dislocations are best seen on CT. The laminar fracture is commonly a green-stick type, extending through the ventral cortex of the lamina close to the spinous process (Fig. 13.15).

CT shows the sagittal fracture of the body that typically extends from the basivertebral vein to the inferior endplate (Fig. 13.16a–c). CT clearly demonstrates the degree of spinal canal compromise by the retropulsed fracture fragments, especially on sagittal reconstructed images (Fig. 13.16d).

MR is useful in assessing the direct effects of the retropulsed fragment on the thecal sac and spinal cord (Fig. 13.17) and the integrity of the spinal ligaments (Fig. 13.3c, d).

13.5.1.3 Flexion-Distraction Injuries

Flexion-distraction injuries of the thoracic and lumbar spine were first described by G. Q. Chance in 1948 (Chance 1948). He described the fracture in general terms as a flexion injury but did not propose details as to the mechanism of the injury. The mechanism has subsequently been characterized as hyperflexion with distraction of the posterior spinal elements.

A Chance fracture is commonly associated with use of a lap seat belt in high-speed motor vehicle crashes involving rear-seat passengers with lap seat

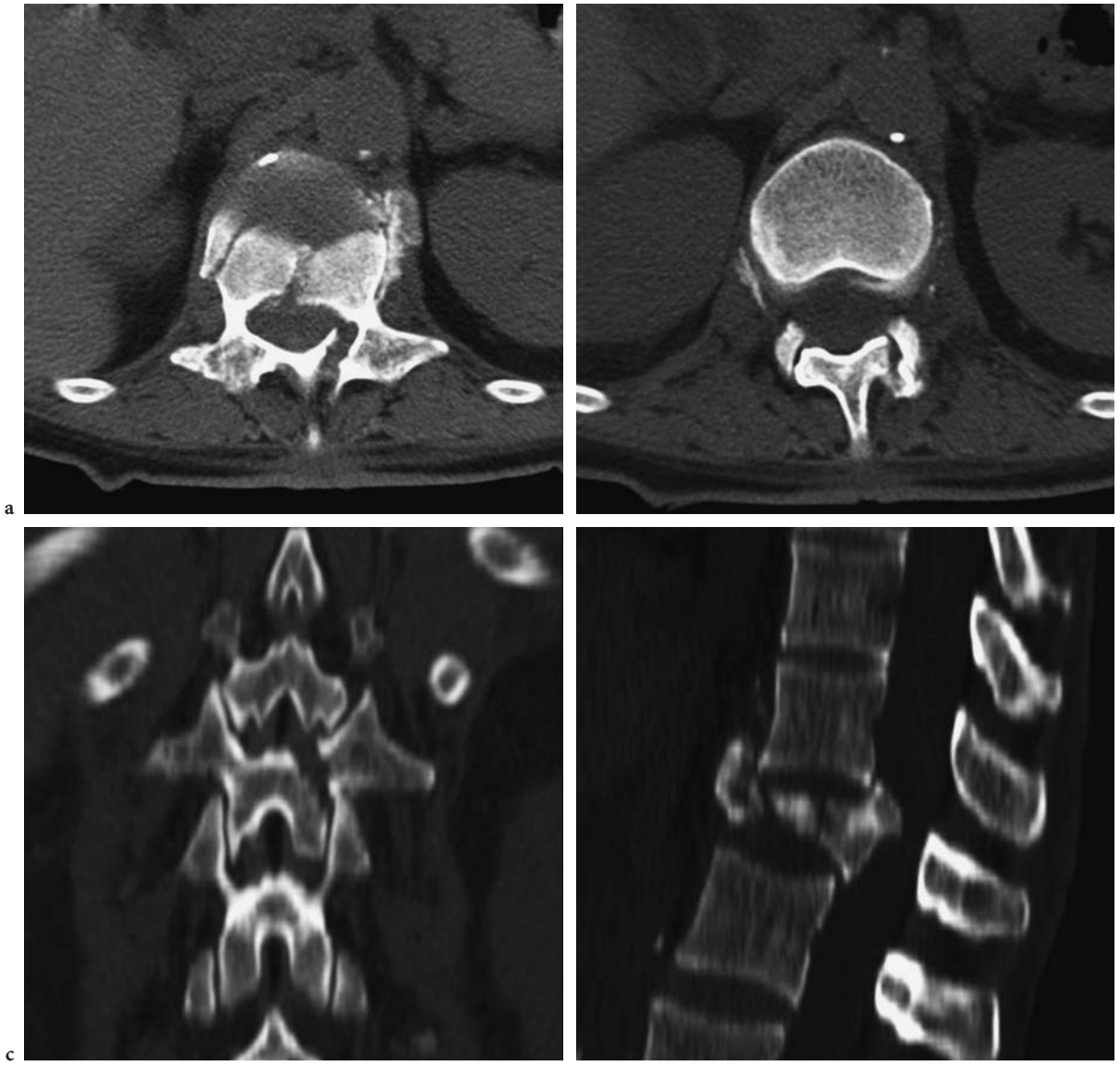

Fig. 13.16a–d. Burst fracture with a rotatory/translational component. **a–c** Axial CT with coronal reconstruction demonstrates the sagittal fracture extending into the endplate from the basivertebral vein, a laminar fracture and facet subluxation. **d** Sagittal reconstructed CT image demonstrates the retropulsed fragment which is typically rotated posterosuperiorly into the canal

belt restraints alone. It is also commonly seen in young children who are too small for the standard seat belt. When a passenger is restrained by a lap belt and not a shoulder harness, he is propelled forward but restrained at the abdominal wall by the lap belt. The fulcrum of force is then located more anteriorly relative to the position of the lap seat belt within the abdominal wall rather than the vertebral column. This results in a distraction force at the level of the spine. The posterior and middle columns fail in distraction and the anterior column can fail in distraction or compression. These injuries comprise about 5% of the series of spinal fractures and 6% of major spinal injuries in Denis's study (Denis 1983).

A Chance fracture is a horizontal vertebral body injury that results from flexion about an axis anterior to the anterior longitudinal ligament, so that the entire vertebral body is pulled apart by strong tensile forces. The lap belt (Chance) injuries include a spectrum of ligamentous and bony injuries. Three types have been described depending on whether there is disruption of bone, ligamentous components, or both.

Fig. 13.17. **a** Sagittal T1, **b** gradient-echo, **c** FSE T2-weighted, and **d** STIR images show the degree of retropulsion, canal compromise, conus compression, and associated ligamentous injury. The fracture line is best visualized on the gradient-echo sequence (**b**, *arrow*), and the STIR sequence is most sensitive for depicting marrow edema (**d**, *arrow*). The anterior longitudinal ligament (ALL) is disrupted and displaced by the fracture fragment and prevertebral hematoma. The posterior longitudinal ligament (PLL) is elevated but appears intact

The classic Chance fracture (**Type 1**) occurs between L1 and L3 (Chance 1948; Smith and Kaufer 1969), but has also been reported to occur in the upper thoracic spine (Davis et al. 2004) as a result of a steering wheel acting as the fulcrum. The fracture is a horizontal avulsion through the posterior arch and pedicles extending anteriorly to involve the posterosuperior aspect of the body just anterior to the neural foramen. The posterior ligaments are intact. This usually involves one level, between L1 and L3.

The second type of horizontal injury (**Type 2**) is also known as the Smith fracture (Chance 1948)

where injury initially disrupts the supraspinous and interspinous ligaments with the fracture occurring at the junction of the lamina and spinous process without involving the spinous process itself and extends to involve the posterior body. The fracture may extend anteriorly to involve the ligamentum flavum, PLL and the disc. On imaging, the widening of the interspinous distance and an intact spinous process helps to differentiate this fracture from the classic Chance fracture.

The third type (**Type 3**) of fracture involves the posterior elements on one side only secondary to a rotational force.

Chance fractures are infrequently associated with neurologic deficits, but if present, should be further evaluated with MR imaging to exclude neural compression. Both MR and CT with sagittal reconstructions are valuable for delineating the path of injury (through bone and/or soft tissues).

Injuries associated with Chance fractures often result in greater morbidity and mortality than the fracture itself (Reid et al. 1990). The presence of transabdominal ecchymosis especially in children in itself is a high predictor of further intraabdominal injury and associated spinal injuries (Voss et al. 1996). Intraabdominal injuries can be seen in 45% of patients and include hollow viscous or visceral lacerations, hematomas, and solid organ contusions. Injuries to the spinal cord, cauda equina, pancreas, and 2nd or 3rd part of the duodenum, as well as small bowel laceration and abdominal muscle abrasions associated with deceleration injuries in passengers wearing lap seat belts constitute the seat belt syndrome (Garrett and Braunstein 1962).

13.5.1.3.1 Imaging

On conventional radiographs the horizontal fractures are best seen on the lateral view. There may be an increase in the distance between the spinous processes, as well as horizontal fractures of the lamina, pedicles, and posterior body. On the AP view there may be lack of overlap between the vertebral body and posterior elements caused by elevation of the posterior elements. While anterior wedging of the vertebral body may be observed, the anterior column is uninvolved and the ALL is intact.

On axial CT images, it may be difficult to appreciate the horizontal fracture as the plane of injury is parallel to the CT cuts. Thin axial cuts and sagittal and coronal reconstructions are essential to detect the fracture and any malalignment due to ligamentous injury (Fig. 13.18). MR will demonstrate subtle

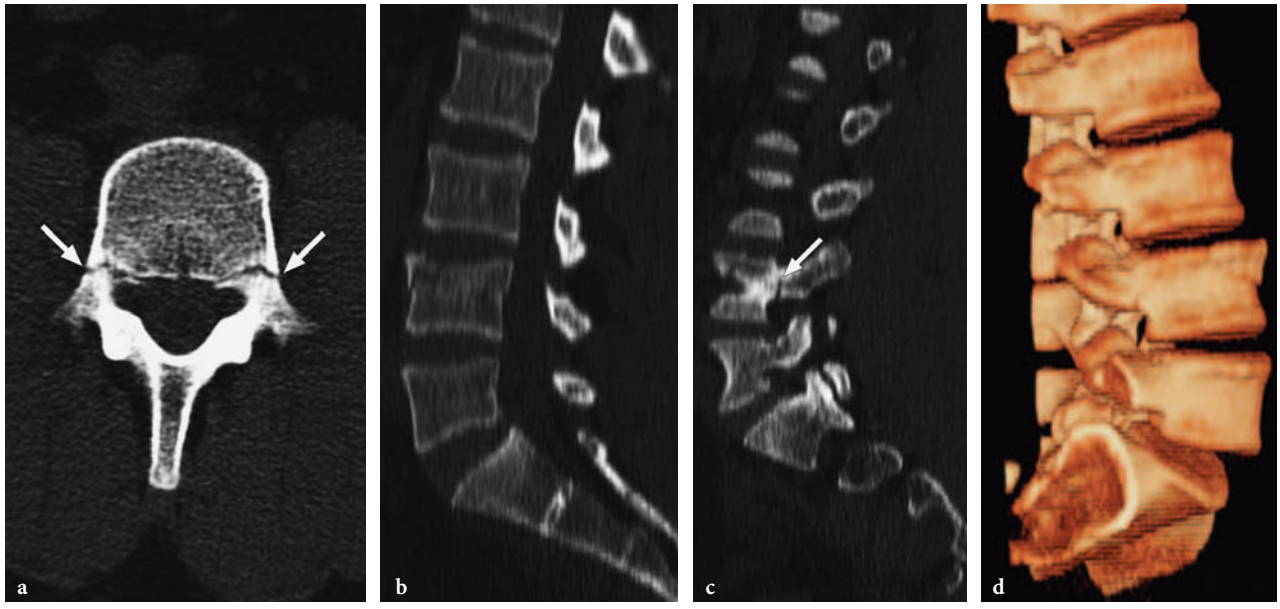

Fig. 13.18a–d. Flexion-distraction injury: seat belt fracture (type 2 horizontal injury – Smith). **a** Axial CT demonstrates the horizontally oriented fracture extending through the posterior aspect of the vertebral body and involving the pedicles (*arrows*). **b**,**c** Sagittal reconstructed CT images demonstrate the characteristic step-off of the anterior cortex and the fracture extending to involve the pedicles (*arrow*), and sparing the spinous processes. **d** Lateral volume-rendered CT image defines the orientation of the fracture line

marrow edema and is also very useful to exclude an associated ligamentous injury (Fig. 13.19). Presence of gas in the posterior subcutaneous soft tissues suggests a possible flexion-distraction injury (Fig. 13.20a).

13.5.1.4 Fracture-Dislocation Injuries

Fracture-dislocations are the result of a violent complex shearing force with failure of all three columns. They account for 15% of all spinal fractures and 20% of all major injuries in Denis's study (Denis 1983). These can occur anywhere along the thoracolumbar spine with a predilection for the thoracolumbar junction. They are extremely unstable.

The main characteristic of fracture dislocations is that there is failure of all columns under compression, tension, rotation, or shear. This leads to subluxation or dislocation. There are three subtypes: flexion-rotation, shear, and flexion-distraction. The rate of neurologic injury is highest (75%) with this injury subtype. Most injuries result from a force directed to the dorsal aspect of the spine (DeOliviera 1978).

- In the *flexion-rotation* injury, the axis of flexion is posterior to the anterior longitudinal ligament. The posterior and middle columns totally rupture under tension and rotation forces leading to a tear of the posterior longitudinal ligament. The anterior column fails under a combination of compression and rotation forces, leading to anterior wedging with stripping off of the anterior longitudinal ligament of the vertebra below (Denis 1983). These fractures are potentially unstable as the ligamentum flavum, interspinous ligament, and supraspinous ligament are usually torn. The injury may either go through the disc (it is then

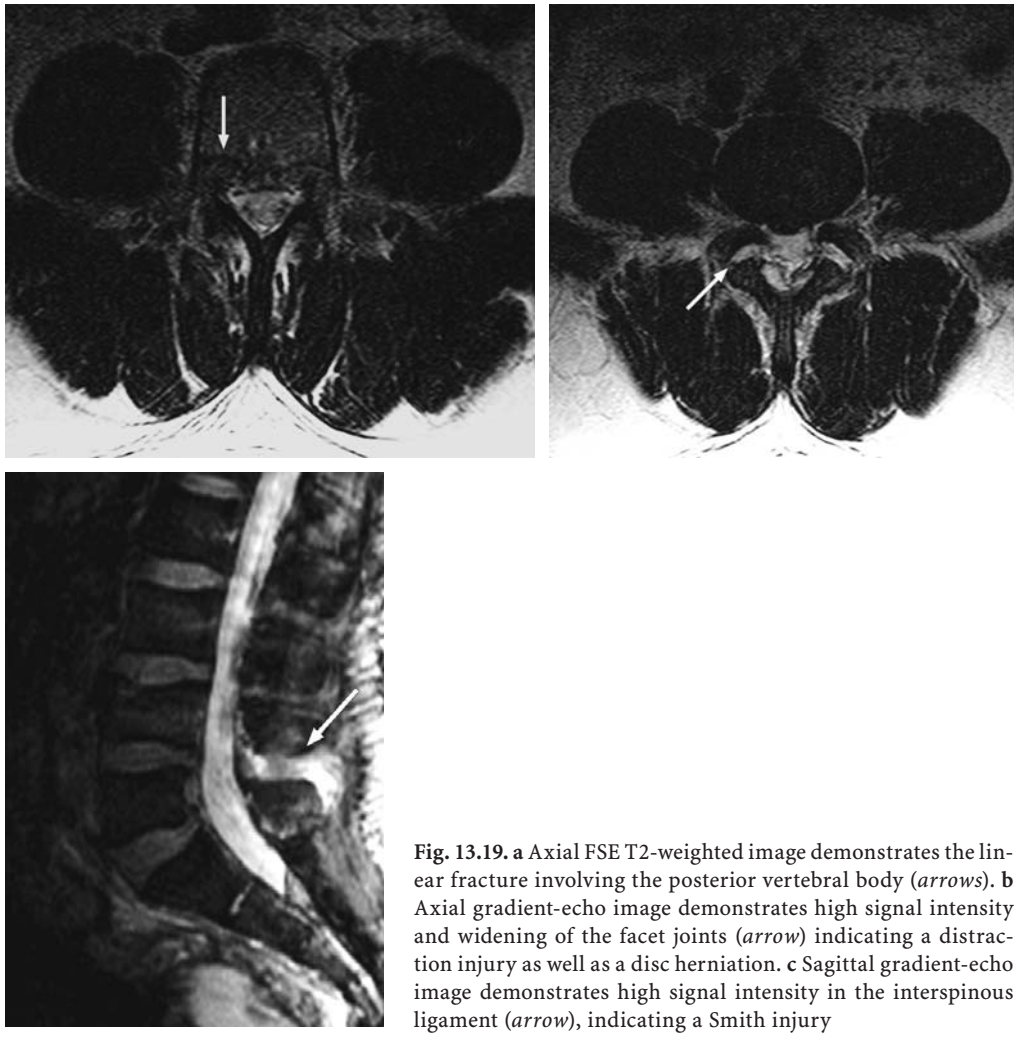

Fig. 13.19. a Axial FSE T2-weighted image demonstrates the linear fracture involving the posterior vertebral body (*arrows*). **b** Axial gradient-echo image demonstrates high signal intensity and widening of the facet joints (*arrow*) indicating a distraction injury as well as a disc herniation. **c** Sagittal gradient-echo image demonstrates high signal intensity in the interspinous ligament (*arrow*), indicating a Smith injury

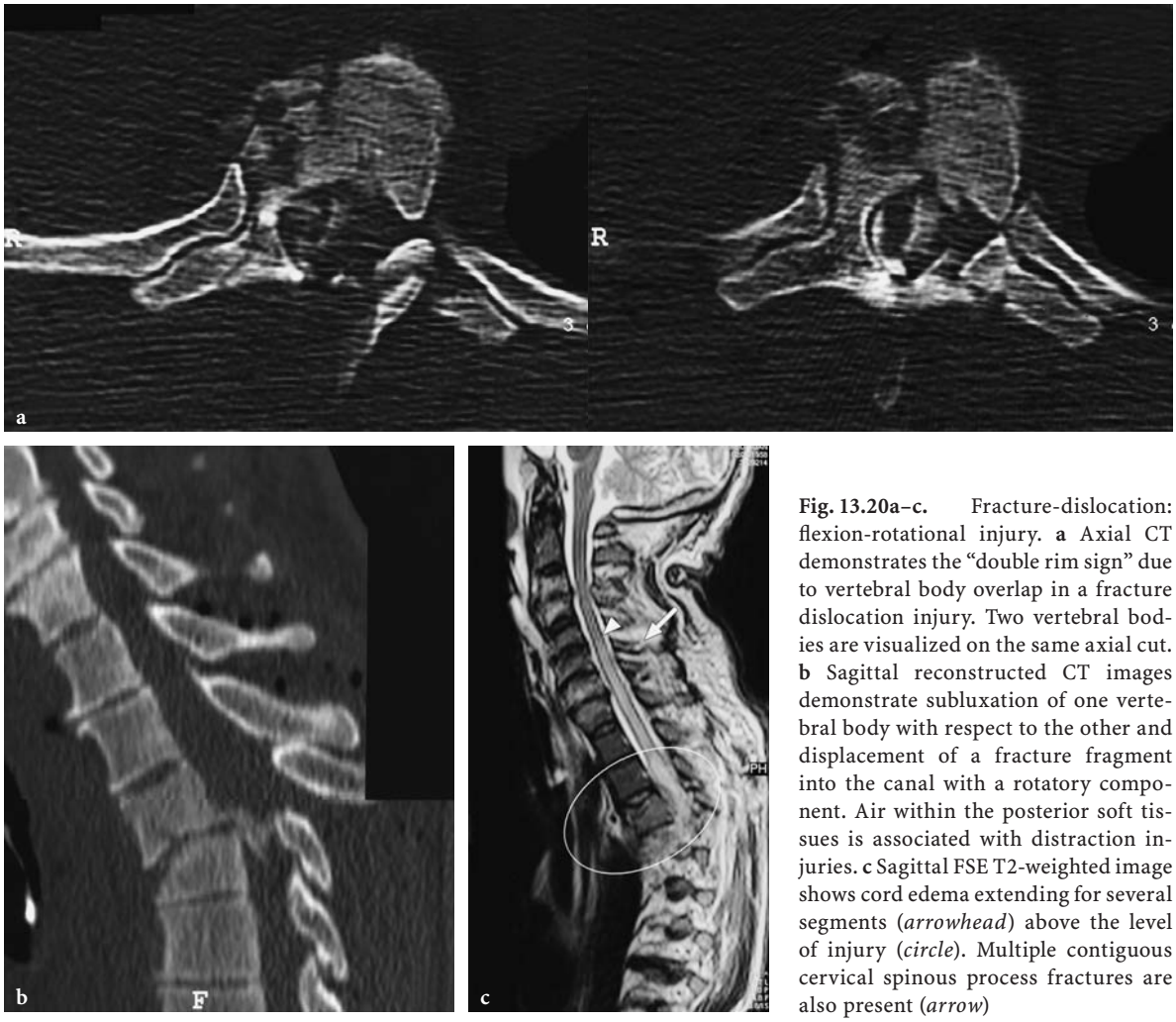

Fig. 13.20a–c. Fracture-dislocation: flexion-rotational injury. **a** Axial CT demonstrates the "double rim sign" due to vertebral body overlap in a fracture dislocation injury. Two vertebral bodies are visualized on the same axial cut. **b** Sagittal reconstructed CT images demonstrate subluxation of one vertebral body with respect to the other and displacement of a fracture fragment into the canal with a rotatory component. Air within the posterior soft tissues is associated with distraction injuries. **c** Sagittal FSE T2-weighted image shows cord edema extending for several segments (*arrowhead*) above the level of injury (*circle*). Multiple contiguous cervical spinous process fractures are also present (*arrow*)

accompanied by wedging of the vertebral body below) or it may go right through the body itself leading to a "slice" type of fracture. There will be fanning of the spinous processes. If the zygapophyseal joint capsules are disrupted there may be subluxation or dislocation of the facet joint, or fractures of the facets may occur.

These fractures are differentiated from burst fractures in that the interpediculate distance remains constant as the ring of the neural arch is not disrupted in this type of injury.

- In *shear fractures*, all three columns are disrupted including the anterior longitudinal ligament. The shearing forces are most often directed from posterior to anterior (PA).
  - In the PA shear, the segment above shears off forward on the segment below. This takes place in an extended position so the vertebral body height is maintained. The posterior arch of the dislocated vertebra is fractured at several levels, there are free floating lamina, fractures of multiple spinous processes in the upper segment, and fracture of the superior facet of the lower vertebra.
  - In the AP shear injury subtype, the segment above shears off on the segment below in a posterior direction. There may be a fracture of the spinous process but no free floating lamina. The anterior segment of the upper vertebral body may be locked on the superior facet of the vertebra below.
- The *flexion-distraction* type injuries resemble the seat-belt type of injury; with both the posterior and middle column rupture under tension and the annulus fibrosus torn, this allows the vertebra above to sublux or dislocate on the vertebra below. The anterior longitudinal ligament is stripped off the vertebral body below, and the continuity of the ligament is disrupted. In this type of injury, there is no rotation between the two vertebrae involved,

and the superior facet fracture of the flexion type injury will be absent.

Locked facets are rarer in the thoracic and lumbar spine than in the cervical spine (Holdsworth 1970; Gellad et al. 1986; Sharafuddin et al. 1990). Three types of facet abnormalities reported with flexion-distraction and flexion-rotation injuries are anteriorly, laterally, and superiorly locked facets.

13.5.1.4.1 Imaging

The hallmark of this group of injuries is displacement or subluxation of one vertebral body with respect to another (Fig. 13.20a). On the AP radiograph, the interspinous distance at the affected level will be widened.

In the flexion-rotation subtype, offset of the vertebra above on the vertebra below is noted with rotation between the two. This rotation can be recognized from the orientation of the pedicles and spinous processes.

CT is optimal for evaluating displacement of vertebral bodies, spinal canal, and facetal involvement, and for detecting dislocated articular processes.

Axial CT images demonstrate the "double rim sign" due to vertebral body overlap (Fig. 13.20b). The flexion component of the injury brings the superior body down inferiorly to the level of inferior body with the result that both are visible on a single section of the CT scan. The "naked facet sign" on axial images (O'Callaghan et al. 1980; Manaster and Osborne 1987) due to dislocated facets may be seen in severe dislocation (Fig. 13.21).

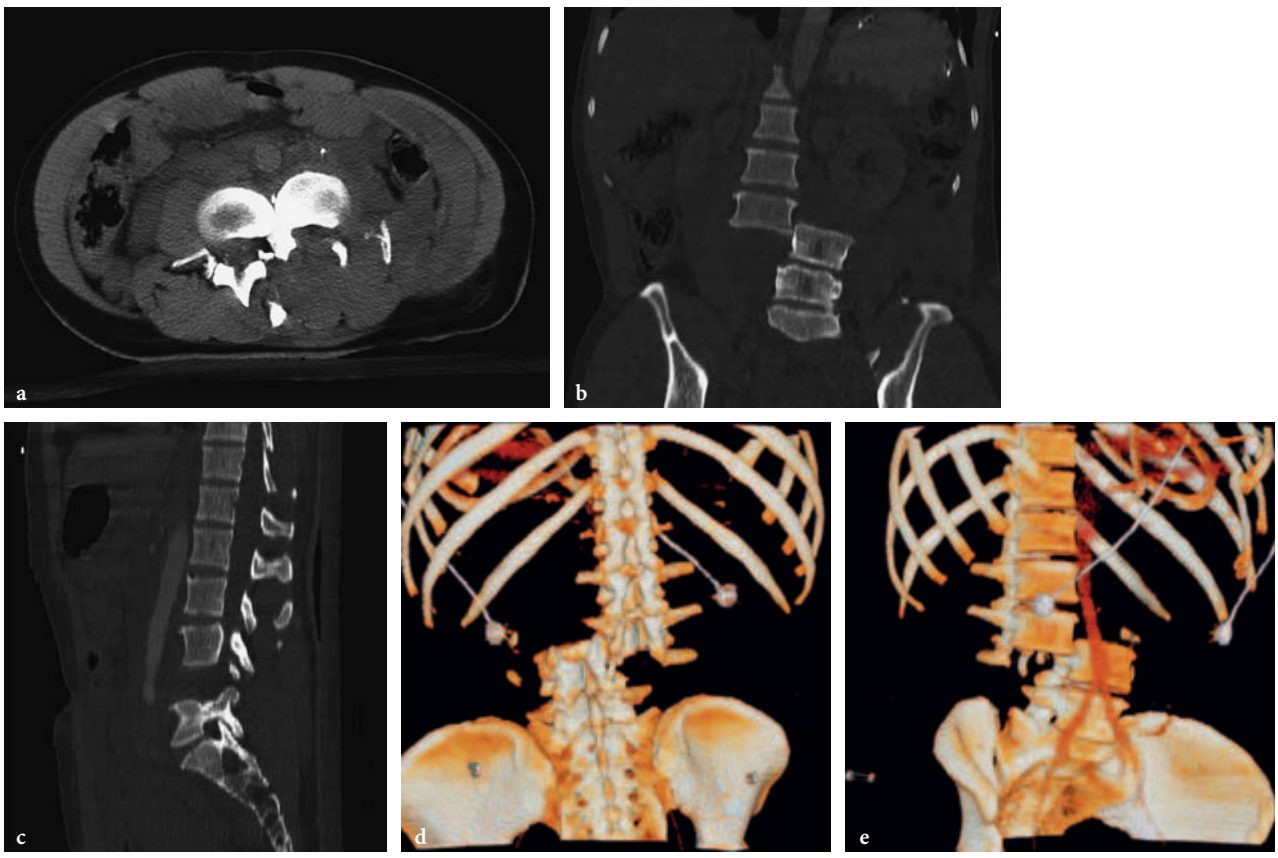

Fig. 13.21a–e. Complete fracture-dislocation/spondyloptosis and complete cauda equina injury: shear type of injury. **a–c** Axial CT with multiplanar reconstructed coronal and sagittal images demonstrate a complete fracture dislocation. The "naked facet sign" due to dislocated facets are seen on the axial image. **d,e** Volume rendered images are very useful for evaluating complex injuries. Posterior view volume rendered images demonstrate the full extent of bony injury and best show the relationship of the dislocated vertebral bodies to one another. Additional transverse process and iliac crest fractures are also noted. The oblique view shows that the major vascular structures are normal, a useful piece of information for surgical planning

Sagittal CT reconstructions and sagittal MR images provide information about the nature and extent of canal compromise (Fig. 13.22). The midsagittal CT reconstruction can also help to determine prognosis. According to Gellad et al. (1986), patients who were neurologically intact or had incomplete lesions at the time of presentation had a midsagittal diameter ranging from 8–15 mm (mean 11.2 mm). Those who were neurologically complete paraplegics at the time of injury had a midsagittal diameter ranging from 5–8.5 mm (mean 6.6 mm).

13.5.1.5 Miscellaneous Fractures

True bilateral fracture dislocations of the lumbar spine are rare and are usually related to major pelvic trauma, fall from a height, or ejection from a motor vehicle. Many are associated with sacral fractures.

Hyperextension injuries are extremely rare in the thoracolumbar spine and, when seen, usually occur in the mid-lumbar region. The resultant deformity is posterior compression and anterior distraction. Radiographic findings include widening of the anterior disc space, retrolisthesis, pars interarticularis fractures, and triangular avulsion fractures from the anterosuperior vertebral body (Fig. 13.23).

Transverse process fractures of the lumbar spine, although classified as minor injuries, may be associated with abdominal injury (Patten et al. 2000; Sturm and Perry 1984). They may result from direct blunt trauma, avulsion of the psoas muscle, violent lateral flexion-extension forces, or Malgaigne fractures of the pelvis (Krueger et al. 1996). When present in a patient with blunt abdominal trauma, further evaluation with CT imaging is recommended to exclude associated genitourinary, hepatic, splenic, or bowel injuries (Sturm and Perry 1984).

13.5.2 Spinal Conditions Predisposing to Trauma

13.5.2.1 Ankylosing Spondylitis

Patients with long standing ankylosing spondylitis are predisposed to fractures of the spine. Horizontal fractures occur through the ossified intervertebral disc space and/or endplate, as well as the posterior

Fig. 13.22a,b. Fracture-dislocation: shear type of injury with cord transection. **a** Sagittal reconstructed CT image demonstrates the vertebral body fracture dislocation of T11 with involvement of the posterior elements and a burst fracture of T8. **b** Sagittal gradient-echo image also shows the fracture through the vertebra with dislocation and associated extensive abnormal hyperintense cord signal intensity and diffuse cord expansion

Fig. 13.23a–d. Hyperextension injury. **a** Sagittal reconstructed CT demonstrates widening of the anterior disc space and malaligned posterior elements. No fracture is noted of the vertebral body. **b,c** Axial CT and volumetric rendering lateral view demonstrate bilateral locked facets (*arrows*). **d** Sagittal FSE T2-weighted MR image demonstrates subtle retrolisthesis and associated spinal cord injury

elements, in the thoracic and lumbar spine (Gelman and Umber 1978). Biomechanically, these fractures resemble the seat belt type of injury because of shifting of the axis of flexion and extension in the ankylosed spine away from its normal location in the center of the nucleus pulposus (Graham and Van Peteghem 1989). Patients can sustain serious spinal injury even after minor trauma. These fractures are unstable and may proceed to a pseudoarthrosis. The pseudoarthrosis places the patient at risk for further vertebral body displacement and subluxation with associated cord injuries. MR is the study of choice in evaluating the degree of spinal canal compromise in the setting of trauma.

13.5.2.2 Diffuse Idiopathic Skeletal Hyperostosis

Diffuse idiopathic skeletal hyperostosis (DISH) also known as Forestier's disease or ankylosing hyper-

ostosis is differentiated from degenerative disc disease and ankylosing spondylitis by certain criteria. These features include flowing ossification along the anterolateral aspect of at least four contiguous vertebral bodies, and preservation of intervertebral disc height, absence of marginal sclerosis, and absence of apophyseal joint fusion. The thoracic spine is most commonly involved.

The mechanism of injury to the spine in patients with DISH is typically hyperextension, and the fracture is always unstable since all three columns are usually involved. Fractures through the region of flowing ossification anteriorly may result in subluxation and disc injury (Fig. 13.24) (Israel et al. 1994).

13.5.3.3 Pathologic Fracture

Malignancy is another cause of vertebral body collapse and must not be overlooked in the setting of trauma, especially in the elderly population. Complete replacement of the normal marrow signal by tissue with abnormal signal and associated collapse is the usual appearance on MR imaging in neoplastic disease. Other MR imaging findings that suggest metastatic collapse include a paraspinal mass, abnormal marrow signal in the adjacent pedicle, and epidural extension (Fig. 13.25). Complementary imaging modalities such as bone scintigraphy should also be considered in the work-up of such patients.

13.5.3 Trauma Mimics

13.5.3.1 Physiologic Wedging

Physiologic wedging typically occurs in the lower thoracic spine between T8 and T12 and is more pronounced in males. A wedging ratio (anterior vertebral body divided by posterior vertebral body height) of 0.80 in males and 0.87 in females at T8–T10 is considered normal (El-Khoury and Whitten 1993).

13.5.3.2 Schmorl's Nodes

Schmorl's nodes are herniations of the nucleus pulposus into the trabecular bone through the vertebral endplate. They appear as shallow concavities along the superior and inferior endplates of vertebral bodies and are often detected incidentally on radiographs. They may occur spontaneously or may result from stress from axial loading, especially in young athletes or related to trauma (Sward et al. 1990). They are most common in the lower thoracic and lumbar spine and should not be confused with acute compression fractures. On plain radiographs and CT, reactive sclerosis around a Schmorl's node may help differentiate it from an acute fracture (Fig. 13.26). On MRI, no signal abnormalities in the vertebral body are present in the asymptomatic individual. Focal high signal intensity on T2 or STIR images, and even enhancement on post gadolinium images, can be seen surrounding the intraosseous hernia in acutely symptomatic patients with back pain (Stabler et al. 1997).

13.5.3.3 Scheuermann's Disease

Scheuermann's disease or juvenile kyphosis is caused by a wedge shaped deformity of usually three to five vertebrae with wedging of at least 5°. They must not be confused with old compression fractures. They most commonly occur in the thoracic spine but the thoracolumbar and lumbar spine may also be involved .The characteristic lesion of Scheuermann's disease is irregularity or ossification of one or more vertebral body endplates (Alexander 1977). The irregular ossification manifests as Schmorl's nodes or vertebral marginal abnormalities. Schmorl's node formation is usually in the anterior aspect of the vertebrae in Scheuermann's disease (Fig. 13.26) ,whereas in the normal spine the node formation is more central. In the scoliotic spine, node formation is posterior (Leatherman and Dickson 1988). The exact pathogenesis of Scheuermann's disease is unknown but mechanical or traumatic factors have been implicated in the pathogenesis (Alexander 1977; Blumenthal et al. 1987). Endplate fractures develop in a weak spine undergoing rapid growth which lead to traumatic growth arrest, followed by narrowed discs, wedging of the vertebral bodies, and kyphosis.

13.5.3.4 Kummell's Disease and Benign Osteoporotic Fracture

Kummell's disease or delayed posttraumatic collapse of a vertebral body should not be confused with acute traumatic wedge compression. The etiology of this entity is uncertain. It is felt to be due to osteonecrosis of the vertebral body as a result of

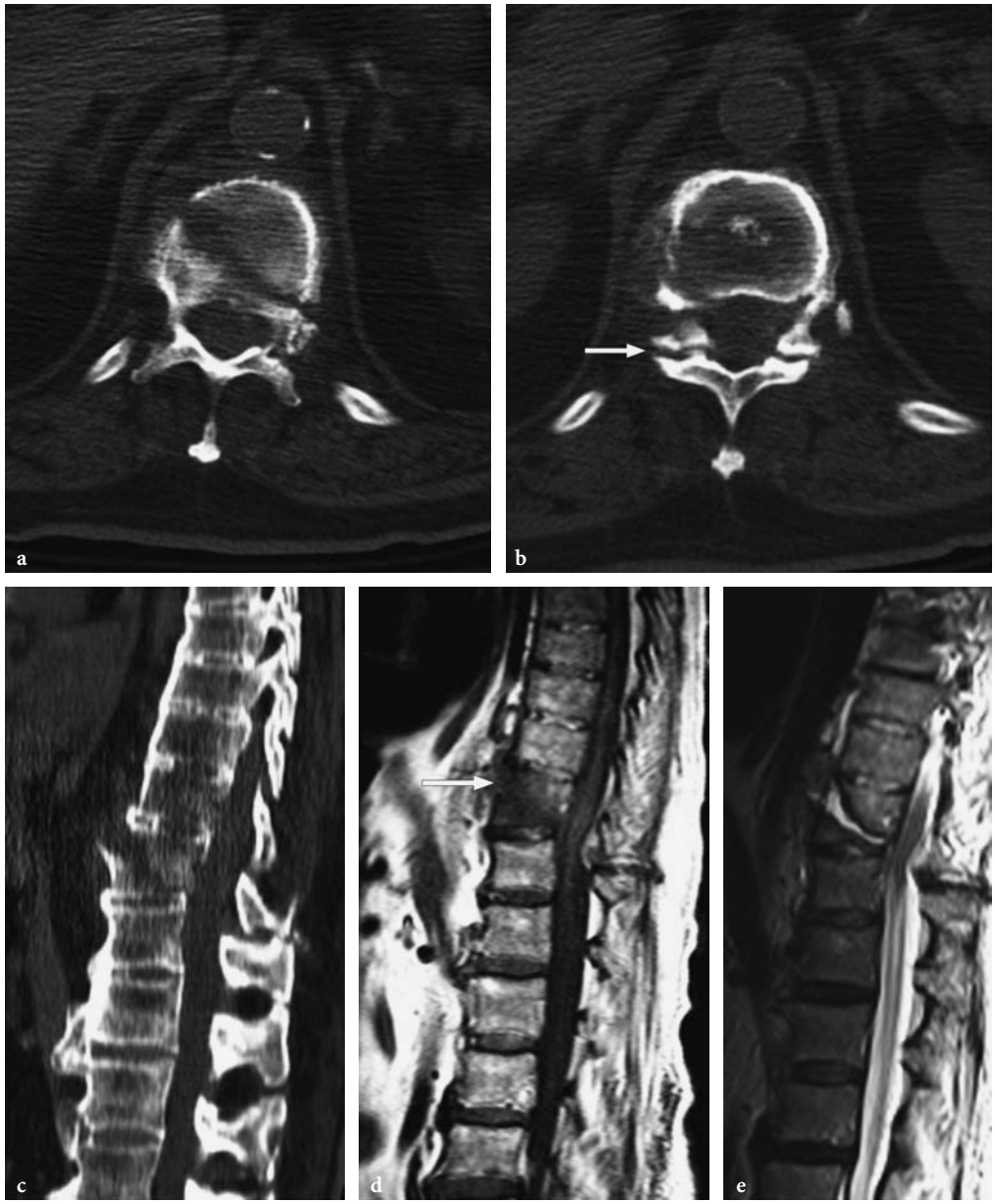

Fig. 13.24a–e. Hyperextension-dislocation in DISH. **a**,**b**Axial CT images demonstrate posterior element involvement and facet dislocation (*arrows*). **c** Sagittal reconstructed CT image demonstrates the oblique fracture of the vertebral body. **d**,**e** Sagittal T1- and FSE T2-weighted images demonstrate an apparent increased height of the vertebral body and disruption of all three columns with dorsal cord compression (*arrow*)

a vascular insult; however, nutritional, vasomotor, traumatic, and neurologic etiologies have also been postulated. Steroids may be a predisposing factor. It is characterized by intravertebral gas and typically the injury causes compression of the vertebral body over a period of 6 weeks or more. It is most common within the thoracic spine. The presence of gas either in the vertebral body or disc space is a reliable predictor of a benign process and is best seen on CT (Fig. 13.27c). These gas collections may fill with fluid that, on MR, typically demonstrate low signal on T1- and high signal on T2-weighted images (Fig. 13.27a,b) (Naul et al. 1989; Dupuy et al. 1996; Yuh et al. 1989; Baur et al. 2002).

MR may show diffuse abnormal signal throughout the vertebral body in an acute compression

Fig. 13.25a–c. Pathologic fracture. **a**,**b** Sagittal T1- and FSE T2-weighted images demonstrate a pathological fracture and complete replacement of the vertebral body by abnormal marrow signal intensit. **c** Post-gadolinium sagittal T1-weighted image with fat saturation technique shows multiple enhancing lesions consistent with metastatic involvement

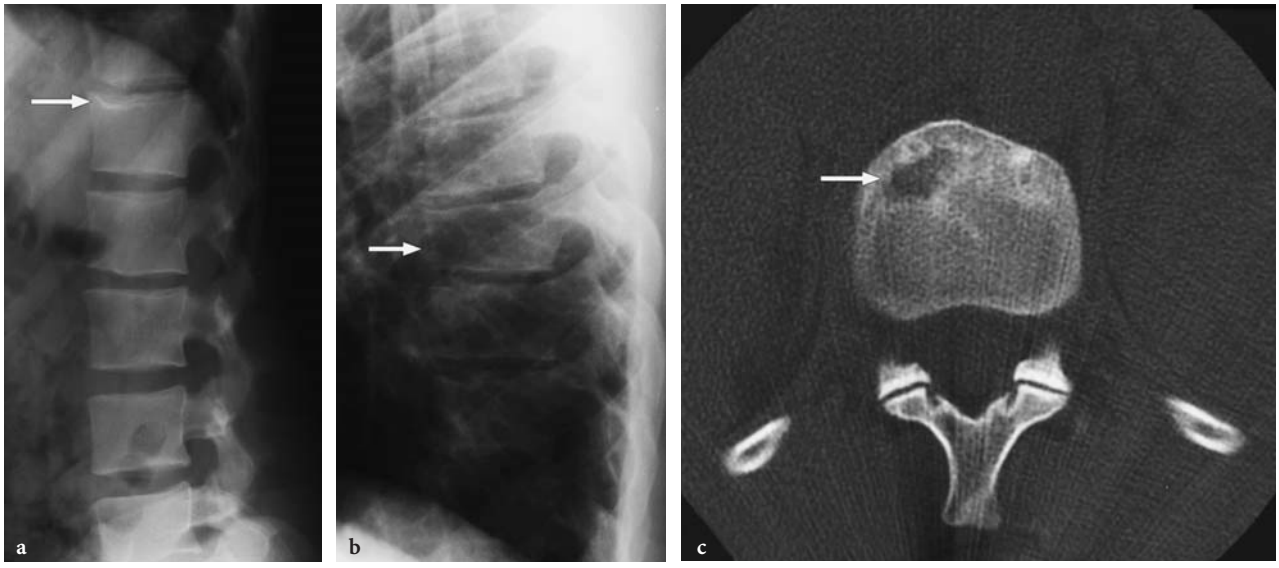

Fig. 13.26a–c. Schmorl's nodes in Scheuermann's disease. These should not be confused with acute compression fractures. **a** Lateral radiograph demonstrates Schmorl's nodes along the anterior aspect of T12 and L1 vertebrae (*arrow*). **b** Lateral radiograph shows anterior wedging of the thoracic vertebra and anteriorly located Schmorl's nodes (*arrow*). **c** Axial CT demonstrates reactive sclerotic margins around the Schmorl node (*arrow*)

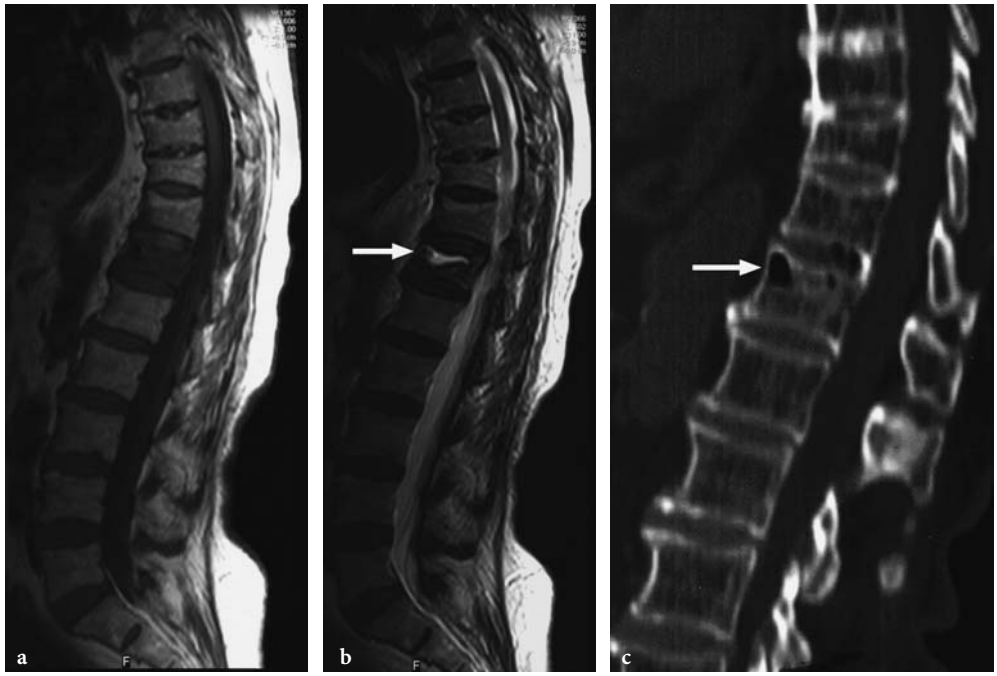

Fig. 13.27a–c. Kummell's disease. **a** Sagittal T1-weighted image shows diffuse low signal intensity and loss of height of the T12 vertebral body. Multiple old compression deformities are also noted. **b** Sagittal FSE T2-weighted image demonstrates linear high T2 signal intensity consistent with fluid within the fracture plane parallel to the superior endplate (*arrow*). **c** Sagittal reconstructed CT image demonstrates air within the cleft – a very reliable indicator of a benign process (*arrow*)

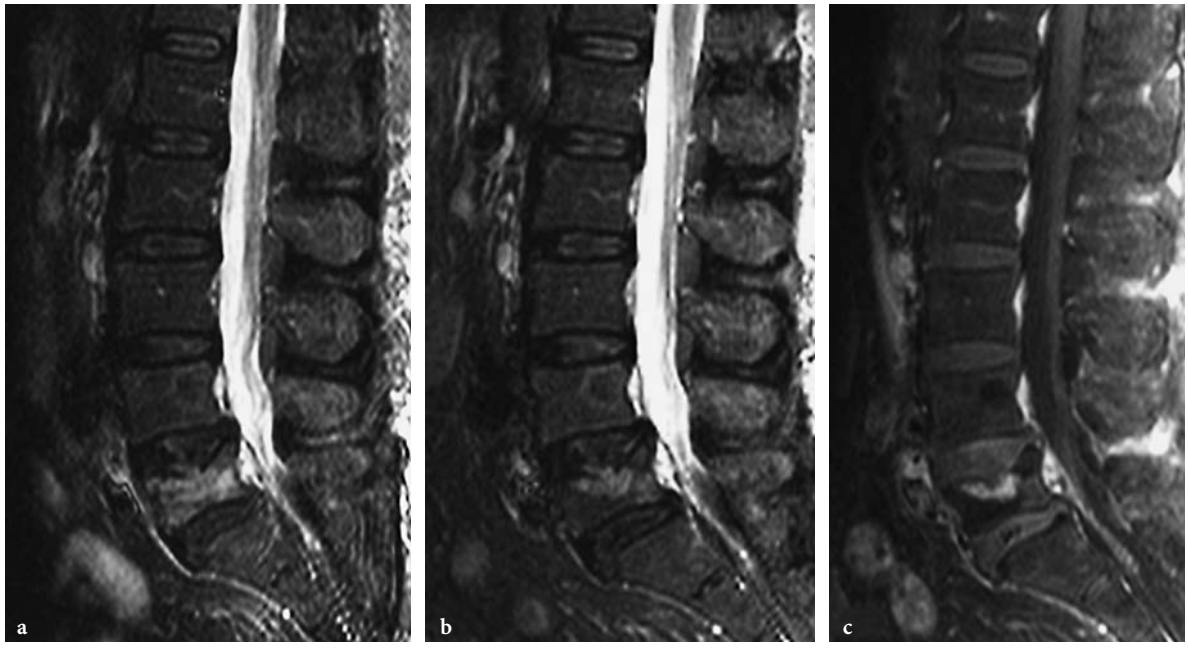

Fig. 13.28a–c. Benign osteoporotic fracture. **a** Sagittal STIR image demonstrates a compression deformity and high T2 signal intensity indicative of marrow edema in L5. **b** Follow-up Sagittal STIR image obtained after 6 weeks demonstrates partial resolution of marrow signal abnormality. **c** Post-gadolinium contrast enhanced T1-weighted image with fat saturation technique demonstrates enhancement that corresponds to the area of residual marrow edema; this finding can be seen in a resolving benign compression fracture

fracture, and it may be difficult to differentiate a benign from a malignant compression. In such instances, it may be advisable to wait for a period of about 6 weeks and repeat the MR imaging .The MR may show resolution of the signal abnormality and demonstrate some normal marrow signal intensity, confirming the benign etiology of the collapse (Fig. 13.28).

13.6 Conclusion

Initial evaluation and diagnosis of thoracolumbar trauma includes characterization of thoracolumbar injuries, as well as prompt recognition of neurological deficits and any other associated injuries. The ultimate therapeutic goals are preservation of neurological function and restoration of anatomy. Imaging plays an integral part in the initial evaluation and decision making process of the trauma patient. Advances in imaging have resulted in greater ease of data acquisition and increased diagnostic accuracy for emergent evaluation of the spine.

Conventional radiography still remains the initial screening method of choice in most hospitals but multidetector CT, when available, is preferred as initial screening in the severely or polytraumatized patient. Multidetector CT is the most commonly used modality in the assessment of thoracolumbar fractures and with its reconstruction capability, provides useful and accurate information to assess for spinal stability and guide patient management. MR provides information about the nature and extent of spinal canal compromise and is the definitive diagnostic modality in the evaluation of spinal cord injury. MR helps to ensure a rational approach to the surgical management of the fractured spine and can sometimes be used to predict outcome.

References

Alexander CJ (1977) Scheuermann's disease: a traumatic spondylodystrophy? Skeletal Radiology 1:209–221

Atlas WS, Regenbogen V, Rogers LF, Kim KS (1986) The radiographic characterization of burst fractures of the spine. AJR Am J Roentgenol 147:575–582

Ballock RT, Mackersie R, Abitbol JJ, Cervilla V, Resnick D, Garfin SR (1992) Can burst fractures be predicted from plain radiographs? J Bone Joint Surg Br 74-B:147–150

Baur A, Stabler A, Arbogast S, Duerr HR, Barti R, Reiser M (2002) Acute osteoporotic and neoplastic vertebral compression fractures: fluid sign at MR imaging. Radiology 225:730–735

Blumenthal SL, Roach J, Herring JA (1987) Lumbar Scheuermann's. A clinical series and classification. Spine 12:929–932

Bohlman HH, Ducker TB, Lucas JT (1982) Spine and spinal cord injury in the spine. In Rothman RH, Simeone FA (eds) The spine, edn. 2. WB Saunders, Philadelphia, pp 661–756

Brandser EA, El-Khoury GY (1997) Thoracic and lumbar spine trauma. Radiol Clin North Am 35:533–557

Brant-Zawadski M, Jeffrey RB, Minagi H, Pitts LH (1982) High resolution CT of thoracolumbar fractures. AJR Am J Roentgenol 138:699–704

Brightman RP, Miller CA, Rea GL, Chakeres DW, Hunt WE (1992) Magnetic resonance imaging of trauma to the thoracic and lumbar spine. Spine 17:541–550

Burgos J, Rapariz JM, Gonzalez-Herranz P (1988) Anterior endoscopic approach to the thoracolumbar spine. Spine 23:2427–2431

Calenoff L, Chessare JW, Rogers LF, Toerge J, Rosen JS (1978) Multiple level spinal injuries: importance of early recognition. AJR Am J Roentgenol 130:665–669

Carpenter MB (1991) Core text of neuroanatomy, 4th edn. Wilkins & Wilkins, Baltimore, MD

Chance GQ (1948) Note on a type of flexion fracture of the spine. Br J Radiol 21:452–453

Cotler JM, Vernace JV, Michalski JA (1986) The use of Harrington rods in thoracolumbar fractures. Orthop Clin North Am 17:87–103

Daffner RH, Deeb ZL, Goldberg AL, Kandabarow A, Rothfus WE (1990) The radiologic assessment of post-traumatic vertebral stability. Skeletal Radiology 19:102–108

Davis JM, Beall DP, Lastine C, Sweet C, Wolff J, Wu D (2004) Chance fracture of the upper thoracic spine. AJR Am J Roentgenol 183:1475–1478

Denis F (1983) The three column spine and its significance in the classification of acute thoracolumbar spinal injuries. Spine 8:817–831

Denis F (1984) Spinal instability as defined by the three-column spine concept in acute spinal trauma. Clin Orthop 189:65–76

De Oliveira JC (1978) A new type of fracture-dislocation of the thoracolumbar spine. J Bone Joint Surg Am 60:481–488

Doi K et al. (2002) Cervical root avulsion in brachial plexus injuries. Magnetic resonance imaging classification and comparison with myelography and computed tomography myelography. J Neurosurgery 96 [3 Suppl]:277–284

Dupuy DE, Palmer WE, Rosenthal DI (1996) Vertebral fluid collection associated with vertebral collapse. AJR Am J Roentgenol 167:1535–1538

El-Khoury GY, Whitten CG (1993) Trauma to the upper thoracic spine: anatomy, biomechanics and unique imaging features. AJR Am J Roentgenol 160:95–102

Ferguson RL, Allen BL Jr (1984) A mechanistic classification of thoracolumbar spine fractures. Clin Orthop 189:77–88

Fessler RG, Masson RL (1996) Management of thoracic frac-

tures. In: Menezes AH, Sonntag VK (eds) Principles of spinal injury. Mc Graw-Hill, New York, pp 899–918
Flanders AE, Tartaglino LM, Friedman DP, Aquilone LF (1992) Magnetic resonance imaging in acute spinal injury. Semin Roentgenol 27:271–298
Garrett JW, Braunstein PW (1962) Seat belt syndrome. J Trauma 2:220–238
Gellad FE, Levine AM, Joslyn JN, Edwards CC, Bosse M (1986) Pure thoracolumbar facet dislocations: clinical features and CT appearance. Radiology 161:505–508
Gelman MI, Umber JS (1978) Fractures of the thoracolumbar spine in ankylosing spondylitis. AJR Am J Roentgenol 130:485–491
Gertzbein SD, Court-Brown CM (1988) Flexion-distraction injuries of the lumbar spine: mechanism of injury and classification. Clin Orthop 227:52–60
Graham B, Van Peteghem PK (1989) Fractures of the spine in ankylosing spondylitis. Diagnosis, treatment and complications. Spine 14:803–807
Guerra J Jr, Garfin SR, Resnick D (1984) Vertebral burst fractures: CT analysis of the retropulsed fragment. Radiology 153:769–772
Gumley G, Taylor TK, Ryan MD (1982) Distraction fractures of the spine. J Bone Joint Surg Br 64:520–525
Hackney DB, Asato R, Joseph PM, Carvlin MJ, Mc Grath JT, Grossman RI, Kassab EA, De Simone D (1986) Hemorrhage and edema in acute spinal cord compression: demonstration by MR imaging. Radiology 161:387–390
Hanley EN Jr, Eskay ML (1989) Thoracic spine fractures. Orthopedics 12:689–696
Henderson RL, Reid DC, Saboe LA (1991) Multiple noncontiguous spine fractures. Spine 16:128–131
Holdsworth FW (1970) Review article. Fractures, dislocations and fracture dislocations of the spine. J Bone Joint Surg (Am) 52:1534–1551
Hubbard D (1974) Injuries of the spine in children and adolescents. Clin Orthop 100:56–65
Israel Z et al. (1994) Hyperextension fracture-dislocation of the thoracic spine with paraplegia in a patient with diffuse idiopathic skeletal hyperostosis. J Spinal Disord 7:455–457
Jelsma RK, Kirsch PT, Rice J, Jelsma LF (1982) The radiographic description of thoracolumbar fractures. Surg Neurol 18:230–236
Keene JS (1987) Thoracolumbar fractures in winter sports. Clin Orthop 216:39–49
Kilcoyne RF, Mack LA, King HA, Ratcliff SS, Loop JW (1983) Thoracolumbar spine injuries associated with vertical plunges: re-appraisal with computed tomography. Radiology 146:137–140
Kerlaske RW, Jaspan T,Worthington BS (1991) Magnetic resonance imaging of spinal trauma. Br J Radiol 64:386–402
King AG (1986) Spinal column trauma. Instruct Course Lect 35:40–51
Kraus JF, Franti CE, Riggins RS, Richards D, Borhani NO (1975) Incidence of traumatic spinal cord lesions. J Chronic Dis 28:471–492
Krueger MA, Green DA, Hoyt D, Garfin SR (1996) Overlooked spine injuries associated with lumbar transverse process fractures. Clin Orthop 327:191–195
Kulkarni MV, McArdle CB, Kopanicky D, Miner M, Cotler HB, Lee KF, Harris JH (1987) Acute spinal cord injury. MR imaging at 1.5 T. Radiology 164:837–843
Leatherman KD, Dickson RA (1988) The management of spinal deformities: Scheuermann's kyphosis. Butterworth and Co, London, pp 123–136
Magerl F, Aebi M, Gertzbein S, Harms J, Nazarian S (1994) A comprehensive classification of thoracic and lumbar injuries. Eur Spine J 3:184–201
Manaster BJ, Osborne AG (1987) CT patterns of facet fracture dislocation in the thoracolumbar region. AJR Am J Roentgenol 148:335–340
McAfee PC, Yuan HA, Lasada NA (1982) The unstable burst fracture. Spine 7:365–373
McAfee PC, Yuan HA, Fredrickson BE, Lubicky JP (1983) The value of computed tomography in thoracolumbar fractures: an analysis of 100 consecutive cases in a new classification. J Bone Joint Surg Am 65-A:461–473
Meyer PR (1989) Fractures of the thoracic spine: T1–T10. In: Meyer PR (ed) Surgery of spine trauma. Churchill Livingstone, New York, pp 525–571
Nagle DA, Koogle TA, Piziali RL, Perkash I (1981) Stability of the upper lumbar spine following progressive disruptions and the application of individual internal and external fixation devices. J Bone Joint Surg 63-A:62–70
Naul LG, Peet GJ, Maupin WB (1989) Avascular necrosis of the vertebral body. Radiology 172:219–222
Nussbaum ES, Sebring LA, Wolf AL, Mirvis SE, Gottlieb R (1992) Myelographic and enhanced computed tomographic appearance of acute traumatic spinal cord avulsion. Neurosurgery 30:43–48
O'Callaghan JP, Ullrich CG, Yuan HA, Kieffer SA (1980) CT of facet distraction in flexion injuries of the thoracolumbar spine: the "naked" facet. AJR Am J Roentgenol 134:563–568
Panjabi MM, Hausfeld JN, White AA III (1981) A biomechanical study of the ligamentous stability of the thoracic spine in man. Acta Orthop Scand 52:315–326
Patten RM, Gunberg SR, Brandenberger DK (2000) Frequency and importance of transverse process fractures in the lumbar vertebra at helical abdominal CT in patients with trauma. Radiology 215:831–834
Petersilge CA, Pathria MN, Emery SE, Masaryk TJ (1995) Thoracolumbar burst fractures: evaluation with MR imaging. Radiology 194:49–54
Post MJD, Green BA (1983) The use of computed tomography in spinal trauma. Radiol Clin North Am 21:327–375
Pratt ES, Green DA, Spengler DM (1990) Herniated intervertebral disc associated with unstable spinal injuries. Spine 15:662–666
Reid AB, Letts RM, Black GB (1990) Pediatric Chance fractures: association with intra-abdominal injuries and seat belt use. J Trauma 30:384–391
Resnick KR, Weller SJ, Benzel EC (1997) Biomechanics of the thoracolumbar spine. In: Neurosurgery clinics of North America. Management of thoracolumbar instability, vol. 8. Saunders, pp 455–469
Saboe LA, Reid DC, Davis LA, Warren SA, Grace MG (1991) Spine trauma and associated injuries. J Trauma 31:43–48
Saifuddin A, Noordeen H, Taylor BA, Bayley I (1996) The role of imaging in the diagnosis and management of thoracolumbar burst fractures: current concepts and a review of literature. Skeletal Radiology 25:603–613
Sharafuddin MF, Hitchon PW, El-Khoury GY, Dyst GN (1990) Locked facets in the thoracic spine: report of three cases and a review. J Spinal Disord 3:255–258

Shellock FG (2002) Magnetic resonance safety update: implants and devices. J Magn Reson Imaging 16:485–496
Shuman WP, Rogers JV, Sickler ME, Hanson JA, Crutcher JP, King HA, Mack LA (1985) Thoracolumbar burst fractures: CT dimensions of the spinal canal relative to post surgical improvement. AJR Am J Roentgenol 145:337–341
Smith WS, Kaufer H (1969) Patterns and mechanisms of lumbar injuries associated with lap seat belts. J Bone Joint Surg Am 51:239–254
Smugar SS, Schweitzer ME, Hume E (1999) MRI in patients with intraspinal bullets. J Magn Reson Imaging 9:151–153
Stabler A, Bellan M, Weiss M, Gartner C, Brossmann J, Reiser MF (1997) MR imaging of enhancing intraosseous disk herniation (Schmorl's nodes). AJR Am J Roentgenol 168:933–938
Sturm JT, Perry JF (1984) Injuries associated with the transverse processes of the thoracic and lumbar vertebrae. J Trauma 24:597–599
Sward L, Hellstrom M, Jacobsson B, Peterson (1990) Back pain and radiological changes in the thoracolumbar spine of athletes. Spine 15:124–129
Teitelbaum GP, Yee CA, Van Horn DD, Kim HS, Colletti PM (1990) Metallic ballistic fragments: MR imaging safety and artifacts. Radiology 175:855–859
Trafton PG, Boyd CA Jr (1984) Computed tomography of thoracic and lumbar spine injuries. J Trauma 24:506–515
Vaccaro AR, Nachwalter RS, Klein GR, Sewards JM, Albert TJ, Garfin SR (2001) The significance of thoracolumbar spinal canal size in spinal cord injury patients. Spine 26:371–376
Volle E, Assheuer J, Hedde JP, Gustorf-Aeckerle R (1992) Radicular avulsion resulting from spinal injury: assessment of diagnostic modalities. Neuroradiology 34:235–240
Voss L, Cole PA, D'Amato C (1996) Pediatric Chance fractures from lapbelts: unique case report of three in one accident. J Orthop Trauma 10:421–428
Weinstein JN, Collalto P, Lehmann R (1988) Thoracolumbar "burst" fractures treated conservatively: a long-term follow-up. Spine 13:33–38
White AA III, Punjabi MM (1990) Clinical biomechanics of the spine, 2nd edn. J. B Lippincott, Philadelphia, pp 1–342
White AA III, Panjabi MM, Posner I (1981) Spinal stability: evaluation and treatment. AAOS Instruct Course Lect 30:457–483
Yuh WT, Zachar CK, Barloon TJ, Sato Y, Sickels WJ, Hawes DR (1989) Vertebral compression fracture: distinction between benign and malignant causes with MR imaging. Radiology 172:215–218

The Postoperative Spine

Surgical Procedures: Discectomy and Herniectomy

14

Erik Van de Kelft

CONTENTS

14.1 Introduction

In this chapter we will discuss the pathology of lumbar disk herniation. The clinical symptoms of a lumbar disk herniation will be discussed as well as the different therapeutical options, especially surgical therapy.

The different surgical techniques will be described in detail with the intention to help the radiologist in interpreting both pre- and postoperative lumbar spine imaging studies. The choice of treatment of a lumbar disc herniation depends increasingly on radiological images. The decision on how to treat the so-called failed back surgery syndrome (FBSS) also depends largely on the specific postoperative imaging findings.

E. Van de Kelft, MD, PhD
Department of Neurosurgery, Nikolaas General Hospital, Moerlandstraat 1, 9100 Sint-Niklaas, Belgium

14.2 Pathology of Lumbar Disc Herniation

Joints are subjected to the ravages of aging, degeneration and trauma. The degeneration of the intervertebral disk is a complex process that involves changes in both composition and function of the disk.

This degenerative process most frequently manifests itself as spondylosis, the development of osteophytes and disc herniation. Indeed, a symptomatic disc herniation without any other sign of disc degeneration is rarely noticed. Even so-called post-traumatic disc herniations usually have an underlying degenerative process. Sudden strains, particularly if associated with rotational torque, may cause tearing and ultimately rupture of the annular ring. More commonly the annulus fibrosus deteriorates more gradually, as a product of cumulative stresses over time, causing microscopic tears rather than a single explosive rupture. A significant compressive force at the level of a healthy disc will cause a fracture of the vertebral body before tearing the annulus. This is important when considering the relationship of a traumatic event to a herniated disc that may manifest itself several years later.

Many procedures have been developed to treat abnormalities and degeneration of the intervertebral disc. The associated pathological entities include disc herniation, degenerative disc disease (DDD) and segmental instability (Mouw and Hitchon 1996; Dowd et al. 1998). Over the past three decades, much attention has been given by clinicians and

KEY-POINTS

- Indications for surgery in patients with lumbar disc herniation:
  - Absolute indications:
    - Cauda equina syndrome
    - Weakness and sensory loss
    - Persistent pain
  - Relative indications:
    - Failure of symptom relief after 2–4 weeks of appropriate conservative therapy
    - Radicular pain in a dermatomal pattern
    - Sensory loss in the same dermatome
    - Weakness in the correct distribution
    - Depressed tendon reflex appropriate to pain, weakness and sensory loss
    - Limited straight-leg raising with reproduction of radicular pain
    - Abnormal neuro-imaging (CT or MRI) consistent with the neurological deficit
- Surgical techniques:
  - Percutaneous disc decompression
  - Micro-endoscopic discectomy
  - Resection of extraforaminal disc herniations
- Risks and benefits of surgery compared to conservative therapy:
  - Risks – complications:
    - Spondylodiscitis
    - Hemorrhage
    - Wound infection
    - Nerve root damage
    - FBSS
  - Benefits:
    - Early pain relief

radiologists to the degeneration of the disc itself as a result of the growing awareness of the clinical entity "lumbar disc herniation", its surgical treatment and the impact this treatment has on national health services. Lumbar discectomies are among the most common elective surgical procedures performed in North America (Taylor et al. 1994). In Belgium, the incidence of lumbar discectomies was 1 in 1000 in 2004.

In the near future, however, pathology of the facet joints will become as important as that of the disc itself. Spine surgeons all over the world are becoming increasingly interested in total disc replacement strategies. The use of lumbar disc prosthesis is already common in Europe and will soon explode in North America, as soon as clinical results can demonstrate its superiority over other surgical treatment options (Geisler et al. 2004). Total disc replacement by a disc prosthesis can only be of any use if the facet joints are intact and are as such not responsible for any clinically relevant pain. When both the intervertebral disc and the facet joints are degenerated and both are responsible for pain, they should both be replaced. Some facet joint implants have already been designed and patented. They are currently undergoing mechanical testing but have not been used in clinical trials. Thus the three degenerated joints (one disc and two facets) will be replaced by three artificial joints (one disc prosthesis and two facet joint prostheses).

14.3 Pathophysiology of Lumbar Disc Herniation

Although the incidence of low back pain is about 60%, the incidence of low back pain with sciatica is only 1%. Sciatica is most commonly due to herniation of parts of a lumbar disc. Since 90% of disc herniations occur at the level of the two lowest lumbar discs, the referred pain is within the distribution of the sciatic nerve, hence the name sciatica. Such a disc herniation, however, may not be a prerequisite for radicular pain.

Root entrapment syndrome may affect the lumbar root in the spinal canal, in the foraminal canal or even outside this foraminal canal. In our own series, we reported such "extraforaminal" location in 13% of all lumbar disc herniations (Van de Kelft et al. 1994). The radiologist, when he has no clinical information, often overlooks this pathology, especially on poor resolution CT images. A clear L4 pathology with a normal spinal canal at L3–L4 should urge the radiologist to look for an extraforaminal location of

an extruded disc fragment at L4–L5. It is also important to notice that a disc bulging or protrusion seldom reaches the root at a foraminal and never at its extraforaminal location. This is only possible for an extruded disc fragment.

In an extreme situation there may be a massive nuclear protrusion in which a large volume of disc material is suddenly thrust into the spinal canal, producing a "profound neurological catastrophe", such as a cauda equina syndrome. In this case progressive sensory loss and motor weakness of the legs is associated with sphincter disturbances. The physician on duty will urge the radiologist for an immediate diagnosis, since this condition has to be treated surgically as soon as possible. The best option for the correct diagnosis is MRI. If unavailable, a CT myelogram should be carried out, even at night, since a poor resolution CT scan may give false negative results; the herniation may be so large that it completely fills the spinal canal making the differentiation from its normal content extremely difficult.

The initial symptoms of sciatica often occur without a precipitating event or following a seemingly trivial movement or maneuver and are typically not particularly incapacitating. At this moment, a tear in the annular ring appears which can be well demonstrated on MRI. As the inflammation (as a result of the annular tear) progresses, the symptoms crescendo in a relentless fashion. Most patients experience paraspinal muscle spasms directed at stabilizing the affected level. At that time the sciatica appears with irradiating pain in the leg according to the dermatomal distribution of the affected nerve root. Through the annular tear, the nucleus pulposus has protruded as a herniated fragment compressing the nerve root. The irradiating pain is the result of mechanical compression of the nerve root. The precise distribution of leg pain varies according to the root involved. Compression of the S1 nerve root usually starts as a dull pain in the back or the thigh or buttock, but can later involve the posterior or lateral aspects of the calf, as well as the heel and the sole of the foot. Compression of the L5 nerve root is characterized by pain that runs more at the anterior side of the leg into the big toe. A typical L4 pain runs more in front of the leg and around the knee, to end half way the tibia. This typical pain is often caused by an extraforaminal disc herniation at L4–L5.

Following mechanical compression, the root becomes inflamed due to this mechanical trauma. This inflammation can be dealt with during the conservative treatment, but is often responsible for a long-lasting dull aching or burning limb pain, even when the nerve root is fully decompressed. The initial goal of conservative therapy is to diminish the pain caused by inflammation. Usual conservative treatment consists of bed rest, non-steroidal anti-inflammatory drugs, muscle relaxation and, if necessary, epidural steroids. There seems to be no significant difference in outcome when conservative treatment is compared to the natural history of sciatica. After the acute onset of sciatica, more than 50% of patients will improve significantly under conservative treatment after 2 months (Saal 1996).

14.4 Surgical Treatment

14.4.1 Indications

There is some controversy about the usefulness of surgery versus nonoperative treatment in managing these patients. The majority of patients with lumbar disc herniations and sciatica will improve over time with conservative treatment. There is a tendency, however, to operate on these patients a few weeks after the onset of their initial symptoms. The surgical technique becomes minimally invasive (nucleoplasty, micro-endoscopic discectomy) and can be performed on an outpatient basis (Foley and Smith 1997; Smith and Foley 1998). It is our task to return a patient with sciatica in a prompt and effective manner to his or her previous level of function as soon as possible.

Indications for surgery can be divided into absolute and relative indications (Table 14.1).

14.4.1.1 Absolute Indications for Surgical Treatment

There are three absolute indications for surgical treatment of acute sciatica due to a herniated lumbar disc which will be discussed in the following sections.

14.4.1.1.1 The Cauda Equina Syndrome

In cauda equina compression with bladder and/or bowel incontinence, which is often not obvious at

Table 14.1. Indications for surgery in patients with a herniated lumbar disc

Absolute indications
Cauda equina syndrome
Weakness and sensory loss
Persistent pain
Relative indications
Failure of symptom relief after 2–4 weeks of appropriate conservative therapy
Radicular pain in a dermatomal pattern
Sensory loss in the same dermatome
Weakness in the correct distribution
Depressed tendon reflex appropriate to pain, weakness and sensory loss
Limited straight-leg raising with reproduction of radicular pain
Abnormal neuro-imaging (CT or MRI) consistent with the neurological deficit

the time of admission, urgent decompression of the cauda is mandatory. This is the only indication for urgent lumbar disc surgery. Every attempt to treat this disorder conservatively will end in court. Often, even after adequate surgical decompression with complete relief of pain, the bowel or bladder incontinence persists for months or becomes permanent.

14.4.1.1.2 Weakness and Sensory Loss

The presence of significant neurological deficits such as weakness and/or sensory loss, which affects 5%–20% of patients with acute sciatica, is a good indication for surgery without delay. It seems obvious that a neurological deficit due to mechanical compression of the nerve root will resolve better the earlier the root can be liberated. Some authors showed, however, that delays of up to 3 months had a minimal effect on the ultimate recovery of strength (Hakelius 1970).

14.4.1.1.3 Severe Persistent Pain

Clearly not all patients have the opportunity to rest and undergo conservative treatment of their sciatica. Busy people with severe incapacitating leg pain due to a herniated disc fragment often urge us to find an immediate yet elegant solution for their problem. The more surgery becomes minimally invasive due to microsurgical and endoscopic techniques, and the more this surgery can be done on an outpatient basis, the more it becomes an attractive alternative for relief of symptoms, even after the first week of symptoms. As will be discussed later, the benefit of surgery is the swift relief of symptoms. The long-term outcome is comparable to that of conservative treatment and even with that of natural evolution.

14.4.1.2 Relative Indications for Surgical Treatment

The American Association of Neurological Surgeons (AANS) and the American Academy of Orthopaedic Surgeons have listed seven indications for surgical treatment of a herniated lumbar disc disease:

- Failure to relieve symptoms after 2–4 weeks of appropriate conservative therapy
- Radicular pain in a dermatomal pattern
- Sensory loss in the same dermatome
- Weakness in the correct distribution
- Depressed tendon reflex appropriate to pain, weakness and sensory loss
- Limited straight-leg raising with reproduction of radicular pain
- Abnormal neuro-imaging (CT scan or MRI) consistent with the neurological deficit (Long et al. 1988)

In these cases it is up to the patient whether he decides to resolve the pain by surgery or whether he prefers to wait for the results of conservative treatment. Weber (1983) reported a prospective, randomized study in which surgery was compared to conservative therapy. The study showed that, although surgery of lumbar disc herniations was superior to nonoperative treatment at 1 year, results at 4- and 10-year follow-up showed no statistical difference (Weber 1983). Although surgery may provide more rapid relief of pain, the ultimate result is approximately the same regardless of treatment, with long-term resolution of sciatica approaching 87%. This study was undertaken 25 years ago; conservative treatment did not change spectacularly in this period; surgery, however, did.

14.4.2 Risks and Benefits

If, according to a 25-year-old study, there is no difference in outcome when surgery is compared to conservative therapy, and if surgery always carries some operative risk, what then is its benefit (Fig. 14.1)

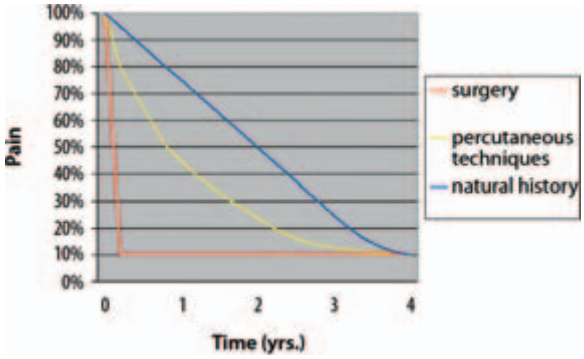

Fig. 14.1. Evolution of pain in patients with a lumbar disc herniation. According to Weber's study, there is no statistical difference in outcome after 4 years when comparing natural history, percutaneous techniques or surgery in the treatment of a lumbar disc herniation. It is obvious, however, that surgery is able to relieve symptoms more quickly. Degenerative disc disease can be responsible for recurrent low back pain in all non-disc-replacing therapeutic options

(Weber 1983)? Clearly there is a benefit in terms of the so-called absolute indications, especially the cauda equina syndrome. For the relative indications the benefit lies in early pain relief in comparison to conservative treatment. Therefore, it is better to operate a patient with acute sciatica of 4 weeks' duration, than one with chronic sciatica over a period of 6 months, since the latter may be close to the spontaneous resolution of his problems. The relative benefit of surgery will be comparatively small in this case. Additionally, recovery of the root might also be problematic after mechanical compression of 6 months' duration.

Most patients are afraid of lumbar disc surgery and many have heard stories of someone who was left plegic following surgery. Although the theoretical risk of serious nerve root damage exists, in practice it almost never occurs. The most serious risk of lumber surgery, with an incidence of 0.04%, is spondylodiscitis (Van Goethem et al. 2000). This involves extreme low back pain occurring weeks to months after surgery and a hospital stay of several weeks since the treatment consists of antibiotics over at least a 6-week period. Wound hematoma and superficial wound infection are minor risks.

Procedures for removal of the herniated disc fragment have two major goals: to relieve pain immediately and to prevent recurrence. The first goal can be accomplished in more than 90% of cases. The second is more difficult. The more the surgeon tries to prevent any recurrence, implying near total disc removal, the more the intervertebral disc will collapse, resulting in facet joint pain. Furthermore, recurrence of a herniated disc is not typical in operated patients: there is no difference in recurrence between operated and non-operated patients (Weber 1983). The disc itself will degenerate once an annular tear has appeared. Consequently, low back pain can occur due to disc degeneration in operated as well as in non-operated patients. Therefore, in the author's opinion, recurrence and persistent low back pain after conservative or surgical therapy is not a complication, but rather a logical consequence of the natural history of disc degeneration (Van de Kelft et al. 1996). In 2004 we started a phase three clinical trial as part of a multicenter study using a mixture of elastin and silk injected into an operated disc to seal the annular tear or the surgically created annular opening. This procedure has two goals: to prevent recurrent herniation of previously operated discs and to restore the disc height by replacing the amount of resected nucleus with the product mentioned above.

A major "complication" after surgery is the so-called FBSS occurring in less than 1% of all operated patients (Samy Abdou and Hardy 1999). Its origin is unknown, but the syndrome consists of a dull burning pain in the limbs, occurring weeks to months after surgery. Successful treatment of these patients requires a correct diagnosis of the underlying process prior to further intervention. Surgery may benefit patients with recurrent disc herniation, segmental instability, or spinal stenosis, but patients with epidural fibrosis and arachnoiditis (together accounting for about 20% of all FBSS patients) are less likely to obtain a satisfactory outcome from surgical re-intervention (Van de Kelft and De La Porte 1994). Spinal cord stimulation may benefit about half of these patients (Samy Abdou and Hardy 1999). Today, there are neither technical guidelines nor products available to prevent peridural scarring (Robertson et al. 1999).

14.4.3 Surgical Technique

As indicated earlier, there is a strong tendency to minimize tissue damage and to operate patients early in order to rehabilitate them faster. Therefore, many percutaneous techniques have been developed in recent years. Other than the chemical dissolution of the nucleus (chymopapain), a technique that is no longer in use, new techniques focus on the mechanical treatment of the pathological disc. It is of extreme importance to notice that all of these

techniques have the same clinical indications as the classical surgical one (i.e. microdiscectomy), but can only be carried out with a reasonable success rate if the herniation is contained by an intact outer annular ring. Even discography cannot help establish this diagnosis.

Minimally invasive intradiscal techniques that provide percutaneous access to the discs are chemonucleolysis, percutaneous nucleotomy, automated percutaneous lumbar discectomy, intradiscal laser discectomy, and intradiscal radiofrequency ablation. Nucleoplasty is a non-heat driven process that employs coblation technology using bipolar radiofrequency technology applied to a conductive medium (i.e. saline) to achieve tissue removal with minimal thermal damage to collateral tissues (Nazariaz 1985).

14.4.3.1 Percutaneous Disc Decompression

The technique we use in our department is a nucleoplasty based on coblation (Robertson et al. 1999; Nazariaz 1985; Singh et al. 2003; Mochida et al. 2001). Percutaneous disc decompression using coblation (nucleoplasty) is performed on an outpatient basis under monitored anesthesia care in the operating room.

All procedures are performed under strict sterile conditions using fluoroscopic guidance with the patient in a prone or semi-oblique position. A 17-gauge 6-in. Crawford-type spinal access cannula is placed at the junction of the annulus and nucleus. A PercDLE wand (ArthroCare, Inc., Sunnyvale, CA) is advanced into the disc via the spinal access cannula. After confirming that proximal and distal channel limits are within the disc, decompression is initiated. The decompression process involves advancing the wand, in ablation mode, to the distal channel limit at a speed of 0.5 cm/s and retraction of the wand in coagulation mode, to the proximal channel limit at the same speed (Fig. 14.2).

Six channels are created at the twelve, two, four, six, eight, and ten o'clock positions. Postoperatively, patients are allowed limited walking, standing and sitting as needed in daily-life activities; however, they are instructed to limit bending, stooping and

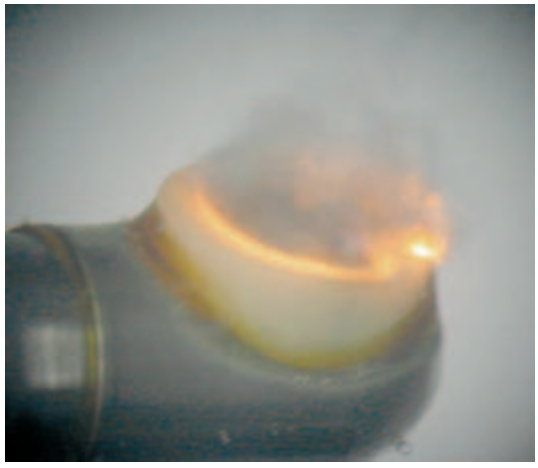

a

b

c

Fig. 14.2a–c. Disc coblation. **a** The coblation technique is based on a heat producing canula that coagulates and aspirates parts of the nucleus. **b** Under fluoroscopic guidance, a 17-gauge spinal cannula is placed in the center of the nucleus. **c** In a forward-backward mode, six channels are created in the nucleus

lifting more than 5 kg (10 lbs) for 2 weeks. Patients with sedentary or light work environments are allowed to return to work after 2 weeks. A qualified instructor provides patients with home exercise instructions.

14.4.3.2 Micro-endoscopic Discectomy

Annular integrity is an important variable in achieving a beneficial outcome in patients undergoing disc decompression. Annular repair occurs very gradually and a large incision into a degenerated-herniated disc will result in a decrease in annular strength during the healing process (Ahlgren et al. 2000). Analysis of proteoglycan synthesis and degradation indicate that replacement of proteoglycan molecules within the disc may take up to 3 years (Stathopoulos and Cramer 1995). Three separate analyses have concluded that the box incision method leads to significantly poorer healing, a decrease in strength of 40%–50%, and an increase in severe and early disc degeneration (Ahlgren et al. 1994; Ethier et al. 1994). Another study indicates that square, circular, cross, and slit incisions each produce a larger range in motion during axial moment loading (Ahlgren et al. 2000). Annular entry with a 2.5-mm OD trocar maintained disc integrity during biomechanical loading (Natarajan et al. 2002). Once the annular ring has been opened, subtotal or total discectomy can be carried out. Biomechanical studies show, however, that translational as well as rotational instability is less following subtotal discectomy (Nazariaz 1985). It is these findings that have further lent support to the approach of discectomy without curettement. In special indications we do remove the total nucleus with the intention of replacing it with a prosthesis like the prosthetic disc nucleus (PDN) (Fig. 14.3). This technique, while very challenging, is also very promising. It is not always obvious to see the PDN on MR, especially if the surgical procedure is not known while interpreting the images.

The most important goals for surgical treatment of lumbar disc herniation are therefore:

- Removal of the herniation causing symptoms.
- If unnecessary, try to avoid making holes in the annulus.
- Remove as little as possible of the remaining disc material.
- Choose a minimally invasive access to promote early recovery and rehabilitation and to minimize hospital stay and cost.

Fig. 14.3. Prosthetic disc nucleus (PDN device). Note the PDN device in the center of the L5–S1 disc (*white arrow*). Without relevant clinical information, recognizing the device itself can be problematic

Bearing these goals in mind, we actually perform a micro-endoscopic discectomy in all patients with an indication for surgical treatment and a contraindication for percutaneous nucleoplasty.

The main advantage of the METRx system (Medtronic Sofamor Danek, Memphis, TN) in comparison to a traditional discectomy is a smaller incision and less damage to the muscles of the spinal column (Foley and Smith 1997). This advantage is achieved by allowing the surgeon to expose the area where the herniated disc is located without making a large incision. A discectomy that is done with the METRx system begins with the surgeon precisely localizing the level of the herniated disk with a very small needle that is inserted through the muscles of the back down to the area where the disk fragments are located (Fig. 14.4). The correct position of this needle is confirmed by fluoroscopy, after which a series of soft-tissue dilators are used to create a small tunnel measuring 16 mm in diameter (less than ¾ of an inch) through the muscles of the back, enabling a hollow tube to be inserted down to the level of the spinal column. This tube, which is called a tubular retractor, contains a highly specialized video camera with a magnifying lens and a fiber optic light source that illuminates the tissues and relays the im-

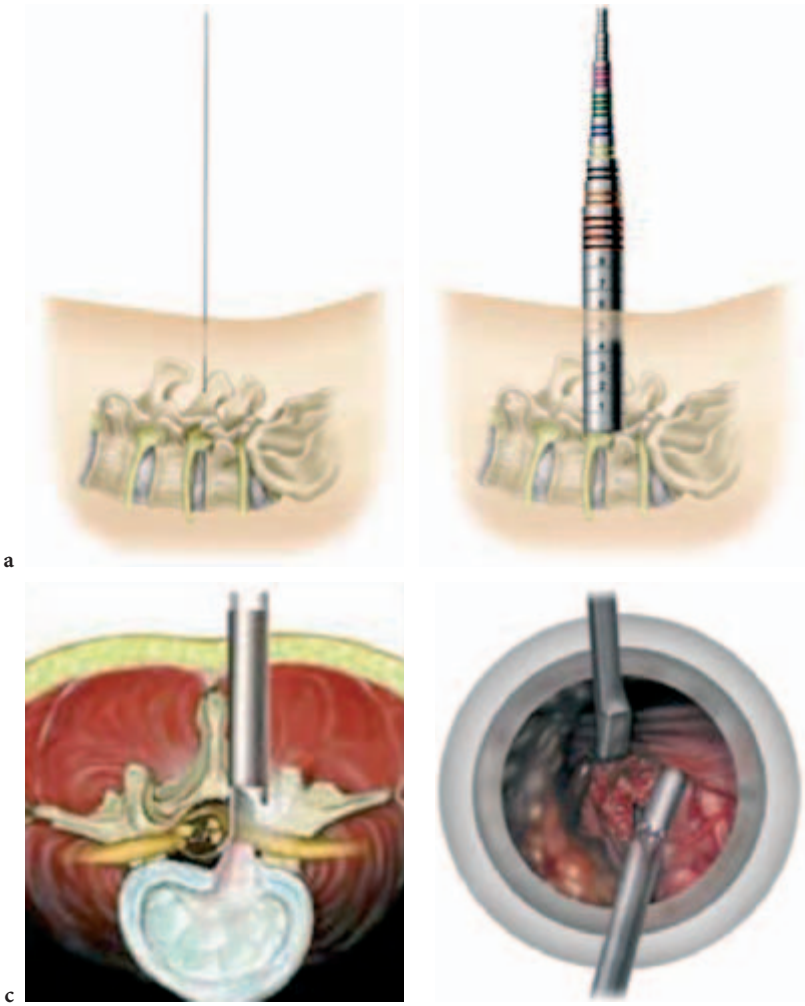

Fig. 14.4a–d. Micro-Endoscopic Discectomy. **a** K-wire inserted percutaneously at the L4–L5 junction. The correct position of this needle is confirmed by fluoroscopy. **b** After the correct position of the needle has been confirmed with fluoroscopic guidance, a series of soft-tissue dilators are used to create a small tunnel that measures 16 mm in diameter (less than ¾ of an inch) through the muscles of the back so that a hollow tube can be inserted down to the level of the spinal column. **c** This tube, which is called a tubular retractor, contains a highly specialized video camera with a magnifying lens and a fiberoptic light source that illuminates the tissues and relays the images to a separate video screen so that the surgeon can operate safely. Once the tubular retractor is in the correct place the surgeon is able to visualize the area where the herniated disk is located. **d** After a small laminotomy and flavectomy, he or she is able to remove the fragments of the disk with special instruments that fit down the inside of the tubular retractor. (Reproduced with permission from Medtronic Sofamor Danek)

ages to a separate video screen so that the surgeon can operate safely.

Once the tubular retractor is in the correct place the surgeon is able to visualize the area where the herniated disc is located. After a small laminotomy and flavectomy, he or she is able to remove the fragments of the disc with special instruments that fit into the tubular retractor. When the operation is finished, the tubular retractor is removed and the incision, which is less than 16 mm (1 in). in length, is closed and the wound is allowed to heal.

14.4.3.3 Resection of Extraforaminal Disc Herniations

It is a relatively common phenomenon to encounter extreme lateral nerve root entrapment in patients with L4 symptoms when one is looking for it (Van de Kelft et al. 1994). In 1994 we presented a surgical technique that approaches the disc fragment not from intraspinally, but from outside the spinal structures (Van de Kelft et al. 1994). In this microsurgical approach the incision is centered on the

spinous process of the upper vertebra, i.e. slightly more upwards compared to the classical interlaminar approach. We prefer a paramuscular approach and therefore retract the muscle by a self-retaining retractor. We then aim for the junction between the pedicle and the transverse process. The nerve root in these cases is always pushed cranially against the pedicle. Once the pedicle is identified, the nerve root can be easily tracked. Caudally we find the extruded fragment. In fact, we only remove this fragment and perform a non-classical discectomy. Once the nerve root is no longer compromised between the disc fragment and the pedicle, we retract the retractor and close the skin. This technique has the advantage of seeing the herniated fragment clearly, as well as the nerve root, while preserving all spinal structures. If one aims for an extraforaminal disc fragment by the classical intraspinal interlaminar approach, one ends up with a destroyed or even removed facet joint, because the herniated fragment can otherwise not be seen or reached.

More recently we carry out the same procedure in an endoscopic way, with the tools as described earlier.

14.5 Conclusions

Once a trial of conservative treatment has been attempted, it may be wise to proceed with a surgical intervention on a patient suffering from sciatica due to a herniated lumbar disc. With the exception of the absolute indications, we see that the relative indications become more popular because of the advent of minimally invasive disc surgery that is performed on an ambulatory basis. Given this, the patient can benefit maximally from surgery as a result of early relief of symptoms and full resumption of previous functions. Nevertheless, the patient should be informed that the long-term outcome is comparable to the outcome of conservative therapy.

References

Ahlgren BD, Lui W, Herkowitz HN et al. (2000) Effect of anular repair on the healing strength of the intervertebral disc: a sheep model. Spine 25:165–170

Ahlgren BD, Vasavada A, Brower RS et al. (1994) Anular incision technique on the strength and multidirectional flexibility of the healing intervertebral disc. Spine 19:948–994

Dowd GC, Rusich GP, Connolly ES (1998) Herniated lumbar disc evaluation and management. Neurosurg Quarterly 8:140–160

Ethier DB, Cain JE, Yaszemski MJ et al. (1994) The influence of annulotomy selection on disc competence. A radiographic, biomechanical, and histologic analysis. Spine 19:2071–2076

Foley KT, Smith MM (1997) Microscopic discectomy. Tech Neurosurg 3:301–307

Geisler FH, Blumenthal SL, Guyer RD et al (2004) Neurological complications of lumbar artificial disc replacement and comparison of clinical results with those related to lumbar arthrodesis in the literature: results of a multicenter, prospective, randomized investigational device exemption study of Charité intervertebral disc. Invited submission from the Joint Section Meeting on Disorders of the Spine and Peripheral Nerves, March 2004. J Neurosurg Spine 1:143–154

Hakelius A (1970) Prognosis in sciatica: a clinical follow-up of surgical and non-surgical treatment. Acta Orthop Scand 121:S1

Long DM, Filtzer DL, BenDebba M (1988) Clinical features of the failed back syndrome. J Neurosurg 69:61–71

Mochida J, Tos E, Nomura T et al. (2001) The risks and benefits of percutaneous nucleotomy for lumbar disc herniation: a 10-year longitudinal study. J Bone Joint Surg Br 83:501–505

Mouw LJ, Hitchon PW (1996) Pathogenesis and natural history of degenerative disc and spinal disease. In: Tindall GT, Cooper PR, Barrows DL (eds) The practice of neurosurgery. Williams & Wilkins, Baltimore, pp 2357–2366

Natarajan RN, Andersson GB, Patwardhan AG et al. (2002) Effect of annular incision type on the change in biomechanical properties in a herniated lumbar intervertebral disc. J Biomech Eng 124:229–236

Nazariaz S (1985) Anatomical basis of intervertebral disc puncture with chemonucleolysis. Anat Clin 7:23–32

Robertson JT, Maier K, Anderson RW, Mule JL, Palatinsky EA (1999) Prevention of epidural fibrosis with Adcon-L in presence of a durotomy during lumbar disc surgery: experiences with a preclinical model. Neurol Res 21[Suppl 1]:S61–S66

Saal JA (1996) Natural history and nonoperative treatment of lumbar disc herniations. Spine 21[Suppl 24]:2S–9S

Samy Abdou M, Hardy Jr RW (1999) Epidural fibrosis and the failed back surgery syndrome: history and physical findings. Neurol Res 21:55–57

Smith MM, Foley KT (1998) Microendoscopic discectomy (MED): the first one hundred cases. Neurosurg 43:702

Stathopoulos PC, Cramer GD (1995) Microscopic anatomy of the zygapophyseal joints and intervertebral discs. In: Cramer GD, Darby SA (eds) Basic and clinical anatomy of the spine, spinal cord and ANS. Mosby Year Book, St. Louis, pp 393–419

Taylor VM, Dey RA, Cherkin DC et al (1994) Low back pain hospitalization. Recent United States trends and regional variations. Spine 19:1207–1213

Van de Kelft E, De La Porte C (1994) Spinal cord stimulation in failed back surgery syndrome. Qual Life Res 3:21–27

Van de Kelft E, Segnarbieux A, Candon E, Bitoun J, Frèrebeau Ph (1994) Disco-computed tomography in extraforaminal and foraminal lumber disc herniations: influence on surgical approaches. Neurosurgery 34:643–648

Van de Kelft E, Van Goethem J, De La Porte Ch, Verlooy J (1996) Early postoperative gadolinium-DTPA-enhanced MR imaging after successful lumbar discectomy. Br J Neurosurg 1:41–49

Van Goethem J, Parizel PM, van den Hauwe L, Van de Kelft E, Verlooy J, De Schepper A (2000) The value of MRI in the diagnosis of postoperative spondylodiscitis. Neuroradiol 42:580–585

Singh V, Piryani C, Liao K (2003) Evaluation of percutaneous disc decompression using coblation in chronic back pain with or without leg pain. Pain Physician 6:273–280293-302

Weber H (1983) Lumbar disc herniation: a controlled, prospective study with ten years of observation. Spine 8:131

Imaging of the Postoperative Spine: Discectomy and Herniectomy

15

Johan W. M. Van Goethem and Rodrigo Salgado

CONTENTS

J. W. M. Van Goethem, MD, PhD
Department of Radiology, University Hospital Antwerp, Wilrijkstraat 10, 2650 Edegem, Belgium
and
Department of Radiology, AZ Nikolaas, Moerlandstraat 1, 9100 Sint-Niklaas, Belgium
R. Salgado, MD
Department of Radiology, University Hospital Antwerp, Wilrijkstraat 10, 2650 Edegem, Belgium

15.1 Introduction

Low-back pain (LBP) is a frequent complaint and a leading cause of disability in the general population. Epidemiological studies have identified many individual, psychosocial, and occupational risk factors for its onset, but the primary causative mechanisms of LBP remain largely undetermined. Psychological factors have an important role in the transition from acute to chronic pain and related disability (Manek and MacGregor 2005). Recent advances show that there is also a significant genetic effect on severe LBP, a condition which is responsible for a substantial loss in productivity. The total costs of LBP in the US exceed $100 billion per year (Katz 2006). Two-thirds of these costs are indirect, due to lost wages and reduced productivity. Each year, the less than 5% of the patients who have an episode of LBP account for 75% of the total costs (Jinkins 1997). Most episodes of LBP have a mechanical origin and are self-limiting, resolving within a few days or weeks (Borenstein 1996). There is considerable scope for prevention of the consequences of LBP such as recurrence, disability, and workloss. Different interventions and outcomes will be appropriate for different target populations, yet inevitably there is an overlap.

Some patients with degenerative disk disease and persisting pain, having exhausted almost every imaginable form of nonoperative therapy, finally seek surgical help. It would not be entirely unjustified for a spine surgeon to adhere to a totally avoidant approach to chronic LBP, rationalized by a reasonably legitimate nihilism regarding the presently available means of surgically managing LBP (Kwon et al. 2003). In cases where surgery is performed, it is the role of imaging studies to assist in diagnosing the cause of the complaints and to determine in which patients surgery is a possible indication. Some investigators suggest that surgery should not be performed unless diagnostic imaging demonstrates nerve-root compromise and/or when symp-

KEY-POINTS

- **Imaging technique:**
  - **Plain film**
    - Has little value in the non-instrumented postoperative spine
    - Assessment of the spine during physiological loading, stability/instability
  - **CT**
    - Shows laminotomy/laminectomy defect
    - Shows marking filament in case of textiloma
    - Is far less accurate than MR in
      - Differentiating recurrent disc from epidural scar
      - Evaluating early complications (hemorrhage, infection, etc.)
    - Helical CT is a valuable technique in evaluating (postoperative) spinal stenosis (central spinal canal, lateral recesses and/or foraminal)
  - **MRI**
    - Preferred imaging technique in the postoperative spine
    - First procedure in imaging the postoperative spine
      - Early complications (hemorrhage, infection, etc.)
      - Differentiating recurrent disc from epidural scar
    - Equal value to CT in the evaluation of spinal stenosis
- **Expected postoperative findings**
  - Interpretation of images in the first 6–8 postoperative weeks must be undertaken with caution
    - Especially on unenhanced images postdiscectomy changes can mimic the preoperative appearance
  - **Bone defect** – when present – is sometimes difficult to see on MRI
  - **Epidural fibrosis** is an expected finding in all postoperative patients
    - >6 Months after surgery: no or only minimal dural sac deformation
    - <6 Months after surgery: up to 25% deformation
  - **Enhancing endplates** in 1 out of 5 patients between 6 and 18 months after surgery
- **Complications**
  - **FBSS** (failed back surgery syndrome) in 10%–40% of patients
  - **Early complications**
    - **Hematoma**
      - <1% of patients
      - Hours to days after surgery
    - **Spondylodiscitis**
      - 0.1%–3% of patients
      - 7–28 days after surgery
      - NO spondylodiscitis unless: high SI of the disc space on T2 and enhancement of the disc space
      - Diagnosis is combination of clinical, laboratory, and imaging findings
    - **Pseudomeningocele**
      - Usually asymptomatic
  - **Recurrent disc herniation**
    - Recurrent herniation may be an indication for repeat surgery (success rate 10 times higher with repeat surgery for recurrent herniation compared to repeat surgery for epidural fibrosis alone)
    - Differentiation from epidural fibrosis:
      - No enhancement of recurrent herniation, but:
      - Peripheral enhancement often seen, represents fibrosis that is always present after surgery
      - Discrete enhancement possible if long period between injection and imaging (>10 min)
      - Natural evolution of recurrent herniation may take months to years, with gradually less non-enhancement representing resorption of disc material
        - Normally no mass effect with epidural fibrosis
        - Fibrosis only along the surgical route
    - Is not necessarily responsible for the patient's complaints
  - **Arachnoiditis**
    - Clumped nerve roots
    - Empty thecal sac
    - and/or enhancing intrathecal mass
  - **Stenosis**
    - Frequent cause of FBSS: 25%–29% of patients with FBSS
    - CT or MR

toms, clinical findings and imaging findings are consistent (Butt 1989).

Imaging assessment of the spine following surgery is complex and depends upon several factors, including the anatomy of the patient, the surgical procedure and the disease process for which it was performed, the age of the patient, the biomechanical condition of the underlying cortical and cancellous bone, intervertebral disc and musculoligamentous tissues, the time elapsed since the surgical procedure, and the duration and nature of the postsurgical syndrome (Van Goethem et al. 2002).

This chapter will only discuss imaging of the non-instrumented postsurgical spine, i.e., after herniectomy and/or discectomy. Imaging of the postsurgical spine with cages, prostheses and/or instrumentation is discussed in Chapter 17.

15.2 Imaging Technique

Imaging of the postsurgical spine is in general performed in patients with complications. These complications usually manifest themselves either as persisting or recurrent pain or as some form of neurological deficit. In the acute stage, surgical complications such as bleeding, infection, meningoceles/dural lacerations, or neurological deficits can be encountered. Recurrent disk herniation, stenosis, textiloma and arachnoiditis usually present as persisting or recurrent pain in a later stage (Table 15.1).

Plain film radiography has almost no use in the diagnostic work-up of the non-instrumented postoperative spine. Plain films do show the surgical laminectomy defect, but this has little value in cases of persisting pain or complications. In chronic postsurgical pain, plain film can be useful in evaluating spinal stability since it is one of the only imaging modalities that can be used in the upright patient both in neutral position and during flexion and extension.

Computed Tomography (CT) is useful in detecting and grading spinal and/or foraminal stenosis and can be used in the follow-up of stenosis after surgery. In the acute postsurgical stage CT has little role. CT can be superior in detecting and differentiating a postsurgical textiloma. The main role of CT in the postsurgical spine, however, is after instrumentation or fusion surgery (see Chap. 17).

Magnetic Resonance Imaging (MRI), because of its superior soft tissue resolution, is the preferred imaging modality in the evaluation of patients with recurrent clinical symptoms after discectomy and/or herniectomy (Grane 1998; Van Goethem et al. 1996). Tissue enhancement is much better detected with MRI than with CT (Bundschuh et al. 1990; Sotiropoulos et al. 1989), making the differential diagnosis of recurrent disc herniation versus epidural fibrosis much easier. Moreover, bone marrow edema, soft tissue inflammation, nerve root enhancement, hemorrhage, and facet joint inflammation are difficult or even impossible to detect on CT. Evaluation of spinal stenosis with MRI is also very accurate.

In routine imaging of the postoperative spine, both sagittal and axial MR images are usually obtained. In the sagittal plane, T1- and T2-weighted images (WI) offer complementary information.

On T2-WI, normal intervertebral discs are bright (i.e., give relatively high signal). With ageing and/or degeneration of the disc, water loss and collagen deposition occur, T2 relaxation time shortens, and the discs gradually become darker (i.e., low-signal degenerative or 'black-disc disease'). However, in fast spin-echo (SE) acquisitions with longer echo trains

Table 15.1. Etiology of FBSS and/or complications after surgery for disc herniation

	Early postsurgical	Late postsurgical
Procedure-related	Bleeding	Textiloma
	Infection	Arachnoiditis
	Dural tear – pseudomeningocoele	
	Nerve root lesion	
Mechanical	Residual disk hemiation	Recurrent disk hemiation
		Stenosis
		Instability
Diagnostic	Failure to identify the cause of pain	Failure to identify the cause of pain

lengths (ETL), normal discs also become somewhat darker due to certain physical effects. Therefore, sagittal T2-WI with a relatively short ETL (<10) are preferable to diagnose disc degeneration (Van Goethem 1999). Sagittal and axial T2-WI are also excellent for showing the spinal cord and the nerve roots of the cauda equina.

The normal epidural fat in the lumbar spine is very bright on T1-WI and contrasts well with the dural sac and the adjacent normal or pathological intervertebral disc. This is why axial T1-WI are of high value in the lumbar region. Furthermore, the high signal of normal epidural fat also contrasts well with postoperative epidural fibrosis which is dark.

Additional axial SE T1-WI after intravenous gadolinium-containing contrast medium (referred to hereafter simply as contrast-enhanced images) are mandatory in patients who have undergone prior disc surgery (Babar and Saifuddin 2002; Bradley 1999; Henk et al. 1999; Jinkins and Van Goethem 2001). The use of contrast medium is important in differentiating scar tissue (fibrosis) from recurrent disc herniation (Bradley 1999; Jinkins and Van Goethem 2001), which is essential since the latter is generally accepted to be a possible indication for further surgery (Suk et al. 2001). Epidural fibrosis shows early enhancement after gadolinium injection (Fig. 15.1). A recent recurrent disc herniation initially shows no enhancement since it has no vascularization (Fig. 15.2). However, it is surrounded by epidural fibrosis that does show enhancement (Fig. 15.3). Contrast medium diffuses from this epidural fibrosis into the disc material causing mild enhancement from the outside in, late after contrast injection. Therefore, images after gadolinium injection should be acquired as quickly as possible after injection (Van Goethem et al. 2002). This late disc enhancement is more pronounced with non-ionic contrast agents. Therefore, an ionic contrast agent is preferable in clinical imaging of patients with (supposed) recurrent herniated discs since the distinction between a disc fragment and scar tissue will be greater after the use of an ionic contrast medium compared to a nonionic one (Haughton et al. 2002).

Furthermore, assessment of the enhancement pattern of nerves, meninges, posterior spinal (zygoapophyseal or facet) joints and paraspinal soft tissues is important in some patients. Fast SE or fluid-attenuated inversion-recovery (FLAIR) T2-WI in addition to or instead of contrast-enhanced T1-WI have also been propagated in the differentiation of recurrent disc herniation from epidural fibrosis (Barrera et al. 2001; Mullin et al. 2000).

In the lumbar spine, fat-suppression techniques before and/or after contrast-enhanced T1-WI can further assist in differentiating between enhanc-

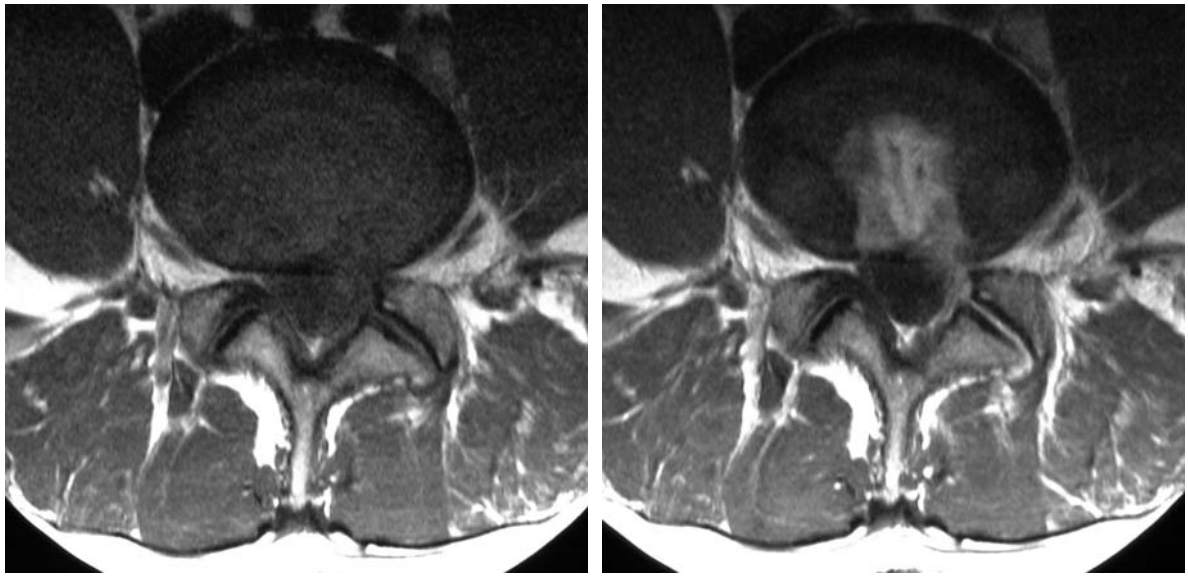

Fig. 15.1a,b. Expected postoperative finding: normal epidural and intervertebral fibrosis. Axial T1-WI before (**a**) and after (**b**) gadolinium enhancement. Patient 6 months after discectomy. Normal enhancing tissue in the left lateral epidural space representing normal epidural fibrosis (epidural scar). Note also extensive and expected intervertebral enhancement representing scar tissue along the discectomy tract. No residual disc herniation, no minimalthecal sac deformation and no spinal stenosis

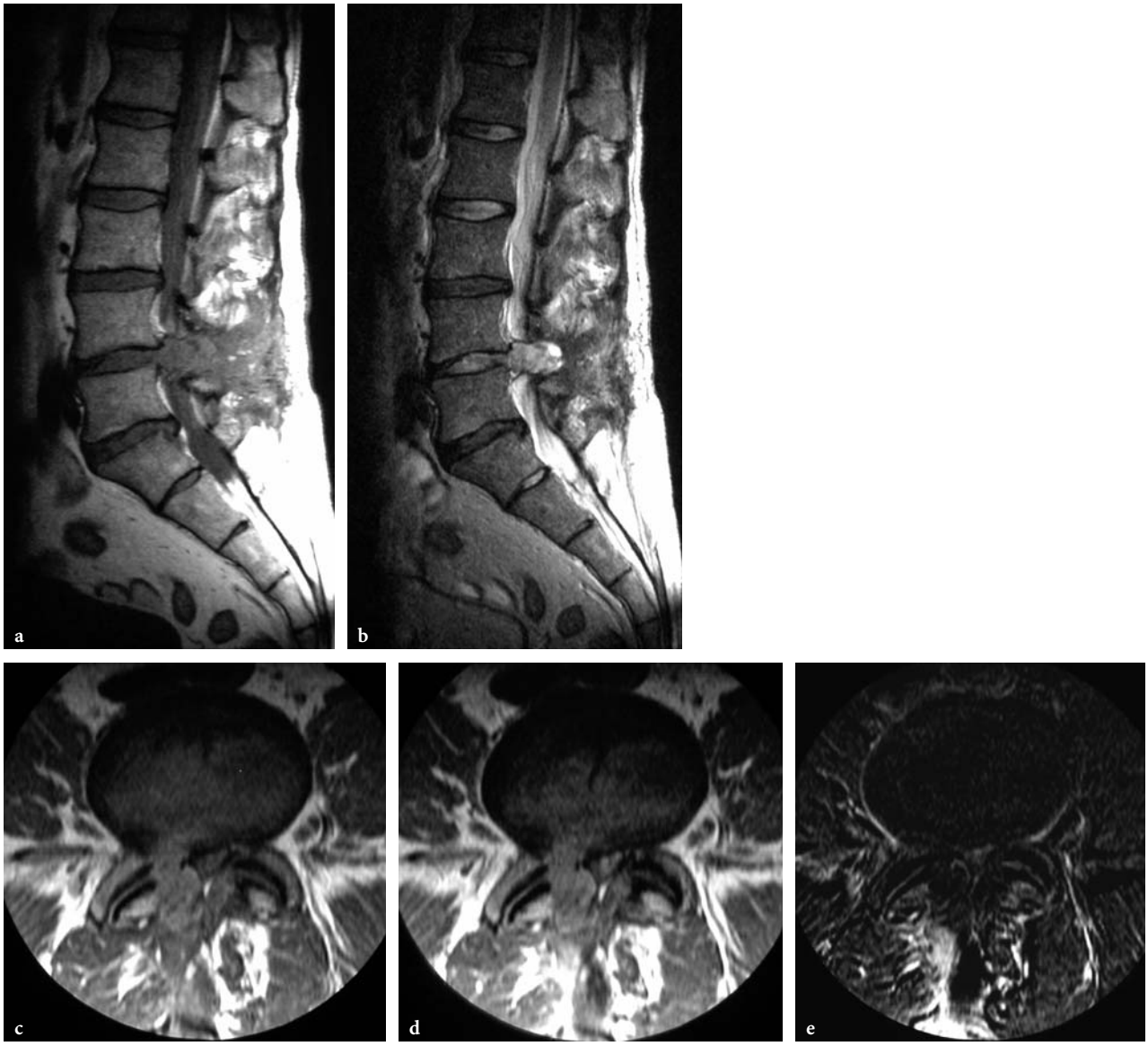

Fig. 15.2a–e. Massive recurrent disc herniation. Sagittal T1-WI (**a**), sagittal T2-WI (**b**), axial T1-WI (**c**), axial T1-WI after gadolinium enhancement (**d**) and subtraction (**e**). Sagittal images show a large mass extending from the intervertebral space in the right lateral epidural space and even through the laminectomy defect. The lesion is iso- to hyperintense on both T1- and T2-WI. The image after gadolinium enhancement only shows minimal peripheral enhancement, only visible on the subtraction image. Compare with the enhancement along the surgical tract lateral of the spinous process more posteriorly. This non-enhancement is the clue to the diagnosis. One should take care to image immediately after gadolinium injection to minimize possible diffusion of contrast medium into the disc fragment. The high signal on the T2-WI is highly suggestive for a recent recurrent herniation

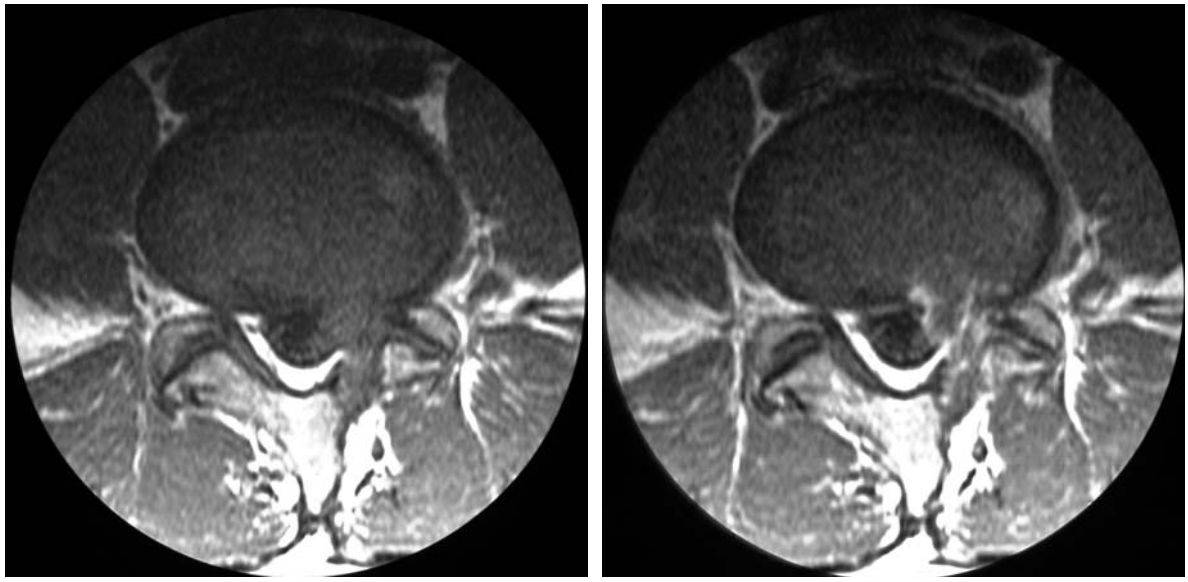

a b

Fig. 15.3a,b. Recurrent disc herniation. Axial T1-WI (**a**) and axial T1-WI after gadolinium enhancement (**b**). The non-enhancing portion of the lesion in the left anterior epidural space represents recurrent disc herniation. As in this case it is typically surrounded by enhancing epidural fibrosis

ing scar tissue and epidural fat and, in rare cases, between postoperative blood and normal epidural fat. Conversely, on fat-suppressed images abnormal postoperative nerve-root enhancement may be more difficult to differentiate from the normal slight pial-root enhancement.

MR myelography without contrast medium can be helpful in addition to standard imaging sequences.

Although spinal stimulators and other electronic implant devices such as cardiac pacemakers are normally a contraindication to MRI, some are MRI-compatible (Liem and van Dongen 1997; Shellock et al. 2000). Some devices must be switched off before entering the room containing the magnet – and switched on again upon exiting the room.

15.3 The Normal Postoperative Spine – Expected Postoperative Findings

Interpretation of images of the lumbosacral spine in the immediate postoperative period, i.e., the first 6–8 postsurgical weeks, must be undertaken with caution. Normal, or at least expected, postoperative changes occur within the bones, as well as the soft tissues, and vary in part depending on the type and extent of surgery and the time since the operation (Van Goethem et al. 1996).

Nowadays, herniectomy is regularly performed without laminotomy or laminectomy. Laminotomy is the partial removal of the lamina, while laminectomy is the complete removal of the lamina. Leaving the lamina intact without bone removal is more frequently seen at the lower lumbar levels, especially L5–S1, since there is more space between the lamina to access the spinal canal. Also, when using newer microsurgical and endoscopic techniques, the access way can be smaller and no bone (or less bone) has to be removed (Choi et al. 2006). In discectomy at the L5–S1 level, typically only the ligamentum flavum is incised and the posterior bony hemiarches are left intact. However, at L4–L5 and particularly at L3–L4, part of the hemiarch above has to be removed to obtain adequate access to the spinal canal (Van Goethem et al. 2002). If the nerve root has to be accessed, the medial border of the inferior articular process of the posterior spinal joint has to be resected at L4–L5 or L3–L4. It is therefore important to know the precise radial location of the herniated disc material in advance in order to preserve as much of the posterior spinal facet joints and the related posterior spinal bony elements as possible. Overzealous laminectomy or facetectomy may contribute to spinal instability and result in progressive spondylolisthesis. On MRI, the postsurgical absence of bone is sometimes difficult to assess,

especially in cases of laminotomy, but can be best demonstrated on axial T1-WI. There is often asymmetry in the paraspinal muscle fat planes posteriorly. The margins of the paraspinal musculature may also be temporarily indistinct secondary to edema in the subacute phase after surgery. The posterior border of the dural sac may expand posteriorly towards the surgical site and laminectomy defect, reflecting relative bony insufficiency (Fig. 15.4). This is an expected, clinically irrelevant finding and does not represent a pseudomeningocele (see 15.4.2.3).

On unenhanced images immediately after surgery, postdiscectomy changes can mimic the preoperative appearance of disc herniation in the epidural space because of disruption of the annulus fibrosus and edema of the epidural tissues. These blur the outline of the dural sac and the posterior margin of the intervertebral disc and may efface the anterior border of the thecal sac.

Homogeneous contrast enhancement of this epidural reaction may be observed (Fig. 15.1). The cause of this finding is granulation tissue and/or fibrosis, which explains the mild local epidural mass effect commonly seen in postoperative imaging of a clinically successful lumbar discectomy. In one study of asymptomatic patients following intervertebral disc surgery, all showed evidence of enhancing epidural fibrosis (Jinkins et al. 1993). In the asymptomatic postsurgical patient the accompanying deformation of the dural sac is minimal (<10% area deformation) 6 months or later after surgery. In the immediate postoperative phase, the deformation can be more extensive but was never more than 25% of the area of the dural sac (Van Goethem 1999).

Enhancing lumbosacral vertebral endplates have been observed between 6 and 18 months after surgery in 19% of patients, and enhancement of the posterior annulus fibrosis has been reported in the majority of asymptomatic patients (Shafaie et al. 1997). These are due to an aseptic reaction that can mimic early postoperative disc infection. Another study of asymptomatic patients showed residual or recurrent disc herniation at the operated level in 24% of patients within 6 weeks of surgery (Van Goethem et al. 1996). In 16% this was associated with mild to moderate mass effect on the dural sac and/or nerve roots or sleeves, and 5% had severe compression of the dural sac. In 78% of these patients with residual or recurrent herniation, there was no progression of the shape of the herniated disc on imaging, nor had the mass effect resolved on MRI after 6 months as compared with 6 weeks after surgery.

Fig. 15.4. Expected postoperative finding: bulging of the dural sac at the laminectomy defect. Sagittal T1-WI. Patient after L4 and L5 laminectomy. Expansion of the dural sac at the site of laminectomy is a reflection of bone insufficiency and does not represent true (pseudo-) meningocele and is clinically irrelevant

15.4 Failed Back Surgery Syndrome and Postoperative Complications

15.4.1 Failed Back Surgery Syndrome

Despite the relatively loose application of criteria for surgical success, lumbosacral spinal surgery has been unsuccessful so often in the past (10%–40% of cases) that failed back surgery is regarded as a syndrome: the failed back surgery syndrome (FBSS) (Shafaie et al. 1997). FBSS is defined as significant persistent back pain with or without radiating pain and/or various degrees of functional incapacity following back surgery. The most common causes include failure to recognize or adequately treat the cause of the pain, incomplete decompression, recurrent disc herniation, and spinal and/or foraminal stenosis (Van Goethem et al. 1997). Conservative estimates reveal that 10%–40% of back surgeries fail, although many studies indicate a much higher

percentage. Spinal surgery continues to dominate neurosurgical malpractice claims with 42% of the total, most from lumbar spine operations (Fager 2006). The best way to prevent FBSS is to avoid surgery that is apt to lead to an unsatisfactory result, hence the critical importance of thorough preoperative imaging evaluation. Still, the number of discectomy procedures in the US alone was around 300,000/year in the period from 1990 to 2000. Even with a conservative guess of 10% of patients with FBSS this represents at least 30,000 new cases in the US each year. In one study carried out among 35,309 patients undergoing an initial discectomy, 4943 (14.0%) had at least one reoperation and 803 (2.3%) had two or more reoperations, and as such patients with one reoperation after lumbar discectomy had a 25.1% cumulative risk of further spinal surgery in a 10-year follow-up (Osterman et al. 2003).

15.4.2 Early Complications

15.4.2.1 Hematoma

Although uncommon, occurring in less than 1% of patients, symptomatic postoperative hemorrhage typically presents hours to days following the spinal surgical procedure. MRI will show mixed blood breakdown products and is more sensitive than CT for both the detection of the hematoma and evaluation of its extent (Fig. 15.5). Some hematomas may reach rather large sizes and can extend into the central spinal canal to compress the spinal nerves and/or cord (Fig. 15.5). Such cases potentially constitute medical emergencies requiring urgent surgical evacuation.

15.4.2.2 Spondylodiscitis

Spondylodiscitis, or discitis combined with vertebral osteomyelitis, is a relatively uncommon but serious complication of spinal (disc) surgery, which may lead to long-lasting and sometimes permanent morbidity. It can be encountered after surgery or chemonucleolysis, but can also occur after diagnostic procedures such as discography and myelography (Fraser et al. 1986; Guyer et al. 1988; Scherbel and Gardner 1960). Postoperative spondylodiscitis occurs in about 0.4% of patients in the cervical spine (Bertalanffy and Eggert 1989), and between 0.1%–3% in the lumbar spine (Bircher et al. 1988; Lindholm and Pylkkanen 1982). Although the incidence of postoperative infection may be progressively decreasing due to better technical and prophylactic measures, it has not been completely eliminated. The infection is mostly due to direct intraoperative contamination (Tronnier et al. 1992), although a pre- or perioperative infection at another anatomical site or an underlying immunocompromising condition can also predispose. The organisms involved are usually *Staphylococcus epidermidis* or *Staphylococcus aureus* (Grane et al. 1998).

Early diagnosis and appropriate treatment are mandatory to shorten the disease course and reduce the severe sequelae of spondylodiscitis. The diagnosis of postoperative spondylodiscitis depends on a combination of clinical, laboratory, and imaging findings. It typically presents clinically with severe pain in the affected spinal region, with or without associated radiculopathy, and commonly 7–28 days after surgery (Dall et al. 1987).

Although diagnosing spondylodiscitis with the help of MRI in the non-operated patient can be quite straightforward, it is typically a more challenging problem in the postoperative spine. The operated disc level always shows more or less extensive changes due to the surgical intervention itself and the accompanying postoperative aseptic inflammatory response (Grane et al. 1998; Van de Kelft et al. 1996; Van Goethem et al. 1996). These alterations may include Modic type I (e.g., marrow edema) changes of the adjacent peridiscal vertebral marrow (Fig. 15.6) (Modic et al. 1988). In addition, normal contrast enhancement can be seen in the intervertebral disc space and along the vertebral endplates postoperatively (Grand et al. 1993).

MRI is probably the only imaging modality able to make a significant contribution to the diagnosis of postoperative spondylodiscitis (Van Goethem et al. 2000) (Fig. 15.7). Key points include:

- The absence of peridiscal marrow changes (i.e., low signal intensity on T1-WI and high signal intensity on T2-WI) makes the diagnosis of septic spondylodiscitis highly unlikely
- The same holds true for absence of enhancement of the intervertebral disc space.
- An enhancing soft tissue mass surrounding the affected spinal level in the perivertebral and epidural spaces is highly suggestive of septic spondylodiscitis, requiring further evaluation of such patients.

Fig. 15.5a–d. Postoperative hematoma. Sagittal T1-WI (**a**), sagittal T2-WI (**b**), axial T1-WI (**c**) and axial T1-WI after gadolinium enhancement (**d**). Patient with numbness in both legs 1 day after L5 laminectomy and L5–S1 discectomy. Emergency MRI shows inhomogeneous lesion with high SI on both T1- and T2-WI. This is the clue to the diagnosis since no other lesion has high SI on T1-WI before gadolinium enhancement. Axial images before and after gadolinium show more or less the same picture with a large hyperintense mass filling the spinal canal and obliterating the dural sac

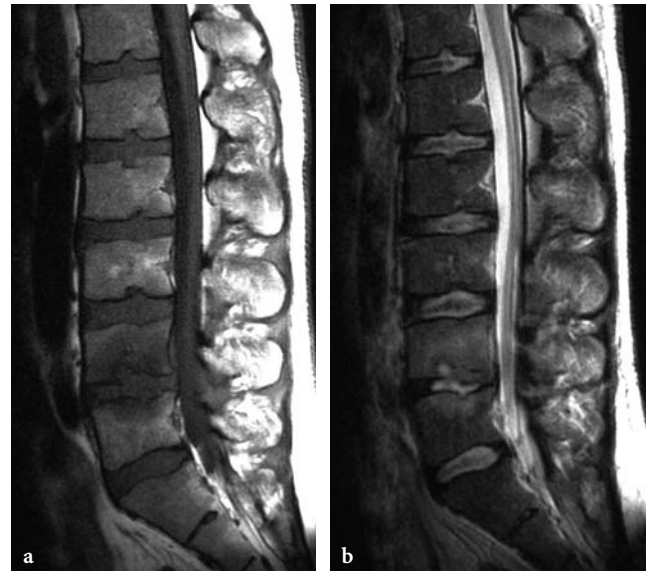

Fig. 15.6a,b. Postoperative 'aseptic' spondylodiscitis. Sagittal T1-WI (**a**) and sagittal T2-WI (**b**). Patient 2 weeks after L4–L5 discectomy with mild recurrent low back pain. High SI on T2-WI and low SI on T1-WI in the vertebral endplates adjacent to the operated intervertebral disc represents bone marrow edema. Also note partially high SI of the disc on T2-WI. The absence of laboratory findings and clinical symptoms consistent with or suggestive of septic spondylodiscitis, and the absence of (an evolution to) a completely bright disc on T2-WI, led to the diagnosis of 'aseptic' spondylodiscitis (inflammatory changes without infection)

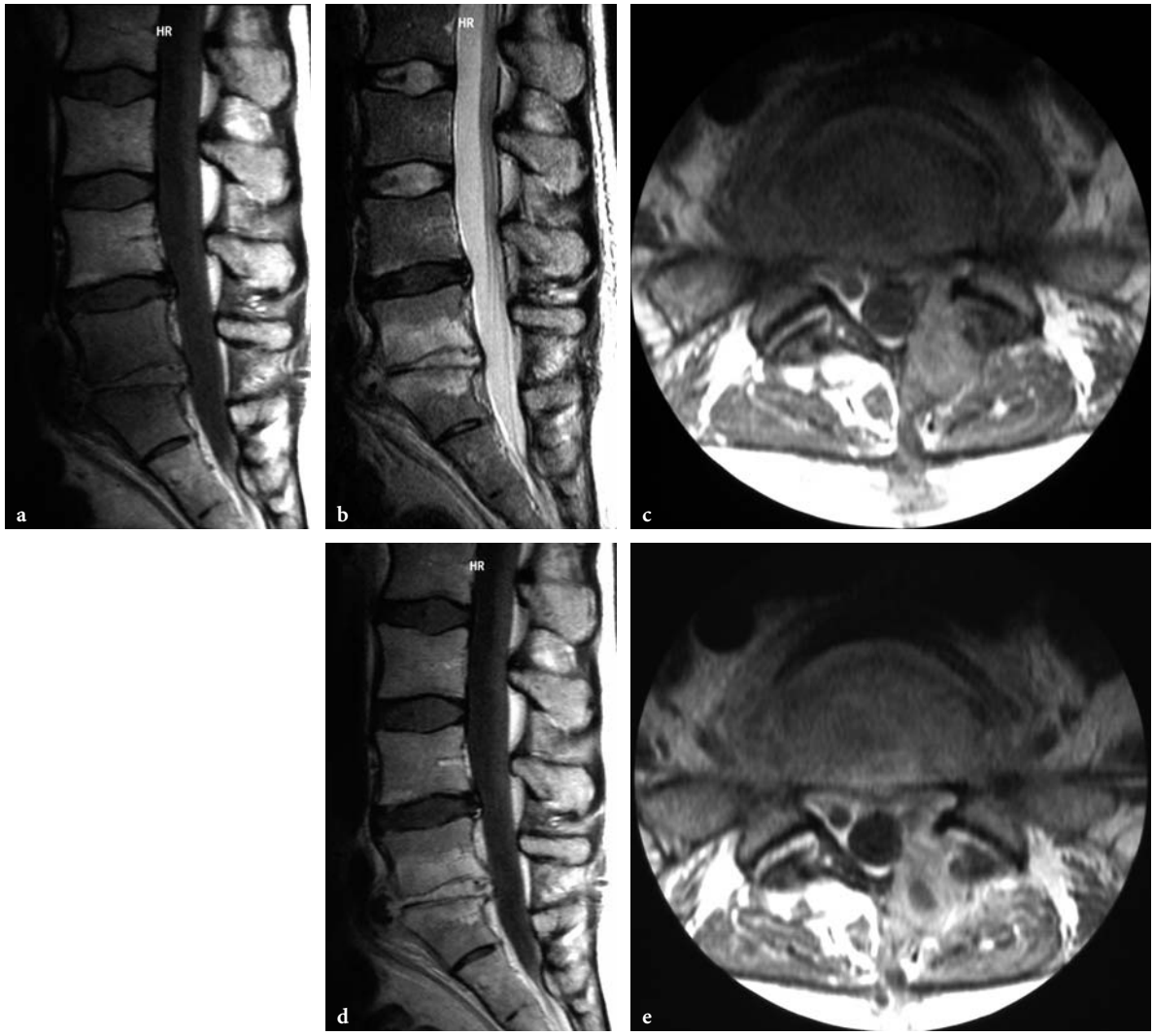

Fig. 15.7a–e. Postoperative spondylodiscitis. Sagittal T1-WI (**a**), sagittal T2-WI (**b**), axial T1-WI (**c**), sagittal (**d**), and axial T1-WI after gadolinium enhancement (**e**). Patient 3 weeks after L5–S1 discectomy with severe recurrent low back pain. In comparison to Fig. 15.6 the complete intervertebral disc has high SI on T2-WI. Also note extensive enhancement in the intervertebral space and in the adjacent bone marrow. In addition there is a large enhancing soft tissue mass in the paravertebral space around the intervertebral disc and along the surgical route with focal abcedation (non-enhancing portion)

However, the role of MRI alone continues to be debated and is not universally accepted (Boden et al. 1992; Grane et al. 1998; Schulitz and Assheuer 1994). Therefore, in inconclusive cases, one should attempt to confirm the diagnosis through percutaneous biopsy (Fouquet et al. 1992). A large bore nucleotome is needed (Onik 1996), since fine-needle aspiration is often negative in septic spondylodiscitis (Demaerel et al. 1994; Grane et al. 1998).

On the other hand, since most postoperative spinal infections are caused by *Staphylococcus aureus,* appropriate antibiotic therapy can be started in cases of probable spondylodiscitis even when no conclusive diagnosis is reached.

15.4.2.3 Pseudomeningocele

Pseudomeningoceles are CSF-filled collections extending from the central spinal canal into the perispinal soft tissues (Horowitz et al. 1990). It is an uncommon complication, being often an incidental finding causing no symptoms. These are not true meningoceles since they have no true

arachnoidal lining, but instead walls of reactive fibrous tissue.

Pseudomeningoceles typically develop after inadvertent surgical laceration of the dural sac during surgery or following incomplete closure of the dural sac in cases of intradural surgery. Usually, they protrude through a surgical bony defect of the posterior spinal elements to form a cystic lesion with imaging characteristics comparable to CSF both on CT and MRI (Fig. 15.8).

In the cervical spine, pseudomeningoceles mostly develop after an anterior approach, and here they may present a difficult challenge to treat (Andrew and Sidhu 2005). Patients with ossification of the posterior longitudinal ligament (OPLL) are especially prone to dural leaks and resultant pseudomeningocele formation.

In some cases, compression of nerve roots and/or the spinal cord may occur, causing symptoms. Spinal cord herniation in the pseudomeningocele is a rare but serious condition, requiring urgent intervention (Hosono et al. 1995).

15.4.3 Late Complications

15.4.3.1 Recurrent Disc Herniation – Epidural Scar Tissue

Differentiation between scar tissue and recurrent or residual disc herniation is important, since the latter is an indication for surgery. A recurrent disc herniation may actually be made up of disc mate-

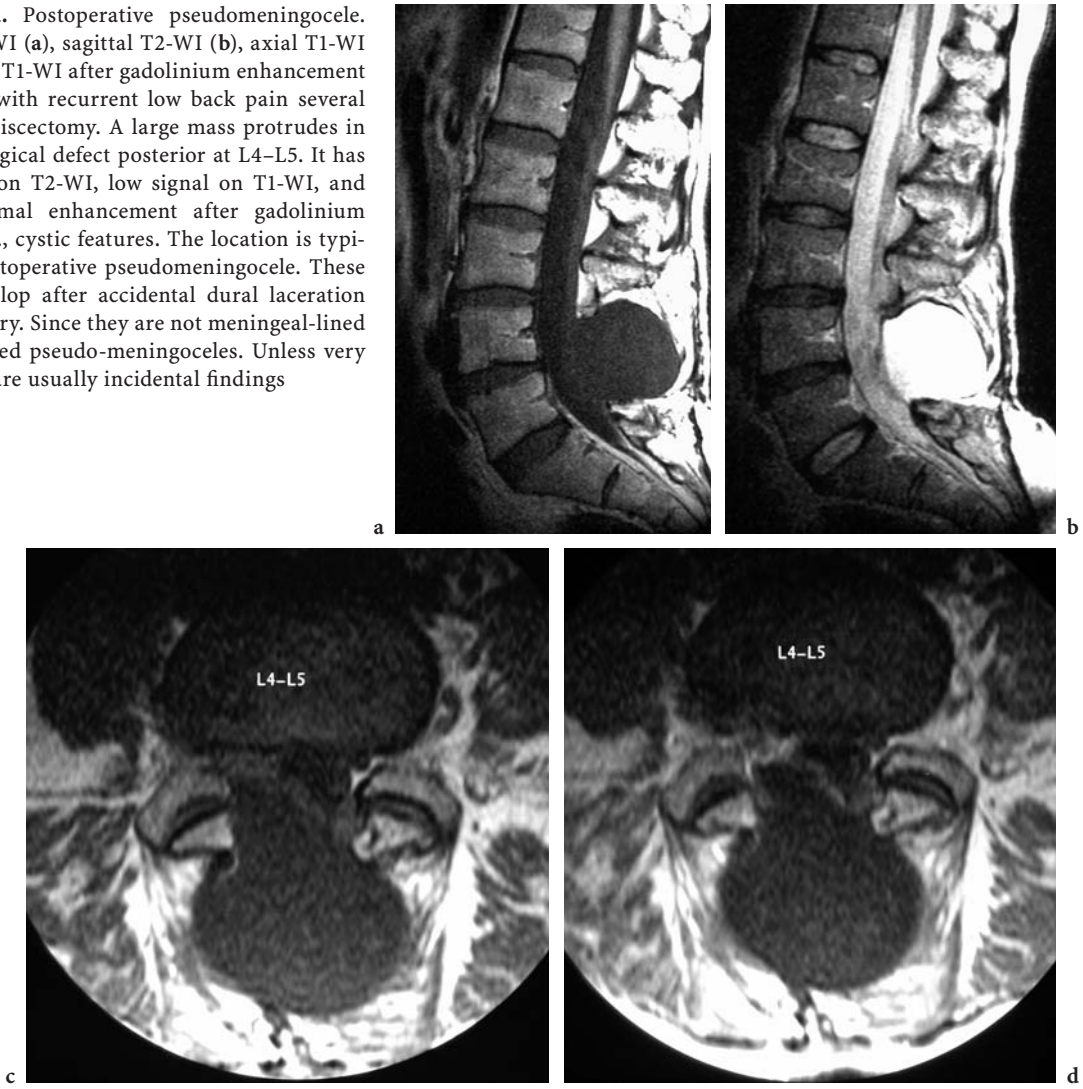

Fig. 15.8a–d. Postoperative pseudomeningocele. Sagittal T1-WI (**a**), sagittal T2-WI (**b**), axial T1-WI (**c**) and axial T1-WI after gadolinium enhancement (**d**). Patient with recurrent low back pain several years after discectomy. A large mass protrudes in the bony surgical defect posterior at L4–L5. It has high signal on T2-WI, low signal on T1-WI, and shows minimal enhancement after gadolinium injection, i.e., cystic features. The location is typical for a postoperative pseudomeningocele. These usually develop after accidental dural laceration during surgery. Since they are not meningeal-lined they are called pseudo-meningoceles. Unless very large, these are usually incidental findings

rial, cartilage, bone, or any combination of these. It is less frequent in the cervical spine compared to the lumbosacral region (Van Goethem et al. 2002). One reason is a different surgical approach, since in the cervical spine an anterior cervical discectomy is often followed by fusion (ACIF), thereby restricting motion and diminishing loading. Furthermore, the cervical spine lacks the broad epidural fat lining in which epidural fibrosis is usually seen. However, it is an important issue in the postoperative lumbar spine.

Adequate differentiation may be achieved with relatively high accuracy on contrast-enhanced CT, but is even better made on contrast-enhanced MRI, which is the imaging modality of choice (Bundschuh et al. 1990; Sotiropoulos et al. 1989).

In the immediate postoperative phase, the epidural space at the site of surgery fills with hemorrhagic and inflammatory tissue and debris. In the first days after surgery this may resemble a residual disc herniation, especially since the mass effect can be considerable and even more pronounced than in the preoperative phase. In the first few days after surgery it may be impossible to make the differentiation with a residual/recurrent disc herniation on imaging alone. In the following weeks there is reorganization and epidural granulation tissue is formed. This epidural granulomatosis shows strong enhancement with gadolinium. If there was residual mass effect, it will reduce in this phase unless a complication exists (hematoma, infection, residual disc material). After several months, this epidural granulation tissue organizes into more ordered collagen fibers to epidural scar formation (epidural fibrosis). At this time there is weaker enhancement.

The distinction between epidural fibrosis and recurrent disc herniation can usually be made using existing criteria (Bundschuh et al. 1988; Bundschuh et al. 1990; Shafaie et al. 997; Sotiropoulos et al. 1989), including on the one hand obliteration of the epidural fat by uniformly enhancing scar tissue in the anterior, lateral, and/or posterior epidural space in epidural fibrosis, or, on the other hand, early central non-enhancement in recurrent or residual disc herniation (Figs. 15.1, 15.2) (Table 15.2). Months after surgery the epidural tissue surrounding a recurrent disc herniation eventually leads to inflammatory changes in the disc material causing more or less enhancement of the recurrent disc material itself (Figs. 15.9, 15.10). This process may lead to complete spontaneous resorption of a recurrent disc herniation and is reflected in changes of volume and enhancement of the prolapsed disc material.

The severity of recurrent symptoms has not been shown to correlate with the amount of epidural scar tissue (Cervellini et al. 1988; Coskun et al. 2000). Studies indicate that epidural fibrosis may be considered as a radiological entity independent of patients' complaints (Coskun et al. 2000). Moreover, epidural fibrosis without significant deformation of the dural sac and/or nerve root sheaths is a normal postoperative finding and as such does not constitute a complication (Van Goethem et al. 2002).

Also, when a residual disc herniation is present one should keep in mind that it is not necessarily responsible for the patient's complaints (Weber 1994). Herniated disc fragments, especially when extruded into the spinal canal (as is often the case in the postoperative phase), can regress spontaneously, mainly via phagocytosis (Komori et al. 1998;

Table 15.2. Recurrent disc herniation vs. epidural fibrosis: findings on MRI

	Recurrent disc herniation	Epidural fibrosis
T1-WI	dark/intermediate	intermediate
T2-WI	usually dark but can be bright especially when recent	intermediate to bright
T1-WI +Gd	dark but may enhance peripherally especially late after injection (+10min)	moderate to strong enhancement
Mass effect	depends on position - can be severe	usually minimal
Morphology	smooth margins	irregular
Natural evolution	shrinks - enhances more	enhances less
Site	can be either site	site of operation
Location	can be anterior, anterolateral or lateral (very rarely posterolateral)	lateral from posterior to anterior

Fig. 15.9a–d. 'Old' recurrent disc herniation. Sagittal T1-WI (**a**), sagittal T2-WI (**b**), axial T1-WI (**c**) and axial T1-WI after gadolinium enhancement (**d**). Patient with longstanding recurrent irradiating leg pain after L4–L5 discectomy. After months, a recurrent disc herniation shows increasing enhancement from the periphery inward. This is due to the replacement of disc material by inflammatory tissue and concomitant ingrowth of microvessels. The natural evolution of a recurrent disc herniation is a gradual transformation of disc material to fibrosis and finally resorption. This is why 'older' recurrent disc herniations can show peripheral enhancement as in this case

Fig. 15.10a–c. 'Old' recurrent disc herniation. Axial T1-WI (**a**), axial T1-WI after gadolinium enhancement (**b**) and subtraction (**c**). In comparison to Fig. 15.9, this recurrent disc herniation shows more diffuse and also central enhancement as seen on the subtracted image. It is an illustration of the continuing process of resorption of recurrent disc material

Weber 1994). Therefore, management of patients with FBSS remains difficult (Hudgins and Clare 1990).

15.4.3.2 Sterile Radiculitis

On MRI, enhancement of the intrathecal spinal nerve roots of the cauda equina following intravenous gadolinium administration at a conventional dosage of 0.1 mmol/kg (0.2 cc/kg) is not a normal observation. With frank compression injury (e.g., by posterolateral disc herniation) to spinal nerves and nerve roots, however, this otherwise relatively intact blood–nerve barrier (BNB) may break down (Fig. 15.11). The complex and as yet poorly understood sequelae of chronic neural trauma and ischemia are believed to be the cause of the abnormal neurophysiologic changes resulting in clinical radiculopathy that may continue long after the disc herniation has been surgically removed (Jinkins 1993).

In a study on asymptomatic postoperative patients, intrathecal nerve root enhancement was seen in 20% of cases 6 weeks after disc surgery, but in only 2% of patients after 6 months (Van Goethem et al. 2000). In a study of symptomatic postoperative patients, enhancement of spinal nerve roots after intravenous gadolinium administration was demonstrated at, and extending cranially and caudally away from, the surgical site in the chronic postoperative period (i.e., more than 6–8 months after surgery) (Jinkins 1993).

15.4.3.3 Sterile Arachnoiditis

The potential factors inciting chronic sterile spinal arachnoiditis are much debated but include the surgical procedure itself, the presence of intradural blood following surgery, diagnostic lumbar

Fig. 15.11a–c. Recurrent disc herniation with radiculitis. Axial T1-WI (**a**), axial T1-WI after gadolinium enhancement (**b**) and axial T1-WI after gadolinium enhancement above the surgical level (**c**). Patient 6 months after surgery with recurrent leg pain. MRI shows the typical image of a recurrent disc herniation. The enhancing tissue posteromedially and intrathecally does not represent scar tissue but are actually enhancing nerve roots. These can be traced upwards (**c**), sometimes all the way up to the conus medullaris

puncture, treated perioperative spinal infection, the previous use of myelographic contrast media (especially older oil-based preparations), and prior intraspinal injection of anesthetic, anti-inflammatory, or chemotherapeutic agents (e.g., steroids, methotrexate). Chronically persistent lumbosacral signs and symptoms in 6%–16% of postsurgical patients have been attributed to sterile arachnoiditis. The three MRI patterns described in adhesive arachnoiditis include: scattered groups of matted or "clumped" nerve roots; an "empty" thecal sac caused by adhesion of the nerve roots to its walls; and an intrathecal soft tissue "mass" with a broad dural base, representing a large group of matted roots, which may obstruct the CSF pathways (Fig. 15.12) (Shafaie et al. 1997). These changes may be focal or diffuse. Contrast enhancement of the thickened meningeal scarring and underlying intrathecal roots may or may not be observed (Jinkins 1993).

15.4.3.4 Textiloma

A surgical sponge or "cottonoid", accidentally left behind in a surgical wound, eventually becomes a textiloma (Guiard et al. 1988). The term "gossybipoma" was used in older literature to denote a mass composed of a cotton matrix (Williams et al. 1978). The foreign body is made of synthetic cotton-like ("cottonoid") fiber ("rayon") usually containing a barium sulphate marking filament, visible on radiographic examinations. The pseudotumor consists of the foreign body itself with perilesional reactive changes, forming a foreign-body granuloma.

MRI can be confusing and misleading because the most typical radiographic sign of a forgotten "cottonoid", the filament, is not visible on MRI. Indeed, this filament consists of barium sulphate, which is neither magnetic nor paramagnetic, and therefore causes no visible magnetic trace on MRI (Fig. 15.13).

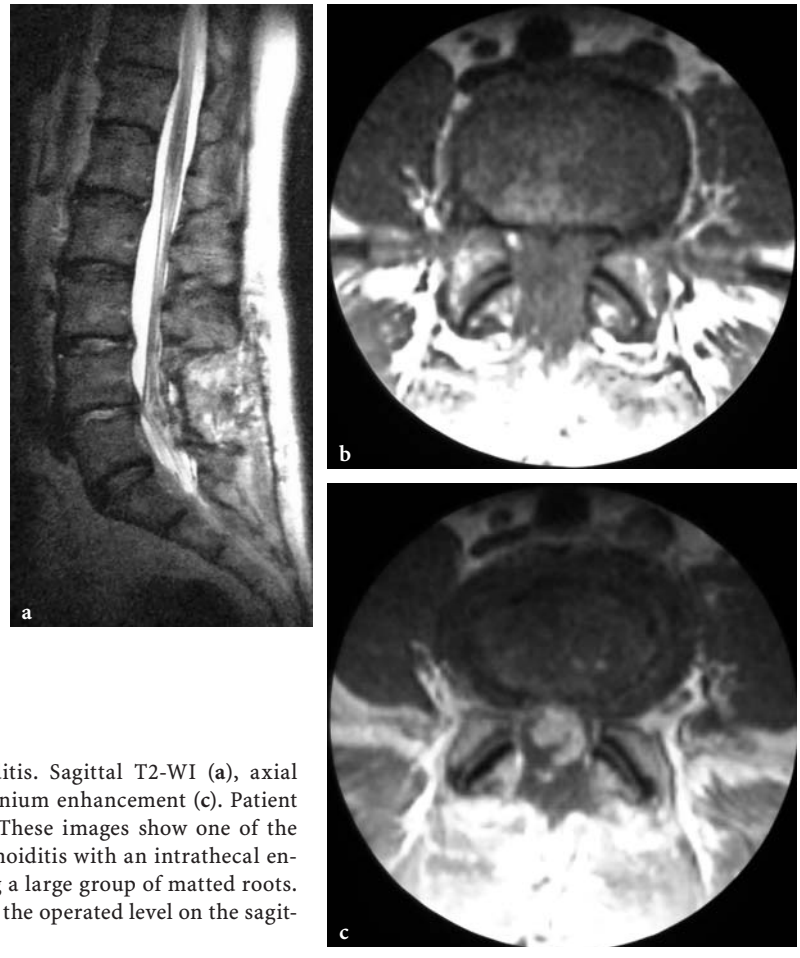

Fig. 15.12a–c. Postoperative arachnoiditis. Sagittal T2-WI (**a**), axial T1-WI (**b**) and axial T1-WI after gadolinium enhancement (**c**). Patient several years after L4–L5 discectomy. These images show one of the typical patterns of postoperative arachnoiditis with an intrathecal enhancing soft tissue "mass" representing a large group of matted roots. Note the spreading of the nerve roots at the operated level on the sagittal T2-WI

a

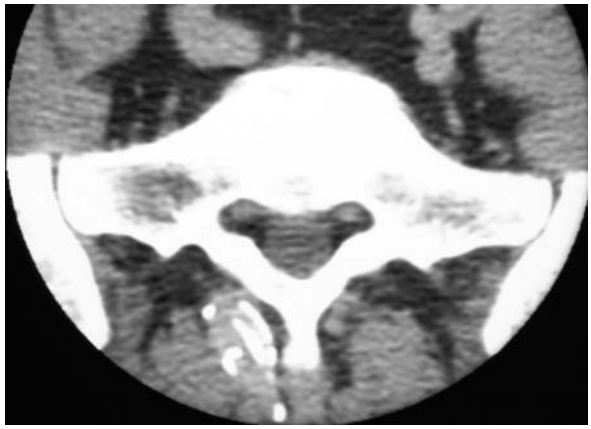

b

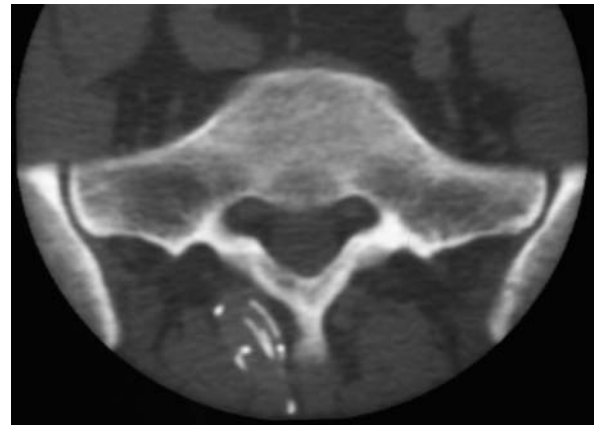

c

Fig. 15.13a-g. Textiloma. AP plain film (**a**), CT soft tissue window (**b**), CT bone window (**c**), and of another patient sagittal T1-WI (**d**), sagittal T2-WI (**e**), axial T1-WI (**f**), and axial T1-WI after gadolinium enhancement (**g**). Textiloma on plain film and CT scan with the typical dense barium-impregnated marking filament. In another patient, MRI shows a mass lesion with an enhancing irregular wall and a characteristic low SI on T2-WI, reflecting a dense fibrous tissue reaction peripherally and central foreign body material lacking mobile protons

These lesions show a moderate degree of peripheral contrast enhancement on T1-WI, believed to be related to an inflammatory foreign-body reaction. On T2-WI, these lesions give low signal, presumably reflecting a dense fibrous tissue reaction peripherally, and central foreign body material lacking mobile protons (De Marco et al. 1991; Van Goethem et al. 1991). This also explains the centrally non-enhancing area on contrast-enhanced T1-WI (Fig. 15.13).

15.4.3.5 Stenosis

One should be aware of the possibility of changes in the size and shape of the spinal structures which may develop as a result of discectomy. One consequence can be secondary stenosis of the central portion or lateral recesses of the central spinal canal, and one or more neural foramina. These are probably an important but under-recognized cause of the FBSS, and may predate or follow spinal surgery. According to some studies, foraminal stenosis is the most common cause of FBSS, seen in 25%–29% of patients with FBSS (Schofferman et al. 2003).

When the stenosis follows surgery, it may present years after the operation, as a result of accelerated degeneration after (partial) discectomy. Loss of intervertebral height, either as a direct effect of discectomy and/or because of (accelerated) postsurgical degeneration, also induces foraminal narrowing and stenosis. Although published studies have methodological biases and small sample

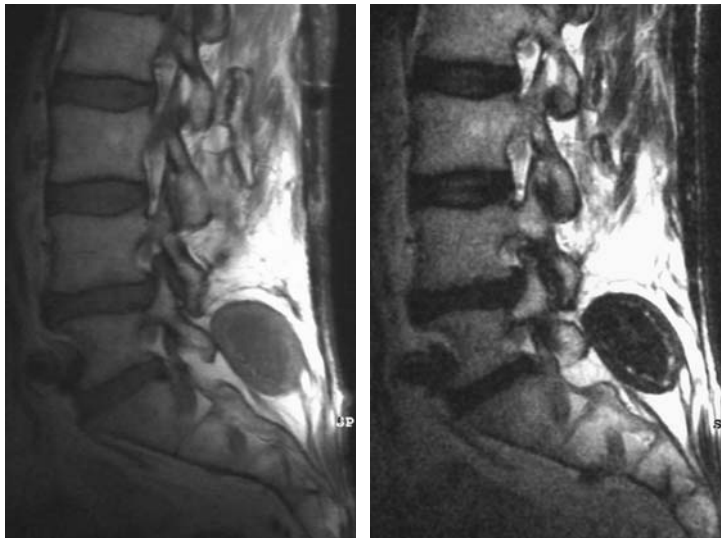

d e

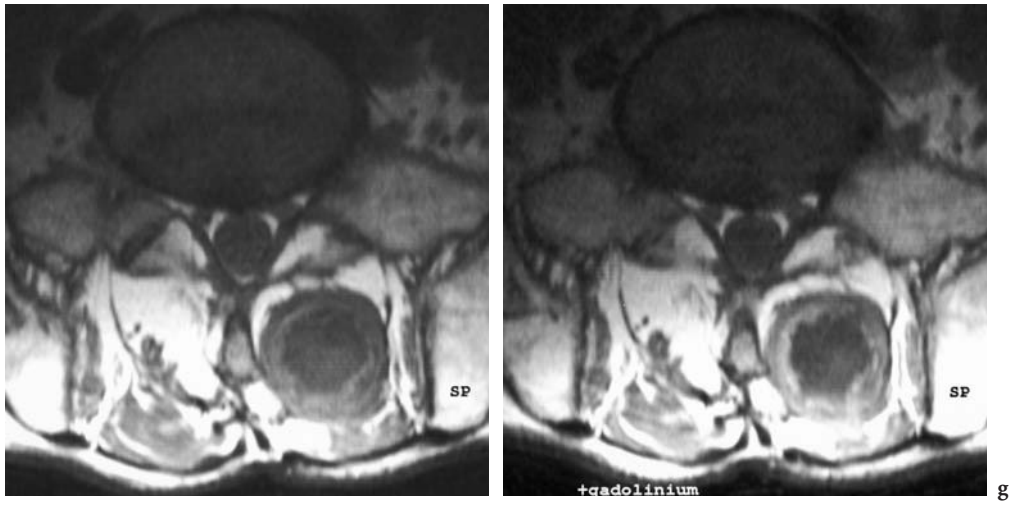

f g

sizes, it appears that the sensitivity to and specificity for spinal stenosis of MRI and CT are similar: true-positive rates of approximately 90%, false-positive rates of approximately 10% (Shafaie et al. 1997).

Lumbosacral neural foramen narrowing is best imaged with direct sagittal T1-WI. Foraminal narrowing with nerve root impingement, due to loss of intervertebral disc height after complete discectomy is not uncommon. Therefore, some surgeons resect only the visibly herniated or sequestered disc material after blunt enlargement of the site of annular rupture in an attempt to preserve the biomechanics of the disc. Unfortunately, this also leaves behind a significant amount of nuclear and annular material, which may lead to recurrent herniation.

15.5 Conclusion

Despite advances in imaging technology, imaging of the postoperative spine remains a challenging and difficult issue. As demonstrated, one or a combination of complimentary medical imaging modalities may be required in a given patient to diagnose the clinically relevant abnormality and to assist the surgeon in deciding whether repeat surgery is necessary, and if so, of what type and at which vertebral level(s). A clear understanding of the indications, limitations, and alternatives available to the imaging specialist will assist the referring physician in achieving the most efficacious triage, as well as promoting the most beneficial and timely outcome for the individual patient.

References

Andrew SA, Sidhu KS (2005) Cervical-peritoneal shunt placement for postoperative cervical pseudomeningocele. J Spinal Disord Tech 18:290–292

Babar S, Saifuddin A (2002) MRI of the post-discectomy lumbar spine. Clin Radiol 57:969–981

Barrera MC, Alustiza JM, Gervas C, Recondo JA, Villanua JA, Salvador E (2001) Post-operative lumbar spine: comparative study of TSE T2 and turbo-FLAIR sequences vs contrast-enhanced SE T1. Clin Radiol 56:133–137

Bertalanffy H, Eggert HR (1989) Complications of anterior cervical discectomy without fusion in 450 consecutive patients. Acta Neurochir (Wien) 99:41–50

Bircher MD, Tasker T, Crawshaw C, Mulholland RC (1988) Discitis following lumbar surgery. Spine 13:98–102

Boden SD, Davis DO, Dina TS, Sunner JL, Wiesel SW (1992) Postoperative diskitis: distinguishing early MR imaging findings from normal postoperative disk space changes. Radiology 184:765–771

Borenstein DG (1996) Chronic low back pain. Rheum Dis Clin North Am 22:439–456

Bradley WG (1999) Use of contrast in MR imaging of the lumbar spine. Magn Reson Imaging Clin N Am 7:439–457, vii

Bundschuh CV, Modic MT, Ross JS, Masaryk TJ, Bohlman H (1988) Epidural fibrosis and recurrent disk herniation in the lumbar spine: MR imaging assessment. AJR Am J Roentgenol 150:923–932

Bundschuh CV, Stein L, Slusser JH, Schinco FP, Ladaga LE, Dillon JD (1990) Distinguishing between scar and recurrent herniated disk in postoperative patients: value of contrast-enhanced CT and MR imaging. AJNR Am J Neuroradiol 11:949–958

Butt WP (1989) Radiology for back pain. Clin Radiol 40:6–10

Cervellini P, Curri D, Volpin L, Bernardi L, Pinna V, Benedetti A (1988) Computed tomography of epidural fibrosis after discectomy: a comparison between symptomatic and asymptomatic patients. Neurosurgery 23:710–713

Choi G, Lee SH, Raiturker PP, Lee S, Chae YS (2006) Percutaneous endoscopic interlaminar discectomy for intracanalicular disc herniations at L5–S1 using a rigid working channel endoscope. Neurosurgery 58:ONS59–68; discussion ONS59–68

Coskun E, Suzer T, Topuz O, Zencir M, Pakdemirli E, Tahta K (2000) Relationships between epidural fibrosis, pain, disability, and psychological factors after lumbar disc surgery. Eur Spine J 9:218–223

Dall BE, Rowe DE, Odette WG, Batts DH (1987) Postoperative discitis. Diagnosis and management. Clin Orthop Relat Res:138–146

De Marco JK, McDermott MW, Dillon WP, Bollen A, Edwards MS (1991) MR appearance of postoperative foreign body granuloma: case report with pathologic confirmation. AJNR Am J Neuroradiol 12:190–192

Demaerel P, van Ongeval C, Wilms G, Lateur L, Baert AL (1994) MR imaging of spondylitis with gadopentetate dimeglumine enhancement. J Neuroradiol 21:245–254

Fager CA (2006) Malpractice issues in neurological surgery. Surg Neurol 65:416–421

Fouquet B, Goupille P, Jattiot F, Cotty P, Lapierre F, Valat JP, Amouroux J, Benatre A (1992) Discitis after lumbar disc surgery. Features of „aseptic“ and „septic“ forms. Spine 17:356–358

Fraser RD, Osti OL, Vernon-Roberts B (1986) Discitis following chemonucleolysis. An experimental study. Spine 11:679–687

Grand CM, Bank WO, Baleriaux D, Matos C, Levivier M, Brotchi J (1993) Gadolinium enhancement of vertebral endplates following lumbar disc surgery. Neuroradiology 35:503–505

Grane P (1998) The postoperative lumbar spine. A radiological investigation of the lumbar spine after discectomy using MR imaging and CT. Acta Radiol Suppl 414:1–23

Grane P, Josephsson A, Seferlis A, Tullberg T (1998) Septic and aseptic post-operative discitis in the lumbar spine – evaluation by MR imaging. Acta Radiol 39:108–115

Guiard JM, Bonnet JC, Boutin JP, Plane D, Guilleux MH, Delorme G (1988) [„Textiloma“: X-ray computed tomographic aspect. Apropos of a case]. Ann Radiol (Paris) 31:49–52

Guyer RD, Collier R, Stith WJ, Ohnmeiss DD, Hochschuler SH, Rashbaum RF, Regan JJ (1988) Discitis after discography. Spine 13:1352–1354

Haughton V, Schreibman K, De Smet A (2002) Contrast between scar and recurrent herniated disk on contrast-enhanced MR images. AJNR Am J Neuroradiol 23:1652–1656

Henk CB, Brodner W, Grampp S, Breitenseher M, Thurnher M, Mostbeck GH, Imhof H (1999) The postoperative spine. Top Magn Reson Imaging 10:247–264

Horowitz SW, Azar-Kia B, Fine M (1990) Postoperative cervical pseudomeningocele. AJNR Am J Neuroradiol 11:784

Hosono N, Yonenobu K, Ono K (1995) Postoperative cervical pseudomeningocele with herniation of the spinal cord. Spine 20:2147–2150

Hudgins PA, Clare CE (1990) Radiographic evaluation of the patient with failed back surgery syndrome (FBSS). Cont Neurosurg 12:23–28

Jinkins JR (1993) Magnetic resonance imaging of benign nerve root enhancement in the unoperated and postoperative lumbosacral spine. Neuroimag Clin North Am:525–541

Jinkins JR (1997) Posttherapeutic neurodiagnostic imaging. Lippincott-Raven, Philadelphia

Jinkins JR, Van Goethem JW (2001) The postsurgical lumbosacral spine. Magnetic resonance imaging evaluation following intervertebral disk surgery, surgical decompression, intervertebral bony fusion, and spinal instrumentation. Radiol Clin North Am 39:1–29

Jinkins JR, Osborn AG, Garrett D, Jr., Hunt S, Story JL (1993) Spinal nerve enhancement with Gd-DTPA: MR correlation with the postoperative lumbosacral spine. AJNR Am J Neuroradiol 14:383–394

Katz JN (2006) Lumbar disc disorders and low-back pain: socioeconomic factors and consequences. J Bone Joint Surg Am 88[Suppl 2]:21–24

Komori H, Okawa A, Haro H, Muneta T, Yamamoto H, Shinomiya K (1998) Contrast-enhanced magnetic resonance imaging in conservative management of lumbar disc herniation. Spine 23:67–73

Kwon BK, Vaccaro AR, Grauer JN, Beiner J (2003) Indications, techniques, and outcomes of posterior surgery for chronic low back pain. Orthop Clin North Am 34:297–308

Liem LA, van Dongen VC (1997) Magnetic resonance imaging and spinal cord stimulation systems. Pain 70:95–97

Lindholm TS, Pylkkanen P (1982) Discitis following removal of intervertebral disc. Spine 7:618–622

Manek NJ, MacGregor AJ (2005) Epidemiology of back disorders: prevalence, risk factors, and prognosis. Curr Opin Rheumatol 17:134–140

Modic MT, Steinberg PM, Ross JS, Masaryk TJ, Carter JR (1988) Degenerative disk disease: assessment of changes in vertebral body marrow with MR imaging. Radiology 166:193–199

Mullin WJ, Heithoff KB, Gilbert TJ Jr, Renfrew DL (2000) Magnetic resonance evaluation of recurrent disc herniation: is gadolinium necessary? Spine 25:1493–1499

Onik G (1996) Automated percutaneous biopsy in the diagnosis and treatment of infectious discitis. Neurosurg Clin N Am 7:145–150

Osterman H, Sund R, Seitsalo S, Keskimaki I (2003) Risk of multiple reoperations after lumbar discectomy: a population-based study. Spine 28:621–627

Scherbel AL, Gardner WJ (1960) Infections involving the intervertebral disks. Diagnosis and management. JAMA 174:370–374

Schofferman J, Reynolds J, Herzog R, Covington E, Dreyfuss P, O'Neill C (2003) Failed back surgery: etiology and diagnostic evaluation. Spine J 3:400–403

Schulitz KP, Assheuer J (1994) Discitis after procedures on the intervertebral disc. Spine 19:1172–1177

Shafaie FF, Bundschuh C, Jinkins JR (1997) The posttherapeutic lumbosacral spine. In: Jinkins JR (ed) Posttherapeutic neurodiagnostic imaging. Lippincott-Raven, Philadelphia, pp 223–243

Shellock FG, Hatfield M, Simon BJ, Block S, Wamboldt J, Starewicz PM, Punchard WF (2000) Implantable spinal fusion stimulator: assessment of MR safety and artifacts. J Magn Reson Imaging 12:214–223

Sotiropoulos S, Chafetz NI, Lang P, Winkler M, Morris JM, Weinstein PR, Genant HK (1989) Differentiation between postoperative scar and recurrent disk herniation: prospective comparison of MR, CT, and contrast-enhanced CT. AJNR Am J Neuroradiol 10:639–643

Suk KS, Lee HM, Moon SH, Kim NH (2001) Recurrent lumbar disc herniation: results of operative management. Spine 26:672–676

Tronnier V, Schneider R, Kunz U, Albert F, Oldenkott P (1992) Postoperative spondylodiscitis: results of a prospective study about the aetiology of spondylodiscitis after operation for lumbar disc herniation. Acta Neurochir (Wien) 117:149–152

van de Kelft EJ, van Goethem JW, de La Porte C, Verlooy JS (1996) Early postoperative gadolinium-DTPA-enhanced MR imaging after successful lumbar discectomy. Br J Neurosurg 10:41–49

Van Goethem JW (1999) Magnetic resonance imaging of the spine. In: Reimer P PP, Stichnoth FA (eds) Clinical MR-imaging, a practical approach. Springer-Verlag, Berlin Heidelberg New York, pp 129–156

Van Goethem JW, Parizel PM, Perdieus D, Hermans P, de Moor J (1991) MR and CT imaging of paraspinal textiloma (gossypiboma). J Comput Assist Tomogr 15:1000–1003

Van Goethem JW, Van de Kelft E, Biltjes IG, van Hasselt BA, van den Hauwe L, Parizel PM, De Schepper AM (1996) MRI after successful lumbar discectomy. Neuroradiology 38[Suppl 1]:S90–96

Van Goethem JW, Parizel PM, van den Hauwe L, De Schepper AM (1997) Imaging findings in patients with failed back surgery syndrome. J Belge Radiol 80:81–84

Van Goethem JW, Parizel PM, van den Hauwe L, Van de Kelft E, Verlooy J, De Schepper AM (2000) The value of MRI in the diagnosis of postoperative spondylodiscitis. Neuroradiology 42:580–585

Van Goethem JW, Parizel PM, Jinkins JR (2002) Review article: MRI of the postoperative lumbar spine. Neuroradiology 44:723–739

Weber H (1994) The natural history of disc herniation and the influence of intervention. Spine 19:2234–2238; discussion 2233

Williams RG, Bragg DG, Nelson JA (1978) Gossypiboma – the problem of the retained surgical sponge. Radiology 129:323–326

Surgical Procedures: Cages, Prostheses, and Instrumentation

16

Robert Gunzburg and Marek Szpalski

CONTENTS

16.1 Introduction

In this chapter the different types of implants and their respective surgical approaches are discussed (Szpalski et al. 1998). Imaging of the instrumented spine is covered in the next chapter.

Implants in spine surgery are used for trauma, deformity, tumors, and degenerative conditions. Surgical treatment of degenerative conditions, however, is still controversial.

Over the years there has been a convergence of orthopedic surgery and neurosurgery towards "spine surgery" as such. A spine surgeon should be able to offer the complete array of surgical approaches and techniques to his patients. Indeed, for some indications, an anterior, posterior, or combined approach may be necessary. In order to use the most adequate imaging technique and to interpret imaging studies it is essential to know what surgical approach was used and what implants or instrumentation was utilized.

The scope of available implants for use in the spine is so vast and so rapidly evolving that it is impossible to make a complete inventory. Instead, the general approaches to spinal instrumentation are discussed.

R. Gunzburg, MD, PhD
Centenary Clinic, Harmoniestraat 68, 2018 Antwerp, Belgium
M. Szpalski, MD
Centre Hospitalier Molière Longchamp, Rue Marconi 142, 1180 Brussels, Belgium

16.2 Approaches

16.2.1 Implants Inserted Through a Posterior Approach

Posterior approaches are mainly midline at the level of the skin, yet the fascia can be incised over the midline or parasagittally as described by Wiltse (1973). Most surgery is aimed at either decompressing neural structures contained in the osteoligamentous structures of the spine, or at fusing two or more vertebrae. When implants are used, it is important to realize that, whereas they may provide an initial stability, their ultimate function is only to provide this stability during the period of bone graft healing which is the final goal of the operation. Screws can be inserted in the pedicles and hooks anchored on laminae or pedicles. These anchorage points are then interconnected rigidly or dynamically, by rods, plates, or elastic devices. Such implants can be made of stainless steel, yet most are of a titanium alloy. The use of pedicle screws was pioneered by Roy-Camille (1970, 1986) and rapidly taken over by surgeons all over the world. The anatomy of the pedicle indeed allows a good and strong purchase of screws. Yet, it is small in size and screw misplacement can have dramatic complications by damaging nearby spinal nerve roots or ganglia (Fig. 16.1).

KEY-POINTS

- Indications: mostly decompression and/or fusion:
  - Trauma
    - Stabilization
    - Vertebroplasty, kyphoplasty
  - Deformity
    - Mainly scoliosis
    - Screws, hooks, and rods
  - Tumor
    - Restoration of stability after resection
  - Degeneration
    - Spondylolisthesis
    - Fusion of painful segment
    - Disc prostheses
- Posterior approaches:
  - Pedicle screws and/or hooks, interconnection with rods, plates or elastic devices
  - Translaminar or transfacet screws
  - Intersomatic devices (PLIF: posterior lumbar interbody fusion)
- Anterior approach:
  - Intersomatic devices (ALIF: anterior lumbar interbody fusion)
  - Plates, staples, wires, and/or rods
  - Route:
    - Upper cervical: transbuccal
    - Lower cervical: paravertebral
    - T1 to T3: difficult
    - Thoracic: transpleural
    - Thoracolumbar: thoraco-phreno-lumbothomy
    - Lumbosacral: retroperitoneal

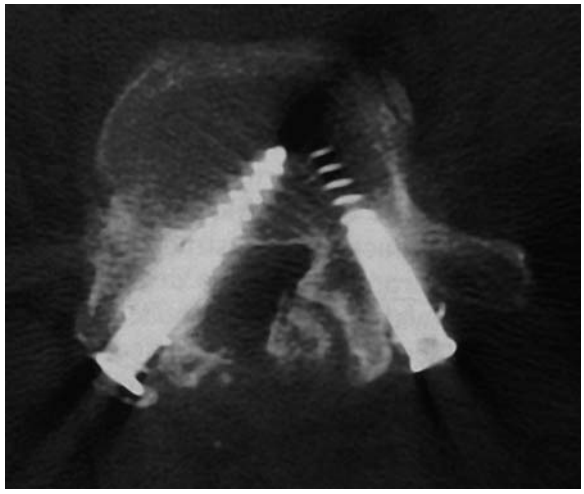

Fig. 16.1. Axial CT image showing pedicle screw misplacement. The right pedicle screw transverses the lateral recess with possible nerve damage

Devices can also be inserted between spinous processes; those are used in spinal stenosis with neurogenic claudication. The rationale is to prevent extension of the motion segment since this causes a decrease of the dural sac diameter by buckling of the ligamentum flavum, and/or a decrease in size of the intervertebral foramen.

Through a posterior approach translaminar or transfacet stainless steel screws can also be inserted (Fig. 16.2).

Intersomatic devices can be inserted in the disc space through a posterior approach in order to achieve a so-called posterior lumbar interbody fusion (PLIF). In order to insert these devices, the neural canal must be opened and the dura retracted widely. This may lead to fibrotic adhesions and even nerve damage. Finally, devices can be inserted intersomatically or in the vertebral bodies via a transpedicular or paravertebral approach.

16.2.2 Implants Inserted Through an Anterior or Antero-lateral Approach

Through an anterior or antero-lateral approach, implants can be placed at the level of the discs (anterior lumbar interbody fusion, ALIF) or longer cages may replace one or several vertebral bodies in cases of

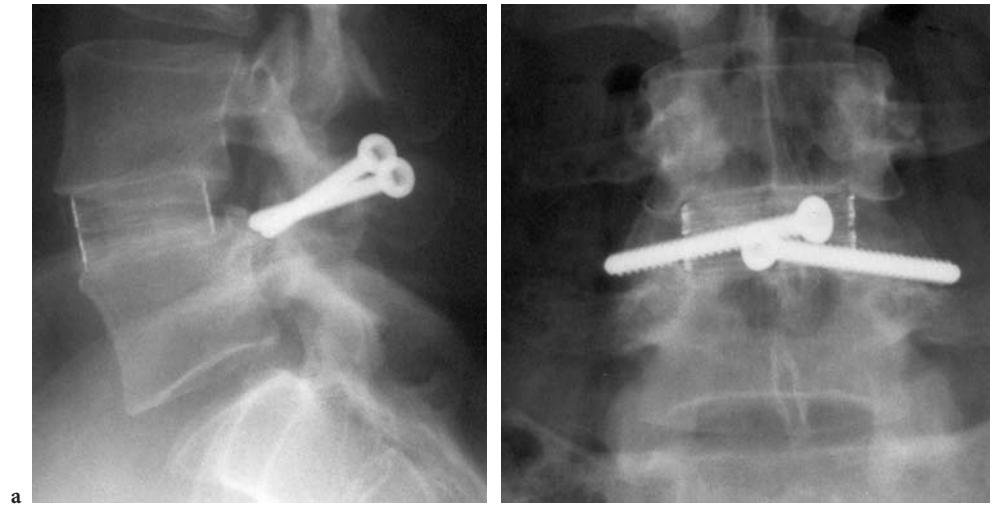

Fig. 16.2a,b. Lateral (**a**) and AP (**b**) plain film of a 360° fusion. Carbon cage between the vertebral bodies (inserted through an anterior retroperitoneal approach: anterior lumbar interbody fusion) and screws through the facet joints at the back

vertebrectomy. There are also plates, staples, wires, rods, or combined devices which may span several vertebral segments.

The approach to the spine can be large and open, small and open, or small and endoscopic. In the cervical area implants are usually inserted via transbuccal route for the upper levels or an anterior paravertebral approach for surgery down to T1. T1 through T3 are difficult to access surgically. Below that, a transpleural approach will allow good access to the spine. For the thoracolumbar area, a thoraco-phreno-lumbotomy will be required, and for the lumbosacral spine a retroperitoneal approach is preferred over a transperitoneal approach. Each of these approaches may lead to specific complications which may require specifically adapted imaging techniques.

16.2.3 The 360° Approach

A combination of interbody devices inserted anteriorly or posteriorly with pedicle or facet fixation at the back is referred to as 360° fusion. (Fig. 16.2).

16.3 Specific Types of Surgery

Tumor surgery, which can be curative or palliative, requires the resection of diseased tissue often resulting in a violation of the structural stability of the spine. Such operations will therefore be completed by an attempt to restore this stability. Implants will consist of posterior instrumentation and/or anterior instrumentation such as cages sometimes reinforced by plates. Bone grafts (vascularized or not), synthetic bone grafts, or even bone cement may be used during these interventions, and all these may affect postoperative imaging.

Trauma surgery is indicated either when fracture stabilization has to be achieved and/or when a deformity needs to be corrected. Recently, new techniques to treat osteoporotic vertebral compression fractures are becoming increasingly popular. One of these techniques relies on percutaneous injection of cement in the vertebra (vertebroplasty) or percutaneous fracture reduction by the inflation of balloons (kyphoplasty) or Dacron bags (Optiplasty) inserted into the collapsed vertebra. Cement or grafts are then inserted to maintain this reduction (Mehbod et al. 2003).

Deformity surgery can be divided into several categories. Adolescent idiopathic scoliosis represents the bulk of these cases. Surgery will require long posterior stabilizations, often combined with anterior releases and stabilizations. The hardware

Fig. 16.3. PA plain film. Long thoracolumbar posterior fusion for idiopathic scoliosis with multiple pedicle screws and two long rods. (Courtesy E. Munting)

in these cases comprises an arrays of screws, hooks, and rods (Fig. 16.3). Kyphotic deformities due to Scheuermann's disease, ankylosing spondylitis, or vertebral compression fractures may require vertebral osteotomies, stabilized with hardware. Deformities in the elderly are mostly at the lumbar level and often need to be fused either in situ or after decompression of the neural structures and an attempt at reduction. The final category of deformity cases consists of major deformities encountered in infants presenting with muscular dystrophies or other congenital anomalies.

Except for a few specific cases, such as lytic and degenerative spondylolisthesis, there are no absolute indications for the use of implants in degenerative spine surgery. Yet the bulk of implants inserted worldwide is for degenerative low back pain. The rationale is to fuse the segments deemed to be responsible for the pain (Fritzell et al. 2001). To which extent the results can be enhanced by the addition of implants for the most part remains uncertain. Only a few well-conducted studies address this problem and most do not show clinical advantages of added instrumentation (Fritzell et al. 2001). One of the most controversial aspects of these procedures is the determination of an acquired fusion vs non-union or pseudarthrosis (Albert et al. 2000; Pearcy and Burrough 1982). The very presence of implants makes imaging difficult, and multiple techniques have been devised to try to assess this problem. These techniques include plain films with or without dynamic imaging, multirow detector CT, MRI, and nuclear medicine (Fig. 16.4). Another aspect of the use of implants, which may prove a problem in the future, is the possibility of wear debris deposits around the spine as polyethylene and metal-on-metal implants are being used more frequently (Hallab et al. 2003).

A full array of implants has been proposed and used. Posterior instrumentation comprises pedicle screws and rods or plates (Fig. 16.5). Alternatively, more dynamic constructs have been introduced. As the pain mostly originates from the intervertebral disc, a resection of this structure followed by

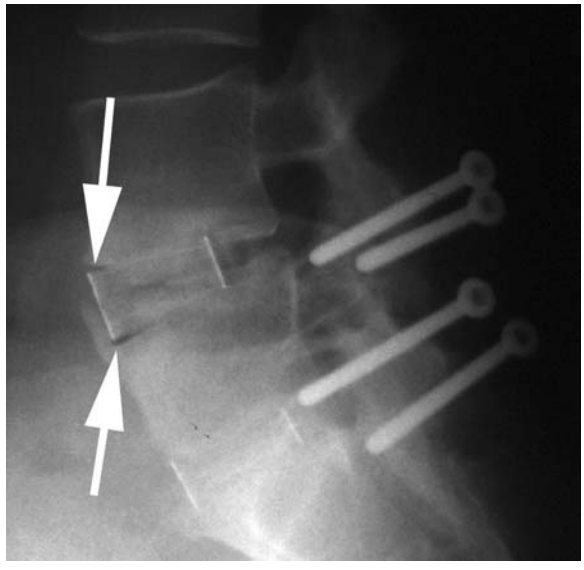

Fig. 16.4. 360° fusion at L4–L5 and L5–S1 with facet screws at the back and carbon cages in the front. The carbon cages have metal markers to improve radiographic visibility. This lateral view extension shows a space between the cage and the bone indicating a non-union at L4–L5 (*arrows*)

some replacement has been proposed and executed through a posterior or anterior approach. Allografts, such as femoral rings, or autografts, such as fibular struts, are employed (Fig 16.6). Alternatively, carbon cages filled with autologous bone or synthetic bone are also being applied (Fig. 16.4). Rigid metal cages of all shapes and sizes have been introduced at the intersomatic level (Fig 16.5).

Intervertebral disc prostheses have been used for several years now, but this technique enjoys a sudden popularity with a spectacular increase in numbers. Numerous implants have been patented (Szpalski et al. 2002), yet only a handful have reached clinical use. The most important point regarding these implants is that they require an absolutely impeccable positioning. Such a prosthesis may not be placed off-center or into the vertebral bodies. Polyethylene cores can be dislodged and compress neural or vascular structures requiring specific imaging methods. What the future of these devices will be in the light of the ever lengthening life expectancy and advancing osteoporosis with age remains an unanswered question. Specific devices are being developed for the cervical and lumbar spine (Figs. 16.7, 16.8).

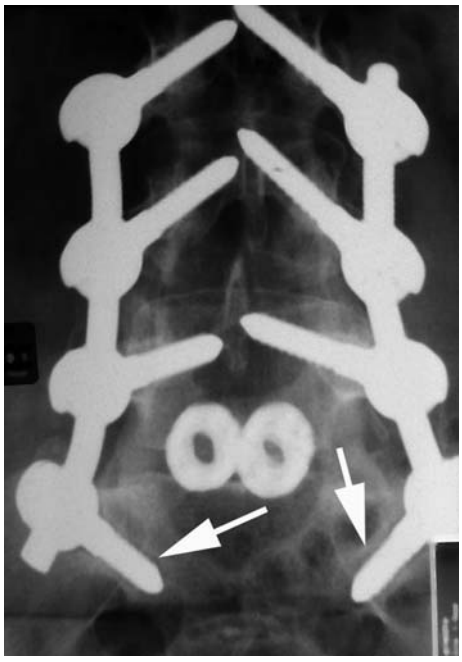

Fig. 16.5. AP plain film. L3–S1 fusion supported by pedicle screws at the back. For an L5–S1 non-fusion (notice loosening around S1 screws; *arrows*) two hollow spherical intersomatic implants were later inserted through a laparoscopic approach

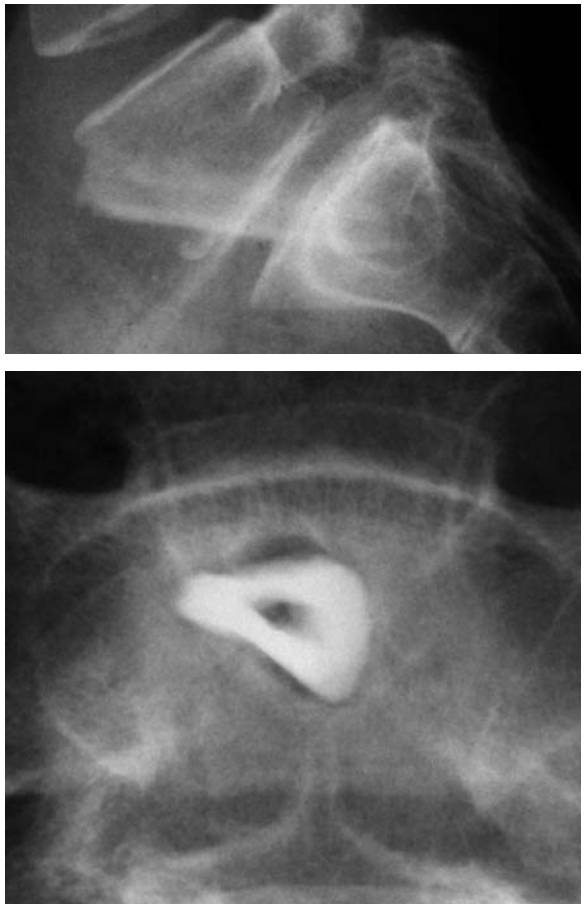

Fig. 16.6a,b. Lateral (**a**) and AP (**b**) plain film. L5–S1 anterior fusion with a fibular autograft

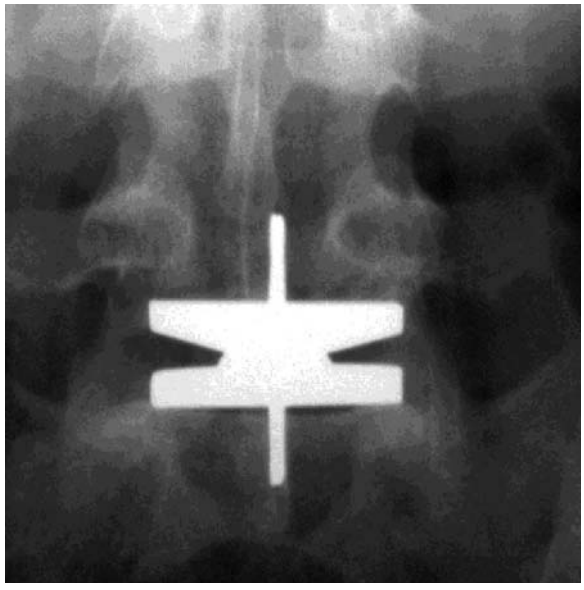

Fig. 16.7. AP plain film perpendicular to a L5–S1 disc prosthesis. In this example a metal-on-metal device was used

Fig. 16.8. Lateral plain film. At L5–S1 a posterolateral fusion was performed with the support of a titanium pedicle screw–rod system. Later an L4–L5 discographically confirmed painful disc was treated with a disc prosthesis. In this example a polyethylene core is contained between two metal plates

References

Albert T, Pinto M, Denis F (2000) Management of symptomatic lumbar pseudarthrosis with anteroposterior fusion: a functional and radiographic outcome study. Spine 25:123–130

Fritzell P, Hagg O, Wessberg P, Nordwall A (2001) Volvo award winner in clinical studies: lumbar fusion versus nonsurgical treatment for chronic low back pain: a multicenter randomized controlled trial from the Swedish Lumbar Spine Study Group. Spine 26:2512–2532

Hallab N, Cunningham B, Jacobs J (2003) Spinal implant debris-induced osteolysis. Spine 28:S125–S138

Heini P, Walchli B, Berlemann U (2000) Percutaneous transpedicular vertebroplasty with PMMA: operative technique and early results. A prospective study for the treatment of osteoporotic compression fractures. Eur Spine J 9:445–450

Mehbod M, Aunoble S, Le Huec J-C (2003) Vertebroplasty for osteoporotic spine fracture: prevention and treatment. Eur Spine J 12:S155–S162

Pearcy M, Burrough S (1982) Assessment of bony union after interbody fusion of the lumbar spine using a biplanar radiographic technique. J Bone Joint Surg Br 64:228–232

Roy-Camille R, Roy-Camille M, Demeulenaere C (1970) Osteosynthesis of dorsal, lumbar, and lumbosacral spine with metallic plates screwed into vertebral pedicles and articular apophyses. Presse Med 78:1447–1448

Roy-Camille R, Saillant G, Mazel C (1986) Internal fixation of the lumbar spine with pedicle screw plating. Clin Orthop 203:7–17

Szpalski M, Gunzburg R (1998) The role of surgery in the management of low back pain. Baillieres Clin Rheumatol 12:141–159

Szpalski M, Gunzburg R, Mayer M (2002) Spine arthroplasty: a historical review. Eur Spine J 11:S65–S84

Imaging of the Postoperative Spine: Cages, Prostheses, and Instrumentation

17

Paul E. Kim and Chi Shing Zee

CONTENTS

P. E. Kim, MD
Assistant Professor of Clinical Radiology, University of Southern California Keck School of Medicine, Room 3740, 1200 N. State Street, Los Angeles, CA 90033, USA
C. S. Zee, MD
Professor of Radiology, Chief, Division of Neuroradiology, University of Southern California Keck School of Medicine, Room 3740, 1200 N. State Street, Los Angeles, CA 90033, USA

17.1 Introduction

Spinal instrumentation has undergone tremendous evolution in the more than 125 years since the first reported internal fixation of the spine in 1888 by B. F. Wilkins, who reduced a dislocated T12–L1 vertebrae by fixing a wire with carbonized silver suture passed around the pedicles of the T12 and L1 vertebrae (Cotler 1999). In 1911 Albee and Hibbs, at two different institutions in New York, performed the first biological fusion procedures of the spine by using autogenous bone graft (Albee 1911; Hibbs 1911). Between these historical events, one of the most significant technological advances to impact the development of spinal instrumentation (and medicine in general) took place: William Roentgen's discovery of X-ray imaging in 1895. Since these early events, the two landmark developments in spinal instrumentation of the past century were the interspinous wiring technique described by Rogers in the early 1940s and the rod/hook instrumentation system of Harrington for treatment of postpoliomyelitis scoliosis in the 1950s (Benzel 1994).

The goal of spinal instrumentation is to maintain or correct anatomic alignment of spinal segments by sharing the loads acting on the spine, usually until a solid biological fusion occurs. Biological fusion refers either to the natural healing of traumatic vertebral fractures or surgically decorticated bony surfaces, or to the incorporation of bone graft material. Autologous bone continues to be the most commonly employed material to establish bony arthrodesis regardless of the fusion procedure type, implant device, or instrumentation used. Morselized autograft, bone chips harvested usually from iliac crest (or spinous processes if concomitant laminectomy is performed) is typically incorporated within or around cage devices and spacers, femoral ring allografts, or threaded allograft bone dowels, as well as along decorticated facet joints and lamina in rod

KEY-POINTS

- Spinal instrumentation:
  - Serves to maintain or correct anatomic alignment
  - Usually until a solid biological fusion occurs
- Role of imaging:
  - Intraoperative image guidance
    - C-arm fluoroscopy
    - C-arm portable CT scan
    - CT – computer-aided surgery (CAS)
  - Positioning of grafts, implants, or hardware
    - Plain film
    - CT, especially MDCT
  - Postoperative assessment of complications
    - CT, especially MDCT
    - MR
- Early postoperative complications (first few weeks or months):
  - Graft extrusion
  - Implant or hardware misplacement
  - Infection
  - Dural leak, pseudomeningocele
- Late postoperative complications (months or years):
  - Pseudarthrosis, non-union
    - Gold standard is surgical exploration combined with clinical data
    - MDCT (and plain film): abnormal lucency with surrounding sclerosis
    - MR: reactive marrow changes (low SI on T1, high SI on T2) and enhancement with gadolinium
  - Graft subsidence, migration, extrusion, fragmentation, and/or collapse
  - Hardware failure
    - Occurs usually with non-union
    - Loosening: lucent halo with surrounding sclerosis

instrumentations and posterior fusions, and along decorticated transverse processes in posterolateral fusions. The relatively recent development of demineralized bone matrix (DBM), bone morphogenetic proteins (BMP), and biocompatible synthetic materials is making greater inroads into this dependency on autologous graft harvesting (Burkus et al. 2002a,b; Price et al. 2003; Sandhu 2004).

17.2 Imaging in Uncomplicated Spinal Fusion

Imaging assumes two principal roles in the evaluation of the intra- and postoperative patient with a spinal implant: intraoperative image guidance for placement of the implant and postoperative assessment of complications. These roles are accomplished primarily with plain X-rays and CT. Nuclear medicine scintigraphy assumes an adjunct role in select cases for assessment of non-union or hardware loosening. Magnetic resonance imaging has thus far not been useful for direct assessment of implants or hardware, but it assumes a primary role for all other operative complications not directly involving grafts, implants, or hardware.

17.2.1 Computed Tomography and Plain X-ray

The relatively recent development of multirow detector CT with near isotropic voxel imaging capability has greatly enhanced the assessment of fused spines, both due to enhanced spatial resolution in three dimensions as well as reduced metallic artifacts. Although routine CT scans may be acquired at 1-mm beam collimation with multiplanar reconstructions formatted at 3-mm intervals, if a specific site is of particular concern, additional imaging at sub-millimeter collimation should be performed with thinner reconstruction intervals. In addition to standard axial, sagittal and coronal multiplanar reconstructions of helical volumetric data sets, angled

or curved reformats should be performed at a postprocessing workstation if needed to address specific concerns. Linear polytomography is only indicated when older stainless steel hardware is present that precludes adequate CT imaging.

17.2.1.1 Posterior and Posterolateral Fusion

Graft material is either autologous (autograft) or allogeneic (allograft). Morselized autograft has been the mainstay of posterior and posterolateral fusion procedures for many years. Posterior fusion is characterized by autograft placed along decorticated facets and/or laminae. The radiographic appearances are quite variable from patient to patient, some showing large solid fusion masses, whereas others demonstrate small, wispy bone graft that may be inapparent on plain X-ray and subtle even on CT, particularly if small amounts of graft were placed only along decorticated facets (Fig. 17.1).

Posterolateral intertransverse fusion masses are usually more apparent on plain films and CT. The early postoperative radiographic appearance is characterized by a coarse, ill-defined gravel-like appearance which may be difficult to visualize. This gradually consolidates over several months into a solid bony fusion within the first postoperative year (Fig. 17.2). Posterior and posterolateral fusions are much more variable in final appearance than interbody fusions, some showing discrete, well-formed solid fusion masses, whereas others demonstrate a somewhat fragmented appearance that belies the intactness of the underlying fusion (Fig. 17.1c).

17.2.1.2 Interbody Grafts and Implants

Tricortical iliac crest grafts are less commonly used for interbody grafting in heavy load-bearing segments such as the lumbar spine due to relative lack of compressive strength compared with cortical allografts and cages, as well as donor site morbidity issues. Femoral ring allografts are widely used in anterior lumbar interbody fusion (ALIF) procedures (Fig. 17.2a). These cortical grafts, made from sectioned cadaveric femurs, have great compressive strength to resist the high axial-loading forces encountered in the lumbar spine. The central cavity is typically packed with autologous bone chips, demineralized bone matrix (DBM), and/or bone morphogenetic protein (BMP) to establish fusion (Burkus et al. 2002a). Threaded allograft bone dowels, also made from dense cortical bone, have good compressive strength and are similar to threaded metal cages in external morphology. These grafts often have a central cavity for packing of autograft, DBM, or BMP. Threaded bone dowels can be implanted by either posterior or anterior approach. In the cervical spine, the original Smith-Robinson procedure utilized tricortical iliac crest autograft for interbody fusion. Presently, the most commonly used interbody grafts for anterior cervical diskectomy and fusion (ACDF) are small fibular allograft plugs, which also have a central core that can be packed with autologous bone chips, DBM, and/or BMP. The radiographic appearance of interbody grafts of all types in the early postoperative period is characterized by a well-defined, dense graft implant with sharp margins. On plain X-ray, an apparent thin perigraft lucency not seen on CT may be present for several months (Fig. 17.2a). The margins gradually blur and disappear as the graft becomes fully incorporated and replaced by new bone. After many years, some interbody fusions can have the appearance of physiologic ankylosis (Fig. 17.3).

Interbody cages are either threaded or impacted, and may also be applied from posterior, anterior, or transforaminal approaches. Threaded interbody cages are cylindrical devices filled with autograft and implanted in a horizontal position. As the term implies, they have a threaded outer contour, which aids in insertion and/or maintaining implant position (Fig. 17.4). Impacted cages are much more variable in design. Smaller upright cages are designed for interbody placement from either posterior or transforaminal approaches (Fig. 17.2b). Currently, the most commonly used material for cage devices is titanium. Newer materials are particularly advantageous from a postoperative imaging perspective. Being essentially radiolucent, they elicit no streak artifact on CT scanning or susceptibility artifacts on MRI (Fig. 17.5).

Simple interbody spacers may be made of allograft bone or a variety of newer synthetic materials made in a tremendous variety of shapes, usually designed for implantation from a posterior approach. Autograft, DBM, and/or BMP are packed around, rather than within, these implants (Fig. 17.6).

On plain films, cages should appear "cleanly" situated within the disc space with no adjacent lucency or sclerosis. On the anteroposterior view, metal cages in intact fusions appear to "float" within the intervertebral space (Fig. 17.4a,b). With multislice helical CT and multiplanar reconstructions less than 3 mm

Fig. 17.1a–d. Posterior lumbar fusion. **a** Lateral plain X-ray of 72-year-old man with old posterior lumbar fusion at L4–L5 and L5–S1 shows solid mature bony arthrodesis of posterior facets and laminae. Many posterior fusion masses are significantly less conspicuous. **b** Magnetic resonance imaging (*arrows*) and **c** multiplanar 3D CT show variable appearances of posterior fusion masses. Fusion masses may be intact yet appear quite irregular and even fragmented (**c**, *arrows*) on any single slice due to multiple irregular surface and internal crevices. Early postoperative posterior fusion graft may be difficult to visualize on plain X-ray, but usually can be seen on CT (**d**, *arrows*)

Fig. 17.2a–c. Anterior lumbar interbody fusion (ALIF) with femoral ring allografts **a** and threaded interbody bone dowels **b**; posterior lumbar interbody fusion (PLIF) with titanium cage **c**. Posterior instrumentation and/or fusion usually accompany interbody fusion: posterolateral fusion and pedicle screw instrumentation **a**; posterior fusion and translaminar facet screw fixation **b**; and posterolateral (intertransverse) fusion without instrumentation **c**. Note gravel-like appearance of intertransverse bone graft in the early postoperative period (**a**, *arrowheads*), and solid appearance of older fusion (**c**, *arrowheads*). Marked variability in radiographic appearance typifies posterior and posterolateral fusions

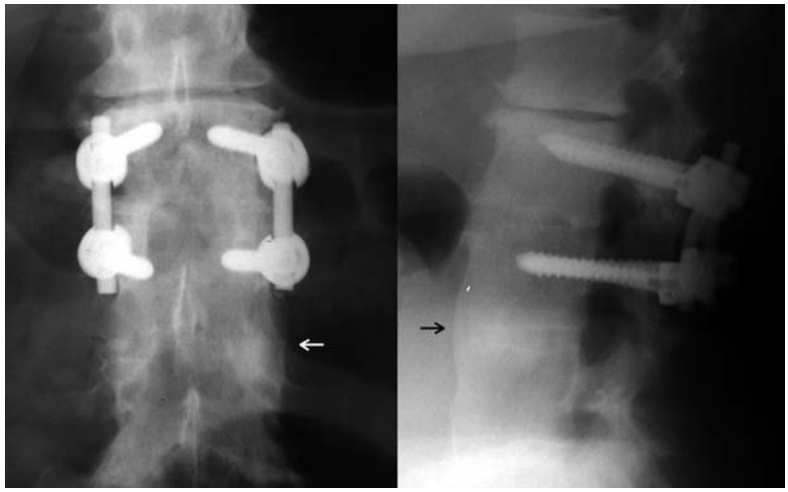

Fig. 17.3. A 68-year old man 12 years after plate/screw interbody fusion at L2–L3 with appearance approaching ankylosis (*arrows*). Posterior fusion and pedicle screw instrumentation at L1–L2 was more recent

thick, continuous bone traversing the openings of the cage can be clearly delineated (Fig. 17.4c). Cages inserted in posterior lumbar interbody fusion (PLIF) or unilaterally in transforaminal lumbar interbody fusion (TLIF) are sometimes positioned somewhat posteriorly within the disc space, and prevertebral vascular clips used in anterior approaches are absent. In the early postoperative period, morselized autograft placed within and/or around these devices is not visible on plain X-rays and is usually only visible radiographically within cages made of radiolucent materials (Fig. 17.5b).

For corpectomy procedures larger strut grafts are used. Femoral strut allografts are designed for use in lumbar or thoracic spine, typically applied with lateral rod or plate instrumentation. Fibular strut allografts or tricortical iliac crest grafts may be used in anterior cervical corpectomy and fusion in combination with anterior plates (Fig. 17.7).

17.2.1.3 Posterior Instrumentation

Posterior instrumentation is of three main types: (a) rods with sublaminar hook or wire fixation; (b) pedicle screw systems with rods or plates; and (c) simple facet joint fixation with lamina facet screws. Combination hook/wire/pedicle screw systems are also used.

The Harrington and Luque rod systems are the prototypes of the rod and hook/wire systems. Numerous modifications to rod and hook designs have taken place over the past several decades in attempts to overcome previous shortcomings, the most common of which were mechanical failure through breakage or hook dislodgement, and flat-back syndrome (Harrington 1960, 1988). Hooks pointed away from the center of the rods provide distraction forces while hooks pointed toward the center of the rods provide compression (Albert et al. 1999). Luque's system, by contrast, used sublaminar wiring with rods to achieve multiple points of fixation and apply horizontally oriented corrective forces for deformity and spinal stabilization (Fig. 17.8) (Luque 1982; Thometz and An 1999). Radiographs seldom show clearly the posterior bony fusion along the facets unless a pseudarthrosis becomes apparent.

Currently, pedicle screws with rods or plates are the most commonly used posterior instrumentation systems. These can now even be placed entirely through a "minimally invasive" percutaneous procedure. Advances in pedicle screw materials have paralleled that for implant devices, including radiolucent bioabsorbable materials such as polylactate.

Translaminar facet joint fixation with cortical screws is a simple method of posterior fixation, and may be applied to add stability to interbody, posterior (facet or interlaminar), or posterolateral (intertransverse) fusions (Fig. 17.2b).

In the cervical spine, posterior instrumentation includes interspinous or sublaminar wiring techniques, interlaminar clamps, and lateral mass fixation constructs consisting of screws with plates or rods (Fig. 17.9).

17.2.1.4 Anterior Instrumentation

Anterior instrumentation can be categorized into two main types: rod-screw systems and plate-screw

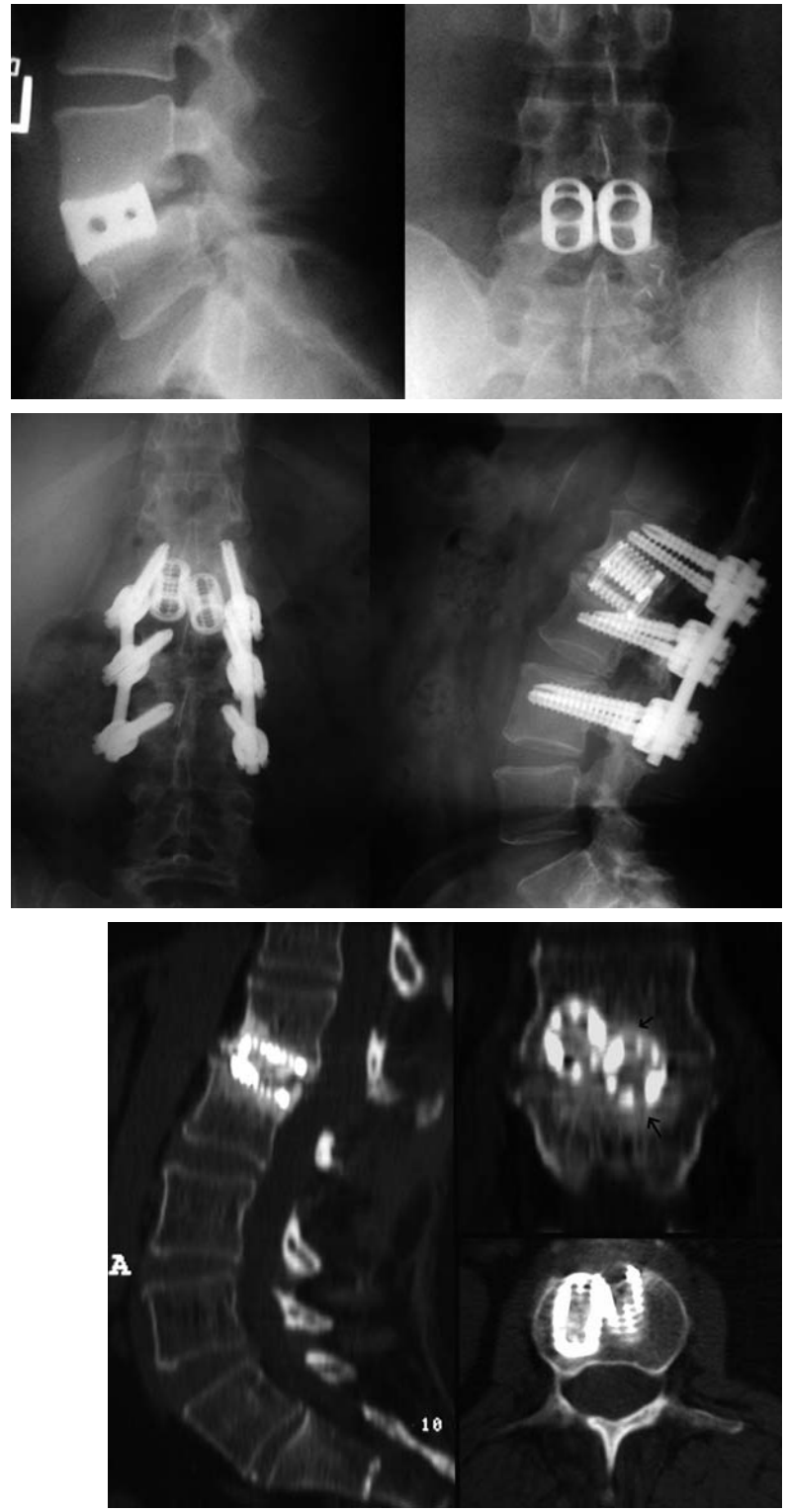

Fig. 17.4a–c. Threaded titanium interbody cages used in ALIF **a** and PLIF **b,c**. Anterior approach (ALIF) is reflected in the presence of vascular clips anterior to left side of L5 as well as relative large size and anterior positioning of the titanium cages. In PLIF note somewhat smaller size of cages, as well as absence of surgical clips anteriorly, and the slightly oblique orientation of the cages reflecting the direction of insertion from posterior approach. Multiplanar 3D CT shows solid bony arthrodesis through the openings of the cage (**c**, *arrows*)

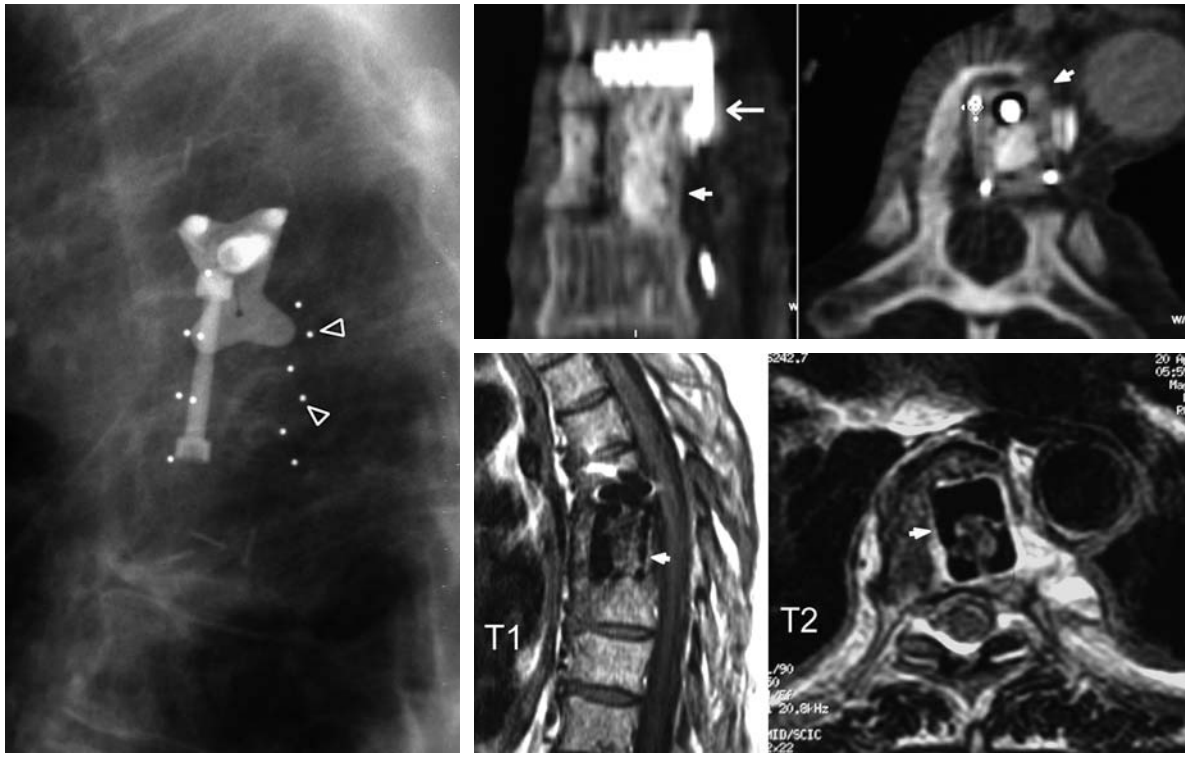

Fig. 17.5a–c. A 62-year-old woman with metastatic breast cancer: T6 anterior corpectomy and fusion using radiolucent carbon-fiber-reinforced polymer (CFRP) cage. Small radio-opaque beads assist intraoperatively in cage placement (**a**, *arrowheads*). In this case, anterior plate/screw instrumentation at left of T5–T6 is used only to prevent lateral graft extrusion (**b**, *arrow*). Radiolucent cage causes no CT streak artifact (**b**, *arrowhead*) or MRI susceptibility artifact (**c**, *arrowheads*). Note autograft bone visible on CT and MRI within the central cavity of the cage

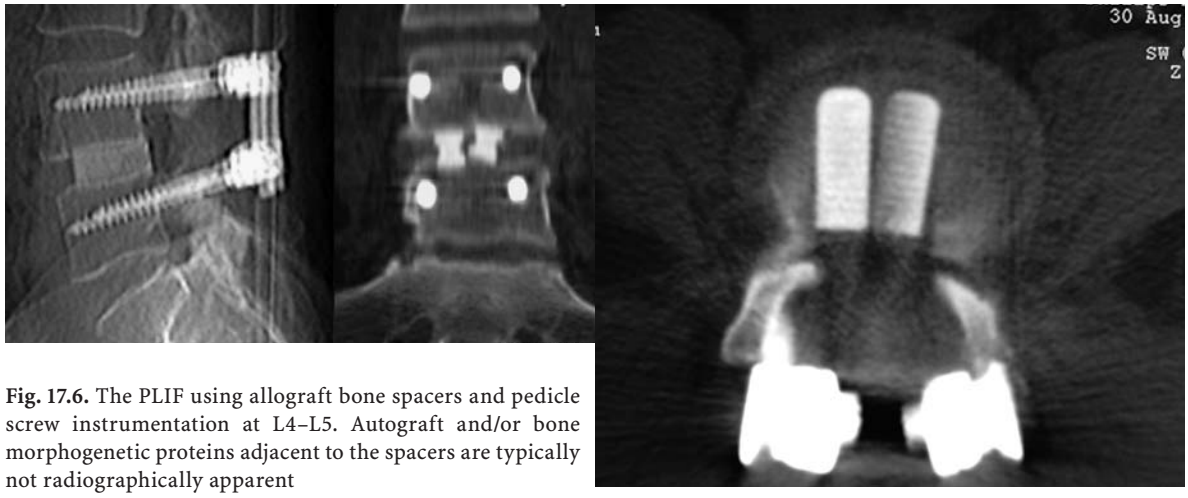

Fig. 17.6. The PLIF using allograft bone spacers and pedicle screw instrumentation at L4–L5. Autograft and/or bone morphogenetic proteins adjacent to the spacers are typically not radiographically apparent

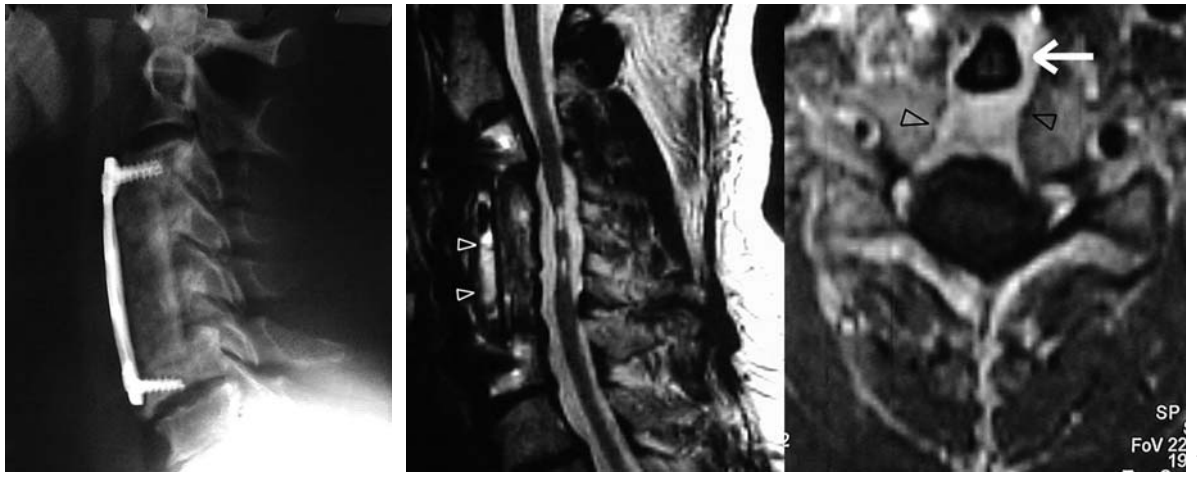

Fig. 17.7a,b. C4, C5 anterior corpectomy and fusion with fibular strut allograft and anterior plate instrumentation. Lateral plain X-ray **a** and MRI **b**. Sagittal T2-weighted image (**b**, *left*) shows typical hyperintense core of fibular allograft (*arrow*) and mild susceptibility artifacts from titanium plate. Post-gadolinium axial T1-weighted image (**b**, *right*) shows contrast enhancement of the "trough" of the corpectomy (*arrowheads*), within which lies the fibular strut (*arrow*)

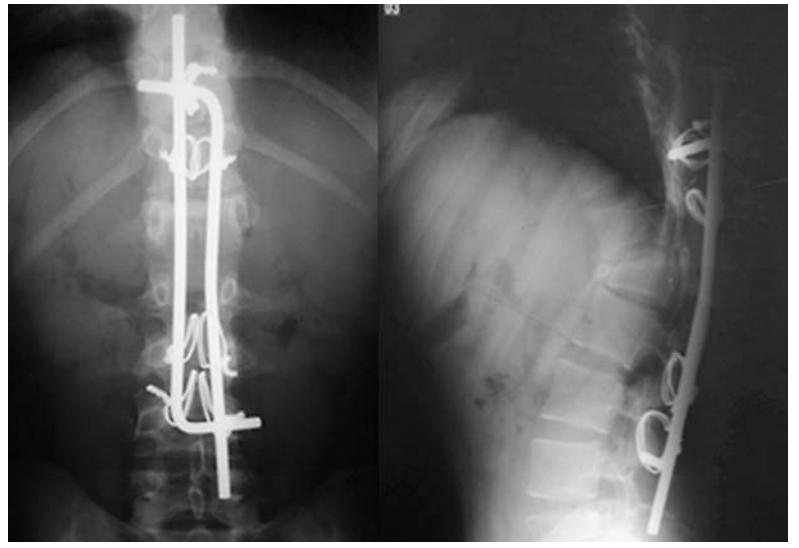

Fig. 17.8 Luque rod posterior instrumentation and fusion

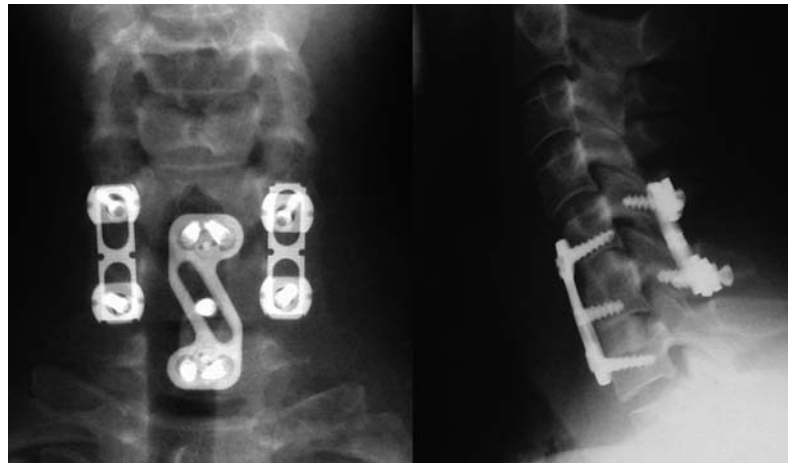

Fig. 17.9 C5–C6–C7 anterior cervical diskectomy and fusion (ACDF) with anterior plate instrumentation and lateral mass plate fixation of C5–C6 after laminectomy

systems. In the thoracic and lumbar spine rods and plates are generally placed laterally along the vertebral bodies and provide load-sharing support to the fixated segments. In the cervical spine, plates are placed anteriorly, and function both to provide load-sharing fixation and to prevent graft extrusion. As with cages and other implants, recent and future work has been toward development of newer materials, such as radiolucent bioabsorbable polymers.

17.2.1.5 New Materials

A number of synthetic materials have recently become available for use in spinal implantation that eliminate all image degradation from metal-related artifacts (Fig. 17.10). Carbon-fiber reinforced polymer and polyether-etherketone (PEEK), both radiolucent polymers, have been used in a variety of cage and spacer designs (Brantigan and Neidre 2003; Cho et al. 2002). In addition, polylactic acid (PLA) polymers, which have been used for some time in resorbable suture materials, are now being used in spinal implantation devices such as cages, plates, and even screws (Fig. 17.11). The PLA cages are radiolucent and provide height restoration and load-sharing alignment support while a solid bony fusion evolves, then resorb after many months (Alexander et al. 2002; Robbins et al. 2004). Radiographically, these devices allow for excellent assessment of the graft/native bone interfaces on CT and better MRI evaluations because of the absence of artifacts (Fig. 17.5c) (Kuklo et al. 2004; Krijnen et al. 2004). Tantalum is a radio-opaque porous metal with good compressive strength that can be fashioned into blocks or cages and conduct new bone formation through small porous interstices (Wigfield and Robie 2004). It causes even less artifacts than titanium on MRI but gives massive streak artifacts on CT. Calcium phosphate ceramic implants have relatively poor compressive strength, so they cannot be used in high-load bearing regions, such as the lumbar spine, but have adequate strength for the cervical spine.

17.2.1.6 Prosthetic Mechanical Discs

These devices were first introduced in the late 1980s. A number of such artificial disc designs have become commercially available (Fig. 17.12). Bao (1996) classified these devices into four categories: (a) low-friction sliding surface; (b) spring-and-hinge systems; (c) contained fluid-filled chambers; and (d) discs comprised of rubber or other elastomers. The materials used by different manufacturers vary considerably, with many different combinations of metals and polymers. Compared with spinal arthrodesis, these devices preserve at least some element of motion at the implanted segment, but the effects on adjacent motion segments and the facets have not been studied. In addition, mechanical wear and fatigue with ultimate device failure are inevitabilities that have not been added to the equation in comparing the overall clinical effectiveness of these devices vis-à-vis spinal arthrodesis procedures.

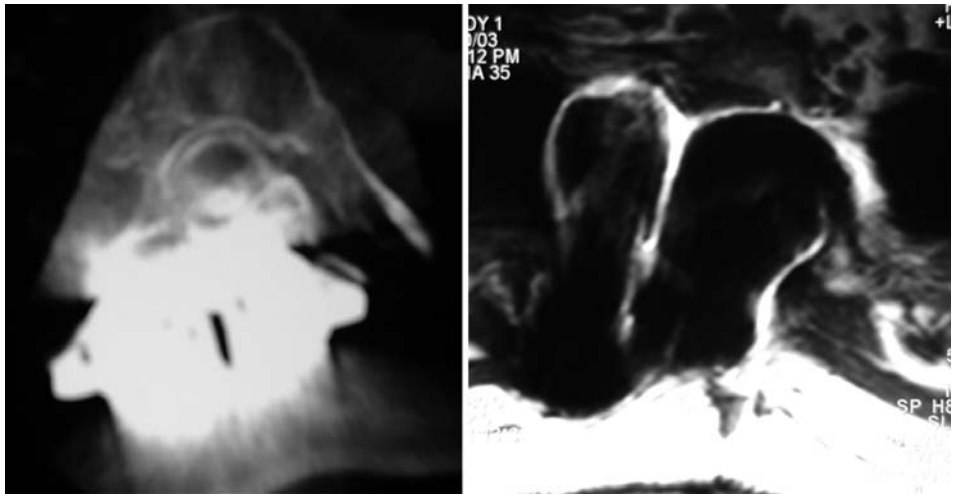

Fig. 17.10. Old stainless steel rods causing severe CT streak artifact (*left*) and MRI susceptibility artifacts (*right*)

Fig. 17.11. Polylactic acid radiolucent resorbable implant devices: plates; cages; and screws. (From Neurosurgical Focus, American Association of Neurological Surgeons)

17.2.2 Magnetic Resonance Imaging

Because CT and plain films provide virtually all relevant diagnostic information, MRI is not currently routinely used to assess grafts, implants, or hardware. It maintains its essential role in evaluating virtually everything else in the postoperative patient: neural structures; infection; disc herniations, etc. With higher field magnets and newer magnetically inert polymers being used for everything from cages to plates to screws, MRI may eventually be able to play a greater role (Fig. 17.13) (Van Goethem et al. 2002; Jinkins and Van Goethem 2001; Krijnen et al. 2004).

17.3 Intraoperative Image Guidance

Until recently, intraoperative image guidance has been limited to C-arm fluoroscopy and portable plain X-rays. While these modalities certainly have been adequate for placement of most implant devices, pedicle screw placement requires a high degree of precision, particularly in the smaller upper thoracic levels. Recent reports suggest that the isocentric C-arm portable CT scanners recently developed for intraoperative use provide a greater level of precision (Wang et al. 2004). Placement of screws using computer-aided surgery (CAS) techniques is also more reliable.

17.4 Imaging of Postoperative Complications

Complications may be categorized broadly into intra/peri-operative, early and delayed complications. Intra- and peri-operative complications are typically well-recognized surgical complications, most commonly direct injury to vascular or neural structures. Imaging of these complications, as well as some of the early postoperative complications, such as infection and dural leak, is essentially covered in the previous chapter on general postoperative spinal imaging and is not specific to spinal instrumentation: for instance, angiography for the assessment of vascular injuries and MRI for assessment of extradural hematomas or acute recurrent disc herniations.

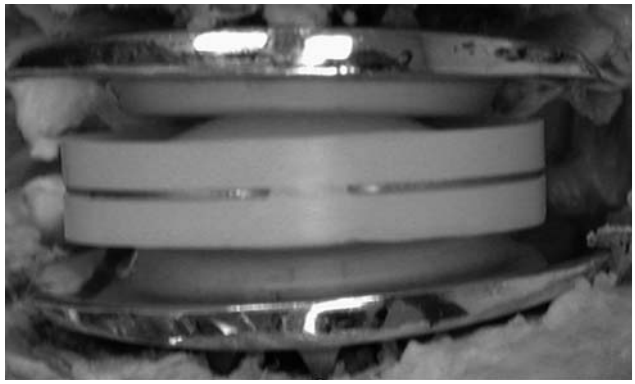

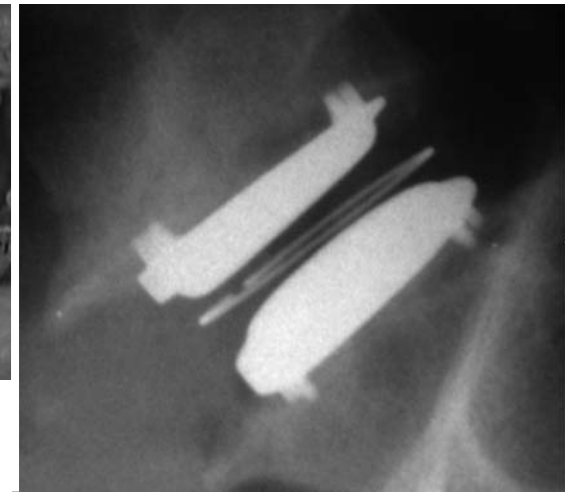

Fig. 17.12. Artificial disc implantation at L5–S1

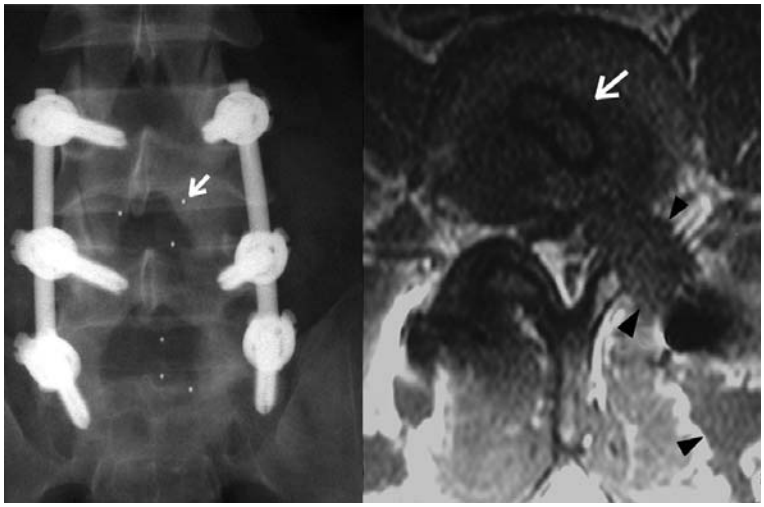

Fig. 17.13. Polyetheretherketone (PEEK) interbody cages (*arrows*) placed via minimally invasive percutaneous transforaminal lumbar interbody fusion (TLIF) at L4–L5 and L5–S1 and pedicle screw fixation. Cages are radiolucent with small radio-opaque beads for intraoperative visualization by C-arm fluoroscopy and X-ray (*left*, *arrow*). Magnetic resonance imaging shows absence of susceptibility artifact and subcutaneous track of transforaminal approach (*right*, *arrowheads*). Subcutaneous track on the contralateral side was for percutaneous pedicle screw placement

17.4.1 Imaging of Early Postoperative Complications

Early postoperative complications are primarily those that occur in the first few postoperative weeks or months: graft extrusion; implant or hardware misplacement; infection; and dural leak (pseudomeningocele). Unless migration is severe, partial graft extrusion may remain asymptomatic, although the risk of delayed union or non-union may increase. Implant or hardware misplacement likewise may remain asymptomatic unless severe enough to impinge on neural structures. Posterior cage migration encroaching on the spinal canal is infrequently encountered. By contrast, pedicle screw misplacement is more commonly seen. Examination in multiple planes by CT should be performed because axial images alone can be misleading as the screw takes an oblique course through the pedicle, particularly if there is violation of the superior or inferior cortical margins of the pedicle (Fig. 17.14).

17.4.2 Imaging Late Postoperative Complications

17.4.2.1 Pseudarthrosis and Nonunion

Pseudarthrosis is defined as failure of attempted spinal fusion to achieve solid bony arthrodesis by 1 year after surgery. The reported incidence of pseudarthrosis varies widely due to a multitude of disparate factors influencing outcomes: from 3–25% in posterolateral lumbar fusion, 4–68% in anterior lumbar interbody fusion, and 3–46% in anterior cervical fusion (An et al 1995; Boleta et al. 2000; Emery et al. 1997; Mutoh et al. 1993; Silcox 1998; Turner et al. 1992). The factors influencing pseudarthrosis rates include such disparate issues as type of fusion procedure and graft type (auto vs allograft); use of instrumentation; BMP, etc.; and patient factors, such as tobacco use, corticosteroid administration, non-steroidal anti-inflammatory medications, and underlying conditions such as scoliosis and osteoporosis.

17.4.2.2 Pseudarthrosis: Imaging Background

Despite the advances in imaging technology, the gold standard for diagnosis of pseudarthrosis continues to be surgical exploration combined with clinical data. The sensitivity and specificity of radiographic studies for assessment of non-union in spinal fusion has historically been low, with overall agreement rates for plain X-ray and surgical findings reported at 68–69% (Blumenthal and Gill 1993; Kant et al. 1995). With the exception of radionuclide bone scans, imaging studies have generally demonstrate good specificity and poorer sensitivity relative to surgical exploration with relatively high interobserver variability. Imaging studies have thus been used largely to confirm a clinical impression of non-union or to exclude other pathology responsible for symptoms. The advent of multislice helical volumetric CT scanning has added greater accuracy to diagnosis by imaging, but clinical impressions remain paramount, as another complicating factor is that some patients with radiographic evidence of pseudarthrosis are asymptomatic.

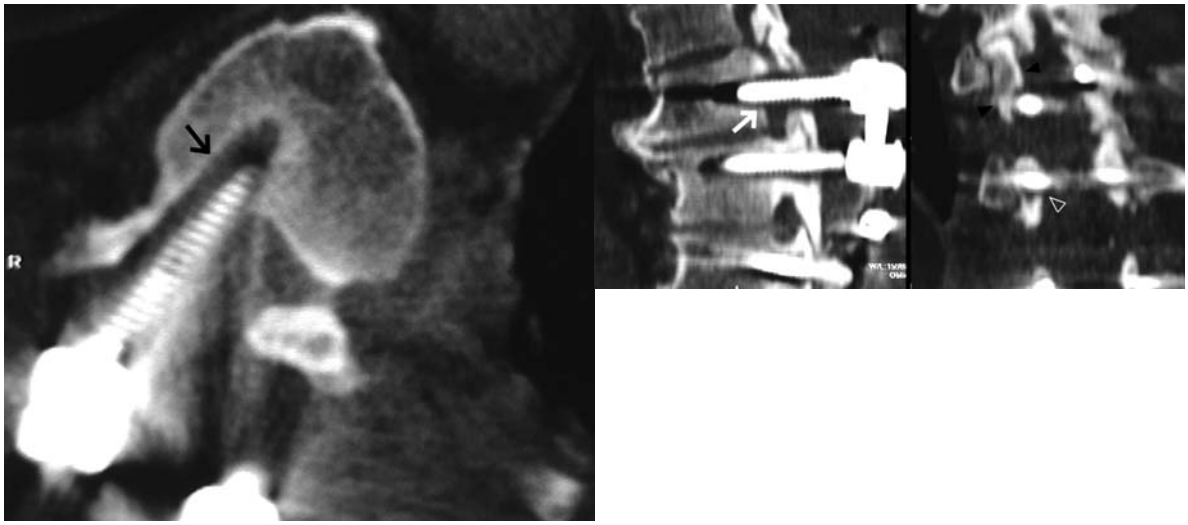

Fig. 17.14. Hardware misplacement and loosening, axial, sagittal, and coronal CT MPR. Lucent halo with surrounding sclerosis (*black arrow*) is the hallmark of hardware loosening. Confirming screw misplacement may require examination of multiple planes, as the oblique orientation of the screw relative to the pedicle can be problematic. Note confirmed violation of inferior margin of right T10 pedicle on sagittal MPR (*white arrow*), with appropriately placed screw at T11 below. Coronal MPR shows relationship of misplaced screw to T10 pedicle (*black arrowheads*), with appropriate screw placement noted at T11 (*white arrowhead*)

17.4.2.3 Radiographic Features

Imaging techniques capable of detecting pseudarthrosis include plain radiographs, X-ray polytomography, CT, and radionuclide imaging with single photon emission computed tomography (SPECT). Three-dimensional helical CT using multiplanar reconstructions (MPR) is the principal method of investigation, and as previously noted, clinical suspicion of pseudarthrosis warrants obtaining a volume data set with the thinnest available collimation and examining the fusion site in multiple planes. Radiographic recognition of pseudarthrosis in posterior and posterolateral fusion masses can be particularly difficult because of the marked variability in normal appearances. In these cases, correlation with nuclear medicine scintigraphy in addition to clinical findings may be helpful.

The radiographic hallmark of pseudarthrosis on plain X-ray or CT is abnormal lucency with surrounding sclerosis (Fig. 17.15). Sclerosis is a reflection of abnormal motion, which is a clinical hallmark of non-union.

Radionuclide bone scanning has yielded inconsistent results in both sensitivity and specificity in the diagnosis of non-union. Generally, bone scans are more sensitive and less specific than plain radiographs. Positive bone scans are present in over half of asymptomatic patients, likely due to continued normal bony remodeling at the fusion site (Hannon and Wetta 1977; Mcmaster and Merrick 1980). Very focal intense activity may better reflect the presence of non-union, as opposed to more ill-defined or diffuse activity that reflects normally increased bone turnover in a fused spine (Fig. 17.16).

Magnetic resonance imaging has not established a significant role in the diagnosis of non-union or instrumentation failure. When findings are present on MRI, pseudarthrosis is seen as a linear hyperintensity on T2-weighted images and subchondral bands of low intensity on T1-weighted images (Ghazi et al. 1992). Reactive marrow changes and enhancement with gadolinium due to abnormal motion may be seen as well (Fig. 17.17) (Salgado et al.), but these findings are inconstant in our experience. Magnetic resonance imaging is more useful to exclude other pathology responsible for pain in the post-fusion patient.

17.4.2.4 Other Graft-Related Delayed Complications

Graft subsidence, or settling of an interbody graft into the endplates of the vertebral bodies, may or

Fig. 17.15a–c. Pseudarthrosis: ALIF with threaded interbody allograft **a**, and threaded titanium cage **b,c**. The radiographic hallmark is perigraft lucency and sclerosis, which may either completely surround the graft (**a**, *arrowheads*), or involve only one of the graft/bone interfaces (**c**, *arrows*), while other interface is intact (**c**, *arrowheads*)

may not be associated with non-union. This complication results in loss of the restoration of disc height, one of the principal goals of spinal fusion surgery. Other graft complications include graft migration or extrusion and graft fragmentation/collapse, both of which typically occur in association with non-union.

17.4.2.5 Hardware Failure

Hardware failure frequently occurs in association with non-union and results from persistent repetitive loading secondary to non-union with subsequent metal fatigue and breakage or loosening. Hardware loosening presents radiographically as a lucent halo surrounding the device. Adjacent bony sclerotic changes may also be present (Fig. 17.18).

17.5 Conclusion

Future avenues of advancement will undoubtedly be towards the further development of synthetic materials to replace the need for autogenous graft harvesting, which is still associated with a high incidence of postoperative morbidity, as well as towards less invasive and more "biologic" approaches to spinal disease, such as disc regeneration. The field of spinal instrumentation surgery, like many medical disciplines, is undergoing continuous change; thus far, changes have essentially been confined within a well-established set of basic principles addressed in this chapter. It would therefore serve the radiologist well to have an understanding of these basic principles when interpreting imaging studies in the postoperative spine patient as the field of spine surgery continues to evolve.

Fig. 17.16a–c. Pseudarthrosis, 13 months postoperative in symptomatic patient: lateral plain X-ray **a**, axial CT **b**, and bone scan **c**. Nonunion is not apparent on plain X-ray and quite subtle on axial CT (**b**, *arrows*). The degree of abnormal focal tracer activity on bone scan **c** is greater than should be expected normally at 13 months post-procedure

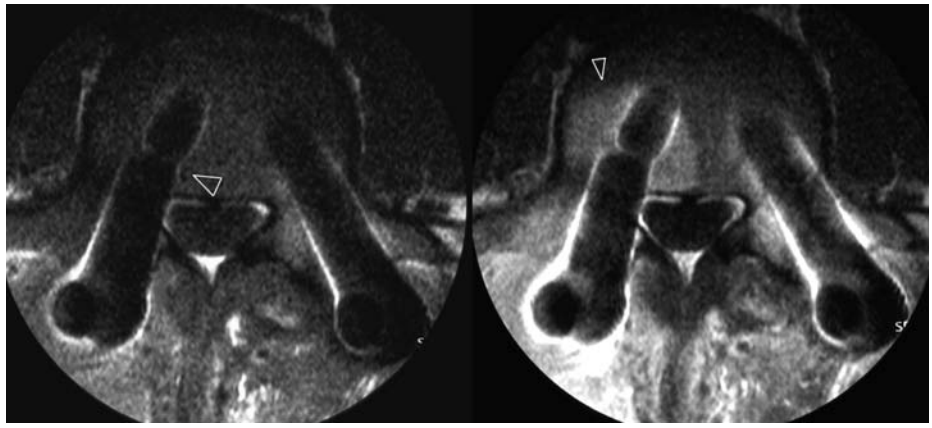

Fig. 17.17. Hardware failure with pedicle screw breakage and loosening. Axial T1-weighted MRI shows broken pedicle screw (*left, arrowhead*). Abnormal enhancement after gadolinium administration indicates loosening (*right, arrowhead*). (Case courtesy of J. Van Goethem)

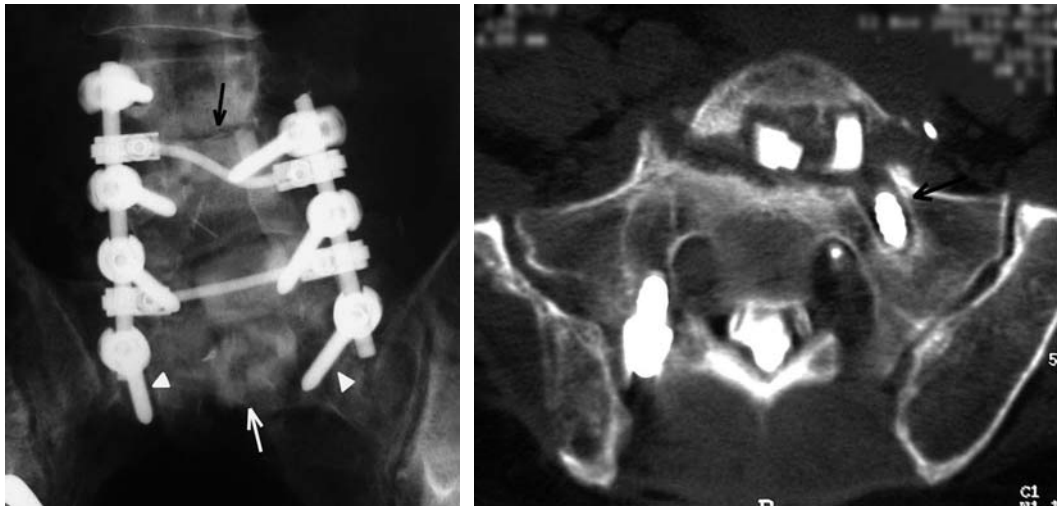

Fig. 17.18a,b. Hardware failure accompanying pseudarthrosis in multilevel ALIF with femoral ring allografts and pedicle screw instrumentation. Abnormal lucency and sclerosis is seen at superior margin of graft at L3–L4 on anteroposterior X-ray (**a**, *black arrow*) and at L5–S1 on axial CT **b**. Graft fragmentation as well as perigraft lucency is noted at L5–S1 (**a**, *white arrow*) with associated pedicle screw loosening characterized by lucent halo on plain X-ray (**a**, *arrowheads*) and axial CT (**b**, *arrow*)

References

Albee FH (1911) Transplantation of a portion of the tibia for Potts disease. J Am Med Assoc 57:885–886

Albert TJ, An HS, Cotler JM, Balderston RA (1999) Harrington instrumentation and modifications. In: An HS, Cotler JM (eds) Spinal instrumentation, 2nd edn. Lippincott Williams and Wilkins, Philadelphia, pp 305–316

Alexander JT, Branch CL Jr, Subach BR, Haid RW (2002) Applications of a resorbable interbody spacer via a posterior lumbar interbody fusion technique. Orthopedics 25:1185–1189

An HS, Simpson JM, Glover JM et al. (1995) Comparison between allograft plus demineralized bone matrix versus autograft in anterior cervical fusion. A prospective multicenter study. Spine 20:2211–2216

Bao QB (1996) The artificial disc: theory, design and materials. Biomaterials 17:1157–1167

Benzel EC, Ball P (1994) History of spinal instrumentation. Neurosurgical topics: spinal instrumentation. American Association of Neurological Surgeons, Rolling Meadows, Illinois

Blumenthal SL, Gill K (1993) Can lumbar spine radiographs accurately determine fusion in postoperative patients? Correlation of routine radiographs with a second surgical look at lumbar fusions. Spine 18:1186–1189

Boleta MJ, Rechtine GR II, Chrin AM (2000) Three- and four-level anterior cervical discectomy and fusion with plate fixation: a prospective study. Spine 25:2040–2044

Brantigan JW, Neidre A (2003) Achievement of normal sagittal plane alignment using a wedged carbon fiber reinforced polymer fusion cage in treatment of spondylolisthesis. Spine J 3:186–196

Burkus JK, Gornet MF, Dickman C, Zdeblick TA (2002a) Anterior interbody fusion using rhBMP-2 with tapered interbody cages. J Spinal Disord Tech 15:337–349

Burkus JK, Transfeldt E, Kitchel SH, Watkins R, Balderston R (2002b) Clinical and radiographic outcomes of anterior lumbar interbody fusion using recombinant human bone morphogenetic protein-2. Spine 27:2396–2408

Cho DY, Liau WR, Lee WY et al. (2002) Preliminary experience using a polyetheretherketone (PEEK) cage in the treatment of cervical disc disease. Neurosurgery 51:1343–1349

Cotler JM (1999) Historical events leading to spine surgery. In: An HS, Cotler JM (eds) Spinal instrumentation, 2nd edn. Lippincott Williams and Wilkins, Philadelphia, pp 3–8

Emery SE, Fisher JR, Bohlman HH (1997) Three-level anterior cervical discectomy and fusion: radiographic and clinical results. Spine 22:2622–2624

Ghazi J, Golimbu CN, Engler G (1992) MRI of spinal fusion pseudarthrosis. J Comput Assist Tomogr 16:324–326

Hannon KM, Wetta WJ (1977) Failure of technetium bone scanning to detect pseudarthrosis in spinal fusion for scoliosis. Clin Orthop 123:42–44

Harrington PR (1960) Surgical instrumentation for management of scoliosis. J Bone Joint Surg 42A:1448

Harrington PR (1988) The history and development of Harrington instrumentation. Clin Orthop 227:3

Hibbs RA (1911) An operation for progressive spinal deformities. NY State J Med 93:1013–1016

Jinkins JR, Van Goethem JW (2001) The postsurgical lumbosacral spine. Magnetic resonance imaging evaluation following intervertebral disk surgery, surgical decompression, intervertebral bony fusion, and spinal instrumentation. Radiol Clin North Am 39:1–29

Kant AP, Daum WJ, Dean SM et al. (1995) Evaluation of lumbar spine fusion: plain radiographs versus direct surgical exploration and observation. Spine 20:2313–2317

Krijnen MR, Smit TH, Strijkers GJ et al. (2004) The use of high-resolution magnetic resonance imaging for monitoring interbody fusion and bioabsorbable cages: an ex vivo pilot study. Neurosurg Focus 16, Article 3, pp 1–8

Kuklo TR, Rosner MK, Polly DW Jr (2004) Computerized tomography evaluation of a resorbable implant after transforaminal lumbar interbody fusion. Neurosurg Focus 16, Article 10, pp 1–6

Luque ER (1982) The anatomic basis and development of segmental spine instrumentation. Spine 7:256–259

McMaster MJ, Merrick MV (1980) The scintigraphic assessment of the scoliotic spine after fusion. J Bone Joint Surg Br 62:65–72

Mutoh N, Shinomiya K, Furuya K et al. (1993) Pseudarthrosis and delayed union after anterior cervical fusion. Int Orthop 17:286–289

Price CT, Connolly JF, Carantzas AC et al. (2003) Comparison of bone grafts for posterior spinal fusion in adolescent idiopathic scoliosis. Spine 28:793–798

Robbins MM, Vaccaro AR, Madigan L (2004) The use of bioabsorbable implants in spine surgery. Neurosurg Focus 16, Article 1, pp 1–7

Sandhu H (2004) Spinal fusion using bone morphogenetic proteins. Orthopedics 27:717–718

Salgado R, Van Goethem JW, van den Hauwe L, Parizel PM (2006) Imaging of the postoperative spine. Semin Roentgenol. 41:312-326

Silcox DH III (1998) Laparoscopic bone dowel fusions of the lumbar spine. Orthop Clin N Am 29:655–663

Thometz JG, An HS (1999) Luque instrumentation with sublaminar wiring. In In: An HS, Cotler JM (eds) Spinal instrumentation, 2nd edn. Lippincott Williams and Wilkins, Philadelphia, pp 317–326

Turner JA, Ersek M, Herron L et al. (1992) Patient outcomes after lumbar spinal fusions. J Am Med Assoc 268:907–911

Van Goethem JW, Parizel PM, Jinkins JR (2002) Review article: MRI of the postoperative lumbar spine. Neuroradiology 44:723–739

Wang MY, Kim KA, Liu CY, Kim P, Apuzzo ML (2004) Reliability of three-dimensional fluoroscopy for detecting pedicle screw violations in the thoracic and lumbar spine. Neurosurgery 54:1138–1142

Wigfield CC, Robie BH (2004) Porous tantalum for spinal interbody fusion. In: Lewandrowski K, Wise D, Trantolo DJ et al. (eds) Advances in spinal fusion. Dekker, New York, pp 775–780

Tumors

Intradural Spinal Tumors

18

Danielle Balériaux and Neslihan Gültaşli

CONTENTS

D. Balériaux, MD
Professor, Department of Radiology, Clinique de Radioneurologie, Hôpital Erasme, Université Libre de Bruxelles, 808 Route de Lennik, 1070 Brussels, Belgium
N. Gültaşli, MD
Department of Radiology, Clinique de Radioneurologie, Hôpital Erasme, Université Libre de Bruxelles, 808 Route de Lennik, 1070 Brussels, Belgium

18.1 Introduction

The spinal cord is especially well protected by the surrounding CSF, the meningeal envelopes and the bony spine. Intradural tumors are rare lesions: they include intramedullary and intradural extramedullary tumors (Fischer and Brotchi 1996). In a general hospital, of all spinal tumors only 5% are intramedullary whereas 40% are intradural extramedullary and 55% are extradural. Some tumors may initially be intramedullary and become eventually exophytic, growing out of the medulla (extramedullary ependymoma, extramedullary astrocytoma). On the contrary, some extramedullary intradural tumors may grow into the cord like schwannomas. Finally, primary intradural extramedullary tumors may expand towards the extra-dural space such as schwannomas or meningiomas. Extradural tumors are most often malignant lesions, rapidly evolving and originating from the epidural or latero-vertebral space: they are described in Chapters 19 and 20.

KEY-POINTS

- Intradural tumors may be either:
  - Intramedullary
  - Intradural extramedullary
- In general, clinical symptoms of spinal tumors include:
  - Pain (most common symptom)
  - Motor and sensory deficits
  - Sphincter disturbances and impotence
- MRI is the imaging modality of choice
- Spinal tumors are classified according to the WHO classification system
- About intramedullary tumors:
  - Astrocytomas and ependymomas are most common intramedullary tumors
  - Occur predominantly in children and young adults
  - Ependymomas are circumscribed, enhancing tumors, and are frequently associated with hemorrhage and satellite cysts
  - Astrocytomas are enhancing, infiltrating spinal cord tumors; they tend to be more heterogeneous and may contain necrotic or cystic components
  - Hemangioblastomas are low grade tumors, rich in capillaries and are seen as intensely enhancing subpial nodules with flow voids; they may be associated with very large intramedullary cysts
  - Intramedullary metastases are focal enhancing spinal cord lesions with extensive edema
- About intradural extramedullary tumors:
  - Neurogenic tumors (schwannomas, neurofibromas) and meningiomas are most common intradural extramedullary tumors
  - Schwannomas originate from the nerve sheath; they are most often purely intradural extramedullary tumors, though 15% are extradural and 15% have a "dumbbell" shape involving both the intra- and extradural space
  - Meningiomas are slow growing dural-based intradural tumors with a female preponderance (fifth/sixth decade)
  - Intradural extramedullary metastases can spread subarachnoidally from CNS tumors ("drop metastases") or through hematogenous dissemination from a primary non-CNS tumor (breast and lung carcinoma)
- Many non-neoplastic intramedullary lesions can simulate tumor infiltration:
  - MS plaques
  - Inflammatory lesions
  - Granulomatous disease (tuberculosis, sarcoid)
  - Abscesses (bacterial, tuberculosis)
  - Radionecrosis

The role of the radiologist is to answer the following major questions posed by the clinician: does the patient have an intracanalar lesion and, if yes, is it a tumor? If it is a tumor, where is this tumor precisely located (extra- versus intramedullary)? Is it a benign or a malignant tumor? Is it surgically removable? Other questions regard prognosis and optimal treatment, as well as follow-up.

18.2 Clinical Symptoms

Spinal cord tumors are mostly (80%) slow growing, low grade tumors; pain is the most frequent and early symptom reported and may be the only symptom at the beginning of the disease. Motor and sensory deficits occur in relation to tumor location. Clinical presentation is poorly specific and, therefore, the diagnosis is frequently delayed (Baleriaux 1999a). In our experience, the mean time between the initial symptoms (first medical consultation) and diagnosis was more than 2 years! Urinary disturbances and impotence are less frequent and usually appear at a later stage in the clinical course of the disease, coincident with motor paralysis of the legs.

In children, pain is also the most frequent symptom, as reported in 42% of cases. Motor regression is present in 36%, gait abnormality in 27%, torticollis in 27% and progressive kyphoscoliosis in 24%. In the pediatric age group, 89% of tumors are low grade lesions (Constantini et al. 1996; Innocenzi et al. 1996).

Hemorrhage can occur within spinal cord tumors (Nemoto et al. 1992) and may be recognized on T1-WI as hyperintense areas, when the hemorrhage is between 1 week to approximately 4 months old. Hemosiderin deposits can later be identified as low signal areas on both T1-WI and T2-WI, preferably obtained in gradient echo sequences. When MRI shows an intramedullary tumor with hypointensity at the margins, it is suggestive, but not pathognomonic, of an ependymoma (Osborn 1994; Nemoto et al. 1992).

Subarachnoid hemorrhage (SAH) of spinal origin is a rare clinical entity and the most common source of SAH is an arteriovenous malformation (Lahanis et al. 1993). Still, a few cases of SAH due to bleeding from hemangioblastoma have been reported in the literature: this etiology should be kept in mind in documented cases of SAH with normal cerebral angiography. In these patients, MRI of the spine should be performed in order to rule out this classical, although very rare, cause of SAH (Minami et al. 1998).

Finally, hydrocephalus may be observed, associated with an intradural spinal tumor; we have encountered this feature once associated with a large lumbar schwannoma, once associated with a huge intramedullary astrocytoma in a child and in a case of a malignant intramedullary tumor with associated leptomeningeal carcinomatous spread (Fig. 18.1). In the literature, this infrequent cause of hydrocephalus has been well documented (Rifkinson-Mann et al. 1990). Consequently, in the presence of childhood hydrocephalus and increased intracranial pressure without a clearly defined etiology, a spinal cord tumor should always be ruled out (Caviness et al. 1998).

18.3 Imaging Techniques

Today, magnetic resonance imaging (MRI) has become the imaging technique of choice to demonstrate intradural tumors. Still, so-called conventional techniques are commonly performed and we will quickly review their usefulness and limitations in the case of an intradural tumor.

18.3.1 X-Ray Films

Plain X-ray films are usually of very limited value in the case of an intramedullary tumor in an adult patient. The cervical spine may loose its normal lordotic aspect in the case of an intramedullary cervi-

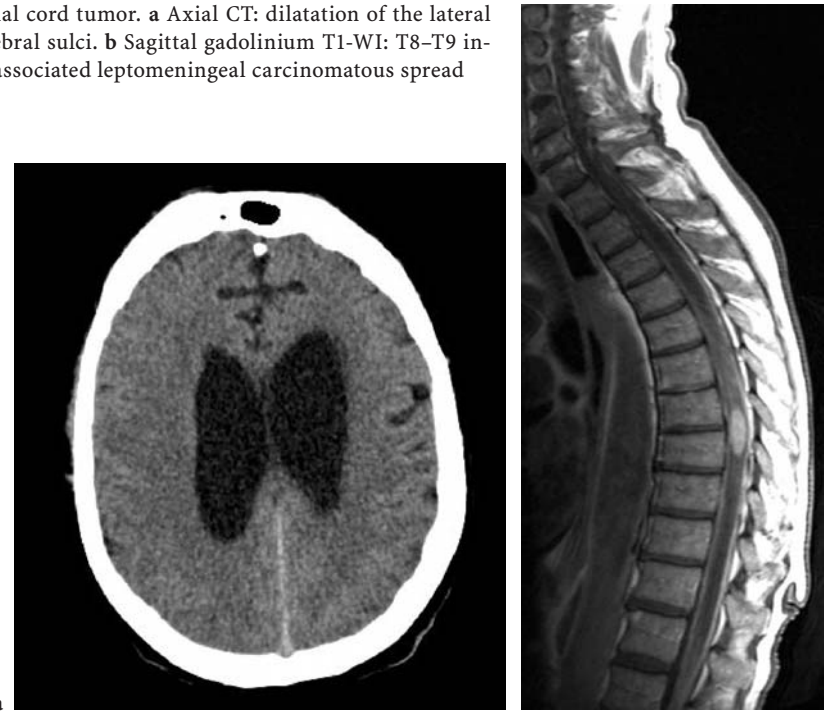

Fig. 18.1a,b. Hydrocephalus and spinal cord tumor. **a** Axial CT: dilatation of the lateral ventricles and effacement of the cerebral sulci. **b** Sagittal gadolinium T1-WI: T8–T9 intramedullary malignant tumor and associated leptomeningeal carcinomatous spread

a b

cal tumor; this is mainly linked to the more or less severe pain experienced by the patient. Whenever an especially "straight" cervical spine is observed, or if the normal curvature is reversed, one should rule out an underlying spinal cord tumor (Fig. 18.2a). The same applies in the case of torticollis, which is often associated with an upper cervical tumor or a foramen magnum lesion. Moreover, a progressive, evolving scoliosis should alert the clinician to the possibility of an underlying intramedullary lesion (Baleriaux et al. 1992).

Although plain films are rarely abnormal in adults with an intramedullary tumor, they may show anomalies in children (58%–81%) demonstrating enlargement of the canal, straightening of the spine or scoliosis. Indeed, in children, a growing spinal cord tumor may expand the bony canal, through pressure erosion, and this enlargement of the spinal canal can be an important feature diagnosed on plain films.

A myxopapillary ependymoma of the conus is typically seen in young adults. Those tumors are often also responsible for enlargement and "scalloping" of the posterior part of the lower thoracic and upper lumbar vertebrae.

Intradural extramedullary tumors typically expand into the extradural and paravertebral space. Enlargement of the spinal foramina can be detected on plain X-ray films as well as intratumoral calcifications, when present.

Today, in our experience, standard X-ray films have almost completely been replaced by multidetector computed tomography (CT).

18.3.2 Computed Tomography

Computed tomography has become the optimal imaging technique for the evaluation of the vertebral bony structures including vertebral bodies, pedicles, articular facets and laminae. Multidetector volume CT allows rapid and extensive visualization of the spine and has replaced standard X-ray films, especially in trauma patients. Secondary 3D reconstructions are obtained almost instantly and provide unique visualization of bony structures. In the case of tumor pathology, CT clearly shows widening of the bony spinal canal and enlargement of the vertebral foramina. Intratumoral calcifications are better depicted on CT compared to MRI but the relation to the soft tissues remain in some cases uncertain (Fig. 18.2b, 18.3a). However, plain CT is not the initial screening modality for intramedullary lesions, given the limited contrast resolution for the content of the spinal canal (although, thanks to technical developments, the density resolution has improved). The diagnosis of an intramedullary cystic lesion is feasible with CT (Fig. 18.2b), especially if the reader is aware of a potential intracanalar pathology suspected by clinical examination!

18.3.3 Myelography and Myelo-CT

Before the arrival of MRI, myelography was the preferred imaging modality for the visualization of the spinal cord. Nowadays, this invasive imaging method should be definitely avoided since the patient's symptoms may occasionally be exacerbated by the procedure. Moreover, only the cord contours are delineated with myelography and no information is obtained concerning the intramedullary appearance. Myelo-CT was used in cases of complete "myelographic bloc" in order to still be able to image the intracanalar space as even small amounts of contrast medium could be better picked up by CT. Cystic tumor components may be detected on delayed myelo-CT performed a few hours after intrathecal water-soluble contrast medium (Baleriaux et al. 1992).

18.3.4 Digital Substraction Angiography

The normal vascularisation of the spinal cord is demonstrated in an optimal way by systematic catheterization of all potential vascular feeders to the cord. Digital substraction angiography (DSA) remains the imaging modality of choice to study spinal cord vascularization and, especially, to identify the artery of Adamkiewicz, spinal cord AVMs, and spinal dural fistula. Spinal vascularization has been perfectly described by Thron et al. (1988), as well as by Lasjaunias et al. (1992). Spinal angiography is a long procedure requiring good knowledge of spinal normal vascularization and should be performed by trained neuroradiologists (Fig. 18.4a). Magnetic resonance angiography (MRA) however, is steadily becoming an alternative imaging procedure that might replace spinal DSA in the near future, mainly for diagnostic purposes and to guide spinal neurointerventional procedures (Backes et al. 2004).

Fig. 18.2a–f. Cervical ependymoma in a 30-year-old male with a 1-year history of left cervicobrachialgia. **a** Lateral X-ray film shows inversion of the normal cervical lordosis. No enlargement or bony erosion of the cervical canal. **b** Series of axial contrast enhanced CT images at the level of C6–C7: careful analysis allows detection of an enlarged spinal cord. An intramedullary cyst may be suspected. **c–f** Series of sagittal MRI images. **c** Sagittal T2-WI. **d** Gradient echo T2-WI. **e** T1-WI. **f** Gadolinium T1-WI images. The tumor is mainly hypointense on T2-WI, isointense on T1-WI and enhances strongly after contrast administration. Signs of chronic bleeding at both extremities of the tumor are best demonstrated on gradient T2-WI: "cap sign". Associated cysts are seen both above and below the solid tumor

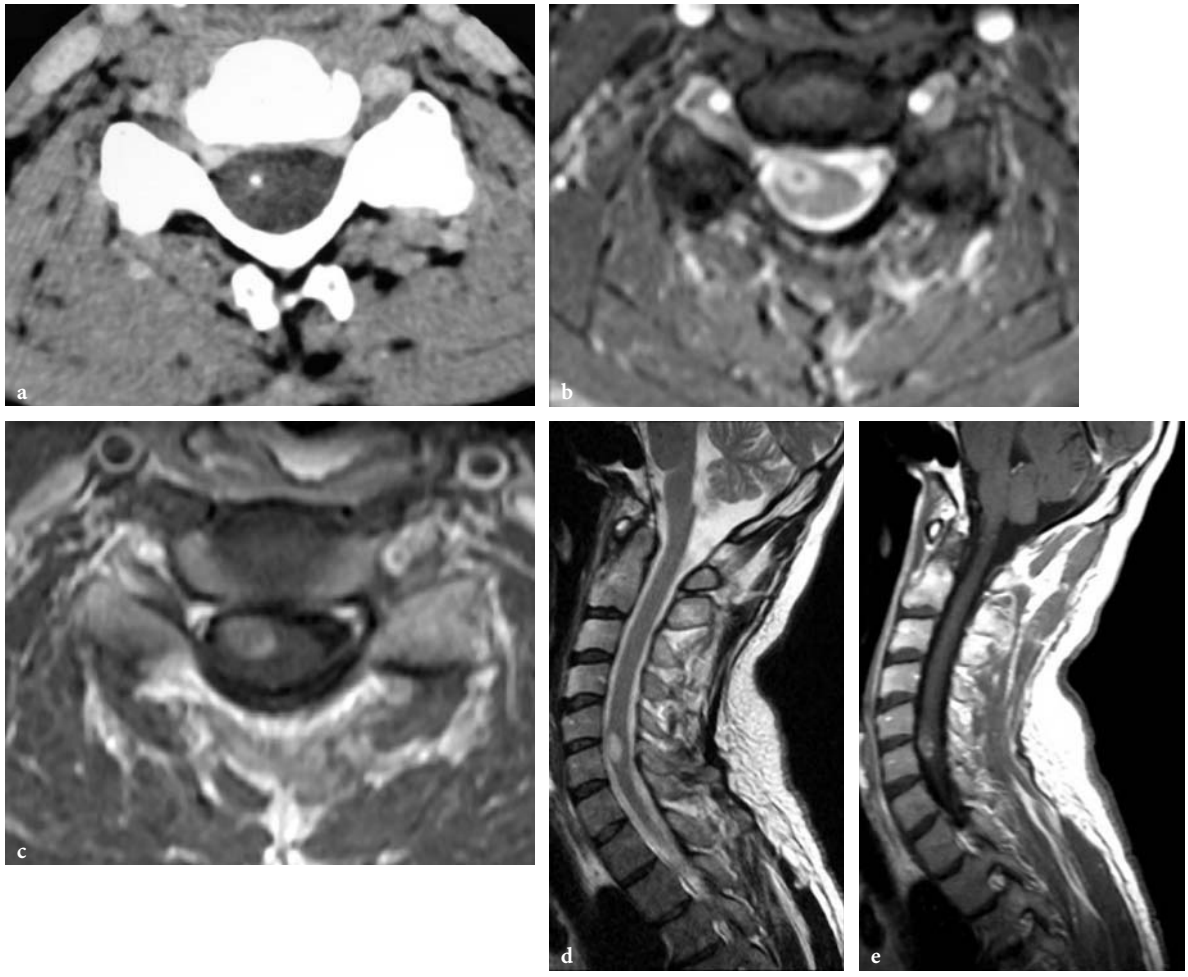

Fig. 18.3a–e. Tumor of unknown histology: incidental finding in an asymptomatic patient. **a** Axial contrast enhanced CT shows a small intracanalar calcification. The precise location within the spinal cord cannot be appreciated on this image. **b** Axial T2-WI. **c** Gadolinium T1-WI much better demonstrates the presence of an intramedullary anterior right mass. The calcification is clearly visible on the T2-WI and is intramedullary. (Reprinted with permission from Baleriaux et al. 2004) **d,e** Sagittal T2- and gadolinium T1-WI: well circumscribed lesion, hyperintense on T2-WI and enhancing strongly after contrast administration. The patient is asymptomatic: no surgical removal has been attempted until now as 5-years follow-up shows no evolution of this lesion!

18.3.5 Magnetic Resonance Imaging

When magnetic resonance imaging (MRI) is used to explore the spinal canal, the following rules must be observed: systematic use of both T1- and T2-weighted images (Bydder et al. 1985) (Figs. 18.2c–f, 18.4b–d), thin slices (≤ 3 mm slice thickness), two different imaging planes (sagittal and axial), and a large field-of-view to allow visualisation of the entire cord (Baleriaux et al. 2004). Gradient echo images are useful in order to detect hemorrhagic components often present in cord tumors (Fig. 18.2d). Contrast injection is indispensable in order to better identify solid enhancing tumor components (Figs. 18.2f, 18.4d,e), and to differentiate tumor cysts whose borders enhance from associated, so-called reactive, cystic components (Baleriaux 1999b; Del Caprio O'Donovan 1998; Li and Holtas 1991; Parizel et al. 1989; Scotti et al. 1987).

18.3.6 Magnetic Resonance Myelography

Heavily T2-weighted fat suppression techniques have been described in order to obtain interesting thin slices resembling conventional myelography with the

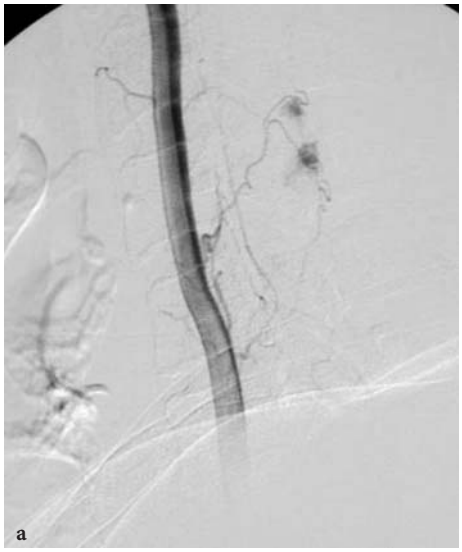

Fig. 18.4a–f. Cervical hemangioblastomas in a case of von Hippel-Lindau syndrome. **a** Vertebral digital substraction angiography best shows the typical hypervascularisation supplied by enlarged arterial branches and the typical vascular stain of hemangioblastomas. **b** Sagittal T2-WI. **c** Sagittal T1-WI. **d** Sagittal gadolinium T1-WI. Small intensely enhancing tumors are located posteriorly to the cord (subpial) at the C4 level. The tumors are hypointense on T2-WI and are surrounded by extensive edema, best seen on this T2-WI (**b**). **e** Axial gadolinium T1-WI help identify the posteriorly, sub-pial location. **f** Sagittal gadolinium T1-WI: post-operative MRI shows complete removal of the multiple hemangioblastomas

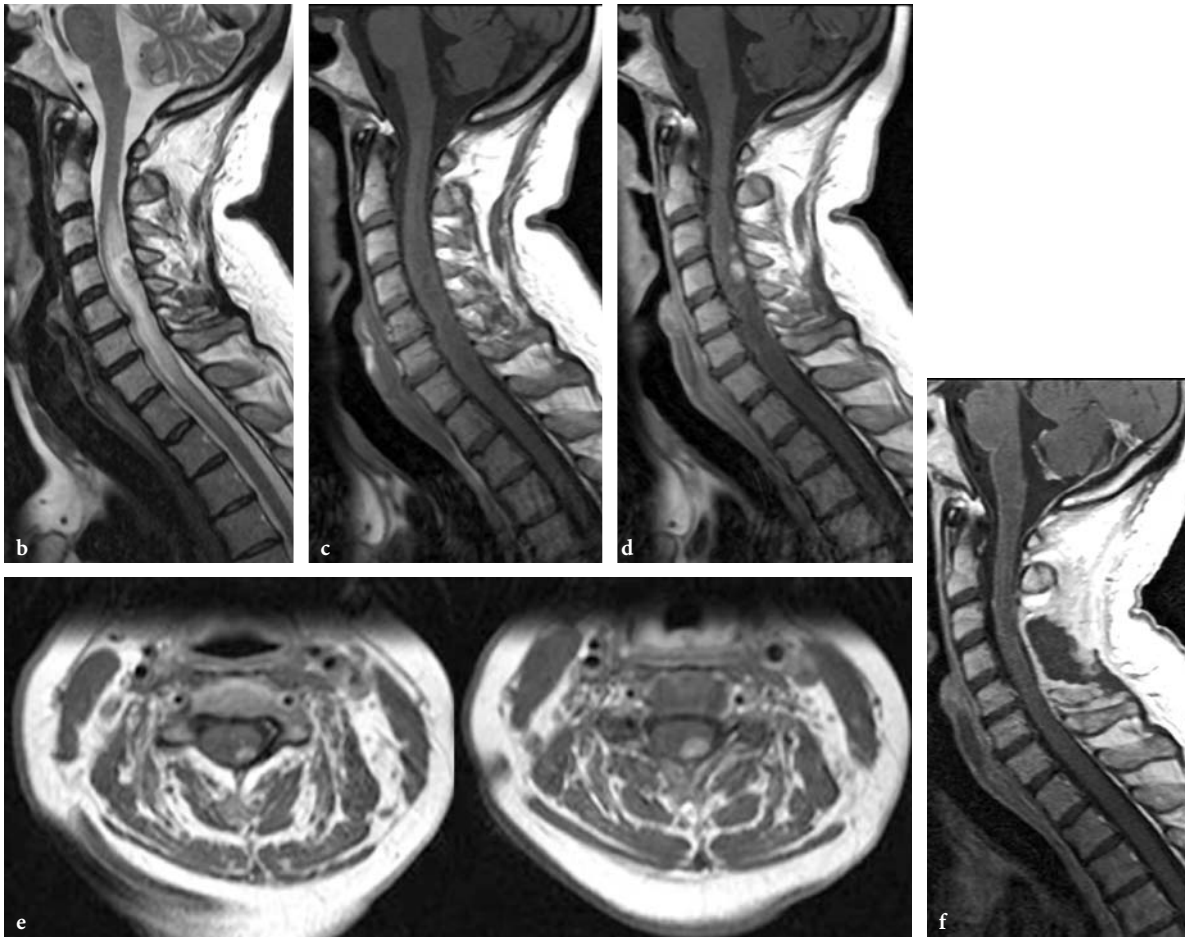

major advantage that no intrathecal contrast injection is required! This technique is mainly useful to detect and better depict extramedullary intracanalar lesions such as small neurinomas (Figs. 18.5d, 18.35b), dilated vascular structures on the surface of the cord (see Fig. 39f.) or traumatic lesions such as pseudomeningoceles (Edal et al. 1997).

18.3.7 Magnetic Resonance Angiography

Multiple MRA techniques are currently available. Time-of-flight (TOF), phase contrast (PC) and contrast-enhanced bolus T1-weighted techniques are routinely used for vascular pathology in the brain. The small size of spinal cord vessels, especially arteries, makes spinal MRA more difficult and challenging. Still, the results of spinal MRA are constantly improving. We recommend the use of T1-weighted sequences with intravenous bolus injection of gadolinium as described by Backes et al. (2004); this method enables systematic visualisation of the artery of Adamkiewicz and provides a very attractive and reliable first angiographic approach of spinal vascular malformations. Spinal MRA is becoming the first diagnostic screening procedure for vascular spinal malformations. In some cases, spinal MRA may obviate the need for unnecessary invasive spinal angiography; in other instances, it may serve as an initial roadmap to guide DSA and embolisation procedures (Fig. 18.6c). Still, spinal DSA with selective catheterization of the spinal feeding arteries remains the modality of choice to study spinal cord vascularization and allows interventional procedures.

18.3.8 Diffusion Techniques

Molecular diffusion nuclear MRI is an extremely interesting imaging technique first described by Le Bihan in 1991. It has been predominantly used for the evaluation of cerebral lesions, especially in cases

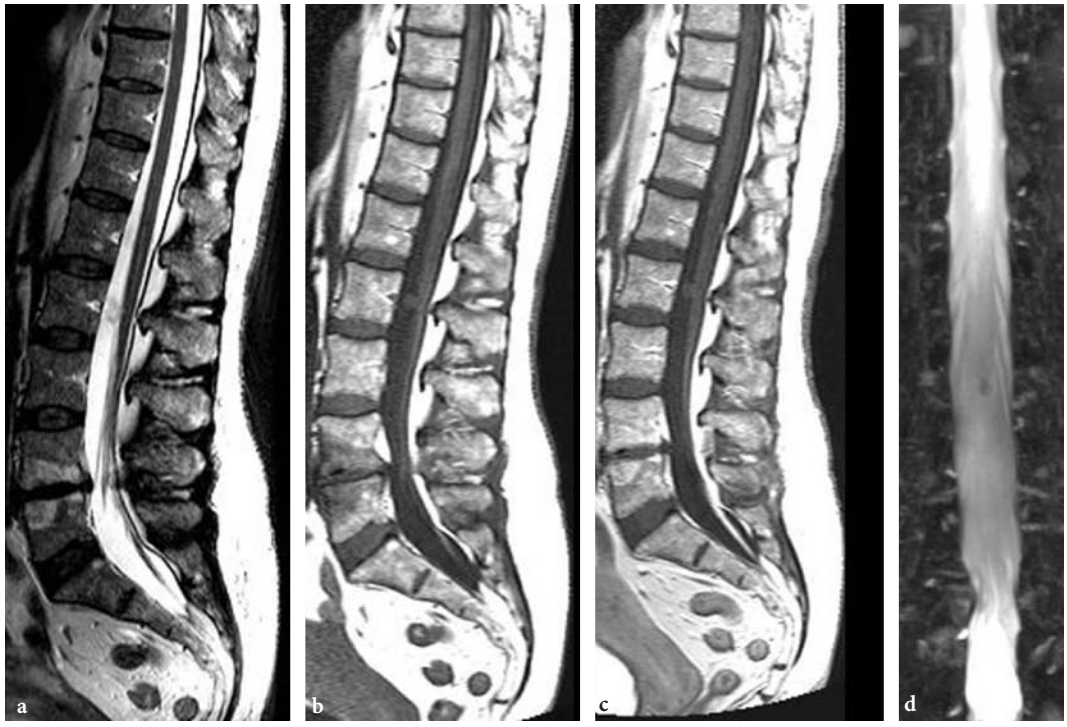

Fig. 18.5a–d. Usefulness of myelo-MRI in a case of a small neurinoma in a patient with a low conus medullaris (L2–L3). **a** Sagittal T2-WI. **b** Sagittal T1–WI. **c** Sagittal gadolinium T1–WI. **d** Coronal myelo-MRI. The lesion is anteriorly located at the L2 level. It is moderately hyperintense on T2-WI compared to the cord, isointense on T1-WI and it mildly enhances after contrast administration. MR myelography nicely demonstrates the relation between the lesion and the adjacent low spinal cord

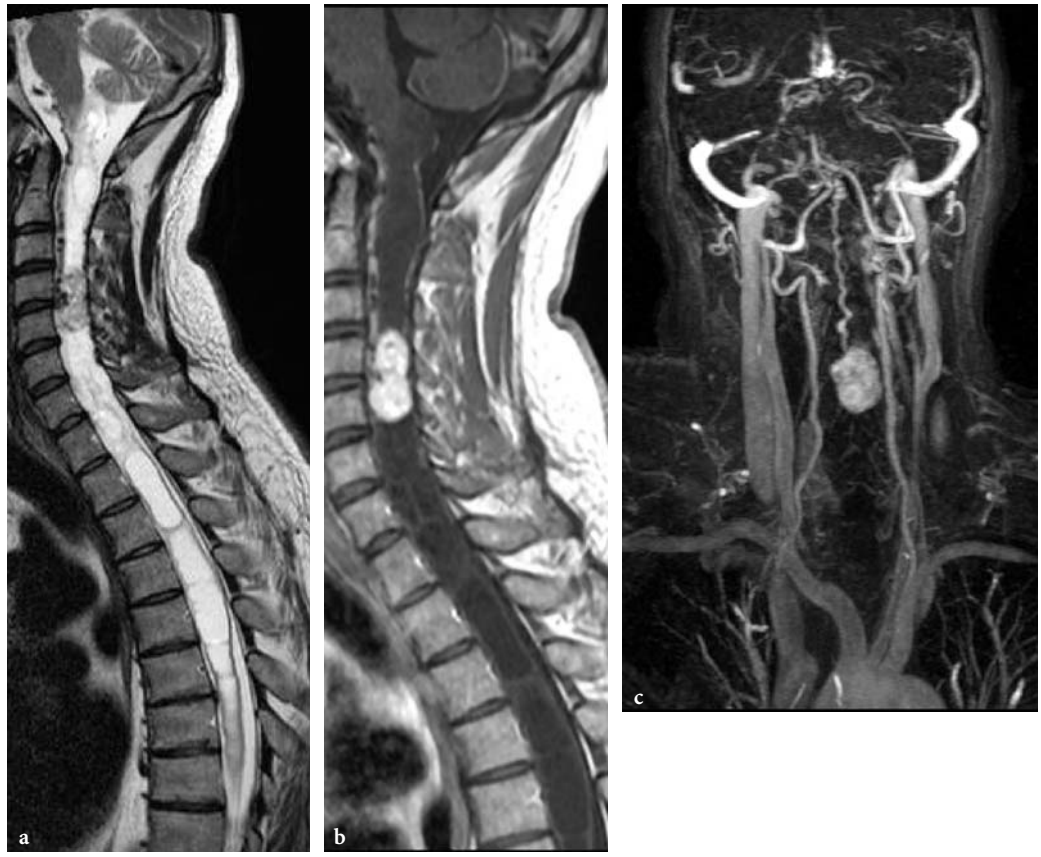

Fig. 18.6a–c. Cervical hemangioblastoma: C4–C5 nodule and multiple, extensive associated cysts. **a** Sagittal T2-WI. **b** Sagittal gadolinium T1-WI. The solid tumor nodule has a mild hypointense aspect on T2-WI with multiple areas of flow void phenomenon due to dilated vascular structures. After gadolinium administration, strong enhancement is seen within the tumor. Enhancement is also visible in the dilated veins located both at the anterior and posterior surface of the enlarged cord. No enhancement is seen at the level of the multiple associated cysts located above and beneath the tumor nodule. **c** Coronal contrast enhanced 3D-MRA. Two feeding arteries can be suspected coming from the right vertebral artery. A large medial anterior draining vein is clearly seen

of ischemia and brain tumors. Diffusion-weighted imaging has also been applied to the spinal cord with variable results (Ries et al. 2000; Schwarts et al. 2002). In our experience this new technique is still experimental as far as spinal tumors are concerned.

18.3.9 Magnetic Resonance Tractography

In contrast, although still also under development, magnetic resonance tractography based on diffusion tensor imaging techniques holds great potential for the study of intramedullary fibres in the cord (Fig. 18.7c). Displacement and/or interruption of the fibres by an intramedullary tumor provides important additional information for guiding the surgical procedure (Facon et al. 2005; Tsuchiya et al. 2005).

18.3.10 Magnetic Resonance Spectroscopy (MRS)

In vivo proton magnetic resonance spectroscopy (MRS) is a widely used technique for tissue characterization of intracranial mass lesions. Spectroscopy is nowadays considered to be a reliable technique for grading gliomas when N-acetyl-aspartate/choline and choline/creatine ratios and presence of lipids are used in combination. Spectroscopy of the spinal cord is more challenging due to the small size of the cord, and the presence of local field inhomogeneities. Re-

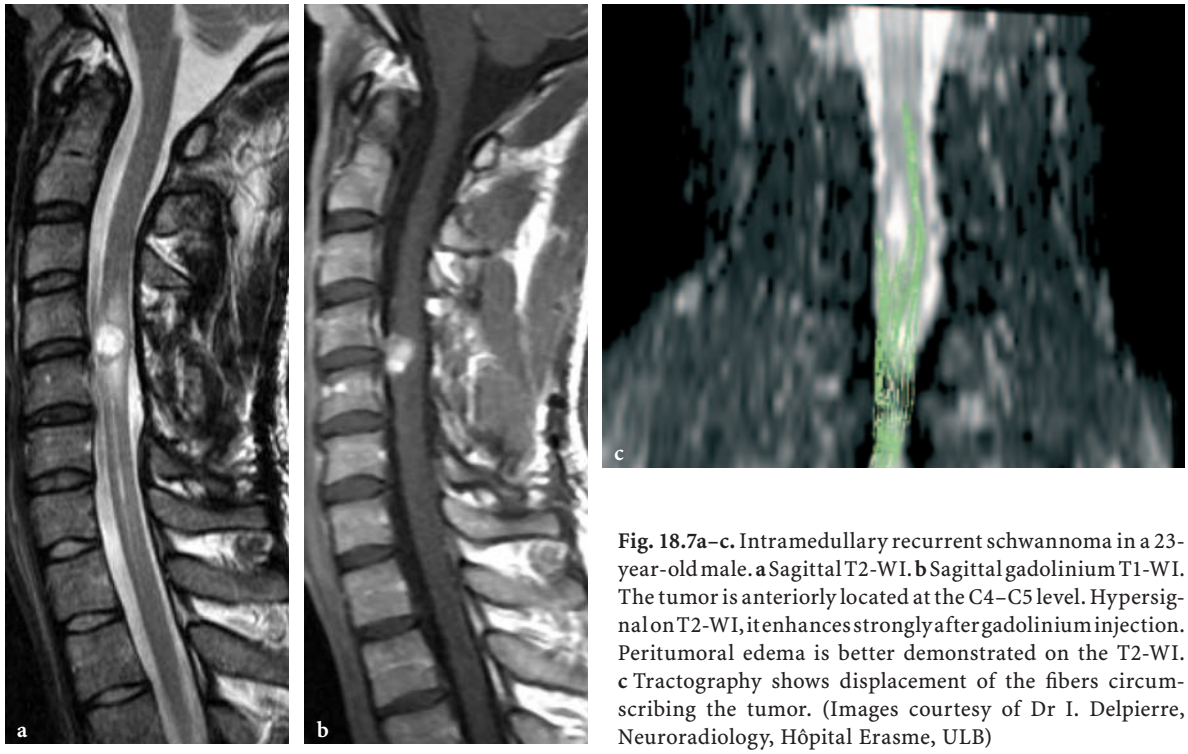

Fig. 18.7a–c. Intramedullary recurrent schwannoma in a 23-year-old male. **a** Sagittal T2-WI. **b** Sagittal gadolinium T1-WI. The tumor is anteriorly located at the C4–C5 level. Hypersignal on T2-WI, it enhances strongly after gadolinium injection. Peritumoral edema is better demonstrated on the T2-WI. **c** Tractography shows displacement of the fibers circumscribing the tumor. (Images courtesy of Dr I. Delpierre, Neuroradiology, Hôpital Erasme, ULB)

cently, Kim et al. (2004) reported that acquisition of in vivo 1H-NMR signals was possible in human spinal mass lesions on a 1.5-T clinical MRI unit. Detection of choline only in the spinal tumors may indicate that there is some potential in using in vivo 1H-MRS to distinguish spinal tumors from disc herniations mimicking spinal cord tumors, non-multiple sclerosis myelitis, and dermoid cysts. However, it was not possible to distinguish between benign diseases with MRS. In our experience, MRS was performed in a case of an enhancing cervical spinal cord lesion and allowed differential diagnosis between neoplasm and multiple sclerosis (MS) (Fig. 18.8c).

18.3.11 Magnetic Resonance Functional Imaging

Magnetic resonance functional imaging (fMRI) with blood oxygen level-dependent (BOLD) contrast has extensively been investigated for the study of local neuronal activation in the human brain. In the past decade, fMRI has become a valuable tool in some clinical settings, such as the pre-operative assessment of brain tumors. It has been shown that, when spinal cord neurons are activated, hemodynamic effects may equally be initiated. Interesting recent studies have been published demonstrating that cervical spinal cord fMRI is feasible in humans. Further research work, especially at higher field strengths, is needed before this new technique can be introduced in a routine clinical work-up of spinal cord tumors. It is, however, anticipated that more physiological information concerning the spinal cord function could improve the management of spinal tumors (Backes et al. 2001; Komisaruk et al. 2002).

18.3.12 Intraoperative Ultrasound

Before the advent of MRI, intraoperative ultrasound (IOU) had been successfully used for intradural spinal tumors at the early stage of surgery, immediately after initial laminectomy.The technique of IOU is especially useful in the case of intramedullary tumors, where it is able to show hyperechoic solid and hypoechoic cystic and necrotic components and may guide the surgical procedure. Still, specific tissue characterization is not possible with IOU (Regelsberger et al. 2005; Maiuri et al. 1997, 2000; Lunardi et al. 1993).

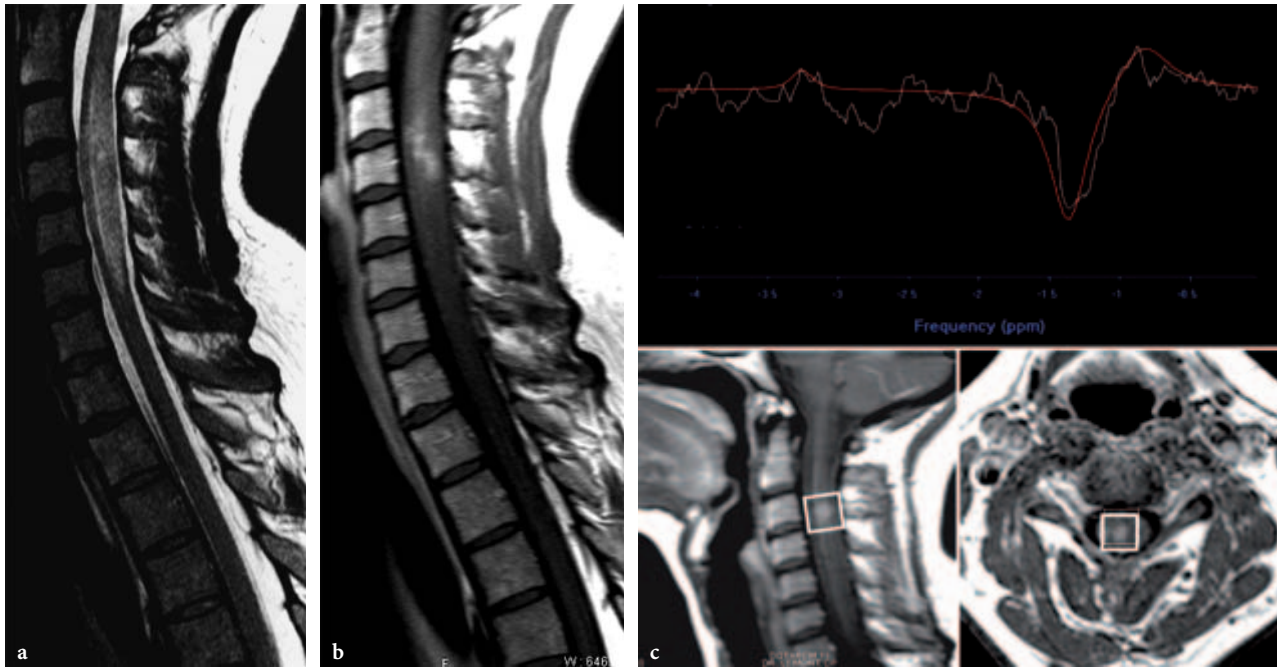

Fig. 18.8a–c. MR Spectroscopy in a case of spinal cord MS. **a** Sagittal T2-WI. **b** Sagittal gadolinium T1-WI. The cervical spinal cord is focally enlarged and a patchy, ill delineated area of enhancement is visible at the C3–C4 level. **c** MRS gives a spectrum different from normal nervous tissue: free lipids and lactate are present (indicating cell membrane degradation and hypoxia). In this particular case, MRS enabled a differential diagnosis between MS and tumor infiltration. (Images courtesy of Dr M Lemort, Bordet Cancer Institute, ULB)

18.3.13 Positron Emission Tomography

18F-Fluorodeoxyglucose positron emission tomography (FDG-PET) is a well-recognized tool used to predict the growth rate of a neoplasm because uptake of FDG in brain gliomas shows good correlation with anaplasia in general (Shimizu et al. 2004). Although no established consensus in interpretation of FDG-PET findings for spinal gliomas exists, Wilmshurst et al. (2000) reported correlation with histologic malignancy. The same authors suggested performing a prospective study of larger numbers of patients with a wider range of tumors, although this might be difficult to achieve given the rarity of spinal cord tumors (Shimizu et al. 2004; Poggi et al. 2001). In our experience, FDG-PET imaging was useful in evaluating tumor progression and identifying the most metabolically active components in spinal cord tumors (Figs. 18.9, 18.10). It was also used for monitoring unusually slow-growing metastases of a brain stem oligo-astrocytoma (Fig. 18.11c.).

18.4 Classification of Spinal Tumors

The World Health Organization (WHO) edited a new comprehensive classification of neoplasms affecting the central nervous system. A modified outline of this classification is proposed by Van Goethem et al. (2004) and is shown in Table 18.1.

18.5 Intramedullary Tumors

18.5.1 Introduction

Spinal cord tumors are rare and account for only 2%–4 % of all tumors of the central nervous system (Sze 1996; Osborn 1994). Since intramedullary tumors are infrequent lesions, the statistics published

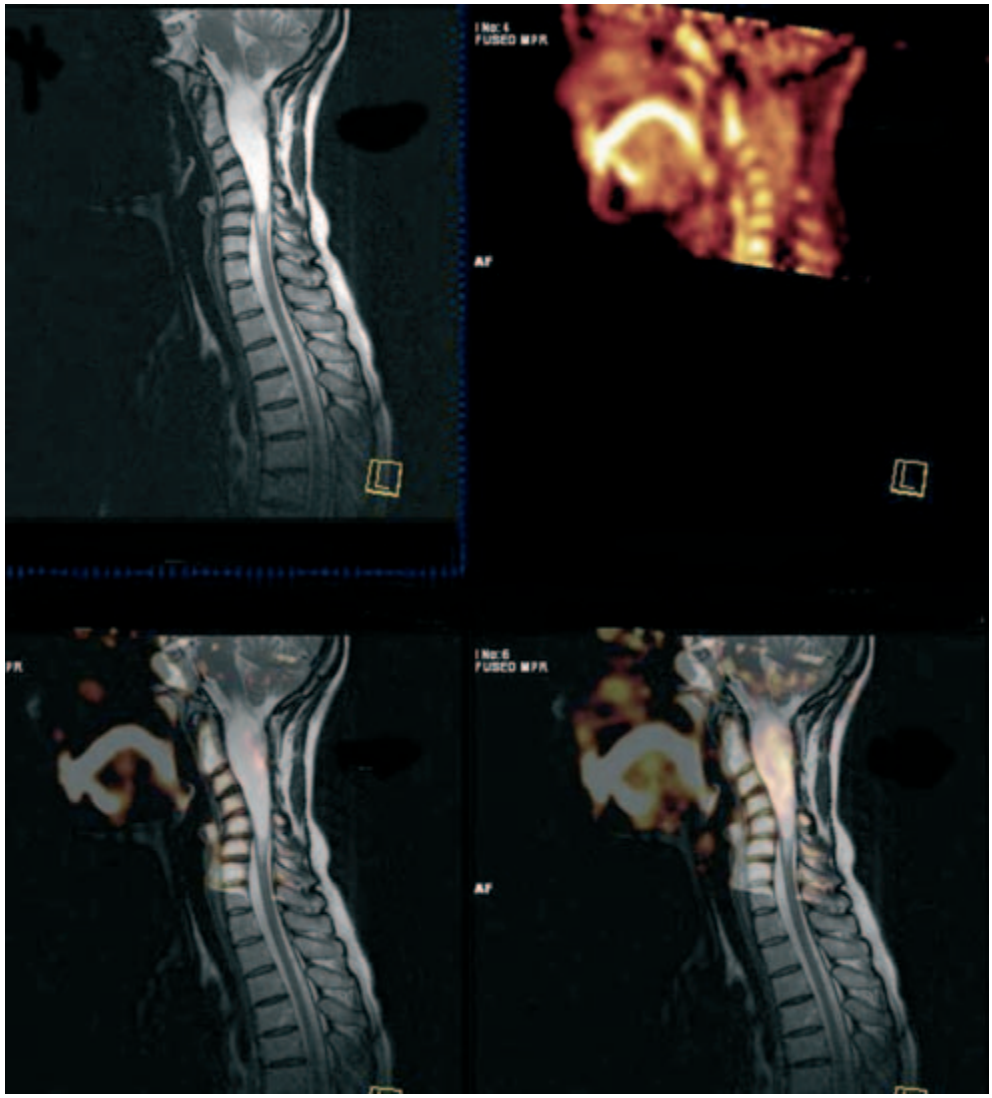

Fig. 18.9. Low grade glioma in a 25-year-old female with a slow growing low grade astrocytoma followed-up over the previous 5 years after biopsy both by MRI and methionine PET. The tumor grows very slowly while PET shows no signs of malignant degeneration. PET methionine and sagittal T2-WI in a hypometabolic low grade astrocytoma. (Images courtesy of Prof. S. Goldman, PET Unit, Hôpital Erasme, ULB)

in the literature often concern limited numbers of cases.

We report here our own statistics concerning 149 surgically proven cases of intramedullary tumors.

The majority of intramedullary tumors are glial tumors: the most frequently encountered neoplasms in adults are ependymoma (40%) and astrocytoma (28%). In children, however, astrocytomas are by far the most frequent tumors. Hemangioblastomas represent 14% of the spinal cord tumors.

Less frequent tumors include intramedullary metastasis, lymphoma, cavernous malformation (cavernoma), epidermoid cyst, lipoma, ganglioglioma, oligodendroglioma, intramedullary schwannoma, and teratoma. It is of note that intramedullary cavernous malformations represent 8% of intramedullary tumors in our series.

The radiologist should analyze carefully and systematically the MR images in order to predict, as accurately as possible, the tentative histological diagnosis: indeed, the surgical approach, the presence or not of a cleavage plane, as well as the prognosis will all be different according to the nature of the tumor. Preoperative assessment has therefore a key role to play.

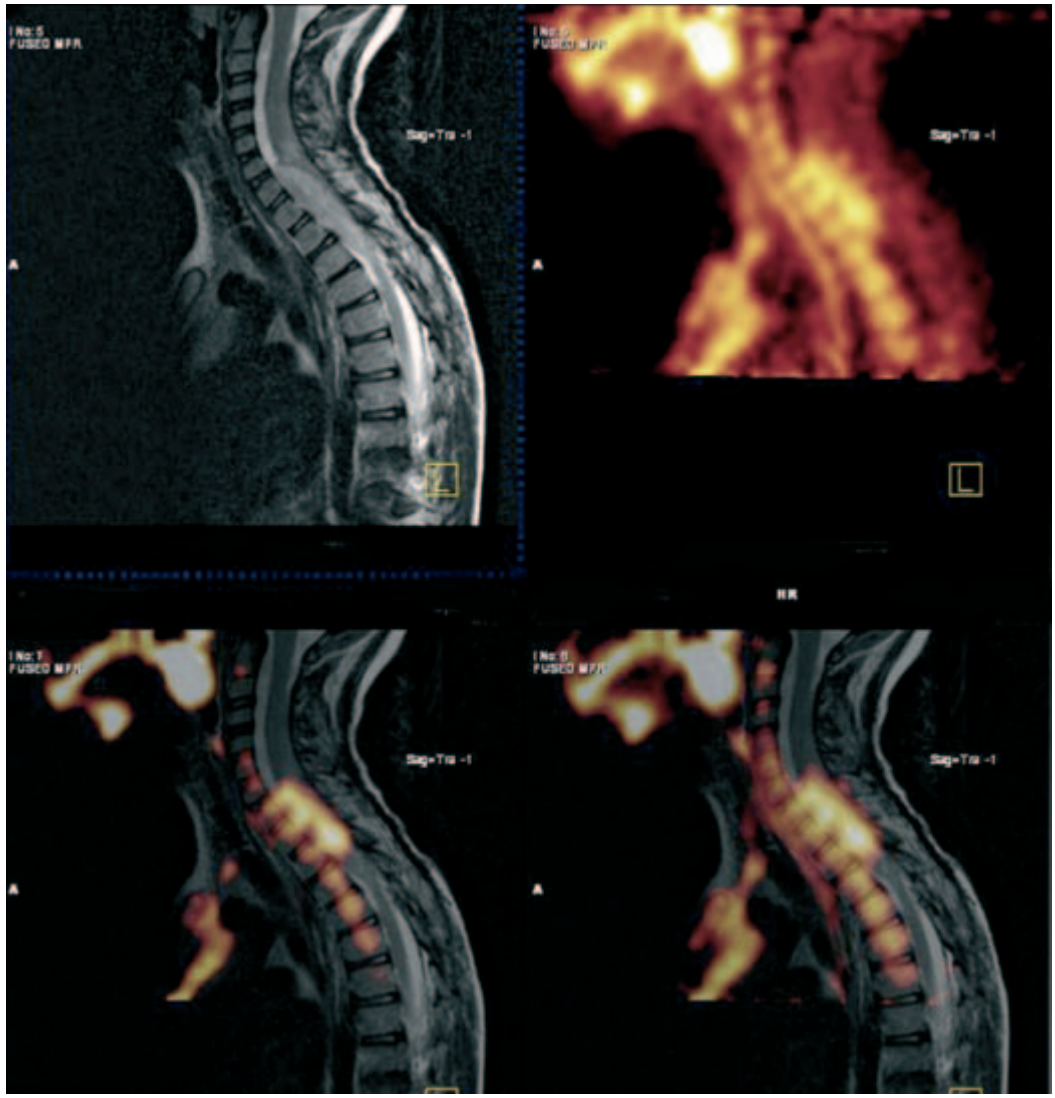

Fig. 18.10. Ganglioglioma. A 4-year-old boy has regular PET and MR examinations in order to follow-up this partially exophytic, slow growing, low grade tumor. Fusion of PET methionine and MR images. (Images courtesy of Prof. S. Goldman, PET Unit, Hôpital Erasme, ULB)

18.5.2 Astrocytoma

Astrocytomas are the most common intramedullary tumors (up to 90%) in children (Przyblski et al. 1997; Tortori-Donati and Rossi 2005) and account for 28% of intramedullary tumors in adults according to our experience. Astrocytomas are mostly encountered in young adult patients (mean age in our series is 34) with a slight predominance among males (55%). Astrocytomas may be found at any spinal level: 33% were limited to the cervical region, 21% were cervicothoracic, whilst 36% were purely thoracic. The remaining 7% corresponded to the thoracolumbar and lumbar region. The mean size of the solid tumor component involves four vertebral segments. However, especially in the pediatric population, the *entire* spinal cord may be involved. Cystic components within the tumor were found in 27% of our cases. Associated satellite cysts and secondary hydromyelia were observed in 50% of astrocytomas. Most tumors are low-grade WHO grade II tumours and are slow-growing. On T1-WI, astrocytomas are mostly hypointense (83%) whilst

Fig. 18.11a–c. Metastases from intracerebral endymoma. **a** Sagittal T2-WI. **b** Sagittal T1-WI. **c** FDG-PET image. Patient with a history of a partially resected tumor of the brain stem followed by radiotherapy. Multiple slow growing spinal metastases are monitored both by MRI and PET over the previous 2 years. (Images courtesy Prof. S. Goldman PET Unit, Hôpital Erasme, ULB)

on T2-WI they are predominantly hyperintense. For the most part, low grade astrocytomas do not enhance (Figs. 18.12, 18.13), although enhancement may be observed. Pilocytic astrocytomas, on the other hand, do enhance intensely. High grade astrocytomas and glioblastoma tend to be more heterogeneous with necrotico-cytic areas and enhance often in a patchy mode (60%) (Figs. 18.14–18.17). Intratumoral hemorrhage (Fig. 18.16a.) may occur (13%) and is best seen on gradient echo T2-WI. Intratumoral cysts and necrosis are common. Associated syringomyelia may occur: the borders of those associated cavities do not enhance after contrast injection.

Astrocytomas frequently have ill-defined borders, reflecting the infiltrative nature of those tumors. At surgery, a cleavage plane is rarely found; under these circumstances, only debulking or limited biopsy will then be performed (although complete removal may sometimes be achieved). Secondary radiation therapy is only applied for highly malignant tumours (Brotchi et al. 1991; Epstein et al 1992).

18.5.3 Ependymoma

Ependymomas are found in young patients as well: the mean age in our series was 42 years with a slight male preponderance (54%). Typically, ependymoma is more frequently found in the cervical spinal cord (50%). Associated satellite cysts are seen in 60% of the cases, and they may be very large (Fig. 18.18, 18.19). A so-called "cap sign" is seen in almost one out of four cases (27%) and corresponds to low signal intensity areas seen on T2-WI and even better on gradient echo T2-WI, capping at both sides the tumor limits. Those caps are hemosiderin deposits due to chronic hemorrhage (Figs. 18.2c,d, 18.20a, 18.21d). Ependymomas do enhance vividly and homogeneously in 91% of the cases, and have usually well-defined borders (Fig. 18.22), (Baleriaux 1999a; Kahan et al. 1996). Still, no contrast enhancement was found in two cases and a ring-like, heterogeneous enhancement in the remaining 8% (Fig. 18.23).

Table 18.1. A modified outline of the classification of neoplasms affecting the nervous system as proposed by Van Goethem et al. (2004)

Neuroepithelial Tumors
Astrocytic tumors (glial tumors)
Pilocytic astrocytoma (WHO grade I)
Fibrillary astrocytoma (WHO grade II)
Pleomorphic xanthoastrocytoma (WHO grade II)
Anaplastic astrocytoma (WHOgrade III)
Glioblastoma multiforma (WHO grade IV)
Oligodendroglial tumors
Oligodendroglioma (WHO grade II)
Anaplastic (malignant) oligodendroglioma (WHO grade III)
Ependymal cell tumors
Subependymoma (WHO grade I)
Myxopapillary ependymoma (WHO grade I)
Ependymoma (WHO grade II)
Anaplastic ependymoma (WHO grade III)
Mixed Gliomas
Mixed oligoastrocytoma (WHO grade II)
Anaplastic (malignant) oligoastrocytoma (WHO grade III)
Neuronal and mixed neuronal-glial tumors
Gangliocytoma (WHO grade I)
Ganglioglioma (WHO grade I/II)
Anaplastic (malignant) ganglioglioma (WHO grade III)
Desmoplastic infantile ganglioglioma (WHO grade I)
Dysembryoplastic neuroepithelial tumor (DNET) (WHO grade I)
Paraganglioma (WHO grade I)
Neuroblastic
Neuroblastoma
Embryonal tumors
Ependymoblastoma (WHO grade IV)
Peripheral nerve tumors
Schwannoma (neurinoma, neurilemoma) (WHO grade I)
Neurofibroma (WHO grade I)
Malignant peripheral nerve sheath tumor (WHO grade III/IV)
Hematopoietic tumors
Primary malignant lymphomas
Plasmacytoma
Leukemia
Germ cell tumors
Embryonal carcinoma
Teratoma
Mixed germ cell tumors
Tumors of the meninges
Meningothelial tumors
Meningioma (WHO grade I)
Atypical meningioma (WHO grade II)
Anaplastic (malignant) meningioma (WHO grade III)
Mesenchymal, non-meningothelial tumors
Lipoma
Angiolipoma
Fibrosarcoma
Hibernoma
Fibrosarcoma
Malignant fibrous histiocytoma
Osteoma, osteosarcoma
Osteochondroma
Hemangioma
Hemangiopericytoma
Melanocytic lesions
Melanocytoma
Malignant melanoma
Meningeal melanocytosis
Tumors of unclear origin
Hemangioblastoma
Metastatic tumors

Fig. 18.12a–d. Low grade cervicothoracic astrocytoma. A 21-year-old female with a 3-year history of weakness of the right foot and atrophy of the quadriceps. The cord is enlarged from C4 to D4. **a** Sagittal T2-WI shows an infiltrating, ill-defined high signal intensity lesion. **b** Sagittal T1-WI. **c,d** Gadolinium T1-WI. The tumor is moderately hypointense and does not enhance after contrast administration

Fig. 18.13a–c. Thoracic low grade astrocytoma. **a** Sagittal T2-WI. **b** Sagittal T1-WI. **c** Gadolinium T1-WI. This 31-year-old male complained of progressive paresis of both lower limbs. A low grade Th6–Th8 tumor was biopsied: no complete resection could be achieved in this infiltrating tumor. A large associated cyst is found below the tumor infiltration. No enhancement after contrast injection

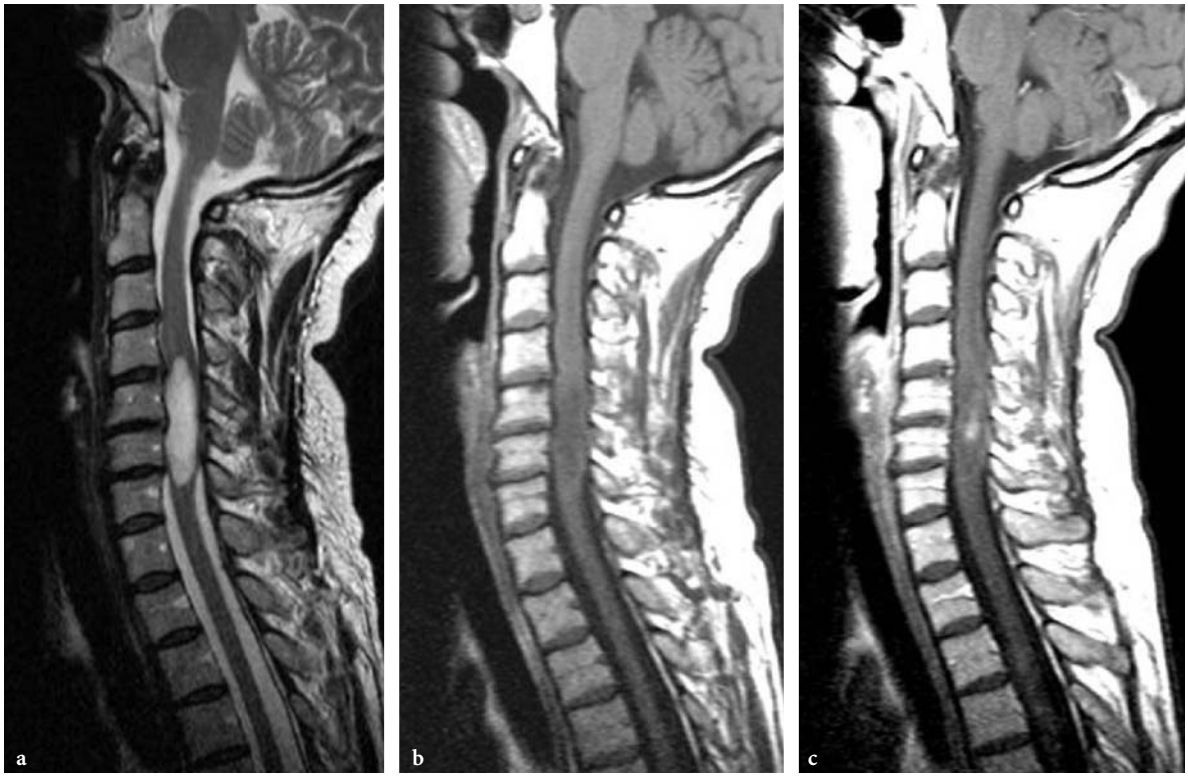

Fig. 18.14a–c. Cervical astrocytoma grade II**. a** Sagittal T2-WI. **b** Sagittal T1-WI. **c** Sagittal gadolinium T1-WI. The tumor is hyperintense on T2-WI, mildly hypointense on T1-WI and enhances only partly and heterogeneously. This 45-year-old female underwent surgery with partial removal of an astrocytoma grade II

Fig. 18.15a–c. Anaplastic astrocytoma. This 22-year-old male presented mainly right cervicobrachialgia and bilateral paresthesia of the superior limbs. Biopsy and widening of the cervical spinal canal could only be performed. **a** Sagittal T1-WI. **b** Sagittal T2-WI. **c** Sagittal gadolinium T1-WI. Extensive C0–T3 tumor infiltration. The lesion is mildly hypointense on T1-WI, hyperintense on T2-WI and enhances strongly but heterogeneously after contrast injection with an irregular pattern

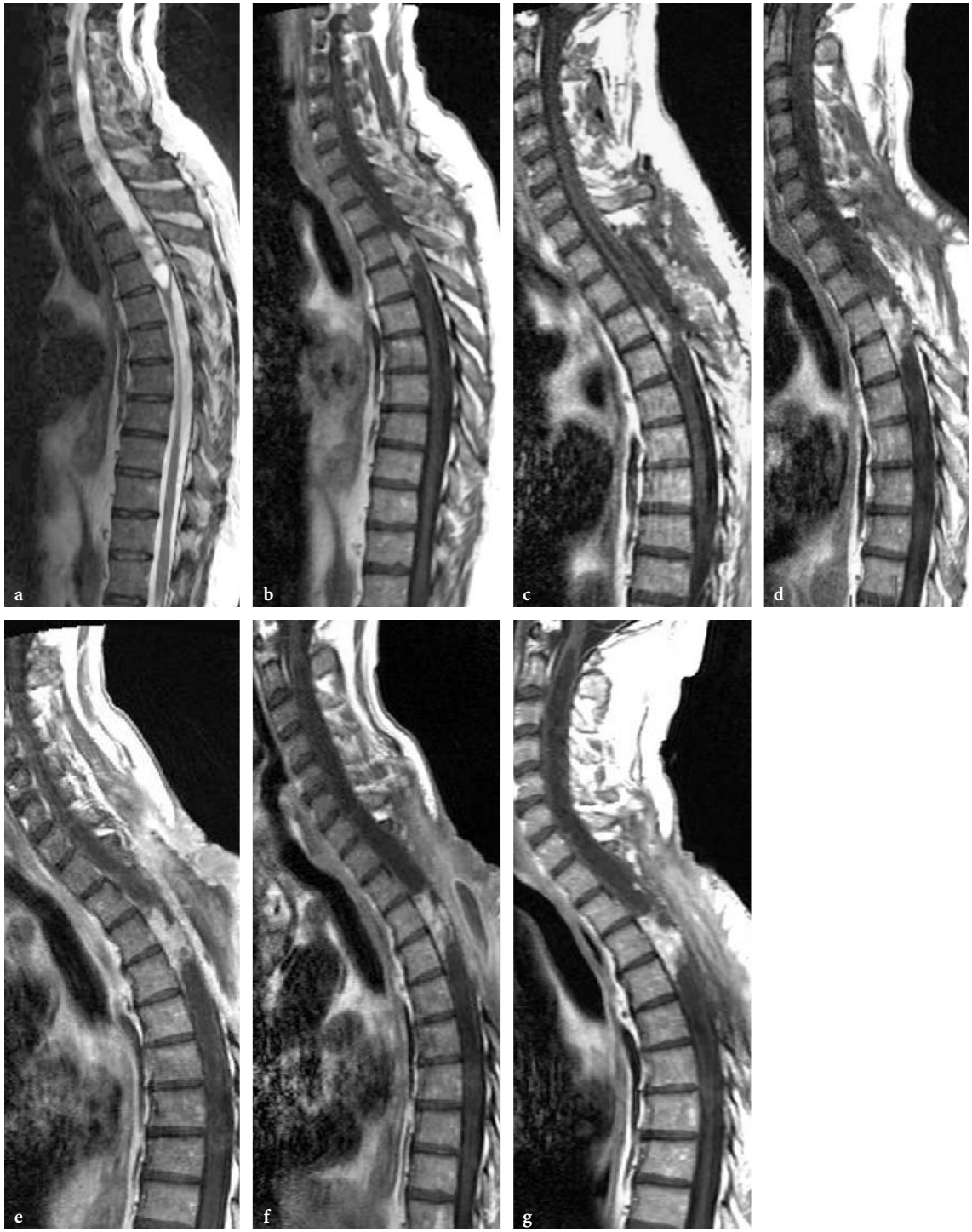

Fig. 18.16a–g. Follow-up MRI examinations in a case of a malignant astrocytoma. **a,b** Pre-operative MRI. **a** Sagittal T2-WI. **b** Sagittal gadolinium T1-WI. A large tumor infiltration is found, involving the entire cervical cord and extending to the upper thoracic spine. Low signal areas are seen on T2-WI at the T2–T3 level indicating chronic intratumoral hemorrhage. The tumor has a very heterogeneous pattern on both T1- and T2-WI. It only partially enhances. **c–g** Follow-up MRI. Series of sagittal gadolinium T1-WI. **c** Control MRI obtained immediately after partial removal. **d** MRI obtained 6 months later. **e–g** Repeated follow-up MRI after chemotherapy on a 24-month period: some response to the treatment is seen on (**f**) but tumor progression is again noticed on (**g**)

Fig. 18.17a–d. Exophytic, multifocal malignant astrocytoma. A 23-year-old male complaining of diffuse neck and lower back pain. At neurological examination, a bilateral pyramidal syndrome is observed. **a** Sagittal T1-WI. **b** Sagittal T2-WI. **c,d** Sagittal gadolinium T1-WI. The tumor involves the entire spinal cord. Metastatic spread is seen within the lumbo-sacral canal

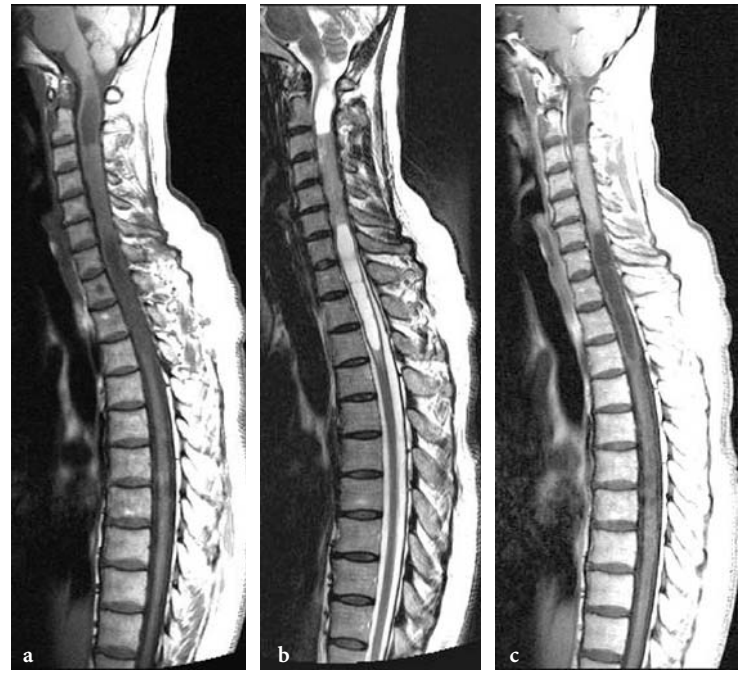

Fig. 18.18a–c. Ependymoma. This patient presents with a 1-year history of sensitive impairment of both superior limbs. **a** Sagittal T1-WI. **b** Sagittal T2-WI. **c** Sagittal gadolinium T1-WI. A solid component is located at the C3–C6 level: it is isointense on T1-WI, isointense on T2-WI and enhances homogeneously. Associated cysts are visible above and below the tumor. The borders of those cysts do not enhance. The cervical spine is straightened

Fig. 18.19a–c. Ependymoma. A 40-year-old female with intermittent neck pain and paresthesias in the right part of the body. **a** Sagittal T1-WI. **b** Sagittal T2-WI. **c** Sagittal gadolinium T1-WI. In this case, the solid nodule has a more heterogeneous aspect. A small associated cyst is seen at the inferior part of the lesion. Still, the tumor is well delineated after contrast injection

Fig. 18.20a–c. Ependymoma. A 53-year-old female with a 2-year history of progressive difficulties walking and chronic cervicothoracic back pain. **a** Sagittal T2-WI. **b** Sagittal T1-WI. **c** Sagittal gadolinium T1-WI. Relatively small heterogeneous tumor shown on the three imaging sequences. The most typical feature is the bilateral hypointense areas capping the tumor: "cap sign" more frequently seen in case of ependymoma. Note the straightening of the cervical spine and disappearance of the normal cervical lordosis

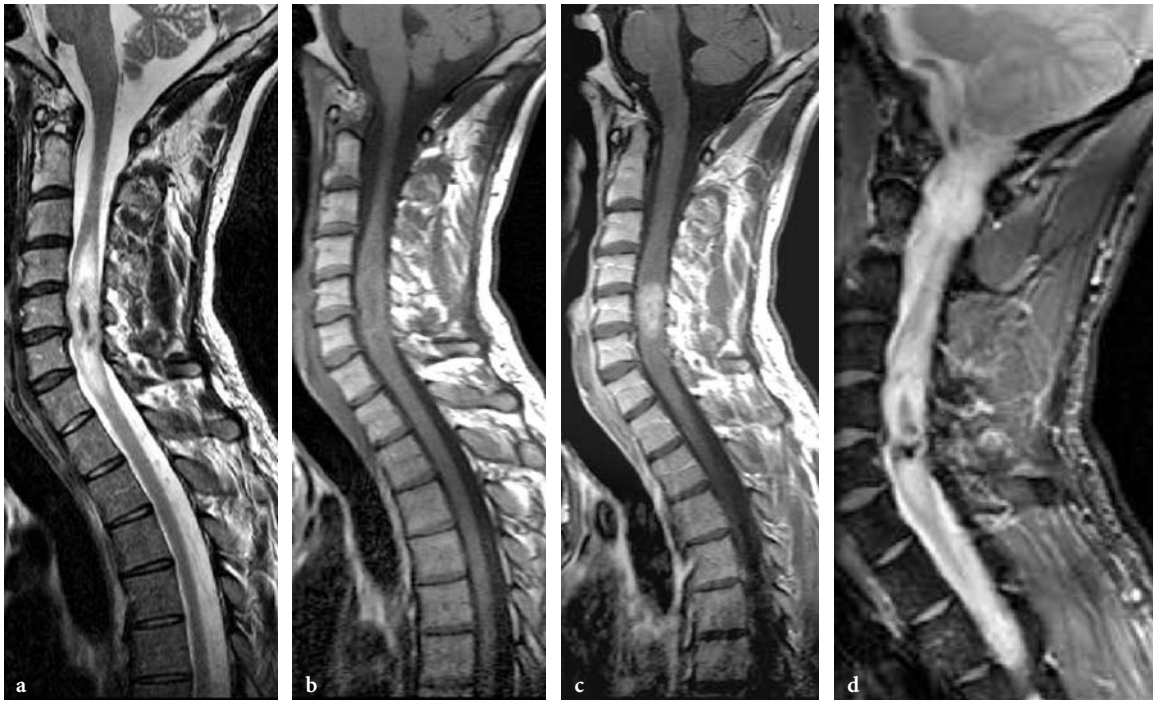

Fig. 18.21a–d. Hemorrhagic ependymoma. A 28-year-old male with a 2-year history of Lhermitte sign believed to be related to chronic cervical trauma! Recently, rapid appearance of a tetraparesis. **a** Sagittal T2-WI. **b** Sagittal T1-WI. **c** Sagittal gadolinium T1-WI. **d** Sagittal gradient echo T2-WI. C5 ependymoma showing an intratumoral hemorrhage best seen on gradient echo T2-WI

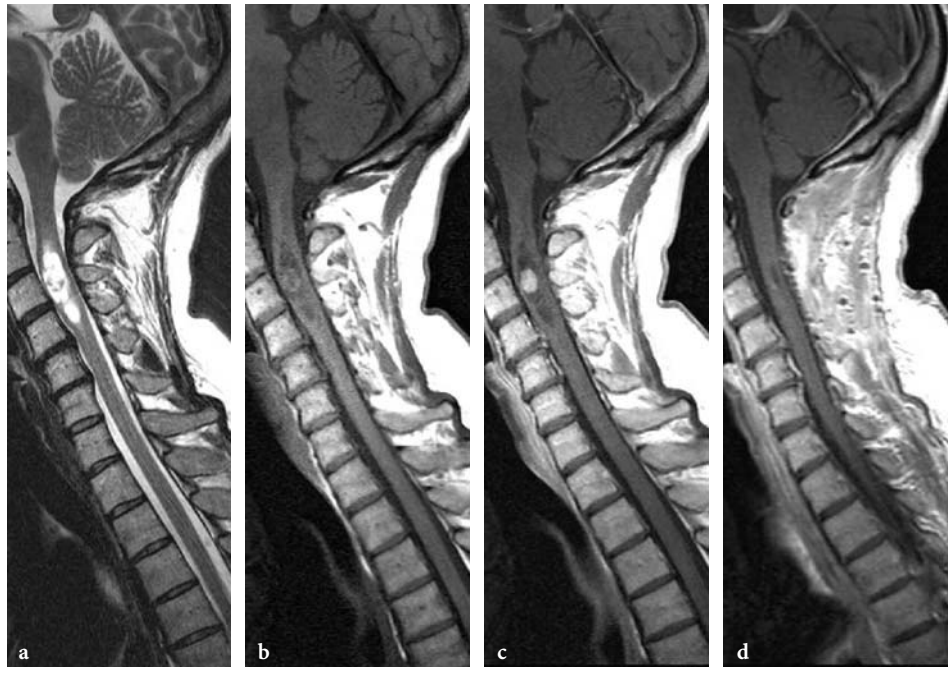

Fig. 18.22a–d. Ependymoma. This 34-year-old female had complained mainly of dysesthesia in the left forearm and hand for several years but more recently observed motor deficit in the left inferior limb. **a** Sagittal T2-WI. **b** Sagittal T1-WI. **c** Sagittal gadolinium T1-WI. **d** Sagittal T1-WI obtained immediately after complete removal of the tumor. The solid tumor nodule is enhancing homogeneously and has sharp borders: complete removal was achieved (**d**)

Fig. 18.23a,b. Cystic ependymoma with mild contrast uptake. A 40-year-old male with right thoracic pain of 1-year's standing. **a** Sagittal T2-WI. **b** Sagittal gadolinium T1-WI. Large tumour infiltration with many cystic components and signs of chronic hemorrhage. There is only a mild, ill-defined area of contrast uptake at the T3–T5 level. [Reprinted with permission from Baleriaux et al. (2004)]

Ependymomas originate from the cells bordering the ependymal canal and, as such, are expected to be more centromedullary located compared to astrocytomas (Fine et al. 1995; Parizel et al. 1989; Sun et al. 2003): this central location was indeed observed in 94% of our cases.

The mean tumor size of the ependymoma corresponds to three vertebral bodies (min. 2 – max. 13), while astrocytomas are usually more extensive, involving 2–19 vertebrae.

18.5.4 Subependymoma

In the literature, rare cases of spinal cord subependymoma are reported and were reviewed by Bret et al. (1997). It is likely that these rare lesions account for less than 2% of all spinal cord tumors. Most of the cases involved the cervical cord or the cervicothoracic junction. No specific pattern could be found on MRI in order to help diagnose those lesions except the tendency for a subependymoma to grow excentrically within the cord or to show an exophytic component.

18.5.5 Myxopapillary Ependymoma

Myxopapillary ependymoma of the conus medullaris and filum terminale is a relatively common spinal intradural neoplasm found predominantly in children (Nagib and O'Fallon 1997) and young adults, although it may be observed at older age. There is a slight male preponderance. Tumor location at the lower thoracic level and lumbar spine is typical. Myxopapillary ependymomas are slow growing tumors: they may become very large before the diagnosis is finally made in patients with a classical long standing history of poorly specific chronic low back pain exacerbated at night. On MRI, the lesion is isointense compared to the cord and hyperintense on T2-WI: it enhances strongly after gadolinium injection (Fig. 18.24). Hemorrhage may occur, explaining the sudden worsening of clinical symptoms with occurrence of leg weakness and sphincter disturbances (Friedman and Hollander 1998).

18.5.6 Hemangioblastoma

Hemangioblastomas are benign, usually richly vascularized spinal cord tumors and represent 2%–6% of all spinal tumors. They are often located superficially, in the subpial region (Figs. 18.4, 18.25). Hemangioblastomas have two different but rather typical presentations: either a small nodular lesion located in the sub-pial compartment and surrounded by extensive intramedullary edema (Fig. 18.4), or a small nodule associated with huge and extensive intramedullary cystic components (Fig. 18.6). Hemangioblastomas can be solitary (in 80% of cases) or multiple, when associated with von Hippel-Lindau disease (Baker et al. 2000) (Figs. 18.4, 18.25). Exophytic hemangioblastoma may occur with minimal cord reaction as well as extramedullary hemangioblastoma.

Fig. 18.24a–d. Myxopapillary ependymoma. This 26-year-old male suffers from severe lower back pain without neurological deficit. **a** Sagittal T1-WI: low signal intensity well-delineated tumor. **b** Sagittal T2-WI: The tumor is hypointense to the CSF but moderately hyperintense compared to the spinal cord. **c** Sagittal gadolinium T1-WI: the tumor enhances intensely after contrast administration. **d** Control postoperative sagittal gadolinium T1-WI shows complete removal of the tumor

On T1-WI, the solid nodule is isointense to hypointense to the spinal cord; on T2-WI it is isointense to slightly hyperintense. A rich vascular network in the tumor, as well as enlarged feeding arteries and dilated draining veins, may best be seen on proton-density and T2-WI. After gadolinium injection, intense and homogeneous contrast uptake is seen (Fig. 18.26) (Baleriaux 1999a; Colombo et al. 1986). Contrast administration is especially useful in order to pick up small, multiple nodules when associated to large cystic components. DSA is still performed to identify the feeding arteries to the tumor and, if possible, to perform pre-operative embolisation in order to reduce the bleeding during surgery of those richly vascularized tumors (Fig. 18.26).

18.5.7 Cavernous Malformation (Cavernoma)

Cavernous malformations (also known as cavernomas) represent, in our experience, 8% of all intramedullary tumors. These vascular malformations may remain clinically silent for a long period of time before an acute and rapidly progressive neurological medullary deficit occurs due to bleeding. Before the advent of MRI these lesions were extremely difficult to diagnose, especially in the spinal cord, as they usually are small and do not enlarge the spinal cord. On MRI, intramedullary cavernous malformations are usually easily recognized thanks to a typical "black and white" appearance due to areas of mixed signal intensity on both T1- and T2- or T2*-WI (Fig. 18.27). Contrast enhancement is variable. Because cavernous malformations may be multiple, we recommend performing an MRI of the brain, whenever the diagnosis of an intramedullary cavernous malformation is suspected. If multiple similar lesions are found in the brain, this should support the final diagnosis of cavernous malformation of the spinal cord (Santoro et al. 2004).

18.5.8 Less Frequent Intramedullary Tumors

18.5.8.1 Metastases

The true incidence of intramedullary metastases is difficult to ascertain and variably reported (Koeller et al. 2000). Studies based on autopsy material are

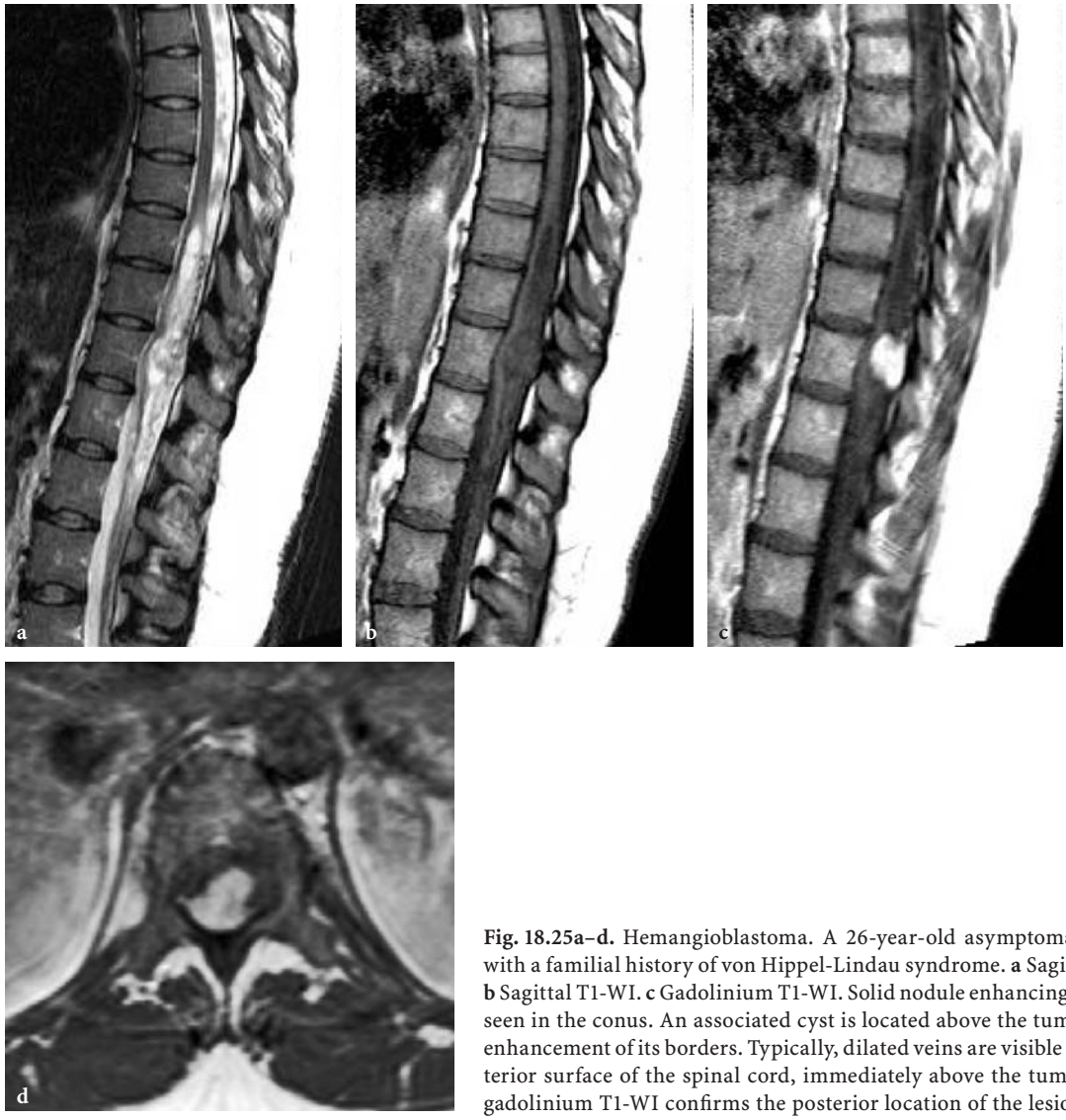

Fig. 18.25a–d. Hemangioblastoma. A 26-year-old asymptomatic female with a familial history of von Hippel-Lindau syndrome. **a** Sagittal T2-WI. **b** Sagittal T1-WI. **c** Gadolinium T1-WI. Solid nodule enhancing strongly is seen in the conus. An associated cyst is located above the tumor with no enhancement of its borders. Typically, dilated veins are visible on the posterior surface of the spinal cord, immediately above the tumor. **d** Axial gadolinium T1-WI confirms the posterior location of the lesion

biased, as the cord is often not systematically examined. Longer survival of cancer patients on the one hand and better imaging techniques on the other hand, enable detection of a higher number of intramedullary metastases. Only 2.4% of metastases removed surgically from the CNS are located in the cord: moreover, it is extremely rare that a spinal cord metastasis represents the first clinical manifestation of a primary cancer. Clinical symptoms are often non-specific, but usually involve root pain (Aryan et al. 2004).

The high sensitivity of MRI enables easy detection of intramedullary metastases: however, there are no specific MRI characteristics. Usually, spinal cord metastases are small, nodular, well-defined lesions, hypointense on T2-WI, surrounded by mild to extensive edema. The enhancement pattern may be either ring-like or homogeneous and intense (Figs. 18.28, 18.29) (Kalayci et al. 2004; Ijaz and Jones 1997).

Melanoma metastasis, in contrast, has a more specific appearance exhibiting a spontaneously hyperintense aspect on T1-WI linked to the presence of melanin. Longer survival of patients with melanoma explains the higher number of those metastases found recently (Conill et al. 2004).

18.5.8.2 Ganglioglioma

Spinal cord gangliogliomas are rare, representing 3.8% of all central nervous system tumors

Fig. 18.26a–d. Hemangioblastoma: role of embolisation. A 24-year-old male with an 1-year history of dysesthesia in the right superior limb and right hand. **a** Sagittal gadolinium T1 weighted images before (**a**) and after (**c**) embolisation. Well-defined tumor located in the posterior upper cervical spine with an associated cyst capping the lesion. **b** Digital substraction angiography shows a typical, richly vascularized tumor (Image courtesy Dr G. Rodesch, Hôpital Erasme, ULB). **d** Post-operative sagittal gadolinium T1-WI obtained 24 h after surgery: complete removal of the tumor is confirmed. The associated cyst is already much smaller whilst the anterior dilated vein located on the anterior surface of the bulbo-medullary region is unchanged

(Hamburger et al. 1997). They mostly involve the upper cervical cord. One third of the gangliogliomas are seen in children. A large series of 27 patients with spinal cord gangliogliomas was reported by Patel et al. (1998). According to these authors, the diagnosis of intramedullary ganglioglioma can be suspected whenever, in young patients (mean age: 12 years), a large tumor is found presenting with a tumoral cyst, no edema, mixed signal intensity on T1-WI and patchy enhancement (Fig. 18.10). Associated bone erosion and scoliosis is reported. However, the ultimate diagnosis needs to be ascertained by histopathology.

18.5.8.3 Gangliocytoma

Gangliocytomas are intramedullary tumors usually involving multiple spinal cord segments. MR findings reported in the literature mention extensive intramedullary mass lesions of heterogeneous signal intensity with heterogenous enhancement and

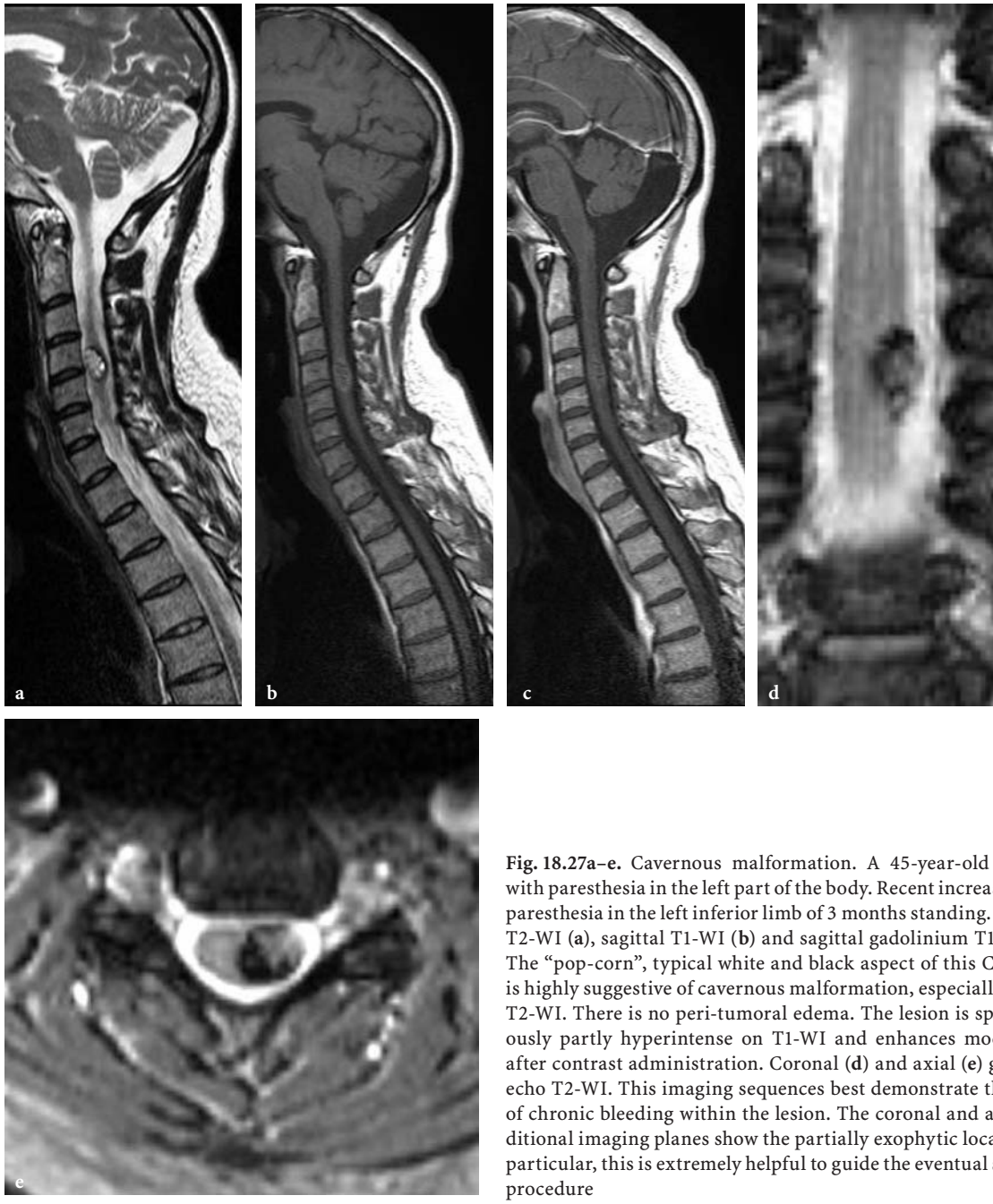

Fig. 18.27a–e. Cavernous malformation. A 45-year-old women with paresthesia in the left part of the body. Recent increase of the paresthesia in the left inferior limb of 3 months standing. Sagittal T2-WI (**a**), sagittal T1-WI (**b**) and sagittal gadolinium T1-WI (**c**). The "pop-corn", typical white and black aspect of this C4 lesion is highly suggestive of cavernous malformation, especially on the T2-WI. There is no peri-tumoral edema. The lesion is spontaneously partly hyperintense on T1-WI and enhances moderately after contrast administration. Coronal (**d**) and axial (**e**) gradient echo T2-WI. This imaging sequences best demonstrate the signs of chronic bleeding within the lesion. The coronal and axial additional imaging planes show the partially exophytic location. In particular, this is extremely helpful to guide the eventual surgical procedure

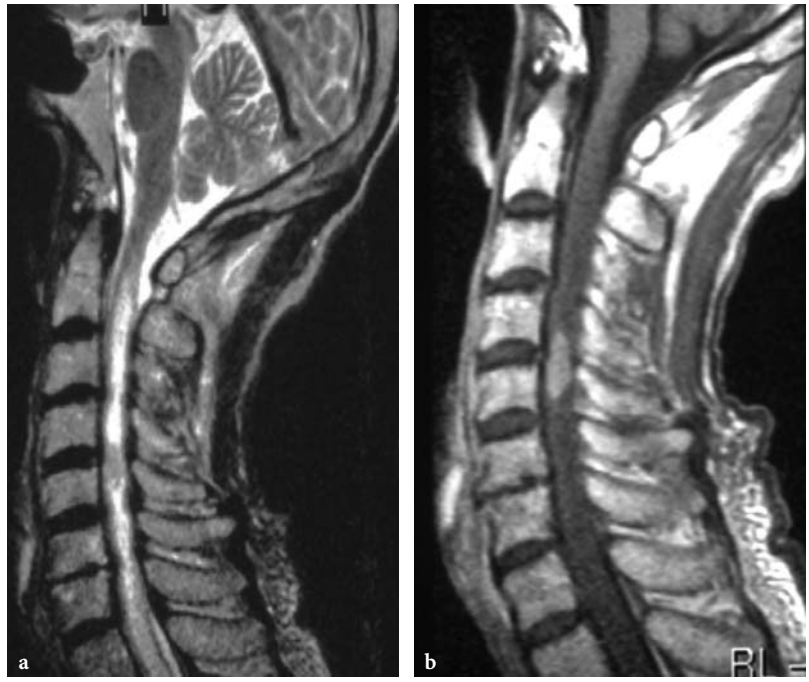

Fig. 18.28a,b. Intramedullary lung metastasis. Sagittal T2-WI (**a**) and sagittal gadolinium T1-WI (**b**). An isointense lesion is seen at the level of C4–C5 on T2-WI, surrounded by an extensive edema. Intense gadolinium uptake confirms the tumor borders in this case of a 55-year-old male with a congenital cervical spinal canal stenosis. The primary lung cancer was unknown at the time of imaging

Fig. 18.29a–c. Metastases of a fronto-ethmoido-orbital carcinoma. Series of adjacent sagittal gadolinium enhanced T1-WI. Multiple enhancing nodules located both in and around the spinal cord

without associated syrinx. Other reports have described extensive cyst formation along with tumor enhancement. There is apparently no reliable way to differentiate a gangliocytoma from a ganglioglioma on the basis of imaging characteristics. Both types of tumors show little propensity for growth and both are treated with surgery (Russo et al 1995).

18.5.8.4 Oligodendroglioma

Oligodendrogliomas are rare in the spinal cord (Fountas et al. 2005). They exhibit no specific MRI characteristics. However, the few cases in our experience were relatively small tumors (two vertebral segments) with ill-defined borders and slight hyperintensity on T1-WI. No peritumoral edema or contrast uptake was observed.

18.5.8.5 Intramedullary Schwannoma, Melanotic Schwannoma

Purely intramedullary schwannomas may be seen as well circumscribed lesions, isointense on T1-WI and hypointense on T2-WI. They enhance homogeneously (Fig. 18.7). Usually, there is only mild or no peritumoral edema, reflecting the slowly growing nature of these tumors (Colosimo et al. 2003). The extra-axial nature of the tumor can only be detected through careful scrutiny of the spinal cord surface. Some schwannomas contain melanin that can be detected thanks to the high signal appearance on T1-WI (Santaguida et al 2004).

18.5.8.6 Dermoid Cyst

Spinal dermoids are most commonly detected in infants, during the first year of life. They can occur both in the intramedullary or extramedullary compartment. Their MR signal behavior is variable, linked to the different nature of their components. Still, a hyperintense appearance is usually found on T1-WI.

18.5.8.7 Lipoma

Lipomas constitute 6% of intramedullary tumors in our series. Intramedullary lipomas must be differentiated from cauda equina lipomas or lipomas associated with dysraphism: the clinical, radiological, and surgical problems raised by these lesions are indeed totally different (Timmer et al. 1993). Although lipomas appear well-defined on MRI, no cleavage plane from the surrounding spinal cord is found at surgery. Therefore, the tumor usually cannot be completely resected without causing severe neurological damage and only widening of the spinal canal allowing further slow tumor growth is beneficial to the patient. The typical hyperintensity of lipomas on T1-WI makes these lesions easy to diagnose with MRI (Fig. 18.30).

18.5.8.8 Lymphoma

Primary intramedullary lymphomas are rare in immunocompetent patients but are more frequent in AIDS patients. The most common MRI findings reported are a solid and homogeneously enhancing mass that is hyperintense on T2-weighted images, without associated syringomyelia (Nakamizo et al. 2002).

18.5.8.9 Vascular Lesions

Intramedullary arteriovenous malformations (AVM) have a relatively specific appearance: flow void phenomena are easily shown on proton density and T2-WI images. Cord enlargement is minimal. In the case of acute bleeding, hemorrhage is shown as low signal intensity on T2-WI with iso- becoming later hyperintense areas on T1-WI (Fig. 18.31). MRA is a helpful tool to ascertain the diagnosis although conventional DSA remains the diagnostic modality of choice; it can be followed immediately by an interventional procedure (Lahanis 1993).

Dural fistulae are more difficult to diagnose: they are often located at the lower thoracolumbar level, although they may also be encountered at the cervical and thoracic level. In many cases, there are no evident abnormalities on T1-WI. However, on T2-WI, the cord exhibits an extensive high signal intensity area that enhances homogeneously after contrast injection. The cardinal diagnostic features are the enlarged arterial and venous structures surrounding the medulla, best seen on thin section T2-WI or MR myelography, and confirmed by MRA. Unfortunately those findings are often misdiagnosed in clinical practice and considered erroneously as tumors!

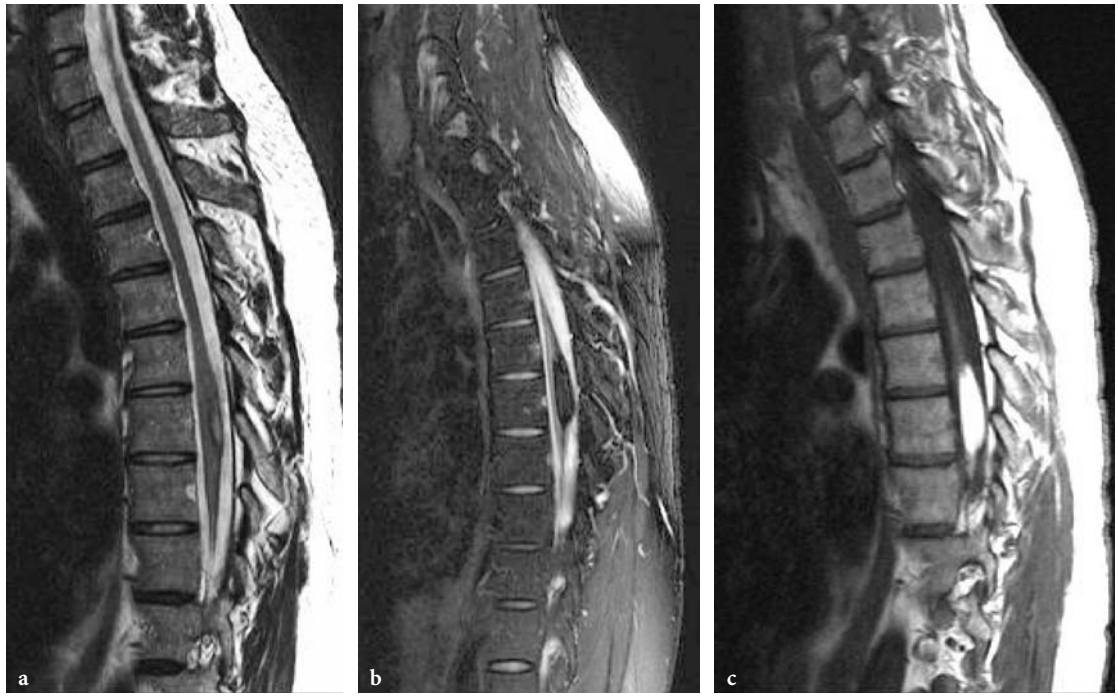

Fig. 18.30a–c. Thoracic intramedullary lipoma. A 30-year-old male with a 2-year history of dysesthesia in the left foot. Sagittal T2-WI (**a**), sagittal T2-WI with fat suppression (**b**), sagittal T1-WI (**c**). Intramedullary T5–T6 lesion with a typical hypointense aspect on T2-WI and hyperintense on T1-WI. The T2-WI with fat suppression technique definitely confirms the fatty nature of the lesion

18.6 Intradural Extramedullary Tumors

Most intradural extramedullary tumors are benign. They originate either in a spinal nerve or in the meninges. Schwannomas, together with meningiomas, account for almost 50% of all intradural extramedullary neoplasms.

18.6.1 Schwannoma and Neurofibroma

Schwannomas are the most common intradural extramedullary tumors. They are usually well encapsulated tumors that can be cystic. Typically, they arise from the dorsal sensory root (De Verdelhan et al. 2005). The majority of neurinomas (70%–75%) are purely intradural extramedullary tumors. Still, 15% are extradural and 15% have a "dumbbell" shape involving both the intra- and extradural space (Fig. 18.32). Neurinomas are found at the cervical and thoracic region in 60% of cases and 40% in the lumbar region. Less than 1% grows inside the cord. Schwannomas are solitary tumors.

CT is useful in order to depict associated bone erosion centred on the foraminal canal and/or vertebral body scalloping. Calcifications are rare (Fig. 18.33). On MRI, neurinomas are isointense to the cord in 70% of the cases while 20% are moderately hypointense on T1-WI. On T2-WI, 95% of those lesions are hyperintense. Of the schwannomas, 40% have a cystic component. Hemorrhage is found in 10% of cases. After contrast injection, almost all schwannomas enhance intensely and homogeneously. A more heterogeneous pattern is seen when cystic. Giant schwannomas are typically encountered at the lumbar level and are then almost indistinguishable from myxopapillary ependymoma (Fig. 18.24) or hemangiopericytoma (Fig. 18.34).

Neurofibromas (Figs. 18.35, 18.36) are not well encapsulated, are ill-defined and often present as multiple tumors. MRI usually does not enable differentiation between a schwannoma and a neurofibroma when the tumor is solitary (Huang et al. 2005). In neurofibromatosis type 1 (Fig. 18.35), multiple plexiform neurofibromas are typically encoun-

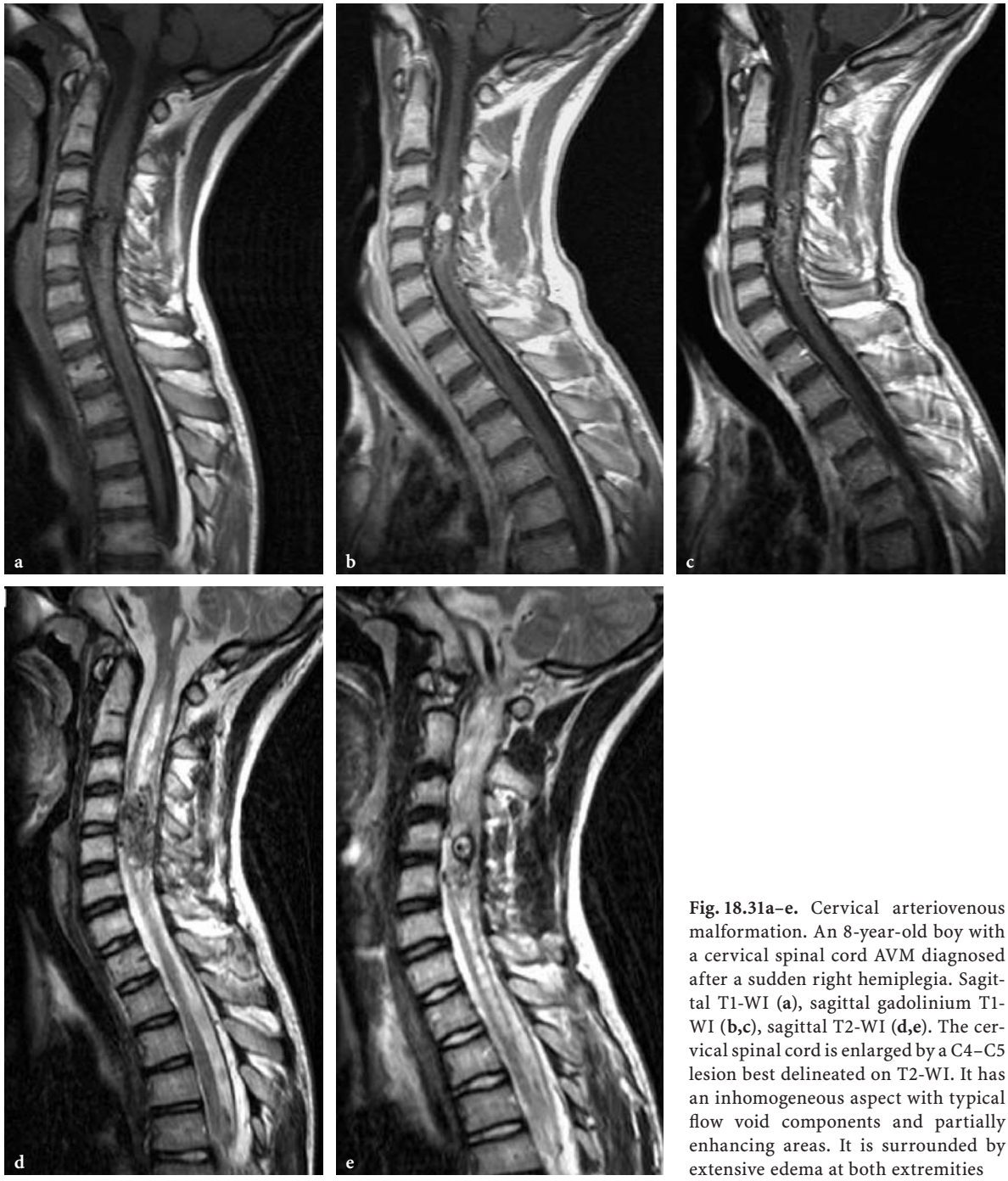

Fig. 18.31a–e. Cervical arteriovenous malformation. An 8-year-old boy with a cervical spinal cord AVM diagnosed after a sudden right hemiplegia. Sagittal T1-WI (**a**), sagittal gadolinium T1-WI (**b,c**), sagittal T2-WI (**d,e**). The cervical spinal cord is enlarged by a C4–C5 lesion best delineated on T2-WI. It has an inhomogeneous aspect with typical flow void components and partially enhancing areas. It is surrounded by extensive edema at both extremities

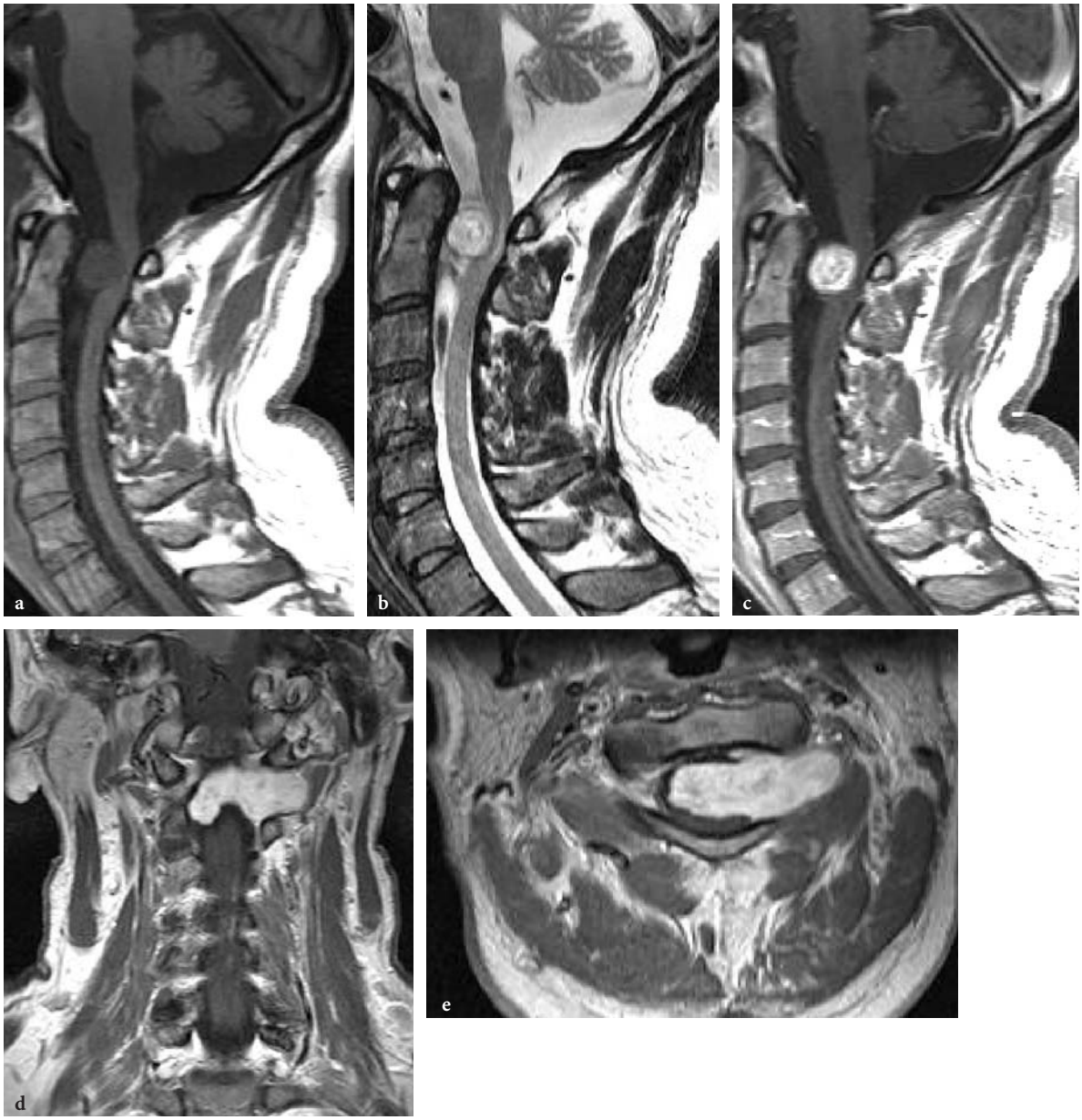

Fig. 18.32a–e. Upper cervical schwannoma. A 35-year-old male with a 1-year history of right arm paresis. Sagittal T1-WI (**a**), sagittal T2 (**b**) and sagittal gadolinium T1-WI (**c**). Well circumscribed extramedullary tumor with homogeneous signal behaviour, hypointense on T1- and hyper-intense on T2-WI. Intense contrast uptake. Coronal (**d**) and axial gadolinium T1-WI (**e**). Those images obtained in different imaging planes best demonstrate the full extent (intra- and extradural location) of the lesion at the C1–C2 left foramen allowing a definite diagnosis of schwannoma

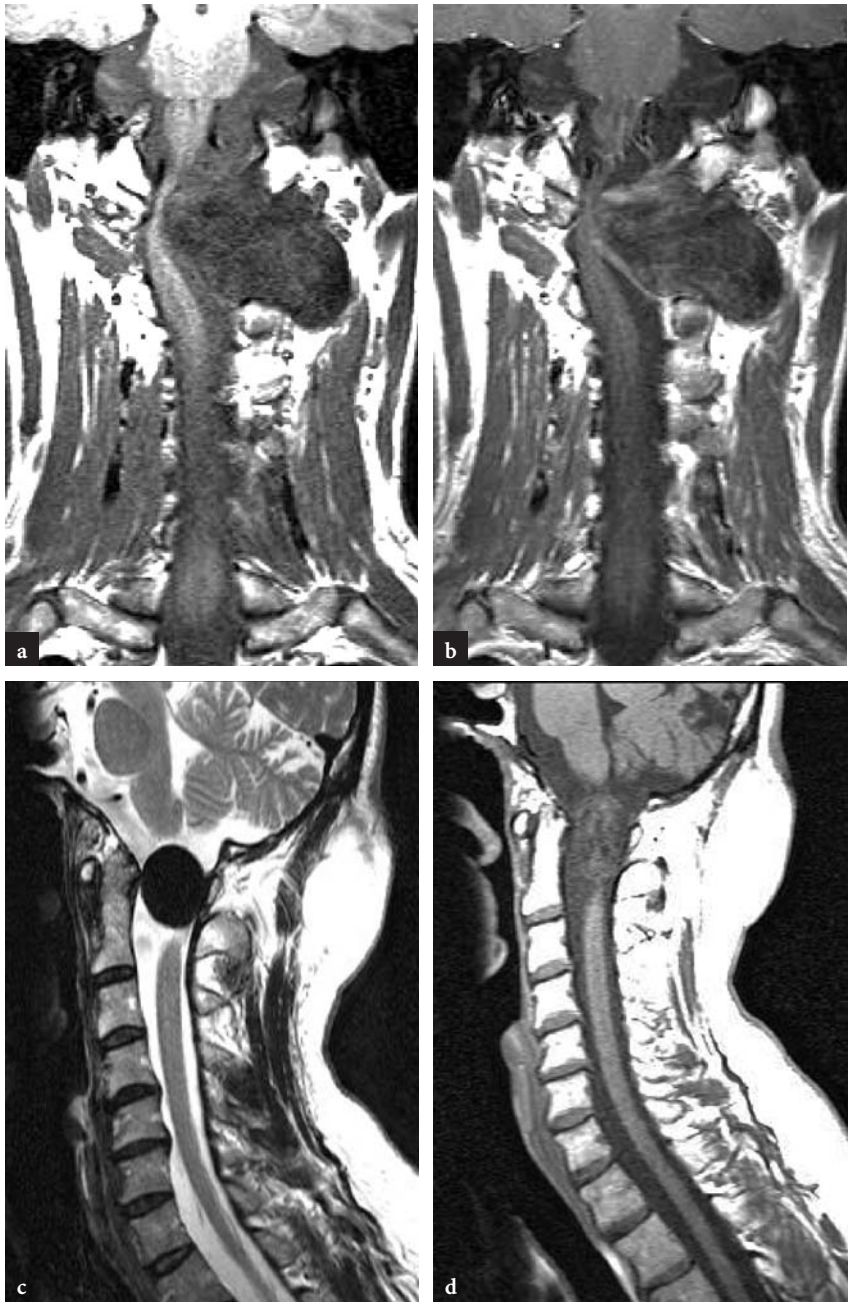

Fig. 18.33a–d. Calcified cervical schwannoma. Incidental finding in a 35-year-old patient investigated by MRI for a huge subcutaneous lipoma. Coronal T1-WI (**a**) and coronal gadolinium T1-WI (**b**). Large upper cervical tumor with a dumbbell shape, mainly hypointense with minimal enhancement at the periphery. Impressive compression and right lateral displacement of the upper cervical cord. Sagittal T2-WI (**c**) and sagittal T1-WI (**d**). This very slowly growing tumor has sharp borders and is calcified. Note the presence of a huge upper cervical lipoma, the reason why in fact this MRI was performed before surgical removal!

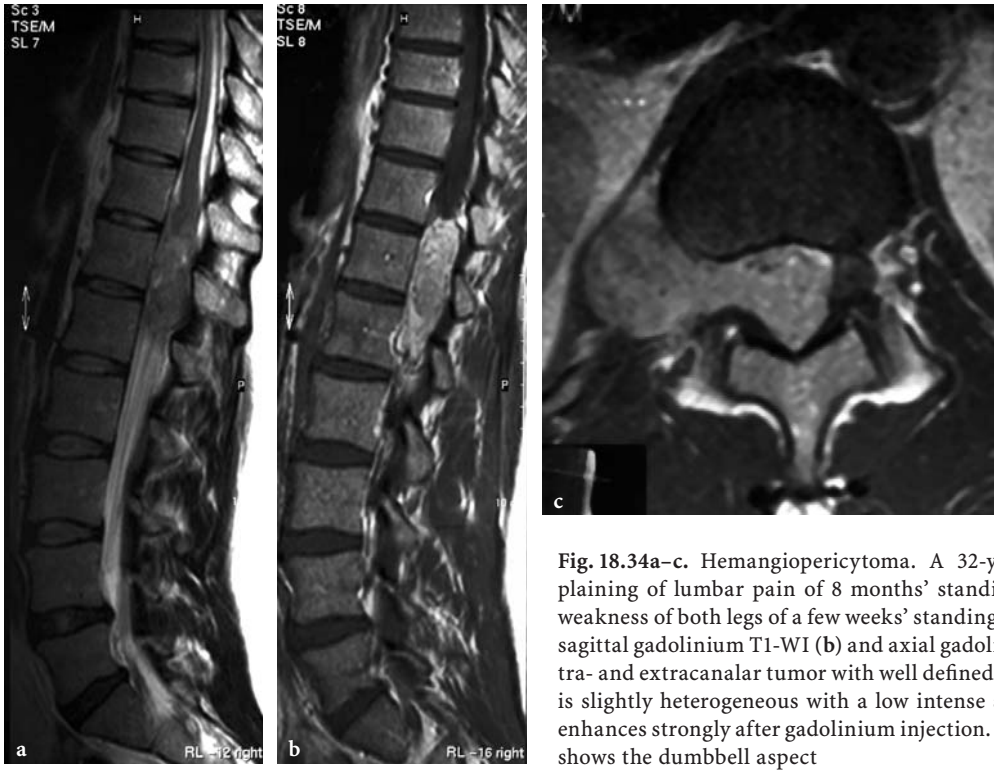

Fig. 18.34a–c. Hemangiopericytoma. A 32-year-old man complaining of lumbar pain of 8 months' standing and progressive weakness of both legs of a few weeks' standing. Sagittal T2-WI (**a**), sagittal gadolinium T1-WI (**b**) and axial gadolinium T1-WI (**c**). Intra- and extracanalar tumor with well defined borders. The tumor is slightly heterogeneous with a low intense aspect on T2-WI. It enhances strongly after gadolinium injection. The axial plane best shows the dumbbell aspect

Fig. 18.35a,b. Neurofibromatosis type 1. Follow-up MRI in a 27-year-old man with known neurofibromatosis type I. Coronal T2-WI (**a**) and coronal myelo-MRI (**b**). Multiple plexiform neurofibromas are nicely shown on those coronal views. The myelographic MIP (**b**) image provides an excellent global view of this massive involvement of most thoracic and lumbo-sacral nerves

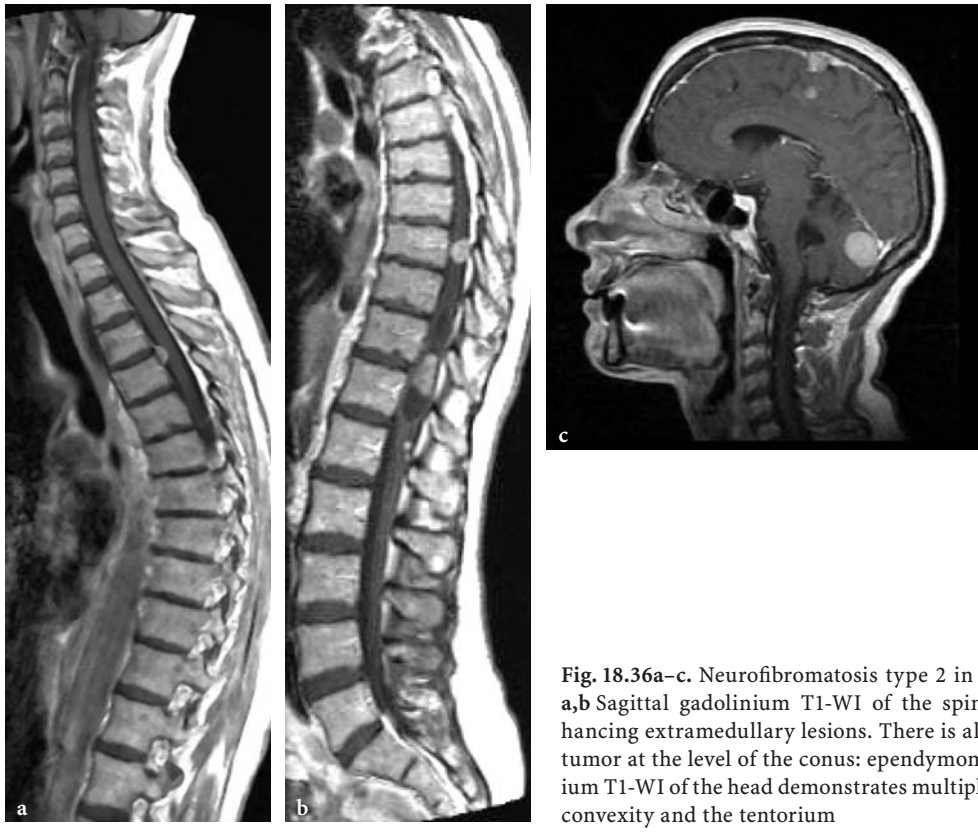

Fig. 18.36a–c. Neurofibromatosis type 2 in a 52-year-old female. **a,b** Sagittal gadolinium T1-WI of the spine show multiple enhancing extramedullary lesions. There is also an intramedullary tumor at the level of the conus: ependymoma. **c** Sagittal gadolinium T1-WI of the head demonstrates multiple meningiomas at the convexity and the tentorium

tered: they are iso-/hyperintense on T2-WI with a "target" aspect (hyperintense rim and low/intermediate center). Enhancement is typically mild. Malignant degeneration does occur rarely, mainly in the case of neurofibromatosis type 2.

18.6.2 Meningioma

Meningiomas are mainly dural-based intradural tumors (95%). Still, the dumbbell presentation may be found in 5% of cases. Overall, 80% of meningiomas are found in the thoracic region, with a female preponderance (fifth/sixth decade); 16% of meningiomas are located in the cervical region and only 4% are lumbar. Multiple meningiomas are rarer than multiple neurinomas. Giant meningiomas have been described. On MRI meningiomas are largely isointense to the spinal cord both on T1-WI and T2-WI. They enhance in a homogeneous and intense manner after gadolinium injection (Figs. 18.37, 18.38). The classical "dural tail" may be seen although this aspect is less frequently and less typically found in the spine compared to the intracranial location (De Verdelhan et al. 2005). Calcifications are more difficult to pick up with MRI than with CT; therefore, CT is a useful complementary procedure.

18.6.3 Paraganglioma

Paragangliomas of the spinal canal may occur anywhere in the spinal canal; still, the lumbosacral level is most commonly affected (Slowinski et al. 2005). The mean age of patients at presentation is around 50 years. Paragangliomas are slow growing, richly vascular tumors that may become very large, eroding the bony canal. Their appearance on MRI is non-specific (Fig. 18.39). Still, the presence of a "flow void" phenomenon can be picked up on T2-WI, indicating a highly vascularized tumor (Perez-Lopez et al. 2004). In general, paragangliomas are relatively benign tumors. Some paragangliomas are more aggressive and may give rise to metastatic spread (Sundgren et al. 1999).

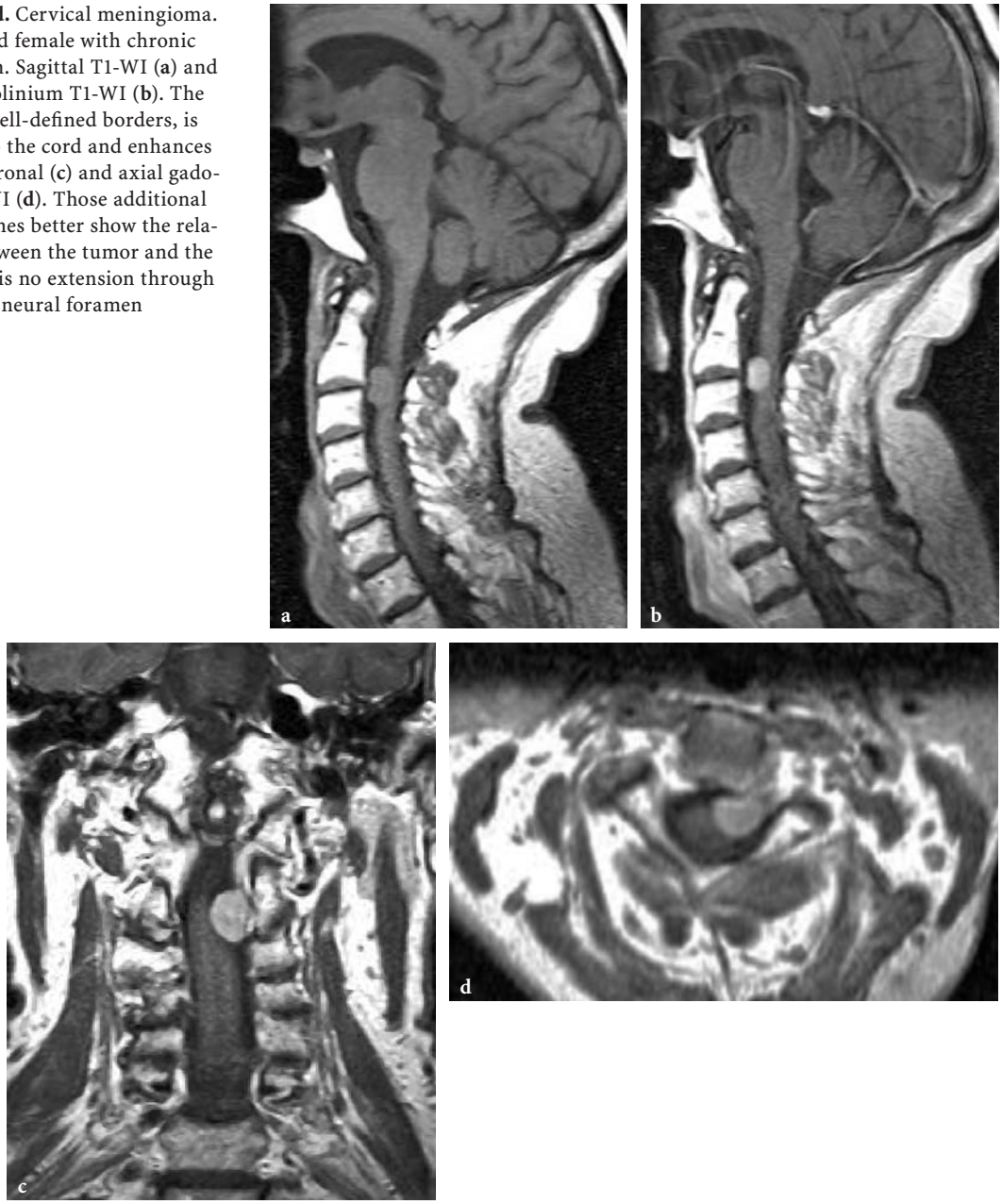

Fig. 18.37a–d. Cervical meningioma. A 73-year-old female with chronic cervical pain. Sagittal T1-WI (**a**) and sagittal gadolinium T1-WI (**b**). The tumor has well-defined borders, is isointense to the cord and enhances strongly. Coronal (**c**) and axial gadolinium T1-WI (**d**). Those additional imaging planes better show the relationship between the tumor and the dura. There is no extension through the adjacent neural foramen

18.6.4 Lipoma

Lipomas are rare, congenital lesions. They occur both as intramedullary or extramedullary intradural lesions. They are classically associated with congenital anomalies (spinal dysraphism, tethered cord, meningoceles, etc.) (Pathi et al. 2003). Their MR presentation is typical because of the high signal intensity on T1-WI. On CT, they also produce a characteristic appearance as strongly hypodense lesions.

18.6.5 Epidermoid

Epidermoid cysts represent 0.5%–1% of all spinal tumors and 10% are found in children. Their origin is either congenital or acquired. When congenital, they are located at the level of the conus or the cauda equina. Acquired epidermoid tumors are probably of iatrogenic origin (adverse complication after lumbar puncture) and are mainly found at the lower lumbar region. On MRI, epidermoid cysts are iso-

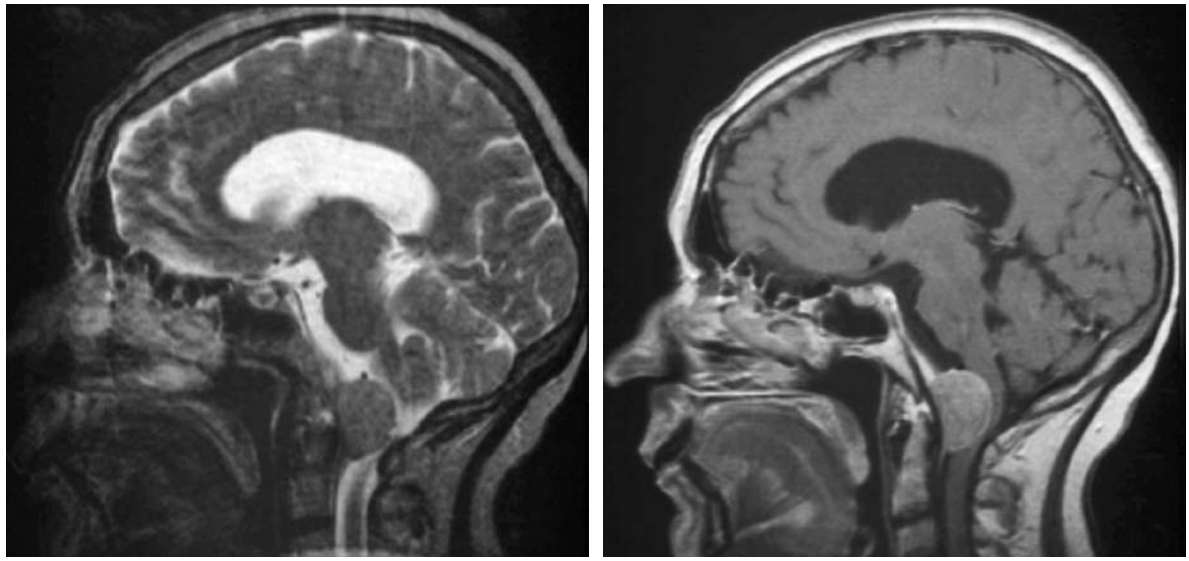

a b

Fig. 18.38a,b. Meningioma of the craniocervical junction. Sagittal T2-WI (**a**), sagittal gadolinium T1-WI (**b**). In this case, the dural base of this anteriorly located tumor is clearly seen. The lesion is isointense on T2-WI and enhances strongly and homogeneously after gadolinium administration

or slightly hypointense to the spinal cord and iso- to hyperintense to CSF on T2-WI (Fig. 18.40). They are better appreciated on T1-WI and proton-density images than on T2-WI. They do not enhance after contrast administration.

18.6.6 Dermoid Cysts

Dermoid cysts are congenital midline cystic tumors. They represent 20% of all intradural tumors seen during the first year of life. Their most common location is the lumbosacral region: 20% of those lesions are associated with a dermal sinus tract. Dermoids typically present a mixed intensity pattern with a fatty component responsible for a hyperintense aspect on T1-WI (Fig. 18.41). Dermoids and epidermoids may rupture and cause chemical meningitis (Gupta et al. 1993).

18.6.7 Metastases

Thanks to MRI, multiple small intradural extramedullary metastases can nowadays easily be diagnosed at a much earlier stage. When they may occur through metastatic spread from a brain tumor, they are preferentially located at the lumbo-sacral level and are called "drop metastases" [ependymoma, medulloblastoma, glioblastoma multiforma, lymphoma (Figs. 18.42, 18.43)]. Alternatively, they can originate from a primary non-CNS tumor: breast and lung carcinoma are the most common origin (Fig. 18.28). PET scanning plays an important role in the diagnosis and monitoring of these lesions, which are highly metabolically active (Fig. 18.11).

18.6.8 Extramedullary Ependymoma

Few cases of purely extramedullary ependymomas have been reported in the literature: imaging findings are non-specific and show a tumor located within the intradural extramedullary space. They may or may not enhance, and can have cystic components (Graca et al. 2006).

18.6.9 Hemangioblastoma

Although hemangioblastomas are usually intramedullary tumors, they may be located entirely outside the medulla. They are well circumscribed, usually small and richly vascular, enhancing after contrast injection (Fig. 18.44). They cannot be differentiated on MRI from schwannomas or metastases. Clinical

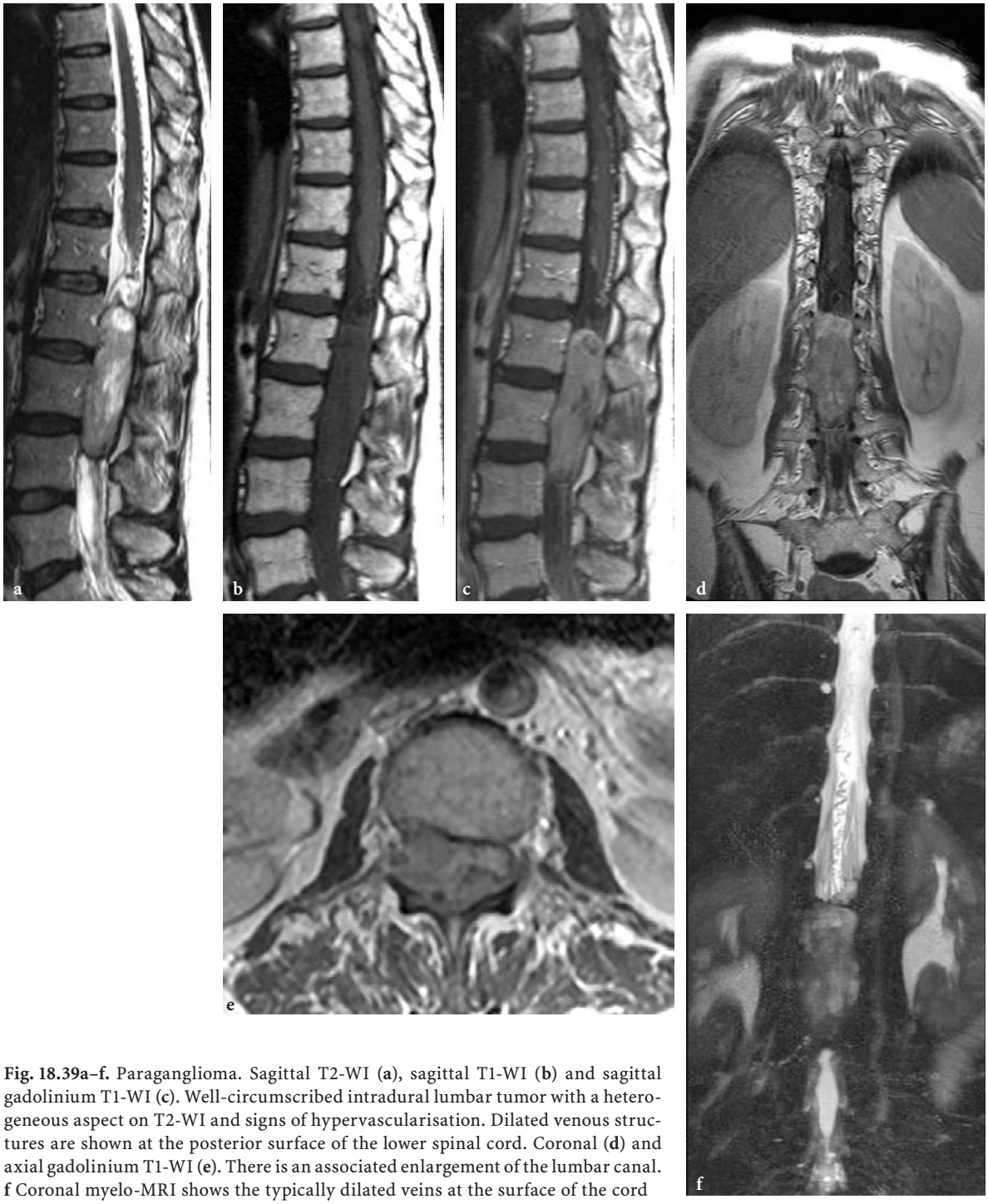

Fig. 18.39a–f. Paraganglioma. Sagittal T2-WI (**a**), sagittal T1-WI (**b**) and sagittal gadolinium T1-WI (**c**). Well-circumscribed intradural lumbar tumor with a heterogeneous aspect on T2-WI and signs of hypervascularisation. Dilated venous structures are shown at the posterior surface of the lower spinal cord. Coronal (**d**) and axial gadolinium T1-WI (**e**). There is an associated enlargement of the lumbar canal. **f** Coronal myelo-MRI shows the typically dilated veins at the surface of the cord

Fig. 18.40a–c. Epidermoid cyst. Sagittal T1-WI (**a**), sagittal T2-WI (**b**), sagittal gadolinium T1-WI (**c**). Intradural mass with a signal behaviour very similar to CSF. No contrast uptake after gadolinium injection

Fig. 18.41a,b. Dermoid cyst. A 16-year-old girl with lumbar pain of a few weeks' standing and walking difficulties. Sagittal T1-WI (**a**) and sagittal T2-WI (**b**). Small fat containing intradural tumor

Fig. 18.42. Metastases from an intracerebral highly malignant gliosarcoma in a 49-year-old man. Sagittal gadolinium T1-WI. After gadolinium injection, intense enhancement due to metastatic spread is seen, surrounding the lower spinal cord and the cauda equina

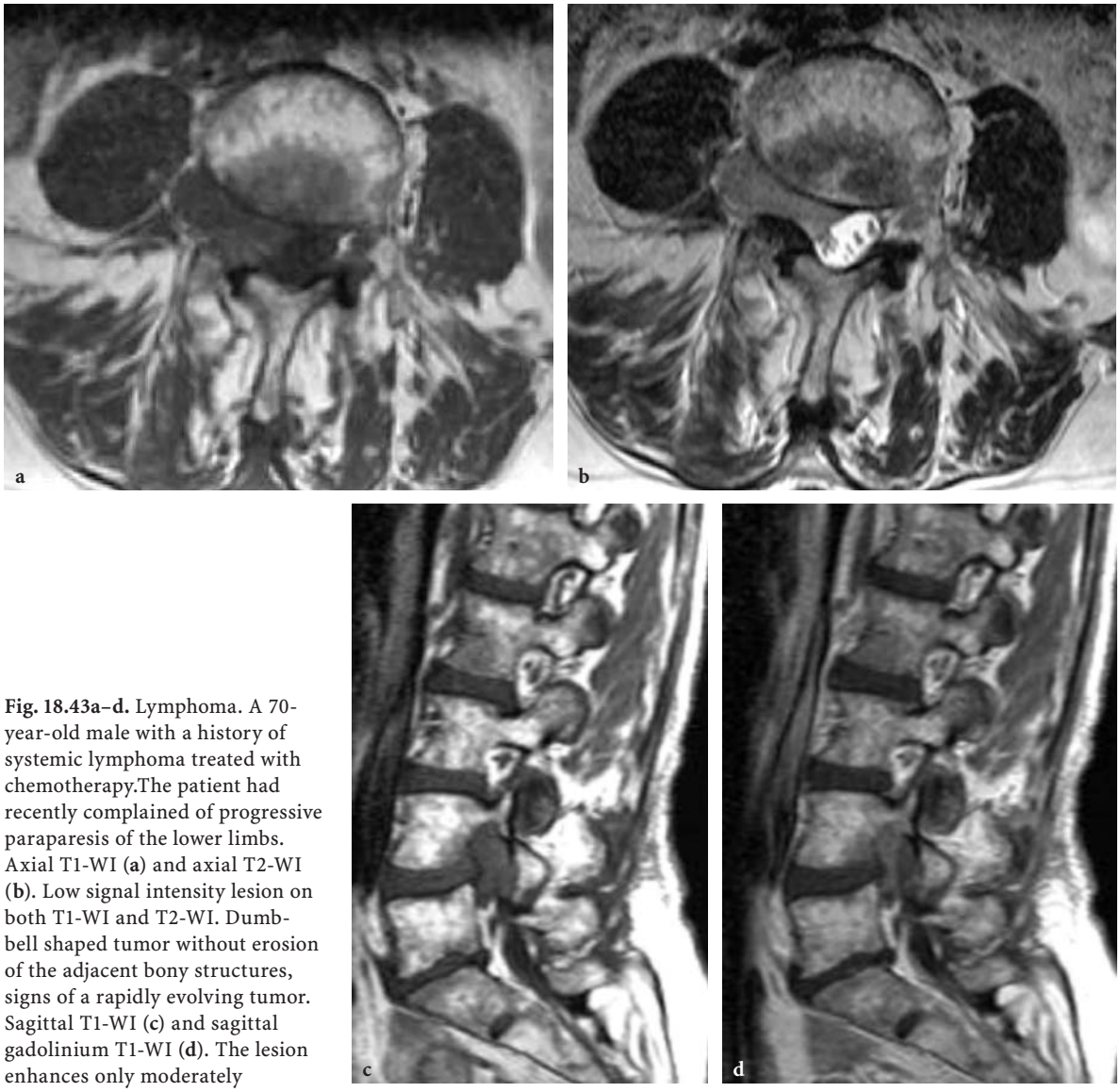

Fig. 18.43a–d. Lymphoma. A 70-year-old male with a history of systemic lymphoma treated with chemotherapy.The patient had recently complained of progressive paraparesis of the lower limbs. Axial T1-WI (**a**) and axial T2-WI (**b**). Low signal intensity lesion on both T1-WI and T2-WI. Dumb-bell shaped tumor without erosion of the adjacent bony structures, signs of a rapidly evolving tumor. Sagittal T1-WI (**c**) and sagittal gadolinium T1-WI (**d**). The lesion enhances only moderately

history and especially the presence of von Hippel-Lindau disease will help to establish the differential diagnosis.

18.7 Differential Diagnosis: Tumor Mimics

18.7.1 Intramedullary Non-tumoral Lesions

Even with MRI, it may be difficult or impossible to differentiate spinal tumors from intramedullary non-neoplastic lesions (Lee et al. 1998). In one series of 212 patients undergoing surgery for intramedullary spinal cord "tumors", investigators reported 4% of non-neoplastic lesions (Lee et al. 1998). Histological examination showed demyelinating disease, sarcoid, amyloid angiopathy, and even a mass of nonneoplastic inflammatory cells of unknown origin! It is therefore essential to know that various non-neoplastic intramedullary lesions can simulate tumor infiltration; they should be properly recognized as such, in order to avoid unnecessary biopsy. The typical spectrum of non-neoplastic intramedullary lesions includes MS plaques, inflammatory lesions, granulomas, abscesses and radionecrosis (Schwartz and McCormick 2000).

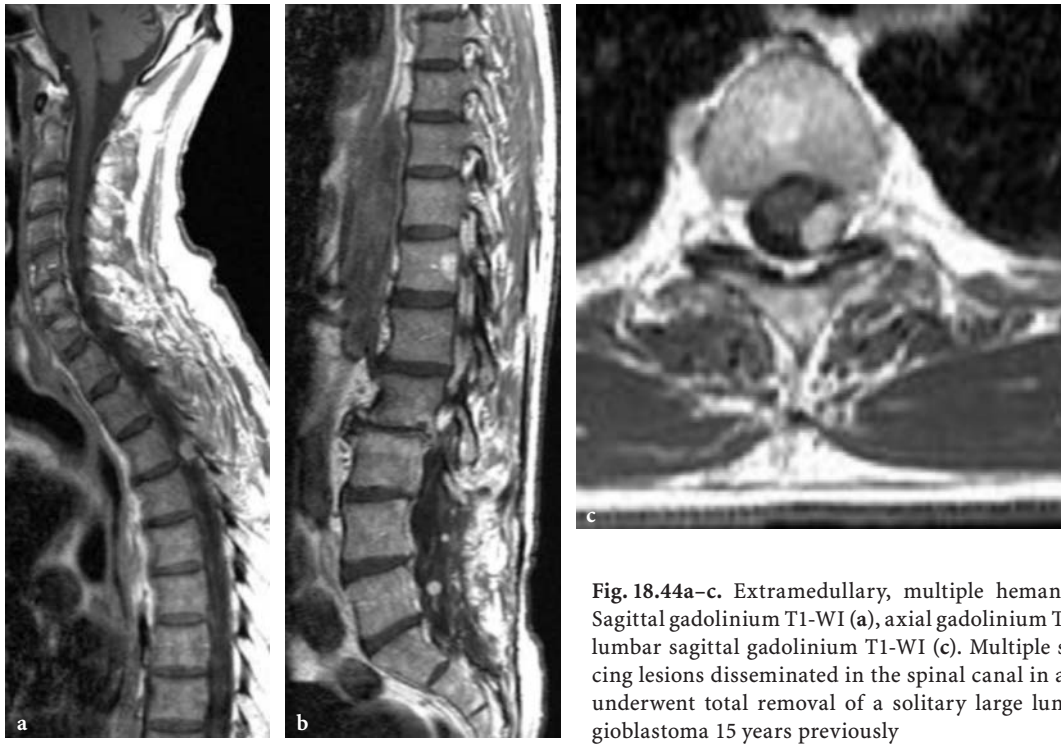

Fig. 18.44a–c. Extramedullary, multiple hemangioblastoma. Sagittal gadolinium T1-WI (**a**), axial gadolinium T1-WI (**b**) and lumbar sagittal gadolinium T1-WI (**c**). Multiple small enhancing lesions disseminated in the spinal canal in a patient who underwent total removal of a solitary large lumbar hemangioblastoma 15 years previously

Radiation necrosis is a rare complication of spinal irradiation: acute necrosis within the spinal cord is seen as a mass lesion with a necrotic center and enhancing rim (Fig. 18.45). Clinical history should guide the differential diagnosis.

18.7.2 Multiple Sclerosis (MS)

An isolated multiple sclerosis (MS) plaque can easily simulate an intramedullary tumor, especially when the lesion causes fusiform enlargement of the cord. MS plaques are usually iso- or hypointense on T1-WI, hyperintense on T2-WI and in the acute phase, enhance mainly in a ringlike mode (Schwartz and McCormick 2000). However, the clinical symptoms usually develop more acutely compared to an intramedullary glioma. MRI of the brain should be performed to rule out cerebral lesions. MRS, when available and technically feasible, may be a helpful tool to rule out a tumor (Fig. 18.8). When dealing with a solitary isolated lesion, and when MS is clinically suspected, a follow-up MRI obtained after 6–8 weeks (and appropriate therapy with corticosteroids) will show size reduction of the lesion (Fig. 18.46). In this way, an unnecessary biopsy or attempt to remove the lesion can be avoided!

18.7.3 Sarcoidosis

Sarcoidosis is rare in the spinal cord. Diagnosis of an intramedullary lesion is facilitated when the patient is known to have systemic sarcoidosis. In two of our cases, the patient had a solitary spinal cord lesion presenting as an intramedullary tumor (Fig. 18.47) (Levivier et al. 1991). MRI demonstrated nonspecific findings of a nodular lesion, with strong enhancement on post-contrast T1-WI. Sarcoidosis should thus be included in the differential diagnosis of a nodular intramedullary lesion. Biopsy may be required and should be performed to establish the diagnosis when there are no systemic signs of sarcoidosis.

18.7.4 Infectious Spinal Cord Diseases

Spinal cord abscesses are rare (Weng et al 2001; Chan et al. 1998). Since the original description in

Fig. 18.45a,b. Radionecrosis. Sagittal T2-WI (**a**) and sagittal gadolinium T1-WI (**b**). Enhancing mass lesion at the C2 level: biopsy confirmed an area of radionecrosis in a patient who had undergone total removal of a posterior fossa malignant ependymoma followed by radiotherapy 2 years previously. [Reprinted with permission from Baleriaux et al. (2004)]

1830, fewer than 100 cases have been reported in the literature (Murphy et al. 1998; Quencer and Post 1997). A spinal cord abscess is easily diagnosed when it occurs as a complication of spinal surgery, or in the setting of infectious spondylodiscitis, because of the continuity with bony lesions. Intramedullary tuberculosis has been reported but again is extremely rare, as are Shistosomiasis and toxoplasmosis, among others. It is mainly in immunocompromised and AIDS patients that these rare infectious complications are found in the spinal cord. Clinical history is usually very helpful (Baleriaux et al. 1992).

Myelitis and transverse myelitis are more common compared to spinal cord abscess and usually are from viral origin, although it should be emphasized that in more than 50% of cases the origin remains unknown. MRI plays a key role since it is the only imaging modality that allows direct visualization of the disease. The spinal cord is usually only mildly enlarged while there are one or multiple foci of ill delineated high signal intensity areas on T2-WI, low or iso-signal on T1-WI and enhancing moderately to strongly after gadolinium enhancement. Differential diagnosis includes mainly multiple sclerosis and metastasis (Baleriaux and Neugroschl 2004). Again, the clinical history is usually very helpful.

18.8 Conclusions

Although spinal intradural tumors are relatively rare lesions, they represent a significant cause of disability and concern mostly younger patients. MRI has played a major role in the diagnosis and management of these patients, who often benefit from major improvement after surgical treatment.

Acknowledgements
Our sincere thanks to Professor Jacques Brotchi, head of the department of Neurosurgery and Dr Florence Lefranc for their invaluable, continuous and fruitful collaboration. Our sincere thanks also go to Professor Isabelle Salmon, head of the department of pathology.

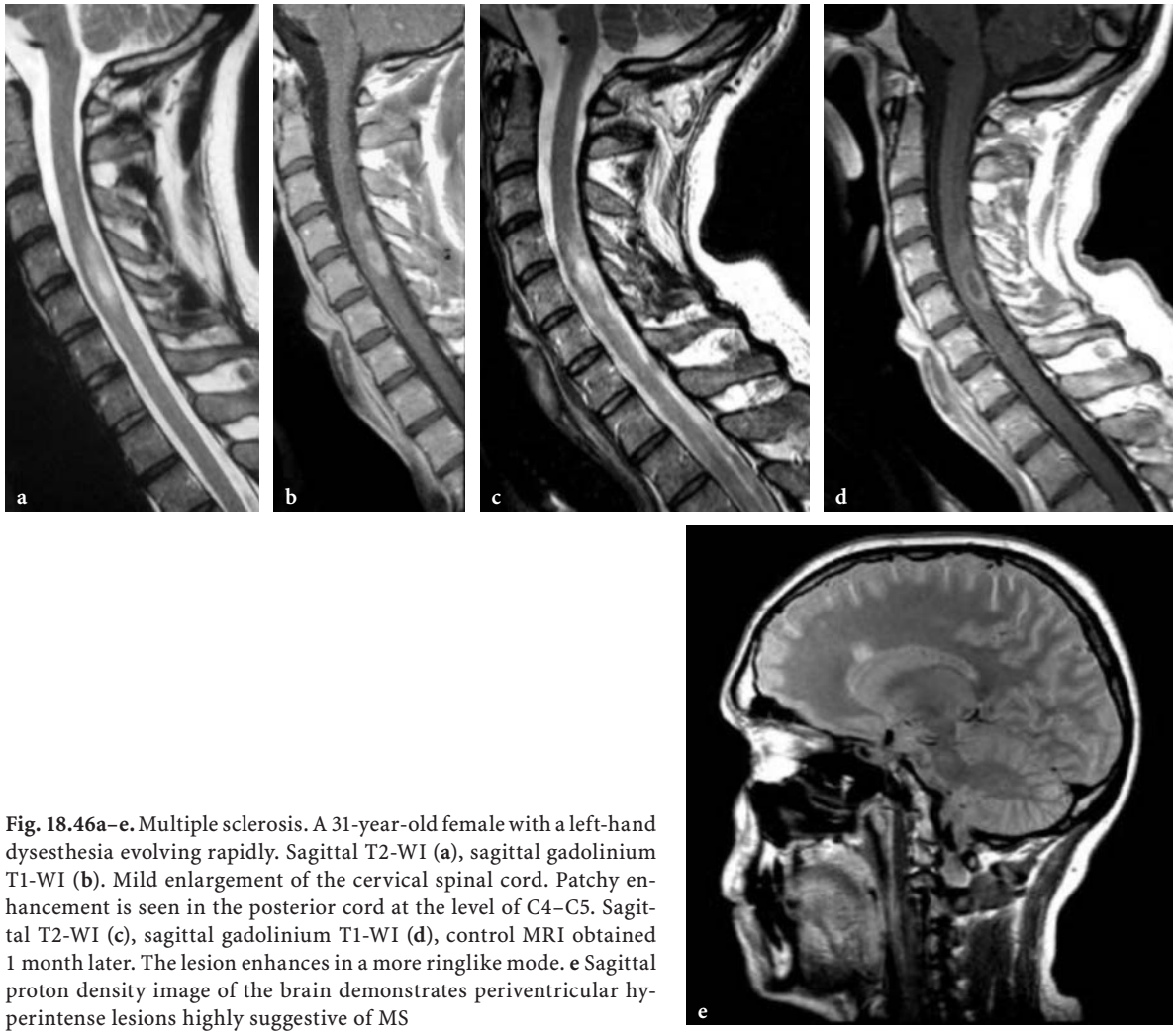

Fig. 18.46a–e. Multiple sclerosis. A 31-year-old female with a left-hand dysesthesia evolving rapidly. Sagittal T2-WI (**a**), sagittal gadolinium T1-WI (**b**). Mild enlargement of the cervical spinal cord. Patchy enhancement is seen in the posterior cord at the level of C4–C5. Sagittal T2-WI (**c**), sagittal gadolinium T1-WI (**d**), control MRI obtained 1 month later. The lesion enhances in a more ringlike mode. **e** Sagittal proton density image of the brain demonstrates periventricular hyperintense lesions highly suggestive of MS

Fig. 18.47a,b. Cervical spinal cord sarcoidosis. Sagittal T1-WI (**a**) and sagittal gadolinium T1-WI (**b**). There is a mild enlargement of the cervical spinal cord at the level of C4. The lesion enhances strongly after gadolinium injection. This finding is non-specific: differential diagnosis includes tumor infiltration and MS. Biopsy was necessary to provide the final diagnosis as there was no evidence of systemic sarcoidosis

References

Aryan HE, Farin A, Nakaji P et al. (2004) Intramedullary spinal cord metastasis of lung adenocarcinoma presenting as Brown-Sequard syndrome. Surg Neurol 61:72–76

Backes WH, Mess WH, Wilmink JT (2001) Functional MR imaging of the cervical spinal cord by use of median nerve stimulation and fist clenching. Am J Neuroradiol 22:1854–1859

Backes WH, Nijenhuis RJ, Mull M et al. (2004) Contrast-enhanced MR angiography of the spinal arteries: current possibilities and limitations. Rivista Di Neuroradiologia 17:282–291

Baker KB, Moran CJ, Wippold FJ 2nd et al. (2000) MR imaging of spinal hemangioblastoma. AJR Am J Roentgenol 174:377–382

Balériaux D, Parizel P, Bank WO (1992) Intraspinal and intramedullary pathology. In: Manelfe C (ed) Imaging of the spine and spinal cord. Raven Press, New York, pp 513–564

Balériaux D (1999a) Spinal cord tumors. Eur Radiol 9:1252–1258

Balériaux D (1999b) MRI of spinal cord diseases. Educational CD ROM edited by Lasion, 2nd edn.

Balériaux DL, Neugroschl C (2004) Spinal and spinal cord infection. Eur Radiol 14[Suppl 3]:E72–83

Balériaux D, Brotchi J, Salmon I (2004) Spinal cord tumours: a pictorial essay. Rivista di Neuroradiologia 17:336–348

Bret P, Bougeard R, Saint-Pierre G et al. (1997) Intramedullary subependymoma of the cervical spinal cord. Review of the literature a propos of a case. Neurochirurgie 43:158–163

Brotchi J, Dewitte O, Levivier M et al. (1991) A survey of 65 tumors within the spinal cord: surgical results and the importance of preoperative magnetic resonance imaging. Neurosurgery 29:651–657

Brotchi J (2002) Intrinsic spinal cord tumor resection. Neurosurgery 50:1059–1063

Bydder GM, Brown J, Niendorf HP et al. (1985) Enhancement of cervical intraspinal tumors in MR imaging with intravenous gadolinium-DTPA. J Comput Assist Tomogr 9:847–851

Caviness JA, Tucker MH, Pia SK et al. (1998) Hydrocephalus as a possible early symptom in a child with a spinal cord tumor. Pediatr Neurol 18:169–171

Chan CT, Gold WL (1998) Intramedullary abscess of the spinal cord in the antibiotic era: clinical features, microbial etiologies, trends in pathogenesis, and outcomes. Clin Infect Dis Sep 27:619–626

Colombo N, Kucharczyk W, Brant-Zawadzki M et al. (1986) Magnetic resonance imaging of spinal cord hemangioblastoma. Acta Radiol (Diagn) 769:734–737

Colosimo C, Cerase A, Denaro L et al. (2003) Magnetic resonance imaging of intramedullary spinal cord schwannomas. Report of two cases and review of the literature. J Neurosurg 99[1 Suppl]:114–117

Conill C, Sanchez M, Puig S et al. (2004) Intramedullary spinal cord metastases of melanoma. Melanoma Res 14:431–433

Constantini S, Houten J, Miller DC, et al. (1996) Intramedullary spinal cord tumors in children under the age of 3 years. J Neurosurg 85:1036–1043

De Verdelhan O, Haegelen C, Carsin-Nicol B (2005) MR imaging features of spinal schwannomas and meningiomas. J Neuroradiol 32:42–49

Del Carpio, O'Donovan R (1998) A pattern approach to the differential diagnosis of intramedullary spinal cord lesions on MR imaging. AJR Am J Roentgenol 170:1645–1649

Edal A, Balériaux D, Metens T et al. (1997) Three-dimensional turbo spin echo cervical magnetic resonance myelography. Int J Neuroradiol 3:130–135

Epstein FJ, Farmer JP, Freed D (1992) Adult intramedullary astrocytomas of the spinal cord. J Neurosurg 77:355–359

Epstein FJ, Farmer JP, Freed D (1993) Adult intramedullary spinal cord ependymomas: the result of surgery in 38 patients J Neurosurg 79:204–209

Facon D, Ozanne A, Fillard P et al. (2005) MR diffusion tensor imaging and fiber tracking in spinal cord compression. AJNR Am J Neuroradiol 26:1587–1594

Fine MJ, Kricheff II, Freed D et al. (1995) Spinal cord ependymomas: MR imaging features. Radiology 197:655–658

Fischer G, Brotchi J (1996) Intramedullary spinal cord tumors. Thieme, Stuttgart New York

Fountas KN, Karampelas I, Nikolakakos LG et al. (2005) Primary spinal cord oligodendroglioma: case report and review of the literature. Childs Nerv Syst 21:171–175

Friedman DP, Hollander MD (1998) Neuroradiology case of the day. Myxopapillary ependymoma of the conus medullaris or filum terminale resulting in superficial siderosis and dissemination of tumor along CSF pathways. Radiographics 18:794–798

Graca J, Gultasli N, Brotchi J et al. (2006) Cystic extra-medullary ependymoma. AJNR Am J Neuroradiol 27:818--821

Gupta S, Gupta RK, Gujral RB, et al. (1993) Signal intensity patterns in intraspinal dermoids and epidermoids on MR imaging. Clin Radiol 48:405–413

Hamburger C, Buttner A, Weis S (1997) Ganglioglioma of the spinal cord: report of two rare cases and review of the literature. Neurosurgery 41:1410–1415

Huang JH, Zhang J, Zager EL (2005) Diagnosis and treatment options for nerve sheath tumors. Expert Rev Neurother 5:515–523

Innocenzi G, Raco A, Cantore G et al (1996) Intramedullary astrocytomas and ependymomas in the pediatric age group: a retrospective study. Childs Nerv Syst 12:776–780

Ijaz T, Jones K (1997) Images in clinical medicine. Intramedullary spinal cord metastases. N Engl J Med 336:768

Kahan H, Sklar EML, Donovan Post MJ et al. (1996) MR characteristics of histopathologic subtypes of spinal ependymoma. AJNR Am J Neuroradiol 17:143–150

Kalayci M, Cagavi F, Gul S et al. (2004) Intramedullary spinal cord metastases: diagnosis and treatment -- an illustrated review. Acta Neurochir (Wien) 146:1347–1354

Kim YG, Choi GH, Kim DH et al. (2004) In vivo proton magnetic resonance spectroscopy of human spinal mass lesions. J Spinal Disord Tech 17:405–411

Koeller KK, Rosenblum RS, Morrison AL (2000) Neoplasms of the spinal cord and filum Terminale: radiologic-pathologic correlation. Radiographics 20:1721–1749

Komisaruk BR, Mosier KM, Liu WC et al. (2002) Functional localization of brainstem and spinal cord nuclei in humans with fMRI. Am J Neuroradiol 23:609–617

Lahanis S, Vlahos L, Gouliamos A et al. (1993) Arteriovenous malformation of the spinal cord mimicking a tumour. Neuroradiology 35:598–599

Lasjaunias P, Berenstein A, Raybaud C (1992) Surgical neuroangiography V. endovascular treatment of spine and

spinal cord lesions. Springer-Verlag, Berlin Heidelberg New York
Le Bihan D (1991) Molecular diffusion nuclear magnetic resonance imaging. Magn Reson Q 7:1–30
Lee M, Epstein FJ, Rezai AR et al. (1998) Nonneoplastic intramedullary spinal cord lesions mimicking tumours. Neurosurgery 43:788–794
Levivier M, Brotchi J, Balériaux D et al. (1991) Sarcoidosis presenting as an isolated intramedullary tumor. Neurosurgery 25:271–276
Li MH, Holtas S (1991) MR imaging of spinal intramedullary tumors. Acta Radiol 32:505–513
Lonjon M, Goh KY, Epstein FJ (1998) Intramedullary spinal cord ependymomas in children: treatment, results and follow-up. Pediatr Neurosurg 29:178–183
Lunardi P, Licastro G, Missori P et al. (1993) Management of intramedullary tumours in children. Acta Neurochir (Wien) 120:59–65
Maiuri F, Iaconetta G, De Divitiis O (1997) The role of intraoperative sonography in reducing invasiveness during surgery for spinal tumors. Minim Invasive Neurosurg 40:8–12
Maiuri F, Iaconetta G, Gallicchio B, Stella L (2000) Intraoperative sonography for spinal tumors. Correlations with MR findings and surgery. J Neurosurg Sci 44:115–122
McCormick PC, Torres R, Post KD et al. (1990) Intramedullary ependymoma of the spinal cord. J Neurosurg 72:523–532
Minami M, Hanakita J, Suwa H, et al. (1998) Cervical hemangioblastoma with a past history of subarachnoid hemorrhage. Surg Neurol 49:278–281
Murphy KJ, Brunberg JA, Quint DJ et al. (1998) Spinal cord infection: myelitis and abscess formation. AJNR Am J Neuroradiol 19:341–348
Nadkarni TD, Rekate HL (1999) Pediatric intramedullary spinal cord tumors: critical review of the literature. Childs Nerv Syst 15:17–28
Nagib MG, O'Fallon MT (1997) Myxopapillary ependymoma of the conus medullaris and filum terminale in the pediatric age group. Pediatr Neurosurg 26:2–7
Nakamizo T, Inoue H, Udaka F et al. (2002) Magnetic resonance imaging of primary spinal intramedullary lymphoma. J Neuroimaging 12:183–186
Nemoto Y, Inoue Y, Tashiro T et al. (1992) Intramedullary spinal cord tumors: significance of associated hemorrhage at MR imaging. Radiology 182:793–796
Osborn AG (1994) Tumors, cysts and tumorlike lesions of the spine and spinal cord. In: Osborn AG (ed) Diagnostic neuroradiology. Mosby, pp 876–918
Parizel PM, Balériaux D, Rodesch G, Segebarth C, Lalmand B, Christophe C, Lemort M, Haesendonck P, Niendorf HP, Flament-Durand J, Brotchi J (1989) Gadolinium-DTPA-enhanced MR imaging of spinal tumors. AJNR Am J Neuroradiol 10:249–258
Patel U, Pinto RS, Miller DC et al. (1998) MR of spinal cord ganglioglioma. AJNR Am J Neuroradiol 19:879–887
Pathi R, Kiley M, Sage M (2003) Isolated spinal cord lipoma. J Clin Neuroscience 10:692–694
Perez-Lopez C, Sarmiento MA, Alvarez-Ruiz F et al. (2004) Paragangliomas of the cauda equina: report of two cases. Neurocirugia (Astur) 15:565–570
Przybylski GJ, Albright AL, Martinez AJ (1997) Spinal cord astrocytomas: long-term results comparing treatments in children. Childs Nerv Syst 13:375–382
Poggi MM, Patronas N, Buttman JA et al. (2001) Intramedullary spinal cord metastasis from renal cell carcinoma: detection by positron emission tomography. Clin Nucl Med 26:837–839
Regelsberger J, Fritzsche E, Langer N et al. (2005) Intraoperative sonography of intra- and extramedullary tumors. Ultrasound Med Biol 31:593–598
Ries M, Jones RA, Dousset V et al. (2000) Diffusion tensor MRI of the spinal cord. Magn Reson Med 44:884–892
Rifkinson-Mann S, Wisoff JH, Epstein F (1990) The association of hydrocephalus with intramedullary spinal cord tumors: a series of 25 patients. Neurosurgery 27:749–754
Russo CP, Katz DS, Corona RJ et al. (1995) Gangliocytoma of the cervicothoracic spinal cord. AJNR Am J Neuroradiol 16:889–891
Quencer RM, Post MJ (1997) Spinal cord lesions in patients with AIDS. Neuroimaging Clin N Am 7:359–373
Santaguida C, Sabbagh AJ, Guiot MC et al.(2004) Aggressive intramedullary melanotic schwannoma: case report. Neurosurgery 55:1430
Santoro A, Piccirilli M, Frati A et al. (2004) Intramedullary spinal cord cavernous malformations: report of ten new cases. Neurosurg Rev 27:93–98
Schwarts ED, Chin CL, Takahashi M et al. (2002) Diffusion-weighted imaging of the spinal cord. Neuroimaging Clin N Am 12:125–146
Schwartz TH and McCormick PC (2000) Non-neoplastic intramedullary pathology. Diagnostic dilemma: to Bx or not to Bx. J Neurooncol 47:283–292
Scotti G, Scialfa G, Colombo N et al. (1987) Magnetic resonance diagnosis of intramedullary tumors of the spinal cord. Neuroradiology 29:130–135
Shimizu T, Saito N, Aihara M et al. (2004) Primary spinal oligoastrocytoma: a case report. Surg Neurol 61:77–81
Slowinski J, Stomal M, Bierzynska-Macyszyn G et al. (2005) Paraganglioma of the lumbar spinal canal – case report. Folia Neuropathol 43:119–122
Sun B, Wang J, Liu A (2003) MRI features of intramedullary spinal cord ependymomas. J Neuroimaging 13:346–351
Sundgren P, Annaertz M, Englund E et al. (1999) Paragangliomas of spinal canal. Neuroradiology 41:788–794
Sze G (1996) Neoplastic disease of the spine and spinal cord. In: Atlas SW (ed) Magnetic resonance imaging of the brain and spine, 2nd edn. Lippincott-Raven, pp 1339–1385
Thron AK, Rossberg C, Mironov A (1988) Vascular anatomy of the spinal cord: neurological investigations and clinical syndromes. Springer-Verlag (Wien), Berlin Heidelberg New York
Timmer FA, Van Rooij WJ, Beute GN et al. (1993) Intramedullary lipoma. Neuroradiology 38:159–160
Tortori Donati P, Rossi A (2005) Tumors of the spine and spinal cord. In: Pediatric neuroradiology. Springer-Verlag, Berlin Heidelberg New York, pp 1609–1653
Tsuchiya K, Fujikawa A, Suzuki Y (2005) Diffusion tractography of the cervical spinal cord by using parallel imaging. AJNR Am J Neuroradiol 26:398–400
Van Goethem JW, Van den Hauwe L, Ozsarlak O et al. (2004) Spinal tumors. Eur J Radiol 50:159–176
Weiner HL, Freed D, Woo HH et al. (1997) Intra-axial tumors of the cervicomedullary junction: surgical results and long-term outcome. Pediatr Neurosurg 27:12–18
Weng TI, Shih FY, Chen WJ et al. (2001) Intramedullary abscess of the spinal cord. Am J Emerg Med 19:177–178
Wilmshurst JM, Barrington SF, Pritchard D et al.(2000) Positron emission tomography in imaging spinal cord tumors. J Child Neurol 15:465–472

Metastatic Disease of the Spine

19

Cosma Andreula, Mario Murrone, and Paul R. Algra

CONTENTS

19.1 Spinal Metastatic Disease

The vertebral column is the most common site for bony metastases in patients with systemic malignancy, and metastatic lesions are the most common tumors of the spine (Harrington 1986). Patients with metastatic spinal tumors may present with pain (most common clinical presentation), neurologic deficit or both. Some tumors on the other hand are asymptomatic and are detected during screening examinations. Treatment options include chemotherapy, hormonal therapy, steroids, surgery, radiation and combinations thereof.

Cosma Andreula
Department of Radiology and Neuroradiology, Anthea Hospital, Bari, Italy
Mario Murrone
Città di Lecce. Lecce, Gruppo Villa Maria Puglia, Italy
Paul R. Algra
Department of Radiology, Medisch Centrum Alkmaar, The Netherlands

Metastases of the spine can occur:
1. Intramedullary
2. Intradural but extramedullary
3. Extradural in the epidural space
4. In the osseous spine

Spinal metastases most often originate from carcinomas of the breast (21%), lung (14%), prostate (7.5%), kidney (5%) and gastrointestinal tract (5%) (Schick et al. 2001; Harrington 1986). These tumors generally involve the bones of the vertebrae or the surface of the spinal cord, but less than 5% of all metastatic spine tumors are intradural (either intra- or extramedullary).

The most common tumors known to spread to meninges are small cell lung cancer (11%), breast cancer (5%) and melanoma.

19.1.1 Intramedullary Metastases

Intramedullary metastases are very rare (1%–3% of cancer patients) and usually originate either from non-CNS tumors (breast and lung cancers). CNS tumors that may also metastasize to the cord are glioblastoma, medulloblastoma and ependymoma. Tumor spread occurs either via blood or through cord penetration from leptomeningeal tumors. Intramedullary metastases may be single or multiple, small and not enlarging the spinal cord, or large enough to completely replace the spinal cord, spreading into the meninges. Cord enlargement is focal in hematogenous spread, whereas the involvement of the spinal cord by direct spread from leptomeningeal tumors results in continuous enlargement of a cord segment.

If the lesion is large enough the cord enlargement has low signal on T1-weighted images (T1-WI), and high signal on T2-weighted images (T2-WI), with heterogeneous contrast enhancement. Viable tissue shows up as the contrast-enhanced lesion, the remainder is edema (Fig. 19.1).

Key Points

- Spinal metastases most often originate from:
  - Breast (21%)
  - Lung (14%)
  - Prostate (7.5%)
  - Kidney (5%)
  - Gastrointestinal tract (5%)
- Bone metastases
  - In up to 50% of patients with cancer
    - Among these 40%–70% are vertebral lesions
  - 10% Unknown origin
- Vertebral metastases
  - 10% of patients with malignant neoplasms
  - Cause the primary symptoms in 10%–40% of these patients
- No sex predilection
- Most frequent in the 5th decade
- Thoracic > lumbar > cervical (4:2:1)
- Imaging
  - Screening asymptomatic patients: scintigraphy
  - But: screening for breast and lung metastases: MRI
  - Suspected lesion (positive scintigraphy): confirm by plain film/CT
  - Neurological symptoms: MRI
- Vertebral collapse/compression fracture:
  - Benign:
    - No cortical destruction,
    - Retropulsion of bone fragments
    - Intravertebral vacuum phenomenon
    - Multiple compression fractures
    - Focal concave collapse
    - Spared normal bone marrow SI of the vertebral body
  - Malignant:
    - Other (vertebral) lesions
    - Abnormal signal intensity of the pedicle or posterior element
    - Expansive
    - Cortical bone lysis
    - An encasing epidural mass or a focal paraspinal mass
    - Focal acute angled collapse
    - Convex posterior border
    - Complete absence of normal bone marrow

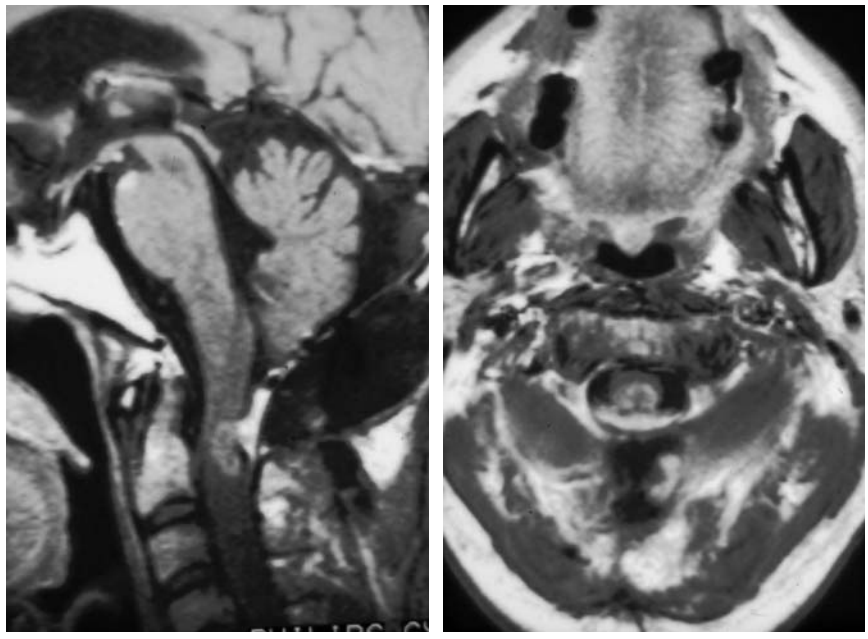

a b

Fig. 19.1a,b. Intramedullary metastasis at the level of C2. Rounded lesion in the central posterior part of the spinal cord on T1-WI (**a**). Contrast enhancement after gadolinium (**b**). The lesion predominantly involves the gray matter and has a necrotic center

Metastatic disease may also be detected by the presence of a syrinx.

In small lesions frequently the only sign is focal contrast enhancement.

The differential diagnosis includes transverse myelitis (vascular location and pattern of contrast enhancement), and an active multiple sclerosis (MS) plaque (different clinical history, less edema, usually multiple).

Fig. 19.2. Drop metastasis of different size and different morphology at L3–L4, L4 and in the cul-de-sac on this T1-WI after gadolinium

19.1.2 Leptomeningeal Metastases

Leptomeningeal metastases have the same origin as intramedullary metastases, with the exception of acute leukemia, which occurs frequently in the dura.

Dural involvement, or carcinomatous meningitis, results in thickened leptomeninges (Fig. 19.2). As the tumor increases, nodules and/or plaques appear.

Specific imaging studies such as myelography or intrathecal contrast-enhanced CT reveal nodular filling defects. Basic MRI has a low sensitivity with 40% false negatives. Contrast-enhanced MRI identifies the nodules directly and dural involvement can also be seen as abnormally strong enhancing and/or thickened leptomeninges. Positive CSF cytology confirms the diagnosis.

In the cauda equina and at the end of the dural sac drop metastases are easily recognized as small isointense nodules with marked contrast enhancement surrounded by hypointense CSF (Fig. 19.3). Their detection may be more difficult on T2-WI. Only if they have relatively low signal compared to CSF are they recognizable.

In carcinomatous arachnoiditis the roots of the cauda equina appear mottled, ill-defined and/or asymmetrically distributed within the thecal sac. However, arachnoiditis due to infection or other etiologies can have the same pattern. The difference is involvement of the spinal ganglion, which is seen in carcinomatosis, but is rare in arachnoiditis due to other pathology.

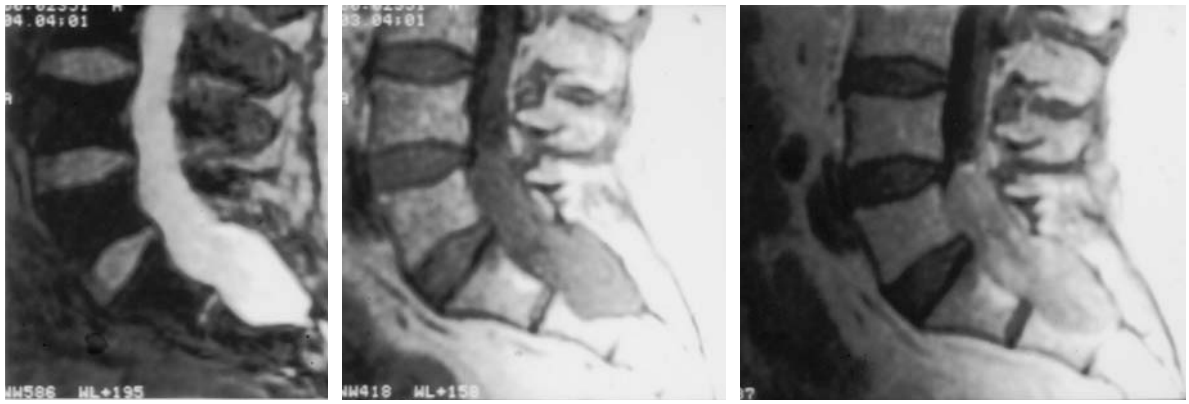

Fig. 19.3. Drop metastases filling the cul de sac on T2-WI and T1-WI before and after gadolinium

19.1.3 Epidural and Paraspinal Lesions

Epidural and paraspinal metastatic disease are closely related to the vertebral bodies (Fig. 19.4). The only epidural location without vertebral involvement occurs in lymphoma, from spread of the retroperitoneum to the paraspinal and epidural spaces through the neural foramina. Dissection of the dura may cause spinal narrowing (Kienstra et al. 2000).

On MRI the tumoral cells infiltrate and replace the fatty epidural spaces, with iso-hypointense signal on T1-WI, marked and homogeneous contrast enhancement and hyperintense signal on T2-WI. Spread of the process along the path of minor resistance forces epidural spaces in the lower thoracic and lumbar spine to assume a biconvex form (curtain sign), related to the ligament of Trolard that runs between the posterior ligament and the anterior part of the dural sac (Fig. 19.5).

Differential diagnosis includes spondylitis, granulomatous inflammatory infectious processes and epidural and paraspinal extension of aggressive vertebral hemangioma (Figs. 19.6, 19.7). In spondylitis the perivertebral collar is more prominent, bone erosion is frequently more patchy and there is almost always involvement of the disk space and endplates. Epidural metastasis could simulate granulomatous infectious disease such as tuberculosis with epidural abscess, but in this case the process is usually more extensive. Aggressive expansile vertebral heman-

Fig. 19.4. Epidural metastasis. At a midthoracic level a posterior epidural plaque compressing the cord posteriorly is seen on this T1-WI after gadolinium. At the same level a vertebral body metastasis with posterior wall erosion is revealed by its hypointense signal

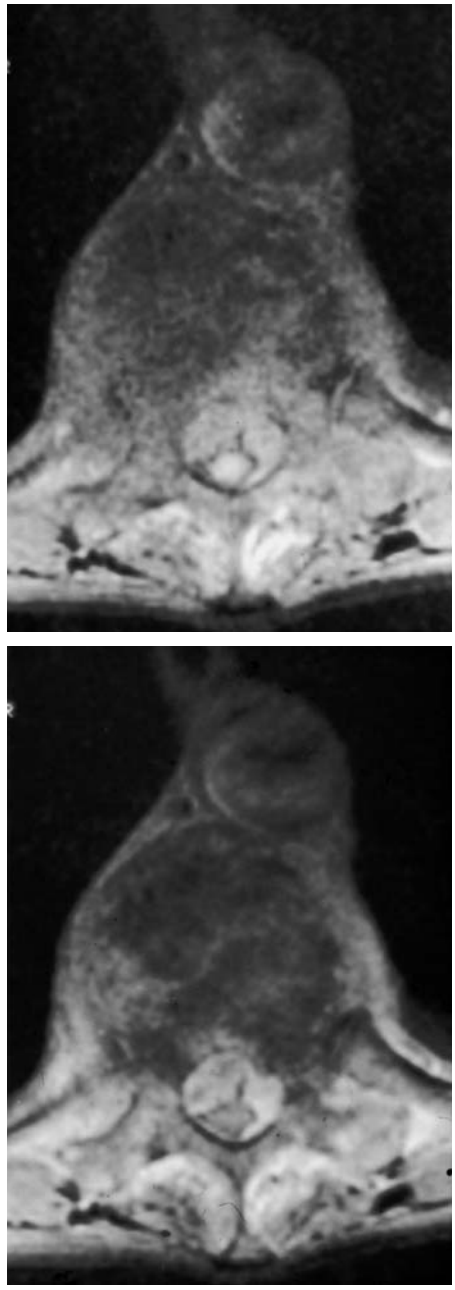

Fig. 19.5a,b. Epidural metastasis. "Curtain sign" of the epidural metastasis with vertebral body involvement on T1-WI before (**a**) and after (**b**) gadolinium and T2-WI

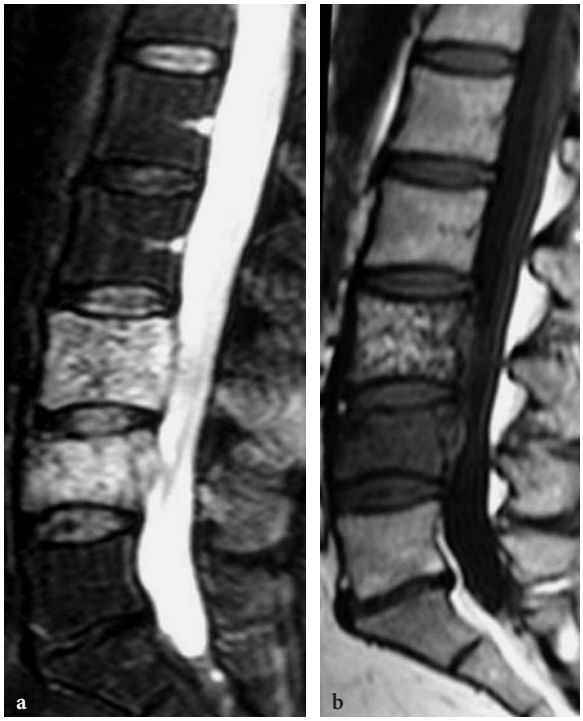

Fig. 19.6a,b. Benign (hemangioma) and malignant collapses in the same patient. Vertebral collapses of L3 and L4. L3 is only minimally decreased in height with erosion of the posterior wall and epidural extension, and high signal SI on T2-WI (**a**). L4 is partially collapsed with osteolysis of the posterior wall and epidural extension with high signal. L3 has a mottled aspect on T1-WI (**b**), whereas L4 is homogeneously hypointense. Vertebral aggressive hemangioma in L3 and metastasis in L4

Fig. 19.7a,b. Metastasis of breast carcinoma: differential diagnosis with spondylitis. Hypointense lesion both on T1-WI (**a**) and T2-WI (**b**), with little paraspinal collar and partially spared disk

gioma has a peculiar mottled signal with a swollen aspect of the vertebral body with cortical "lamellar" erosion due to compression, whereas metastasis infiltrates the cortex of the vertebra with osteolysis.

19.1.4 Vertebral Metastases

Vertebral metastases are the most frequent tumors of the spine.

Bone metastases occur in up to 50% of patients with cancer, and among these 40%–70% are vertebral lesions. In 10% of the patients with neoplastic disease, the original tumor is unknown. Vertebral metastases occur in 10% of patients with malignant neoplasms (Schiff et al. 1997) and cause the primary symptoms in 10%–40% of these patients, usually as vertebral collapse and/or spinal cord compression.

They can occur at any age and have no sex predilection, but are most frequent in the 5th decade. The incidence of spinal metastases increases with age.

Most of the metastases are located in the thoracic spine, less frequently in the lumbar spine and infrequently in the cervical spine (factors 4:2:1).

Pain is the most frequent clinical presentation and is related to metastatic vertebral compression fracture, and in 10% of patients the clinical presentation of cancer. Neurological symptoms can occur due to a posterior dislocated bone fragment, epidural extension of bone involvement or both (Schiff et al. 1997).

Symptoms depend on the vertebrae involved, and include local radiculopathy with bands of hypoesthesia and/or hyperesthesia, amyotrophia, loss of reflexes and vasomotor disturbances. Under the level of the lesion motor, sensory and sphincter disorders are related to spinal cord compression. Anterior compression more often causes motor symptoms, posterior compression deep sensitive signs and in lateral compression Brown-Sequard symptoms can occur.

Sometimes vertebral metastases are asymptomatic.

Metastasis involves primarily the medullary bone and causes osteoclastic and osteoblastic activation with subsequent lysis (70%), osteosclerosis (9%) or both (21%). Osteosclerosis is a reactive phenomenon (increased osteoblastic activity) and is not necessarily formed by the tumor itself.

Spread of tumors to the spine is believed to occur by three mechanisms:

- Direct extension
- Hematogenous spread through the arterial system
- Retrograde spread through the venous system via Batson's venous plexus

Metastases show a strong predilection for the high vascular bone marrow and replace the normal fat cells with tumor.

Lung carcinoma metastasizes arterially, prostate and breast carcinomas disseminate venously related to a complex system with communicating intraspinal and extraspinal veins, favoring tumor localization to the vertebral column (thoracic spine for breast cancer, and lumbar spine for pelvic tumors).

19.2 Imaging

Imaging modalities should be tailored to detect lesions, assess localization and the compartments involved (intramedullary, intradural, extradural and/or vertebral) and ideally suggest therapeutic strategies (Andreula and Murrone 2005).

19.2.1 Imaging Technique

In patients suffering from a carcinoma with a tendency to metastasize to the skeleton, who are clinically suspected of having metastases, Technetium-99m-methylene diphosphonate (Tc-MDP) scintigraphy allows assessment of the entire skeleton in one single examination. The high sensitivity of Tc-MDP scintigraphy in the detection of osseous metastases makes it ideal in the screening of the skeleton. However, its low specificity necessitates the diagnosis to be confirmed by plain film radiography (positive if >50% of bone is destroyed, can be negative otherwise), CT or MRI.

Because of their excellent specificity, compared with MDP bone scans, Technetium-99m-sestamibi (Tc-MIBI) scans may play an important complementary role in differentiating vertebral metastases from traumatic vertebral fractures (Buyukdereli et al. 2006).

MRI is more sensitive in the detection of skeletal metastases than is bone MDP scintigraphy (Algra et al. 1991a,b). MRI is positive in 15% of patients with negative bone scans, and reveals 20% more lesions in patients with positive bone scans.

The factors contributing to the discrepancies between bone scintigraphy and MRI are related to the size and location of the lesions. Increased osteoblastic activity is necessary to have positive scintigraphy and intratrabecular lesions without a high osteoblastic turnover remain undetected by bone scans. For this reason some authors suggest MRI in the screening for breast and lung metastases (Eustace et al. 1997; Steinbborn et al. 1999; Layer et al. 1999).

In patients with neurological symptoms (localized pain and /or spinal cord compression signs), MRI is mandatory, and is the first choice examination for detecting and defining spinal metastases.

CT is not suited as a screening examination because of the use of ionising radiation, but it is useful in evaluating lesions detected by scintigraphy, but not confirmed by plain film. It reveals trabecular and cortical bone lysis, invasion of the paraspinal tissues and the relative speed of growth of the tumor by identifying a sclerotic peritumoral reaction. CT depicts the tumor growth ratio starting from grade 1: lysis with sclerotic border, over grade 2: lysis without sclerotic border to grade 3: lysis with ill-defined border.

Again MRI is the most important modality for investigating the whole spine with a panoramic view and a high contrast resolution.

Given the high sensitivity of MRI in the detection of skeletal metastases, whole-body MRI is advocated when metastases are suspected (Eustace et al. 1997). Screening of the entire skeleton can be achieved in 40–45 min using STIR T1-WI. In a comparative study PET has a sensitivity of 90%, whole body MRI of 82% and 99m Tc scintigraphy of 71%.

19.2.2 MRI

Suggested MRI protocol:

1. SE T1-WI. Anatomic sequence with high contrast resolution between red bone marrow (isointense), fatty bone marrow (hyperintense) and metastasis with cellular bone marrow replacement (hypointense).
2. FSE T2-WI: "water" sequence with hyperintensity of the tumoral lesion.
3. STIR or SPIR: also known as "fat suppression sequences" with hyperintense tumoral lesion in a "dark" background of normal suppressed bone marrow.

Infiltrative processes such as malignant neoplasms tend to replace the normal bone marrow components completely. Normal hematopoietic marrow in the axial skeleton has fat and water components (red marrow 40% fat and yellow marrow 80% fat content). Theoretically, the replacement of fat by a neoplastic process should result in a decreased loss of signal intensity on out-of-phase images compared with in-phase images.

Chemical shift imaging makes use of the slight difference in Larmor frequencies between fat and water protons (Wismer et al. 1985). Bone marrow in the vertebral bodies displays a somewhat variable behavior at chemical shift MR imaging. Results suggest that a decrease in signal intensity greater than 20% on out-of-phase images compared with in-phase images should be used as a cutoff threshold for normalcy to allow distinction between benign and malignant causes of vertebral marrow abnormalities (Zajick et al. 2005).

Gadolinium chelates as an intravenous contrast agent may be helpful in the diagnosis and differential diagnosis of spinal metastatic disease (Verstraete et al. 1994; Montazel et al. 2003; Baur et al. 1997). Use of an intravenous contrast medium in T1-WI with fat suppression avoid confusion between contrast-enhanced lesions and fat 'spots'. It is mandatory to obtain images without contrast-enhancement first, because sometimes the enhanced lesion matches the signal of the normal adjacent bone marrow making it much less conspicuous (ghost tumor). Contrast enhanced images on the other hand define better the extraosseous component, the "pseudocapsule" if present, epidural extension and dural invasion.

STIR images are very sensitive in detecting bone marrow pathology (Mehta et al. 1995) and negative STIR exclude metastases obviating the use of intravenous contrast (Mahnken et al. 2005).

On T1-WI spinal osteolytic metastases are hypointense signal in relation to the normal bone, whereas on T2-WI they are hyperintense, especially on STIR and SPIR sequences (Figs. 19.8–19.10).

On the contrary, osteosclerotic metastasis (from carcinoma of the prostate, for example) have low signal on T1- and T2-WI (Figs. 19.11, 19.12). Sometimes sclerotic lesions, seen on plain films can present with high signal on T2-WI due to the presence of an infiltrating component.

Cortical bone destruction can be seen on T1-WI and even better on proton density images as a lack of hypointense signal of the vertebral body contour.

In osteolytic metastases contrast enhancement of the lesion is massive and marked, whereas in sclerotic lesions the enhancement is heterogeneous and peripheral.

Fig. 19.8a–c. Breast carcinoma with lytic metastases. Abnormal low signal in the body and pedicle on T1-WI (**a**) corresponding to high SI lesions on STIR images (**b**). After intravenous contrast medium administration the signal matches the normal bone marrow except at the border, revealed by a thin dark line (**c**)

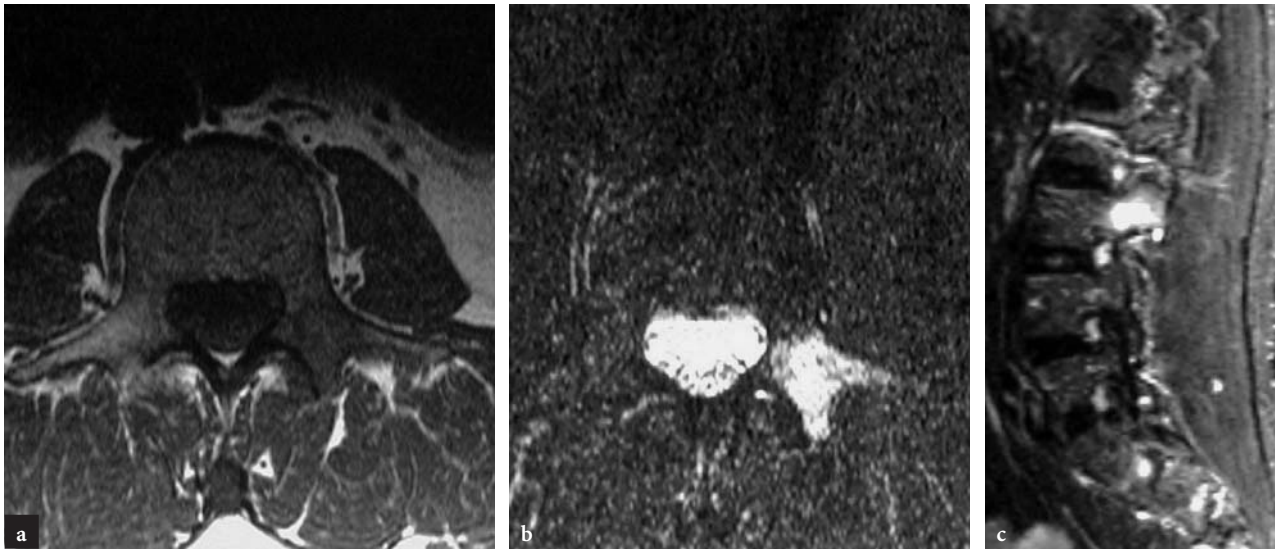

Fig. 19.9a–c. Vertebral metastasis in the left pedicle of L3. Subtle abnormal low signal is seen on T1-WI (**a**), better seen on the STIR images as areas of high SI (**b**,**c**)

Fig. 19.10a,b. Value of the STIR images in detecting metastasis. A slight change in morphology of the body and the pedicle of L1, without any valuable signal intensity change, is seen on the sagittal T1-WI (**a**). On STIR images neoplastic infiltration is much clearer (**b**)

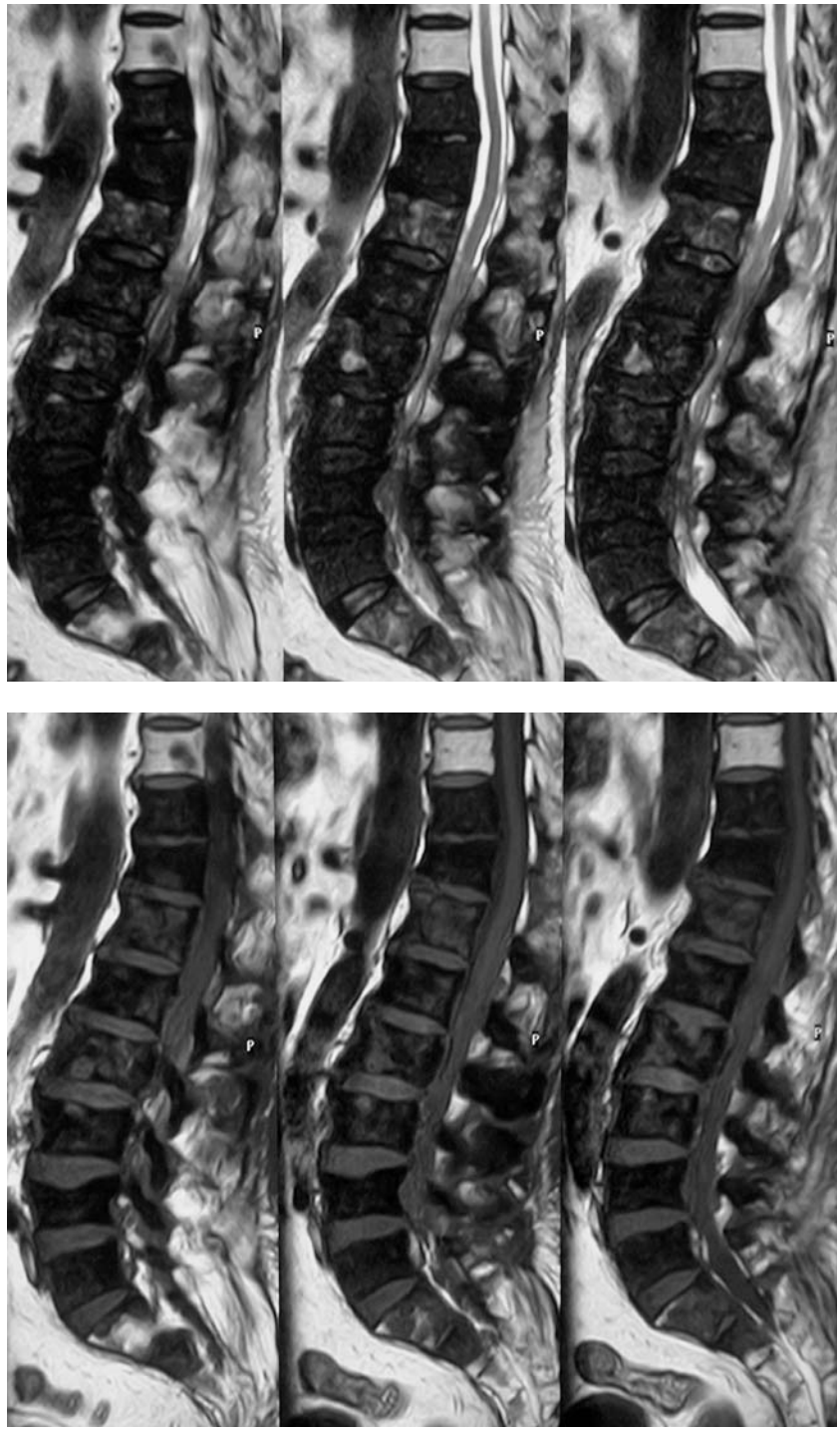

Fig. 19.11a,b. Prostate carcinoma with osteoblastic and mixed type metastases. Abnormal low signal on T1-WI (**a**) and STIR images (**b**) in Th10, Th11, L3, L4 and L5, whereas Th12, L1 and L2 have mixed signal on T1-WI and STIR images. In this case both osteoblastic and mixed lesions are present. The Th9 vertebral body has high signal on T1-WI and STIR images related to post-radiotherapy fatty transformation of the bone marrow

Fig. 19.12a–c. Prostate carcinoma with osteoblastic metastasis. A hypointense lesion in the body of L2 is seen on axial T1-WI (**a**). The T2-WI show a slight hypertense signal corresponding to an osteosclerotic rim and an infiltrative core [FSE T2-WI (**b**) and GRE T2-WI (**c**)]

The combination of non-contrast-enhanced T1-WI and contrast-enhanced sequences is advised to determine the presence of spinal metastases in children with neuroblastoma, particularly those children who are 1 year and older (Meyer et al. 2005; Daldrup-Link et al. 2001).

19.3 Differential Diagnosis

Some non-tumoral lesions may mimic metastases.

Physiological or pathological changes of the bone marrow, for example in young people with an inverted ratio of red and fat marrow, in medullar hyperplasia (caused by anemia, smoking), or related to stimulation of hematopoiesis may cause low signal of the bone marrow on T1-WI. Also red (hematopoietic) bone marrow islands may suggest infiltrating metastases. Usually these have less marked hypointensity and they lack the marked contrast enhancement of metastases.

In some degenerative changes like degenerative osteochondritis, edema of the bone marrow may mimic a metastatic lesion: in such cases contrast enhancement could be marked, and only concomitant osteophytosis with "pointed" margins can be helpful in the differential diagnosis.

A recent Schmorl (intraspongeous) herniation in the endplate with reactive edema of the subchondral zone could raise the suspicion of a metastatic localization, which can be excluded by multiplanar reformation in order to define the cortical bone depression caused by the disc material and the close relationship between edema and node.

In cases of isolated vertebral body collapse the differential diagnosis between recent (less than 3 months) non-tumoral lesions (osteoporosis or osteopenia) and tumoral (metastatic) lesions can be difficult. In both cases the signal will be low on T1-WI and high on T2-WI and fat suppression sequences. A benign lesion should be considered if the hypointensity on the T1-WI is under the concave endplate as a stripe- or band-like pattern (Modic et al. 1988a,b; Kuisma et al. 2006). Different patterns of contrast enhancement are helpful: marked and heterogeneous in metastases, arranged as a stripe in osteoporosis.

MR imaging (Yuh et al. 1989; Baur et al. 1998) and CT (Laredo et al. 1995) may be helpful in distinguishing benign from malignant causes of vertebral

Fig. 19.13a–c. Chronic and acute benign vertebral collapse in the same patient. Lateral plain film shows vertebral collapses of L3 and L4. The vertebral body of L4 has a biconcave aspect, whereas L3 has an angled aspect of the inferior plate (**a**). MRI shows involvement of the upper part of the vertebral body of L3 with signal changes, hypointense on T1-WI (**b**) and hyperintense on T2-WI (**c**), band-like suggesting recent collapse. The vertebral body of L4 has a "normal" (degenerative signal), suggesting chronic benign osteopenic collapse

fracture. This is of particular importance since spinal metastases tend to occur in the elderly in whom osteoporotic fractures are also very common.

On CT benign collapses show fractures without cortical destruction, retropulsion of bone fragments into the spinal canal, intravertebral vacuum phenomenon and absent or small soft tissue mass (Laredo et al. 1995). Of course, other small infiltrative vertebral lesions, pedicles and posterior element involvement with expansive features, cortical bone lysis and paravertebral and epidural invasion suggest malignant collapse (Algra et al. 1992).

MR imaging findings suggestive of metastatic compression fractures include: a convex posterior border of the vertebral body, abnormal signal intensity of the pedicle or posterior element, an epidural mass, an encasing epidural mass, a focal paraspinal mass and other spinal metastases. MR imaging findings suggestive of acute osteoporotic compression fractures include: a low-signal-intensity band on T1- and T2-WI, spared normal bone marrow signal intensity of the vertebral body, retropulsion of a posterior bone fragment and multiple compression fractures (Figs. 19.6, 19.13). The signal intensity on fast spin-echo T2-WI obtained without fat suppression played little role in distinguishing between metastatic compression fractures and acute osteoporotic compression fractures (Jung et al. 2003; Park et al. 2004).

Morphologically focal concave collapse predicts a benign lesion, whereas focal acute angled collapse suggests malignancy, especially if the posterior border of the body is convex. The convex posterior vertebral body and the disappearance of the basivertebral vein (Algra et al. 1991) are early signs of tumor tissue growing from the vertebral body and extending into the epidural space.

Chronic benign fractures show isointense bone marrow signal intensity. Fat images show only partial replacement of the normal fatty marrow in contrast to the complete absence of marrow signal intensity typical of pathologic fractures. In-phase and opposed-phase MR imaging may also give valuable clues as to the nature of the lesion (Disler et al. 1997; Zampa et al. 2002; Zajick et al. 2005).

Gadolinium enhanced and unenhanced MR images can be useful in the differentiation of vertebral collapses by showing the enhanced convex posterior body, epidural mass, and enhancement of the low signal intensity T1 lesions (Cuenod et al. 1996).

The use of dynamic contrast enhancement could be helpful in suggesting metastases: high peak of enhancement is present either in malignant lesions as acute benign compression fractures, but not in the chronic ones. However, in metastases the dynamic pattern is a rapid wash-in with early wash-out.

Moreover, collapses where the major static forces apply, with anterior-posterior symmetry, involvement of one discal plate, restricted to the body without posterior wall lesions, spared lateral and posterior elements and gaseous disc degeneration suggest a benign lesion.

Some authors postulated that the presence of a fluid spot (fluid sign) close to the fractured end plate should suggest a benign lesion This sign related to medullar edema is absent in secondary fractures (Baur et al. 2002).

Nevertheless the differential diagnosis between benign and malignant vertebral collapses is very difficult (Vanel et al. 1998).

The use of diffusion-weighted imaging (Baur et al. 2001, 2003), quantitative diffusion imaging (Zhou et al. 2002) and ADC values has been suggested to discriminate benign and malignant collapses: a pathologic vertebral compression fracture has been reported to be hyperintense to normal bone marrow, and benign collapse has shown hypointense or isointense signal. The theory is based on the increased tumor hypercellularity which restricts the water movements (Fig. 19.14) (Spuentrup et al. 2001). However, other authors do not report such results (Castillo et al. 2000; Maeda et al. 2003).

Diffusion-weighted imaging is of value in the follow-up after therapy. With successful therapy, the bone marrow will return to decreased signal intensity on diffusion-weighted images (Byun et al. 2002).

References

Algra PR, Bloem JL, Verboom LJ et al. (1991a) MRI vs scintigraphy in the detection of vertebral metastases. Radiographics 11:219–232

Algra PR, Bloem JH, Valk J (1991b) Loss of visibility of the basivertebral vein: a new MR sign of diffuse bone marrow disease. AJR Am J Roentgenol 157:1129–1130

Algra PR, Heimans JJ, Valk J et al. (1992) Do metastases begin in the body or pedicle? Imaging study in 45 patients. AJR Am J Roentgenol 158:1275–1279

Andreula C, Murrone M (2005) Metastatic disease of the spine. Eur Radiol 15:627–632

Baur A, Stäbler A, Bartl R et al. (1997) MRI gadolinium enhancement of bone marrow: age related changes in normals and in diffuse neoplastic infiltration. Skeletal Radiol 26:414–418

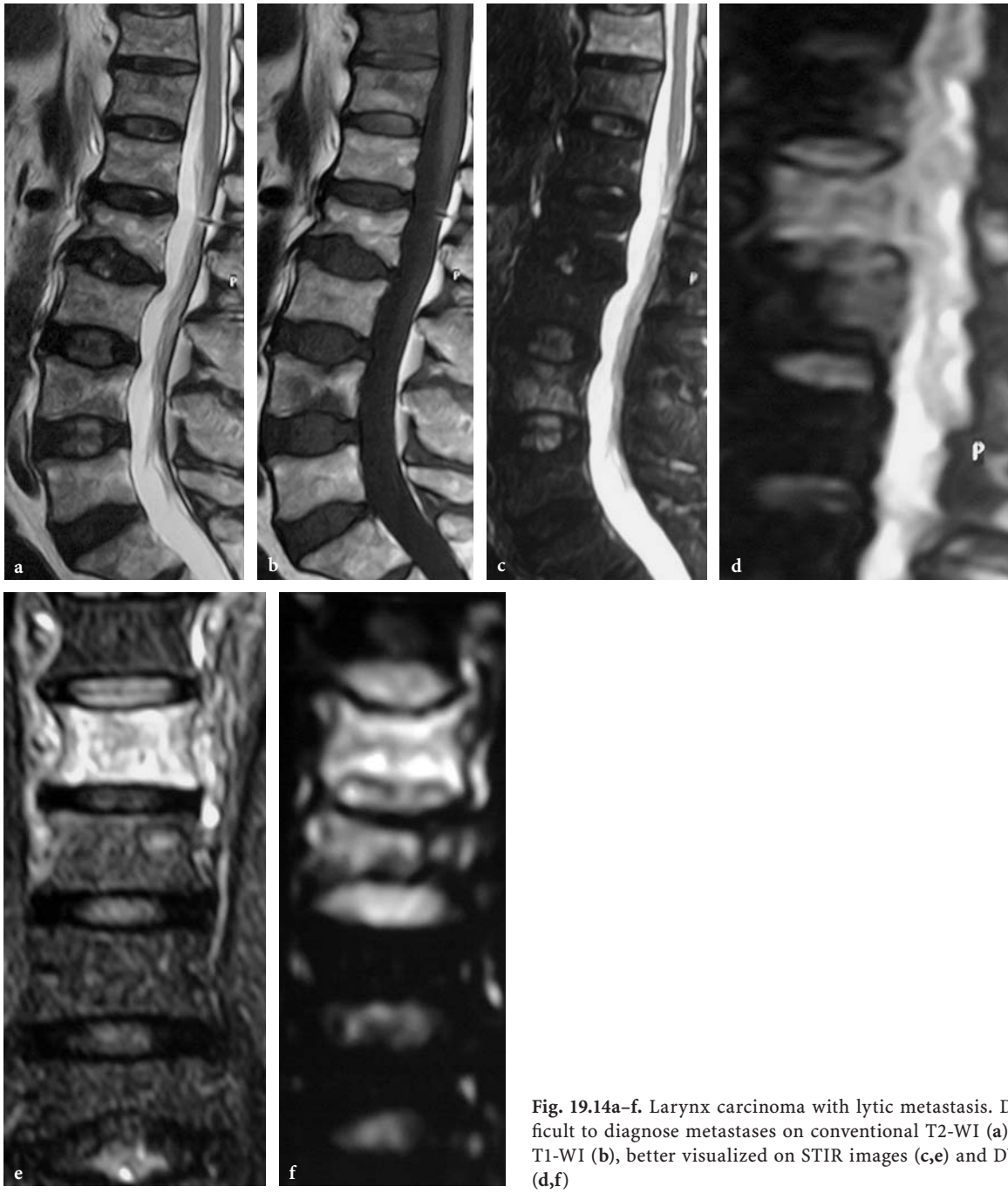

Fig. 19.14a–f. Larynx carcinoma with lytic metastasis. Difficult to diagnose metastases on conventional T2-WI (**a**) or T1-WI (**b**), better visualized on STIR images (**c,e**) and DWI (**d,f**)

Baur A, Stäbler A, Bruning R et al. (1998) Diffusion-weighted MR imaging of bone marrow: differentiation of benign versus pathologic compression fractures. Radiology 207:349–356

Baur A, Huber A, Ertl-Wagner B et al. (2001) Diagnostic value increased diffusion weighting of a steady-state free precession sequence for differentiating acute benign osteoporotic fractures from pathologic vertebral compression fractures. Am J Neuroradiol 22:366–372

Baur A, Stäbler A, Arbogast S, Duerr HR, Bartl R, Reiser M (2002) Acute osteoporotic and neoplastic vertebral compression fractures: fluid sign at MR imaging. Radiology 225:730–735

Baur A, Dietrich O, Reiser M (2003) Diffusion weighted imaging of bone marrow. Eur Radiol 13:1699–1708

Buyukdereli G, Ermin T, Kara O, Kibar M (2006) Tc-99m MIBI uptake in traumatic vertebral fractures and metastatic vertebral lesions: comparison with Tc-99m MDP. Adv Ther 23:33–8

ByunWM, Shin, SO, Chang Y et al. (2002) Diffusion-weighted MR imaging of metastatic disease of the spine: assessment of response to therapy. AJNR Am J Neuroradiol 23:906–912

Castillo M, Arbelaez A, Smith JK, Fisher LL (2000) Diffusion weighted MR imaging offers no advantage over routine noncontrast MR imaging in the detection of vertebral metastases. Am J Neuroradiol 21:948–953

Cuenod CA, Laredo JD, Cheveret S et al. (1996) Acute vertebral collapse due to osteoporosis or malignancy: appearance on unenhanced and gadolinium-enhanced MR images. Radiology 199:541–549

Daldrup-Link HE, Franzius C, Link TM et al. (2001) Whole body MR imaging for detection of bone metastases in children and young adults: comparison with skeletal scintigraphy and FDG PET. AJR Am J Roentgenol 177:229–236

Disler DG, McCauley TR, Ratner LM, Kesack CD, Cooper JA (1997) In-phase and out-of-phase MR imaging of bone marrow: prediction of neoplasia based on the detection of coexistent fat and water. AJR Am J Roentgenol 169:1439–1447

Eustace S, Tello R, DeCarvalho V et al. (1997) A comparison of whole body turbo STIR MR imaging and planar 99mTc-methylene diphosphonate scintigraphy in the examination of patients with suspected skeletal metastases. AJR Am J Roentgenol 169:1655-1661

Harrington KD (1986) Metastatic disease of the spine. J Bone Joint Surg Am 68:1110–1115

Jung HS, Jee WHJ, McCauley TR et al. (2003) Discrimination of metastatic from acute osteoporotic compression spinal fractures with MR imaging. Radiographics 23:179–187

Kienstra GE, Terwee CB, Dekker FW, Canta lR, Borstlap AC, Tijssen JG (2000) Prediction of spinal epidural metastases. Arch Neurol 57:690–695

Kuisma M, Karppinen J, Niinimäki J, Kurunlahti M, Haapea M, Vanharanta H, Tervonen O (2006) A three-year follow-up of lumbar spine endplate (Modic) changes. Spine 31:1714–1718

Laredo JD, Lakhdari K, Bellaïche L et al. (1995) Acute vertebral collapse: CT findings in benign and malignant nontraumatic cases. Radiology 194:41–48

Layer G, Steudel A, Schuller H, van Kaick G, Grunwald F, Reiser M, Schild HH (1999) Magnetic resonance imaging to detect bone marrow metastases in the initial staging of small cell lung carcinoma and breast carcinoma. Cancer 85:1004–1009

Maeda M, Sakuma H, Maier SE et al. (2003) Quantitative assessment of diffusion abnormalities in benign and malignant vertebral compression fractures by line scan diffusion-weighted imaging. AJR Am J Roentgenol 181:1203–1209

Mahnken AH, Wildberger JE, Adam J et al. (2005) Is there a need for contrast-enhanced T1-weighted MRI of the spine after inconspicuous short tau inversion recovery imaging? Eur radiol 15:1387–1392

Mehta RC, Marks MP, Hinks RS et al. (1995) MR evaluation of vertebral metastases: T1-weighted, short-inversion-time inversion recovery, fast spin echo, and inversion-recovery fast spin-echo sequences. AJNR Am J Neuroradiol 16:281–288

Meyer JS, Siegel MJ, Farooqui SO et al. (2005) Which MRI sequence of the spine best reveals bone-marrow metastases of neuroblastoma? Pediatr Radiol 35:778–785

Modic MT, Steinberg PM, Ross JS (1988) Degenerative disk disease: assessment of changes in vertebral bone marrow with MR imaging. Radiology 166:193–199

Modic MT, Masaryk TJ, Ross JS et al. (1988) Imaging of degenerative disk disease. Radiology 168:177–186

Montazel JL, Divine M, Lepage E (2003) Normal spinal bone marrow in adults: dynamic gadolinium-enhanced MR imaging. Radiology 229:703–709

Park SW, Lee JH, Ehara S, Park YB, Sung SO, Choi JA, Joo YE (2004) Single shot fast spin echo diffusion-weighted MR imaging of the spine; is it useful in differentiating malignant metastatic tumor infiltration from benign fracture edema? Clin Imaging 28:102–108

Schick U, Marquardt G, Lorenz R (2001) Intradural and extradural spinal metastases. Neurosurg Rev 24:1–5

Schiff D, O'Neill BP, Suman VJ (1997) Spinal epidural metastasis as the initial manifestation of malignancy: clinical features and diagnostic approach. Neurology 49:452–456

Spuentrup E, Buecker A, Adam G et al. (2001) Diffusion-weighted MR imaging for differentiation of benign fracture edema and tumor infiltration of the vertebral body. AJR Am J Roentgenol 176:351–358

Steinborn MM, Heuck AF, Tilling R et al. (1999) Whole body bone marrow MRI in patients with metastatic disease to the skeletal system. JCAT 23:123–129

Vanel D, Bittoun J, Tardivon A (1998) MRI of bone metastases. Eur Radiol 8: 1345–1351

Verstraete KL, De Deene Y, Roels H et al. (1994) Benign and malignant musculoskeletal lesions: dynamic contrast enhanced MR imaging. Radiology 192:835–843

Wismer GL, Rosen BR, Buxton R, Stark DD, Brady TJ (1985) Chemical shift imaging of bone marrow: preliminary experience. AJR Am J Roentgenol 145:1031–1037

Yuh WTC, Zachar CK, Barloon TJ et al. (1989) Vertebral compression fractures: distinction between benign and malignant causes with MR imaging. Radiology 172:215–218

Zajick DC, Morrison WB, Schweitzer ME et al. (2005) Benign and malignant processes: normal values and differentiation with chemical shift MR imaging in vertebral marrow. Radiology 237:590–596

Zampa V, Cosottini M, Michelassi C, Ortori S, Bruschini L, Bartolozzi C (2002) Value of opposed-phase gradient-echo technique in distinguishing between benign and malignant vertebral lesions. Eur Radiol 12:1811–1818

Zhou XJ, Leeds NE, McKinnon GC et al. (2002) Characterization of benign and metastatic vertebral compression fractures with quantitative diffusion MR imaging. AJNR Am J Neuroradiol 23:165–170

Primary Tumors of the Osseous Spine

20

S. H. M. Khan and Arthur M. De Schepper

CONTENTS

S. H. M. Khan, FRCR
Cownsultant Radiologist, Department of Radiology, East Lancashire NHS Trust, Blackburn Royal Infirmary, Bolton Road, Blackburn, Lancashire, BB2 3LR UK
A. M. De Schepper, MD, PhD
Consultant – Professor of Radiology, Leiden University Medical Centre, Albinusdreef 2, PO Box 9600, 2300 RC, Leiden, The Netherlands
and
Emeritus Professor of Radiology, University Hospital Antwerp, Edegem, Belgium

20.1 Introduction

The majority of primary spinal bone tumors are lymphoproliferative disorders including multiple myeloma and lymphoma. Solitary lesions are rare and have a wide and varied differential diagnosis.

Most benign lesions are asymptomatic; if not, the clinical presentation is generally back pain with or without neurological symptoms.

Initial imaging is usually plain radiography, which is not very sensitive because of the complex anatomy

KEY-POINTS

- Extradural spinal tumors
  - Most frequent group of spine tumors in general
  - Most originate from the vertebrae
  - Most frequent extradural tumor is metastasis
  - Primary bone tumors are much less common
- Solitary vertebral lesions are less common than tumors with multiple locations
- Benign lesions are usually
  - Asymptomatic
  - Incidental findings
- Malignant vertebral tumors
  - Cause back pain
  - Sometimes manifest neurologic symptoms, especially in children
- Diagnosis is based on
  - Imaging findings
    - Morphology
      - Border
      - Matrix
      - Expansile character
      - Soft tissue extension
    - Density/signal intensity
    - Pattern of morphology
  - Age of the patient
  - Multiplicity
  - Location of the lesion(s)
- Common benign spinal tumors
  - Hemangioma
  - Enostosis
  - Osteochondroma
  - Osteoid osteoma
  - Osteoblastoma
  - Aneurysmal bone cyst
  - Giant cell tumor
  - Eosinophilic granuloma
- Common malignant spinal tumors
  - Solitary
    - Chordoma
    - Chondrosarcoma
    - Ewing Sarcoma
  - Multiple
    - Multiple myeloma
    - Lymphoma

of the vertebrae. Cross-sectional imaging is required to adequately assess and characterize a spinal lesion. Magnetic resonance imaging (MRI) is the imaging modality of choice for evaluation and subsequent follow-up after treatment of most tumors. However, computed tomography (CT) is the imaging modality of choice in some posterior element lesions.

20.2 Imaging Strategy

There is a wide variety of lesions that affect the spine. It is possible to detect and characterize the lesions based on the basis of age, number, position in the spine and location in the vertebra. The differential diagnosis can be narrowed down by evaluating the imaging findings including morphology, density or signal intensity of lesions on CT and MRI, as well as enhancement following administration of contrast media.

In the first part of this chapter we propose a pragmatic and analytical approach to a spinal lesion. This should enable the reader to characterize lesions with a greater degree of certainty prior to biopsy. More importantly, however, better accuracy avoids unnecessary intervention and the consequent morbidity and anxiety suffered by patients with benign lesions.

20.2.1 Single/Multiple Lesion(s)

Initially, it is important to determine whether the lesion(s) is (are) solitary or multiple. Multiple lesions

are most commonly seen in metastases from breast and lung in women and prostate and lung in men. Multiple lesions are seen in 30% of metastases (Van Goethem et al. 2004).

Past or concurrent history of a primary tumor is generally available to suggest this diagnosis, but may need to be ascertained if the history is absent. History from the patient may divulge valuable information not mentioned on the request card!

The most common multiple primary spinal tumors are lymphoproliferative lesions such as multiple myeloma and lymphoma (Fig. 20.1; Table 20.1).

The presence of multiple lesions may be noted on plain radiography but is more likely to be seen on bone scintigraphy or MRI, including whole body MRI. However, both plain radiographs and MRI may be normal in 20% of cases of multiple myeloma (Van Goethem et al. 2004).

Another condition that can rarely present as multiple lesions is eosinophilic granuloma (EG), which needs to be considered in children. Fibrous dysplasia occasionally involves the spine at multiple sites (Fig. 20.2). A third of spinal hemangiomas involves multiple levels (Fig. 20.3).

Solitary lesions have a wider differential and would require meticulous analysis of the imaging features to arrive at the correct diagnosis.

Table 20.1. Most common benign and malignant primary spinal bone tumors

Common benign spinal tumors	
Hemangioma	
Enostosis	
Osteochondroma	
Osteoid osteoma	
Osteoblastoma	
Aneurysmal bone cyst	
Giant cell tumor	
Eosinophilic granuloma	
Common malignant spinal tumors	
Solitary	Chordoma
	Chondrosarcoma
	Ewing Sarcoma
Multiple	Multiple myeloma
	Lymphoma

20.2.2 Clinical Information

This is of utmost importance in the evaluation of spinal lesions. A good clinical history can augment diagnostic confidence in characterizing a lesion.

Fig. 20.1a–c. Multiple myeloma. Plain film of the lumbar spine in a patient with multiple myeloma, showing multiple osteolytic lesions and decreased height of several vertebrae (**a**). MRI demonstrates multiple low signal intensity lesions on T1-WI without gadolinium in several thoracic vertebral bodies (**b,c**)

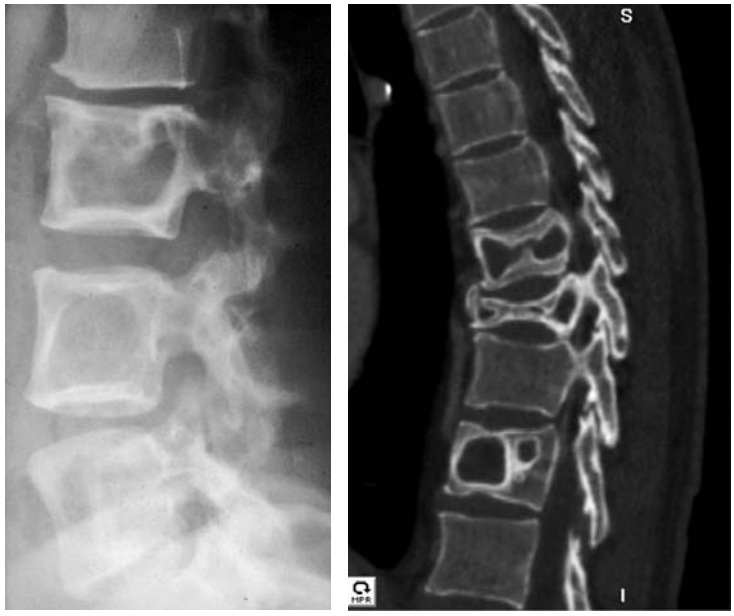

a b

Fig. 20.2a,b. Polyostotic fibrous dysplasia. Well-defined non-expansile osteolytic lesions with a thin sclerotic rim in several lumbar vertebral bodies in a case of spinal fibrous dysplasia (**a**). Sagittal reformatted CT in a different case of polyostotic fibrous dysplasia (**b**).

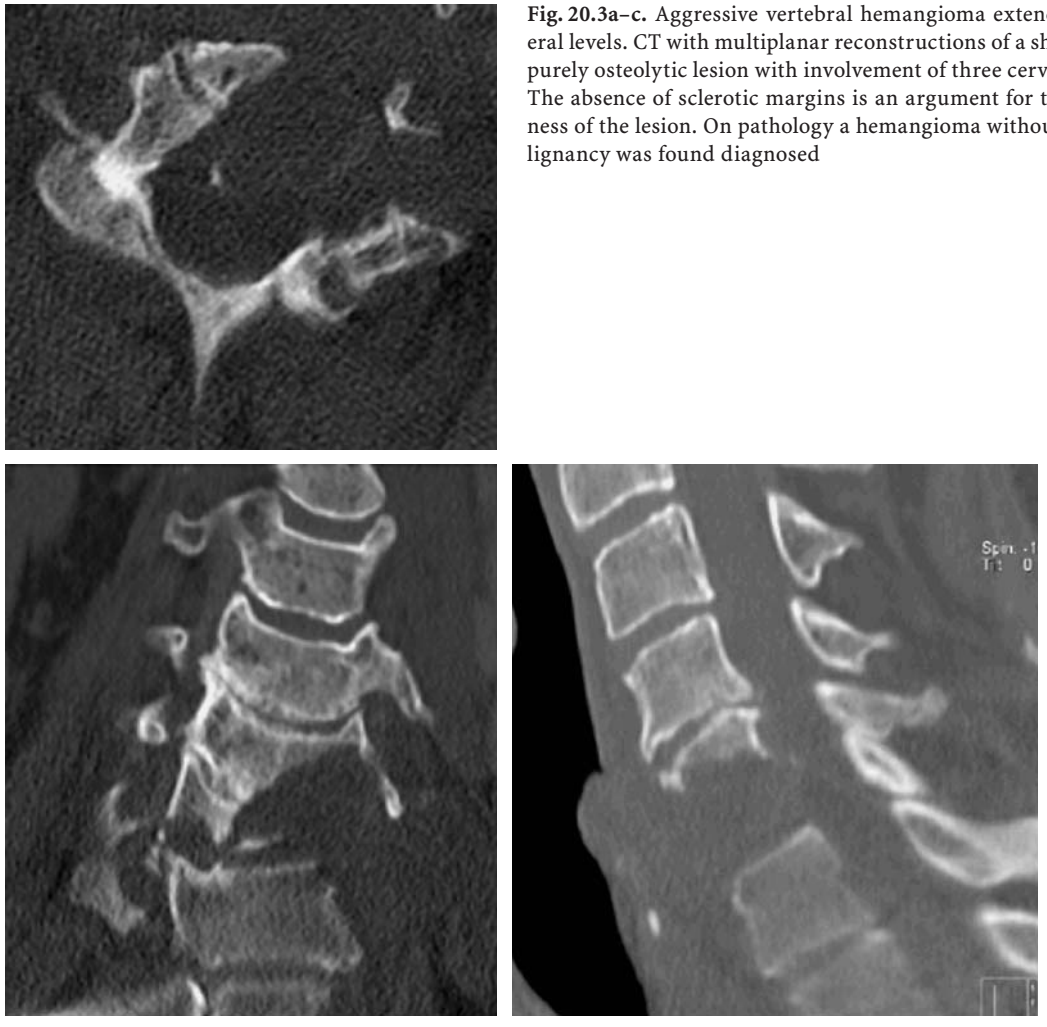

a b c

Fig. 20.3a–c. Aggressive vertebral hemangioma extending over several levels. CT with multiplanar reconstructions of a sharply defined, purely osteolytic lesion with involvement of three cervical vertebrae. The absence of sclerotic margins is an argument for the aggressiveness of the lesion. On pathology a hemangioma without signs of malignancy was found diagnosed

Multiple lesions in the spine with a known history of primary lung or breast tumor are most likely to be metastases and knowing the history makes the diagnosis that much easier. Presence of clinical symptoms is related to the type of tumor, its location and its extension. In this regard, osteoid osteoma, aggressive hemangioma and malignancies are mostly symptomatic (Fig. 20.4). History of night pain and recent-onset painful scoliosis should alert us to search carefully for osteoid osteoma. This condition has a predilection for the posterior elements, which is a difficult area to assess due to the complex anatomy and partial volume effects.

The age of the patient is valuable in the assessment of these lesions. In a young patient, osteoid osteoma, aneurysmal bone cyst (ABC) and Ewing's sarcoma predominate, whereas giant cell tumor is normally seen in the middle aged and chordoma in the elderly.

Tumors that are mostly asymptomatic may occasionally become symptomatic due to associated pathology such as a disc herniation.

20.2.3 Topography

20.2.3.1 Location

The location of a tumor in the spine is useful in determining the nature of the lesion.

The cervical spine is the predilection site for osteoblastoma and osteochondroma. It is also commonly involved in EG, particularly C2 in adults (Bertram et al. 2002).

The thoracic spine is the preferred site in more than 50% of hemangioma (Fig. 20.5), enostosis (particu-

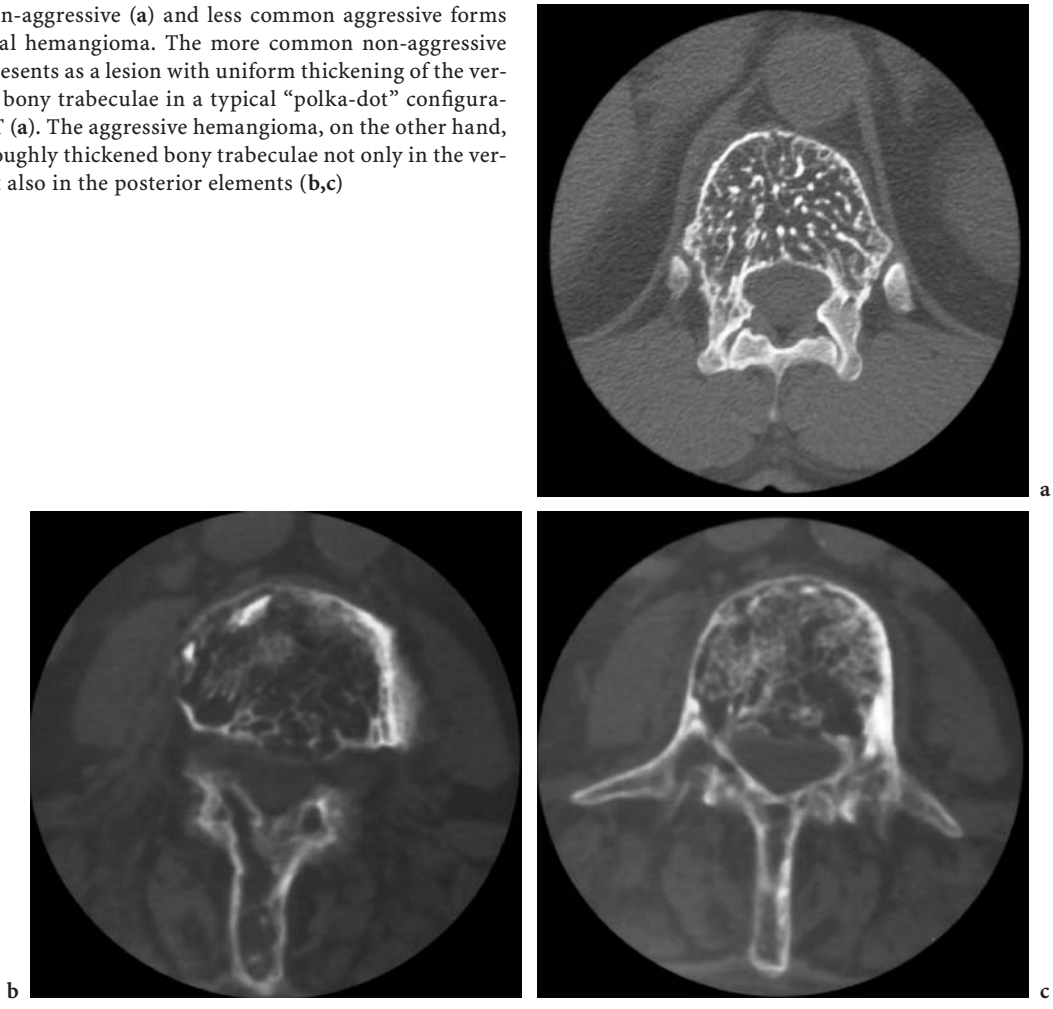

Fig. 20.4a-c. Non-aggressive (**a**) and less common aggressive forms (**b,c**) of vertebral hemangioma. The more common non-aggressive hemangioma presents as a lesion with uniform thickening of the vertically oriented bony trabeculae in a typical "polka-dot" configuration on axial CT (**a**). The aggressive hemangioma, on the other hand, presents with roughly thickened bony trabeculae not only in the vertebral body, but also in the posterior elements (**b,c**)

Fig. 20.5. Topography of primary tumors of the spine. Thoracic aggressive vertebral hemangioma. Aggressive hemangioma of the thoracic spine with a bony component and a soft tissue component in the posterior epidural space. A total of 50% of all vertebral hemangiomas are located in the thoracic spine

larly T1–T7) and chondrosarcoma (Van Goethem et al. 2004; Flemming et al. 2000; Murphey et al. 1996). ABC also frequently occurs at the thoracic spine but most commonly involves the lumbosacral spine.

Enostosis and osteoid osteomas have strong affinity for the lumbar spine (Ozaki et al. 2002).

Chordoma, giant cell tumor (GCT) and plasmacytoma have a penchant for the sacrum. Indeed, GCT comprises 71% of benign sacral tumors (Disler and Miklic 1999). Ewing's sarcoma is a rare cause of sacral spine tumor (Ilaslan et al. 2004).

20.2.3.2 Site

The body of the vertebra is mainly affected by benign conditions such as hemangioma, bone islands and GCT (Fig. 20.6a). The vast majority of hemangiomas is seen in the vertebral body, varying in size from very small to complete involvement. However, about 10% of hemangiomas may involve the posterior elements. The vertebral body is also favored by chordomas and Ewing's sarcomas.

Benign conditions commonly involving the posterior elements are osteoid osteoma, osteoblastoma, ABC and osteochondroma (Fig. 20.6b).

Not all lesions stay confined to the body or the posterior elements and may extend into one or the other. Plasmacytoma and multiple myeloma prefer the body but tend to spread to the posterior elements. ABC, in contrast, mainly affects the pedicles but may extend into the body (Fig. 20.6c).

The position of a lesion within the body is useful in narrowing the diagnosis. Chordoma and Ewing's sarcoma are centrally sited (Fig. 20.7), whereas GCT tends to lie eccentrically (Fig. 20.8).

20.2.4 Morphology

20.2.4.1 Border

The appearance of the lesion seen in various imaging modalities is useful for characterization.

A well-defined border (so-called geographic) is seen with benign conditions such as hemangioma, enostosis, osteoid osteoma, osteoblastoma and ABC (Fig. 20.9).

A permeative appearance with a broad zone of transition indicating aggressive biologic activity is seen in aggressive hemangioma and malignant tumors such as osteosarcoma, Ewing's sarcoma and metastatic disease (Fig. 20.10).

Periosteal reaction is rarely seen in vertebral lesions and is difficult to assess. If present, the possibility of an osteosarcoma should be considered (Fig. 20.11).

20.2.4.2 Matrix

Solid dense cortical bone seen within the spongy bone of the vertebral body is characteristic of enostosis (Fig. 20.9b). Calcification within a lucent nidus surrounded by extensive reactive sclerosis is a feature of osteoid osteoma (Fig. 20.12). Osteoblastoma is histologically similar yet radiologically distinct from osteoid osteoma but is expansile and larger than 1.5 cm in diameter (Fig. 20.13). The matrix also contains prominent areas of calcification (Fig. 20.6b).

Ring- and arc-type calcification is typically seen in chondroid tissues such as osteochondroma and chondrosarcoma (Figs. 20.14 and 20.15). This pat-

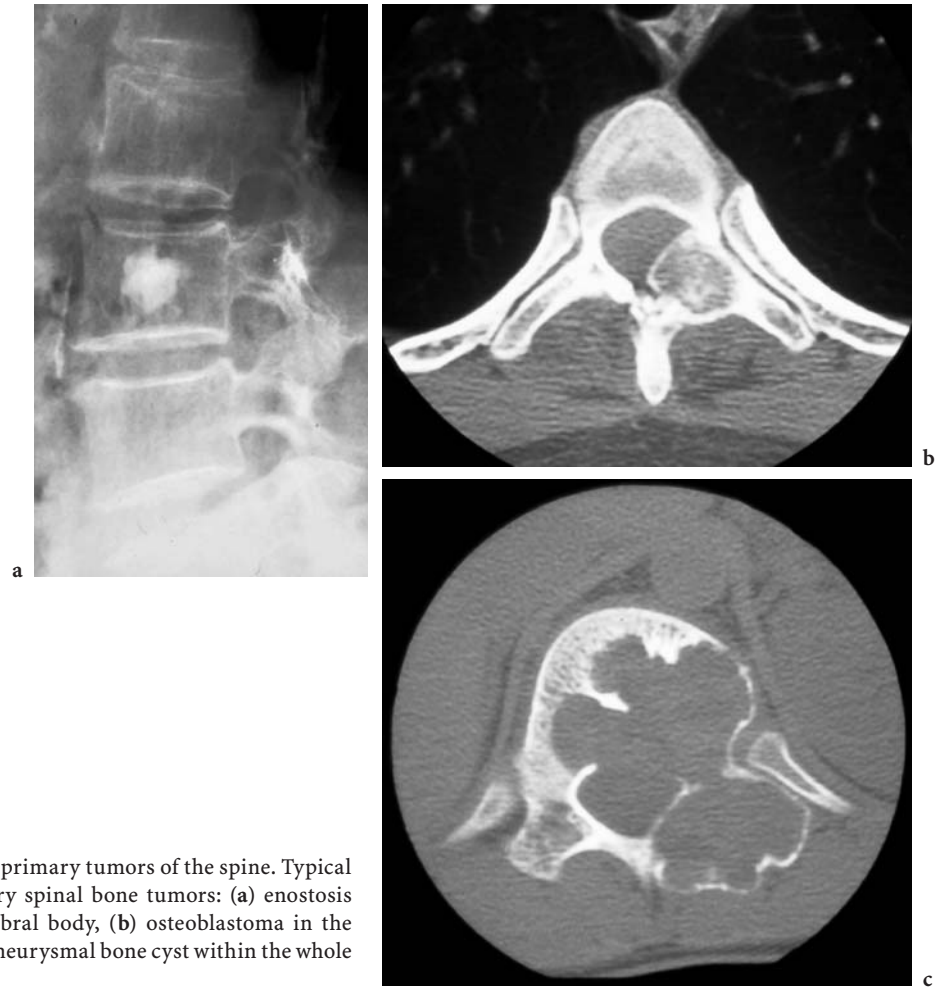

Fig. 20.6a–c. Topography of primary tumors of the spine. Typical location of different primary spinal bone tumors: (**a**) enostosis or bone island in the vertebral body, (**b**) osteoblastoma in the posterior elements and (**c**) aneurysmal bone cyst within the whole vertebra

Fig. 20.7a,b. Topography of primary tumors of the spine. Axial T1-WI (**a**) before and sagittal T1-WI (**b**) after gadolinium enhancement. Central position of a chordoma with invasion of the anterior epidural space and characteristic "curtain" sign


a


b

c

Fig. 20.8a–c. Topography of primary tumors of the spine. CT in an eccentrically located giant cell tumor of the vertebral body (**a**). Sagittal T1-WI (**b**) and fat suppressed axial T1-WI after gadolinium enhancement (**c**) in another case of giant cell tumor of the transverse process extending into the spinal canal

tern may also be seen in osteoblastoma and sometimes in chondroid types of chordoma.

20.2.4.3 Expansile Character

Expansile lesions are seen in ABC (Figs. 20.9a, 20.16), osteoblastoma (Fig. 20.13) and occasionally in aggressive hemangioma. Malignant lesions like chordoma, Ewing's sarcoma and chondrosarcoma also demonstrate expansion along with soft tissue extension. This feature may also be seen in relatively benign conditions such as osteoblastoma and GCT (Fig. 20.8).

20.2.4.4 Soft Tissue Extension

Some of the primary spinal tumors have a proclivity for soft tissue extension. It is not only seen with malignant conditions such as Ewing's sarcoma (Fig. 20.17) or chordoma but also in benign lesions like osteoblastoma. Occasionally, hemangiomas may be associated with an extensive soft tissue component and is then referred to as an aggressive hemangioma (Fig. 20.5). These lesions tend to be symptomatic.

20.2.5 Density (Hounsfield Units)

The density of the lesion may be helpful for its characterization. Fatty lesions such as lipoma have a low density on CT (–50 to –100 HU) (Fig. 20.18). Measuring the density enables differentiation from air (–800 to –1000), which is occasionally seen in the vertebral body and originates from degenerative disc disease.

Enostosis appears very dense, similar in density to cortical bone, lying within the cancellous vertebral body.

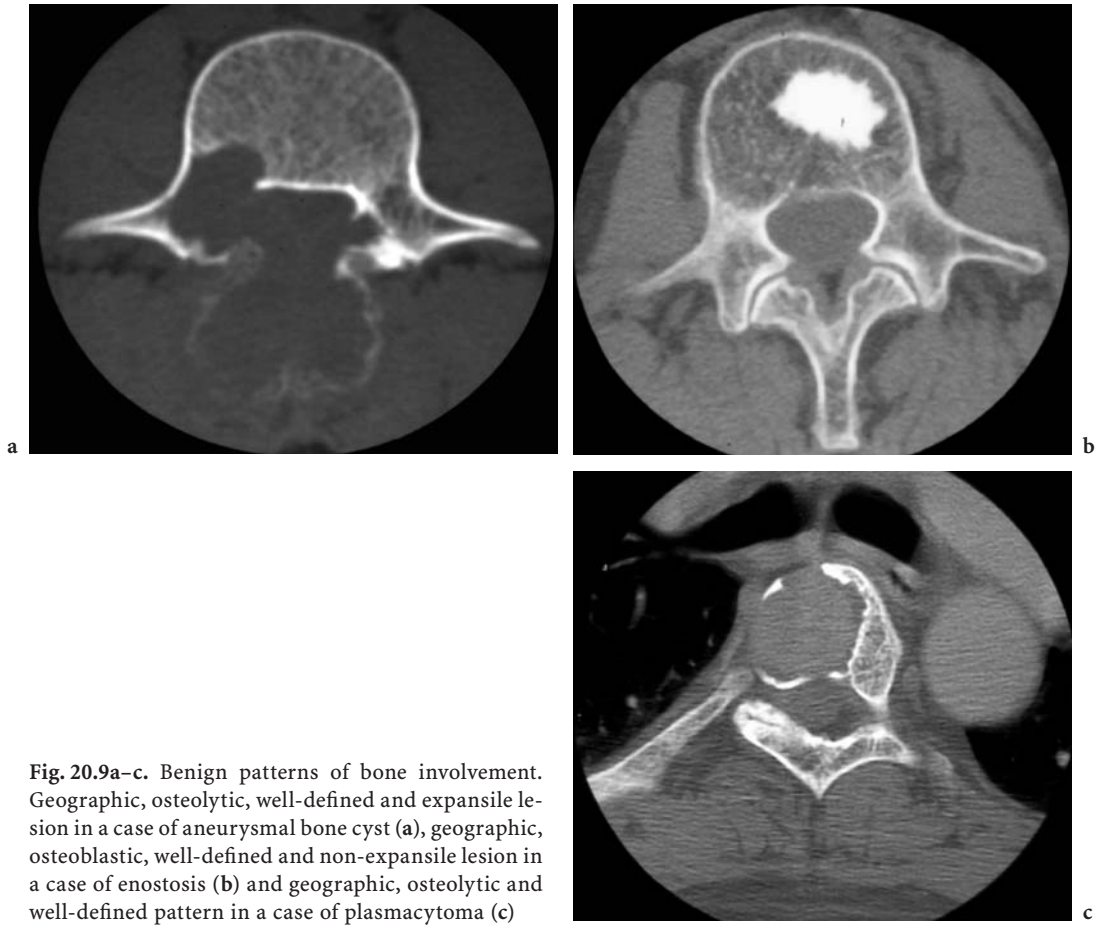

Fig. 20.9a–c. Benign patterns of bone involvement. Geographic, osteolytic, well-defined and expansile lesion in a case of aneurysmal bone cyst (**a**), geographic, osteoblastic, well-defined and non-expansile lesion in a case of enostosis (**b**) and geographic, osteolytic and well-defined pattern in a case of plasmacytoma (**c**)

20.2.6 Signal Intensity

Most pathological lesions tend to have low signal intensity on T1-weighted images (T1-WI) and high signal intensity on T2-weighted images (T2-WI). This reflects the high relaxing value of water on long TE sequences. A typical example is the high signal intensity on T2-WI of the cartilage cap of an exostosis because of the high water content of its chondroid tissue (Fig. 20.19).

Hemangioma and EG tend to have increased signal intensity on T1-WI indicating the presence of fat (Fig. 20.20a). Low signal intensity on T2-WI is seen in GCT due to high collagen content, hemosiderin and increased cellularity of the lesion (Fig. 20.20b) (Murphey et al. 2001). Bone islands demonstrate low signal intensity on all MR sequences, as these are basically cortical bone (Fig. 20.21).

Contrast enhancement following administration of gadolinium chelates can help characterize the tumor. A ring and arc pattern of enhancement is characteristic of a chondroid tumor (Fig. 20.22).

20.2.7 Pattern of Morphology

There are some morphological patterns seen in the spine using various imaging modalities and which have a very specific differential diagnosis.

Vertebra plana is typical for eosinophilic granuloma, though it can sometimes also be noted in other tumors such as giant cell tumor (Fig. 20.23). "Honeycombing" or "corduroy" pattern seen on plain radiograph and a "polka-dot" appearance on axial CT sections is characteristic of hemangioma (Fig. 20.24).

A lucent center (nidus) with variable central mineralization surrounded by extensive reactive sclero-

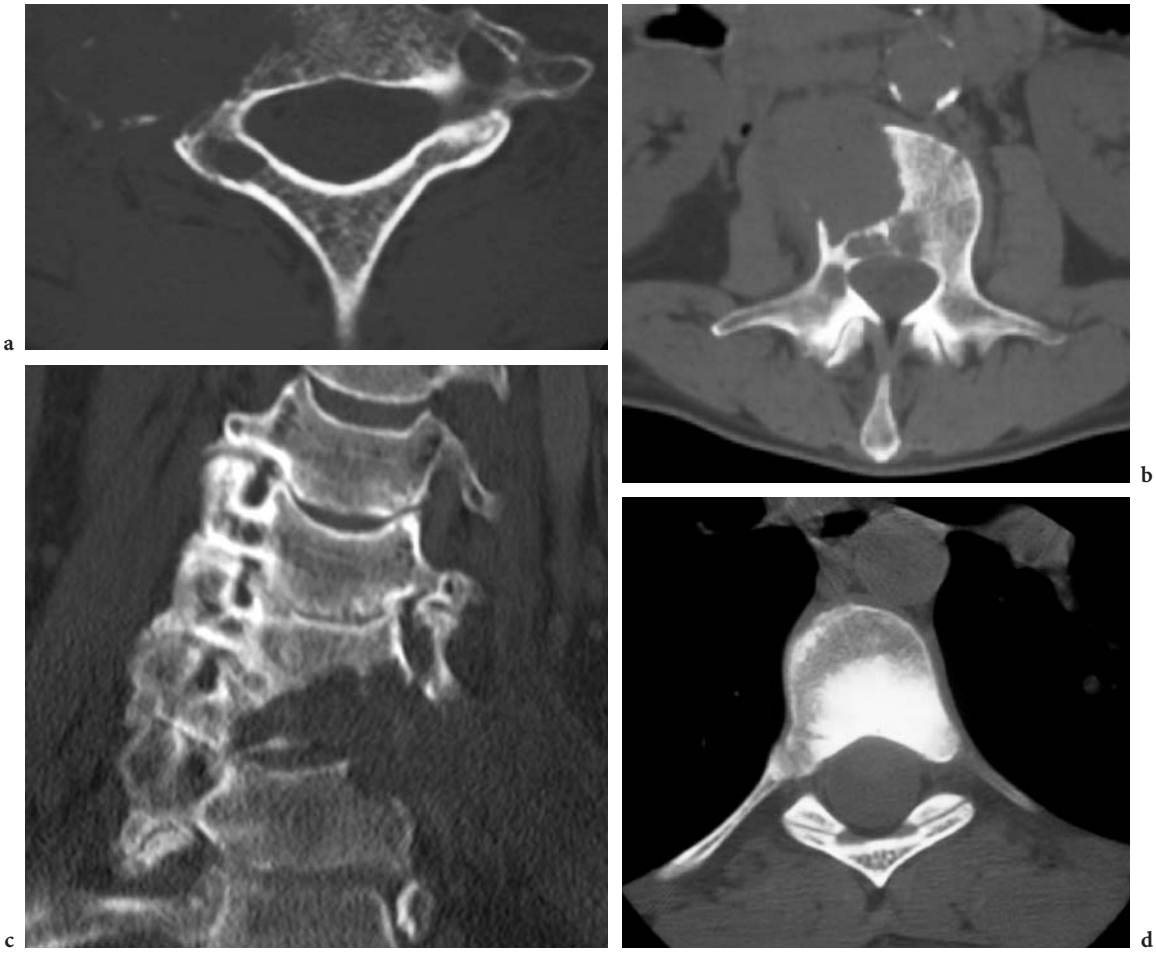

Fig. 20.10a–d. Malignant/aggressive patterns of bone destruction. Osteolytic permeative pattern in cases of Ewing sarcoma (**a**), metastatic disease (**b**) and aggressive hemangioma (**c**). Geographic, osteoblastic, less well-defined and non-expansile in a case of osteosarcoma (**d**)

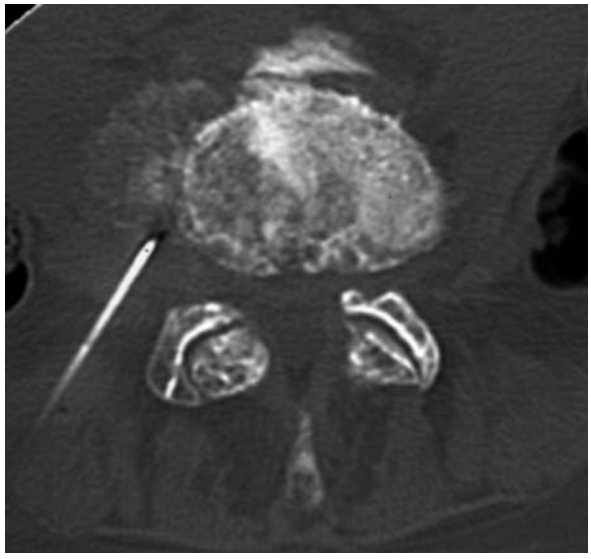

Fig. 20.11. Patterns of bone involvement – periosteal reaction. Periosteal reactions are rare in the spine. This case with inhomogeneous lytic and sclerotic areas and accompanying periosteal reaction proved to be an osteosarcoma

Fig. 20.12a,b. Osteoid osteoma. Osteoid osteoma of the inferior endplate of L5. T1-WI before (**a**) and after (**b**) gadolinium enhancement shows a central markedly enhancing nidus surrounded by non-enhancing sclerotic bone and a less enhancing peripheral zone of edema

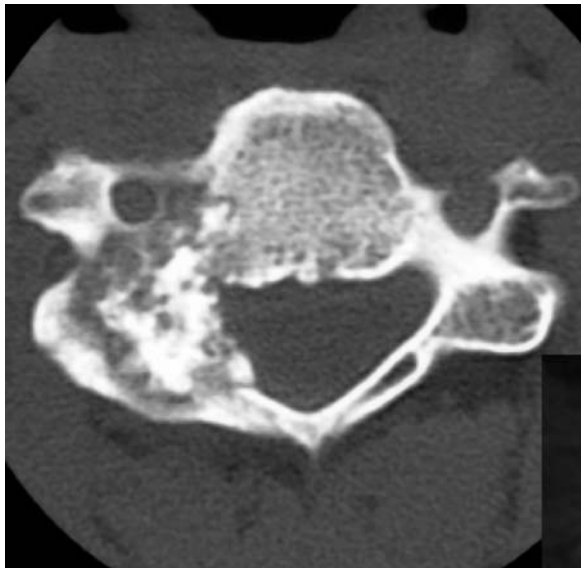

Fig. 20.13. Osteoblastoma. Calcified or ossified matrix in a case of osteoblastoma of the cervical spine. The lesion is typically located in the posterior elements of the vertebra

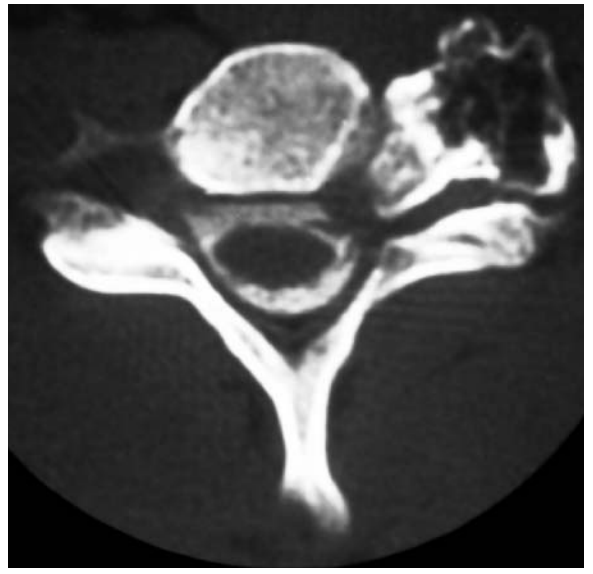

Fig. 20.14. Chondrosarcoma. CT myelogram in a case of cervical foraminal chondrosarcoma. Dense ring and arc type of calcification of the chondroid matrix of the tumor

sis is seen in osteoid osteoma on plain films, CT and MRI (Fig. 20.12).

Marked sclerosis with expansion of the whole vertebral body, which is referred to as "ivory vertebra", is seen in lymphoma or Paget's disease (Fig. 20.25).

Fluid-fluid levels are characteristically seen in ABC due to sedimentation of blood degradation products (Fig. 20.16) (Hudson 1984; Beltran et al. 1986). However, this is not specific and may also be seen in osteoblastoma and osteosarcoma. Indeed, in

Fig. 20.15a–e. Chondrosarcoma of C2 on axial CT (**a**), sagittal reformatted CT (**b**) and oblique plain film (**c**) with extensive intraspinal and intraforaminal extension. The associated soft tissue component extending into the right neuro foramen is shown on T1-WI before (**d**) and after (**e**) gadolinium enhancement

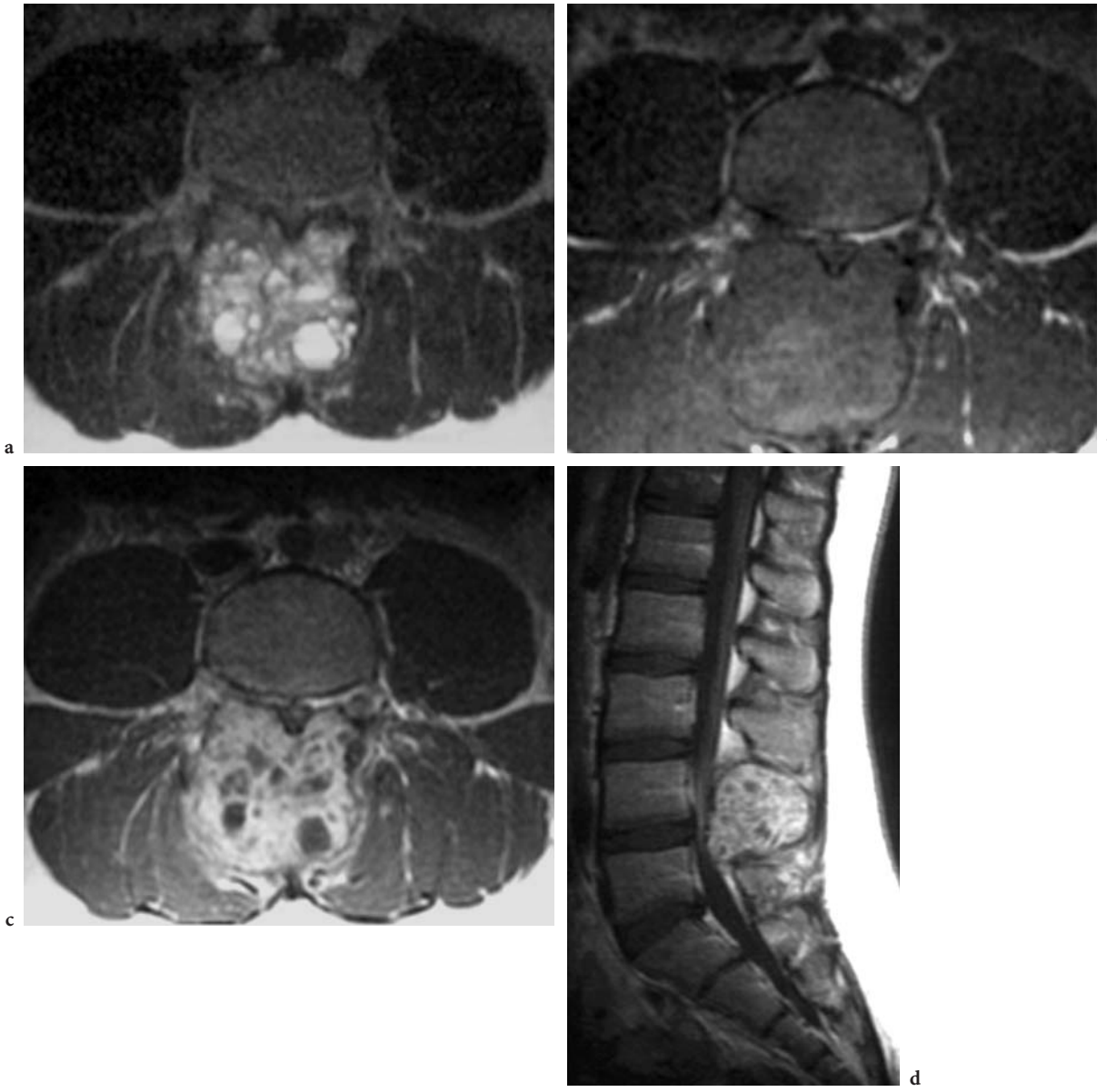

Fig. 20.16a-d. Aneurysmal bone cyst. MRI shows a large expansile lesion of the posterior elements with cystic components with high signal on T2-WI (**a**) and low signal on T1-WI (**b**). Some of the cystic lesions show fluid-fluid levels on T2-WI, typical for ABC but sometimes also seen in other tumors. Strong enhancement of the non-cystic components after gadolinium enhancement (**c**,**d**)

secondary cases of ABC, the same may occur in conditions such as osteoblastoma, GCT and fibrous dysplasia. A feature that may distinguish primary ABC from other causes is the presence of solid tissue in the secondary cases. This is not usually seen in primary ABC unless there has been a pathological fracture.

A "mini-brain" appearance is seen in plasmacytoma mimicking the MR appearance of brain (Fig. 20.26) (Major et al. 2000).

A "dumbbell" or "mushroom" shape may be seen in chordoma together with preservation of the disc space (Fig. 20.27).

The patterns mentioned are useful in characterizing the lesions but need to be cautiously interpreted, taking all other features into account.

The "spider pattern" is an interesting example we have observed on CT. This pattern is noted in plasmacytoma but also in hemangioma (Fig. 20.28).

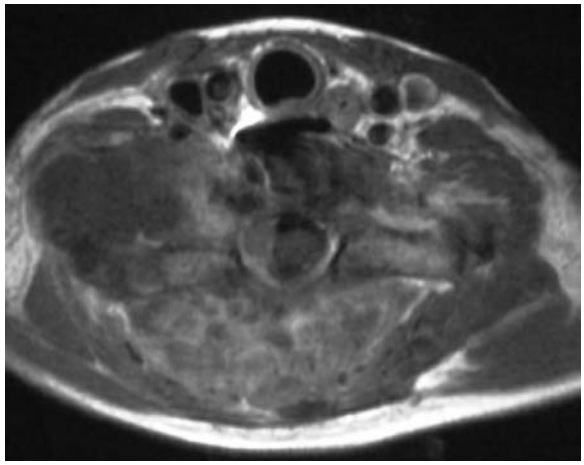

Fig. 20.17. Extensive soft tissue extension in a case of Ewing's sarcoma.

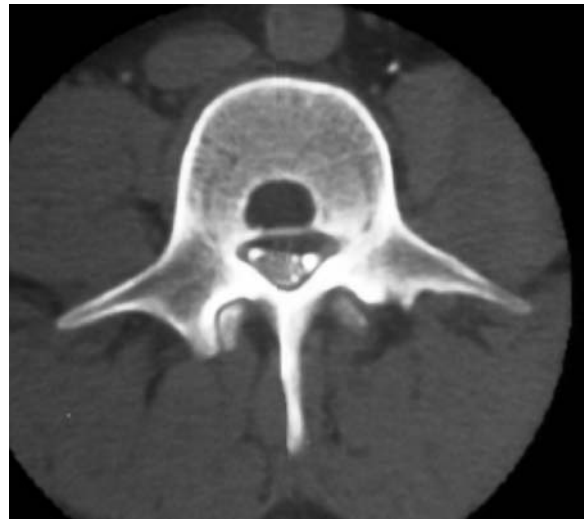

Fig. 20.18. Lipoma of the bony spine. Sharply demarcated intravertebral lesion with very typical low density (<0 HU) on CT in a case of intravertebral spinal lipoma

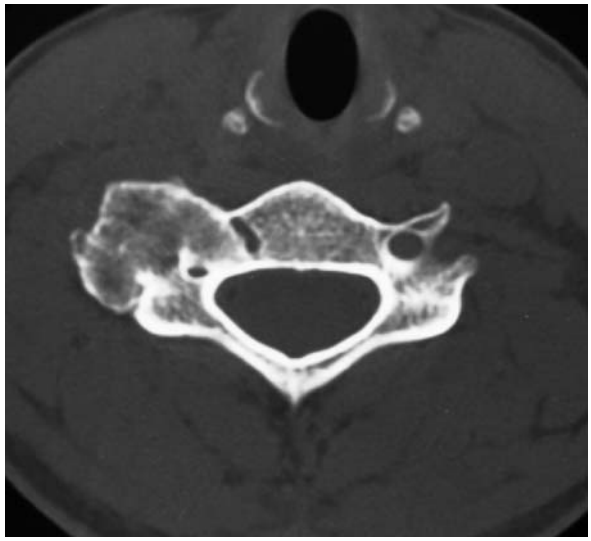

a

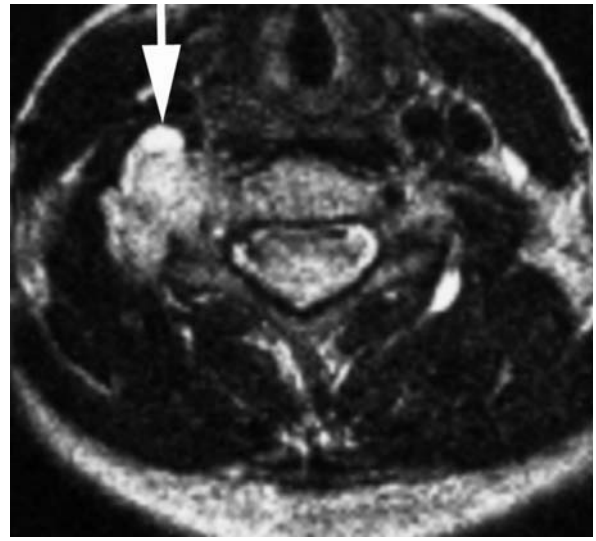

b

Fig. 20.19a,b. Signal intensity patterns on MR: exostosis. Osteo-cartilaginous exostosis (**a**) with a small cartilaginous cap that is bright on T2-WI (**b**). This enables the thickness of the cartilage cap to be measured

20.3 Primary Tumors of the Osseous Spine

In general, extradural lesions constitute the most frequent group of spine tumors. Most originate from the vertebrae. The most frequent extradural tumor is metastasis, while primary bone tumors are much less common. Solitary vertebral lesions are less common than tumors with multiple locations. Benign lesions are usually asymptomatic, incidentals findings, while malignant vertebral tumors cause back pain and sometimes manifest neurologic symptoms, especially in children. Besides imaging findings, the age of the patient and the multiplicity and location of the lesion(s) are most important in the differential diagnosis (Van Goethem et al. 2004) (Table 20.2).

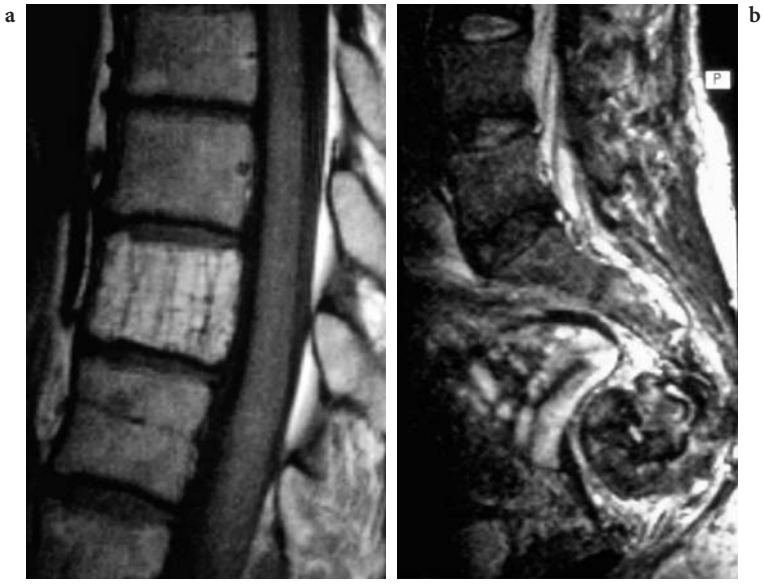

Fig. 20.20a,b. Infrequent SI-patterns on MR. Typically high signal intensity on T1-WI (**a**) in a vertebral hemangioma due to its fatty contents and low signal intensity on T2-WI (**b**) in a sacral giant cell tumor because of high collagen content, hemosiderin and/or increased cellularity

Fig. 20.21a,b. Low signal intensity patterns on MR: enostosis. Enostosis presenting with low signal intensity on all MR sequences. All sclerotic (portions of) vertebral tumors present with this signal intensity pattern

20.3.1 Vertebral Hemangioma

20.3.1.1 General

The incidence of vertebral hemangiomas increases with age, peaking around the fourth to sixth decades. There are two types of vertebral hemangioma: asymptomatic lesions, and aggressive, symptomatic types, with compression of the spinal cord (Laredo et al. 1986). The symptomatic lesions in particular occur somewhat more frequently in women. Vertebral hemangioma is the most common benign spinal tumor. More than half of all vertebral hemangiomas are seen in the thoracic region, one third in the lumbar region and the remainder in the cervical and sacral region. About one third are multiple. Most occur in the vertebral body, but about 10% extend to the posterior elements. Extraosseous lesions are rare (1%).

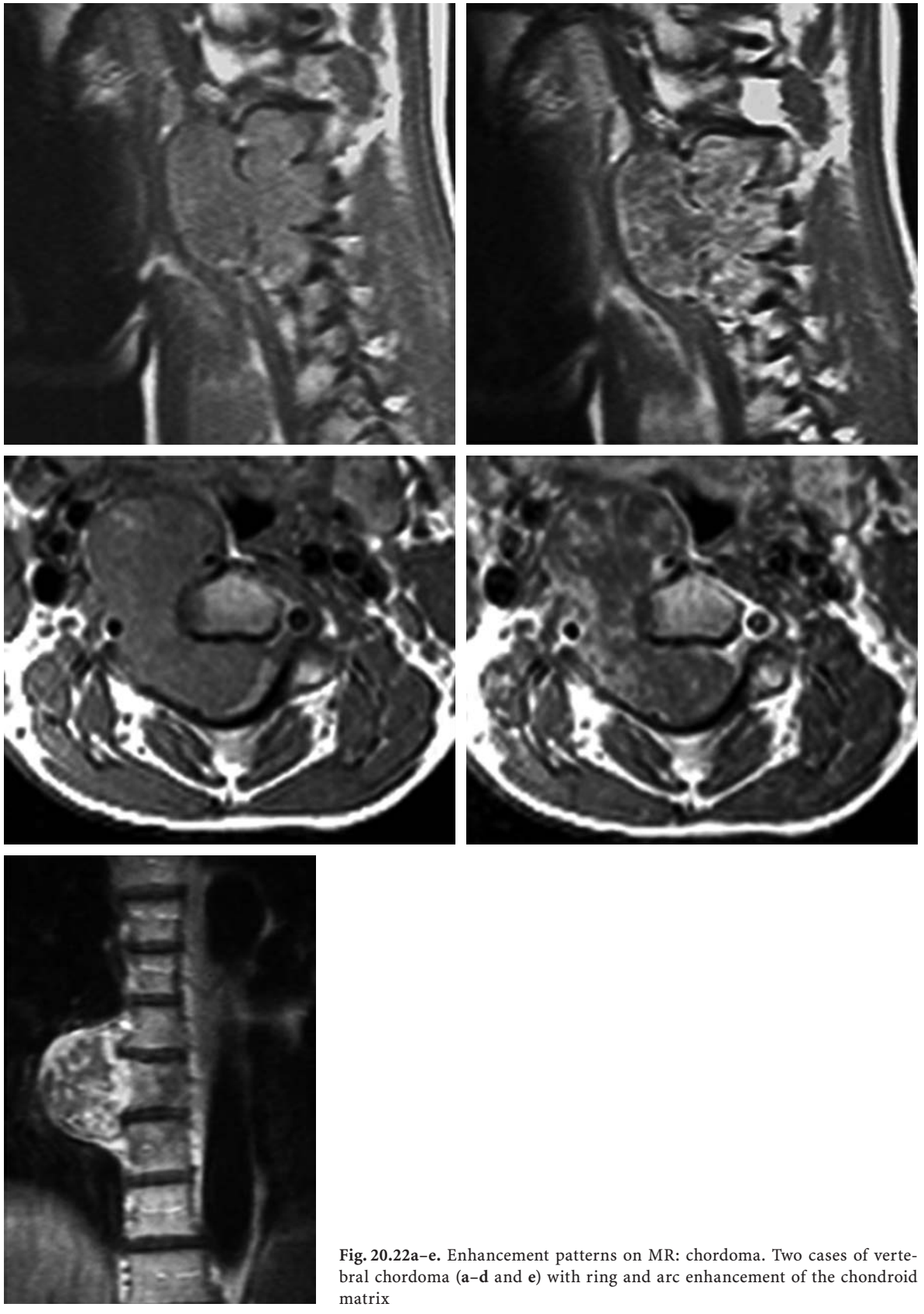

Fig. 20.22a–e. Enhancement patterns on MR: chordoma. Two cases of vertebral chordoma (**a–d** and **e**) with ring and arc enhancement of the chondroid matrix

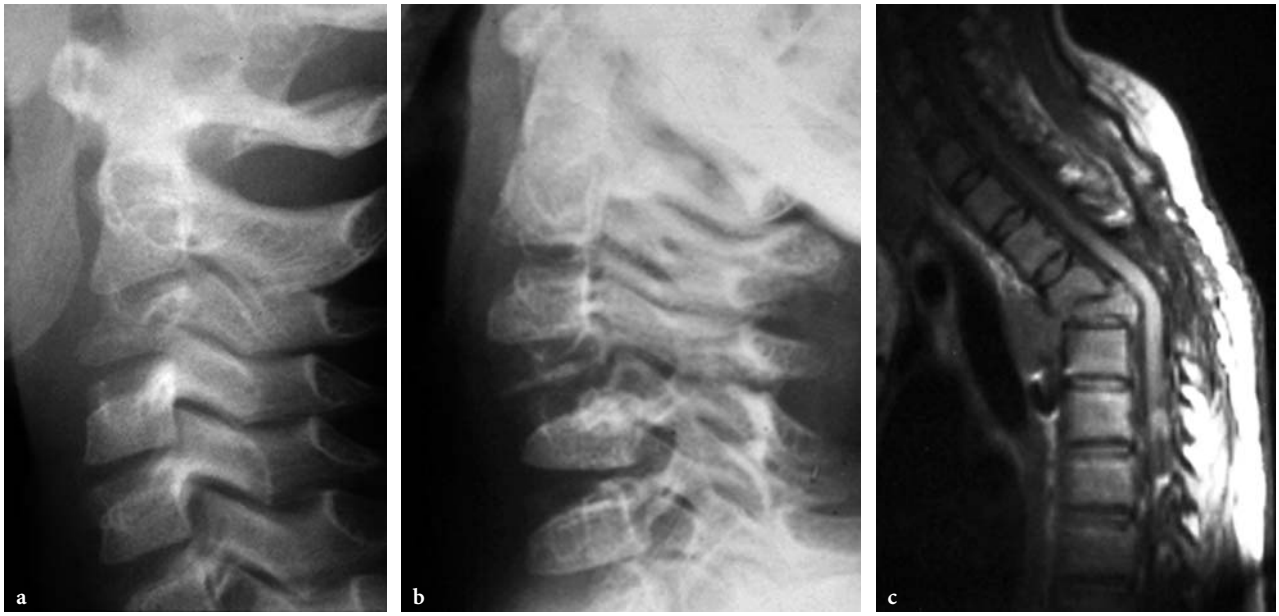

Fig. 20.23a-c. Vertebra plana. Two cases of vertebra plana. **a**,**b** This C4 vertebra collapsed over an interval of only 2 weeks in a case of eosinophilic granuloma. Vertebra plana, however, is also noted in other pathology, as in this case of a thoracic giant cell tumor (**c**)

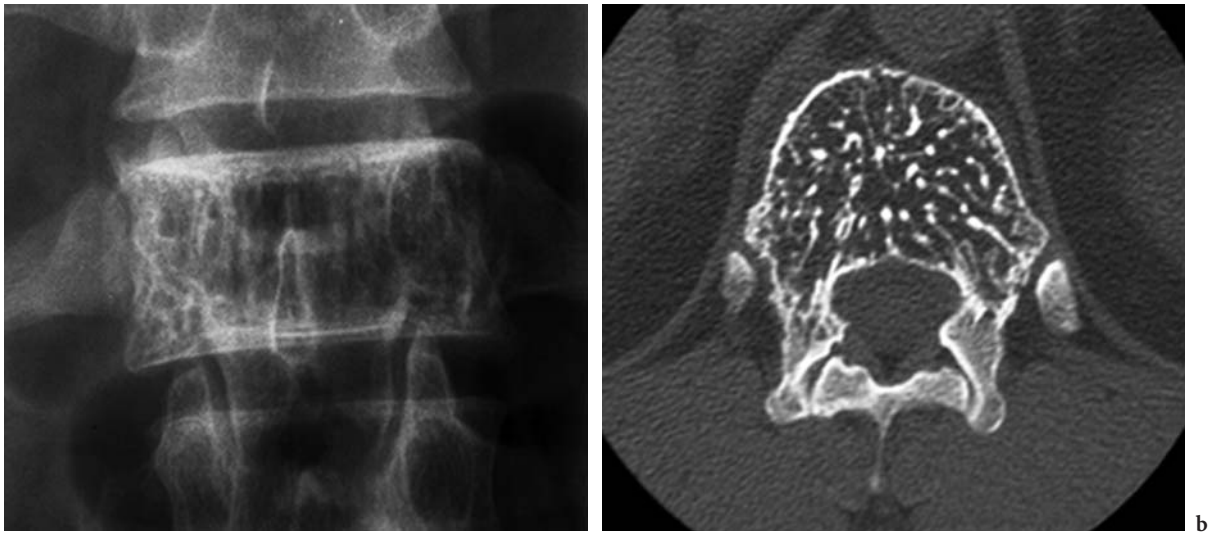

Fig. 20.24a,b. Vertebral hemangioma. A common, non-aggressive and asymptomatic vertebral hemangioma with "honeycombing" or "jail bar" appearance on plain film (**a**) and corresponding "polka-dot" sign on CT (**b**)

20.3.1.2 Clinical Presentation

The vast majority of vertebral hemangiomas are discovered incidentally. Sometimes local pain or tenderness is present. Symptoms of cord or nerve compression are rare and are due to tumor extension rather than vertebral collapse. Compression fractures are unusual because of the thickened trabeculae.

20.3.1.3 Pathology

Vertebral hemangioma consists of endothelium lined vascular structures. They can be of either capillary, cavernous or venous origin. Because of destruction of some of the bone trabeculae the remainder tends to increase in thickness.

a

b

c

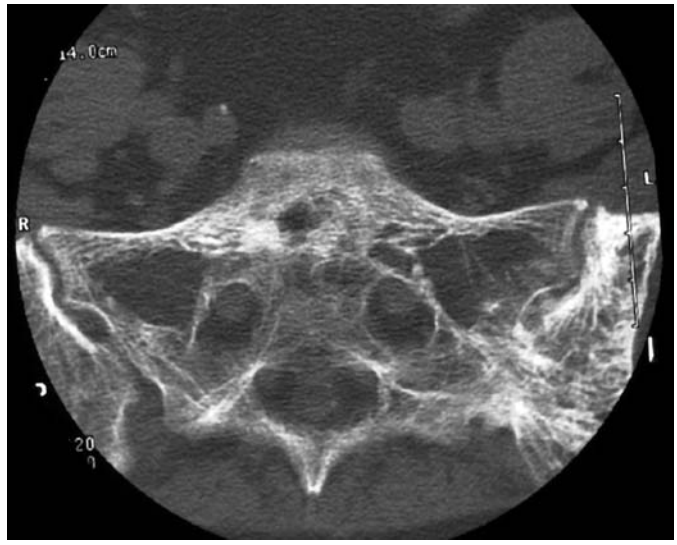

d

Fig. 20.25a–d. Paget's disease. Ivory vertebra on plain film (**a**) and CT scan (**b**) in a case of Paget's disease. Thickened sclerotic margins may lead to a so-called "picture frame" appearance here in a lumbar vertebra (**c**) and the sacrum (**d**). Note the involvement of all vertebral elements

20.3.1.4 Imaging

The thickened vertical bone trabeculae in vertebral hemangioma give rise to its typical "jail bar" or "honeycombing" appearance on plain films (Figs. 20.4, 20.24). On axial CT this is seen as a spotted appearance, known as "polka dot". On MR imaging these lesions are well circumscribed and have a typical high signal intensity both on T1- and T2-WI. This high signal is caused by a high fatty content (Baudrez et al. 2001). Some lesions, however, have low signal on T1-WI, and these tend to be more aggressive. Hemangiomas show enhancement, which is especially noticeable in the more aggressive lesions that have a lower signal on T1-WI to start with.

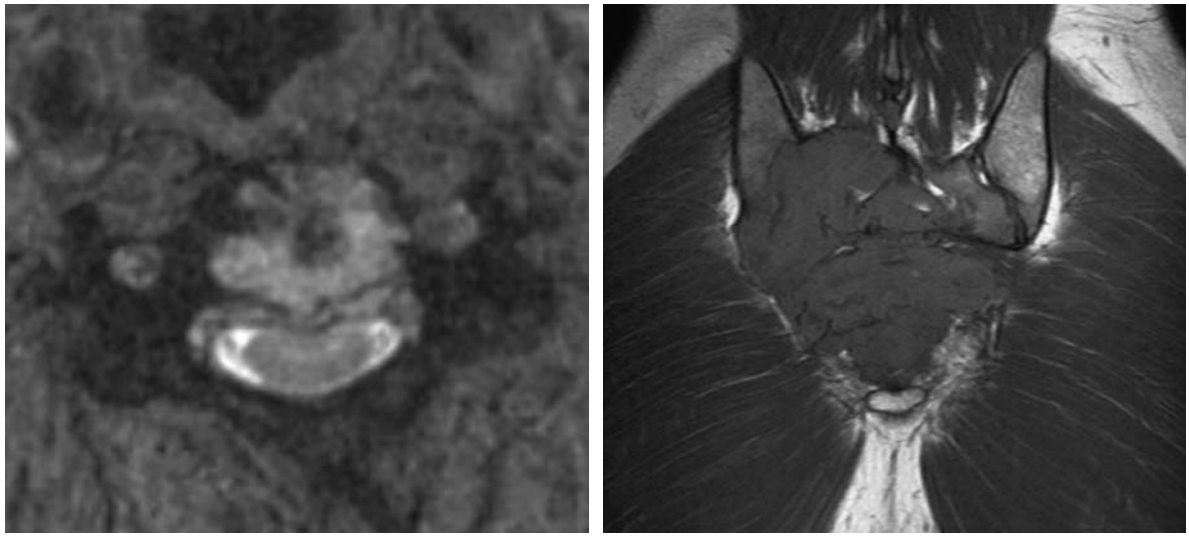

Fig. 20.26a,b. Plasmacytoma. Typical "mini-brain" appearance of a plasmocytoma of a cervical vertebral body (**a**) and in another case in the sacral spine (**b**)

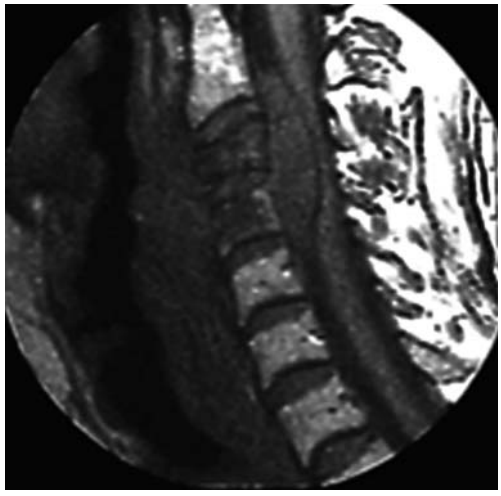

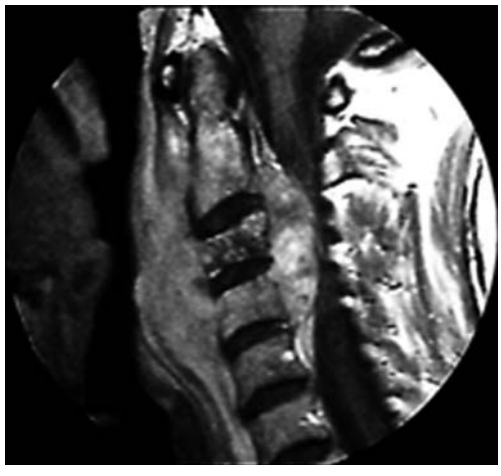

Fig. 20.27a–c. Chordoma. Two cases of chordoma of the cervical spine. Case 1 (**a**,**b**) shows multilevel involvement and a marked inhomogeneous enhancing soft-tissue component with dumbbell and clover leaf-shape. Case 2 (**c**) demonstrates high signal intensity of the soft tissue components on T2-WI. Both cases demonstrate preserved intervertebral discs typical of chordoma

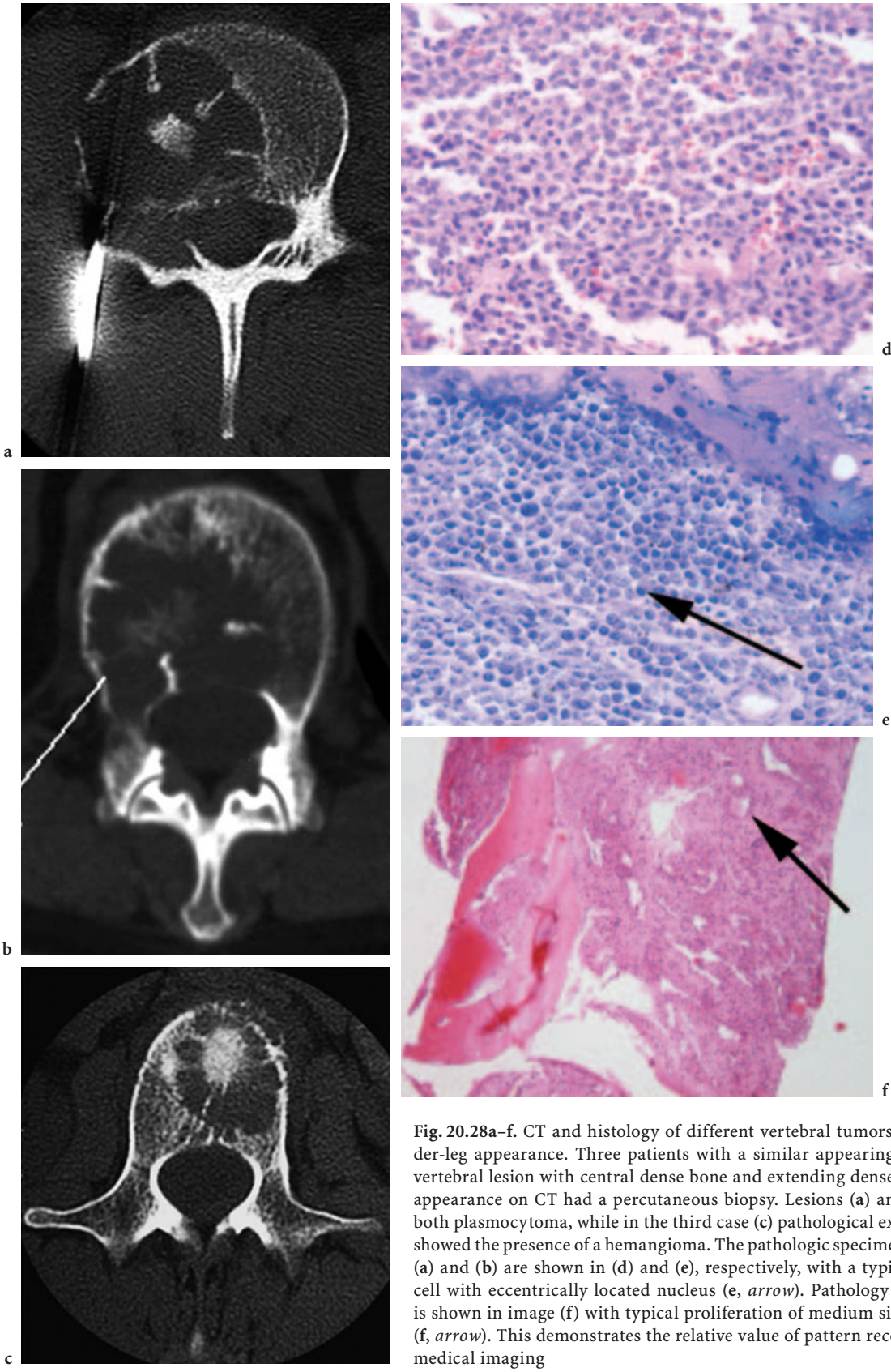

Fig. 20.28a–f. CT and histology of different vertebral tumors with "spider-leg appearance. Three patients with a similar appearing osteolytic vertebral lesion with central dense bone and extending dense spider-leg appearance on CT had a percutaneous biopsy. Lesions (**a**) and (**b**) were both plasmocytoma, while in the third case (**c**) pathological examination showed the presence of a hemangioma. The pathologic specimens of cases (**a**) and (**b**) are shown in (**d**) and (**e**), respectively, with a typical plasma cell with eccentrically located nucleus (**e**, *arrow*). Pathology in case (**c**) is shown in image (**f**) with typical proliferation of medium sized vessels (**f**, *arrow*). This demonstrates the relative value of pattern recognition in medical imaging

20.3.2 Plasmacytoma

20.3.2.1 General

The peak incidence for spinal plasmacytoma is in the fifth to sixth decade. Men are more affected than women. Solitary plasmacytoma is an uncommon tumor occurring in 3%–7% of patients with plasma cell neoplasms. The lesion is commonly found in the axial skeleton (25%–60%). Plasmacytoma is a lesion of the vertebral body but involvement of the posterior elements is the rule. Often, the lesion is present for many years as an isolated lesion but, on occasion, multiple plasmacytomas can develop.

20.3.2.2 Clinical Presentation

Local or irradiating pain is the most common presenting complaint. Sudden intense pain may be caused by acute compression fracture. Radicular or cord symptoms occur with compression of neurologic structures, often after vertebral collapse. The thoracic spine is the commonest site involved, followed by lumbar spine, cervical spine and sacrum in descending order. Most patients have an indolent course with a median survival rate of 10 years.

20.3.2.3 Pathology

Plasmacytomas are considered to represent the early stages of multiple myeloma, but plasmacytoma can precede laboratory evidence of multiple myeloma for many years. There are no signs of myeloma cells on bone marrow examination.

20.3.2.4 Imaging

On plain film plasmacytoma presents as a lytic and usually expansile bone lesion with thickened trabeculae and multicystic appearance (Shah et al. 2000). Often fractures or even frank collapse exists. MR imaging shows a low signal intensity on T1-WI and high signal intensity on T2-WI involving the entire vertebral body. Diffuse enhancement with intravenous contrast medium is the rule, but in some cases only peripheral enhancement is noted. Curvilinear low-signal-intensity structures on all imaging sequences extending partially through the vertebral body and resembling sulci seen in the brain, causing a "mini-brain" appearance on axial images, is very typical (Fig. 20.26) (Major et al. 2000). These low-signal-intensity structures are likely caused by thickened cortical bone caused by the slow growing nature of plasmacytoma. This appearance can also be seen on CT of plasmacytoma.

20.3.3 Multiple Myeloma

20.3.3.1 General

The peak incidence of multiple myeloma is in the sixth to seventh decades. The spine and especially the vertebral bodies are the most common location, frequently with epidural extension. It is the most frequent primary malignant tumor of the spine.

20.3.3.2 Clinical Presentation

Bone pain, usually involving the back or sternum, from tumor expansion is the most common presenting symptom. Less common presentations of multiple myeloma include vague symptoms of fatigue, weakness or weight loss. Often, however, the disease is discovered while the patient is being examined for other medical problems. Routine radiographs demonstrating bony lesions can be the first sign of multiple myeloma.

20.3.3.3 Pathology

Multiple myeloma is a monoclonal proliferation of malignant plasma cells usually affecting bone. Monoclonal gammopathies are a premalignant condition of multiple myeloma.

20.3.3.4 Imaging

The typical imaging findings on conventional radiography and CT include punched out lytic bone lesions, diffuse osteopenia, fractures and, rarely, osteosclerosis. On MR imaging different signal patterns, ranging from normal-appearing bone marrow to focal lesions or diffuse bone marrow in-

Table 20.2. The common primary spinal bone tumors with their salient features

	Location	Location	Clinical symptoms	Plain film	CT	MR
Hemangioma	T>L>C	VB	Asymptomatic, occasionally painful	Corduroy or jail bar	Polka dot	High SI on both T1- and T2-WI
Enostosis	T>L	VB	Asymptomatic	Cortical bone density with spiculated margin	Same density as cortex	Low SI on both T1- and T2-WI
Osteochondroma	C	PE		Continuity of marrow and cortex with the underlying bone	Continuity of marrow and cortex with the underlying bone. Cartilage cap	Cartilage cap with high SI on T2-WI
Osteoid Osteoma	L>T>C	PE	Unrelenting pain, worse at night; sensitive to aspirin	Radiolucent nidus with surrounding sclerosis, mineralization of nidus	Radiolucent nidus with surrounding sclerosis, mineralization of nidus	Strong enhancement of nidus. Surrounding low SI.
Osteoblastoma	T>L	PE		Expansile lesion with calcified matrix and soft tissue mass; >1.5 cm	Expansile lesion with calcified matrix and soft tissue mass; >1.5 cm	Expansile lesion with calcified matrix and soft tissue mass; >1.5 cm
Aneursymal Bone Cyst	T>L	PE>VB	Local pain	Expansile multiloculated lesion	Expansile multiloculated lesion. Fluid-fluid levels	Cysts with fluid-fluid levels
Giant Cell Tumor	S>C>T	VB; eccentric location	Local pain	Expansile lytic lesion of vertebral body	Expansile lytic lesion of vertebral body	Low SI on T2-WI
Eosinophilic Granuloma	T>L>C	VB	Variable; sensitive to aspirin	Well defined lytic lesion, may lead to vertebra plana	Well defined lytic lesion, may lead to vertebra plana	Well defined lytic lesion, may lead to vertebra plana. Strong enhancement.
Chordoma	S	VB; centrally located	Painful	Destructive lesion; may affect multiple vertebrae and extend across the discs. Amorphous calcification	Destructive lesion; may affect multiple vertebrae and extend across the discs. Amorphous calcification	Destructive lesion; may affect multiple vertebrae and extend across the discs
Chondrosarcoma	T	VB	Symptomatic		Destructive bone lesion with ring and arc calcification	Ring and arc enhancement
Ewing's Sarcoma	L>S	VB	Symptomatic	Permeative lesion with associated soft tissue mass	Permeative lesion with associated soft tissue mass	Permeative lesion with associated soft tissue mass
Multiple Myeloma	T>L	VB	Local pain	Multiple lesions; lytic lesions or diffuse osteopenia or vertebral collapse	Multiple lesions; lytic lesions or diffuse osteopenia or vertebral collapse. "Mini-brain"	Low SI on T1-WI and high SI on T2-WI. "Mini-brain"

C, cervical; *T*, thoracic; *L*, lumbar; *S*, sacral; *VB*, vertebral body; *PE*, posterior elements; *SI*, signal intensity

filtration, are seen. On T1-WI, a low signal intensity is typically noted (Fig. 20.1), with marked enhancement after the administration of contrast material. Even in advanced stages of this disease, up to 20% of radiographs and MR examinations can have normal findings. Spiral CT allows imaging of the entire spine and provides detailed information on osseous involvement in multiple myeloma. Especially in anatomically complex regions like the pelvis and the thoracic spine, it is superior to conventional radiography. Compared with conventional radiography and MR imaging, spiral CT provides more detailed information on the risk of vertebral fracture (Lecouvet et al. 1997). For evaluating diffuse bone marrow changes, MR imaging is still the imaging modality of choice. Because MR imaging of the spine shows normal findings in up to 20% of patients with proven bone marrow infiltration, the initial staging of multiple myeloma should include MR imaging in combination with spiral CT.

20.3.4 Chordoma

20.3.4.1 General

The peak incidence for chordoma is in the fifth to sixth decades. The average age at presentation is 55 years (York et al. 1999). Men are more often affected than women (2:1). Half of these tumors are found in the sacrum, 35% in the clivus and the rest in the vertebrae (Smolders et al. 2003).

20.3.4.2 Clinical Presentation

Local pain is the most frequent presenting symptom. Symptoms of spinal cord or nerve root compression can occur if they grow large enough.

20.3.4.3 Pathology

Chordomas arise from remnants of the notochord. They are composed of large vacuolated physaliphorous cells with intervening fibrous septae (Crapanzano et al. 2001). A fluid and gelatinous mucoid substance (associated with recent and old hemorrhage) and necrotic areas are found within the tumor; in some patients, calcification and sequestered bone fragments are also found. In addition to conventional chordomas, chondroid chordomas are identified by their hyaline cartilage content.

Chordomas are malignant tumors that show local invasion, and especially vertebral body cases show distant metastasis.

20.3.4.4 Imaging

On plain film bone destruction, often with amorphous calcification, is seen. CT can show paravertebral and especially epidural extension (Fig. 20.27) (Wippold et al. 1999). Due to the variety of components most lesions are heterogeneous on MR imaging. They are iso-intense on T1-WI and hyperintense on T2-WI. Enhancement after contrast injection varies from little to prominent (Fig. 20.7). Often internal septations and a low signal surrounding capsule can be seen (Fig. 20.22). Sometimes hemorrhage and cyst formation is present.

20.3.5 Osteoid Osteoma

20.3.5.1 General

The peak incidence for osteoid osteoma is in the second decade. The average age at presentation is 17 years. Men are more commonly affected than women (2–4:1). It accounts for about 10% of all bone tumors involving the spine. An osteoid osteoma is a benign lesion that has a unique tendency to affect the posterior part of the vertebra and occurs primarily in the pedicle and the posterior elements, not in the vertebral body. The lumbar spine is the most affected, followed by the cervical, thoracic and sacral regions (Ozaki et al. 2002).

20.3.5.2 Clinical Presentation

It typically presents as unrelenting pain, clearly worse at night, which is extremely sensitive to aspirin or non-steroidal anti-inflammatory drugs (NSAIDs). Not infrequently patients with spinal osteoid osteoma have a painful scoliosis (Saifuddin et al. 1998).

20.3.5.3 Pathology

Osteoid osteoma has a central nidus of vascular fibrous connective tissue with a surrounding osteoid matrix. Multinucleated giant cells and osteoclasts are frequently observed. They are surrounded by bone sclerosis. Lesions larger than 1.5 cm are usually categorized as osteoblastoma.

20.3.5.4 Imaging

Plain film shows a lucent nidus, frequently with a small cental calcification. Surrounding the nidus is variable bone sclerosis. Bone scintigraphy is highly sensitive for osteoid osteoma. Especially when there is extensive bone sclerosis the nidus is much easier to distinguish on CT (Youssef et al. 1996). On MR imaging calcifications and bone sclerosis have a low signal both on T1- and T2-WI. The non-calcified portion of the nidus has high signal on T2-WI. After contrast administration intense enhancement of the nidus is seen (Fig. 20.12). Sometimes adjacent bone marrow and soft tissue changes are seen.

20.3.6 Osteoblastoma

Osteoblastomas are related to osteoid osteomas and, by definition, are larger than 1.5 cm in diameter (Fig. 20.13). They also have the tendency to affect the posterior part of the spine and present with pain (Fig. 20.6b). Osteoblastomas can be more aggressive than osteoid osteomas and more often require surgical resection. The recurrence rate is about 10%, which is also higher than that seen with osteoid osteomas.

20.3.7 Aneurysmal Bone Cyst

20.3.7.1 General

The peak incidence for ABC is in adolescence, and 80% occur before the age of 20. Women are somewhat more affected than men. The lumbosacral spine is the most affected and the tumor may affect the posterior elements of the spine or expand to the pedicles and the vertebral body itself.

20.3.7.2 Clinical Presentation

These tumors may present with pain and in some cases, fractures and cord or nerve root compression with neurological symptoms.

20.3.7.3 Pathology

ABCs are benign tumors of unknown etiology. In almost half of all cases they are associated with a preexisting bone lesion. They are large, expansile and multiloculated lesions with high vascularization.

20.3.7.4 Imaging

Plain film shows an expansile, osteolytic lesion with thin surrounding cortical bone. CT and MR imaging typically show a multiloculated lesion with fluid-fluid levels (Fig. 20.16). Sometimes internal septations and lobulations are present. MR imaging demonstrates blood degradation products.

20.3.8 Giant Cell Tumor

20.3.8.1 General

The peak incidence for giant cell tumor is in the third through fifth decades. There is no sex predilection, but there is a female preponderance in spinal giant cell tumors, which are seen in particular in the sacrum, but are rare in other spinal locations. It is the most frequent benign tumor of the sacrum. It tends to affect the vertebral body (front of the spine).

20.3.8.2 Clinical Presentation

Giant cell tumors present with local pain. Neurologic complications are not uncommon.

20.3.8.3 Pathology

Despite being technically "benign", they can be very aggressive and sometimes spread elsewhere. They extend to the cortex, but usually do not transgress

the periosteum. Giant cell tumors contain monocytes, macrophages and multinucleated giant cells. On pathologic examination they are indistinguishable from brown tumors and may resemble chondroblastoma, chondromyxoid fibroma, ABC and osteosarcoma. Incomplete removal of a vertebral giant cell tumor can lead to possible malignant transformation, seen in about 10% of cases.

20.3.8.4 Imaging

Plain films show a lytic and expansile spinal lesion, typically in the sacrum. MR imaging demonstrates an inhomogeneous multiloculated cystic mass (Fig. 20.8). They may show low SI on T2-WI since they frequently contain blood degradation products and/or have a high cellularity.

20.3.9 Eosinophilic Granuloma

20.3.9.1 General

The peak incidence for eosinophilic granuloma of the spine is in the first decade. There is a clear male predilection. Eosinophilic granuloma is one of the presenting forms of Langerhans cell histiocytosis. Lesions may be single or multiple. Most lesions are seen in the cervical spine, especially mid-cervical in children and at C2 in adults (Bertram et al. 2002).

20.3.9.2 Clinical Presentation

Eosinophilic granuloma has a highly variable clinical presentation ranging from non-existent to very painful, sometimes worsening at night and sensitive to NSAIDs. The presenting symptoms of cervical eosinophilic granuloma are usually pain and restricted range of motion. Sometimes scoliosis is the presenting symptom. In contrast to eosinophilic granuloma of the thoracic spine and lumbar spine, the neurologic symptoms are less frequent.

20.3.9.3 Pathology

Eosinophilic granuloma is a benign nonneoplastic disorder with unknown etiology. They tend to evolve from small cystic and hemorrhagic to larger fatty and fibrous lesions. Initially they contain many eosinophils and lymphocytes.

20.3.9.4 Imaging

Plain film shows a lytic lesion with sharp borders. It is a classic cause of a single collapsed vertebral body (vertebra plana) (Fig. 20.23). Nevertheless, "vertebra plana" is a rare sign in cervical eosinophilic granuloma. On MR imaging it has a high signal on T2-WI and a variable signal on T1-WI (De Schepper et al. 1993). It enhances strongly with gadolinium. When the vertebral body is involved it is usually affected in its entirety.

20.4 Relative Merit of CT and MRI

MRI is the method of choice for imaging the majority of spinal tumors as it has superior soft tissue characterization and multiplanar capability. It can also delineate the extent of neurological compromise. However, it is limited by poor imaging of calcification and cortical bone.

CT, on the other hand, has superior ability to detect tiny specks of calcification and subtle cortical bone lesions. With the advent of multi-slice CT, imaging has become much quicker with virtually the same multi-planar capability as MR.

CT has the advantage of being able to detect small lesions in the posterior elements which have a complex anatomy and may be difficult to discern on MRI. Thus, CT is the imaging modality of choice in conditions such as osteoid osteoma, osteoblastoma and osteochondroma (Flemming et al. 2000; Youssef et al. 1996). It plays a very useful role in terms of guidance in biopsy of lesions and in therapeutic ablation of tumors such as osteoid osteoma.

References

Baudrez V, Galant C, Vande Berg BC (2001) Benign vertebral hemangioma: MR-histological correlation. Skeletal Radiol 30:442–446

Beltran J, Simon DC, Levy M, Herman L, Weis L, Mueller CF (1986) Aneurysmal bone cysts: MR imaging at 1.5 T. Radiology 158:689–690

Bertram C, Madert J, Eggers C (2002) Eosinophilic granuloma of the cervical spine. Spine 27:1408–1413

Crapanzano JP, Ali SZ, Ginsberg MS, Zakowski MF (2001) Chordoma: a cytologic study with histologic and radiologic correlation. Cancer 93:40–51

De Schepper AM, Ramon F, Van Marck E (1993) MR imaging of eosinophilic granuloma: report of 11 cases. Skeletal Radiol. 22:163-166

Disler DG, Miklic D (1999) Imaging findings in tumors of the sacrum. AJR Am J Roentgenol 173:1699–1706

Flemming DJ, Murphey MD, Carmichael BB, Bernard SA (2000) Primary tumors of the spine. Semin Musculoskelet Radiol 4:299–320

Hudson TM (1984) Fluid levels in aneurysmal bone cysts: a CT feature. AJR Am.J.Roentgenol. 142:1001–1004

Ilaslan H, Sundaram M, Unni KK, Dekutoski MB (2004) Primary Ewing's sarcoma of the vertebral column. Skeletal Radiol 33:506–513

Laredo JD, Reizine D, Bard M, Merland JJ (1986) Vertebral hemangiomas: radiologic evaluation. Radiology 161:183–189

Lecouvet FE, Malghem J, Michaux L, Michaux JL, Lehmann F, Maldague BE, Jamart J, Ferrant A, Vande Berg BC (1997) Vertebral compression fractures in multiple myeloma. Part II. Assessment of fracture risk with MR imaging of spinal bone marrow. Radiology 204:201–205

Major NM, Helms CA, Richardson WJ (2000) The „mini brain": plasmacytoma in a vertebral body on MR imaging. AJR Am J Roentgenol 175:261–263

Murphey MD, Andrews CL, Flemming DJ, Temple HT, Smith WS, Smirniotopoulos JG (1996) From the archives of the AFIP. Primary tumors of the spine: radiologic pathologic correlation. Radiographics 16:1131–1158

Murphey MD, Nomikos GC, Flemming DJ, Gannon FH, Temple HT, Kransdorf MJ (2001) From the archives of AFIP. Imaging of giant cell tumor and giant cell reparative granuloma of bone: radiologic-pathologic correlation. Radiographics 21:1283–1309

Ozaki T, Liljenqvist U, Hillmann A, Halm H, Lindner N, Gosheger G et al. (2002) Osteoid osteoma and osteoblastoma of the spine: experiences with 22 patients. Clin Orthop Relat Res 397:394–402

Saifuddin A, White J, Sherazi Z, Shaikh MI, Natali C, Ransford AO (1998) Osteoid osteoma and osteoblastoma of the spine. Factors associated with the presence of scoliosis. Spine 23:47–53

Shah BK, Saifuddin A, Price GJ (2000) Magnetic resonance imaging of spinal plasmacytoma. Clin Radiol 55:439–445

Smolders D, Wang X, Drevelengas A, Vanhoenacker F, De Schepper AM (2003) Value of MRI in the diagnosis of non-clival, non-sacral chordoma. Skeletal Radiol. 32:343-350

Van Goethem JW, van den Hauwe L, Ozsarlak O, De Schepper AM, Parizel PM (2004) Spinal tumors. Eur J Radiol 50:159–176

Wippold FJ, Koeller KK, Smirniotopoulos JG (1999) Clinical and imaging features of cervical chordoma. AJR Am J Roentgenol 172:1423–1426

York JE, Kaczaraj A, Abi-Said D, Fuller GN, Skibber JM, Janjan NA, Gokaslan ZL (1999) Sacral chordoma: 40-year experience at a major cancer center. Neurosurgery 44:74–79

Youssef BA, Haddad MC, Zahrani A, Sharif HS, Morgan JL, al-Shahed M, al-Sabty A, Choudary R (1996) Osteoid osteoma and osteoblastoma: MRI appearances and the significance of ring enhancement. Eur Radiol 6:291–296

Bone Marrow

Spinal Bone Marrow Disorders

21

Philippe Demaerel

CONTENTS

21.1 Introduction

The normal bone marrow and its physiological conversion from the newborn to the elderly will be reviewed.

Although bone marrow alterations can be observed in many vertebral disorders, only intrinsic haematological bone marrow disorders will be dealt with in this chapter. Vertebral metastases and infectious vertebral pathology are discussed in Chapters 19 and 22.

Although in most of the diseases that will be discussed here, extraspinal bone involvement can be observed, this falls outside the scope of this chapter. However, it should be emphasized that a systematic assessment of the pelvic bone marrow is strongly recommended (Vande Berg et al. 1996).

P. Demaerel, MD
Professor, Department of Radiology, University Hospital K.U.L., Herestraat 49, 3000 Leuven, Belgium

21.2 Normal Bone Marrow

The normal bone marrow contains a variable amount of yellow and red marrow, depending on age and on significant interindividual variations within the same age group (Vogler and Murphy 1988; Ricci et al. 1990; Sze et al. 1991). In adulthood, red marrow can be found in the axial skeleton and in the proximal femora and humeri. Red marrow is characterized by the presence of hematopoietic cells (60%), while yellow marrow consists of 95% adipocytes. Both marrow types contain fat but the amount of fat is twice as high in yellow marrow. Red marrow contains about three times more water than yellow marrow.

Although X-ray and CT still play a role in the work-up of the patient with a suspected bone marrow disorder, magnetic resonance imaging (MRI) is the preferred technique whenever neurological symptoms occur, in order to visualize the spinal cord and/or nerve root compression. Because of the different fat/water ratios in yellow and red marrow, MRI is an exquisite technique to visualize the bone marrow. MRI is less sensitive to cortical and trabecular bone changes and should therefore be considered as a complementary examination compared to X-ray or CT.

In normal physiological circumstances there is a progressive conversion of red marrow into yellow marrow. MRI can be used as a guide to follow this conversion but it should be mentioned that there is an overestimation of the fat content (Moore and Dawson 1990). At birth, bone marrow is predominantly red marrow, involved in the production of red cells, white cells and platelets (Fig. 21.1). The adult marrow distribution is reached by the age of 25 years. The marrow conversion continues during adulthood but slower than during the first two decades. On the other hand, red marrow will appear different with increasing age, reflecting the increasing amount of fat. The red marrow distribution is symmetrical and is often located near the end plates.

KEY-POINTS

- Normal bone marrow:
  - Variable amount of yellow marrow (95% adipocytes) and red marrow (60% hematopoietic cells), depending on the age of the patient
  - Progressive conversion of red marrow into yellow marrow
- Benign bone marrow hyperplasia:
  - Signal corresponds to red marrow on all sequences
  - Observed in obesity, athletes and heavy smokers
  - Seen in association with chronic anemia, chronic infection or treatment
  - SI on T2-weighted images is usually less pronounced
  - Gadolinium-enhancement is absent
- Imaging:
  - X-ray and CT: cortical and trabecular bone changes
  - MRI: exquisite technique to visualize the bone marrow
    - preferred imaging sequences
      - T1-weighted SE images (pre- and post-contrast)
      - STIR images
      - opposed-phase GRE images
    - "whole-body MRI" approach
    - imaging abnormalities are non-specific
      - neoplastic
      - non-neoplastic (infectious disease, bone marrow hyperplasia)

Multiple myeloma (morbus Kahler)

- Role of spinal imaging:
  - Detection of bone marrow infiltration (MRI) and bone resorption (X-ray/CT)
  - focal mass lesion
    - diffuse disease
  - Depicting vertebral compression fractures (MRI and CT)
  - Assessing spinal cord compression/CNS involvement (MRI with gadolinium)
  - Assessing the response to therapy
- Bone marrow infiltration
  - MRI may be normal
  - Focal involvement
    - focal lesions with low signal on T1-weighted images, sometimes surrounded by a halo on T2-weighted images (active disease)
    - "salt and pepper" pattern: multiple tiny foci of low signal on T1-weighted images, intermediate to high signal on fat-suppressed T2-weighted images, enhancement on post-contrast images
  - Diffuse involvement
    - decreased signal on T1-weighted images
    - "bright disc" sign
  - Staging (MRI added to clinical staging system of Durie and Salmon)
- Vertebral compression fractures
  - Due to bone marrow involvement and bone resorption
  - In up to 70% of MM patients
  - > 60% Of the vertebral fractures are benign
    - partial preservation of normal marrow
    - only displacement of the posterior wall
    - no involvement of the pedicles
    - no soft-tissue component
- Leptomeningeal spread
  - Very rare (1%)
  - MR findings resemble those of leptomeningeal metastases or pial involvement by lymphoma
- Follow-up
  - Value of MRI seems limited
    - T1-weighted images before and after Gd injection better than T2-weighted images
    - role of iron-oxide based contrast agents?
    - post-treatment changes
      - response to treatment
      - decrease or disappearance of the focal lesions or diffuse disease
    - decrease of contrast enhancement
    - reappearance of fatty marrow
      - treatment-related changes
    - myelofibrosis
    - amyloidosis
  - FDG-PET

Lymphoma

- Bone marrow involvement is uncommon at diagnosis
  - Hodgkin: 10%–15% of marrow infiltration in relapses
    - MRI better than bone marrow biopsy
  - Non-Hodgkin: detection on MRI depends on the histological subtype
    - low-grade lymphoma:
      - rather diffuse bone marrow involvement
      - biopsy is warranted
      - often associated with normal MRI findings (follicular or paratrabecular)
    - intermediate and high-grade lymphoma:
      - focal marrow lesions
      - MRI plays a more important role
- Primary leptomeningeal lymphoma:
  - Without vertebral abnormalities is extremely rare
  - Arise from lymphocytes in the vicinity of the meninges
  - Diffuse enhancement of the nerve roots; nodular lesions along the cauda equina
- Primary spinal epidural lymphoma:
  - Slightly more common than the leptomeningeal subtype
  - Mechanism: epidural extension from adjacent vertebral lesions versus haematogenous spread
  - Differential diagnosis with metastases
    - infiltrative growth through the foramen is typical for lymphoma
    - epidural masses are more common in lymphoma than in metastases

Leukaemia

- Diffuse decrease of the bone marrow signal on T1-weighted images
- Signal intensity may correlate with the aggressiveness in CLL
- However, MR findings may be normal

Langerhans cell histiocytosis
(histiocytosis X)

- Preservation of the disc space
- An associated epidural soft tissue mass may be present. **Differentiating** haematological malignancies from metastases
  - Lymphoproliferative disorders
    - diffuse involvement
    - predilection for the posterior elements
    - "wrap-around" sign: paravertebral soft tissue mass, not affecting the shape or contour of the bone
      - typical for lymphoma
      - never observed in myeloma
  - Metastases
    - (multi)focal involvement
    - involvement of the anterior vertebral elements

The signal of red marrow on T1-weighted spin-echo images is higher than the signal of muscle or intervertebral disc, but lower than the signal of yellow marrow.

On T1-weighted spin-echo images, four main patterns of marrow distribution are identified throughout the spine according to age (Ricci et al. 1990). In young adults, high signal can be seen in the region of the basivertebral vein (Fig. 21.2). After 30 years of age, bandlike or triangular regions can be identified near the endplates, possibly to some extent related to degenerative changes (Fig. 21.2). Two other patterns that can be observed consisting of numerous dots of only a few millimeters and larger areas of 0.5–1.5 cm (Fig. 21.2).

Benign bone marrow hyperplasia has been observed in obesity, athletes and heavy smokers. In these cases, the marrow signal should correspond to red marrow on all sequences. Differences have been demonstrated between male professional cyclists and male volunteers on spin-echo T1-weighted sequences (Altehoefer et al. 2002). There was only a borderline correlation with hematocrit and not with hemoglobin, erythrocyte or reticulocyte count. Red marrow hyperplasia can also be seen in association with chronic anemia, chronic infection or treatment.

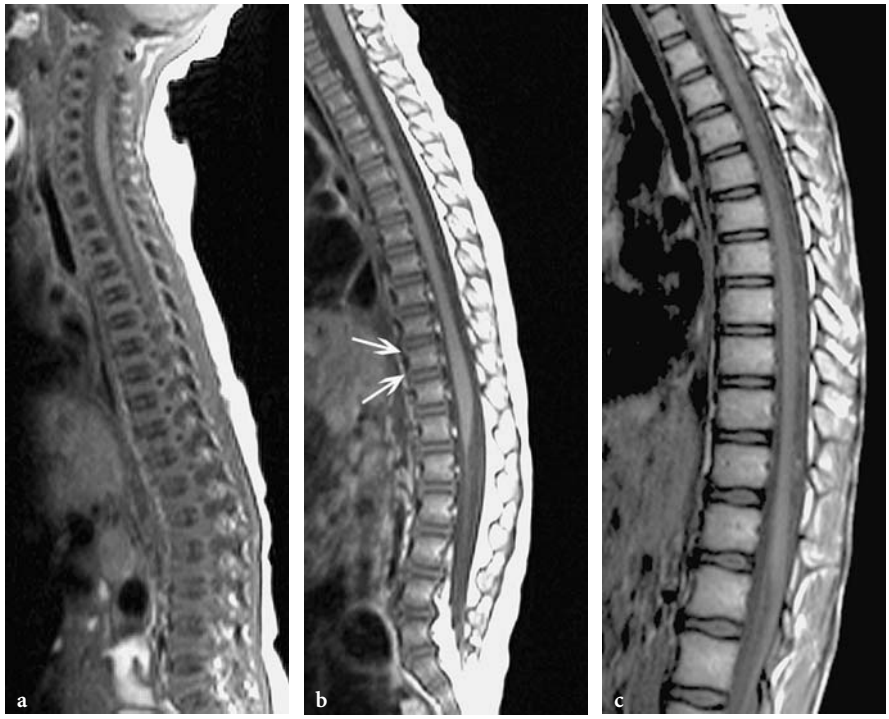

Fig. 21.1a–c. Sagittal T1-weighted SE images in a neonate (**a**), a 1-year-old boy (**b**) and a 14-year-old girl (**c**). Note the predominantly hematopoietic red marrow in the newborn (**a**) and the progressive conversion to yellow marrow (**b,c**). In the 1-year-old boy red marrow is seen at the endplates (**b**, *arrows*)

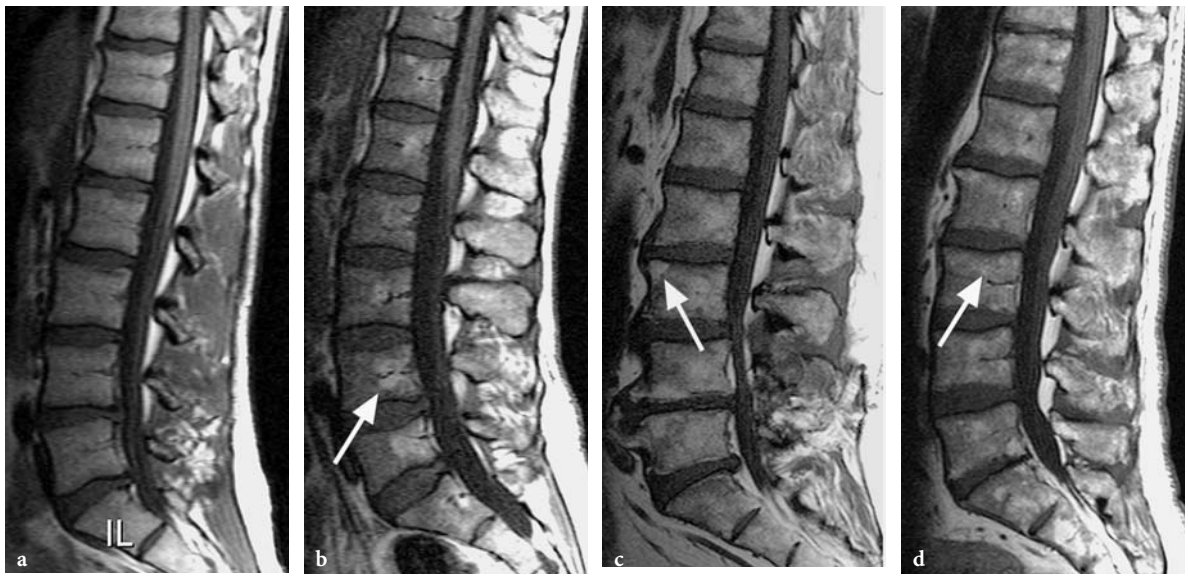

Fig. 21.2a-d. Sagittal T1-weighted SE images in a 28-year-old (**a**), a 41-year-old (**b**), a 50-year-old (**c**) and a 74-year-old (**d**) volunteer. A rather low bone marrow signal is seen in the younger volunteer, except for a linear area of high signal superior and inferior to the basivertebral vein (**b**, *arrow*). With increasing age, areas of linear or triangular hyperintensity become visible near the end plates and at the corners of the vertebral body (**c**, *arrow*). In addition, focal areas, ranging in size from 0.5 to 1.5 cm, and/or small dots measuring a few millimeters can be seen (**d**, *arrow*)

Bone marrow reconversion depends on numerous factors and the extent depends on the severity and duration of the stimulus (Weinreb 1990). The spine is affected first.

21.3 Imaging Approach

T1-weighted spin-echo images are recommended when the bone marrow is studied. Additional sequences are usually necessary, particularly when the signal of the red marrow is decreased, e.g. in infants or in adults with spontaneous or treatment-induced red marrow hyperplasia. Short tau inversion recovery (STIR) images are therefore routinely obtained in the study of the bone marrow (disorders). This technique, where an inversion time is chosen to cancel the signal of fat, yields T2-weighted images with fat suppression. Alternatively, one may choose opposed-phase gradient-echo images. By choosing an echo-time resulting in different phases of fat and water protons, the red marrow (containing equal amounts of fat and water) will return a low signal on the opposed-phase images compared to the in-phase images where yellow and red marrow cannot be differentiated. Bone marrow infiltration will behave in a similar way on in-phase and opposed-phase images (Seiderer et al. 1999).

T2-weighted fast spin-echo images are less useful in analyzing bone marrow disorders but are usually obtained to evaluate possible spinal cord compression and to exclude spinal cord pathology.

Following the injection of gadolinium chelates, the limited signal increase of normal bone marrow is less than 10% and is often barely or not visible. In bone marrow infiltration there will be a significant increase. Precontrast images are always necessary because the pathological enhancement may return a signal similar to that of the uninvolved yellow marrow. The main reason for obtaining gadolinium-enhanced images is the demonstration of intraspinal abnormalities.

Diffusion-weighted MR imaging has been successfully applied in differentiating benign osteoporotic fractures from malignant fractures and in assessing response to radiation and/or chemotherapy (Baur et al. 1998; Park et al. 2004). Malignant vertebral compression fractures return a high signal on diffusion-weighted MR images while benign compression fractures remain hypointense. This statement should be handled with caution because it has been demonstrated that vertebral metastases can return a low signal on diffusion-weighted images (Castillo et al. 2002). Diffusion-weighted images have been used to monitor the response to therapy (Byun et al. 2002). The authors found a decrease in the signal of metastases as early as 1 month after successful therapy.

Iron-oxide-based MR contrast agents have been administered in patients with malignancies of the hematopoietic system. Superparamagnetic iron oxides are taken up by the reticuloendothelial system in the red marrow, but not by neoplastic bone marrow (Daldrup-Link et al. 2002). The authors have used T1- and T2-weighted turbo spin-echo and STIR images, the latter being the best sequence for demonstrating signal changes after iron oxide administration.

More recently, dynamic contrast-enhanced MRI has been used in the hope of solving some of the remaining uncertainties in the analysis of the bone marrow. The authors have used a turbo FLASH T1-weighted technique and have shown that the maximum enhancement occurs within 1 min (Montazel et al. 2003). Differences were noted with increasing age and fat content. The maximum percentage of enhancement was higher in patients younger than 40 years. These high values in young patients probably correlate with the presence of hematopoietic bone marrow.

These authors have used the same technique to demonstrate that the maximum enhancement increased with the degree of bone marrow involvement reflecting angiogenesis in lymphoproliferative disorders (Scherer et al. 2002; Rahmouni et al. 2003).

Although bone marrow disorders of the spine are the main focus of this chapter, the "whole-body MRI" approach merits mention (Laffan et al. 2004). In this technique one sequence, usually a coronal STIR sequence, is repeated between two and four times (each 14–16 slices) to cover the head, neck, thorax, abdomen, pelvis, femora, tibiae and fibulae with a slice thickness that varies from 4 to 6 mm according to the region that was examined. In children with a suspected bone marrow disorder, this technique may prove to be a useful additional tool.

21.4 Bone Marrow Infiltration

Bone marrow lesions are not specific and can be seen in non-neoplastic as well as in neoplastic disorders.

The distribution of the lesions correlates with the hematopoietic marrow.

21.4.1 Multiple Myeloma

Multiple myeloma or morbus Kahler is characterized by a proliferation of plasma cells of B-lymphocyte origin, which produce monoclonal immunoglobulin. Monoclonal gammopathies are a premalignant condition of multiple myeloma. As a result of this infiltration and the bone resorption, abnormalities may be detected on X-rays or CT (Fig. 21.3). The appropriate therapy depends on the disease activity and may vary from alkylating agents and prednisone to high-dose chemotherapy, bone marrow transplantation and thalidomide therapy (Barlogie 2001; Kyle 2001). High-dose chemotherapy appears to be superior over conventional chemotherapy and bisphosphonates are frequently associated because of their anti-osteoclastic action (leading to fewer vertebral fractures). Thalidomide with its anti-angiogenetic activity has been shown to improve outcomes. Recently, a consensus report was published on the guidelines for treating myeloma (Durie et al. 2003). These consensus guidelines are largely based on the guidelines that have been compiled by the Guidelines Working Group of the UK Myeloma Forum (UK Myeloma Forum 2001).

Fig. 21.3. Sagittal reformatted spiral CT in a 57-year-old patient with M. Kahler, treated with thalidomide. Note the diffuse osteolytic areas and the thinning of the cortex in several vertebral bodies. A collapse of vertebral body L1 is seen with near disappearance of the posterior wall

The main role of imaging consists of: (1) detecting an expansile focal mass or diffuse disease, (2) depicting vertebral compression fractures, (3) assessing spinal cord compression and (4) assessing the response to therapy.

On MRI, the abnormalities are usually seen in the vertebrae, the proximal femur and humerus, corresponding to the adult areas of the red marrow distribution. This can be explained by the vascularity of red marrow. MRI of the pelvis is recommended in the diagnostic work-up (Fig. 21.4).

Three MRI patterns have been described: (1) normal (up to 20% of patients with stage III multiple myeloma), (2) focal involvement and (3) diffuse involvement (Vande Berg et al. 1998). Typically the bone marrow infiltration is characterized by a decreased signal (compared to the intervertebral disc) on spin-echo T1-weighted images. This has been called the "bright disc sign" (Castillo et al. 1990). The focal lesions may be surrounded by a halo on T2-weighted images corresponding to active disease (Schweitzer et al. 1993).

The so-called "salt and pepper" pattern consists of multiple tiny foci of low signal on T1-weighted spin-echo images with enhancement on postcontrast images (Moulopoulos et al. 1997) (Fig. 21.5). On the fat-suppression T2-weighted images there is intermediate to high signal.

The diffuse involvement carries the worst prognosis while the "salt and pepper" and the "normal" MR pattern have a significantly better outcome.

The bone marrow involvement and bone resorption lead to osteoporosis and an increased risk of vertebral fractures in patients with multiple myeloma (Fig. 21.6). Vertebral fractures occur in up to 70% of the patients with multiple myeloma (Lecouvet et al 1997a). The differential diagnosis between benign and malignant vertebral fractures will be discussed in Chap. 10. More than 60% of the vertebral fractures in multiple myeloma are benign and are characterized by the partial preservation of normal marrow, the displacement of the posterior wall usually without involvement of the pedicles and without soft-tissue component (Fig. 21.7). This is thought to be due to osteoclast activating factors that may play a role in addition to the marrow infiltration (Moulopoulos et al. 1992).

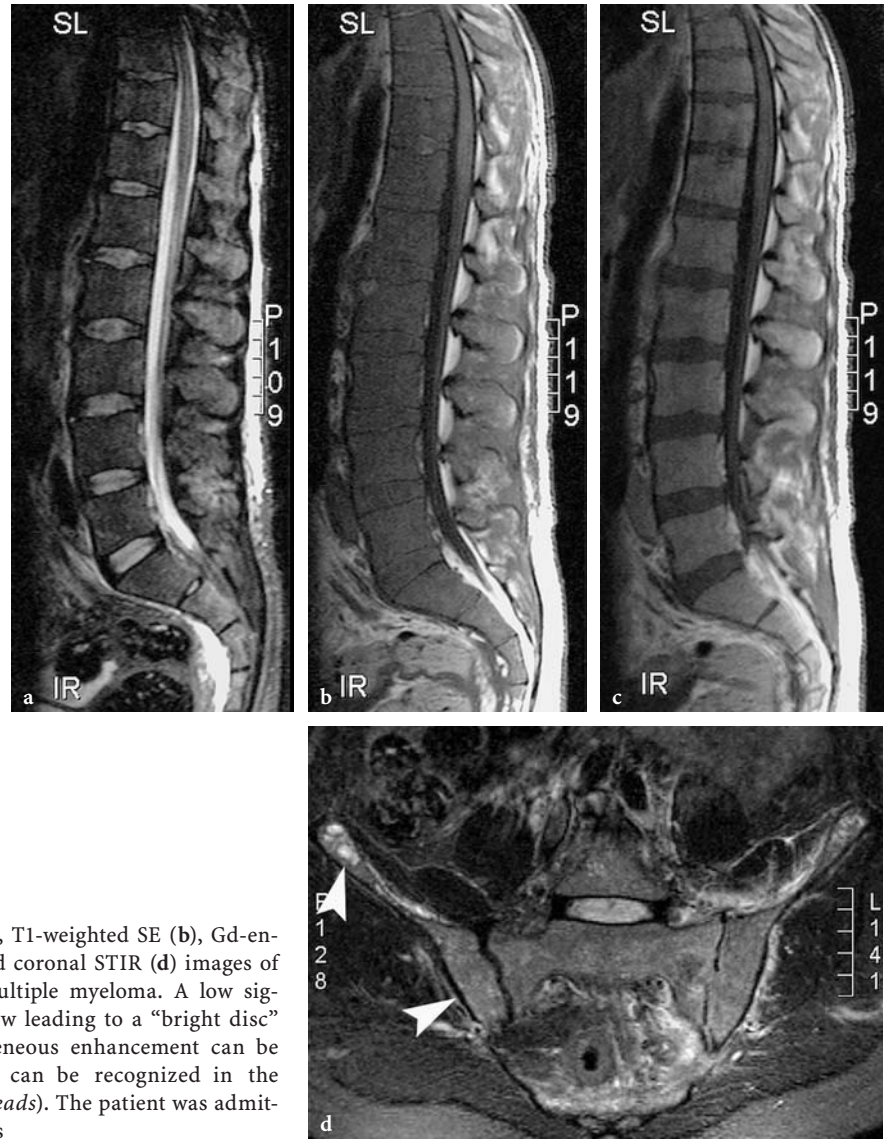

Fig. 21.4a–d. Sagittal STIR (**a**), T1-weighted SE (**b**), Gd-enhanced T1-weighted SE (**c**) and coronal STIR (**d**) images of a 43-year-old patient with multiple myeloma. A low signal is seen in the bone marrow leading to a "bright disc" sign and a moderate homogeneous enhancement can be observed (**b,c**). Multiple foci can be recognized in the sacrum and ilium (**d**, *arrowheads*). The patient was admitted with a left-sided sacroiliitis

Leptomeningeal spread of multiple myeloma within the central nervous system occurs in approximately 1% of the patients (Fassas et al. 2002). The MR findings resemble those of leptomeningeal metastases or pial involvement by lymphoma (Fig. 21.8). It is of interest to note that this manifestation of multiple myeloma seems to be associated with chromosome 13 deletion, plasmablastic cells on histology, other extramedullary sites of disease and plasma cell leukemia (Fassas et al. 2002).

MRI does not only play a role in the diagnostic work-up of a suspected multiple myeloma patient but also has a prognostic value. Recently, MRI has been added as a supplement to the clinical staging system of Durie and Salmon (Durie and Salmon 1975; Baur et al. 2002). That clinical staging system is based on the detection of a monoclonal M protein in serum and urine (and serum hemoglobin and calcium), the presence of bone lesions on X-ray and renal function. Patients with lytic lesions on X-ray correspond to stage III multiple myeloma. Patients with more than ten focal lesions or with diffuse bone marrow involvement are considered stage III patients and at are a higher risk for vertebral fractures (Lecouvet et al 1997b; Baur et al 2002). The use of a dynamic contrast material-enhanced turbo FLASH T1-weighted technique has been successfully applied in a limited number of patients to differentiate vertebrae that fracture during follow-up from those that do not (Scherer et al. 2002). These are

Fig. 21.5a–d. Sagittal T2-weighted TSE (**a**), STIR (**b**), T1-weighted SE (**c**) and Gd-enhanced T1-weighted SE (**d**) of a 73-year-old patient with multiple myeloma. The bone marrow appears heterogeneous with multiple tiny focal areas of low signal which enhance following the administration of Gd (**c,d**). This is characteristic of the so-called "salt and pepper" pattern. Note the recent collapse of vertebral body C6 (**b**, *arrow*)

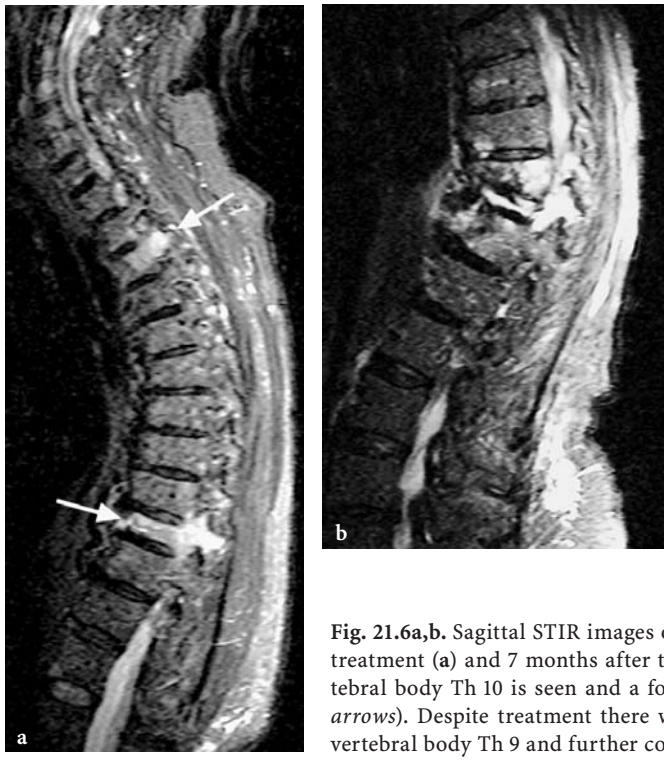

Fig. 21.6a,b. Sagittal STIR images of a 70-year-old patient with multiple myeloma before treatment (**a**) and 7 months after treatment with chemotherapy (**b**). The collapse of vertebral body Th 10 is seen and a focal lesion is clearly visible in vertebral body Th 3 (**a**, *arrows*). Despite treatment there was a progression of the disease with involvement of vertebral body Th 9 and further collapse of Th 10 (**b**)

Fig. 21.7a–c. Sagittal STIR (**a**), T1-weighted SE (**b**) and axial Gd-enhanced T1-weighted SE (**c**) images in a 60-year-old patient with multiple myeloma. There is bone marrow infiltration at the level C4–C6 with collapse of the vertebral body C5, resulting in spinal cord compression (**a**, *arrowheads*). On the axial image the extent of the paraspinal and epidural component is clearly visible (**c**, *arrowheads*)

Fig. 21.8a–d. Sagittal T1-weighted SE (**a,b**) and Gd-enhanced T1-weighted SE (**c,d**) in a 48-year-old patient with multiple myeloma. Note the collapse of vertebral body Th 10 and to a lesser extent Th 5 and the presence of both an epidural mass (**a**, *black arrowhead*) and enhancing pial lesions along the cauda equina (**c**, *white arrowheads*). These lesions have disappeared following autologous bone marrow transplantation and radiotherapy (**b,d**)

preliminary but hopeful results. Patients without MR changes are considered stage I patients. Patients with stage I disease and bone marrow abnormalities on MR show a more progressive disease (Vande Berg et al. 1996). The remainder of the patients are stage II. A tumour mass index on MRI correlates plasma cell percentage and serum beta-2 microglobulin levels (Carlson et al. 1995). In a series of 77 patients it was shown that without taking into account the MR findings, about one third of the patients are understaged (Baur et al. 2002).

A radiological classification and grading of the bone marrow changes has been proposed (Laroche et al. 1996; Mahnken et al. 2002). Multidetector CT using thin-collimation protocols proved particularly useful for assessing the thoracic spine. Diffuse osteopenic bone is considered grade 1, lacunae > 5 mm grade 2 and nodular lesions grade 3a or, if fractured, grade 3b.

Patients with a solitary bone lesion without systemic involvement and with limited serum and biopsy changes may benefit from an MR screening of the spine and pelvis. Most of these patients will develop morbus Kahler and the detection of abnormalities in these patients is correlated with an earlier development of systemic disease. The detection of additional bone marrow lesions is associated with a poor response to the therapy.

Posttreatment changes may vary from unchanged appearance to decreasing size of the lesions and of the enhancement. Response to treatment has been found to correlate with a decrease or disappearance of the focal lesions or diffuse disease (Lecouvet et al. 2001) (Fig. 21.9). The reappearance of fatty marrow can also be observed (Fig. 21.10). Myelofibrosis or amyloidosis can develop secondary to the treatment. The latter consists of focal areas of low signal in the bone marrow while myelofibrosis can be recognized as a diffuse conversion of the bone marrow with low signal on both T1-weighted images and STIR images.

Until now the value of MRI in the follow-up after treatment is limited. T2-weighted images have been considered less useful because lesions remained hyperintense even in good and partial responders. This has been related to necrotic changes. Until now it is accepted that the T1-weighted images before and after administration of contrast are the best way of demonstrating the effect of treatment, although there is no proof of its clinical value. There have been attempts to assess the prognostic significance of MRI before and after bone marrow transplantation but without clear conclusions (Figs. 21.6, 21.8 and 21.9) (Agren et al 1998; Lecouvet et al. 2001). With the introduction of new high-dose chemotherapeutic agents and new angiogenesis drugs, which induce a reconversion of the yellow marrow with increase in cellularity, it has become more difficult to differentiate bone marrow reconversion from cellular infiltration. One of the interesting paths to solve this problem is the administration of iron-oxide based contrast agents. The reconverted bone marrow will take up the iron oxides while tumorous marrow infiltration will not (Daldrup-Link et al. 2002).

On the other hand, positron emission tomography with fluorodeoxyglucose (FDG-PET) has been found useful in the detection of recurrent (extra)medullary disease in patients with normal routine imaging findings (Schirrmeister et al. 2002).

Some attention should be paid to monoclonal gammopathy of uncertain significance (MGUS). This is usually an incidental finding but the disease can evolve to multiple myeloma, chronic lymphocytic leukemia or lymphoma in 11%–24% of the patients (Fig. 21.9) (Bellaiche et al. 1997). In a series of patients with MGUS, abnormalities were found on MR in 20% of the cases (Vande Berg et al. 1997). Treatment was required within 5 years of diagnosis in 55% of the patients with MR changes, but not in the patients without MR changes.

21.4.2 Malignant Lymphoma

Involvement of the bone marrow is uncommon at diagnosis, but Hodgkin's disease is associated with 10%–15% of marrow infiltration in relapses (Smith et al. 1991). The involvement is detected more often with MRI than with bone marrow biopsy (Varan et al. 1999). The value of a bone marrow biopsy is controversial in Hodgkin's disease and only a small proportion of the patients have positive bone marrow aspirates in the early stages (Sandrasegaran et al. 1994).

The detection of non-Hodgkin lymphoma on MRI depends on the histological subtype, which will determine therapy and prognosis. Low-grade lymphoma can remain undetectable partly due to the rather diffuse bone marrow involvement. In these patients a biopsy is warranted. The follicular or paratrabecular low-grade lymphoma is often associated with normal MR findings.

Fig. 21.9a–c. Sagittal T1-weighted SE (**a**) and STIR (**b,c**) images in an 80-year-old patient with monoclonal gammopathy of unknown significance. Several focal bone marrow lesions can be recognized (**a,b**, *arrowheads*). Note the disappearance of the lesions following treatment (**c**)

Fig. 21.10. Sagittal T1-weighted SE images in a 45-year-old patient who underwent radiotherapy of the lower abdominal region. Note the fatty replacement of the bone marrow in the lower lumbar spine

Intermediate and high-grade lymphoma present as focal marrow lesions and hence MRI plays a more important role in the diagnostic work-up (Fig. 21.11).

Primary leptomeningeal lymphoma without vertebral abnormality is extremely rare (Fig. 21.12) (Carlson et al. 2003). This subtype is thought to arise from lymphocytes that can be found in the vicinity of the meninges. Usually diffuse enhancement of the nerve roots can be observed although occasionally nodular lesions can be seen along the cauda equina. The recognition of the MR abnormalities in the adequate clinical context may aid in a rapid diagnosis. Early treatment with corticosteroids and irradiation with/without intrathecal chemotherapy is the treatment that has been suggested. Although there have been reports on successful treatments, prognosis is usually poor with a median survival time of 8 months.

Primary spinal epidural lymphoma is slightly more common than the leptomeningeal subtype (Boukobza et al. 1996). In this subtype both epidural extension from adjacent vertebral lesions and haematogenous spread have been put forward as possible mechanisms. The infiltrative growth through the foramen is typical of lymphoma and can be used in the differential diagnosis with metastases. Epidural masses are more common in lymphoma than in metastases.

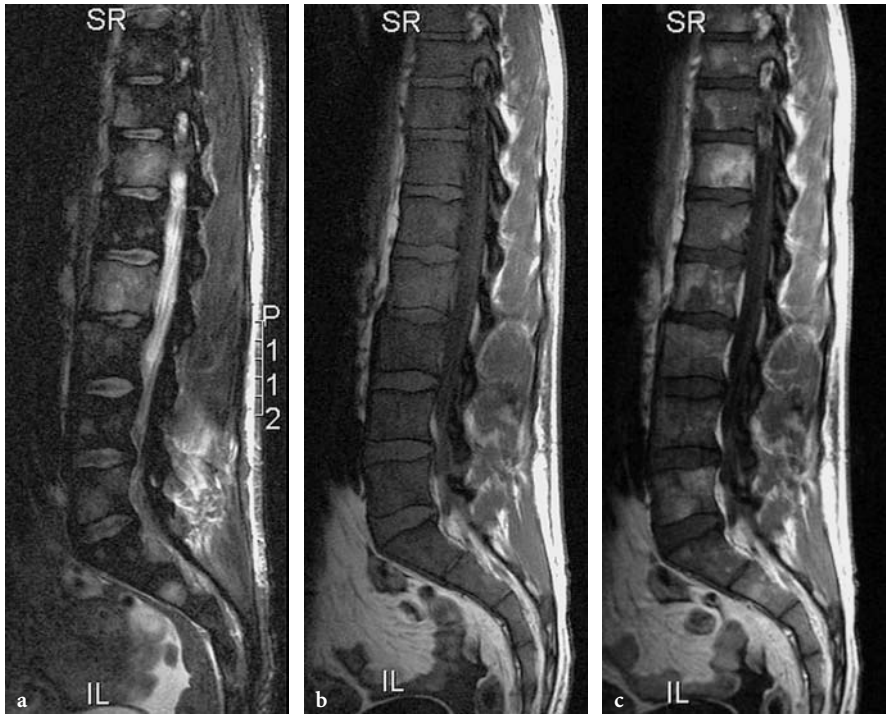

Fig. 21.11a–c. Sagittal STIR (**a**), T1-weighted SE (**b**) and Gd-enhanced T1-weighted SE (**c**) images in a 40-year-old patient with an anaplastic cutaneous T-cell lymphoma. Note the multifocal diffuse bone marrow involvement (**a,c**) and the diffuse low signal of the bone marrow (**b**)

Fig. 21.12a,b. Sagittal T1-weighted SE (**a**) and Gd-enhanced T1-weighted SE (**b**) images in a 58-year-old patient, known to have had M. Kahler for 8 years, with a non-Hodgkin B-cell lymphoma. Note the leptomeningeal lymphoma (**b**, *arrowheads*). The bone marrow changes may reflect lymphoma and/or the residual changes after treatment for M. Kahler

21.4.3 Leukaemia

Leukaemias are composed of marrow accumulations of mature and immature granulocytes in myeloid and lymphocytes in lymphocytic leukaemia. While immature cells proliferate in acute leukaemia, more differentiated cells are encountered in chronic leukaemia. A myelodysplastic syndrome, characterized by peripheral cytopenia, a (hyper)cellular bone marrow and frequent cytogenic abnormalities, may precede acute leukaemia.

MRI usually demonstrates a diffuse decrease of the bone marrow signal on T1-weighted spin-echo images but in one series of 21 patients two-thirds of the patients with early chronic lymphocytic leukaemia had normal MR findings (Lecouvet et al. 1997c) (Fig. 21.13). Perhaps the signal intensity correlates with the aggressiveness of the chronic lymphocytic leukaemia, but the clinical experience of MRI in leukaemia is limited (Vande Berg et al. 1998). The hope that methods such as bulk T1 relaxation time measurement, chemical shift imaging or spectroscopy might improve the demonstration of marrow involvement seems until now only partly fulfilled. Sequential quantitative MRI proved valuable for the prediction of response in patients with acute lymphatic leukaemia but not in those with acute myeloid leukaemia (Vande Berg et al. 1995).

21.4.4 Langerhans Cell Histiocytosis

Langerhans cell histiocytosis (histiocytosis X) is a neoplastic disorder associated with bone marrow histiocytosis and is therefore classified in a group of diseases including myeloid leukaemia, non-Hodgkin's lymphoma and Hodgkin's disease. In this chapter attention will only be briefly paid to multifocal histiocytosis (Fig. 21.14). We refer to Chapter 20 for a review of the solitary eosinophilic granuloma.

The bone and the bone marrow are involved and the diagnosis is usually made by the demonstration of Langerhans cells on the biopsy. There is a predilection for the flat bones, particularly the skull, followed by the pelvis, spine and mandible.

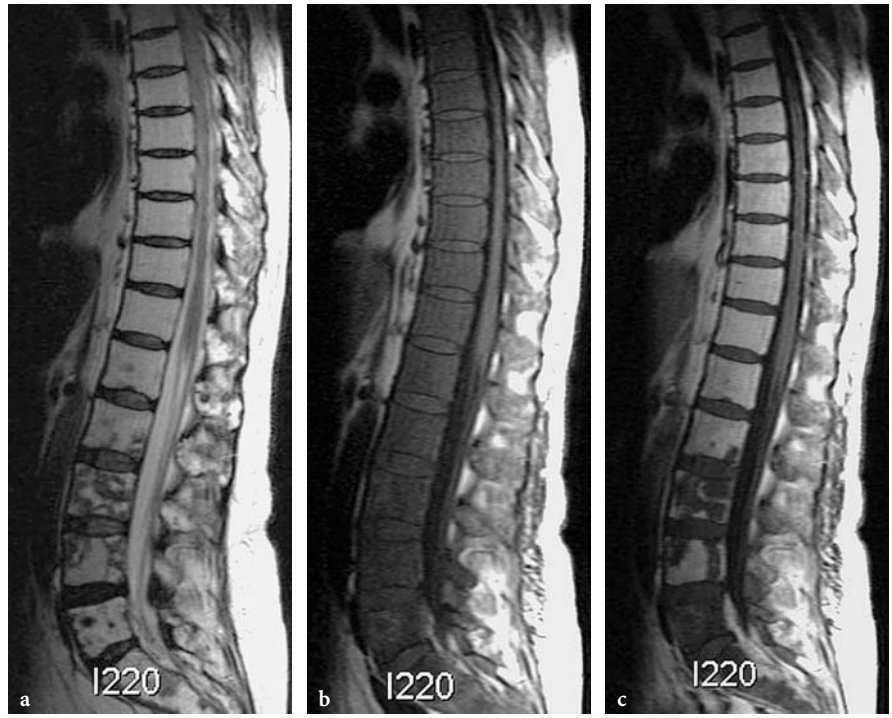

Fig. 21.13a–c. Sagittal T2-weighted TSE (**a**), T1-weighted SE (**b**) and Gd-enhanced T1-weighted SE (**c**) in a 53-year-old patient treated for a carcinoma of the cervix and who developed chronic myelogenous leukaemia. The bone marrow returns a homogeneous low signal (**b**). Following the administration of Gd, there is a multifocal enhancement in the lower lumbar vertebrae and a homogeneous pathological enhancement in the thoracolumbar spine

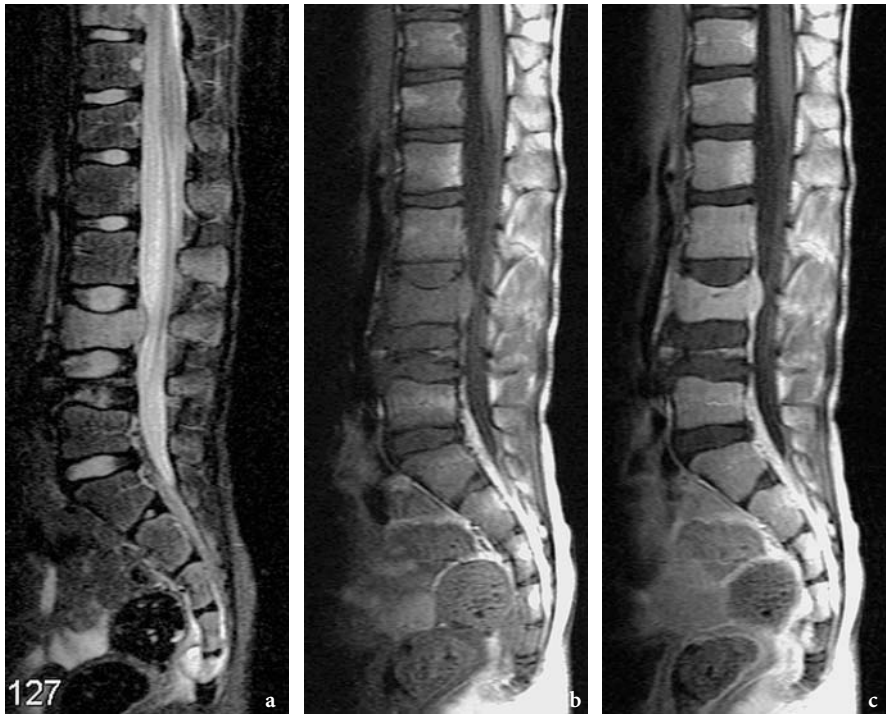

Fig. 21.14a–c. Sagittal STIR (**a**), T1-weighted SE (**b**) and Gd-enhanced T1-weighted SE (**c**) images in a 12-year-old patient with Langerhans cell histiocytosis. Apart from the "vertebra plana" L4 and the partial collapse of vertebra L3, several focal lesions can be observed. Note the involvement of S5 and the bulging of the posterior wall of vertebral body L3

Vertebral body involvement may cause collapse, resulting in vertebra plana.

MRI shows a clear preservation of the disc space, which is an important observation in differentiating the lesion from infection (Tan et al. 2004; Azouz et al. 2004). The classical appearance consists of two intervertebral discs in apposition without intervening vertebral body. There may be an associated epidural soft tissue mass.

Bone marrow involvement by Langerhans cell histiocytosis should be distinguished from metastatic disease, leukaemia and large cell lymphoma.

Recently, whole-body STIR MRI has been compared to (99m)Tc-methylene diphosphonate scintigraphy in children with multiple bone lesions and MRI proved to be feasible as a screening modality in, e.g., Langerhans cell histiocytosis in children (Mentzel et al. 2004).

21.4.5 Differential Diagnosis

Several aspects merit discussion here. It is important to realize that bone marrow involvement is a non-specific observation that may be observed in neoplastic as well as in non-neoplastic bone marrow disorders.

The observation of reactive bone marrow changes in unaffected vertebrae of patients with infectious spondylitis is probably the best illustration of the non-specificity of this finding (Stäbler at al. 2000). It should be borne in mind that reactive bone marrow stimulation may occur in many instances leading to changes in bone marrow cellularity. Bone marrow cellularity does not always reflect a bone marrow disease and may be influenced by smoking, endurance activities, various drug therapies and hemolytic disorders (see Fig. 21.2). The MR signal changes, however, are similar to those occurring in malignant disease, myeloproliferative diseases and haematological neoplasia and may therefore represent a difficult differential diagnosis.

The distinction between haematological malignancies and metastases is not always clear.

Lymphoproliferative disorders tend to lead to a diffuse involvement while metastases are characterized by a (multi)focal involvement. Involvement of the anterior elements of vertebrae is unusual in hematopoietic malignancies which seem to have a pre-

dilection for the posterior vertebral elements (Kim et al. 1999) (Figs. 21.6, 21.7).

There have been attempts to differentiate lymphoma from myeloma and metastases (Moulopoulos et al. 1999). The authors found a paravertebral soft tissue mass without affecting the shape or contour of the bone in 92% of their patients with stage IV lymphoma. They introduced the term "wrap-around" sign. This sign was never observed in their patients with myeloma and metastases when contour alterations and/or cortical destruction were always present (Fig. 21.7).

Finally, it can be very difficult to differentiate haematological malignancies from red marrow hyperplasia. In red marrow hyperplasia the signal intensity on T2 is usually less pronounced and gadolinium-enhancement is absent.

References

Agren B, Rudberg U, Isberg B et al. (1998) MR imaging of multiple myeloma patients with bone marrow transplants. Acta Radiol 39:36–42

Altehoefer C, Schmid A, Büchert M et al. (2002) Characterization of hematopoietic bone marrow in male professional cyclists by magnetic resonance imaging of the lumbar spine. J Magn Res Imag 16:284–288

Azouz E, Saigal G, Rodriguez MM et al. (2004) Langerhans' cell histiocytosis: pathology, imaging and treatment of skeletal involvement. Pediatric Radiology 35:103–115

Barlogie B (2001) High-dose therapy and innovative approaches to treatment of multiple myeloma. Semin Hematol 38:21–27

Baur A, Stäbler A, Bruning R et al. (1998) Diffusion-weighted MR imaging of bone marrow: differentiation of benign versus pathologic compression fractures. Radiology 207:349–356

Baur A, Stäbler A, Nagel D et al. (2002) Magnetic resonance imaging as a supplement for the clinical staging system of Durie and Salmon. Cancer 95:1334–1345

Bellaiche L, Laredo JD, Liote F et al. (1997) Magnetic resonance appearance of monoclonal gammopathies of unknown significance and multiple myeloma. Spine 22:2551–2557

Boukobza M, Mazel C, Touboul E (1996) Primary vertebral and spinal epidural non-Hodgkin's lymphoma with spinal cord compression. Neuroradiology 38:333–337

Byun WM, Shin SO, Chang Y et al. (2002) Diffusion-weighted MR imaging of metastatic disease of the spine: assessment of response to therapy. Am J Neuroradiol 23:906–912

Carlson K, Astrom G, Nyman R et al. (1995) MR imaging of multiple myeloma in tumour mass measurement of diagnosis and during treatment. Acta Radiol 36:9–14

Carlson CL, Hartman R, Ly JQ et al. (2003) Primary leptomeningeal lymphoma of the lumbar spine. J Clin Imaging 27:389–393

Castillo M, Malko JA, Hoffman JC Jr (1990) The bright intervertebral disk: an indirect sign of abnormal spinal bone marrow on T1-weighted MR images. Am J Neuroradiol 11:23–26

Castillo M, Arbelaez A, Smith JK et al. (2002) Diffusion-weighted MR imaging offers no advantage over routine noncontrast MR imaging in the detection of vertebral metastasis. Am J Neuroradiol 21:948–953

Daldrup-Link HE, Rummeny EJ, Ihssen B et al. (2002) Iron-oxide-enhanced MR imaging of bone marrow in patients with non-Hodgkin's lymphoma: differentiation between tumor infiltration and hypercellular bone marrow. Eur Radiol 12:1557–1566

Durie BGM, Salmon SE (1975) A clinical staging system for multiple myeloma: correlation of measured myeloma cell mass with presenting clinical features, response to treatment and survival. Cancer 36:842–854

Durie BGM, Kyle RA, Belch A et al (2003) Myeloma management guidelines: a consensus report from the Scientific Advisors of the International Myeloma Foundation. Hematol J 4:379–398

Fassas A, Muwalla F, Berryman T et al. (2002) Myeloma of the central nervous system: association with high-risk chromosomal abnormalities, plasmablastic morphology and extramedullary manifestations. Br J Haematol 117:103–108

Kim HJ, Ryu KN, Choi WS et al. (1999) Spinal involvement of hematopoietic malignancies and metastasis: differentiation using MR imaging. Clin Imaging 23:125–133

Kyle RA (2001) Multiple myeloma: diagnostic challenges and standard therapy. Semin Hematol 38:11–14

Laroche M, Assoun J, Sixou L et al. (1996) Comparison of MRI and computed tomography in the various stages of plasma cell disorders: correlation with biological and histological finding. Clin Exp Rheumatol 14:171–176

Laffan EE, O'Connor R, Ryan SP (2004) Whole-body magnetic resonance imaging: a useful additional sequence in paediatric imaging. Pediatr Radiol 34:472–480

Lecouvet FE, Vende Berg BC, Maldague BE et al. (1997a) Vertebral compression fractures in multiple myeloma. Part I. Distribution and appearance at MR imaging. Radiology 204:195–199

Lecouvet FE, Malghem J, Michaux L et al. (1997b) Vertebral compression fractures in multiple myeloma. Part II. Assessment of fracture risk with MR imaging of spinal bone marrow. Radiology 204:201–205

Lecouvet FE, Vande Berg BC, Michaux L et al. (1997c) Early chronic lymphocytic leukemia: prognostic value of quantitative bone marrow MR imaging findings and correlation with hematologic variables. Radiology 204:813–818

Lecouvet FE, Dechambre S, Malghem J et al. (2001) Bone marrow transplantation in patients with multiple myeloma: prognostic significance of MR imaging. AJR Am J Roentgenol 176:91–96

Mahnken AH, Wildberger JE, Gehbauer G et al. (2002) Multidetector CT of the spine in multiple myeloma: comparison with MR imaging and radiography. AJR Am J Roentgenol 178:1429–1436

Mentzel HJ, Kentouche K, Sauner D et al. (2004) Comparison of whole-body STIR-MRI and (99m)Tc-methylene diphosphonate scintigraphy in children with suspected multiple bone lesions. Eur Radiology 14(12):2297-302

Montazel J-L, Divine M, Lepage E et al. (2003) Normal spinal bone marrow in adults: dynamic gadolinium-enhanced MR imaging. Radiology 229:703–709

Moore SG, Dawson KL (1990) Red and yellow marrow in the femur: age-related changes in appearance at MR imaging. Radiology 175:219–223

Moulopoulos LA, Varma DGK, Dimopoulos MA et al. (1992) Multiple myeloma: spinal MR imaging in patients with untreated newly diagnosed disease. Radiology 185:833–840

Moulopoulos L, Dimopoulos M (1997) Magnetic resonance imaging of the bone marrow in hematological malignancies. Blood 90:2127–2147

Moulopoulos LA, Dimopoulos MA, Vourtsi A et al. (1999) Bone lesions and soft-tissue mass: magnetic resonance imaging diagnosis of lymphomatous involvement of the bone marrow versus multiple myeloma and bone metastases. Leuk Lymphoma 34:179–184

Park S-W, Lee J-H, Ehara S et al. (2004) Single shot fast spin echo diffusion weighted MR imaging of the spine. Is it useful in differentiating malignant metastatic tumor infiltration from benign fracture edema. Clin Imaging 28:102–108

Rahmouni A, Montazel J-L, Divine M et al. (2003) Bone marrow with diffuse tumor infiltration in patients with lymphoproliferative diseases: dynamic gadolinium-enhanced MR imaging. Radiology 229:710–717

Ricci C, Cova M, Kang YS et al. (1990) Normal age related patterns of cellular and fatty bone marrow distribution in the axial skeleton: MR imaging study. Radiology 177:83–88

Sandrasegaran K, Robinson PJ, Selby P (1994) Review: staging of lymphoma in adults. Clin Radiol 49:149–161

Scherer A, Strupp C, Wittsack H-J et al. (2002) Dynamic contrast-enhanced MRI for evaluating bone marrow microcirculation in malignant hematological diseases before and after thalidomide therapy. Radiologe 42:222–230

Scherer A, Wittsack H-J, Strupp C et al. (2002) Vertebral fractures in multiple myeloma: first results of assessment of fracture risk using dynamic contrast-enhanced magnetic resonance imaging. Ann Hematol 81:517–521

Schirrmeister H, Bommer M, Buck AK et al. (2002) Initial results in the assessment of multiple myeloma using F-18 FDG PET. Eur J Nucl Med Mol Imaging 29:361–366

Schweitzer ME, Levine C, Mitchell DG et al. (1993) Bull's eyes and halos: useful MR discriminators of osseous metastases. Radiology 188:249–252

Seiderer M, Stäbler A, Wagner H (1999) MRI of bone marrow: opposed-phase gradient-echo sequences with long repetition time. Eur Radiol 9:652–661

Smith SR, Williams CE, Edwards RH et al. (1991) Quantitative magnetic resonance studies of lumbar vertebral marrow in patients with refractory or relapsed Hodgkin's disease. Ann Oncol 2[Suppl 2]:39–42

Stäbler A, Doma AB, Baur A et al. (2000) Reactive bone marrow changes in infectious spondylitis: quantitative assessment with MR imaging. Radiology 217:863–868

Sze G, Bravo S, Baierl P et al. (1991) Developing spinal column: gadolinium-enhanced MR imaging. Radiology 180:497–502

Tan G, Samson I, De Wever I et al. (2004) Langerhans cell histiocytosis of the cervical spine: a single institution experience in four patients. J Ped Orthop B 13:123–126

UK Myeloma Forum (2001) Guideline: diagnosis and management of multiple myeloma. Br J Haematol 115:522–540

Vande Berg BC, Schmitz PJ, Scheiff M et al. (1995) Acute myeloid leukemia: lack of predictive value of sequential quantitative MR imaging during treatment. Radiology 197:301–305

Vande Berg BC, Lecouvet FE, Michaux L et al. (1996) Stage I multiple myeloma: value of MR imaging of the bone marrow in the determination of prognosis. Radiology 201:243–246

Vande Berg BC, Lecouvet FE, Michaux L et al. (1997) Nonmyelomatous monoclonal gammopathy: correlation of bone marrow MR images with laboratory findings and spontaneous clinical outcome. Radiology 202:247–251

Vande Berg BC, Lecouvet FE, Michaux L et al. (1998) Magnetic resonance imaging of the bone marrow in hematological malignancies. Eur Radiol 8:1335–1344

Varan A, Cila A, Buyukpamukcu M (1999) Prognostic importance of magnetic resonance imaging in bone marrow involvement of Hodgkin disease. Med Pediatr Oncol 32:267–271

Vogler JB, Murphy WA (1988) Bone marrow imaging. Radiology 168:679–693

Weinreb JC (1990) MR imaging of bone marrow: a map could help. Radiology 177:23–24

Infection and Inflammation

Spinal Infections

22

Majda M. Thurnher

CONTENTS

22.1 Introduction

Spinal infection is a significant cause of morbidity. Despite advances in antibiotic treatment regimens, the incidence is not decreasing. Several factors can make people more vulnerable to spinal infections, including immunodeficiency secondary to human immunodeficiency virus (HIV) infection or intravenous drug abuse, old age, chronically debilitated individuals, the widespread use of broad-spectrum antibiotics, the use of corticosteroids and immunosuppressive drugs and parenteral alimentation. Clinical symptoms most often include back pain, sensory motor deficits, fever, and obtundation. Fever, however, may not be prominent, and body temperature can be normal in patients with chronic infection. Mechanical compression is the most common cause of functional compromise of the spinal cord, and deterioration secondary to ischemic compromise is often seen. Magnetic resonance imaging is the method of choice and gold standard in detecting infectious spine diseases. Sensitivity, specificity, and accuracy are reported as 96, 92, and 94%, respectively (Tins and Cassar-Pullicino 1996). The MR imaging protocol should include unenhanced T1-weighted images (WI) and T2WI, short tau inversion recovery (STIR) T2WI, and contrast-enhanced T1WI. The most detailed information is provided by contrast-enhanced T1WI with fat suppression (Longo et al. 2003).

The pathogens can reach the spine by four principal routes of spread: (a) the arterial hematogenous route from distant septic foci; (b) the venous hematogenous route; (c) from septic foci of adjacent soft tissue; and (d) direct inoculation (iatrogenic during surgery or interventional procedures). Iatrogenic spinal infections constitute 2.5% of all spinal infections (Tins and Cassar-Pullicino 2004). The infection risk of discography is reported to be approximately 1%, and for open surgery this rises to 3–13%. Myelography, chemonucleolysis, vertebroplasty, and kyphoplasty are other known causes of spinal infection. The use of vertebroplasty for the treatment of osteoporotic compression fractures has been described and recommended in the medical literature; however, in addition to possible complications that include nerve entrapment, and complications related to cement or fat emboli, serious pyogenic spondylitis has been reported (Yu et al. 2004).

M. M. Thurnher, MD
Associate Professor of Radiology, Neuroradiology Section, Department of Radiology, University Hospital Vienna, Waehringer Guertel 18–20, 1090 Vienna, Austria

KEY-POINTS

- Clinical symptoms of spinal infection
  - Back pain
  - Sensory motor deficits
  - Fever: sometimes not prominent especially in chronic infection
- MR is the imaging method of choice with an accuracy of 94%
  - Should include T1WI and T2WI, especially fat-suppressed T2WI (STIR)
  - Should also include gadolinium-enhanced fat-suppressed T1WI
- Possible routes of infection:
  - Arterial from distant septic foci
  - Venous
  - Adjacent infected tissue
  - Direct inoculation (trauma, interventions, and surgery): 2.5% of all spinal infections
- Most common infectious agents:
  - Overall: Staphylococcus aureus (62%)
  - For each category:
    - Bacterial: Staphylococcus aureus followed by Enterobacter, Salmonella, Pseudomonas, and Serratia
    - Viral: cytomegalovirus and herpes simplex
    - Fungal: Candida followed by Aspergillus
    - Parasitic: Toxoplasmosis, Cysticercosis
- Bacterial spondylodiscitis:
  - Symptoms for >3 months in 50% of patients
  - Fever in 50% of patients
  - Elevated sedimentation rate in 50% of patients
  - Elevated white blood cell count in 50% of patients
  - 50% in lumbar, 35% thoracic
  - MR
    - Vertebral bodies:
      - Low SI on T1WI
      - High SI on T2WI
      - Strong enhancement
    - Intervertebral disk:
      - High SI on T2WI
      - Loss of intranuclear cleft
      - Peripheral enhancement
- Bacterial epidural abscess:
  - Peak in sixth and seventh decade
  - Predisposing factors:
    - Diabetes
    - IV drug abuse
    - Chronic renal failure
    - Immunodeficiency
    - Cirrhosis
  - Sometimes difficult to visualize on T2WI, postcontrast imaging essential
- Tuberculous spondylodiscitis/spondylitis:
  - Subligamentous spread with consecutive involvement of adjacent vertebrae
  - Sometimes multiple vertebrae at multiple sites
  - Skip lesions in 4% of cases
  - Paraspinal soft tissue involvement in three of four adults and 98% of children
- TB versus pyogenic:
  - TB: well-defined paraspinal changes, smooth enhancement of abscess walls
  - Pyogenic: ill-defined paraspinal changes, thick, irregular abscess wall
- Viral infections:
  - HIV
    - Vacuolar myelopathy
    - Sensorimotor deficit in lower extremities, gait, and urinary disorders
    - Bilaterally symmetrical high SI on T2WI, predominantly in lateral and dorsal parts of the spinal cord
  - CMV and herpes simplex:
    - Polyradiculitis
    - Myelitis
- Fungal infections:
  - Primarily opportunistic in immuno-compromised patients
  - Spondylodiscitis/spondylitis
- Parasitic infections
  - Toxoplasmosis:
    - AIDS patients but even then rare
  - Cysticercosis
    - Spinal involvement in 0.7–5.9% of cases
    - All patients with spinal cysticercosis have cerebral involvement
    - Most commonly subarachnoid infection

Staphylococcus aureus is the predominant organism and is found in 62% of all spinal infections. Proteolytic enzymes enable the spread of the infection into the vertebral bodies and the disc. The spread of the infection in pathogens that do not produce proteolytic enzymes (e.g., *Mycobacterium tuberculosis*) is much more slowly with late clinical presentation.

22.2 Bacterial Infections

Pyogenic infections have a peak age incidence in the sixth to seventh decades. The number of cases of spondylodiscitis is on the rise in industrial countries due to immigration, the spread of acquired immunodeficiency syndrome (AIDS), and the use of intravenous drugs. The most common cause is *Staphylococcus aureus*, followed by *Enterobacter, Salmonella, Pseudomonas*, and *Serratia* species.

22.2.1 Bacterial Spondylodiscitis

The infection usually starts in the anterior portion of the vertebra due to its rich arterial supply and then spreads to the rest of the vertebral body, along the medullary spaces. Through the disk space, which is usually involved in pyogenic infections, the infection spreads to the contiguous vertebrae. Due to the disappearance of the vascular anastomotic connections in the vertebral bodies after childhood, in adults a large area of bone remains susceptible to infarction and infection from hematogenous septic emboli (Smith and Blaser 1991).

Clinical symptoms of spondylodiscitis include localized back pain, limited range of motion, and fever. According to the "rule of 50%", 50% of the patients will have increased erythrocyte sedimentation rate (ESR), 50% of patients have symptoms for at least 3 months before presentation, fever will be present in 50% of patients and white blood cell count will be increased in 50% of patients. In spinal infections after surgery or trauma, ESR is unreliable and increase in pain may be the only feature (Tins and Cassar-Pullicino 2004). Blood cultures are positive in 25–50% but biopsy reveals positive results in 50–90% of cases with open biopsies being the most reliable.

The lumbar region is most commonly affected (50%), the thoracic spine is involved in 35% of cases, and the cervical spine is less frequently involved (Van Tassel 1994). The extent of vertebral and epidural space abnormalities in cases of cervical infection is greater than in the thoracic or lumbar region (Friedman and Hills 1994).

The radiologic diagnosis of spondylodiscitis is based on magnetic resonance imaging (MRI) findings, although spine radiographs, bone scans, and computed tomography (CT) can provide additional information. Radiographs of the spine are not helpful in the early stage of spondylodiscitis. Disk space narrowing and irregularity of vertebral body margins can be seen after 2–4 weeks on plain radiographs. Bone scans are sensitive in the early phase but not specific. Increased bone turnover from surgery, fracture, and degenerative changes cannot be distinguished from inflammatory changes. Disc flattening and destruction of vertebral endplates can be demonstrated on CT and paravertebral extension and epidural abscess can be delineated after contrast administration. The relationship of the spinal cord and epidural space cannot be reliably evaluated without use of intrathecal contrast agent application (Smith and Blaser 1991).

Magnetic resonance imaging is the method of choice for the diagnosis of pyogenic spondylodiscitis. Affected vertebral bodies show low signal on T1WI and high signal on T2WI with strong enhancement on postcontrast T1WI (Fig. 22.1). The MR signal abnormalities are assumed to correspond to the extent of the inflammatory process and increased water content in exudates containing polynuclear leukocytes and fibrin (Smith and Blaser 1991). The changes in signal intensity in pyogenic spondylodiscitis are relatively constant and do not correlate with the etiologic agent (Maiuri et al. 1997); however, cases of *Brucella* spondylodiscitis may have long T1 and T2 relaxation times. Abnormal enhancement can be observed in the affected bone, disk, and epidural abscess formations (Post et al. 1990). The improved delineation of epidural collections from the compressed thecal sac was one of the major advantages of postcontrast images.

The extension of the infection can be well visualized and documented using fat-suppressed postcontrast T1WI. Involved disks show high signal on T2WI ("hot disk") with loss of intranuclear cleft and peripheral enhancement (Maiuri et al. 1997). Destruction of the bone results first in subchondral erosions and sequestrations, followed by vertebral body de-

Fig. 22.1a–c. Pyogenic spondylodiscitis. **a** On T1WI the vertebral bodies L4 and L5 show low signal intensity. **b** Sagittal T2WI shows narrowing of the disc space L4–L5 with high signal intensity of the disc and affected vertebral bodies. **c** Homogenous enhancement of the vertebral bodies L4 and L5 is seen on postcontrast T1WI with fat suppression. The disk shows inhomogeneous, patchy enhancement

struction. Bony sequestrations are recognized as low signal intensity structures on postcontrast images surrounded by inflammatory tissue, and disappear with time due to osteolysis. Soft tissue involvement is present in 20% of pyogenic spinal infections with paravertebral abscesses and pleural effusions with spread through the parietal pleura when the dorsal spine is involved (Bass et al.1998). A case of osteomyelitis of the thoracic spine caused by *Salmonella* with pleural effusion was described recently (Gupta et al. 2004). Salmonella osteomyelitis is usually seen in immunocompromised patients, and accounts for approximately 0.5% of all osteomyelitis cases. When the infection passes through the posterior longitudinal ligament, inflammatory masses extend along several segments and form epidural abscesses.

Reactive bone marrow changes can be also found in unaffected vertebral bodies in patients with pyogenic spondylitis (Stäbler et al. 2000). A recent study suggests that in patients with chronic bacterial spondylitis, alterations in bone marrow signal is due to reactive bone marrow stimulation. This was found in about 25% of patients with infectious spondylitis (Stäbler et al. 2000).

The differential diagnosis includes degenerative changes Modic type-I, rheumatic diseases, and neoplasms. In cases of infection the disk is hyperintense on T2WI, whereas a dehydrated disk shows a typically low signal on T2-weighted MR images. On postcontrast images, degenerative changes can show enhancement of the vertebral bodies and the disk due to the presence of vascularized fibrous tissue and edema in the bone marrow (Jevtic 2001). After discectomy, 20% of patients show enhancement of the disk, which is considered normal up to 3 months after surgery. Rheumatoid arthritis usually involves the craniocervical junction, and demonstrates characteristic laboratory and clinical data. Primary or secondary neoplastic lesions of the vertebral bodies usually can be easily distinguished from infections because disk involvement is only rarely present; however, myeloma and chordoma may develop near or even within the disk space (Longo et al. 2003). Spinal erosive changes have been described in patients with chronic renal failure, usually in patients being on dialysis for more than 3 years (Sundaram et al. 1987). Decreased signal intensity on both T1- and T2-weighted MR images, normal signal of the intervertebral disk, lack of associated soft tissue abnormality, and normal bone scan suggest the correct diagnosis.

22.2.2 Bacterial Epidural Abscess

The peak incidence of epidural abscesses of bacterial origin occurs in the sixth and seventh decades of life (Danner and Hartmann 1987). Diabetes mellitus,

intravenous drug abuse, chronic renal failure, immunodeficiency syndromes, and cirrhosis are the primary predisposing factors (Cross and Howell 2003). In 50% of cases, no obvious source of infection can be identified (Panagiotopoulos et al. 2004).

Staphylococcus aureus is the most common agent (45%). Fever and localized tenderness over the spine are common early symptoms, but often the symptoms are nonspecific, resulting in delayed diagnosis. Based on their age, spinal epidural abscesses are classified as: (a) acute abscess formations with frank pus in the epidural space; and (b) chronic epidural abscesses with granulation tissue.

The MR imaging characteristics of an epidural abscess are high signal on T2WI and low signal on T1WI with two types of enhancement (Figs. 22.2–22.6; Friedman and Hills 1994). A homogenous enhancement corresponds to an abscess with inflammatory tissue without purulent collection; a peripheral enhancement indicates a true abscess formation with purulent fluid (Sandhu and Dillon 1991). The necrotic center of the abscess is not perfused and is a relatively inaccessible extravascular space with low accumulation of contrast material. This avascular core will not be accessible to intravenous antibiotics, and usually requires surgical drainage. In the case of suspected epidural abscess, due to the continuity of the epidural space, the entire spine should be examined.

Precontrast T2WI usually fail to show an epidural abscess because both CSF and abscess formation show high signal intensity. Precontrast T1WI are helpful for detection of low signal intensity of associated affected vertebral bodies and involved disks. The subtle changes in the signal intensity of CSF on T1WI may indicate widespread involvement, compression of the thecal sac, and associated meningitis. Both T1- and T2WI show no different histologic zones of abscess formations. Postcontrast images delineate the histologic zones and the extent of an abscess, as well as the degree of spinal cord compression. Two additional patterns of enhancement are present: linear enhancement along the dura mater; and engorgement of the epidural or basivertebral veins. Linear enhancement repre-

Fig. 22.2a–c. Pyogenic spondylodiscitis with epidural extension. **a** Sagittal T1WI shows low signal intensity of vertebral body L2 and L3 with low signal intensity disc and loss of cortical continuity of the adjacent endplates. An additional isointense mass is seen in the anterior epidural space extending from L1 to L3 level. **b** On T2WI the disk shows high signal intensity with low signal intensity of the mass in the epidural space. **c** Patchy enhancement of the affected vertebral bodies and peripheral enhancement of the disc is seen on postcontrast T1WI representing spondylodiscitis. Epidural collection also shows peripheral enhancement

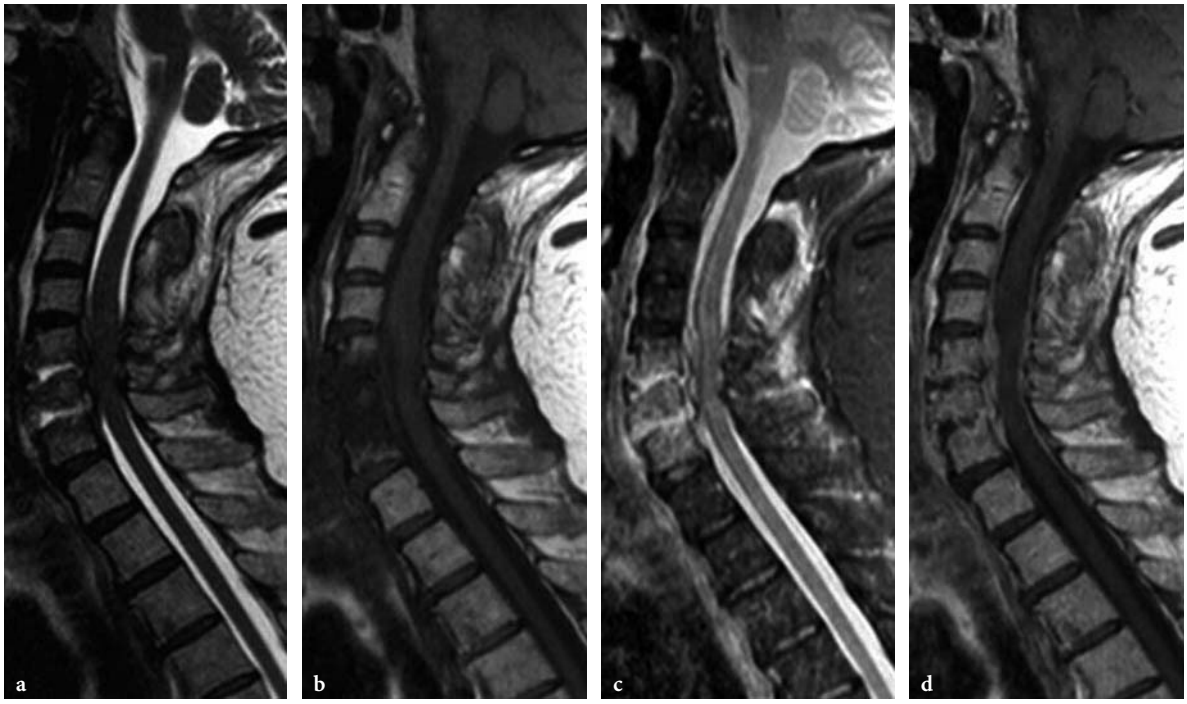

Fig. 22.3a–d. Pyogenic spondylodiscitis with epidural extension. **a** Sagittal T2WI of the cervical spine shows high signal intensity of the disc C5–C6 and C6–C7 with narrowing of the disc spaces on both levels. **b** Affected discs and vertebral bodies appear hypointense on T1WI with irregularity of the subchondral regions of the vertebral bodies. **c** Hyperintensity of the vertebral bodies is most prominent on sagittal short tau inversion recovery (STIR) image representing inflammatory bone marrow edema. **d** After gadolinium injection, the extent of the infection is evident with enhancement of vertebral bodies C5–C7 and the disk spaces. Epidural extension of the infection is clearly delineated on postcontrast images with enhancement of the epidural phlegmon in the anterior epidural space

sents extension of inflammation into the dura mater, and venous engorgement can be observed below and above an epidural collection, which is the result of extension of the inflammation along the venous plexus or mechanical obstruction of venous drainage (Numaguchi et al. 1993).

Follow-up imaging of epidural abscesses is crucial whether the treatment is surgical or nonsurgical. Increased or diminished intensity of contrast enhancement at the site of an epidural abscess correlates well with clinical deterioration or improvement respectively (Numaguchi et al. 1993). Immediate surgical decompression is indicated in patients who exhibit neurologic deterioration during antibiotic therapy. Abscesses located posteriorly are easier to drain and are associated with less postoperative morbidity. Recent reports suggest minimally invasive techniques, such as mild continuous suction, are a promising and successful alternative treatment (Panagiotopoulos et al. 2004). In the past decade surgical interventions in cases of spondylodiscitis and epidural abscess have been replaced by conservative therapy, and percutaneous drainage of the abscesses. Immobilization, as well as antibiotic and anti-inflammatory therapy, is usually required in spondylodiscitis. A CT-guided percutaneous drainage is necessary in cases of large paravertebral masses. Monitoring treatment response is therefore critical, especially in immunocompromised patients. When the infection process begins to diminish and responds well to medical treatment, the change in signal intensity tends to regress in 6 weeks to several months. A high signal intensity rim on the T1WI at the edge of the lesion has been described as one of the earliest signs representing healing (Gillams et al.1996). Replacement of abnormal hypointense signal in the vertebral bone marrow on T1WI with hyperintense fat also indicates healing. Gradual decrease in T2WI can be observed on follow-up MR scans. Gadolinium enhancement may increase in degree and extent in some patients, persists for several weeks, and does not indicate deterioration or treatment failure (Gillams et al.1996).

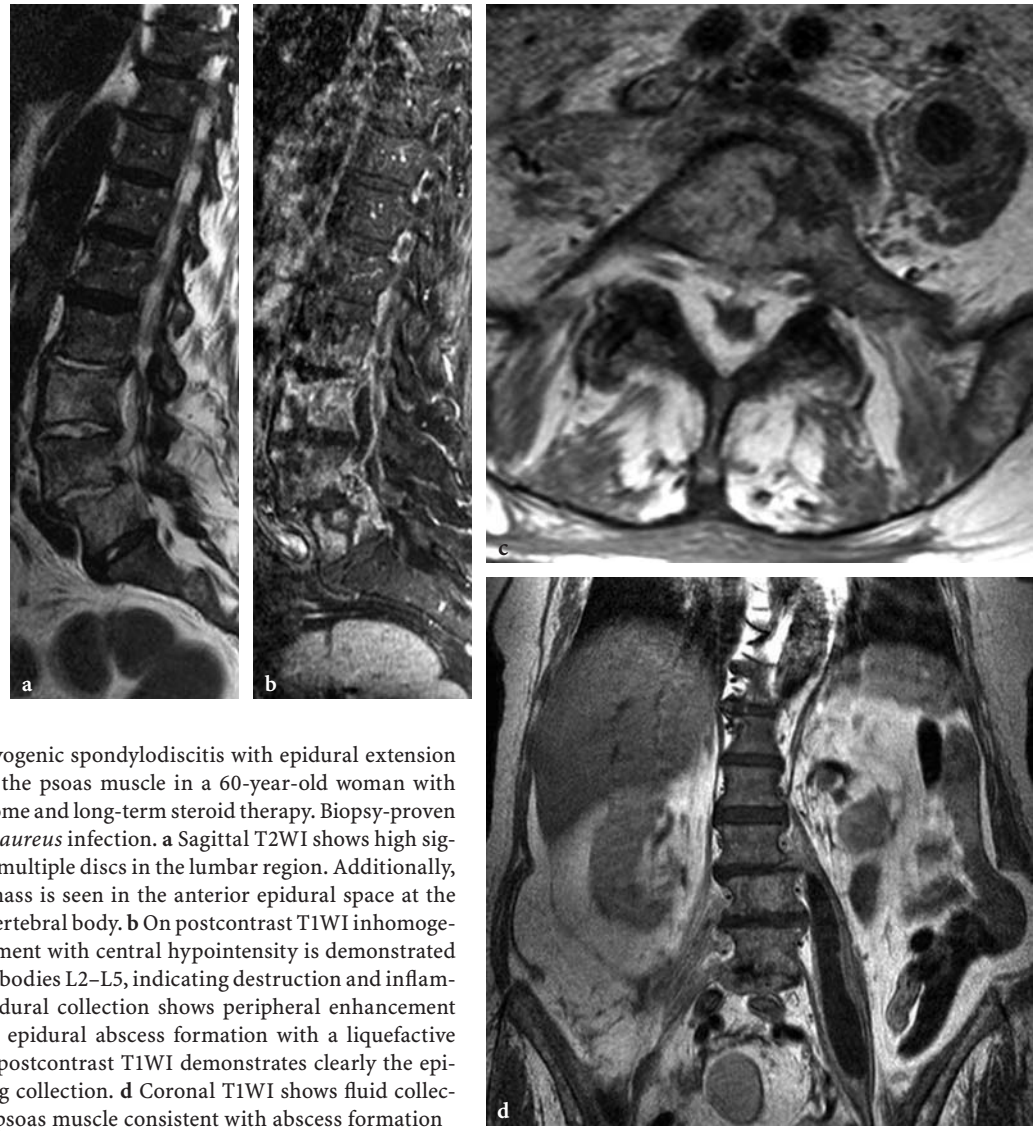

Fig. 22.4a–d. Pyogenic spondylodiscitis with epidural extension and abscess in the psoas muscle in a 60-year-old woman with Cushing syndrome and long-term steroid therapy. Biopsy-proven *Staphylococcus aureus* infection. **a** Sagittal T2WI shows high signal intensity of multiple discs in the lumbar region. Additionally, an isointense mass is seen in the anterior epidural space at the level of the L3 vertebral body. **b** On postcontrast T1WI inhomogeneous enhancement with central hypointensity is demonstrated in the vertebral bodies L2–L5, indicating destruction and inflammation. An epidural collection shows peripheral enhancement consistent with epidural abscess formation with a liquefactive center. **c** Axial postcontrast T1WI demonstrates clearly the epidural enhancing collection. **d** Coronal T1WI shows fluid collection in the left psoas muscle consistent with abscess formation

22.2.3 Bacterial Myelitis and Spinal Cord Abscess

The occurrence of intramedullary abscess formation is rare, with only a few cases described in the literature, with the thoracic spine the most commonly involved area (Candon and Frerebeau 1994). *Staphylococcus aureus* and *Streptococcus* are the most common bacterial organisms to invade the spinal cord. Hematologic spread is the most common route of infection. It has been postulated that bacterial spinal abscesses only occur in a setting of systemic bacteremia (Babu et al. 1992). In one series, however, in 25% of the patients, a primary source of infection was never found (Murphy et al. 1988). Contiguous spread through a congenital dermal sinus may be a mechanism of infection in children (Chan and Gold 1988). The clinical signs and symptoms depend on the location of the lesion. Patients usually present with motor and sensory neurologic deficits, back and/or radicular pain (60% of patients), and fever (40% of patients). The erythrocyte sedimentation rate tends to be elevated in all patients regardless of the clinical findings (Candon and Frerebeau 1994). The CSF cultures usually remain sterile.

Development of an abscess in the spinal cord may be similar to the pathologic evolution of abscess in the brain: (a) early stage of infectious myelitis; (b) late stage of myelitis; and (c) intramedullary cord abscess formation (Murphy et al. 1988). High signal on T2WI

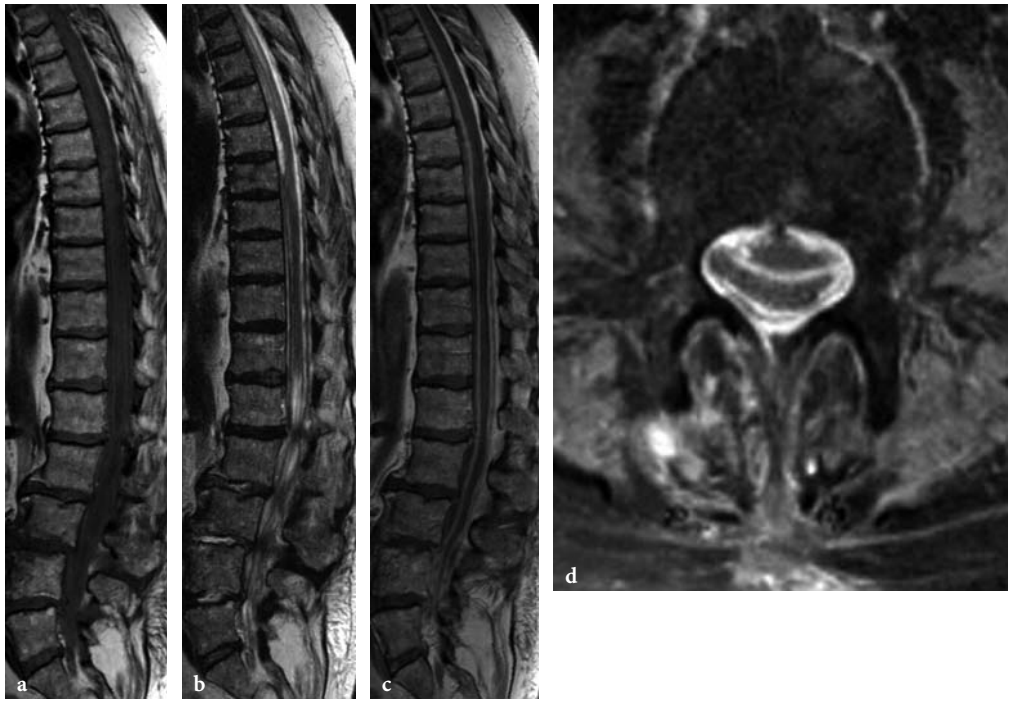

Fig. 22.5a–d. Epidural abscess. **a** On sagittal T1WI an isointense abnormality is observed in the anterior and posterior epidural space in the thoracic and lumbar region. **b** Poor contrast between the spinal cord and cerebrospinal fluid (CSF) is shown on T2WI. The dura is seen as a low signal intensity line, indicating a process in the epidural space. **c,d** On postcontrast sagittal **c** and axial **d** T1WI an intense enhancement of the dura is shown with clear delineation of a fluid collection in the anterior and posterior epidural space representing epidural abscess formation

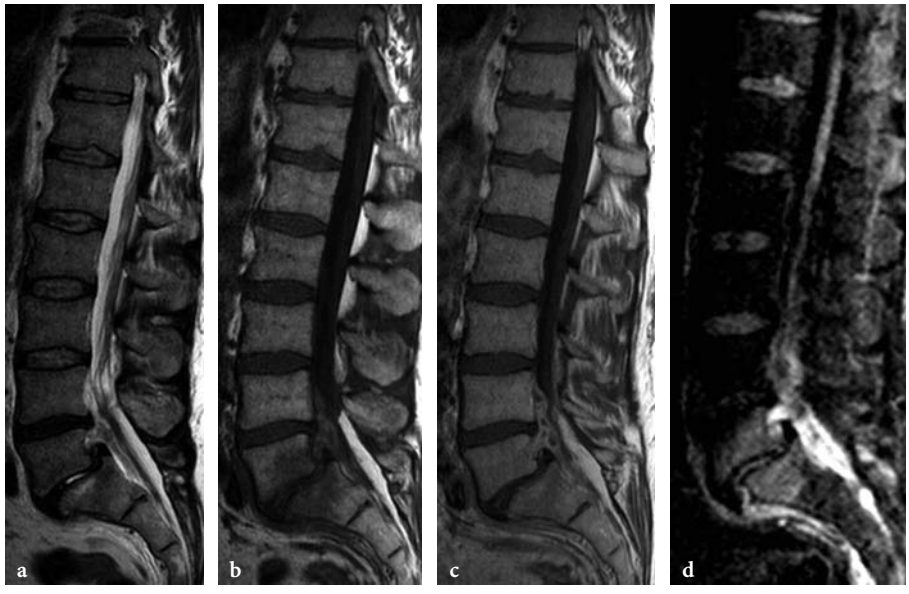

Fig. 22.6a–d. Pyogenic spondylodiscitis with epidural abscess in the lumbar spine. **a** On sagittal T2WI linear high signal is noted in the disc L5–S1 with a low signal intensity mass in the anterior epidural space at the same level. **b** The vertebral bodies L5 and S1 show low signal on T1WI with narrowing of the disc space L5–S1. An epidural mass appears slightly hyperintense to CSF on T1WI. **c** Postcontrast T1WI demonstrates enhancement of the affected vertebral bodies (now isointense compared with normal vertebral bodies) and enhancement of the epidural collection. **d** On sagittal diffusion-weighted image vertebral bodies L5 and S1 have high signal most probably representing inflammatory edema. High signal is also shown in the epidural collection suggesting restricted diffusion due to the highly viscous content of the epidural abscess

with poorly defined enhancement are the typical MR imaging findings in the early stage. Clearly defined peripheral enhancement with surrounding edema is present in the late stage of myelitis, corresponding to capsular formation and inflammatory changes in the late stage of cerebritis. The earliest well-defined enhancement is observed 7 days after the onset of symptoms (Murphy et al. 1988), and this is thought to represent the beginning of abscess formation within the spinal cord. In one study, a case of staphylococcal myelitis of the cervical spinal cord presented as a homogeneously enhancing lesion without cavitation (Friess and Wasenko 1997). Multiple ring-enhancing lesions were found in the brain in that particular patient. Since the patient improved clinically and radiologically after antibiotic treatment, the authors postulated that the imaging findings represented early bacterial myelitis resembling pathologically early cerebritis.

Syphilitic myelitis is a very rare manifestation of neurosyphilis (Tsui et al. 2002). It is a form of meningovascular syphilis with thrombosis of the spinal vessels due to syphilitic endarteritis. High signal abnormality on T2WI, with enhancement predominantly on the surface of the cord, has been described in a few cases of proven syphilitic myelitis (Tsui et al. 2002). The disappearance of the spinal cord abnormalities suggests the reversible nature of the lesions. In one case, high signal intensity abnormality was present in the entire spinal cord (Tsui et al. 2002). Since the clinical and imaging findings are nonspecific, this potentially treatable entity should be included in the differential diagnosis of acute transverse myelitis. The final diagnosis can be made with serum and CSF tests.

22.2.4 Tuberculosis

The worldwide rise of AIDS is in part responsible for an increased incidence in tuberculosis (TB). At present, approximately 30% of patients with tuberculosis are HIV-positive (Whitemann et al. 1995). Extrapulmonary and disseminated forms are much more common in immunocompromised hosts than in the healthy population (Thurnher et al. 1997; Villoria et al. 1995).

Tuberculosis of the spine was first described as a distinct entity by Sir Percival Pott in England in 1779 (Pott 1779). Vertebral TB is the most common form of skeletal TB, and thoracic involvement is usually seen in 50% of the cases. The most common affected vertebral body is L1 (Sklar et al. 1993). Depending on the location of the disease, the age of the patient and the number of vertebrae affected, the patient may present with symptoms ranging from systemic upsets or back pain to severe spinal deformity and neurologic deficits. Knowing that a delay in diagnosis may have devastating consequences, especially spinal deformity, it is crucial to establish early diagnosis of spinal tuberculous infection. The spine is usually affected through the spread of the *Mycobacterium tuberculosis* from a primary focus located outside the CNS.

Tuberculous infection of the spine may present as: (a) tuberculous spondylodiscitis; (b) tuberculous radiculitis; or (c) intramedullary tuberculoma.

22.2.4.1 Tuberculous Spondylodiscitis

Typically, the anteroinferior part of the vertebral body is affected first with contiguous subligamentous spread and consecutive involvement of the adjacent vertebral bodies with abscess formation and avascular necrosis. Tuberculous infection causes destruction through a delayed hypersensitivity reaction of the vertebral body with the formation of granuloma and Langerhans giant cells. Although the involvement of the posterior elements can occur secondarily, occasionally the posterior elements can be affected primarily. In one study, 5% of spinal TB was located in the posterior elements (Kumar 1985). In another recently published series about spinal TB, 24% of patients had posterior element involvement, with isolated posterior element involvement in 3% (Narlawar et al. 2002). Spread of the infection posteriorly into the spinal canal causes epidural abscess formations and spinal cord compression.

Tuberculosis may also involve multiple vertebrae at multiple sites, sometimes creating diagnostic problems. Skip lesions occur in up to 4% of the cases (Smith and Blaser 1991). For this reason, as large a section of the spine as possible should be imaged in all cases of suspected spinal TB to avoid overlooking distant foci.

Because of its multiplanar capability and sensitivity in detecting osseous and soft tissue changes associated with osteomyelitis, MR imaging should be considered the method of choice for imaging spinal TB (Figs. 22.7, 22.8). On MR imaging the affected vertebral bodies show high signal on T2WI, and low signal on T1WI, representing acute edematous changes. The height of the disk is preserved until the later stages of the infection. Loss of the intranuclear cleft

Fig. 22.7a–d. Early tuberculous spondylitis in an 18-year-old HIV-negative intravenous drug abuser. **a** Low signal intensity is shown in the vertebral bodies L3 and L4 on T1WI. **b** On T2WI low signal and reduction of the disk height L3–L4 is shown. The affected vertebral bodies have a slightly higher signal intensity compared with the normal ones. **c** High signal was present in the vertebral bodies L3 and L4 on STIR sequence. **d** The signal of the affected vertebral bodies becomes almost similar to the normal ones on postcontrast T1WI. The presence of the prevertebral enhancing mass at that level is suggestive of tuberculous spondylitis (without disk involvement) with anterior spread of the infection

and hyperintensity of the disk on T2WI are signs of disk involvement (46–72% of cases; Al-Mulhim et al. 1995; Gouliamos et al. 2001; Lindahl et al. 1996; Liu et al. 1993). The intervertebral disk is involved by direct spread from affected neighboring vertebral bodies or soft tissue. On postcontrast images, a rim enhancement around the disk can be seen.

The imaging findings in tuberculous spondylitis in children are similar to those in adults, but are more extensive (Andronikou et al. 2002). In a large pediatric study, vertebral body involvement was central, with collapse commencing anteriorly (Hoffmann et al. 1993). In their series, all pediatric patients had two or more vertebral bodies involved. Direct involvement of the disk by blood-borne pathogens occurs only in the pediatric age group because of persistent fetal blood supply to the disk. The affected disks are hypointense on T2WI compared with the high signal intensity characteristic of a normal disk. Kyphosis and cord compression are the most common complications (Andronikou et al. 2002).

Paraspinal soft tissue involvement accompanies vertebral destruction, and has been reported in 73.9% of the cases in adults, and in an even higher percentage in children (98%; Andronikou et al. 2002; Hoffmann et al. 1993). Paravertebral abscesses are seen as posterior mediastinal masses when they are thoracic and psoas abscesses in the lumbar spine (Fig. 22.9). A psoas abscess may extend into the groin and thigh with calcifications after healing. According to one study, paravertebral masses do not correlate well with the site of the initial vertebral body lesion, and psoas abscesses are known to be located below the level of spondylitis (Loke et al. 1997). Paravertebral soft tissue masses reach a maximum size within 2 months of presentation and may take up to 15 months to resolve (Sharif et al. 1995). In the acute stage paravertebral tissues are usually hypointense on T1WI and hyperintense on T2WI with disappearance of the fat and increased size of the homolateral psoas muscle. In the chronic stage, scar formation in the fat tissue is observed (Maiuri et al. 1997). On postcontrast scans strong rim enhancement around multiloculated fluid collections is present. Multilocular and calcified paraspinal masses with a thick rim and associated vertebral body fragmentation is strongly suggestive of tuberculous infection.

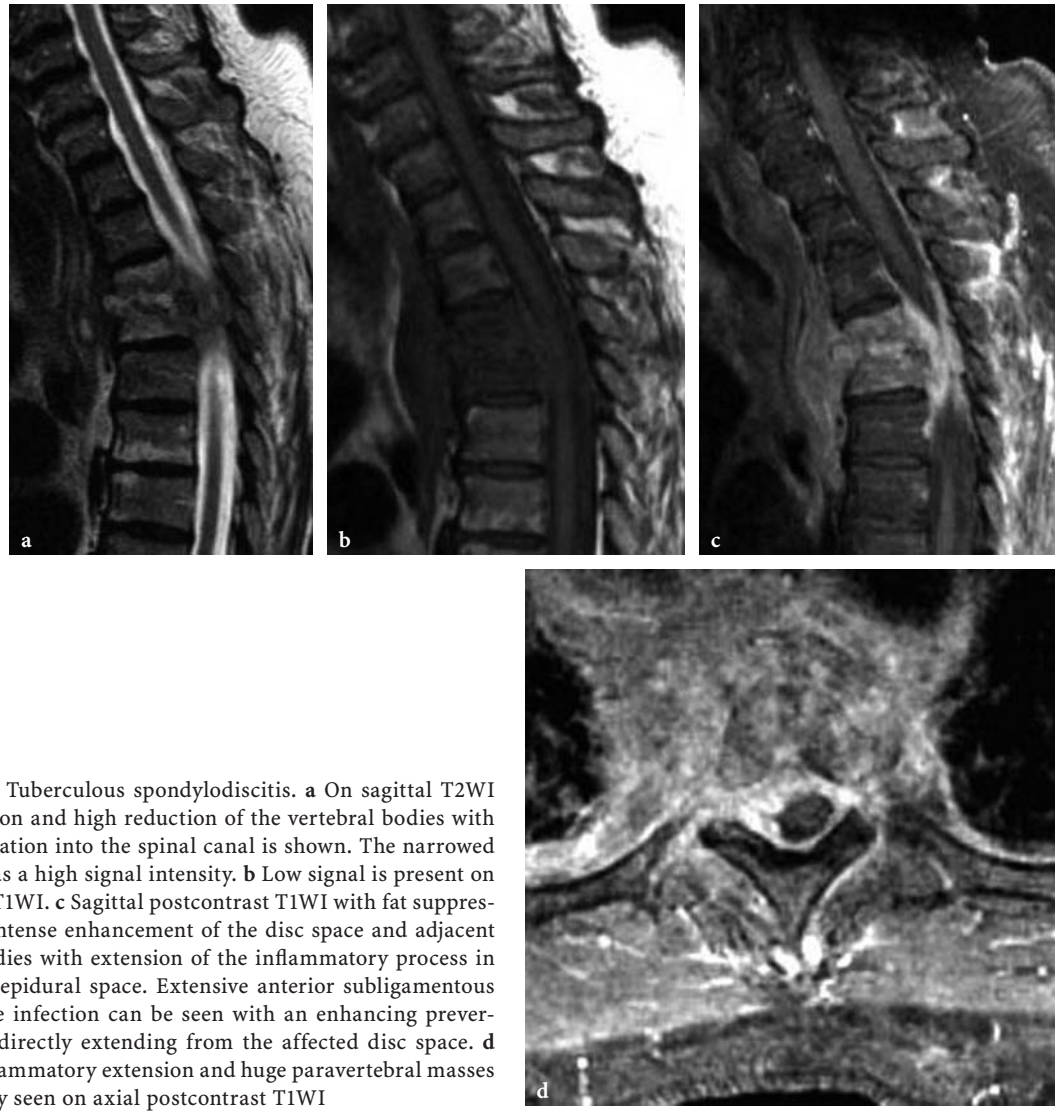

Fig. 22.8a–d. Tuberculous spondylodiscitis. **a** On sagittal T2WI the destruction and high reduction of the vertebral bodies with dorsal dislocation into the spinal canal is shown. The narrowed disc space has a high signal intensity. **b** Low signal is present on precontrast T1WI. **c** Sagittal postcontrast T1WI with fat suppression shows intense enhancement of the disc space and adjacent vertebral bodies with extension of the inflammatory process in the anterior epidural space. Extensive anterior subligamentous spread of the infection can be seen with an enhancing prevertebral mass directly extending from the affected disc space. **d** Epidural inflammatory extension and huge paravertebral masses can be clearly seen on axial postcontrast T1WI

Calcifications within or surrounding paraspinal abscesses are considered pathognomonic for TB (Sharif et al. 1995). Paraspinal soft tissue masses extend in an anterolateral direction, but posterior extension into the spinal canal are also seen.

One of the rare complications of TB spinal infection is fistulization of spondylodiscitis to the skin or abdominal viscera.

Differentiation between tuberculous and pyogenic spondylitis is difficult both clinically and radiologically. Clinical information is not helpful, although a more insidious onset favors a tuberculous origin. In one comparative study, the two most reliable MRI findings indicative of a tuberculous infection were thin and smooth enhancement of the abscess wall and well-defined paraspinal signal abnormality. Thick and irregular enhancement of the abscess wall and ill-defined paraspinal abnormal signal were suggestive of pyogenic spondylitis (Jung et al. 2004). An air–fluid level within an abscess is said to exclude TB (Loke et al. 1997).

Osseous TB has been reported in 1–3% of patients with TB (Evangelista et al. 2004), with involvement of the dorsolumbar spine in 50% and sacroiliac joints in 10% of patients. The diagnosis of bone TB is challenging, on the one hand because of nonspecific clinical symptoms and nonspecific radiologic findings, and, on the other hand, due to the low prevalence in Western countries. Atypical forms of osseous TB mostly affect diabetic or immunocompromised patients. Imaging findings in atypical bone TB differ from Pott's disease. The neural arch is most commonly in-

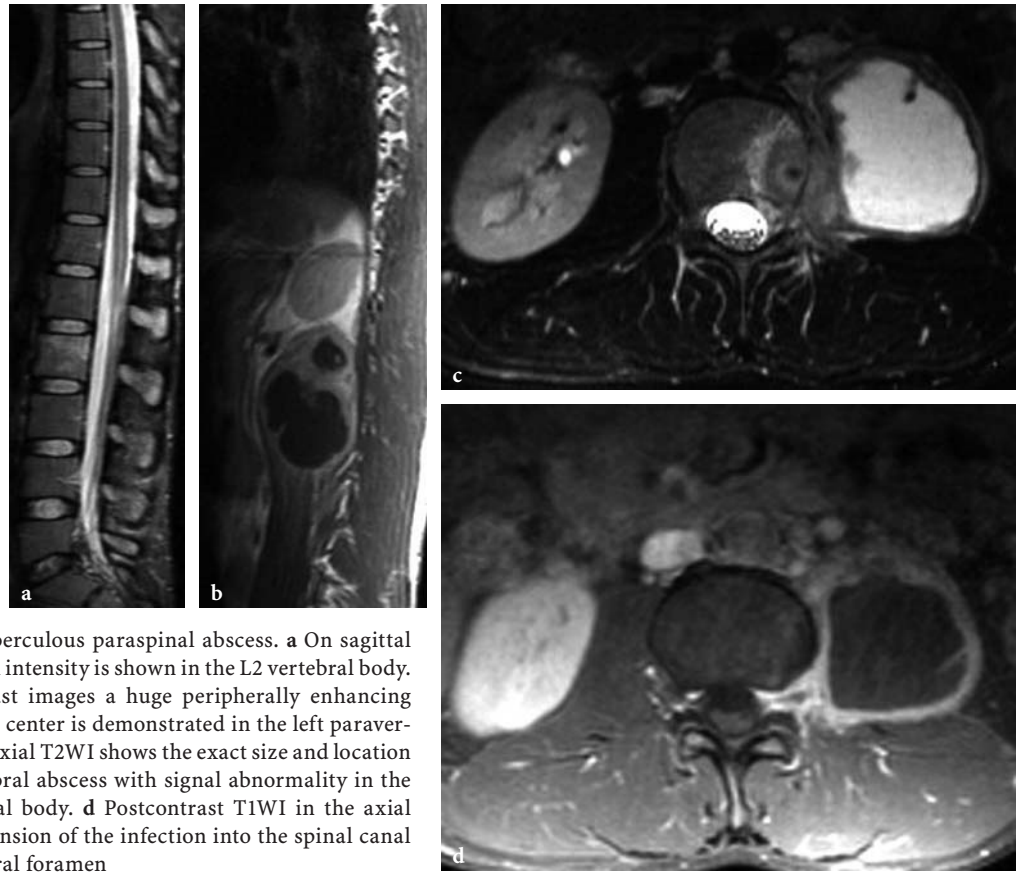

Fig. 22.9a–d. Tuberculous paraspinal abscess. **a** On sagittal T2WI high signal intensity is shown in the L2 vertebral body. **b** On postcontrast images a huge peripherally enhancing mass with a fluid center is demonstrated in the left paravertebral region. **c** Axial T2WI shows the exact size and location of the paravertebral abscess with signal abnormality in the adjacent vertebral body. **d** Postcontrast T1WI in the axial plane shows extension of the infection into the spinal canal through the neural foramen

volved, with sparing of the vertebral body and disks. Furthermore, skin lesions are often present, and lesions may manifest as solid tumor-like masses with no evidence of abscess formation. Hypercaptation on bone scan can anticipate radiographic abnormalities by 2–5 months in cases of osseous TB and help guide a biopsy site (Evangelista et al. 2004).

In the past 20 years, plain films have been replaced by CT and MRI in the assessment of spinal TB. Early bone marrow edema, epidural and paraspinal masses, as well as cord compression can be detected on CT and MR before plain radiograph changes appear. Plain-film changes may lack the pathologic alterations in tuberculous infection of the spine by up to 8 weeks, radionuclide scanning is sensitive but nonspecific. Bone destruction at the vertebral endplates with fragmentation is well demonstrated on CT scan.

22.2.4.2 Tuberculous Arachnoiditis

Tuberculosis is a rare cause of spinal arachnoiditis. Classification is based on the site of origin: (a) primary TB radiculomyelitis; (b) radiculomyelitis secondary to vertebral TB; and (c) radiculomyelitis secondary to intracranial TB meningitis. The clinical features of spinal TB arachnoiditis include paraplegia, quadriplegia, pain, and root symptoms. Pathologically, the meninges of the cord show a variable degree of congestion and inflammatory changes throughout their course. Spinal cord and nerve roots are edematous and surrounded by gelatinous exudate. Associated tuberculomas may be located within the thecal sac, and are usually closely adherent to the inner aspect of the dura mater and to the spinal cord.

The diagnosis of tuberculous arachnoiditis is usually suspected on the basis of a history of cranial tuberculous meningitis, the clinical picture, and CSF analysis. MR imaging is the method of choice in the detection of tuberculous arachnoiditis. The intrathecal space is usually hyperintense on all MR imaging sequences. On postcontrast MR imaging, enhancement of the dura–arachnoid complex is usually seen. The nerve root thickening reflects edematous swelling in the acute stage, and adhesions in the chronic stage (Fig. 22.10; Bötzel 1993;

Fig. 22.10a–f. Tuberculous radiculitis with epidural tuberculoma in 7-year-old child with tuberculous meningitis. **a** Sagittal postcontrast T1WI of the cervical spine shows linear enhancement on the anterior and posterior surface of the spinal cord representing leptomeningeal disease. **b** Enhancement and clumping of the cauda equina is demonstrated on postcontrast images of the lumbar region. **c** Axial T1WI after gadolinium injection shows typical arachnoiditis-type enhancement of the cauda equina due to extensive tuberculous infection. **d** Low signal intensity mass located in the anterior epidural space of the thoracic spine is shown on T1WI. **e** The lesion has low signal compared with CSF on T2WI. **f** Axial postcontrast T1WI with fat suppression shows epidural mass in the anterior epidural space to the best advantage, representing epidural tuberculoma

Chang et al. 1989). Other imaging findings, such as irregular margins of the thecal sac, irregular cord outline, and irregular filling or obliteration of the subarachnoid space, can also be visualized on myelograms.

An unusual case of intradural, extramedullary tuberculoma as a complication of tuberculous meningitis was described recently (Skendros et al. 2003). MR imaging demonstrated an intradural, extramedullary mass that extended from Th2 to the lumbar spine. The spinal cord showed intramedullary hyperintensity consistent with edema.

22.2.4.3 Intramedullary Tuberculoma

Intramedullary TB infection remains an extremely rare disease entity. Only 148 cases have been reported in the international literature, although numerous recent reports from developing countries, and

in HIV-positive patients, increase this number. Intramedullary tuberculomas are seen only in 0.002% of the cases of TB and in 0.2% of the cases of CNS TB (Citow and Ammirati 1994). The ratio of intracranial to intraspinal tuberculomas ranges from 20:1 and 42:1 (Jinkins 1995). Histologically, mature tuberculoma have a central area of solid caseation necrosis and a capsule of collagenous tissue, epithelioid cells, multinucleated giant cells, and mononuclear inflammatory cells (Whiteman et al. 1995).

Fusiform swelling of the cord was noted in six of seven cases of intramedullary tuberculoma with iso- or hyperintensity on T1WI (Parmar et al. 2000). Hypo- or isointensity on T2WI with surrounding hyperintense edema was present in 2 patients, a finding suggestive of tuberculoma (Fig. 22.11); however, in 5 patients, a hyperintense center on T2WI was noted due to the lesser degree of caseation and liquefaction. Solid or ring-like enhancement is usually present on postcontrast images. A case of intramedullary tuberculoma of the thoracic spinal cord was recently reported (Torri et al. 2004). The patient presented with a 2-month history of progressive paraparesis and sphincter dysfunction, and MR showed a ring-enhancing mass with perifocal edema within the cord (Torri et al. 2004). In another series five cases of spinal intramedullary tuberculoma and abscess were reported (Devi et al. 2002). On postcontrast images ring-enhancing lesions with central hypointensity were described. The lesions were treated successfully surgically and/or with antituberculous therapy. Intramedullary tuberculoma was also reported in patients with AIDS (Melhem and Wang 1992).

Tuberculous involvement of the subdural and intramedullary compartment is uncommon; however, a case of combined subdural spinal tuberculous empyema and intramedullary tuberculoma in an HIV-positive patient was described (Alessi et al. 2003). A lentiform lesion with rim enhancement at the level Th2 was seen in the cord on postcontrast MR images. Additionally, an enhancing subdural collection was present from C5 and further downward along the complete thoracic spine with compression of the spinal cord.

22.3 Viral Infections

22.3.1 Human Immunodeficiency Virus

As the human immunodeficiency virus (HIV)/AIDS epidemic approaches its 20th anniversary, researchers and clinicians continue to grapple with the complexities of the virus. An estimated 36 million people worldwide are currently living with HIV, and some 20 million people have already died from AIDS.

Vacuolar myelopathy (VM) is a common neurologic complication of AIDS. Petito et al. first described in 1985 the neuropathologic findings in a previously uncharacterized progressive myelopathy in AIDS patients (Petito et al. 1985). Pathologically, VM is characterized by vacuolization in the lateral

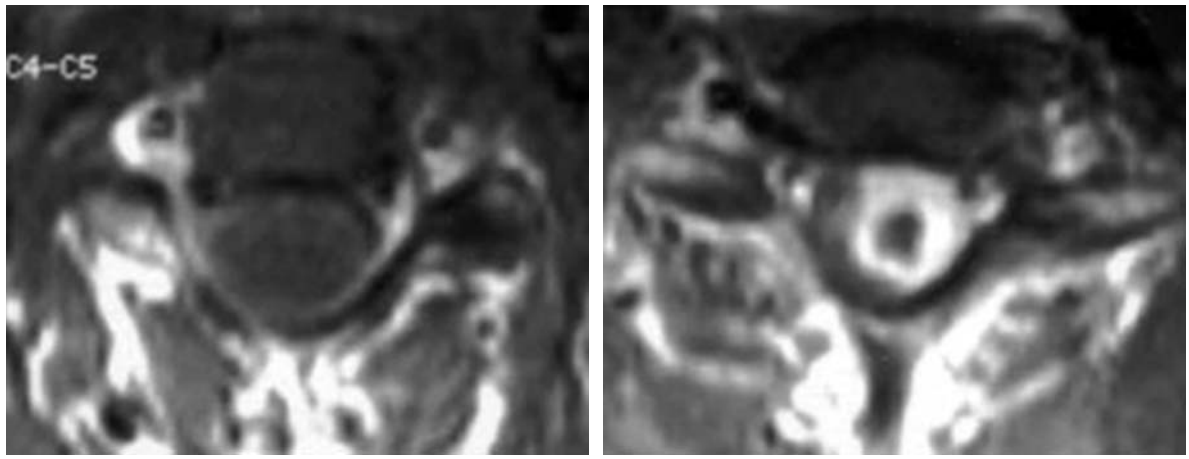

a b

Fig. 22.11a,b. Intramedullary tuberculoma in a patient with known cerebral tuberculosis. **a** On axial T1WI enlargement of the cord with central hypointensity is shown. **b** Axial postcontrast T1WI reveals an intramedullary ring-like enhancing lesion, representing intramedullary tuberculous granuloma

and posterior columns of the thoracic spinal cord, resembling changes seen in vitamin B12 deficiency. Vacuoles are the result of edematous swelling within myelin, with splitting of the lamellae. The axons are usually normal until severe vacuolation and secondary Wallerian degeneration and axonal disruption occurs (Artigas et al. 1990; Dal Pan et al. 1994; Gray et al. 1990; Petito et al. 1985). The vacuolization is not, however, confined to specific white matter tracts. Twenty to 55% of patients with AIDS have evidence of spinal cord disease consistent with VM. The exact cause of VM remains unclear. The pathogenesis of VM may be secondary to a combination of immune-mediated myelin and oligodendrocyte injury, and simultaneous impairment of repair mechanisms due to a deficiency of S-adenosylmethionine (SAM; Tan and Guiloff 1998). Published reports support an indirect relation between HIV and the pathogenesis of vacuolar myelopathy, peripheral neuropathy, and dementia. Because of the overlap between these syndromes, it is not completely clear whether we are dealing with disease entities or parts of a spectrum of tissue damage (Bergmann et al. 1993).

Clinically, patients present with slowly progressive weakness of the lower extremities, gait disorder, sensory abnormalities in the legs, impotence in men, and urinary disturbances (Rocco et al. 2004). The diagnosis is based on the clinical course and exclusion of other causes of myelopathy. The MR imaging findings include bilaterally symmetrical increased signal intensity on T2WI, predominantly located in the lateral and dorsal parts of the cord (Fig. 22.12; Sartoretti-Schefer et al. 1997; Thurnher et al. 2000). In one study symmetrical, triangular, high-signal lesions were found within the gracile tract over several spinal segments, which correlated well with histopathologic findings (Sartoretti-Schefer et al. 1997). Since the inflammatory component is missing in VM, the blood–brain barrier is not damaged, and no enhancement is present on postcontrast images.

The differential diagnosis includes HIV myelitis and herpes simplex or cytomegalovirus (CMV) radiculitis, which is easily distinguishable from VM on MR imaging.

22.3.2 Cytomegalovirus and Herpes Simplex

Cytomegalovirus and herpes simplex virus (HSV), both herpes viruses, are the most common viral agents that cause spinal infections. Between 40 and 100% of individuals in the general population are seropositive for CMV. Almost all homosexual men with HIV are co-infected with CMV (Griffiths 2004). Cytomegalovirus is a common pathogen in AIDS patients, most often causing retinitis, pneumonia, or gastrointestinal infection. With the advent of highly active antiretroviral therapy (HAART), a significant decrease in the rate of CMV disease has been reported (Palella et al. 1998). Cytomegalovirus infection may also involve the central and peripheral nervous system (Chimelli et al. 1990; Morgello et al. 1987; Said et al. 1991). Clinical CMV disease of the CNS accounts for less than 1% of all CMV manifestations.

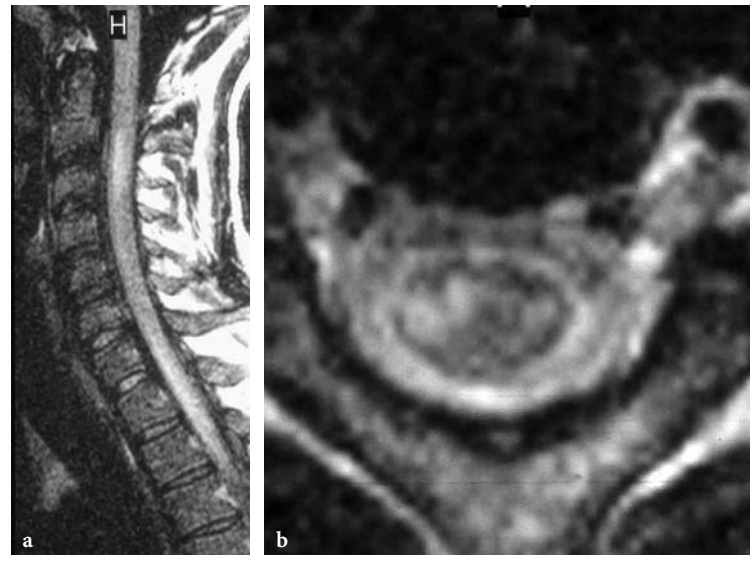

Fig. 22.12a,b. Vacuolar myelopathy in a male HIV-positive patient with progressive lower extremity weakness and urinary incontinence. His CD4 count was 20 cells/mm^2, and viral load level 100,000 copies/ml. **a** On sagittal fluid-attenuated inversion recovery MR image of the cervical spine hyperintensity without cord enlargement is demonstrated in the spinal cord. **b** Axial T2WI clearly shows typical lateral location of the HIV-associated lesions consistent with vacuolar myelopathy

Necrotizing polyradiculitis and myelitis of the spinal cord are pathologic forms of this infection in the spine (Chimelli et al. 1990, Morgello et al. 1987). The CMV polyradiculitis presents with progressive weakness, hyporeflexia, urinary retention, and perianal sensory disturbances. Cerebrospinal fluid analysis is usually nonspecific with findings such as elevated protein level and cellular pleocytosis with polymorphonuclear predominance (Mahieux et al. 1989). Culture of the CSF for CMV is insensitive, and often negative. The introduction of CSF polymerase chain reaction (PCR) has allowed better characterization and improved diagnosis of CMV infection of the CNS.

The MR imaging findings include enhancement and clumping of the nerve roots of the cauda equina and leptomeninges of the spinal cord, predominantly in the region of the conus medullaris (Figs. 22.13, 22.14; Bazan et al. 1991; Whiteman et al. 1994; Talpos et al. 1991; Thurnher et al. 2000). The differential diagnosis for CMV polyradiculitis in AIDS patients includes lymphoma, HSV infection, distal symmetric polyneuropathy, and vacuolar myelopathy. Enhancement pattern in patients with intradural extramedullary inflammatory changes have also been seen in patients with leptomeningeal spread of tumor; thus, the MR findings alone cannot differentiate infection from tumor (Gero et al. 1991).

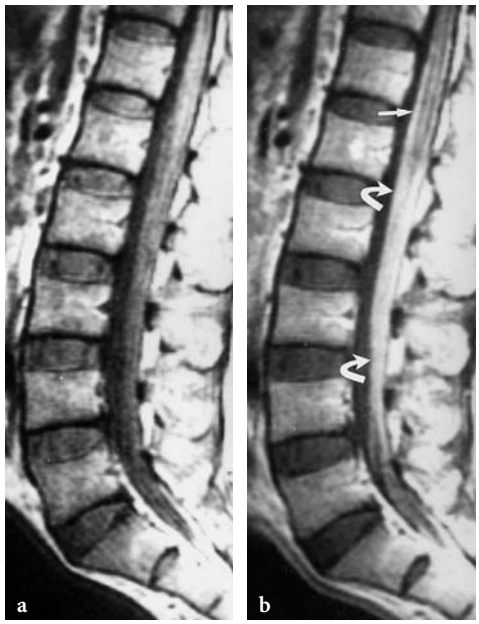

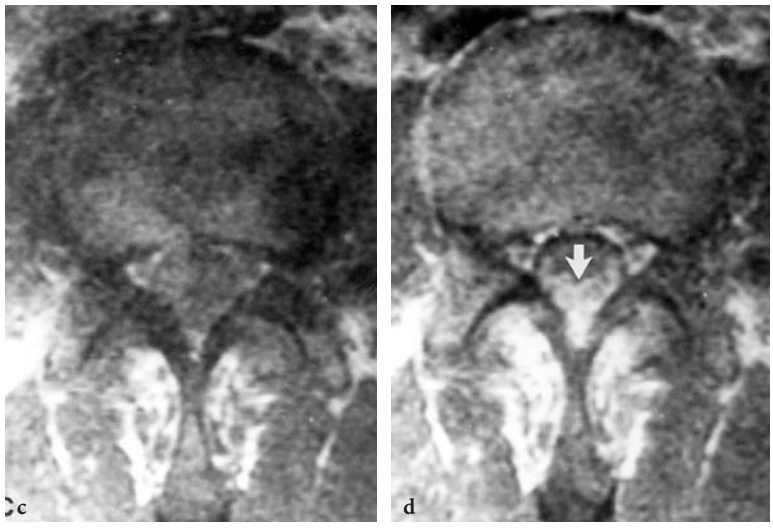

Fig. 22.13a–d. Cytomegalovirus (CMV) polyradiculopathy in a 39-year-old patient with AIDS with simultaneously present CMV retinitis. **a,c** On sagittal and axial T1-weighted MR images of the lumbar spine slightly increased signal of the CSF **a** and nerve roots clumping is present **c**. **b,d** Sheet-like enhancement around the conus medullaris (**b**, *straight arrow*) and enhancement of the cauda equina (**b**, *curved arrows*) is clearly shown on postcontrast image (**d**, *arrow*). The CSF analysis revealed increased cell count and positive PCR for CMV

22.4 Fungal Infections

Fungal infections of the spine are noncaseating infections that occur primarily as opportunistic infections in immunocompromised patients. By far, the most frequent cause of fungal infections are *Candida* species, followed by *Aspergillus* and others. In addition to being uncommon pathogens, fungal organisms are slow growing and difficult to identify by culture (Farkas 1986). These infections mainly present as discitis/osteomyelitis in the spine.

Most reviews of fungal spinal infections have included a limited number of patients and short follow-up. In one study, 11 patients with fungal osteomyelitis from three institutions in 16 years have been collect-

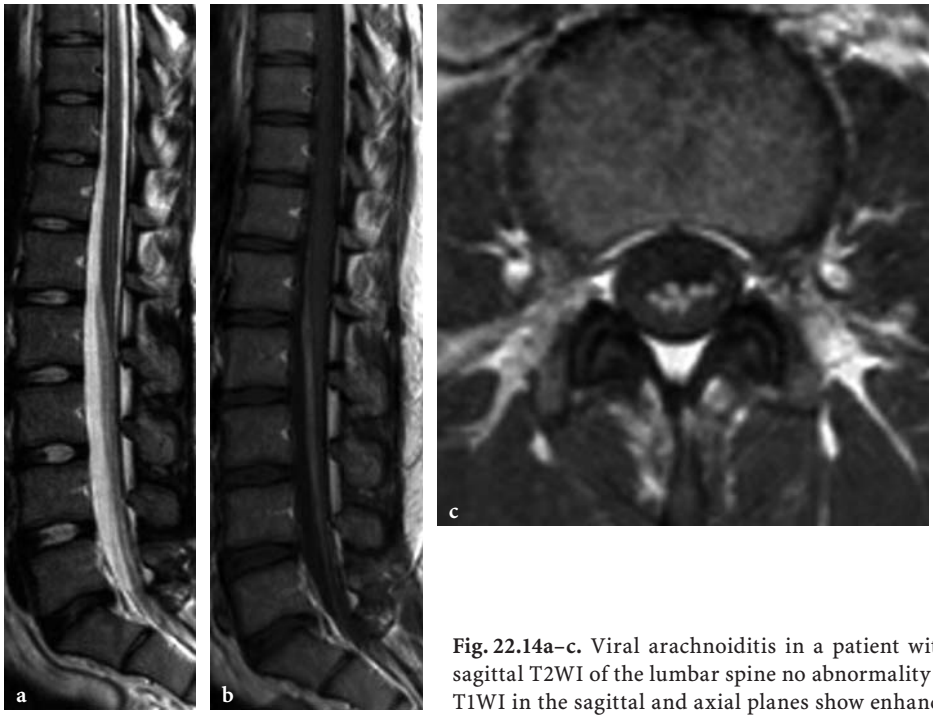

Fig. 22.14a–c. Viral arachnoiditis in a patient with Evans syndrome. **a** On sagittal T2WI of the lumbar spine no abnormality is shown. **b,c** Postcontrast T1WI in the sagittal and axial planes show enhancement of the nerve roots

ed (Frazier et al. 2001). In 7 of 11 cases, the cause was *Candida* species. A case of spinal intramedullary abscess caused by *Candida albicans* was also published (Lindner et al. 1995). These spinal infections may originate either from contiguous spread from an adjacent involved organ (lung), hematogenous spread from a distant focus, or iatrogenic inoculation (Saigal et al. 2004; Woods and Goldsmith 1990).

The incidence of invasive aspergillosis infection has been estimated at 12/1,000,000 per year. In one series, over a period of 20 years, 71 patients with invasive aspergillosis have been encountered; 42 have shown CNS involvement, and only 2 had myelitis (Kleinschmidt-DeMasters 2002). Granulomatous lesions are a result of contiguous spread, whereas hematogenous dissemination results in intramedullary abscess formation. Spread of the infection from vertebral osteomyelitis to the epidural space with development of an extradural abscess is a rare manifestation (Vaishya and Sharma 2004).

The MR imaging features of fungal spondylodiscitis are distinct from pyogenic osteomyelitis and include absence of disk hyperintensity and preservation of the intranuclear cleft on T2WI (Williams et al. 1999). Hypointensity of the vertebral bodies on T1-weighted MR images was observed in three cases of fungal spondylodiscitis in posttransplant patients (Williams et al. 1999). Only minimal hyperintensity was present on T2WI, which was probably caused by the absence of an acute inflammatory reaction that is usually present in immunocompetent patients. None of the cases in this particular series showed high signal within the intervertebral disk on T2WI, which is typical of pyogenic infection. This could be attributable to factors inherent to fungi, including the presence of paramagnetic and ferromagnetic elements. The long-term clinical outcome is not related to the specific species of fungus, but rather to the time between onset of the symptoms and treatment of the infection (Frazier et al. 2001). Recognition of the imaging characteristics of fungal spondylitis should lead to prompt biopsy and influence management, especially in the immunocompromised host.

Recently, a case of epidural abscess in the cervical spine in a diabetic patient was published (Chi et al. 2003). The patient presented with a prolonged history of neck pain and progressive weakness, and surgical decompression revealed an *Aspergillus flavus* abscess. In another case of fungal discitis in a patient with lymphoblastic leukemia, *Aspergillus terreus* was isolated (Park et al. 2000). A case of thoracic intradural *Aspergillus* abscess formation following epidural steroid injection was also reported recently (Saigal et al. 2004). A spinal epidural abscess as the initial appearance of aspergillosis has

been reported in renal transplant recipients (Byrd et al. 1982; Ingwer et al. 1978). In two reports, epidural abscess was the first clinical manifestation of the *Aspergillus* infection in an AIDS patient (Woods and Goldsmith 1990; Go et al. 1993).

Coccidioidomycosis of the spine involves multiple vertebral bodies with sparing of the disks, and sometimes paravertebral soft tissue involvement (Sklar et al. 1993).

Blastomycosis may produce lytic vertebral lesions and perispinal inflammation.

22.5 Parasitic Infection

22.5.1 Toxoplasmosis

Cerebral toxoplasmosis is the most common opportunistic infection of the CNS in AIDS patients. Spinal cord *Toxoplasma gondii* infection occurs rarely in AIDS patients and is always associated with coexisting cerebral infection. In one series, 7.3% of 55 patients with AIDS patients had spinal cord toxoplasmosis (Thurnher et al. 2000). Clinical symptoms include weakness of the lower extremities and paralysis. In the majority of studies, an enhancing mass was described in the cord with low signal on T1WI and high signal intensity on T2WI (Fig. 22.15; Fairley et al. 1992; Harris et al. 1990; Mehren et al. 1988; Poon et al. 1992; Resnick et al. 1995; Thurnher et al. 2000). In one reported case of toxoplasmosis of the conus medullaris in a patient with hemophilia-associated AIDS, no abnormalities were present on T1WI or T2WI (Kayser et al. 1990); however, after gadolinium injection, a homogeneously enhancing lesion was detected in the conus without enlargement of the cord.

The correct diagnostic approach in intramedullary lesions in HIV-positive patients is difficult and includes balancing the risks of surgery against empirical treatment. Treatment experience with spinal toxoplasmosis remains limited, and the standard treatment for cerebral toxoplasmosis (long-standing suppressive treatment) considered satisfactory for controlling spinal cord disease.

22.5.2 Cysticercosis

Cysticercosis is the most common parasitic infection, affecting the CNS with spinal involvement in 0.7–5.9% of cases (Leite et al. 1997). All patients with spinal cysticercosis have cerebral involvement.

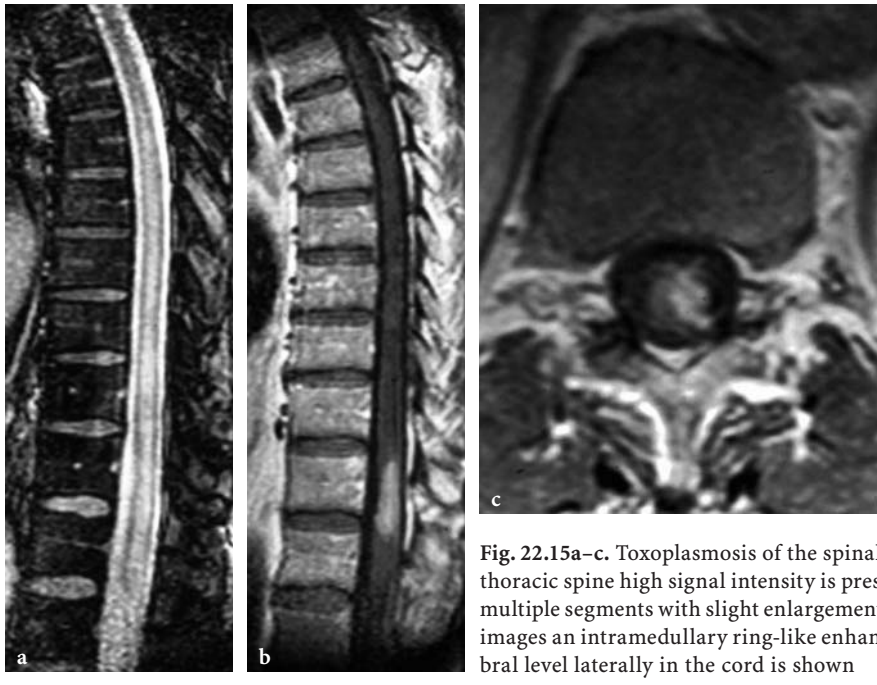

Fig. 22.15a–c. Toxoplasmosis of the spinal cord. **a** On sagittal T2WI of the thoracic spine high signal intensity is present in the spinal cord extending multiple segments with slight enlargement of the cord. **b,c** On postcontrast images an intramedullary ring-like enhancing lesion extending one vertebral level laterally in the cord is shown

The infection is caused by *Taenia solium* larvae, and it is endemic in the developing countries of Latin America, Asia, and Africa.

The subarachnoid space is the most common location, with intramedullary involvement more rare, and an epidural location very rare. A pathologic classification of spinal cysticercosis includes: (a) isolated spinal infestation; (b) spinal infestation with multifocal disease; (c) direct spinal extension of intracranial cysticercosis; and (d) cervical pachymeningitis with cord degeneration accompanying posterior fossa involvement (AKIGUCHI et al. 1979). Clinical symptoms result from the mass effect of cysts or vasogenic edema. Patients with spinal cysticercosis present with spastic paraplegia, bladder or bowel incontinence, pain, and sexual impotence (PARMAR et al. 2001).

On MR imaging an intact cysticercus is seen as a cystic area that is isointense to CSF. The scolex is recognized as a mural nodule within the cyst. The cyst fluid is clear as long as the parasite is alive. Peripheral enhancement will be present after the death of the parasite and an intense inflammatory reaction of the host can then be seen. Empirical treatment with antihelminthic drugs for 2 months usually leads to complete recovery.

References

Akiguchi I, Fujiwara T, Matsuyama H et al. (1979) Intramedullary cysticercosis. Neurology 29:1531–1534

Alessi G, Lemmerling M, Nathoo N (2003) Combined spinal subdural tuberculous empyema and intramedullary tuebrculoma in an HIV-positive patient. Eur Radiol 13:1899–901

Al-Mulhim FA, Ibrahim EM, el Hassan AY, Moharram HM (1995) Magnetic resonance imaging of tuberculous spondylitis. Spine20:2287–2292

Andronikou A, Jadwat A, Dois H (2002) Patterns of disease on MRI in 53 children with tuberculous spondylitis and the role of gadolinium. Pediatr Radiol 32:798–805

Artigas J, Grosse G, Niedobitek F (1990) Vacuolar myelopathy in AIDS. A morphologic analysis. Path Res Pract186:228–237

Babu R, Jafar JJ, Huang PP et al. (1992) Intramedullary cord abscesses associated with spinal cord ependymoma. Neurosurgery30:121–124

Bass SN, Ailani RK, Shekar R, Gerblich AA (1998) Pyogenic vertebral osteomyelitis presenting as exudative pleural effusion: a series of five cases. Chest 114:642–647

Bazan C III, Jackson C, Jinkins JR, Barohn RJ (1991) Gadolinium-enhanced MRI in a case of cytomegalovirus polyradiculopathy. Neurology 41:1522–1523

Bergmann M, Gulotta F, Kuchelmeister K, Masini T, Angeli G (1993) AIDS-myelopathy. A neuropathological study. Path Res Pract 189:58–65

Bötzel K (1993) Tuberkulöse Radiculomyelitis: gut therapierbar nur bei frühem Erkennen. Nervenarzt 64:281–283

Byrd BF, Weiner MH, McGee ZA (1982) *Aspergillus* spinal epidural abscess. J Am Med Assoc 248:3138–3139

Candon E, Frerebeau P (1994) Bacterial abscesses of the spinal cord. Review of the literature (73 cases). Rev Neurol 150:370–376

Chan CT, Gold WL (1998) Intramedullary abscess of the spinal cord in the antibiotic era: clinical features, microbial etiologies, trends in pathogenesis, and outcomes. Clin Infect Dis 27:619–626

Chang KH, Han MH, Choi YW et al. (1989) Tuberculous arachnoiditis of the spine: findings on myelography, CT, and MR imaging. Am J Neuroradiol 10:1255–1262

Chi Cy, Fung CP, Liu CY (2003) Aspergillus flavus epidural abscess and osteomyelitis in a diabetic patient. J Microbiol Immunol Infect 36:145–148

Chimelli L, Freitas MRG de, Bazin AR et al. (1990) Encephalo-myelo-radiculite a cytomegalovirus au cours du syndrome dímmuno-deficience acquise. Rev Neurol 146:354–360

Citow JS, Ammirati M (1994) Intramedullary tuberculoma of the spinal cord: case report. Neurosurgery 35:327–330

Cross RK Jr, Howell C (2003) Two cases of spontaneous epidural abscess in patient with cirrhosis. South Med J 96:291–293

Dal Pan GJ, Glass JD, McArthur JC (1994) Clinicopathologic correlations of HIV-1-associated vacuolar myelopathy. Neurology 44:2159–2164

Danner RL, Hartmann BJ (1987) Update of spinal epidural abscess: 35 cases and review of the literature. Rev Infect Dis 9:265–274

Devi BI, Chandra S, Mongia S et al. (2002) Spinal intramedullary tuberculoma and abscess: a rare cause of paraparesis. Neurol India 50:494–496

Evangelista E, Itti E, Malek Z et al. (2004) Diagnostic value of 99mTc-HMDP bone scan in atypical osseous tuberculosis mimicking multiple secondary metastases. Spine 1: E85–E87

Fairley CK, Wodak J, Benson E (1992) Spinal cord toxoplasmosis in a patient with human immunodeficiency virus infection. Int J STD AIDS 3:366–368

Farkas V (1986) Morphology and structure of fungi. In: Braude AI, Davis CE, Fierer J (eds) Infectious diseases and medical microbiology, 2nd edn. Saunders, Philadelphia, pp 113–124

Frazier DD, Campell DR, Garvey TA et al. (2001) Fungal infections of the spine. J Bone Joint Surg 83:560–565

Friedman DP, Hills JR (1994) Cervical epidural spinal infection: MR imaging characteristics. Am J Radiol 163:699–704

Friess HM, Wasenko JJ (1997) MR of staphylococcal myelitis of the cervical spinal cord. Am J Neuroradiol 18:455–458

Gero B, Sze G, Sharif H (1991) MR imaging findings of intradural inflammatory diseases of the spine. Am J Neuroradiol 12:1009–1019

Gillams AR, Chaddha B, Carter AP (1996) MR appearance of the temporal evolution and resolution of infectious spondylitis. Am J Roentgenol 166:903–907

Go BM, Ziring DJ, Kountz DS (1993) Spinal epidural abscess due to *Aspergillus* sp in a patient with acquired immunodeficiency syndrome. South Med J 8:957–960

Gouliamos AD, Kehagias DT, Lahanis S et al. (2001) MR imaging of tuberculous vertebral osteomyelitis: pictorial review. Eur Radiol 11:575–579

Gray F, Gherardi R, Trotot P, fenelon G, Poirier J (1990) Spinal cord lesions in acquired immune deficiency syndrome. Neurosurg Rev 13:189–194

Griffiths P (2004) Cytomegalovirus infection of the central nervous system. Herpes 11:95A–104A

Gupta SK, Pandit A, White DG, Evans PD (2004) Salmonella osteomyelitis of the thoracic spine: an unusual presentation. Postgrad Med J 80:110–111

Harris TM, Smith RR, Bognanno JR, Edwards MK (1990) Toxoplasmic myelitis in AIDS: gadolinium-enhanced MR. J Comput Assist Tomogr14:809–811

Hoffman EB, Crosier JH, Cremin BJ (1993) Imaging children with spinal tuberculosis. A comparison of radiography, CT and MRI. J Bone Joint Surg Br 75:233–239

Ingwer I, McLeish KR, Tight RR et al. (1978) *Aspergillus fumigatus* epidural abscess in a renal transplant recipient. Arch Intern Med 138:153–154

Jevtic V (2001) Magnetic resonance imaging appearances of different discovertebral lesions. Eur Radiol 11:1123–1135

Jinkins JR, Gupta R, Chang KH et al. (1995) MR imaging of central nervous system tuberculosis. Radiol Clin North Am 33:771–786

Jung NY, Jee WH, Ha KY, Park CK, Byun JY (2004) Discrimination of tuberculous spondylitis from pyogenic spondylitis on MRI. Am J Radiol 182:1405–1410

Kayser K, Campbell R, Sartorious C, Bartlett M (1990) Toxoplasmosis of the conus medullaris in a patient with hemophilia A-associated AIDS. J Neurosurg 73:951–953

Kleinschmidt-DeMasters BK (2002) Central nervous system aspergillosis: a 20-year retrospective study. Hum Pathol 33:116–124

Kumar K (1985) A clinical study and classification of posterior spinal tuberculosis. Int Orthop 9:147–152

Leite CC, Jinkins JR, Escobar BE et al. (1997) MR imaging of intramedullary and intradural–extramedullary spinal cysticercosis. Am J Radiol 169:1713–1717

Lindahl S, Nyman RS, Brismar J et al. (1996) Imaging of tuberculosis: spinal manifestations in 63 patients. Acta Radiol 37:506–511

Lindner A, Becker G, Warmuth-Metz M et al. (1995) Magentic resonance imaging findings of spinal intramedullary abscess caused by *Candida albicans*: case report. Neurosurgery 36:411–412

Liu GC, Chou MS, Tsai TC et al. (1993) MR evaluation of tuberculosis spondylitis. Acta Radiol 34:554–558

Loke TK, Ma HT, Chan CS (1997) MRI of tuberculous spinal infection. Australas Radiol 41:7–12

Longo M, Granata F, Ricciardi GK, Gatea M, Blandino A (2003) Contrast-enhanced MR imaging with fat suppression in adult-onset septic spondylodiscitis. Eur Radiol 13:626–637

Maiuri F, Iaconetta G, Gallicchio B, Manto A, Briganti F (1997) Spondylodiscitis: clinical and magnetic resonance diagnosis. Spine22:1741–1746

Mahieux F, Gray F, Fenelon G et al. (1989) Acute myeloradiculitis due to cytomegalovirus as the initial manifestation of AIDS. J Neurol Neurosurg Psychiatry 52:270–274

Mehren M, Burns PJ, Mamani F, Levy CS, Laureno R (1988) Toxoplasmic myelitis mimicking intramedullary spinal cord tumor. Neurology 38:1648–1650

Melhem ER, Wang H (1992) Intramedullary spinal cord tuberculoma in a patient with AIDS. Am J Neuroradiol 13:986–988

Morgello S, Cho ES, Nielsen S et al. (1987) Cytomegalovirus encephalitis in patients with acquired immunodeficiency syndrome: an autopsy study of 30 cases and a review of the literature. Hum Pathol 18:289–297

Murphy KJ, Brunberg JA, Quint DJ, Kazanjian PH (1988) Spinal cord infection: myelitis and abscess formation. Am J Neuroradiol 19:341–348

Narlawar RS, Shah JH, Pimple MK et al. (2002) Isolated tuberculosis of posterior elements of spine. Spine 27:275–281

Numaguchi Y, Rigamonti D, Rothman MI et al. (1993) Spinal epidural abscess: evaluation with gadolinium-enhanced MR imaging. RadioGraphics 13:545–559

Palella FJ Jr, Delaney KM, Moorman AC et al. (1998) Declining morbidity and mortality among patients with advanced human immunodeficiency virus infection. HIV Outpatients Study Investigators. N Engl J Med 338:853–860

Panagiotopoulos V, Konstantinou D, Solomou E et al. (2004) Extended cervicolumbar spinal epidural abscess associated with paraparesis successfully decompressed using a minimally invasive technique. Spine 29:300–303

Park KU, Lee HS, Kim CJ, Kim EC (2000) Fungal discitis due to Aspergillus terreus in a patient with acute lymphoblastic leukemia. J Korean Med Sci 15:704–707

Parmar H, Shah J, Patkar D, Varma R (2000) Intramedullary tuberculomas. MR findings in seven patients. Acta Radiol 41:572–577

Parmar H, Shah , Pathwardhan V et al. (2001) MR imaging in intramedullary cysticercosis. Neuroradiology 43:961–967

Petito CK, Navia BA, Cho ES et al. (1985) Vacuolar myelopathy pathologically resembling combined degeneration in patients with the acquired immunodeficiency syndrome. N Engl J Med 312:874–879

Poon TP, Tchertkoff V, Pares F et al. (1992) Spinal cord toxoplasma lesion in AIDS: MR findings. J Comput Assist Tomogr 16:817–819

Post MJD, Sze G, Quencer RM et al. (1990) Gadolinium-enhanced MR in spinal infection. J Comput Assist Tomogr 14:721–729

Pott P (1997) Remarks of that kind of palsy of the lower limbs which is frequently found to accompany a curvature of the spine. J. Johnson, London

Resnick DK, Comey CH, Welch WC et al. (1995) Isolated toxoplasmosis of the thoracic spinal cord in a patient with acquired immunodeficiency syndrome. J Neurosurg 82:493–496

Rocco A di, Werner P, Bottiglieri T et al. (2004) Treatment of AIDS-associated myelopathy with L-methionine: a placebo-controlled study. Neurology 63:1270–1275

Said G, Lacroix C, Chemouilli P et al. (1991) Cytomegalovirus neuropathy in acquired immunodeficiency syndrome: a clinical and pathological study. Ann Neurol 29:139–146

Saigal G, Post MJD, Kozic D (2004) Thoracic intradural aspergillus abscess formation following epidural steroid injection. Am J Neuroradiol 25:642–644

Sandhu FS, Dillon WP (1991) Spinal epidural abscess: evaluation with contrast-enhanced MR imaging. Am J Neuroradiol 12:1087–1093

Sartoretti-Schefer S, Blättler T, Wichmann W (1997) Spinal MRI in vacuolar myelopathy, and correlation with histopathological findings. Neuroradiology 39:865–869

Sharif HS, Morgan JL, Al Shahed MS, Al Thagafi MYA (1995) Role of CT and MRI in the management of tuberculous spondylitis. Radiol Clin N Am 33:787–804

Skendros P, Kamaria F, Knotopoulos V, Tsitouridis I, Sidiropoulos L (2003) Intradural, extramedullary tuberculoma of the spinal cord as a complication of tuberculous meningitis. Infection 31:115–117

Sklar EM, Post MJD, Lebwohl NH (1993) Imaging of infection of the lumbosacral spine. Neuroimaging Clin North Am 3:577–590

Smith AS, Blaser SI (1991) Infectious and inflammatory processes of the spine. Radiol Clin N Am 29:809–827

Stäbler A, Doma AB, Baur A, Krüger A, Reiser MF (2000) Reactive bone marrow changes in infectious spondylitis: quantitative assessment with MR imaging. Radiology 217:863–868

Sundaram M, Seelig R, Pohl D (1987) Vertebral erosions in patients undergoing maintenance hemodyalisis for chronic renal failure. Am J Roentgenol 149:323–327

Talpos D, Tien RD, Hesselink JR (1991) Magnetic resonance imaging of AIDS-related polyradiculopathy. Neurology 41:1996–1997

Tan SV, Guiloff RJ (1998) Hypothesis on the pathogenesis of vacuolar myelopathy, dementia, and peripheral neuropathy in AIDS. J Neurol Neurosurg Psychiatry 65:23–28

Tins BJ, Cassar-Pullicino VN (2004) MR imaging in spinal infection. Semin Musculoskelet Radiol 3:215–229

Thurnher MM, Jinkins RJ, Post MJD (1997) Diagnostic imaging of infections and neoplasms affecting the spine in patients with AIDS. Neuroimaging Clin North Am 7:341–357

Thurnher MM, Post MJD, Jinkins JR (2000) MRI of infections and neoplasms of the spine and spinal cord in 55 patients with AIDS. Neuroradiology 42:551–563

Tins BJ, Cassar-Pullicino VN (2004) MR imaging in spinal infection. Semin Musculoskelet Radiol 8:215–229

Torri H, Takahashi T, Shimizu H, Watanabe M, Tominaga T (2004) Intramedullary spinal tuberculoma: case report. Neurol Med Chir 44:266–268

Tsui EYK, Ng SH, Chow L et al. (2002) Syphilitic myelitis with diffuse spinal cord abnormality on MR imaging. Eur Radiol 12:2973–2976

Vaishya S, Sharma MS (2004) Spinal *Aspergillus* vertebral osteomyelitis with extradural abscess: case report and review of literature. Surg Neurol 61:551–555

Van Tassel P (1994) Magnetic resonance imaging in spinal infections. Top Magn Reson Imaging 6:69–81

Villoria MF, Fortea F, Moreno S, Munoz L, Manero M, Benito C (1995) MRI and CT of CNS tuberculosis in the patients with AIDS. Radiol Clin N Am 33:805–819

Whiteman ML, Dandapari BK, Shebert RT, Post MJD (1994) MRI of AIDS-related polyradiculomyelitis. J Comput Assist Tomogr 18:7–11

Whiteman M, Espinoza L, Post MJ et al. (1995) Central nervous system tuberculosis in HIV-infected patients: clinical and radiographic findings. Am J Neuroradiol 16:1319–1327

Williams RL, Fukui MB, Meltzer CC et al. (1999) Fungal spinal osteomyelitis in the immunocompromised patient: MR findings in three cases. Am J Neuroradiol 20:381–385

Woods GL, Goldsmith JC (1990) *Aspergillus* infection of the central nervous system in patients with acquired immunodeficiency syndrome. Arch Neurol 47:181–184

Yu AW, Chen WJ, Lin WC et al. (2004) Serious pyogenic spondylitis following vertebroplasty: a case report. Spine 10:209–211

Seronegative Spondylarthropathy

23

Claude Manelfe and Filip M. Vanhoenacker

CONTENTS

C. Manelfe, MD
Service de Neuroradiologie, CHU Purpan, Place du Docteur Baylac, 31059 Toulouse, France
F. M. Vanhoenacker, MD, PhD
Department of Radiology, University Hospital Antwerp, Wilrijkstraat 10, 2650 Edegem, Belgium

23.1 Introduction

Seronegative spondylarthropathy consists of a spectrum of chronic inflammatory disorders that lack the presence of rheumatoid factor and are clearly distinct from rheumatoid arthritis.

Whereas rheumatoid arthritis involves predominantly the synovial joints, significant abnormalities in the cartilaginous joints, entheses, as well as synovial articulations are seen in spondylarthropathic processes (Resnick 2002b).

The age of onset ranges from 20 to 40 years, and the overall prevalence is estimated to be as high as 0.2–2%, with ankylosing spondylitis (AS) and psoriatic arthritis (PA) being the most prevalent. Moreover, both AS and PA may cause severe functional disability of the affected patients.

Ankylosing spondylitis has a predilection for the axial skeleton, resulting in progressive stiffness, flattening of the lumbar lordosis, and exaggeration of the thoracic kyphosis, together with a limitation in spinal flexion (Levine et al. 2004). A peripheral polyarthritis with predilection for the lower limbs occurs less commonly.

Psoriatic arthritis may involve both the appendicular and the axial skeleton and is characterized by a chronic course (Klecker and Weissman 2003).

Other less frequent spondylarthropathies include:

- Reiter's syndrome
- Enteropathic arthropathies
- SAPHO (synovitis, acne, pustulosis palmoplantaris, hyperostosis and osteitis)

Generally, all spondylarthropathic disorders are characterized by several common features, including (Table 23.1):

- Disease onset in young adults (between 20 and 40 years).
- Inflammation not limited to the synovial membrane, but involving different target sites, includ-

KEY-POINTS

- Common features of seronegative spondylarthropathies:
  - Chronic inflammatory disorders
  - Lack the presence of rheumatoid factor
  - Inflammation involving:
    - The cartilaginous joints
    - Entheses
    - Synovial articulations
  - Involvement of both the axial and appendicular skeleton
  - Onset in young adults
  - Genetic predisposition (HLA-B27 antigen, familial occurrence)
  - Frequent association with extra-articular manifestations
  - Chronic disease course
- Age of onset ranges from 20 to 40 years
- Overall prevalence is 0.2–2%
- Most frequent:
  - Ankylosing spondylitis
  - Psoriatic arthritis
  - Reiter's syndrome
  - Enteropathic arthropathies
  - SAPHO (synovitis, acne, pustulosis palmoplantaris, hyperostosis and osteitis)
- Ankylosing spondylitis:
  - Young men
  - Genetic factor
  - Initially low back pain and/or sacroiliac pain
  - Leading to painful stiffening of the spine
  - Imaging:
    - Sacroiliac:
      - Blurring of the subchondral cortex, erosions
      - Sclerosis
      - Ankylosis
    - Spine:
      - Especially thoracolumbar and lumbosacral
      - Spondylitis anterior (Romanus lesion)
      - Vertebral squaring
      - Andersson lesion
      - Ankylosis
- Psoriatic arthritis
  - 10–15% of patients with psoriasis
  - Age of onset 30–50 years
  - Cutaneous disease usually precedes joint disease
  - Usually oligoarticular, asymmetrical, DIP hands and feet, also PIP, MCP, and MTP
  - Symmetric sacroiliitis in 20%
  - Spondylitis in 20–40%, usually with peripheral disease
  - Resembles AS in the spine, but milder, bigger, and asymmetric syndesmophytes

ing the entheses, synovial joints, as well as the cartilaginous joints (Fournie 1993; Godfrin et al. 2004; Resnick 2002b). Three pathological processes, namely inflammation, bony repair, and ossification, will occur at these target sites, resulting in the radiopathological picture in the individual patient. These processes will be explained more in detail in the section on ankylosing spondylitis. As opposed to the situation in rheumatoid arthritis, however, the inflammatory changes in spondylarthropathies are less intense. On the contrary, the hallmark of spondylarthropathy is a generalized enthesopathy in which the inflammatory changes within the synovial joints may be secondary to enthesopathy. The proclivity to osseous fusion of certain synovial joints, such as the apophyseal and sacroiliac articulations, especially in ankylosing spondylitis, can be related to abnormalities occurring at the capsuloligamentous attachments, perhaps reflecting another manifestation of enthesopathy (Resnick 2002b).

- Involvement of both the axial and appendicular skeleton
- Genetic predisposition (HLA-B27 antigen, familial occurrence)
- Frequent association with extra-articular manifestations, including acute anterior uveitis, cardiovascular involvement
- Typical chronic disease course, resulting in a progressive functional disability in the worse sce-

nario, accounting for 10% of cases. Many cases, however, are mild presenting with only pain, tenderness, and stiffness, with no other features

From an epidemiological point of view, different prevalences of spondylarthropathy have been reported in different countries: Scotland, 0.2% (Steven 1992); Germany, < 1% (Braun et al. 1998); U.S., 0.2% (Lawrence et al. 1998); China, 0.3%; and France (Wigley et al. 1994), 0.5% (Saraux et al. 1999). Besides genetic predisposition (HLA-B27 positive), numerous exogenous factors, such as infectious etiology (human immunodeficiency virus and associated infection of the gastrointestinal tract) and Arabic origin are exacerbating factors (Cuellar and Espinoza 2000; Solinger 2003).

23.2 Ankylosing Spondylitis

23.2.1 Definition and Epidemiology

Ankylosing spondylitis (AS) is a chronic, idiopathic, inflammatory arthritis with a predilection for the axial skeleton. The prevalence has been estimated to be as high as 0.2–1.6% (Vinson and Major 2003). The disease is most common in young men, with an age of onset usually between 20 and 40 years. Men are more commonly affected than women, and the male/female ratio is estimated to be 4 to 1 (El-Khoury et al. 1996). Moreover, radiographic changes of AS are more pronounced in men and there has been concern that early AS is underreported in women, as the disease may be more subtle and more difficult to diagnose in women (El-Khoury et al. 1996). Although the mode of inheritance remains unknown, there is a clear genetic component, with a strong association between AS and the HLA-B27 allele (Barozzi et al. 1998; Olivieri et al. 1998). This histocompatibility antigen is expressed in up to 96% of patients with AS, although the exact role of HLA-B27 in the pathogenesis of AS remains unknown (Vinson and Major 2003). Approximately 10% of HLA-B27-positive individuals ultimately develop the disorder (Haller and Hofmann 2001). Because the overall prevalence of HLA-B27 expression (9% of the general population) outnumbers largely the amount of affected patients, numerous exogenous factors, including infectious etiologies, have been suggested as inciting or exacerbating factors.

Table 23.1. Common features of spondylarthropathies

Onset in young adults
Inflammation involving entheses, synovial joints, as well as the cartilaginous joints
Involvement of both the axial and appendicular skeleton
Genetic predisposition (HLA-B27 antigen, familial occurrence)
Frequent association with extra-articular manifestations
Chronic disease course

The absence of HLA-B27 expression in an individual patient does not exclude the diagnosis of AS.

Various diagnostic criteria have been developed for AS and related disorders, including the modified New York Criteria, which combine clinical and radiological criteria in classifying and grading AS. Most of these criteria require decreased spinal mobility, decreased chest expansion, and radiographically evident sacroiliitis for the diagnosis of AS (Resnick 2002c; Van der Linden et al. 1984; Vinson and Major 2003); however, many patients with early disease may fail to meet these criteria (Van der Linden and Van der Heijde 1998; Vinson and Major 2003).

23.2.2 Clinical Features

Classically, AS presents as an insidious onset of low back pain persisting for more than 3 months and associated with morning stiffness. Pain or tenderness over the gluteal or sacroiliac regions can be prominent in the early phases of the disease. Other possible early clinical signs include chest pain and later mild to moderate reduction in chest expansion, owing to costovertebral and costosternal involvement. Peripheral articular manifestations, most commonly synovitis of hips or shoulders, are eventually seen in as many as 50% of patients, but are mild and overshadowed by more prominent manifestations in the central skeleton (Resnick 2002c).

The lower limbs are more frequently involved than the upper limbs. In 20–25% of AS patients, peripheral articular symptoms may precede axial manifestations. Painful tendinopathy occurs in about 10% of patients (Haller and Hofmann 2001).

The complete picture of AS leads to a painful stiffening of the entire spine, severe thoracic kyphosis,

and a rigid thorax. Associated extra-articular manifestations include acute anterior uveitis (25–30%), cardiovascular involvement, especially aortitis (10%), inflammatory bowel disease, amyloidosis, and, occasionally, pulmonary fibrosis (Resnick 2002c).

23.2.3 Laboratory Findings Other Than HLA-B27 Antigen

Generally, laboratory parameters are not very useful in diagnosing or monitoring patients with AS. The erythrocyte sedimentation rate and C-reactive protein are frequently elevated during the active phase and may become normal in later phases of the disease (Resnick 2002c).

Results of serological tests for rheumatoid arthritis and LE factors are characteristically negative, although 1–2% of patients with AS may be positive for rheumatoid factor (Resnick 2002c).

23.2.4 Basic Radio-Pathological Correlation

Three pathological processes, namely inflammation, bony repair, and ossification, are at the basis of the radiopathological changes of AS and may occur either consecutively or simultaneously in an individual patient (Fig. 23.1; Table 23.2). Different target sites, including the entheses and both the synovial and the cartilaginous joints, can be involved (Table 23.3). Each basic histopathological process is reflected by non-specific radiographic changes, occurring at different target sites (Table 23.2).

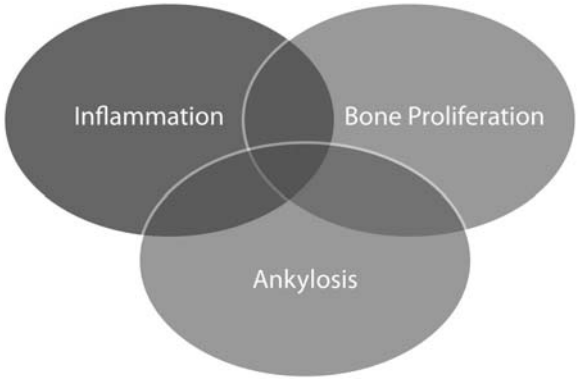

Fig. 23.1. Basic histopathological processes occurring consecutively or simultaneously. (From Lambrecht et al. 2005)

Generally, the inflammatory destruction presents as erosions on plain radiography, whereas subchondral sclerosis and ligamentous ossification are the radiological hallmarks of reactive bone formation, leading to ankylosis due to osseous bridging of the articulations. The different locations of the disease have quite characteristic radiographic features. The resulting radiographic picture will depend on the underlying histopathological processes. Destruction, subchondral sclerosis, and osseous ankylosis may exist in any combination and lead to the typical "variegated picture" of the disease.

23.2.5 Conventional Radiographic Findings in Ankylosing Spondylitis

23.2.5.1 Sacroiliac Joints and Pelvis

Sacroiliitis is the hallmark of ankylosing spondylitis. Previous studies have shown that sacroiliitis is the earliest radiographic sign in 99% of cases of AS (Bennett et al. 2004; Dihlman 1985; El-Khoury et al. 1996).

Although sacroiliitis alone is a non-specific finding and is not sufficient for the diagnosis of AS, changes in the sacroiliac joints are considered ubiquitous among patients with AS (El-Khoury et al. 1996; Vinson and Major 2003).

Both the synovial and ligamentous (superior and posterior) portions of the joint are involved. Classically, the involvement is symmetric and bilateral (Taylor et al. 2004), but – particularly very early in the course of the disease – unilateral disease may occur.

The above-mentioned basic radiopathological processes contribute to the ultimate radiographic picture of sacroiliac joint involvement (Table 23.2).

Among the signs of sacroiliac inflammation (Fig. 23.2) are blurring of the subchondral cortex with ill-defined articular contours and hazy structure of the subchondral cancellous trabeculae, resulting in pseudodilatation of the joint (Dihlman 1985). This finding is followed by the development of small, succinct erosions, giving the joint margin the appearance of the perforated edge of a postage stamp or a saw blade. Small erosions lined up one behind the other at corresponding sites of the ilium and the sacrum resemble a string of beads or rosary.

Table 23.2. Basic histopathological features that occur in ankylosing spondylitis, and its radiological counterparts (From Lambrecht et al. 2005)

Basic histopathological process	Radiographic counterpart
Inflammation	Erosions, joint widening/dilatation, erosive fibro-osteitis
Bony repair	Sclerosis, productive fibro-osteitis
Progressive ossification	Ankylosis

Table 23.3. Target sites for ankylosing spondylitis involvement of the axial skeleton (Modified from Lambrecht et al. 2005)

Synovial joints	Cartilaginous joints	Entheses
Sacroiliac joints	Discovertebral joints	Spine: posterior and interspinous ligamentous attachments; Sharpey's fibers anteriorly
Facet joints	Symphysis pubis	Pelvis
Costovertebral joints	Manubriosternal joint	Shoulder
Atlanto-axial joint		
Shoulder, hip		

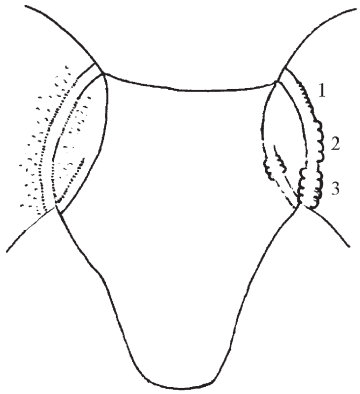

Fig. 23.2. Reactive bone proliferation at the sacroiliac joints. Inflammatory changes at the sacroiliac joint. Blurring of the articular contours and hazy structure of the subchondral bone at the right sacroiliac joint, resulting in pseudodilatation of the joint. On the left side typical erosions resembling the perforated edge of a postage stamp (*1*), a saw blade (*2*), and a rosary (*3*). (From Lambrecht et al. 2005)

The erosions usually develop earlier on the iliac than on the sacral side of the joint, possibly because the cartilage covering the sacrum is approximately twice as thick as that covering the ilium (1–4 mm vs 0.5–2 mm; Vinson and Major 2003).

Reactive bone proliferation (Fig. 23.3) is seen radiographically as sclerosis of the adjacent cancellous bone with a variable pattern (diffuse, band shaped, spotty, triangular). Ossifications of the joint capsule and its reinforcing ligaments present as bony hooks below the linea terminalis and as a striated structure above this line, forming the so-called star sign at the superior border of the joint. In addition to the destruction of cartilage with narrowing of the joint space, slim bony bridges connecting the ilium with the sacrum enlarge and become fused with one another, resulting in complete bony ankylosis. Radiographically, parts of the articular contour that remain visible following the advent of ankylosis are described as "phantom joint."

The simultaneous triad of sacroiliac destruction, sclerosis, and discrete ankylosis reflects a mode of reaction that is characteristic of AS and is described on plain radiography as the "variegated sacroiliac picture" (Fig. 23.4; Dihlman 1985; Lambrecht et al. 2005).

Early sacroiliac changes can be occult on plain radiography with plain radiographic findings of sacroiliitis lagging behind the clinical findings by several years (Resnick and Shields 1994). Because an early diagnosis of AS allows an earlier start of appropriate treatment, other imaging techniques, namely CT and MRI, have been proposed for the evaluation of the sacroiliac joints (Vinson and Major 2003).

Other changes in the pelvis may be associated with the changes in the sacroiliac joints. Ossifica-

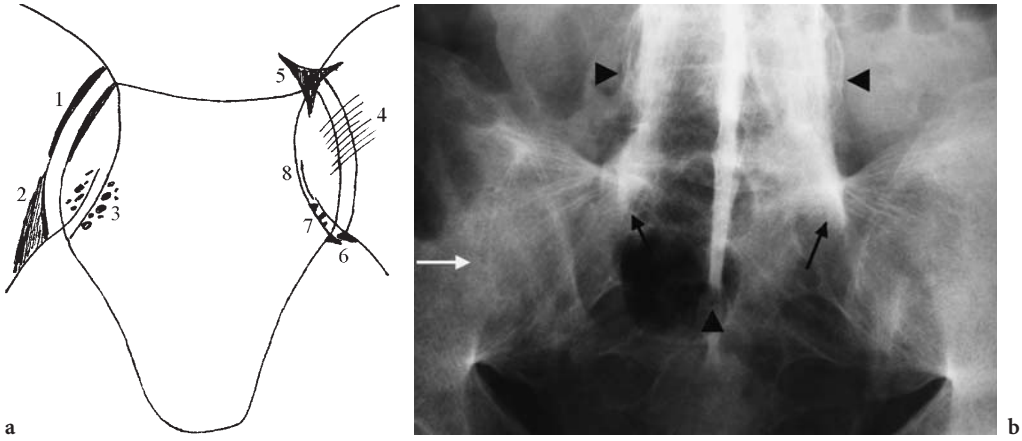

Fig. 23.3a. The variable appearance of reactive bone proliferation. Different types of subchondral sclerosis on the iliac and sacral side of the right sacroiliac joint: band-like (*1*); triangular (*2*); and spotty (*3*). At the left joint there are different types of ossification according to the location toward the linea terminalis. Above the linea terminalis a striated appearance (*4*) is seen, resulting in a star sign (*5*) at the upper part of the joint. There are hook-like bony projections (*6*) below the linea terminalis, at the inferior part of the joint. There are bony bridges (*7*) across the joint, resulting in complete ankylosis of the joint, sometimes appearing as a phantom joint (*8*). **b** Standard radiograph of the sacroiliac joints, demonstrating bilateral ankylosis. Note the "phantom sign" at the inferior part of the joint (*white arrow*). Ankylosis of the facet joints gives rise to the "trolley-track sign" (*arrowheads*). Ossification of the interspinous ligaments are seen as the "dagger sign" (*arrowhead*). Bilateral "star-sign" (*black arrows*) due to ossification of capsuloligamentous structures at the superior part of the sacroiliac joint. (From Lambrecht et al. 2005)

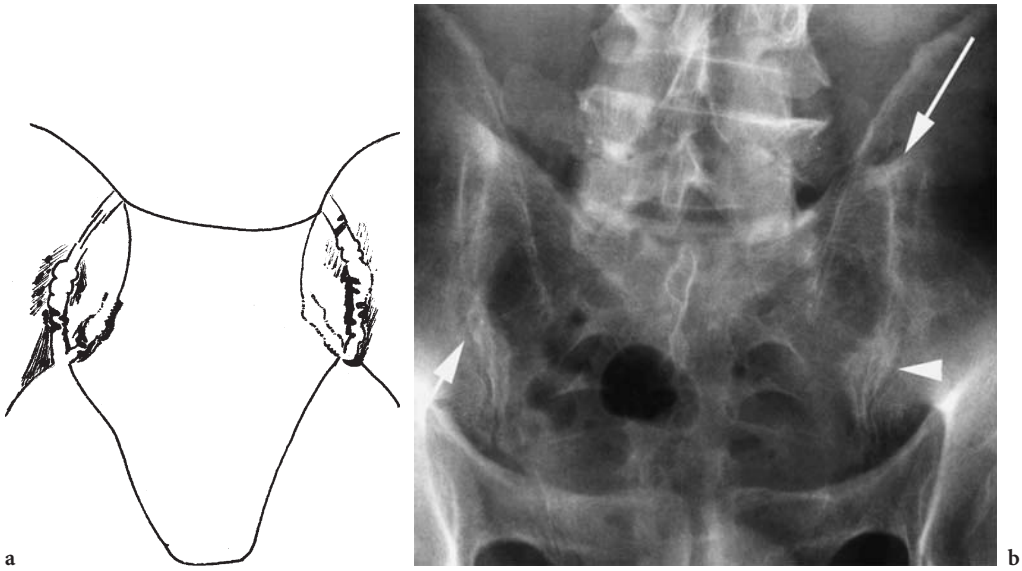

Fig. 23.4a,b. "Variegated sacroiliac picture." **a** Schematic drawing. **b** Anteroposterior radiograph of bilateral variegated sacroiliitis. Erosive and hazy subchondral cortex on the right side (*small arrow*), subchondral sclerosis (*arrowhead*), and beginning ankylosis with bony bridges (*arrow*) on the left side. (From Lambrecht et al. 2005)

tion and/or erosion of the ligamentous attachments to the iliac crest and ischial tuberosities leads to the so-called whiskered appearance. The pubic symphysis are involved in 23% of patients with AS (Vinson and Major 2003), with small succinct erosions and adjacent sclerosis, followed by total ankylosis.

23.2.5.2 The Spine

Abnormalities of the spine can be seen at the discovertebral junctions, apophyseal joints, costovertebral joints, posterior ligamentous attachments, and

atlantoaxial joints. Classically, changes are initially noted at the thoracolumbar and lumbosacral junctions. Spinal extension to the midlumbar, as well as the upper thoracic and cervical vertebrae, occurs with disease progression but may be arrested at any stage (Resnick 2002c).

During the course of AS, the spine may present destructive changes as well as features due to bone proliferation and ankylosis.

There is a spectrum of inflammatory and destructive lesions of the spine in AS that predominantly involves the cartilaginous discovertebral junction. One of the earliest plain-film findings of spinal involvement, typically seen at vertebrae T10 through L2, is the so-called **Romanus lesion**, also known as spondylitis anterior (Fig. 23.5). Inflammation (active enthesitis and fibro-osteitis) at the attachments of the outer fibers of the annulus fibrosus and longitudinal ligaments at the vertebral body causes small erosions at the anterosuperior and anteroinferior vertebral body corners (Ball 1979). Less frequently, this defect is seen at the posterior vertebral body corners. As the erosions heal, reactive sclerosis produces a "shiny-corner" configuration (Aufdermaur 1989).

Bony proliferation in the connective tissue between the anterior longitudinal ligament and the anterior surface of the vertebral body fills the concavity of the anterior vertebral surface. In combination with osseous erosion of the vertebral body rim, this results in a flattened or even convex anterior surface, creating a squared or barrel-shaped contour (Fig. 23.5). The "squaring phenomenon" is best identified on a lateral view of the lumbar spine, because a straightened anterior contour also occurs as a normal variant in the cervical and thoracic spine (Dihlman 1985).

Further along the spectrum of destructive discovertebral lesions are the **Andersson lesions**. Two types have been described. Andersson lesion type A is an inflammatory reaction with focal destruction of the intervertebral disc and the adjacent vertebral endplates, characterized histologically by herniation or invasion of disc material through the vertebral endplate. Plain-film radiographs characteristically show disc-space narrowing (usually), a circumscribed defect in the neighboring vertebral bodies or irregularities along the endplates, and a wide area of reactive sclerosis in the surrounding cancellous bone (Vinson and Major 2003). Differentiation from mechanically induced "erosive" osteochondrosis, which has a predilection for L4–S1, is sometimes difficult (Haller and Hofmann 2001). The "inflammatory type" develops primarily during the first 9 years of the disease and may be asymptomatic or cause acute (Dihlman 1985) focal back pain that, in contradiction to the typical pattern of AS pain, worsens with movement (Vinson and Major 2003).

The "noninflammatory" type B usually develops later in the evolution of the disease, after ankylosis has occurred. The ankylosed spine is vulnerable to fracture. The type-B Andersson lesion is thought to be a pseudarthrosis following a discovertebral fracture of the demineralized and extensively ossified, stiff axial skeleton (Haller and Hofmann 2001). It is usually located at the thoracolumbar or cervicothoracic junction, around an area of skipped ossification which has become the single point of motion in the entire spine and therefore undergoes degeneration with extensive, irregular destruction of the vertebral end plates extending into the subchondral bone of two neighboring vertebral bodies. Alternatively, it

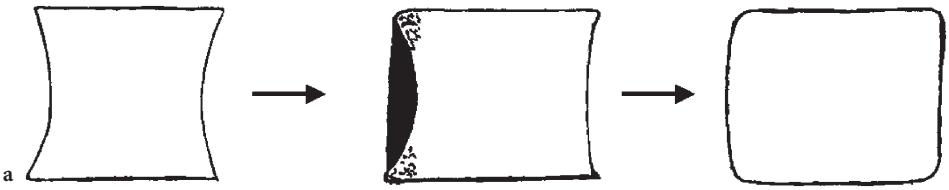

Fig. 23.5a,b. Radiographic appearance of anterior corner osteitis (Romanus lesion). **a** The inflammatory process and reactive sclerosis at the anteroinferior and anterosuperior corner of the vertebral bodies. The evolution from a normal vertebral body to a squared or barrel-shaped appearance is illustrated. **b** Lateral radiograph of the lumbar spine demonstrates several Romanus lesions at the anterior corners; some are completely sclerotic (shiny corner; *arrow*), others consist of a small erosion with surrounding sclerosis (*small arrow*). At the level of L3 and L4 there is extension of bone formation along the anterior margin of the vertebra resulting in a barrel-shaped appearance (*arrowhead*). (From Lambrecht et al. 2005)

may develop around an area of true fracture through the ankylosed apophyseal joints. On plain-film radiographs, there is destruction of the entire discovertebral junction with a normal or widened disc space and reactive sclerosis in the adjacent vertebral bodies (Vinson and Major 2003). The radiographic findings may mimic infectious spondylodiscitis or a neuropathic spine (Bennett et al. 2004).

Morphologically, Cawley et al. (1971, 1972) classified the lesions into three types: (a) those that involve the central portions of the discovertebral junction and are covered by the cartilaginous endplate (type I); (b) those that involve the peripheral portions of the discovertebral junction and are not covered by the cartilaginous endplate (type II); and (c) those that involve both the peripheral and the central portions of the discovertebral junction (type III). Type-I and type-II lesions may occur in the early or late stages of the disease, whereas type-III lesions are infrequently observed without spinal ankylosis (Jajic et al. 1982; Rasker et al. 1996; Rivelis and Freiberger 1969). Type-III lesions are believed to represent a "noninflammatory" type-B lesion, in which trauma, rather than inflammation, is the major factor in the production of these lesions (Fang et al. 1988; Pastershank and Resnick 1980; Resnick 2002c). The pathogenesis of type-I and type-II lesions is still debated. Both inflammatory factors (enthesopathy at the anterior or posterior corners in type-II lesions) or noninflammatory mechanical factors (cartilaginous node formation aggravated by osteoporosis, kyphosis, or instability from apophyseal joint disease in type-I and type-II lesions) may be etiological factors (Resnick 2002c).

Localized endplate defects accompanying Andersson lesions may mimic simple intravertebral herniations of Schmorl, but their delineation is usually more irregular and accompanied by more extensive adjacent reactive changes of the subchondral bone (Cawley et al. 1971).

The frequency of Andersson lesions in AS patients is estimated to be between 2.7 and 28% (Bennett et al. 2004; Vinson and Major 2003).

The erosive vertebral abnormalities are associated with bone formation. Ossification first takes place in the outer portion of the annulus fibrosus, where Sharpey's fibers attach to the vertebral body. This ossification will extend from Sharpey's fibers along the deep layers of the longitudinal ligaments, forming initially thin, vertical outgrowths along the contour of the disc. These syndesmophytes ossify one vertebral body to the adjacent vertebral body in a succinct fashion (Fig. 23.6a,b). The disc spaces are generally preserved. With disease progression, the syndesmophytes thicken (Fig. 23.6c) and involve the anterior longitudinal ligament and paravertebral soft tissues. The end result is the so-called bamboo spine (Fig. 23.7; Haller and Hofmann 2001). Syndesmophytes must be differentiated from vertebral osteophytes which are (sub)marginal ossifications caused by disk degeneration and grow horizontally.

Disuse osteoporosis of the spine may result from immobilization due to ankylosis. Decreased nutrition of the intervertebral disk may promote premature disk calcification in late stage disease. Furthermore, due to osteoporotic deformity of the vertebral body, the intervertebral disc appears biconvex, better known as "discal ballooning" (Fig. 23.7b).

Other target locations in the spine are summarized in Table 23.3 and are reviewed briefly.

The apophyseal joints may demonstrate erosions due to inflammation and reactive bone formation with subchondral sclerosis and ankylosis. Narrowing and osseous fusion of these joints can be apparent on standard radiography. Especially in the cervical spine, apophyseal joint ankylosis can be very striking (Fig. 23.8).

On the other hand, the triad of erosion, sclerosis, and ankylosis is more difficult to demonstrate on standard radiographs at the level of the costovertebral joints, because of superposition of adjacent structures.

Like in rheumatoid arthritis, inflammatory changes of the synovial and adjacent ligamentous structures in the atlantoaxial articulations can lead to erosions of the dens (Fig. 23.8) and even, although much less frequently, to atlantoaxial subluxation (Resnick and Shields 1994).

Enthesitis of the posterior ligamentous attachments of the spine leads to subligamentous erosion and ossification. On frontal radiographs ossification of the supraspinous and interspinous ligaments can be seen as a single central radiodense line, known as the "dagger sign" (Fig. 23.3b). Ossification of the apophyseal joint capsules forming two vertical radiodense lines lateral to this central line is apparent as the "trolley-" or "tram-track sign" on frontal view (Bennett 2004).

23.2.5.3 Other Joints

Besides the axial skeleton and the pelvis, shoulders and knees are the most commonly involved joints,

a

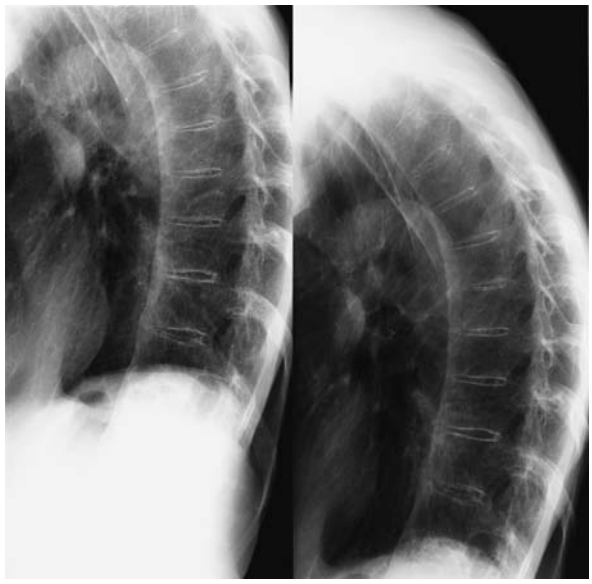

c

b

Fig. 23.6a–c. Typical radiographic appearance of syndesmophytes. **a** Anteroposterior view of an early-phase syndesmophyte. **b** Lateral tomograph of an early phase syndesmophyte. Presence of thin lateral outgrowths (**a**) and anterior outgrowths (**b**), extending in a vertical fashion from one vertebral body to another. In the early stage, those thin outgrowths represent ossifications of the annulus fibrosus itself. **c** Lateral radiograph of the thoracic spine. Ankylosed spine with more advanced syndesmophyte formation, in which the ossification process has spread to the anterior longitudinal ligament

but virtually every joint can be affected. The calcaneus is the most common site of extra-axial enthesopathy. Radiographically, these enthesopathies appear as whisker- and blister-like fibro-osteoses, serrated contour irregularities, and erosions.

23.2.6 Scintigraphy

Evaluation of sacroiliac, spinal, and peripheral abnormalities in AS with scintigraphy has been attempted with varying degrees of success (Resnick 2002c). At any location, an abnormal scintigraphic tracer uptake is not very specific, and accurate diagnosis necessitates correlation with clinical and imaging studies (Resnick 2002c).

Focal areas of augmented radionuclide accumulation in the spine usually indicate the site of an acute fracture or chronic "pseudarthrosis" (Gaucher et al. 1987), and the exact diagnosis can then be substantiated by plain films and CT scan (Resnick 2002c).

Moreover, scintigraphy lacks sensitivity, and even in patients with advanced disease of the sacroiliac joints and the spine (Godfrin et al. 2004), radionuclide uptake may be normal (Resnick 2002c). This poor sensitivity, which does not apply for peripheral enthesopathies, is attributed to the superposition of different anatomical structures (Bollow et al. 1995); therefore, scintigraphy is not advocated as a

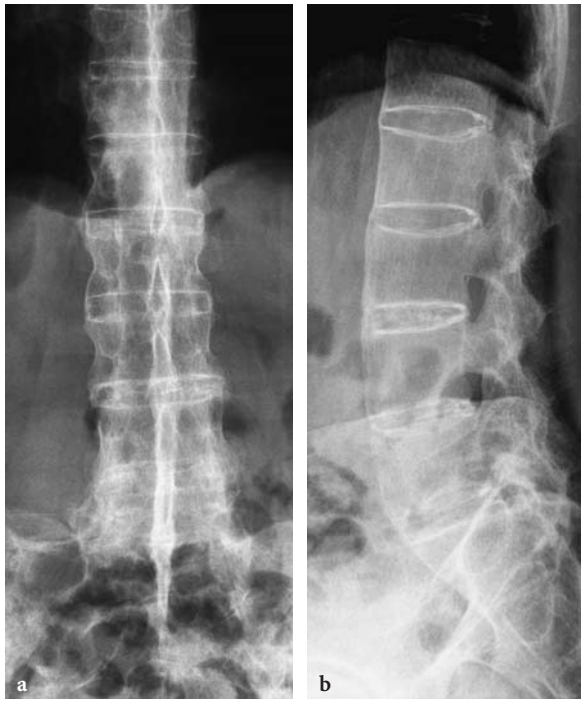

Fig. 23.7a,b. Late-stage ankylosing spondylitis. **a** Anteroposterior view of the lumbar spine. Multiple syndesmophytes bridging adjacent vertebral bodies. Note also ankylosis of the facet joints and ossification of the interspinous ligaments, resulting in a "trolley-track" (combining a central "dagger" sign and a peripheral tram-like track). **b** Lateral view of the lumbar spine in a second patient. Severe osteoporosis of the vertebral bodies with discal calcifications in a completely ankylosed so-called bamboo spine. (From Lambrecht et al. 2005)

Fig. 23.8 Ankylosing spondylitis of the cervical spine. Lateral spot view of the upper cervical spine. Severe osteoporosis due to longstanding ankylosis with very striking ossifications of the facet joints. There are also erosive changes and concomitant sclerosis at the dens axis, resulting in an increased atlanto-dental distance. (From Lambrecht et al. 2005)

useful screening tool in the assessment of axial involvement of AS.

23.2.7 Computed Tomography

Because of the difficulty in detecting early changes in the sacroiliac joints on plain film, CT has been advocated to delineate early sacroiliitis. Results, however, are conflicting (Resnick 2002c). Interpretation of CT scans must be accomplished by a knowledgeable radiologist who is well aware of the normal variations of the sacroiliac joint that can simulate inflammation (Resnick 2002c).

Other indications for CT scan are areas that are difficult to evaluate on plain radiography. Abnormalities of the facet, costovertebral, costotransverse, and atlantoaxial joints can be documented by CT (Levine et al. 2004). Computed tomography is also superior in the assessment of spinal fractures, spinal stenosis due to ossification of the ligamenta flava, and thecal diverticula (Resnick 2002c). A CT scan, however, is not very accurate for early detection of Romanus lesions. In general, therefore, the value of CT scan is limited.

23.2.8 Magnetic Resonance Imaging

23.2.8.1 Sacroiliac Joints

The presence of subchondral bone marrow edema on fluid-sensitive sequences in the sacroiliac joints is very suggestive for early sacroiliitis (Levine et al. 2004; Wittram et al. 1996; Yu et al. 1998).

Recent studies have focused on the benefits of using dynamic enhanced MRI for early detection of sacroiliitis (Bollow et al. 1995). Findings characteristic of AS include loss of the normal thin band of intermediate signal intensity representing cartilage on T1-weighted images, with replacement by a zone of heterogeneous mixed signal intensity, showing enhancement after gadolinium contrast administration. Dynamic enhanced MRI demonstrates distinct and rapid contrast enhancement of the joint space, in which both the degree and the rate of enhancement correspond to the severity of the inflammation (Bollow et al. 1995). The routine use of gadolinium is not required for diagnosis in all patients (Levine et al. 2004).

Erosions are shown as foci of high signal intensity in the subchondral bone, whereas subchondral sclerosis is seen as low signal intensity on all sequences (Fig. 23.9). In advanced disease, ankylosis can be noted as continuity of the medullary bone across the obliterated joint space (Levine et al. 2004).

23.2.8.2 The Spine

The typical MR appearances of an early vertebral osteitis (Romanus lesion) consists of low signal intensity on T1-weighted images, with marked contrast enhancement after gadolinium contrast administration and high signal intensity on T2-weighted images (Fig. 23.10) (Jevtic et al. 2000). These features are thought to reflect edema and hyperemia of inflammation, due to active enthesitis and osteitis at the attachments of the annulus fibrosis and longitudinal ligaments, where the disc, the anterior ligament, and the vertebral body meet

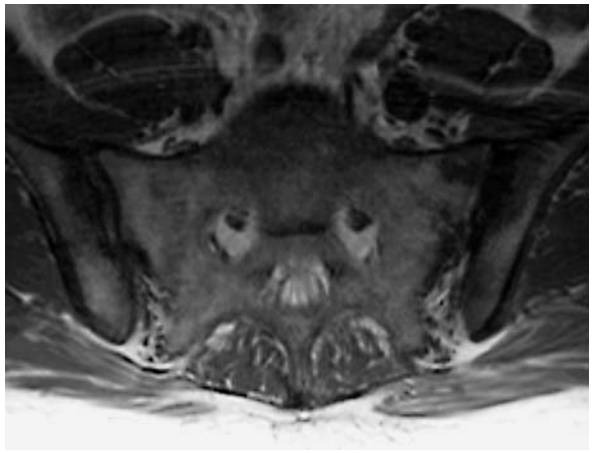

a

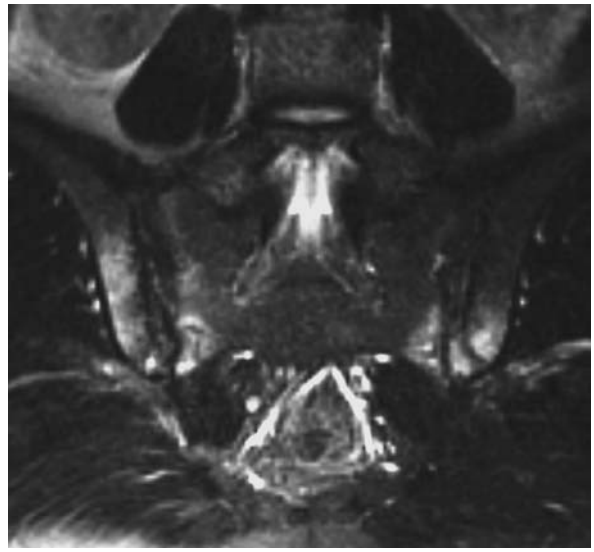

b

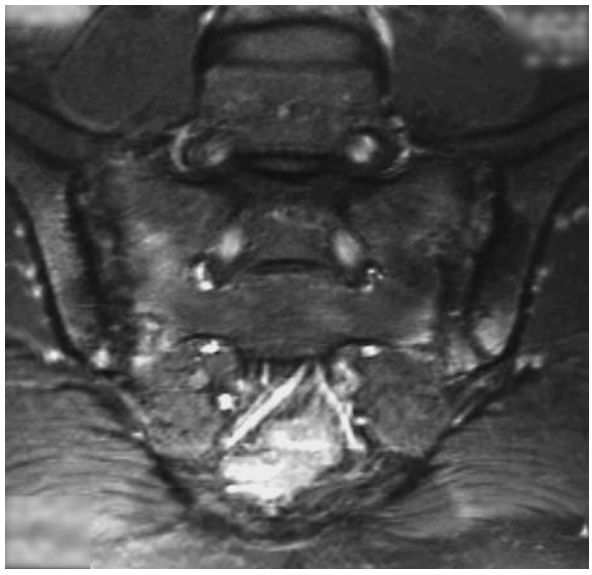

c

Fig. 23.9a–c. The MRI appearance of established sacroiliitis. **a** Coronal oblique spin-echo T1-weighted image. **b** Coronal oblique fat-suppressed fast spin-echo T2-weighted image. **c** Coronal oblique spin echo T1-weighted image with fat suppresion after intravenous gadolinium contrast administration. Areas of subchondral sclerosis are hypointense on all pulse sequences. Erosions are hyperintense on T2-weighted image. Furthermore, extensive bone marrow edema is seen parallel to the sacroiliac joints

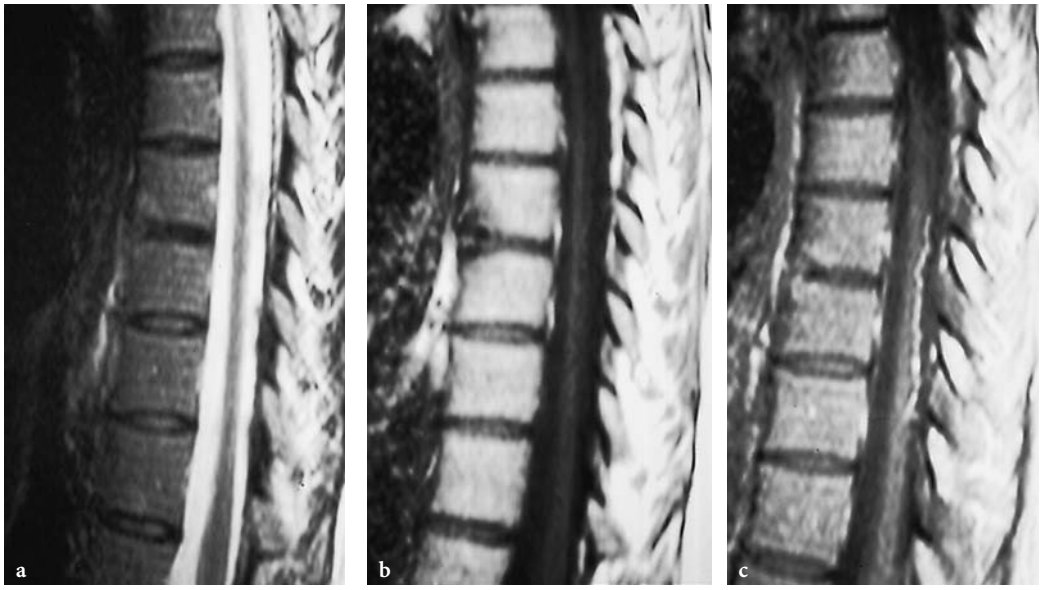

Fig. 23.10a–c. The MRI appearance of a Romanus lesion. **a** Sagittal fast spin-echo T2-weighted image. **b** Sagittal spin-echo T1-weighted image. **c** Sagittal spin-echo T1-weighted image after intravenous gadolinium contrast administration. Note focal anterior corner destruction and associated bone marrow edema at the thoracolumbar junction. There is contrast enhancement of the anterior corner lesions

(Levine et al. 2004). Magnetic resonance imaging is more sensitive than conventional radiography as an indicator of early inflammatory changes at the vertebral body corners (Levine et al. 2004; Vinson and Major 2003). According to some authors, vertebral enthesitis resembles peripheral enthesitis and these signal changes on MRI may be observed in absence of clinical or radiographic evidence of AS (Marc et al. 1997; Rasker et al. 1996).

In the healing phase of enthesitis with plain radiographic evidence of marginal syndesmophyte formation, MRI shows high signal intensity at the vertebral corners on T1- and T2-weighted images with no significant contrast enhancement, thought to represent yellow marrow accumulation (Levine et al. 2004; Oostveen and van de Laar 2000).

Some discovertebral junctions display low signal intensity on T1- and T2-weighted images, likely due to marginal osteosclerosis (Jevtic et al. 2000).

Further along the spectrum of discovertebral diseases are the more destructive lesions, such as Andersson lesions. As discussed previously, three types are distinguished:

- Type I shows central focal endplate destruction with intraosseous disc herniation and associated reactive endplate changes, the nature of which depends on the age of the lesion (Levine et al. 2004). In the relatively acute stage, marrow edema is identified, with enhancement after intravenous gadolinium contrast administration (Fig. 23.11).
- Type-II lesions are located more at the periphery of the discovertebral junction.
- Type-III lesions involving both the central and the peripheral portions may be difficult to differentiate from infectious spondylodiscitis (Fig. 23.12). The absence of an anterior paraspinal soft tissue mass and the predominant low signal intensity of the intervertebral disc on T2-weighted images (with only possible minor areas of high signal intensity adjacent to vertebral erosions) indicate a noninfectious Andersson lesion.

Disc calcifications in patients with AS are traditionally believed to cause low signal on all sequences; however, some patients with long-standing disease show foci of increased signal intensity within the disc on T1-weighted images. This hyperintensity of the calcified discs is thought to be related to the physical structure of the calcium deposits (Levine et al. 2004; Tyrell et al. 1995). Moreover, high signal intensity areas on T2-weighted images have been described within calcified discs (Tyrell et al. 1995). Here, the absence of associated vertebral marrow changes and correlation with plain radiography is the clue in the differential diagnosis with infectious spondylodiscitis.

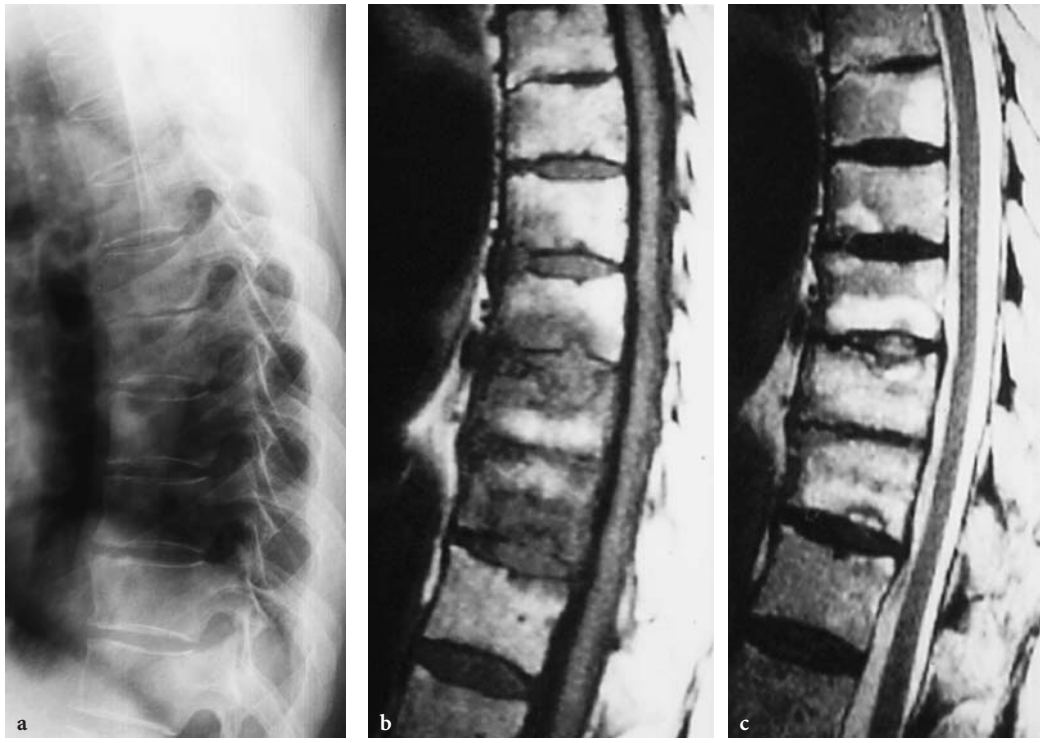

Fig. 23.11a–c. Type-1 and type-2 discovertebral lesions of Andersson. **a** Lateral radiograph. **b** Sagittal spin-echo T1-weighted image. **c** Sagittal fast spin-echo T2-weighted image. The plain radiograph (**a**) shows typical multifocal osteitis at the anterior corners of the lower thoracic vertebrae. Radiographically, there is erosion and reactive sclerosis. Note a more extensive lesion at the midthoracic spine, in which there is a more uniform irregular delineation of the end plates and associated narrowing of the disc space. On MRI (**b**, **c**), both central (type 1) and peripheral (type 2) discovertebral lesions are seen. Type-1 lesions demonstrate intraosseous disc herniations (Schmorl's nodes). Note also the presence of bone marrow edema on both sides of the disc space

Other potential applications of MRI in the assessment of spinal AS are involvement of the facet, costovertebral, and costotransverse joints, and spinal stenosis due to involvement of the ligamenta flava. Involvement of the small joints of the spine is demonstrated on MRI initially as subchondral edema, which progresses to sclerosis and eventually to ankylosis (Levine et al. 2004). Involvement of the ligamenta flava, as well as the interspinous and supraspinous ligaments, may initially result in thickening of these structures. Later, ossification results in increased signal intensity on all sequences corresponding to fatty bone marrow signal characteristics (Levine et al. 2004).

Magnetic resonance imaging is also the preferred imaging technique for the assessment of specific spinal complications of AS, such as fractures, vertebral pseudarthrosis, and cauda equina syndrome

The AS patients are particularly susceptible to fracture as a consequence of their spinal rigidity and osteoporosis (de Peretti et al. 2004; Devogelaer et al. 1992; Koivikko et al. 2004; Pedrosa et al. 2002). Fractures through the disc space, the weakest point in the ankylosed spine, are the most common, especially in the cervical spine.

Although CT is still preferred for identifying the site and extent of fractures, MRI is invaluable in the evaluation of (paravertebral) hematoma, disruption of ligamentous structures, the intervertebral disc, vertebral bone marrow edema, and associated spinal cord injury (Fig. 23.13). Catastrophic spinal cord injuries include hemorrhagic cord contusion, intramedullary hematoma, and complete cord transection.

Posttraumatic cord contusion may even occur in the absence of overt fracture (Levine et al. 2004).

Cauda equina syndrome is a rare complication of AS, the mechanism of which remains unclear (Mitchell et al. 1990). Magnetic resonance imaging shows widening of the dural sac with arachnoid diverticula. Posterior vertebral body erosion may be an associated finding (Levine et al. 2004).

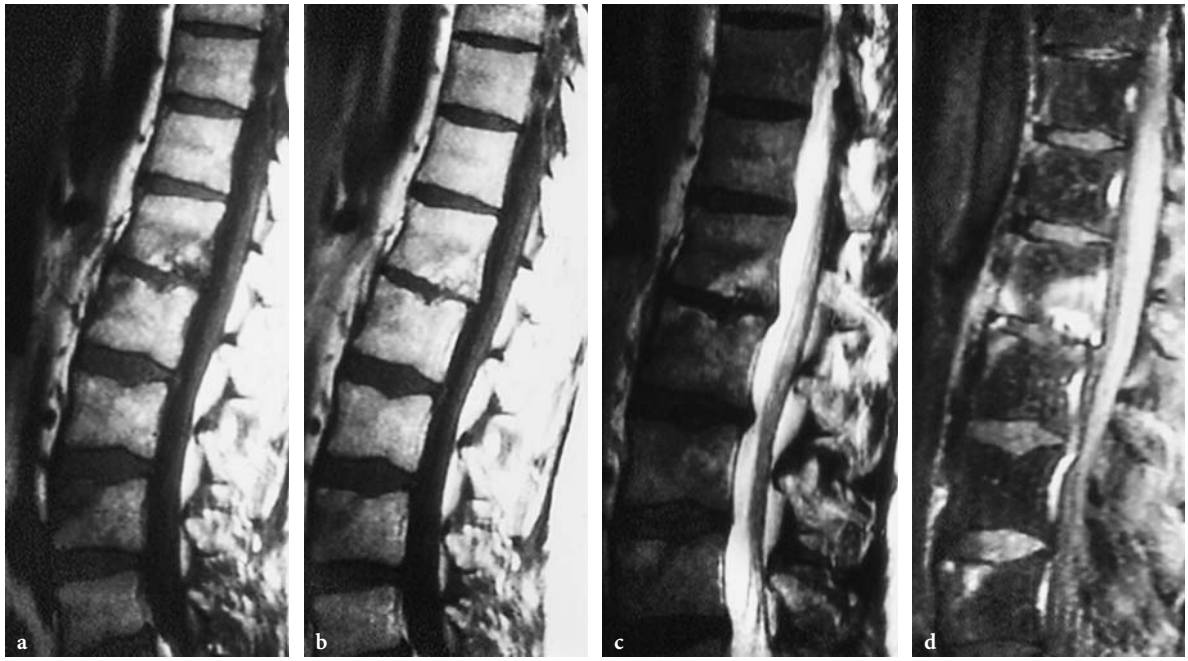

Fig. 23.12a–d. Type-3 discovertebral lesions of Andersson. **a** Sagittal spin-echo T1-weighted image. **b** Parasagittal spin-echo T1-weighted image. **c** Sagittal fast spin-echo T2-weighted image. **d** Sagittal spin-echo T1-weighted image with fat suppression after gadolinium contrast enhancement. Type-3 lesions involve both the central and peripheral portions of the discovertebral junctions. Note extensive contrast enhancement of the lesions

Fig. 23.13. Thoracic fracture through the disc space in an ankylosed spine. Sagittal fast spin-echo T2-weighted image, demonstrating a fracture through the disc space, extending posteriorly through the ossified interspinous ligaments. There is focal narrowing of the spinal canal. Note an associated type-3 destructive discovertebral lesion on an adjacent level

Atrophy of the paraspinal muscles may also be readily identified on CT and MRI in longstanding AS, and is believed to be secondary to limitation of mobility (Vinson and Major 2003).

23.2.8.3 Role of MRI in Diagnosis and Management of AS

Magnetic resonance imaging may enable early diagnosis of spinal manifestations of AS by an increased sensitivity for identification of early-stage sacroiliitis or vertebral osteitis.

Magnetic resonance imaging is also superior to other imaging techniques for differential diagnosis of Andersson lesions vs infectious spondylodiscitis and in the evaluation of most acute and chronic spinal complications of AS.

Also, MRI has been used to assess the effect of tumor necrosis factor alpha block with drugs in the management of acute inflammatory lesions (Braun et al. 2003; Marzo-Ortega et al. 2001).

23.3 Psoriatic Arthritis

23.3.1 Definition and Epidemiology

Psoriatic arthritis (PA) is a seronegative spondylarthropathy that occurs in 10–15% of people with psoriasis. For many years the joint abnormalities associated with psoriasis were considered to be part of the spectrum of rheumatoid arthritis. Since 1964 the disease has been defined as a separate and distinct articular disorder by the American Rheumatism Association (Helliwell and Wright 1994).

Psoriatic arthritis can affect synovial and cartilaginous joints and sites of tendon and ligament attachment to bone in both the appendicular and the axial skeleton. In this regard, it is similar to Reiter's syndrome and AS, and differs from rheumatoid arthritis, in which significant alterations of cartilaginous and tendinous attachments are less frequent (Resnick 2002a).

The usual age of onset is between 30 and 50 years (Klecker and Weissman 2003). Cutaneous disease commonly precedes joint disease by months or years. In 15% of cases skin abnormalities and articular disease coincide, and in 10% arthritis antedates skin disease (Martel et al. 1980). Men and women are equally affected (Klecker and Weissman 2003).

The pathogenesis of the disease is not completely understood. A familial occurrence has been described, and histocompatibility typing in patients with psoriatic arthritis has revealed a 25–60% incidence of HLA-B27 antigen (Klecker and Weissman 2003; Moll and Wright 1973; Moll 1979; Schumacher et al. 1978).

AIDS has been associated with severe exacerbation of rapidly evolutive and therapy resistant PA (Cuellar and Espinoza 2000; Solinger 2003).

23.3.2 Clinical Features

In order of frequency, Moll and Wright (1973) described five broad clinical categories of PA:

- Type 1: The most common form (70%) presents as oligoarticular, asymmetrical involvement, first appearing in the distal interphalangeal joints of the hands and feet. The interphalangeal, metacarpophalangeal, and metatarsophalangeal joints are asymmetrically involved. The so-called sausage digit is associated with this group.
- Type 2 resembles rheumatoid arthritis with multiple joint involvement frequently of the hands, knees, ankles, and feet but in an asymmetrical fashion. It accounts for 15% of PA. Systemic symptoms such as fever, weight loss, fatigue, and anemia may be present. The final deformity, however, is usually less extensive, and the laboratory findings characteristic of rheumatoid arthritis are absent.
- Type 3 consists of patients with a deforming type of arthritis with widespread ankylosis and, occasionally, "arthritis mutilans" (accounting for 5% of PA).
- Type 4 is a polyarthritis characterized by predominant involvement of the distal interphalangeal joints (5% of cases).
- Type 5: The predominant feature in this category is sacroiliitis and spondylitis resembling ankylosing spondylitis (5% of cases).

In daily clinical practice, this classification is difficult to handle. Moreover, the most common presentation is that of polyarthritis, often mimicking rheumatoid arthritis (Helliwell et al. 1991; Taylor et al. 2004). The prognosis is variable but often better than rheumatoid polyarthritis.

Other clinical features are the typical macular or papular rash with characteristic silver scales predominantly located over the extensor surfaces. Nail abnormalities and ocular manifestations occur frequently as well.

23.3.3 Conventional Radiographic Findings of PA

23.3.3.1 Sacroiliac Joints and Pelvis

The sacroiliac joints are affected in 20% of patients with PA (Moll 1979). The sacroiliitis accompanying psoriasis is usually bilateral and symmetrical. Although asymmetrical or unilateral involvement is uncommon, this feature may help in the differential diagnosis with AS; in the latter, sacroiliac joint changes are always symmetrical (Helliwell and Wright 1994; Resnick 2002a; Schumacher et al. 1978). The radiographic picture resembles AS, but ankylosis is much less common than in AS (Klecker and Weissman 2003).

23.3.3.2 The Spine

Spondylitis is uncommon in the absence of sacroiliitis. Approximately 5% of patients with PA have exclusive spine involvement. Spinal involvement with one of the forms of peripheral joint disease is more common and seen in 20–40% of patients (Klecker and Weissman 2003).

Although spinal manifestations of PA resemble those seen in AS, there are some features that may distinguish spinal PA from AS.

Firstly, PA is characterized by a progressive noncontiguous involvement of the spine, and its disease course is milder compared to AS (Moll and Wright 1973).

Secondly, the paravertebral ossifications seen in PA differ from the syndesmophytes of AS and spondylitis in inflammatory bowel disease. Indeed, they are of bigger size, and have a unilateral or asymmetrical distribution. These arise typically beyond the margin of the vertebral body, and are therefore designated as nonmarginal paravertebral ossification or parasyndesmophytes.

The large and bulky aspect of these overgrowths may reflect the process of extensive bone proliferation, which is the hallmark of PA. The nonmarginal bridging occurs in a random, asymmetrical fashion and is most common in the thoracolumbar spine, usually sparing the lumbar spine (Klecker and Weissman 2003). These outgrowths occasionally involve the cervical spine (Fig. 23.14).

The paravertebral ossifications may resemble diffuse idiopathic skeletal hyperostosis (DISH), also known as Forrestier's disease (Helliwell and Wright 1994).

Occasionally, however, the slender, central and symmetric outgrowths in PA are identical to the syndesmophytes of ankylosing spondylitis. In addition to the pattern and distribution of bony outgrowths, other features of PA differ from those in classic AS.

In PA there is relative sparing of the apophyseal joints (Klecker and Weissman 2003). According to some investigators, the large size of the paravertebral ossifications in PA is due to less involvement of the apophyseal joints. Indeed, the relatively normal posterior spinal mobility leads to greater tensile forces anteriorly and promotes paravertebral inflammation and bone formation (De Vlam et al. 1996; Resnick 2002a).

Furthermore, osteitis and squaring of the anterior surfaces of the vertebral bodies are relatively infrequent in PA. Discovertebral erosions in the thoracolumbar spine are rare in PA compared with AS (Resnick 2002a).

Fig. 23.14. Psoriatic arthritis of the cervical spine. Lateral radiograph. The vertical syndesmophytes at the anterior aspect of the spine are larger than those seen in ankylosing spondylitis. There is fusion of most of the visible facet joints, which is unusual in psoriatic arthritis and is more frequently seen in ankylosing spondylitis

In psoriatic spondylitis of the cervical spine, erosions may arise anywhere along the surface of the vertebral body, the apophyseal joints, or the spinous processes.

Anterior ligament calcification has been seen in 19% of radiographs of patients with PA (Klecker and Weissman 2003).

Atlanto-axial subluxation may be associated with sclerosis and erosion of both the dens and the arch of the atlas (Klecker and Weissman 2003; Lassoued et al. 1989).

23.3.4 Imaging Other Than Plain Radiography

The use of MRI in PA has received little emphasis (Resnick 2002a). Generally, MRI could be a useful imaging tool for early detection of spinal and sacroiliac manifestations by demonstrating bone mar-

row edema. On the other hand, in the more chronic phase, MRI could be helpful to assess disease activity and for follow-up of response to treatment.

Scintigraphy and computed tomography are not promoted as routine screening tools in the assessment of PA.

23.4 Reiter's Syndrome

23.4.1 Definition and Epidemiology

Reiter's syndrome is a subgroup of reactive arthritis that occurs following an infection at a site remote from the involved joint. Reactive arthritis may be triggered by enteric or urogenital infection (Klecker and Weissman 2003).

The syndrome was first described by Hans Reiter in 1916, who incorrectly identified the causative agent as a spirochete. In the same year, Fiessinger and LeRoy correctly attributed the syndrome to *Shigella*. Subsequently, other infectious agents have been associated with Reiter's syndrome.

It is historically characterized by the triad of arthritis, urethritis (or cervicitis), and conjunctivitis. In some patients, balanitis or buccal ulcerations may also be present as a fourth manifestation of the disease. Currently, it is recognized that many patients with Reiter's syndrome do not demonstrate the entire clinical triad. Most patients are between 15 and 40 years of age.

The presence of HLA-B27 antigen is strongly associated in 60–85% of patients. In these cases prognosis is worse, and an evolution to spondylarthropathy is seen in 30–50% of cases.

23.4.2 Articular Symptoms

Characteristically, acute asymmetric arthritis of the lower extremity becomes evident in Reiter's syndrome, often within 1–3 weeks of the inciting episode of urethritis or diarrhea. Initially, the most commonly affected joints are the knee and the ankle, followed by the metatarsophalangeal joints, heel, shoulder, wrist, hip, and lumbar spine. Subsequently, more widespread articular changes can occur (Resnick 2002a). Heel pain is a common manifestation of Reiter's syndrome.

The arthritic attacks of Reiter's syndrome are usually self-limiting and of short duration, although recurrences are frequent. Residual disability and deformity occurs in approximately 5% of patients (Resnick 2002a).

23.4.3 Imaging Findings of the Axial Skeleton

Radiological manifestations of Reiter's syndrome of the sacroiliac joints and the spine are very similar to those of psoriatic arthritis (Klecker and Weissman 2003; Resnick 1989). In chronic Reiter's syndrome, 40–60% of patients may have radiographic evidence of sacroiliitis (Klecker and Weissman 2003). Bilateral sacroiliac involvement is common, but, as in PA, unilateral or asymmetrical involvement can occur, especially early in the disease course.

Paravertebral ossifications resemble parasyndesmophytes of PA, with relative sparing of the anterior surface of the spine (Klecker and Weissman 2003). The facet joints are only rarely involved (Fig. 23.15).

The clue to the differential diagnosis is the association with the classical clinical triad, either in its complete or incomplete form, and the knowledge of

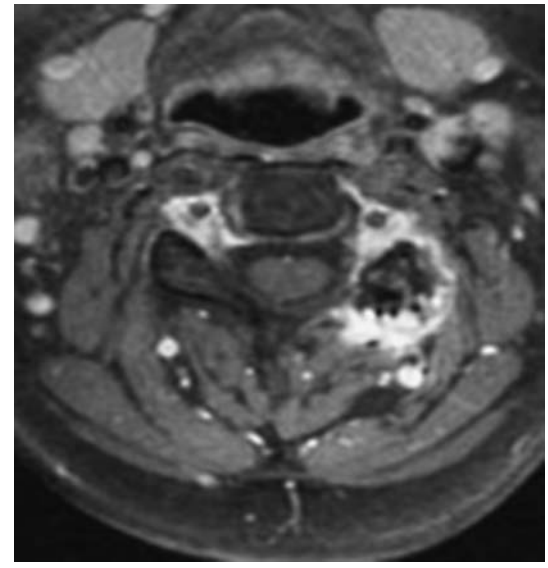

Fig. 23.15. Reiter's syndrome of the cervical spine. Axial fat-suppressed T1-weighted image after gadolinium contrast administration. Note unusual involvement of the left facet joint, demonstrating irregular delineation and enhancement on both sides of the joint space

recurrent attacks of peripheral asymmetric oligoarthritis, predominantly of the joints of the lower extremities.

Furthermore, the cervical spine is often spared in Reiter's syndrome (Klecker and Weissman 2003), although this is not true in all cases (Fig. 23.15).

23.5 Enteropathic Spondylarthropathy

23.5.1 Definition and Epidemiology

The appearance of arthritis in patients with inflammatory intestinal disease (ulcerative colitis, Crohn's disease, and Whipple's disease) has been described since 1950 (Gravallese and Kantrowitz 1988). These abnormalities have been designated enteropathic arthritis (Resnick 2002a).

Both the peripheral joints and the axial skeleton (spondylarthropathy) may be involved in enteropathic arthritis. The axial skeleton is involved in about 10% of patients (Gravallese and Kantrowitz 1988).

23.5.2 Imaging Findings of the Axial Skeleton

Radiological manifestations of enteropathic spondylarthropathy (sacroiliitis and spondylitis) are indistinguishable from AS (Fig. 23.16) (Gravallese and Kantrowitz 1988).

Axial involvement is poorly correlated with activity of bowel disease, whereas a close temporal association exists between exacerbations of intestinal disease and peripheral joint inflammation (Gravallese and Kantrowitz 1988; Resnick 2002a).

23.6 SAPHO

23.6.1 Definition and Terminology

The acronym SAPHO (synovitis, acne, pustulosis, hyperostosis, osteitis) is considered as a spondylarthropathy associated with different types of cutaneous pustules (Chamot et al. 1987). According to

Fig. 23.16a,b. Enteropathic spondylarthropathy in a patient with Crohn's disease. **a**,**b** Lateral radiographs of the lumbar spine in two different patients. Typical anterior corner lesion (**a**). Ankylosed spine, with associated disc calcification in long-standing disease (**b**). On imaging, the lesions are similar to those seen in ankylosing spondylitis

some authors, however, the term pustulotic arthro-osteitis (PAO) is more appropriate (Freyschmidt and Freyschmidt-Paul 2001). Indeed, acne-associated skeletal changes are usually associated with chronic recurrent multifocal osteomyelitis (CRMO) (Yu et al. 1998; Vanhoenacker 1998), whereas skin lesions associated with PAO or SAPHO consist of palmoplantar pustulosis (PPP). Hyperostosis is usually the result of chronic aseptic osteitis. Furthermore, not all patients have synovitis. This means that S for synovitis, A for acne, and H for hyperostosis are superfluous or redundant in the term SAPHO, leaving only P and O. Since the sternocostoclavicular region is nearly always involved, it is appropriate to insert A for arthropathy, resulting in the acronym PAO.

23.6.2 Clinical Findings

Patient age usually ranges from 20 to 60 years, and there is no gender predilection. HLA-B27 association has been reported, but precise data are not available. The key clinical finding to the diagnosis is the presence of PPP, a chronic condition of the palms of the hands and soles of the feet. It is characterized by recurring eruptions of sterile pustules on an initially normal skin. With time, the pustules dry up and desquamate, leaving a heterogeneous pattern of yellowish dried pustules and small brown scaly crusts. The PPP may be superimposed on classic psoriasis, supporting the idea that PPP is a variant of psoriasis. Moreover, because of the similarities of skeletal changes in SAPHO and the other spondylarthropathies, SAPHO can be classified as a seronegative spondylarthropathy.

The earliest articular symptoms consist of swelling and redness located at the manubrial region. Spinal involvement may manifest as chronic low back pain associated with painful stiffening.

23.6.3 Imaging Findings of the Axial Skeleton

In about 33–50% of cases, the sacroiliac joints are involved. Typically, unilateral sacroiliitis is found with large erosions and an important reactive sclerosis.

In more than 50% of patients, the spine is involved. Radiologically, SAPHO presents with a combination of osteolytic and sclerotic changes. Spinal involvement can be misinterpreted as primary subacute to chronic bacterial spondylitis or spondylodiscitis (Chamot et al. 1987). This accounts for many unnecessary biopsies when the radiologist fails to recognize the systemic nature of the changes.

Usually two or more vertebral bodies are affected including the intervertebral space. Often the changes are accompanied by syndesmophytes or mixed-osteophyte-type outgrowths (Resnick and Niwayama 2002). Other features consist of vertebral squaring and erosions of the anterior vertebral corners. These features may support the relationship between SAPHO and other spondylarthropathies, such as AS, PA, and Reiter's syndrome.

Plain radiography is usually sufficient for the diagnosis, but CT scan may allow an early diagnosis in some patients (Fig. 23.17).

Magnetic resonance imaging is rarely required but may be helpful in excluding tumoral or infectious disease. In essence, MRI findings consist of an enthesopathy of the anterior vertebral corners, as described in other spondylarthropathies (Laredo et al. 2003). This inflammatory focus may extend in different directions, including the adjacent vertebral end-

Fig. 23.17a,b. The SAPHO (synovitis, acne, pustulosis palmoplantaris, hyperostosis and osteitis) syndrome (pustulotic arthro-osteitis). **a** Lateral radiograph of the thoracic spine revealing multifocal irregular end-plate delineation, reactive sclerosis (particularly at the anterior cortex of the vertebral bodies), and narrowing of the disc space at the midthoracic spine. Note a vertebral fracture at the lumbar spine with associated end-plate sclerosis. **b** On a sagittal reformatted CT scan, these findings are more accurately demonstrated

plate, along the anterior vertebral cortex or towards the anterior corner of the adjacent vertebral body.

In rare cases, the disc is of high signal intensity and enhances after contrast administration, making a differential diagnosis with infectious spondylodiscitis very difficult.

23.6.4 Other Skeletal Manifestations

Involvement of the sternocostoclavicular, manubriosternal joints, and the appendicular skeleton are cardinal characteristics of the SAPHO syndrome.

23.7 Conclusion

Whereas newer techniques, such as MRI, certainly have a role in early diagnosis, assessment of spinal complications, and monitoring of treatment response in spondylarthropathies, standard radiography is the mainstay in the overall evaluation of the different spinal manifestations of this group of diseases.

References

Aufdermaur M (1989) Pathogenesis of square bodies in ankylosing spondylitis. Ann Rheum Dis 48(8):628–631

Ball J (1979) Articular pathology of ankylosing spondylitis. Clin Orthop Relat Res (143):30–37

Barozzi L, Olivieri I, De Matteis M, Padula A, Pavlica P (1998) Seronegative spondylarthropathies: imaging of spondylitis, enthesitis and dactylitis. Eur J Radiol 27 (Suppl 1): S12–S17

Bennett DL, Ohashi K, El-Khoury GY (2004) Spondyloarthropathies: ankylosing spondylitis and psoriatic arthritis. Radiol Clin North Am 42:121–134

Bollow M, Braun J, Hamm B et al. (1995) Early sacroiliitis in patients with spondyloarthropathy: evaluation with dynamic gadolinium-enhanced MR imaging. Radiology 194(2):529–536

Braun J, Bollow M, Remlinger G et al. (1998) Prevalence of spondylarthropathies in HLA-B27 positive and negative blood donors. Arthritis Rheum 41(1):58–67

Braun J, Baraliakos X, Golder W et al. (2003) Magnetic resonance imaging examinations of the spine in patients with ankylosing spondylitis, before and after successful therapy with infliximab: evaluation of a new scoring system. Arthritis Rheum 48:1126–1136

Cawley MI, Chalmers TM, Ball J (1971) Destructive lesions of vertebral bodies in ankylosing spondylitis. Ann Rheum Dis 30(5):539–540

Cawley MI, Chalmers TM, Kellgren JH, Ball J (1972) Destructive lesions of vertebral bodies in ankylosing spondylitis. Ann Rheum Dis 31(5):345–358

Chamot AM, Benhamou CL, Kahn MF, Beraneck L, Kaplan G, Prost A (1987) Le syndrome acné, pustulose, hyperostose, ostéïte. Resultats d'une enquête nationale. A propos de 85 cas. Rev Rhum Mal Osteoartic 54(3):187–196

Cuellar ML, Espinoza LR (2000) Rheumatic manifestations of HIV-AIDS. Baillieres Best Pract Res Clin Rheumatol 14(3):579–593

De Vlam K, Mielants H, Veys EM (1996) Association between ankylosing spondylitis and diffuse idiopathic skeletal hyperostosis: Reality or fiction? Clin Exp Rheumatol 14:5

Devogelaer JP, Maldague B, Malghem J, Nagant de Deuxchaisnes C (1992) Appendicular and vertebral bone mass in ankylosing spondylitis. A comparison of plain radiographs with single- and dual-photon absorptiometry and with quantitative computed tomography. Arthritis Rheum 35(9):1062–1067

Dihlman W (1985) Joints and vertebral connections. Thieme, Stuttgart

El-Khoury GY, Kathol MH, Brandser EA (1996) Seronegative spondyloarthropathies. Radiol Clin North Am. 34:343–357

Fang D, Leong JC, Ho EK, Chan FL, Chow SP (1988) Spinal pseudarthrosis in ankylosing spondylitis. Clinicopathological correlation and the results of anterior spinal fusion. J Bone Joint Surg Br 70(3):443–447

Fournie B (1993) La région enthésique: le concept étendu de territoire enthésique. Presse Med 22(35):1767–1769

Freyschmidt J, Freyschmidt-Paul P (2001) SKIBO diseases: a concept to avoid bloody diagnostic procedures in ambiguous skeletal lesions. Eur Radiol 11:1729–1742

Gaucher A, Pere P, Regent D, Grandhaye P, Aussedat R, Vivard T (1987) Spondylarthropathies ou polyenthésites ossifiantes, arguments scintigraphiques et scanographiques. Rev Rhum Mal Osteoartic 54(3):243–248

Godfrin B, Zabraniecki L, Lamboley V, Bertrand-Latour F, Sans N, Fournie B (2004) Spondyloarthropathy with entheseal pain. A prospective study in 33 patients. Joint Bone Spine 71(6):557–562

Gravallese EM, Kantrowitz FG (1988) Arthritic manifestations of inflammatory bowel disease. Am J Gastroenterol 83(7):703–709

Haller J, Hofmann J (2001) Ankylosing spondylitis. In: Bohndorf K (ed) Musculoskeletal imaging. A concise multimodality approach. Thieme, Stuttgart, pp 346–351

Helliwell P, Wright V (1994) Psoriatic arthritis: clinical features. In: Klippel JH, Dieppe P(eds) Rheumatology. Mosby-Year Book, London, pp 1–8

Helliwell P, Marchesoni A, Peters M, Barker M, Wright V (1991) A re-evaluation of the osteoarticular manifestations of psoriasis. Br J Rheumatol 30(5):339–345

Jajic I, Furst Z, Vuksic B (1982) Spondylitis erosiva: report on 9 patients. Ann Rheum Dis 41(3):237–241

Jevtic V, Kos-Golja M, Rozman B, McCall I (2000). Marginal erosive discovertebral "Romanus" lesions in ankylosing spondylitis demonstrated by contrast enhanced Gd-DTPA magnetic resonance imaging. Skeletal Radiol 29(1):27–33

Klecker RJ, Weissman BN (2003) Imaging features of psoriatic arthritis and Reiter's syndrome. Semin Musculoskelet Radiol 7(2):115–126

Koivikko MP, Kiuru MJ, Koskinen SK (2004) Multidetector computed tomography of cervical spine fractures in ankylosing spondylitis. Acta Radiol 45(7):751–759

Lambrecht V, Vanhoenacker FM, Van Dyck P, Gielen J, Parizel PM (2005). Ankylosing spondylitis: What remains of the standard radiography anno 2004? JBR-BTR 88:25–41

Laredo J, Lagier R, Vuillemin-Bodaghi V, Bard H (2003) L'IRM des spondylarthropathies. In: Bard H (ed) Tendons et enthèses. Sauramps, Montpellier, pp 145–156

Lassoued S, Hamidou M, Fournie B, Fournie A (1989) Cervical spine involvement in psoriatic arthritis. J Rheumatol 16(2):251–252

Lawrence RC, Helmick CG, Arnett FC et al. (1998) Estimates of the prevalence of arthritis and selected musculoskeletal disorders in the United States. Arthritis Rheum 41(5):778–799

Levine DS, Forbat SM, Saifuddin A (2004) MRI of the axial skeletal manifestations of ankylosing spondylitis. Clin Radiol 59:400–413

Marc V, Dromer C, Le Guennec P, Manelfe C, Fournie B (1997) Magnetic resonance imaging and axial involvement in spondylarthropathies. Delineation of the spinal entheses. Rev Rhum Engl Ed 64(7–9):465–473

Martel W, Stuck KJ, Dworin AM, Hylland RG (1980) Erosive osteoarthritis and psoriatic arthritis: a radiologic comparison in the hand, wrist, and foot. Am J Roentgenol 134(1):125–135

Marzo-Ortega H, McGonagle D, O'Connor P, Emery P (2001) Efficacy of etanercept in the treatment of the entheseal pathology in resistant spondylarthropathy: a clinical and magnetic resonance imaging study. Arthritis Rheum 44:2112–2117

Mitchell MJ, Sartoris DJ, Moody D, Resnick D (1990) Cauda equina syndrome complicating ankylosing spondylitis. Radiology 175(2):521–525

Moll JM (1979) The clinical spectrum of psoriatic arthritis. Clin Orthop (143):66–75

Moll JM, Wright V (1973) Psoriatic arthritis. Semin Arthritis Rheum 3(1):55–78

Olivieri I, Barozzi L, Padula A, De Matteis M, Pavlica P (1998) Clinical manifestations of seronegative spondylarthropathies. Eur J Radiol 27 (Suppl 1):S3–S6

Oostveen JC, van de Laar MA (2000) Magnetic resonance imaging in rheumatic disorders of the spine and sacroiliac joints. Semin Arthritis Rheum 30(1):52–69

Pastershank SP, Resnick D (1980) Pseudoarthrosis in ankylosing spondylitis. J Can Assoc Radiol 31(4):234–235

Pedrosa I, Jorquera M, Mendez R, Cabeza B (2002) Cervical spine fractures in ankylosing spondylitis: MR findings. Emerg Radiol 9(1):38–42

Peretti F de, Sane JC, Dran G, Razafindratsiva C, Argenson C (2004). Fractures du rachis sur ankylose étendue par spondylarthrite ou hyperostose vertébrale: diagnostic et complications. Rev Chir Orthop Reparatrice Appar Mot 90(5):456–465

Rasker JJ, Prevo RL, Lanting PJ (1996) Spondylodiscitis in ankylosing spondylitis, inflammation or trauma? A description of six cases. Scand J Rheumatol 25(1):52–57

Resnick D (1989) Inflammatory disorders of the vertebral column: seronegative spondyloarthropathies, adult-onset rheumatoid arthritis, and juvenile chronic arthritis. Clin Imaging 13(4):253–268

Resnick D (2002a) Psoriatic arthritis. In: Resnick D (ed) Diagnosis of bone and joint disorders, 4th edn. Saunders, Philadelphia, pp 1082–1109

Resnick D (2002b) Rheumatoid arthritis and the seronegative spondylarthropathies: radiographic and pathologic concepts. In: Resnick D (ed) Diagnosis of bone and joint disorders, 4th edn. Saunders, Philadelphia, pp 837–890

Resnick D (2002c) Ankylosing spondylitis. In: Resnick D (ed) Diagnosis of bone and joint disorders, 4th edn. Saunders, Philadelphia, pp 1023–1081

Resnick DK, Shields P (1994) Cystic lesion of the second cervical vertebral body. Case report. J Spinal Disord 7(6):533–539

Resnick D, Niwayama G (2002) Enostosis, hyperostosis and periostitis. In: Resnick D (ed) Diagnosis of bone and joint disorders, 4th edn. Saunders, Philadelphia, pp 4844–4919

Rivelis M, Freiberger RH (1969) Vertebral destruction at unfused segments in late ankylosing spondylitis. Radiology 93(2):251–256

Saraux A, Guedes C, Allain J et al. (1999) Prevalence of rheumatoid arthritis and spondyloarthropathy in Brittany, France. Societe de Rhumatologie de l'Ouest. J Rheumatol 26(12):2622–2627

Schumacher TM, Genant HK, Kellet MJ, Mall JC, Fye KH (1978) HLA-B27 associated arthropathies. Radiology 126(2):289–297

Solinger AM (2003) Rheumatic manifestations of human immunodeficiency virus. Curr Rheumatol Rep 5(3):205–209

Steven MM (1992) Prevalence of chronic arthritis in four geographical areas of the Scottish Highlands. Ann Rheum Dis 51(2):186–194

Taylor WJ, Marchesoni A, Arreghini M, Sokoll K, Helliwell PS (2004) A comparison of the performance characteristics of classification criteria for the diagnosis of psoriatic arthritis. Semin Arthritis Rheum 34(3):575–584

Tyrell PN, Davies AM, Evans N, Jubb RW (1995). Signal changes in the intervertebral discs on MRI of the thoracolumbar spine in ankylosing spondylitis. Clin Radiol 50:377–383

Van der Linden S, van der Heijde D (1998) Ankylosing spondylitis: clinical features. Rheum Dis Clin North Am 24:663–676

Van der Linden S, Valkenburg HA, Cats A (1984) Evaluation of diagnostic criteria for ankylosing spondylitis: a proposal for modification of the New York Criteria. Arthritis Rheum 27:361–368

Vanhoenacker FM, Baekelandt J, Vanwambeke K, Willemen D, De Schepper AM (1998) Chronic recurrent multifocal osteomyelitis. J Belge Radiol 81:84–86

Vinson EN, Major NM (2003) MR imaging of ankylosing spondylitis. Semin Musculoskelet Radiol 7:103–113

Wigley RD, Zhang NZ, Zeng QY et al. (1994) Rheumatic diseases in China: ILAR-China study comparing the prevalence of rheumatic symptoms in northern and southern rural populations. J Rheumatol 21(8):1484–1490

Wittram C, Whitehouse GH, Williams JW, Bucknall RC (1996) A comparison of MR and CT in suspected sacroiliitis. J Comput Assist Tomogr. 20:68–72

Yu W, Feng F, Dion E, Yang H, Jiang M, Genant HK (1998) Comparison of radiography, computed tomography and magnetic resonance imaging in the detection of sacroiliitis accompanying ankylosing spondylitis. Skeletal Radiol 27:311–320

Sacrum

Imaging of the Sacrum

24

Andrew Y. Choi, A. Orlando Ortiz, Douglas S. Katz, and Steven J. Lypen

CONTENTS

24.1 Introduction

The sacrum is a large bone composed of five fused vertebrae, which contributes stability and strength to the pelvis, transmitting the weight of the body to the pelvic girdle. It is located at the crossroads of the pelvis and lower extremities, and the anatomy and pathology of the sacrum is of interest to neuroradiologists as well as to body imagers. Plain films are often non-diagnostic for this region, due to the relatively complex anatomy of the sacrum and the adjacent pelvic bones and due to overlying bowel. Therefore, depending on the specific clinical situations, a variety of cross-sectional imaging techniques are of value for sacral imaging, including CT, MRI, and nuclear medicine studies, and in some of these situations these techniques are complementary to each other. Cross-sectional imaging is also valuable for guiding interventional procedures on the sacrum.

A. Y. Choi, MD; A. O. Ortiz, MD, MBA; D. S. Katz, MD
Department of Radiology, Winthrop-University Hospital, 259 First Street, Mineola, NY 11501, USA
S. J. Lypen, BS
239 Douglas Rd, Staten Island, NY 10304, USA

A wide variety of congenital conditions, inflammatory processes, infections, and tumors may affect the sacrum, with which radiologists need to be familiar. Congenital lesions of the sacrum include common benign entities such as transitional vertebrae, as well as serious disorders of neural tube closure including myelodysplasia. The most common developmental tumor of the sacrum is the teratoma, which is classified by its predominant location. The seronegative spondyloarthropathies include ankylosing spondylitis, psoriatic arthritis, and arthritis related to inflammatory bowel disease, all of which may affect the sacroiliac joints. The sacrum is also a relatively common location for Paget's disease. Sacral and sacroiliac joint infections result from contiguous spread from adjacent infection in the pelvis or subcutaneous tissues, as well as from hematogenous spread from Batson's plexus of paravertebral veins. Metastases represent the most common tumor of the sacrum in adults, with involvement occurring in cancer of the lung, breast, and prostate, as well as in lymphoma. Primary tumors of the sacrum are much less common, with chordoma, a malignant tumor arising from notochordal remnants, and giant cell tumor, a usually benign neoplasm, being the most common types. CT and MRI are quite valuable for the diagnosis of all of these conditions and disorders.

Sacral fractures, which usually occur in conjunction with other pelvic fractures, are often missed on initial clinical evaluation and may be difficult to appreciate on plain radiographs. Such fractures carry a significant risk of complications, especially neurological sequelae. Fatigue stress fractures of the sacrum are relatively rare but occur most frequently in long-distance runners. Insufficiency stress fractures are much more common, and are increasingly recognized as a cause of low back pain in older adults. A high index of suspicion is needed for clinical diagnosis of fatigue as well an insufficiency fractures; plain films are of limited utility for accurate diagnosis, but the diagnosis can be confirmed with nuclear bone scintigraphy supplemented by MRI or CT as needed.

KEY-POINTS

- **Anatomy – embryology**
  - The sacrum develops in the **first trimester**
  - Residual disc S1–S2 is not uncommon, especially in young adults
  - Sacrum is composed of **five fused vertebrae**
  - Normal **lumbosacral angle:** 130°–160°
  - **Sacral hiatus** is the defect within the posterior wall at S5
  - Four pairs of foramina both on anterior and posterior surface
  - **Sacral plexus:** L4–S4
  - **Sciatic nerve:** L3–S3
- **Congenital**
  - **Transitional vertebrae** reported prevalence up to 20%
    - may not in and of itself be clinically symptomatic
    - incorrect numbering may lead to intervention at the wrong level
  - **Spinal dysraphism:** see also Chap. 1
  - **Sacral cysts**
    - perineural and Tarlov cysts communicate with the subarachnoid space – mostly asymptomatic
    - arachnoid and intrasacral cysts do not communicate with the subarachnoid space – may be symptomatic
  - **Congenital neoplasms:** epidermoids, dermoids, and teratomas
- **Inflammation**
  - **Seronegative spondyloarthropathies:** sacroiliitis and negative tests for rheumatoid factor
    - ankylosing spondylitis
    - psoriatic arthritis
    - reactive arthritis
    - associated with inflammatory bowel disease
    - unclassified
  - **Paget's disease**
    - cortical thickening may lead to encroachment on the sacral canal and foramina
- **Infection**
  - **Contiguous spread** from an intra-abdominal process or from a decubitus lesion
  - **Arterial seeding** from a distant infectious process
  - Sacral involvement in **tuberculous spondylitis** is rare
  - **Septic sacroiliitis** is uncommon
- **Neoplasm**
  - **Metastases** most common
    - sacrum is a common target (large volume)
    - common primary sites include lung, breast, prostate, and kidney
  - **Primary neoplasms**
    - **chordoma:**
      - 50% of primary sacral tumor
      - 4th to 7th decade
      - 2:1 male-to-female ratio
      - calcification in 90%
    - **giant cell tumor**
      - second most common primary sacral tumor
      - predilection for the sacrum
      - 3rd to 4th decade
      - sacral lesions show female preponderance
    - **chondrosarcoma**
      - 7–12% involve the spine, sacrum most common location
- **Trauma**
  - Often in **combination** with other pelvic fractures
  - More **often missed** and more neurological injury than other pelvic fractures
  - Usually **high velocity impacts** (MVA and falls from significant height)
  - **Dennis classification** of traumatic fractures
    - zone I: ala without foramina or sacral canal
    - zone II: one or more foramina but not the sacral canal with or without zone I
    - zone III: sacral canal with or without zone I/II
  - **Fatigue stress fractures**
    - normal bone, abnormal stress
    - **very rare**
    - pain in lower back or buttocks
    - female athletes
    - frequently unilateral
  - **Insufficiency stress fractures**
    - normal stress, abnormal bone
    - elderly, especially women with osteoporosis
    - low back pain
    - usually extend vertically within the sacral alae
    - usually bilateral

24.2 Embryology

Sacral development commences during the first trimester and continues into the third decade of life. Spinal axis development is initiated in the 15th and 16th days of embryogenesis when ectodermal cells proliferate along the midline surface of the embryo to form the primitive streak with its most cranial end referred to as the primitive pit (Barkovich 2000). During the 16th gestational day, the notochordal process extends from the primitive pit to the prochordal plate. The notochord induces mesodermal and ectodermal differentiation and determines the organization of the spinal axis. This leads to formation of the neural plate and tube. Neuroepithelial cells fuse within the caudal end of the notochord in the tail fold of the embryo, thus forming a caudal cell mass. At the 30th gestational day, multiple cell clusters and cysts form within the caudal cell mass. In the process of canalization, in what will become the conus medullaris, ventriculus terminus, and filum terminale, these microcysts coalesce to form an ependymal-lined tube that fuses with the more cephalad portion of the neural tube. Through the process of retrogressive differentiation, in the 38th day, the caudal cell mass and associated central lumen decrease in size. The cloaca, which forms the anorectal and lower genitourinary structures, lies just ventral to the caudal cell mass. Disturbances that occur during this phase of development, the mesenchymal or membranous stage, can result in the most severe of the congenital spine anomalies, including caudal mass migration abnormalities and myelodysplasias. The notochord also contributes to formation of the nucleus pulposus of the intervertebral disc. Notochord cell remnants are often observed within the cranial and caudal aspects of the spinal axis. These residual notochordal cells are the predecessors to chordomas and account for the increased prevalence of these tumors within these respective locations (Parke 1992).

The notochord induces mesodermal differentiation into paraxial mesoderm. This paraxial mesoderm undergoes further segmentation that by the end of the fifth gestational week results in the formation of 42–44 somites (Verbout 1985). Three major components comprise the somite. They include the sclerotome, the myotome, and the dermatome. The adjacent halves of two sclerotomes fuse to form the membranous precursor of what eventually is the vertebra (Verbout 1985). Alterations in this segmentation process can result in vertebral anomalies such as fused vertebrae, hemi-vertebrae, or transitional vertebrae. In the second, or chondrification stage, the membranous vertebral column develops a cartilaginous framework. Enchondral ossification occurs during the third or primary ossification stage. Three primary ossification centers are observed within each vertebra – central, neural, and costal – of the axial skeleton. The central ossification center forms the central portion of each sacral vertebra. Two neural ossification centers form the neural arch at each sacral level. The costal ossification centers contribute to the lateral mass of the sacrum, while three ossification centers help form the sacral ala. It is during the fourth stage, secondary ossification, that further ossification of the vertebral epiphyses completes the formation of the sacral vertebral body. The sacral vertebrae are separated by intervertebral discs during childhood with subsequent fusion of the S4–S5 and S3–S4 levels in late adolescence and fusion of the S2–S3 and S1–S2 levels by the third decade of life. It is not uncommon to observe a residual disc at S1–S2 levels on imaging studies, especially in young adults. When this disc space is prominent, care must be exercised so as not to incorrectly count intervertebral disc space levels.

24.3 Anatomy

The sacrum is a large, triangular wedge-shaped bone normally composed of five fused sacral vertebrae. The sacrum is concave along its anterior aspect and has a convex outer surface. It forms the roof and posterior and superior wall of the pelvic cavity. The sacrum contributes stability and strength to the pelvis and transmits weight from the body to the pelvic girdle (Moore and Dalley 1999). Superiorly, the sacrum articulates with the fifth lumbar vertebra. The superior surface of the S1 vertebra forms the base of the sacrum. The sacral promontory is the anterior protrusion of the superior border of S1 (Fig. 24.1). S1 is the largest of the sacral vertebral bodies and provides support during axial loading. The inferior half of the sacrum is not weight bearing and is diminished in size relative to its superior half. The apex of the sacrum inferiorly articulates with the coccyx. The sacrum articulates bilaterally with the iliac bones at the sacroiliac joints. The sacrum is angled posteriorly with L5, forming the lumbosacral angle, which normally ranges from

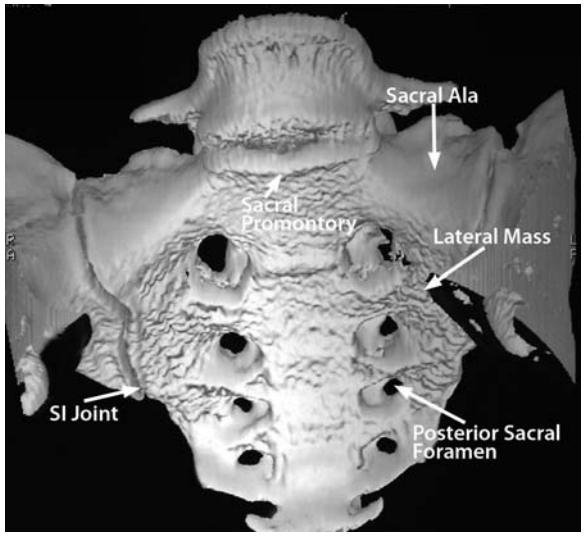

Fig. 24.1. Three-dimensional CT reformation demonstrating an anterior view of the sacral anatomy

130° to 160° (Moore and Dalley 1999). The medial sacral crest is seen posteriorly, and is formed by spinous tubercles resulting from the fusion of the spinous processes. The transverse processes of the fused sacral vertebrae form the lateral crests. The sacral crest divides into two sacral cornua at the S4 level. The sacral hiatus is the defect within the posterior wall of the sacrum at the S5 level and is the point in which the epidural space terminates (Fig. 24.2). The sacral hiatus is formed due to the absence of the laminae and spinous process of S5. The sacral hiatus is connected to the sacral canal, which is the caudal continuation of the lumbar spinal canal. The sacral canal contains the meninges, the lower portion of the cauda equina (sacral and coccygeal nerve roots), the filum terminale, and fibrous and fatty tissue (Fig. 24.3). There are four pairs of foramina on both the anterior and posterior surfaces of the sacrum, which provide the passageways for the S1–S4 rami. Lateral to the sacral foramina are paired blocks of bone termed the lateral masses (Diel et al. 2001). The sacral ala is the wing-shaped bone found lateral to the S1 vertebral body.

The sacroiliac joints are strong, weight-bearing synovial joints between the lateral aspects of the sacral alae and the iliac bones. The interosseous and sacroiliac ligaments suspend the sacrum between the iliac bones. The interosseous sacroiliac ligament is a ligamentous joint which comprises the superior two-thirds to one-half of the joint. The inferior one-half of the joint is formed by the synovial sacroiliac joint. The synovial sacroiliac joint is lined by 3–5 mm of hyaline cartilage on its sacral side and by 1 mm of fibrocartilage layer on its iliac side (Diel et al. 2001). The sacrotuberous and sacrospinous ligaments join the sacrum to the ischium. The sacrotuberous ligament unites the sacrum to the sciatic tuber. The sacrospinous ligament unites the sacrum to the sciatic spine and separates the greater from the lesser sciatic foramen (Dietemann et al. 1992).

The sacral plexus is formed by the ventral rami of L4–S4. The L4–L5 nerves join to form the lumbosacral trunk. The lumbosacral trunk is found medial to the psoas muscle and descends adjacent to the sacral promontory and courses inferolaterally. The S1–S4 rami enter the pelvis through their respective foramina and also course inferolaterally (Gierada et al. 1993). The lumbosacral trunk joins the S1 ventral rami within the pelvis to form the larger superior band. The S2–S4 ventral rami join to form the smaller inferior band. The sacral plexus nerve roots lie between the internal iliac vessels anteriorly and the piriformis muscle posteriorly. The sciatic nerve (L3–S3), the largest nerve in the body, is the continuation of the sacral plexus. The sciatic nerve leaves the pelvis through the greater sciatic foramen to enter the thigh. The common iliac vessels and bifurcations are present anteromedial to the lumbosacral trunk at the level of the sacral promontory. The superior gluteal vessels run between the lumbosacral trunk and the S1 nerve. The superior gluteal vessels exit the pelvis superior to the piriformis muscle and are often seen in the superiormost aspect of the greater sciatic foramen (Moore and Dalley 1999). The inferior gluteal vessels also exit the pelvis via the greater sciatic foramen, passing inferior to the piriformis muscle.

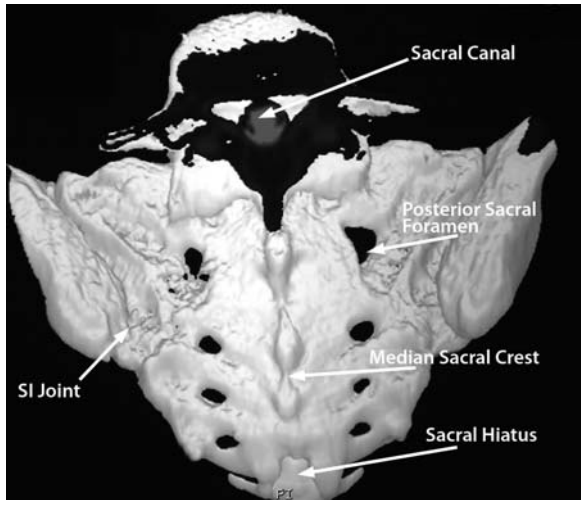

Fig. 24.2. Three-dimensional CT reformation demonstrating a posterior view of the sacral anatomy

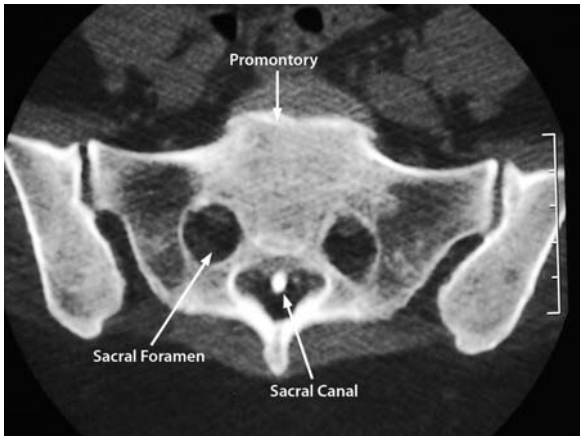

Fig. 24.3. Non-enhanced axial CT image shows the sacral promontory, sacral foramen, and sacral canal

24.4 Congenital

Congenital lesions of the sacrum include benign entities such as transitional vertebra to more extreme conditions such as myelodysplasia and caudal dysplasias. Transitional vertebrae are frequently observed during spine imaging. These developmental variants have been reported in up to 20% of human skeletons. Depending upon the segmentation of the spinal column that occurs during the mesenchymal stage, with respect to the sacrum, these transitions may occur at the lumbosacral or sacrococcygeal junctions (Banna 1985). Transitional vertebrae that occur at the lumbosacral junction consist of either a "lumbarized" S1 vertebra or a "sacralized" L5 vertebra. While the presence of a transitional vertebra may not in and of itself be clinically symptomatic, their major impact is on the localization of lesions at other levels of the lumbar spine. An incorrect numerical labeling of the lumbar spine can lead to unnecessary surgical intervention at the wrong level. In those instances where a subsequent spine intervention may be performed, it may be prudent to obtain a full survey of the spine, either fluoroscopically, radiographically, or with MRI sagittal scout sequences, in order to accurately characterize the type of transitional vertebra and to correctly identify the intended level for intervention. The transitional vertebra itself will show a hybrid appearance with combined features of a lumbar and a sacral vertebra.

Disorders of neural tube closure during development result in the dysraphic myelodysplasias that often affect the sacrum. There is defective midline closure of the spine with a cutaneous defect, spina bifida aperta, or with the skin intact, occult spinal dysraphism. Cutaneous stigmata, nevertheless, are almost always observed and include external neural placode, hypertrichosis, nevus, hemangioma, subcutaneous lipoma, or dermal sinus tracts. The clinical presentation, moreover, depends upon the severity and timing of the congenital insult such that patient presentation may range from asymptomatic to multiple malformations that involve the genitourinary tract, the anus and rectum, and the lower extremities. The myelodysplasias can present with neural tissue containing masses that are observed in open neural tube defects such as myeloceles and myelomeningoceles. Alternatively, in closed neural tube defects, patients may present with lipomyelomeningocele, meningocele, myelocystocele, dermal sinus, neurenteric cyst, or lipoma. Associated abnormalities of the spinal cord such as hydromyelia, tethering, or diastematomyelia, may also be present.

Lipomyelomeningoceles are the most common of the occult myelodysplasias and account for up to one-half of all cases of occult spinal dysraphisms (Lemire et al. 1971). These malformations are due to failure of non-disjunction of cutaneous ectoderm from neuroectoderm. Imaging of the lumbosacral junction will show a bony defect in the posterior elements, associated with a cystic and/or lipomatous mass that extends to the subcutaneous fat (Fig. 24.4). The spinal cord may be low-lying or tethered. The spinal canal is enlarged and there may be varying types of vertebral anomalies such as partial or complete sacral agenesis. Meningoceles are uncommon masses that consist of focal cerebrospinal fluid containing dural sacs which protrude through either a sacral defect or foramina. Posterior meningoceles are more common than anterior meningoceles, and the latter may present as a pelvic mass. Anterior meningoceles may be associated with varying degrees of sacral agenesis as well as with genitourinary and anorectal malformations. Meningoceles that involve the sacral foramina may be observed in patients with neurofibromatosis or Marfan's syndrome. Imaging with MRI or CT will reveal a cystic mass that is continuous with the thecal sac. It is important to identify whether or not a nerve root is present within the cyst prior to surgical treatment. CT will often demonstrate remodeling of the sacrum with an associated osseous defect or enlarged neural foramen.

Sacral agenesis is part of the spectrum of caudal dysplasias that include lower limb anomalies as well as anorectal and genitourinary malformations. This

Fig. 24.4. Sagittal T2-weighted MR image shows a large lipomyelomeningocele (*arrows*) in a 5-month-old male. (Courtesy of Donald B. Price, MD, Winthrop-University Hospital, Department of Radiology)

appears to be due to an insult to the caudal mesoderm, including the caudal cell mass and cloaca, prior to the fourth week of gestation. The caudal regression syndrome constitutes part of this spectrum. Caudal regression is observed in 0.01% of the population and in up to 0.2% of children of diabetic mothers. Conversely, one out of six children with this syndrome has a diabetic mother. Additionally, the severity of sacral agenesis may vary and other spinal anomalies, including tethered cord, syrinx, lipoma, and lipomyelomeningocele, may be present (O'Neill et al. 1995). MRI shows the characteristic wedge-shaped conus medullaris that is located at a higher than normal position within the spinal canal. The extent of sacral agenesis can be classified with plain radiography, CT, or MRI into four types: (1) partial unilateral sacral agenesis; (2) partial bilateral symmetric sacral defects with iliac bones articulating with S1; (3) complete sacral agenesis with iliac bones articulating with lumbar spine; and (4) total sacral agenesis with fusion of the iliac bones (Banna 1985).

Developmental tumors of the sacrum may include cysts, such as meningeal and arachnoid cysts, dermoids, epidermoids and teratomas. Meningeal cysts are abnormal focal dilatations of the meninges within the sacral canal and/or foramina. These cysts are commonly seen at the sacral level and demonstrated an incidence of 5% in routine lumbar spine MR imaging (Paulsen et al. 1994). Meningeal cysts are commonly seen as incidental findings during pelvic CT evaluation. They are also referred to as perineural cysts, Tarlov cysts, sacral arachnoid cysts and occult intrasacral meningoceles (Fig. 24.5). Perineural cysts and Tarlov cysts demonstrate communication with the subarachnoid space whereas arachnoid cysts and intrasacral meningoceles do not. The cysts can remodel the involved portion of the sacral canal or foramen as a result of pressure erosion due to transmitted cerebrospinal fluid pulsations or increased intraspinal pressure. These cysts can occur as single or multiple entities. MRI shows a well-circumscribed oval, round, or lobulated cystic mass that is hypointense on T1-weighted images, hyperintense on T2-weighted MR images, and does not enhance after contrast administration. Communication or the lack thereof may be demonstrated with MR CSF flow studies or on post-myelogram CT examinations with immediate and delayed images (Davis et al. 1993). The relationship of the cyst to the exiting nerve root(s) is well seen on MR. The remodeled sacral canal or foramen with thin or deficient cortical margins is best seen on CT. Whereas the majority of these meningeal cysts are asymptomatic, non-communicating large cysts may be symptomatic (Davis et al. 1993). Symptomatic cysts have shown a variable treatment response to percutaneous aspiration. Anecdotal reports that involve injection of the cyst with various agents including steroid or fibrin glue have been described (Patel et al. 1997). Special care must be taken to avoid introducing these agents into the subarachnoid space as they may cause meningitis. Surgical treatment involving duroplasty with or without shunts has also been attempted with varying amounts of success.

Epidermoids, dermoids, and teratomas can present in the sacrum. These congenital neoplasms represent 4% of pediatric spine tumors (Steinbok et al. 1992). Sacrococcygeal teratomas are by far the most common of these developmental tumors to present within the sacrum (Fig. 24.6). Teratomas are comprised of cells that arise from ectoderm, mesoderm, and endoderm and possibly develop from rests of undifferentiated cells in the caudal cell mass (Schey et al. 1977). Since they are developmental neoplasms, they are most frequently observed at birth, with an incidence of 1/40,000 births. Rarely, teratomas can also present in adults as an occult mass (Ng et al. 1999). There is a rare familial autosomal dominant presentation in which the teratoma is associated

Fig. 24.5a–c. Tarlov cysts (*arrows*) shown on multiple imaging modalities. **a** Contrast-enhanced axial CT image. **b** Coronal T2-weighted MR image. **c** Image from a lumbar myelogram

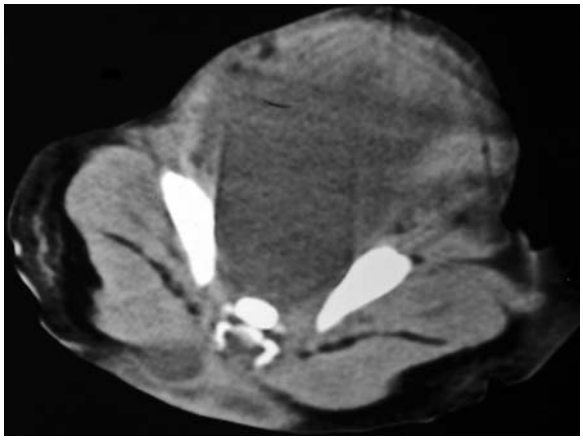

Fig. 24.6. Non-enhanced axial CT image of a sacral teratoma in a female neonate. The mass is partially cystic and fills the pelvis

with a malformed sacrum and anorectal and lower genitourinary tract anomalies. There is a 4:1 female-to-male ratio. Two-thirds of these tumors are benign mature teratomas and the remainder are either immature or anaplastic teratomas with malignant potential.

Teratomas can be classified by their predominant location (Schey et al. 1977). Type 1 teratomas (47%) are predominantly posterior and present as a gluteal mass. Type 2 teratomas (35%) are also located posteriorly but extend into the pelvis. Type 3 teratomas (8%) are located within the pelvis and abdomen, and Type 4 (10%) teratomas have a presacral location. Given that these tumors arise from all three germ cell layers, it is common for imaging with CT or MRI to show a complex solid and cystic mass. There is associated osseous destruction of the involved portions of the sacrum, lumbar spine, and coccyx. CT will show calcification in 60% of cases. Fluid-fluid levels may be observed on CT or MRI. On MRI, teratomas are isointense or hypointense on

T1-weighted images, and isointense or hyperintense on T2-weighted images. Enhancement of the solid portions of the tumor will be seen following contrast agent administration on CT or MRI.

Approximately 22% of epidermoids are found within the lumbosacral region while 60% of dermoids occur in this location (Barkovich 2000). Epidermoids contain epidermal tissue elements and may arise from congenital tissue rests or may be secondary to post-procedural implantation such as lumbar puncture or myelomeningocele repair (Barkovich 2000). Dermoids are derived from ectodermal elements, and therefore contain epidermal and dermal tissue elements. They may show lipid-containing components on CT or MRI. These lesions show attenuation similar to that of cerebrospinal fluid on CT and are isointense to cerebrospinal fluid or hypointense on T1-weighted MR images and hyperintense on T2-weighted MR images. A fluid attenuation inversion recovery (FLAIR) sequence may distinguish the hyperintense mass from hypointense cerebrospinal fluid (Barkovich 2000). These lesions do not usually demonstrate contrast enhancement unless they have been infected. Both of these lesions may be associated with a tethered cord, dermal sinus, or abscess (Fig. 24.7). Between 20% and 30% of epidermoids and dermoids are associated with a dermal sinus tract (Barkovich 2000). Ruptured dermoids may present with chemical meningitis.

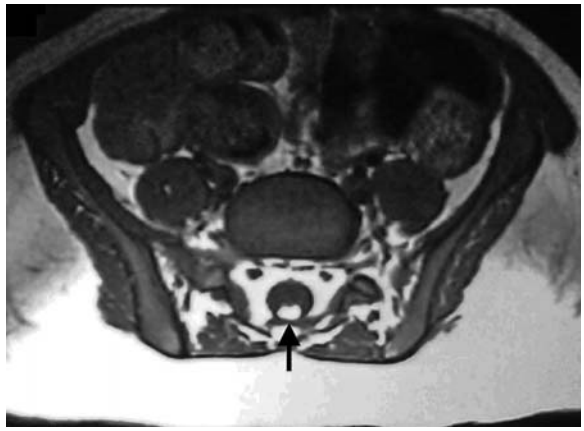

Fig. 24.7. Axial T1-weighted MR image of a 2-year-old girl shows a tethered cord with a lipoma (*arrow*)

Fig. 24.8. Frontal abdominal and pelvic radiograph of a middle-aged woman with a history of inflammatory bowel disease. There is prominent sclerosis at both sacroiliac joints (*arrows*)

24.5 Inflammation

The seronegative spondyloarthropathies are a group of arthritic diseases that affect multiple organ systems and are thought to have a significant genetic component to their origin. The seronegative spondyloarthropathies include ankylosing spondylitis, psoriatic arthritis, reactive arthritis, arthritis associated with inflammatory bowel diseases (Fig. 24.8), and unclassified seronegative spondyloarthropathies (Dougados et al. 1991). Negative tests for rheumatoid factor and sacroiliitis as a common initial manifestation are uniting features of the seronegative spondyloarthropathies.

Although conventional radiography is the first imaging modality for diagnosing sacroiliitis, results are often equivocal due to the anatomic configuration and obliquity of the joints. Plain radiographs may demonstrate a range of findings including sclerosis, erosions, cartilage space narrowing, and complete bony ankylosis, or may demonstrate completely normal sacroiliac joints (Fig. 24.9). Technetium-99m labeled methylene diphosphonate (99mTc-MDP) bone scintigraphy is a more sensitive modality for demonstrating abnormalities of the sacroiliac joints. The study characteristically demonstrates increased uptake of radionuclide at the sacroiliac joint(s), although this finding is highly non-specific. CT is a more sensitive and accurate modality than plain films in the evaluation of sacroiliitis. Early findings notable on CT include cortical erosions and subchondral sclerosis. Later findings of the disease include joint space narrowing and bony ankylosis.

Fig. 24.9. An 85-year-old woman with a history of breast cancer. Biopsy of the anterior sclerotic focus in the left sacrum (*arrow*) was consistent with osteoarthritis and not tumor. Note the subtle vacuum phenomenon in the left sacroiliac joint, with nitrogen gas formation

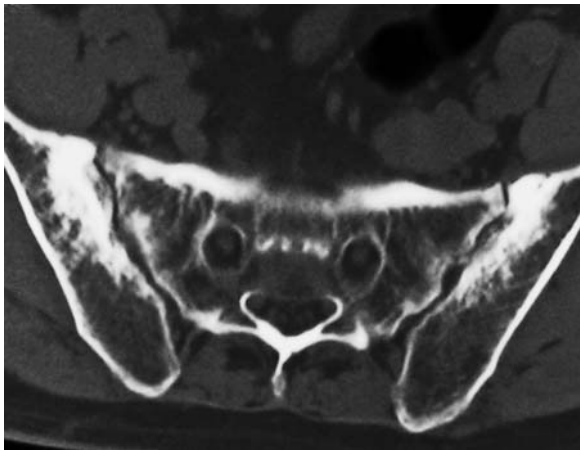

Fig. 24.10. Non-enhanced axial CT image in a 45-year-old man with a history of ankylosing spondylitis shows marked sclerosis at the iliac portions of the sacroiliac joints

The anatomy and pathologic changes to the sacroiliac joint are more clearly demonstrated on CT than on plain radiography (Borlaza et al. 1981. An advantage of CT over plain radiographs is the ability to demonstrate findings which were normal or equivocal on plain radiographs (Luong and Salonen 2000). MRI is the most sensitive means for detecting early sacroiliitis, and is better for detecting active inflammatory sacroiliitis than CT (Puhakka et al. 2003). MR imaging enables delineation between the two compartments of the sacroiliac joint, the ligamentous segment containing adipose tissue, and the synovial compartment demonstrating cartilage signal intensity (Murphy et al. 1991). Initially in sacroiliitis, there may be loss of the normal thin band of intermediate signal intensity representing cartilage on T1-weighted images. T1-weighted images can also demonstrate cortical erosions and subchondral sclerosis (Wittram et al. 1996). Spin-echo T2-weighted images demonstrate bone marrow edema adjacent to the involved sacroiliac joint. Short TI inversion recovery images (STIR) demonstrate inflammation at the periarticular bone marrow while suppressing the normally increased fat signal. STIR-imaging is considered more sensitive than T2-weighted imaging for demonstrating subchondral bone edema.

Ankylosing spondylitis has a strong association with the histocompatibility antigen HLA-B27, and is more common in men than in women (4:1). Patients generally present with an insidious onset of low back pain, which persists for more than 3 months. Classically, ankylosing spondylitis causes symmetric and bilateral sacroiliac joint involvement (Fig. 24.10). Sacroiliitis is the initial radiographic finding in the overwhelming majority of patients. Initially, there is blurring of the subchondral cortex at the sacroiliac joints. Small erosions may develop along the iliac side of the joint initially, while progressing to the sacral side as the erosions become larger. This may occur since the sacral surface of hyaline cartilage is thicker in comparison to the ilial surface. Widening of the joint space, sclerosis, and eventual ankylosis occur as the disease progresses.

Psoriatic arthritis affects 5%–8% of patients with psoriasis. Approximately half of the patients with severe psoriasis have sacroiliitis, usually presenting bilaterally and asymmetrically. Patients may present with spondylitis with or without associated sacroiliitis. As opposed to ankylosing spondylitis, the erosions involving the sacroiliac joint are large. These erosions undergo subsequent repair, leading to subchondral sclerosis, although eventual ankylosis of the sacroiliac joints is relatively uncommon (Bennett et al. 2004). Rheumatoid arthritis, like ankylosing spondylitis, is associated with bilateral symmetrical sacroiliitis. Reiter syndrome, psoriatic arthritis, inflammatory bowel disease, and osteoarthritis are usually associated with asymmetric bilateral sacroiliitis, although all of these entities can also present with unilateral involvement. Bilateral symmetric sacroiliac joint involvement is typical of osteitis condensans ilii, a condition most commonly seen in young multiparous women (Fig. 24.11). The findings usually consist of a triangular area of subchondral sclerosis on the anteroinferior aspect of the iliac side of the joint, unassociated with erosions or joint space narrowing (Diel et al. 2001). Infec-

Fig. 24.11. Non-enhanced axial CT image of a 37-year-old woman reveals bilateral osteitis condensans ilii and an anterior bridging osteophyte at the right sacroiliac joint

tion, trauma, and metastatic cancer are most commonly associated with unilateral sacroiliitis. Gouty arthritis, although rare, should be considered in a patient with acute unilateral sacroiliitis and a history of gout (Fig. 24.12).

Involvement of the sacrum in Paget's disease is often polyostotic, although it can also be isolated. Paget's disease is predominantly located in the axial skeleton, with the most commonly affected sites being the pelvis (30%–75% of cases), spine (30%–75%), and skull (25%–65%). The three phases of Paget's disease are the lytic, mixed, and blastic phases. Areas of osteolysis, which reflect unopposed osteoclastic activity, are demonstrated on radiographs during the early lytic phase of Paget's disease. Findings during the mixed phase include coarsening and thickening of the trabecular pattern and cortex. These radiographic findings represent areas of osteoblastic repair. The blastic phase is characterized by areas of sclerosis which can be extensive, replacing areas of previous trabecular thickening. Bone enlargement is a common finding during the blastic phase (Smith et al. 2002). The presence of bone expansion and cortical and trabecular bone thickening is pathognomonic for Paget's disease. Sacral involvement during the blastic phase includes cortical thickening affecting the sacral foramina and the sacral side of the sacroiliac joints. Eventually encroachment on the sacral canal and foramina may ensue as a result of cortical thickening and osseous expansion (Diel et al. 2001). Paget's disease produces enlargement of all the vertebral elements.

MR imaging findings of Paget's disease vary depending on the phase of the disease. During the lytic phase, the fibrovascular matrix may appear hypointense on T1-weighted images and hyperintense on T2-weighted images. Areas of blastic activity during the later blastic phase appear as regions of low intensity on T1- and T2-weighted images. MR images during the blastic phase can have a similar appearance to metastatic disease or osteomyelitis, and correlation with other forms of imaging is often needed to differentiate amongst these entities.

Neoplastic transformation, most frequently osteosarcoma, is a rare complication which occurs in fewer than 1% of patients with Paget's disease. The risk of developing sarcomatous transformation increases with age, and most commonly affects the pelvis, sacrum and femur (Llauger et al. 2000). Patients may experience pain, a palpable mass, weight loss, and neurologic complications. Findings of cortical destruction and the presence of an adjacent soft tissue mass in addition to findings of Paget's disease on imaging studies are highly suggestive of sarcomatous transformation (Fig. 24.13). Both CT and MRI are accurate in demonstrating tumor development and for assessing tumor spread, as well as for serving as a guide for a biopsy to confirm the diagnosis.

24.6 Infection

Sacral and sacroiliac joint infections are usually the result of contiguous spread from adjacent infectious processes. As with infections involving the spine elsewhere, sacral infections can also occur as the result of hematogenous spread of infectious agents. Spread of infection may occur hematogenously through Batson's plexus of paravertebral veins (Batson 1995). Sacral infection can occur in intravenous drug abusers or immunosuppressed patients (Horton et al. 2002). Osteomyelitis of the sacrum may result from extension of an intra-abdominal abscess into the pelvic bones or extension from a decubitus ulcer. *Staphylococcus aureus* is the most common infecting organism. Osteomyelitis can also occur via arterial seeding of microorganisms from distant infectious processes. The typical appearance of sacral osteomyelitis is a destructive lesion of the sacrum with associated soft tissue swelling (Fig. 24.14). Osteomyelitis involving a single vertebral body can rapidly spread to the adjacent disk and vertebral body via vascular and subligamentous routes. A corresponding abscess may develop within the presacral soft tissues, adjacent articulations, or sacral epidural space.

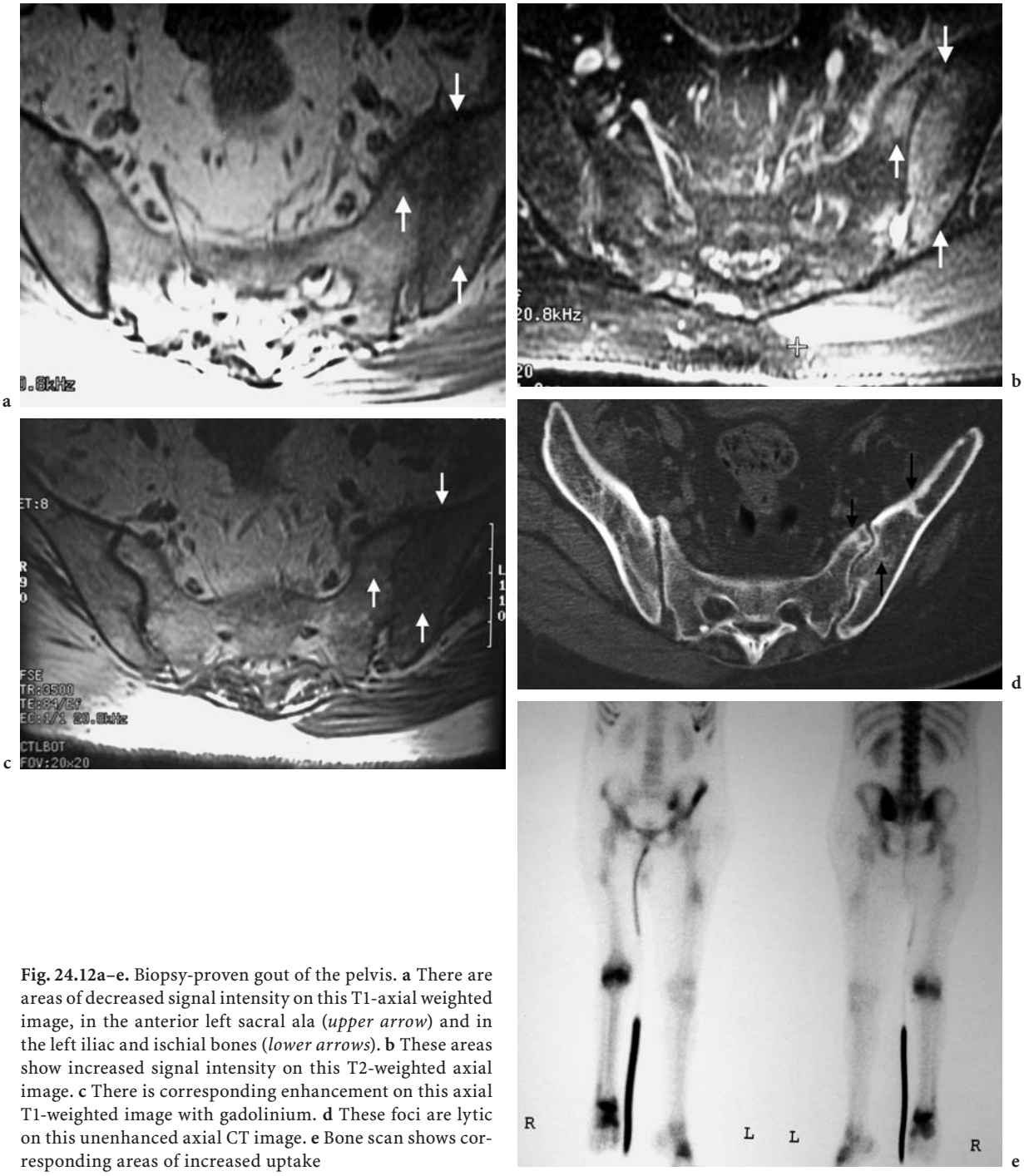

Fig. 24.12a–e. Biopsy-proven gout of the pelvis. **a** There are areas of decreased signal intensity on this T1-axial weighted image, in the anterior left sacral ala (*upper arrow*) and in the left iliac and ischial bones (*lower arrows*). **b** These areas show increased signal intensity on this T2-weighted axial image. **c** There is corresponding enhancement on this axial T1-weighted image with gadolinium. **d** These foci are lytic on this unenhanced axial CT image. **e** Bone scan shows corresponding areas of increased uptake

The conventional radiographic hallmark of spondylodiscitis is irregularity of the vertebral endplates with narrowing of the intervening disc space (Latchaw 1990). However, due to the possible lag time between symptomatology and the plain-film findings of the disease, a normal plain film does not exclude osteomyelitis. Radionuclide bone scans are very sensitive for the detection of early osteomyelitis, demonstrating increased uptake in the affected regions. The earliest finding on CT of osteomyelitis is an increase in intramedullary density due to the accumulation of infected debris within the bone marrow. This finding is non-specific, as an increase in the intramedullary density can be a result of in-

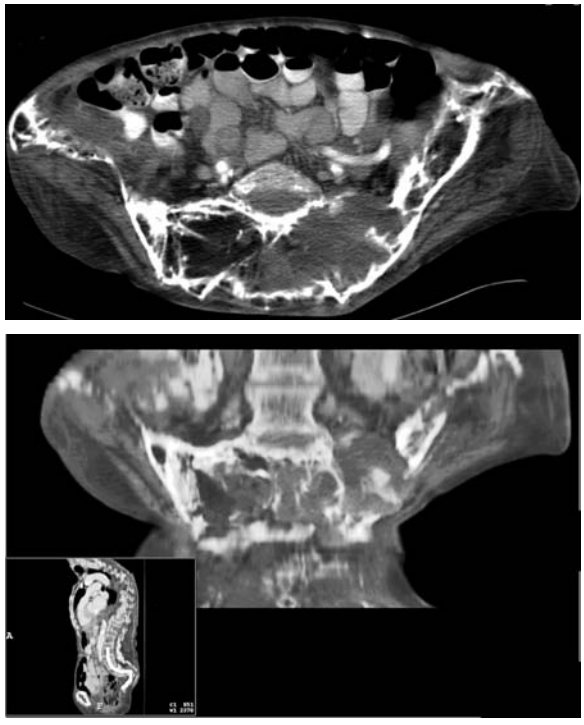

Fig. 24.13a,b. Paget's disease complicated by sarcomatous transformation in this elderly patient with low back pain. There is a soft-tissue mass in the left sacrum. Note the diffusely thickened cortical bone. **a** Contrast-enhanced axial CT image. **b** Coronal CT reformation

Fig. 24.14. Non-enhanced axial CT image showing sacral infection

fection, hemorrhage, stress fracture, irradiation, or neoplasm (Helms et al. 1981). CT is a very accurate modality for detecting cortical destruction, intraosseous gas, periosteal reaction, soft tissue extension, and abscess formation. Although an uncommon manifestation of osteomyelitis, intraosseous gas is pathognomonic for infection, and the presence of gas within the sacral foramina has been described (Merine et al. 1988). A biopsy may be required in order to establish a definitive diagnosis. MRI is more sensitive for the detection of early disease than plain films. On T1-weighted images, the vertebral bone marrow appears low in signal. Contrast enhancement of the bone marrow on T1-weighted images is typical of osteomyelitis. High signal intensity of the disc is observed on T2-weighted images. Sagittal images demonstrate disc space narrowing characteristic of infectious discitis.

Although tuberculous spondylitis is the most common form of skeletal tuberculosis, sacral involvement in spinal tuberculosis is rare. The MR appearance of tuberculous osteomyelitis is not different from other forms of osteomyelitis, although involvement of the posterior elements is more characteristic of tuberculous than pyogenic osteomyelitis. Sacroiliac joint involvement is common in patients with tuberculous osteomyelitis. Manifestations on MR include a widened sacroiliac joint, often containing fluid along with evidence of inflammatory tissue in the neighboring sacrum or ilium (Patankar et al. 2000). Sacral tuberculosis is often associated with a presacral mass or abscess.

Septic sacroiliitis is an uncommon entity resulting from either the spread of infection hematogenously, the direct introduction into the joint during surgery or trauma, or spread from adjacent soft tissue or bone. *Staphylococcus aureus* is the most common organism isolated in septic sacroiliitis, although other bacterial, mycobacterial, and fungal organisms can also be responsible. Early diagnosis allows for the appropriate administration of antibiotics and resolution of the disease without surgical intervention. Nuclear bone scans demonstrate increased radiotracer uptake at the sacroiliac joints within 1 week of onset of symptoms. These findings can be demonstrated earlier than on plain radiographs. CT shows findings that are similar to those recognized on plain radiographs, such as erosions and widening of the joint space. CT better demonstrates the involvement of bone and soft tissues more clearly than plain radiographs or nuclear bone scans. Infiltration of the fat around the iliopsoas muscles or asymmetry of the muscles are findings seen on CT which are suggestive of the disease. CT can be used to delineate abscess formation and to distinguish cortical from medullary bone involvement, and also demonstrates other bony abnormalities.

MRI is a sensitive modality for detecting early septic sacroiliitis, and has the capability to demon-

strate abnormal regions of fluid and/or inflammation. These abnormal regions are characteristically found in the sacroiliac joint space, in the bone marrow of the sacrum and/or ilium, and in the iliopsoas muscle. MRI findings include low signal intensity on T1-weighted images and increased signal intensity on T2-weighted and STIR-images, at the joint space, periarticular muscle tissue, and subperiosteal infiltration. The presence of fluid tracking posterior to the iliopsoas muscle seems to be specific for septic sacroiliitis, as this finding is absent in other causes of sacroiliitis (Klein et al. 1991). Hyperintensity in the anterior or posterior joint space which tracks subperiosteally along the periarticular bone also appears to be specific for septic sacroiliitis (Stürzenbecker et al. 2000). Advanced stages of the disease leads to erosion, sequestration, and abscess formation, which are also absent in other forms of sacroiliitis. The presence of unilateral sacroiliac joint involvement should be regarded as highly suspicious for joint infection.

24.7 Neoplasm

Primary neoplasms of the bony sacrum are much less common than metastases in this location (Disler and Miklic 1999). Of these primary tumors, chordoma is the most frequently encountered neoplasm. Chordomas arise from notochordal elements and account for 2%–4% of malignant bone tumors and approximately one-half of primary sacral bone tumors (Murphey et al. 1996). Chordomas are usually diagnosed in the fourth to seventh decades of life. A 2:1 male-to-female ratio has been observed. Patients typically present with sacrococcygeal pain and/or bowel or bladder disturbances. Chordomas are slow-growing, infiltrative neoplasms (Fig. 24.15). This growth pattern not only accounts for their delayed clinical presentation, but also for the challenge associated with treating large infiltrative tumors. Metastases to the lung, liver, or lymph nodes occur in 5%–40% of cases. Imaging with plain radiography or CT shows a large soft-tissue mass that involves the sacrum. Calcification is seen in 90% of cases on CT. There is expansion and destruction of the involved portions of the sacrum and adjacent bones. Extension across the sacroiliac joint can occur, as can extension into the sacral canal and/or presacral involvement. Tumor extent can be assessed with CT or MRI, but is most optimally characterized with MRI. On MRI, chordomas are hypointense on T1-weighted images, very hyperintense on T2-weighted MR images, and show variable enhancement following contrast administration (Fig. 24.16). These masses demonstrate a tumor stain on catheter angiography.

Giant cell tumor is the second most common primary sacral neoplasm (Murphey et al. 1996). While accounting for only 7% of spinal neoplasms, this tumor shows a predilection for the sacrum (Fig. 24.17). These neoplasms tend to present within the third and fourth decades of life. Sacral lesions show a female preponderance. Giant cell tumors are usually benign neoplasms, but in 5%–10% of cases, malignant tumor behavior with metastases has been observed. Imaging with plain radiography or CT will show a large expansile lytic lesion that may extend across the sacroiliac joint (Diel et al. 2001). Fluid-fluid levels may occur secondary to intra-tumoral hemorrhage in what is a relatively hypervascular lesion; these can be observed either with CT or MRI, as can prominent contrast enhancement within soft tissue components. When they present with multiple fluid-fluid levels, giant cell tumors can simulate the appearance of aneurysmal bone cysts, which also present as expansile lytic lesions with hematocrit levels. Aneurysmal bone cysts, however, rarely occur within the sacrum (Diel et al. 2001). On MRI, giant cell tumors are hypointense on T1-weighted images, intermediate to hyperintense on T2-weighted images, and show a relatively hypointense pseudocapsule. Imaging with skeletal scintigraphy shows increased peripheral radiotracer uptake, the so-called "donut" sign. As these are hypervascular tumors, catheter angiography will show a prominent tumor stain with neovascularity.

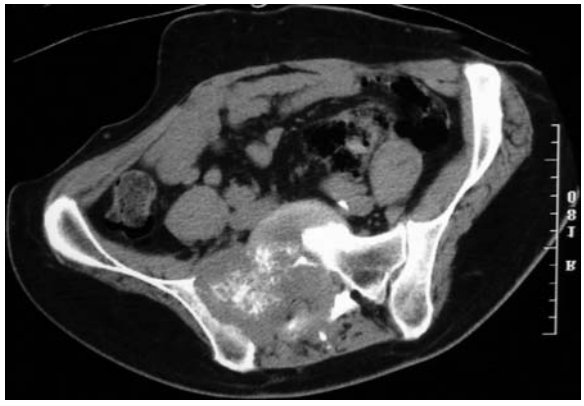

Fig. 24.15. A 57-year-old man with a chordoma, which is demonstrated on this non-enhanced axial CT image

Fig. 24.16a,b. An 81-year-old man with a 2-year history of low back pain and increasing weakness in the lower extremities. A large lobulated heterogeneous mass is present. **a** Sagittal T2-weighted image. **b** Sagittal T1-weighted image with gadolinium

Fig. 24.17. A 32-year-old woman with a giant cell tumor of the sacrum. A lytic soft-tissue mass replaces most of the left sacrum

Primary sarcomas are malignant tumors that can occur within the sacrum. Approximately 7%–12% of chondrosarcomas involve the spine, with the sacrum being the most common location (Nguyen et al. 1993). Chondrosarcomas can arise as primary lesions within the sacrum or secondary to pre-existing lesions such as osteochondromas or Paget's disease. On imaging, these tumors present as destructive masses on plain radiography. CT shows a soft mass that extends beyond the normal margins of the sacrum and contains areas of calcification or mineralization (Fig. 24.18). The tumors are hypointense on T1-weighted MR images and heterogeneously hyperintense on T2-weighted MR images. Though Ewing's sarcoma infrequently involves the spine, the sacrum is the most common site of origin when spinal involvement occurs (Whitehouse and Griffiths 1976). This tumor is found in a younger age group, 90% of whom are between 5 and 30 years of age. It typically presents as a lytic, destructive lesion that can extend across the intervertebral disc; the latter situation may therefore simulate infection. Ewing's sarcoma can also present as a sclerotic lesion. When a destructive lesion is seen within the sacrum in a child, the differential diagnosis should include Ewing's sarcoma, leukemia, and metastatic neuroblastoma. Primary sarcomas, such as osteosarcoma and fibrosarcoma, rarely involve the sacrum. There have been sporadic reports of other malignant tumors, including carcinoid and primitive neuroectodermal tumor, presenting with primary sacral involvement (Schnee et al. 1994).

The majority of primary benign neoplasms that occur within the spine rarely involve the sacrum. Cavernous hemangiomas are the most common primary neoplasm of the spine, but are infrequently found within the sacrum. These lesions, though benign, can occasionally show an atypical or aggressive lytic appearance, with an epidural soft-tissue component that may compromise neural structures

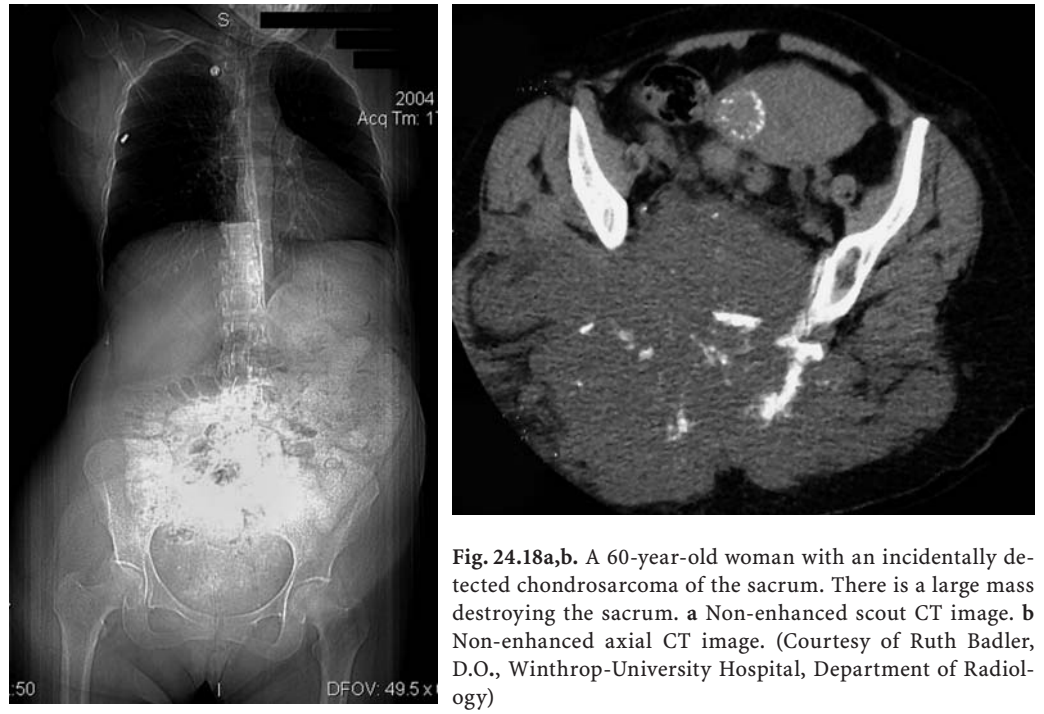

Fig. 24.18a,b. A 60-year-old woman with an incidentally detected chondrosarcoma of the sacrum. There is a large mass destroying the sacrum. **a** Non-enhanced scout CT image. **b** Non-enhanced axial CT image. (Courtesy of Ruth Badler, D.O., Winthrop-University Hospital, Department of Radiology)

and cause pain. Osteoid osteomas account for 10% of spine tumors, yet only 2% are located within the sacrum (Murphey et al. 1996). Osteoid osteomas present in males in their second decade of life. A history of nocturnal pain that responds to salicylates may be observed. These are small lesions that are characterized by the presence of a prominent hypervascular, hence enhancing, nidus that is surrounded by an edematous zone of low attenuation on CT or hypointensity on T1-weighted images and hyperintensity on T2-weighted images. A peripheral zone of reactive sclerosis may be identified on CT. Osteoblastomas, which share pathologic features with osteoid osteomas but tend to involve the posterior elements, are exceedingly rare within the sacrum. Primary neoplasms that occur within the sacral canal are either derived from exiting nerve roots or the filum terminale and adjacent epidural fat. Lipomas are most often associated with a tethered cord and with other dysraphic findings. Tumors that involve the exiting lumbosacral nerve roots include schwannoma, neurofibroma and, even more rarely, meningioma. These tumors are usually benign and can attain a large size prior to clinical presentation (Ortolan et al. 1996). Schwannomas and neurofibromas, therefore, tend to present in adults (Fig. 24.19). Furthermore, as a result of this slow growth, the involved portions of the sacral canal and neural foramen will show expansion on imaging. It may not be possible to distinguish between a schwannoma and neurofibroma; however, when multiple neural tumors are seen, the diagnosis of neurofibromatosis should be suspected (Fig. 24.20). Imaging with CT or MRI will show a variably-sized, enhancing soft-tissue mass that involves a nerve segment and is associated with bony remodeling of the sacral foramen and/or canal. Ependymomas can also rarely present as isolated tumors within the sacral canal. These ependymomas tend to be of the myxopapillary type and occur along the distal filum terminale (Moelleken et al. 1992).

Metastases account for the majority of sacral neoplasms (Fig. 24.21). The relatively large volume of the sacrum and its hematopoietic marrow content makes this structure a common target for hematogenous metastases. Common primary tumor sites include lung, breast, prostate, and kidney (Disler and Miklic 1999). Metastatic disease is often initially imaged with skeletal scintigraphy and lesions usually present as foci of increased radiotracer uptake not only within the sacrum but also within other portions of the axial and appendicular skeleton. Imaging with plain radiography or CT will often demonstrate single or multiple variably-sized osteolytic lesions (Fig. 24.22). Sclerotic lesions can be observed with breast or prostate metastases. MRI will show well-circumscribed or ill-defined hypointense foci of marrow replacement on T1-weighted

a b

Fig. 24.19a,b. A 74-year-old woman with a sacral schwannoma. There is a heterogenous mass extending anteriorly from the sacrum, with areas of increased signal intensity on the T2-weighted image and marked enhancement with gadolinium. **a** Axial contrast-enhanced T1-weighted MR image. **b** Sagittal T2-weighted MR image

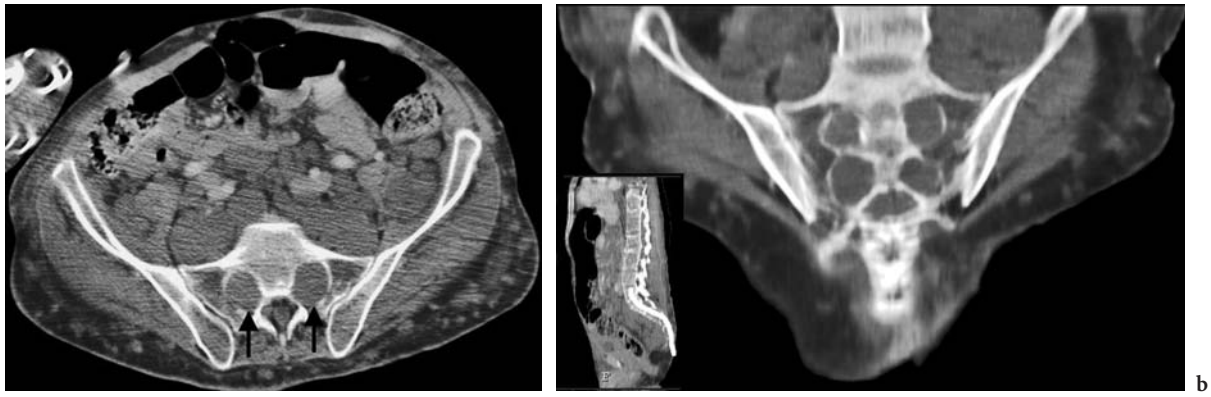

a b

Fig. 24.20a,b. Neurofibromatosis, incidentally detected on a CT scan of the abdomen and pelvis which was performed for unrelated reasons. **a** There is enlargement of the neural foramina in the sacrum (*arrows*) on this axial CT image. There are innumerable masses anterior to the sacrum and iliac bones, as well as in the subcutaneous tissues. **b** Coronal CT reforma-

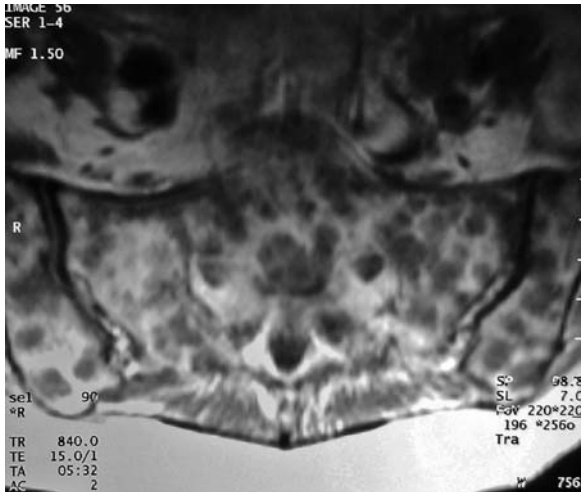

Fig. 24.21. Axial non-enhanced T1-weighted axial image shows numerous focal lesions representing metastases in this 53-year-old woman

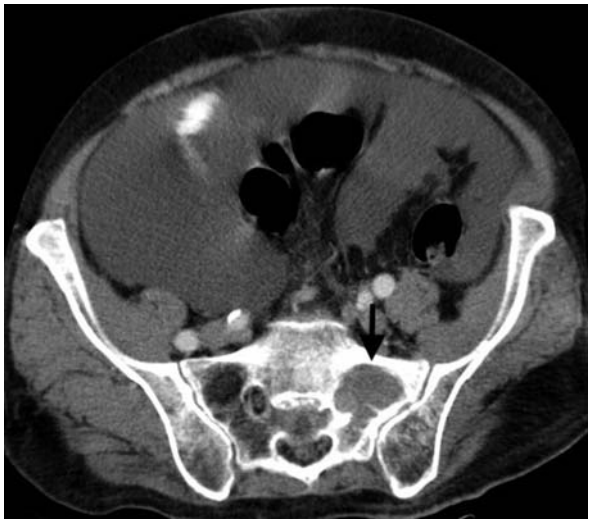

a

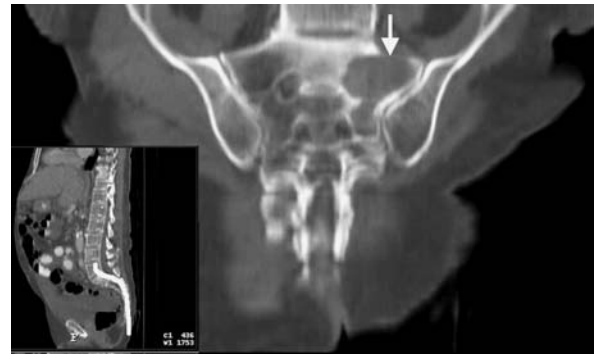

b

Fig. 24.22a,b. Metastasis from hepatocellular carcinoma. **a** Contrast-enhanced axial CT image demonstrates a focal lytic lesion in the left sacrum (*arrow*). **b** Coronal CT reformation displayed with a bone window

images with variable hyperintensity on T2-weighted images. Contrast enhancement is best demonstrated with fat-suppressed T1-weighted images. Given that the sacral canal is the most dependent portion of the spinal canal, this location is a frequent site for central nervous system neoplasms which disseminate into the subarachnoid space. High grade astrocytomas, ependymomas, medulloblastomas, pineal parenchymal tumors, and choroid plexus tumors are examples of neoplasms that can be associated with implants in the distal thecal sac at the level of the sacral canal. Contrast-enhanced MRI is the study of choice for assessing not only the distal sacral involvement but also the entire neuraxis. Another source of secondary tumor involvement of the sacrum is contiguous spread from adjacent pelvic neoplasms such as rectal carcinoma, prostate carcinoma, or uterine carcinoma. Regardless of the method of extension into the sacrum and sacral canal, patients with these lesions can present with sacral pain, sacral plexopathy or cauda equina syndrome. Multiple myeloma may simulate the imaging appearance of metastatic disease with osteolytic lesions present in the sacrum and remainder of the spine. Isolated involvement of the sacrum by plasmacytoma has also been reported (Lanzieri et al. 1987). Lymphoma is another malignant neoplasm that may infiltrate the sacrum or present as an epidural soft-tissue mass that involves the sacral canal and foramina (Fig. 24.23). When multiple lesions are present within the spinal axis, including the sacrum, the differential diagnosis should include metastases, multiple myeloma, and lymphoma. Clinical and biopsy correlation are often required in order to establish the diagnosis.

24.8 Trauma

Sacral fractures resulting from acute traumatic injury carry a significant risk of morbidity and long-term complications, most frequently in the form of neurological sequelae. Though they may be solitary, more often they occur in combination with other pelvic fractures (Denis et al. 1988). Injuries causing sacral fractures are usually high velocity impacts such as motor vehicle accidents and falls from a significant height, where stress is transmitted through the pelvic ring to the sacrum (Hart et al. 2004). Despite an incidence of 10%–45% in pelvic ring injury, sacral fractures are often missed initially or sometimes entirely, as the other pelvic fractures are usually more readily apparent (Denis et al. 1988; Gibbons et al. 1990). Though pelvic fractures are more common, they rarely result in neurological deficit without a concurrent sacral fracture (Denis et al. 1988; Gibbons et al. 1990; Hart et al. 2004). Pelvic fractures have a 3%–15% incidence of neurological injury, which increases to 34%–45% when only cases of pelvic fractures with concomitant sacral fracture are considered (Bellabarba et al. 2003). Unfortunately, these neurological deficits may become chronic if not properly localized and promptly treated (Denis et al. 1988). An association between non-contiguous thoracolumbar fractures and sacral fractures has been reported, which was noted in 26% of sacral fractures in one series (Albert et al. 1993).

The Denis classification system draws connections between the mechanism of injury, the stabil-

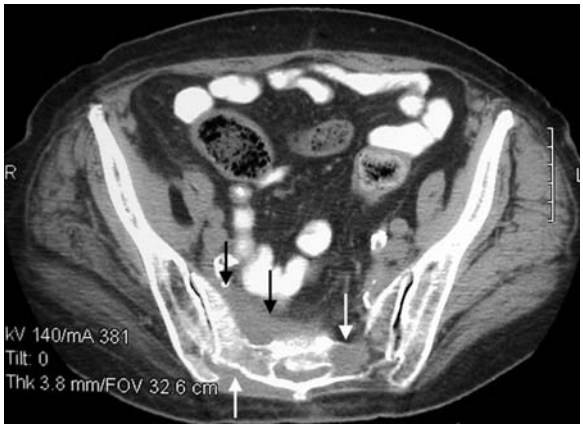

Fig. 24.23. B-cell lymphoma. Non-enhanced axial CT image shows tumor involving the sacrum and adjacent soft tissue (*arrows*)

ity of the resulting sacral fracture, and the extent and type of associated neurological involvement, and helps to predict neurological sequelae (Denis et al. 1988; Gibbons et al. 1990). In this system, zone I fractures involve the ala without extension into either the foramina or the sacral canal; zone II fractures involve one or more foramina and may involve the ala, but do not extend to the central sacral canal; and zone III fractures involve the sacral canal but may also pass through the other two zones (Denis et al. 1988). In an analysis of 236 patients with sacral fractures, the incidence of neurological involvement was 5.9% in zone I fractures, 28% in zone II fractures, and 56% in zone III fractures. The types of neurological deficit also varied, with the most serious deficits resulting from zone III fractures (Denis et al. 1988).

Zone III fractures are the most likely to result in significant neurological damage, usually in the form of bowel and bladder dysfunction. Fractures involving the sacral canal frequently result in bilateral nerve root injury, which has been shown to be necessary to cause sphincter dysfunction. Zone III fractures can occur in both vertical and transverse orientations. Vertical fractures usually result from lateral compression and vertical shear injuries, and are complicated by extensive pelvic involvement. Transverse fractures through the canal are less common injuries that may occur without concurrent pelvis fractures, and are caused by direct force applied to the sacrum which is usually seen in falls from a height. If the transverse fracture occurs above S4, severe neurological injury including bowel and bladder dysfunction is likely, whereas transverse fractures below this level are not likely to cause significant deficits (Denis et al. 1988; Gibbons et al. 1990).

Accurate imaging of traumatic sacral fractures can be challenging. Plain radiography is usually the first imaging test performed, but is often inadequate. Up to 35% of sacral fractures may go undetected and may only be appreciated in retrospect (White et al. 2003). The natural curvature of the sacrum precludes accurate assessment of its superior aspect on frontal projection radiographs, and the lower portions are often obscured on lateral views (Denis et al. 1988). Bowel gas, bladder, calcified arteries, and pelvic pathology may obscure the sacrum and contribute to the low accuracy for plain film assessment. CT, therefore, is the preferred technique for imaging sacral trauma (Albert et al. 1993; Hart et al. 2004). CT can provide information on the location and orientation of fractures, which can be used to aid in clinical and surgical management and allow for more accurate assessment of neurological injury (Fig. 24.24). Multidetector CT with its ability to provide high quality multiplanar reformations facilitates this task. While it is not utilized in the acute phase of injury, MRI is often used to assess the location and extent of neural injury.

Fatigue stress fractures occur in normal bone that is subjected to abnormal stress, usually in young, healthy, physically active individuals. While stress fractures in general are not uncommon in athletes, fatigue stress fractures of the sacrum are relatively rare (Ahovuo et al. 2004; Major and Helms 2000). Vertical body forces are concentrated and transmitted from the spine to the sacrum and sacral alae before further dissipating onto the iliac wings. When bone is subject to excessive repetitive stress, its normal mechanisms for remodeling may be overwhelmed; this causes a deficit in the degree of bone reformation compared to bone resorption, which makes bone more vulnerable to stress fractures (Johnson et al. 2001). Correspondingly, the most significant risk factor for developing sacral stress fractures is an increase in impact activity secondary to an increase in exercise intensity (Johnson et al. 2001). Sacral stress fractures are more common in women, and it is theorized that this may be partly nutritionally-based. Amenorrhea is also common in high-performance female athletes, which often results in a decrease in bone density and increases the risk of fatigue stress fractures (Major and Helms 2000). Because of their tendency to present with non-specific symptoms, sacral fatigue stress frac-

tures are often misdiagnosed as sciatica or lumbar spinal disc disease. This problem is compounded by a lack of awareness that this type of fracture can occur. Sacral stress fractures typically present with pain in the lower back or buttocks. Less often, pain may be referred to the groin or lower leg, and patients may develop tenderness that localizes to the region of the sacrum or sacroiliac joint (Ahovuo et al. 2004; Johnson et al. 2001; Major and Helms 2000). With a high index of suspicion based on patient history and physical examination, the diagnosis can be made by correlation with appropriate imaging studies (Johnson et al. 2001).

Fatigue stress fractures of the sacrum are frequently unilateral. In a recent series of 31 patients, unilateral fracture was seen in 26 cases, with only five having bilateral involvement (Ahovuo et al. 2004). Plain radiographic findings include periosteal, endosteal, or medullary new bone formation. Discrete fracture lines are less often seen, as plain radiographs have a high false-negative rate. Skeletal scintigraphy is a highly sensitive test for the detection of stress fractures, but exact fracture localization may be difficult in some cases (Johnson et al. 2001). Typical findings include a round area of focal uptake in the ala, though some cases show more diffuse uptake in the sacral wing extending into the sacroiliac joint. A normal bone scan virtually excludes the possibility of sacral stress fracture. A typical positive bone scan appearance coupled with appropriate history and physical findings may not need confirmation with CT or MRI, especially if the patient subsequently shows an expected level of improvement following treatment. Multidetector CT with multiplanar reformations readily depicts suspected stress fractures. The characteristic findings are a vertical or oblique cortical disruption and sclerosis in the superior ala that extends into the first or second sacral foramina; cortical bone shows lucency and thickening, while cancellous bone develops focal sclerosis (Johnson et al. 2001; Major and Helms 2000). MRI also allows for accurate localization of sacral stress fractures. Characteristic MRI findings include bone edema manifest as hypointense foci within the sacral ala on T1-weighted images, with corresponding high signal intensity on T2-weighted and STIR-images. Linear low signal may also be present on all MR sequences, extending obliquely from the upper ala to the first or second sacral foramina, indicating a discrete fracture line (Ahovuo et al. 2004; Major and Helms 2000). MRI is considered to be as sensitive as bone scintigraphy in the detection of sacral stress fractures, though neither is as specific as

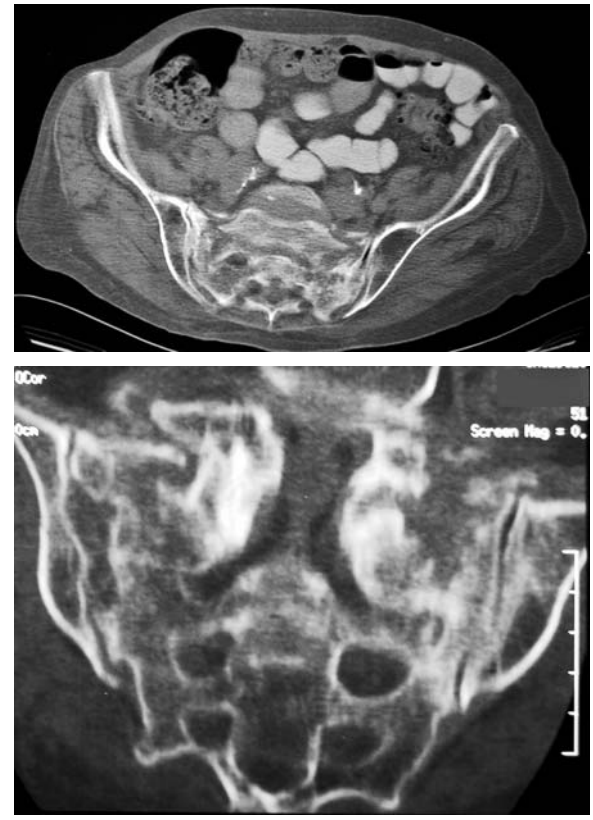

Fig. 24.24a,b. Sacral insufficiency stress fracture in a 76-year-old woman. **a** Non-enhanced axial CT image. **b** Non-enhanced coronal CT image

CT (Ahovuo et al. 2004). In cases where MRI is non-diagnostic, and there is increased suspicion for this diagnosis, CT evaluation is recommended. Each of these modalities has proven useful in detecting stress injury to the sacrum, but, to our knowledge, there is no general consensus as to which is the best study or combination of studies to obtain.

Insufficiency stress fractures occur when normal stress is applied to bone that is either weakened or displays decreased elastic resistance. In the last 20 years, insufficiency fractures of the sacrum have gained increasing attention as a source of low back pain in the elderly population (Cooper et al. 1985; Peh et al. 1996; Schneider et al. 1985). Non-specific presenting symptoms and subtle radiographic findings have traditionally caused such fractures to be under-diagnosed. Though improvements in imaging studies have been partly responsible for the greater attention being paid to sacral insufficiency fractures, increased awareness has also played a large part. Osteoporosis has been implicated as the central predisposing factor for developing sacral insufficiency frac-

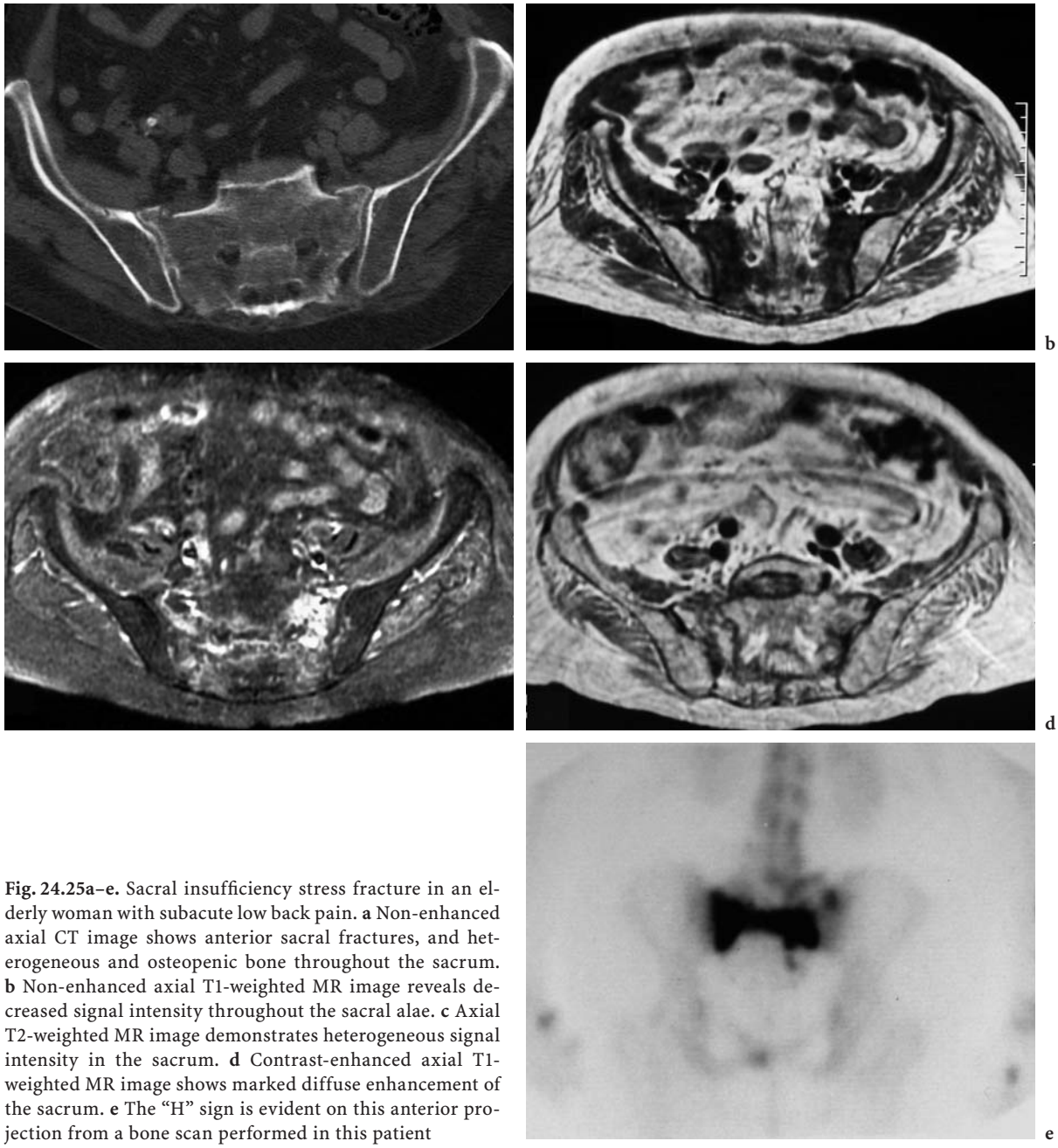

Fig. 24.25a–e. Sacral insufficiency stress fracture in an elderly woman with subacute low back pain. **a** Non-enhanced axial CT image shows anterior sacral fractures, and heterogeneous and osteopenic bone throughout the sacrum. **b** Non-enhanced axial T1-weighted MR image reveals decreased signal intensity throughout the sacral alae. **c** Axial T2-weighted MR image demonstrates heterogeneous signal intensity in the sacrum. **d** Contrast-enhanced axial T1-weighted MR image shows marked diffuse enhancement of the sacrum. **e** The "H" sign is evident on this anterior projection from a bone scan performed in this patient

tures (Gotis-Graham et al. 1994). The vast majority of these fractures are seen in women. Radiation therapy of the pelvis is another major risk factor (Rafi et al. 1988). Exposure above 40 Gy has been shown to induce atrophy of bone secondary to vascular supply damage, and irradiation may further weaken bone by exerting a direct effect on osteocytes (Rafi et al. 1988). Slow to present, these changes are not usually radiographically detectible for the first year after treatment. Fractures are more likely to occur as the changes manifest, often seen progressing up to the 3rd to 5th year post-irradiation (Rafi et al. 1988). Other common predisposing factors are long-term steroid use and rheumatoid arthritis (Cooper et al. 1985).

Clinically diagnosing sacral insufficiency fractures is difficult due to the non-specific presentation (Schneider et al. 1985). These fractures usually occur without an inciting incident. When a patient reports a history of trauma, it is usually limited to a minor event (Cooper et al. 1985; Peh et al. 1996).

Patients typically present with low back pain, often in the region of the sacroiliac joints (Cooper et al. 1985; Stroebel et al. 1991). The pain may be acute in onset and exacerbated by weight bearing and ambulation. Suggestive of radicular compression, the pain commonly radiates to the buttock, hip, or lower extremities (Schneider et al. 1985). Local sacral tenderness and decreased range of lower back motion are common. Neurological findings are otherwise normal (Gotis-Graham et al. 1994; Stroebel et al. 1991).

Sacral insufficiency fractures usually extend vertically within the sacral alae, lateral to the margin of the lumbar spine (Fig. 24.25) (Cooper et al. 1985; Rafi et al. 1988). Body weight is transmitted from the spine to the sacrum and sacral alae, then to the iliac wings. The location of sacral insufficiency fractures is consistent with this transfer of force as the causal mechanism (Gotis-Graham et al. 1994). Sacral insufficiency fractures are usually bilateral at the time of diagnosis (Cooper et al. 1985; Rafi et al. 1988). It is thought that the fracture, which may initially be unilateral, becomes bilateral with more intense or continued stress. Further stress can also result in the development of a horizontal component, and this, in turn, may progress to completion of the fracture, where the upper fragment is sometimes seen displaced anteriorly on the lower fragment (Gotis-Graham et al. 1994). Sacral insufficiency fractures are often seen in association with other insufficiency fractures of the pelvis, most commonly the pubic bone and often involving the ilium.

Plain radiography is of limited use for specifically diagnosing sacral insufficiency fractures, as these patients are osteoporotic. The main radiographic finding is sclerosis, which results from endosteal callus formation and trabecular compression (Cooper et al. 1985; Gotis-Graham et al. 1994; Stroebel et al. 1991). These sclerotic changes may be very subtle, are often only appreciated in retrospect, or may be impossible to detect, especially in cases of very recent fractures that have not yet produced callus (Gotis-Graham et al. 1994; Rafi et al. 1988; Schneider et al. 1985). Skeletal scintigraphy has proven to be a useful test for detecting sacral insufficiency fractures and is capable of demonstrating abnormalities before they are evident on plain films (Cooper et al. 1985; Peh et al. 1996). The typical scintigraphic manifestation of a sacral insufficiency fracture is the "H" sign, which corresponds to increased uptake in the sacral alae as well as a transverse component corresponding to the sacral body (Peh et al. 1996; Schneider et al. 1985; Stroebel et al. 1991). While this pattern is considered pathognomonic, several incomplete variants may also be observed. It has recently been shown that sacral insufficiency fractures are also detectable with positron emission tomography (PET). Fractures inadvertently detected during metastatic screening may be misinterpreted as sites of tumor, as findings characteristic for insufficiency fractures are not well-defined for PET. Correlation with cross-sectional imaging, especially with PET-CT, can help to differentiate fractures from metastases (Fayad et al. 2003).

CT can be used to evaluate sacral insufficiency fractures. CT images frequently show cortical disruption or fracture lines that are not visible on plain radiographs (Cooper et al. 1985; Peh et al. 1996). Sclerotic foci may also be identified with CT. The CT findings in sacral insufficiency fractures, however, can be subtle. MRI can reveal fracture lines earlier in the clinical course as compared to CT. MRI shows edema as an area of decreased signal intensity on T1-weighted images and increased signal intensity on T2-weighted images, but discrete fracture lines can also be seen. Detection is improved with the addition of contrast-enhanced fat-suppressed images.

References

Ahovuo JA, Kiuru MJ, Visuri TV (2004) Fatigue stress fractures of the sacrum: diagnosis with MR imaging. Eur Radiol 14:500–505

Albert TJ, Levine MJ, An HS et al. (1993) Concomitant noncontiguous thoracolumbar and sacral fractures. Spine 18:1285–1291

Banna M (1985) Clinical radiology of the spine and the spinal cord. Aspen, Gaithersburg, MD

Barkovich AJ (2000) Pediatric neuroimaging, 3rd ed. Lippincott Williams & Wilkins, Philadelphia, pp 621–683

Batson OV (1995) The function of the vertebral veins and their role in the spread of metastases. Clin Orthop 312:4–9

Bellabarba C, Stewart JD, Ricci WM et al. (2003) Midline sagittal sacral fractures in anterior-posterior compression pelvic ring injuries. J Orthop Trauma 17:32–37

Bennett DL, Ohashi K, El-Khoury GY (2004) Spondyloarthropathies: ankylosing spondylitis and psoriatic arthritis. Radiol Clin N Am 42:121–134

Borlaza GS, Seigel R, Kuhns LR,et al. (1981) Computed tomography in the evaluation of sacroiliac arthritis. Radiology 139:437–440

Cooper KL, Beabout JW, Swee RG (1985) Insufficiency fractures of the sacrum. Radiology 156:15–20

Davis SW, Levy LM, LeBihan DJ et al. (1993) Sacral meningeal cysts: evaluation with MR imaging. Radiology 187:445–448

Denis F, Davis S, Comfort T (1988) Sacral fractures: an important problem: retrospective analysis of 236 cases. Clin Orthop 227:67–81

Diel J, Ortiz O, Losada R et al. (2001) The sacrum: pathologic spectrum, multimodality imaging, and subspecialty approach. Radiographics 21:83–104

Dietemann JL, Caille JM, Manelfe C et al. (1992) The sacrum: normal and pathological aspects. In: Manelfe, C (ed) Imaging of the spine and spinal cord. Lippincott Williams & Wilkins, New York

Disler DG, Miklic D (1999) Imaging findings in tumors of the sacrum. Am J Roentgenol 173:1699–1706

Dougados M, van der Linden S, Juhlin R et al. (1991) The European spondylarthropathy study group preliminary criteria for the classification of spondylarthropathy. Arthritis Rheum 34:1218–1227

Fayad LM, Cohade C, Wahl RL et al. (2003) Sacral fractures: a potential pitfall of FDG positron emission tomography. AJR 181:1239–1243

Gibbons KJ, Soloniuk DS, Razack N (1990) Neurological injury and patterns of sacral fractures. J Neurosurg 72:889–893

Gierada DS, Erickson SJ, Haughton VM et al. (1993) MR imaging of the sacral plexus: normal findings. Am J Roentgenol 160:1059–1065

Gotis-Graham I, McGuigan L, Diamond T et al. (1994) Sacral insufficiency fractures in the elderly. J Bone Joint Surg [Br] 76:882–886

Hart DJ, Wang MY, Griffith P et al. (2004) Pediatric sacral fractures. Spine 6:667–670

Helms CA, Cann CE, Brunelle FO et al. (1981) Detection of bone-marrow metastases using quantitative computed tomography. Radiology 140:745–750

Horton KM, Ho AC, Frassica F et al. (2002) Optimal imaging of the sacrum: the role of spiral CT and 3D CT imaging – a pictorial review. Crit Rev Comput Tomogr 43:39–67

Johnson AW, Weiss CB, Sento K,et al. (2001) Stress fractures of the sacrum: an atypical cause of low back pain in the female. A J Sports Med 29:498–508

Klein MA, Winalski CS, Wax MR et al. (1991) MR imaging of septic sacroiliitis. J Comput Assist Tomogr 15:126–132

Lanzieri CF, Sacher M, Solodnik P et al. (1987) Unusual patterns of solitary sacral plasmacytoma. Am J Neuroradiol 8:566–567

Latchaw RE (1990) MR and CT imaging of head, neck and spine, 2nd ed. Mosby-Year Book, Chicago

Lemire RJ, Graham CB, Beckwith JB (1971) Skin–covered sacrococcygeal masses in infants and children. J Pediatr 79:948–954

Llauger J, Palmer J, Amores S et al. (2000) Primary tumors of the sacrum: diagnostic imaging. Am J Roentgenol 174:417–424

Luong AA, Salonen DC (2000) Imaging of the seronegative spondyloarthropathies. Curr Rheumatol Rep 2:288–296

Major NM, Helms CA (2000) Sacral stress fractures in long-distance runners. AJR 174:727–729

Merine D, Fishman EK, Magid D (1988) CT detection of sacral osteomyelitis associated with pelvic abscesses. J Comput Assist Tomogr 12:118–121

Moelleken SM, Seeger LL, Eckardt JJ et al. (1992) Myxopapillary ependymomas with extensive sacral destruction: CT and MR findings. J Comput Assist Tomogr 16:164-166

Moore KL, Dalley AF (1999) Clinically oriented anatomy, 4th ed. Lippincott Williams & Wilkins, New York

Murphey MD, Andrews CL, Flemming DJ et al. (1996) Primary tumors of the spine: radiologic–pathologic correlation. Radiographics 16:1131–1158

Murphey MD, Wetzel LH, Bramble JM et al. (1991) Sacroiliitis: MR imaging findings. Radiology 180:239–244

Ng EW, Porcu P, Loehrer PJ Jr (1999) Sacrococcygeal teratoma in adults: case reports and a review of the literature. Cancer 86:1198–1202

Nguyen BD, Daffner RH, Dash N et al. (1993) Case report 790. Mesenchymal chondrosarcoma of the sacrum. Skeletal Radiol 22:362–366

O'Neill OR, Piatt JH Jr, Mitchell P et al. (1995) Agenesis and dysgenesis of the sacrum: neurosurgical implications. Pediatr Neurosurg 22:20–28

Ortolan EG, Sola CA, Gruenberg MF et al. (1996) Giant sacral schwannoma. Spine 21:522–526

Parke WW (1992) Development of the spine. In: Rothman RH, Simeone FA, eds. The spine. 3rd edn. Saunders, Philadelphia

Patankar T, Krishnan A, Patkar D et al. (2000) Imaging in isolated sacral tuberculosis: a review of 15 cases. Skeletal Radiol 29:392–396

Patel MR, Louie W, Rachlin J (1997) Percutaneous fibrin glue therapy of meningeal cysts of the sacral spine. Am J Roentgenol 168:367–370

Paulsen RD, Call GA, Murtagh FR (1994) Prevalence and percutaneous drainage of cysts of the sacral nerve root sheath (Tarlov cysts). Am J Neuroradiol 15:293–297

Peh WCG, Khong P, Yin Y et al. (1996) Imaging of pelvic insufficiency fractures. Radiographics 16:335–348

Puhakka KB, Jurik AG, Egund N, Schiottz-Christensen B et al. (2003) Imaging of sacroiliitis in early seronegative spondyloarthropathy. Acta Radiologica 44:218–229

Rafii M, Firooznia H, Golimbu C et al. (1988) Radiation induced fractures of sacrum: CT diagnosis. J Comput Assist Tomogr 12:231–235

Schey WL, Shkolnik A, White H (1977) Clinical and radiographic considerations of sacrococcygeal teratomas. An analysis of 26 new cases and review of the literature. Radiology 125:189–195

Schnee CL, Hurst RW, Curtis MT et al. (1994) Carcinoid tumor of the sacrum: case report. Neurosurgery 35:1163–1167

Schneider R, Yacovone J, Ghelman B (1985) Unsuspected sacral fractures: detection by radionuclide bone scanning. AJR 144:337–341

Smith SE, Murphey MD, Motamedi K et al. (2002) From the archives of the AFIP: radiologic spectrum of paget disease of bone and its complications with pathologic correlation. Radiographics 22:1191–1216

Steinbok P et al. (1992) Intramedullary spinal cord tumors in children. In: Berger MS (ed) Pediatric neuro-oncology. Saunders, Philadelphia, pp 931–945

Stroebel RJ, Ginsburg WW, McLeod A (1991) Sacral insufficiency fractures: an often unsuspected cause of low back pain. J Rheumatol 18:117–119

Stürzenbecher A, Braun J, Paris S et al. (2000) MR imaging of septic sacroiliitis. Skeletal Radiol 29:439–446

Verbout AJ (1985) The development of the vertebral column. Adv Anat Embryol Cell Biol 90:1–122

White JH, Hague C, Nicolaou S et al. (2003) Imaging of sacral fractures. Clin Radiol 58:914–921

Whitehouse GH, Griffiths GJ (1976) Roentgenologic aspects of spinal involvement by primary and metastatic Ewing's tumor. J Can Assoc Radiol 27:290–297

Wittram C, Whitehouse GH, Williams JW et al. (1996) A comparison of MR and CT in suspected sacroiliitis. J Comput Assist Tomogr 20:68–72

Subject Index

D

E

F

G

H

I

J

K

L

M

N

O

P

R

S

T

U

V

W

Y

Z

List of Contributors

Paul R. Algra, MD
Department of Radiology and Neuroradiology
Medisch Centrum Alkmaar
Alkmaar
The Netherlands

Cosma Andreula, MD
Director, Neuroradiology and Radiology
Anthea Hospital Bari
Città di lecce Hospital Lecce
Gruppo Villa Maria
via C. Rosalba 35-37
70100 Bari
Italy

Danielle Balériaux, MD
Professor, Department of Radiology
Clinique de Neuroradiologie
Hôpital Erasme
Université Libre de Bruxelles
808 Route de Lennik,
1070 Brussels
Belgium

Stephen M. Belkoff, PhD
Associate Professor and Director
International Center for Orthopaedic Advancement
Department of Orthopaedic Surgery
Johns Hopkins University / Johns Hopkins
Bayview Medical Center
4940 Eastern Avenue, A674
Baltimore, MD 21224-2780
USA

Rita G. Bhatia, MD
Department of Radiology
Neuroradiology Section
Jackson Memorial Hospital / Miller School of Medicine
1611 NW 12th Avenue
Miami, FL 33136
USA

Brian C. Bowen, MD, PhD
Department of Radiology
Neuroradiology Section
Jackson Memorial Hospital / Miller School of Medicine
1611 NW 12th Avenue
Miami, FL 33136
USA

Oznur Boyunaga, MD
Associate Professor
Department of Radiology
Divisions of Neuroradiology and Pediatric Radiology
Gazi University School of Medizine
Besevler 06510 Ankara
Turkey

Armando Cama, MD
Head, Department of Pediatric Neuroradiology
G. Gaslini Children's Research Hospital
Largo G. Gaslini 5
16147 Genoa
Italy

Silvia Capoccia, MD
Department of Radiology
Hospital "S. Maria della Stella"
Piazza Duomo
05018 Orvieto
Italy

Roberto Cartolari, MD
Hospital Belcolle
Department of Neuroradiology
Via R. Capocci 13
01100 Viterbo
Italy

Andrew Y. Choi, MD
Department of Radiology
Winthrop-University Hospital
259 First Street
Mineola, NY 11501
USA

Mauro Colajacomo, MD
Department of Radiology
Paediatric Hospital "Bambino Gesù" Palidoro
Via Torre di Palidoro
00050 Passoscuro (Fiumicino)
Roma
Italy

Concetto Cristaudo, MD
Director of Neuroradiology
Department of Neuroradiology
Hospital Cannizzaro
Via Messina 829
95127 Catania
Italy

Philippe Demaerel, MD
Professor, Department of Radiology
University Hospitals K.U.L.
Herestraat 49
3000 Leuven
Belgium

Arthur M. De Schepper, MD, PhD
Consultant – Professor of Radiology
Leiden University Medical Centre
Albinusdreef 2
PO Box 9600
2300 RC, Leiden
The Netherlands
and
Emeritus Professor of Radiology
University Hospital Antwerp
Edegem
Belgium

Massimo Gallucci, MD
Department of Radiology
University of L'Aquila
Ospedale Nuovo S. Salvatore
Località Coppito
67100 L'Aquila
Italy

Carlo Gandolfo, MD
Staff Neuroradiologist,
Department of Pediatric Neuroradiology
G. Gaslini Children's Research Hospital
Largo G. Gaslini 5
16147 Genoa
Italy

Neslìhan Gültaşli, MD
Department of Radiology
Clinique de Neuroradiologie
Hôpital Erasme
Université Libre de Bruxelles
808 Route de Lennik,
1070 Brussels
Belgium

Robert Gunzburg, MD, PhD
Centenary Clinic
Harmoniestraat 68
2018 Antwerp
Belgium

S. H. M. Kahn, FRCR
Consultant Radiologist
Department of Radiology
East Lancashire NHS Trust
Blackburn Royal Infirmary
Bolton Road
Blackburn
Lancashire, BB2 3LR
UK

Douglas S. Katz, MD
Department of Radiology
Winthrop-University Hospital
259 First Street
Mineola, NY 11501
USA

Paul E. Kim, MD
Assistant Professor of Clinical Radiology
University of Southern California Keck School of Medicine
1200 N. State Street, Room 3740
Los Angeles, CA 90033
USA

Bart Koes, PhD
Department of General Practice
Erasmus MC-University Medical Center Rotterdam
3062 PA Rotterdam
Burgemeester Oudlaan 50
The Netherlands

Jostein Kråkenes, MD, PhD
Head of Section of Neuroradiology
Haukeland University Hospital
5021 Bergen
Norway

Steven J. Lypen, BS
239 Douglas Rd.
Staten Island, NY 10304
USA

Menno Maes, MD
Department of Radiology
Sint-Vincentius Hospital
Sint-Vincentiusstraat 20
2018 Antwerp
Belgium

Claude Manelfè, MD
Service de Neuroradiologie
CHU Purpan
Place du Docteur Baylac
31059 Toulouse
France

Luigi Manfré, MD
Department of Neuroradiology
Hospital Cannizzaro
Via Messina 829
95127 Catania
Italy

Mario Murrone, MD
Citta di lecce Hospital
Va Provinciale per Arnesano 4
73100 Lecce
Italy

A. Orlando Ortiz, MD, MBA
Department of Radiology
Winthrop-University Hospital
259 First Street
Mineola, NY 11501
USA

Özkan Özsarlak, MD
Department of Radiology
University Hospital Antwerp
Wilrijkstraat 10
2650 Edegem
Belgium

Paul M. Parizel, MD, PhD
Department of Radiology
University Hospital Antwerpen
Wilrijkstraat 10
2650 Edegem
Belgium

Andrea Rossi, MD
Senior Staff Neuroradiologist
Department of Pediatric Neuroradiology
G. Gaslini Children's Research Hospital
Largo G. Gaslini 5
16147 Genoa
Italy

Rodrigo Salgado, MD
Department of Radiology
University Hospital Antwerp
Wilrijkstraat 10
2650 Edegem
Belgium

Marek Szpalski, MD
Centre Hospitalier Molière Longchamp
Rue Marconi 142
1180 Brussels
Belgium

Turgut Tali, MD
Professor, Department of Radiology
Divisions of Neuroradilogy and Pediatric Radiology
Gazi University, School of Medicine
Besevler Ankara 06510
Turkey

Majda M. Thurnher, MD
Associate Professor of Radiology
Neuroradiology Section
Department of Radiology
University Hospital Vienna
Waehringer Guertel 18–20
1090 Vienna
Austria

Paolo Tortori-Donati, MD
Head, Department of Pediatric Neuroradiology
G. Gaslini Children's Research Hospital
Largo G. Gaslini 5
16147 Genoa
Italy

Guido Trasimeni, MD
Department of Neuroradiology
Hospital Sant'Andrea
University La Sapienza Rome
Via di Grottarossa 1035
00189 Rome
Italy

Anja Van Campenhout, MD
Department of Orthopaedics
University Hospital Leuven
Pellenberg
Weligervfeld 1
3212 Pellenberg
Belgium

Erik van de Kelft, MD, PhD
Department of Neurosurgery
AZ Nikolaas
Moerlandstraat 1
9100 Sint-Niklaas
Belgium

Luc van den Hauwe, MD
Department of Radiology
University Hospital Antwerpen
Wilrijkstraat 10
2650 Edegem
Belgium
and
Department of Radiology
AZ KLINA
Augustijnslei 100
2930 Brasschaat
Belgium

Johan W. M. Van Goethem, MD, PhD
Department of Radiology
University Hospital Antwerpen
Wilrijkstraat 10
2650 Edegem
Belgium
and
Department of Radiology
AZ Nikolaas
Moerlandstraat 1
9100 Sint-Niklaas
Belgium

Filip M. Vanhoenacker, MD, PhD
Department of Radiology
University Hospital Antwerp
Wilrijkstraat 10
2650 Edegem
Belgium

Maurits van Tulder, MD, PhD
Institute for Research in Extramural Medicine (EMGO)
VU University Medical Center and
Institute for Health Sciences
Faculty of Earth & Life Sciences
Van der Boechorststraat 7
1081 BT Amsterdam
The Netherlands

Mauritis Voormolen, MD, PhD
Department of Radiology
University Hospital Antwerpen
Wilrijkstraat 10
2650 Edegem
Belgium

Chi Shing Zee, MD
Professor of Radiology
Chief, Division of Neuroradiology
University of Southern California
Keck School of Medicine
1200 N. State Street, Room 3740
Los Angeles, CA 90033
USA

Medical Radiology Diagnostic Imaging and Radiation Oncology

Titles in the series already published

Diagnostic Imaging

Innovations in Diagnostic Imaging
Edited by J. H. Anderson

Radiology of the Upper Urinary Tract
Edited by E. K. Lang

The Thymus - Diagnostic Imaging, Functions, and Pathologic Anatomy
Edited by E. Walter, E. Willich, and W. R. Webb

Interventional Neuroradiology
Edited by A. Valavanis

Radiology of the Pancreas
Edited by A. L. Baert, co-edited by G. Delorme

Radiology of the Lower Urinary Tract
Edited by E. K. Lang

Magnetic Resonance Angiography
Edited by I. P. Arlart, G. M. Bongartz, and G. Marchal

Contrast-Enhanced MRI of the Breast
S. Heywang-Köbrunner and R. Beck

Spiral CT of the Chest
Edited by M. Rémy-Jardin and J. Rémy

Radiological Diagnosis of Breast Diseases
Edited by M. Friedrich and E.A. Sickles

Radiology of the Trauma
Edited by M. Heller and A. Fink

Biliary Tract Radiology
Edited by P. Rossi, co-edited by M. Brezi

Radiological Imaging of Sports Injuries
Edited by C. Masciocchi

Modern Imaging of the Alimentary Tube
Edited by A. R. Margulis

Diagnosis and Therapy of Spinal Tumors
Edited by P. R. Algra, J. Valk, and J. J. Heimans

Interventional Magnetic Resonance Imaging
Edited by J. F. Debatin and G. Adam

Abdominal and Pelvic MRI
Edited by A. Heuck and M. Reiser

Orthopedic Imaging
Techniques and Applications
Edited by A. M. Davies and H. Pettersson

Radiology of the Female Pelvic Organs
Edited by E. K.Lang

Magnetic Resonance of the Heart and Great Vessels
Clinical Applications
Edited by J. Bogaert, A.J. Duerinckx, and F. E. Rademakers

Modern Head and Neck Imaging
Edited by S. K. Mukherji and J. A. Castelijns

Radiological Imaging of Endocrine Diseases
Edited by J. N. Bruneton in collaboration with B. Padovani and M.-Y. Mourou

Trends in Contrast Media
Edited by H. S. Thomsen, R. N. Muller, and R. F. Mattrey

Functional MRI
Edited by C. T. W. Moonen and P. A. Bandettini

Radiology of the Pancreas
2nd Revised Edition
Edited by A. L. Baert. Co-edited by G. Delorme and L. Van Hoe

Emergency Pediatric Radiology
Edited by H. Carty

Spiral CT of the Abdomen
Edited by F. Terrier, M. Grossholz, and C. D. Becker

Liver Malignancies
Diagnostic and Interventional Radiology
Edited by C. Bartolozzi and R. Lencioni

Medical Imaging of the Spleen
Edited by A. M. De Schepper and F. Vanhoenacker

Radiology of Peripheral Vascular Diseases
Edited by E. Zeitler

Diagnostic Nuclear Medicine
Edited by C. Schiepers

Radiology of Blunt Trauma of the Chest
P. Schnyder and M. Wintermark

Portal Hypertension
Diagnostic Imaging-Guided Therapy
Edited by P. Rossi
Co-edited by P. Ricci and L. Broglia

Recent Advances in Diagnostic Neuroradiology
Edited by Ph. Demaerel

Virtual Endoscopy and Related 3D Techniques
Edited by P. Rogalla, J. Terwisscha Van Scheltinga, and B. Hamm

Multislice CT
Edited by M. F. Reiser, M. Takahashi, M. Modic, and R. Bruening

Pediatric Uroradiology
Edited by R. Fotter

Transfontanellar Doppler Imaging in Neonates
A. Couture and C. Veyrac

Radiology of AIDS
A Practical Approach
Edited by J.W.A.J. Reeders and P.C. Goodman

CT of the Peritoneum
Armando Rossi and Giorgio Rossi

Magnetic Resonance Angiography
2nd Revised Edition
Edited by I. P. Arlart, G. M. Bongratz, and G. Marchal

Pediatric Chest Imaging
Edited by Javier Lucaya and Janet L. Strife

Applications of Sonography in Head and Neck Pathology
Edited by J. N. Bruneton in collaboration with C. Raffaelli and O. Dassonville

Imaging of the Larynx
Edited by R. Hermans

3D Image Processing
Techniques and Clinical Applications
Edited by D. Caramella and C. Bartolozzi

Imaging of Orbital and Visual Pathway Pathology
Edited by W. S. Müller-Forell

Pediatric ENT Radiology
Edited by S. J. King and A. E. Boothroyd

Radiological Imaging of the Small Intestine
Edited by N. C. Gourtsoyiannis

Imaging of the Knee
Techniques and Applications
Edited by A. M. Davies and V. N. Cassar-Pullicino

Perinatal Imaging
From Ultrasound to MR Imaging
Edited by Fred E. Avni

Radiological Imaging of the Neonatal Chest
Edited by V. Donoghue

Diagnostic and Interventional Radiology in Liver Transplantation
Edited by E. Bücheler, V. Nicolas, C. E. Broelsch, X. Rogiers, and G. Krupski

Radiology of Osteoporosis
Edited by S. Grampp

Imaging Pelvic Floor Disorders
Edited by C. I. Bartram and J. O. L. DeLancey
Associate Editors: S. Halligan, F. M. Kelvin, and J. Stoker

Imaging of the Pancreas
Cystic and Rare Tumors
Edited by C. Procacci and A. J. Megibow

High Resolution Sonography of the Peripheral Nervous System
Edited by S. Peer and G. Bodner

Imaging of the Foot and Ankle
Techniques and Applications
Edited by A. M. Davies, R. W. Whitehouse, and J. P. R. Jenkins

Radiology Imaging of the Ureter
Edited by F. Joffre, Ph. Otal, and M. Soulie

Imaging of the Shoulder
Techniques and Applications
Edited by A. M. Davies and J. Hodler

Radiology of the Petrous Bone
Edited by M. Lemmerling and S. S. Kollias

Interventional Radiology in Cancer
Edited by A. Adam, R. F. Dondelinger, and P. R. Mueller

Duplex and Color Doppler Imaging of the Venous System
Edited by G. H. Mostbeck

Multidetector-Row CT of the Thorax
Edited by U. J. Schoepf

Functional Imaging of the Chest
Edited by H.-U. Kauczor

Radiology of the Pharynx and the Esophagus
Edited by O. Ekberg

Radiological Imaging in Hematological Malignancies
Edited by A. Guermazi

Imaging and Intervention in Abdominal Trauma
Edited by R. F. Dondelinger

Multislice CT
2nd Revised Edition
Edited by M. F. Reiser, M. Takahashi, M. Modic, and C. R. Becker

Intracranial Vascular Malformations and Aneurysms
From Diagnostic Work-Up to Endovascular Therapy
Edited by M. Forsting

Radiology and Imaging of the Colon
Edited by A. H. Chapman

Coronary Radiology
Edited by M. Oudkerk

Dynamic Contrast-Enhanced Magnetic Resonance Imaging in Oncology
Edited by A. Jackson, D. L. Buckley, and G. J. M. Parker

Imaging in Treatment Planning for Sinonasal Diseases
Edited by R. Maroldi and P. Nicolai

Clinical Cardiac MRI
With Interactive CD-ROM
Edited by J. Bogaert, S. Dymarkowski, and A. M. Taylor

Focal Liver Lesions
Detection, Characterization, Ablation
Edited by R. Lencioni, D. Cioni, and C. Bartolozzi

Multidetector-Row CT Angiography
Edited by C. Catalano and R. Passariello

Paediatric Musculoskeletal Diseases
With an Emphasis on Ultrasound
Edited by D. Wilson

Contrast Media in Ultrasonography
Basic Principles and Clinical Applications
Edited by Emilio Quaia

MR Imaging in White Matter Diseases of the Brain and Spinal Cord
Edited by M. Filippi, N. De Stefano, V. Dousset, and J. C. McGowan

Diagnostic Nuclear Medicine
2nd Revised Edition
Edited by C. Schiepers

Imaging of the Kidney Cancer
Edited by A. Guermazi

Magnetic Resonance Imaging in Ischemic Stroke
Edited by R. von Kummer and T. Back

Imaging of the Hip & Bony Pelvis
Techniques and Applications
Edited by A. M. Davies, K. J. Johnson, and R. W. Whitehouse

Imaging of Occupational and Environmental Disorders of the Chest
Edited by P. A. Gevenois and P. De Vuyst

Contrast Media
Safety Issues and ESUR Guidelines
Edited by H. S. Thomsen

Virtual Colonoscopy
A Practical Guide
Edited by P. Lefere and S. Gryspeerdt

Vascular Embolotherapy
A Comprehensive Approach
Volume 1: *General Principles, Chest, Abdomen, and Great Vessels*
Edited by J. Golzarian. Co-edited by S. Sun and M. J. Sharafuddin

Vascular Embolotherapy
A Comprehensive Approach
Volume 2: *Oncology, Trauma, Gene Therapy, Vascular Malformations, and Neck*
Edited by J. Golzarian. Co-edited by S. Sun and M. J. Sharafuddin

Head and Neck Cancer Imaging
Edited by R. Hermans

Vascular Interventional Radiology
Current Evidence in Endovascular Surgery
Edited by M. G. Cowling

Ultrasound of the Gastrointestinal Tract
Edited by G. Maconi and G. Bianchi Porro

Imaging of Orthopedic Sports Injuries
Edited by F. M. Vanhoenacker, M. Maas, J. L. M. A. Gielen

Parallel Imaging in Clinical MR Applications
Edited by S. O. Schoenberg, O. Dietrich, and F. M. Reiser

MR and CT of the Female Pelvis
Edited by B. Hamm and R. Forstner

Ultrasound of the Musculoskeletal System
S. Bianchi and C. Martinoli

Spinal Imaging
Diagnostic Imaging of the Spine and Spinal Cord
Edited by J. W. M. Van Goethem, L. Van den Hauwe, and P. M. Parizel

Radiation Dose from Adult and Pediatric Multidetector Computed Tomography
Edited by D. Tack and P. A. Gevenois

Computed Tomography of the Lung
A Pattern Approach
J. A. Verschakelen and W. De Wever

Clinical Functional MRI
Presurgical Functional Neuroimaging
Edited bei C. Stippich

Springer

Medical Radiology Diagnostic Imaging and Radiation Oncology

Titles in the series already published

Radiation Oncology

Lung Cancer
Edited by C.W. Scarantino

Innovations in Radiation Oncology
Edited by H. R. Withers
and L. J. Peters

Radiation Therapy
of Head and Neck Cancer
Edited by G. E. Laramore

Gastrointestinal Cancer –
Radiation Therapy
Edited by R.R. Dobelbower, Jr.

Radiation Exposure
and Occupational Risks
Edited by E. Scherer, C. Streffer,
and K.-R. Trott

Radiation Therapy of Benign Diseases
A Clinical Guide
S. E. Order and S. S. Donaldson

Interventional Radiation
Therapy Techniques – Brachytherapy
Edited by R. Sauer

Radiopathology of Organs and Tissues
Edited by E. Scherer, C. Streffer,
and K.-R. Trott

Concomitant Continuous Infusion
Chemotherapy and Radiation
Edited by M. Rotman
and C. J. Rosenthal

Intraoperative Radiotherapy –
Clinical Experiences and Results
Edited by F. A. Calvo, M. Santos,
and L.W. Brady

Radiotherapy of Intraocular
and Orbital Tumors
Edited by W. E. Alberti and
R. H. Sagerman

Interstitial and Intracavitary
Thermoradiotherapy
Edited by M. H. Seegenschmiedt
and R. Sauer

Non-Disseminated Breast Cancer
Controversial Issues in Management
Edited by G. H. Fletcher and S.H. Levitt

Current Topics in
Clinical Radiobiology of Tumors
Edited by H.-P. Beck-Bornholdt

Practical Approaches to
Cancer Invasion and Metastases
A Compendium of Radiation
Oncologists' Responses to 40 Histories
Edited by A. R. Kagan with the
Assistance of R. J. Steckel

Radiation Therapy in Pediatric Oncology
Edited by J. R. Cassady

Radiation Therapy Physics
Edited by A. R. Smith

Late Sequelae in Oncology
Edited by J. Dunst and R. Sauer

Mediastinal Tumors. Update 1995
Edited by D. E. Wood and C. R. Thomas, Jr.

Thermoradiotherapy
and Thermochemotherapy
Volume 1:
Biology, Physiology, and Physics
Volume 2:
Clinical Applications
Edited by M.H. Seegenschmiedt,
P. Fessenden, and C.C. Vernon

Carcinoma of the Prostate
Innovations in Management
Edited by Z. Petrovich, L. Baert,
and L.W. Brady

Radiation Oncology
of Gynecological Cancers
Edited by H.W. Vahrson

Carcinoma of the Bladder
Innovations in Management
Edited by Z. Petrovich, L. Baert,
and L.W. Brady

Blood Perfusion and
Microenvironment of Human Tumors
Implications for Clinical Radiooncology
Edited by M. Molls and P. Vaupel

Radiation Therapy of Benign Diseases
A Clinical Guide
2nd Revised Edition
S. E. Order and S. S. Donaldson

Carcinoma of the Kidney and Testis,
and Rare Urologic Malignancies
Innovations in Management
Edited by Z. Petrovich, L. Baert,
and L.W. Brady

Progress and Perspectives in the
Treatment of Lung Cancer
Edited by P. Van Houtte,
J. Klastersky, and P. Rocmans

Combined Modality Therapy of
Central Nervous System Tumors
Edited by Z. Petrovich, L. W. Brady,
M. L. Apuzzo, and M. Bamberg

Age-Related Macular Degeneration
Current Treatment Concepts
Edited by W. A. Alberti, G. Richard,
and R. H. Sagerman

Radiotherapy of Intraocular
and Orbital Tumors
2nd Revised Edition
Edited by R. H. Sagerman,
and W. E. Alberti

Modification of Radiation Response
Cytokines, Growth Factors,
and Other Biolgical Targets
Edited by C. Nieder, L. Milas,
and K. K. Ang

Radiation Oncology for Cure and Palliation
R. G. Parker, N. A. Janjan,
and M. T. Selch

Clinical Target Volumes in Conformal and
Intensity Modulated Radiation Therapy
A Clinical Guide to Cancer Treatment
Edited by V. Grégoire, P. Scalliet,
and K. K. Ang

Advances in Radiation Oncology
in Lung Cancer
Edited by Branislav Jeremić

New Technologies in Radiation Oncology
Edited by W. Schlegel, T. Bortfeld,
and A.-L. Grosu

Technical Basis of Radiation Therapy
4th Revised Edition
Edited by S. H. Levitt, J. A. Purdy,
C. A. Perez, and S. Vijayakumar

Clinical Practice of Radiation Therapy for
Benign Diseases Contemporary Concepts
and Clinical Results
Edited by M. H. Seegenschmiedt,
H.-B. Makoski, K.-R. Trott, and
L. W. Brady

Springer